AD/A-003 801

WIND MODELS FOR FLIGHT SIMULATOR CERTIFICATION OF LANDING AND APPROACH GUIDANCE AND CONTROL SYSTEMS

Neal M. Barr, et al

Boeing Commercial Airplane Company

Prepared for:

Federal Aviation Administration

December 1974

NOTICE

This document is disseminated under the sponsorship of the Department of Transportation in the interest of information exchange. The United States Government assumes no liability for its contents or use thereof.

TECHNICAL REPORT STANDARD TITLE PAGE

1 Report No. FAA-RD-74-206	2. Government Accession No.	3. Recipient's Catalog No. AD/A-003 801
4 Title and Subtitle WIND MODELS FOR FLIGHT SIMULATOR CERTIFICATION OF LANDING AND APPROACH GUIDANCE AND CONTROL SYSTEMS		5 Report Date December 1974 6. Performing Organization Code
7 Author(s) Neal M. Barr, Dagfinn Gangsaas, and Dwight R. Schaeffer		8. Performing Organization Report No.
9. Performing Organization Name and Address Boeing Commercial Airplane Company P.O. Box 3707 Seattle, Washington 98124		10. Work Unit No. TRAIS- 45149 11. Contract or Grant No. DOT-FA72WA-2934
12. Sponsoring Agency Name and Address U.S. Department of Transportation Federal Aviation Administration Systems Research and Development Service Washington, D.C. 20590		13. Type of Report and Period Covered Final Report 14 Sponsoring Agency Code

15 Supplementary Notes

16. Abstract

Analytic and probabilistic descriptions of low-altitude mean wind and turbulence have been investigated and a description selected. The effects of wind and turbulence on aerodynamics and aircraft motion have been analyzed. A model of wind and turbulence, suitable for the certification of landing and approach guidance and control systems by flight simulations, has been developed, and consideration has been given to implementation.

17. Key Words	18. Distribution Statement
Approach and landing Atmospheric boundary layer Guidance and control systems Mean wind Simulation Turbulence	Document is available to the public through the National Technical Information Service, Springfield, Virginia 22151. PRICES SUBJECT TO CHANGE

19. Security Classif. (of this report)	20. Security Classif. (of this page)	21. No. of Pages	22. Price
Unclassified	Unclassified	622	$15.25

Form DOT F 1700.7 (8 69)

PREFACE

This report was prepared under the direction of Kenneth Kraus, from the Federal Aviation Administration. Boeing project manager and co-principal investigator was Dwight R. Schaeffer, flight dynamicist. Co-principal investigator responsible for Section 3, "Probabilistic Description of the Low Altitude Atmosphere," was Neal M. Barr, meteorologist. Dagfinn Gangsaas, aerodynamicist, served as associate investigator and studied the variances of low-altitude turbulence and simulation techniques for generating random noise.

CONTENTS

	Page
1.0 INTRODUCTION, SUMMARY, AND PROPOSED MODEL	1
1.1 Introduction	1
1.2 Nomenclature	3
1.3 Summary	7
1.3.1 Mean Wind	8
1.3.2 Turbulence	37
1.4 Wind Model for Automatic Landing System Certification	62
APPENDIX 1A COMPARISON OF PROPOSED MODEL WITH ARB MODEL	69
Mean Wind	69
Turbulence	73
APPENDIX 1B COMPARISON OF PROPOSED MODEL WITH FAA MODEL	81
Mean Wind	81
Turbulence	85
APPENDIX 1C COMPARISON OF PROPOSED MODEL WITH MILITARY MODEL	91
Mean Wind	91
Turbulence	91
2.0 ANALYTIC DESCRIPTION OF LOW ALTITUDE WIND PHENOMENA	101
2.1 Nomenclature	102
2.2 Classification of Wind Phenomena	106
2.3 Mean Wind	108
2.3.1 Ekman Spiral	110
2.3.1.1 Derivation	110
2.3.1.2 Description	112
2.3.2 Logarithmic Profile	114
2.3.2.1 Development and Description	115
2.3.2.2 Roughness Length	116
2.3.2.3 Minimum Valid Altitude	121
2.3.2.4 Maximum Valid Altitude	121
2.3.3 The Power Law	122
2.3.3.1 Exponent Value	123
2.3.3.2 Relationship with Logarithmic Profile: Conditions for Validity	126
2.3.4 Influence of Nonadiabatic Thermal Conditions	128
2.3.4.1 Atmospheric Stability	128
2.3.4.2 Log-Linear Profile	130
2.3.4.3 Extension from the Log-Linear Profile	134
2.3.4.4 Deacon Wind Profile	139
2.3.4.5 Extension from the Power Law	140

CONTENTS (CONTINUED)

Page

2.3.5 Extension of the Mean Wind Profile to the Boundary Layer . . . 141
2.3.5.1 Boundary Layer Thickness and the Altitude Dependence of Friction Velocity . . . 143
2.3.5.2 Modification of the Mean Wind Profile From Similarity Theory . . . 148
2.3.6 Selection of Mean Wind Description . . . 152
2.4 Turbulence . . . 164
2.4.1 Statistical Functions for Turbulence Description . . . 166
2.4.1.1 Correlation Functions . . . 167
2.4.1.2 Probability Functions . . . 169
2.4.1.3 Spectrum Functions . . . 178
2.4.2 Isotropic Turbulence . . . 182
2.4.2.1 Fundamental Correlation Functions . . . 182
2.4.2.2 Interrelationships of Spectrum Functions . . . 185
2.4.2.3 Integral Scale . . . 187
2.4.2.4 Isotropic Turbulence Spectra Forms . . . 188
2.4.3 Low Altitude Turbulence . . . 199
2.4.3.1 Conditions of Limited Isotropy . . . 202
2.4.3.2 Low Altitude Power Spectra . . . 203
2.4.3.3 Low Altitude Cross Spectrum . . . 205
2.4.4 Magnitude of Turbulence . . . 208
2.4.4.1 Kinetic Energy in Turbulence Near the Ground . . . 208
2.4.4.2 Magnitude of the Turbulence Components . . . 216
2.4.5 The Scale of Low Altitude Turbulence . . . 243
2.4.5.1 Measurement of Turbulence and Integral Scales . . . 245
2.4.5.2 The Scale of Vertical Turbulence . . . 247
2.4.5.3 The Scale of Horizontal Turbulence . . . 252
2.4.6 Selection of a Low Altitude Turbulence Description . . . 257
2.4.6.1 Selected Assumptions . . . 257
2.4.6.2 Requirements for Statistical Functions . . . 260
2.4.6.3 Selected Turbulence Variance Description . . . 261
2.4.6.4 Selected Integral Scale Description . . . 267
2.4.6.5 Selected Cospectrum Description . . . 269
2.4.6.6 Composite Turbulence Description Selected . . . 281
2.5 References . . . 283

APPENDIX 2A EXTENSION OF MEAN WIND MODEL TO BOUNDARY LAYER 289

3.0 PROBABILISTIC DESCRIPTION OF THE LOW ALTITUDE ATMOSPHERE . 295
3.1 List of Symbols . . . 295
3.2 Near-Surface Wind and Wind Shear Information . . . 295
3.2.1 Evaluation of Surface (20-Foot)Wind Descriptions . . . 296
3.2.1.1 Wind Speed . . . 296
3.2.1.2 Wind Direction . . . 297
3.2.1.3 Crosswinds . . . 301
3.2.1.4 Headwind-Tailwind Description . . . 301

CONTENTS (CONTINUED)

Page

3.2.2 Mean Profiles From Instrumented Towers 301
3.2.3 Evaluation of Near-Surface Wind Shear Information From the Literature 307
3.2.3.1 Survey of World Locations 309
3.2.3.2 Summary 333
3.3 Evaluation of Tower Data 333
3.3.1 General Description 335
3.3.1.1 Cape Kennedy 335
3.3.1.2 Cedar Hills 336
3.3.2 Wind Speed 337
3.3.2.1 Evaluation Methods 337
3.3.2.2 Distribution at 20 Feet Elevation 337
3.3.2.3 Distribution with Height 337
3.3.3 Richardson's Number 337
3.3.3.1 Evaluation Methods 337
3.3.3.2 Distribution at 20 Feet Elevation 344
3.3.3.3 Richardson's Number and Speed at 20 Feet Elevation . . . 362
3.3.4 Wind Direction Shear 362
3.3.4.1 Evaluation Methods 362
3.3.4.2 Distribution with Speed at 20 Feet Elevation 362
3.3.4.3 Distribution with Height 369
3.3.5 Wind Speed Shear 369
3.3.5.1 Evaluation Methods 369
3.3.5.2 Distribution with Speed at 20 Feet Elevation 369
3.3.5.3 Distribution with Height for Two Speed Intervals at 20 Feet Elevation 373
3.3.6 Regression Equations and Correlation Coefficients 377
3.3.6.1 Evaluation Methods 377
3.3.6.2 Richardson's Number and Speed 377
3.3.6.3 Speed and Direction Shear 378
3.3.6.4 Richardson's Number and Direction Shear 385
3.3.6.5 Speed and Speed Shear 385
3.3.7 Comparison with Literature, Section 3.2.3 385
3.4 Selected Description 386
3.4.1 Airport Wind Speed Description 386
3.4.2 Airport Wind Direction Description 386
3.4.3 Description of Wind Direction Variation with Height 386
3.4.4 Richardson's Number-Wind Speed Description 386
3.5 References 388

4.0 ANALYSIS AND SIMULATION MODELING 395
4.1 Nomenclature 395
4.2 Effects of Winds on Aircraft Motion 405
4.2.1 Small Disturbance Analysis 405

CONTENTS (CONCLUDED)

Page

4.2.1.1 Effects of Mean Wind, Point Lift 408
4.2.1.2 Effects of Mean Wind, Distributed Lift 426
4.2.1.3 Effects of Turbulence 437
4.2.2 Large Disturbance Effects of Winds 486
4.3 Sorting Out the Axis Systems 491
4.3.1 Transformations 492
4.3.2 Isotropic Turbulence 499
4.3.3 Low Altitude Turbulence 504
4.3.4 Significance of Mean Wind Axis Cospectra 509
4.4 Noise Generation for Turbulence Simulation 512
4.4.1 Analog Computer Methods 513
4.4.1.1 Analog Random Noise Generators 513
4.4.1.2 A Hybrid Analog-Digital Pseudo-Random Noise Generator . 514
4.4.2 Digital Computer Methods 520
4.4.2.1 Random Numbers with a Uniform Distribution 521
4.4.2.2 Random Numbers with Nonuniform Distribution 527
4.4.2.3 The Normal Distribution 529
4.4.2.4 The Power Spectrum of a Digital Noise Generator . . . 537
4.4.2.5 Digital Computer Application 543
4.5 Modeling for Simulation 546
4.5.1 Probability Model 548
4.5.2 Mean Wind Model 559
4.5.3 Turbulence Model 570
4.5.3.1 Noise Generator 571
4.5.3.2 Turbulence Statistics, Mean Wind Axis 572
4.5.3.3 Turbulence Filters 572
4.5.4 Transformations 579
4.5.5 Aerodynamic Parameters 581
4.5.6 Aerodynamic Forces and Moments 591
4.5.7 Model Simplifications 593
4.6 Analysis of Touchdown Performance 597
4.7 References 602

APPENDIX 4A DERIVATION OF GENERAL RELATIONSHIP BETWEEN INERTIAL AND AERODYNAMIC ANGLES 605

APPENDIX 4B BODY AXIS-RELATIVE WIND AXIS VECTOR TRANSFORMATION 609

ILLUSTRATIONS

No.		Page
1-1	Schematic Spectrum of Wind Speed Near the Ground Estimated From a Study of Van Der Hoven (1957)	8
1-2	Selected Nondimensional Shear Description	15
1-3	Nondimensional Shear	16
1-4	Contribution of Non-Neutral Stability to Mean Wind	17
1-5	Contribution of Non-neutral Stability to Mean Wind, Log Plot	18
1-6	Low Altitude Richardson's Number Profile	19
1-7	Mean Wind Proportionality Constant	20
1-8	Variable Shear Stress Correction to Wind Profile	22
1-9	Mean Wind Cumulative/Exceedance Probability	24
1-10	Total Crosswind Information Compiled From 24 U.S. Airports	25
1-11	Headwind Tailwind Description Compiled From 24 U.S. Airports	26
1-12	Total Headwind/Tailwind, Mean of 24 U.S Airports	27
1-13	Probability of Exceedance of R_i for All Wind Speeds	28
1-14	Percent Frequency of Occurrence, Wind Speed VS R_i Cape Kennedy, 1966-68	29
1-15	Cumulative Percent Frequency of Occurrence of R_i at Given Wind Speeds, 0 to 12 Knots	30
1-16	Cumulative Percent Frequency of Occurrence of R_i at Given Wind Speeds, 12 to 24 Knots	31
1-17	Cumulative Percent Frequency of Occurrence of R_i at Given Wind Speeds, 24 to 30 Knots	32
1-18	Transformations	34
1-19	Wind Heading Cumulative Probability Model	35
1-20	Von Karman and Dryden Correlation and Spectra Functions	42
1-21	Comparison: Dryden and Von Karman Variance Density	45
1-22	Schematic for Turbulence Filters	46
1-23	Approximate Longitudinal Turbulence Filter Accuracy	47
1-24	Approximate Transverse Turbulence Filter Accuracy	48
1-25	σ_w/u_* Variation with Stability	51
1-26	Profile of Vertical Turbulence RMS, Selected Description	52
1-27	Selected Description for Variances of Horizontal Turbulence Components	53
1-28	Selected Integral Scale Description	55
1-29	Turbulence Pitch and Yaw Rate Spectra	60
1-30	Probability Model Schematic	63
1-31	Scaling Length	65
1-32	Computation Flow Diagram	67
1A-1	Comparison of Wind Speed Descriptions	71
1A-2	ARB Model Spectrum Comparison with Measured Spectra at 100 FT	75
1A-3	ARB Model Spectrum Comparison with Measured Spectra at Different Altitudes	77
1A-4	Comparison of Horizontal Turbulence in Direction of the Mean Wind	78
1A-5	Comparison of Horizontal Turbulence Perpendicular to Direction of Mean Wind	79
1A-6	Comparison of Vertical Turbulence	80

ILLUSTRATIONS (CONTINUED)

No.		Page
1B-1	Thrust Required to Hold 3° Glideslope in Headwind, 170 kt Approach Speed	84
1B-2	FAA Turbulence Model Implementation	86
1B-3	Frequency for Maximum Vertical Turbulence Energy Comparison	87
1C-1	Effective Turbulence Roll Rate Power Spectrum	96
1C-2	Effective Turbulence Roll Component Low-Frequency Power Spectrum	97
1C-3	Turbulence Pitch and Yaw Rate Spectra	99
2-1	Schematic Spectrum of Wind Speed Near the Ground Estimated From a Study of Van Der Hoven (1957)	107
2-2	Wind Profile, Ekman Spiral	113
2-3	Idealization of Wind Directions Near the Ground and at High Altitude (Northern Hemisphere)	114
2-4	Mean Wind Profile	117
2-5	Logarithmic Mean Wind Profile	118
2-6	Mean Wind Shear	119
2-7	Surface Roughness Lengths	120
2-8	Log-Linear Mean Wind Profile	132
2-9	Nondimensional Wind Shear, Effect of Stability	135
2-10	Diabatic Mean Wind Profile Function, Unstable Conditions	138
2-11	Power Law Exponent, Effect of Stability	142
2-12	Effect of Shear Stress Variation on Wind Profiles	151
2-13	Low Altitude Richardson's Number Profile	155
2-14	Universal Mean Wind Function for Diabatic Conditions	156
2-15	Proportionality Constant, Diabatic Wind Profile	157
2-16	Scaling Length Determination	158
2-17	Mean Wind Profile, Effect of Stability	160
2-18	Selected Nondimensional Shear Description	162
2-19	Variable Shear Stress Correction to Wind Profile	163
2-20	Probability Functions and Characteristics	171
2-21	Turbulence Probability Densities	175
2-22	Comparison: Normal Distribution and Sum of Two Normal Distributions	177
2-23	Fundamental Correlation Functions	184
2-24	Evaluation of $\Omega^{-5/3}$ Asymptote	191
2-25	Von Karman and Dryden Correlation and Spectra Functions	194
2-26	Von Karman and Dryden One-Dimensional Power Spectra	195
2-27	Von Karman and Dryden Nondimensional Spectra	196
2-28	Dryden and Von Karman Fundamental Correlation Functions	197
2-29	Typical Comparison of Experimental Spectra with Von Karman and Dryden Mathematical Expressions	200
2-30	Experimental/Mathematical Spectra Comparisons	201
2-31	Axis System for Low Altitude Turbulence	202
2-32	Cross Spectrum to Vertical Power Spectrum Ratio, Effect of Wind Shear	206

ILLUSTRATIONS (CONTINUED)

No.		Page
2-33	Variation of Energy Dissipation with Height	211
2-34	Three-Dimensional Turbulent Kinetic Energy at Brookhaven, N. Y Rough Terrain	214
2-35	Three Dimensional Turbulent Kinetic Energy at O'Neill, Nebr. Smooth Terrain	214
2-36	Theoretical and Observed Variation of σ_w/u_* with Instability	220
2-37	Standard Deviation of Vertical Velocity at 23 M or 29 M Over Smooth Terrain as a Function of Wind Speed at 2 M	222
2-38	Standard Deviations of Vertical Velocity at 2M at O'Neill, Nebraska as a Function of Wind Speed at 1 M	223
2-39	Standard Deviation of Vertical Velocity at Brookhaven, N. Y. as a Function of Wind Speed at 11 M	224
2-40	Observed σ_w/u_* as a Function of h/ℓ'	226
2-41	Standard Deviation of Lateral Velocity at Brookhaven, N. Y. as a Function of Wind Speed at 11 M	228
2-42	Standard Deviation of Lateral Velocity at South Dartmouth, Mass., as a Function of Wind Speed at 11 M	228
2-43	Variance of Lateral Wind Components at 18M as a Function of Friction Velocity at 18M	229
2-44	Standard Deviation of Lateral Velocity at South Dartmouth, Mass. as Function of Wind Speed at 11 M	231
2-45	Standard Deviation of Lateral Velocity at O'Neill, Nebr. as Function of Wind Speed at 11 M	231
2-46	Ratio of Variance of Lateral Wind Components to the Friction Velocity at 18 M as a Function of Richardson's Number at 18 M	232
2-47	Standard Deviation of Lateral Velocity at O'Neill, Nebr. at 2 M at Night as Function of 3/2 Power of Wind Speed at 11 M	233
2-48	Standard Deviation of Lateral Velocity at South Dartmouth, Mass. at 2 M at Night as Function of 3/2 Power of Wind Speed at 11 M	233
2-49	Variance of the Longitudinal Wind Components at 18 M as a Function of Friction Velocity at 18 M	235
2-50	Observed Ratio of Standard Deviation of Longitudinal Velocity to Friction Velocity as a Function of h/ℓ'	238
2-51	Ratio of the Variance of Longitudinal Wind Components to the Friction Velocity at 18 M as a Function of Richardson's Number at 18 M	238
2-52	Difference of Variance of Lateral Wind Component at 18 M and 150 M as a Function of Mean Wind at 18 M	239
2-53	Difference of Variances of Longitudinal Wind Component at 18 M and 150 M as a Function of Mean Wind at 18 M	240
2-54	R.M.S. Turbulence Interrelationship, Military Models	244
2-55	Effect of Nonhomogeneity on Spectrum Shape	246
2-56	Vertical Turbulence Spectrum, Estimation of Scale	249

ILLUSTRATIONS (CONTINUED)

No.		Page
2-57	Integral Scale Estimate for Vertical Spectrum	251
2-58	Alternate Representations of the Integral Scale for Horizontal Turbulence	255
2-59	Integral Scale Representation	256
2-60	Integral Scale Estimate for Horizontal Spectra	258
2-61	σ_w/u_* Variation with Stability	263
2-62	σ_w/u_* Variation with Stability, Log Plot	264
2-63	Profile of Vertical Turbulence RMS, Selected Description	265
2-64	Selected Description for Variances of Horizontal Turbulence Components	270
2-65	Selected Integral Scale Description	271
2-66	Cospectrum Data Fitting	273
2-67	Cospectrum Break Frequency	275
2-68	Cospectrum Correction Factor	276
2-69	Qualitative Cospectrum Shape	278
3-1	Annual Percent Probability of Mean Wind Speed Equaling or Exceeding Given Values	298
3-2	Wind Speed Description, Normalized Probability of Occurrence, 24 U.S. Airports	299
3-3	Comparison of Wind Speed Descriptions	300
3-4	Wind Direction Histogram, 24 U.S. Airports	302
3-5	Crosswind Description Compiled From 24 U.S. Airports	303
3-6	Total Crosswind Information Compiled From 24 U.S. Airports and ARB Model	304
3-7	Headwind Tailwind Description Compiled From 24 U.S. Airports	305
3-8	Total Headwind Tailwind, Mean of 24 U.S. Airports	307
3-9	Mean Annual Wind Speed Profiles for Three Locations	308
3-10	Wind Shear Magnitudes, Montreal and Whiteshell, Canada	310
3-11	Directional Shear, Whiteshell, Canada	311
3-12	Directional Shear, Hanford, Washington	312
3-13	Wind Shear Magnitudes, Canada	313
3-14	Wind Shear Magnitudes, Whiteshell, Canada	314
3-15	Component Wind Shear Magnitudes, Thumba, India	316
3-16	Component Wind Shear, Tokyo	317
3-17	Wind Shear vs Speed Averaging Time	319
3-18	Distribution of Average and Maximum Wind Shear From Surface Level to 110 Ft as a Function of Surface Wind Speed	321
3-19	Relative Frequencies of Wind Shear and Temperature Differences According to Ramsey	322
3-20	Wind Shear Magnitudes, Cardington, England	324
3-21	Wind Shear and Stability From Russian Balloon Data	325
3-22	Annual Relative Frequency Distribution of Wind Shear Speed	331

ILLUSTRATIONS (CONTINUED)

No.		Page
3-23	Wind Shear Magnitude, Oklahoma City	332
3-24	Wind Speed at 20 Feet, Cape Kennedy, 1966-68	338
3-25	Wind Speed at 20 Feet, Cedar Hills, Texas, 1960-62	339
3-26	Comparison of Wind Speeds, Cape Kennedy and 24 U.S. Airports	340
3-27	Comparison of Wind Speeds, Cedar Hills, Texas and Mean of 24 U.S. Airports	341
3-28	Percent Frequency of Exceedance of Wind Speed at Several Heights, Cape Kennedy, 1966-68	342
3-29	Percent Frequency of Exceedance of Wind Speed at Several Heights, Cedar Hills, Texas, 1960-1962	343
3-30	Probability of Exceedance of R_i for All Wind Speeds	345
3-31	R_i at 20 Feet, Cape Kennedy, 1966-68, All Wind Speeds	346
3-32	R_i at 20 Feet, Cape Kennedy, 1966-68, Wind Speeds 0-2 Kt	347
3-33	R_i at 20 Feet, Cape Kennedy, 1966-68, Wind Speeds 2-4 Kt	348
3-34	R_i at 20 Feet, Cape Kennedy, 1966-68, Wind Speeds 4-6 Kt	349
3-35	R_i at 20 Feet, Cape Kennedy, 1966-68, Wind Speeds 6-8 Kt	350
3-36	R_i at 20 Feet, Cape Kennedy, 1966-68, Wind Speeds 8-10 Kt	351
3-37	R_i at 20 Feet, Cape Kennedy, 1966-68, Wind Speeds 10-12 Kt	352
3-38	R_i at 20 Feet, Cape Kennedy, 1966-68, Wind Speeds 12-14 Kt	353
3-39	R_i at 20 Feet, Cedar Hills, Texas, 1960-62, All Wind Speeds	354
3-40	R_i at 20 Feet, Cedar Hills, Texas, 1960-62, Wind Speeds 0-2 Kt	355
3-41	R_i at 20 Feet, Cedar Hills, Texas, 1960-62, Wind Speeds 0-4 Kt	356
3-42	R_i at 20 Feet, Cedar Hills, Texas, 1960-62, Wind Speeds 4-6 Kt	357
3-43	R_i at 20 Feet, Cedar Hills, Texas, 1960-62, Wind Speeds 6-8 Kt	358
3-44	R_i at 20 Feet, Cedar Hills, Texas, 1960-62, Wind Speeds 8-10 Kt	359
3-45	R_i at 20 Feet, Cedar Hills, Texas, 1960-62, Wind Speeds 10-12 Kt	360
3-46	R_i at 20 Feet, Cedar Hills, Texas, 1960-62, Wind Speeds 12-14 Kt	361
3-47	Percent Frequency of Occurrence, Wind Speed vs Richardson's No. Cape Kennedy, 1966-68	363
3-48	Percent Frequency of Occurrence, Wind Speed vs Richardson's No., Cedar Hills, Texas, 1960-62	364
3-49	Wind Direction Shear for Various Wind Speeds at 20 Ft (33-10 Ft), Cape Kennedy, 1966-68	365
3-50	Wind Direction Shear for Various Wind Speeds at 46 Ft (70-30 Ft), Cedar Hills, Texas, 1960-62	366
3-51	Percent Frequency of Occurrence, Wind Speed vs Directional Shear, Cape Kennedy, 1966-68	367
3-52	Percent Frequency of Occurrence, Wind Speed vs Directional Shear, Cedar Hills, Texas, 1960-62	368
3-53	Wind Direction Shear for Several Heights, All Wind Speeds, Cape Kennedy, 1966-69	370
3-54	Wind Direction Shear for Several Heights, All Wind Speeds, Cedar Hills, Texas, 1960-62	371
3-55	Distribution of Wind Direction Shear with Height, Cape Kennedy	372
3-56	Distribution of Wind Direction Shear with Height, Cedar Hills, Texas	373
3-57	Examples of Wind Direction Profiles	374

ILLUSTRATIONS (CONTINUED)

No.		Page
3-58	Cape Kennedy, 1966-68, Wind Speed Shear at 20 Ft	375
3-59	Cedar Hills, Texas 1960-62, Wind Speed Shear at 20 Ft	376
3-60	Percent Frequency of Occurrence, Wind Speed vs Speed Shear at 20 Ft, Cape Kennedy, 1966-68	377
3-61	Percent Frequency of Occurrence, Wind Speed vs Speed Shear at 20 Ft, Cedar Hills, Texas, 1960-62	378
3-62	Cape Kennedy, 1966-68, Variation with Height of Wind Speed Shear, 2-4 Kt Speed at 20 Ft	379
3-63	Cedar Hills, Texas, 1960-62, Variation with Height of Wind Speed Shear, 2-4 Kt Speed at 20 Ft	380
3-64	Cape Kennedy, 1966-68, Distribution of Wind Speed Shear vs Height, 20 Ft Wind Speed = 2-4 Kt	381
3-65	Cedar Hills, Texas, 1960-62, Distribution of Wind Speed Shear vs Height, 20 Ft Wind Speed 2-4 Kt	382
3-66	Cape Kennedy, 1966-68, Distribution of Wind Speed Shear vs Height, 20 Ft Wind Speed > 12 Kt	383
3-67	Cedar Hills, Texas, 1960-62, Distribution of Wind Speed Shear vs Height, 20 Ft Wind Speed > 12 Kt	384
3-68	Percent Frequency of Occurrence, Wind Speed vs R_j, Cape Kennedy, 1966-68	389
3-69	Cumulative Percent Frequency of Occurrence of R_j, at Given Wind Speeds, 0 to 12 Knots	390
3-70	Cumulative Percent Frequency of Occurrence of R_j at Given Wind Speeds, 12 to 24 Knots	391
3-71	Cumulative Percent Frequency of Occurrence of R_j at Given Wind Speeds, 24 to 30 Knots	392
4-1	Linearized Equations of Motion for Still Air	406
4-2	Linearized Equations of Motion for Level Flight in Wind	407
4-3	Body Axis Mean Wind Components	409
4-4	Characteristic Equations, Effects of Mean Wind	410
4-5	Effect of Mean Wind Magnitude, No Crosswind	412
4-6	Effect of Mean Wind Magnitude on Altitude Transfer Function Zeros—No Crosswind	414
4-7	Change of $\partial(T/W)_{REQ}/\partial V_A$ with Flight Path	415
4-8	Pitch Attitude Required to Hold a Glideslope	416
4-9	Effect of Wind Shear, No Crosswind	418
4-10	Wind Shear Root Locus, Short Period Approximation, No Crosswind	421
4-11	Wind Shear Root Locus, Low Frequency Behavior, No Crosswind	423
4-12	Wind Shear Root Locus, Phugoid Approximation, No Crosswind	425
4-13	Effect of Longitudinal Component of Shear on Control Transfer Functions	427
4-14	Wind Shear Distribution Across an Airplane Wing	428
4-15	Perturbations of Effective Angular Components of Mean Wind	430
4-16	Distributed Lift Effects of Longitudinal Wind Shear on Characteristic Lateral -Directional Motion	432
4-17	Root Locus of Lateral-Directional Characteristic Motion Due to Wind Shear	434
4-18	Bank Angle to Control Transfer Function Zeros, Effect of Wind Shear	436
4-19	Equations for Turbulence Responses	438
4-20	Density of Turbulence Variance, Von Karman Spectra	441

ILLUSTRATIONS (CONTINUED)

No.		Page
4-21	Frequency Limitation of Linear Turbulence Field Representation	450
4-22	Cross Spectra for Treatment of Nonuniform Spanwise Gusts	452
4-23	Spectrum Function $\Phi_{uu}/\sigma^2 L$	454
4-24	Spectrum Function $\Phi_{vv}/\sigma^2 L$	455
4-25	Spectrum Function $\Phi_{ww}/\sigma^2 L$	456
4-26	Effective Turbulence Roll Rate Power Spectrum	458
4-27	Effective Trubulence Roll Component, Low Frequency Power Spectrum	459
4-28	Turbulence Pitch and Yaw Rate Spectra	462
4-29	Transport Lead(Lag) Approximations	467
4-30	Lift Growth Amplitude Frequency Responses	471
4-31	Spectrum Asymptotes, Effect of Speed and Scale	473
4-32	Variance Density Asymptotes, Effect of Speed and Scale	474
4-33	Turbulence Angular Components, Effect of Speed and Scale.	476
4-34	Load Factor to Gust Frequency Response	478
4-35	Normal Load Factor P.S.D. Due to w_g, Effect of Speed	479
4-36	Load Factor Response to Vertical Gust, Effect of Speed	480
4-37	Load Factor Response to Longitudinal Gust, Effect of Speed	481
4-38	Normal Load Factor P.S.D. Due to u_g, Effect of Speed	482
4-39	Normal Load Factor P.S.D. Due to u_g and w_g, Effect of Speed	483
4-40	Power Spectrum of Altitude Rate of Change Due to Turbulence, Effect of Speed	484
4-41	Frequency Response of Flight Path Attitude Due to Turbulence, Effect of Speed	485
4-42	Response to a Set of Random Inputs	493
4-43	Axis Transformations	494
4-44	Mean Wind Axis to Body Axis Transformation of Spectra	495
4-45	Relative Wind Axis Variances and Covariances	496
4-46	Body Axis Variances and Covariances	498
4-47	Body Axis Spectra, Isotropic Turbulence	500
4-48	Body Axis Covariance Density, Isotropic Turbulence	501
4-49	Body Axis Cospectra, Isotropic Turbulence	502
4-50	Relative Wind To Body Axis Transformation Effect on Vertical P.S.D.	507
4-51	Low Frequency Vertical P.S.D. Level, Effect of Axis Rotation	508
4-52	Generation and Transformation of Turbulence Components	510
4-53	Cospectrum Break Frequency	511
4-54	A Practical Pseudo-Random Noise Generator System	515
4-55	Power Spectrum and Autocorrelation Function of a Binary Sequence Generator	517
4-56	Numerical Approximation to Obtain the Inverse of Cumulative Distribution Function	528
4-57	Approximate Gaussian Amplitude Distributions, Linear Plot	531
4-58	Approximate Gaussian Amplitude Distributions, Log Plot	532
4-59	Deviations of Approximate Gaussian Amplitude Distributions From the True Gaussian Distribution	533

ILLUSTRATIONS (CONCLUDED)

No.		Page
4-60	Power Spectrum and Autocorrelation Function of a Digital Random Number Generator	538
4-61	Digital Random Number Generator Power Spectrum	541
4-62	Noise Power Spectrum, Log-Log Scale	542
4-63	White Noise Generation Steps	544
4-64	Wind Model Schematic	547
4-65	Example: Joint Probability for Correlated Parameters	550
4-66	Example: Generation of Joint Distribution	551
4-67	Probability Model Schematic	553
4-68	Wind Heading Cumulative Probability Model	554
4-69	Mean Wind Cumulative/Exceedance Probability	555
4-70	Cumulative Probability of R_i at Given Wind Speeds, 0 to 12 Kt	556
4-71	Cumulative Probability of R_i at Given Wind Speeds, 12 to 24 Kt	557
4-72	Cumulative Probability of R_i at Given Wind Speeds, 24 to 30 Kt	558
4-73	Nondimensional Shear	560
4-74	Contribution of Nonneutral Stability to Mean Wind	561
4-75	Contribution of Non-Neutral Stability to Mean Wind	562
4-76	Variable Shear Stress Correction to Wind Profile	563
4-77	Mean Wind Proportionality Constant	565
4-78	Scaling Length	566
4-79	Schematic of Calculation of Parameters	568
4-80	Mean Wind and Wind Shear Model Schematic	569
4-81	Generation of Turbulence Velocity Schematic	570
4-82	Schematic of Calculation of Mean Wind Axis Turbulence Statistics	573
4-83	σ_w/u_* Variation with Stability	574
4-84	Vertical Turbulence Standard Deviation, Effect of Stability	575
4-85	Selected Description for Variances of Horizontal Turbulence Components	576
4-86	Turbulence Filter Design	578
4-87	Comparison: Dryden and Von Karman Variance Density	580
4-88	Turbulence Filters	581
4-89	Approximate Longitudinal Turbulence Filter Accuracy	582
4-90	Approximate Transverse Turbulence Filter Accuracy	583
4-91	Schematic for Turbu! ıce Filters	584
4-92	Transformations	585
4-93	Wing-Body Body Axis Aerodynamic Parameters	592
4-94	Tail Body Axis Aerodynamic Parameters	593
4-95	Number of Digital Simulation Runs Required for Simulation	600

TABLES

No.		Page
2-1	Influence of Surface Roughness on Power Law Exponent[a]	124
2-2	Energy Budget Between 11 M and 125 M at Brookhaven, New York	212
2-3	Kinetic Energy	215
2-4	Values of the Constant of Proportionality C between σ_w and u_*	219
2-5	Summary of Estimates of Vertical Turbulence in Neutral Conditions	221
2-6	Values of the Constant of Proportionality C Between σ_v and u_*	227
2-7	Values of the Constant of Proportionality C Between σ_u and u_*	236
2-8	Ratios Between σ_u, σ_v, and σ_w	242
3-1	Wind Rose Model Relative to Runway Orientation	306
3-2	Frequencies of Occurrence of Vector Wind Shear Magnitude Durations for 830- to 350-Ft Interval	318
3-3	Vector Wind Shear Magnitudes at Oblinsk, Russia	320
3-4	Variation of Wind Shear with Windspeed and Height Interval During Neutral Conditions–Russia	326
3-5	Variation of Wind Shear with Height Interval and Stability–Russia	326
3-6	Means and Standard Deviations for 20- to 200-Ft Shears	327
3-7	Variation of Number of Extreme Shear Occurrences From Gaussian Distribution Relative to Upper-Wind Directions	328
3-8	Mean Shear Values--Two-Tower Experiment	329
3-9	Probabilities of Shear	329
3-10	Windspeed Relationship to Gustiness at Essendon, England	330
3-11	Mean Lapse Rates in the Boundary Layer Defined by Singer and Smith	330
3-12	Wind Shear Summary	334
3-13	Percent Frequency of Exceedance of Windspeed–Cape Kennedy 1966-68	344
4-1	Asymptotes of Turbulence Transfer Functions	443
4-2	Lift Growth Functions for Mach = 0	469
4-3	Gaussian Distribution Generation: Comparison of Computation Time	536

1.0 INTRODUCTION, SUMMARY, AND PROPOSED MODEL

1.1 INTRODUCTION

This document reports an investigation performed to provide the information for improved accuracy of low-altitude wind and turbulence models to be used for the certification by flight simulation of approach and landing guidance and control systems.

Historically, the structural designers were first to recognize the requirement for a mathematical model and initially used only the discrete 1-cosine gust for the design limit case. As airplanes became lighter and more flexible, fatigue life became more critical and the need for a more accurate description became greater. This led to the application of the statistical power spectra. Attempts to fit a mathematical model to measured data began seriously in the late 1950s and has progressed to the point of "which model do I use?"

Automatic controls were used initially to provide modest improvements of airplane stability and to provide guidance during noncritical flight phases (altitude, attitude, and heading hold). Automatic control authority tended to be low. Hence, the interaction of the control system with wind and turbulence was unimportant; it was not a concern for flight safety.

For typical flight controls analysis, such as handling qualities, ride qualities, and controllability, concern was for a qualitative, rather than quantitative, answer: that is, does a parameter variation (in the aircraft or control system) improve or degrade the particular output? A forced change of this philosophy occurred when the autoland systems began to appear in the early 1960s. The dependence upon an automatic landing system rather than the highly adaptive pilot required analytic proof that the landing would be performed with adequate safety. The problem is now quantitative rather than qualitative and a gross error in the approach wind model could be very serious; parameters of the wind model have effects comparable to parameters of the aircraft and guidance system. Certification of autoland systems is dependent upon demonstration of very low orders of risk of fatal accidents. Obtaining adequate statistical data to validate remote probabilities of fatal accidents is impractical without heavy reliance upon simulation.

The search for a low-altitude wind model, providing a better representation of low-altitude wind phenomena than provided by existing certification wind models, was principally concerned with the region from the surface to about 1000 feet. The model for this altitude region tends to be the most general and complex due to the strong dependence of wind characteristics upon altitude and surface terrain and the orientation dependence of turbulence characteristics. Additionally, the landing approach task is the most difficult and critical task for which relatively small changes of wind characteristics may result in large changes in maneuver performance. The low airspeed during approach tends to couple vertical motion with longitudinal wind components and longitudinal motion with vertical wind components, increases the nonlinearity of aircraft responses to winds, and increases the significance of the distribution of winds over the aircraft. Hence, the aerodynamic model incorporating the effects of winds tends also to be most general and complex.

The main objective of the investigation was to define a model suitable for certification. A model for design must be simplified to reduce the wind model parameters to enable evaluation of a large number of aircraft and control system design parameters.

The studies were concerned with the "average" airport, although it is recognized that the "average" airport may not exist. It is both impractical and undesirable to represent unique characteristics of any particular airport for the certification of an aircraft that will land at many different airports. "Average" airport is used in regard to possible unique operating procedures and terrain features and does not imply "average" winds at the "average" airport.

Consideration is not for the wind alone, but for aircraft responses in wind environments, so the investigation included the representation of aerodynamic forces due to winds and a brief analysis of the effects of winds on aircraft motion.

No original work on the description of low-altitude winds is intended. The wind model is a combination of the work of others. The structure of the model has been parameterized to enable incorporation of new material and updating of parts without discarding the entire model.

For virtually every aspect of low-altitude winds there are conflicting descriptions. Some descriptions are based on undocumented data collection, analysis techniques, and test conditions. Some general considerations used for selecting one among competion descriptions are:

- Weight of evidence
- Physical and intuitive reasonableness
- Substantiation
- Existing specifications, when the choice appears arbitrary
- Compatibility with the description of other parameters
- Validity of the assumptions
- Avoidance of descriptions providing unreasonable discontinuities

Analytic descriptions of wind phenomena are presented. Where possible, a deterministic description is preferred in the presumption that all physical processes have cause-and-effect relationships. When relationships are too complex to permit quantitative understanding or when deterministic descriptions are impractical, probabilistic descriptions are used, with the statistical parameters defined deterministically as much as possible.

For those parameters defying analytic description, probabilistic descriptions have been sought. Probabilistic descriptions were first sought from the literature. For those aspects not well defined by the literature, descriptions have been sought by reducing and evaluating tower data.

A brief analysis of the effects of winds on aircraft motion has been conducted to gain an appreciation of what needs to be modeled. The axes transformations required between wind and turbulence components in their inherent axis system and in the airplane's axis system are shown. Techniques of providing a random process on computers for the representation of turbulence are presented. A simulation model is presented that combines all the foregoing components.

Each section has been designed to be relatively independent of the other sections. Each section has its own nomenclature and reference list, and tables and figures are numbered by section.

1.2 NOMENCLATURE

b	Wing span
C_p	Specific heat at constant pressure
$\bar{c}$	Mean chord
d	Atmospheric boundary layer thickness
e	Exponential function
f	Coriolis parameter, $f = 2\omega_E \sin \lambda$
$f(h/\ell')$	Contribution of nonneutral atmospheric stability to the mean wind
$f(\xi)$, $g(\xi)$	Fundamental longitudinal and transverse correlation functions for isotropic turbulence, respectively
G_u, G_v, G_w	Filters for producing u, v, and w components of turbulence
g	Acceleration due to gravity
$g(h/\ell')$	Contribution of atmospheric stability to mean wind caused by variation of shear stress
H	Heat flux, positive upward
h	Altitude

h_{REF}	Reference altitude
h_I	Altitude above which turbulence is isotropic
k	Von Karman constant, k = 0.4
L	Longitudinal isotropic turbulence integral scale
L_H, L_V	Integral scales for horizontal and vertical turbulence components
L_p, L_N	Longitudinal and transverse integral scales for turbulence components parallel and normal to the displacement vector, respectively
L_u, L_v, L_w	Integral scales corresponding to the longitudinal, transverse, and vertical turbulence components, respectively
ℓ, ℓ'	Monin-Obukov scaling length and Monin-Obukov scaling length modified by ratio of eddy conductivity to eddy vicosity
ℓ_T	Distance from the wing-body aerodynamic center to the tail aerodynamic center along the x body axis, positive aft
$M(\omega)$	Frequency response amplitude
p	Inertial body axis roll rate
p_T	Effective roll rate of the air mass due to turbulence relative to the earth
q	Inertial body axis pitch rate
$\bar{q}$	Dynamic pressure
q_T	Effective body axis pitch rate due to turbulence with respect to the earth
R_i, $R_{i_{20}}$	Richardson's number and that at 20-foot altitude
R_{ij}	Correlation function for the i and j turbulence components
r	Inertial body axis yaw rate
$\vec{r}$	Displacement vector
r_A	Yaw rate relative to the air mass

r_T	Effective body axis yaw rate due to turbulence relative to the earth
$r_W, \bar{r}_W$	Effective yaw rate due to the wind and mean wind relative to the earth
s	Laplace transform variable
T	Absolute temperature
t	Time
u	Inertial linear velocity along the x body axis
u_*, u_{*0}	Friction velocity (shear stress/density)$^{1/2}$ and that at the surface
u_A	Linear velocity with respect to the air mass along the x body axis
$u_{A_{TG}}$	Component of airspeed along the x turbulence generation axis
u_p, u_N	Turbulence velocity parallel and normal to the displacement vector
$u_T, u_{T_{TG}}$	Linear turbulence velocity along the x body axis and the x turbulence generation axis relative to the earth
$u_{T_{TAIL}}$	u_T at the tail
$u_W, \bar{u}_W$	Linear velocity of the wind and mean wind with respect to the earth along the x body axis
$\bar{V}_W, \bar{V}_{20}$	Mean wind speed and that at 20-foot altitude
V_A	Total air speed
v	Inertial linear velocity along the y body axis relative to the earth
v_A	Linear velocity with respect to the air mass along the y body axis
$v_T, v_{T_{TG}}$	Linear turbulence velocity along the y body axis and the y turbulence generation axis relative to the earth at the center of gravity
$v_W, \bar{v}_W$	Linear velocity of the wind and mean wind along the y body axis relative to the earth

w	Inertial linear velocity along the z body axis
w_A	Linear velocity along the z body axis relative to the air mass
w_T	Linear turbulence velocity along the z body axis relative to the earth
w_W, $\bar{w}_W$	Linear velocity of the wind and the mean wind along the z body axis relative to the earth
z_0	Surface roughness length
α	Angle of attack
β	Sideslip angle
γ	Glide slope
θ	Euler pitch angle
$\theta_{ij}(\vec{\Omega})$	Three-dimensional spectrum function for the i and j turbulence components
λ	Latitude
λ_1, λ_2	Turbulence wavelength along the x and y axes
$\vec{\xi}$, ξ	Position displacement vector and magnitude
σ_i	Standard deviation for parameter i
σ_H, σ_V	Standard deviation of horizontal and vertical turbulence
σ_u, σ_v, σ_w	Standard deviations of the u, v, and w components of turbulence
σ_{ij}^2	Covariance between the i and j turbulence components
τ	Time displacement
τ, τ_0	Shear stress and that measured at the surface
Φ_I, Φ_O	Input and output power spectra
$\Phi_i(\Omega_1)$	One-dimensional power spectrum for parameter i
$\Phi_{ij}(\Omega_1)$	One-dimensional spectrum function for the i and j turbulence components

Φ_N	Random noise power spectrum
$\Phi_{NN}(\Omega_1)$, $\Phi_{pp}(\Omega_1)$	Isotropic one-dimensional spectrum functions for u_N and u_p
$\Phi_u(\Omega_1)$, $\Phi_v(\Omega_1)$, $\Phi_w(\Omega_1)$	One-dimensional power spectra for components of turbulence along the x, y, and z axes
$\Phi_{uw}(\Omega_1)$	One-dimensional cospectrum for components of turbulence along the x and z axes
$\phi(h/\ell')$	Universal function of h/ℓ' defining nondimensional wind shear: $\frac{kh}{u_{*0}} \frac{\partial \bar{V}_W}{\partial h} = \phi(h/\ell')$
ϕ	Euler bank angle
$\psi_{ij}(\Omega_1, \Omega_2)$	Two-dimensional spectrum function for the i and j turbulence components
ψ	Euler heading angle
$\bar{\psi}_W$	Heading to which the mean wind is blowing
$\vec{\Omega}$, Ω	Spacial frequency vector and spacial frequency magnitude
Ω_1	Component of spacial frequency along the x axis
ω	Temporal frequency, rad/sec
ω_E	Angular velocity of the earth

Note: Dotted terms refer to derivatives with respect to time. Overbar indicates an average. Other terms defined where used.

1.3 SUMMARY

Wind phenomena are classified in Section 2.2 as being mean wind, turbulence, and discrete gusts. Mean wind and turbulence are statistical parameters that appear together with turbulence being a random deviation of wind velocity about the mean. Distinction between the mean wind, which eventually is variable given enough time or space, is made on a frequency basis using the Van der Hoven bimodal wind speed spectrum (Fig. 1-1).

Discrete gusts are deterministic phenomena caused by localized terrain or atmospheric inhomogeneities of which there are an infinite number of possibilities. So long as conditions of reasonably homogeneous terrain and atmospheric features or restrictions on the proximity to inhomogeneities are justified, consideration of discrete gusts is unnecessary.

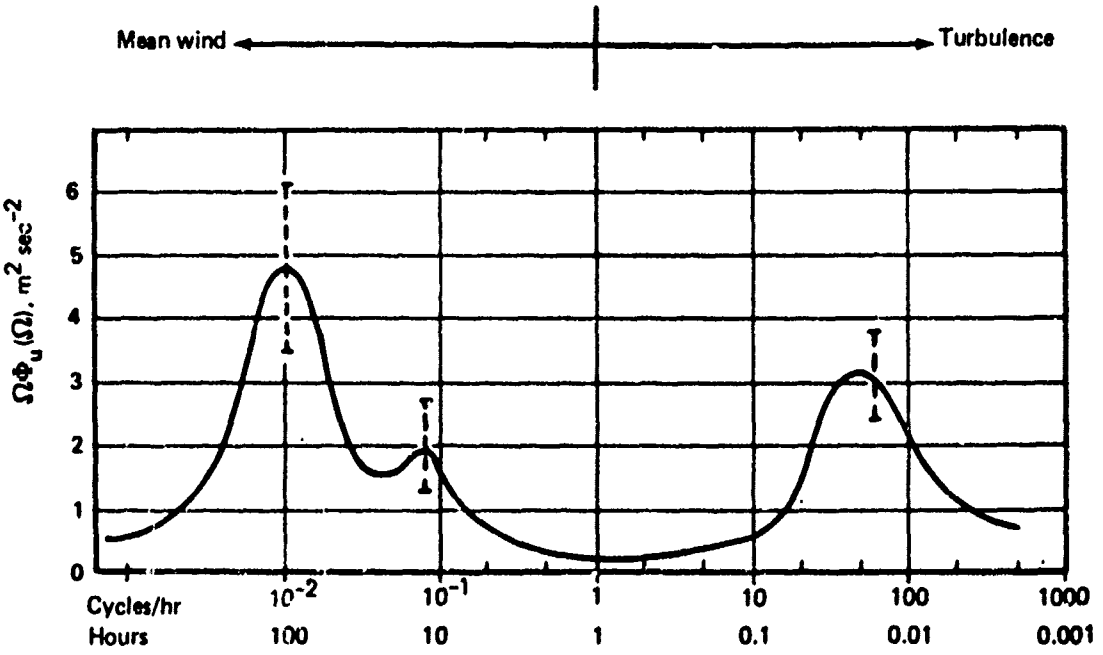

FIGURE 1-1.– SCHEMATIC SPECTRUM OF WIND SPEED NEAR THE GROUND ESTIMATED FROM A STUDY OF VAN DER HOVEN (1957)

1.3.1 Mean Wind

The mean wind is characterized by:

- Zero vertical component
- Zero wind speed at the surface
- Invariant with altitude above the atmospheric boundary layer

The mean wind model having the greatest acceptance, both theoretically and empirically, is that developed from dimensional analysis. The parameters involved are:

$\frac{\partial \bar{V}_W}{\partial h}$ = mean wind shear

τ = shear stress

ρ = atmospheric density

C_p = specific heat at constant pressure

h = altitude

g = gravitational acceleration

H = heat flux

T = absolute temperature

$\frac{\partial T}{\partial h}$ = lapse rate

This inclusive list assumes:

- Pressure gradients are invariant with altitude, at least over a sufficiently constrained altitude region.
- Viscous forces dominate pressure and Coriolis forces.
- The flow of air is fully rough so that molecular viscosity is not a significant parameter.

The parameters appear in the combinations

$$u_* = \sqrt{\frac{\tau}{\rho}} = \text{friction velocity}$$

$$\frac{kh}{u_*}\frac{\partial \bar{V}_W}{\partial h} = \text{nondimensional shear}$$

(k = 0.4 = Von Karman's constant)

$$\ell = \frac{u_*^3 C_p \rho T}{kgH}$$

Dimensional analysis then predicts

$$\frac{kh}{u_*}\frac{\partial \bar{V}_W}{\partial h} = \phi(h/\ell)$$

where (h/ℓ) is some specific function.

It is additionally assumed that shear stress and density are invariant with altitude for a sufficiently constrained altitude region. Then

$$\bar{V}_W = \frac{u_{*0}}{k}\int_{z_0}^{h}\frac{(h/\ell)}{h}\,dh$$

where

z_0 = the altitude at which the mean wind speed formally goes to zero

u_{*0} = $u_*(h = 0)$

The scaling length, ℓ, is difficult to measure due to the difficulty of measuring heat flux, so an alternate scaling length, ℓ', is introduced:

$$\ell' = \frac{u_{*_0}^{\,T} \frac{\partial \bar{V}_W}{\partial h}}{kG\left[\frac{\partial T}{\partial h} + \frac{g}{C_p}\right]}$$

This alternate scaling length is equal to the dimensional analysis scaling length multiplied by the ratio of eddy conductivity to eddy viscosity and is assumed to be a constant, implying that there is a one-to-one relationship of the wind and temperature shears independent of altitude.

The alternate scaling length can be related to a more conventional and still more easily measured parameter reflecting atmospheric stability, Richardson's number:

$$R_i = \frac{\frac{g}{T}\left(\frac{\partial T}{\partial h} + \frac{g}{C_p}\right)}{\left(\frac{\partial \bar{V}_W}{\partial h}\right)^2}$$

$$\frac{h}{\ell'} = \left[\frac{\frac{g}{T}\left(\frac{\partial T}{\partial h} + \frac{g}{C_p}\right)}{\left(\frac{\partial \bar{V}_W}{\partial h}\right)^2}\right]\left(\frac{kh}{u_{*_0}} \frac{\partial \bar{V}_W}{\partial h}\right) = R_i\, \phi(h/\ell')$$

Richardson's number is a nondimensional ratio between the mechanical wind shear that tends to displace air and the buoyancy force, which may damp or amplify this tendency (Sec. 2.3.4). Richardson's number thus gives rise to the notion of atmospheric stability, a dynamic concept:

$R_i,\ h/\ell' > 0 \rightarrow \frac{\partial T}{\partial h} > \frac{-g}{C_p}$: stable (weak lapse or inversion)

$$R_i,\ h/\ell' = 0 \rightarrow \frac{\partial T}{\partial h} = \frac{-g}{C_p} = -0.00536^\circ R/ft;\ \text{neutral (adiabatic lapse)}$$

$$R_i\ \ h/\ell' < 0 \rightarrow \frac{\partial T}{\partial h} < \frac{-g}{C_p};\ \text{unstable (strong lapse)}$$

Given the nature of $\phi(h/\ell')$, the variation of R_i is known with altitude and R_i could be used in place of h/ℓ'. However, it is simpler to use h/ℓ' as it varies linearly with altitude. The greater ease involved in measuring R_i provides an indirect means of computing ℓ'.

Investigators have examined $\phi(h/\ell')$ for different regions of stability. For neutral stability $\phi(h/\ell') = 1$ and

$$\frac{\partial \bar{V}_W}{\partial h} = \frac{u_{*0}}{kh}$$

$$\bar{V}_W = \frac{u_{*0}}{k} \ln\left(\frac{h}{z_0}\right) \qquad \text{(Sec. 2.3.2)}$$

or, after an axis system shift to provide $\bar{V}_W = 0$ at $h = 0$,

$$\bar{V}_W = \frac{u_{*0}}{k} \ln\left(\frac{h + z_0}{z_0}\right)$$

For neutral stability, the shear is inversely proportional to altitude and the mean wind is described by the logarithmic profile. The term z_0 reflects surface roughness and is larger for greater roughness. The relationship between z_0 and roughness of the terrain has been investigated in Section 2.3.2.2. In Section 2.3.6, it is concluded that $z_0 = 0.15$ foot, as provided by the British specification, and is representative for autoland applications.

If the mean wind, V_{REF} is known at some altitude, h_{REF}, the friction velocity, u_{*0}, may be found from the equation for the mean wind profile:

$$u_{*0} = \frac{k\bar{V}_{REF}}{\ln\left(\frac{h_{REF} + z_0}{z_0}\right)}$$

For a given wind speed at h_{REF} an increase in roughness length, z_0, is related to an increase in friction velocity, which in turn provides an increase of the shear at every altitude, a decrease in wind speed for $h < h_{REF}$, and an increase in wind speed for $h > h_{REF}$.

For near neutral stability, $\phi(h/\ell')$ may be estimated from the first two terms of a Taylor series expansion about neutral stability:

$$\phi(h/\ell') = 1 + \alpha' h/\ell', \; h/\ell' \ll 1$$

$$\alpha' = \text{constant}$$

Thus,

$$\bar{V}_W = \frac{u_{*0}}{k}\left[\ln\left(\frac{h + z_0}{z_0}\right) + \alpha' h/\ell'\right] \qquad \text{(Sec. 2.3.4.2)}$$

which is the log-linear mean wind profile. For stable conditions ($h/\ell' > 0$), the effect of stability appears to cause an increase in the mean wind speed and shear. Unstable conditions appear to cause a decrease in the shear and mean wind speed.

For the log-linear profile, friction velocity can be determined from the mean wind speed at a given altitude by

$$u_{*0} = \frac{k\bar{V}_{REF}}{\ln\left(\frac{h + z_0}{z_0}\right) + \alpha' h_{REF}/\ell'}$$

Stable conditions result in a decrease and unstable conditions result in an increase of friction velocity.

Combining the effects of stability on friction velocity and the nondimensional wind shear gives

$$\frac{\partial \bar{V}_W}{\partial h} = \frac{\bar{V}_{REF}}{h}\left[\frac{1 + \alpha' h/\ell'}{\ln\left(\frac{h_{REF} + z_0}{z_0}\right) + \alpha' h_{REF}/\ell'}\right]$$

Stable conditions cause the shear to be greater than for neutral conditions above some altitude, but less than the neutral stability shear below that altitude. The reverse is true for unstable conditions.

For near neutral stability, the constant ℓ' can be determined by knowing Richardson's number at some altitude, h_{REF}:

$$h/\ell' = R_i \phi(h/\ell') = R_i(1 + \alpha' h/\ell'), \; h/\ell' \ll 1$$

$$1/\ell' = \frac{R_{i_{REF}}}{h_{REF}(1 - R_{i_{REF}})} \cong \frac{R_{i_{REF}}}{h_{REF}}$$

The general form of the mean wind profile may be reformulated to represent the contribution of neutral conditions plus the increment due to nonneutral conditions:

$$\bar{V}_W = \frac{u_{*0}}{k}\left[\ln\left(\frac{h + z_0}{z_0}\right) + f(h/\ell')\right]$$

where

$$f(h/\ell') = \int_0^h \frac{\theta(\xi) - 1}{\xi} d\xi$$

Different investigators have developed expressions for the mean wind shear for various regions of stability (Sec. 2.3.4.3.). For unstable conditions,

$$\phi(h/\ell) = \frac{1}{1 - \beta' R_i^{1/2}} \quad \text{, small negative } R_i$$

$$\beta' = \text{constant}$$

$$\frac{\partial \bar{V}_W}{\partial h} \sim h^{-4/3} \quad \text{, strong instability.}$$

A form that matches the logarithmic, log-linear, and the above two expressions is the KEYPS equation:

$$\phi(h/\ell') = \frac{1}{(1 - \gamma' R_i)^{1/4}}, \; R_i \leq 0$$

$$\gamma' = 2\beta' = 4\alpha' = \text{constant}$$

This form has been adopted in Section 2.3.5 along with the $\gamma' = 18$, which implies $\alpha' = 4.5$, values in good agreement with measurements. The corresponding relationship between nondimensional altitude and Richardson's number is

$$h/\ell' = \frac{R_i}{(1 - \gamma' R_i)^{1/4}}$$

An explicit expression for the mean wind shear and, consequently, the mean wind speed in terms of h/ℓ' cannot be found, but such a relationship can be determined numerically.

For stable conditions, the log-linear relationship has been found to hold for suprisingly large values of h/ℓ'; for very stable conditions, knowledge is poor. The best expression found for very stable conditions is

$$\phi(h/\ell') = (1 + \alpha')$$

which once again results in a shear inversely proportional to altitude. The corresponding mean wind profile is

$$\bar{V}_W = \frac{u_{*0}}{k}\left\{\ln\left(\frac{h + z_0}{z_0}\right) + \alpha'\left[1 + \ln(h/\ell')\right]\right\}, \quad h/\ell' > 1$$

For $h/\ell' > 1$, Richardson's number and nondimensional altitude are related by

$$h/\ell' = (1 + \alpha')R_i$$

Combining the descriptions of $\phi(h/\ell')$ adopted provides the nondimensional shear as a function of h/ℓ', as shown in Figures 1-2 and 1-3. The corresponding function $f(h/\ell')$ for the mean wind equation is shown in Figures 1-4 and 1-5. The combined relationships between h/ℓ' and R_i are shown in Figure 1-6.

The wind above the edge of the boundary layer (geostrophic wind) is that which remains invariant with surface conditions and atmospheric stability in the boundary layer. There are little data on geostrophic winds, and relationships between winds near the surface and above the boundary layer are poor. Rather than relating low-altitude wind conditions to the geostrophic wind, the wind profile is extrapolated from low-altitude winds. The American standard for airport wind measurements is 20 feet. The extrapolation of winds and shears based on wind speeds at 20 feet is performed through the determination of friction velocity:

$$u_{*0}/k = \frac{\bar{V}_{20}}{\ln\left(\frac{20.15}{0.15}\right) + f(h_{REF}/\ell')} \quad \text{(Fig. 1-7)}$$

Figure 1-7 shows friction velocity to continually decrease for increasing stability. The nondimensional shear, Figures 1-2 or 1-3, is constant for $h/\ell' > 1$. Thus, the shear, given by

$$\frac{\partial \bar{V}_{20}}{\partial h} = \frac{\bar{V}_{20}}{h}\left(\frac{u_{*0}/k}{\bar{V}_{20}}\right)\left(\frac{kh}{u_{*0}}\frac{\partial \bar{V}_W}{\partial h}\right)$$

must decrease for $h/\ell' > 1$.

The scaling length, ℓ', may be determined for Richardson's number measured at another altitude different from 20 feet, but since the choice appears arbitrary, $1/\ell'$ is determined from Figure 1-6 for Richardson's number measured at 20 feet. The description provided

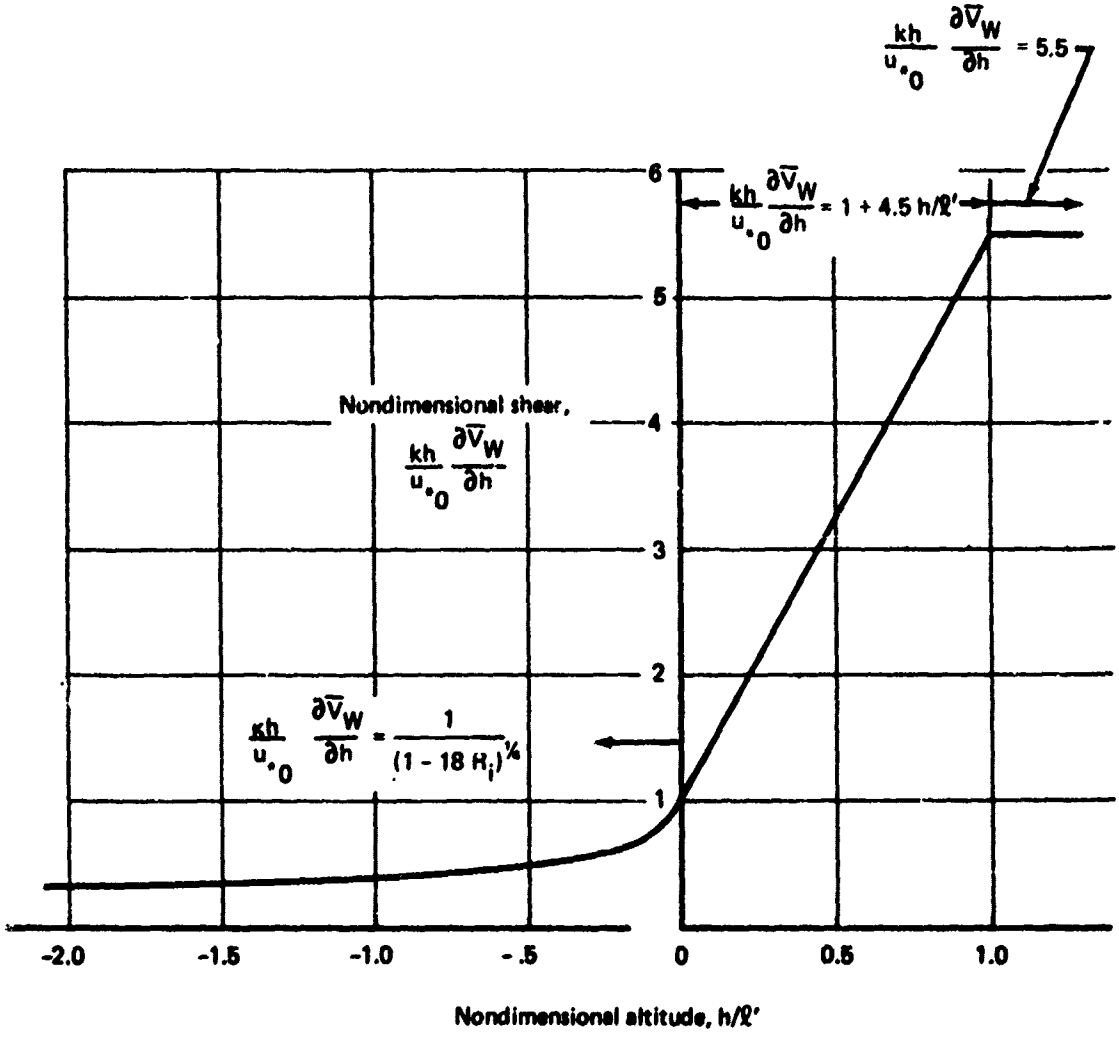

FIGURE 1-2.– SELECTED NONDIMENSIONAL SHEAR DESCRIPTION

thus far still suffers from a restriction: the dimensional analyses descriptions are valid only over the altitude region for which shear stress differs insignificantly from that at the surface. Insignificant variations of the shear stress have been variously estimated to occur up to 65 to 650 feet (sec. 2.3.2.4), significantly less than the objective of 1000 feet. At progressively higher altitudes, a progessively greater overestimation of the mean wind speed and shear occur; the description of the mean wind never does provide a constant mean wind with altitude above the boundary layer. A mechanism for adjusting the description has been found through descriptions of shear stress (friction velocity) variations throughout the boundary layer in Section 2.3.5.1.

By expanding shear stress with altitude about conditions at the boundary layer (where shear stress is zero) using a Taylor series, expressions for friction velocity variations with altitude and for the boundary layer depth, d, are developed:

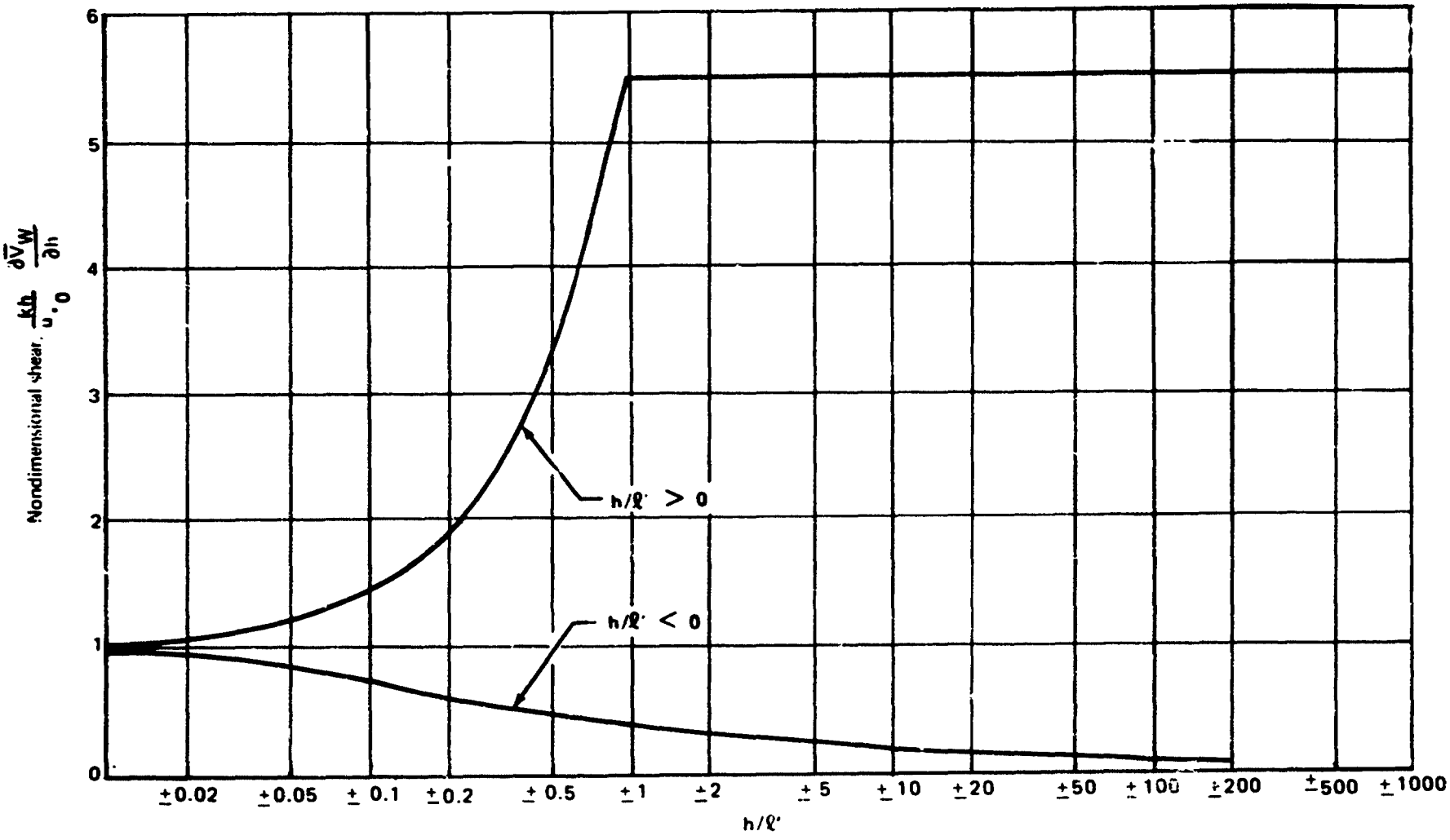

FIGURE 1-3.– NONDIMENSIONAL SHEAR

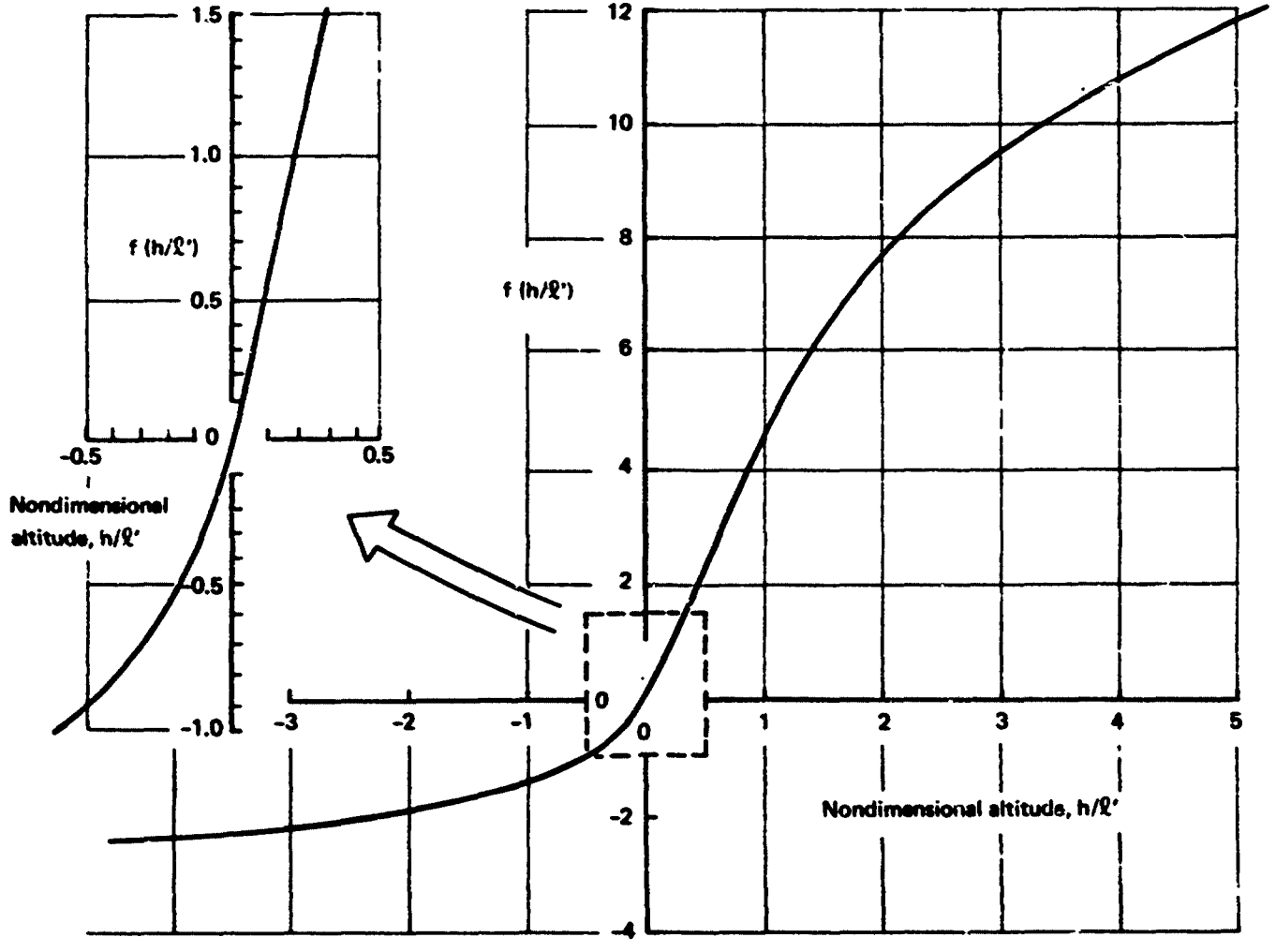

FIGURE 1-4.–CONTRIBUTION OF NON-NEUTRAL STABILITY TO MEAN WIND

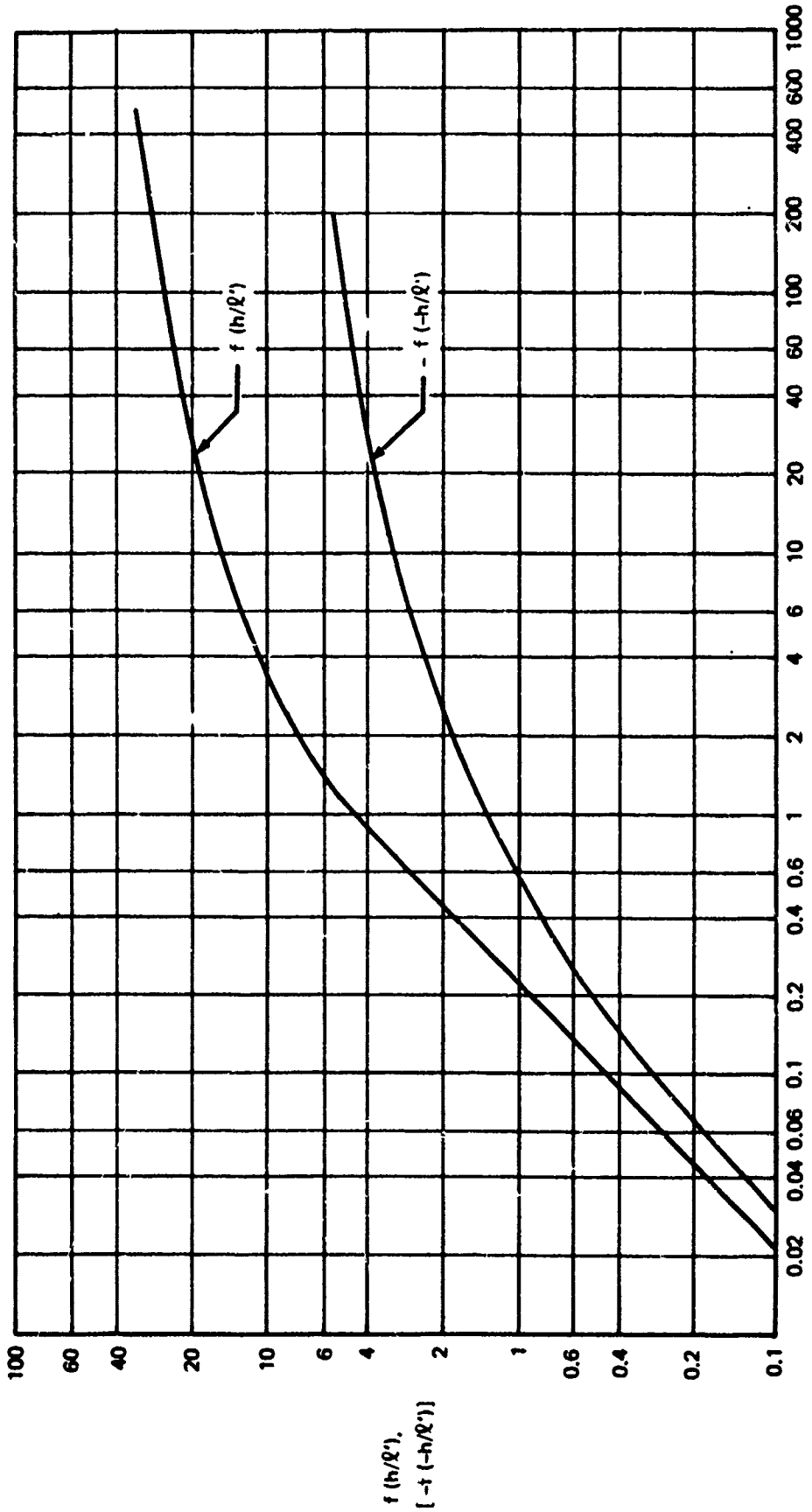

FIGURE 1-5.—CONTRIBUTION OF NON-NEUTRAL STABILITY TO MEAN WIND, LOG PLOT

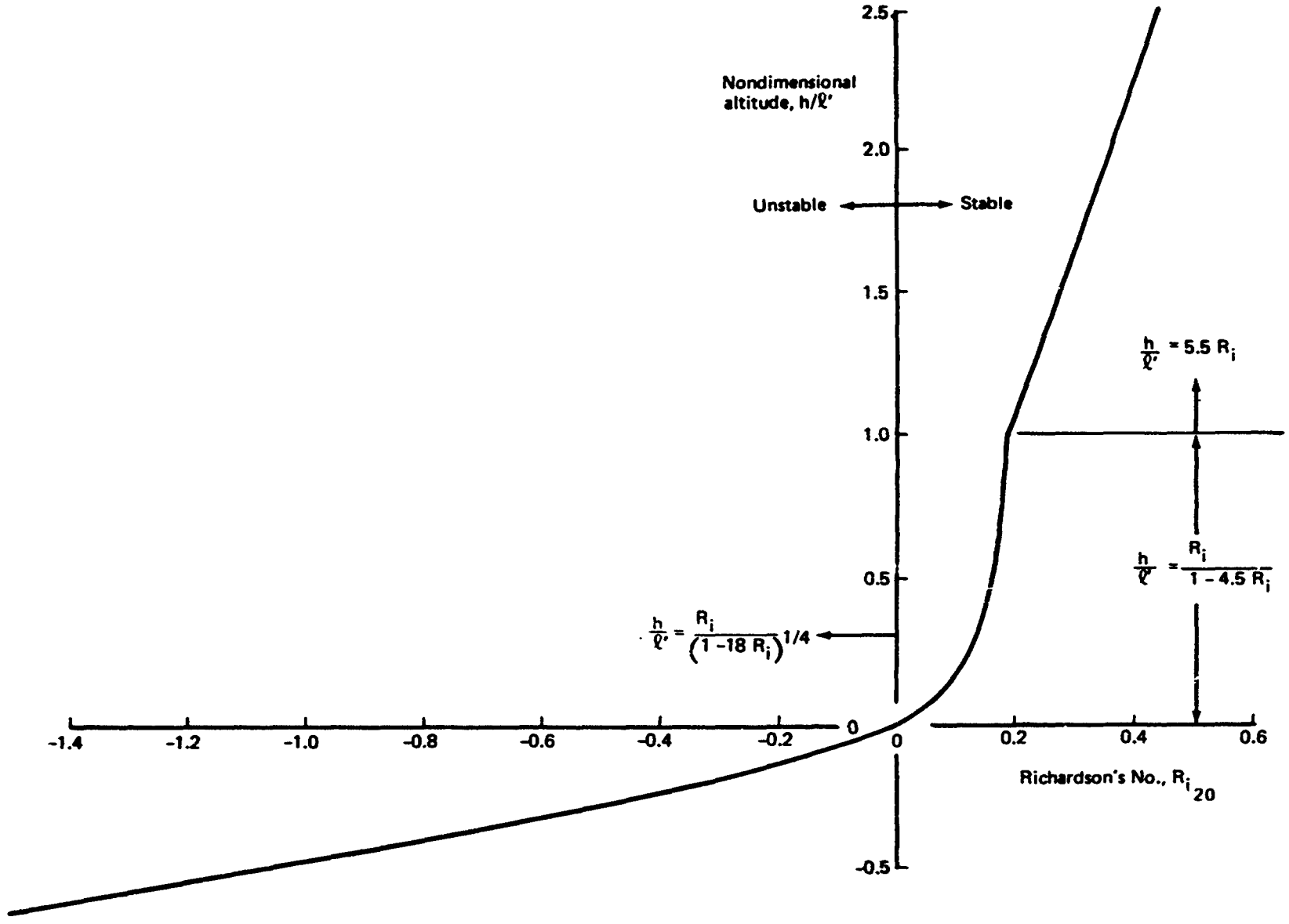

FIGURE 1-6.– LOW ALTITUDE RICHARDSON'S NUMBER PROFILE

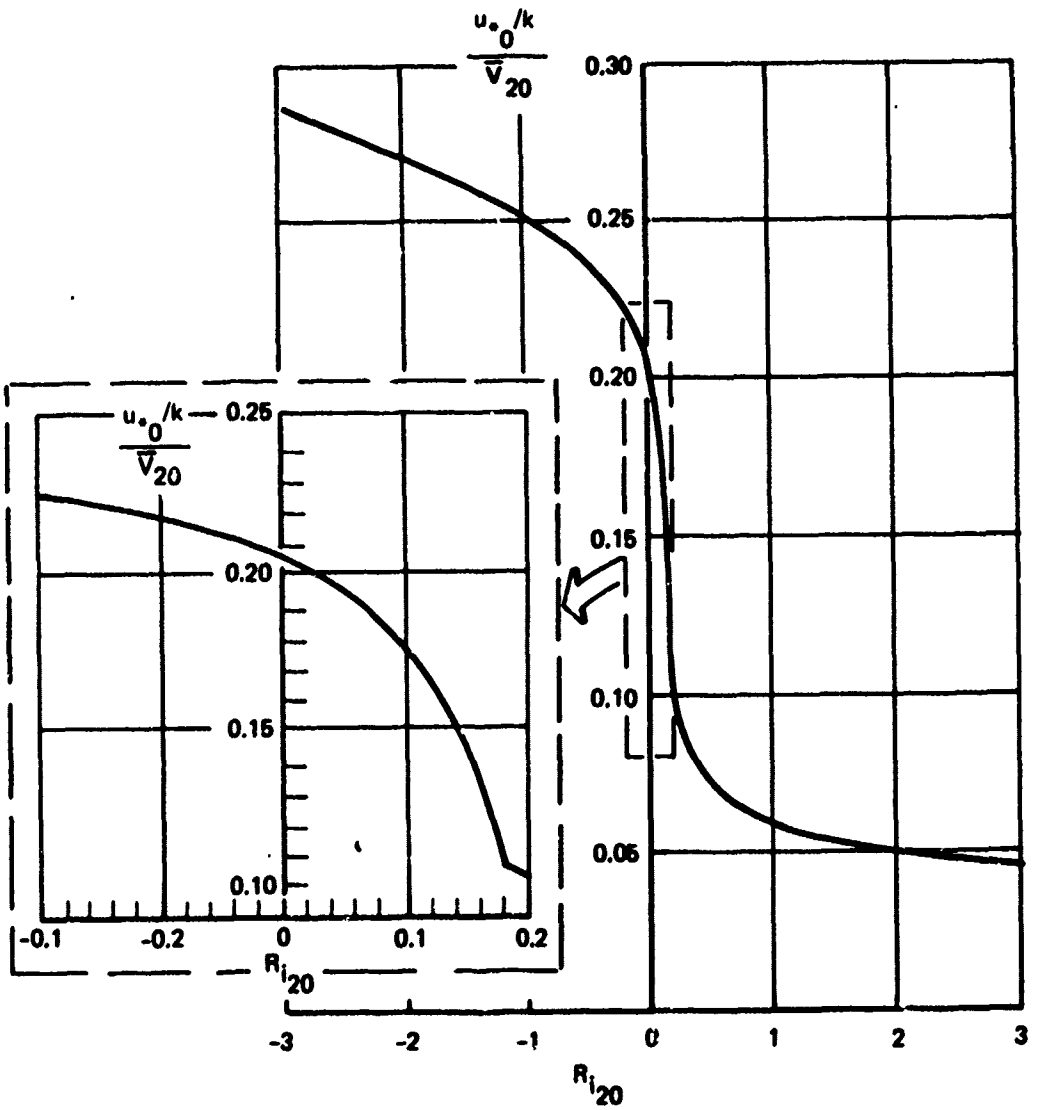

FIGURE 1-7.– MEAN WIND PROPORTIONALITY CONSTANT

$$u_* = u_{*_0}(1 - h/d)$$

$$d = u_{*_0}/5.35f$$

where

f = Coriolis parameter

$= 2\omega_E \sin\lambda$

ω_E = angular velocity of the earth

λ = latitude

Most of the United States and a majority of the world airport activity lies between 30° and 50° latitude, so a fixed latitude, $\lambda = 40°$, is adopted for determining the boundary layer depth. Then,

$$d = 2000\, u_{*_0}$$

To incorporate the shear stress variation into the mean wind description, the assumption that the shear is proportional to friction velocity at the surface is dropped, and it is assumed that the shear is proportional to the local level of friction velocity. Then,

$$\frac{\partial \bar{V}_W}{\partial h} = \frac{u_*}{kh}\phi(h/\ell') = \left(\frac{u_*}{u_{*_0}}\right)\frac{u_{*_0}}{kh}\left(\frac{kh}{u_*}\frac{\partial \bar{V}_W}{\partial h}\right)$$

$$= \left(1 - \frac{h}{d}\right)\frac{\bar{V}_{20}}{h}\left(\frac{u_{*_0}/k}{\bar{V}_{20}}\right)\left(\frac{kh}{u_*}\frac{\partial \bar{V}_W}{\partial h}\right)$$

The shear now smoothly decreases to zero at the edge of the boundary layer with increasing altitude. Near the surface, where $h/d \cong 0$, the constant shear stress model is unaffected.

The corresponding expression for the mean wind speed, developed in Section 2.3.5.2, is

$$\bar{V}_W = \bar{V}_{20}\left(\frac{u_{*_0}/k}{\bar{V}_{20}}\right)\left[\ln\left(\frac{h + z_0}{z_0}\right) + f(h/\ell') - \frac{h}{d}g(h/\ell')\right]$$

The function $g(h/\ell')$ (Fig. 1-8) is derived from $f(h/\ell')$. It is always positive, is equal to one for neutral stability, and increases with increasing stability.

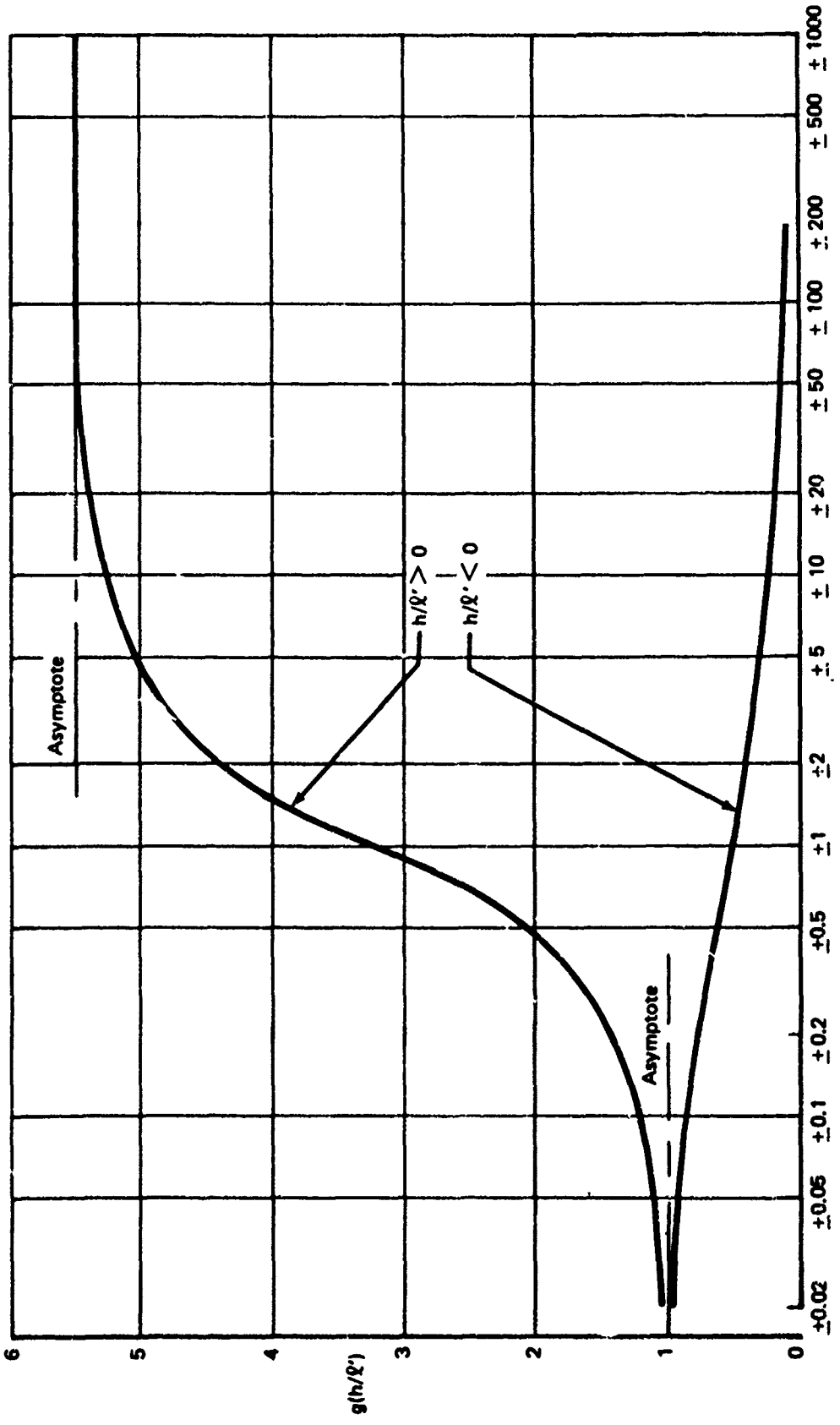

FIGURE 1-8.– VARIABLE SHEAR STRESS CORRECTION TO WIND PROFILE

The additional parameters required to complete the description of the mean wind speed and mean wind shear are specifications for wind speed and Richardson's number at a 20-foot altitude. Probabilistic descriptions are developed in Section 3.0.

Based on Weather Service reports at U.S. airports, a description of airport wind speeds has been developed in Section 3.2 that describes 10-minute averages measured each hour for 10 years. The data were taken prior to establishing 20 feet as a standard anemometer height, so anemometer heights varied widely from airport to airport. From data for 132 U.S. airports, data were selected from 24 sites where anemometer heights varied from 20 to 35 feet with an average height of about 26 feet. The remaining sites have anemometers located from above 35 to 120 feet above the ground and were considered to be too high to represent wind speeds at 20 feet. In developing a composite description for all 24 airports, the distributions from each site were weighted equally. The resulting descriptions, Figure 1-9, provide for 8 knots exceeded 50% of the time and 22.8 knots exceeded 1% of the time. For 39 of the same 132 sites, data for the wind speed distribution when visibility was less than 0.5 mile (prepared by the Weather and Flight Service Station Branch of the FAA) are presented. For low visibility, wind speeds are much lower than for clear conditions, for low visibility, 4.5 knots is exceeded 50% of the time and 14 knots is exceeded 1% of the time.

From the data for the 24 U.S. airports, distribution of wind components along and across runways were developed, assuming the runway is aligned to the prevailing wind (Secs. 3.2.1.3 and 3.2.1.4). Crosswinds from the left and right were found to be equally likely. The distribution of crosswind magnitude, Figure 1-10, provides for exceeding a 5-knot crosswind 50% of the time and a 19-knot crosswind 1% of the time. When the distribution of crosswinds are plotted for both positive and negative crosswinds, the distribution is closely Gaussian (standard deviation equal to 6.5 knots), with deviations from a Gaussian distribution occurring in the tails (1.65 standard deviations from zero crosswind).

The distribution of down runway components is also closely Gaussian (Fig. 1-11) with a mean and standard deviation of 1 and 7 knots, respectively. The probability of a wind component in the direction of the prevailing wind is 59%. The distribution for the magnitude of the component of mean wind aligned to the runway (Fig. 1-12) provides for 5 knots exceeded 50% of the time and 19 knots exceeded 1% of the time.

Distribution of mean wind shears were also investigated in Section 3.0. Distributions were much broader near the surface than at higher altitudes, conforming to the analytic description The introduction of atmospheric stability into the mean wind description in such a way that wind shears increase with increasing stability (up to a point), as well as with wind speed and the finding that atmospheric stability is inversely related to wind speed, introduce confusion as to whether maximum shears occur at high wind speeds where stability is close to neutral or at low wind speeds where stability is high. Data from the literature, presented in Section 3.2.3.1, show the greatest shears occur at the most stable lapse rates and at low wind speeds (both average and maximum wind shears decrease monotonically with increasing wind speeds at high wind speeds), conflicting with commonly employed wind models that assume neutral stability and increasing shears with wind speed, thus emphasizing the importance of atmospheric stability as a mean wind parameter.

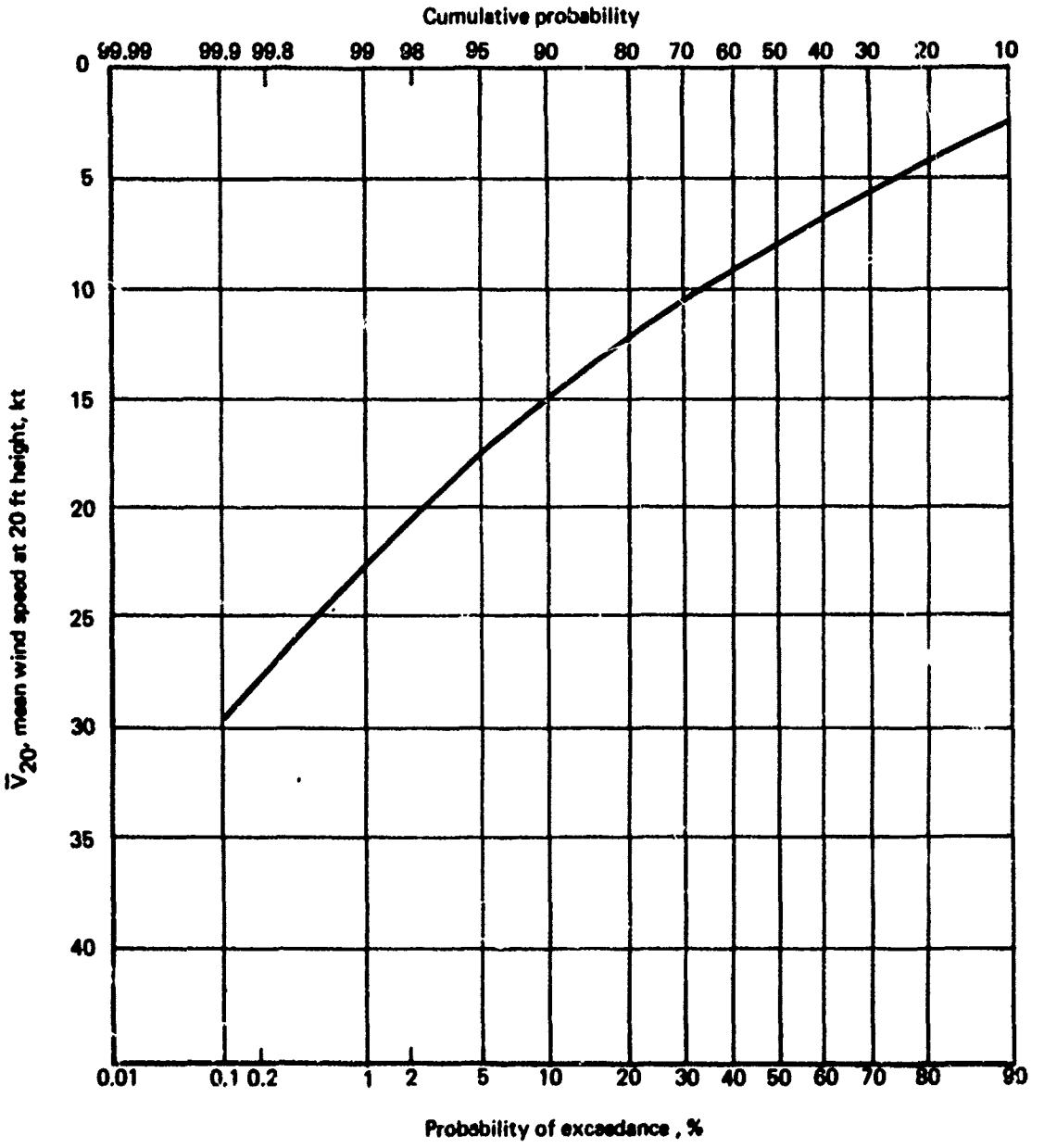

FIGURE 1-9.– MEAN WIND CUMULATIVE/EXCCEDANCE PROBABILITY

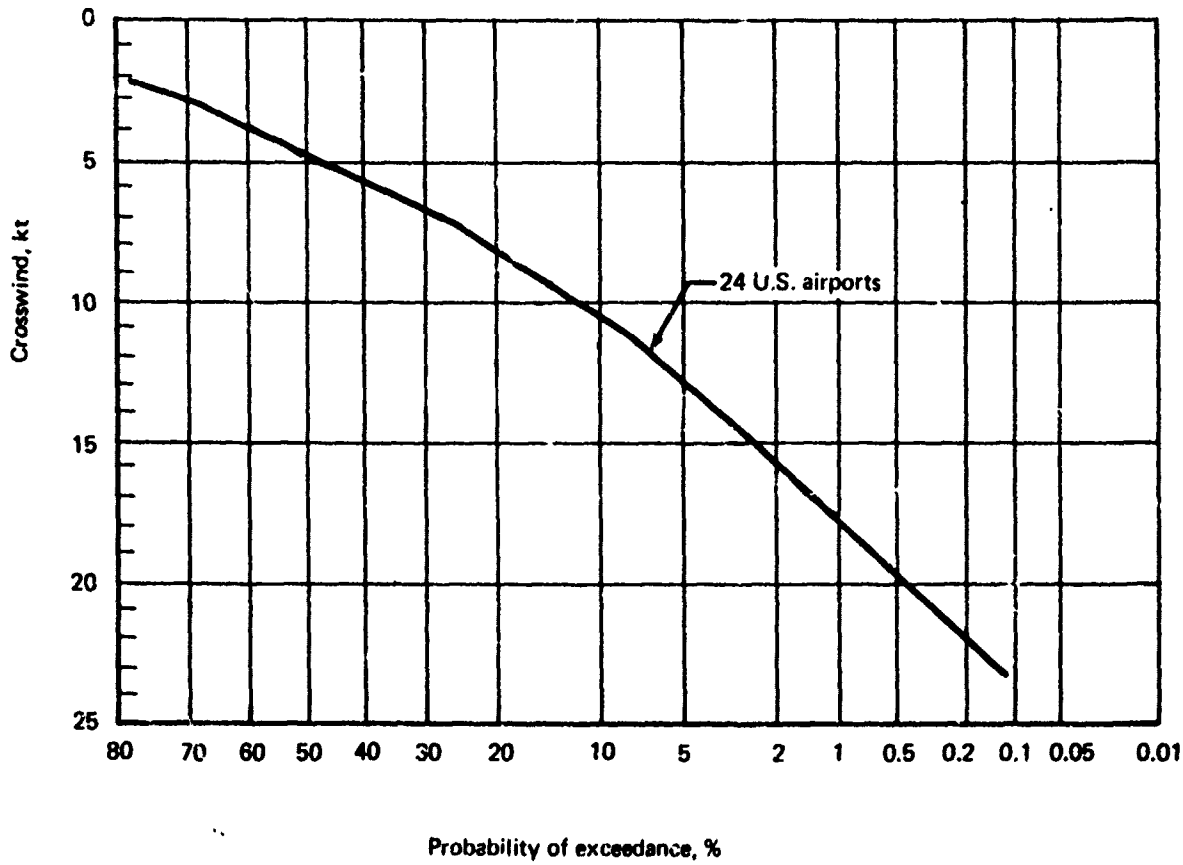

FIGURE 1-10.–TOTAL CROSSWIND INFORMATION COMPILED FROM 24 U.S. AIRPORTS

The literature was not productive for describing distributions of atmospheric stability, so probability distributions were generated by reducing data from towers located at Cedar Hills, Texas, and Cape Kennedy, Florida (Sec. 3.3.3.). The distributions for the two sites differed substantially (Fig. 1-13), with the Cedar Hills data being more stable. Evaluation of the climatology and wind characteristics of the two sites led to the conclusion that the Cape Kennedy stability data were more representative of average airport conditions. Consequently, the Cape Kennedy data were selected for use with the model. Although the Cape Kennedy data reflected the lesser stability over 70% of the cases at the site were stable (versus 90% of the cases at Cedar Hills).

The strong interdependence between the distribution of atmospheric stability and near-surface wind speed can be seen in Figure 1-14. Although the atmospheric stability distribution narrows substantially about neutral conditions at increasing wind speeds, the distribution remains significantly broad at high wind speeds. The data in Figure 1-14 were faired and extrapolated to account for the relatively small data sample (one site for 3 years with near-calm wind speed conditions excluded) and have been cross plotted at constant 20-foot-altitude wind speeds in Figures 1-15, 1-16, and 1-17.

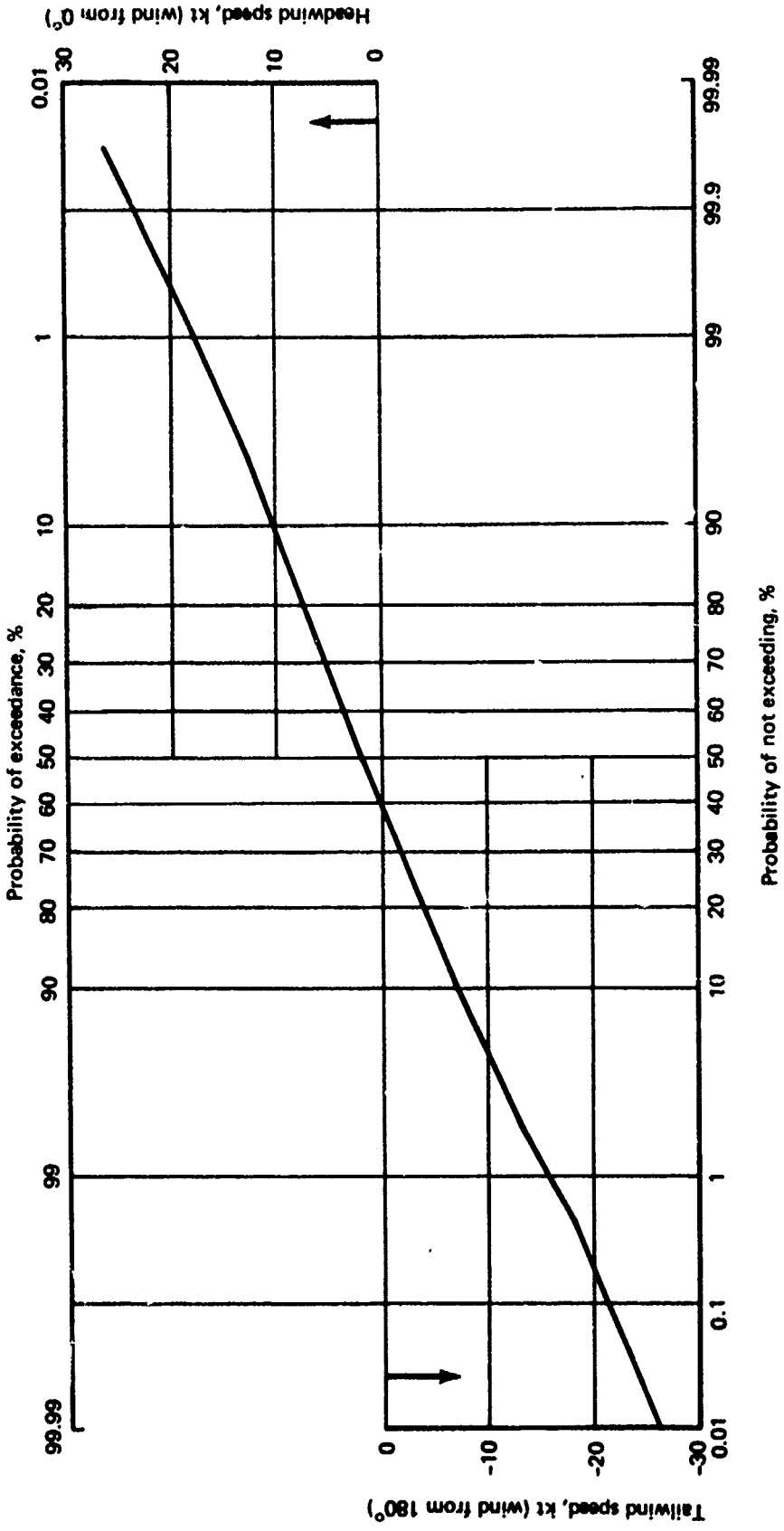

FIGURE 1-11.– HEADWIND–TAILWIND DESCRIPTION COMPILED FROM 24 U.S. AIRPORTS

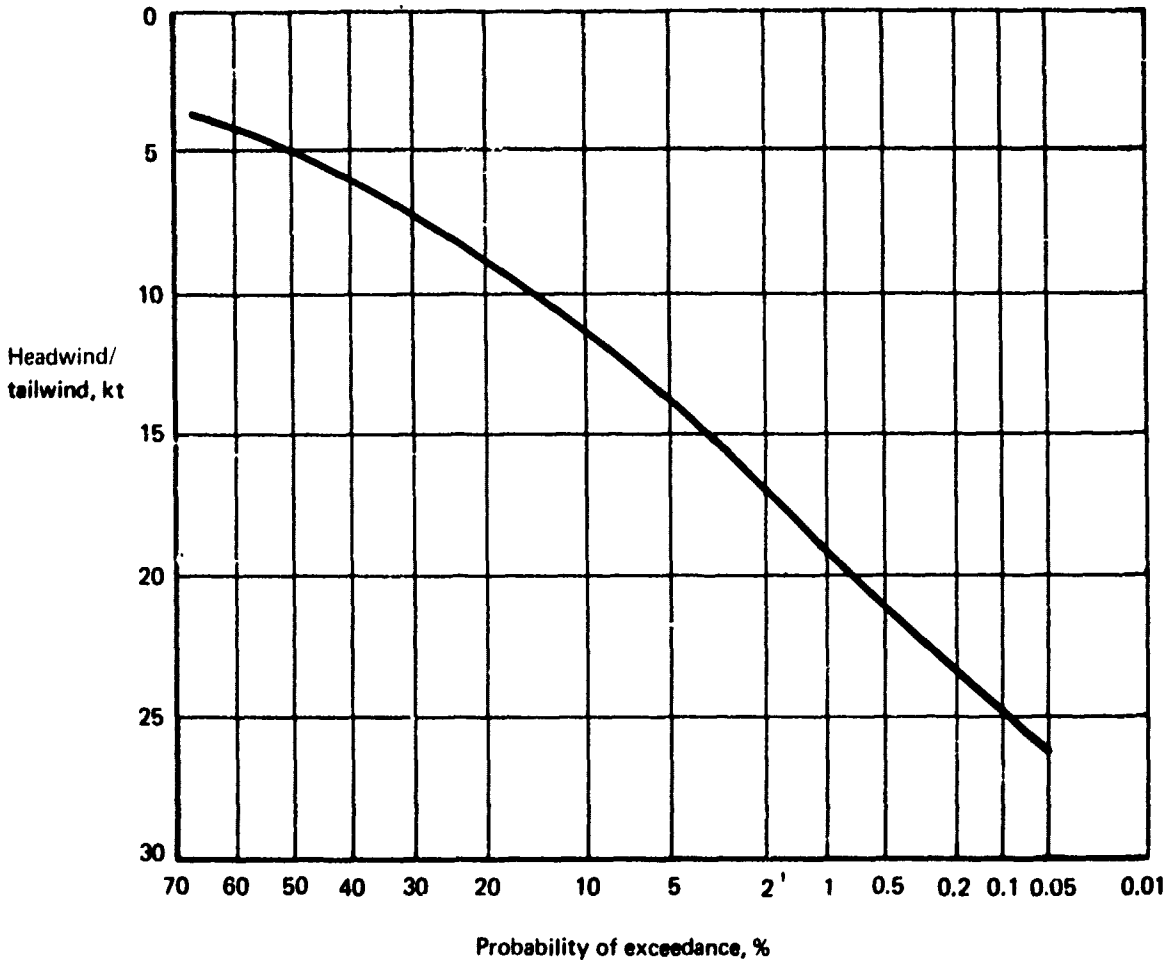

FIGURE 1-12.– TOTAL HEADWIND–TAILWIND MEAN OF 24 U.S. AIRPORTS

The mean wind speed and atmospheric stability distribution curves may be used by (1) defining wind speed/stability regions and assigning average values of wind speed and Richardson's number to each region; (2) by simulating the aircraft for each wind speed/Richardson's number combination; and (3) by combining the results of the simulation according to the joint probabilities of each region. Alternatively, the simulation may be used to define random combinations of mean wind speed and Richardson's number. A random number generator, providing a uniform distribution between zero and one, is used to determine two random numbers. A mean wind speed at an exceedance probability equal to one of the random number generators is found. The Richardson's number associated with the exceedance probability for the mean wind speed determined equal to the second random number is found. The Richardson's number and mean wind speed then determine the mean wind speed and shear profiles. When this process is repeated, the joint distribution of wind speed and Richardson's number is reproduced. This procedure is defined in more detail in Section 4.5.1.

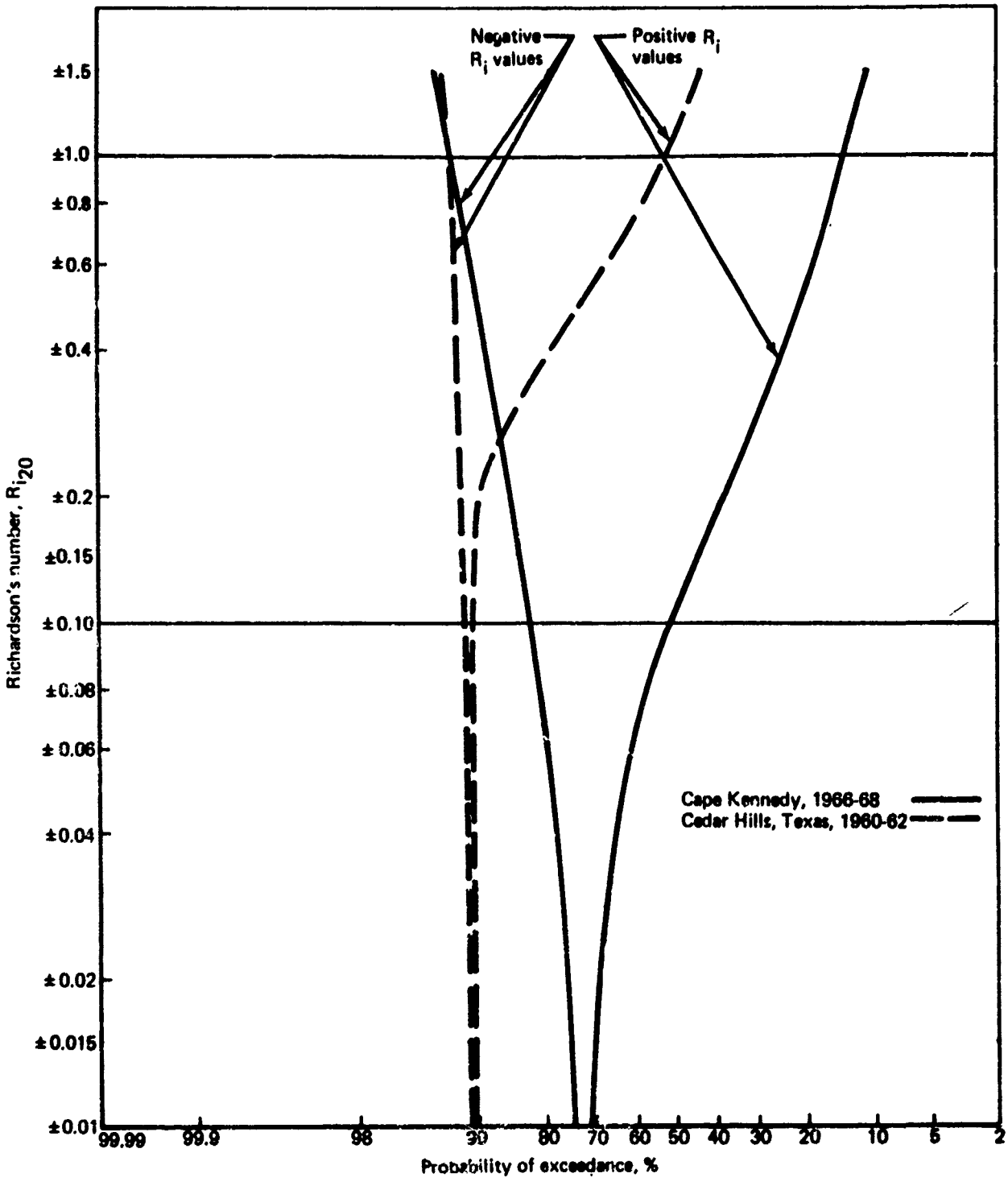

FIGURE 1-13.– PROBABILITY OF EXCEEDANCE OF R_i FOR ALL WIND SPEEDS

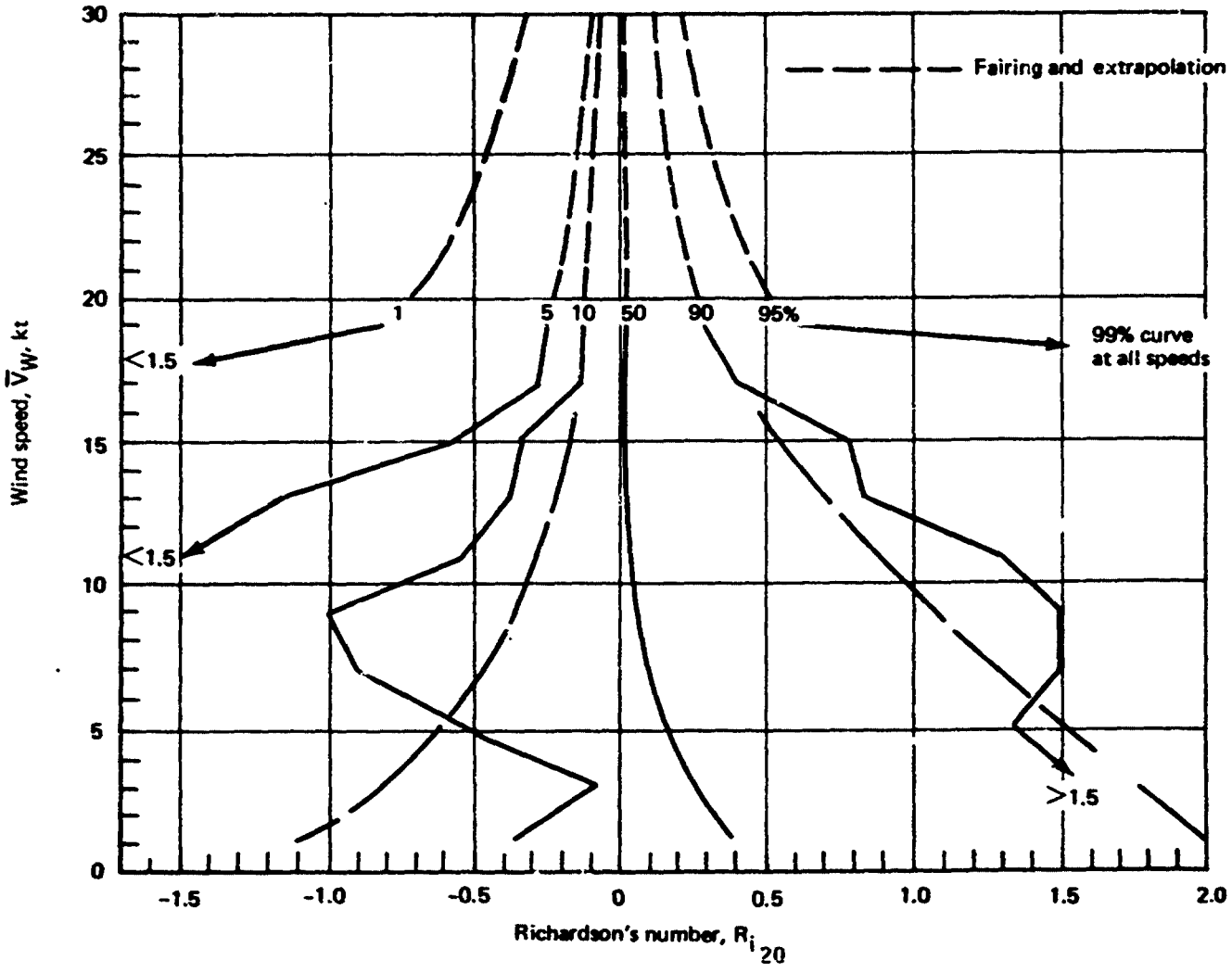

FIGURE 1-14.– PERCENT FREQUENCY OF OCCURRENCE, WIND SPEED VS R_i, CAPE KENNEDY, 1966-68

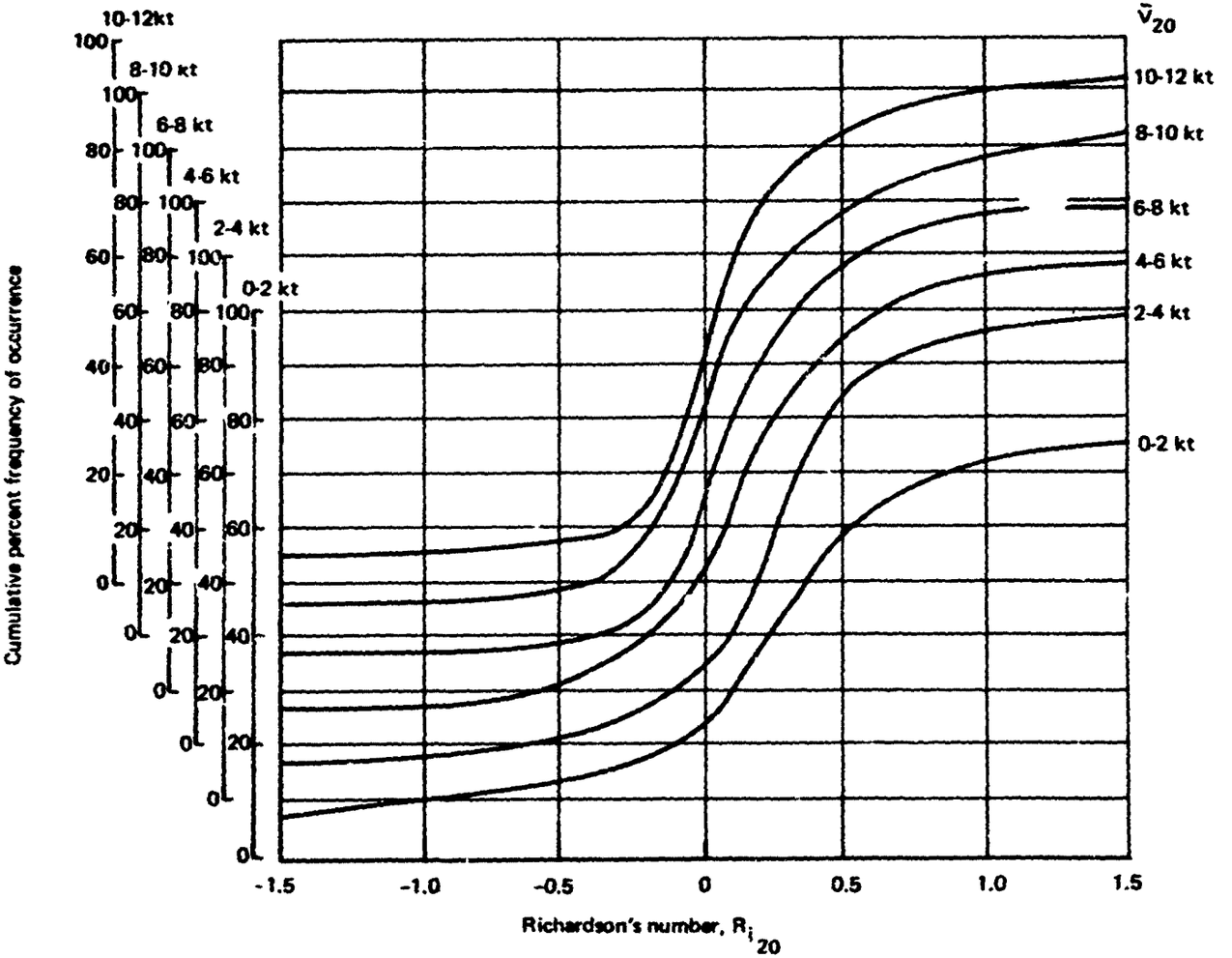

FIGURE 1-15.– CUMULATIVE PERCENT FREQUENCY OF OCCURRENCE OF R_i AT GIVEN WIND SPEEDS, 0 TO 12 KNOTS

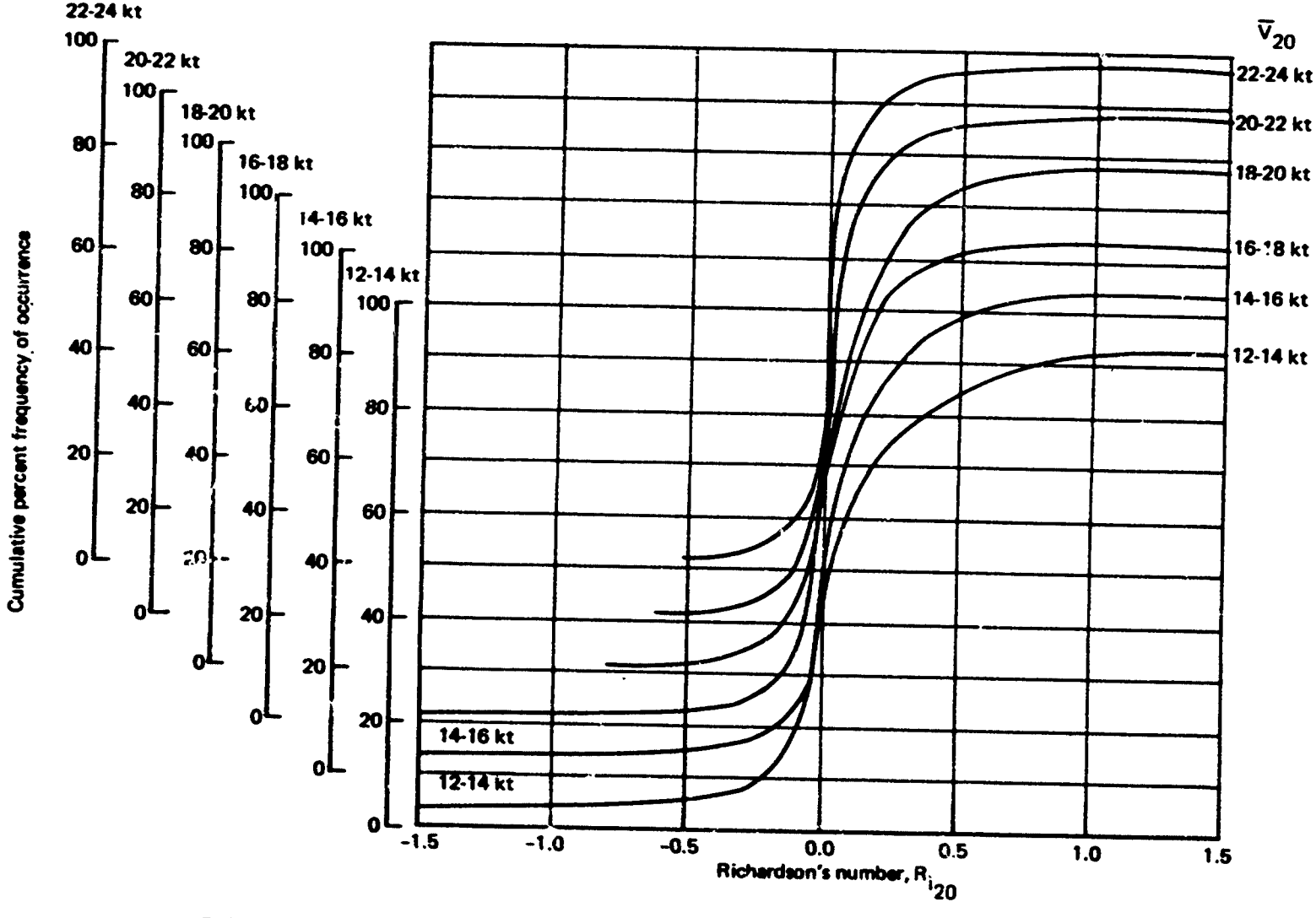

FIGURE 1-16.– CUMULATIVE PERCENT FREQUENCY OF OCCURRENCE OF R_i AT GIVEN WIND SPEEDS, 12 TO 24 KNOTS

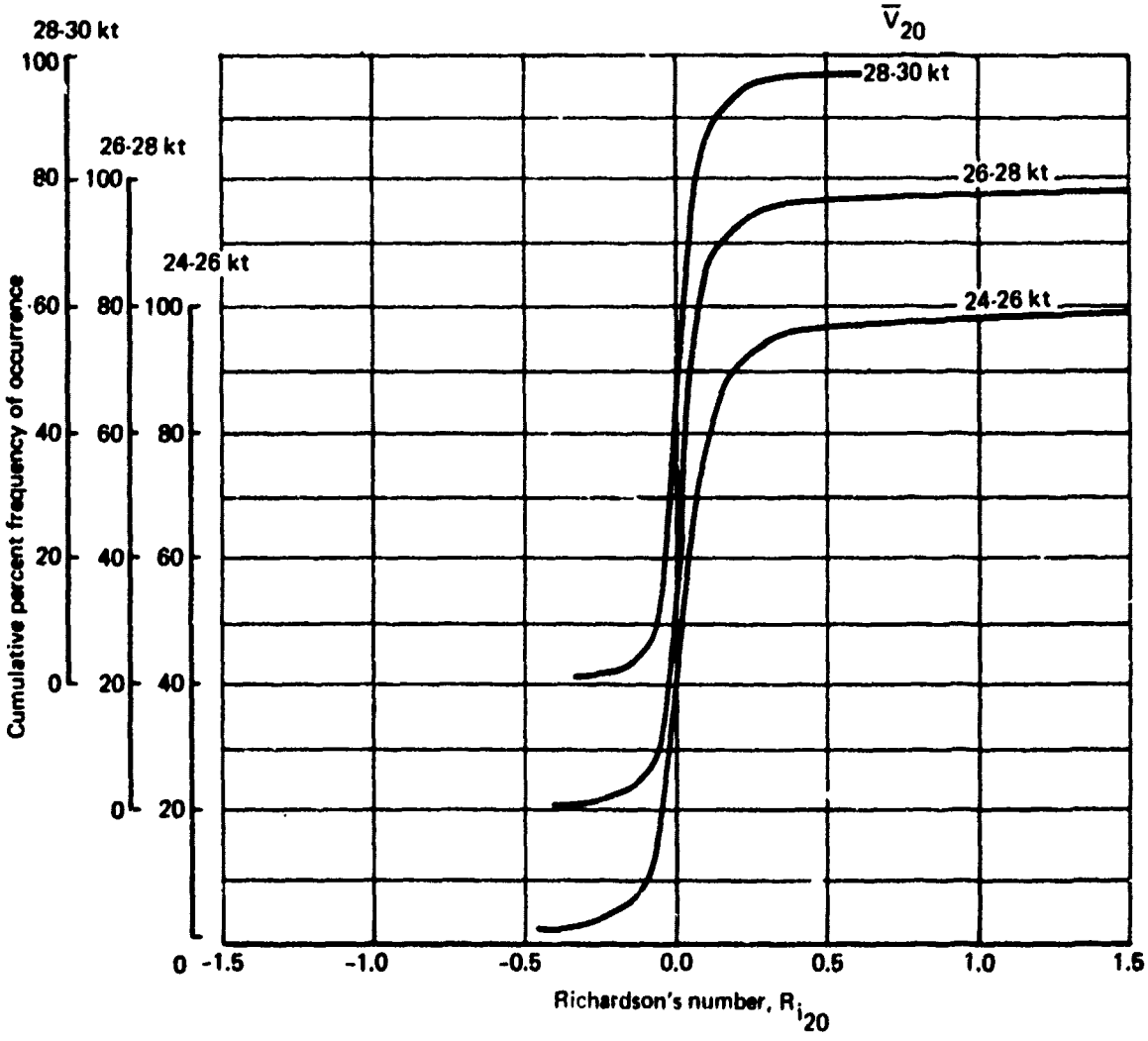

FIGURE 1-17.– CUMULATIVE PERCENT FREQUENCY OF OCCURRENCE OF R_i AT GIVEN WIND SPEEDS, 24 TO 30 KNOTS

In order to determine the aerodynamic forces and moments, the mean wind must be resolved into body axis components, an axis system attached to the airplane. The transformation required is presented in Figure 1-18 and depends on the orientation of the airplane's body axis with respect to the wind, defined by the Euler yaw, pitch, and roll angles and the direction to which the wind is blowing (negative of conventional wind heading). The introduction of wind heading presents an additional mean wind parameter that must be known at each altitude. As shown in Section 4.2.1.1.2, a variation of wind heading with altitude (heading shear) has an effect on the shear that the airplane sees that is added to the mean wind speed shear effect.

Analytic descriptions for the variation of wind heading with altitude are provided in Sections 2.3.1 and 2.3.5.1, but these descriptions lack empirical support. A small amount of heading shear probability distribution data was found in the literature and is reported in Section 3.2.3.1. The data indicate a majority of heading shears are within ±3°/100 feet and a greater tendency to rotate counterclockwise while approaching the surface. The tower data used to determine the atmospheric stability distribution were also evaluated for heading shear information in Section 3.3.4. Distributions tended to be larger near the surface but constant above about 150 feet. No consistent trend of the profile shapes could be found. Heading shear was found to be uncorrelated with both wind speed and atmospheric stability (Sec. 3.3.6). In order for the heading shear to be significant, the wind speed must also be large (body axis shear components involve the combination $\bar{V}_W \, d\bar{\psi}_W/dh$ only). The probability of having a large heading shear and wind speed shear is sufficiently remote and the information for specifying the variation of wind heading with altitude is sufficiently poor so that a representation of wind heading dependence upon altitude is not attempted; the wind heading is assumed to remain constant and equal to that at the surface. The distribution of wind heading at the surface was developed from wind roses for the same 24 sites used to determine the wind speed distribution (Sec. 3.2.1.3) and is presented in Figure 1-19.

A major factor to which longitudinal touchdown dispersions are attributed is the longitudinal wind shear component. Considerable literature has been written on the subject, but conflicting conclusions are provided. Some predict a headwind shear will cause an overshoot, while others predict an undershoot. The subject is evaluated in Section 4.2.2. Some of the differences of opinion can be attributed to different trim and operation procedures. However, it is concluded that one of two airplanes can overshoot while the other undershoots due to a wind shear, even if both are operated in the same manner.

The effect of a steady wind is to alter the pitch attitude (θ) at which to trim to hold a given glideslope (γ):

$$\theta \cong \left[1 + \frac{\bar{V}_W \cos(\psi - \bar{\psi}_W)}{V_A}\right]\gamma + \alpha$$

where $\bar{\psi}_W = 0$ is a tailwind. For a headwind and a negative glideslope, the pitch attitude must be increased by $(\bar{V}_W/V_A)\gamma$ from that for still air and the thrust increased by $\Delta(\text{thrust}) = W\Delta\theta$, or the airplane will touch down short.

BODY AXIS MEAN WIND COMPONENTS

$$\begin{Bmatrix} \bar{u}_W \\ \bar{v}_W \\ \bar{w}_W \end{Bmatrix} = \begin{Bmatrix} \cos(\psi - \bar{\psi}_W)\cos\theta \\ \cos(\psi - \bar{\psi}_W)\sin\theta\sin\phi - \sin(\psi - \bar{\psi}_W)\cos\phi \\ \cos(\psi - \bar{\psi}_W)\sin\theta\cos\phi + \sin(\psi - \bar{\psi}_W)\sin\phi \end{Bmatrix} \bar{V}_W$$

BODY AXIS MEAN WIND SHEAR COMPONENTS

$$\begin{Bmatrix} \frac{\partial \bar{u}_W}{\partial h} \\ \frac{\partial \bar{v}_W}{\partial h} \\ \frac{\partial \bar{w}_W}{\partial h} \end{Bmatrix} = \begin{bmatrix} \cos(\psi - \bar{\psi}_W)\cos\theta & \sin(\psi - \psi_W)\cos\theta \\ \cos(\psi - \bar{\psi}_W)\sin\theta\sin\phi - \sin(\psi - \bar{\psi}_W)\cos\phi & \sin(\psi - \psi_W)\sin\theta\sin\phi + \cos(\psi - \psi_W)\cos\phi \\ \cos(\psi - \bar{\psi}_W)\sin\theta\cos\phi + \sin(\psi - \bar{\psi}_W)\sin\phi & \sin(\psi - \psi_W)\sin\theta\cos\phi - \cos(\psi - \psi_W)\sin\phi \end{bmatrix} \frac{d\bar{V}_W}{dh}$$

BODY AXIS TURBULENCE COMPONENTS

$$u_{A_P} = \left[\cos\alpha\cos\beta\cos\theta + \sin\beta\sin\theta\sin\phi + \sin\alpha\cos\beta\sin\theta\cos\phi\right] V_{A_{CG}}$$

$$v_{A_P} = \left[\sin\beta\cos\phi - \sin\alpha\cos\beta\sin\phi\right] V_{A_{CG}}$$

$$\Delta\psi = -\tan^{-1}\frac{v_{A_{TG}}}{u_{A_{TG}}} \cong -\beta$$

$$\begin{Bmatrix} u_T \\ v_T \\ w_T \end{Bmatrix} = \begin{bmatrix} \cos\Delta\psi\cos\theta & \sin\Delta\psi\cos\theta & -\sin\theta \\ \cos\Delta\psi\sin\theta\sin\phi + \sin\Delta\psi\sin\theta\sin\phi & \sin\Delta\psi\sin\theta\sin\phi + \cos\Delta\psi\cos\phi & \cos\theta\sin\phi \\ \cos\Delta\psi\sin\theta\cos\phi + \sin\Delta\psi\sin\phi & \sin\Delta\psi\sin\theta\cos\phi - \cos\Delta\psi\sin\phi & \cos\theta\cos\phi \end{bmatrix} \begin{Bmatrix} u_{T_{TG}} \\ v_{T_{TG}} \\ w_{T_{TG}} \end{Bmatrix}$$

FIGURE 1-18.– TRANSFORMATIONS

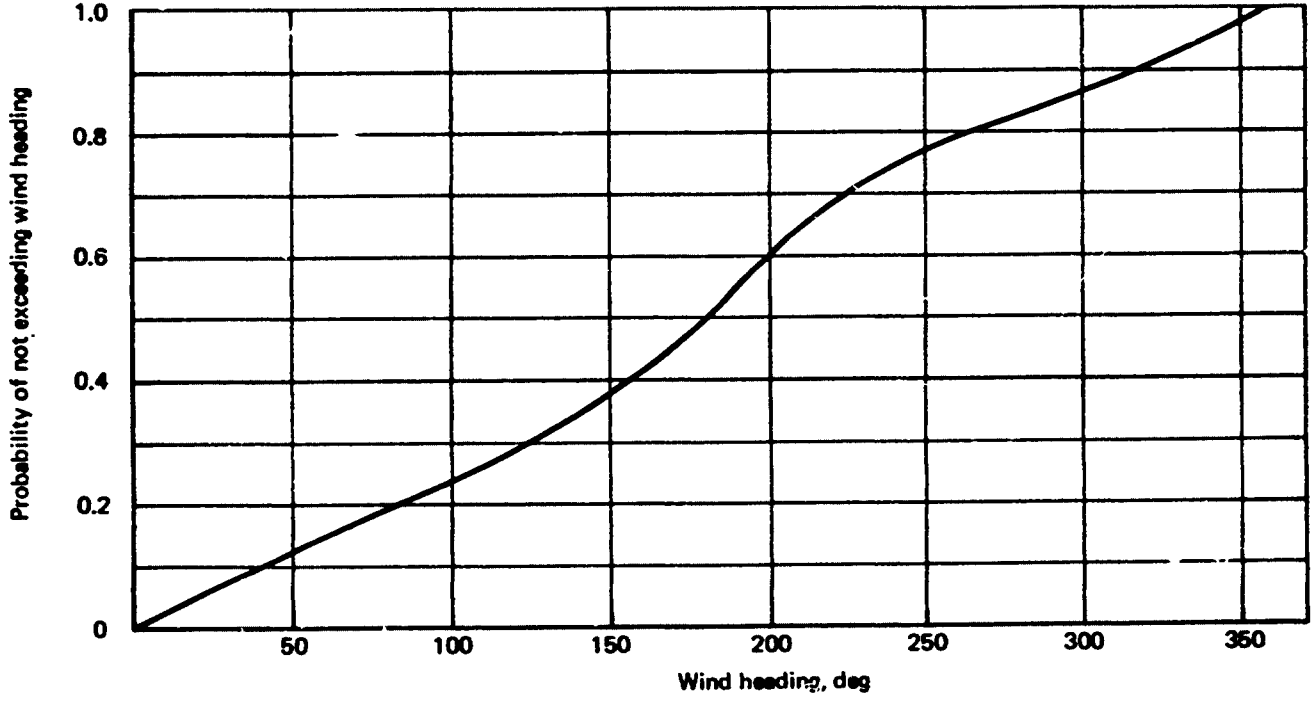

FIGURE 1-19.— WIND HEADING CUMULATIVE PROBABILITY MODEL

If the airplane is trimmed for a headwind at a high altitude and the headwind decreases with altitude, the pitch attitude must be decreased throughout the approach and thrust correspondingly decreased, or else the airplane will touch down long due to the attitude effect.

There is also a second effect of a wind shear. If the approach is to be performed at constant airspeed, changes in the wind speed must be matched with changes in the inertial speed. To provide inertial acceleration, thrust must be changed by

$$\Delta(\text{thrust}) \cong \frac{W(V_A + \bar{V}_W)}{g} \frac{d\bar{V}_W}{dh} \gamma$$

For a headwind that diminishes during an approach

$$\frac{d\bar{V}_W}{dh} \gamma > 0$$

and thrust must be increased or the touchdown will be short.

The combination of the attitude and acceleration effects is

$$\frac{\Delta T}{W} \cong \gamma \left[\frac{\Delta \bar{V}_W}{V_A} + \frac{(\bar{V}_A + \bar{V}_W)}{g} \frac{d\bar{V}_W}{dh} \right]$$

So long as the magnitude of the wind increases with altitude and the airplane is trimmed for the high attitude wind, the two terms have opposite signs. For airplanes with low airspeeds, the attitude effect tends to dominate. For a given airplane, the acceleration effect will be stronger at lower altitudes where the shear is relatively strong compared to the total change of wind speed. This evaluation presumes the airplane is controlled in an open-loop manner. The ability to attain closed-loop control, either by the pilot or the autoland system, depends in part upon the open-loop stability of the aircraft-autoland system.

Airplane stability is affected by the wind shear, as shown in Sections 4.2.1.1. and 4.2.1.2: aerodynamic forces and moments are dependent on the components of wind speed, motion is dependent on aerodynamic forces and moments, and the components of wind speed are dependent on airplane motion. If the aerodynamic characteristics can be considered to be concentrated at the center of gravity, only longitudinal stability, principally phugoid or long period stability, is affected by wind shears. A headwind shear can either stabilize or destabilize the phugoid, depending on the characteristics of the airplane's stability derivatives. If a headwind shear has stabilizing effects, a tailwind has destabilizing effects, and vice-versa.

The effects of a wind shear may not be adequately represented by considering the aerodynamic characteristics to be concentrated at the center of gravity. Due to the change of wind speed with altitude, there is a distribution of wind speed over the vertical tail that

introduces a rolling moment. When the airplane is disturbed from zero pitch attitude and wings level, the different parts of the airplane in the plane of the wings will be at different altitudes and there will be a distribution of wind speed about the airplane and a corresponding change in the distribution of lift.

The distribution of wind about the airplane may well be represented as being linear in three dimensions. Then the components of wind at some point (x,y,z) are represented by

$$\bar{u}_W = \bar{u}_{W_{CG}} + \frac{\partial \bar{u}_W}{\partial x}x + \frac{\partial \bar{u}_W}{\partial y}y + \frac{\partial \bar{u}_W}{\partial z}z$$

$$\bar{v}_W = \bar{v}_{W_{CG}} + \frac{\partial \bar{v}_W}{\partial x}x + \frac{\partial \bar{v}_W}{\partial y}y + \frac{\partial \bar{v}_W}{\partial z}z$$

$$\bar{w}_W = \bar{w}_{W_{CG}} + \frac{\partial \bar{w}_W}{\partial x}x + \frac{\partial \bar{w}_W}{\partial y}y + \frac{\partial \bar{w}_W}{\partial z}z$$

The derivative of body axis wind components are expressible in terms of the mean wind shear (Sec. 4.2.1.2) and can be interpreted as effective angular components of wind. For example, the distribution of the lateral component of wind about the vertical dimensions of the fin appears as a roll rate, which generates a rolling moment proportional to the fin's contribution to the roll rate derivative of rolling moment.

Linear analysis predicts that the distributed lift effects of the mean wind shear appear primarily for lateral-directional motion. These effects are due to the headwind-tailwind component of the shear. The wind shear alters all of the lateral-directional stability characteristics, but the sensitivity of the characteristic roots to wind shear are configuration dependent.

Representation of the distributed lift effects is the only reason for computing the mean wind shear at each altitude. If the distributed lift effects can be shown to be insignificant, the computation of the shear can be left out of the simulation.

1.3.2 Turbulence

For unstable atmospheric conditions, amplified displacement of air particles from their initial positions due to buoyancy forces cannot increase without bound. Turbulence is the mechanism by which the effects of instability are constrained through the mixing of hot and cold air particles, which produces equilibrium locally. The appearance and disappearance of turbulence with changing atmospheric stability involves a hysteresis effect, but it is predicted to occur at the critical Richardson's number, related to the log-linear mean wind profile constant:

$$R_{i_{CRIT}} = \frac{1}{\alpha'} = 0.222 \text{ for } \alpha' = 4.5$$

The equations of motion for turbulence have been developed from the Navier-Stokes equations, but the severe nonlinearity of these equations has prevented their solution. Even if they could be solved, it is questionable as to whether they could be practically applied. From observations relating to these equations, some characteristics have been determined:

- Turbulence transports energy from large eddies, where it is generated mechanically and thermally to smaller eddies until it is finally dissipated viscously.
- Turbulence can only occur nonlinearly in three dimensions.
- Turbulence is diffusive and far more efficient for the transport of mass, momentum, and heat properties than molecular motion.
- Turbulence is a continuum having a smallest dynamically significant scale much larger than molecular or intermolecular dimensions.
- Turbulence is approximately an equilibrium phenomenon for homogeneous terrain having very low rates of change of kinetic energy.
- The diffusive, continuous, and equilibrium characteristics tend to produce homogeneity for turbulence in a horizontal plane.

Using these properties of turbulence, a statistical description of turbulence is developed (Sec. 2.4.1). The basic statistical function is the average product of two turbulence components measured at two points of time and space, the correlation function:

$$R_{ij}(t_1, t_2, \vec{r}_1, \vec{r}_2) = \overline{u_i(t_1, \vec{r}_1)\, u_j(t_2, \vec{r}_2)}$$

When $\vec{r}_1 = \vec{r}_2$ (measured at the same point in space) and $t_1 = t_2$ (measured at the same time), the correlation function becomes the covariance. When, in addition, $i = j$, the correlation function is the variance.

By invoking homogeneity (turbulence properties independent of absolute position in space) and stationarity (turbulence properties independent of absolute time), the parameters reduce to just the displacements in position and time between the measured components:

$$R_{ij}(t_1, t_2, r_1, r_2) = R(\tau, \vec{\xi})$$

$$\tau = t_2 - t_1$$

$$\xi = \vec{r}_1 - \vec{r}_2$$

By additionally applying Taylor's hypothesis (frozen field concept), which assumes airplanes fly at speeds large compared to turbulent velocities and their rates of change, the time displacement can be related to a component of the position displacement, leaving statistical turbulence properties defined only in terms of space.

The correlation function can be transformed into the three-dimensional spectrum function by applying the Fourier integral:

$$\theta_{ij}(\vec{\Omega}) = \frac{1}{(2\pi)^3}\int_{-\infty}^{\infty} R_{ij}(\vec{\xi})e^{-i\vec{\Omega}\vec{\xi}}\, d\vec{\xi}$$

The parameter $\vec{\Omega}$ is the spacial frequency vector having units of rad/ft and is related to distance as temporal frequency in rad/sec is to time. The transformation can be reversed by the inversion formula:

$$R_{ij}(\vec{\xi}) = \int_{-\infty}^{\infty} \theta_{ij}(\vec{\Omega})e^{i\vec{\Omega}\vec{\xi}}\, d\vec{\Omega}$$

When $\vec{\xi} = 0$, the correlation function becomes the covariance and the spectrum function can be seen to be the distribution of the covariance with spacial frequency:

$$\sigma_{ij}^2 = \int_{-\infty}^{\infty} \theta_{ij}(\vec{\Omega})d\vec{\Omega}$$

Simulation of turbulence can be performed only by a temporal process, but only one component of spacial frequency (that in the direction of flight) can be related to time or temporal frequency through Taylor's hypothesis, $\omega = \Omega_1 V_A$. To obtain a spectrum function in terms of the component associated with the coordinate in the direction of flight ($\Phi(\Omega_1)$) integration of the spectrum function over the other two components is performed. Then

$$\sigma_{ij}^2 = \int_{-\infty}^{\infty} \Phi(\Omega_1)d\Omega_1$$

Important characteristics of the one-dimensional spectrum function, $\Phi_{ij}(\Omega_1)$, have been derived by Batchelor for the special case of isotropic turbulence (Sec. 2.4.2),for which the statistical properties of turbulence are invariant with coordinate system rotation or translation. Batchelor showed that there were but two one-dimensional spectrum functions: one for two parallel longitudinal turbulence components (components aligned to the vector separating them), $\Phi_{pp}(\Omega_1)$, and one for parallel transverse components (components normal to the vector separating them), $\Phi_{NN}(\Omega_1)$. All spectra for orthogonal components are zero. The variances for all components are equal. The two spectra are related by

$$\Phi_{NN}(\Omega_1) = \frac{1}{2}\left[\Phi_{pp}(\Omega_1) - \Omega_1 \frac{d\Phi_{pp}(\Omega_1)}{d\Omega_1}\right]$$

Determination of one of the isotropic spectrum functions provides the other.

Corresponding to the two spectrum functions are two nondimensional (divided by variance) scalar correlation functions: one, $f(\xi)$, for two parallel longitudinal components, and the other, $g(\xi)$, for two parallel transverse components, which are also interrelated:

$$f(\xi) = \frac{\overline{u_p^2(\xi)}}{\sigma_2}$$

$$g(\xi) = \frac{\overline{u_N^2(\xi)}}{\sigma_2}$$

$$g(\xi) = f(\xi) + \frac{\xi}{2}\frac{df(\xi)}{d\xi}$$

The fundamental correlation functions are analogous to serial correlation functions.

A measure of the average eddy size, the integral scale (Sec. 2.4.2.3) may be determined from the fundamental correlation functions:

$$L_P = \int_0^\infty f(\xi)d\xi$$

$$L_N = \int_0^\infty g(\xi)d\xi$$

For a separation distance, ξ, equal to the integral scale, the area under the corresponding correlation function is divided into equal parts. Through the relationship between the fundamental correlation functions, it can be shown

$$L_P = 2\,L_N$$

The integral scales provide means for normalizing distance. It is then postulated that $f(\xi/L_P)$ and $g(\xi/L_N)$ are universal functions. The one-dimensional spectrum functions must correspondingly have the form

$$\Phi_{ii}(\Omega_1) = \sigma_{ii}^2 G(L_i, L_i\Omega_1)$$

That is, spacial frequency appears only in combination with the integral scales.

Theory and empirical investigation have led to additional requirements for the isotropic one-dimensional spectra (Sec. 2.4.2.4):

- The high frequency asymptotes (excluding viscous dissipation) of the spectra are of the form $\Phi_{ii}(\Omega_1) \sim \Omega^{-5/3}$. This leads to a ratio of the transverse-to-longitudinal spectrum equal to 4/3 at high frequencies.

- The low-frequency asymptotes are frequency invariant. This leads to a ratio of the transverse-to-longitudinal spectrum equal to 1/2.

- Isotropic spectra must be symmetric about $\Omega_l = 0$.

A number of isotropic spectra forms have been proposed. The best-known forms for aeronautical applications are the Dryden and Von Karman forms, presented with related functions in Figure 1-20.

The Dryden form is simpler and is based on an exponential shape of the fundamental correlation functions. The Dryden function fails to meet the high-frequency requirement.

The Von Karman forms result from a curve fitting expression for the energy spectrum and satisfy all isotropic requirements. In numerous investigations the Von Karman forms have been shown to be superior to the Dryden forms. The Von Karman one-dimensional spectra are those accepted for the model.

Although high-altitude turbulence is well represented by isotropy, low-altitude turbulence (Sec. 2.4.3) is clearly nonisotropic. Specifically:

- The statistical functions describing the field of turbulence are not invariant with coordinate rotation; variances of turbulence components are not equal and the longitudinal and transverse integral scales vary with coordinate rotations.

- Low-altitude turbulence exhibits a lack of homogeneity with altitude; the variances and integral scales of turbulence vary with altitude.

- A non-zero correlation between turbulence in the direction of the mean wind and vertical turbulence has been found. Isotropic turbulence requires zero correlation between orthogonal components.

There are, however, limited conditions of isotropy found to hold for low-altitude turbulence:

- At sufficiently high spacial frequencies (short separation distances), low-altitude turbulence is isotropic. This is referred to as "local isotropy" and requires the high-frequency spectrum asymptotes to be invariant with coordinate rotations.

- The existence of a single non-zero correlation function between the downwind and vertical components of turbulence is compatible with horizontal isotropy (invariance of the horizontal statistical functions with rotations of the axis system in the horizontal plane). Horizontal isotropy must be viewed as an approximate characteristic for low-altitude turbulence, for the variance of horizontal turbulence perpendicular to the mean wind is frequently reported as being somewhat greater than the variance of the component in the direction of the mean wind.

The spectra that have been developed specifically for low altitude tend to be for small regions of altitude near the surface and do not tend to full isotropy at higher altitudes. A

Von Karman	Dryden
Longitudinal correlation function:	
$f(\xi) = \frac{2^{2/3}}{\Gamma(1/3)}\left(\frac{\xi}{aL}\right)^{1/3} K_{1/3}\left(\frac{\xi}{aL}\right)$	$f(\xi) = e^{-\xi/L}$
Transverse correlation functions:	
$g(\xi) = \frac{2^{2/3}}{\Gamma(1/3)}\left(\frac{\xi}{aL}\right)^{1/3}\left[K_{1/3}\left(\frac{\xi}{aL}\right) - \frac{\xi}{2aL} K_{2/3}\left(\frac{\xi}{aL}\right)\right]$	$g(\xi) = e^{-\xi/L}\left[1 - \frac{\xi}{2L}\right]$
Longitudinal one-dimensional power spectrum:	
$\Phi_{PP} = \frac{\sigma^2 L}{\pi} \frac{1}{\left[1 + (aL\Omega_1)^2\right]^{5/6}}$	$\Phi_{PP} = \frac{\sigma^2 L}{\pi} \frac{1}{\left[1 + (L\Omega_1)^2\right]}$
Transverse one-dimensional power spectrum:	
$\Phi_{NN} = \frac{\sigma^2 L}{2\pi} \frac{1 + 8/3\,(aL\Omega_1)^2}{\left[1 + (aL\Omega_1)^2\right]^{11/6}}$	$\Phi_{NN} = \frac{\sigma^2 L}{2\pi} \frac{1 + 3(L\Omega_1)^2}{\left[1 + (L\Omega)^2\right]^2}$
Energy spectrum:	
$E(\Omega) = \frac{55}{9\pi}\sigma^2 L \frac{(aL\Omega)^4}{\left[1 + (aL\Omega)^2\right]^{17/6}}$	$E(\Omega) = \frac{8\sigma^2 L}{\pi} \frac{(L\Omega)^4}{\left[1 + (L\Omega)^2\right]^3}$

Definitions:

$a = 1.339$

$\Omega = |\vec{\Omega}| = |\Omega_1 \hat{i} + \Omega_2 \hat{j} + \Omega_3 \hat{k}|$

Φ_{PP} and Φ_{NN} such that $\sigma^2 = \int_{-\infty}^{\infty} \Phi_{PP}\, d\,\Omega_1 = \int_{-\infty}^{\infty} \Phi_{NN}\, d\Omega_1$

$$L = \int_0^{\infty} f(\xi)\, d\,\xi = 2\int_0^{\infty} g(\xi)\, d\,\xi$$

$K_{1/3}\left(\frac{\xi}{aL}\right)$ and $K_{2/3}\left(\frac{\xi}{aL}\right)$ are modified Bessel functions of the second kind.

FIGURE 1-20.– VON KARMAN AND DRYDEN CORRELATION AND SPECTRA FUNCTIONS

frequently employed technique that is employed in this report is to adopt isotropic spectra for low altitude by permitting the variances and integral scales to be different for each component. The Von Karman spectra are used. These low-altitude forms become:

$$\Phi_u(\Omega_l) = \frac{\sigma_u^2 L_u}{\pi} \frac{1}{\left[1 + (1.339\, L_u \Omega_l)^2\right]^{5/6}}$$

$$\Phi_v(\Omega_l) = \frac{\sigma_v^2 L_v}{2\pi} \frac{1 + 8/3\,(1.339\, L_v \Omega_l)^2}{\left[1 + (1.339\, L_v \Omega_l)^2\right]^{11/6}}$$

$$\Phi_w(\Omega_l) = \frac{\sigma_w^2 L_w}{2\pi} \frac{1 + 8/3(1.339\, L_w \Omega_l)^2}{\left[1 + (1.339\, L_w \Omega_l)^2\right]^{11/16}}$$

These spectra were all originally written in terms of the longitudinal integral scale, which is twice the transverse integral scale for isotropy, so L_v and L_w must be redefined as twice the area under the corresponding correlation functions.

Although a cross spectrum, Φ_{uw}, has been found to exist and was modeled in Section 2.4.6.5, it has been concluded that the cross spectrum has a significant magnitude only at frequencies too low to be important.

The spectra in terms of temporal frequency are obtained by substituting $\Omega_l = \omega/V_A$ (Taylor's hypothesis) and by requiring the variance to be the same in either domain:

$$\sigma_i^2 = \int_{-\infty}^{\infty} \Phi_i(\omega) d\omega = \int_{-\infty}^{\infty} \Phi_i(\Omega_l) d\Omega_l$$

Then

$$\Phi_i(\omega) = \frac{1}{V_A} \Phi_i\left(\Omega_l = \frac{\omega}{V_A}\right)$$

When a random variable is modified by a transfer function, the output spectrum is given by

$$\Phi_O(\omega) = M^2(\omega)\Phi_N(\omega) \qquad \text{(Sec. 4.2.1.3.1)}$$

where:

$\Phi_O(\omega)$ = output spectrum

$M(\omega)$ = amplitude frequency response of the transfer function

$\Phi_N(\omega)$ = power spectrum of the random function or noise

Turbulence is represented by finding a transfer function such that

$$M(\omega) = \sqrt{\frac{\Phi_O(\omega)}{\Phi_N(\omega)}}$$

where the output frequency response is equal to that desired. When white noise is used, $\Phi_N = 1$ by definition. Then to match a desired power spectrum, it is only necessary to find a transfer function with a frequency response equal to the square root of the spectrum.

It is not possible to exactly reproduce the Von Karman spectra with linear transfer functions (filters) due to exponents of frequency that are noneven integers, so an approximation is sought.

The significant criteria for evaluating an approximation to a power spectra is to require the contribution of each incremental frequency range to the variance to be correct for the frequency range in which the airplane's response is important. Directly plotting $\Phi(\omega)$ versus ω lacks resolution over the entire frequency range. Plots of $\omega\Phi(\omega)$ versus log (ω) provide the necessary resolution and the area under such a curve is also equal to the contribution to the variance:

$$\Delta\sigma^2 = \int_{\omega_1}^{\omega_2} \Phi(\omega)d\omega = \int_{\text{Log } \omega_1}^{\text{Log } \omega_2} \omega\Phi(\omega)d(\log \omega)$$

The validity of transfer functions representing spectra may be assessed by comparing plots of this type for the transfer function frequency response squared and the power spectrum.

Filters exactly duplicating the Dryden spectra are often assumed to match the Von Karman spectra well for rigid airplane responses even though it is conceded the Dryden spectra are not substantiated by theory and empirical evidence. This is seen not to be true in Figure 1-21, for the Dryden spectra provide greater contributions to the variance than the Von Karman spectra by as much as 25% at frequencies where contributions to the variance are greatest. Approximate filters that do a much better job of matching the Von Karman spectra are presented in Section 4.5.3.3 and in Figure 1-22 (where the corresponding mechanization is also shown). Comparisons of the filters in Figure 1-22 with the Von Karman spectra are shown in Figures 1-23 and 1-24.

The white noise may be generated by either hardware or software (digitally). There are several methods available, as discussed in Section 4.4.2, each with different shortcomings.

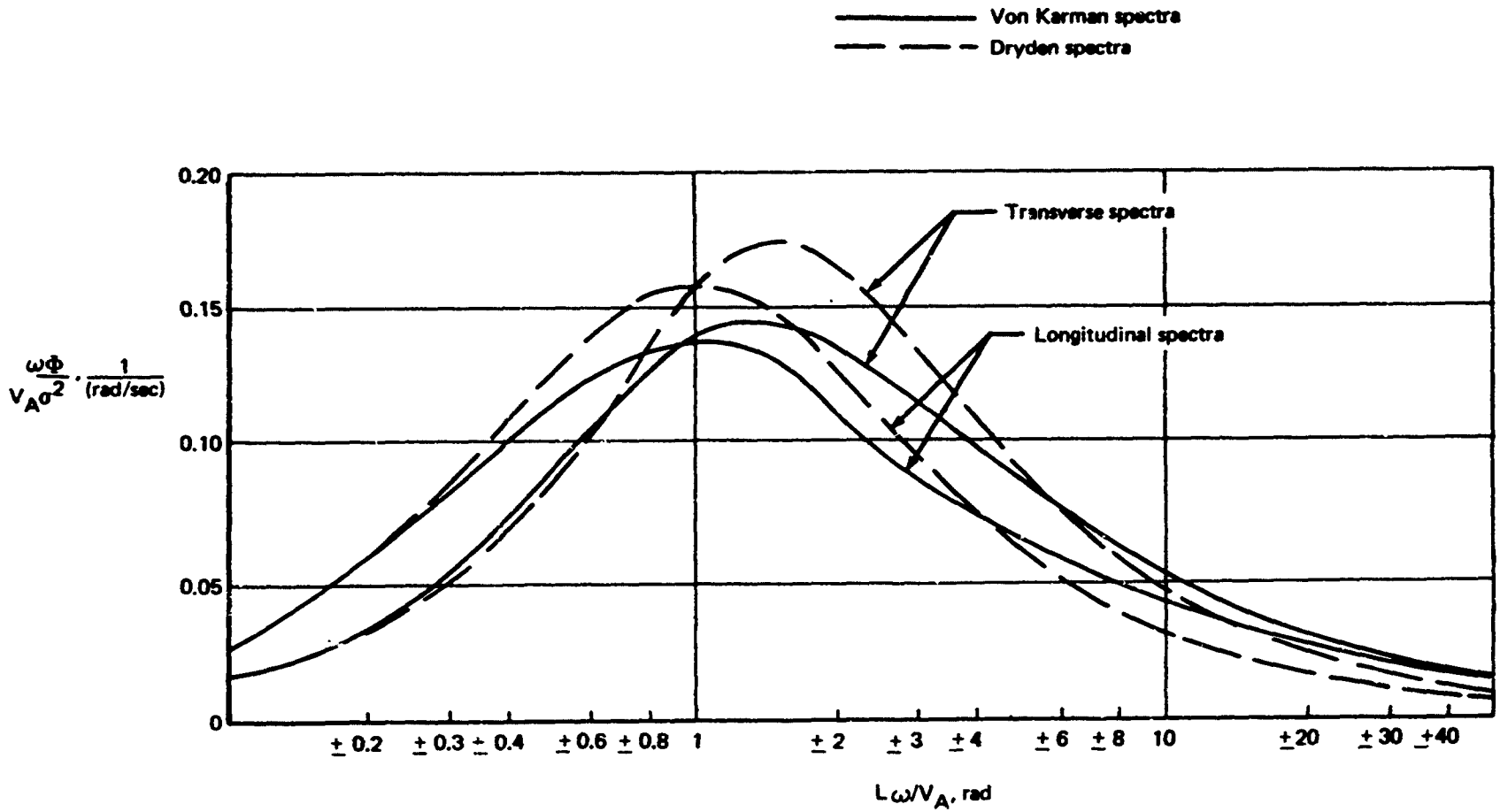

FIGURE 1-21.—COMPARISON: DRYDEN AND VON KARMAN VARIANCE DENSITY

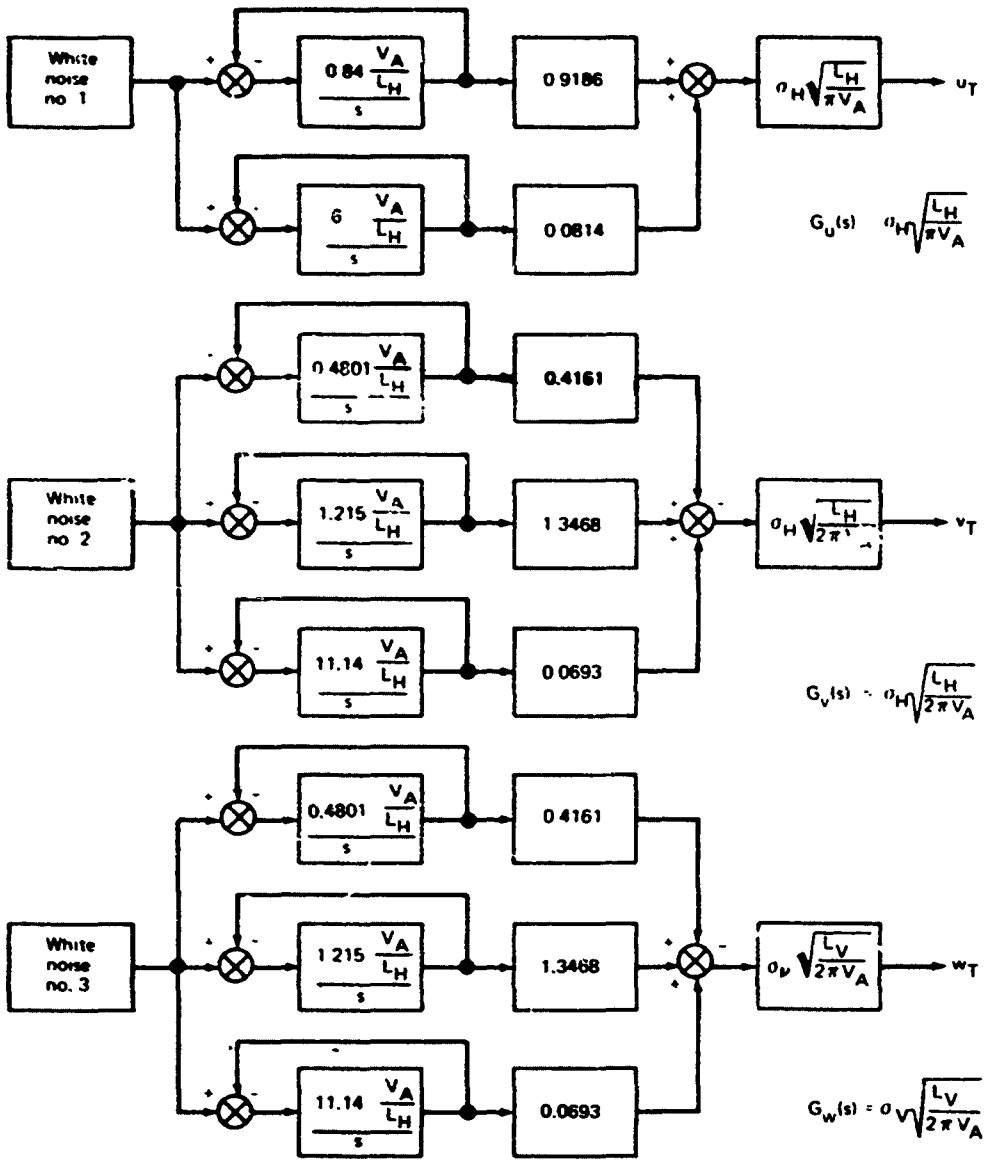

$$G_u(s) = \sigma_H\sqrt{\frac{L_H}{\pi V_A}}\,\frac{1 + 0.25\frac{L_H}{V_A}s}{(1 + 1.19\frac{L_H}{V_A}s)(1 + 0.167\frac{L_H}{V_A}s)}$$

$$G_v(s) = \sigma_H\sqrt{\frac{L_H}{2\pi V_A}}\,\frac{(1 + 2.618\frac{L_H}{V_A}s)(1 + 0.1298\frac{L_H}{V_A}s)}{(1 + 2.083\frac{L_H}{V_A}s)(1 + 0.823\frac{L_H}{V_A}s)(1 + 0.08977\frac{L_H}{V_A}s)}$$

$$G_w(s) = \sigma_v\sqrt{\frac{L_V}{2\pi V_A}}\,\frac{(1 + 2.618\frac{L_V}{V_A}s)(1 + 0.1298\frac{L_V}{V_A}s)}{(1 + 2.083\frac{L_V}{V_A}s)(1 + 0.823\frac{L_V}{V_A}s)(1 + 0.08977\frac{L_V}{V_A}s)}$$

FIGURE 1-22.— SCHEMATIC FOR TURBULENCE FILTERS

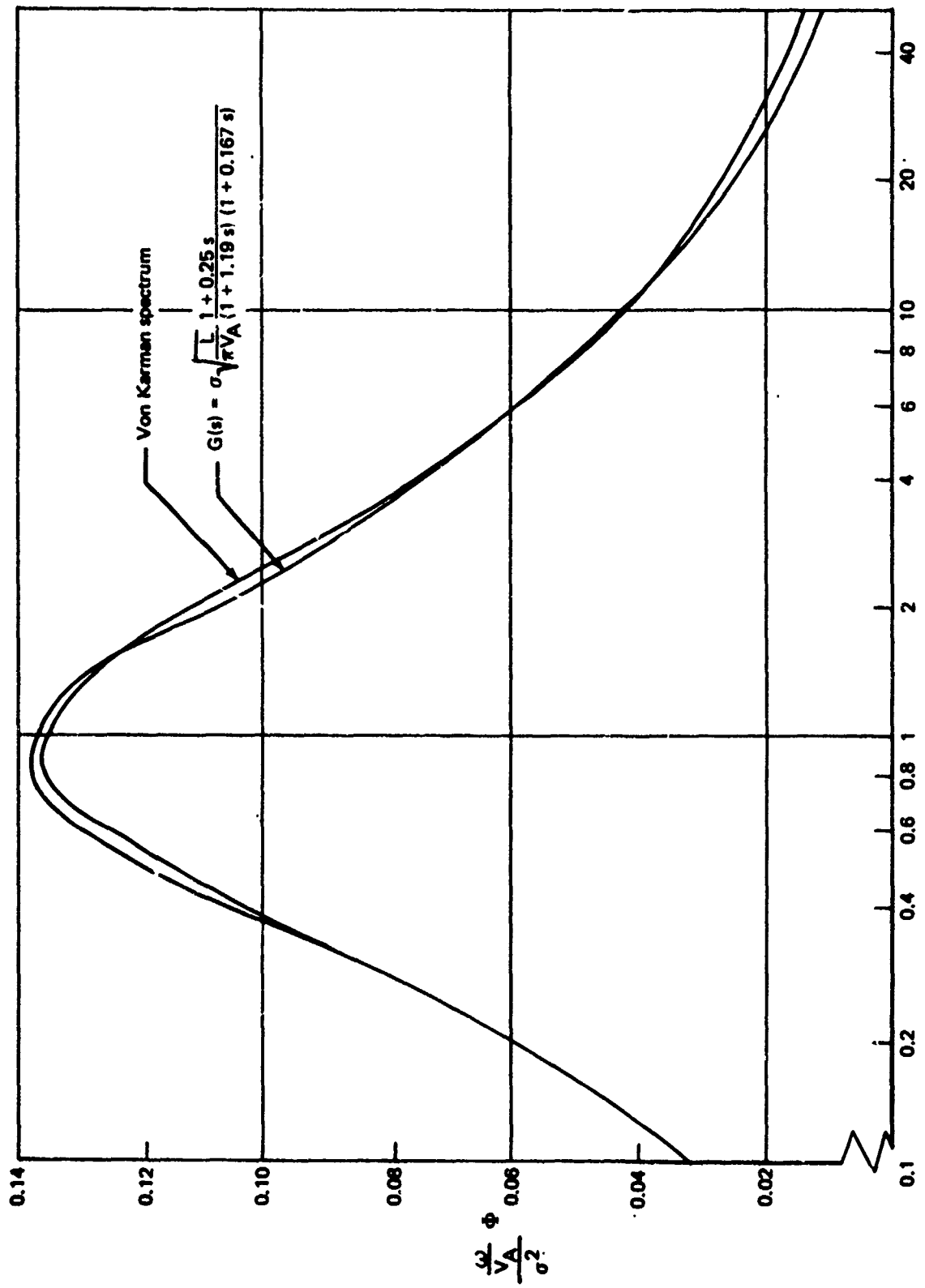

FIGURE 1-23.– APPROXIMATE LONGITUDINAL TURBULENCE FILTER ACCURACY

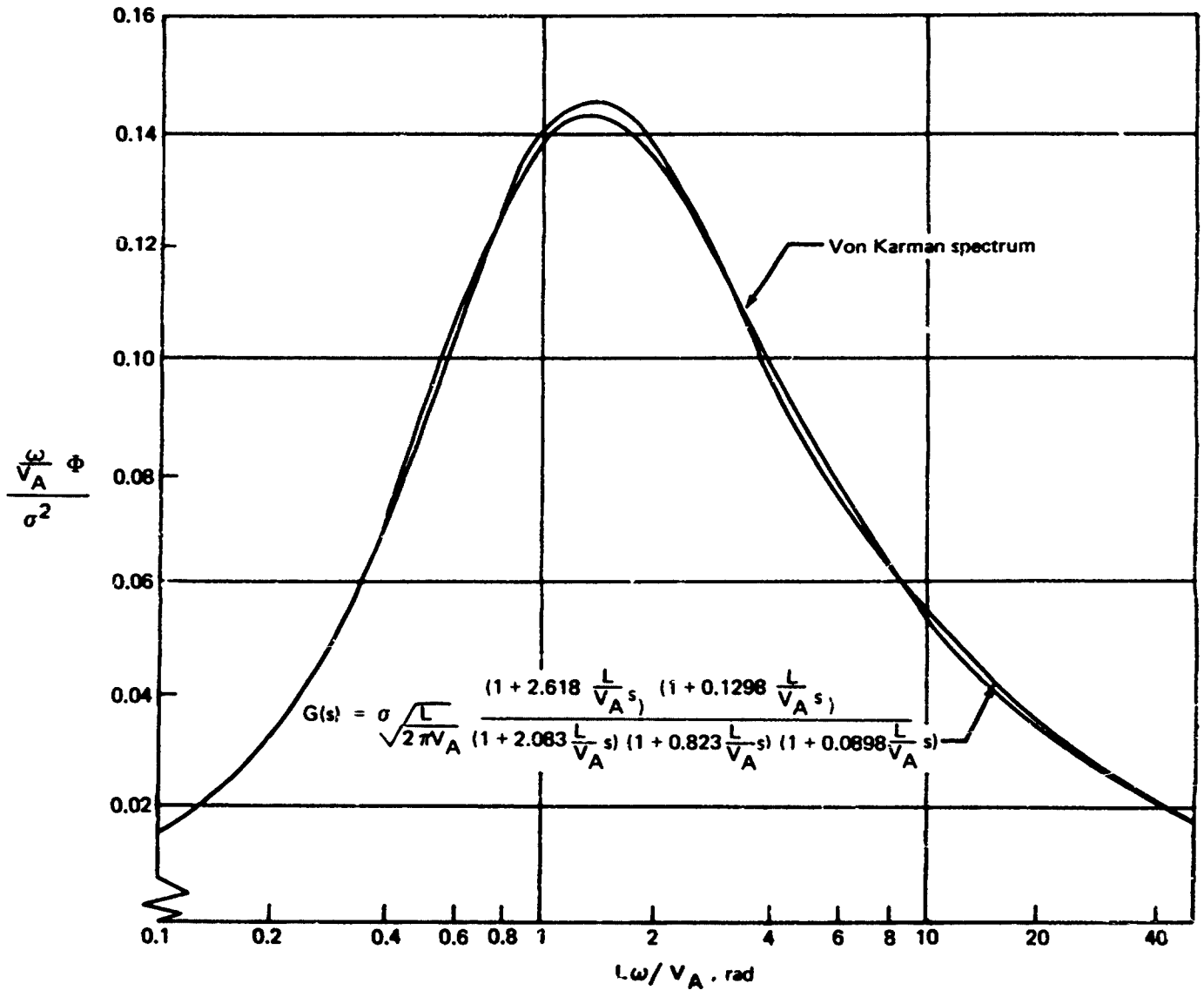

FIGURE 1-24.— APPROXIMATE TRANSVERSE TURBULENCE FILTER ACCURACY

When the noise is generated digitally, it is only approximately random and the noise spectrum is only approximately flat and equal to one. The digital generation of white noise consists of three main steps:

1) Random numbers having a uniform distribution between 0 and 1 are generated.

2) From the uniform distribution, the distribution assumed to hold for turbulence is generated.

3) The noise thus far produced will have a unit variance and a spectrum amplitude of $\Delta t/2\pi$ (Δt = frame time or sampling interval) no matter what distribution is used in 2). To provide white noise for which the spectrum amplitude is one, the output from 2) is multiplied by $\sqrt{2\pi/\Delta t}$.

Turbulence velocities within a single patch of turbulence are assumed to form a Gaussian distribution (Sec. 2.4.1.2). Although the distribution of turbulence velocities for the sum of all turbulence patches have been shown to be non-Gaussian, this is not inconsistent with a Gaussian distribution for a single patch of turbulence.

The simulator model for turbulence in Figure 1-22 lacks definition of the variances and integral scales. The measurements and theory for these statistical parameters of turbulence, measured in an axis system aligned to the mean wind, are presented in Sections 2.4.4 and 2.4.5.

Dimensional analysis leads to a description of the vertical turbulence standard deviation for unstable condition given in Section 2.4.4.2.1:

$$\frac{\sigma_w}{u_*} = C\left[\frac{kh}{u_*}\frac{\partial \bar{V}_W}{\partial h} - \left(\frac{D}{C}\right)^3 \frac{h}{\ell'}\right]^{1/3}$$

D and C are constants

For neutral conditions where the nondimensional shear at the surface $(kh/u_*)/\partial \bar{V}_W/\partial h)$ is 1,

$$\frac{\sigma_w}{u_*} = 1.3 = C$$

is well accepted. For extremely unstable conditions, the nondimensional shear is negligible and the equation reduces to

$$\frac{\sigma_w}{u_*} = D\left(-\frac{h}{\ell'}\right)^{1/3}$$

The constant D is well represented by 1.7, hence

$$\frac{\sigma_w}{u_*} = 1.3\left[\left(\frac{kh}{u_*}\frac{\partial \bar{V}_W}{\partial h}\right) - 2.236\left(\frac{h}{\ell'}\right)\right]^{1/3}$$

The nondimensional shear has been described as a function of h/ℓ' only, so σ_w/u_* is also completely described by h/ℓ'. For near neutral conditions and slightly stable conditions, the shape of σ_w/u_* versus h/ℓ' has been made to match that of measured data. The standard deviation of vertical turbulence is reduced abruptly beginning at $h/\ell' = 1$, above which the nondimensional shear is constant, to $\sigma_w/u_* = 0$ at $h/\ell' = 1.22$, which corresponds to the critical Richardson's number ($Ri_{CRIT} = 0.222$). The combined description for σ_w/u_* is presented in Figure 1-25. The procedure for computing the rms level of turbulence vertical to the earth is:

$$\sigma_w = u_*\left[\frac{\sigma_w}{u_*}\left(\frac{h}{\ell'}\right)\right]$$

$$= 0.4\bar{V}_{20}\left(\frac{u_{*_0}/k}{\bar{V}_{20}}\right)\left(\frac{u_*}{u_{*_0}}\right)\left[\frac{\sigma_w}{u_*}\left(\frac{h}{\ell'}\right)\right]$$

where:

$\frac{u_{*_0}/k}{\bar{V}_{20}}$ determined for the mean wind model

$\frac{u_*}{u_{*_0}} = 1-\frac{h}{d}$, as determined from the mean wind model

$d = 2000\, u_{*_0}$, as determined for the mean wind model

The standard deviation for vertical turbulence is described as being proportional to the mean wind speed at 20 feet, as decreasing and finally disappearing with increasing atmospheric stability, and as tending toward zero as altitude approaches the boundary layer. The variation of σ_w with altitude for different surface wind and atmospheric stability conditions is shown in Figure 1-26.

Dimensional analysis relationships for the variances of horizontal components of turbulence have not had good empirical support. At the surface, the magnitudes of the horizontal components are significantly greater than magnitude of the vertical component with the component in the direction of the mean wind frequently reported as greater than the horizontal component normal to the mean wind. The data in Section 2.4.4.2.5 do not indicate any clear relationship between the variances for the horizontal turbulence components but do show them to be approximately equal, so horizontal isotropy ($\sigma_u = \sigma_v$, $L_u = L_v$) is assumed. This enables describing turbulence characteristics according to whether

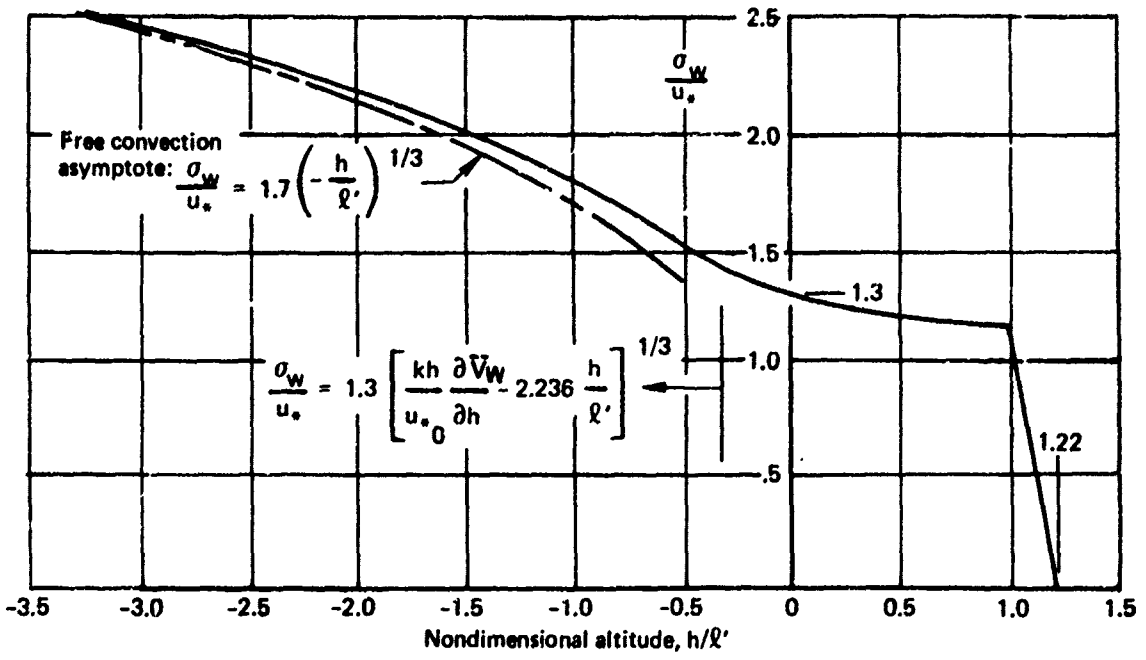

FIGURE 1-25.– σ_w/u_* VARIATION WITH STABILITY

turbulence components are vertical or horizontal. A corresponding change of nomenclature is adopted: σ_V replaces σ_w, L_V replaces L_w, σ_H replaces σ_u and σ_v, and L_H replaces L_u and L_v (subscripts H and V refer to horizontal and vertical components).

The change in nomenclature aids in differentiating between turbulence components aligned to the mean wind and turbulence components aligned to other axis systems.

It is assumed that the horizontal components of turbulence have variances that change identically with stability. Qualitatively, this is not correct, but any other quantitative descriptions based on the information in hand would be just as arbitrary but more complex. As a result, the standard deviation for horizontal turbulence may be described by

$$\sigma_H = \left(\frac{\sigma_H}{\sigma_V}\right)\sigma_V$$

At the surface $\sigma_H/\sigma_V = 2$ is a good compromise of the data. Above a sufficiently high altitude where complete isotropy begins, h_I, $\sigma_H/\sigma_V = 1$. There is little information to describe the variation of σ_H/σ_V with altitude, so in Sections 2.4.6.3 and 2.4.6.4 an interpolation equation,

$$\frac{\sigma_H}{\sigma_V} = \begin{cases} \dfrac{1}{\left[0.177 + 0.823\dfrac{h}{h_I}\right]^{0.4}}, & h < h_I \\ 1, & h \geq h_I \end{cases} \qquad \text{(Fig. 1-27)}$$

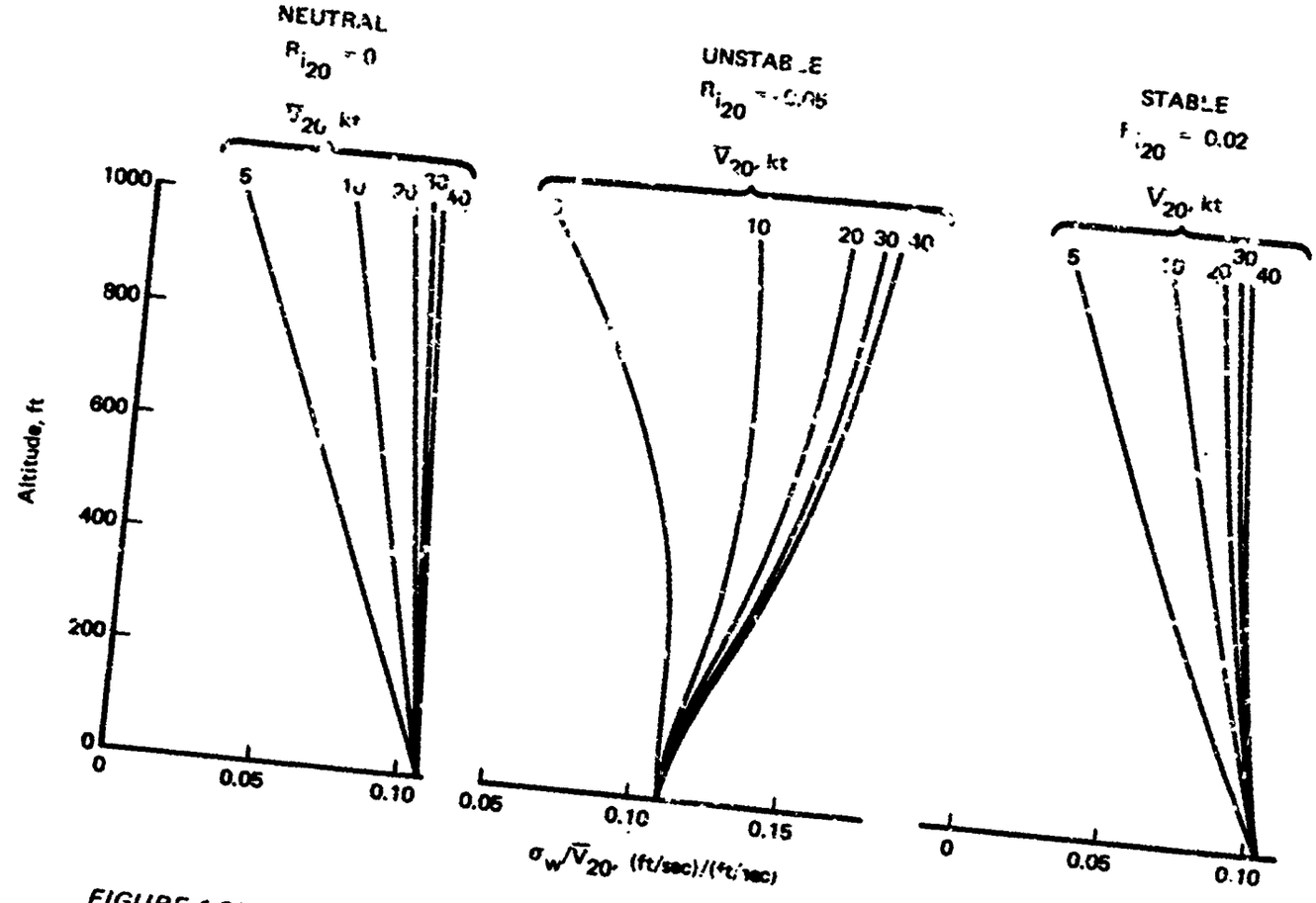

FIGURE 1-26.– PROFILE OF VERTICAL TURBULENCE RMS, SELECTED DESCRIPTION

$$\frac{\sigma_u}{\sigma_w} = \frac{\sigma_v}{\sigma_w} = \begin{cases} \dfrac{1}{\left[0.177 + 0.823\, h/h_l\right]^{.4}}, & h < h_l \\ 1.0, & h \geq h_l \end{cases}$$

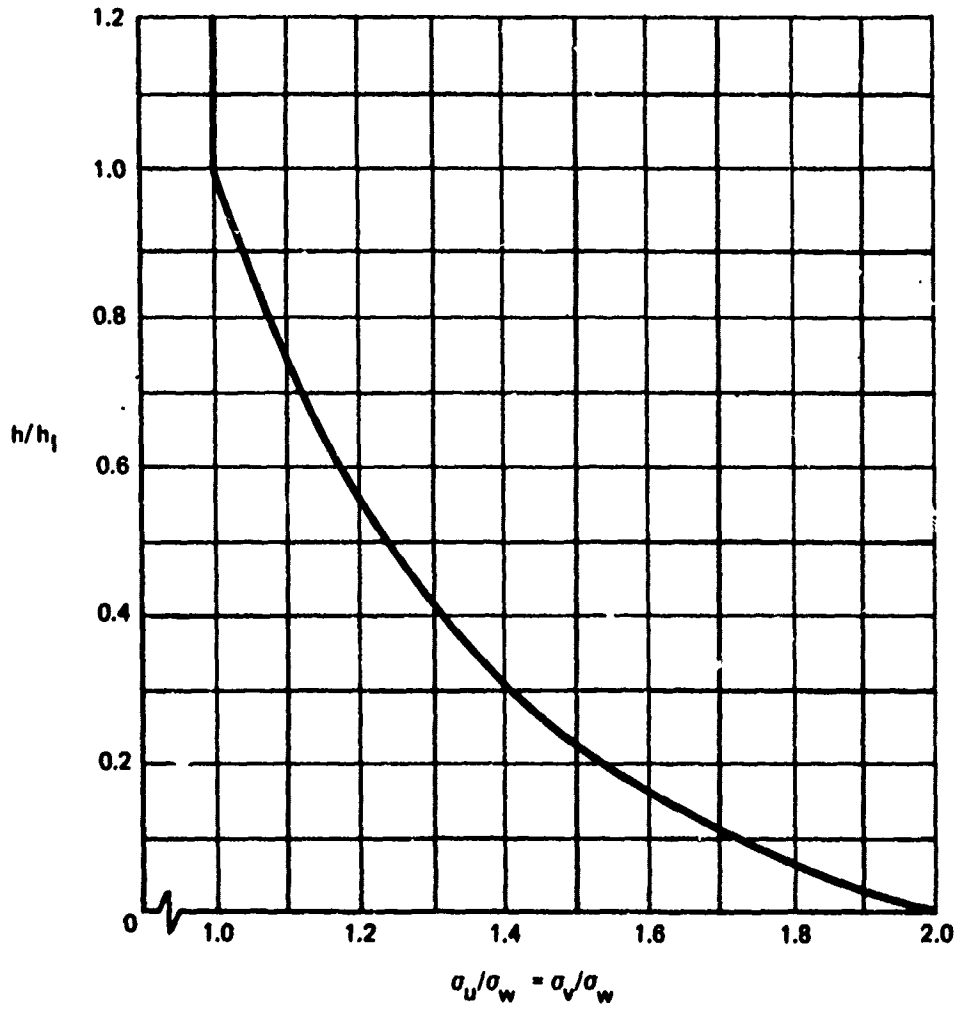

FIGURE 1-27.– SELECTED DESCRIPTION FOR VARIANCES OF HORIZONTAL TURBULENCE COMPONENTS

was developed that is qualitatively similar to other variations proposed.

Implied estimates for the altitude above which isotropy exists (h_I) range from 300 to 2500 feet. The latter number is an extreme. A value of h_I = 1000 feet is chosen, is adequately supportable, and provides integral scales comparable with other models.

The integral scale for vertical turbulence is predicted by dimensional analysis to have the form

$$L_V = [B(R_i)]\ h \qquad \text{(Sec. 2.4.5)}$$

That is, the vertical turbulence integral scale is linearly related to altitude with the proportionality constant dependent upon stability.

The atmospheric stability dependence of the proportionality constant is apparently weak, at least for a wide range of stability conditions, and is assumed to be constant. Estimates for B range from 0.125 to greater than 4, with most estimates centered about 0.5 and 1. Unit proportionality is assumed. The estimates about 0.5 may be for the literal definition of integral scale equal to the integral of the correlation function rather than the redefinition of twice that area. Hence, the estimates of 0.5 may be consistent with the unit proportionality assumed for the redefinition. In keeping with isotropy about 1000 feet, L_V = 1000 feet for $h \geq 1000$ feet.

The integral scale for horizontal turbulence is the parameter for which knowledge is poorest. It may be derived from the condition of local isotropy at low altitudes, which can be shown to require (Sec. 2.4.3.1):

$$L_H = \left(\frac{\sigma_H}{\sigma_V}\right)^3 L_V \qquad \text{(Fig. 1-28)}$$

This description provides a horizontal turbulence integral scale greater or equal to that vertical turbulence. At the surface, $L_H = 8\ L_V$. Above 1000 feet, where isotropy is assumed to exist, the integral scales are equal. These characteristics are in agreement with observations (Sec. 2.4.5.3).

There is an inconsistency in the turbulence model developed: the power spectra are for turbulence components aligned to the airplane's velocity with respect to the air mass and the standard deviations and integral scales are for turbulence components aligned with respect to the plane of the earth and the mean wind heading. Both sets of components can, in general, coincide only for an observer whose position with respect to the earth is fixed. This inconsistency of axis systems is examined in Section 4.3.

One exact approach for resolving the differences in axis systems consists of transforming the variances and integral scales from the mean wind axis system to the axis system attached to the relative wind where the spectra shapes are known. Turbulence components would then be generated in the relative wind axis and transformed to the body axis. Transformations for the integral scales and variances have been developed, but are quite complex. Complete tensor transformations have been developed and reveal that when the airplane's relative

$$L_w = \begin{cases} h, h < h_I \\ d, h = h_I \end{cases}$$

$$L_u = \begin{cases} L_w \left(\frac{\sigma_u}{\sigma_w}\right)^3 = \frac{h}{\left[0.177 + 0.823\, h/h_I\right]^{1.2}} & , h < h_I \\ d & , h \geq h_I \end{cases}$$

$$L_v = L_u$$

h_I = Altitude above which turbulence is isotropic

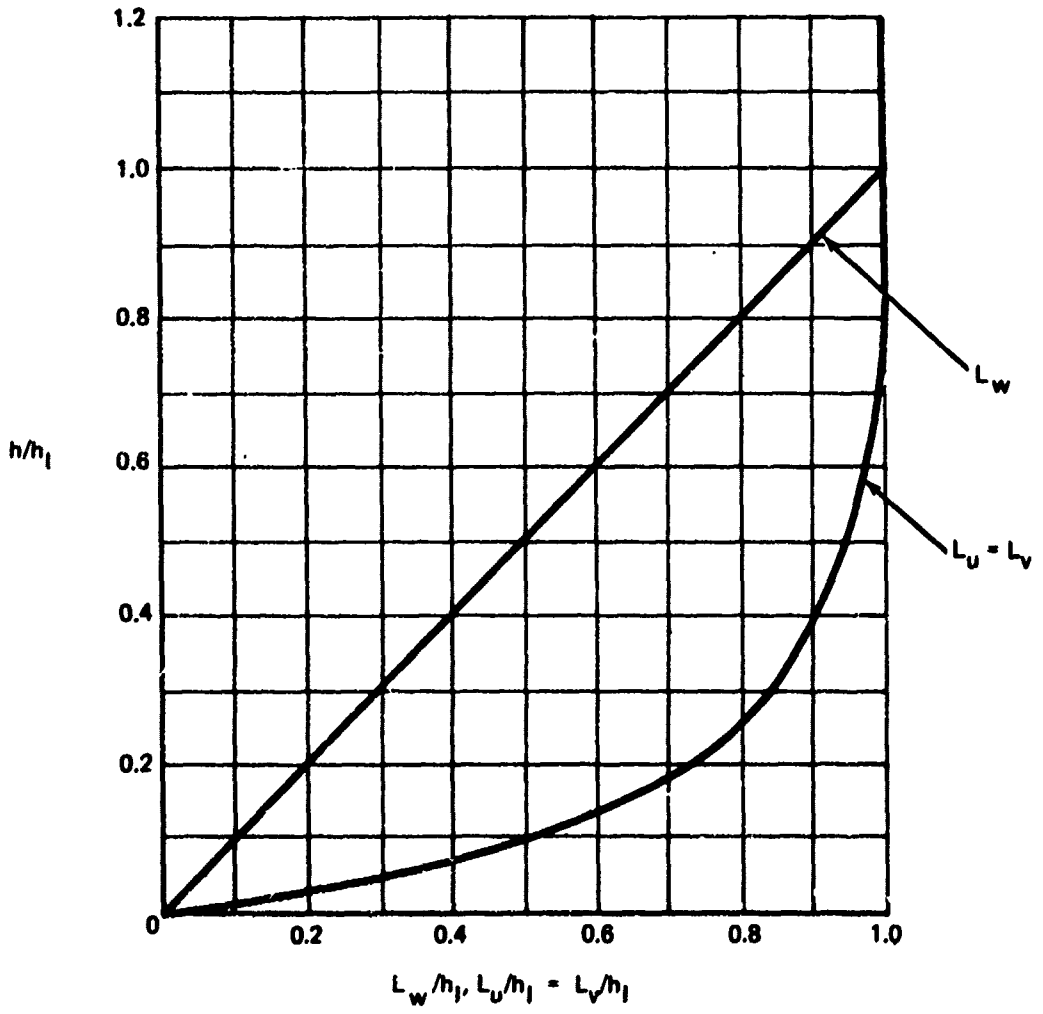

FIGURE 1-28.– SELECTED INTEGRAL SCALE DESCRIPTION

velocity is not aligned to the mean wind and when wings are nonlevel, nonnegligible cospectra exist in the body axis (components of body axis turbulence are correlated). Since the power spectra shapes are in general not known in the mean wind axis system and the cospectra forms are not known for a body axis system, the exact method cannot be performed.

Errors from approximate methods were examined. It was revealed that for low-altitude turbulence, it is much more important to have the correct alignment for the variances and integral scales than for the spectra shapes. The greatest error in the spectra magnitude at any frequency for turbulence normal to the airplane that can occur due to misalignment of the spectra shape is a factor of 2, while the greatest error possible due to misalignment of the statistical parameters is a factor of 64. The best compromise found was to generate turbulence in an axis system that is in the plane of the earth but aligned to the heading of the airplane's relative velocity vector with the filters in Figure 1-22 and the specified rms levels and integral scales. The components of turbulence are then transformed to the body axis system. The transformation required is presented in Figure 1-18.

When the aircraft can be adequately represented as though the aerodynamic forces and moments were concentrated at the center of gravity, turbulence affects forces and moments through the computation of body axis velocities relative to the air mass:

$u_A = u - u_W,\ u_W = \bar{u}_W + u_T$

$v_A = v - v_W,\ v_W = \bar{v}_W + v_T$

$w_A = w - w_W,\ w_W = \bar{w}_W + w_T$

$V_A = u_A^2 + v_A^2 + w_A^2$

u, v, w = inertial velocity components along the x, y, and z body axis coordinates

$u_A\ v_A\ w_A$ = components of airplane velocity relative to the air mass

$u_W\ v_W\ w_W$ = components of wind relative to the earth

$\bar{u}_W,\ \bar{v}_W\ \bar{w}_W$ = components of mean wind relative to the earth

$u_T\ v_T\ w_T$ = components of turbulence velocities relative to the earth

The relative velocity components are used to determine the parameters, which in turn determine the aerodynamics forces and moments:

$$\alpha = \tan^{-1}\frac{w_A}{u_A} = \text{angle of attack}$$

$$\beta = \sin^{-1}\frac{v_A}{V_A} = \text{sideslip angle}$$

$$\bar{q} = \tfrac{1}{2}\rho V_A^2 = \text{dynamic pressure}$$

$$\dot{\alpha} = \frac{u_A\dot{w} - w_A\dot{u}}{u_A^2 + w_A^2}$$

$$\dot{\beta} = \frac{(u_A^2 + w_A^2)\dot{v} - v_A(u_A\dot{u} + w_A\dot{w})}{V_A^2\sqrt{u_A^2 + w_A^2}}$$

Note that for the point representation, $\dot{u}_W = \dot{v}_W = \dot{w}_W = 0$.

The attenuation of the high-frequency response of forces and moments due to the fact that lift cannot respond instantaneously to changes in angle of attack (unsteady aerodynamics) can be handled approximately through use of the Kussner and Wagner lift growth functions in the manner described in Section 4.2.1.3.4.

In general, it is not adequate to assume the aerodynamics may be represented by a point for the purpose of simulating the effects of turbulence; there is a distribution of turbulence about the airplane that causes a change in the distribution of lift. The point representation has been estimated in Section 4.2.1.3.3 to be accurate only up to:

$$\lambda_1 > 120\ell_T$$

$$\omega < 60\bar{c} \text{ for tailless aircraft or for the wing only}$$

or

$$< 0.1\, V_A/\ell_T$$

$$< 0.05\frac{V_A}{\bar{c}} \text{ for tailless aircraft or for the wing only}$$

$$\lambda_2 > \pi b$$

where:

λ_1, λ_2 = wavelengths in the longitudinal and lateral directions, respectively

ℓ_T = tail length

b = wing span

$\bar{c}$ = mean chord

Only one method of representing all the distributed lift effects suitable for simulation has been found. This method represents the distribution of turbulence linearly, just as was done

for the distributed lift effects of the mean wind. The derivatives of turbulence with respect to the coordinates are related to effective angular components of turbulence:

Effective Turbulence Angular Velocities

Wing	Tail
$p_T = -\frac{\partial w_T}{\partial y}$	$p_T = \frac{\partial v_T}{\partial z}$
$q_T = \frac{\partial w_T}{\partial x}$	$q_T = \frac{\partial w_T}{\partial x}$
$r_T = \frac{\partial u_T}{\partial y}$	$r_T = -\frac{\partial v_T}{\partial x}$

p_T, q_T, r_T = effective body axis roll, pitch, and yaw rates due to turbulence with respect to the earth

The effective angular velocities are generated through matching the spectra for the turbulence derivatives and their cospectra with the linear velocities of turbulence in a manner similar to that used for generating linear components of turbulence.

The effective angular velocities affect body axis forces and moments in the same way as did the linear components of turbulence. For example, the yaw rates of the airplane with respect to the air mass are computed by

$$r_A = r - r_W, \quad r_W = \bar{r}_W + r_T$$

Separate yaw rates for wing and tail are computed as the effective yaw rates of the wind are different. A total force or moment due to yaw rate is the sum of the contribution of the wing force or moment derivative with respect to yaw rate times the wing yaw rate with respect to the air mass and the contribution of the tail to the force or moment derivative with respect to yaw rate times the tail yaw rate with respect to the air mass.

At lower and lower turbulence frequencies, the linear representation of the distribution becomes exact. The linear distribution becomes poor at high frequencies; relating effective angular velocities to turbulence derivatives produces infinite variances of angular velocities due to the error of the representation at high frequencies. The spectra for the angular velocities must be attenuated at high frequencies or truncated.

A comparison of representing the distribution of turbulence in this manner with the point representation is made in Section 4.2.1.3.3. It is concluded that a factor of 10 improvement in the maximum frequency to which the representation is valid occurs for representing the longitudinal distributions. However, no improvement over the point representation occurs for representing the lateral and vertical distributions. This does not mean that the lateral and

vertical distributions of turbulence are insignificant just that they can't be accurately modeled. However, from a simple analysis in Section 4.2.1.3.3, it is concluded that the rolling moment due to turbulence roll rate will generally be insignificant compared to the roll rate caused by the lateral component of turbulence.

The power spectra and cross spectra for turbulence pitch and yaw rates that provide longitudinal distributions of turbulence are represented by simply filtering the vertical and lateral components of turbulence by

$$q_T = -\frac{1}{V_A}\frac{s}{1+\frac{4\ell_T}{\pi V_A}s} w_T$$

$$r_T = \frac{1}{V_A}\frac{s}{1+\frac{4\ell_T}{\pi V_A}s} v_T$$

The terms $1/V_A\ s\ w_T$ and $1/V_A\ s\ v_T$ represent the derivatives of turbulence with respect to the longitudinal coordinate:

$$\frac{\partial}{\partial x} = \frac{\partial}{\partial t}\frac{dt}{dx} = \frac{1}{V_A}s$$

s = Laplace transform operator

The additional filter

$$\frac{1}{1+\frac{4\ell_T}{\pi V_A}s}$$

attenuates the effective angular velocity at the maximum frequency to which the representation is valid assuming eight straight line segments are the minimum number that can adequately represent a sine wave. That is, the effective angular velocities are attenuated at a frequency corresponding to a wavelength that is eight times the distance over which the distribution of turbulence is provided. The power spectra that result are shown in Figure 1-29. There are also body axis accelerations due to distributed lift:

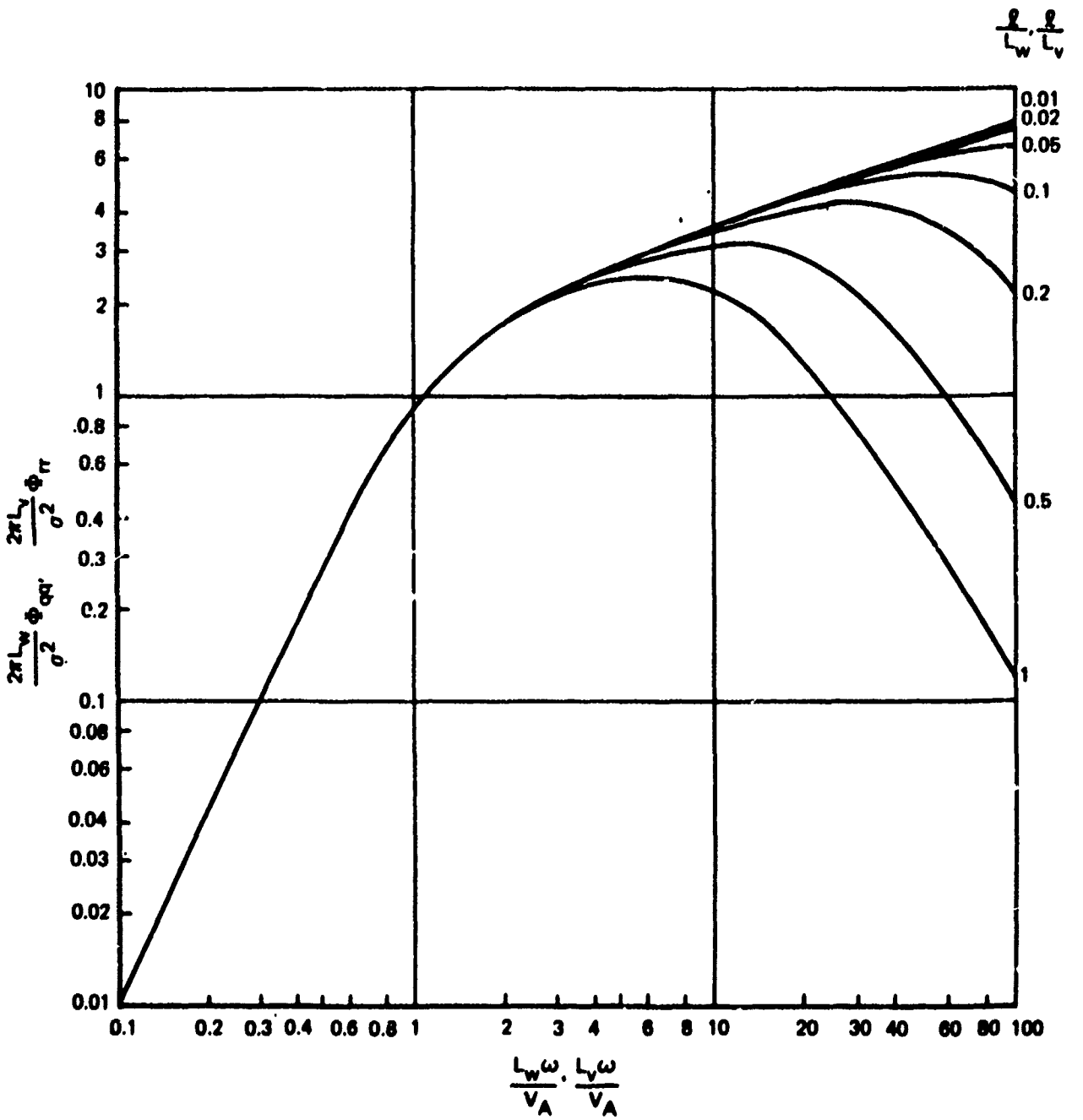

FIGURE 1.29.– TURBULENCE PITCH AND YAW RATE SPECTRA

$$\dot{u}_T = \frac{\partial u_T}{\partial x}\frac{dx}{dt} = \left[\frac{s}{1+\frac{4\ell_T}{\pi V_A}s}\right]u_T$$

$$\dot{v}_T = \frac{\partial v_T}{\partial x}\frac{dx}{dt} = \left[\frac{s}{1+\frac{4\ell_T}{\pi V_A}s}\right]v_T$$

$$\dot{w}_T = \frac{\partial w_T}{\partial x}\frac{dx}{dt} = \left[\frac{s}{1+\frac{4\ell_T}{\pi V_A}s}\right]w_T$$

To accommodate the linear accelerations due to turbulence, the equations for $\dot{\alpha}$ and $\dot{\beta}$ are revised to

$$\dot{\alpha} = \frac{u_A\dot{w}_A - w_A\dot{u}_A}{u_A^2 + w_A^2}$$

$$\dot{\beta} = \frac{(u_A^2 + v_A^2)\dot{v}_A - v_A(u_A\dot{u}_A + w_A\dot{w}_A)}{V_A^2\sqrt{u_A^2 + v_A^2}}$$

where

$$\dot{u}_A = \dot{u} - (\dot{\bar{u}}_W + \dot{u}_T)$$

$$\dot{v}_A = \dot{v} - (\dot{\bar{v}}_W + \dot{v}_T)$$

$$\dot{w}_A = \dot{w} - (\dot{\bar{w}}_W + \dot{w}_T)$$

For the representation of the longitudinal distribution of turbulence only (gust penetration), there is an alternate technique based on the frozen field hypothesis. The turbulence velocities may be considered to be frozen with respect to the air mass as rates of change of turbulence velocities are small compared to the speed and dimensions of an aircraft. The turbulence velocities that strike the airplane at its center of gravity will occur at the tail a time $\Delta t = \ell_T/V_A$ later. The turbulence at the tail may be represented on a digital simulator by storing turbulence velocities occurring at the cg for the appropriate time lag, then using them for turbulence velocities at the tail. If digital noise generation is used, two identical random number sequences displaced in time by $\Delta t = \ell_T/V_A$ may be used. Additionally, linear filter representations for a transport lag are provided in Section 4.2.1.3.3. Separate buildups of angle of attack, sideslip angle, and dynamic pressure are provided for the tail, and the forces and moments due to the tail are built up separately from those due to the wing-body. This method is described in more detail in Sections 4.2.1.3 3 and 4.5.5.

The highest frequency to which gust penetration is accurate using the transport lag method is

$$\omega < 0.1 \frac{V_A}{\bar{c}}$$

which may not be as good as the restriction for the linear distribution method of

$$\omega < 0.5 \frac{V_A}{\ell_T}$$

The two methods may be combined by separate wing and tail representations using the transport lag plus a linear distribution representation for the wing. The maximum frequency then increases to

$$\omega < \frac{V_A}{\ell_T}$$

The need to provide more and more accurate representations, or rather the sufficiency of any approximation, depends on whether the variance of airplane motion parameters are significantly altered. Some considerations involved for determining the sufficiency of an approximation are provided in Sections 4.2.1.3.1 and 4.2.1.3.2. Approximations that can be shown to be conservative may be acceptable for certification but provide economic penalties due to overdesign. Care must be taken to demonstrate the suitability of assumptions. As the airplane descends, the frequency at which the greatest turbulent energy occurs changes by a factor of 50, drastically altering the response of the airplane (Sec. 4.2.1.3.5). Generally, the lower the speed of an airplane, the more accurate the representation required and the greater the coupling between forces and moments along one coordinate with wind and turbulence components along another coordinate (Sec. 4.2.1.3.5).

Finally, care must be taken with the way data are analyzed. Far fewer simulations than conventionally performed may provide a more precise statement of results with fewer assumptions (Sec. 4.6).

1.4 WIND MODEL FOR AUTOMATIC LANDING SYSTEM CERTIFICATION

The applicant should account for the aerodynamics of the airplane being evaluated including aeroelasticity, plus the distributed lift effects of steady winds and the longitudinal distribution of lift due to turbulence, unless it can be shown that these effects are insignificant.

The surface mean wind is defined as that at 20 feet above the ground. The automatic landing system need not be certified for surface wind speeds exceeding 25 knots nor for tailwind components exceeding 10 knots. The probability distribution of surface wind speeds ($\bar{V}_{20}$) is presented in Figure 1-9. The probability distribution for the direction to

which the wind is belowing, ($\bar{\psi}_W$), is presented in Figure 1-19 and is uncorrelated with the surface wind speed. The probability distribution of atmospheric stability as defined in terms of Richardson's number, (R_{i20}), is correlated with wind speed and is presented in Figures 1-15 and 1-16. The stochastic combinations of surface wind speed and heading and atmospheric stability may be generated by the model in Figure 1-30.

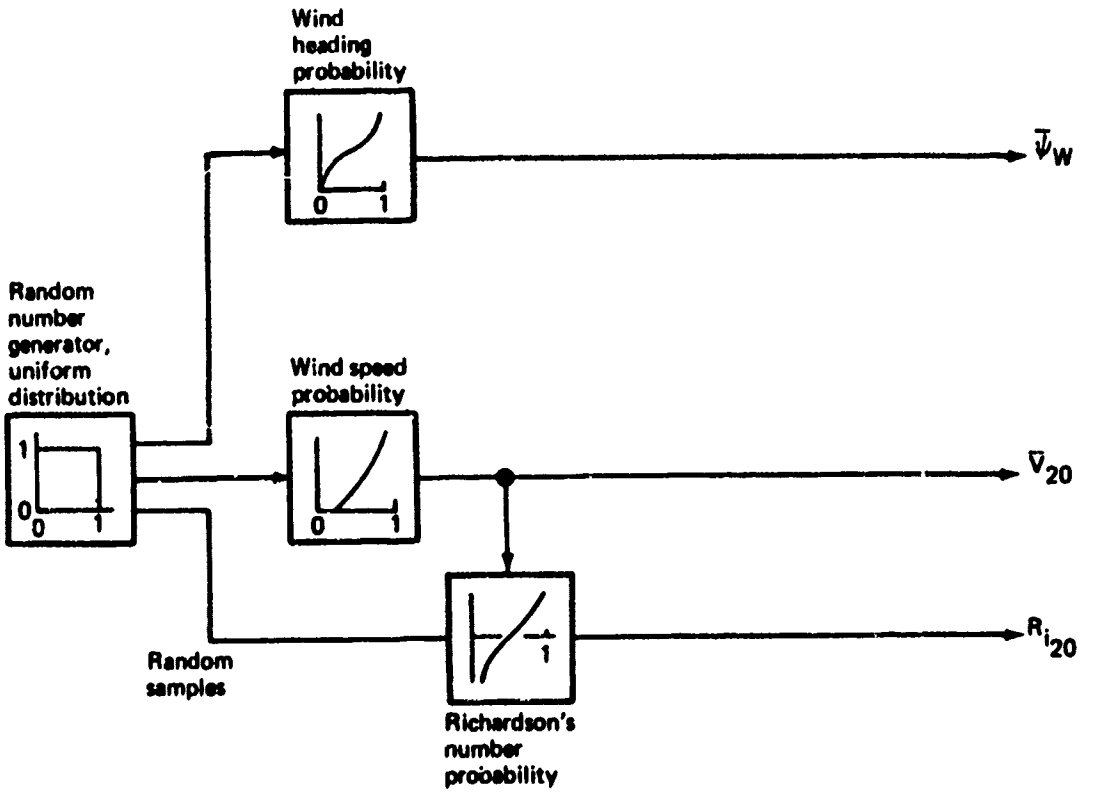

FIGURE 1-30.– PROBABILITY MODEL SCHEMATIC

The mean wind at any altitude is computed from the equation:

$$\bar{V}_W(h) = \bar{V}_{20}\left(\frac{u_{*_0}/k}{\bar{V}_{20}}\right)\left[\ln\left(\frac{h}{0.15}\right) + f(h/\ell') - \frac{h}{d}g(h/\ell')\right]$$

where

$\frac{u_{*_0}/k}{\bar{V}_{20}}$ is given on Figure 1-7 as a function of R_{i20}

$$d = 800 \frac{u_{*_0}/k}{\bar{V}_{20}} \bar{V}_{20}$$

$h \leq d$ no matter what the actual altitude

$1/\ell'$ is given in Figure 1-31 as a function of $R_{i_{20}}$

$f(h/\ell')$, $g(h/\ell')$ are described in Figures 1-4, or 1-5 and 1-8, respectively.

The mean wind shear at any altitude, needed only to define the distributed lift effects of the mean wind, is given by

$$\frac{\partial \bar{V}_W}{\partial h}(h) \left(\frac{u_{*_0}/k}{\bar{V}_{20}}\right) \left(1 - \frac{h}{d}\right) \phi\left(\frac{h}{\ell'}\right)$$

where $\phi(h/\ell')$ is described in Figures 1-2 and 1-3, and where, once again $h \leq d$ no matter what the actual altitude.

The power spectra for uncorrelated components of turbulence in an axis system parallel to the earth but aligned to the direction of the airplane's airspeed vector are given by

$$\Phi_u(\omega) = \frac{\sigma_H^2 L_H}{\pi V_A} \frac{1}{\left[1 + (1.339 L_H \omega/V_A)^2\right]^{5/6}} \sim \frac{(ft/sec)^2}{rad/sec}$$

$$\Phi_v(\omega) = \frac{\sigma_H^2 L_H}{2\pi V_A} \frac{1 + 8/3(1.339 L_H \omega/V_A)^2}{\left[1 + (1.339 L_H \omega/V_A)^2\right]^{11/6}} \sim \frac{(ft/sec)^2}{rad/sec}$$

$$\Phi_w(\omega) = \frac{\sigma_V^2 L_V}{2\pi V_A} \frac{1 + 8/3(1.339 L_V \omega/V_A)^2}{\left[1\ 3\ (1.339 L_V \omega/V_A)^2\right]^{11/6}} \sim \frac{(ft/sec)^2}{rad/sec}$$

where the spectra are defined such that

$$\sigma_H^2 = \int_{-\infty}^{\infty} \Phi_u(\omega) d\omega = \int_{-\infty}^{\infty} \Phi_v(\omega) d\omega$$

= variance of a horizontal component of turbulence

$\sigma_w^2 = \int_{-\infty}^{\infty} \Phi_u(\omega) d\omega$ = variance of the vertical component of turbulence and where

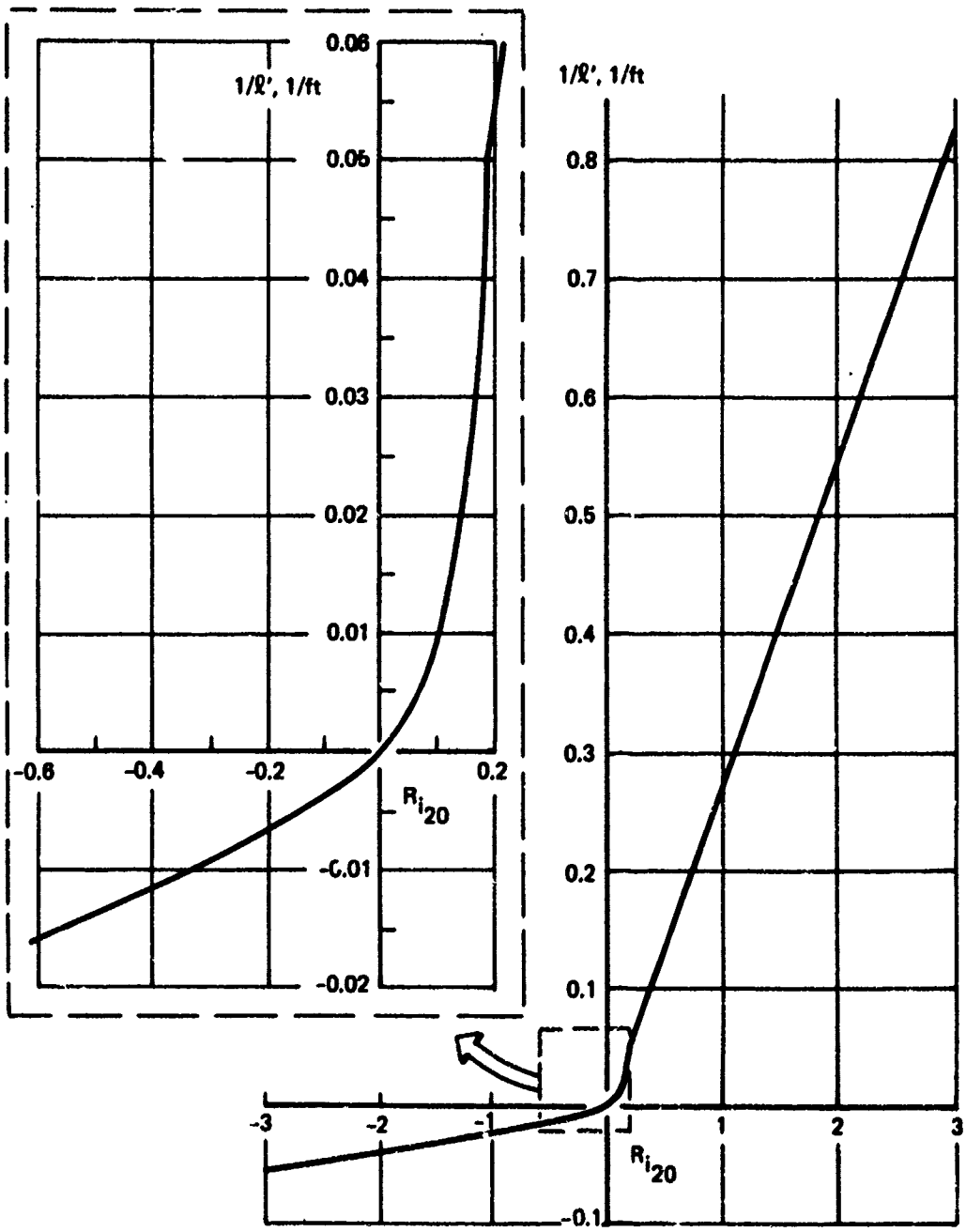

FIGURE 1-31.– SCALING LENGTH

$$\sigma_V = 0.4\bar{V}_{20}\left(\frac{u_{*_0}/k}{\bar{V}_{20}}\right)\left(1 - \frac{h}{d}\right)\left(\frac{\sigma_V}{u_*}\right)$$

$\frac{\sigma_V}{u_*}$ defined on Figure 1-25 is a function of h/ℓ'

$$\sigma_H = \left(\frac{\sigma_H}{\sigma_V}\right)\sigma_V$$

$\frac{\sigma_H}{\sigma_V}$ given as function of altitude on Figure 1-27.

$$L_V = \begin{cases} h & , h < 1000 \text{ ft} \\ 1000 \text{ ft} & , h \geq 1000 \text{ ft} \end{cases}$$

$$L_H = L_V(\sigma_H/\sigma_V)^3$$

The spectra are well represented by generating turbulence components equal to passing uncorrelated Gaussian white noise through the filters in Figure 1-22.

Body axis components of mean wind, mean wind shear, and turbulence are found by means of the transformations in Figure 1-18.

The interrelationships between the components of the wind model and the other elements of the simulation are described in Figure 1-32.

This model is compared with the current British, FAA, and military models in Appendixes 1-A, 1-B, and 1-C.

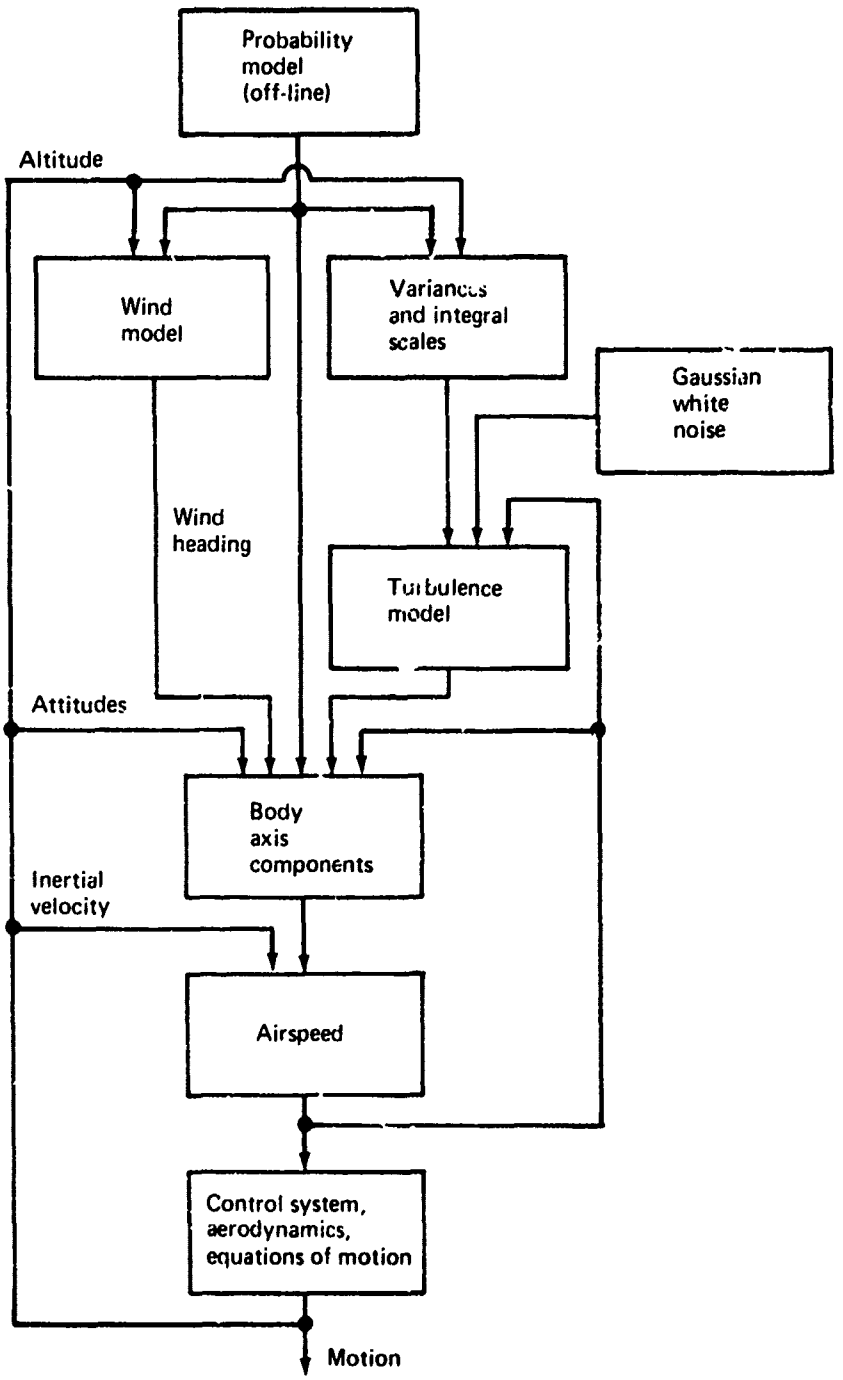

FIGURE 1-32.–COMPUTATION FLOW DIAGRAM

APPENDIX 1A

COMPARISON OF PROPOSED MODEL WITH ARB MODEL

This appendix provides a comparison of the model proposed in Section 1.4 with the Air Registration Board (ARB) model defined in the following reference: "Air Registration Requirements," Paper No. 367, Issue 3, June 1970.

MEAN WIND

The ARB mean wind model provides for a mean wind variation with altitude given by

$$\bar{V}_W = \bar{V}_{REF}\left[0.43 \log_{10}(h) + 0.35\right]$$

$$\bar{V}_{REF} = \bar{V}_W(h = 10 \text{ meters})$$

which can be rewritten as

$$\bar{V}_W = \frac{u_{*0}}{k} \ln\left(\frac{h}{z_0}\right)$$

$$z_0 = 0.15 \text{ feet}$$

$$\frac{u_{*0}}{k} = \frac{\bar{V}_{REF}}{\ln(32.18/0.15)}$$

The proposed model, given by

$$\bar{V}_W = \frac{u_{*0}}{k}\left[\ln\left(\frac{h + z_0}{z_0}\right) + f\left(\frac{h}{\ell'}\right) - \frac{h}{d} g\left(\frac{h}{\ell'}\right)\right]$$

$$z_0 = 0.15 \text{ feet}$$

$$\frac{u_{*0}}{k} = \frac{\bar{V}_{REF}}{\ln\left(\frac{h_{REF} + z_0}{z_0}\right) + f\left(\frac{h_{REF}}{\ell'}\right)}$$

$$h_{REF} = 20 \text{ feet}$$

reduces to approximately the same form when neutral stability ($h/\ell' = 0$) and low altitudes ($h/d \cong 0$) are assumed:

$$\bar{V}_{REF} \cong \frac{u_{*0}}{k} \ln\left(\frac{h + z_0}{z_0}\right)$$

The only other difference is that the ARB model uses a wind speed measured at 10 meters, the British standard, while the proposed model uses a wind speed measured at 20 feet, the American Standard.

The explanation for the ARB model assuming neutral conditions appears to be contained in the following statement contained in the reference:

> "Large wind shears can exist in stable conditions, which usually occur at night with wind speeds less than 20 ft/sec. However, these will be less severe circumstances overall, since the turbulence will then be less . . ."

The qualitative explanation of the effect of stability agrees with the proposed model. The above statement implies that turbulence and wind shears have the same effect, which does not agree with the analysis performed in Section 4.2. Even though the reference is concerned with determining the risk of a fatal landing, the above statement implies that this risk must be determined with the most severe wind conditions, an attitude that leads to overdesign. The use of atmospheric stability in the proposed model is an attempt to provide wind conditions as they appear; since about 70% of the cases for the proposed model are for stable conditions, the proposed model will tend to be less severe than the ARB model if the above statement can be believed.

The term $(h/d)\, g(h/\ell')$ was provided in the proposed model to ensure the shear diminished to zero at the edge of the boundary layer. Since no comparable term exists in the ARB model, the ARB model will provide greater shears and wind speeds at high altitudes. This difference is unimportant if the wind and wind shear above the altitudes where $(h/d)\, g(h/\ell')$ is significant has no effect on touchdown performance. The parameters most likely to be influenced by high-altitude wind conditions are the touchdown dispersion parameters.

Because the mean wind speed increases with altitude and the probabilistic distribution of reference wind speeds ($\bar{V}_{REF}$) for the ARB model is presumed to be measured at a higher altitude than is the data for the proposed model, it would be expected that for a given exceedance probability the ARB description would provide the higher reference wind speeds. This relationship has been found to hold, as seen in Figure 1A-1. The ARB model provides an average wind speed of 9.1 knots at 10 meters. Using the neutral stability ARB model, the average wind speed at 20 feet is

$$\bar{V}_W(h = 20) = \frac{9.1 \ln\left(\frac{20}{0.15}\right)}{\ln\left(\frac{32.15}{0.15}\right)} = 8.3 \text{ kt.}$$

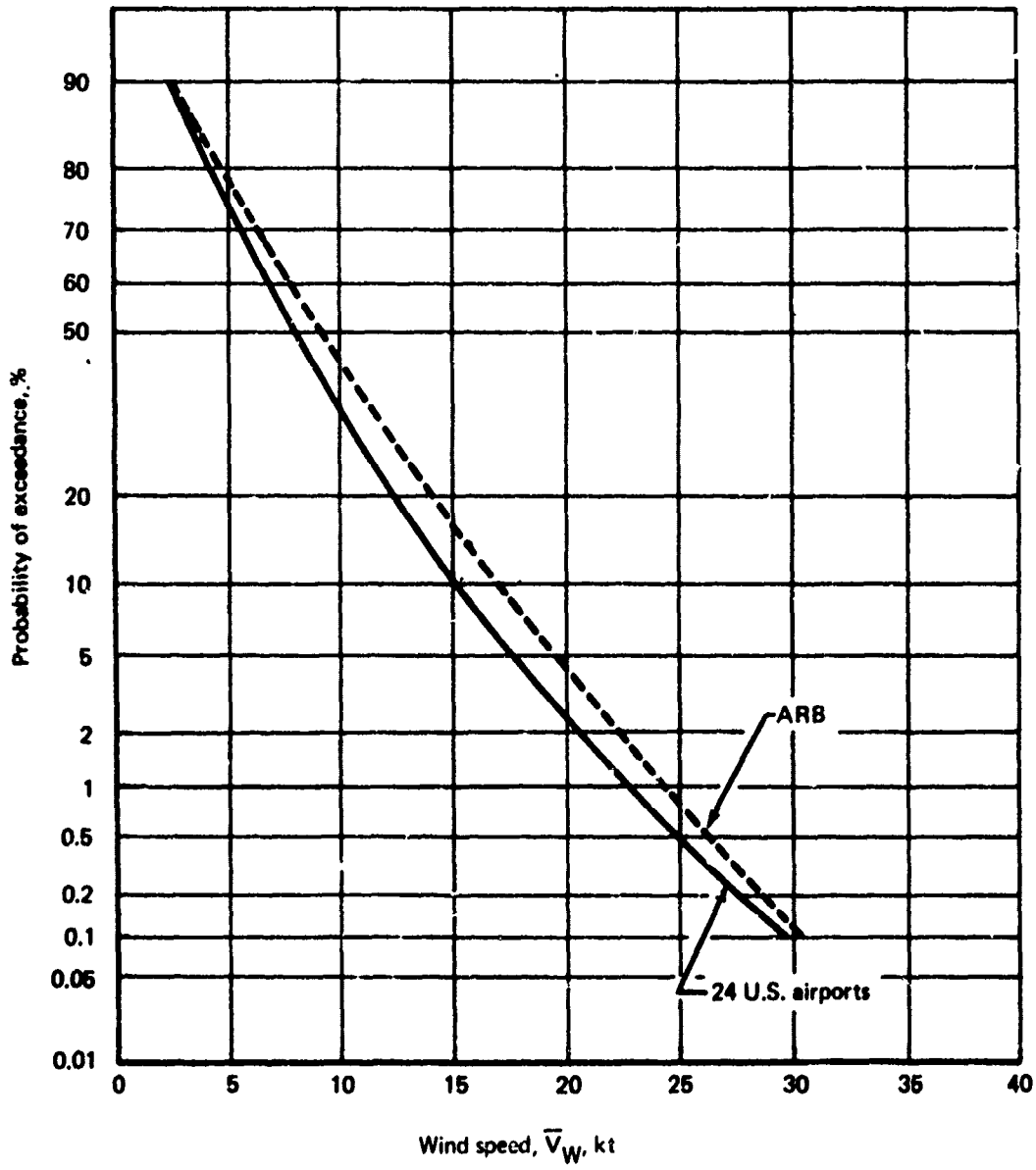

FIGURE 1A-1.–COMPARISON OF WIND SPEED DESCRIPTIONS

which is reasonably close to the 8-knot average wind speed at 20 feet provided by the proposed model. The lack of precise agreement can be attributed to the following.

1) The average level of atmospheric stability is more stable at lower altitudes. Since wind speed decreases with increasing stability, the average wind speed at 20 feet would be less than would be predicted by a constant atmosphere stability model such as the ARB model.

2) The data employed by the two models are different, measured at different locations.

The ARB wind speed exceedance probability data is said to be "... based on worldwide in-service operations of U.K. airlines (sample size about 1,000)."

The technique of taking data corresponding to in-service operations is superior to the approach taken for the proposed model if the samples were random, for conditions at a specific airport would tend to be weighted according to the activity at that airport. Whether or not the samples were taken randomly is not known. Although the ARB model presumes the wind speeds were taken at 10 meters, anemometer heights vary widely from airport to airport. Even if the average anemometer height were 10 meters, deviations of individual anemometers from 10 meters would influence the tails of the distribution. The main advantage of the probabilistic description of wind speeds in the proposed model are the constraints of anemometer heights and the much larger data sample (about 170,000 data points), which provides a better description for the more remote exceedance probabilities.

For six-degree-of-freedom simulations, the distribution of wind heading is needed as well as the distribution of wind speed in order to provide the combinations of down-runway and cross-runway wind components in proportion to their joint probabilities. If separate down-runway and cross-runway wind component distributions are provided, then the correlation between the components must also be provided. If separate longitudinal and lateral-direction simulations can be justified, only the distributions for down-runway and cross-runway wind components are needed.

The heading and wind speed distributions were provided in the proposed model. Distributions for the components were also developed during the study. The ARB model provides a strange combination of data: the distributions of the total wind speed and for the cross-runway component are provided. This information is incomplete for either six-degree-of-freedom or separate longitudinal and lateral-directional simulations.

The ARB model does not explicitly provide an equation for the wind shear at any altitude nor does it mention accounting for the distribution of the mean wind over the airplane. Hence, the ARB model implies the distributed lift effects due to the mean wind are insignificant. From the analysis in Section 4.2.1.2, it can be concluded that the significance of the distributed lift effects due to the mean wind are configuration dependent.

TURBULENCE

The ARB turbulence model employs the same power spectrum form for all three components:

$$\Phi(\Omega_l) = \frac{2\sigma^2 L}{\pi} \frac{1}{1 + (L\Omega_l)^2}.$$

This form corresponds to the one-sided Dryden spectrum for the longitudinal component of turbulence. By one-sided, it is meant that the spectrum is redefined to provide

$$\sigma^2 = \int_0^\infty \Phi(\Omega_l)\, d\Omega_l$$

rather than the literal definition of the power spectrum, which provides

$$\sigma^2 = \int_{-\infty}^\infty \Phi(\Omega_l)\, d\Omega_l.$$

If a turbulence filter operating on white noise is made to match the one-sided spectrum,

$$G(S) = \sqrt{\frac{2L}{\pi V_A}} \frac{1}{1 + LS/V_A},$$

the resulting variance will be high by a factor of two.

The use of a single spectrum for all three turbulence components prevents turbulence from meeting well-established requirements:

- Local isotropy (isotropy at high frequencies) will not result
- Turbulence will not tend toward isotropy for increasing altitude

Failure to meet these requirements means the relationship between the transverse spectra to the longitudinal spectrum is incorrect.

The Dryden longitudinal spectrum was found to be inferior to the Von Karman form in Section 2.4.2.4 and was found to be a poor approximation to the Von Karman form in Section 4.5.3.3.

The ARB model defines rms turbulence intensities and integral scales relative to the mean wind, just as was done in the proposed model. However, the reference does not indicate how to resolve the problem of spectra defined for components aligned to the relative wind and turbulence parameters defined relative to the mean wind.

Vertical rms turbulence in the ARB model is 9% of the mean wind speed at 10 meters and horizontal rms turbulence is twice the vertical turbulence level. Rms intensities are defined as invariant with altitude and are said to be representative for neutral stability.

In the proposed model, vertical turbulence decreases slowly with altitude and horizontal turbulence decreases more rapidly with altitude until it is equal to the level of vertical turbulence at 1000 feet. All proposed turbulence levels increase with decreasing stability in the same manner. At the surface, horizontal rms turbulence is twice the level for vertical turbulence, just as for the ARB model. For neutral conditions, the proposed model provides rms vertical turbulence equal to 10.6% of the mean wind speed at 20 feet. For neutral conditions, the wind speed at 20 feet is 91.3% of the wind speed at 10 meters. Hence, the proposed model provides rms vertical turbulence equal to 9.7% of the mean wind speed at 10 meters, which is close to the level specified in the ARB model. Near the surface for neutral conditions, the two models provide for nearly equal rms intensities.

The failure of the ARB model to provide for the effects of atmospheric stability on turbulence, the decrease of turbulence levels with increasing atmospheric stability, and the evidence indicating the atmosphere is stable for a majority of the time mean the ARB model is overpredicting the average level of turbulence. The invariance of ARB turbulence levels with altitude means the ARB model tends to overpredict turbulence levels away from the surface.

The reference provides for turbulence generated by a Gaussian process, but qualifies the acceptability of the Gaussian distribution with the following statement:

> "Whilst giving an adequate description of measured wind decreases, the Gaussian model underestimates the probability of large wind increases. In accepting the Gaussian model the assumption has been made that critical touchdown performance parameters are primarily influenced by wind decreases."

The qualification is unnecessary. Although evidence shows that for the sum of all patches of turbulence the distribution of turbulence is non-Gaussian, there is nothing to indicate that the distribution of turbulence velocities for a single patch of turbulence (that which is being simulated) is anything but Gaussian (Sec. 2.4.1.2).

The ARB model specifies an integral scale for vertical turbulence equal to the altitude except below 30 feet, where it is 15 feet. Why the vertical turbulence integral scale is held constant near the surface is unknown. Above 30 feet, the ARB vertical turbulence integral scale is half that in the proposed model. This causes the turbulence for the ARB model to be greatest about a frequency that is twice that for the proposed model. The use of the longitudinal turbulence spectra for vertical turbulence reduces this difference.

The ARB model specifies 600 feet invariant with altitude for the horizontal integral scale. The reference states that this was determined by approximating a "mean smoothed" spectrum from six 1-hour runs (Fig. 1A-2). The use of 1-hour runs implies the mean wind was the average of a 1-hour sample of data, and turbulence is taken as the deviation from that mean. One hour is a very long period for determining the mean wind (10 minutes is more common). Within 1 hour, "mean" conditions vary and changes in the mean wind are

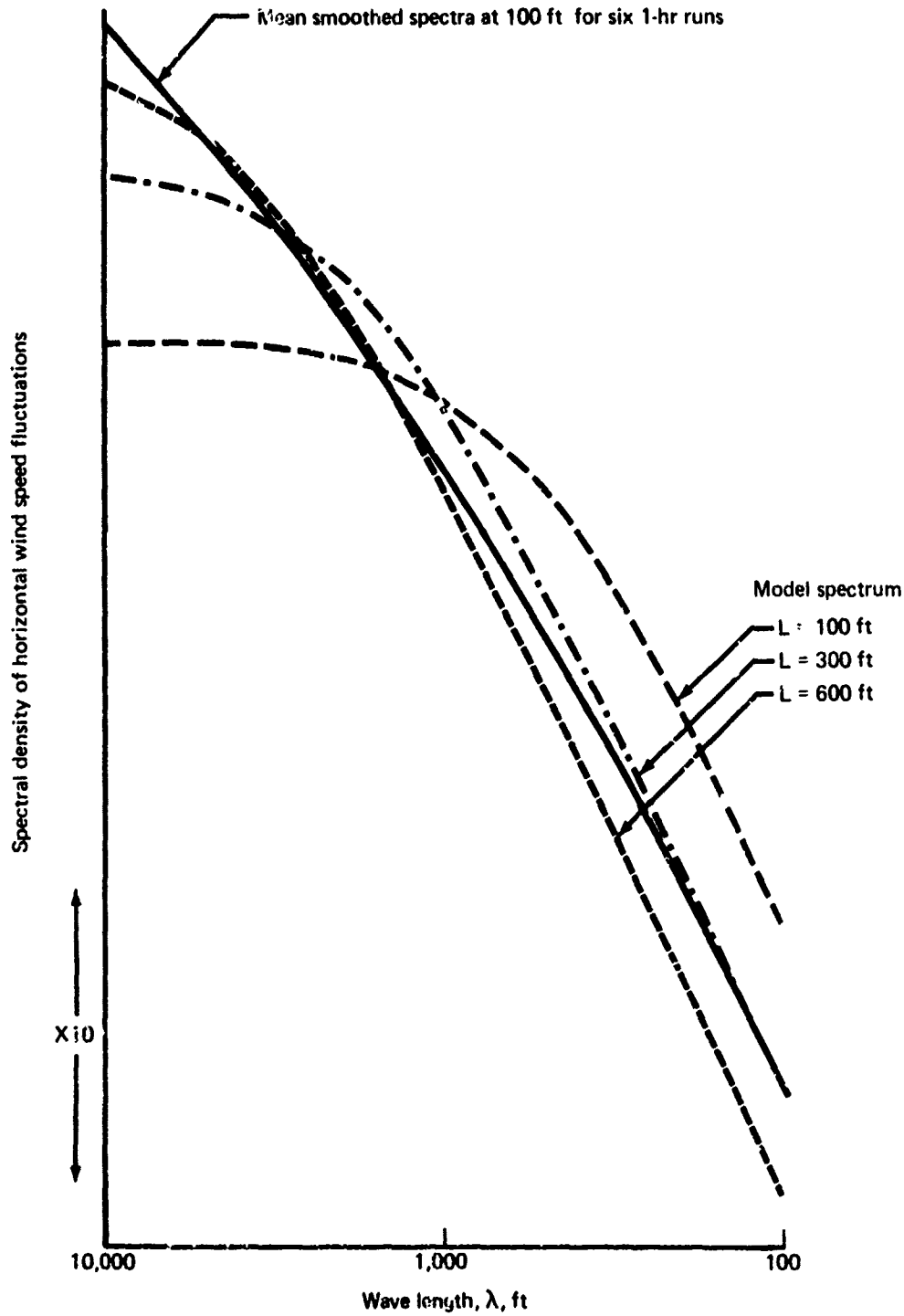

Mean smoothed spectrum at 100-ft height compared with model spectra having the same rms and various values of scale length, L.

$$\text{Model spectrum} \sim \frac{L}{1+(2\pi L/\lambda)^2} = \frac{L}{1+\Omega^2 L^2}$$

FIGURE 1A-2.–ARB MODEL SPECTRUM COMPARISON WITH MEASURED SPECTRA AT 100 FT

interpreted as turbulence. The effect is to overpredict the spectrum at low frequencies and to overpredict integral scales. However, the ARB spectrum model underpredicts the "mean smoothed" spectrum at low frequencies, as seen in Figure 1A-2, to compensate for this error. At 100 feet, the proposed model predicts an integral scale of 500 feet, which is not far different from the ARB specification.

Although the reference implies the integral scale for horizontal turbulence changes with altitude through Figure 1A-3, no provisions for varying the horizontal integral scale with altitude were made. In contrast, the integral scale for horizontal turbulence increases with altitude for the proposed model.

The best comparison between the two models is a comparison of the complete spectra, including the specified rms levels and integral scales. Comparisons of $\Omega\Phi$ are made for the three components aligned to the mean wind in Figures 1A-4, 1A-5, and 1A-6. The ARB spectrum has been divided by two to provide the two-sided spectrum compatible with the proposed model. The areas under these curves are proportional to the variances of the components. Hence, the curves define the distribution of turbulence variance with frequency.

The proposed turbulence model and the ARB model do not agree well for any of the components. For the horizontal components (Figs. 1A-4 and 1A-5), the maximum contribution to the variance at low altitudes is at a lower frequency for the ARB model than for the proposed model. The vertical turbulence spectra compare much better at low altitudes (Fig. 1A-6). This is due to a cancellation of differences:

- The use of the Dryden spectra causes the maximum value of $\Omega\Phi_w$ for the ARB model to be greater, but the use of the horizontal turbulence spectrum for vertical turbulence causes the maximum of $\Omega\Phi_w$ to be less.

- The use of a smaller integral scale shifts the ARB spectra to higher frequencies but the use of the Dryden horizontal turbulence spectrum for vertical turbulence shifts the ARB spectrum back to lower frequencies.

Even though the rms levels provided by each model are comparable at low altitudes, the ARB model provides greater maximum values for $\Omega\Phi_u$ and $\Omega\Phi_v$; thus the ARB model provides for a greater concentration of turbulent energy about the frequency for maximum $\Omega\Phi$.

At higher altitudes, the airplane response to turbulence is clearly greater for the ARB model. The ARB model will generally have more severe airplane responses at low altitudes, although the conclusion as to which model is most severe at low altitudes is heavily dependent upon airspeed and particular airplane-control system characteristics.

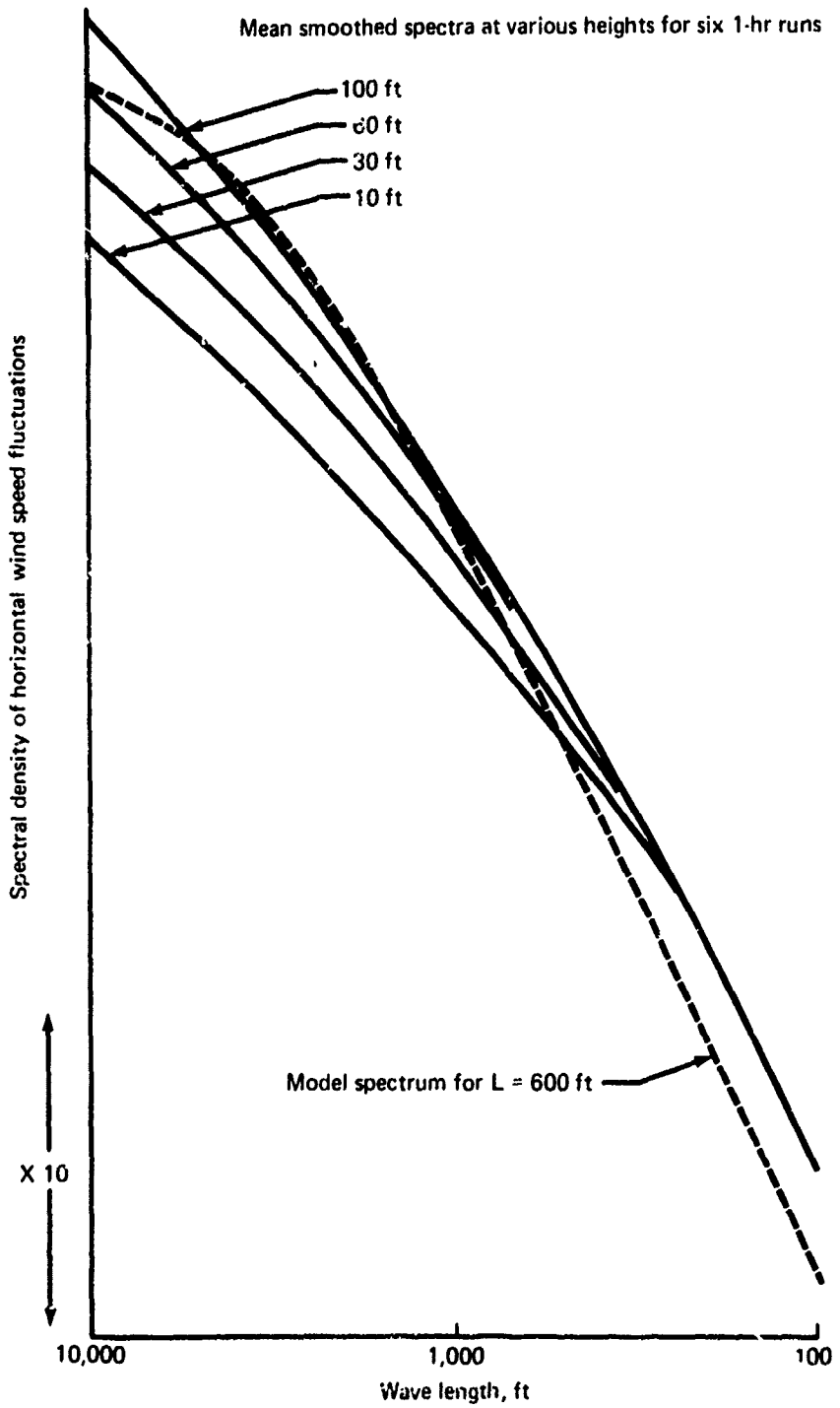

Mean smoothed spectra for six 1-hr runs, fitted to give same spectral density at short wavelengths.

For comparison the model spectrum is shown having L = 600 ft and the same rms as the 100-ft measured spectrum.

FIGURE 1A-3.–ARB MODEL SPECTRUM COMPARISON WITH MEASURED SPECTRA AT DIFFERENT ALTITUDES

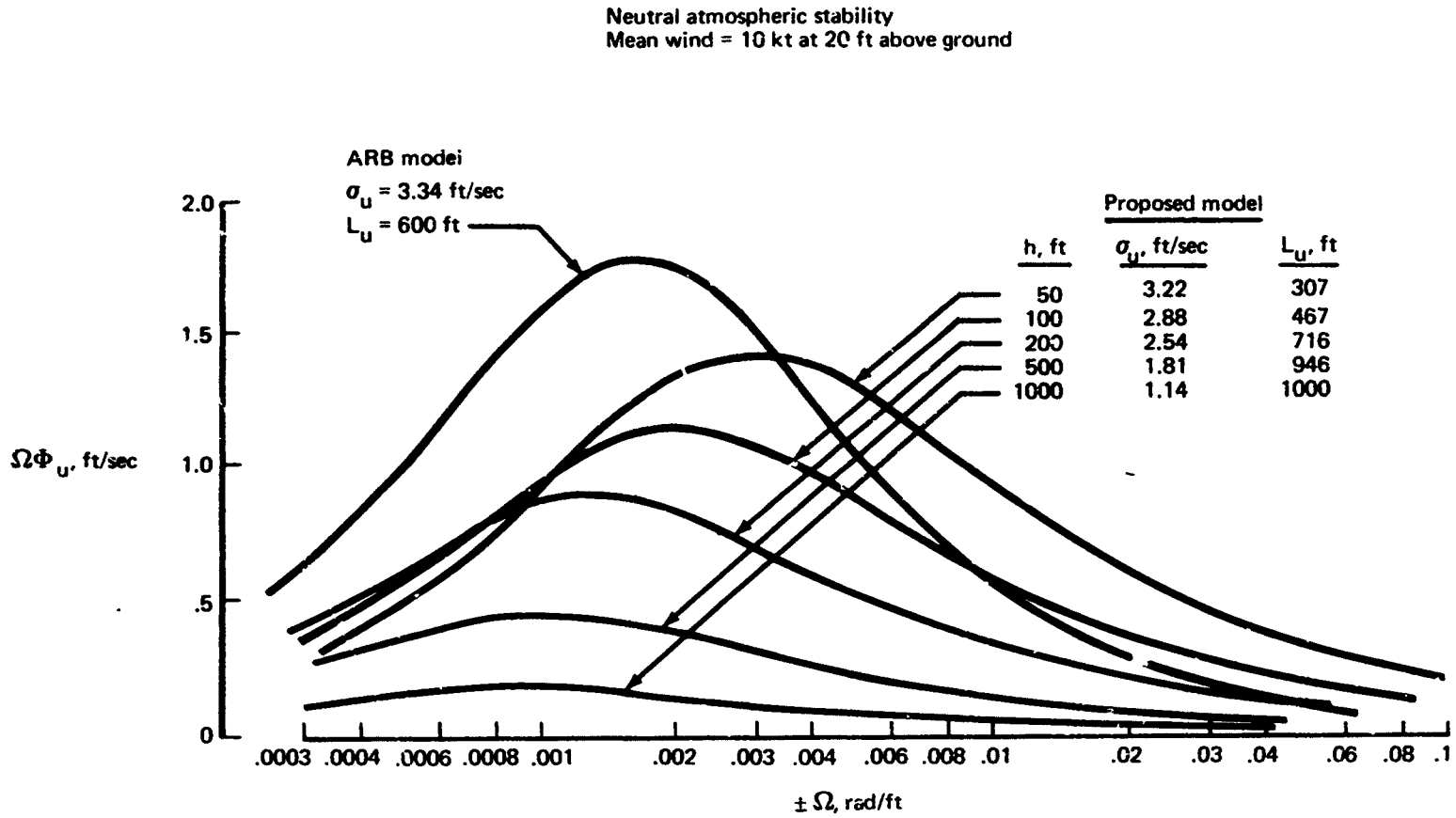

FIGURE 1A-4.—COMPARISON OF HORIZONTAL TURBULENCE IN DIRECTION OF THE MEAN WIND

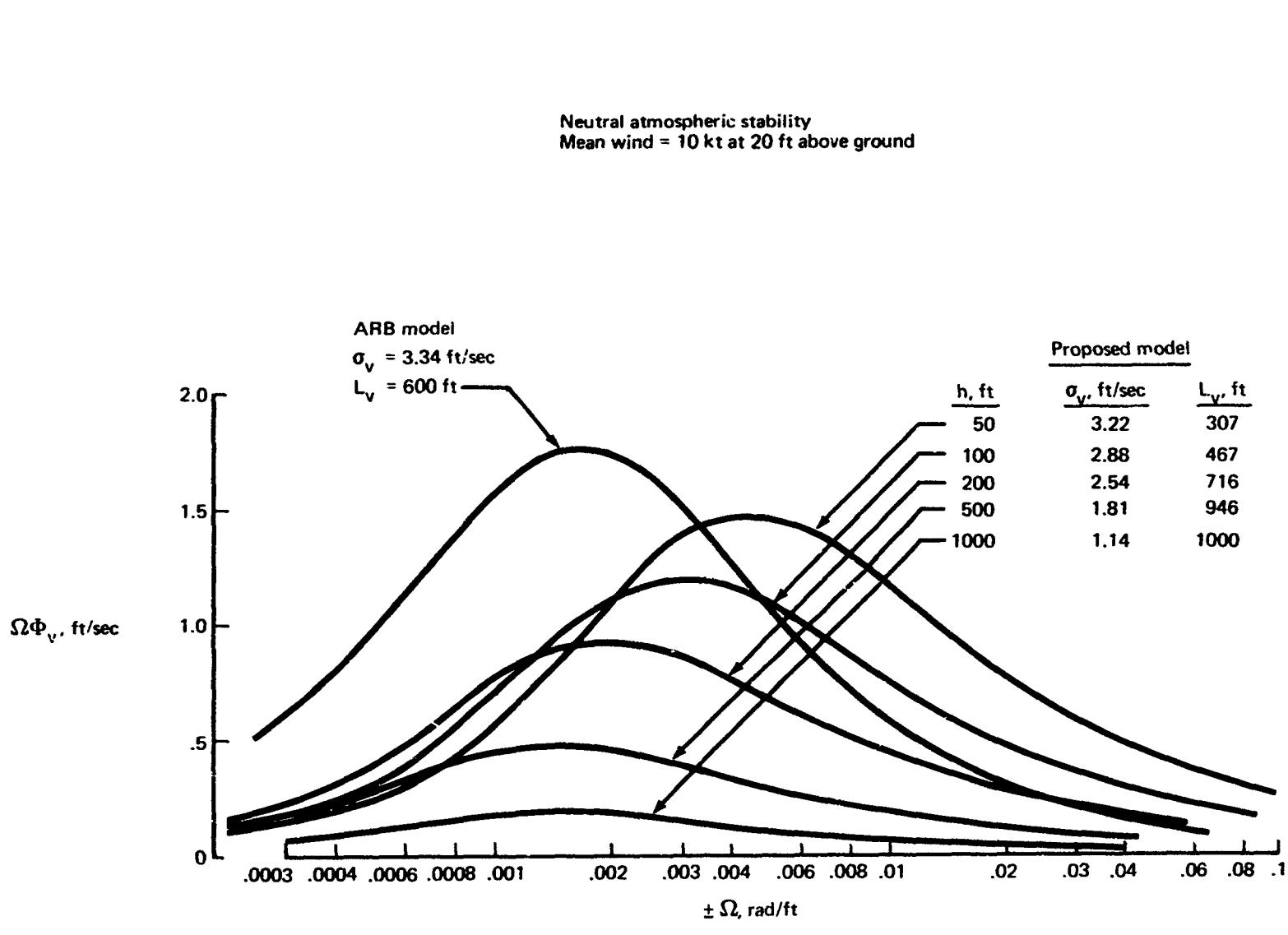

FIGURE 1A-5.—COMPARISON OF HORIZONTAL TURBULENCE PERPENDICULAR TO DIRECTION OF MEAN WIND

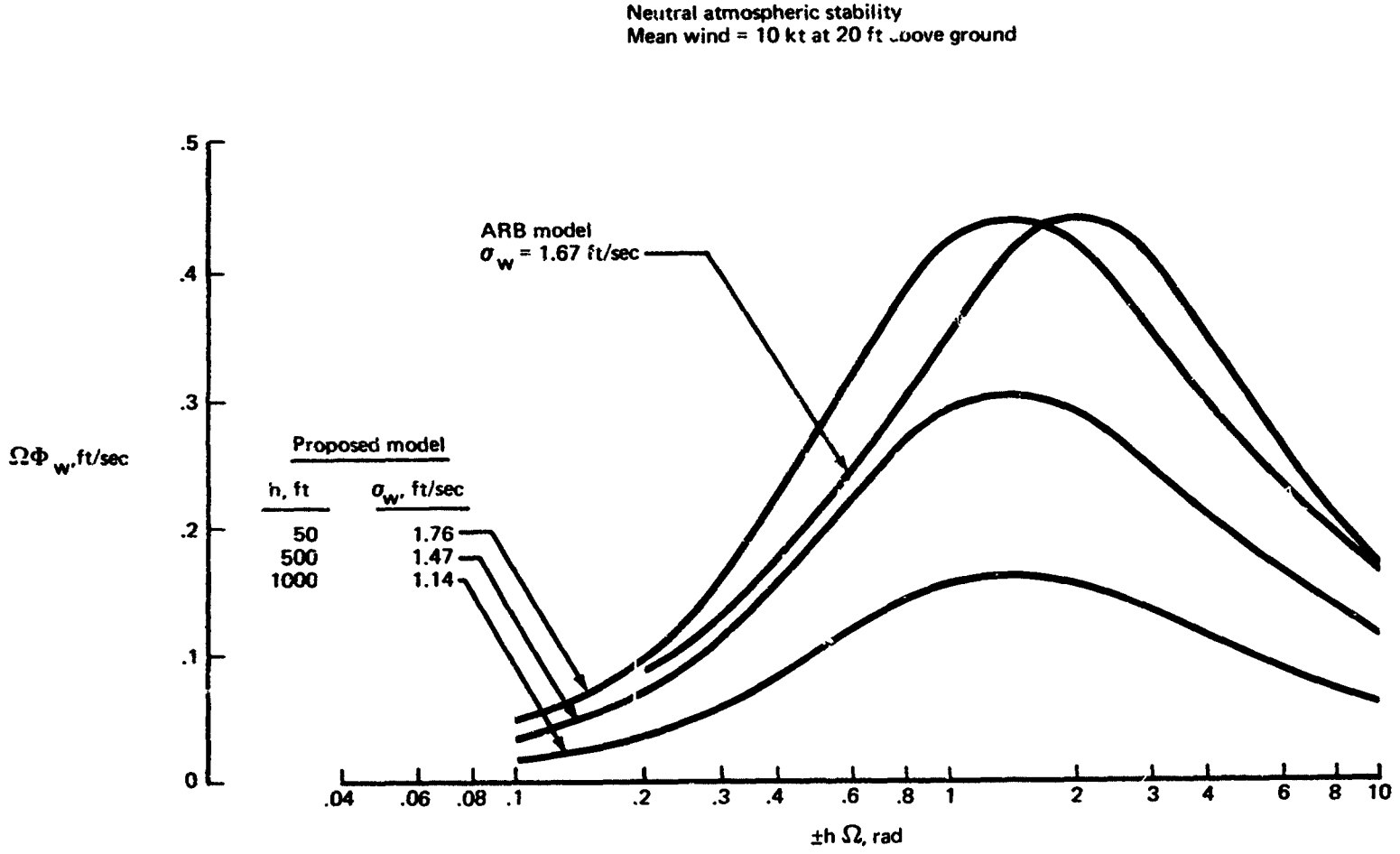

FIGURE 1A-6.—COMPARISON OF VERTICAL TURBULENCE

APPENDIX 1B

COMPARISON OF PROPOSED MODEL WITH FAA MODEL

This appendix provides a comparison of the model proposed in Section 1.4 with the Federal Aviation Administration model defined in the following reference: Advisory Circular 20-57A, "Automatic Landing Systems," Federal Aviation Administration, 12 January 1971.

MEAN WIND

The reference requires demonstrating adequate touchdown performance for "reasonable" combinations of headwinds up to 25 knots, tailwinds up to 10 knots, crosswinds up to 15 knots, wind shear of 8 knots per 100 feet from 200 feet to touchdown, and moderate turbulence. Probability distributions are specified for mean wind speeds identical to those appearing in the ARB model except the "total wind" speed distribution in the ARB model has been redesignated "downwind." Since the reference is dated later than the reference for the ARB model, the probability distribution has likely been taken from the ARB model.

Using the total wind distribution for the distribution of the downwind component significantly overpredicts the downwind component associated with a given exceedance probability. For example, the average wind speed at 20 feet for the proposed model is 8 knots, while the corresponding average downwind component is only 5 knots. Alternately, a 5-knot downwind component corresponds to an exceedance probability of 0.5, while an 8-knot downwind component corresponds to an exceedance probability of 0.25, twice as remote.

The altitude at which the probability distributions of wind speeds are to apply are not specified. Furthermore, it is not clear how variable levels of wind speed are to be combined with a fixed shear. Several interpretations are possible, as shown below.

1) The user may arbitrarily select the altitude at which to apply the wind speeds. The wind speed varies linearly with altitude about that point at the rate of 8 knots/100 feet. This will result in a finite wind speed at the surface or a wind speed that decreases to zero with decreasing altitude, then reverses direction and increases with further decreases of altitude. Both of these descriptions of the mean wind are unreasonable.

2) The user is to evaluate the effects of a steady wind and a shear separately, then combine results.

   A steady wind has little influence on touchdown performance except through the decrab maneuver, if one is provided. It is possible to represent a wind shear without representing the corresponding change in wind speed through linear equations. However, as discussed in Section 4.2.2, this will cause the touchdown dispersions to be overpredicted.

To hold constant airspeed along a glideslope in a decreasing headwind requires an acceleration to increase the groundspeed. If throttles are not advanced, the airplane will tend to touch short. This is the effect of the shear.

The decrease in headwind requires the pitch attitude to be decreased in order to hold the glideslope. Less thrust is required to maintain lesser attitudes. Unless throttles are retarded, the decreasing wind speed will cause the touchdown to be long. This is the effect that would be ignored if only the wind shear were to be represented.

3) The user is to represent the mean wind by

$$\bar{V}_W = 0.08\,h$$

$$\bar{V}_W \sim \text{knots}$$

$$h \sim \text{feet}$$

and the probability distribution of wind speeds is to be used only for determining turbulence levels. This would make the relationship between the mean wind and turbulence arbitrary. In contrast, the proposed model provides a definite relationship between the level of wind and the level of turbulence and the shear is described as varying inversely with altitude.

The proposed mean wind model cannot be well approximated by a constant shear. To demonstrate that this is true, consider an example where atmospheric stability is neutral. The wind profile for the proposed model is then

$$\bar{V}_W = 0.204\,\bar{V}_{20}\ln\left(\frac{h+0.15}{0.15}\right).$$

If the shear in FAA model is supposed to correspond to the shear computed by the difference in wind speeds at the surface and 200 feet, the wind speed at 200 feet for the proposed model should also be 16 knots.

Then,

$$\bar{V}_{20} = \frac{16}{\ln\left(\frac{200.15}{0.15}\right)} = 10.9 \text{ knots}$$

$$\bar{V}_W = (0.204)(10.9)\ln\left(\frac{h+0.15}{0.15}\right) = 2.224\ln\left(\frac{h+0.15}{0.15}\right)$$

$$\frac{d\bar{V}_W}{dh} = \frac{2.224}{h+0.15}$$

The FAA and proposed wind profiles and shears are compared on Figure 1B-1.

To assess the relative effects of the two wind profiles, an airplane approaching into the wind at a constant 120-knot airspeed along a 3° glideslope is considered. In Section 4.2.2, an approximate expression for the change of thrust required from that used to trim the airplane initially was developed for such a maneuver:

$$\left(\frac{\Delta T}{W}\right)_{REQ.} = \left[\frac{\bar{V}_W}{V_A} + \frac{V_A + \bar{V}_W}{g}\frac{d\bar{V}_W}{dh}\right]$$

where

$$\bar{V}_W, \frac{d\bar{V}_W}{dh} < 0 \text{ and } \Delta\bar{V}_W > 0$$

for an approach into a headwind. If the airplane is trimmed for the glideslope at 200 feet

$$\Delta\bar{V}_W = \bar{V}_W(h) - \bar{V}_W(h = 200)$$

$$\Delta(T/W) = \frac{T}{W}(h) - \frac{T}{W}(h = 200).$$

The change in thrust-to-weight ratio represents the throttle activity required to maintain constant airspeed on a fixed glideslope or, conversely, it represents the airplane deceleration if the throttles are not moved.

As seen in Figure 1B-1, the FAA model requires only a single throttle correction, while the throttles for the proposed model must be increased at an increasing rate as the ground is approached. If no throttle corrections are made, touchdown will be far more short of the glideslope intercept for the FAA model than for the proposed model. Without a throttle adjustment, a high deceleration will occur for the FAA model from 200 feet while a high deceleration only occurs near the ground for the proposed model, too late to cause a significant touchdown dispersion.

The differences between the two models is even greater because the shear for the FAA model is always constant, while that for the proposed model will change substantially with changing atmospheric stability and wind levels. Figure 1B-1 makes it clear that a wind shear invariant with altitude cannot represent the effects of the shear in the proposed model.

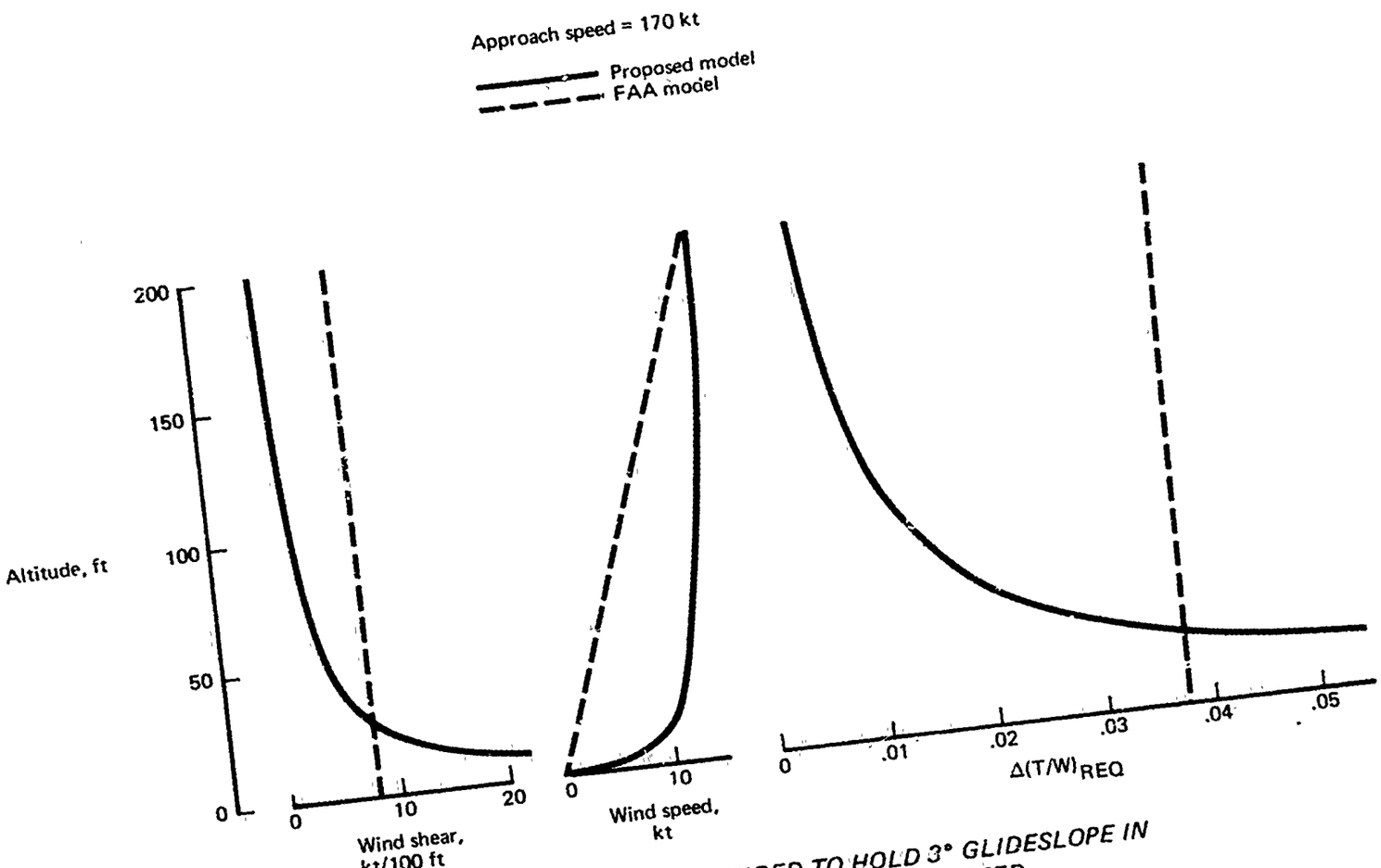

FIGURE 1B-1.—THRUST REQUIRED TO HOLD 3° GLIDESLOPE IN HEADWIND, 170 KT APPROACH SPEED

TURBULENCE

The turbulence model in the reference is similar to, and appears to be taken from, the ARB model except for the following significant differences.

1) The integral scale for vertical turbulence is a constant 30 feet.

2) The rms level for vertical turbulence is set at a constant 1.5 knots independent of wind speed, atmospheric stability, and altitude.

3) The rms levels of the horizontal turbulence components are linearly related to downwind and crosswind components of the mean wind.

4) Components of turbulence are to be generated directly in an axis system attached to the orientation of the airplane (Fig. 1B-2).

5) Undefined concepts of "span averaging" and "area averaging" are shown to affect longitudinal and vertical turbulence, respectively (Fig. 1B-2).

The explanation provided for item 2) in the reference is "The effect of vertical turbulence is small and a constant level is satisfactory." The reason vertical turbulence has been found to have small effect is because of item 1): the very small constant integral scale of 30 feet for vertical turbulence shifts the power of turbulence to frequencies above those at which the aircraft can respond. For the power spectra provided in the reference, which is the same as for the ARB model, the greatest vertical turbulence energy is about a frequency computed from

$$\frac{L\omega}{V_A} = 1.$$

Hence, for the FAA model and a 120-knot approach speed, maximum turbulence energy occurs at

$$\omega = \frac{(120)(1.688)}{20} = 6.752 \text{ rad/sec.}$$

This is far beyond the short-period natural frequencies of most commercial aircraft. For the proposed model, where the integral scale for vertical turbulence is equal to altitude, the airplane will respond to vertical turbulence until very close to the ground. This is shown in Figure 1B-3. At higher altitudes, not only will the short period respond to the vertical turbulence from the proposed model, but the phugoid will also respond.

The description of the rms levels of the turbulence components provided by items 2) and 3) is: horizontal turbulence occurs only in the direction of the mean wind while vertical turbulence occurs regardless of the wind level or even if there isn't any wind. This description is contrary to the empirically substantiated theory presented in Section 2.4.4. Turbulence can only occur in three dimensions, as can be observed from the equations of motion governing turbulent motion. Rms turbulence levels are proportional to the mean

LONGITUDINAL TURBULENCE

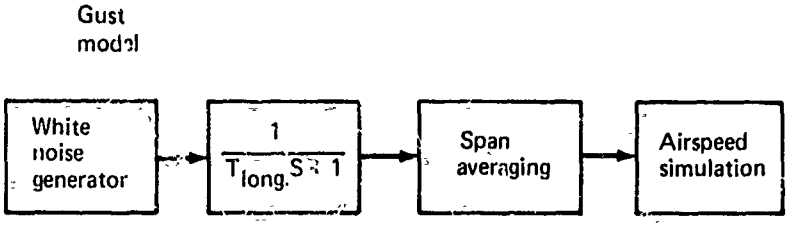

$T_{long.}$ is L/V: where L is longitudinal scale length = 600 ft
V = approach speed (ft/sec)

VERTICAL TURBULENCE

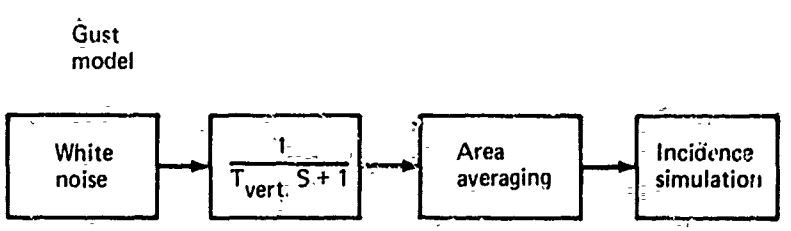

$T_{vert.}$ is L/V: where L is vertical scale length ≅ 30 ft
V = approach speed (ft/sec)

LATERAL TURBULENCE

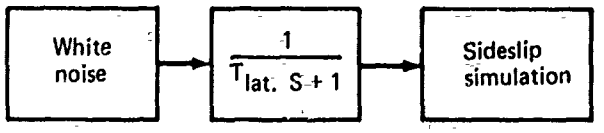

$T_{lat.}$ is L/V: where L is lateral scale length = 600 ft
V = approach speed (ft/sec)

T represents time constant τ
S represents the Laplace operator $\mathcal{L}$ where t denotes a real variable and S a complex variable:

$$\mathcal{L}[f(t)] = \int_0^\infty e^{-st} f(t)\, dt$$

FIGURE 1B-2.—FAA TURBULENCE MODEL IMPLEMENTATION

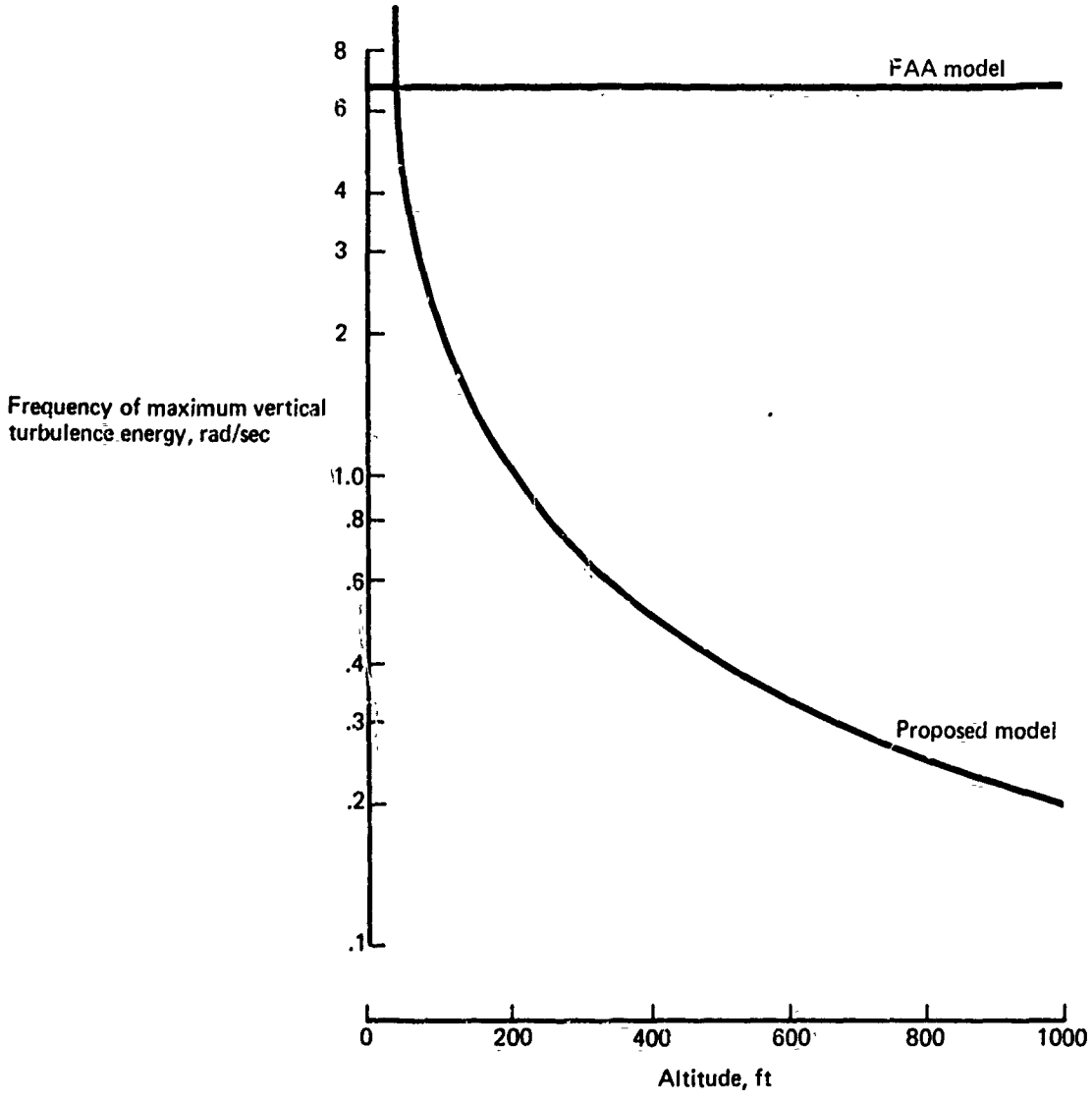

FIGURE 1B-3.–FREQUENCY FOR MAXIMUM VERTICAL TURBULENCE ENERGY COMPARISON

wind speed at a given altitude, with the constant of proportionality determined by the state of atmospheric stability. It is possible to have significant levels of turbulence for low levels of mean wind speed for very unstable conditions, but then turbulence levels would vary strongly with altitude.

The constant level of vertical turbulence does not even constitute a good average value. Near the surface and/or during high mean wind conditions, the proposed model defines the rms vertical turbulence level to be 10.6% of the mean wind speed at a 20-foot altitude. Thus, a 1.5-knot rms vertical turbulence level would correspond to a mean wind speed of 14.2 knots. The probability of exceeding a 20-foot mean wind speed of 14.2 knots is not 50% but 12.5%.

The setting of rms levels of horizontal components of turbulence equal to 15% of the respective components of mean wind corresponds to the 18% of the total mean wind speed at 10 meters specified by the ARB model for neutral atmospheric stability. Thus, the reference specifies a reduced percentage of a reduced wind speed.

Specifying turbulence to be generated directly in an axis system attached to the airplane, item 4), implies the rms levels of turbulence and the integral scales depend upon the orientation of the airplane. The theory and empirical investigation presented in Sections 2.4.4 and 2.4.5 clearly define the statistical properties of turbulence to be aligned to the heading of the mean wind. Directly generating turbulence in an airplane referenced axis system was found in Section 4.3 to be a poor approximation for vertical turbulence. Near the surface, for a 5° pitch attitude generating turbulence directly in the airplane body axis will cause the low-frequency portion of the vertical turbulence spectrum to be underestimated by a factor of two.

"Span averaging" and "area averaging" are apparently intended to represent the distributed lift effects of turbulence. Although the reference does not specify the nature of these operations, Figure 1B-2 implies that they are linear operations such as filtering. The representation of the distribution of turbulence about an airplane is discussed in Section 4.2.1.3.3. No suitable method corresponding to Figure 1B-2 was discovered. The only suitable method found for simulating the spanwise distribution of turbulence was through generating an effective roll rate due to turbulence by filtering the vertical body axis component of turbulence. However, the proponent of this method has found that representing an effective turbulence roll rate does not improve the fidelity of the airplane response to turbulence.

Two methods of representing the longitudinal distribution of turbulence (gust penetration) were determined and both may be used in combination. One method consists of generating effective pitch and yaw rates due to turbulence by filtering the vertical and lateral body axis components of turbulence by:

$$q_T = \frac{1}{V_A} \frac{S}{1 + \frac{4\ell}{\pi V_A} S} w_T$$

$$r_T = \frac{1}{V_A} \frac{S}{1 + \frac{4\ell}{\pi V_A} S} v_T$$

where ℓ = length from wing aerodynamic center to tail aerodynamic center.

The turbulence pitch and yaw rates are subtracted from the inertial pitch and yaw rates to form the airplane pitch and yaw rates with respect to the air mass, respectively, which in turn are multiplied by the aerodynamic pitch rate derivatives and yaw rate derivatives due to the longitudinal velocity distribution.

The second method employs the frozen field concept. Turbulence velocities are assumed to be frozen in space. Turbulence at the tail is the same as that at the wing occurring a time increment earlier equal to that required to traverse the distance from the wing aerodynamic center to the tail aerodynamic center. Upon computing turbulence velocities at the wing, these velocities are stored for a time $\Delta t = \ell/V_A$ and then are used as the turbulence velocities at the tail. Approximate methods of representing the transport lag are also discussed in Section 4.2.1.3.3. The transport lag method of representing distributed lift effects requires separate buildups of tail angle of attack and tail aerodynamics but will provide a better representation than using just effective turbulence angular velocities. An even better representation is provided by using effective turbulence angular velocities with the wing contributions to yaw rate and pitch rate aerodynamic derivatives in addition to the transport lag method.

The representation of the distributed lift due to turbulence is not an unnecessary luxury. It is generally required for approach speeds to eliminate significant errors caused by using a point lift representation of the airplane. As discussed in Section 4.2.1.2 and as provided for in the model in Section 1.4, it may be necessary to represent the distributed lift effects of the mean wind also.

In summary, the average turbulence condition provided by the FAA model will generally be more severe than that provided by the proposed model because the FAA model does not account for the diminishing or disappearance of turbulence for stable atmospheric conditions nor for increasing altitude, which occur for a majority of the time. On the other hand, the FAA model generally underpredicts the effects of the more severe turbulence conditions for the following reasons.

- An unrealistically short integral scale for vertical turbulence causes the aircraft to not respond to vertical turbulence.
- Horizontal turbulence rms levels are too low of a percentage of wind speed and are incorrectly based on components of the mean wind speed rather than the total wind speed.
- The increase of turbulence levels for increasingly unstable atmospheric conditions are not accounted for.

- The reference incorrectly implies turbulence components may be attenuated for distributed lift effects.

- The vertical body axis turbulence tends to be underpredicted because the reference incorrectly permits the generation of turbulence directly in the airplane's body axis system.

APPENDIX 1C

COMPARISON OF PROPOSED MODEL WITH MILITARY MODEL

This appendix provides a comparison of the model proposed in Section 1.4 with the military model defined in the following reference: Chalk, C. R., Neal, T. P., Harris, F. E., and Pritchard, F. E., "Background Information and User Guide for MIL-F-8785B(ASG), Military Specification–Flying Qualities of Piloted Airplanes," Technical Report AFFDL-TR-69-72, August, 1967.

MEAN WIND

The most notable shortcoming of the military model is the absence of a mean wind model for low altitudes.

TURBULENCE

The reference recommends use of the Von Karman power spectra forms, which are identical to the spectra approximated by the filters in Section 1.4 except the reference employs the one-sided redefinition of the spectra, which have twice the gain of the literal two-sided spectra. That is, the reference defines the spectra such that

$$\sigma^2 = \int_0^\infty \Phi(\Omega)\, d\Omega$$

rather than

$$\sigma^2 = \int_{-\infty}^{\infty} \Phi(\Omega)\, d\Omega.$$

The reference also permits use of the Dryden spectra "... when it is not feasible to use the Von Karman form, ..." The reference also provides filters which, when modifying white noise, are to represent the Dryden spectra. However, in developing the filters, an error has occurred. The transformation to the time domain from the frequency domain (Fourier integral inversion) is:

$$x(t) = \int_{-\infty}^{\infty} \Phi(\omega)\, e^{i\omega t}.$$

Hence, no matter if a spectrum is defined as one-sided, the time simulation will treat its filter representation as corresponding to a two-sided spectrum. The effect of the reference's

filter representing a one-sided spectrum is to provide turbulence with a variance that is too high by a factor of two.

The reference describes rms vertical turbulence levels probabilistically in terms of the expected level as a function of altitude, the probability of encountering turbulence (also a function of altitude), and the Rayleigh distribution. The reference notes that "... The model described here neglects any effects on the turbulence due to terrain roughness, mean wind magnitude, or any other meteorological factor except height (altitude). This means that the model describes an average of all conditions for clear air turbulence." If the mean wind and mean wind shear are unimportant, the representation for rms vertical turbulence levels as provided by the reference would be satisfactory provided it could be ensured that the weighted average conditions yielding the statistical functions are representative for the applications to which the model is intended.

The reference shows an expected rms vertical turbulence level that is 6.7 ft/sec^2 at the surface and which declines slowly with altitude, similar to the variation provided by the proposed model.

The reference provides for determining horizontal turbulence levels from the condition of local isotropy,

$$\frac{\sigma_u^2}{L_u^{2/3}} = \frac{\sigma_v^2}{L_v^{2/3}} = \frac{\sigma_w^2}{L_w^{2/3}}$$

and the assumption of horizontal isotropy,

$$\sigma_u = \sigma_v$$

$$L_u = L_v$$

These same assumptions were used to develop the proposed model (Sec. 2.4.6). However, rather than specifying σ_w, $L_u = L_v$, and L_w then determining $\sigma_u = \sigma_v$ from the conditions of local isotropy as done in the reference, $\sigma_u = \sigma_v$, σ_w and L_w were specified and $L_u = L_v$ were determined from the condition of local isotropy in arriving at the proposed model.

The variation of the vertical turbulence integral scale with altitude is the same in the reference as in the proposed model ($L_w = h$) except the linear variation with altitude is continued to 2500 feet in the reference as opposed to 1000 feet in the proposed model. The reference notes that it chose 2500 feet because that value is currently being used in other military specifications (for high altitudes). Additionally, the reference notes that 1750 feet, used as the altitude above which the integral scales are invariant with altitude with its Dryden model, exceeds values commonly used in the past. The 1000-foot value used in the proposed model was found to agree more closely with low-altitude measurements.

The reference provides for horizontal integral scales that vary with the cube root of altitude. This variation is qualified by:

> "The variation of L_u and L_v at low altitudes according to the one-third power of altitude above ground level is simply a mechanism that forces the scales of the two horizontal components to be larger than the vertical scale. Although these formula produce the correct trends, there are little data available that can be used to substantiate the $h^{1/3}$ as used in MIL-F-8785B. It is merely a formula that produces reasonable results."

One bad feature of $h^{1/3}$ variation for L_u and L_v is that it causes rms horizontal turbulence levels to go to zero near the ground, although this may be no practical problem as an airplane's aerodynamic center is always substantially above the ground. In order for there to be a finite rms horizontal turbulence level at the surface as indicated by theory and measurements (Sec. 2.4.4), the variation of the horizontal turbulence integral scale with altitude must approach linear near the ground. This is a characteristic of the proposed model.

The observation in the reference that there is little good information concerning the variation of the horizontal integral scale with altitude is agreed with, and the variation resulting from the proposed model was also determined from a somewhat arbitrary interpolation formula, which provides for horizontal integral scales greater than vertical integral scales. The objectionable decrease of the horizontal rms turbulence level near the surface was overcome in the proposed model. Additionally, observations providing ratios of horizontal-to-vertical turbulence levels and integral scales of about 2 and 8 near the surface, respectively (Secs. 2.4.4 and 2.4.5), were matched.

The reference permits constant integral scales and variances equal to those at 500 feet to be used for landings. This simplification is not agreed with (Sec. 4.5.7).

The reference notes that:

> "Atmospheric turbulence should be described mathematically in an axis (coordinate) system related explicitly to the turbulence field itself; but instead, for MIL-F-8785B, the turbulence is described relative to the airplane body-axis system. . . . The implication of these assumptions [isotropy in horizontal planes only] is that flight paths must be within a degree or so of being horizontal near the ground; otherwise special consideration should be given to the non-isotropic and non-homogeneous nature of turbulence."

These comments are in agreement with the analysis in Section 4.3, which shows that generating turbulence directly in the body axis system causes turbulence vertical to the plane of the airplane to be greatly underestimated at low frequencies due to using statistical parameters of turbulence known only in an axis system attached to the mean wind. An exact method for the generating turbulence for flight simulation could not be found in Section 4.3, but rather than resigning to the airplane's body axis system as done in the reference, a better approximation was found: Generate turbulence in the plane of the earth but in an axis system aligned to the relative (to the air) velocity of the airplane, then

transform the turbulence to the body axis system. This method correctly aligns the statistical properties of turbulence and provides only a small error due to the misalignment of the spectra forms.

The reference provides a model to represent the distributed lift effects of turbulence, said to be based on the work of Etkin, which is reported in Section 4.2.1.3.3. Etkin approximated the turbulence field about an airplane with the first two terms of a Taylor series, expanded about the airplane's cg. For example, the vertical component of turbulence would be represented in the plane of the airplane by:

$$w_g(x,y) \cong w_{g_{CG}} + \left(\frac{\partial w_g}{\partial x}\right)_{CG} x + \left(\frac{\partial w_g}{\partial y}\right)_{CG} y.$$

The first-order derivatives are equivalent to introducing angular velocity components of turbulence:

$$\left(\frac{\partial w_g}{\partial x}\right)_{CG} = q_g, \left(\frac{\partial w_g}{\partial y}\right)_{CG} = -p_g.$$

These expressions become exact as frequency approaches zero, but very seriously overpredict the turbulent velocities away from the cg at high frequencies.

Etkin recognized this. In an attempt to alleviate the problem, he first formed the three-dimensional spectra of the derivatives in terms of the three-dimensional spectra for the cg turbulence velocities:

$$\Theta_{\frac{\partial w_g}{\partial x}\frac{\partial w_g}{\partial x}}(\Omega_x, \Omega_y, \Omega_z) = -\Omega_x^2 \Theta_{w_g w_g}(\Omega_x, \Omega_y, \Omega_z)$$

$$\Theta_{\frac{\partial w_g}{\partial x} w_g}(\Omega_x, \Omega_y, \Omega_z) = i\Omega_x \Theta_{w_g w_g}(\Omega_x, \Omega_y, \Omega_z).$$

The three-dimensional spectra are the Fourier integrals of the turbulence velocities described in three-dimensional space. Only one of the spacial frequencies, corresponding to the coordinate along the airplane's relative velocity vector, can be used to convert spacial frequency into time. To eliminate the other two coordinates, integrations are performed with respect to the transverse coordinates to successively obtain the two- and one-dimensional spectra;

$$\psi(\Omega_x, \Omega_y) = \int_{-\infty}^{\infty} \Theta(\Omega_x, \Omega_y, \Omega_z)\, d\Omega_z$$

$$\Phi(\Omega_x) = \int_{-\infty}^{\infty} \psi(\Omega_x, \Omega_y)\, d\Omega_y.$$

Etkin, rather than integrating from $-\infty$ to ∞, performed the integration over the frequency region for which the Taylor series approximation was valid. The airplane's vertical dimensions are generally small and the distribution of turbulence vertically are relatively unimportant, so he performed truncated integrations only for the lateral component of spacial frequency:

$$\Phi(\Omega_x) = \int_{-\Omega_{y_{max}}}^{\Omega_{y_{max}}} \psi(\Omega_x, \Omega_y)\, d\Omega_y.$$

The integration from $-\Omega_{y_{max}}$ to $\Omega_{y_{max}}$ is analogous to truncating the two-dimensional spectra at $\pm\Omega_{y_{max}}$, an arbitrary but convenient method of modifying the two-dimensional spectra. Using the Dryden spectral forms, only because of the simpler and more easily determinable results, Etkin obtained the one-dimensional roll-rate spectra on Figure 1C-1. Etkin reasoned that the truncation frequency, $\Omega_{y_{max}}$, could be estimated by assuming that a sine wave could be adequately represented by no less than eight straight line segments. Thus,

$$\Omega_{y_{max}} = \frac{2\pi}{8(b/2)} = \frac{\pi}{2b}.$$

Substituting this expression into the approximate roll-rate spectra from the reference yields

$$\Phi p_g = \frac{\sigma_w^2}{L_w} \frac{0.8(k_2'/2)^{1/3}}{1 + (2k_1/k_2')^2}$$

$$k_1 = L_w \Omega_x.$$

$$k_2 = L_w \Omega_{y_{max}}$$

Comparing the gain at zero frequency to those from Etkin's work on Figure 1C-2 shows that the approximate spectra seriously overestimates the Etkin low-frequency gain, being about 140% higher for large integral scales and/or high spacial frequencies and orders of magnitude too high for small integral scales and/or low spacial frequencies. Additionally, the shape of the approximate spectrum does not compare well with Etkin's spectra, as seen on Figure 1C-1.

More significant than the poor match of the approximate roll-rate spectrum is the conclusion from Etkin's latest book: *The Taylor Series method for lateral distributions is accurate to no higher lateral spacial frequencies than is the point representation. Representing turbulence roll rates provides no better results than does the point representation.* Etkin reached this conclusion by comparing and examining complex

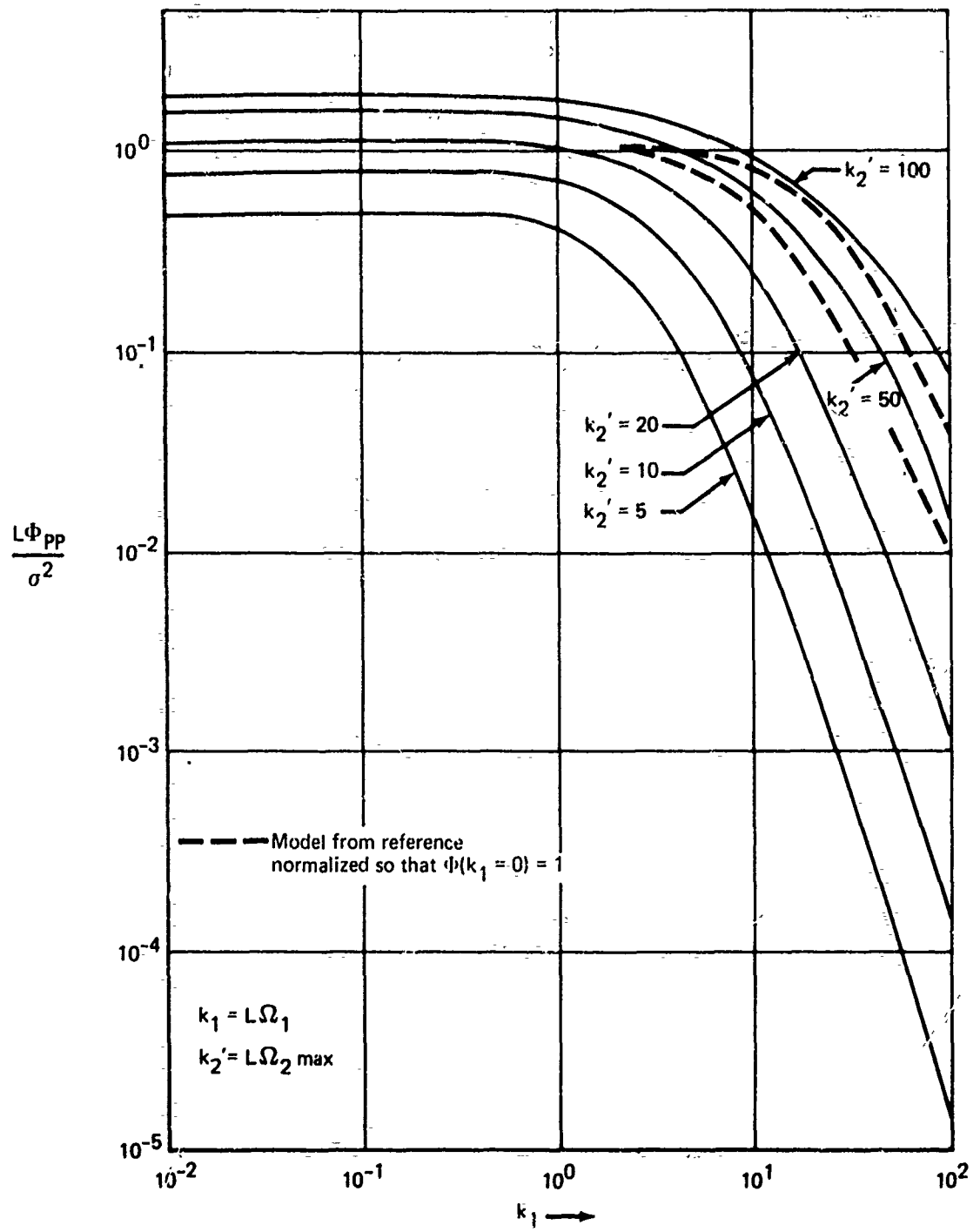

FIGURE 1C-1.–EFFECTIVE TURBULENCE ROLL RATE POWER SPECTRUM

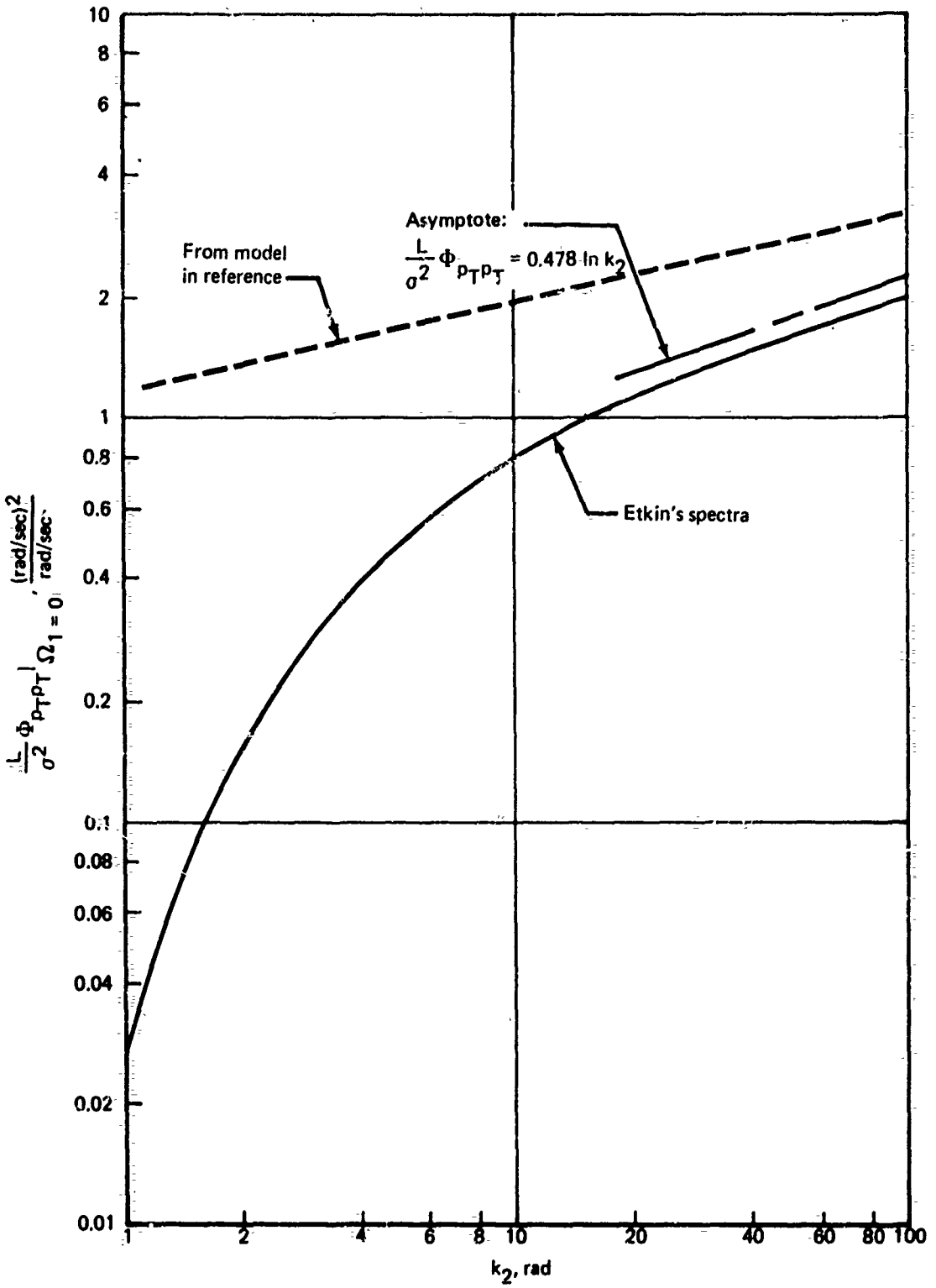

FIGURE 1C-2.–EFFECTIVE TURBULENCE ROLL COMPONENT LOW-FREQUENCY POWER SPECTRUM

amplitudes of force and moment components produced on a finite wing flying through a sinusoidal gust field. The Taylor series method was compared to an exact solution and the maximum frequency was set where the error reached 10%.

The Taylor series method increased the maximum frequency by a factor of 10 for the longitudinal distribution. That is, representing q_g and r_g provides an improvement. As a consequence, the spectra for turbulence pitch and yaw rates in the reference misses the point. Attenuating these spectra should not be performed for lateral dimensions, but for longitudinal dimensions. The one-dimensional spectra should be truncated for wavelengths less than eight times the airplane's tail arm.

Rather than truncating the spectra, the spectra were filtered at the maximum valid frequency in Section 4.2.1.3.3. This is no less arbitrary and more realistic as wings are unlikely to have a response to the effective angular components equal to that at zero frequency up to a given frequency and no response beyond. The filter forms for turbulence pitch and yaw rates become:

$$q_g = -\frac{1}{V_A}\left[\frac{S}{1+\frac{4}{\pi}\frac{\ell_H}{V_A}S}\right]w_g \qquad \text{(Fig. 1C-3)}$$

$$r_g = \frac{1}{V_A}\left[\frac{S}{1+\frac{4}{\pi}\frac{\ell_V}{V_A}S}\right]w_g \qquad \text{(Fig. 1C-3)}$$

where ℓ_H, ℓ_V = horizontal and vertical tail lengths

An approach that is accurate to higher frequencies is to provide separate wing and tail representations. The turbulence at the tail is that at the wing delayed by a transport lag equal to the time required to traverse the distance from the wing to the tail (ℓ/V_A). The distributions of turbulence over just the wing may then be represented by the Taylor series approach.

Although there are significant differences in application and modeling, the assumptions in the proposed turbulence model are the same as in the reference and, except for the dependence of turbulence upon the mean wing, the proposed turbulence model agrees more closely with the military specifications than with either the FAA or ARB models.

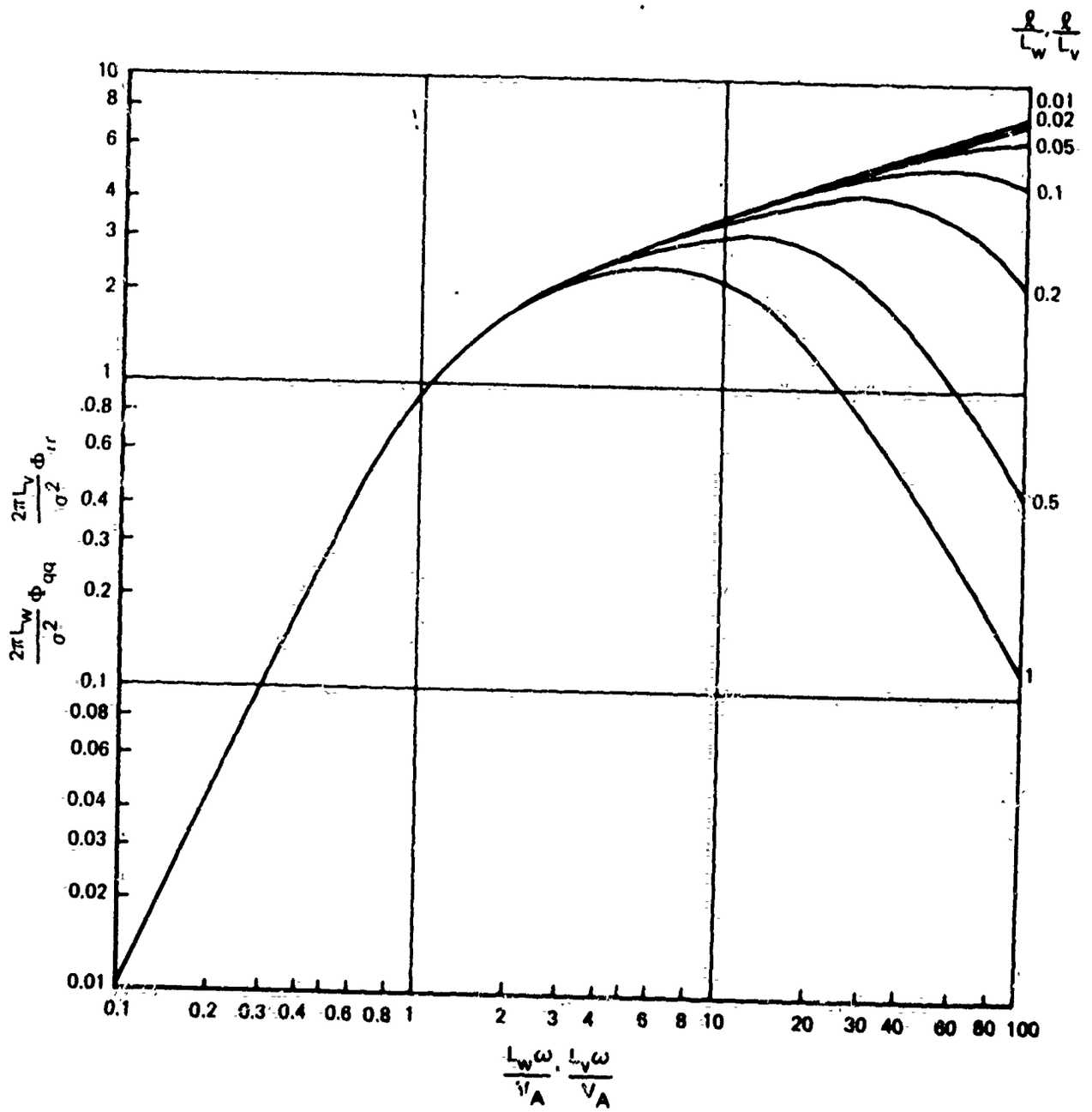

FIGURE 1C-3.--TURBULENCE PITCH AND YAW RATE SPECTRA

2.0 ANALYTIC DESCRIPTION OF LOW ALTITUDE WIND PHENOMENA

This section presents a review, comparison, and analysis of the descriptions of low altitude wind phenomena provided by the literature. The emphasis is on an analytic description that provides for continuity with respect to the parameters, as opposed to a qualitative description.

The objective of the analytic description is to provide a standard for developing, evaluating, and comparing flight simulation models. Although the resulting composite description may be unique, no new scientific work has been done. Rather, engineering judgment was applied to provide analytic descriptions leading to a simulation based on information supplied by the literature. The resulting description is a composite of work provided by many authors. Selection of one of several alternate or conflicting descriptions for a particular subject was based on the weight of evidence, quality of substantiation, appropriateness, and engineering judgment.

Much of the information presented is not restricted to any particular application. However, to restrict the magnitude of the task, it has been found necessary to restrict some of the subject matter to the application of interest. Thus, there are specializations to simulator usage, application to aircraft, and the performance of their autoland systems during the approach and landing phase, and low altitudes (below 1000 feet).

Additionally, the model is developed for the "average" airport. It is recognized that such an average probably does not exist, but when the distribution of airport characteristics and the appropriate weighting of each airport according to its activity are not available, "average" characteristics are selected.

Emphasis is on the more probable events (say, with exceedance probabilities less than 10^{-3}) rather than the extreme events (with probabilities of exceedance as remote as 10^{-9}). The implication is that the following discussion is not directed at flight-critical control system design. If an autoland system should fail, the pilot has recourse to manual control. If more remote and more severe levels of wind should occur, the pilot has recourse to landing at an alternate airport. For flight safety features that must be designed for extremely remote occurrences, critical values rather than average values should be selected, or perhaps a description for a single critical airport should be developed.

Analytic descriptions can be classified as either deterministic or stochastic. In actuality, all physical events are likely to be deterministic. However, when the deterministic relationships are unknown, are too complex, or when the relevant differential equations have not been solved, a stochastic description is used. A deterministic description enables parametric evaluation and understanding of the problem but generally has to be simplified, either merely to avoid complexity or because not all of the parameters and their effects are known. Stochastic descriptions have statistical parameters which, in turn, may be described deterministically or stochastically. Stochastic descriptions suffer from the inability to measure data for all combinations of events, incompatibility of measurement and application conditions, measurement inaccuracies, and data misinterpretations.

Stochastic descriptions are often misapplied. For example, if exceedance probability curves are given for the steady wind and for turbulence, how are the data to be combined? If the engineer is given a design probability, he might choose steady wind and turbulence levels so that the product of their exceedance probabilities is equal to the design probability, or he might choose levels so that the probability of each is equal to the design probability. The former approach implies zero correlation between the steady wind and turbulence while the latter approach implies perfect correlation, neither of which is likely to be valid. Even if he were given the correlation, he could not be sure that the correlation given applies for the conditions of interest. Thus, deterministic descriptions of stochastic processes are required.

The approach taken is to describe deterministically the effects of the important parameters to the greatest extent possible, i.e., so far as the parameters are measurable. Then, all the parameters are related to the smallest number of parameters possible so as to reduce the amount of knowledge required by the user. Ultimately, it is desired to relate all parameters to a single design probability, but this section will deal only with the description in terms of basic parameters.

It must be appreciated that a great number of simplifications are required to arrive at even the most complex description permitted by the state of the art. Discontinuities are not accounted for. To account for such things as low level inversion layers, inhomogeneous terrain, low level squalls and the like, geometrically increases the magnitude of the task and is generally beyond the state of the art.

This section begins with definitions and interrelationships of different classes of wind phenomena and then discusses what is known about each class. Although this section is intended to be independent of other sections, the material within the section is presented in building block format whereby the description of a topic is dependent upon description of previous topics.

2.1 NOMENCLATURE

$A(\Omega), B(\Omega)$	Scalar functions defining isotropic three-dimensional power spectrum
C_p	Specific heat at constant pressure
d	Atmospheric boundary layer thickness
e	Energy or exponential function
$E(\Omega)$	Energy spectrum function
f	Coriolis parameter, $f = 2\omega_E \sin \lambda$
$f(h/\ell')$	Universal function of h/ℓ' defining the incremental change of mean wind due to nonadiabatic thermal conditions

$f(\xi)$, $g(\xi)$	Fundamental longitudinal and transverse correlation functions for isotropic turbulence, respectively
$F(\xi)$, $G(\xi)$	Scalar function defining isotropic turbulence correlation functions
g	Acceleration due to gravity
G	Geostrophic wind speed
h, h_{REF}	Altitude, reference altitude
h_I	Altitude above which turbulence is isotropic
H	Heat flux, positive upward
k	Von Karman constant, k = 0.4
k	Ekman spiral parameter, $k = \sqrt{f/2km}$
k_H, k_M	Eddy conductivity and viscosity, respectively
$K_{1/3}(\ )$, $K_{2/3}(\ )$	Modified Bessel functions of the second kind of orders 1/3 and 2/3, respectively
ℓ, ℓ'	Monin-Obukov scaling length and that modified by ratio of eddy conductivity to eddy viscosity, $\ell' = k_H/k_M \ell$, respectively
L_P, L_N	Longitudinal and transverse integral scales for turbulence components parallel and normal to the displacement vector, respectively
L_u, L_v, L_w	Integral scales corresponding to the longitudinal, transverse, and vertical turbulence components, respectively
p	Pressure
$P\{\ \}$	Probability function
$\vec{r}$	Position vector
R	Gas constant
R_i	Gradient Richardson's number $R_i = \frac{g}{T}\left(\frac{dT}{dh} + \frac{g}{C_p}\right) / \left(\partial \bar{V}_W/\partial h\right)^2$
R_{ij}	Correlation function for the i and j turbulence components

$\hat{R}_{ij}$	Normalized correlation function, $R_{ij} = R_{ij}/\sigma_{ij}^2$
S	Entropy
s	Nondimensional mean wind shear; $s = \frac{kh}{u_{*_0}} \frac{\partial \bar{V}_W}{\partial h}$
t	Time
T	Absolute temperature
u_*, u_{*_0}	Friction velocity and friction velocity at the surface, respectively; $u_* = \sqrt{\tau/\rho}$
$u_P\ u_N$	Turbulence velocity components parallel and normal to the displacement vector
u, v, w	Velocity components along the x, y, and z axis, respectively
$\bar{V}_W, \bar{V}_{REF}$	Mean wind speed and mean wind speed at a reference altitude, respectively
V_A	Airspeed
x, y, z	Position components
z_0	Small-scale roughness length of surface topography
α, α_0	Heading angle between the mean wind and the geostrophic wind and heading angle between the surface wind and the geostrophic wind, respectively
α, α'	Log-linear mean wind profile constant and that constant modified by the ratio of eddy conductivity to eddy viscosity; $\alpha' = \frac{k_H}{k_M} \alpha$
$\beta(\ )$	Probability density function
β	Deacon wind profile exponent
γ, γ'	Mean wind profile constant for KEYPS equation and that modified by the ratio of eddy conductivity to eddy viscosity; $\gamma' = \frac{k_H}{k_M} \gamma$

$\Gamma(\ )$	Gamma function
ϵ	Rate of energy dissipation
$\vec{\xi}, \xi,$ ξ_1, ξ_2, ξ_3	Displacement vector, displacement magnitude and components of the displacement vector, respectively
θ	Potential temperature $\theta = \text{constant} \times \frac{T}{p^{R/C_p}}$
$\theta_{ij}(\vec{\Omega})$	Three-dimensional spectrum function for the i and j turbulence components
λ	Latitude
ρ	Density
$\sigma_{PP}^2, \sigma_{NN}^2$	Variances (square of standard deviation or root mean square) of turbulence components parallel and normal to the displacement vector, respectively
$\sigma_u^2, \sigma_v^2, \sigma_w^2$	Variances of turbulence components along the x, y and z axis, respectively
σ_{ij}^2	Covariance between the i and j turbulence components
σ_{uw}^2	Covariance between turbulence components along the x and z axis
τ	Time displacement
$\vec{\tau}, \tau$ τ_x, τ_y, τ_z	Shear stress vector, shear stress magnitude, and shear stress components along the x, y and z axis, respectively
$\phi(f_1, f)$	Indicator function; zero when $f \leq f_1$, one when $f > f_1$
$\phi(h/\ell')$	Universal function of h/ℓ' defining nondimensional wind shear; $\frac{kh}{u_{*_0}} \frac{\partial \bar{V}_W}{\partial h} = \phi(h/\ell')$
$\Phi_{ij}(\Omega_1)$	One-dimensional spectrum function for the i and j turbulence components

$\Phi_u(\Omega_1)$, $\Phi_v(\Omega_1)$, $\Phi_w(\Omega_1)$	One-dimensional spectrum functions for the u, v, and w turbulence components, respectively
$\Phi_{uw}(\Omega_1)$	One-dimensional cospectrum function for the u and w turbulence components
$\psi_{ij}(\Omega_1, \Omega_2)$	Two-dimensional spectrum function for the i and j turbulence components
ω	Temporal frequency
ω_E	Angular velocity of the earth
$\vec{\Omega}, \Omega,$ $\Omega_1, \Omega_2, \Omega_3$	Spacial frequency vector, spacial frequency magnitude, and components of the spacial frequency vector, respectively

2.2 CLASSIFICATION OF WIND PHENOMENA

By convention, wind phenomena are divided into three categories: discrete gusts, turbulence, and mean winds. However, the distinction between the three is not always clear.

Turbulence and mean wind are statistical quantities appearing in combination. A sample of wind fluctuations is divided into a constant bias about zero plus the deviations about the bias. The bias is the mean wind, assumed to be invariant. Deviations about the bias represent turbulence. The distribution of the fluctuations between mean wind and turbulence will be dependent upon the size of the sample. In a sample of a single data point, all the wind would be mean wind. If a large sample were broken into smaller samples, it could reasonably be expected that the mean value would vary between subsamples. In a sufficiently large sample, nearly all the fluctuation may be turbulence. This is the implication of Figure 2-1, where the widely quoted (Refs. 2-1, -2, -3, and -4, among others) Van der Hoven estimates of the intensity distribution (multiplied by frequency) with frequency are shown. The presumed existence of the distinct peaks leads to the standard distinction between turbulence and mean wind: turbulence is represented by the peak to the right and the mean wind is made up of the distribution at all lower frequencies. Technically, all the intensity of the mean wind should occur at zero frequency.

The definition of the mean wind is also relaxed to include deterministic variations of horizontal winds with altitude at low altitudes. Thus, to obtain a mean from a low-altitude sample, the sample must be collected at constant altitude.

By definition, the term "discrete gust" refers to a discontinuous, individual, and distinct sudden rush of air. In contrast with turbulence, it implies a deterministic fluctuation of wind. That is, a discrete gust has a specific physical shape definable in terms of certain parameters. Local variations of the mean wind may also be classified as discrete gusts. Thus, in a small sample of winds, there may be no distinction between a mean wind and a discrete gust.

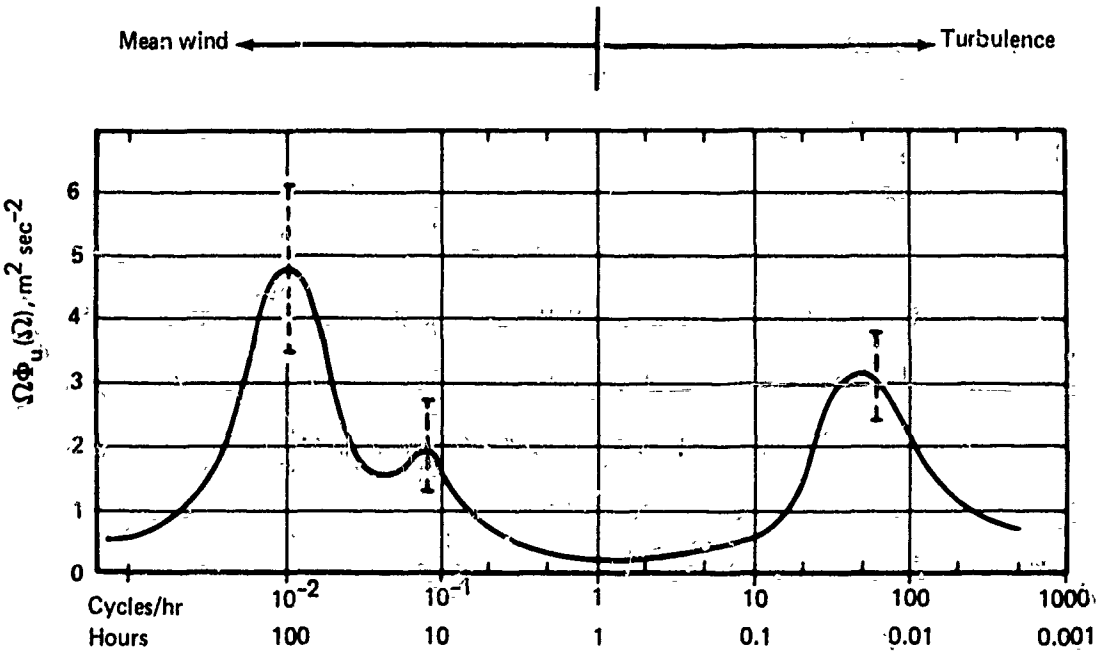

FIGURE 2-1.–SCHEMATIC SPECTRUM OF WIND SPEED NEAR THE GROUND ESTIMATED FROM A STUDY OF VAN DER HOVEN (1957)

The distinction between deterministic discrete gusts and random turbulence may also be difficult. A wind fluctuation may be deterministic in the extremely small scale but random on a much larger scale. In fact, turbulence may be represented by the random superposition of a large number of discrete gusts with varying shapes and magnitudes. In a sufficiently large sample, the contribution of a single discrete gust to the statistical characteristics of turbulence will be negligible. In a small sample, the effects will not be negligible and are difficult to separate out without prior knowledge of the existence of the discrete gust.

From the above discussion, it may appear that the difficulty in distinguishing the character of winds might be alleviated by using only large samples of winds. However, the wind characteristics must be defined in terms of analytic descriptions. In order to match the assumptions inherent in the analytic descriptions and to constrain variations in the large number of parameters, the sample size must be kept relatively small.

In this report, the analytic description of winds assumes the distinction between mean wind and turbulence provided by Figure 2-1. "Discrete gusts" refers to wind phenomena which are generated by local conditions not compatible with the assumptions of the analytic description of mean wind and statistical characteristics of turbulence.

2.3 MEAN WIND

From the definition of mean wind, two additional characteristics are deduced:

- Time variations of mean wind velocity relative to the earth are so slow that wind accelerations may be considered to be zero.
- Since winds due to local conditions have been classified as discrete gusts, the mean wind is considered to be homogeneous in the horizontal plane over the region of interest.

Definition of the mean wind, then, consists of defining the variation of the mean wind vector with altitude under various atmospheric conditions and for different terrain features. The significant classifications of atmospheric conditions are adiabatic (no vertical heat transfer) and nonadiabatic conditions. Under adiabatic conditions, the variation of mean wind with altitude, or the mean wind shear, is generated only mechanically. For the nonadiabatic conditions there is also a transfer of momentum through heat transfer.

Some general qualitative characteristics of mean winds in the atmospheric boundary layer can be deduced. As mean winds are either invariant with time, or are very slowly changing, there must be an equilibrium of forces acting on an element of air mass such that the time derivative of wind vector with respect to the earth is zero. The principal forces involved are:

- Coriolis
- Centrifugal
- Gravitational
- Pressure gradients
- Viscous
- Shear stresses

Coriolis and centrifugal forces result from inertial accelerations. If a particle of air is unaccelerated with respect to the earth, it must be accelerated with respect to an inertial reference system due to the angular velocity of the earth. These forces are actually only part of the expression for the acceleration of a particle in a rotating frame of reference derived in Reference 2-5 by:

$$\vec{a} = \vec{a}_0 + \frac{\vec{\delta^2 r}}{\delta t^2} + \frac{\vec{\delta \omega}}{\delta t} \times \vec{r} + 2\vec{\omega} \times \frac{\vec{\delta r}}{\delta t} + \vec{\omega} \times (\vec{\omega} \times \vec{r})$$

where

$\vec{a}_0$ = acceleration of center of earth with respect to space

$\frac{\vec{\delta 2}_r}{\delta t^2}$ = mean wind acceleration = 0

$2\vec{\omega} \times \frac{\vec{\delta r}}{\delta t}$ = Coriolis acceleration

$\vec{\omega} \times (\vec{\omega} \times \vec{r})$ = centrifugal acceleration

$\vec{\omega}$ = angular velocity of earth

$\vec{r}$ = radius of earth plus altitude to the point in question

The acceleration of the earth with respect to space is assumed to be negligibly small.

Centrifugal acceleration acts perpendicular to the axis of the earth and has a component normal to the earth that varies with the cosine of the latitude but is small at all latitudes compared with gravity. The component at constant altitude of the centrifugal acceleration varies with the sine of the latitude and is negligible near the equator.

Coriolis force is proportional to wind velocity. For constant velocity, it has a component normal to the earth that varies with the cosine of the latitude but is small at all latitudes compared with gravity for reasonable wind velocities. Its component tangent to the earth varies with the sine of the latitude.

To maintain homogeneous mean wind conditions, the latitude variation must be restricted so that changes in horizontal centrifugal and Coriolis force components are small compared to other forces.

Viscous forces oppose the motion of the particle and produce one type of shear stress. The magnitude of the viscous forces depends on the scale of the problem considered. If the scale is very small, molecular motion and viscosity is relevant. For mean winds, the scale is large and the relevant motion is the eddy motion, leading to eddy viscosity, which is on the order of 10^4 greater than molecular viscosity (Ref. 2-6). For the study of mean winds, eddy viscosity is relevant (Ref. 2-7).

Other shear stresses arise from the interaction of winds with the earth's surface, the influence of which can be expected to diminish with increased altitude, and temperature gradients which provide different levels of energy at different altitudes.

At the boundary condition at the earth's surface, there must be zero wind velocity. Thus, the wind must increase in some fashion, at least for small distances from the earth. At high altitudes away from the influence of the surface, the wind can be expected to tend toward a

value equal to the product of the earth's angular velocity and the distance from the earth due to the tendency of a mass to remain fixed in space in the absence of forces. Such a wind would blow from east to west.

The mathematical relationships between the parameters influencing the horizontal components of the mean wind are provided by the equations of motion derived from the Navier-Stokes equations and are, as taken from Reference 2-4:

$$\frac{d\bar{u}}{dt} = 0 = f\bar{v} - \frac{1}{\rho}\left[\frac{\partial p}{\partial x} - \frac{\partial \tau_x}{\partial z}\right]$$

$$\frac{d\bar{v}}{dt} = 0 = -f\bar{u} - \frac{1}{\rho}\left[\frac{\partial \bar{p}}{\partial y} - \frac{\partial \tau_y}{\partial z}\right]$$

where f is the Coriolis parameter describing the variation of the force: $f = 2\omega_E \sin\lambda$. Horizontal components of centrifugal acceleration are neglected. The primary difficulty in solving for the mean wind components is in describing the variation of the shear stress components, τ_x and τ_y, with altitude (z).

Three major analytic descriptions of the mean wind in the earth's boundary layer for adiabatic conditions will be discussed: the Ekman spiral, the logarithmic profile, and the power law. Additionally, the theory of the logarithmic profile has been expanded to include nonadiabatic conditions.

2.3.1 Ekman Spiral

The Ekman spiral describes the variation of the components of mean wind with altitude from the top of the boundary layer to the surface for the following rather restrictive assumptions:

- Motion is horizontal
- Flow is laminar (zero turbulent stresses)
- Isobars are straight, parallel, and constant with altitude
- Above the boundary layer, the wind (geostrophic wind) is constant with altitude
- Eddy viscosity and density are constant with altitude
- Temperature conditions are adiabatic

2.3.1.1 Derivation

The assumptions of constant winds above the boundary layer, the character of the isobars, and constant density leads to constant shear stresses above the boundary layer through the equations of motion and defines the components of the geostrophic wind:

$$G \cos \alpha_0 = -\frac{1}{\rho f} \frac{\partial \bar{p}}{\partial y}$$

$$G \sin \alpha_0 = \frac{1}{\rho f} \frac{\partial \bar{p}}{\partial x}$$

where the axis system is aligned with the x axis along the direction of the surface wind and α_0 is the angle between the geostrophic and surface winds. The equations of motion now reduce to

$$-f(\bar{v} - G \sin \alpha_0) = \frac{d\tau_x}{dz}$$

$$f(\bar{u} - G \cos \alpha_0) = \frac{d\tau_y}{dz}$$

The assumption of laminar flow permits a simple relationship between shear stress and velocity components:

$$\tau_x = k_M \frac{\partial \bar{u}}{\partial z}$$

$$\tau y = k_M \frac{\partial \bar{v}}{\partial z}$$

where k_M is the coefficient of eddy viscosity, which has been assumed to be constant with altitude. Substitution into the equations of motion yields the differential equations

$$\frac{\partial^2 \bar{u}}{\partial z^2} + \frac{f}{k_M} \bar{v} = \frac{f}{k_M} G \sin \alpha_0$$

$$\frac{f}{k_M} \bar{u} - \frac{\partial^2 \bar{v}}{\partial z^2} = -\frac{f}{k_M} G \cos \alpha_0$$

Assuming the form of the solution as

$$\bar{u} = A + B e^{\lambda z}$$

$$\bar{v} = C + D e^{\lambda z}$$

yields a solution for λ of

$$\lambda^4 = -\left(\frac{f}{k_M}\right)^2$$

or

$$\lambda = \begin{cases} \pm\sqrt{\frac{f}{k_M}}\,(1+i) \\ \pm\sqrt{\frac{f}{k_M}}\,(1-i) \end{cases}$$

Only the roots which satisfy the condition of a finite wind speed are retained. Applying the boundary condition of zero velocity at zero height leads to the solution given in Reference 2-6 for an axis system rotated to align the x axis with the geostrophic wind:

$$\bar{u} = G\left|1 - e^{kz}\cos kz\right|$$

$$\bar{v} = G\,e^{-kz}\sin kz$$

where

$$k = \sqrt{\frac{f}{2k_M}} = \sqrt{\frac{\omega_E \sin\lambda}{k_M}}$$

The resulting profiles of the wind vector magnitude and heading are shown on Figure 2-2. The magnitude provides a shear that increases with decreasing altitude. The heading change with altitude is near linear at low altitudes and rotates counterclockwise with decreasing altitude in the northern hemisphere. The solution provides a heading that approaches the geostrophic wind heading asympotically. The total heading change is 45°.

2.3.1.2 Description

This phenomenon is described in Reference 2-8 by a tendency of the wind "to align itself with the pressure gradient (from high to low) near the ground, and to align itself with the Coriolis-produced 'cyclone swirls' (that are perpendicular to the pressure gradient) at higher altitudes." This effect is described on Figure 2-3.

The "cyclone swirls" are generated in part by the shear at a constant altitude produced by the reduction of the Coriolis effect toward the equator. The alignment of winds perpendicular to the pressure gradient is caused by a balance between the pressure gradient and the centrifugal acceleration. As the altitude decreases, the viscous forces increase, slowing the wind down, reducing the centrifugal forces, and causing the wind to turn toward the pressure gradient.

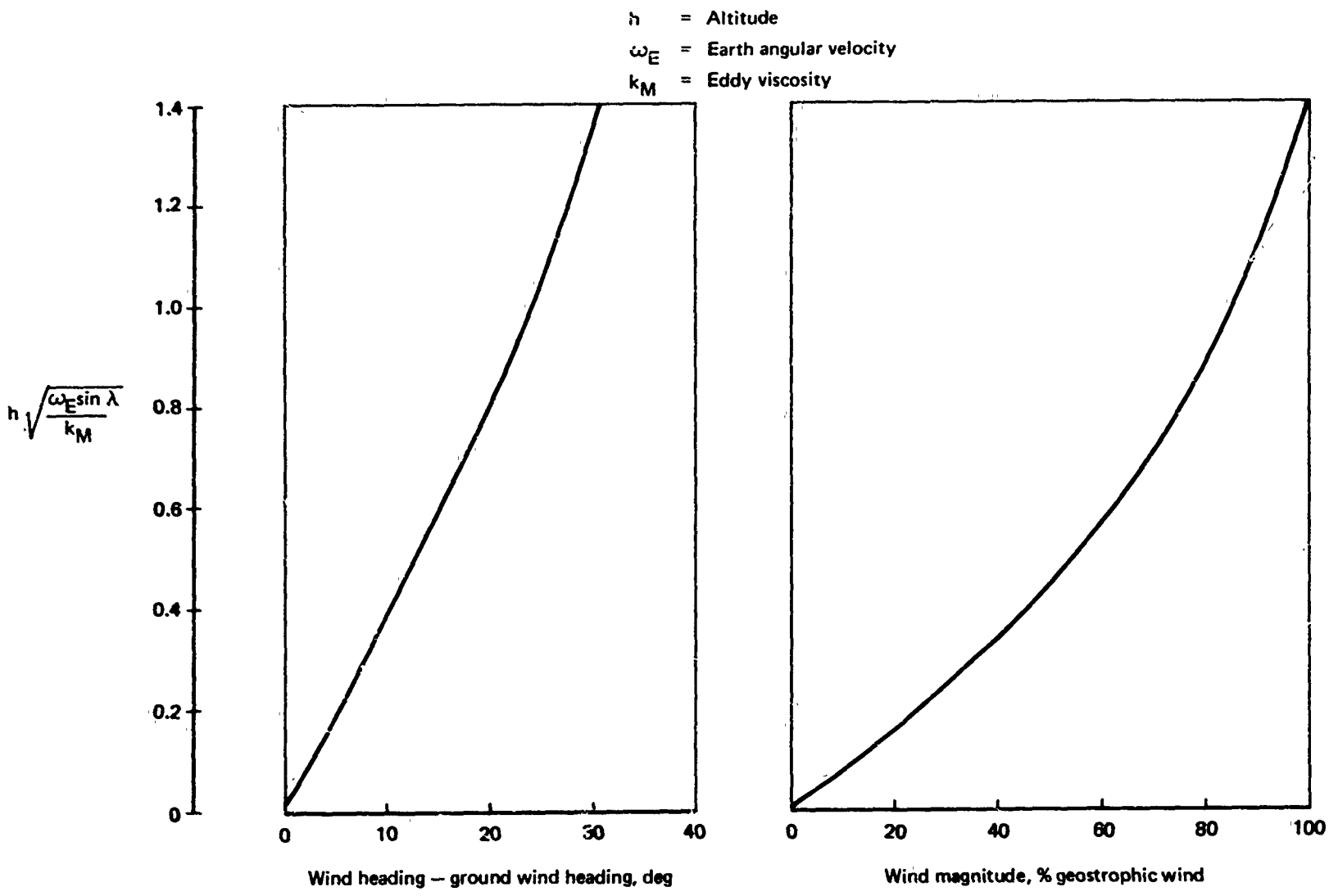

FIGURE 2-2.—WIND PROFILE, EKMAN SPIRAL

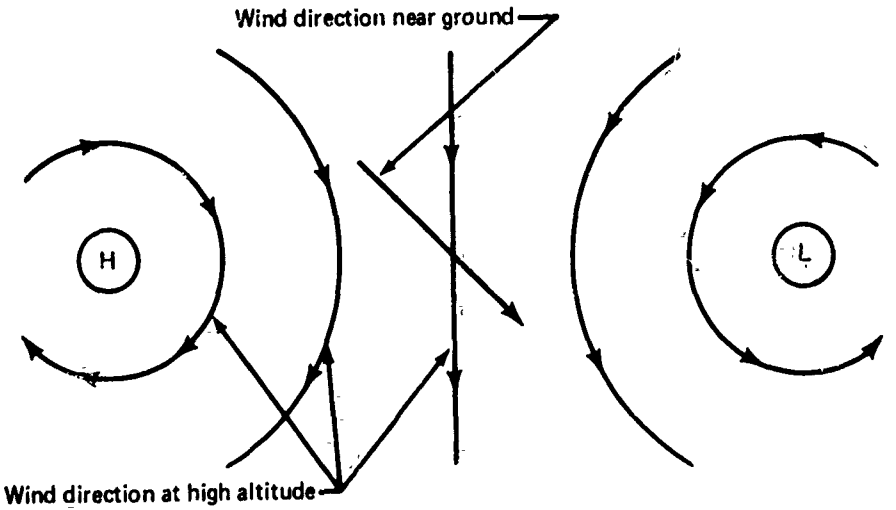

FIGURE 2-3.–IDEALIZATION OF WIND DIRECTIONS NEAR THE GROUND AND AT HIGH ALTITUDE (NORTHERN HEMISPHERE)

The severity of a wind shear component will be dependent upon the magnitude of the geostrophic wind and the depth of the boundary layer. From the altitude scaling factor on Figure 2-2, it can be deduced that the boundary layer thickness must be inversely proportional to the latitude (or Coriolis factor, f). Thus, the thickness would be infinite at the equator, invalidating the solution there. Reference 2-9 provides such an inverse relationship (boundary layer thickness $\sim f^{-1}$). For moderate latitudes, ($f = 1.14 \times 10^{-4}$/sec) the thickness is given at about 3500 feet for adiabatic conditions.

The conditions required for the solution of the Ekman spiral are seldom met. Reference 2-9 notes that a 45° turning angle exceeds any observed, and at moderate latitudes the angle does not exceed 23°. It additionally notes that the solution for the Ekman spiral is particularly poor for turbulent flow (assumed not to exist). The assumption of constant eddy viscosity is probably quite poor near the ground as the eddy size, to which eddy viscosity is proportional, is constrained by the presence of the ground. Finally, the assumption of straight isobars would restrict the size of the field to which the solution would be applicable, depending on the distances to the high and low pressure centers.

The idealized Ekman spiral solution is valuable, however, for the qualitative description and understanding of wind profiles in the boundary layers. It shows the probable existence of mean wind heading changes and increased change of wind magnitudes with lower altitudes that diminish in severity as the equator is approached.

2.3.2 Logarithmic Profile

The logarithmic wind profile is the most widely accepted form describing the altitude variation of mean wind in the lower part of the boundary layer. It is reported in References 2-1, -4, -6, -7, -9, and -10 through -14, among others. The derivation assumes that near the ground

- Shearing stress and pressure gradient are independent of height
- Coriolis force is negligible compared to other forces
- Pressure force can be neglected with respect to viscous forces
- The flow is fully rough; thus, molecular viscosity is not a significant parameter

The assumptions of constant shearing stress and pressure gradient are validated simply by restricting the maximum height under consideration until the variations fall within tolerance. The assumption of constant stress leads to the consequence that near the ground the heading must be constant, and permits the definition of a "friction velocity," u_{*_0}, given by

$$u_{*_0} = \sqrt{\frac{\tau_0}{\rho}} \text{ (measured at the surface)}$$

that remains constant with height. The assumption that the flow is fully rough is validated by not applying the law to extremely small heights, which is relative to the scale of the surface roughness.

2.3.2.1 Development and Description

The only parameters in the equations of motion and in the identification of shear stress remaining are wind shear, altitude, and friction velocity. Panofsky (Ref. 2-7), who states that there are many derivations of the law and that the solution is insensitive to the manner of its derivation, uses dimensional analysis (similarity theory) to show that these parameters must be related by

$$\frac{\partial \bar{V}_W / \partial z}{u_{*_0}} = \frac{1}{kz}$$

where k is a constant of proportionality (Von Karman's constant, equal to 0.4). Integration yields

$$\bar{V}_W = \frac{u_{*_0}}{k} \ln\left(\frac{z}{z_0}\right)$$

or, if the axis system is translated to coincide with the ground,

$$\bar{V}_W = \frac{u_{*_0}}{k} \ln\left(\frac{z + z_0}{z_0}\right)$$

The logarithmic profile is thus derived by assuming that the wind shear magnitude is inversely proportional to altitude. Although the profile formally goes to zero at zero height,

the equation is theoretically valid only when height is large compared to the surface roughness reflected by z_0, the roughness length or height.

The logarithm coefficient need not be calculated directly for modeling. Rather, a reference height at which the mean wind is known is used to extrapolate for all other altitudes:

$$\bar{V}_W = \bar{V}_{REF} \frac{\ln\left(\frac{h + z_0}{z_0}\right)}{\ln\left(\frac{h_{REF} + z_0}{z_0}\right)}$$

Using this form, the mean wind profile is plotted on Figures 2-4 and 2-5 and the corresponding wind shear is plotted on Figure 2-6, all for a reference height selected at 20 feet. An increase in roughness length is seen to cause an increase in wind shear at all altitudes. Small roughness lengths tend to cause a nearly constant mean wind speed down to low altitudes.

2.3.2.2 Roughness Length

Several authors have attempted to associate the roughness length with types of topography. A summary of the results of their studies is provided on Figure 2-7. Reference 2-9 points out that the roughness length may change with wind speed. For example, higher wind levels over water will introduce larger waves, causing an increase of roughness length. On the other hand, vegetation will bend more in high winds, reducing the roughness length, with the effect more significant for taller crops.

For "average" conditions, Reference 2-9 provides a rule of thumb that the roughness length is 15% of the crop height. Reference 2-13 disagrees, however, and recommends 3-1/3% of the "average dimension of the typical roughness particle on the surface," although "this ratio of roughness length z_0 to the actual roughness may show a rather wide range of values." The 3-1/3% relationship is supported by Reference 2-6, but is only applied to very small roughness particles (sand).

The mean wind profile is influenced not only by the terrain immediately below, but also by upwind topography. Thus, for a specific landing field, the effective roughness length will be a function of wind heading. Such is the manner that roughness lengths are presented in Reference 2-15 for the Kennedy Space Center. Perhaps it can be expected that roughness lengths will be greater for winds across runways than down runways.

The special case of a sharp transition in surface roughness along a line perpendicular to the wind direction has been treated in References 2-16, -17, and -18. An internal boundary layer height downwind of the transition is defined, below which the mean wind profile is influenced by the downwind topography. The internal boundary layer height increases with

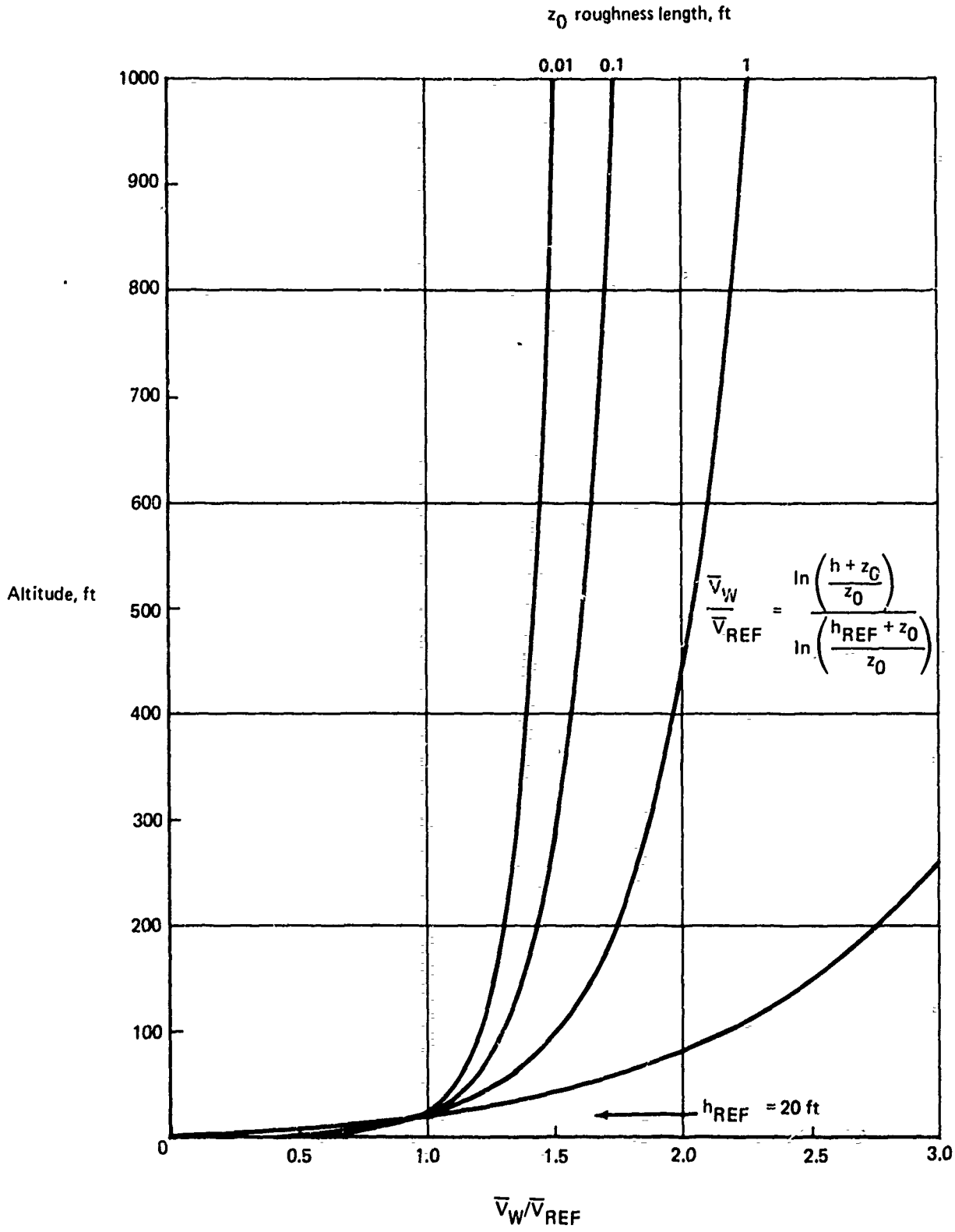

FIGURE 2-4.–MEAN WIND PROFILE

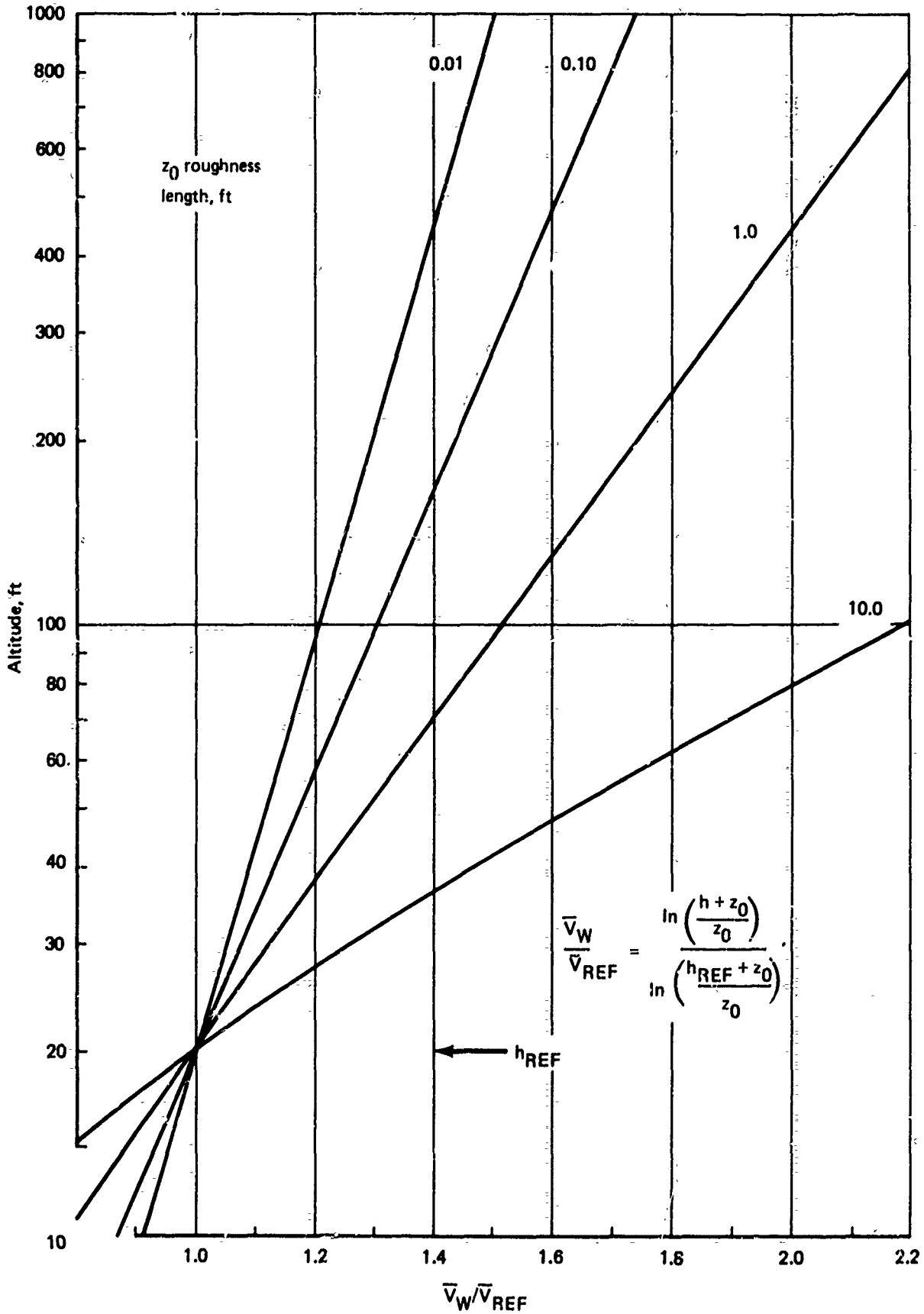

FIGURE 2-5.—LOGARITHMIC MEAN WIND PROFILE

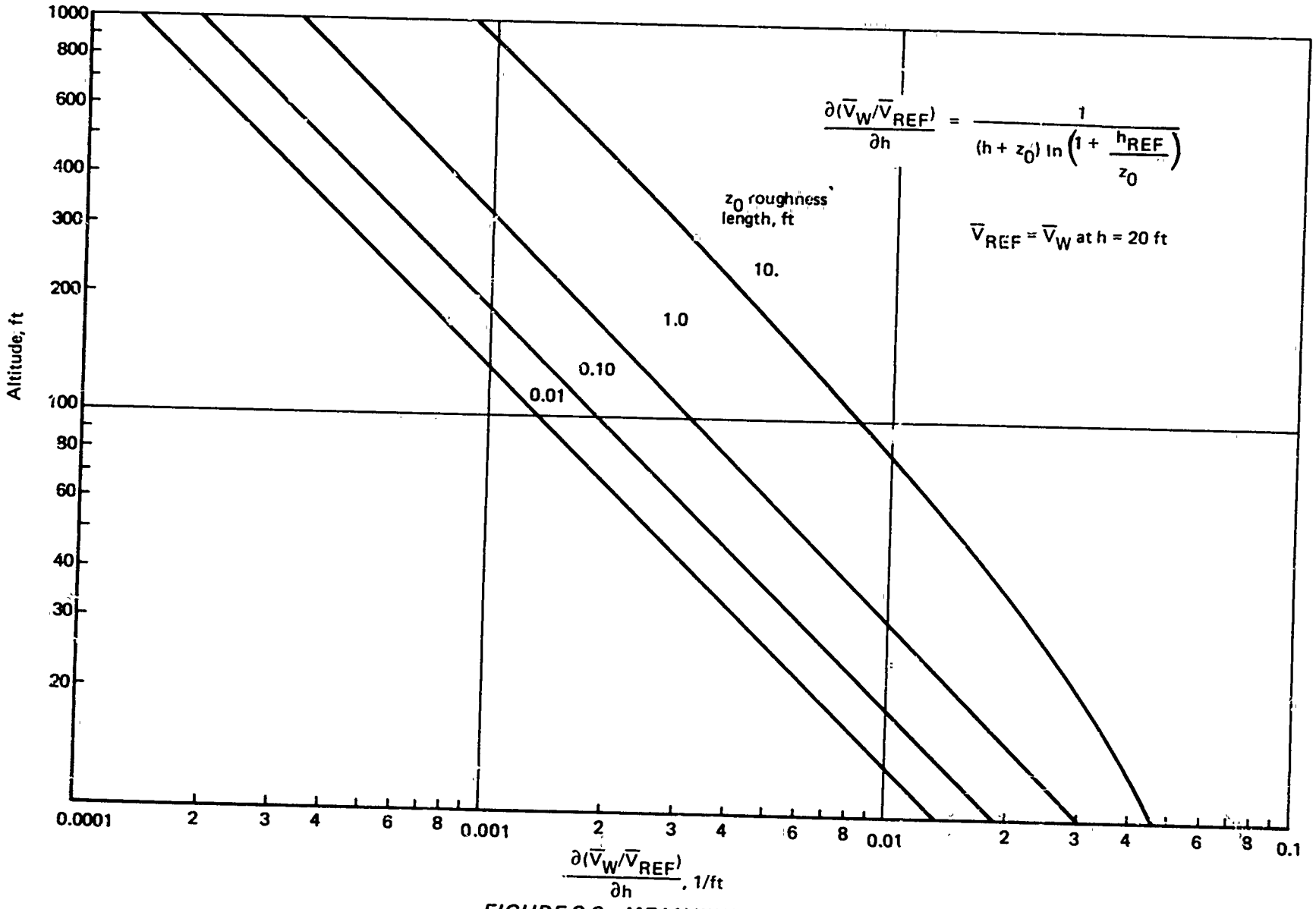

FIGURE 2-6.—MEAN WIND SHEAR

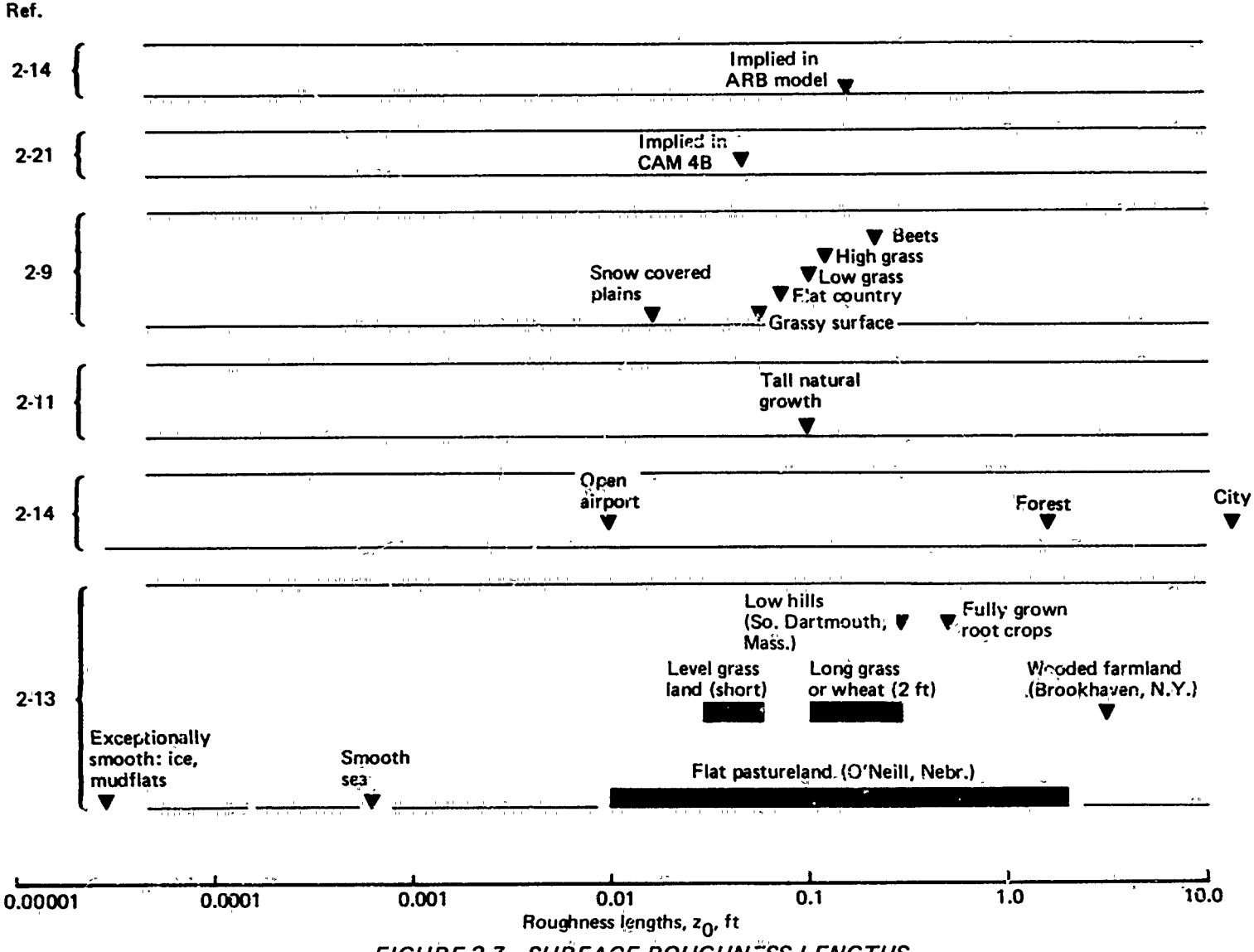

FIGURE 2-7.–SURFACE ROUGHNESS LENGTHS

the downwind distance from the transition. The solution, however, is too restrictive for general application, but future work may lead to significant analytic descriptions.

2.3.2.3 Minimum Valid Altitude

The altitude range for which the logarithmic flow is valid is dependent on the error the user is willing to tolerate. The literature, however, does provide some guidelines. To maintain the assumption of fully rough flow, the minimum altitude must be much greater than the roughness length. Reference 2-9 states that the minimum altitude should be twice the height of the crops, or using the relationship that the roughness length is 15% of the crop height, about 13 times the roughness length. Reference 2-14 states: "It is generally accepted that in neutral conditions, the wind profile between 10 feet and 300 feet may be given by [the logarithmic profile]." The statement is made without regard to any specific roughness length, but a roughness length of 0.15 feet is later recommended. Reference 2-13 states that the logarithmic profile should be good to two or three times the roughness length (for a roughness length of 3 feet).

The relevant altitude to compare with the minimum altitude for applying the logarithmic profile is that near the height of the wing chord plane with the airplane on the ground. For "average" airport conditions with the roughness length at about 0.15 feet as used in the Air Registration Board model in Reference 2-14, there will normally be no problem. If the roughness length is relatively large compared to the wing chord plane, there may still be no problem if the time spent below the minimum altitude of validity is small, particularly since the trend provided (reduced mean wind speed with reduced altitude) is correct. For extreme roughness, such as that occurring while flying within an area influenced by buildings, the problem becomes that of a discrete gust.

2.3.2.4 Maximum Valid Altitude

As stated in Reference 2-9, unambiguous evidence for establishing the upper altitude limit for application of the logarithmic profile is not available. Several authors have, however, estimated the upper limits by testing the assumptions leading to the derivation of the profile.

It can be recognized that when the altitude is very high with respect to the roughness length, the surface roughness will have only a weak influence and should not be included as a parameter. Thus, perhaps the maximum altitude is a multiple of the roughness length, z_0. Reference 2-13 states that the logarithmic profile is accurate to altitudes of the order of 1000 times z_0 (150 feet for $z_0 = 0.15$ as implied in the model of Ref. 2-14).

More commonly, the upper altitude limit is tied to a total change of the shearing stress (the profile assumes constant shear stress). Reference 2-4 estimates a 100-foot limit at moderate latitudes for a 10% total change of shear stress. Reference 2-7 provides an upper limit range of 65 to 650 feet for a 20% change in shear stress.

Reference 2-9 adds the level of turbulence as an additional parameter for determining the upper limit of validity. It is noted that the logarithmic law holds for the lower 15% of the boundary layer for flow over a flat plate but to the center of the pipe for pipe flow,

analagous to the entire boundary layer. Thus, it is deduced that the upper limit increases with the level of turbulence (pipe flow is more turbulent). As a consequence, the logarithmic profile should extend to above 15% of the earth's boundary layer or to above 525 feet for the 3500-foot boundary layer at moderate latitudes previously discussed. A 10% shear stress change criterion was applied.

Reference 2-15 applies the logarithmic profile to the first 100 feet, and Reference 2-14 specifies 300 feet without qualification. Tower data have been evaluated in Reference 2-19, and the logarithmic profile is found to hold up to 100 feet, the highest level for data measurement.

The effect of changing shear stress on the mean wind profile is not clear. It may be assumed that some change of wind heading may occur. If, for small shear stress changes, the logarithmic profile is accurate, then because the mean wind and the mean wind shear are proportional to the square root of the shear stress (through the friction velocity), the error in mean wind and mean wind shear would be approximately half the change in shear stress. Thus, a 10% change in shear stress may be too restrictive, and the upper limit for application of the logarithmic profile associated with a 10% change may be too low.

Application of the logarithmic profile at the extreme upper end of the boundary layer must certainly be criticized, for there it would generate the geostrophic wind from surface conditions. The literature (Refs. 2-4 and 2-9) has overcome this objection by dimensional analysis in the "overlap" region, the region that is influenced by both the surface winds and the winds near the upper part of the boundary layer. By equating dimensionless universal functions for the mean wind above and below the overlap region, the logarithmic profile is again found to be valid but, additionally, relationships between the components of the geostrophic wind and the friction velocity, u_{*_0}, are found. The implication is that the logarithmic profile extends somewhat beyond the region of constant or nearly constant shear stress, particularly if the constant heading restriction is not maintained.

An additional rationale can be made for extending the logarithmic profile beyond the constant stress region very near the surface for approach and landing applications. If it can be accepted that aircraft motion performance parameters are most important when measured at or near touchdown, then it can be reasoned that the most important wind characteristics are for altitudes near the surface and that errors in the wind description are less important as the altitude at which they occur increases. This is particularly true since at higher altitudes the adiabatic mean wind shear diminishes. Large errors in the description of a small shear may be insignificant.

Combining the arguments, it appears reasonable to extend the logarithmic mean wind profile to 1000 feet altitude for approach and landing applications.

2.3.3 The Power Law

An empirical relationship for the wind profile over the entire boundary layer that is widely used, particularly in meteorology, is the power law. It simply extrapolates the mean wind measured at one altitude to all other altitudes by altitude raised to some power:

$$\frac{\bar{V}_W}{\bar{V}_{REF}} = \left(\frac{h}{h_{REF}}\right)^p$$

This description is often preferred because of the simplicity of its form.

For adiabatic conditions, the exponent will depend strongly on the surface roughness and, according to Reference 2-20, slightly on the magnitude of the mean wind. Surface roughness may cause the exponent to vary from something greater than zero to unity. The shear consequently increases less strongly with decreasing altitude than the inverse relationship for the logarithmic profile.

2.3.3.1 Exponent Value

Average values of the exponent are often quoted for three classifications of surface roughness: smooth, moderate, and rough. "Smooth" applies to water, open country, prairie grassland, tundra, and the like. "Moderate" is used with respect to wooded countryside, parkland, towns, and the outskirts of large cities. "Rough" denotes the centers of large cities. The exponent is increased for increased surface roughness.

Panofsky, who has contributed greatly to the development of the logarithmic profile, is said in Reference 2-1 to have recommended exponents of 0.12, 0.25, and 0.38 for the three classifications. Davenport (Ref. 2-20) summarizes his more complete study (shown in Table 2.1) with exponents of 1/3, 1/3.5, and 1/2.5. Davenport's results are often quoted (Refs. 2-3 and 2-9).

The 1/7 exponent is the familiar value used for aircraft approach and landing, perhaps because it is the aircraft design value specified in Reference 2-21 for civil operations. Reference 2-22 also affirms that 1/7 is a "typical" value.

The influence of a magnitude increase of "surface" winds on the exponents is described in Reference 2-20 as an increase of 0.02 for each 10 miles per hour of wind. Reference 2-14 disagrees and prescribes an inverse relationship between the exponent and wind speed for the extrapolation of winds with altitude at the Kennedy Space Center from winds at 18 meters:

$$p = \frac{b}{(u_{18})^{3/4}} \quad (u_{18} \sim \text{m/sec})$$

(b is normally distributed; $b = 0.52 \pm 0.36$)

By comparison, the wind level affects the logarithmic profile only through the roughness length. For winds over land, it is expected that increased winds reduce roughness (through the bending of vegetation) and percentage changes of wind with altitude, analogous to a reduced exponent. The difference in the trends of exponents with wind speed may be explained by differences in the altitude range for which the winds are being curve fitted.

TABLE 2-1.—INFLUENCE OF SURFACE ROUGHNESS ON POWER LAW EXPONENT[a]

Source	Location	Upper limit of investigation (ft)	Description of terrain in site locality	P	Remarks
Goptarev	Caspian Sea (off Apsheron Peninsula)	166	Coastal waters of inland sea	1/10.5	
Juul	Masbedsund, Denmark	182	Flat shore on "Ocean of Small Islands"	1/8.5	
Scrase	Salisbury Plain, England	43	Open grassland without hedgerows or trees	1/7.7	
Wing	Ballybunion, Ireland	492	Flat treeless grassland, Atlantic Ocean 1/2 mile distant	1/7.4	
Sherlock	Ann Arbor, Michigan, U.S.	250	Open, slightly rolling farmland	1/7	
Taylor	Salisbury Plain, England	–	Open grassland without hedgerows or trees	1/7	
Giblett	Cardington, Beds., England	150	Open level agricultural land with only isolated trees	1/7.8	
Frost	Cardington, Beds., England	350	Same as above	1/5.9	
Frost	Cardington, Beds., England	1000	Same as above	1/6.7	
Deacon	Sale, Victoria, Australia	503	Gently rolling grazing land with few trees	1/6.25	
Heywood	Leafield, Oxfordshire, England	313	Open fields divided by low stone walls and hedges	1/5.9	
Kamei	Japan	–	Rough coast	1/5	Observations not necessarily typical of level country
Wax	Orkney Islands	118	Flat-topped grass hill, 1/3 mile inland from high cliff overlooking the sea	1/4.6	
Huss and Portman	Akron, Ohio, U.S.	352	Gently rolling country with many bushes and small trees	1/4.55	
Francken-berger and Rudloff	Quickborn, Germany	230	Relatively level meadowland but with numerous hedges and trees around the small fields	1/4.35	

[a]From Reference 20

TABLE 2-1.—Concluded

Source	Location	Upper limit of investigation (ft)	Description of terrain in site locality	P	Remarks
Smith	Upton, Long Island, New York, U.S.	410	Level country uniformly covered with scrub oak and pine to a height of 30 ft	1/4	Hurricanes Carol and Edna 1954 (fastest 1-min mean speed)
Panofsky	Upton, Long Island, New York, U.S.	410		1/3.85	
U.S. Weather Bureau	Upton, Long Island, New York, U.S.	410		1/3.3	
U.S. Weather Bureau	Upton, Long Island, New York, U.S.	410		1/2.9	(Fastest 6-min mean speed)
Kamei	Japan	–	Three Japanese towns	1/3	
Dines	Farnborough, England	1650	Wooded and treed farmland	1/2.8	
Jensen	Copenhagen, Denmark	242	Center of a large city	1/2.3	
Taylor	Paris, France (Eiffel Tower)	900	Center of a large city	1/2	
Rathbun	New York (Empire State Building)	1263	Center of a large city	1/1.6	

2.3.3.2 Relationship with Logarithmic Profile: Conditions for Validity

Skelton has shown (Ref. 2-1) that the power law can be derived from the logarithmic profile. From the equations for the wind at any altitude and at a reference altitude,

$$\bar{V}_W = \frac{u_{*0}}{k} \ln\left(\frac{h + z_0}{z_0}\right)$$

$$\bar{V}_{REF} = \frac{u_{*0}}{k} \ln\left(\frac{h_{REF} + z_0}{z_0}\right)$$

A difference equation as a fraction of the wind speed at the reference altitude is formed:

$$\frac{\bar{V}_W - \bar{V}_{REF}}{\bar{V}_{REF}} = \frac{\ln\left(\frac{h + z_0}{h_{REF} + z_0}\right)}{\ln\left(\frac{h_{REF} + z_0}{z_0}\right)}$$

or

$$\exp\left[\frac{\bar{V}_W - \bar{V}_{REF}}{\bar{V}_{REF}}\right] = \left[\frac{h + z_0}{h_{REF} + z_0}\right]^p$$

The exponential is represented by the first two terms of its power series:

$$e^a = 1 + a + \frac{a^2}{2} + \frac{a^3}{6} + - - - -$$

$$\cong 1 + a \qquad \text{for } a \ll 1$$

Thus, if

$$\frac{\bar{V}_W - \bar{V}_{REF}}{\bar{V}_{REF}} \ll 1$$

$$\frac{\bar{V}_W}{\bar{V}_{REF}} \cong \left[\frac{h + z_0}{h_{REF} + z_0}\right]^p$$

or if, in addition, the roughness length is always small compared to the reference altitude and the altitude in question

$$\frac{\bar{V}_W}{\bar{V}_{REF}} \cong \left(\frac{h}{h_{REF}}\right)^p$$

where

$$p = \frac{1}{\ln\left(\frac{h_{REF} + z_0}{z_0}\right)} = \frac{u_{*_0}/k}{\bar{V}_{REF}}$$

If the logarithmic profile is accepted as valid for low altitude, then the above derivation leads to the following conditions for the validity of the power law:

- The wind velocity must not differ excessively from that at the reference altitude. An error of 20% of the wind speed would correspond to a deviation from the wind speed at the reference altitude of ±44.7%, as estimated from the third term in the exponential power series. This restriction most severely restricts the altitude range for rough terrain.

- The exponent for the power law varies approximately with the ratio of reference altitude to roughness length. The reference wind speed must be evaluated at the same altitude as the exponent.

- The altitude to which the wind speed is extrapolated and the reference altitude must both be large with respect to the roughness length.

- All other restrictions applied to the logarithmic profile apply to the power law.

As an example, if the wind speed is known at 20 feet altitude and the roughness length is 0.15 feet, the value used in Reference 2-14, the wind speed error will be less than 20% for $2 < h < 180$ feet. A 20% error in the shear would occur above 490 feet or below 20 feet. Thus, the shear provides a more restrictive lower altitude limit. An accurate altitude range could be increased by selecting a higher reference altitude, but the penalty would be a higher minimum altitude.

The derivation provides an analytic relationship between the exponent and the roughness length. The 1/7 exponent corresponds to a roughness length of 0.046 feet when calculated from the corresponding reference height of 50 feet specified in Reference 2-21. Spotting this value in Figure 2-7 indicates that this corresponds to short grass in level land. Thus, there is no compromise provided for the influence of the taller growth or greater roughness often found around airports.

2.3.4 Influence of Nonadiabatic Thermal Conditions

Up to this point, the mean wind profiles with altitude considered have been those for "adiabatic" conditions, or for conditions of no vertical heat flux. Many authors ignore or dismiss the more general case of nonadiabatic atmospheric conditions, arguing that the critical design case occurs for high mean winds and, for high mean winds, conditions of near neutral stability exist. This argument cannot be readily accepted at this point, because a tradeoff between turbulence levels and mean wind levels may appear with atmospheric stability as a parameter. Turbulence and mean wind influence aircraft response in different ways, and a generalization as to which is more important for all aircraft and aircraft systems cannot be made, particularly without reference to the exceedance probabilities, the nearness of "near neutral stability", and the associated levels of mean wind and turbulence. Consequently, the more general case of unconstrained atmosphere stability will be considered for the mean wind profile.

The Ekman spiral is strictly an adiabatic profile. However, the literature provides theory and empirical matching for an extension of the logarithmic profile to nonadiabatic conditions. The power law, as an empirical law, is provided with empirical measures of its exponent for nonadiabatic conditions. First, however, it is appropriate to discuss atmospheric stability and the corresponding atmospheric conditions, its implications, and the methods for its classification.

2.3.4.1 Atmospheric Stability

Atmospheric stability is measured by the temperature profile with altitude (the temperature shear). A decrease in temperature with altitude is referred to as a lapse rate or lapse condition. An increase of temperature with altitude is called an inversion.

During daytime hours, solar radiation heats the earth more than it does the atmosphere. Conduction from the earth causes the air near the earth to be warmer than that above, and a lapse rate results. At night, with clear skies, the earth cools by giving up radiant heat and the air next to it cools by conduction, thus leading to inversions.

These general associations of temperature gradients with time of day are noted in Reference 2-7, where it is additionally stated that near-adiabatic conditions occur at dawn and dusk on clear days and on windy and overcast days and nights.

Atmospheric stability is measured by the tendency of air displaced vertically from its equilibrium condition to return to its original position. Stability can thus be measured by the sign and the magnitude of the "spring constant" of air, and is a dynamic concept. Skelton, in Reference 2-1, has derived the expression for the restoring force, implying the spring constant:

$$F(h_1 + dh) = dh \frac{R}{\rho} \frac{dp}{dh} \left| \frac{dT}{dh} + \frac{g}{C_p} \right|$$

The derivatives are evaluated at the equilibrium altitude h_i ($F(h_i) = 0$) where

$$\frac{dp}{dh} = -\rho g$$

for negligible density and gravitational acceleration gradients.

There will be a restoring force (stable) when the force on the parcel of air is negative. This leads to stability conditions based on the absolute temperature gradient:

$\frac{dT}{dh} > \frac{-g}{C_p}$, stable (weak lapse or inversion)

$\frac{dT}{dh} = \frac{-g}{C_p}$, neutral (adiabatic lapse)

$\frac{dT}{dh} < \frac{-g}{C_p}$, unstable (strong lapse)

A lapse rate of about 0.00536° R/ft is required for dynamic stability. However, when the equation of state,

$$p = \rho RT$$

is used in the equation for the pressure gradient at equilibrium, the temperature gradient required for hydrostatic equilibrium is given as

$$\frac{dT}{dh} = \frac{-g}{R} \qquad \text{(Ref. 2-1)}$$

or a lapse rate of about 0.0188° R/ft In Reference 2-1 it is argued that the air on the average will be in hydrostatic equilibrium: A greater lapse rate than that for hydrostatic equilibrium will cause the air to rise on its own accord and be added to cooler air, raising the temperature above, reducing the lapse rate, and reducing the forces on the rising parcels of air. Similar results are obtained for a lesser lapse rate. If indeed hydrostatic equilibrium is the average condition, then on the average there will be instability as the lapse rate for hydrostatic equilibrium is greater than that for dynamic stability. Alternately, it could be said that instability is more probable than stability.

An alternate parameter, potential temperature, is commonly defined to specify stability. Potential temperature, θ, is defined from the equation for a change of entropy:

$$dS = \frac{C_p}{T} dT - R \frac{dp}{p} \equiv C_p \frac{d\theta}{\theta} \qquad \text{(Ref. 2-7)}$$

thus, θ = constant x $(T/p^{R/C_p})$.

Constant entropy (isentropic) coincides with adiabatic conditions. Thus, adiabatic conditions are represented by constant potential temperature with altitude. The restoring force may be written in terms of potential temperature:

$$F(h_1 + dh) = -dh\frac{g}{\theta}\frac{d\theta}{dz} \text{ (Ref. 2-1)}$$

The term $(g/\theta)\,(d\theta/dz)$ is a measure of the restoring force, and $d\theta/dz$ can replace the comparison of lapse rates as a measure of stability:

$\frac{d\theta}{dz} > 0$, stable

$\frac{d\theta}{dz} = 0$, neutral

$\frac{d\theta}{dz} < 0$, unstable

The potential temperature derivative by itself is not the final parameter used for measuring stability. Rather, a nondimensional ratio of the buoyancy force (spring constant) to inertia force, called the gradient Richardson number, is formed:

$$R_i = \frac{\frac{g}{\theta}\frac{d\theta}{dh}}{(\partial\bar{V}_W/\partial h)^2} = \frac{\frac{g}{T}\frac{dT}{dh} + \frac{g}{C_p}}{(\partial\bar{V}_W/\partial h)^2}$$

Alternately, the gradient Richardson number may be thought of as a relationship between the mechanical shear that tends to displace air and the buoyancy force that may damp (or amplify) this tendency. Atmospheric instability, as applied to mean winds, is a measure of the efficiency by which heat and momentum may be transported to different altitudes by mechanical means.

2.3.4.2 Log-Linear Profile

The most widely accepted description of the mean wind profile at low altitudes for various stability conditions is that developed from similarity arguments (dimensional analysis), the original development of which is attributed to Monin and Obukhov.

First, the conditions leading to the development of the logarithmic profile are applied except for the requirement of adiabatic lapse rate. Similar to the assumption of constant shear stress, the heat flux is assumed to be constant with altitude, and a scaling length analogous to the friction velocity, u_{*0}, is introduced:

$$\ell = \frac{-u_{*0}^3 C_p T}{kgH}$$

(The use of a script "ℓ" is a change from conventional nomenclature. The upper case "L" is reserved to represent a turbulence parameter, used later.)

If the changes of absolute temperature are small for the altitude region of application, the scaling length is essentially constant with altitude. For unstable conditions, the heat flux, H, is positive and the scaling length, ℓ, is negative.

The introduction of the scaling length provides three parameters that are independent of height, the other two being friction velocity and surface roughness length. The surface roughness length enters only through integration of the velocity profile from the surface boundary condition, and need not be included for postulating the form of the mean wind shear. Then, according to References 2-7 and 2-23, a nondimensional shear can be described as some universal function of only the nondimensional altitude:

$$\frac{kh}{u_{*0}} \frac{\partial \bar{V}_W}{\partial h} = \phi\left(\frac{h}{\ell}\right)$$

For adiabatic conditions, the universal function must reduce to unity and lead to the logarithmic profile. Using this knowledge, the universal function is expanded into a Taylor series about adiabatic thermal conditions. Retaining only the linear term of the series for small h/ℓ, the nondimensional shear becomes:

$$\frac{kh}{u_{*0}} \frac{\partial \bar{V}_W}{\partial h} = 1 + \alpha \frac{h}{\ell}$$

or, after integrating,

$$\bar{V}_W = \frac{u_{*0}}{k}\left[\ln\left(\frac{h + z_0}{z_0}\right) + \alpha \frac{h}{\ell}\right]$$

where the origin of the axis system has been shifted to coincide with the surface of the earth. The characteristics of this equation are the logarithmic portion of the mean wind, representing the adiabatic contribution, and the nonadiabatic (or diabatic) contribution that provides an incremental change of the mean wind that increases linearly with altitude. These parts are well described in the name of the profile, the "log-linear" profile.

This description is provided graphically on Figure 2-8. The nonadiabatic, or diabatic increment to the wind shear is invariant with altitude. For instability, the scaling length is negative and reduces or even reverses the shear. Stability provides for an increase of shear and mean wind. Figure 2-8 provides trends that agree well with those of measured profiles such as those found in Reference 2-24.

Application of this profile requires knowledge of the scaling length, ℓ, and the proportionality constant, α. The scaling length is difficult to measure as it depends on the

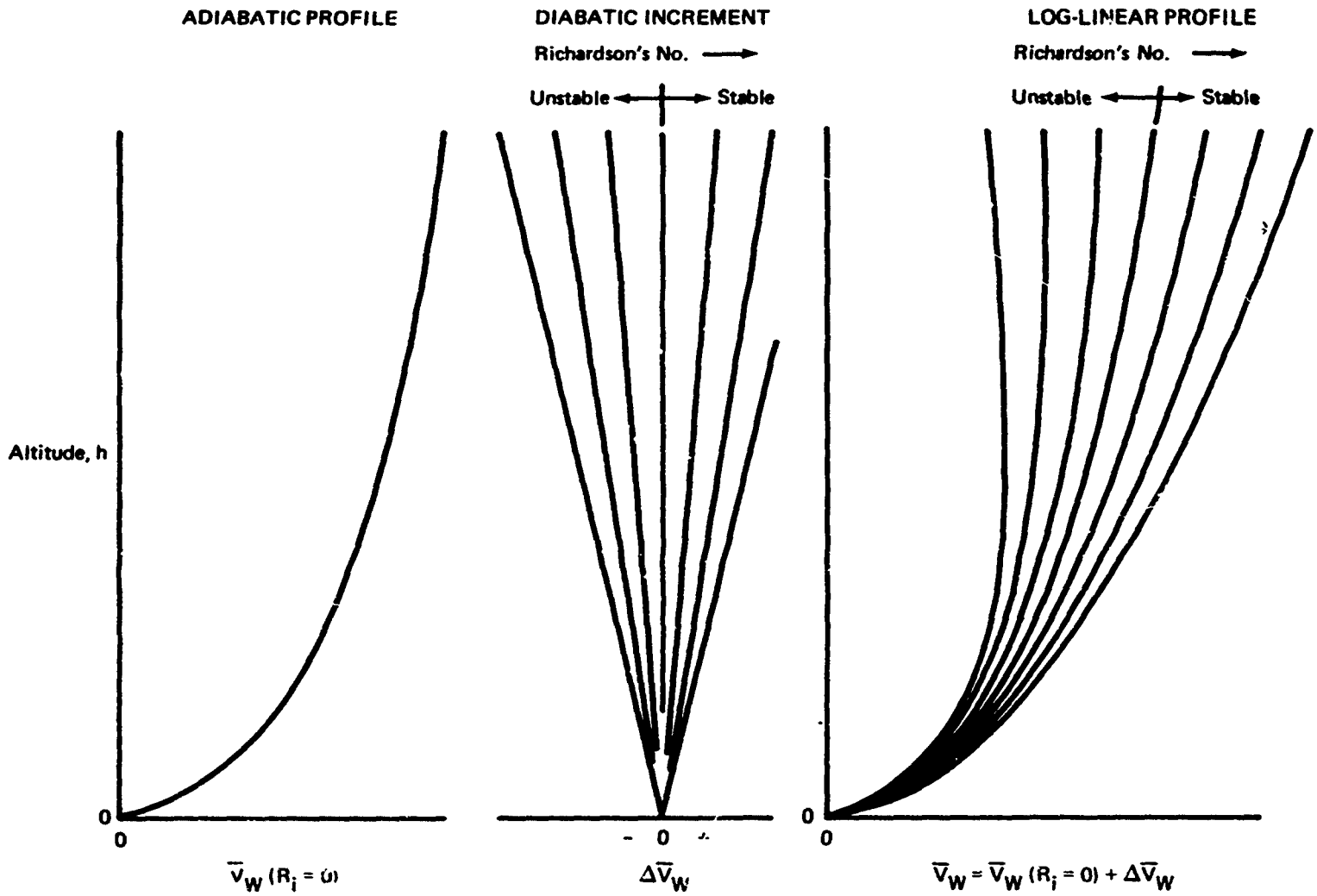

FIGURE 2-8.—LOG-LINEAR MEAN WIND PROFILE

heat flux. Consequently, the literature (Refs. 2-1, -7, -23, and -25) introduces an alternate scaling length, ℓ', given by

$$\ell' = \frac{u_{*0}\theta(\partial\bar{V}_W/\partial h)}{kg(\partial\theta/\partial h)}$$

The alternate scaling length differs from the first one by the ratio of eddy conductivity to eddy viscosity. This ratio of the scaling lengths is said by Reference 2-7 to be either constant with stability near unity or at least a function only of Richardson's number. Note that a constant ratio with altitude, which Reference 2-7 argues is the conclusion of most investigators, implies a ratio between the mean wind and potential temperature that is invariant with altitude. That is, the normalized mean wind and temperature profiles are identical.

The nondimensional altitude may be written in terms of the more readily measurable Richardson's number using the log-linear mean wind profile:

$$\frac{h}{\ell'} = \left[\frac{\frac{g}{\theta}\frac{\partial\theta}{\partial h}}{\left(\frac{\partial\bar{V}_W}{\partial h}\right)^2}\right]\frac{kh}{u_{*0}}\frac{\partial\bar{V}_W}{\partial h} = R_i(1 + \alpha' h/\ell')$$

where α' has been developed by multiplying α by the ratio of eddy conductivity to eddy viscosity so as to make α'/ℓ' equal to α/ℓ.

The resulting expressions for Richardson's number and nondimensional altitude are

$$R_i = \frac{h/\ell'}{1 + \alpha' h/\ell'}$$

$$h/\ell' = \frac{R_i}{1 - \alpha' R_i}$$

The Richardson's number equation predicts that stability or instability will increase with increasing altitude. For very small Richardson's numbers (or small h/ℓ', an adequate approximation is

$$h/\ell' = R_i \qquad |R_i| \text{ very small}$$

Using this approximation further restricts the region of validity. The resulting wind profile becomes

$$\bar{V}_W = \frac{u_{*0}}{k}\left[\ln\left(\frac{h + z_0}{z_0}\right) + R_i\right] \quad , \quad |R_i| \text{ very small}$$

Note that the nonlinear equations restrict Richardson's number to

$$R_i < \frac{1}{\alpha'}$$

The constant of proportionality, α', has had different estimates attributed to it. For unstable conditions, Reference 2-7 argues for a value of 4.5 but notes that other investigators have estimated 4 and 6. Reference 2-26 states that $\alpha' = 4.5$ within a standard error of 10%. An original estimate by Monin and Obukhov of 0.6 is discounted by References 2-7 and 2-9, which argue that it was measured at sufficiently nonadiabatic conditions that the nonlinear terms in the Taylor series expansion were significant. Reference 2-9 quotes values of 3 and 4 obtained from different investigators.

For stable conditions, Reference 2-23 recommends $\alpha' = 7$ but notes that other studies have found values from 2 to 10, although the ranges for application were not qualified. Reference 2-26 has found $\alpha' = 5.2$ for stable conditions but notes that this may not be sufficiently different from the unstable estimate of 4.5 to warrant differentiating between them.

The restrictions for applying the linear part of the log-linear profile are measures of the linearity of the universal function, $\phi(h/\ell)$. Restrictions apply directly to h/ℓ and indirectly to Richardson's number. There is a maximum altitude restriction that becomes more severe as the deviation from an adiabatic lapse rate increases at a fixed altitude ($|\ell'|$ becomes smaller).

Reference 2-7 restricts the log-linear profile to unstable Richardson's numbers more positive than -0.03, a number agreed with in References 2-9 and 2-26.

For stable conditions, Reference 2-7 restricts positive h/ℓ' to 0.3 or Richardson's number to 0.1. Reference 2-23 permits extension up to a Richardson's number of 0.14, only slightly below his estimate of the critical Richardson's number ($1/\alpha'$). Reference 2-7 states that there is no simple relationship for the mean wind with h/ℓ' for conditions more stable than $h/\ell' = 0.3$. A more recent study (Ref. 2-26) disagrees and finds the log-linear profile accurate up to $h/\ell' = 1$ for $\alpha' \cong 5$ ($R_i \cong 0.16$).

2.3.4.3 Extension from the Log-Linear Profile

The data on Figure 2-9 indicate that a linear representation of the universal function $\phi(h/\ell)$ is not a good one for moderately negative (unstable) h/ℓ' ($h/\ell' < 0.03$). Additional solutions for the velocity profile at larger levels of instability but with minimum instability restrictions are presented in References 2-7 and 2-9. Of more interest, however, is a solution that can be applied within a wide range of stability and instability, allowing application to relatively high altitudes.

References 2-7, -9, -15, and -25 present an interpolation formula which has shown good results for matching characteristics over a very large range of instability. The interpolation equation, called the "KEYPS" equation, is given by

$$s^4 - \frac{\gamma' h}{\ell'} s^3 = 1$$

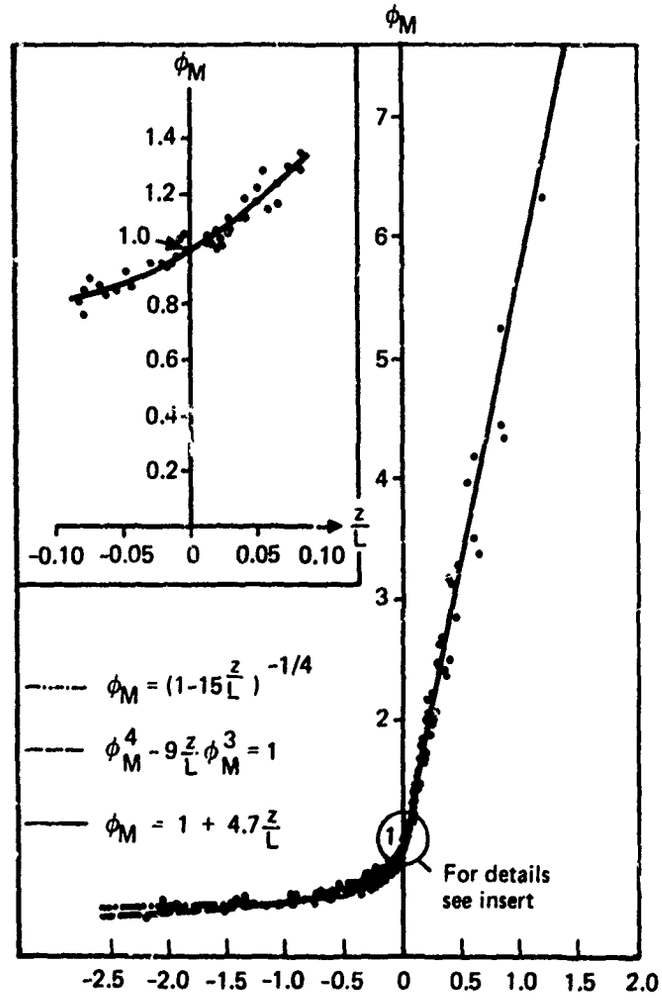

FIGURE 2-9.–NONDIMENSIONAL WIND SHEAR, EFFECT OF STABILITY (FROM REF. 2-9)

where s is the nondimensional wind shear,

$$s = \frac{kh}{u_{*0}} \frac{\partial \bar{V}_W}{\partial h}$$

As was shown for the logarithmic profile, the definition of the scaling length, ℓ', permits an identity between the nondimensional altitude and Richardson's number:

$$h/\ell' = R_i s$$

Substituting this identity into the interpolation formula provides the following equation for shear:

$$\frac{\partial \bar{V}_W}{\partial h} = \frac{u_{*0}}{kh(1 - \gamma' R_i)^{1/4}}$$

Using the same two equations but eliminating s instead provides

$$\frac{h}{\ell'} = \frac{R_i}{(1 - \gamma' R_i)^{1/4}}$$

Both of these equations reduce to the log-linear forms for very small levels of instability provided $\gamma' = 4\alpha'$. Reference 2-7 also indicates good agreement with the form

$$s = \frac{1}{(1 - \frac{\gamma'}{2} R_i)^{1/2}}$$

attributed to Holzman (Refs. 2-7, -9, and -25) for small Richardson's number and the law

$$\frac{\partial \bar{V}_W}{\partial h} \sim h^{-4/3}$$

attributed to Priestly (Refs. 2-7, -9, and -25), for strong instability.

In keeping with its recommendation for $\alpha' = 4.5$, Reference 2-7 recommends $\gamma' = 18$.

In order to integrate the shear to obtain the mean wind profile, Richardson's number must be expressed in terms of altitude, a relationship that requires the solution of a fourth order equation. The mean wind profile must consequently be found by numerical integration.

The form of the resulting mean wind profile proposed in Reference 2-7 is given by:

$$\bar{V}_W = \frac{u_{*0}}{k} \left[\ln\left(\frac{h + z_0}{z_0}\right) + f\left(\frac{h}{\ell'}\right) \right]$$

where the universal function $f(h/\ell')$ corresponds to the non-constant terms of the Taylor series expansion of the universal function $\phi(h/\ell')$ and can be found from the shear equation by ϕ

$$f(h/\ell') = \int_0^{-h/\ell'} \frac{\phi(\xi) - 1}{\xi} d\xi$$

where

$$\phi\left(\frac{h}{\ell'}\right) = \frac{kh}{u_{*0}} \frac{\partial \bar{V}_W}{\partial h}$$

The function $f(h/\ell')$ is shown graphically on Figure 2-10 for the representation

$$\phi = \frac{1}{(1 - \gamma' R_i)^{1/4}}$$

$$h/\ell' = \frac{R_i}{(1 - \gamma' R_i)^{1/4}}$$

and is taken from Reference 2-7. This curve has been fitted by an equation in Reference 2-15 given by

$$f\left(\frac{h}{\ell'}\right) = -\left(-100\frac{h}{\ell'}\right)^{1.0674 - 0.678 \ln\left(-100 \frac{h}{\ell'}\right)}$$

for $R_i < -0.01$.

An extension to strong stability is provided by Webb in Reference 2-20. Webb first argues that the log-linear profile holds for h/ℓ' up to unity. For h/ℓ' greater than unity up to $R_j = 1$, Webb finds the mean wind shear to be given by

$$\frac{\partial \bar{V}_W}{\partial h} = \frac{u_{*0}}{kh}(1 + \alpha') \quad , \quad (1 + \alpha' > h/\ell' \geq 1)$$

for $\alpha' = 5$. The corresponding expression for Richardson's number is given by

$$R_i = \frac{h/\ell'}{1 + \alpha'} \quad , \quad (1 + \alpha' \geq h/\ell' \geq 1).$$

The resulting mean wind is found by integrating from the altitude h_1 where $h_1/\ell' = 1$:

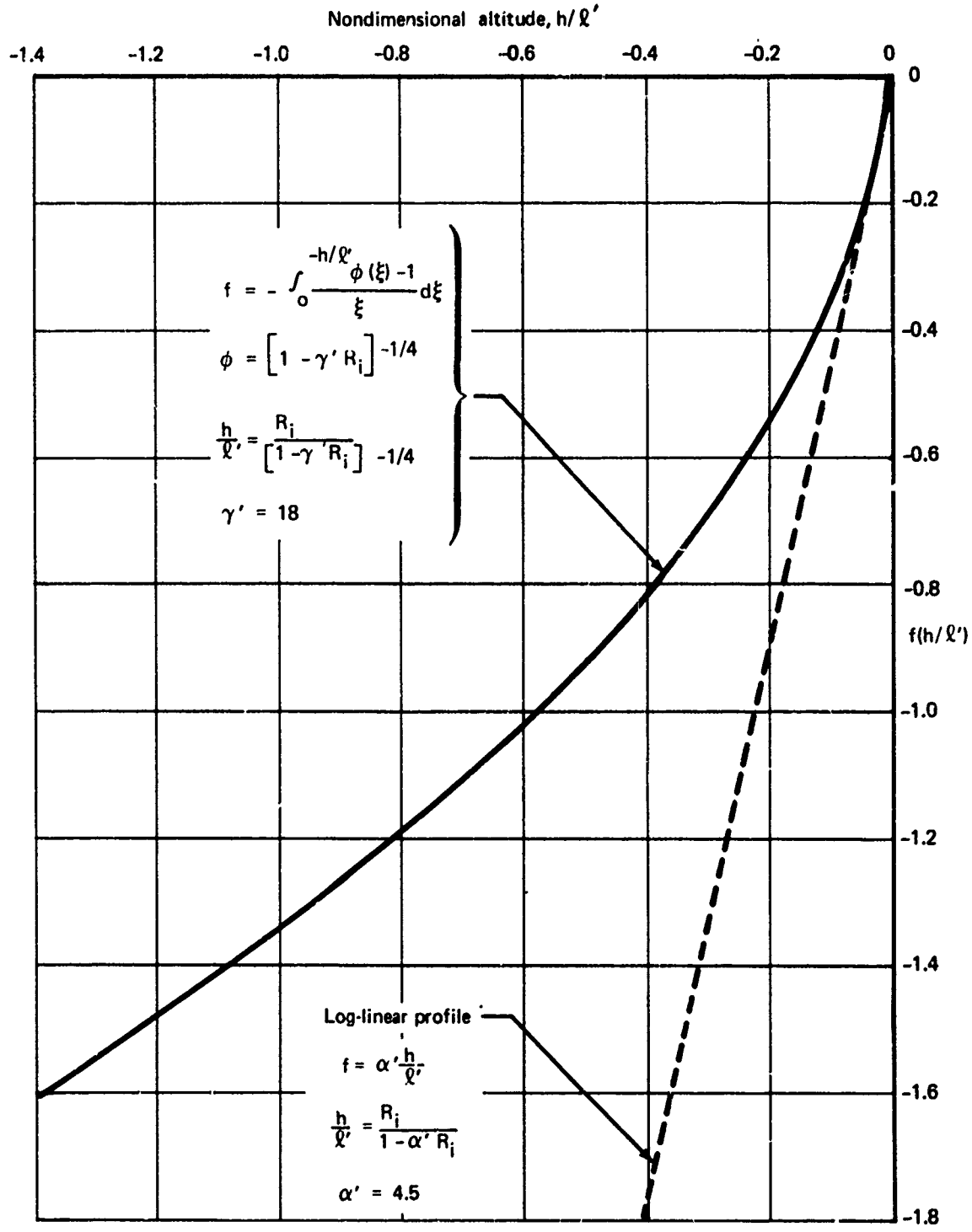

FIGURE 2-10.–DIABATIC MEAN WIND PROFILE FUNCTION, UNSTABLE CONDITIONS (FROM REF. 2-7)

$$\bar{V}_W(h) - \bar{V}_W(h_1) = \frac{u_{*0}}{k}(1+\alpha')\left|\ln(h) - \ln(h_1)\right| \quad , h \gg z_0$$

$$= \frac{u_{*0}}{k}(1+\alpha')\ln(h/\ell')$$

Thus, the change of velocity from h_1 is a pure logarithmic function of altitude. Substituting for $\bar{V}_W(h_1)$,

$$\bar{V}_W(h_1) = \frac{u_{*0}}{k}\left[\ln\left(\frac{h_1 + z_0}{z_0}\right) + f\left(\frac{h_1}{\ell'} = 1\right)\right]$$

$$f\left(\frac{h}{\ell'}\right) = \alpha' \frac{h}{\ell'} \text{ for } R_1 > 0, h/\ell' < 1$$

the mean wind equation becomes

$$\bar{V}_W = \frac{u_{*0}}{k}\left[(1+\alpha')\ln(h/\ell') + \ln\left(\frac{h_1 + z_0}{z_0}\right) + \alpha'\right] \quad , \quad h/\ell' \geq 1$$

or

$$\bar{V}_W = \frac{u_{*0}}{k}\left|\ln(h/z_0) + \alpha' + \alpha'\ln(h/\ell')\right| \quad , \quad h/\ell' \geq 1, h \gg z_0$$

In terms of the universal function from Reference 2-7,

$$f(h/\ell') = \alpha' + \alpha'\ln(h/\ell')$$

2.3.4.4 Deacon Wind Profile

There has been an attempt by Deacon to model the mean wind shear profile for all stability conditions with a single explicit equation. The form of the equation is given by

$$\frac{\partial \bar{V}_W}{\partial h} = Ch^{-\beta} \text{ (Ref. 2-27)}$$

For low altitudes where C and β are independent of height and depend on stability:

$\beta > 1$, unstable ($R_i < 0$)

$\beta = 1$, neutral ($R_i = 0$)

$\beta < 1$, stable ($R_i > 0$)

The mean wind profiles are given by (Ref. 2-27).

$$\bar{V}_W = \frac{u_{*0}}{k(1-\beta)}\left[\left(\frac{h}{z_0}\right)^{1-\beta} - 1\right] \quad , \quad \beta \neq 1$$

$$\bar{V}_W = \frac{u_{*0}}{k}\ln\left(\frac{h}{z_0}\right) \quad , \quad \beta = 1$$

for $\bar{V}_W = 0$ at $h = z_0$.

The assumptions of this profile, specifically the independence of β with height for nonadiabatic conditions, have been tested in Reference 2-27 and have been found to be invalid.

An independent check on the dependence of β with height is provided in Reference 2-25. There it is said that Deacon's β is given by

$$\beta = -\frac{h\dfrac{\partial^2 \bar{V}_W}{\partial h^2}}{\dfrac{\partial \bar{V}_W}{\partial h}}$$

Using the interpolation formula,

$$s^4 - \frac{\gamma' h}{\ell'} s^3 = 1 \quad , \quad \left[s = \frac{kh}{u_{*0}}\frac{\partial \bar{V}_W}{\partial h}\right]$$

a relationship between Richardson's number and β is derived:

$$R_i = (1-\beta)/(1-\tfrac{3}{4}\beta)$$

Thus, if β were independent of height, so must be Richardson's number, in conflict with the results of the interpolation formula and the log-linear profile.

2.3.4.5 Extension from the Power Law

The empirical power law,

$$\frac{\bar{V}_W}{\bar{V}_{REF}} = \left(\frac{h}{h_{REF}}\right)^p$$

is extended to nonadiabatic conditions by altering the exponent with stability. Qualitatively, Reference 2-15 indicates that the exponent increases with increasing stability and may approach zero for conditions of extreme instability.

In Reference 2-25, the logarithmic of the power law equation is taken and derivatives are performed to yield the expression:

$$p = \frac{\partial(\ln \bar{V}_W)}{\partial(\ln h)} = \frac{h}{\bar{V}_W} \frac{\partial \bar{V}_W}{\partial h} = \frac{u_{*_0} s}{k \bar{V}_W}$$

where

$$s = \frac{kh}{u_{*_0}} \frac{\partial \bar{V}_W}{\partial h}$$

By solving the interpolation equation,

$$s^4 - \gamma \frac{h}{\ell'} s^3 = 1$$

for the nondimensional shear and integrating numerically for the mean wind, the exponent that gives the same shear-mean wind relationship at a given altitude can be found for various roughness lengths and levels of stability. Generally, there will be a different exponent for each altitude, but for a sufficiently small altitude range the error from considering the exponent invariant with altitude will be small. For $\gamma' = 18$ and altitudes from 11 to 46 meters, the exponents are shown as a function of the scaling length, ℓ', and the roughness length, z_0, on Figure 2-11, as taken from Reference 2-25. Contrary to that qualitatively described in Reference 2-15, increasing instability (decreasing $1/\ell'$) corresponds to an increasing exponent, a difference that can be due to the altitude and altitude range considered (see Fig. 2-8). The altitude and altitude range restrictions for applying the power law to diabatic thermal conditions can generally be considered to be more severe than those for applying the power law for adiabatic conditions.

2.3.5 Extension of the Mean Wind Profile to the Boundary Layer

The mean wind profiles investigated have been for the lower levels of the boundary layer where accurate knowledge is most important. All the models presented, with the exception of the Ekman spiral, continue to increase with increasing altitude, although at a decreasing rate, so that the boundary condition of a constant wind at and above the boundary layer is not met. If some estimate of the boundary layer thickness, d, could be made, then an artificial restriction, $\bar{V}_W(h) \leq \bar{V}_W(d)$, could be imposed. The artificial restriction would not relieve the overprediction just below the boundary layer.

Overprediction of the mean wind and mean wind shear near the boundary layer may not present any problem for most cases. However, sufficiently severe overestimates could prevent attainment of a glideslope in tailwinds due to inability to produce enough drag or to reduce thrust sufficiently or could prevent the attainment of a positive groundspeed in a headwind at an airplane's nominal approach airspeed.

More importantly, a significant overprediction of the mean wind at the boundary layer implies the model becomes inaccurate at some lower altitude. When mean wind models at nonneutral atmospheric conditions become inaccurate for large deviations from neutral

$$\frac{\bar{V}_W}{V_{REF}} = \left(\frac{h}{h_{REF}}\right)^P$$

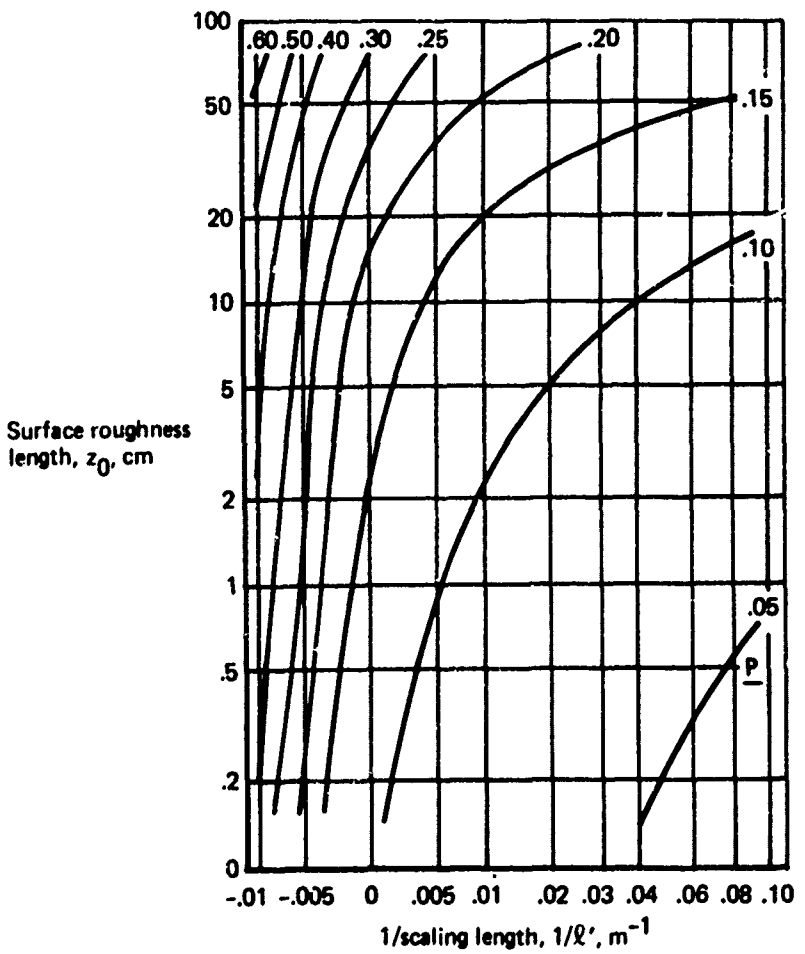

FIGURE 2-11.–POWER LAW EXPONENT, EFFECT OF STABILITY, 11 M < h < 46 M (FROM REF. 2-25)

stability (large h/ℓ'), the altitude at which the model becomes inaccurate is lowered. When the model is accurate to some h/ℓ', large deviations from neutral stability implies small ℓ'; therefore, the limiting altitude becomes small. The position is taken that a model that accurately describes the wind at low altitudes and satisfies the boundary conditions without artificial constraints is more accurate at intermediate altitudes than a model that fails to meet the boundary condition.

A mechanism for correcting the mean wind in the upper part of the boundary has been found for the profiles developed from dimensional analysis: relaxation of the constant shear stress assumption.

2.3.5.1 Boundary Layer Thickness and the Altitude Dependence of Friction Velocity

The Monin-Obukhov similarity theory starts with the hypothesis that in the atmospheric boundary layer the properties of the turbulent velocity fluctuations are uniquely determined by the height h and the following three scaling parameters:

Friction velocity, $u_* = \left(\frac{\tau}{\rho}\right)^{1/2}$

Scaling temperature, $T^* = -\frac{H}{ku_*C_p\rho}$

Scaling length, $\ell = -\frac{u_*^3 C_p \rho T}{kgH}$

These parameters are implicitly independent of height. τ is the horizontal surface stress in the direction of the surface wind, ρ is the air density, H is the upward heat flux, C_p is the specific heat of air at constant pressure, T is the average air absolute temperature, g is the earth's gravitational acceleration, and k = 0.4 is Von Karman's constant. Additionally, upon integration of the equations of motion, the small scale roughness length z_0 is introduced. The roughness length is defined as the height at which the mean wind speed formally goes to zero.

The thickness of the layer in which the Monin-Obukhov similarity theory applies is determined by the height over which the fall in the shear stress and the change in the heat flux remain negligible. This part of the atmospheric boundary layer is normally referred to as the constant-stress layer. Reference 2-28 gives the thickness as approximately 30 feet, while Reference 2-7 infers that the stress changes by less than 10% within a region having a thickness varying from 30 to 300 feet, depending on the magnitude of the ground shear stress. It was concluded that the heat flux is essentially constant with height near the surface except when the flux is small.

Our interest extends beyond the constant stress layer up to about 1000 feet above the surface. The atmospheric boundary layer may be regarded as the layer from which momentum is extracted to overcome aerodynamic friction. Contrary to classical ideas, the thickness of the boundary layer is not constant. The effective range of the turbulent momentum transport is controlled by the thermal stratification of the atmosphere.

Reference 2-4 states that during daytime over land, the top of the boundary layer is usually defined by the existence of a stable layer beginning in the range between 1500 and 6000 feet above ground. Further, at night the stable air generated by ground cooling may suppress the turbulent motion except immediately above the ground, the boundary layer then being very shallow.

In the boundary layer above the constant-stress layer, the semiempirical analysis becomes extremely complex. The simplifying assumptions of the similarity theory are no longer valid, partly due to the decrease in the stress with height and the increasing effect of Coriolis force. Additional complications are introduced by the effect of variable terrain roughness and large-scale horizontal variations of temperature.

For heights over which the decrease of u_* may not be neglected, it is suggested that the mean wind speed and shear remain proportional to the local value of friction velocity, $u_*(h)$, which may be estimated by considering a simplified form of the Navier-Stokes equations of motion.

If $\tau(h)$ is the shear stress at the height h then let

$$[u_*(h)]^2 = \frac{\tau(h)}{\rho}$$

Assuming that the velocity vector and the shear stress vector are parallel at the elevation h, then from Reference 2-9

$$\frac{\partial [u_*(h)]^2}{\partial h} = - fG \sin \alpha$$

where $u_*(h)$ is the value of the friction velocity at the height h, f is Coriolis parameter, G is the geostrophic wind speed, and α is the angle between the geostrophic wind vector and the wind vector at the height h. When the surface wind blows to the left of the geostrophic wind, α is positive. At the surface $\alpha = \alpha_0$ and at the top of the boundary layer $\alpha = 0$. Near the surface $[u_*(h)]^2$ may be expanded in a Taylor series about $h = 0$ and $\alpha = \alpha_0$.

$$[u_*(h)]^2 = [u_*(0)]^2 - hfG \sin \alpha_0 - \frac{h^2}{2} fG \cos \alpha_0 \left. \frac{d\alpha}{dh} \right|_0$$

+ higher order terms.

According to References 2-4, -7, -9, and -29, the term $[d\alpha/dh]$ is small in the lower part of the boundary layer, therefore neglecting second and higher order terms in the expansion

$$u_*(h) \cong u_*(0) \left[1 - \frac{G \sin \alpha_0}{[u_*(0)]^2} h \right]^{1/2}$$

This expression is identical to those derived in References 2-4 and 2-29 and similar to the one derived in Reference 2-9. The cross-isobar angle α_0 varies between 15° for very unstable conditions to 35° for very stable conditions. Reference 2-4 lists

$$\sin \alpha_0 = 0.3$$

as a typical value and reports that observations give

$$\left[G/u_*(0)\right]^2 \cong 10^3$$

Selecting G = 60 feet/sec and assuming 45° latitude, then

$$f \cong 10^{-4}$$

and

$$u_*(h) = u_*(0)\left[1 - 0.5 \cdot 10^{-3}h\right]^{1/2}$$

where h is measured in feet. Given the specified conditions, this formula predicts the following decrease in u_* with height valid for the lower part of the boundary layer:

Height, ft	$100[u_*(0) - u_*(h)]/u_*(0)$
50	1.0%
100	2.5%
300	8.0%
1000	29.0%
2000	100.0%

The variation of the cross-isobar angle α with height is assumed to be negligible in the layer under consideration. However, as the height increases the formula will tend to overestimate the decrease in the friction velocity, because the effect of the variation of α in decreasing the shear correction is not considered in the formula.

A second derivation of the altitude dependence of friction velocity is obtained by a Taylor series expansion about conditions at the edge of the boundary layer.

At the edge of the boundary layer the distributions of velocity and shear stress smoothly join the flow aloft, where $\tau = 0$, $\bar{\nabla}_W = G$, and $\alpha = 0$, everywhere independent of height. This requires the first derivative of the shear stress to be zero. Thus, a simplified expression for $u_*(h)$ may be obtained by expanding $[u_*(h)]^2$ in Taylor series about $h = d$ and $\alpha = 0$ where d is the thickness of the boundary layer.

$$[u_*(h)]^2 = [u_*(d)]^2 - (h-d)\,fG\sin\alpha - \frac{(h-d)^2}{2} fG \left.\frac{d\alpha}{dh}\right|_d$$

+ higher order terms. Thus

$$[u_*(h)]^2 \cong -f\frac{G}{2}\left.\frac{d\alpha}{dh}\right|_d (h-d)^2$$

Also

$$\sin\alpha \cong -\left.\frac{d\alpha}{dh}\right|_d (d-h)$$

Reference 2-9 reports that the quadratic dependency of the shear stress on height and the linear distribution of sin α with height have been confirmed by observations. The quantities $[d\alpha/dh|_d]$ and d must be determined to complete the solution. Reference 2-9 postulates that the expressions may be obtained by assuming that the upper profile is everywhere determined by the asymptotic form and thus in the overlap region of the lower and higher profiles as well. From Reference 2-9

$$\sin\alpha_0 = \left.\frac{d\alpha}{dh}\right|_d d = 10.7\frac{u_*(0)}{G}$$

Thus

$$\sin\alpha = 10.7\frac{u_*(0)}{G}\left(1-\frac{h}{d}\right)$$

and

$$\frac{u_*(h)}{u_*(0)} = \left[5.35\frac{df}{u_*(0)}\right]^{1/2}\left(1-\frac{h}{d}\right)$$

Reference 2-9 makes this expression satisfy the boundary conditions at the surface, i.e., for $h = 0$, $u_*(h)/u_*(0) = 1$. Hence,

$$\frac{u_*(h)}{u_*(0)} = \left|1-\frac{h}{d}\right|$$

Since

$$5.35\frac{df}{u_*(0)} = 1$$

and

$$d = C\frac{u_*(0)}{f}$$

then

$$d = \frac{u_*(0)}{5.35f}$$

and

$$\left.\frac{d\alpha}{dh}\right|_d = -57.2\frac{f}{G}$$

Substituting for d

$$\frac{u_*(h)}{u_*(0)} = \left|1 - 5.35\,\frac{fh}{u_*(0)}\right|$$

Assuming

$$\sin\alpha_0 = 0.3$$

then

$$\frac{G}{u_*(0)} = 32.1$$

which is in good agreement with the value

$$\left|\frac{G}{u_*(0)}\right|^2 \approx 10^3$$

quoted earlier

Selecting G = 60 feet/sec and assuming 45° latitude as before,

$$f \approx 10^{-4}$$

and

$$u_*(h) = u_*(0)\,[1 - 0.286 \cdot 10^{-3}h]$$

where h is measured in feet. Given the specified conditions, this formula predicts the following decrease in u_* with height valid for the upper boundary layer:

Height, ft	$100[u_*(0) - u_*(h)]/u_*(0)$
50	1.5%
100	2.9%
300	8.6%
1000	28.6%
2000	57.2%
3500	100.0%

The expressions for the asymptotic behavior of the shear stress near the ground and at the upper edge of the boundary layer agree very well when both are extrapolated to the lower midrange levels in the boundary layer. It appears that the high level asymptotic expansion will give good results over most of the boundary layer, except for perhaps at the extreme lower part where the low level asymptotic expansion will give better results. The indications are that the latter method will overestimate the decrease in u_* by a considerable amount at levels higher than one-third the boundary layer thickness. It should be noted that for the given geostrophic wind and relationship between the latter and the surface stress, this theory predicts a boundary layer thickness of 3500 feet. This is in good agreement with atmospheric measurements performed under similar conditions (Ref. 2-9).

2.3.5.2 Modification of the Mean Wind Profile From Similarity Theory

Mean wind profiles from dimensional analysis are obtained from

$$\frac{\partial \bar{V}_W}{\partial h} = \frac{u_*}{kh}\phi(h/\ell')$$

Formerly, it was assumed that

$$u_* = u_*(h = 0) = u_{*0}$$

A zero wind shear at the boundary layer is obtained by recognizing the altitude dependence of friction velocity that provides for zero friction velocity at the edge of the boundary layer. Using the expression developed from the Taylor series expansion about conditions at the edge of the boundary layer.

$$u_* = u_{*0}\left(1 - \frac{h}{d}\right)$$

the expression for the mean wind shear becomes

$$\frac{\partial \bar{V}_W}{\partial h} = \left(\frac{u_*}{u_{*0}}\right)\frac{u_{*0}}{kh}\phi(h/\ell') = \left(1 - \frac{h}{d}\right)\frac{u_{*0}}{kh}\phi(h/\ell')$$

The corresponding equation for boundary layer depth, d, is

$$d = \frac{u_{*_0}}{5.35f}$$

For a 40° latitude, the Coriolis parameter, f, is such that

$$d = 2000\, u_{*_0} \sim \text{ft}$$

Accounting for the variation of shear stress with altitude ensures that the wind shear goes to zero at the edge of the boundary layer, as it should to be compatible with the idealized description. At low altitudes, where h/d is small, the previous equation for the

nondimensional shear is unaltered. Reducing the shear at altitudes where it is already small is inconsequential, but reflecting the reduction of the shear on the wind speed can lead to a substantial reduction in the high altitude wind speed.

No justification for incorporating the shear stress reduction in the shear profile has been found in the literature. It is merely presumed that matching requirements at low altitudes and at the boundary layer will provide better results at the intermediate altitudes than just matching requirements at low altitudes and extrapolating to high altitudes.

The integration of the shear to provide the wind profile is performed in Appendix 2A and provides:

$$\bar{V}_W = \frac{u_{*0}}{k}\left[\ln\left(\frac{h + z_0}{z_0}\right) - \frac{h}{d} + f\left(\frac{h}{\ell'}, \frac{h}{d}\right)\right]$$

The two parameters of the function $f(h/\ell', h/d)$, which represents the contribution of nonneutral atmospheric stability to the profile, are separable and the function may be describable in terms of the constant shear stress functions:

$$f\left(\frac{h}{\ell'}, \frac{h}{d}\right) = f\left(\frac{h}{\ell'}\right) - \frac{1}{d}\int_0^h \left[\Phi\left(\frac{h}{\ell'}\right) - 1\right] dh$$

$$= f\left(\frac{h}{\ell'}\right) - \frac{(h/d)}{(-h/\ell')}\int_0^{-h/\ell'} \left[\phi(\xi) - 1\right] d\xi,\ 1/\ell' < 0$$

$$= f\left(\frac{h}{\ell'}\right) - \frac{(h/d)}{(-h/\ell')}\int_0^{h/\ell'} \left[\phi(\xi) - 1\right] d\xi,\ 1/\ell' > 0$$

or

$$f\left(\frac{h}{\ell'}, \frac{h}{\ell}\right) = f\left(\frac{h}{\ell'}\right)\left(1 - \frac{h}{d}\right) + \frac{h/d}{(-h/\ell')}\int_0^{-h/\ell'} f(\xi)\, d\xi,\ 1/\ell' < 0$$

$$= f\left(\frac{h}{\ell'}\right)\left(1 - \frac{h}{d}\right) + \frac{h/d}{h/\ell'}\int_0^{h/\ell'} f(\xi)\, d\xi,\ 1/\ell' > 0$$

For stable conditions, explicit functions are derived in Appendix 2A. For unstable conditions, the functions are derived by numerical integration.

The mean wind equations may be alternately defined as

$$\bar{V}_W = \frac{u_{*0}}{k}\left[\ln\left(\frac{h + z_0}{z_0}\right) + f\left(\frac{h}{\ell'}\right) - \frac{h}{d}g\left(\frac{h}{\ell'}\right)\right]$$

The function $f(h/\ell')$ is identical to that used for the constant friction velocity profile.

The function $g(h/\ell')$ describes the reduction of the wind due to the decrease of shear stress with increasing altitude. For neutral stability, $g(0) = 1$. For low altitudes, where h/d is very small, the mean wind description reduces to that for constant shear stress.

Derivations providing modified expressions for the particular conditions of neutral stability ($\phi(h/\ell') = 1$) and near neutral stability ($\phi(h/\ell') = 1 + \alpha' h/\ell$), are performed in Appendix 2A and provide the following expressions:

Neutral stability: $h/\ell' = 0, \phi(h/\ell') = 1$

$$\bar{V}_W = \frac{u_{*0}}{k}\left[\ln\left(\frac{h + z_0}{z_0}\right) - \frac{h}{d}\right]$$

For low altitudes, $h/d \cong 0$ and the logarithmic profile is obtained.

Near neutral stability: $\phi(h/\ell') = 1 + \alpha' h/\ell'$

$$\bar{V}_W = \frac{u_{*0}}{k}\left[\ln\left(\frac{h + z_0}{z_0}\right) - \frac{h}{d} + \alpha' \frac{h}{\ell'}\left(1 - \frac{1}{2}\frac{h}{d}\right)\right]$$

For low altitudes, $h/d \cong 0$ and the log-linear profile is obtained.

Appendix 2A also provides a derivation for the stable profile represented by $\phi(h/\ell') = 1 + \alpha'$ for $h/\ell' > 1$:

$$\bar{V}_W = \frac{u_{*0}}{k}\left\{\ln\left(\frac{h + z_0}{z_0}\right) + \alpha'\left[1 + \ln\left(\frac{h}{\ell'}\right)\right] - \frac{h}{d}\left[1 + \alpha' - \frac{1}{2(h/\ell')}\right]\right\}$$

To prevent negative friction velocities from occurring for $h > d$, an additional constraint is imposed:

$$\frac{\partial \bar{V}_W}{\partial h} \geq 0$$

$$\bar{V}_W(h) = \bar{V}_W(d) \quad \text{for } h \geq d$$

The effect of the altitude variation of shear stress is negligible for unstable conditions but can be appreciable for stable conditions, as shown on Figure 2-12.

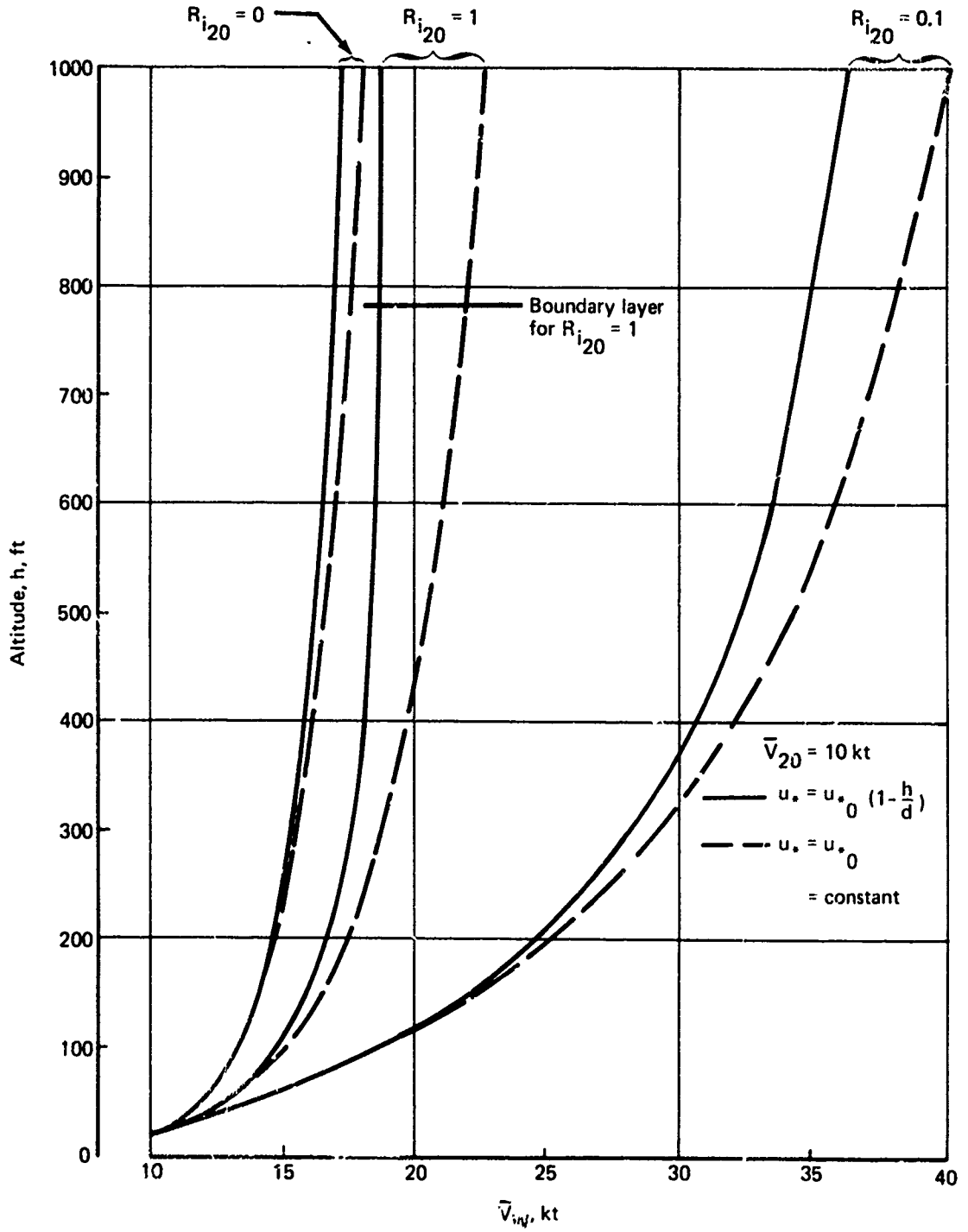

FIGURE 2-12.–EFFECT OF SHEAR STRESS VARIATION ON WIND PROFILES

2.3.6 Selection of Mean Wind Description

The major analytic descriptions for low altitude have been provided; from these, a description for specific application to the approach and landing maneuver is to be selected.

The critical area for the evaluation of aircraft motion during approach and landing is at and near touchdown, where success or failure of the maneuver is determined. Here, accurate correlation of airspeed with ground speed must be made to avoid large touchdown dispersions. This region requires very accurate control of rate of sink, airplane attitude, and angular velocities to avoid structural damage. At higher altitudes, greater tolerances on aircraft motion can be accepted as the consequences are less.

Aircraft motion at or near touchdown is not solely dependent on the conditions in that region, but is also a consequence of conditions experienced before that region is reached. However, it may be reasoned that the effect of conditions at a given altitude on the touchdown performance are inversely proportional to altitude; what happens high above the ground has less effect on the touchdown than what happens at some altitude nearer the ground. Thus, the first requirement for the description selected is accurate representation at the altitude corresponding to that at touchdown (height of the aerodynamic center above ground at touchdown). Then the descriptions are weighted according to their accuracies at increasing altitudes. This effectively rules out the Ekman spiral, whose validity at any altitude is questionable but which is most descriptive for wind conditions at the top of the atmospheric boundary layer.

If thermal conditions were restricted to adiabatic conditions, the choice would be between the logarithmic profile and the power law. The literature argues that the power law has the simpler form, but this cannot be accepted for simulation applications. Either requires a series approximation or a table lookup for digital simulation and a table lookup for analog simulation. The power law has been seen to be an approximation to the logarithmic profile and deviates from the logarithmic profile significantly at higher altitudes. However, the logarithmic profile may be suspect at these altitudes, and the difference at higher altitudes may have little impact.

A decision on whether or not to restrict thermal conditions to adiabatic conditions shall not be made at this point. Rather, a description is sought which accounts for nonadiabatic conditions so that their significance may be evaluated. Descriptions accounting for such effects provide for an increase in the magnitude of stability or instability with increasing altitude (but not a transition between stability and instability with changing altitude). Consequently, a restriction on the range of stable or unstable conditions results in restrictions on the maximum and minimum altitudes to which the description may be applied. An approach and landing from 1000 feet in virtually any condition except for adiabatic conditions will result in passing from strong stability to slight stability or strong instability to slight instability. Hence, the description must be continuous over a wide range of stability and instability. This eliminates the log-linear profile for instability, as well as perhaps for stability and other models restricted to small ranges of stability conditions, such as the law attributed to Priestly. However, it does not eliminate combinations of descriptions, provided such combinations provide a total description that is continuous with stability.

The Deacon profile satisfies these requirements mathematically, but it implies constant stability with altitude, a condition found empirically to be invalid. The power law by itself does not have a well-defined description of the exponent for various stability conditions and surface roughness. Such an exponent description can be obtained by comparison with other wind descriptions, such as was done on Figure 2-11, but the altitude range for accurate application is too restrictive.

A description that best satisfies the requirement for neutral and unstable conditions is the KEYPS equation, which apparently agrees well with restrictive models for regions of instability. For stability, the log-linear profile is well accepted for limited Richardson's number. The only model available for strong stability is that from Reference 2-26, which, although admittedly fitted to data with considerable scatter, provides continuity with the log-linear profile. The data scatter about the strong stability description is not a particular concern as probable occurrences of strong stability are at higher altitudes.

The combination of descriptions just selected is summarized as follows, using the universal function $f(h/\ell')$ for each of the descriptions:

$$\bar{V}_W = \frac{u_{*0}}{k}\left[\ln\left(\frac{h + z_0}{z_0}\right) + f(h/\ell')\right]$$

For $R_i < 0$:

$$h/\ell' = \frac{R_i}{(1 - \gamma' R_i)^{1/4}}$$

$f(h/\ell')$ is given by Figure 2-10

For $R_i > 0$, $h/\ell' < 1$:

$$h/\ell' = \frac{R_i}{1 - \alpha' R_i}$$

$$f(h/\ell') = \alpha' h/\ell'$$

For $R_i > 1/1 + \alpha'$, $h/\ell' > 1$:

$$h/\ell' = (1 + \alpha') R_i$$

$$f(h/\ell') = \alpha' + \alpha' \ln(h/\ell')$$

For continuity, $\gamma' = 4\alpha'$

The combined relationships for R_i and h/ℓ' and for defining (h/ℓ') are presented graphically on Figures 2-13 and 2-14, respectively.

Low altitude winds are probably generated from the geostrophic winds, but the relationship is not clear–the geostrophic wind data are not well documented, and the geostrophic wind has little physical significance. A more meaningful height from which to extrapolate winds, and a height for which more wind data are available, is the tower height. There is a present effort to standardize the tower height at 20 feet and this is the height that will be used. Not only shall the mean wind be specified at 20 feet, but also the Richardson's number, needed to determine the scaling length, ℓ', and, in conjunction with the mean wind at 20 feet, the constant u_{*_0}/k.

Given the Richardson's number and the mean wind at 20 feet, the constants are found by:

$$\frac{u_{*0}}{k} = \frac{\bar{V}_{20}}{\ln\left(\frac{20+z_0}{z_0}\right) + f\left(\frac{20}{\ell'}\right)} \qquad \text{(Fig. 2-15)}$$

$$1/\ell' = \begin{cases} \dfrac{0.05\, R_{i_{20}}}{(1-\gamma' R_{i_{20}})^{1/4}} & , \quad R_{i_{20}} < 0 \\ \dfrac{0.05\, R_i}{1-\alpha' R_{i_{20}}} & , \quad R_{i_{20}} \geq 0, \dfrac{20}{\ell'} < 1 \\ 0.05\,(1+\alpha')\, R_{i_{20}} & , \quad 20/\ell' \geq 1 \end{cases} \qquad \text{(Fig. 2-16)}$$

Note that the constants are calculated before, not during, the simulation.

Still remaining are the specifications for roughness length and α'. The roughness length could be specified for each particular airport and would perhaps be a function of wind direction, distance, height, season, and wind speed. However, the problem at hand involves "average" conditions for all airports, and a number representative for all the above factors for the "average" airport is needed.

The roughness length selected is 0.15 feet, partly because that number appears to qualitatively represent surface conditions in the vicinity of the "average" airport, as seen by Figure 2-7, and partly because that number is used in an existing British Aeronautical Review Board (ARB) autoland certification specification.

It is likely that the "open airport" roughness length of 0.01 feet from Reference 2-14 is too small, since few airports qualify completely as being "open" due to the presence of many aircraft and structures on and around the airport. On the other hand, it is unlikely that the average roughness will correspond to that for the surrounding structures. Airports tend to be

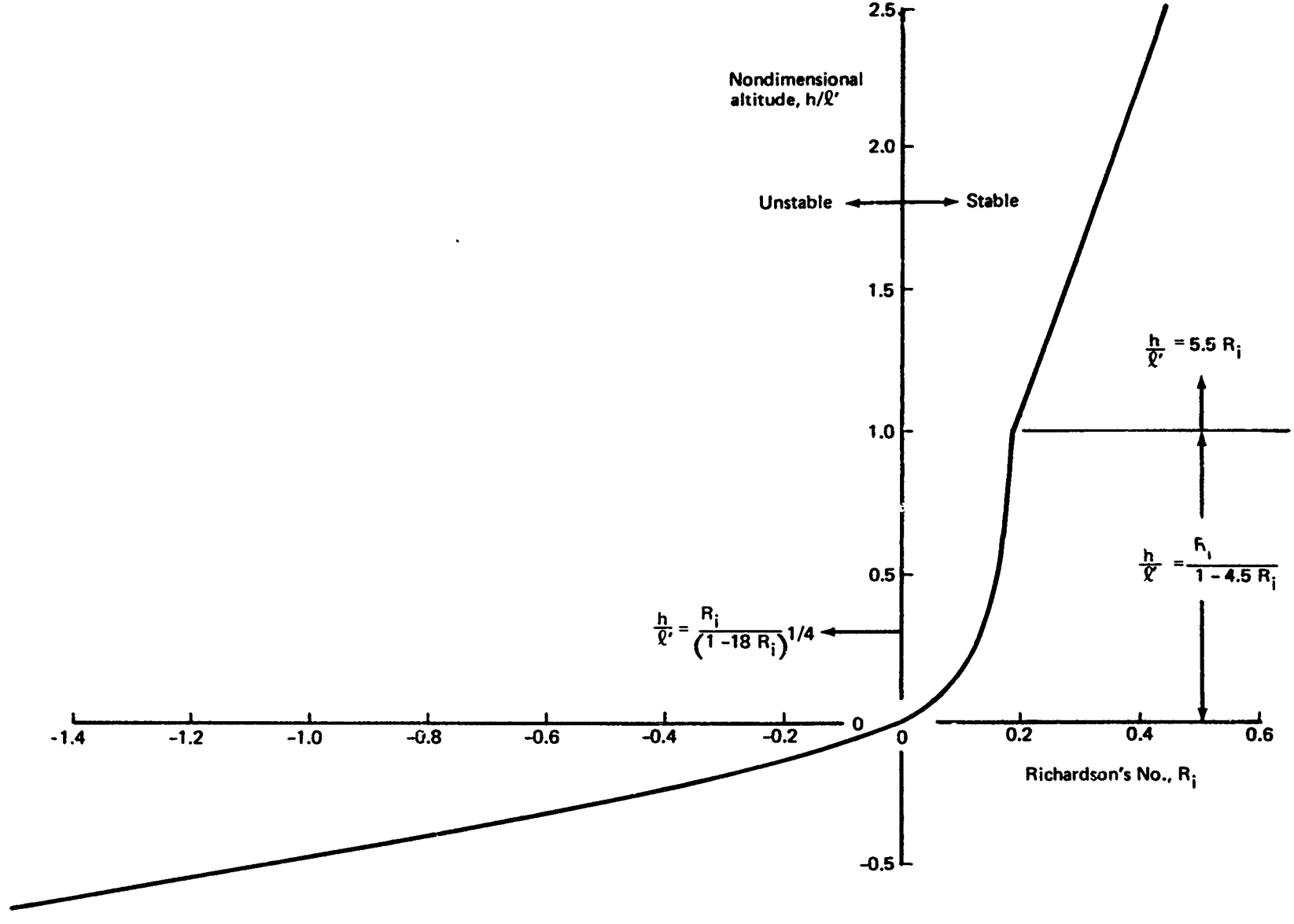

FIGURE 2-13.—LOW ALTITUDE RICHARDSON'S NUMBER PROFILE

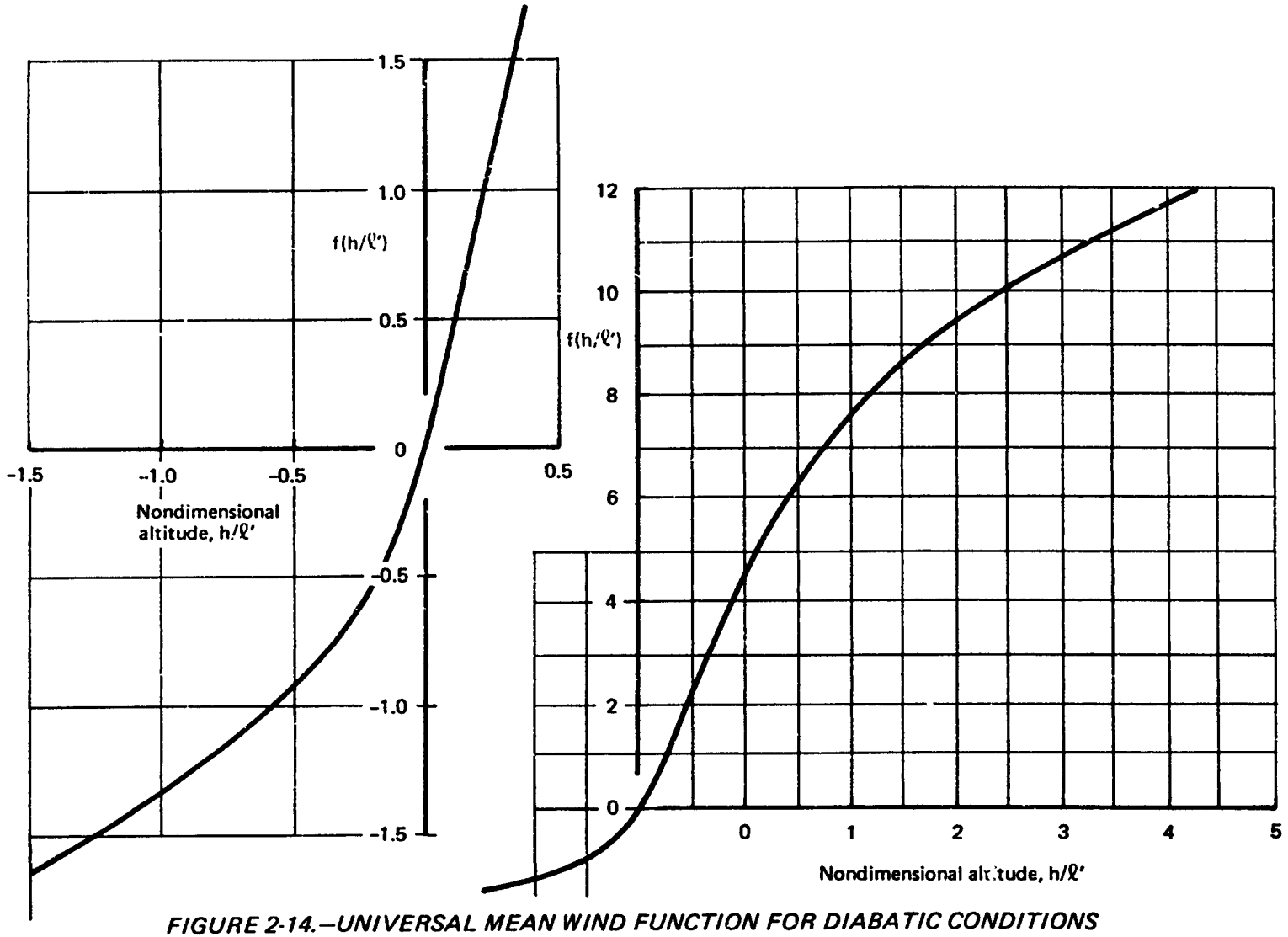

FIGURE 2-14.—UNIVERSAL MEAN WIND FUNCTION FOR DIABATIC CONDITIONS

$$\bar{V}_W = \bar{V}_{20} \frac{u_*/k}{\bar{V}_{20}} \left[\ln\left(\frac{h + z_0}{z_0}\right) + f(h/\ell') \right]$$

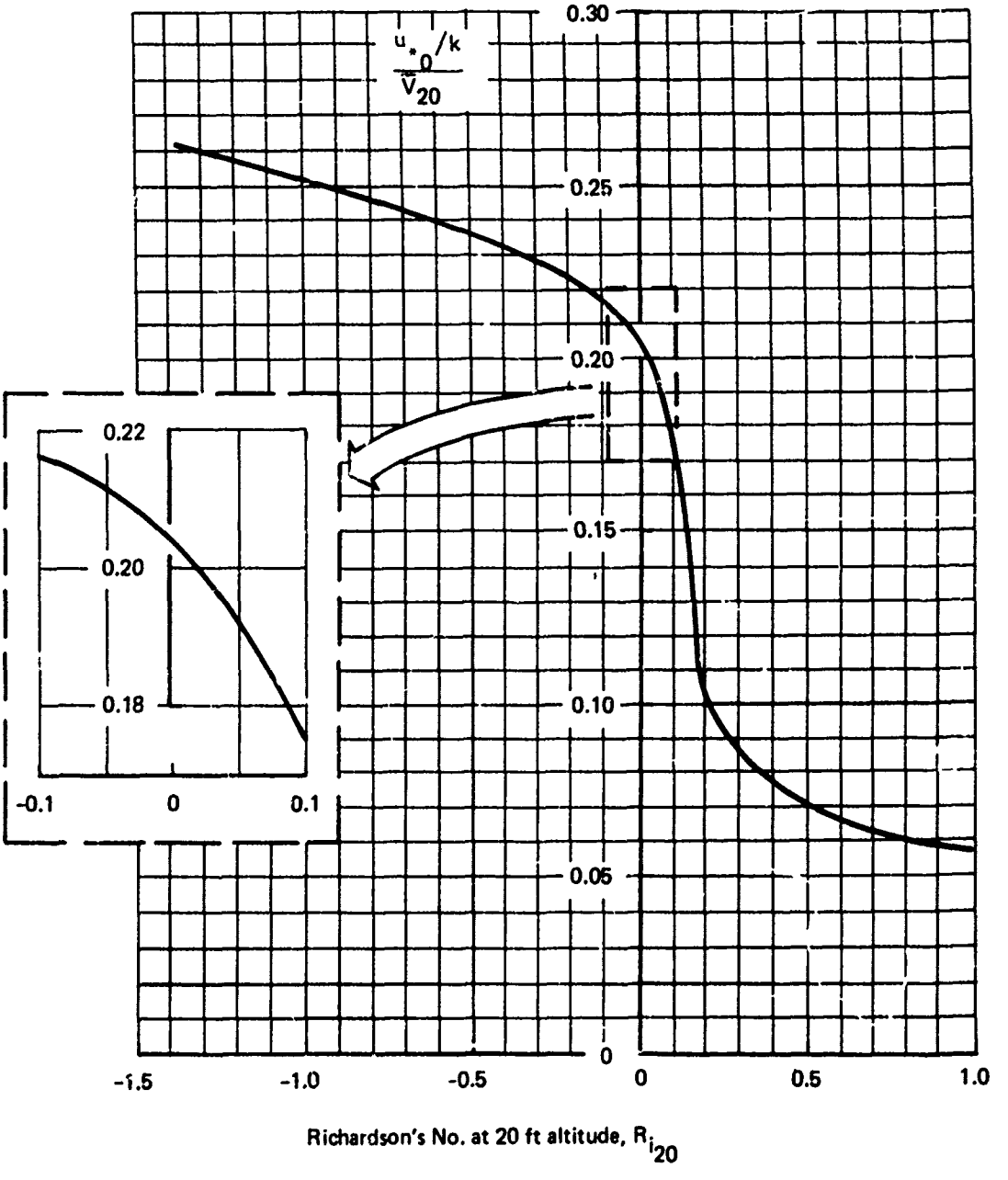

FIGURE 2-15.–PROPORTIONALITY CONSTANT, DIABATIC WIND PROFILE

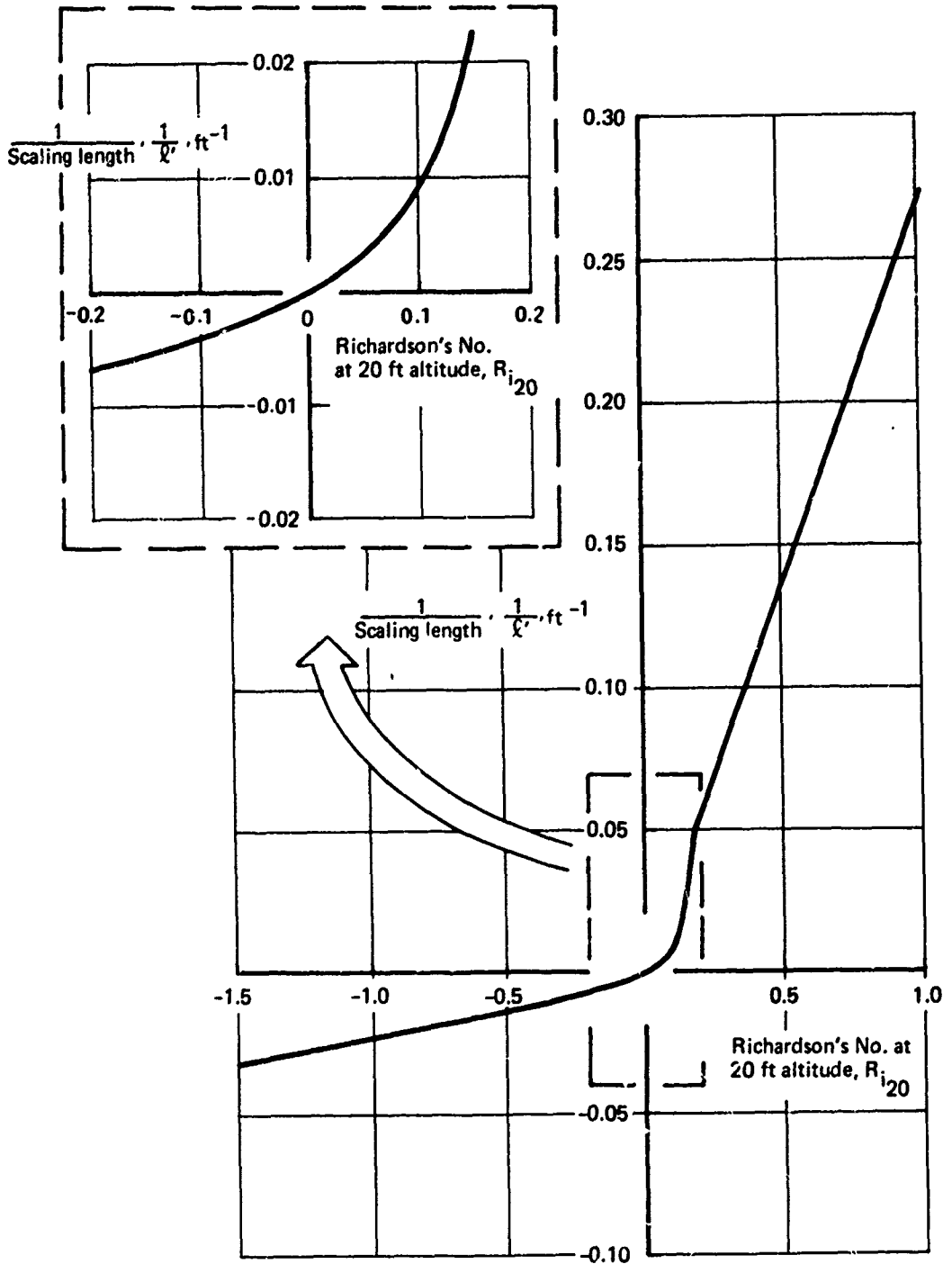

FIGURE 2-16.–SCALING LENGTH DETERMINATION

aligned to the prevailing wind and, due to operation procedures, large down-runway components will be headwinds. From a conversation with Dr. Panofsky (coauthor of Ref. 2-7), the internal boundary layer dissipates after about a mile. Since most runways tend to open for more than a mile, and using a one-in-ten slope for the downwind rise of the internal boundary layer from the terrain discontinuity, it may be concluded that pure headwind approaches will have a roughness dominated by the airfield. Tailwinds, at lower wind speeds, will have a greater roughness associated with the terrain along the approach path. The greatest roughness affecting the wind is likely to be for pure crosswinds: The lateral displacements of obstacles are likely to be within the 1 mile specified. Roughness lengths for pure crosswinds are altitude dependent, with lower altitudes providing smaller roughness lengths approaching that associated with the runway. Since, for aircraft operation the lowest altitudes are generally the most important, there should be a weighting in favor of the smaller lengths.

A qualitative averaging of the various considerations does not indicate that a roughness length of 0.15 feet is out of line. For airports where the surrounding terrain is very rough, the same arguments can be extended to support an effective roughness length substantially less than that associated with the surrounding terrain.

The constant α' is selected as 4.5 for both stable and unstable conditions (to provide continuity of the slope of $f(h/\ell')$ at adiabatic conditions), resulting in $\gamma' = 18$. The main reason for selecting 4.5 is the substantiation given by Reference 2-7. This number appears to agree reasonably well with estimates by other investigators.

The mean wind profiles that result from this description are shown on Figure 2-17. Stable conditions are seen to result in more severe shears and higher winds above 20 feet, for the same reference mean wind. However, since the wind is propagated from the geostrophic wind, it might be expected that greater stability at the reference height will be associated with lower mean winds at the same height, and consequently, the differences in the shears between stable and unstable conditions may not be so great.

In order to provide for a mean wind shear that disappears at the edge of the boundary layer and an increase of the maximum altitude to which the model is accurate, a modification of the wind and wind shear models incorporating friction velocity variation with altitude is adopted.

Two models for the variation of friction velocity with altitude have been provided, both derived using Taylor series expansions. One, providing a quadratic relationship, is most accurate near the surface. The other, a linear relationship, is most accurate near the boundary layer. Either is sufficiently accurate near the surface of the earth where the effect is insignificant. Thus, the linear relationship is selected as it provides a more accurate description at higher altitudes where the decrease in friction velocity is more significant. That is

$$u_* = u_{*_0}\left(1 - \frac{h}{d}\right)$$

where d is depth of the boundary layer.

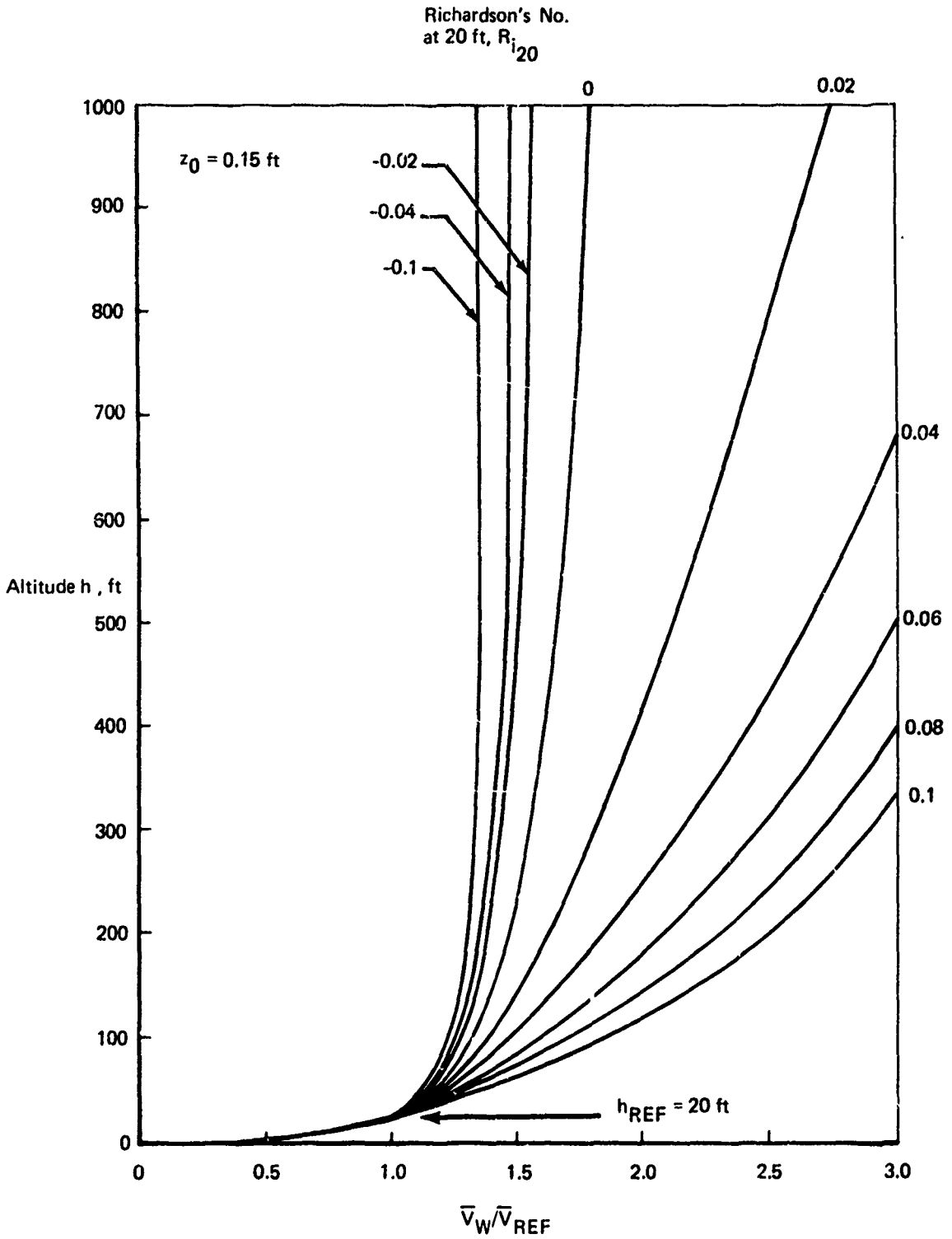

FIGURE 2-17.--MEAN WIND PROFILE, EFFECT OF STABILITY

The depth of the boundary layer has been given by

$$d = \frac{u_{*_0}}{10.7\omega_E \sin\lambda}$$

This equation is undoubtedly incorrect at the equator where the boundary layer is predicted to be infinite. Since u_{*_0} can be related to the surface wind, it provides for less decay of friction velocity for higher surface wind conditions. Above the boundary layer, turbulence due to the propagation of the geostrophic wind to the surface is zero. This does not account for turbulence generated by convectional clouds, inversion layers, low level jetstreams, and other phenomena that produce mean wind shears and heat convection at high altitudes.

The equation for the boundary layer thickness is more acceptable for larger latitudes. Most of the United States and the majority of world airport activity lies between 30° and 50° latitude. A latitude of 40° shall be assumed to be representative of United States operations. Recognizing that $\omega_E = 7.2685 \times 10^{-5}$ rad/sec,

$$d = 2000\, u_{*_0} \sim \text{ft}$$

$$u_{*_0} \sim \text{ft/sec}$$

Richardson's numbers at 20 feet is expected to fall within a small range and hence the effect of stability on boundary layer thickness is small. However, the boundary layer is linearly related to the mean wind at 20 feet. For a 10-knot wind at 20 feet, the boundary layer thickness is computed to be 2750 feet for adiabatic conditions.

The final form for the mean wind and mean wind shear models becomes:

$$\frac{\partial \bar{V}_W}{\partial h} = 0.4\bar{V}_{20}\left(\frac{u_{*_0}/k}{\bar{V}_{20}}\right)\left(1 - \frac{h_W}{d}\right)\phi\left(\frac{h_W}{\ell'}\right)$$

$\phi\left(\frac{h_W}{\ell'}\right)$ given on Figure 2-18

$$\bar{V}_W = \bar{V}_{20}\left(\frac{u_{*_0}/k}{\bar{V}_{20}}\right)\left[\ln\left(\frac{h + z_0}{z_0}\right) + f\left(\frac{h_W}{\ell'}\right) - \frac{h_W}{d}\, g\left(\frac{h_W}{\ell'}\right)\right]$$

$$h_W = \begin{cases} h, & h < d \\ d, & h \geq d \end{cases}$$

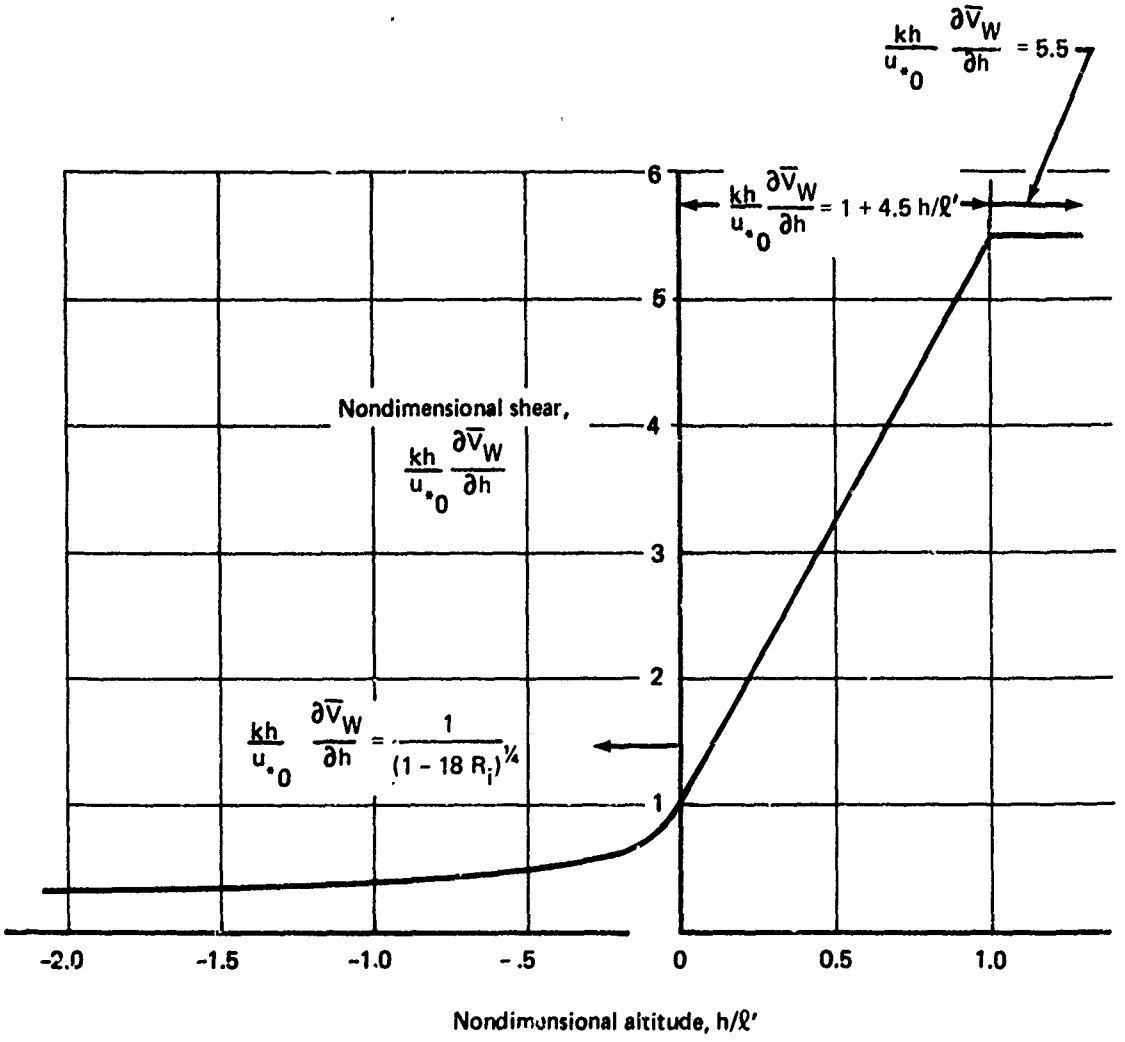

FIGURE 2-18.–SELECTED NONDIMENSIONAL SHEAR DESCRIPTION

The function $g(h/\ell')$ has been obtained from $f(h/\ell')$ and numerical integration according to:

$$g\left(\frac{h}{\ell'}\right)\begin{cases} f\left(\frac{h}{\ell'}\right) - \frac{1}{(-h/\ell')} \int_0^{-h/\ell'} f(\xi)d\xi\,, & \frac{1}{\ell'} < 0 \\ f\left(\frac{h}{\ell'}\right) - \frac{1}{(h/\ell')} \int_0^{h/\ell'} f(\xi)d\xi\,, & \frac{1}{\ell'} > 0 \end{cases}$$

and is shown on Figure 2-19.

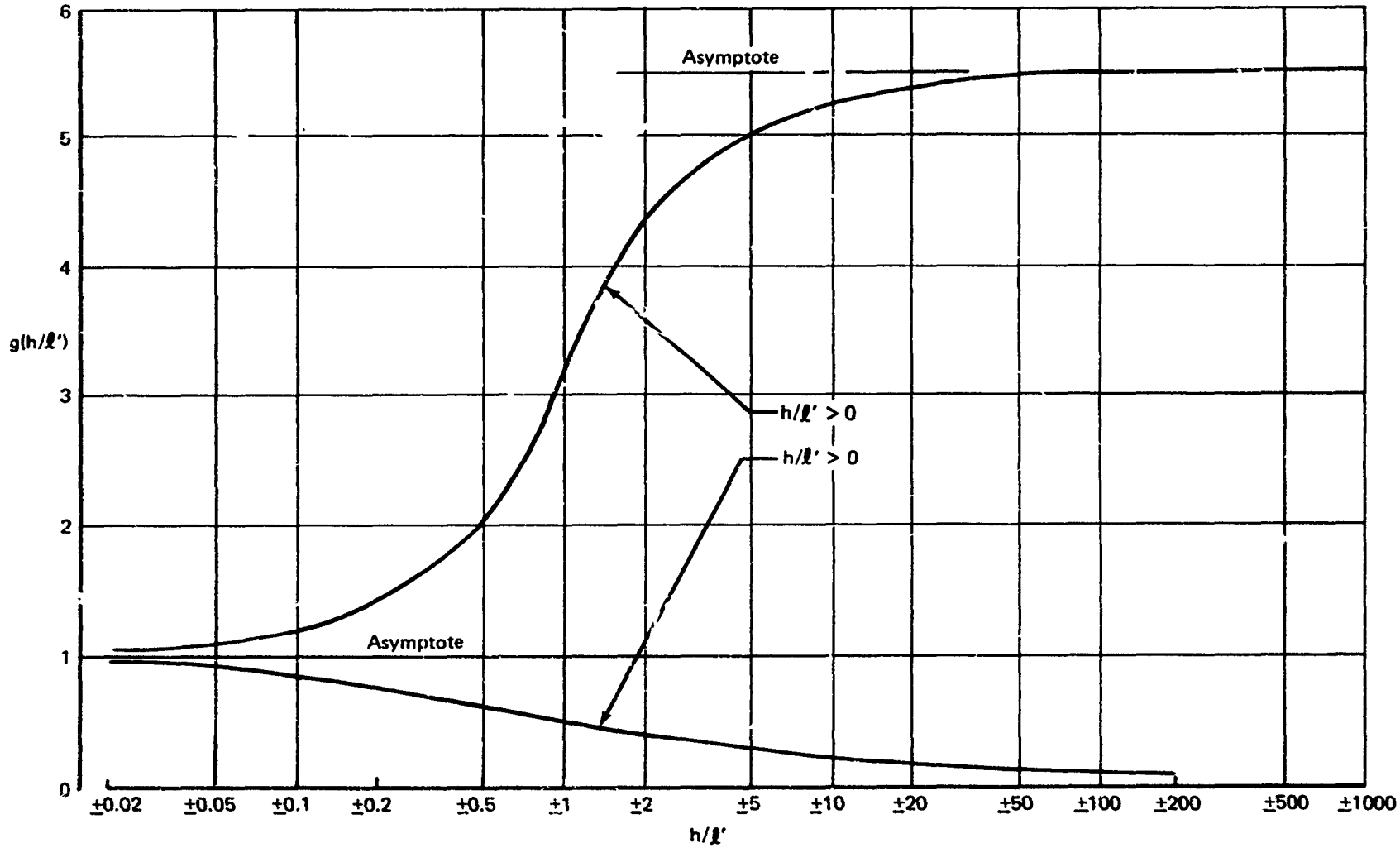

FIGURE 2-19.—VARIABLE SHEAR STRESS CORRECTION TO WIND PROFILE

2.4 TURBULENCE

Wind shears will act to displace air particles vertically. If unstable atmospheric conditions exist, buoyancy forces will tend to amplify the displacement. For physical systems, unstable divergences cannot increase without bound. Produced by the wind shear and buoyancy forces, turbulence is a mechanism by which increasing atmospheric instability is constrained. According to Reference 2-1: "In turbulent air the mixing of hotter and colder air parcels will tend to produce thermal equilibrium locally." This does not mean that turbulent air occurs only for negative Richardson's numbers, but rather that the buoyancy forces must be large enough to remove energy as fast as they are introduced by the shear forces for turbulence not to exist on a self-sustaining basis. The ratio of buoyancy forces removing energy (for stable atmospheric conditions) to the inertia (wind shear) energy production is the Richardson's number, and a value of one might be expected to specify the existence of turbulence. However, as stated in Reference 2-7, "This does not mean that a Richardson's number of unity gives the criterion for the onset or disappearance of turbulence; an instability or some other source must first generate large disturbances; the value of (Richardson's number) then determines when they can be self-supporting."

There apparently is a Richardson's number hysteresis effect determining the existence of turbulence. This is explained in Reference 2-7: "Existing turbulence would not ordinarily be expected to vanish at the same value [of Richardson's number associated with the generation of turbulence from laminar motion.] since disturbances present are already large, ..."

The production of turbulence from laminar flow has been predicted by linear analysis to occur at $R_i = 0.25$, as reported in Reference 2-7. The same reference also notes that turbulence is seldom found above $R_i = 0.2$ in the atmosphere, and the existence of turbulence is related to the "critical" Richardson's number, equal to $1/\alpha'$ where α is the constant appearing in the log-linear mean wind profile. Reference 2-7 provides estimates of critical Richardson's number of from 0.14 to 0.22.

Since turbulence can only exist under conditions of atmospheric stability, its discussion is not separable from stability considerations; limiting consideration of turbulence to adiabatic conditions cannot be justified at this point. The classifications "stable" and "unstable" as applied to turbulence (i.e., its absence or presence) are not the same as for mean wind. In this connection, "stable" and "unstable" are related to a positive critical Richardson's number rather than to 0. The discussion of turbulence applies only for Richardson's numbers less tahn the critical Richardson's number.

The equations of motion for turbulence have been developed from the Navier-Stokes equations and are presented in References 2-7, -9, and -30, among others. From observations relating to these equations, some physical characteristics of turbulence have been determined (Ref. 2-7).

- Turbulence provides a transport of energy from the generation of energy mechanically and convectively to internal energy. The energy transport process occurs through a cascade of eddies of diminishing size, which finally ends in viscous dissipation.

- Turbulence is three-dimensional and nonlinear; the transfer of energy from one size eddy to another can only take place nonlinearly in three dimensions.

- Turbulence is diffusive, much as the molecules in a gas. That is, a tagged point in a turbulence field will wander farther and farther away from its original location, accounting for the transport of mass, moment, and heat properties. Turbulence transport of physical properties "is usually far more effective than the transport due to molecular motion."

- Turbulence is a continuum phenomenon with a smallest dynamically significant scale being much larger than intermolecular distances or molecular dimensions.

- Turbulence is approximately an equilibrium phenomenon for homogeneous terrain. "Except for transitional periods, the local rate of change of kinetic energy is of the order of a few $(m/sec)^2$ in several hours while the largest terms in the energy equation are of [two orders of magnitude larger] in the boundary layer."

The diffusive, continuous, and equilibrium characteristics of turbulence lead to the property of homogeneity of turbulence in the horizontal plane over homogeneous terrain, the condition that has been previously specified. That is, the average properties of turbulent motion are independent of horizontal position, so long as we constrain ourselves to consideration of a region smaller than the entire turbulence field.

The concept for the horizontal homogeneity of turbulence is not universally accepted, and there has been considerable recent work based on turbulence consisting of local concentrations of energy (Refs. 2-31, -32, and -33). However, the description of inhomogeneous turbulence can be understood by relating it to homogeneous turbulence.

The nonlinearity of the equations of motion for turbulence has prevented unique solutions for given sets of conditions. As stated in Reference 2-7, "the uniqueness of the solution seems likely; however, the solution appears (in the unstable regime) to be so sensitive to minute changes in the conditions that we never know these finely enough to predict the detailed structure of the flow." As a consequence, the tool of ignorance, the statistical description, must be used.

The starting point for describing turbulence is the specification of the statistical tools and description of their application. Even using statistics, a great number of assumptions must be made to achieve a description that can be applied to practical problems.

Upon identifying the statistical characteristics, their variations and the parameters causing the variations need to be found. For example, it is intuitive that there is a magnitude of turbulence and a scale relating to the size of the turbulence eddies. The question arises as to whether the statistical characteristics can be described deterministically or whether they, in turn, must be described statistically.

2.4.1 Statistical Functions for Turbulence Description

Turbulence has been defined as the difference between the instantaneous wind velocity and the mean wind velocity. We wish to deal with this difference only, which has thus far been assumed to be a random process and to be homogeneous (the statistical properties are invariant with the location at which they are measured).

The most fundamental statistical property is the arithmetic mean or average. However, the mean may be taken with respect to many parameters. As stated in Reference 2-7, "... in measuring wind velocity, we can speak of the average of wind velocity at a number of different times at the particular measuring station, or of the average of the wind velocity at a number of different places at a particular instant, or of the average of the wind velocity at a particular place, at a particular time of day during a number of occurrences of the same weather conditions. This last is probably the most fundamental idea, the concept of an 'ensemble' of experiments."

For example, assume that for atmospheric conditions constrained to be the same, a turbulence component, u, is a function of time and location, and that N samples have been obtained for the same conditions. Then, using $< >$ to denote an ensemble average,

$$< u(\vec{r}, t, N) > = (1/N) \left[u(\vec{r}, t, 1) + u(\vec{r}, t, 2) + \cdots + u(\vec{r}, t, N) \right]$$

To determine the ensemble average for the entire population of samples, the limit as $N \to \infty$ is considered:

$$< u(\vec{r}, t) > = \lim_{N \to \infty} < u(\vec{r}, t, N) >$$

Two assumptions about the character of turbulence are introduced at this point. First, it shall be assumed that the ensemble average is independent of the absolute time so that

$$< u(\vec{r}, t) > = < u(\vec{r}) >$$

Satisfaction of this assumption is called "stationarity." Stationarity is said to exist when the mean and higher order averages (averages of products of turbulence components) are independent of the absolute value of time, but not necessarily independent of time differences. The second assumption is that time and ensemble averages are the same. A process exhibiting this property is said to be "ergodic." Reference 2-3 states that the ergodic property follows when turbulence is both homogeneous and stationary. From the ergodic property, we have

$$< u(\vec{r}) > = \bar{u}(\vec{r}) = \lim_{T \to \infty} \int_{-T/2}^{T/2} u(\vec{r}, t)\, dt$$

where the over-bar implies a time average.

By definition of turbulence,

$$\bar{u}(\vec{r}) = 0$$

This can be automatically assured if turbulence is considered to be the total wind measured with respect to an axis system attached to the mean wind.

The mean value of turbulence is trivial, but it is only one of many averages that may be taken. In general, averages may be taken of products of turbulence components and their derivatives which may be displaced in time and space from each other. The averages of these products are used to evaluate interrelationships or correlations, and results of the averaging process are called "correlation" functions.

The mean is also but one description defining the probability density function, a second statistical function. Finally, the last statistical function of concern is the spectrum function, which is simply the description of the correlation function in the frequency domain.

2.4.1.1 Correlation Functions

In general, a turbulence correlation function $R_{ij}(\vec{r}_1, \vec{r}_2, t_1, t_2)$ may be defined as:

$$R_{ij}(\vec{r}_1, \vec{r}_2, t_1, t_2) = \langle u_i(\vec{r}_1, t_1) \cdot u_j(\vec{r}_2, t_2) \rangle$$

That is, the correlation function is the ensemble average of the product of the i and j components of turbulence measured at positions $\vec{r}_1$ and $\vec{r}_2$ and at times t_1 and t_2, respectively. The correlation function may more generally involve a product of any number of turbulence components but, for the purposes of this report, only the product of two components will be considered. "Turbulence components" is used in a very general sense and includes space and time derivatives of turbulent velocities.

The correlation function describes the average relationship between two components. If two components are "uncorrelated" for all time and space relationships, their correlation function will be zero. If the two components are the same and are measured at the same time and position, the correlation function becomes the "variance":

$$R_{ii}(\vec{r}_1, t_1) = \langle u_i^2(\vec{r}_1, t_1) \rangle = \sigma_{ii}^2(\vec{r}_1, t_1)$$

Note that the attachment of the turbulence axis system to the mean wind alleviates the need to subtract the mean from the total velocity to achieve the variance.

More generally, the correlation function of two different components evaluated at the same time and point in space leads to the covariance:

$$R_{ij}(\vec{r}_1, t_1) = \langle u_i(\vec{r}_1, t_1)\, u_j(\vec{r}_1, t_1) \rangle = \sigma_{ij}^2(\vec{r}_1, t_1)$$

The correlation function can be simplified considerably by invoking the assumptions previously made:

- *Homogeneity:* The statistical properties of turbulence are independent of position. Thus, if $\vec{r}_2 = \vec{r}_1 + \vec{\xi}$, where $\vec{\xi}$ is the displacement vector between the components,

$$R_{ij}(\vec{r}_1, \vec{r}_2, t_1, t_2) = R_{ij}(\vec{\xi}, t_1, t_2)$$

- *Stationarity:* The statistical properties are independent of the absolute time. Thus, if $t_2 = t_1 + \tau$, where τ is the time displacement between two components,

$$R_{ij}(\vec{\xi}, t_1, t_2) = R_{ij}(\vec{\xi}, \tau)$$

- *Ergodicity:* Ensemble and time averages are identical; therefore,

$$R_{ij}(\vec{\xi}, \tau) = \lim_{T \to \infty} \int_{-T/2}^{T/2} u_i(\vec{r}, t)\, u_j(\vec{r} + \xi, t + \tau)\, dt$$

This equation is equivalent to saying that for specific combinations of relative time and space displacements of the two components, the correlation function is found by averaging over all time. When time averages for all combinations of relative displacement and time have been found, the composite of all the averages provides a correlation function as a function of relative space and time displacement.

If the two components for whose product the average is taken are the same, the correlation function is known as the "autocorrelation." Otherwise, it is referred to as the "cross correlation." The expressions for the variance and covariance reduce to:

$$\sigma_{ij}^2 = R_{ij}(0, 0)$$

and provide a means for normalizing the correlation function:

$$\hat{R}_{ij}(\vec{\xi}, \tau) = \frac{R_{ij}(\vec{\xi}, \tau)}{\sigma_{ij}^2}$$

Note that $\hat{R}_{ij}(0, 0) = 1$.

For the application of turbulence to aircraft, an additional simplification may be made, referred to as "Taylor's hypothesis." The essence of this hypothesis, as described in Reference 2-3, is as follows: "Airplanes fly for the most part at speeds large compared to the turbulence velocities and to their rates of change. Thus the vehicle can traverse a relatively large patch of turbulence in a time so short that the turbulence velocities have not

had time to change very much. This amounts to neglecting t in the argument $\vec{u}(\vec{r}, \tau)$, i.e., to treating the turbulence as a frozen pattern in space. This assumption is known as 'Taylor's hypothesis'. Its consequence is that

$$R_{ij}(\vec{\xi}, \tau) = R_{ij}(\vec{\xi})$$

The application of Taylor's hypothesis is of immense importance for the ability to simulate turbulence.

The correlation function has been presented perhaps abstractly without indicating its relationship to the simulation of turbulence. Unfortunately, this relationship cannot be described without completion of the turbulence description.

A considerable number of assumptions have been introduced to enable the correlation function to be defined in terms of only the spacial separation between the two turbulence components involved. These assumptions are not universally accepted and can be applied only with restrictions.

Certainly, homogeneity at low altitudes is dependent upon homogeneous terrain. Homogeneity and stationarity require equilibrium of turbulence energy, which in turn is dependent on the slow rate of change of atmospheric conditions.

Perhaps most restrictive is the application of Taylor's hypothesis, which at least restricts the minimum airspeed of aircraft to which it may be applied. Most certainly, it cannot apply at zero airspeeds such as for near hover conditions. Reference 2-1 has concluded that the Taylor hypothesis is valid for airspeeds greater than one-third the mean wind velocity in the direction of flight, based on permitting a vertical turbulence standard deviation error of 20% and a presumed "true" space-time relationship.

Reference 2-7 indicates qualitatively that the Taylor hypothesis must fail to some extent for large eddy turbulence contributions, associated with large scale vertical motion during unstable conditions, as these eddy motions must remain fixed with respect to the ground to some extent. Taylor's hypothesis implies that turbulence eddies must move with respect to the ground at the mean wind speed.

It shall be assumed that the conditions required to satisfy the assumptions made are met, for the applications required, and that the correlation function is dependent on spacial separations only.

2.4.1.2 Probability Functions

Such quantities as the variance obtained from the autocorrelation function provide a measure of the average level of turbulence, but do not quantify the distribution of the magnitude of turbulence velocities nor the likelihood of encountering a particular turbulence level. The functions that provide such information shall be referred to as probability functions.

Probability is simply the number of specific occurrences divided by the total number of observations. For example, the probability that a function g lies between the values g_L and g_U is given by:

$$P\left\{g_L \leq g \leq g_U\right\} = \frac{\left[\begin{array}{l}\text{No. of observations where g lies in the region} \\ g_L \leq g \leq g_U\end{array}\right]}{\text{Total number of observations}}$$

When the lower limit g_L is allowed to approach $-\infty$, the probability function is the "cumulative probability," or the probability that g will not exceed g_U. When the upper limit, g_U, is allowed to approach $+\infty$ the probability function is the "exceedance probability," or the probability that g will not be less than g_L. Note that a probability can never be less than zero nor greater than one. The exceedance probability is equal to one minus the cumulative probability and vice versa.

When g_U is allowed to approach g_L, the probability function is the probability that g will equal g_L, or the "probability of occurrence." When g is a discrete function that takes on only specific values in the region, the probability of occurrence may take on non-zero values. If, however, g is a continuous function that may assume any of the values in the region $g_L \leq g \leq g_U$ the probability of occurrence is zero as there are an infinite number of values that g may assume.

For a continuous analytic function, the above definitions are somewhat cumbersome. An alternate approach is provided by Reference 2-7, in which an indicator function, $\phi(g_L, g)$, is first defined.

$$\phi(g_L, g) = \begin{cases} 1, & g \leq g_L \\ 0, & g > g_L \end{cases}$$

That is, the indicator function is unity when the function g is less than or equal to g, and zero otherwise. This is illustrated on Figure 2-20. Now, the average of the indicator function provides the relative portion of time that g is less than g_L, which is precisely the cumulative probability:

$$P\left\{g \leq g_L\right\} = \phi\left|g_L, g(t)\right| = \lim_{T \to \infty} \frac{1}{T} \int_{-T/2}^{T/2} \phi\left|g_L, g(t)\right| \, dt$$

The probability that g lies in the region $g_L \leq g \leq g_U$ can be found from the cumulative probability:

$$P\left\{g_L \leq g \leq g_U\right\} = P\left\{g \leq g_U\right\} - P\left\{g \leq g_L\right\}$$

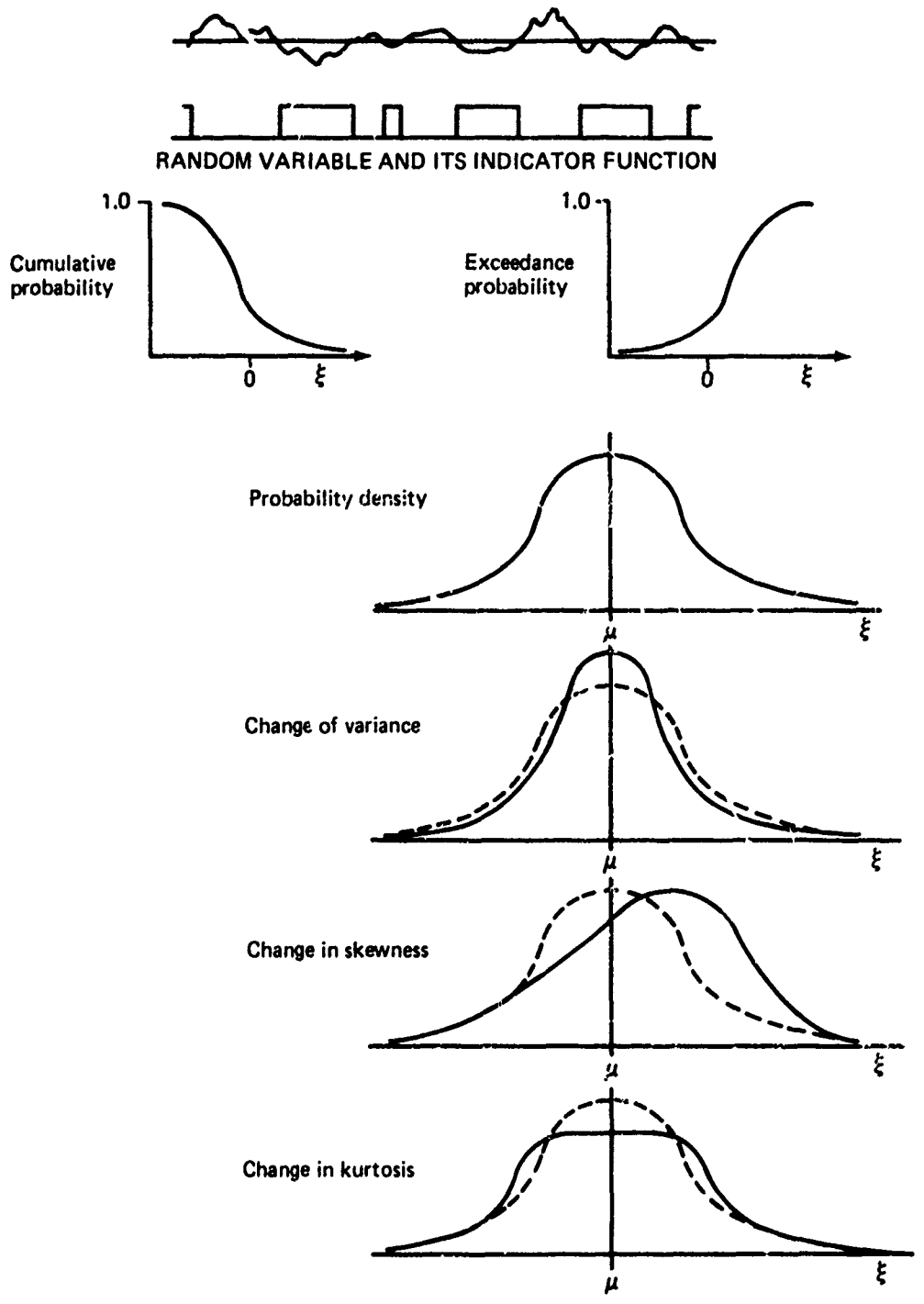

FIGURE 2-20.–PROBABILITY FUNCTIONS AND CHARACTERISTICS

As previously stated, shrinking the region to zero (letting g_U approach g_L) will only provide a probability of occurrence equal to zero for a continuous function. Rather, the ratio of the probability to the width of the region, $(g_U - g_L)$ is considered as g_U approaches g_L. This amounts to taking the derivative of the cumulative distribution, and the result is called the "probability density" function, $\beta(g)$:

$$\beta(g = g_L) = \lim_{g_U \to g_L} \frac{P|g \leq g_U| - P|g \leq g_L|}{g_U - g_L}$$

$$= \frac{d}{dg_L} P|g \leq g_L|$$

Conversely, the cumulative probability is found by integrating the probability density function:

$$P|g \leq g_L| = \int_{-\infty}^{g_L} \beta(g)\, dg$$

Typically, the probability density function approaches zero for increasing large positive and negative g, as illustrated in Figure 2-20.

The probability density function can be used to determine ensemble averages for single parameter functions, as shown in Reference 2-3, by:

$$\langle g \rangle = \int_{-\infty}^{\infty} g(\xi)\, \beta(\xi)\, d\xi$$

This equation is referred to as the "theorem of the mean," and can be used to quantify many characteristics of the probability density function. By letting $g(\xi)$ take on various powers of the parameter ξ,

$$g(\xi) = \xi^n, \; n = 1, 2, 3, \text{---}$$

the "moments" of the distribution are obtained:

$$\langle \xi \rangle = \int_{-\infty}^{\infty} \xi \beta(\xi)\, d\xi \qquad \text{, 1st moment}$$

$$\langle \xi^2 \rangle = \int_{-\infty}^{\infty} \xi^2 \beta(\xi)\, d\xi \qquad \text{, 2nd moment}$$

$$\langle \xi^3 \rangle = \int_{-\infty}^{\infty} \xi^3 \beta(\xi)\, d\xi \qquad \text{, 3rd moment}$$

and so on. The first moment is identified as the mean, which locates the distribution. The second moment is the variance, which defines the breadth of the distribution. All odd-number moments refer to the symmetry or lack of symmetry of the probability density distribution about its mean, with zero values corresponding to symmetry. Specifically, the third moment is used to measure skewness, a normalized measure of the separation between the mean and the mode. The fourth moment is used to measure the "kurtosis" or flatness factor. Higher moments measure other characteristics and generally have diminishing importance. Some of the characteristics of the probability density function are illustrated on Figure 2-20.

The concepts of probability functions can be extended to joint probability functions. Consider two components of a vector, g_1 and g_2. The indicator function is defined by:

$$\phi_1 (g_{1_L}, g_1)\, \phi_2 (g_{2_L}, g_2) = \begin{cases} 1, g_1 \leq g_{1_L} \text{ and } g_2 \leq g_{2_L} \\ 0 \text{ otherwise} \end{cases}$$

The joint cumulative distribution and the joint probability density functions are given by

$$P\left\{g_1 \leq g_{1_L}, g_2 \leq g_{2_L}\right\} = \overline{\phi_1 (g_{1_L}, g_1)\, \phi_2 (g_{2_L}, g_2)}$$

$$\beta\left(g_1 = g_{1_L}, g_2 = g_{2_L}\right) = \frac{\partial^2}{\partial g_{1_L} \partial g_{2_L}} P\left\{g_1 \leq g_{1_L}, g_2 \leq g_{2_L}\right\}$$

or

$$P\left\{g_1 \leq g_{1_L}, g_2 \leq g_{2_L}\right\} = \int_{-\infty}^{g_{2_L}} \int_{-\infty}^{g_{1_L}} \beta(g_1, g_2)\, dg_1\, dg_2$$

Now, invoking the theorem of the mean, the correlation functions may be determined from the joint distribution:

$$R_{12} = \langle g_1 \cdot g_2 \rangle = \int_{-\infty}^{\infty}\int_{-\infty}^{\infty} g_1\, g_2\, \beta(g_1, g_2)\, dg_1\, dg_2$$

For the special case when g_1 and g_2 are independent functions such that the probability density distribution of one of them is not dependent upon the value of the other, the joint probability density distribution is equal to the product of the individual probability density distributions and the correlation function is equal to the product of the individual means:

$$\beta(g_1, g_2) = \beta(g_1)\, \beta(g_2)$$

$$R_{12} = \langle g_1 \rangle \langle g_2 \rangle$$

For two uncorrelated turbulence components, the correlation function is zero.

The most widely used description of the probability density distribution is the "Gaussian" or "normal" distribution. This distribution has great theoretical importance. Many other distributions will asymptotically approach the normal distribution as sample sizes increase. The distribution of sample means, no matter what the distribution of the population, is normal, a characteristic provided by the "central limit theorem."

Assumption of a Gaussian probability density distribution is convenient for developing simple expressions for other types of probability functions, such as for the number of exceedances per mile (number of times a given turbulence level is exceeded in 1 mile of flight), and joint distributions between many possible combinations of turbulence components and their derivatives.

For the simulation of turbulence, assumption of a Gaussian distribution permits the use of relatively simple techniques of generating random or pseudo-random noise needed for the production of turbulence. Analog simulation is heavily dependent upon turbulence having a distribution that is either Gaussian or can be generated from a Gaussian distribution, particularly when time must be scaled by large factors. Techniques are available for real-time digital simulation of turbulence having virtually any distributions.

There is some evidence that turbulence probability density distributions are not Gaussian, particularly for very low and very high turbulence levels. Reference 2-34 states that Reference 2-35 contains an analysis of all three gust components at both high and low altitude showing that atmospheric turbulence is definitely non-Gaussian. The results indicate that low altitude turbulence is more nearly Gaussian than that at high altitudes, but at all altitudes the probability density exceeds that of a Gaussian distribution for both small and large values of gust velocities. Figure 2-21, from Reference 2-35, is presented in Reference 2-34 in support of these arguments. The line labeled "modified Bessel" is the distribution presumed in Reference 2-34 and is obtained by multiplying two random samples of a Gaussian distribution.

Reference 2-35 states that although a probability distribution of all turbulence is non-Gaussian, "... the observational results are in accord with a hypothesis that the turbulence is patchy and that the velocities are distributed locally in a Gaussian manner." As a consequence, a Gaussian representation of turbulence is justified if a patch of turbulence is large in relation to the aircraft and the region covered during a simulation. The patch would have a constant variance, all other factors remaining constant. The variance of turbulence for all patches would be described by a separate probability density function. That is, a Gaussian distribution of turbulence is justified for the simulation of a patch of turbulence having a variance with a constant probability of exceedance. This is the standard procedure.

Even if turbulence patches are not sufficiently large, Figure 2-21 would appear to indicate that a Gaussian distribution of turbulence is representative at low altitudes for all but the very extreme levels. This, however, would require a variance for all of turbulence.

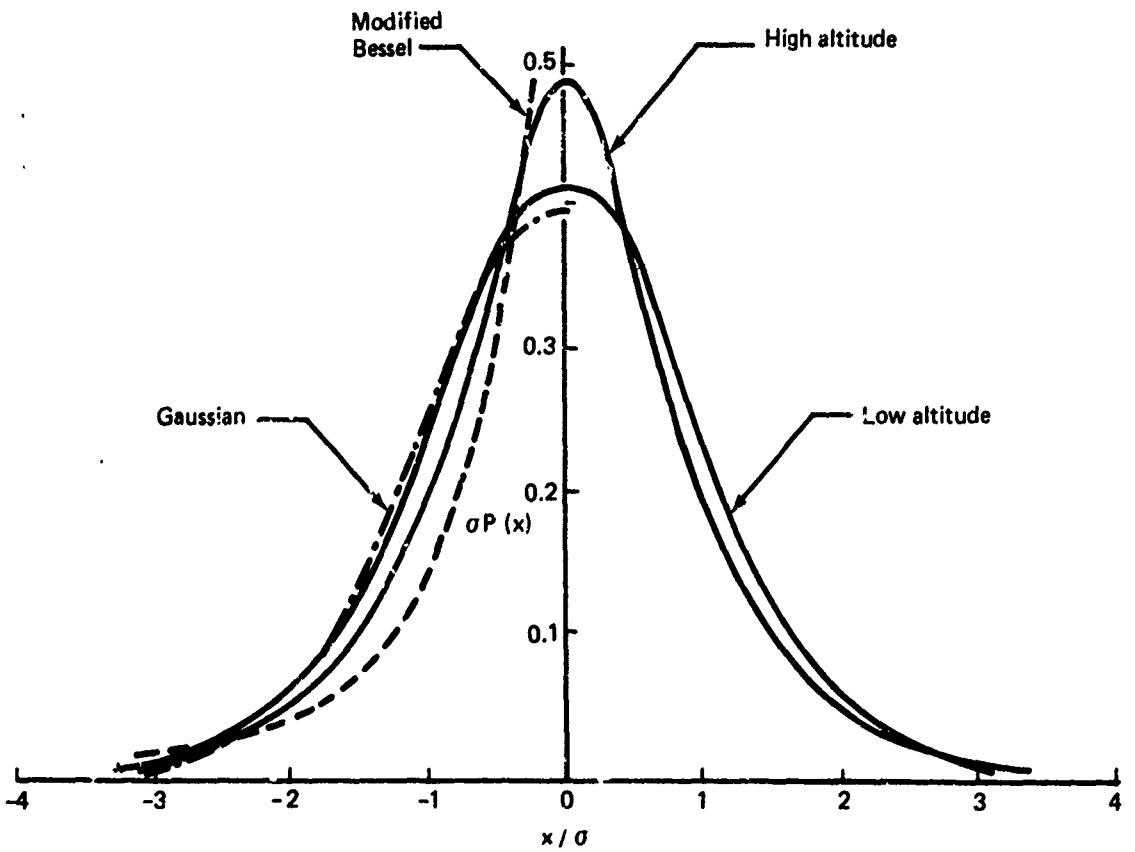

FIGURE 2-21.—TURBULENCE PROBABILITY DENSITIES (FROM REF. 2-34)

It can be shown that a distribution of several patches of turbulence that is non-Gaussian, as shown on Figure 2-21, actually supports the hypothesis that a patch of turbulence is Gaussian. For simplicity, it is assumed that all the world's turbulence is divided into two patches, one with a standard deviation of one and the other with a standard deviation of two. The normal distributions for the two individual patches are ρ_1 and ρ_2 on Figure 2-22. Also, assume that there is equal probability of being in either patch so that the probability of being in one patch is 0.5. The two patches are mutually exclusive. That is, it is not possible to be in both patches at the same time. For mutually exclusive events, the combined probability density function is given by

$$\rho = P_1 \rho_1 + P_2 \rho_2$$

where

P_1 = probability of being in patch 1

P_2 = probability of being in patch 2

The combined probability density function is shown as $(\rho_1 + \rho_2)/2$ on Figure 2-22.

The variance, for discrete samples, is given by

$$\sigma^2 = \frac{\sum_{i=1}^{n} x_i^2}{n-1} \cong \frac{\sum_{i=1}^{n} x_i^2}{n}$$

where x_i = i^{th} sample deviation from the mean. This may be expanded into the standard deviation of patch 1 having n_1 samples and the standard deviation of patch 2 having n_2 samples:

$$\sigma^2 = \frac{\sum_{i=1}^{n_1} x_{1_i}^2 + \sum_{j=1}^{n_2} x_{2_j}^2}{n_1 + n_2}$$

$$= \frac{n_1 \sigma_1^2 + n_2 \sigma_2^2}{n_1 + n_2}$$

The term $n_1/(n_1 + n_2)$ represents the probability of being in patch 1 and the term $n_2/(n_1 + n_2)$ represents the probability of being in patch 2.

$$\sigma^2 = P_1 \sigma_1^2 + P_2 \sigma_2^2$$

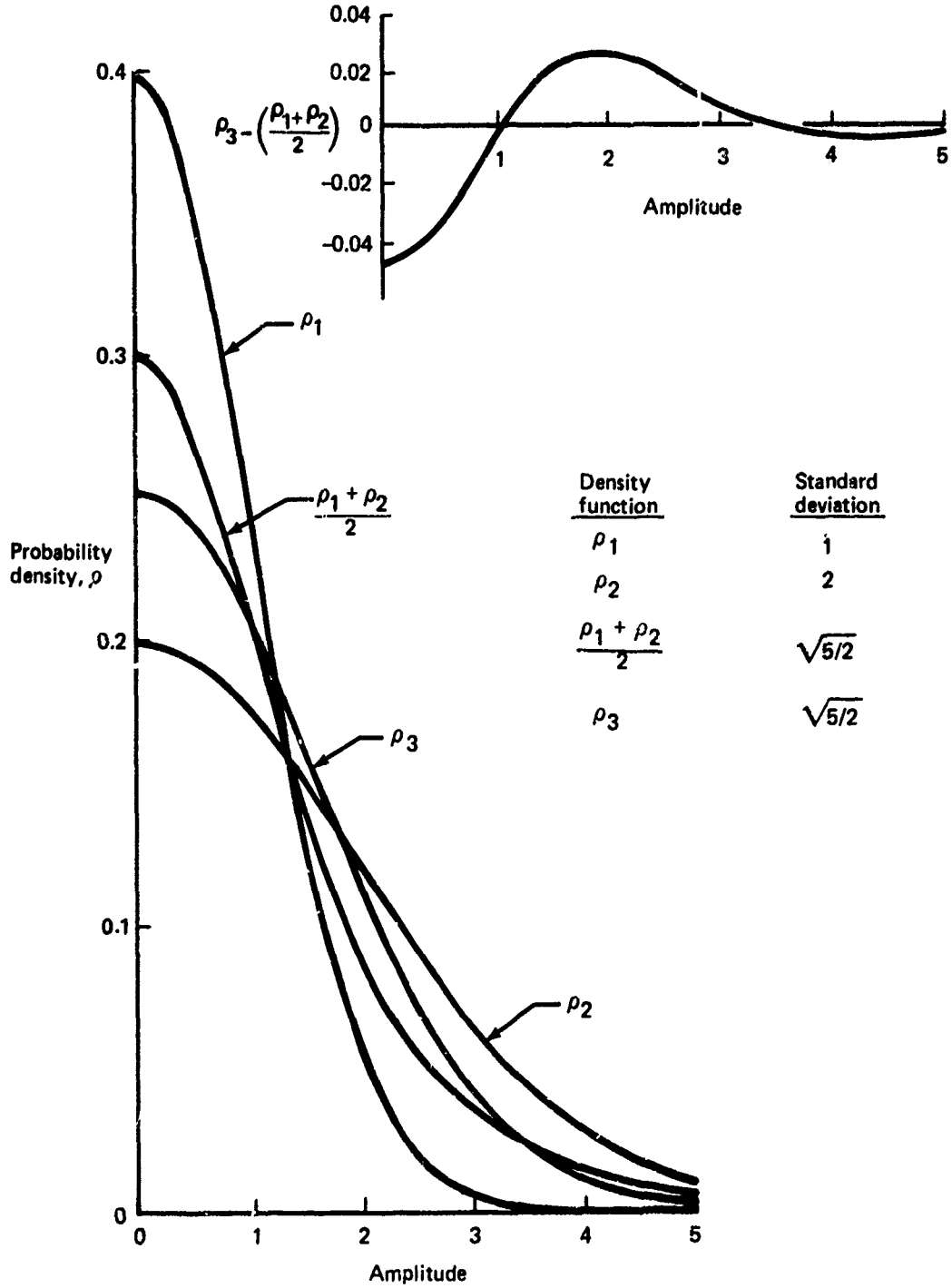

FIGURE 2-22.–COMPARISON: NORMAL DISTRIBUTION AND SUM OF TWO NORMAL DISTRIBUTIONS

For the example, the combined standard deviation is $\sigma = \sqrt{5/2}$. Substituting the combined standard deviation into the equation for the probability density function for a normal distribution,

$$\rho = \frac{1}{\sigma\sqrt{2\pi}} e^{-\frac{1}{2}\left(\frac{x}{\sigma}\right)},$$

gives the distribution on Figure 2-22 labeled ρ_3.

If the actual combined distribution $[(\rho_1 + \rho_2)/2]$ is compared to the Gaussian distribution having the same standard deviation (ρ_3), it is seen that the Gaussian fit underestimates the actual distribution at both small and large amplitudes and overestimates the actual distribution at intermediate amplitudes, exactly the observation on Figure 2-21 made by Reference 2-34.

The non-Gaussian nature of Figure 2-21 actually supports the hypothesis that the velocity distribution of a single patch of turbulence is Gaussian as do the assumptions of homogeneity, stationarity, and diffusiveness, characteristics of turbulence vigorously supported by References 2-7 and 2-30. Perhaps a non-Gaussian description of a single patch of turbulence is best suited for the conditions where these characteristics do not hold.

2.4.1.3 Spectrum Functions

The spectrum function is by definition the Fourier integral of the correlation function. If the correlation function is described in terms of a time displacement, the spectrum function is described in terms of radians/time. If the correlation function is described in terms of a spacial displacement, the spectrum function is in terms of radians/distance.

Consider a one-dimensional correlation function, $R_{ij}(\xi)$. The spectrum function is given by:

$$\Phi_{ij}(\Omega) = \frac{1}{2\pi} \int_{-\infty}^{\infty} R_{ij}(\xi)\, e^{-i\Omega\xi}\, d\xi$$

where Ω = radians/distance. The existence of the spectrum function is assured provided the correlation function vanishes as $\xi \to \pm\infty$.

By the inversion formula for Fourier integrals,

$$R_{ij}(\xi) = \int_{-\infty}^{\infty} \Phi_{ij}(\Omega)\, e^{i\Omega\xi}\, d\Omega$$

When i = j, the spectrum function is called the "power spectral density," or the "power spectrum." When $i \neq j$ the spectrum function is called the "cross-power spectral density" or the "cospectrum."

When the correlation function is for two turbulence components measured at the same location, the integral of the cospectrum yields the covariances.

$$\sigma_{ij}^2 = R_{ij}(0) = \int_{-\infty}^{\infty} \Phi_{ij}(\Omega)\, d\Omega$$

or, for i = j

$$\sigma_{ii}^2 = R_{ii}(0) = \int_{-\infty}^{\infty} \Phi_{ii}(\Omega)\, d\Omega$$

Now, the physical significance of the power spectrum and cospectrum function is seen. The power spectrum and cospectrum function provide the distribution of the variance (or turbulence power) and covariance with frequency. The units of the one-dimensional spectrum function is $(\text{velocity})^2/\text{rad/sec}$. The $(\text{velocity})^2$ term is analogous to power for a unit mass.
The spectrum function is defined for both positive and negative frequencies, is positive everywhere, and is an even function so that $\Phi(-\Omega) = \Phi(\Omega)$. These properties are often used in loads and ride qualities analyses to enable the definition of the "one-sided power spectrum."

$$\sigma_{ii}^2 = \int_{-\infty}^{\infty} \Phi_{ii}(\Omega)\, d\Omega$$

$$= 2\int_{0}^{\infty} \Phi_{ii}(\Omega)\, d\Omega$$

$$= \int_{0}^{\infty} \Phi'_{ii}(\Omega)\, d\Omega;\ \Phi'_{ii}(\Omega) = 2\Phi_{ii}(\Omega)$$

That is, rather than integrating from $-\infty$ to ∞ to obtain the variance, the integral is performed from 0 to ∞ and doubled. Definition of the spectrum function in terms of the one-sided spectrum for the purposes of simulation should be avoided since an erroneous model may result, as is discussed later.

Reference 2-3 and others show that the application of the Fourier integral to a random function results from representing the function with a Fourier series over a finite region, say from $-\lambda$ to λ (the function is zero outside this region), and then taking the limit as the region the function is defined for becomes infinite ($\lambda \to \infty$). The need to consider an infinite

region arises because representation over a finite region from $-\lambda$ to λ will result in a periodic Fourier series with period 2λ, while the random function to be represented is not periodic.

Representation over a finite region results in a "line spectrum" where the spectrum function has non-zero values only at discrete frequencies with the separation between the discrete frequencies being inversely proportional to the size of the region. Use of the Fourier integral will in general attribute a non-zero contribution to the variance at wavelengths approaching infinity. Although this is not physically appealing, a finite patch of turbulence sufficiently large will cause the contributions due to the larger wavelengths to be insignificant and the frequencies at which the disparity exists to be far below the lowest frequencies of interest.

The spectrum function could alternately be represented by the Fourier transform rather than the Fourier integral. The power spectrum function and the corresponding inversion formula would be:

$$\Phi_{FT_{ij}} = \int_{-\infty}^{\infty} R_{ij}(\xi)\, e^{-i\Omega\xi}\, d\xi$$

$$R_{ij}(\xi) = \frac{1}{2\pi} \int_{-\infty}^{\infty} \Phi_{FT_{ij}}(\Omega)\, e^{i\Omega\xi}\, d\Omega$$

The Fourier transform and the Fourier integral spectrum functions are just related by 2π:

$$\Phi_{ij} = 2\pi\, \Phi_{FT_{ij}}$$

The Fourier transform is an acceptable means for producing a power spectrum, but the Fourier integral is used by convention. To avoid possible misinterpretation, any form specified for a spectrum function should be accompanied by the equation for the correlation function or the variance/covariance.

Reference 2-7 discusses alternate techniques for the presentation of the one-dimensional spectrum function. The most direct method is a linear plot of $\Phi(\Omega)$ vs Ω. This plot also has the advantage of graphically presenting the contribution of each frequency to the variance or covariance. However, several decades of frequency and a corresponding range of power may be of interest, thus dictating the form of log (Φ) vs log (Ω). The log-log plot has the advantage of permitting straight-line asymptotic approximations but also the disadvantage of distorting the contribution of each frequency to the total variance or covariance. The form used on Figure 2-1, $\Omega\Phi(\Omega)$ vs log (Ω), combines most of the advantages of the other two forms. Both axes are collapsed (assuming $\Phi(\Omega)$ decreases as $|\Omega|$ increases) and since $\Omega\Phi(\Omega)d$ (log Ω) = $\Phi(\Omega)d\Omega$, the contribution of each frequency range to the total variance/covariance is represented. It may also be noted that a change in the units of frequency (spacial frequency, ordinary frequency, circular frequency) leaves the quantity $\Omega\Phi(\Omega)$ unchanged.

This far, only a one-dimensional spectrum has been considered, where the number of dimensions refers to the number of parameters for which the correlation function and the spectrum function are defined. The number of dimensions does not refer to the number of turbulence components assumed to exist–there are always three turbulence components. The more general case is when the spacial displacement defining the correlation functions is a vector and that has three dimensions. The Fourier transform defining the three-dimensional spectrum function is:

$$\theta_{ij}(\vec{\Omega}) = \frac{1}{(2\pi)^3} \int_{-\infty}^{\infty} R_{ij}(\vec{\xi})\, e^{i\vec{\Omega}\vec{\xi}}\, d\vec{\xi}$$

or

$$\theta_{ij}(\Omega_1, \Omega_2, \Omega_3) = \frac{1}{8\pi^3} \iiint_{-\infty}^{\infty} R_{ij}(\xi_1, \xi_2, \xi_3)\, e^{-i(\Omega_1 \xi_1 + \Omega_2 \xi_2 + \Omega_3 \xi_3)}\, d\xi_1\, d\xi_2\, d\xi_3$$

The inversion formula gives

$$R_{ij}(\xi_1, \xi_2, \xi_3) = \iiint_{-\infty}^{\infty} \theta_{ij}(\Omega_1, \Omega_2, \Omega_3)\, e^{i(\Omega_1 \xi_1 + \Omega_2 \xi_2 + \Omega_3 \xi_3)}\, d\Omega_1\, d\Omega_2\, d\Omega_3$$

This formulation is compatible with the results of the assumptions made, but is not suitable for simulation. Simulation requires that turbulence be generated as a function of time. Taylor's hypothesis provides a tool for converting only one spacial coordinate, that in the direction of flight, into time. The disparity between the three-dimensional spectrum and simulation requirements and the corresponding solution have been observed in Reference 2-30: "Although three-dimensional Fourier transforms are appropriate to a function of a vector argument, the experimenter can make a Fourier analysis (by passing an electronic signal proportional to the velocity through a filter circuit, or wave analyses) with respect to one space coordinate only. The resulting spectrum is a one-dimensional Fourier transform of the velocity correlation sensor, and is obtained from the spectrum tensor $\theta_{ij}(\vec{\Omega})$ by integrating overall values of the lateral components of $\vec{\Omega}$." That is, first the axis system of the turbulence is oriented so that ξ_1 and Ω_1 are measured in the direction of flight, or the "relative wind axis system." Then the three-dimensional spectrum function is integrated successively over the other two components of spacial frequency (Ω_2 and Ω_3) to reduce the three-dimensional spectrum to a one-directional spectrum:

$$R_{ij}(\xi_1, \xi_2) = \iint_{-\infty}^{\infty} \Psi_{ij}(\Omega_1, \Omega_2)\, e^{i(\Omega_1 \xi_1 + \Omega_2 \xi_2)}\, d\Omega_1\, d\Omega_2$$

$\Psi_{ij}(\Omega_1, \Omega_2)$ = two-dimensional spectrum

$$= \int_{-\infty}^{\infty} \theta_{ij}(\Omega_1, \Omega_2, \Omega_3)\, d\Omega_3$$

$$R_{ij}(\xi_1) = \int_{-\infty}^{\infty} \Phi_{ij}(\Omega_1)\, e^{i\Omega_1\xi_1}\, d\Omega_1$$

$$\Phi_{ij}(\Omega_1) = \int_{-\infty}^{\infty} \Psi_{ij}(\Omega_1, \Omega_2,)\, d\Omega_2$$

Thus, the three-dimensional spectrum is reduced to the one-dimensional spectrum.

An additional spectrum of importance is the "energy spectrum function" which distributes kinetic energy with spacial frequency (also called "wave number") magnitude, $\Omega = |\vec{\Omega}|$

$$\tfrac{1}{2}\left[\overline{u_{11}^2} + \overline{u_{22}^2} + \overline{u_{33}^2}\right] = \int_{-\infty}^{\infty} E(\Omega)d\Omega$$

2.4.2 Isotropic Turbulence

The condition of isotropy means that the average functions describing the field of turbulence are independent of direction of the axis system. As a consequence, in the words of Reference 2-7, "... the spectrum function homogeneous in three spacial directions, which is also isotropic, cannot be a function of the separate components of the wave number vector, for a rotation to the new coordinate system would change those. It can be a function only of the length of the vector, for that is the only quantity characterizing $\vec{\Omega}$ which does not remain unchanged under a rotation." Isotropic turbulence exhibits spherical symmetry, and the root mean square intensities for all velocity components must be equal.

It is generally agreed that turbulence at high altitudes is well represented by isotropy. It is also generally agreed that low altitude turbulence is not isotropic. For example, in view of the changes of wind shears and atmospheric stability with altitude at low altitudes, which produce turbulence, it may be reasoned that averages taken normal to the earth will not be the same as averages taken in a direction parallel to the earth. A justified question is: why, when the concern is with low altitude turbulence only, is isotropic turbulence considered? The answer is simply that theory for the general case of nonisotropic turbulence leading to explicit forms of spectrum functions does not exist. Rather, low altitude turbulence spectra are treated as extensions of isotropic turbulence.

2.4.2.1 Fundamental Correlation Functions

The fundamental concept for isotropic turbulence is the form of the correlation function. Reference 2-30 shows that an isotropic second-order two-point tensor, $R_{ij}(\vec{\xi})$, must have the form:

$$R_{ij}(\vec{\xi}) = F(\xi)\xi_i\xi_j + G(\xi)\delta_{ij}$$

where

$\xi = |\vec{\xi}|$

$\delta_{ij} = \begin{cases} 1, & i = j \\ 0, & i \neq j \end{cases}$

$F(\xi), G(\xi)$ = scalar functions.

A second condition for the correlation function is continuity, or conservation of mass. For incompressible conditions, continuity is assured if the divergence of velocity vanishes. In terms of the correlation functions, satisfaction of continuity requires:

$$\sum_{i=1}^{3} \frac{\partial R_{ij}}{\partial \xi_i}(\vec{\xi}) = 0 \qquad \sum_{i=1}^{3} \frac{\partial R_{ij}}{\partial \xi_j} = 0 \qquad \text{(Refs. 2-7, 2-30)}$$

or, simply

$$4F(\xi) + \xi \frac{dF(\xi)}{d\xi} + \frac{1}{\xi} G(\xi) = 0$$

Thus, the continuity equation relates the two scalar functions so that only one of them can be independent.

The scalar functions $F(\xi)$ and $G(\xi)$ have been arbitrary, and as such have had little physical significance. In an important step, two nondimensional correlation functions are introduced. They are the nondimensional correlation functions for parallel turbulence components separated by the displacement vector, $\vec{\xi}$, along and normal to the direction of the displacement vector. The geometry of these correlation functions is shown on Figure 2-23. The functions are defined by:

$$f(\xi) = \hat{R}_{pp}(\xi) = \frac{R_{pp}(\xi)}{\sigma_{pp}^2} = \frac{\langle u_p(\vec{r})\, u_p(\vec{r} + \vec{\xi}) \rangle}{\sigma_{pp}^2}$$

$$g(\xi) = \hat{R}_{NN}(\xi) = \frac{R_{NN}(\xi)}{\sigma_{NN}^2} = \frac{\langle u_N(\vec{r})\, u_N(\vec{r} + \vec{\xi}) \rangle}{\sigma_{NN}^2}$$

The functions $f(\xi)$ and $g(\xi)$ are referred to as the "longitudinal" and "transverse" correlation functions, respectively. It is important to note that $f(\xi)$ and $g(\xi)$ do not depend on the orientation of the displacement vector; it is only required that they be measured for turbulence components parallel and normal to the displacement vector. The general shape of the fundamental correlation function is shown on Figure 2-23, as taken from Reference 2-30.

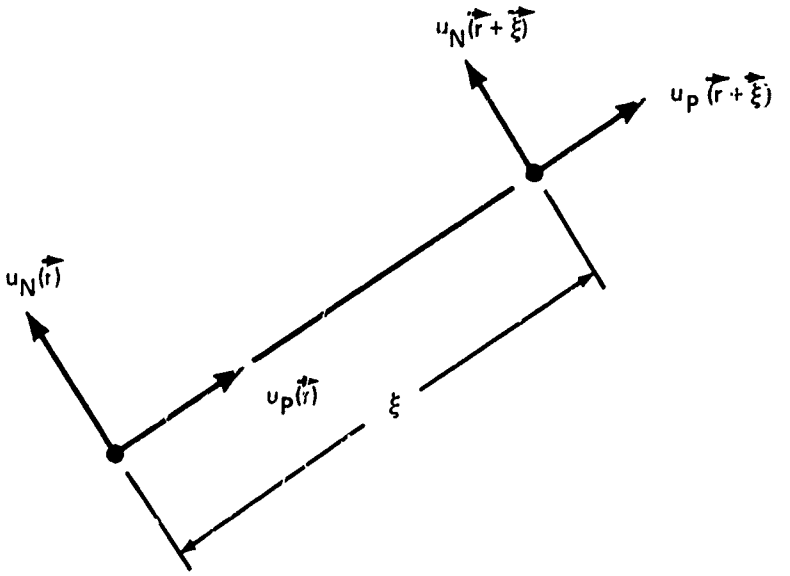

$$f(\xi) = \hat{R}_{PP}(\xi) = \frac{\langle u_P(\vec{r})\, u_P(\vec{r}+\vec{\xi})\rangle}{\sigma_{PP}^2}$$

$$g(\xi) = \hat{R}_{NN}(\xi) = \frac{\langle u_N(\vec{r})\, u_N(\vec{r}+\vec{\xi})\rangle}{\sigma_{NN}^2}$$

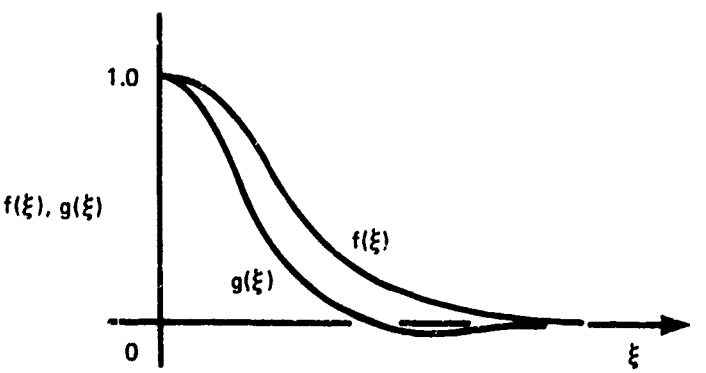

FIGURE 2-23.–FUNDAMENTAL CORRELATION FUNCTIONS (FROM REF. 2-30)

Solving for the relationship of the fundamental correlation functions with the scalar functions using the general form of the correlation function yields:

$$f(\xi) = \frac{R_{ii}(\xi)}{\sigma^2} = \frac{F(\xi)\xi^2 + G(\xi)}{\sigma^2}$$

$$g(\xi) = \frac{R_{jj}(\xi)}{\sigma^2} = \frac{G(\xi)}{\sigma^2}$$

$$\frac{F(\xi)}{\sigma^2} = \frac{f(\xi) - G(\xi)/\sigma^2}{\xi^2} = \frac{f(\xi) - g(\xi)}{\xi^2}$$

$$\frac{1}{\sigma^2}\frac{dF(\xi)}{d\xi} = \frac{-2}{\xi^3}[f(\xi) - g(\xi)] + \frac{1}{\xi^2}\left[\frac{df(\xi)}{d\xi} - \frac{dg(\xi)}{d\xi}\right]$$

$$\frac{1}{\sigma^2}\frac{dG(\xi)}{d\xi} = \frac{dg(\xi)}{d\xi}$$

Substituting these relationships into the continuity equation and solving for $g(\xi)$ gives:

$$g(\xi) = f(\xi) + \frac{\xi}{2}\frac{df(\xi)}{d\xi}$$

Substituting for the scalar function into the equation for the correlation function gives

$$R_{ij}(\xi) = \sigma^2\left[\frac{f(\xi) - g(\xi)}{\xi^2}\xi_i\xi_j + g(\xi)\,\delta_{ij}\right]$$

where

$$\delta_{ij} = \begin{cases} 1, & i = j \\ 0, & i \neq j \end{cases}$$

Note that this equation specifies that cross correlations (R_{ij}, $i \neq j$) are zero for isotropic turbulence.

Now, once the longitudinal correlation function has been determined, the correlation function for two turbulence velocities at any relative displacement in an isotropic turbulence field can be determined.

2.4.2.2 Interrelationships of Spectrum Functions

Arguments similar to those used to develop the interrelationships between the fundamental correlation functions can be used to develop interrelationships between spectrum functions. The following development is taken from Reference 2-30.

As the three-dimensional spectrum functions are a second-order two-point tensor, they may be described in terms of scalar functions for isotropy:

$$\theta_{ij}(\vec{\Omega}) = A(\Omega)\Omega_i\Omega_j + B(\Omega)\delta_{ij}$$

where

$$\Omega = |\vec{\Omega}|$$

$$\delta_{ij} = \begin{cases} 1, i = j \\ 0, i \neq j \end{cases} \quad \begin{cases} 0, i \quad j \end{cases}$$

Using the relationship between the three-dimensional spectrum and the correlation function,

$$R_{ij}(\vec{\xi}) = \int_{-\infty}^{\infty} \theta_{ij}(\vec{\Omega})\, e^{i\vec{\Omega}\cdot\vec{\xi}}\, d\vec{\Omega}$$

the continuity equation

$$\sum_{i=1}^{3} \frac{\partial R_{ij}}{\partial \xi_i}(\vec{\xi}) = \sum_{i=1}^{3} \frac{\partial R_{ij}}{\partial \xi_j}(\vec{\xi}) = 0$$

can be expressed in terms of the three-dimensional spectrum function as

$$\sum_{i=1}^{3} \Omega_i \theta_{ij}(\vec{\Omega}) = \sum_{i=1}^{3} \Omega_j \theta_{ij}(\vec{\Omega}) = 0$$

This form of the continuity equation provides the relationship between the scalar functions:

$$B(\Omega) = -\Omega^2 A(\Omega)$$

Using expression for the three-dimensional power spectrum in terms of the scalar functions

$$\tfrac{1}{2}\theta_{ii}(\vec{\Omega}) = \tfrac{1}{2}\left|\Omega^2 A(\Omega) + 3B(\Omega)\right| = B(\Omega) = -\Omega^2 A(\Omega),$$

and the relationship between the energy spectrum and the three-dimensional power spectrum provided in Reference 2-30,

$$E(\Omega) = 4\pi\Omega^2\theta_{ii}(\vec{\Omega})$$

a description for the three-dimensional spectrum function is found in terms of the energy spectrum:

$$\theta_{ij}(\vec{\Omega}) = \frac{E(\Omega)}{4\pi\Omega^2}(\Omega^2\delta_{ij} - \Omega_i\Omega_j)$$

This equation now permits defining all the isotropic spectrum functions in terms of a single scalar function, the energy spectrum, and is analogous to defining all correlation functions in terms of a single fundamental correlation function. In particular, the one-dimensional longitudinal and transverse power spectra are given by (Ref. 2-30):

$$\Phi_{pp}(\Omega_1) = \frac{1}{2}\int_{\Omega_1}^{\infty}\left(1 - \frac{\Omega_1^2}{\Omega^2}\right)\frac{E(\Omega)}{\Omega}\,d\Omega$$

$$\Phi_{NN}(\Omega_1) = \frac{1}{4}\int_{\Omega_1}^{\infty}\left(1 + \frac{\Omega_1^2}{\Omega^2}\right)\frac{E(\Omega)}{\Omega}\,d\Omega$$

Subscripts P and N refer to directions parallel and normal to the separation vector, $\vec{\xi}$. The one-dimensional power spectra may also be written in terms of each other:

$$\Phi_{NN}(\Omega_1) = \frac{1}{2}\Phi_{pp}(\Omega_1) - \frac{1}{2}\Omega_1\frac{d\Phi_{pp}(\Omega_1)}{d\Omega_1}$$

All cross spectra for velocity components parallel and normal to the separation vector are zero in isotropic turbulence.

2.4.2.3 Integral Scale

As stated in Reference 2-3: "There is an intuitive notion of the scale of turbulence. Clearly there are significant differences of 'size' between the turbulence in the wing boundary layer, in the wake of the airplane, and the atmosphere itself."

The parameters used to define the scale of turbulence are the "integral scales," of which there are two for isotropic turbulence. The integral scales are the areas under the fundamental correlation functions:

$$L_p = \int_0^{\infty} f(\xi)\,d\xi$$

$$L_N = \int_0^{\infty} g(\xi)\,d\xi$$

The implication of the integral scales is that when the separation distance is normalized by the integral scale, the fundamental correlation functions become universal functions for all scales of turbulence. That is, the functions $f(\xi/L_P)$ and $g(\xi/L_N)$ are not functions of ξ, L_P, or L_N alone.

The integral scales can also be seen to represent the average correlation distance as the lines $\xi = L_P$ and $\xi = L_N$ divide the areas under the longitudinal and transverse correlation functions into equal parts.

As seen on Figure 2-23, the transverse correlation function crosses zero. This crossover point will be proportional to the transverse integral scale, and the transverse integral scale can be thought of as a measure of the distance between transverse components for zero correlation.

If the fundamental correlation functions are expressable in terms of integral scales, then so are the spectrum functions. The frequency-dependent characteristics of the power spectrum functions will be inversely proportional to the integral scales. In particular, the peak to the right on Figure 2-1 occurs at a frequency inversely proportional to the integral scale, and the integral scale can be thought of as a measure of the dominant eddy size.

Just as the fundamental correlation functions are not independent, neither are the longitudinal and transverse integral scales. Integrating the relationship between the correlation functions,

$$g(\xi) = f(\xi) + \frac{\xi}{2}\frac{df(\xi)}{d\xi}$$

from 0 to ∞ yields the relationship between integral scales:

$$L_N = L_P + \left[\frac{\xi}{2} f(\xi)\Big|_0^\infty - \int_0^\infty \frac{f(\xi)\, d\xi}{2}\right] = \frac{L_P}{2}$$

$$\lim_{\xi \to \infty} \xi\, f(\xi) = 0$$

By convention, all isotropic turbulence functions are defined in terms of the longitudinal integral scale. Although the integral scale is a parameter defined in terms of isotropic functions, its use has been extended to nonisotropy.

2.4.2.4 Isotropic Turbulence Spectra Forms

Specification of components of turbulence requires knowledge of the one-dimensional spectra, as previously discussed. Specification of two- or three-dimensional spectra, the energy spectrum, or the correlation functions will lead to the description of the one-dimensional spectra.

As the integral of the one-dimensional spectra provides the turbulence variance, which is the same for all three components of isotropic turbulence, the one-dimensional spectra can be written as:

$$\Phi(\Omega_1) = \sigma^2 G(\Omega_1)$$

where

$$\int_{-\infty}^{\infty} G(\Omega_1)\, d\Omega_1 = 1$$

This form separates out the magnitude of turbulence, allowing it to be independently specifiable.

If the fundamental correlation functions are universal when expressed in terms of the ratio of separation distance to the integral scale, a universal description of the isotropic one-dimensional spectra can be found to be

$$\Phi(\Omega_1) = \sigma^2 G(L, L\Omega_1)$$

where by convention the longitudinal integral scale is used in all the one-dimensional spectra.

The objective is to establish an analytic form for $G(L, L\Omega_1)$, the one-dimensional spectra of turbulence with unity root mean square amplitude. Theory has been able to establish asymptotic forms for different spacial frequency ranges.

At the lowest spacial frequencies, where energy is being added to turbulence, the three-dimensional spectrum must be analytic and finite. Reference 2-36 states that it has been shown with a power series expansion that these restrictions lead to a Ω^4 proportionality of the energy spectrum at low frequencies. That is,

$$\lim_{\Omega_1 \to 0} E(\Omega) \sim K\Omega^4 \quad (K = \text{constant})$$

This relationship leads to the one-dimensional spectra being invariant with frequency at low frequencies:

$$\lim_{\Omega_1 \to 0} \Phi(\Omega_1) = C \quad (C = \text{constant})$$

For one-dimensional power spectra equal to a constant, the ratio between the longitudinal and transverse power spectra must be 2 as seen by the relationship between these two spectra:

$$\Phi_{NN} = \frac{1}{2}\Phi_{PP} - \frac{1}{2}\Omega_1 \frac{d\Phi_{PP}}{a\Omega_1}$$

where

$$\Phi_{PP} = \quad C, \Phi_{NN} = \frac{C}{2}$$

The constant variation of the one-dimensional power spectra is generally well accepted. References 2-7 and 2-37 reject proposed analytic forms which do not contain this feature.

In the "inertia subrange" where turbulent energy is being transported to higher frequencies without energy additions or losses, a variation of one-dimensional spectral energy with $\Omega^{-5/3}$ has been derived by Kolmogoroff from similarity theory. This variation of the energy spectrum also leads to the same variation of the one-dimensional power spectra. The $\Omega^{-5/3}$ variation has been verified by numerous authors. Perhaps one of the most extensive verifications has been performed in the LO-LOCAT study presented in Reference 2-37 from which Figure 2-24 is taken.

A $\Omega^{5/3}$ variation of the one-dimensional spectra requires the longitudinal and transverse components to be related asymptotically by the ratio of 3/4:

$$\Phi_{NN} = \frac{1}{2}\Phi_{PP} - \frac{1}{2}\Omega_1 \frac{d\Phi_{PP}}{d\Omega_1}$$

$$\Phi_{PP} = C\Omega^{-5/3}$$

$$\Phi_{NN} = \frac{\Phi_{PP}}{2} + \frac{5}{6}\Omega_1 C\Omega_1^{-8/3} = \frac{\Phi_{PP}}{2} + \frac{5}{6}\Phi_{PP} = \frac{4}{3}\Phi_{PP}$$

At very high spacial frequencies, where viscous dissipation takes place, References 2-7 and 2-36 report a Ω^{-7} variation of the energy spectrum predicted by Heisenberg. Reference 2-7 states that available data provide an exponential variation. The discrepancy is of no concern, as the frequency of onset is far beyond the highest of interest for simulation (Ref. 2-37 assigns this region to wavelengths of less than 0.01 foot). Few power spectrum models have attempted to model this region.

In addition to the low and high frequency asymptotes, a frequency of transition from one asymptotic character to the other is needed. One technique is to observe the value of $L\Omega_1$, at which the peak of $\Omega_1\Phi(\Omega_1)$ occurs.

As an example, the unity rms one-dimensional power spectrum

$$G(L, L\Omega_1) = \frac{A(L)}{(1 + aL\Omega_1)^{5/3}}$$

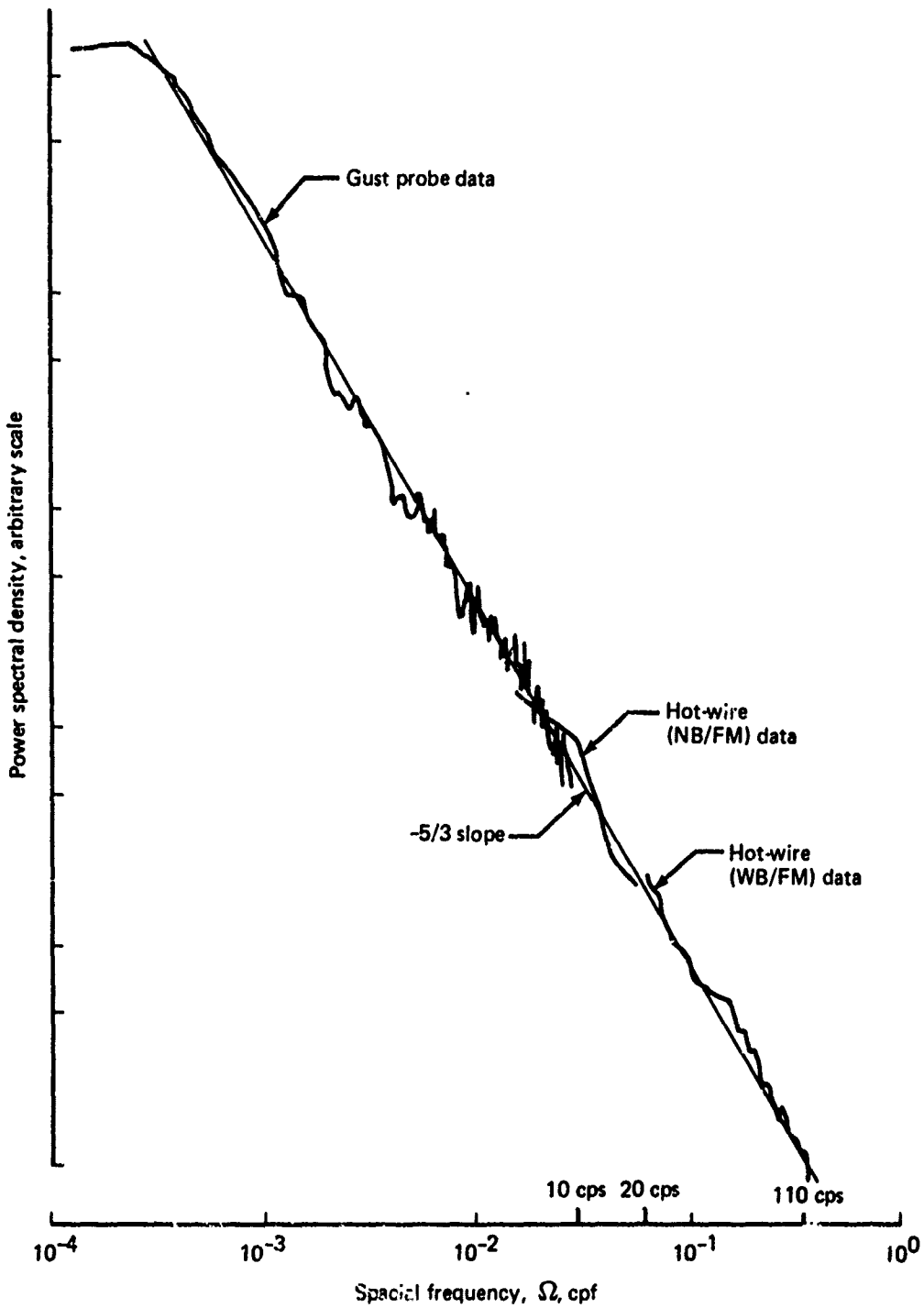

FIGURE 2-24.– EVALUATION OF $\Omega^{-5/3}$ ASYMPTOTE (FROM REF. 2-37)

where a and A(L) are constants, satisfies the asymptotic characteristics. The constant A(L) is found by requiring the rms to be unity:

$$1 = \int_{-\infty}^{\infty} \frac{A(L)}{(1 + aL\Omega_1)^{5/3}} d\Omega_1 = 2\,A(L) \int_{0}^{\infty} \frac{d\Omega}{(1 + aL\Omega_1)^{5/3}} = \frac{3A}{aL}$$

where

$$A = \frac{aL}{3}$$

Thus,

$$\Phi = \sigma^2 \frac{aL}{3} \frac{1}{(1 + aL\Omega_1)^{5/3}}$$

The greatest density of variance with frequency occurs when $d(\Omega_1 \Phi)/d\Omega_1 = 0$, or $\Omega_{1max} = 3/2aL$. The above power spectrum form could then be written in terms of Ω_{max}:

$$\Phi = \sigma^2 \frac{\frac{1}{2}\Omega_{max}}{\left[1 + \frac{3}{2}\frac{\Omega_1}{\Omega_{max}}\right]^{5/3}}$$

If this form were accepted as that for the longitudinal spectrum, the transverse spectrum is found from the previously discussed relationship,

$$\Phi_{NN}(\Omega_1) = \frac{1}{2}\left[\Phi_{pp}(\Omega) - \Omega_1 \frac{d\Phi_{pp}(\Omega_1)}{d\Omega_1}\right]$$

or

$$\Phi_{NN}(\Omega_1) = \sigma^2\left(\frac{aL}{3}\right)\left(\frac{1 + \frac{8}{3}(aL\Omega_1)}{(1 + aL\Omega_1)^{8/3}}\right)$$

The transverse power spectrum also satisfies the asymptotic requirements, but the maximum of Φ_{NN} occurs at different frequencies (Ω = -0.244/aL, 2.3/aL). Hence, if the spectra are written in terms of the frequency where the greatest variance density occurs, two parameters (at least) must be used to replace the longitudinal integral scale.

The form postulated must be rejected on the basis that it does not provide power spectra that are even functions, $\Phi(\Omega) \neq \Phi(-\Omega)$.

A much more satisfying form has been developed by Von Karman, who fitted the energy spectrum with the equation:

$$E(\Omega) = \frac{A\sigma^2(\Omega/\Omega_0)^4}{\left[1 + (\Omega/\Omega_0)^2\right]^{17/6}}$$

The one-dimensional power spectra and the corresponding fundamental correlation functions that result are shown on Figure 2-25. That the Von Karman spectra satisfy the asymptotic requirement for the one-dimensional spectra is shown on Figure 2-26. The relationship between the longitudinal integral scale and the dominant frequencies is shown on Figure 2-27, where dominant frequencies refer to those having the greatest contributions to total kinetic energy or variance. Finally, the fundamental correlation functions, found from the inverse Fourier integrals of the one-dimensional power spectra, are plotted on Figure 2-28.

Reference 2-37 attributes an alternate form for the longitudinal spectrum to Lumley and Panofsky:

$$\Phi_{pp} = \sigma^2 \frac{A}{1 + (B\Omega)^{5/3}}$$

This form, although meeting asymptotic requirements, does not provide symmetry about $\Omega = 0$ and should at least be modified as follows:

$$\Phi_{pp} = \sigma^2 \frac{A}{1 + \left[(B\Omega)^2\right]^{5/6}}$$

The primary difference between this form and the Von Karman form are found in the intermediate frequencies, but these differences are small. The same form has been attributed to Busch and Panofsky for the transverse spectrum by Reference 2-38. However, using the same form does not satisfy the interrelationships between the longitudinal and the transverse isotropic spectra.

Another form presented in References 2-7 and 2-38 and attributed to Inoue is given by:

$$\Phi_{pp} = \left(\frac{\sigma^2}{\Omega}\right)\left(\frac{(\Omega/\Omega_0)}{\left[1 + (\Omega/\Omega_0)^2\right]^{4/3}}\right)$$

Although the $\Omega^{-5/3}$ asymptotic is satisfied, the spectrum goes to zero at zero spacial frequency and has a maximum at $\Omega_0 = (4/7)\Omega_0$. Due to the last characteristic, this form has been discounted by both References 2-7 and 2-38.

A different approach to spectra modeling begins with fitting a fundamental correlation function with an equation, then by deriving all the spectra from that equation. The most

Von Karman (From ref. 2-3)	Dryden (From ref. 2-7)

Longitudinal correlation function:

$$f(\xi) = \frac{2^{2/3}}{\Gamma(1/3)}\left(\frac{\xi}{aL}\right)^{1/3} K_{1/3}\left(\frac{\xi}{aL}\right) \qquad f(\xi) = e^{-\xi/L}$$

Transverse correlation functions:

$$g(\xi) = \frac{2^{2/3}}{\Gamma(1/3)}\left(\frac{\xi}{aL}\right)^{1/3}\left[K_{1/3}\left(\frac{\xi}{aL}\right) - \frac{\xi}{2aL} K_{2/3}\left(\frac{\xi}{aL}\right)\right] \qquad g(\xi) = e^{-\xi/L}\left[1 - \frac{\xi}{2L}\right]$$

Longitudinal one-dimensional power spectrum:

$$\Phi_{PP} = \frac{\sigma^2 L}{\pi} \frac{1}{\left[1 + (aL\Omega_1)^2\right]^{5/6}} \qquad \Phi_{PP} = \frac{\sigma^2 L}{\pi} \frac{1}{\left[1 + (L\Omega_1)^2\right]}$$

Transverse one-dimensional power spectrum:

$$\Phi_{NN} = \frac{\sigma^2 L}{2\pi} \frac{1 + 8/3\,(aL\Omega_1)^2}{\left[1 + (aL\Omega_1)^2\right]^{11/6}} \qquad \Phi_{NN} = \frac{\sigma^2 L}{2\pi} \frac{1 + 3(L\Omega_1)^2}{\left[1 + (L\Omega)^2\right]^2}$$

Energy spectrum:

$$E(\Omega) = \frac{55}{9\pi}\sigma^2 L \frac{(aL\Omega)^4}{\left[1 + (aL\Omega)^2\right]^{17/6}} \qquad E(\Omega) = \frac{8\sigma^2 L}{\pi} \frac{(L\Omega)^4}{\left[1 + (L\Omega)^2\right]^3}$$

Definitions:

$a = 1.339$

$\Omega = |\vec{\Omega}| = |\Omega_1 \hat{i} + \Omega_2 \hat{j} + \Omega_3 \hat{k}|$

Φ_{PP} and Φ_{NN} such that $\sigma^2 = \int_{-\infty}^{\infty} \Phi_{PP}\, d\Omega_1 = \int_{-\infty}^{\infty} \Phi_{NN}\, d\Omega_1$

$$L = \int_0^{\infty} f(\xi)\, d\xi = 2\int_0^{\infty} g(\xi)\, d\xi$$

$K_{1/3}\left(\frac{\xi}{aL}\right)$ and $K_{2/3}\left(\frac{\xi}{aL}\right)$ are modified Bessel functions of the second kind.

FIGURE 2-25.—VON KARMAN AND DRYDEN CORRELATION AND SPECTRA FUNCTIONS

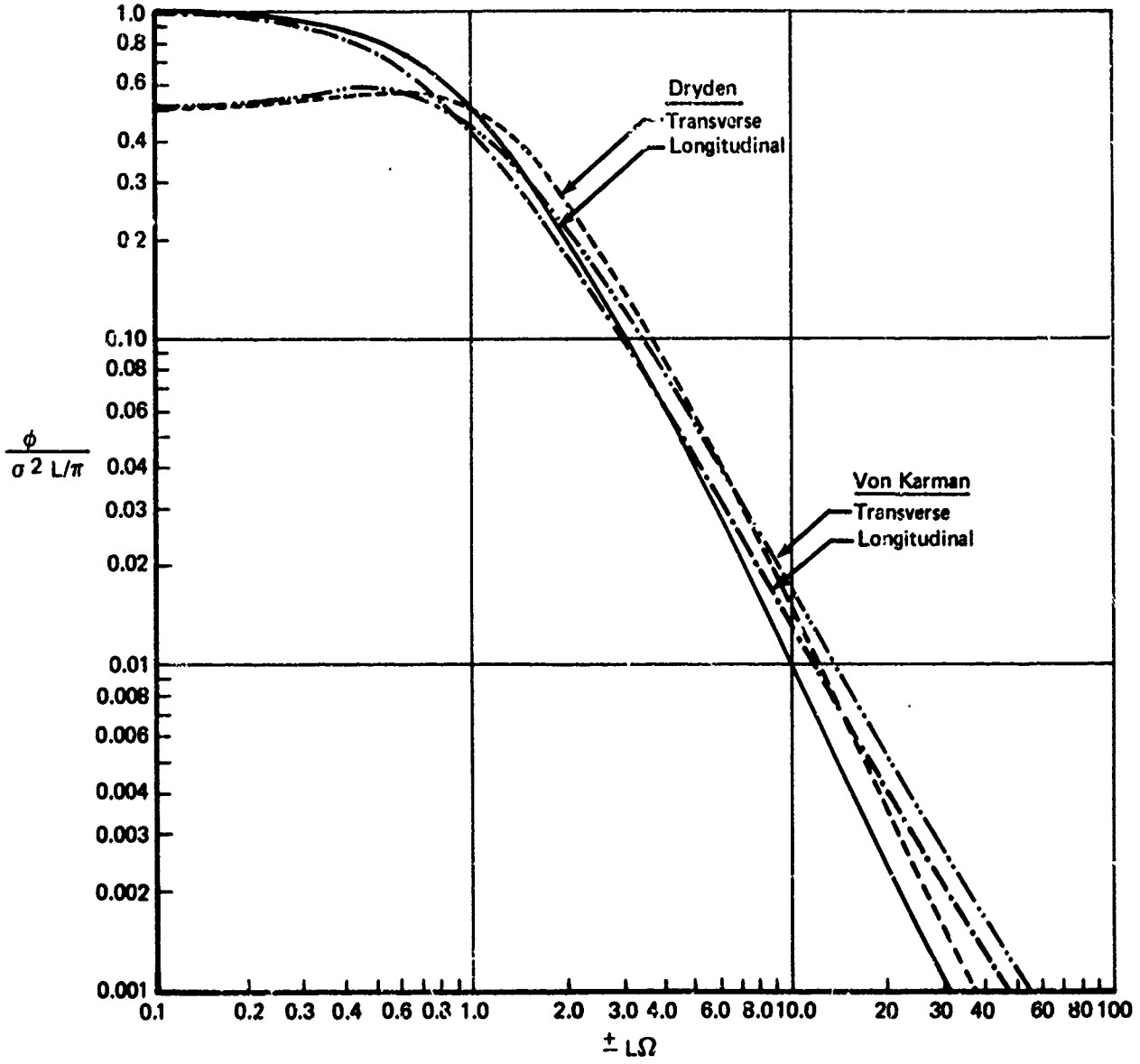

FIGURE 2-26.—VON KARMAN AND DRYDEN ONE-DIMENSIONAL POWER SPECTRA

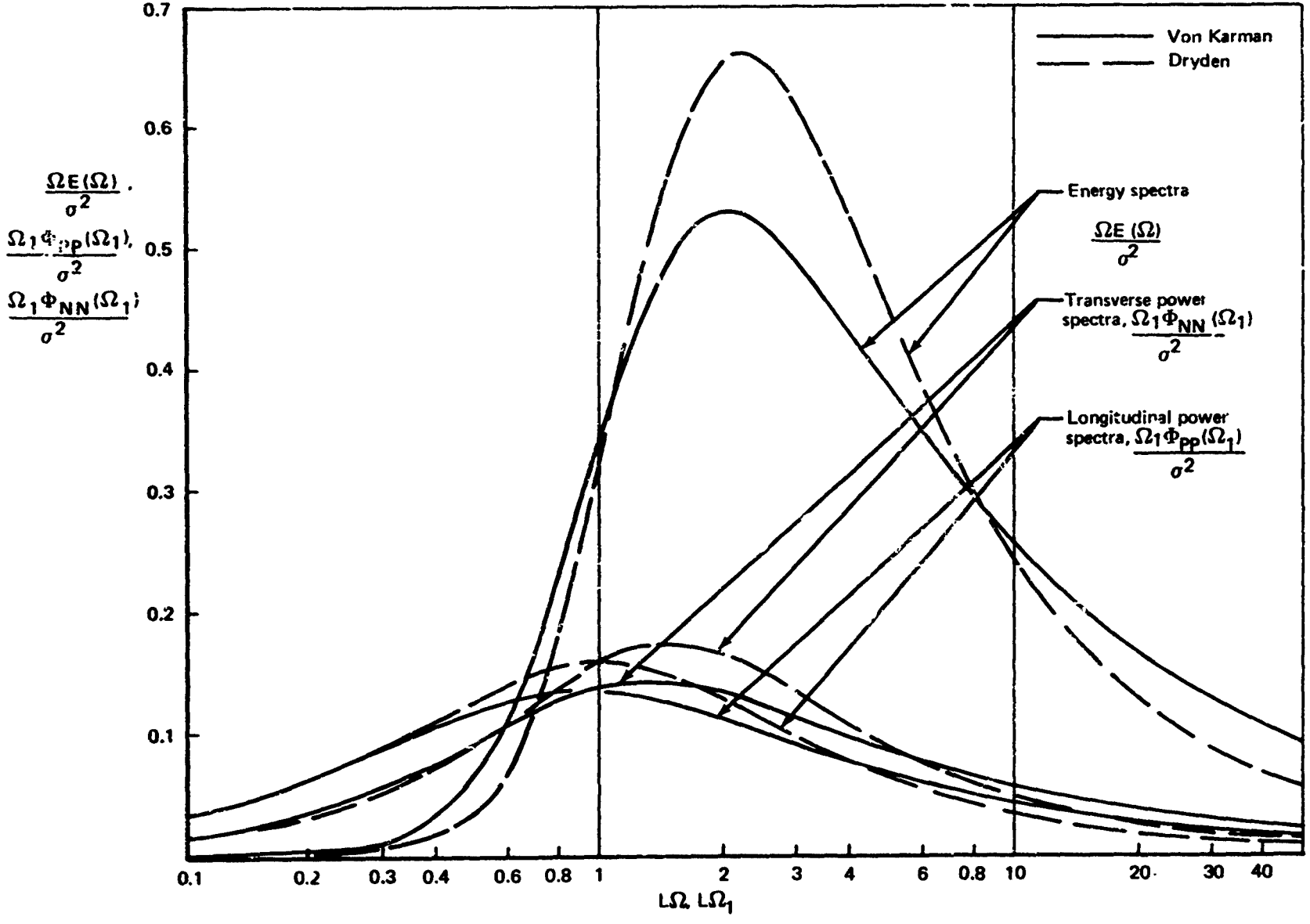

FIGURE 2-27.—VON KARMAN AND DRYDEN NONDIMENSIONAL SPECTRA

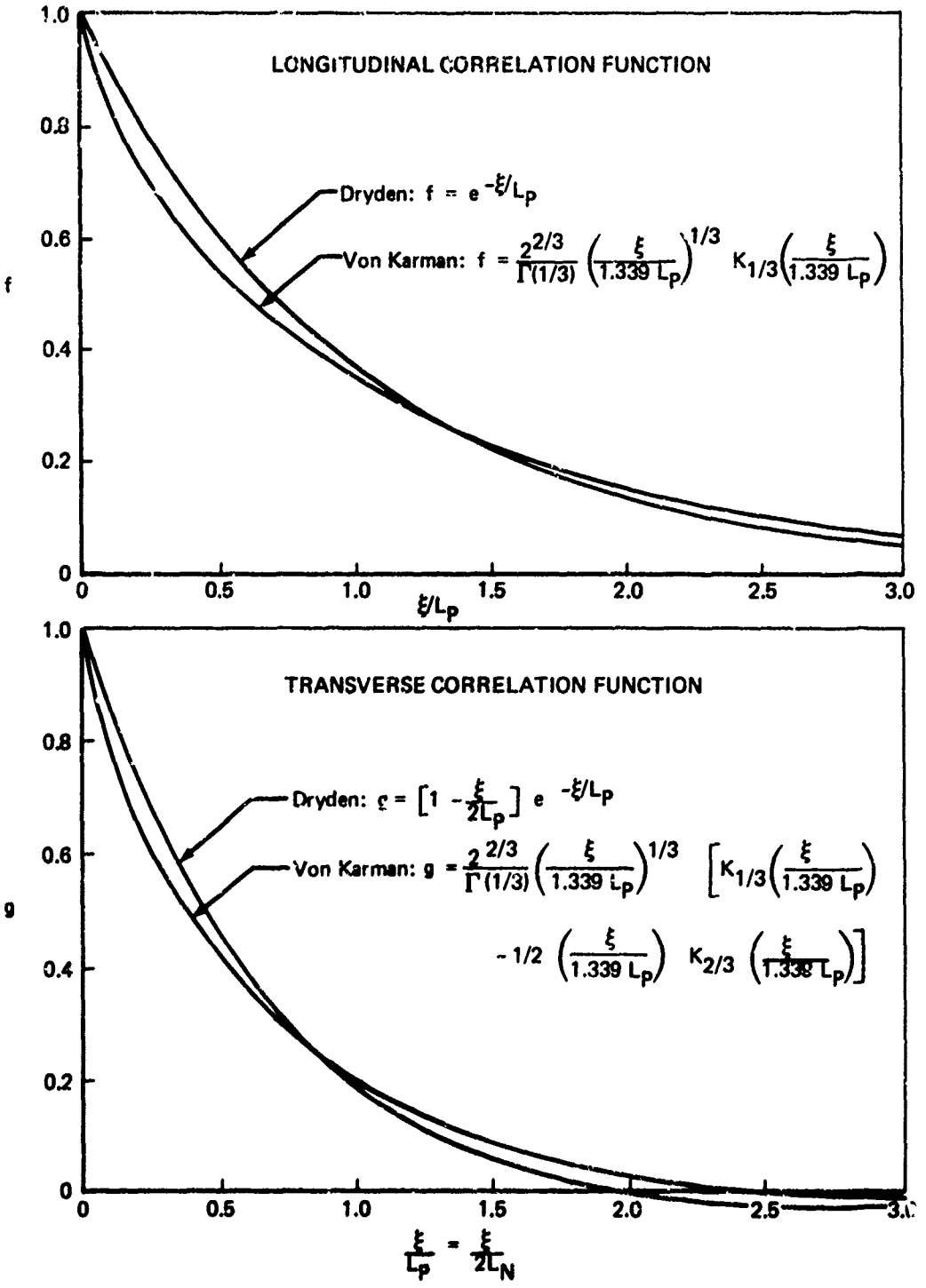

FIGURE 2-28.–DRYDEN AND VON KARMAN FUNDAMENTAL CORRELATION FUNCTIONS

widely used spectrum models that result from this approach are the Dryden spectra. The longitudinal correlation function is assumed to have an exponential form given by:

$$f(\xi) = e^{-\xi/L}$$

Reference 2-7 argues that this form "is physically seriously unrealistic in tha. the curvature at the origin is infinite, and it almost surely decreases too rapidly at infinity; however, it crudely resembles at least some data, . . . ".

The one-dimensional power spectra and the energy spectrum equations for the Dryden formulation are presented on Figure 2-25. As can be seen, they provide a considerable simplification in form over the Von Karman forms.

The Dryden one-dimensional power spectra are seen to satisfy the low frequency asymptotic on Figure 2-26 with the same aplitude as the Von Karman spectra. The Dryden spectra have a greater bandwidth than the Von Karman spectra, exceed the Von Karman spectra at intermediate values, and are progressively lower at increasing high frequencies. As is seen on Figure 2-27, the dominant frequencies for the Dryden spectra are greater than those for the Von Karman spectra.

Although the Von Karman and Dryden spectra are defined in terms of the longitudinal integral scale, the longitudinal integral scales do not have the same values as the fundamental correlation functions because the two forms are not identical, as shown on Figure 2-28. The Dryden model provides higher correlations at small spacial separations and lower correlations at high separations. The Dryden model provides uncorrelated parallel transverse turbulence components at a separation distance equal to four times the transverse integral scale (twice the longitudinal integral scale). The corresponding separation distance for the Von Karman model is about five times the transverse integral scale.

Other authors have also postulated models having the same asymptotic characteristics as the Dryden model. A longitudinal spectrum presented in Reference 2-38 attributed to Zbrozek has a form identical to the Dryden model. Reference 2-38 also presents an early longitudinal spectrum attributed to Panofsky and a transverse spectrum attributed to Pritchard having identical forms:

$$\Phi = \frac{\sigma^2 A}{(1 + B\Omega)^2}$$

This form lacks symmetry about $\Omega = 0$. The same form in Reference 2-37 is said to be recommended by Lappe for both the longitudinal and transverse spectra, although using the same form for both spectra does not satisfy the interrelationship between isotropic spectra.

An empirical form presented in Reference 2-39 for low altitude horizontal spectra is:

$$\Phi_i(\Omega_1) = \frac{u_{*0} A_i B_i h}{\left[1 + 1.5(B_i h \Omega_1)^{r_i}\right]^{5/3 r_i}}$$

This form generalizes several other forms, including the Von Karman for the longitudinal spectrum ($r_u = 2$). Reference 2-40 used this form with $r_u = r_v = 1$, $r_w = 5/3$. Although the resulting spectra lack symmetry about $\Omega = 0$ and fail to provide complete isotropy at high altitudes, the differences between the spectra shapes in Reference 2-39 and those of the Von Karman forms appear at low frequencies when data scatter is large.

A comparison between the Ω^{-2} asymptote as represented by the Dryden model and the $\Omega^{-5/3}$ asymptote as measured by the Von Karman model was made, using measured data, in Reference 2-37 and is shown on Figure 2-29. The Von Karman model is seen to be clearly superior. Additional comparisons between specific models were performed in the same reference and are shown on Figure 2-30. Comparisons are between the Von Karman and Lumley-Panofsky forms, having $\Omega^{-5/3}$ asymptotes, and the Dryden and Lappe forms, having Ω^{-2} asymptotes. Again, it must be concluded that the $\Omega^{-5/3}$ asymptote is superior.

2.4.3 Low Altitude Turbulence

Thus far, the development of turbulence description has been oriented to the definition of isotropic turbulence. However, there is overwhelming evidence that low altitude turbulence is nonisotropic. Specifically:

1) The average functions describing the field of turbulence are not invariant with rotations of the turbulence axis system. That is, the variances of turbulence components are not necessarily equal, and the longitudinal and transverse integral scales may vary with orientation.

2) Low altitude turbulence exhibits a lack of homogeneity with altitude. That is, the turbulence components and the integral scales tend to vary with altitude.

3) A non-zero correlation has been found to exist between turbulence in the direction of the mean wind and turbulence in the vertical direction. Isotropic turbulence requires zero correlation between orthogonal components.

The evidence of a nonisotropic character of low altitude turbulence at first suggests that the theory developed for the special case of isotropy be abandoned and more general theory developed instead. Reference 2-30 provides some of the required fundamental relationships. For the next most restrictive case, that for invariance for rotation about an axis (axisymmetry), the correlation functions are defined in terms of five scalar functions as opposed to two for isotropy. The most general case of no symmetry requires that the correlation functions be defined in terms of 31 scalar functions. The different scalar functions must still be interrelated by the continuity equations, which are much more numerous and complex for nonisotropic conditions.

For nonisotropic conditions, a concept as simple as the fundamental correlation functions is probably not possible, and the isotropic one-dimensional power spectra derived from this concept are not applicable.

The great complexity of the nonisotropic case has prevented solutions comparable to those for the isotropic case. There is, however, considerable evidence that limited conditions of

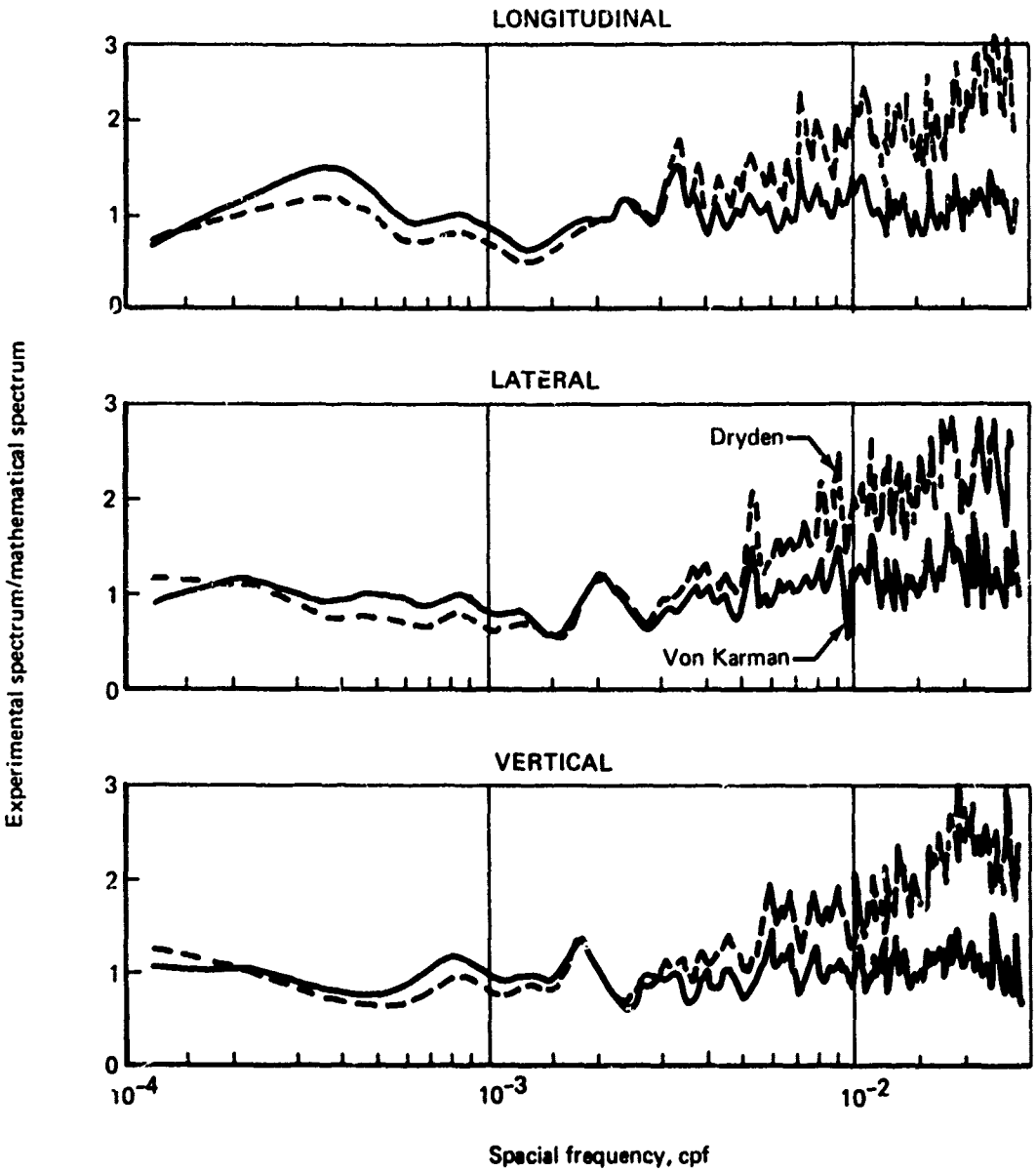

FIGURE 2-29.–TYPICAL COMPARISON OF EXPERIMENTAL SPECTRA WITH VON KARMAN AND DRYDEN MATHEMATICAL EXPRESSIONS (FROM REF. 2-37)

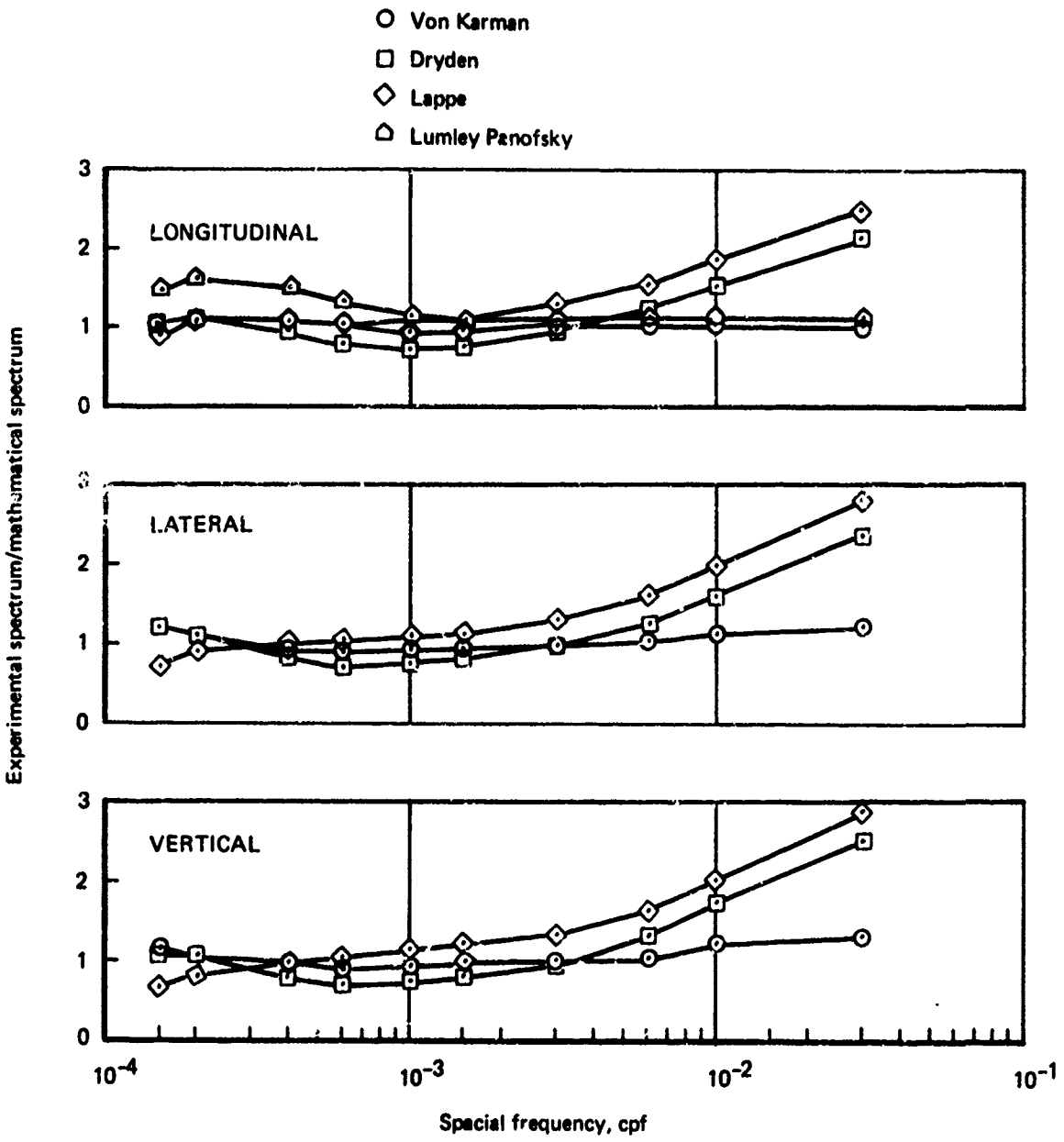

FIGURE 2-30.–EXPERIMENTAL/MATHEMATICAL SPECTRA COMPARISONS (FROM REF. 2-37)

isotropy exist for low altitudes. This evidence has been used to rationalize adaptations of isotropic models for low altitude turbulence. This is fortunate, for as stated in Reference 2-41: "... there would seem to be no recourse, in the present state of the subject, but to use the isotropic model of the one-dimensional power spectra for the low level case as well as for high altitudes. The complexity of the problem is even then quite sufficient."

The majority of statistical data available for low altitude turbulence are for a turbulence axis system aligned to the mean wind. Rather than having longitudinal and transverse turbulence components, with no preferred orientation of the transverse components, a specific orientation of the low altitude turbulence axis system is employed, as shown on Figure 2-31.

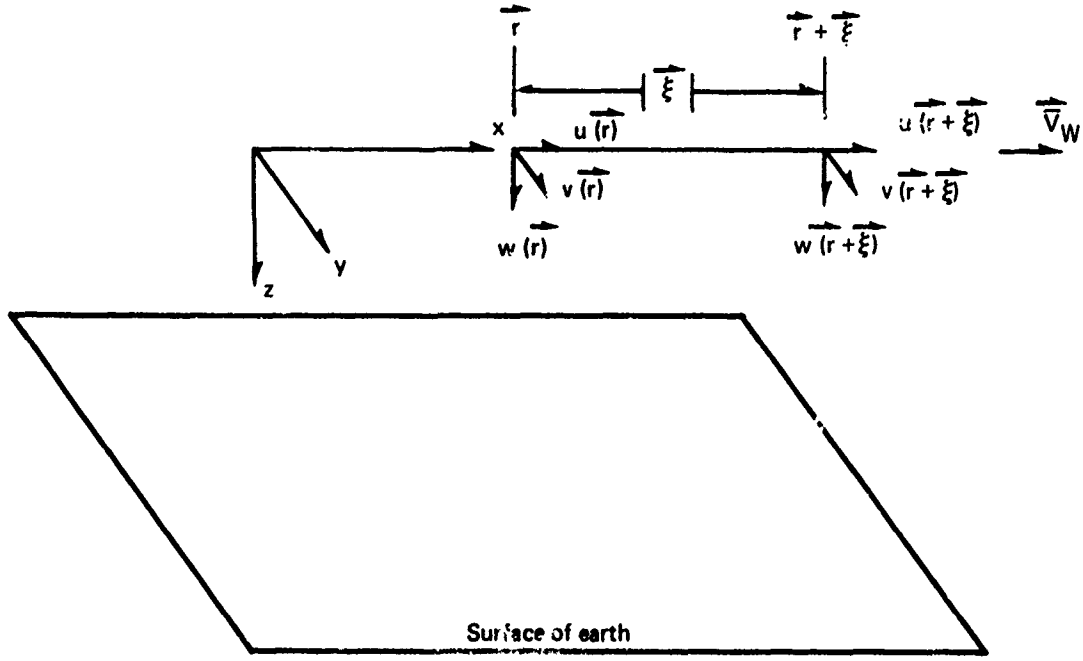

u, v, and w are components of turbulence along x, y, and z axes.
x axis; spacial separation vector, $\vec{\xi}$, and mean wind vector, $\vec{V}_W$ are aligned on x-y plane parallel to earth.
. downward normal to earth.

FIGURE 2-31.--AXIS SYSTEM FOR LOW ALTITUDE TURBULENCE

2.4.3.1 Conditions of Limited Isotropy

The form of the correlation function for axisymmetric turbulence (invariance of turbulence for rotations in the plane parallel to the earth, also called "horizontal isotropy") from Reference 2-30 leads to a single non-zero correlation function between the u and w turbulence components measured at the same point for the system shown on Figure 2-31.

Reference 2-7 reports that: "Attempts to find non-zero cospectra between different velocity components recorded at the same points on the surface layers have been successful only for the longitudinal and vertical components." Disagreement with this statement has not been found in any of the other literature.

Isotropy in the horizontal plane is not assured by the existence of only the single cross-correlation function; the variance of turbulence components in the plane must be found to be equal ($\sigma_u^2 = \sigma_v^2$) and the integral scales must obey the isotropic relationship ($L_u = 2L_v$). Reference 2-41 implies that these conditions are met: "If the terrain is homogeneous and isotropic, then the turbulence will be closely axisymmetric . . . ". Acceptance of this conclusion shall not be immediately made, but shall be dependent upon examination of the data for variances and integral scales.

Reference 2-7 argues that at sufficiently high spacial frequencies, the turbulence is completely isotropic. The implication is that the cross spectrum exists only at the low spacial frequencies and falls off more rapidly with increasing frequency than do the power spectra. Isotropy at high spacial frequencies leads to the "hypothesis of local isotropy" presented in Reference 2-7: "Small eddies may have considerable energy but do not contribute to the correlation between u and w." Specifically, the region of local isotropy is given to be in the inertial subrange.

2.4.3.2 Low Altitude Power Spectra

The constant low frequency asymptote of the power spectra is not dependent upon isotropy. Even if the $\Omega^{-5/3}$ asymptote in the inertial subrange were dependent upon isotropy, there would be no change of that asymptote if isotropy exists at high spacial frequencies. Hence, low altitude turbulence could be expected to have the same asymptotic character. Whether or not the curve-fitting equation that results in the isotropic spectra shape is the same for low altitudes is a matter of conjecture, for even the spectra shapes for isotropy are not known with certainty. The assumption that the shapes of the spectra for low and high altitudes are the same (with frequency suitably normalized) is probably as good as any other.

With the orientations of axis defined on Figure 2-31, the longitudinal power spectrum becomes the u power spectrum (Φ_u), and the transverse power spectrum becomes the v and w power spectra (Φ_v, Φ_w). To account for possible unequal variances of the components, σ^2 in the isotropic forms is replaced by σ_u^2, σ_v^2, and σ_w^2 for the u, v, and w power spectra, respectively.

Adaptation of the concept of integral scales for low altitude turbulence is much more troublesome as the concept is defined in terms of the fundamental correlation functions, which no longer apply at low altitudes, at least not for all three turbulence components. A reference spacial frequency could be used to normalize spacial frequency (i.e., $\Omega_1/\Omega_{1_{REF}}$) instead and is recommended by some authors. Alternately, the integral scales could be redefined to mean the area under the normalized autocorrelation functions, even though the autocorrelation functions may not all be uncorrelated. The integral scales are perhaps

preferred, as they provide better physical interpretation of the eddy sizes and a means for normalizing the autocorrelation arguments. Integral scales determined from the autocorrelation are determined independent of the spectra forms.

There is an alternate procedure used for defining integral scales when specific spectra forms are presumed. The scale lengths are defined to be simply those which enable the presumed spectra to fit the data. In isotropic turbulence, if the spectra forms are valid, determining integral scales from correlation functions and from the spectra forms should provide the same answers, except that the practice for the latter technique is to simply replace the longitudinal integral scale in the transverse spectrum with L_v and L_w. In isotropic turbulence, L_v and L_w would be twice the area under the transverse correlation function. That is, transverse integral scales are substituted for the isotropic longitudinal integral scale.

As an example, the Von Karman isotropic spectra from Figure 2-25 would be adapted for low altitudes as follows:

Isotropic	Low altitudes
$\Phi_{PP} = \frac{\sigma^2 L}{\pi} \frac{1}{\left[1 + (1.339\, L\Omega_1)^2\right]^{5/6}}$	$\Phi_u = \frac{\sigma_u^2 Lu}{\pi} \frac{1}{\left[1 + (1.339\, L_u\Omega_1)^2\right]^{5/6}}$
$\Phi_{NN} = \frac{\sigma^2 L}{2\pi} \frac{1 + \frac{8}{3}(1.339\, L\Omega_1)^2}{\left[1 + (1.339\, L\Omega_1)^2\right]^{11/16}}$	$\Phi_v = \frac{\sigma_v^2 L_v}{2\pi} \frac{1 + \frac{8}{3}(1.339\, L_v\Omega_1)^2}{\left[1 + (1.339\, L_v\Omega_1)^2\right]^{11/6}}$
	$\Phi_w = \frac{\sigma_w^2 L_w}{2\pi} \frac{1 + \frac{8}{3}(1.339\, L_w\Omega_1)^2}{\left[1 + (1.339\, L_w\Omega_1)^2\right]^{11/16}}$

When applying isotropic spectra to low altitudes, the significant matters are to use integral scales in the manner for which their values are defined and to remember that the variances and integral scales are generally defined for the spectra oriented to the mean wind.

The condition of local isotropy leads to an interrelationship of the variances and integral scales. Reference 2-7 argues that the nonisotropy of low altitude turbulence occurs only for large eddies. Then, the $\Omega_1^{-5/3}$ asymptote holds for low altitude turbulence, and turbulence is isotropic at least above some frequency in the inertial subrange, requiring that the v and w spectra be greater than the u spectrum by the ratio of 4/3. Equal variances and the two-to-one integral scale relationships that hold for isotropic turbulence cannot be expected to hold as isotropy at all frequencies is required. However, using the interrelationship between isotropic one-dimensional spectra, the following asymptotic ratios between spectra should hold:

$$\lim_{\Omega_1 \to \infty} \frac{\Phi_v}{\Phi_u} = \lim_{\Omega_1 \to \infty} \frac{\Phi_w}{\Phi_u} = \frac{4}{3} \frac{\sigma_v^2}{\sigma_u^2} \frac{L_u}{L_v} = \frac{4}{3} \frac{\sigma_w^2}{\sigma_u^2} \frac{L_u^{2/3}}{L_w^{2/3}} = \frac{4}{3}$$

or

$$\frac{\sigma_u^2}{L_u^{2/3}} = \frac{\sigma_v^2}{L_v^{2/3}} = \frac{\sigma_w^2}{L_w^{2/3}}$$

where the isotropic form for the transverse spectra has been adapted for low altitude Φ_v and Φ_w by replacing L_{pp} with L_v and L_w, respectively. These relationships are the same as those provided for the low altitude turbulence model in Reference 2-42.

2.4.3.3 Low Altitude Cross Spectrum

A non-zero cross spectrum has been said to exist at low altitudes only between the u and w components at low frequencies. Reference 2-7 defines an "isotropic limit" which defines the maximum spacial frequency at which the cross spectrum is significant, although the level of significance is not specified.

The frequency for the isotropic limit is said to be inversely proportional to altitude, based on studies by Corsin and Priestly. In fact, Priestly is said to define a wavelength of 1.7 times the height as the maximum where the cross spectrum is significant.

Reference 2-7 argues that empirical data and similarity theory suggest a form for the real part (amplitude relationship) of the u-w cross spectrum given by:

$$\omega \phi_{uw}(\omega) = u_*^2 \quad F\left(\frac{h\omega}{V_W}, \frac{h}{\ell}\right)$$

Where F is a universal function and ω is frequency in rad/sec. The square of friction velocity (equal to the ratio of shear stress to density) is identically the covariance. Hence, the universal function F must satisfy the relationship

$$\int_{-\infty}^{\infty} \frac{F}{\Omega_1} d\Omega_1 = 1$$

Reference 2-7 also combines the two parameters of F to provide an alternate form:

$$\Phi_{uw} = \sqrt{\Phi_u \Phi_w}\, G\left(\frac{1}{\omega} \frac{\partial \bar{V}_W}{\partial h}\right)$$

where G is an alternate universal function. Expanding G about zero argument (infinite frequency, where G must be zero) with a first order Taylor series gives:

$$\Phi_{uw}(\omega) = A\sqrt{\Phi_u \Phi_w}\ \ \frac{1}{\omega}\frac{\partial \bar{V}_W}{\partial h}$$

where A is a positive constant.

At infinite frequency, the cospectrum is zero, agreeing with local isotropy. The positive correlation (for the axis system defined), or the correlation of downwind turbulence with turbulence moving vertically downward, is explained in Reference 2-7 as follows: ". . the wind in the surface layer increases upward so that downward moving air tends to have large velocity components in the direction of the mean wind, no matter how large the eddies that produce the vertical exchange."

The first order Taylor series can be expected to be accurate only at high frequencies. At these frequencies, the u and w power spectra differ only by a constant, and the high frequency cospectrum equation can be written as:

$$\Phi_{uw}(\omega) = A'\ \Phi_w\ \frac{1}{\omega}\ \frac{\partial \bar{V}_W}{\partial h}$$

Generally speaking, it would be expected that this would hold only for

$$\frac{1}{\omega}\ \frac{\partial \bar{V}_W}{\partial h} \ll 1,$$

but Reference 2-7 provides data presented in Figure 2-32 showing good agreement up to $(1/\omega)(\partial \bar{V}_W/\partial h) = 2$, with the constant $A' = 1/2$.

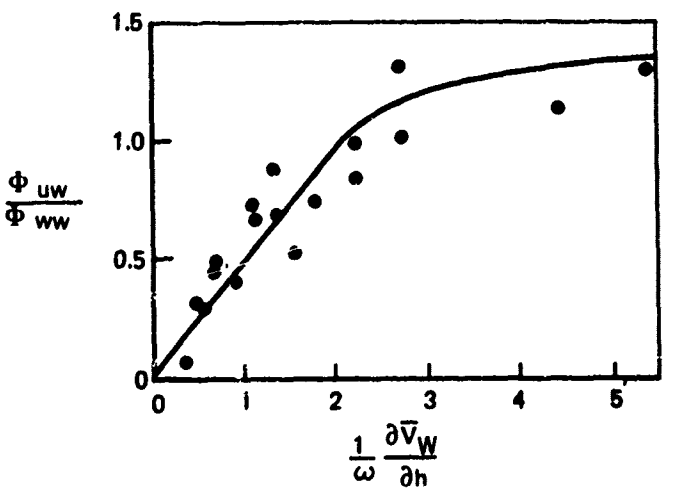

FIGURE 2-32.--CROSS SPECTRUM TO VERTICAL POWER SPECTRUM RATIO, EFFECT OF WIND SHEAR (FROM REF. 2-7)

Reference 2-7 notes that the last cospectrum expression cannot be realistic at low frequencies, since the cospectrum would approach infinity as the frequency approaches zero. Furthermore, at low frequencies, the u and w power spectra can no longer be expected to differ only by a constant. Figure 2-32 indicates that the cospectrum may have a constant low frequency asymptote.

An alternate form for the low altitude cospectrum is recommended by Reference 2-3:

$$\Phi_{uw} = \frac{\sigma_u \sigma_w \gamma_0}{\left[1 + \frac{L\Omega_1}{10}^2\right]^{1/2}} \left[\frac{\Phi_u}{\sigma_u^2} \frac{\Phi_v}{\sigma_v^2}\right]^{1/2}$$

It is presumed that the use of the v power spectrum rather than the w power spectrum is simply an error. The term L is not defined. A representative value of the constant γ_0 is given as 0.5. The formulation is interesting in that it does provide a constant low frequency asymptote and a break frequency dependent on spacial frequency, in line with the "isotropic limit" concept.

A third formulation of the cospectrum is found in Reference 2-34:

$$\Phi_{uw}(\omega) = \frac{2\sqrt{2}\sigma_u \sigma_w}{\alpha^2} \left(\frac{L_w}{\bar{V}_W}\right)^2 \left(\frac{L_u}{\bar{V}_W}\right) \frac{1 + 3\left(\frac{\alpha}{2}\omega\right)^2}{\left[1 + \left(\frac{\alpha}{2}\omega\right)^2\right]^2}$$

where α is a constant.

This formulation provides the same high frequency variation as for the power spectra recommended in the same reference, in contrast with the preceding formulations. If the constant α were equal to $2L_w/\bar{V}_W$, the expression in terms of the w power spectra would be:

$$\Phi_{uw}(\omega) = \frac{B}{\bar{V}_W} \Phi_w$$

where B is a constant.

That is, the cospectrum would differ from the w power spectrum only by a constant at a given speed.

In general, the cross spectrum should also contain phase information as well as amplitude information. That is, it should have an imaginary part, called the "quadrature spectrum." Even less is known about the quadrature spectrum, but its magnitude and effects are generally considered to be negligible.

2.4.4 Magnitude of Turbulence

In the evaluation of the stability and control requirements of an aircraft flying through a turbulent atmosphere, the magnitude of the random wind fluctuations and the associated spectral compositions are of foremost concern. The mean square values of the three wind components are a measure of the magnitude of the wind fluctuations and represent the kinetic energy in the turbulence. The corresponding three power spectra describe the frequency distributions of this energy, but these will not be discussed in this section. However, Reference 2-7 states in the discussion of the magnitude of turbulent fluctuations that in order to conduct experimental observations and the associated analysis in a meaningful manner, it was necessary to assume at least a qualitative description of the spectra.

In the formulation of a turbulence model, it is necessary to establish the mean square value of each of the three wind components in a statistical sense, and to relate these statistics to easily measured parameters such as:

- Atmospheric stability
- Wind shear (or wind speed at a given height)
- Ground roughness
- Height above ground

Although the three fluctuating velocity components have different characteristics, it is convenient to begin the study of the magnitude of turbulent fluctuations by considering the properties of the total kinetic energy in turbulence.

2.4.4.1 Kinetic Energy in Turbulence Near the Ground

The following discussion relies heavily on the work reported in Reference 2-7. The balance of the kinetic energy for horizontally homogeneous turbulence in equilibrium is best described by the energy equation, which is given by Reference 2-7 as

$$u_*^2 \frac{\partial \bar{V}_W}{\partial h} + \frac{gH}{C_p \rho T} = \frac{\partial \overline{ew}}{\partial h} + \frac{\partial \overline{wP/\rho_0}}{\partial h} + \epsilon$$

where the bars denote averages and

$u_*^2 \frac{\partial \bar{V}_W}{\partial h}$ production of mechanical energy through wind shear

$\frac{gH}{C_p \rho T}$ production of convective energy through heating

$\frac{\partial \overline{ew}}{\partial h}$ loss of energy through kinetic energy transport

$\frac{\partial \overline{wP/\rho_0}}{\partial h}$ loss of energy through pressure transport

ϵ local dissipation of energy

According to Reference 2-7, the local rate of change of kinetic energy and the advection of energy over reasonably homogeneous terrain in several hours is two orders of magnitude less than the larger terms in the energy equation, except during periods of transition of the turbulent regime. In view of this, the assumption of equilibrium is justified.

In the neutrally stable atmosphere, the term

$$u_*^2 \frac{\partial \bar{V}_W}{\partial h} = \frac{u_*^3}{kh}$$

and since

$$\bar{V}_W = \frac{u_*}{k} \ln\left(\frac{h}{z_0}\right)$$

the production of mechanical energy is given by

$$u_*^2 \frac{\partial \bar{V}_W}{\partial h} = \frac{k^2 \bar{V}^3}{h\left[\ln\left(\frac{h}{z_0}\right)\right]^2}$$

where $\bar{V}_W$ is the mean wind velocity at the height h, k is the Von Karman constant approximately equal to 0.4, and z_0 is the small scale ground roughness length, which is small compared to h so that $h + z_0 \approx h$. Thus, in neutral air the production of mechanical energy is proportional to the cube of the wind speed, inversely proportional to height, and increases with increasing surface roughness.

In an unstable atmosphere the term producing mechanical energy is given by

$$u_*^2 \frac{\partial \bar{V}_W}{\partial h} = s \frac{u_*^3}{kh}$$

where s is found from

$$s^4 - \frac{\gamma' h}{\ell'} s^3 = 1$$

Since ℓ' is negative in unstable air it can be shown that s will decrease from its value of unity at low levels toward smaller values with increasing height. Thus, the production of mechanical energy will decrease even more rapidly with height in unstable air than in neutral air.

Reference 2-7 assumes that the heat flux, H, varies little with height near the ground except when the heat flux is small. However, in the latter case, the convective energy may be neglected provided that the wind is sufficiently strong. Therefore, an assumption of invariance of the term $gH/C_p\rho T$ with height near the ground, producing convective energy, is essentially valid, except for conditions of near neutral atmospheric stability combined with light wind. The determination of this term directly, which involves the measurement of the heat flux, H, is not very practical. Reference 2-7 describes a method where an approximate value may be obtained by multiplying the term for mechanical energy production, $u_*^2(\partial\bar{V}_W/\partial h)$, by Richardson's number, R_i. From the definition of R_i it is possible to write the following expression

$$gH/C_p\rho T = -(k_H/k_M)R_i u_*^2 (\partial\bar{V}_W/\partial h)$$

where (k_H/k_M) is the ratio between the turbulent transport coefficients for heat and mechanical energy, respectively.

Close to the ground the mechanical energy term is usually much larger than the convective energy term. Higher up the two contributions can become of the same order of magnitude, particularly in light wind conditions.

Reference 2-7 lists four methods used to estimate the energy dissipation term ϵ. Close to the ground all the terms in the energy equation can be neglected except the term representing the production of mechanical energy and the energy dissipation term, giving the following relationship

$$\epsilon \approx u_*^2 \frac{\partial\bar{V}_W}{\partial h}$$

The energy dissipation may be determined by integrating the turbulence spectrum over the dissipation range. By determining the correlation function of a turbulence component for small separations corresponding to the inertial subrange, the energy dissipation may be determined from the following relation

$$R_{xx}(x) = A\epsilon^{2/3}x^{2/3}$$

In the same manner, the spectrum in the inertial subrange may also be used to determine ϵ from

$$\phi_{xx}(k) = a\epsilon^{2/3}K^{-5/3}$$

where K is the wave number.

Finally, the energy dissipation may be obtained by measuring the time after which the size of a diffusing cluster becomes proportional to the cube of the elapsed time. The following expression for the time at which the diffusion law changes from a square law to a cube law has been suggested

$$t \approx y_0^{2/3}\epsilon^{-2/3}$$

where y_0 is the initial size of the cluster. Combined estimates using various methods show that the energy dissipation decreases rapidly with height except for large values in convective clouds (Fig. 2-33).

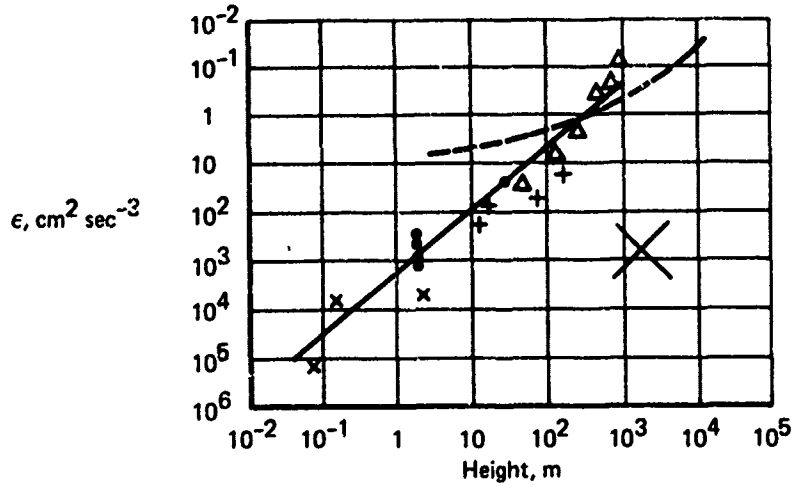

*For details, see original paper. Large cross in lower right gives dissipation calculated for strong convection.

FIGURE 2-33.—VARIATION OF ENERGY DISSIPATION WITH HEIGHT, ACCORDING TO BALL (1961) (FROM REF. 2-7)*

According to Reference 2-7, the measurements of the pressure spectra show little energy in the small scale meteorological range. Thus, the term $\partial(\overline{wP/\rho_0})/\partial h$ is normally neglected near the ground.

Reference 2-7 reports that early attempts at estimating the various terms in the energy equation close to the ground indicated that the divergence of energy flux, $\partial\overline{ew}/\partial h$, was small. However, at higher levels this divergence may be significant. Several investigators, as reported in Reference 2-7, presume that more energy is produced at low levels than is being dissipated locally and thus there is a net energy flux upwards, this energy being dissipated at higher levels. Cross-spectral analysis has revealed that only the low-frequency components of the vertical wind fluctuations contributed to the energy flux. This indicates that the flux is produced by the larger eddies which are prevalent in thermal turbulence. Thus, it may be concluded that the energy flux divergence is only significant under unstable atmospheric conditions. Table 2-2, reproduced from Reference 2-7, shows that the flux divergence may be a significant part of the energy balance. The table also suggests that the rate of energy production by heating is approximately balanced by the energy flux divergence, and therefore the production of mechanical energy is balanced by the local dissipation, even in unstable atmospheric conditions.

It is reasonable to assume that turbulence will be strong where the rate of production of kinetic energy is large. Thus, horizontal and vertical wind shears and atmospheric instability will contribute significantly to the level of turbulence. Restricting considerations to the

TABLE 2-2.–ENERGY[a] BUDGET BETWEEN 11M AND 125 M AT BROOKHAVEN, NEW YORK

Richardson's number	$u_* \frac{2\partial V}{\partial z}$	$\frac{gH}{C_p \rho T}$	Net production	Flux divergence	Dissipation	Net loss
-.03	211	14	225	-24	360	336
-.12	291	3	294	50	188	238
-.60	123	62	185	79	102	181
-.33	177	62	239	119	185	304
-.52	145	96	241	106	147	253
-.53	43	26	69	29	87	116
-.46	280	129	409	108		
.03	612	-19	593	37		
.04	290	-12	278	15		

[a]All entries in ergs gm^{-1} sec^{-1} (from Ref. 7)

atmospheric layer extending from the surface to 1000 feet above the ground, it may be concluded that strong turbulence is likely to occur in the following areas:

- Over rough terrain and in the lee of large physical obstructions, i.e., mountains, hills, buildings, trees, etc., where large wind shears may be present.
- In and near convective clouds and dry thermals where buoyancy effects predominate.

The energy production by wind shear mainly adds directly to the longitudinal turbulence component, which through redistributing action feeds energy into the lateral and vertical turbulence components. In an unstable and a neutrally stable atmosphere, the turbulence level increases until the mechanical energy production is balanced by dissipation. In a stable atmosphere the mechanical energy production is balanced by the combined actions of dissipation and negative buoyancy. Thus, for a given wind level increasing atmospheric stability will tend to reduce the turbulence level.

With increasing atmospheric instability and increasing height from the ground, turbulence due to wind shear decreases until at some height the turbulence will become driven entirely by free convection. However, even under strongly unstable atmospheric conditions, there will always exist in shear flow a layer close to the ground where the mechanical energy production predominates.

The total kinetic energy in turbulence is a function of wind shear, temperature lapse rate, height above ground, and large and small scale terrain roughness. Similarly, theory predicts that the total kinetic energy of turbulence near the ground has the following functional form

$$\overline{e} = u_* f\left(\frac{h}{\ell}\right)$$

where $f(h/\ell')$ is a universal function. Under neutral atmospheric conditions, the preceding equation reduces to

$$\bar{e} = C \frac{\bar{V}_W^2}{\left[\ln\left(\frac{h}{z_0}\right)\right]^2}$$

where $\bar{V}_W$ is the mean wind speed at the height h. Therefore, for a given location the kinetic energy will be proportional to the square of the wind speed at a given height. Figures 2-34 and 2-35, from Reference 2-7, show that this conclusion is confirmed by observations. Figure 2-34 contains observations in unstable air and indicates that any effect of atmospheric stability is indiscernible over relatively rough terrain. However, Figure 2-35 clearly shows that over smooth terrain there is a marked increase in the turbulence level with decreasing atmospheric stability. The effect of increasing atmospheric instability is to increase the production of convective energy, which decreases the wind shear and therewith the production of mechanical energy. Over relatively rough terrain, the turbulence due to wind shear predominates, and the convective energy is not a significant part of the energy balance; an increase in the convective energy may be offset by the resulting decrease in the energy produced by wind shear. Over smooth terrain the convective energy is a more significant part of the energy balance, and the level of turbulence is therefore more sensitive to changes in atmospheric stability.

Reference 2-7 concludes that the variation of kinetic energy with small scale roughness, as suggested by the preceding equation, is in disagreement with experimental observations. It has been shown that for a given wind level there is stronger turbulence over rough terrain (Fig. 2-34) than over smooth terrain (Fig. 2-35), but the difference is not as great as would be expected from the respective small scale roughness lengths. This is demonstrated by the best-fit expressions for the energy under neutral atmospheric conditions for two roughness lengths, as reproduced from Reference 2-7:

For $z_0 = 100$ cm:

$$\bar{e} = 0.78\, \bar{V}_W^2 / \left[\ln\left(\frac{h}{z_0}\right)\right]^2$$

For $z_0 = 0.7$ cm:

$$\bar{e} = 1.36\, \bar{V}_W^2 / \left[\ln\left(\frac{h}{z_0}\right)\right]^2$$

where $\bar{V}_W$ is the mean wind speed at the height h. The roughness length, z_0, is primarily a measure of the vertical dimensions of the small scale surface features. However, the surface is characterized by irregularities of all sizes, and it is reasonable to assume that the total kinetic energy is a function of all of these. Reference 2-7 suggests that the properties of the vertical component of the turbulent velocity fluctuations are primarily related to the vertical small scale roughness characteristics, while the longitudinal and lateral components are also influenced by the presence of large obstructions, i.e., mountains, hills, buildings,

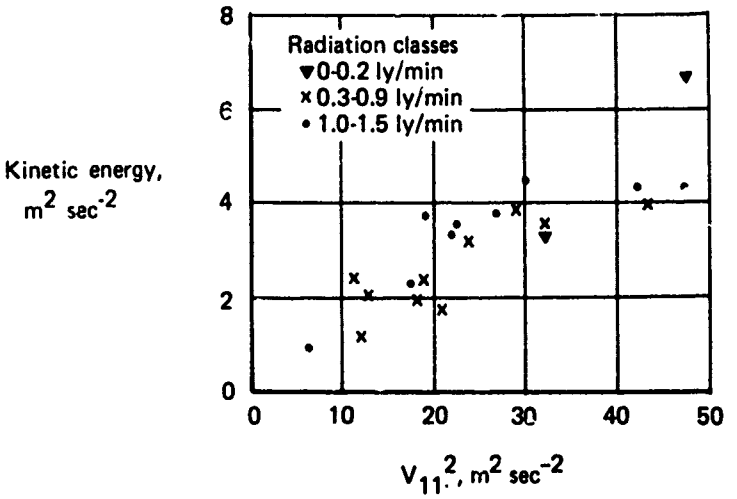

FIGURE 2-34.–THREE-DIMENSIONAL TURBULENT KINETIC ENERGY AT BROOKHAVEN, N.Y.- ROUGH TERRAIN (FROM REF. 2-7)

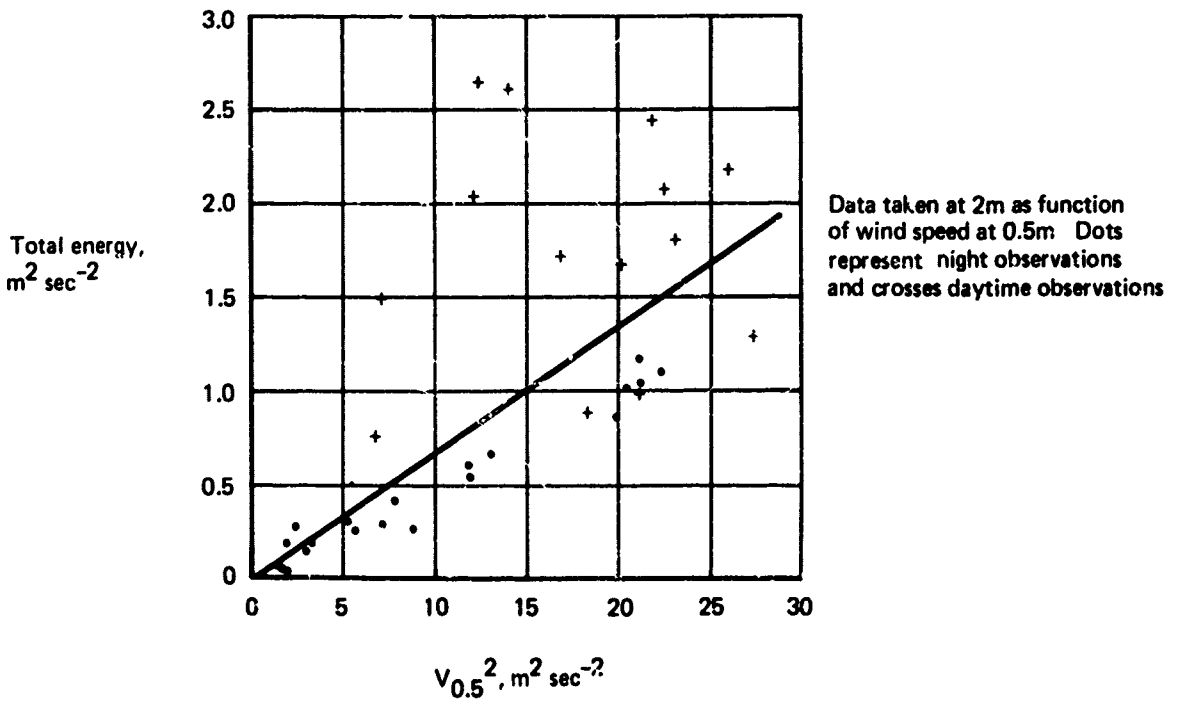

FIGURE 2-35.–THREE DIMENSIONAL TURBULENT KINETIC ENERGY AT O'NEILL, NEBR.--SMOOTH TERRAIN (FROM REF. 2-7)

trees, etc. Thus, the turbulence level will be less in generally flat terrain than in hilly terrain for the same small scale roughness factor z_0.

The preceding discussion suggests that in neutral air the kinetic energy is independent of height. Based on observations, Reference 2-7 concludes that this appears to be true. Within the experimental accuracy, Table 2-3 suggests a remarkable invariance of the kinetic energy with height.

TABLE 2-3.–KINETIC ENERGY, M^2 SEC^{-2}

Height (m)	O'Neill		Brookhaven	
	Night	Day	Night	Day
1.5	0.58	1.41		
3.0	0.58	1.51		
6.0	0.56	1.62		
12.0	0.64	1.82		
23			0.20	4.0
46			0.18	4.3
91			0.20	3.4

A good analytic description of the variations of the total kinetic energy with wind speed and height has been given. However, a constant must be determined by experiment to account for the influence of the large scale surface features at each particular location being considered. Due to relatively few available observations and the complexity of the problem, there are few qualitative estimates of the effect of atmospheric stability on the total kinetic energy in turbulence. As pointed out earlier, the effect of temperature lapse rate is considerable over smooth terrain, while over rough terrain mechanical turbulence predominates and very little dependence on atmospheric stability can be observed. According to Reference 2-7, since

$$\bar{V}_W = \frac{u_*}{k}\left[\ln\left(\frac{h}{z_0}\right) + f\left(\frac{h}{\ell'}\right)\right]$$

then

$$\bar{e} = \frac{k^2 \bar{V}_W^2 f\left(\frac{h}{\ell'}\right)}{\left[\ln\left(\frac{h}{z_0}\right) + f\left(\frac{h}{\ell'}\right)\right]^2}$$

where $\bar{V}_W$ is the wind level at the height h, and if $|h/\ell'|$ is significant the function $f(h/\ell')$, which is negative in unstable air, is not negligible. This equation suggests the dependence of the total kinetic energy in turbulence on atmospheric stability.

2.4.4.2 Magnitude of the Turbulence Components

Many experimental investigations, notably References 2-37, 2-43, and several reported in Reference 2-7, have performed measurements of the mean square values of the three turbulence velocity components. These observations have covered a wide range of atmospheric conditions, heights and topographies. Due to the complexity of the experimental conditions and measurement inaccuracies, any functional relationships between the turbulence intensities and parameters such as season, time of day, altitude, terrain, and the small and large scale meteorological conditions are difficult to extract. The data from these observations are generally presented as statistics and are used to establish trends rather than direct functional dependence. However, the analyses of experimental data have revealed that the following categories of parameters exert the primary influence on the mean square values of the gust velocities.

- Terrain characteristics
- Height above ground
- Wind speed at a given height
- Atmospheric stability

The degree of correlation between the turbulence intensities and any one of these parameters is a function of the state of the other parameters.

Turbulence is more severe over rough terrain than over smooth terrain. The vertical gust component is primarily a function of the small scale roughness features of the ground, whereas the lateral and longitudinal component is also influenced by large scale surface features. The variations of the gust intensities with height depend upon surface roughness and atmospheric stability. Over smooth terrain and under unstable conditions, the turbulence level tends to increase with height due to an increasing effect of convective turbulence. Under stable atmospheric conditions, the turbulence level decreases with height. Over rough terrain where mechanical turbulence predominates, the variation of turbulence with height shows the least correlation with atmospheric stability.

Increasing wind increases the intensity of turbulence, more severely over rough terrain than over smooth terrain. The correlation between the magnitude of turbulence and the wind speed increases with decreasing height. The vertical gust velocity component shows less correlation with wind speed, as do the longitudinal and lateral components.

Low turbulence levels are generally associated with stable atmospheric conditions. The intensity of the gusts normally increases with decreasing atmospheric stability. This effect is more predominant at the higher altitudes and over smooth terrain. There is a high probability of encountering turbulence at Richardson's numbers less than 1.0, and the probability of increased turbulence becomes significantly higher when the Richardson's number is less than the critical Richardson's number, about 0.2.

To determine the appropriate turbulence level for a given wind shear, atmospheric stability, and terrain roughness, it is necessary to define a relationship between these variables and the standard deviation of each of the turbulence components.

2.4.4.2.1 Variance of the Vertical Component–An analytical description of the characteristics of the standard deviation of the vertical velocity fluctuations has been developed and substantiated by Reference 2-7. The following analysis largely follows this work except for a few changes in notation.

The standard deviation of the vertical turbulence component σ_w is a function of atmospheric stability and wind shear near the ground, height, and ground roughness. Monin-Obukhov similarity theory predicts that the standard deviation is defined by an expression of the form

$$\sigma_w = u_* f\left(\frac{h}{\ell}\right)$$

where u_* is the friction velocity, $f(h/\ell)$ is a universal function of h/ℓ, h is height above ground, and ℓ is a scaling length defined by similarity theory as

$$\ell = \frac{u_*^3 C_p \rho T}{kgh}$$

The standard deviation can also be expressed as a function of the height h, the rate of production of mechanical energy by wind shear $u_*^2 \partial \bar{V}_W/\partial h$, and the rate of supply at convective energy by heating $gH/C_p\rho T$. Dimensional analysis predicts the following general equations,

$$\sigma_w = \left(hu_*^2 \frac{\partial \bar{V}_W}{\partial h}\right)^{1/3} F_1\left[(gH/C_p\rho T)/u_*^2 \frac{\partial \bar{V}_W}{\partial h}\right]$$

In the particular case of free convection

$$\sigma_w = A(gHh/C_p\rho T)^{1/3}$$

where A is a constant. Hence the general function must have the form

$$\sigma_w = B\left[h\left(u_*^2 \frac{\partial \bar{V}_W}{\partial h} + \frac{\delta gh}{C_p\rho T}\right)\right]^{1/3}$$

where B and δ are constants.

The nondimensional wind shear, s, is defined as

$$s = \frac{kh}{u_*} \frac{\partial \bar{V}_W}{\partial h}$$

Hence

$$\sigma_w = Cu_*\left(s - \delta\frac{h}{\ell}\right)^{1/3}$$

where

$$C = B/(k)^{1/3}$$

Since in practice only the quantity ℓ' is available, the transformation

$$\ell = \ell'(k_M/k_H)$$

must be used. k_M/k_H is the ratio between the turbulent transport coefficients for mechanical and heat energy, respectively.

Substituting for ℓ gives

$$\sigma_w = Cu_* \left[s - \delta \frac{k_H}{k_M} \frac{h}{\ell'} \right]^{1/3}$$

For neutral and unstable atmospheric conditions, this equation defines the relationship between the standard deviation of the vertical velocity fluctuations and wind shear, small scale surface roughness, atmospheric stability near the ground, and height. Reference 2-7 shows that with the proper selection of the constants C and δ, this theoretical relation agrees well with observations. It is argued that two of the reasons for this agreement are that the presence of the ground surface prevents low frequency components from forming, and the small scale surface roughness length z_0 serves sufficiently well to account for the terrain effect.

Since s is a unique function of h/ℓ', a general function $G(h/\ell')$ may be defined as

$$G(h/\ell') = \left[s - \frac{k_H}{k_M} \frac{h}{\ell'} \right]^{1/3}$$

Hence

$$\sigma_w/u_* = CG(h/\ell')$$

In the case of a neutral atmosphere, $G(h/\ell')$ is a constant equal to one, and

$$\sigma_w/u_* = C$$

Therefore, under adiabatic conditions the standard deviation of the vertical velocity fluctuations is proportional to the friction velocity. This implies that it is proportional to the mean wind speed at a given height, increases with increasing small scale roughness, and is invariant with height. The standard deviation may be expressed in terms of the mean wind speed $\bar{V}_W$ at a height h, and the roughness length z_0:

$$\sigma_w = \frac{0.4\, C \bar{V}_W}{\ln(h/z_0)}$$

The literature lists several values for the constant C. Atmospheric observations have produced values ranging from 0.7 to 1.37, as shown on Table 2-4. There is evidence that the value of 0.7 is too low for a factor of 1.5 (Ref. 2-7). On the other hand, the value of 1.33 also reported in Reference 2-7 may be an overestimate since this value was obtained by equating the standard deviation of the vertical velocity fluctuations to the product of the standard deviation of the vertical angle fluctuations and the mean wind. This is known to produce an overestimate due to the correlation between the vertical angle and mean wind speed. Wind tunnel measurements have consistently produced values close to approximately 1.05, which Reference 2-7 assumes to be a good compromise between the divergent atmospheric observations, the reasoning being that C must be a universal constant.

*TABLE 2-4.–VALUES OF THE CONSTANT OF PROPORTIONALITY C BETWEEN σ_w AND u**

$\sigma_w/u_* = C$	Source	Comments
1.37	Reference 44	Based on u* at 30 m, from TOLCAT data
1.33	Reference 7	Based on measurements of standard deviation of the vertical angle fluctuations
1.30	References 1, 29, and 34	
1.29	Reference 38	Assumed valid within 50 ft of the ground for a wide range of atmospheric stability
1.25	References 7, 4	Based on fitting of observations in neutral and unstable conditions
1.2	Reference 40	
1.05	Reference 7	Based on measurements in pipe flow
1.05	Reference 7	Based on wind tunnel measurements in boundary layer
0.99	Reference 45	
0.87	Reference 7	
0.70	Reference 7	There is evidence that C was underestimated by a factor of 1.5 (0.70 x 1.5 = 1.05)

An additional argument presented in Reference 2-7 for C = 1.05 is provided on Figure 2-36: For $C > 1.05$, σ_w/u_* initially decreases for small decreases of stability from neutral, a characteristic regarded as physically unlikely.

Dr. Panofsky (coauthor with Lumley of Ref. 2-7) has indicated in a conversation that he no longer supports C = 1.05 because of substantial recent evidence, such as the survey on Table 2-5 taken from Reference 2-46, but that he now accepts C = 1.3.

Selecting σ_w/u_* for adiabatic conditions, straight lines representing the theoretical relationship between σ_w and the mean wind speed at a given height were added to Figures 2-37, -38, and -39, which are reproduced from Reference 2-7. Considering the data scatter normally associated with atmospheric observations, there seems to be good agreement between the theoretical estimations and the observed values. This supports the supposition

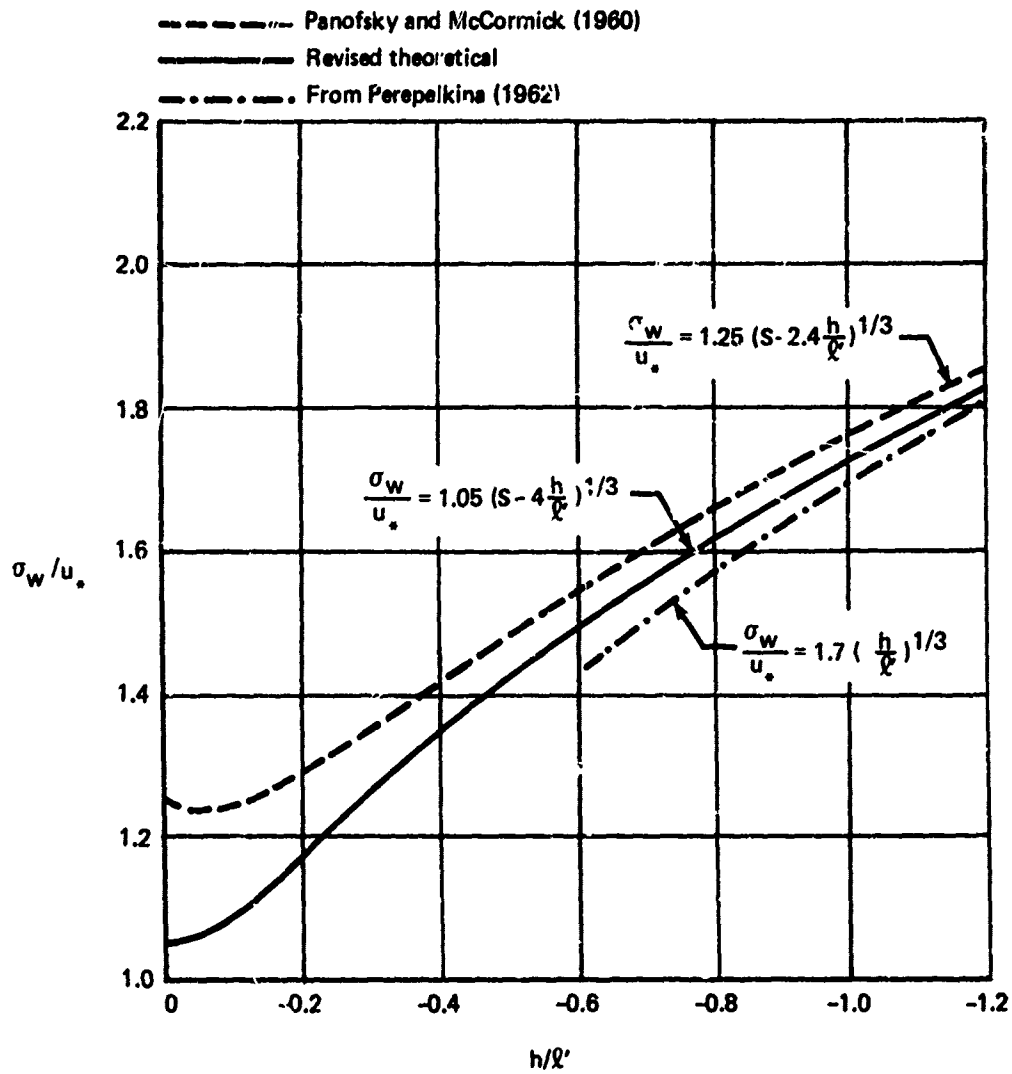

FIGURE 2-36.–THEORETICAL AND OBSERVED VARIATION OF σ_w / u_* WITH INSTABILITY (FROM REF. 2-7)

TABLE 2-5.–SUMMARY OF ESTIMATES OF VERTICAL TURBULENCE IN NEUTRAL CONDITIONS

Site	Height of measurement (m)	Instruments used for σ_w	Source of u_*	σ_w/u_*	Reference for estimates of σ_w/u_*
Brookhaven, U.S.	91	Vane	(a)	1.25	Panofsky and McCormick (1960)
O'Neill, U.S.	12	Sonic anemometer	(a)		
Edithvale, Australia	2, 12, 29	Hot-wire inclinometer	(a)		
Porton	1/2-16	Hot-wire inclinometer	(a)	1·33[2]	Pasquill (1962)
O'Neill, U.S.	1·5-12	Vane	(b)	1·2	Koug (1965)
Various in U.S.	1-55	Various	(a) and (b)	1·2	Panofsky and Prasad (1965)
Rostov, USSR	4	Sonic anemometer	(b)	1·2	Mordukhovich and Tsvang (1966)
Hay, Australia	4	Sonic anemometer	(a)	1·3[3]	Businger et al. (1967)
Hanford, U.S.	3 & 6·1	Heated thermo-couple wires	(b)		Busch and Panofsky (1968)
Kansas	5·7, 22·6	Sonic anemometer	(b)	1·35	Haugen et al. (1971)
British Columbia	2	Sonic anemometer	(b)	1·4	McBean (1971)

Notes:
1. (a) Wind profile (b) eddy correlation.
2. An estimate of the correction required for the approximate use of angular inclination in deriving σ_w reduces this to 1·25.
3. This value is stated by the authors to be low, possibly by as much as 15%, on account of omission of high-frequency contributions to σ_w.
4. Information from Reference 46.

that the theoretical expression represents the variation of σ_w, with the small scale roughness length and the mean wind speed at a given level. Further, it is borne out that for neutral atmospheric conditions σ_w is invariant with height, which is consistent with the theory.

Selecting the roughness length

$$z_0 = 0.15 \text{ feet}$$

as typical for airports, the vertical component of turbulence may be expressed in terms of the mean wind speed at 20 and 33 feet, respectively, for neutral atmospheric conditions.

For C = 1.3

$$\sigma_w = 0.0964\, \bar{V}_{33}$$

$$\sigma_w = 0.106\, \bar{V}_{20}$$

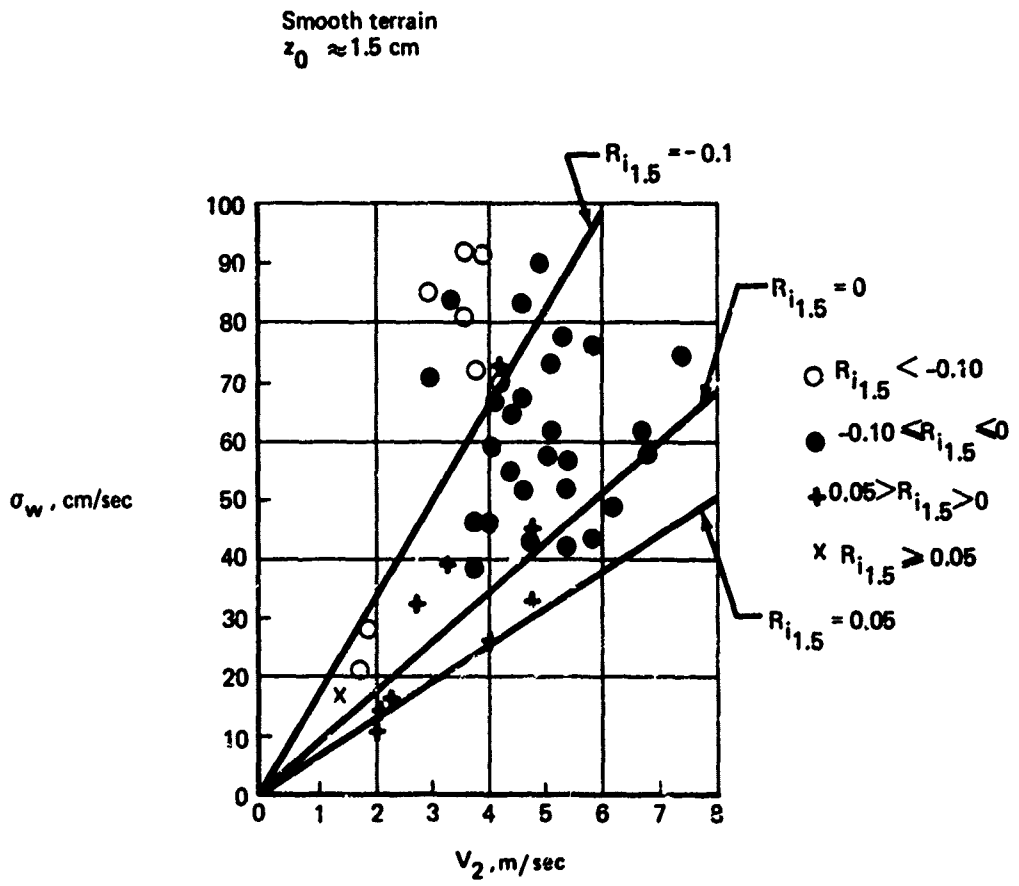

Lines indicate theoretical relationships for various atmospheric stability conditions.

FIGURE 2-37.—STANDARD DEVIATION OF VERTICAL VELOCITY AT 23 M OR 29 M OVER SMOOTH TERRAIN AS A FUNCTION OF WIND SPEED AT 2 M (FROM REF. 2-7)

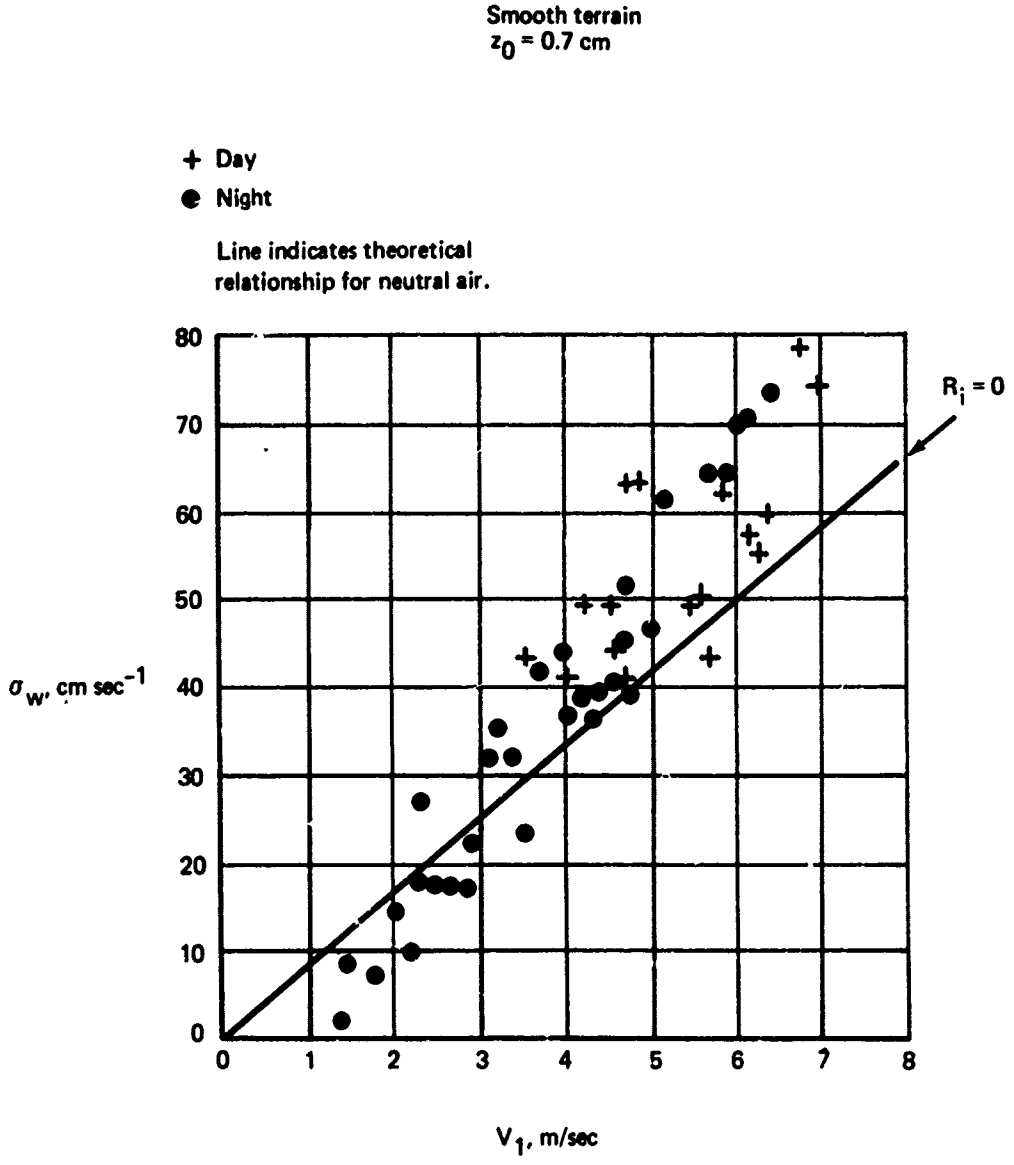

FIGURE 2-38.—STANDARD DEVIATIONS OF VERTICAL VELOCITY AT 2M AT O'NEILL, NEBRASKA AS A FUNCTION OF WIND SPEED AT 1 M (FROM REF. 2-7)

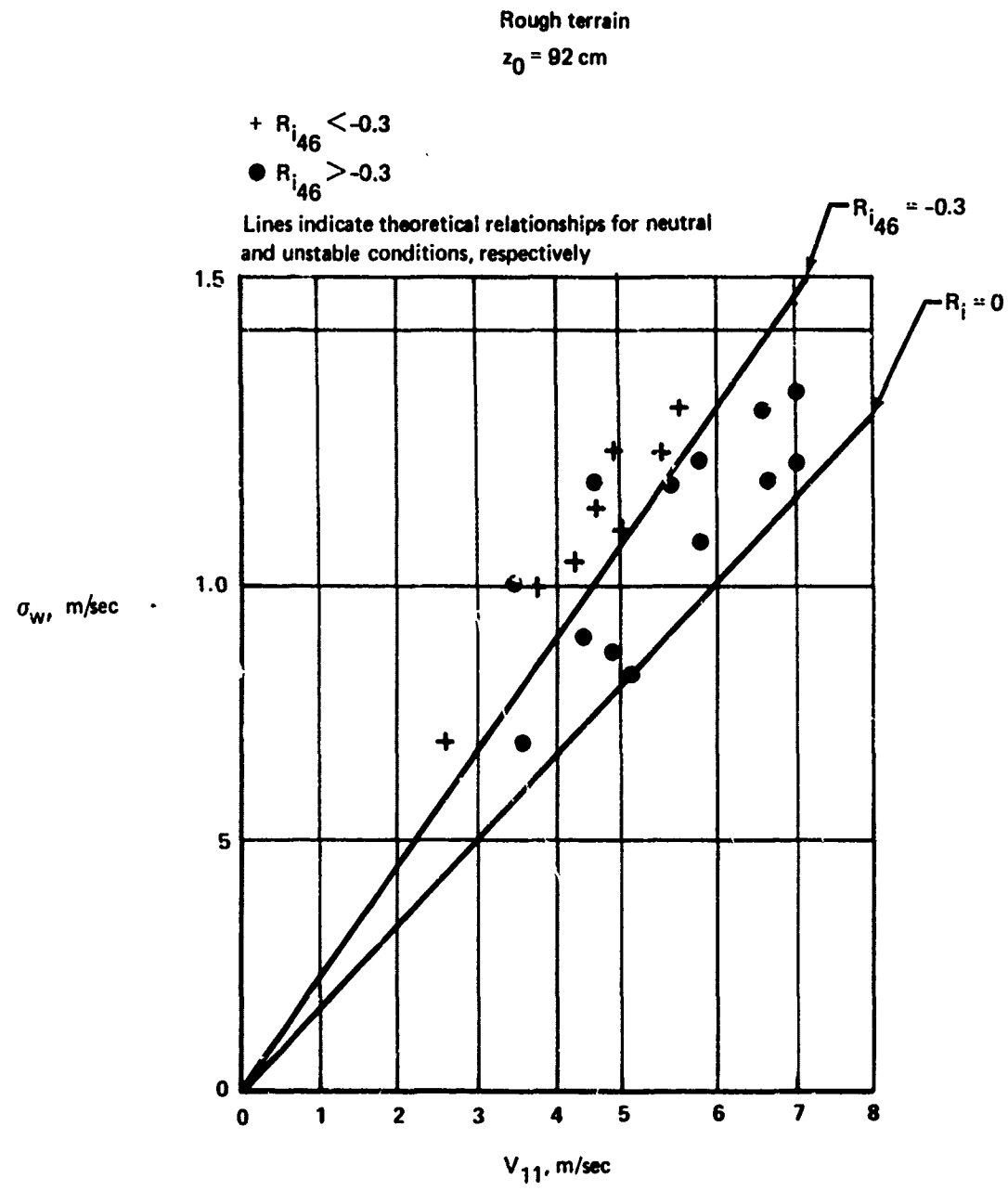

FIGURE 2-39.–STANDARD DEVIATION OF VERTICAL VELOCITY AT BROOKHAVEN, N.Y. AS A FUNCTION OF WIND SPEED AT 11 M (FROM REF. 2-7)

For comparison, the proposed ARB model (Ref. 2-14) specifies for neutral atmospheric conditions

$$\sigma_w = 0.09\,\bar{V}_{33}$$

where $z_0 = 0.15$ feet has been selected. This is based on the assumption that

$$\sigma_w = 0.5\,\sigma_u$$

where

$$\sigma_u = \sigma_v = 0.18\,\bar{V}_{33}$$

which is specified as typical for airports under neutral atmospheric conditions. The ARB model further assumes that these relationships are valid for heights between 10 and 300 feet.

In free convection, equivalent to very unstable conditions where the nondimensional shear is negligible, σ_w is given by:

$$\sigma_w = A(gHh/C_p\rho T)^{1/3}$$

$$\frac{\sigma_w}{u_*} = D\left(\frac{h}{\ell}\right)^{1/3}$$

Therefore, the vertical turbulence component varies as $(h)^{1/3}$ under conditions of free convection. Independent observations reported in Reference 2-7 establish a value of D equal to 1.7. Assuming that the ratio (k_H/k_M) is close to unity the equation for σ_w/u_* becomes

$$\frac{\sigma_w}{u_*} = C\left[s - \left(\frac{D}{C}\right)^3 \frac{h}{\ell'}\right]^{1/3}$$

That is, $\delta = (D/C)^3$

or, for C = 1.3 and D = 1.7,

$$\frac{\sigma_w}{u_*} = 1.3\left[s - 2.236\frac{h}{\ell'}\right]^{1/3}$$

The fact that δ is larger than unity implies that the convective forces are more efficient in producing vertical velocity fluctuations than the wind shear forces. Reference 2-7 lists two possible explanations. Convection directly causes vertical motions, while wind shear first produces horizontal motions. The vertical velocity fluctuations due to wind shear are caused by redistribution of the energy contained in the horizontal fluctuations. The second hypothesis postulates that the convective portion of the vertical velocity fluctuations is characterized by larger eddy sizes than the mechanical portion. For this reason, the effect of convection is relatively more efficient.

The preceding discussions have shown that for a given wind level at a fixed height the standard deviation of the vertical velocity fluctuations is invarlant with height in neutral air and increases with height in unstable air. This is in general agreement with most observations. Experimental observations reported in the literature show that in a stable atmosphere σ_w decreases with increasing altitude. However, Reference 2-7 maintains that the function $G(h/\ell')$ is not valid for positive values of h/ℓ'. Figure 2-40 indicates the variation of σ_w/u_* with h/ℓ' in stable air. For a given level of stability the figure implies a reduction in σ_w with height. The decrease in the value of u_* through the function $f(h/\ell')$ accounts for a general decrease in σ_w at all levels with increasing atmospheric stability.

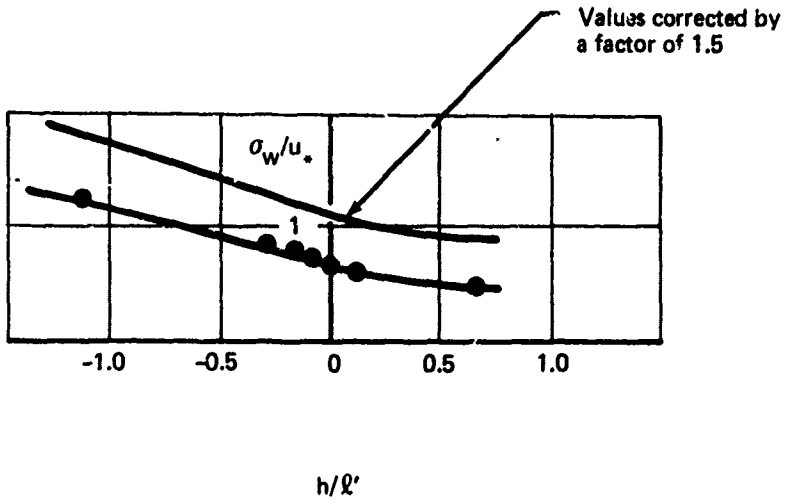

FIGURE 2-40.–OBSERVED σ_w/u_* AS A FUNCTION OF h/ℓ' (FROM REF. 2-7)

In summary, the standard deviations of the vertical velocity fluctuations σ_w are primarily controlled by the wind speed, atmospheric stability, and small scale surface roughness. In neutral air σ_w is invariant with height, increases with height in unstable air, and decreases with height in stable air. For a given wind shear near the ground the value of σ_w at all levels increases with decreasing atmospheric stability. The effect of varying atmospheric stability is small at lower levels and over rough terrain, but increases with height and becomes considerable at higher levels, especially over smooth terrain. The analytical descriptions presented agree well with experimental observations.

2.4.4.2.2 Variance of the Lateral Component–Consider the standard deviation of the lateral velocity fluctuations, σ_v, as a function of wind speed and roughness in a neutrally stable atmosphere. Similarity theory predicts that σ_v is proportional to the friction velocity u_*, i.e.,

$$\sigma_v = Cu_*$$

or

$$\sigma_v = \frac{Ck\bar{V}_W}{\ln(h/z_0)}$$

where $\bar{V}_W$ is the mean wind speed at the height h, z_0 is the small scale roughness length, and C is a constant of proportionality. Again this implies that the standard deviation is proportional to the wind speed at a given height, increases with increasing surface roughness, and is invariant with altitude. Experimental observations at a given location confirm this hypothesis. Figures 2-41, -42, and -43, which have been reproduced from the literature, indicate that σ_v is proportional to the wind speed at a given height and appears to be invariant with height. The straight lines giving the least squares fit to the experimental points in both figures have almost identical slopes, although the roughness lengths associated with the two locations are different by a factor of ten. This implies that the constant C is different for the two locations, a result which is typical when the observed relations between σ_v and u_* for various places are compared. The large spread in the values of C shown in Table 2-6 is sufficient to indicate a systematic difference. As a result, it may be postulated that the small scale roughness length z_0 alone will not account for the effect of terrain roughness on the standard deviation of the lateral velocity fluctuations. Reference 2-7 maintains that z_0 must be replaced by a measure of large scale roughness that depends on large scale surface features such as hills. Actually, the ground is characterized by irregularities of all sizes, ranging from grains of sand and blades of grass, to buildings, hills, and mountains. Some investigators have suggested that the intensity of turbulence should be related to the whole surface spectrum. On the other hand, it appears that for a given location the proportionality between σ_v and u_* holds, and by determining the constant of proportionality C for each location being considered, the effect of large scale roughness may be taken into account.

TABLE 2-6.—VALUES OF THE CONSTANT OF PROPORTIONALITY C BETWEEN σ_v AND u_*

$\sigma_v/u_* = C$	Source	Height	Comments
a) 2.6	Reference 7	2 m	Same location as d)
b) 2.2	Reference 7	12 m	
c) 2.2	Reference 44	30 m	
d) 2.0	Reference 7	2 m	Same location as b)
e) 3.0	Reference 7	300 ft	
f) 2.0	Reference 38	50 ft	Claimed to be valid for a wide range of stabilities within 50 ft of the ground
g) 2.0	References 1 and 34		
h) 1.5	Reference 7		Wind tunnel, boundary-layer measurements
i) 1.5	Reference 7		Pipe flow measurements
j) 1.3	Reference 7	All levels	
k) 1.64	Reference 40	5.06, 11.3, 22.6 m	

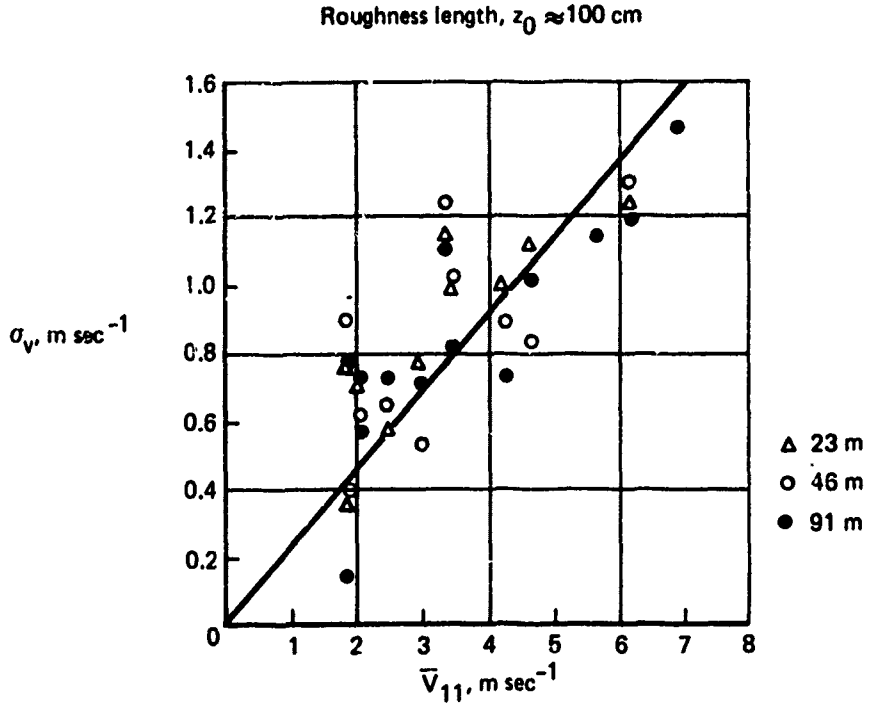

FIGURE 2-41.—STANDARD DEVIATION OF LATERAL VELOCITY AT BROOKHAVEN, N.Y. AS A FUNCTION OF WIND SPEED AT 11 M (FROM REF. 2-7)

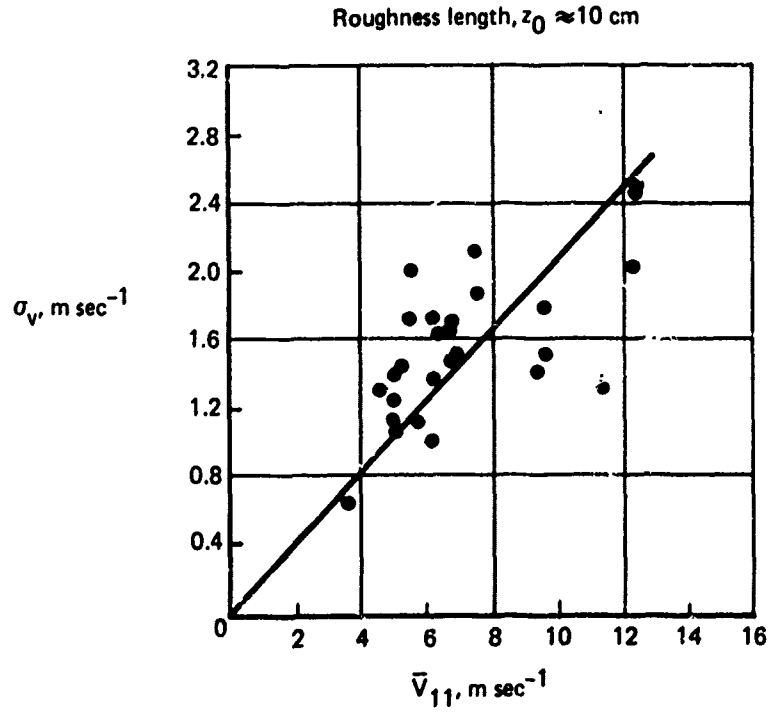

FIGURE 2-42.—STANDARD DEVIATION OF LATERAL VELOCITY AT SOUTH DARTMOUTH, MASS., AS A FUNCTION OF WIND SPEED AT 11 M (FROM REF. 2-7)

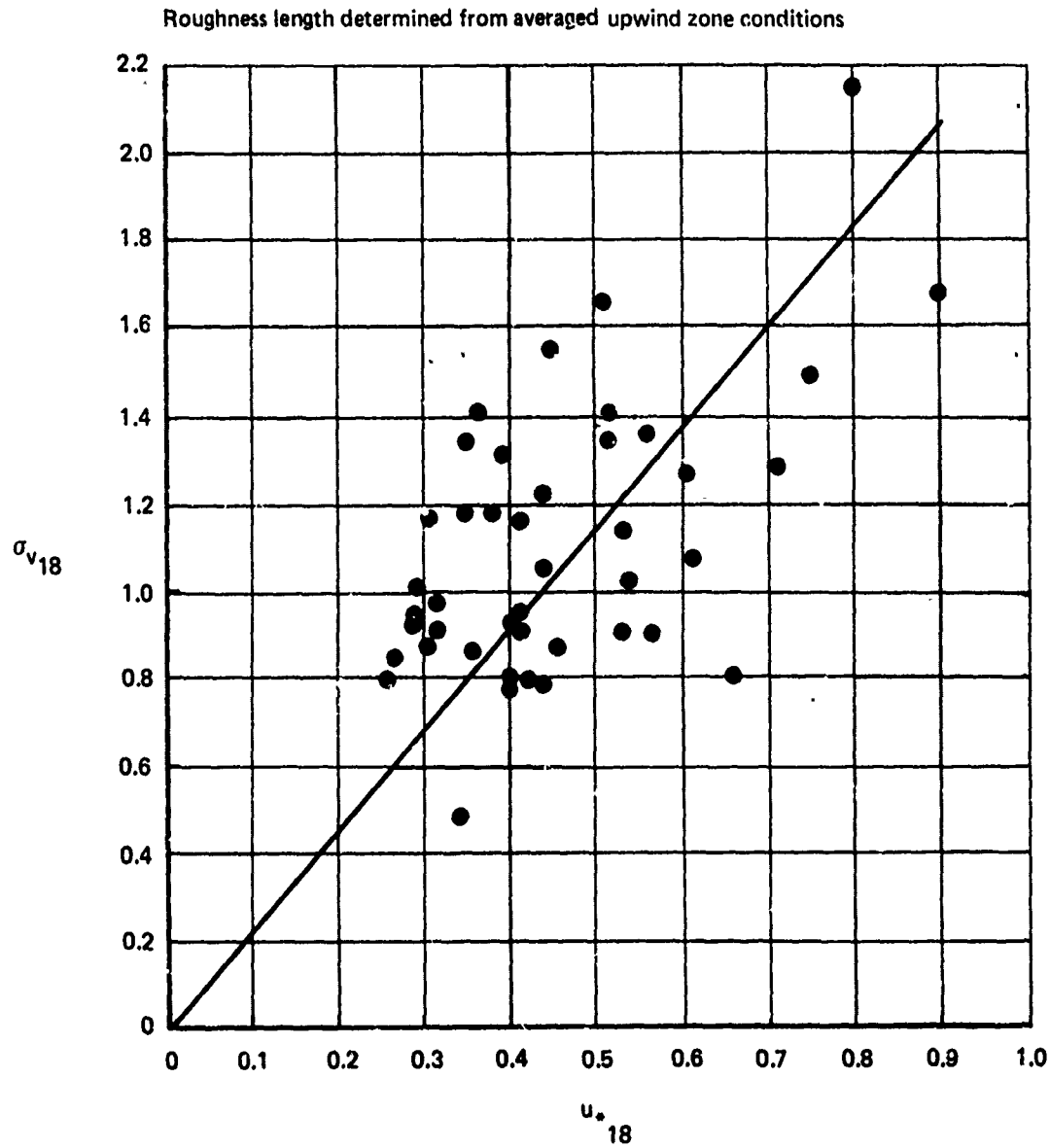

FIGURE 2-43.– VARIANCE OF LATERAL WIND COMPONENTS AT 18M AS A FUNCTION OF FRICTION VELOCITY AT 18M (FROM REF. 2-47)

Selecting the roughness length

$$z_0 = 0.15 \text{ feet}$$

and

$$\sigma_v = 2.6\, u_*$$

as representative of a typical airport, the lateral component of turbulence may be expressed in terms of the mean wind speed at 20 and 33 feet, respectively, for neutral atmospheric conditions.

$$\sigma_v = 0.193\, \bar{V}_{33}$$

$$\sigma_v = 0.212\, \bar{V}_{20}$$

For comparison, the proposed ARB model (Ref. 2-14) specifies for neutral atmospheric conditions

$$\sigma_v = 0.18\, \bar{V}_{33}$$

where z_0 = 0.15 feet has been selected. The ARB model further assumes that this relationship is valid for heights between 10 and 300 feet.

The standard deviation of the lateral velocity fluctuations σ_v at a given location in neutral air is proportional to the friction velocity u_*. The constant of proportionality may differ from one location to another. As in the case of the vertical velocity fluctuations, it may be hypothesized that

$$\sigma_v = Cu_* f(h/\ell)$$

for stable and unstable atmospheric conditions. However, Reference 2-7 maintains that this formulation is incorrect. Observations show that σ_v is insensitive to changes in height but is very sensitive to changes in atmospheric lapse rate, especially at lower wind speeds. At the higher wind speeds when mechanical energy predominates, lapse rate seems to be of less significance.

Observations of σ_v in very unstable air are characterized by considerable data scatter, showing that even hourly averages are influenced by random variations. This indicates that the lateral velocity fluctuations are dominated by heat convection, which is characterized by large eddy sizes, and are controlled by the lapse rate. For a given wind speed the effect of decreasing atmospheric stability is a significant increase in the intensity of the lateral velocity fluctuations. This is borne out well by Figures 2-44, -45, and -46, which have been reproduced from the literature. For the unstable lapse rates the correlation between wind speed and σ_v is weak, especially over smooth terrain, and the effect of surface roughness is small up to moderate wind speeds.

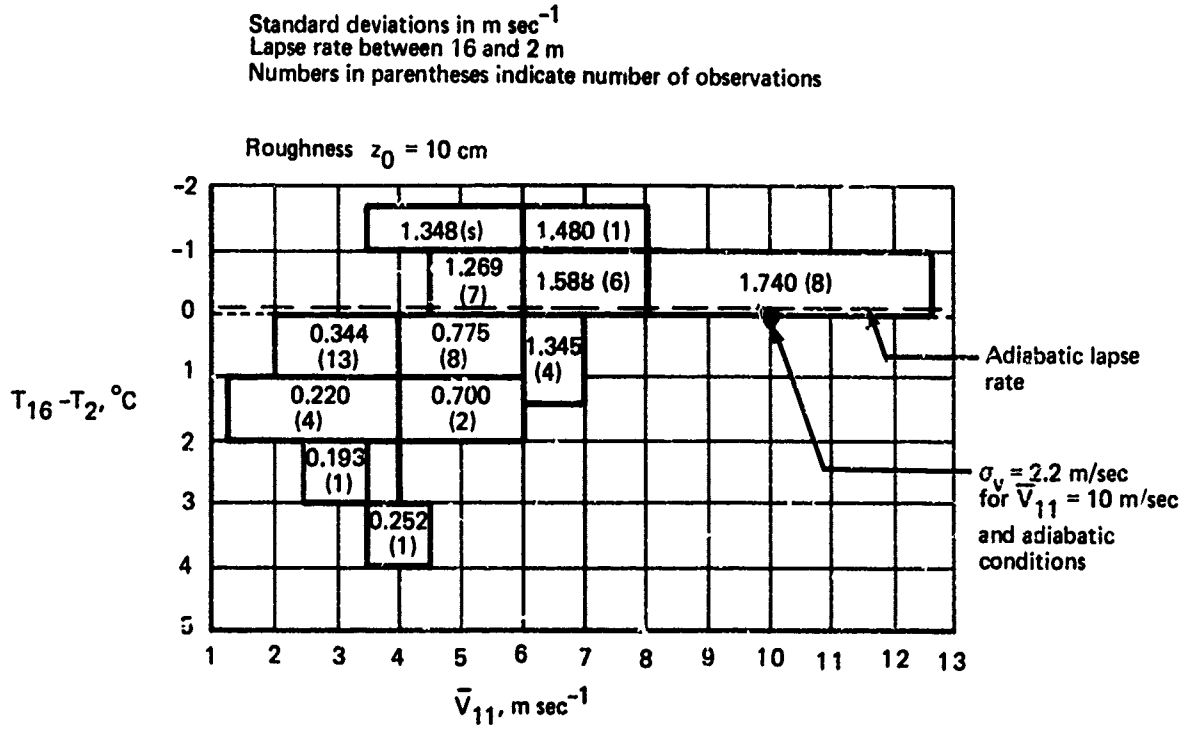

FIGURE 2-44.–STANDARD DEVIATION OF LATERAL VELOCITY AT SOUTH DARTMOUTH, MASS. AS FUNCTION OF WIND SPEED AT 11 M (FROM REF. 2-7)

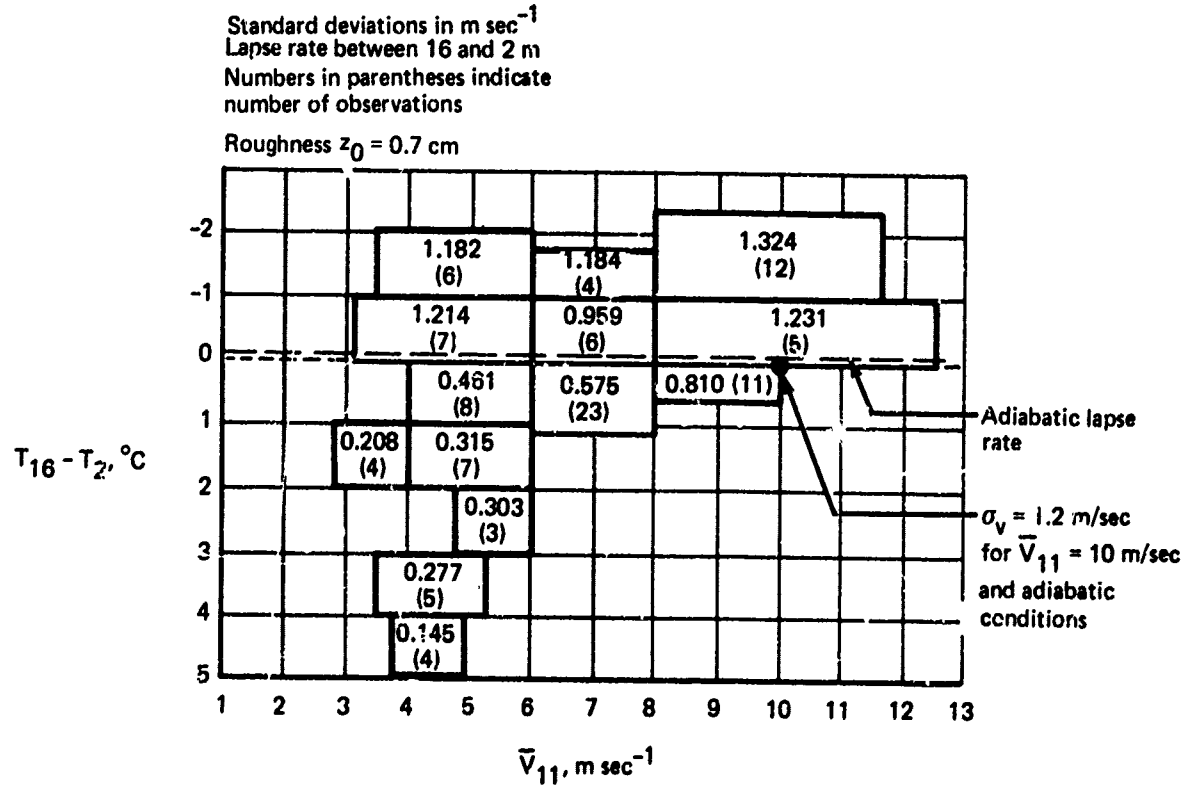

FIGURE 2-45.–STANDARD DEVIATION OF LATERAL VELOCITY AT O'NEILL, NEBR. AS FUNCTION OF WIND SPEED AT 11 M (FROM REF. 2-7)

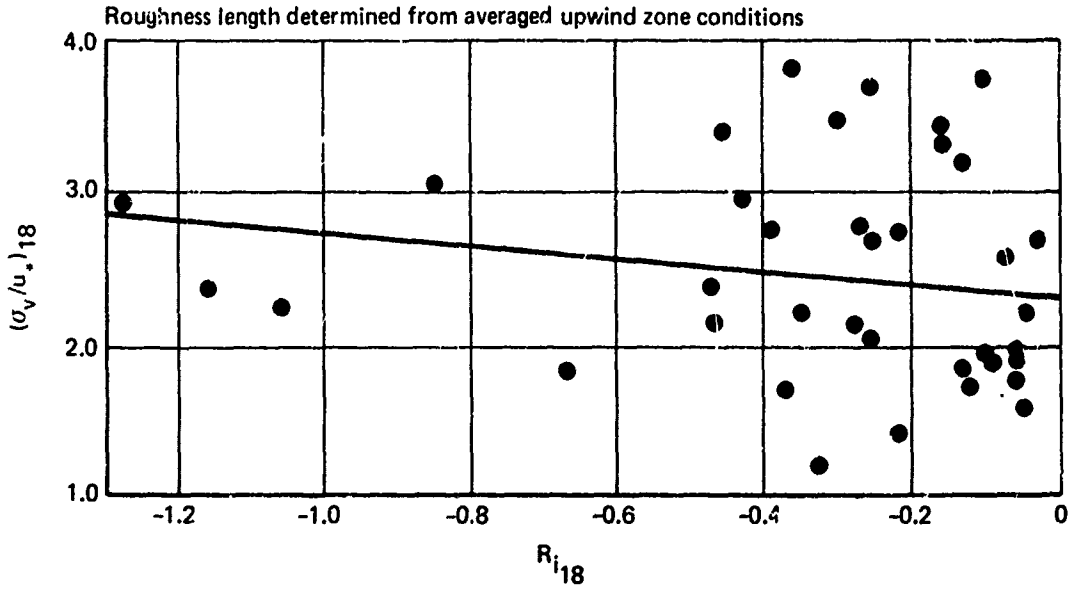

FIGURE 2-46.—RATIO OF VARIANCE OF LATERAL WIND COMPONENTS TO THE FRICTION VELOCITY AT 18 M AS A FUNCTION OF RICHARDSON'S NUMBER AT 18 M (FROM REF. 2-47)

In contrast to σ_W, very little vertical variation of σ_v with height has been observed from the surface up to a height of 300 feet. Reference 2-7 concludes that σ_v probably increases with height by a small amount near the surface in unstable air. This is based on observations taken at heights less than 300 feet above the ground. References 2-37 and 2-43 present observations which indicate that σ_v decreases from 250 to 750 feet over both rough and smooth terrain in unstable air. This decrease in σ_v is more pronounced over rough terrain than over smooth terrain.

The two main results of increasing atmospheric stability are a marked reduction in the magnitude of the lateral velocity fluctuations and an increasing correlation between σ_v and wind speed, and surface roughness. The observations presented in Figures 2-47 and 2-48 indicate that σ_v is approximately proportional to $(\bar{V}_W)^{1.5}$ in stable air:

Least squares fit in Figure 2-47:

$$\sigma_v = 0.03\,(\bar{V}_{11})^{1.5}$$

Least squares fit in Figure 2-48:

$$\sigma_v = 0.07\,(\bar{V}_{11})^{1.5}$$

Where $\bar{V}_{11}$ is the wind speed at 11 m and σ_v is given in m/sec. Reference 2-7 qualitatively explains the 1.5 power as a linear variation, with a decreased effect of the inversion imposed at the higher speeds. The difference in the constants of proportionality again reflects the difference in the large scale surface features between the two locations associated with the figures. Reference 2-7 reports gradual but large azimuth fluctuations in light wind

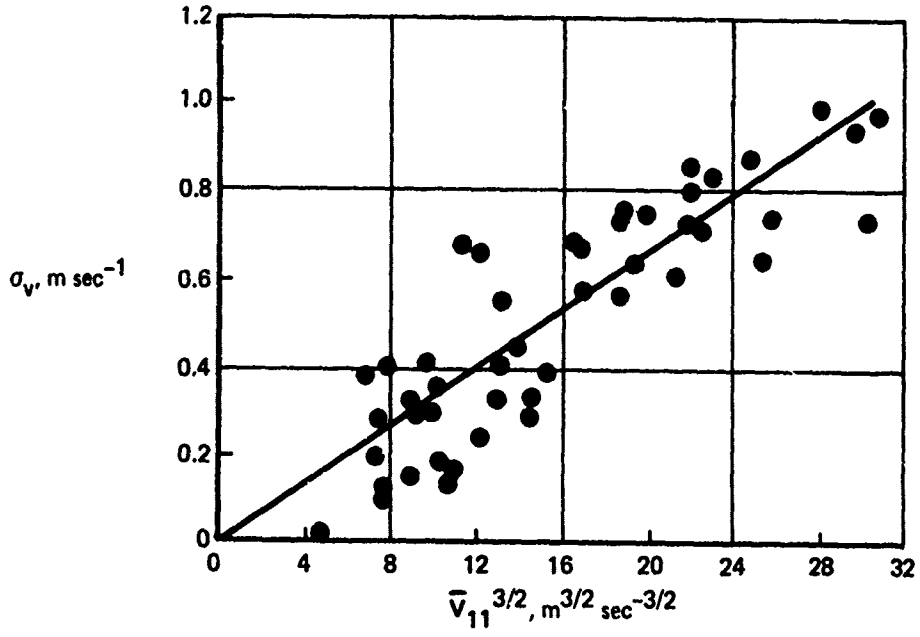

FIGURE 2-47.—STANDARD DEVIATION OF LATERAL VELOCITY AT O'NEILL, NEBR. AT 2 M AT NIGHT AS FUNCTION OF 3/2 POWER OF WIND SPEED AT 11M (FROM REF. 2-7)

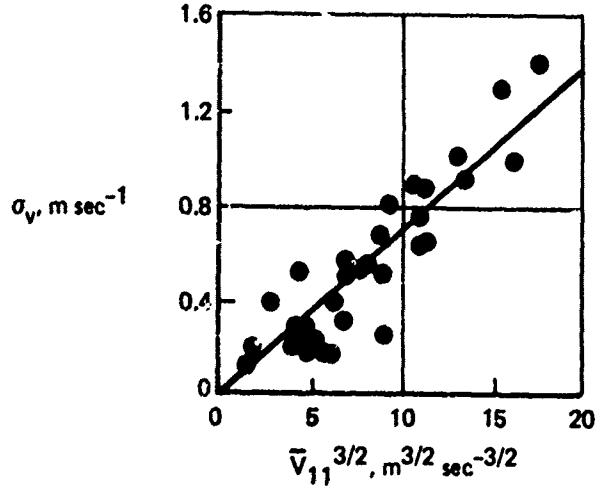

FIGURE 2-48.—STANDARD DEVIATION OF LATERAL VELOCITY AT SOUTH DARTMOUTH, MASS. AT 2 M AT NIGHT AS FUNCTION OF 3/2 POWER OF WIND SPEED AT 11 M (FROM REF. 2-7)

conditions and stable air. For sufficiently long sampling periods this will give rise to considerable data scatter as well as unexpectedly large values of the observed standard deviation. This gradual shift in wind direction cannot be associated with mechanical turbulence, which is small in light winds, nor can it be associated with heat convection, which is absent in stable air. The literature fails to give a satisfactory explanation of this phenomenon.

In contrast to σ_w, observations show little vertical variation of σ_v in stable air. Reference 2-7 notes that the high frequency component of σ_v decreases with altitude. Therefore, some observations may have underestimated σ_v close to the surface through neglect of the high frequency portion of the lateral wind fluctuations. Reference 2-7 concludes that some decrease of σ_v with height in stable air may be anticipated. Observations presented in Reference 2-37 show that the average σ_v decreases from 250 to 750 feet in stable air both over rough and smooth terrain, whereas observations presented in Reference 2-43 show little variation of σ_v in the same altitude range and under the same atmospheric stability conditions.

To summarize, in neutrally stable conditions the standard deviation of the lateral velocity fluctuations σ_v may be assumed to be proportional to the friction velocity u_*, where the constant of proportionality is a function of the large scale surface roughness. The magnitude of the standard deviation increases with decreasing atmospheric instability, and at low wind speeds the lapse rate has the dominant influence on the turbulence strength. The correlation between σ_v and wind speed, and surface roughness is small in unstable air but becomes considerably stronger in stable air. For the latter condition, σ_v increases with increasing wind speed and surface roughness. The vertical variation of σ_v is small in both stable and unstable air. The analytic description presented agrees well with experimental observations in neutral air, provided the constant of proportionality C is adjusted to account for the large scale surface roughness at various locations. No satisfactory analytical relationships for σ_v under unstable and stable atmospheric conditions have been developed.

2.4.4.2.3 Variance of the Longitudinal Component–As in the case of the vertical and lateral velocity fluctuations, experimental observations indicate that the standard deviation of the horizontal velocity fluctions, σ_u, is proportional to the friction velocity u_* in a neutrally stable air mass.

$$\sigma_u = Cu_*$$

This implies that σ_u is proportional to the wind speed at a given height and is more or less invariant with height (see Fig. 2-49).

$$\sigma_u = \frac{Ck\bar{V}_w}{\ln(h/z_0)}$$

As in the case of σ_v, it turns out that the value for the constant of proportionality C varies with terrain as indicated in Table 2-7. Reference 2-7 notes that the values for C are different enough to suggest that a real discrepancy exists, and attributes this to the difference in the large scale surface features from one location to another. By selecting the proper value for C for each location being considered, the effect of large scale roughness may be taken into

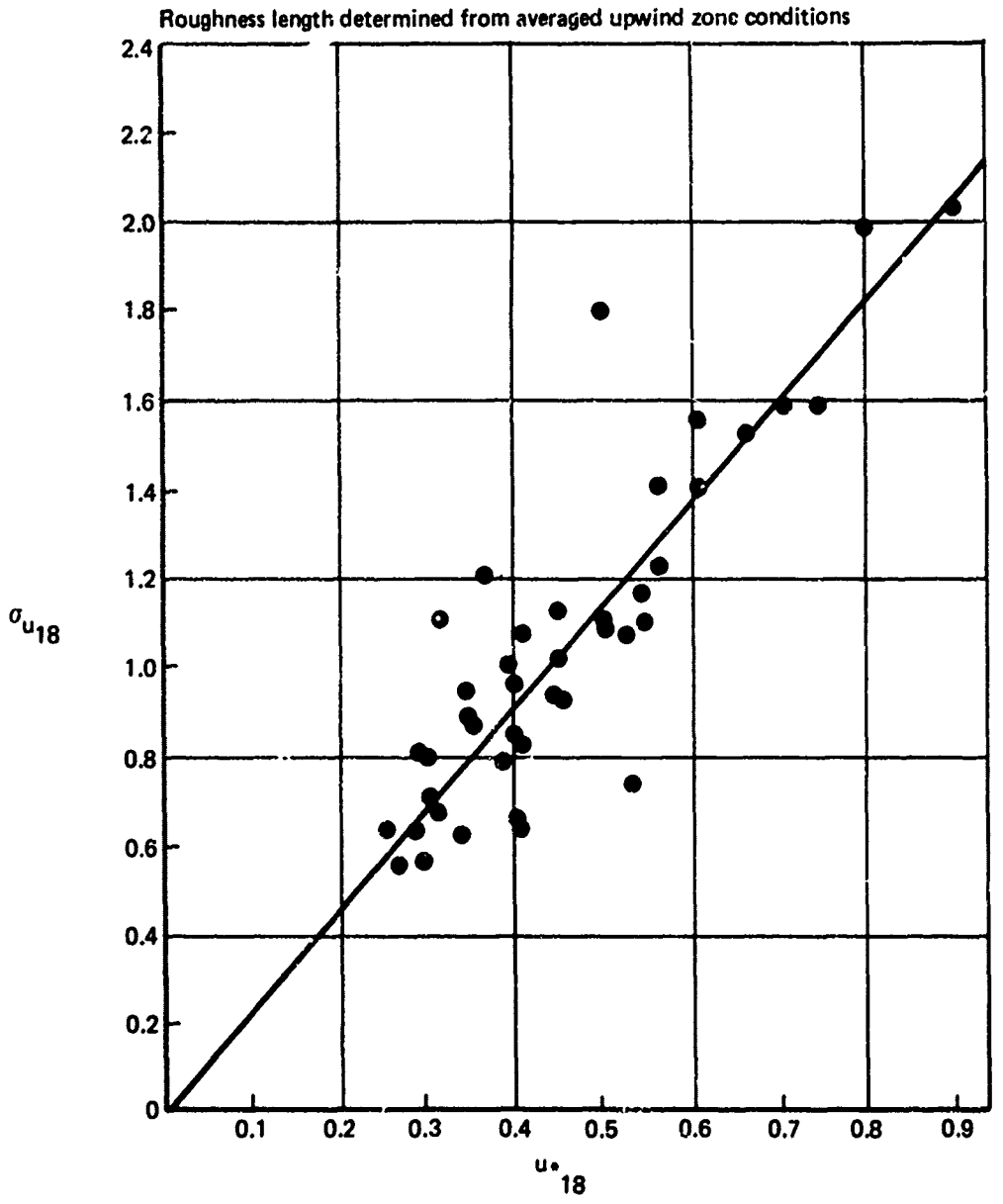

FIGURE 2-49.—VARIANCE OF THE LONGITUDINAL WIND COMPONENTS AT 18 M AS A FUNCTION OF FRICTION VELOCITY AT 18 M (FROM REF. 2-47)

TABLE 2-7.–VALUES OF THE CONSTANT OF PROPORTIONALITY C BETWEEN σ_u AND u_*

$\sigma_u/u_* = C$	Source	Comments
2.90	Reference 7	
2.80	Reference 34	
2.75	Reference 34	
2.50	Reference 38	Recommended for first 50 ft for a wide range of stabilities
2.50	Reference 7	
2.45	Reference 7	Averaged for various types of terrain
2.30	Reference 7	
2.20	Reference 7	Pipe flow measurements
2.20	Reference 44	Measured at 30 m
2.19	Reference 40	
2.10	Reference 7	

account. The conclusions reached by Reference 2-7 are primarily based on atmospheric data taken near the ground up to approximately 300 feet. References 2-37 and 2-43 present observations which indicate that σ_u decreases from 250 to 750 feet over both rough and smooth terrain in neutral air.

Selecting the roughness length

$$z_0 = 0.15 \text{ feet}$$

and

$$\sigma_u = 2.6\, u_*$$

as representative of a typical airport, the longitudinal component of turbulence may be expressed in terms of the mean wind speed at 20 and 33 feet, respectively, for neutral atmospheric conditions.

$$\sigma_u = 0.193\, \bar{V}_{33}$$

$$\sigma_u = 0.212\, \bar{V}_{20}$$

For comparison, the proposed ARB model (Ref. 2-14) specifies for neutral atmospheric conditions

$$\sigma_u = 0.18\, \bar{V}_{33}$$

where $z_0 = 0.15$ feet has been selected. The ARB model further assumes that this relationship is valid for heights between 10 and 300 feet.

For nonadiabatic atmospheric conditions the properties of σ_w are in good agreement with what would be expected from similarity theory, whereas the properties of σ_v are not. Reference 2-7 states that in general, the properties of σ_u are intermediate. The variation of the magnitude of the longitudinal velocity fluctuations with atmospheric stability for a fixed u_* is significant, but is not as strong as that of the lateral velocity fluctuations. Reference 2-7 states that for unstable atmospheric conditions σ_u is invariant with height, but is sensitive to changes in atmospheric lapse rate, particularly at low wind speeds. However, in unstable air the effect of wind is more predominant than in the case of the lateral component, particularly over rough terrain and at low heights. The effect of increasing wind speed or decreasing atmospheric stability is to increase the magnitude of the longitudinal velocity fluctuations. Observations presented in References 2-37 and 2-43 show this to be true in the range between 250 and 750 feet, except that σ_u decreased with increasing height over both rough and smooth terrain in unstable air.

Increasing atmospheric stability always decreases the magnitude of σ_u at all heights. Reference 2-7 maintains that in stable air it appears that the standard deviation remains nearly constant with height, but there is a shift from high frequency fluctuations near the ground to slower wind speed variations at greater heights. Observations presented in Reference 2-37 indicate that σ_u decreases from 250 to 750 feet over both smooth and rough ground in stable air. The same general trends are borne out by observations presented in Reference 2-43, except that there is negligible variation in the average σ_u over rough terrain.

Reference 2-7 refers to Figure 2-50 as an illustration of the variation of σ_u with atmospheric stability at fixed u_*. However, if σ_u/u_* is a function of h/ℓ' it is implied that σ_u will vary with height in nonadiabatic conditions. This contradicts the earlier supposition of the invariance of σ_u with height. This contradiction may be resolved in Figure 2-50. This figure is interpreted as describing the relation between σ_u/u_* and h/ℓ' at a given height, i.e., h is considered a constant and $1/\ell'$ is the independent variable. On the other hand Figure 2-51 does not exhibit any strong dependence of σ_u/u_* upon stability.

To summarize, the standard deviation of the longitudinal velocity fluctuations σ_u is proportional to the friction velocity u_* in neutrally stable air. The constant of proportionality is a function of the large scale surface roughness. The magnitude of the standard deviation increases with decreasing atmospheric stability, and increasing wind speed and surface roughness. The vertical variation of σ_u is small in both stable and unstable air. The analytic description presented agrees well with the experimental observations in neutral air, provided that the constant of proportionality is adjusted to account for the large scale surface roughness at various locations. No satisfactory analytic relationships for σ_u under unstable and stable atmospheric conditions have been developed.

2.4.4.2.4 Effect of Altitude Dependence of Friction Velocity–The similarity theory predicts that the standard deviations σ_u, σ_v, and σ_w are invariant with height in neutrally stable air. This is implied from the assumption of the constancy of u_* with height. For heights over which the decrease of u_* may not be neglected it has been suggested that the standard deviations remain proportional to the local value of the friction velocity (Refs. 2-4 and 2-29):

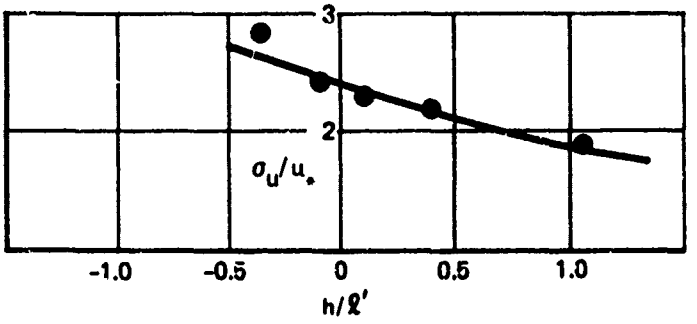

FIGURE 2-50.–OBSERVED RATIO OF STANDARD DEVIATION OF LONGITUDINAL VELOCITY TO FRICTION VELOCITY AS A FUNCTION OF h/ℓ' (FROM REF. 2-7)

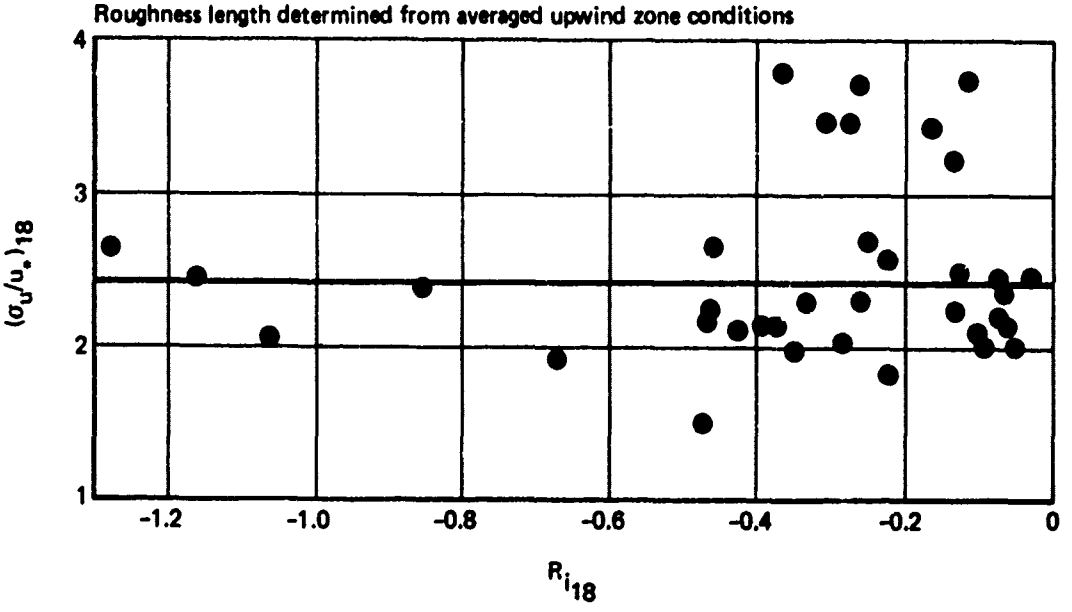

FIGURE 2-51.–RATIO OF THE VARIANCE OF LONGITUDINAL WIND COMPONENTS TO THE FRICTION VELOCITY AT 18 M AS A FUNCTION OF RICHARDSON'S NUMBER AT 18 M (FROM REF. 2-47)

$$\sigma = \left(\frac{\sigma}{u_*}\right) u_* = \left(\frac{\sigma}{u_*}\right) \left[\frac{u_*}{u_{*0}}(h)\right] u_{*0}$$

Assuming that the standard deviations of the velocity fluctuations remain proportional to the local shear stress, the low level asymptotic expansion implies that the change in the σ^2's between two levels at a given location should be proportional to the wind speed at a given height. Reference 2-4 quotes the data presented in Reference 2-47 in support of this. Figures 2-52 and 2-53 reproduced from Reference 2-47 show how σ_u and σ_v vary from one level to another as a function of the wind speed at a given level. The high level asymptotic expansion implies that the change in the σ's between two levels at a given location remain constant, i.e., the slope $\partial u_*(h)/\partial h$ is not a function of the wind level. Reference 2-47 supports this hypothesis by stating that the ratio $G \sin \alpha / u_*$ is theoretically a constant, not only in neutral air but in unstable air as well.

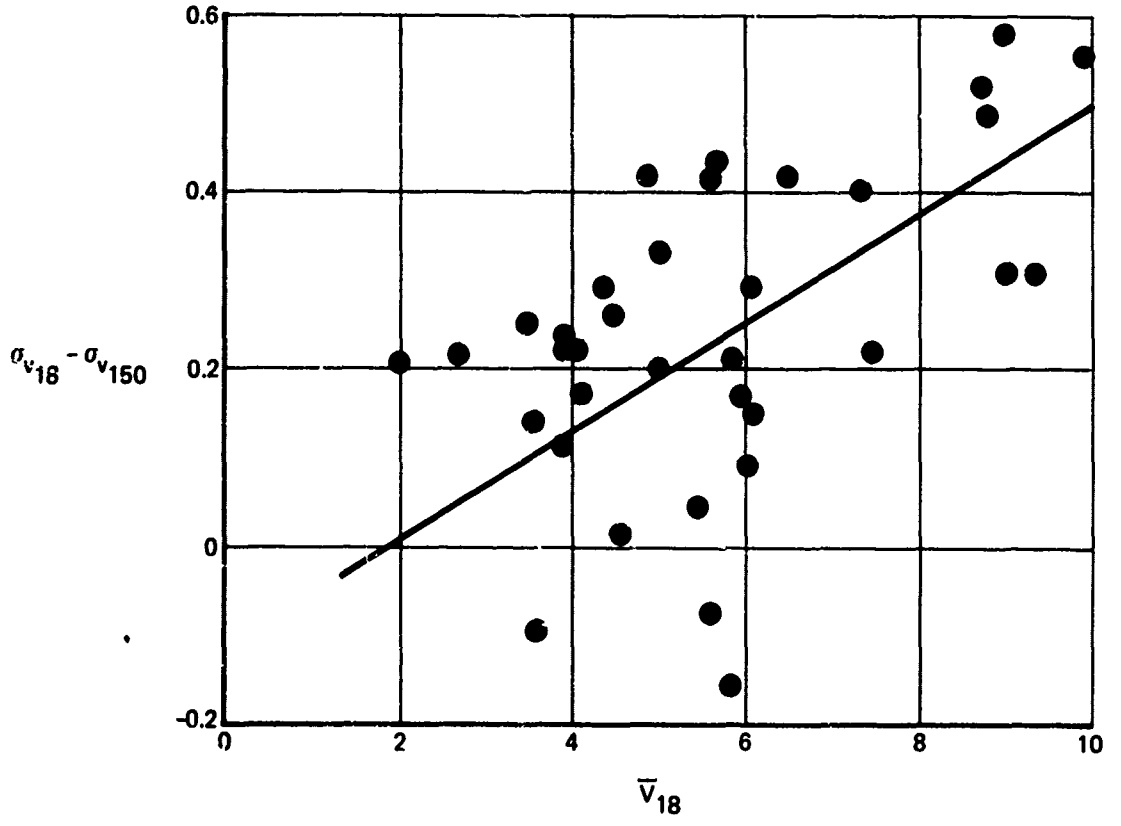

FIGURE 2-52.–DIFFERENCE OF VARIANCE OF LATERAL WIND COMPONENT AT 18 M AND 150 M AS A FUNCTION OF MEAN WIND AT 18 M (FROM REF. 2-47)

Let

$$\frac{\partial u_*(h)}{\partial h} = -\frac{fG \sin \alpha}{2u_*(h)}$$

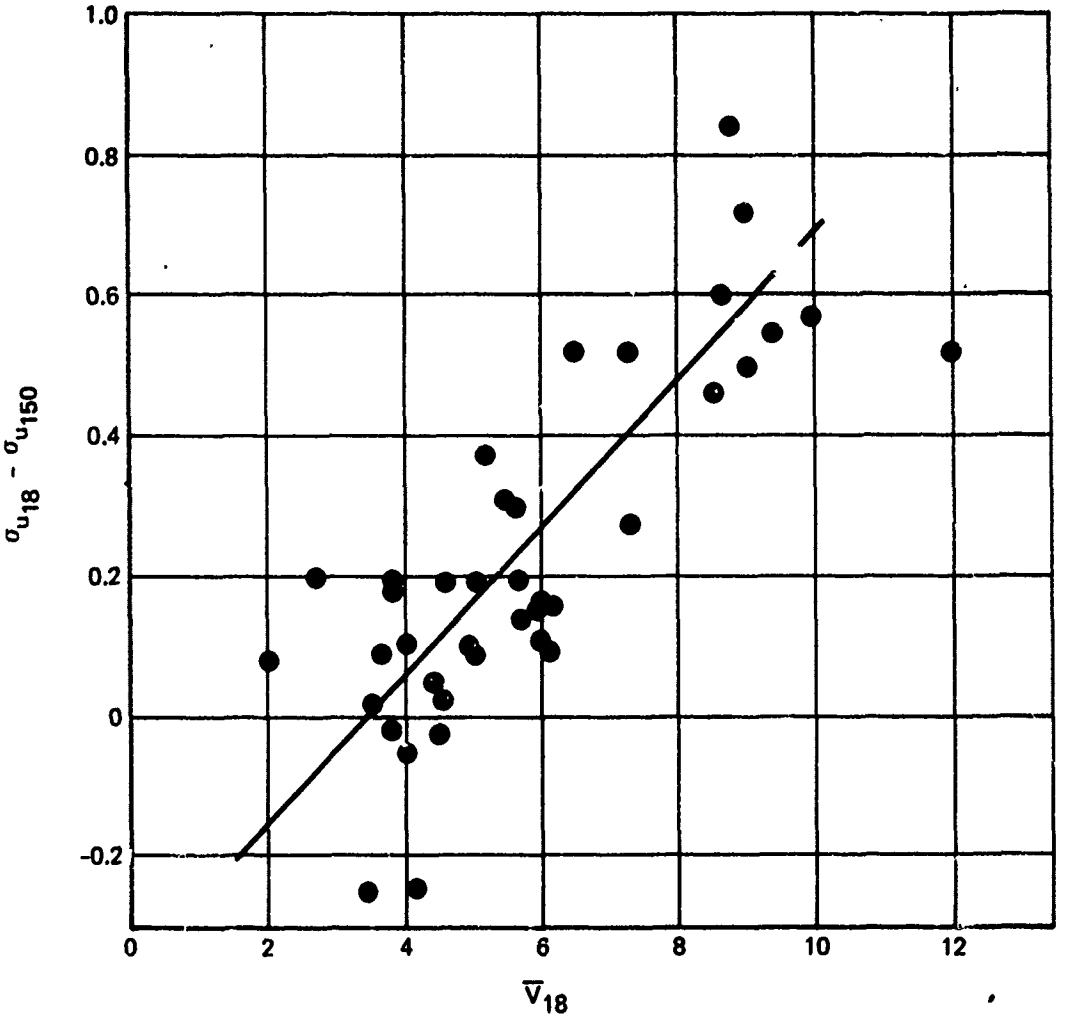

FIGURE 2-53.–DIFFERENCE OF VARIANCES OF LONGITUDINAL WIND COMPONENT AT 18 M AND 150 M AS A FUNCTION OF MEAN WIND AT 18 M (FROM REF. 2-47)

It has been shown that

$$u_*(h) = u_*(0)\left[1 - \frac{h}{d}\right]$$

and

$$d = u_*(0)/f5.35$$

then

$$\frac{\partial u_*(h)}{\partial h} = -\frac{u_*(0)}{d} = -5.35f$$

and

$$\frac{G \sin\alpha}{u_*(h)} = 10.7$$

It can be seen that the slope of u_* versus h is only a function of Coriolis parameters.

Based on the preceding discussion, the intensity of turbulence may be expected to decrease with increasing height under neutral atmospheric conditions. Indeed, all the experimental data presented in References 2-37 and 2-43 consistently show the expected turbulence levels to decrease in going from 250 to 750 feet above the ground under unstable, stable, and neutral atmospheric conditions.

2.4.4.2.5 Ratios Between the Standard Deviations of the Turbulence Components–For an isotropic turbulence field the standard deviations of the turbulent velocity fluctuations are related as follows

$$\sigma_u = \sigma_v = \sigma_w$$

Although these relations are very attractive because of the inherent simplicity, they certainly cannot be recommend ! as being realistic for low altitude turbulence. Table 2-8 lists a wide range of estimates for the σ ratios in low altitude turbulence. The large variations between the estimates may be attributed to differences in meteorological conditions, topography, height, and experimental techniques. With reference to the latter, it should be noted that all measured standard deviations lack contributions from both the high and low frequency ends of the power spectra. The former is due to limited frequency response of the instrumentation and the latter is due to finite sampling times. At the lower levels, the frequency contents of the three turbulence components are different, and therefore the truncation of the standard deviations will affect the ratio between them as well as their absolute value.

Selecting a fixed ratio between the standard deviations may appear a crude approximation. It is obvious that changing terrain features, atmospheric conditions, and height do not affect the three turbulence components in the same way. However, except for the establishment of

TABLE 2-8.–RATIOS BETWEEN σ_u, σ_v AND σ_w

$\sigma_u/\sigma_v/\sigma_w$	Source	Comments
2. 4/1.9/1	References 1 and 7	
2/1.6/1	Reference 3	Valid for below 300 ft
2.2/1.5/1	References 1 and 34	
1.3/1.6/1	References 1 and 34	
1.9/1.6/1	Reference 38	Valid for below 50 ft at a wide range of stabilities
1/1.2/1	Reference 48	
3/2/1	Reference 49	Valid for below 50 ft
1.82/1.37/1	Reference 51	
$\sigma_u/\sigma_w = \sigma_v/\sigma_w/\sigma_w$ $= 1.2 - 1.7 \cdot 10^{-4} h$	Reference 49	Stable and neutral conditions $50 ft < h < 1100 ft$
$\sigma_u/\sigma_w = \sigma_v/\sigma_w$ $= 1.3 - 5.8 \cdot 10^{-4} h$	Reference 49	Unstable conditions $50 ft < h < 1100 ft$
1/1/1	Reference 49	Above 1100 ft in stable and neutral conditions
2/2/1	Reference 14	Near neutral conditions
$\frac{\sigma_u}{\sigma_w} = \frac{\sigma_v}{\sigma_w} = \left(\frac{h}{2500}\right)^{-2/9} > 1$	Reference 42	Dryden spectra — Based on isotropy at high frequencies and presumed integral scale profiles
$\frac{\sigma_u}{\sigma_w} = \frac{\sigma_v}{\upsilon_w} = \left(\frac{h}{1750}\right)^{-1/6} > 1$	Reference 42	Von Karman spectra — Based on isotropy at high frequencies and presumed integral scale profiles

trends, the literature fails to provide any practical functional relationships which would enable accurate predictions of the ratios between the magnitude of the turbulence components for a given set of conditions.

The literature indicates that close to the ground turbulence is strongly anisotropic with respect to the ratios σ_u/σ_w and σ_v/σ_w. The height at which this becomes significant will depend upon the predominant eddy size in the turbulence field. Table 2-8 indicates that below 50 feet measurements consistently confirm that σ_u and σ_v are larger than σ_w. Reference 2-49 maintains that below 50 feet as the effect of the ground becomes more important the ratios σ_u/σ_w and σ_v/σ_w change rather drastically and as height decreases to within a foot or so of the ground, these ratios must increase rapidly because the vertical turbulence is restricted by the close presence of the ground. However, this argument is subject to criticism. Reference 2-7 maintains that for a small range of altitudes above the ground where shear stress is essentially constant, the rms levels of the turbulence components are invariant with altitude. The effect of the proximity of the ground restricts the eddy sizes, causing turbulence power to occur at higher frequencies. In the limit at the ground, the rms level would be finite, but would be spread over an infinite frequency range, with the power spectral density at any frequency being zero. Most likely, any description within inches of the ground will be inadequate, but this is of no consequence as the vertical aerodynamic centers of aircraft are substantially away from the surface when the aircraft is on the ground.

Table 2-8 indicates that σ_u is generally larger than σ_v at the lower heights, indicating anisotropy in the horizontal plane. However, this tendency is not so strong as that exhibited in the vertical plane, and it is common for models to assume equal variances for horizontal components. The models of References 2-42 and 2-49 provide for horizontal isotropy, but permit the ratios of horizontal to vertical turbulence rms levels to decrease to one at a sufficiently high altitude, presumably at an estimate of the boundary layer thickness. Reference 2-49 provides for a linear decrease of the ratio until an isotropic ratio is achieved at 1100 feet. Reference 2-42, however, derives its altitude-varying ratio by requiring isotropy at high frequencies. Then, from presumed models of the vertical turbulence variance and the integral scales, the horizontal turbulence rms levels are found by

$$\sigma_u = \sigma_v = \begin{cases} \sigma_w \left(\frac{L_u}{L_w}\right)^{1/3} = \sigma_w \left(\frac{h}{2500}\right)^{-2/9}, & \text{Von Karman spectra} \\ \sigma_w \left(\frac{L_u}{L_w}\right)^{1/2} = \sigma_w \left(\frac{h}{1750}\right)^{-1/6}, & \text{Dryden spectra} \end{cases}$$

These relationships are plotted on Figure 2-54. At the surface, the ratios go to infinity, but this effect is not necessarily important as such low altitudes are not achieved by aircraft. Reference 2-42 recommends the Von Karman spectra; hence, the representation for the Dryden spectra may be viewed as providing an approximation to the Von Karman spectra. Certainly, the variance, integral scales, and the boundary layer thickness are not dependent on the spectral form assumed, but perhaps the combination of parameters meets some criteria for matching the two power spectra models.

It is not clear whether the use of 2500 feet is based on measured data or whether it was used to provide compatibility with existing military specifications.

The rapid reduction of difference between horizontal and vertical turbulence levels provided by Figure 2-54 may permit using an isotropic relationship at an altitude below that specified for isotropy.

2.4.5 The Scale of Low Altitude Turbulence

At low altitudes the eddy sizes, as reflected by the integral scales, are constrained by the presence of the ground. The integral scale for the vertical component of turbulence is constrained directly by the distance to the ground. The scales for the horizontal components are affected indirectly, presumably through the breakdown of the eddies as the eddies are flattened. As the ground is approached, the eddy sizes and the integral scales can be expected to go to zero. As altitude increases, the turbulence becomes isotropic and, redefining L_v and L_w to be twice the areas under the v and w autocorrelation functions, the integral scales are equal. In between, it can be assumed (as is done in Refs. 2-32 and 2-49) that the integral scale for the vertical component of turbulence will be less than those for the horizontal components because the influence of the ground is greater for the vertical components. These conditions are summarized by:

Von Karman spectra:

$$\sigma_u/\sigma_w = \sigma_v/\sigma_w = \begin{cases} \left(\frac{h}{2500}\right)^{-2/9} & , h < 2500 \text{ ft} \\ 1.0 & , h \geq 2500 \text{ ft} \end{cases}$$

Dryden spectra:

$$\sigma_u/\sigma_w = \sigma_v/\sigma_w = \begin{cases} \left(\frac{h}{1750}\right)^{-1/6} & , h < 1750 \text{ ft} \\ 1.0 & , h \geq 1750 \text{ ft} \end{cases}$$

σ_w invariant with altitude and same for both models

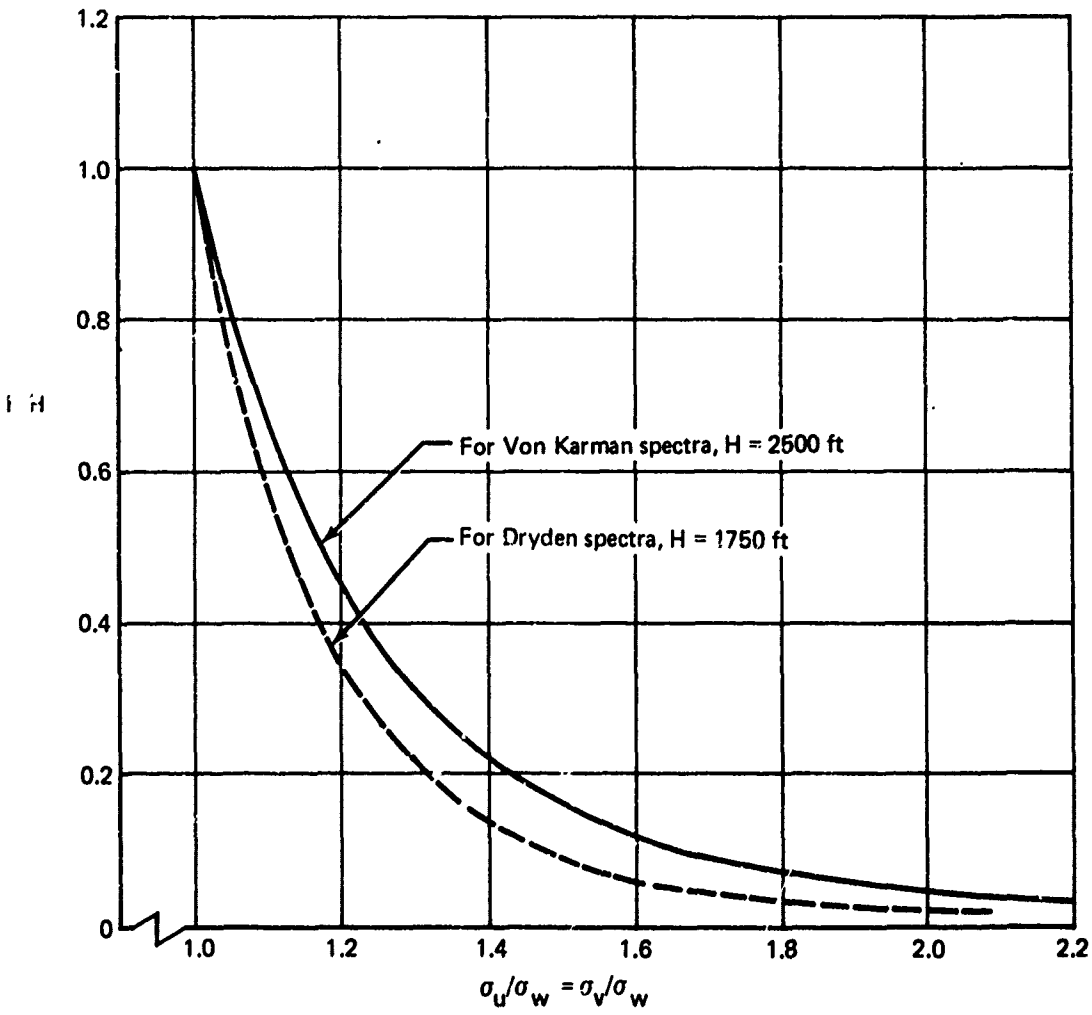

FIGURE 2-54.--R.M.S. TURBULENCE INTERRELATIONSHIP, MILITARY MODELS (FROM REF. 2-42)

$$h = 0,\ L_u = L_v = L_w = 0$$

$$h \rightarrow \infty,\ L_u/L_v/L_w \rightarrow 1/1/1$$

$$L_w \leq L_u,\ L_w \leq L_v$$

Specific questions about low altitude integral scales are:

- What are the magnitudes of integral scales?
- What are the variations of the integral scales with altitude?
- At what altitude does isotropy exist?
- What interrelationships exist between the integral scales?

Before the evidence is examined, it is appropriate to qualify the data by noting that measurement of the integral scales involves several assumptions and small measurement errors result in large distortions of measured values, and by examining measurement techniques and their effects on the resultant data.

2.4.5.1 Measurement of Turbulence and Integral Scales

Atmospheric turbulence is usually measured either by a probe on an airplane or by anemometers mounted on towers. Because aircraft can cover a large distance in a short period of time, aircraft turbulence measurements enable extensions to low spacial frequencies without large changes in the mean wind and atmospheric conditions. However, it is difficult to accurately measure the wind heading magnitude from an aircraft, making difficult the association between turbulence characteristics and the mean wind. At low frequencies, the "rigid" aircraft motion interferes with the measurements, and at high frequencies the data are distorted by structural motion. When covering larger distances, it is quite difficult to maintain homogeneous terrain. The effect of inhomogeneous terrain is to increase the apparent integral scale over that for the mean conditions, as shown on Figure 2-55. Finally, flight safety prevents measurements near the ground.

Inability to separate mean wind from turbulence (Fig. 2-1) by proper selection of the averaging time can also cause an overestimation of the integral scale. If the sample time is held constant while airspeed is increased, more and more of the power due to the mean wind will be included as turbulence, and the low frequency turbulence power and integral scale estimates will increase.

Tower data permit measurements from homogeneous terrain, and the correlation of turbulence with mean wind eliminates the influence of aircraft response on measurements at low frequencies and permits very low altitude measurements. However, it also introduces other problems. Anemometers are characteristically sluggish and attenuate high frequency responses. Low frequency data can be measured accurately, but now the mean airspeed is just the mean wind speed, and very long time periods are required for measurements at low spacial frequencies, enabling significant changes of the mean conditions.

For either method of measurement, the power spectrum is known accurately for only a certain range of spacial frequencies, usually in the inertial subrange. The area under the

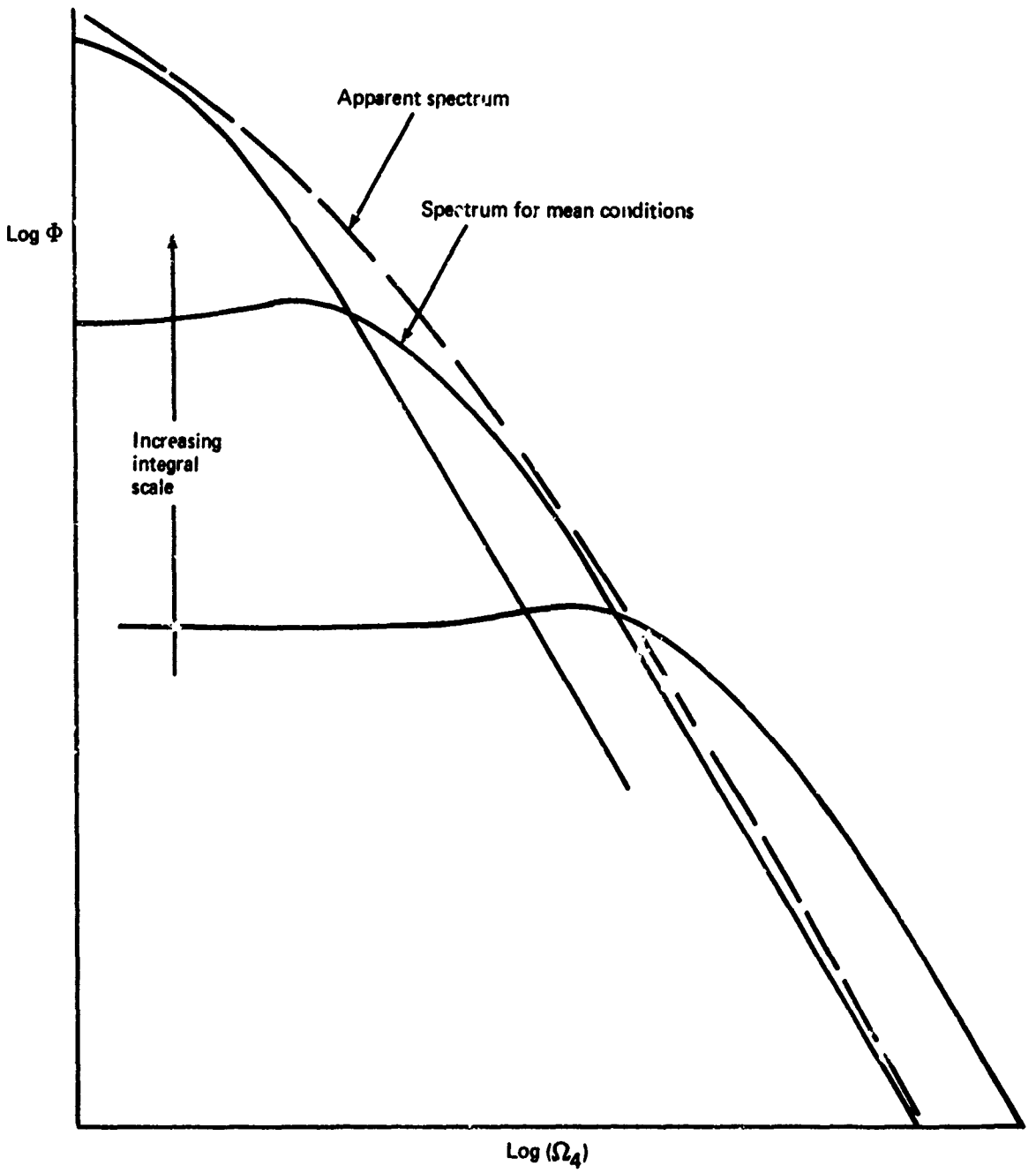

FIGURE 2-55.—EFFECT OF NONHOMOGENEITY ON SPECTRUM SHAPE

segment of the power spectrum can be computed to give a truncated variance. If only the variance is desired, the spectral form and an almost arbitrary integral scale may be assumed to relate the total variance to the truncated variance. Alternately, the contribution of frequencies below and above the region of measurement may be ignored or assumed negligible.

Knowing the amplitude of the power spectrum at some spacial frequencies, or, as in References 2-37 and 2-43, the truncated variance between some spacial frequencies and assuming the asymptotic form of some presumed spectrum permits writing the integral scale in terms of the total variance. For the Von Karman and Dryden spectra, these relationships are:

Von Karman $$L_i = C_{vK_i} \sigma_i^3$$

Dryden $$L_i = C_{D_i} \sigma_i^2$$

where

i = u, v, w

C = known constant in terms of spacial frequencies and the power spectrum at that frequency or truncated variance between spacial frequencies

The first observation from these equation is: Given a measured spectrum segment and the total variance for the spectrum, the computed integral scale is quite dependent on the spectrum assumed; quoted values of integral scales must be qualified by the spectral form assumed in deriving them.

A second observation is: If an error is introduced by calculating the total rms from a truncated rms (which is difficult to avoid), computing the integral scale from the total rms will magnify the error, in addition to any error introduced by assuming asymptotic forms.

The errors from computing total variance and integral scale are in addition to the errors inherent in the measurement technique. As a consequence, quoted integral scales exhibit a wide variation, undoubtedly in addition to their natural variations. John Houbolt has discussed measurement problems and alternative techniques more extensively in several of his publications.

2.4.5.2 The Scale of Vertical Turbulence

At high altitudes, where isotropy exists, all the integral scales are assumed to be invariant with altitude, and various values from 200 to 5000 feet have been prescribed (Ref. 2-50). At low altitudes, however, there is considerable evidence that the integral scales for three components are not equal and that they are not invariant with altitude.

Reference 2-7 states that the nondimensional form of the one-dimensional spectrum for the vertical component of turbulence is predicted by similarity theory (assuming Taylor's hypothesis) as:

$$\Omega_1 \Phi_w(\Omega_1) = \sigma_w^2 \, f(\Omega_1 h, R_i)$$

where f is a universal function. Since the integral scale and spacial frequency only appear in combination for this form of the spectra, this is equivalent to

$$L_w = C(R_i)h$$

That is, the integral scale for the vertical component is linearly proportional to altitude, and the constant of proportionality may be dependent on atmospheric stability. The linear altitude dependence is further said to apply to heights "of perhaps a few 100 m., above which the scale approaches a constant."

Reference 2-7 states that the qualitative effect of decreasing stability is to shift the spectrum to lower frequencies, equivalent to increasing the integral scale, and that this is explained by convective turbulence occurring at lower frequencies than mechanical turbulence.

Large scale terrain roughness is introduced as an additional parameter in Reference 2-51. The integral scale for the vertical turbulence spectrum, assuming a vertical turbulence spectrum identical to the longitudinal Dryden spectrum, is recommended as

$$L_w = h_0 + L_h h$$

where h_0 and L_h are given as follows:

Terrain class	L_h	h_0
Farmlands	0.75	50
Woodlands	0.625	175
Low mountain	0.5	300
High mountain	0.125	675

For this model, the integral scale does not go to zero at the surface. The model provides for greater scale lengths that are less sensitive to altitude for greater large scale roughness. At 1000 feet, variations with large scale roughness disappear.

References 2-37 and 2-43 verify that large scale terrain roughness is a very strong influence on the integral scale for vertical turbulence for measurements taken at 250 feet but a weak influence for measurements at 750 feet.

An attempt to combine the effects of stability and altitude with a quantitative model for the Dryden spectrum is presented on Figure 2-56, taken from Reference 2-49. The nonlinear

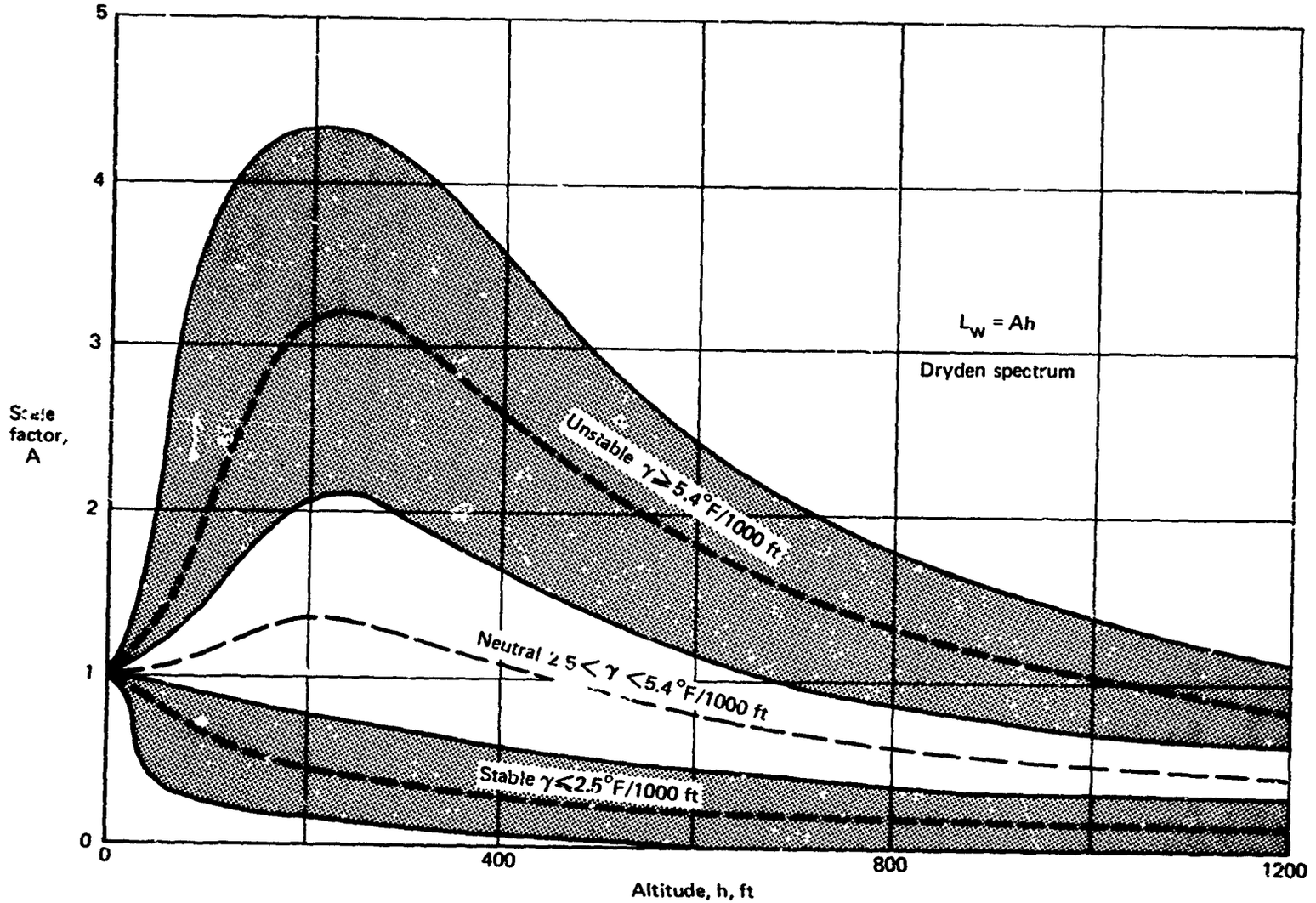

FIGURE 2-56.– VERTICAL TURBULENCE SPECTRUM, ESTIMATION OF SCALE (FROM REF. 2-49)

variation of the constant of proportionality would seem to indicate that the integral scale is not linearly related with altitude. However, when the integral scale is plotted against altitude, as on Figure 2-57, a linear variation at low altitudes and an invariance with altitude at higher altitudes is seen to be a good approximation. The use of lapse rate for a measure of stability does not agree with the use of Richardson's number in similarity theory. The same author has recommended, in Reference 2-42, integral scales for average conditions given by

$$\text{Dryden spectrum:} \qquad L_w = \begin{cases} h, & h \leq 1750 \text{ feet} \\ 1750 \text{ ft}, & h > 1750 \text{ feet} \end{cases}$$

$$\text{Von Karman spectrum:} \qquad L_w = \begin{cases} h, & h \leq 2500 \text{ feet} \\ 2500 \text{ ft}, & h > 2500 \text{ feet} \end{cases}$$

References 2-1 and 2-13 support $L_w = h$.

The data in Reference 2-40 provides spectra shapes at various levels of stability that tend to support the stability trends of Figures 2-56 and 2-57. For stable conditions, a marked decrease of the proportionality constant with increasing stability occurs but, for unstable conditions, the trend is not clear.

Reference 2-41 recommends a linear variation but with a constant of proportionality of 0.9 for the Dryden spectrum. An altitude above which the integral scale is invariant with altitude is not specified. The same author has later recommended, in Reference 2-3, integral scales for the Von Karman spectrum given as follows:

- For the boundary layer as a whole, $L_w = 0.4\ h$
- For $h > 200$ feet, better values given by $L_w = 2.1\ h^{0.73}$

The final model presented is taken from Reference 2-14. For a vertical turbulence spectrum having the same shape as the Dryden longitudinal spectrum, an integral scale equal to 50% of the altitude for altitudes from 30 to 1000 feet is recommended. A constant value of 15 feet is recommended for altitudes less than 30 feet.

Several other models of the vertical spectrum using a constant integral scale based on an "average" altitude exist. The validity of the use of the integral scale at an "average" altitude will be examined later.

As noted, most of the models that do attempt to account for the effect of altitude do not account for stability or large scale roughness. Large scale roughness can be constrained by restricting consideration to a certain type of terrain. Ignoring the effects of stability may not be very reasonable for, although the theory predicts stability effects, the effect may be small, and Reference 2-7 states that ". . . the shape of the vertical velocity spectrum at low levels is essentially independent of stability . . . .".

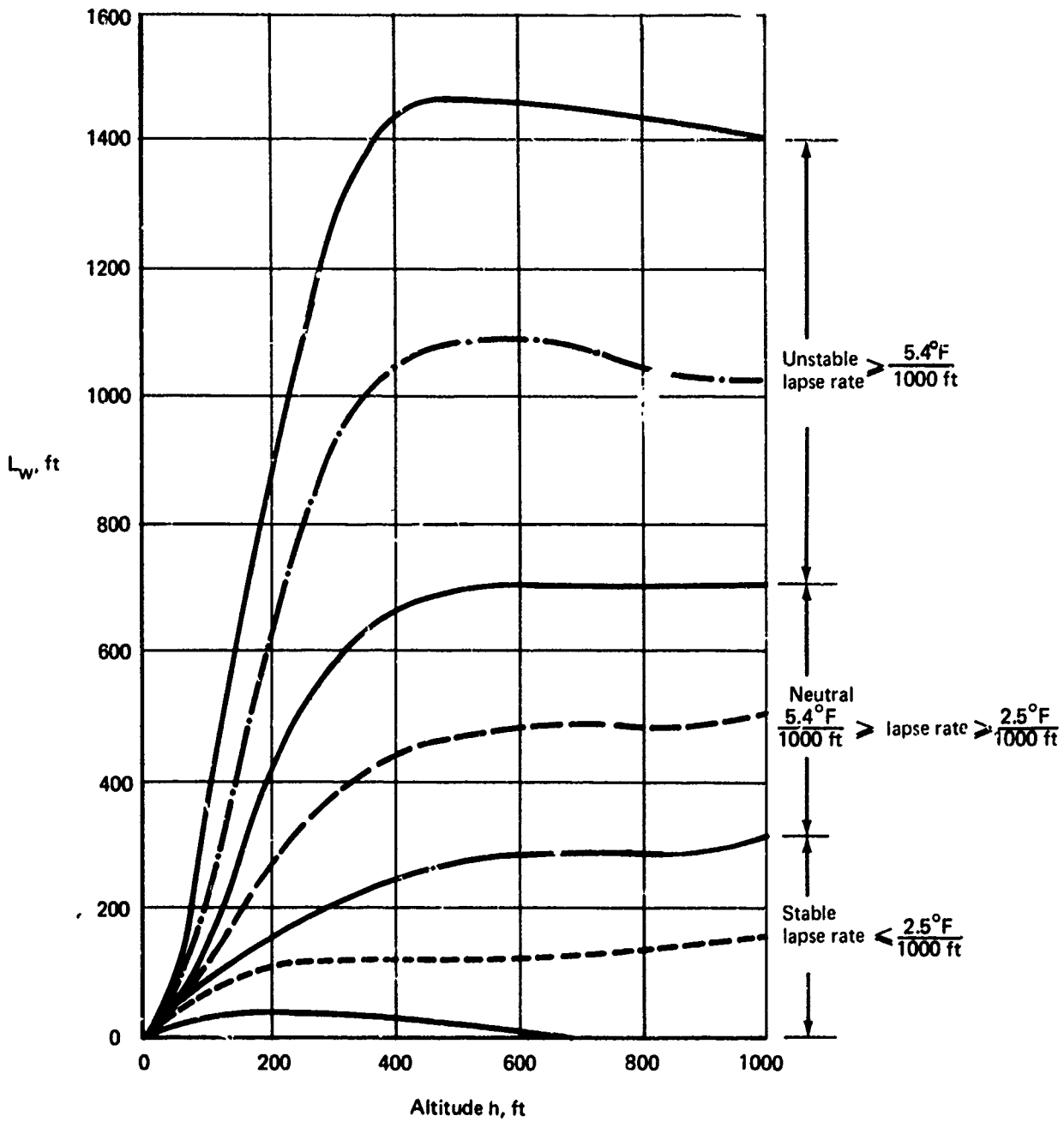

FIGURE 2-57.–INTEGRAL SCALE ESTIMATE FOR VERTICAL SPECTRUM (FROM REF. 2-49, DRYDEN SPECTRA)

2.4.5.3 The Scale of Horizontal Turbulence

The integral scales for the three components are differentiated in Reference 2-7 according to the sensitivity of their shapes to atmospheric stability. The effect on the vertical (w) turbulence spectrum is said to be weak, the effect on the lateral (v) velocity spectrum drastic, and the effect on the longitudinal (u) velocity spectrum intermediate. Furthermore, the sensitivity of the horizontal components of wind velocity spectra is differentiated according to high and low frequency. However, in Reference 2-7, the discussion on spectra is not limited to just turbulence, but is for all of the wind velocity (i.e., Fig. 2-1) and the distinction for high and low frequencies is not clear. (That is, low frequencies may refer to what has been termed in this report as mean wind.) As the spectra of the entire velocity components are being examined, the spectra of "mean wind" heading are reflected at low frequencies.

With this qualification in mind, the effect of atmospheric stability is said to occur primarily at the low frequencies for the horizontal components. Mechanical turbulence is said to have an influence on the low frequency portion of the longitudinal turbulence spectrum, but not the lateral spectrum. If indeed there are separate mechanical and thermal effects on the longitudinal spectrum shape, as implied, then it may be inappropriate to use a single parameter as the integral scale from isotropic turbulence to represent their combined effects.

Reference 2-7 states that applications of similarity theory to the lateral spectrum have been unsuccessful. However, height is concluded to be only a minor factor.

Similarity theory predicts the same spectral form for the longitudinal component as for the vertical component, with integral scale linearly related to altitude. However, Reference 2-7 cites studies supporting not only a linear relationship, but invariance and a square root variation with altitude. A particular difficulty in assessing the scale of longitudinal turbulence occurs and is described in Reference 2-7: "The difficulty lies in the fact that the 'peak' in the frequency-weighted spectrum, which determines the scale, lies at frequencies usually at the low end of the frequency domain analyzed; in this region the resolving power of spectrum analysis is poor and the results unprecise."

Reference 2-7 argues that because the longitudinal spectrum has more energy at the low frequencies and because the law of the inertial subrange extends to lower frequencies, "The larger eddies in neutral and unstable air are elongated in the wind direction." Of course, even isotropic turbulence provides a longitudinal component with twice the low frequency power as in the transverse components (Fig. 2-20).

Quantitative measures of horizontal integral scales that provide L_u and L_v equal, implying horizontal isotropy, and invariant with altitude are found in the model of Reference 2-14 and the two models of Reference 2-52:

Reference	$L_u = L_v$	Spectra
2-14	600 ft	$\Phi_u = \Phi_v = \frac{\sigma^2 L}{(1 + \Omega^2 L^2)}$
2-50	500 ft	Dryden
2-50	600 ft	$\Phi_u = \Phi_v = \frac{0.8 L^2}{(1 + \Omega L)^{1.8}}$

Reference 2-14 presents data showing variations of the integral scale with altitude for the horizontal components but has apparently used some kind of average integral scale. The values from Reference 2-52 are acknowledged to be average values for the first 1000 feet. Hence, none of these models are necessarily implying support for invariance of horizontal scales with altitude.

Another model resulting in a linear variation with altitude for the horizontal turbulence integral scales is that of Reference 2-13. The proportionality constants have been found by requiring all the spectra to be equal in the inertial subrange. By employing the same spectrum for each component equal to the longitudinal Dryden spectrum, the horizontal components are given in terms of ratios of the variances.

$$L_u = \left(\frac{\sigma_u}{w}\right)^2 h$$

$$L_v = \left(\frac{\sigma_v}{w}\right)^2 h$$

Presumed values of $\sigma_u/\sigma_w = 2.5$ and $\sigma_v/\sigma_w = 1.75$ give $L_u = 6.25$ h and $L_v = 3$ h.

Equal integral scales for horizontal turbulence components having a cube root variation with altitude are found in Reference 2-42:

Von Karman spectra: $$L_u = L_v = \begin{cases} 184\, h^{1/3}, & h \leq 2500 \text{ ft} \\ 2500 \text{ ft}, & h > 2500 \text{ ft} \end{cases}$$

Dryden spectra: $$L_u = L_v = \begin{cases} 145\, h^{1/2}, & h \leq 1750 \text{ ft} \\ 1750 \text{ ft}, & h > 1750 \text{ ft} \end{cases}$$

The author concedes that "although these formulas produce correct trends, there are little data available that can be used to substantiate the $h^{1/3}$ as used in MIL-F-8785B. It is merely a formula that produces reasonable results." These formulas are designed to produce zero

integral scales at zero altitude, greater integral scales for the horizontal turbulence components than for the vertical component, and a value corresponding to that specified in the military specification at high altitudes.

Unpublished piloted flight simulations at The Boeing Company using the Von Karman form produced pilot comments indicating the cube root variations were unrealistically long at low altitudes. A brief test comparing $L_u = L_v = h$, $L_u = L_v = 50\,h^{1/2}$, and $L_u = L_v = 184\,h^{1/3}$, produced a marked qualitative preference for the square root form, a form satisfying the same requirements as the cube root form. The three alternate forms tested are presented on Figure 2-58.

Reference 2-3 provides integral scales with implications that differ from other models. The lateral and vertical turbulence integral scales are set equal and are differentiated from that for longitudinal turbulence, implying isotropy in a vertical plane normal to the mean wind. Furthermore, for altitudes above 200 feet, integral scales for all components are given about a 3/4 power of altitude variation. Although the integral scales recommended are for the adaptation of the isotropic Von Karman spectral form, implying that the integral scales for the transverse components are defined as twice the areas under the corresponding autocorrelation functions, the integral scale for the longitudinal component is recommended as twice those for the transverse components for altitudes above 200 feet. The boundary layer thickness is not defined. The integral scales recommended in Reference 2-3 are as follows:

"For the boundary layer as a whole,

$$L_u = 20\,h^{1/2}$$

$$L_v = L_w = 0.4\,h$$

above about 200 feet, slightly better values are given by

$$L_u = 4.2\,h^{0.73}$$

$$L_v = L_w = 2.1\,h^{0.73}$$"

These equations are plotted on Figure 2-59.

One attempt to relate the integral scales for the horizontal components with atmospheric stability was found in Reference 2-49. The Dryden spectra and the integral scale for the vertical component on Figures 2-56 and 2-57 are employed. The integral scales for the horizontal components are set equal to each other, and both are defined in terms of that for the vertical component, which in turn is defined in terms of lapse rate:

$$L_u = L_v = \begin{cases} (1.3 - 0.0006\,h)\,L_w, & 50 \leq h \leq 500 \text{ ft} \\ 1 & h > 500 \text{ ft} \end{cases}$$

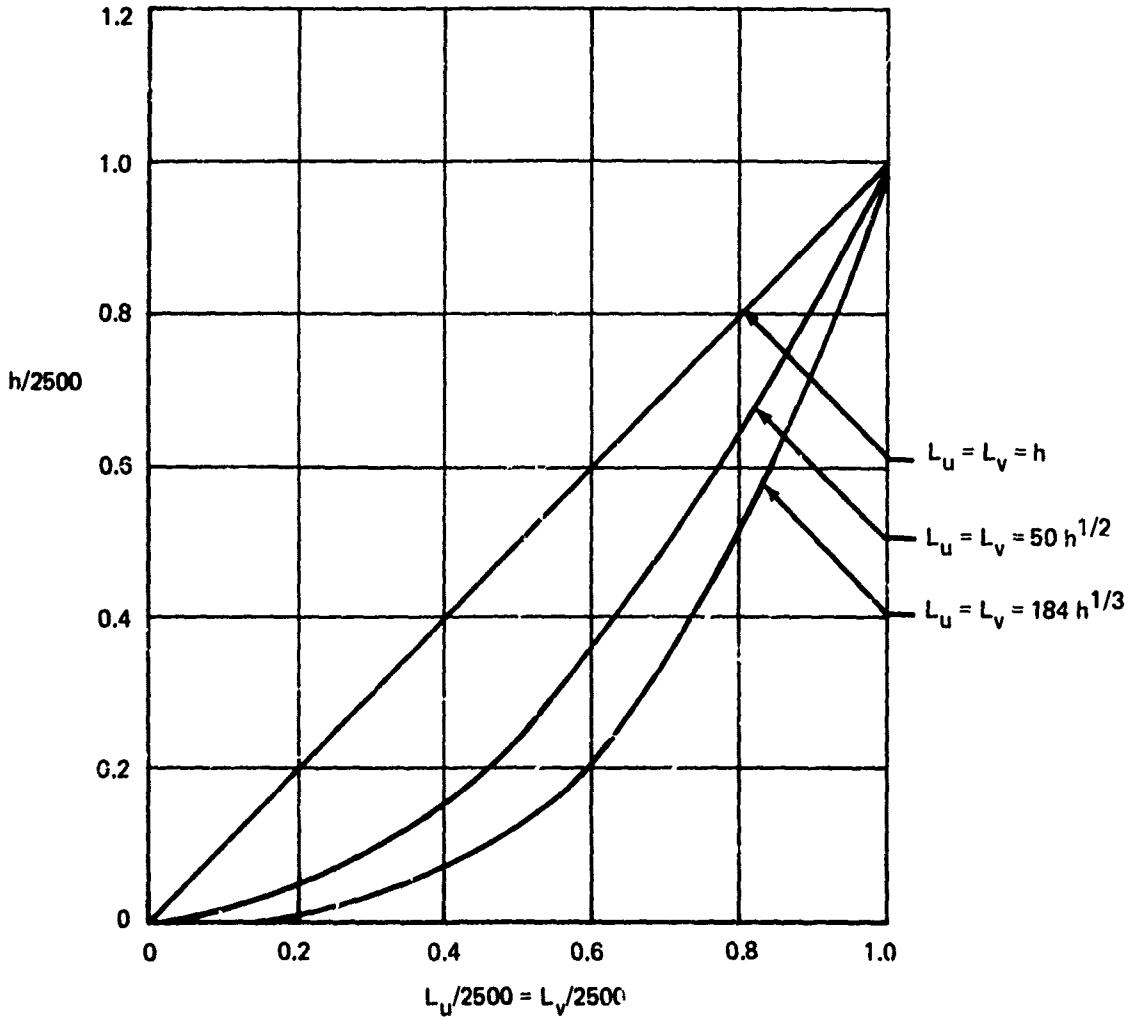

FIGURE 2-58.—ALTERNATE REPRESENTATIONS OF THE INTEGRAL SCALE FOR HORIZONTAL TURBULENCE (FROM REF. 2-42, VON KARMAN SPECTRA)

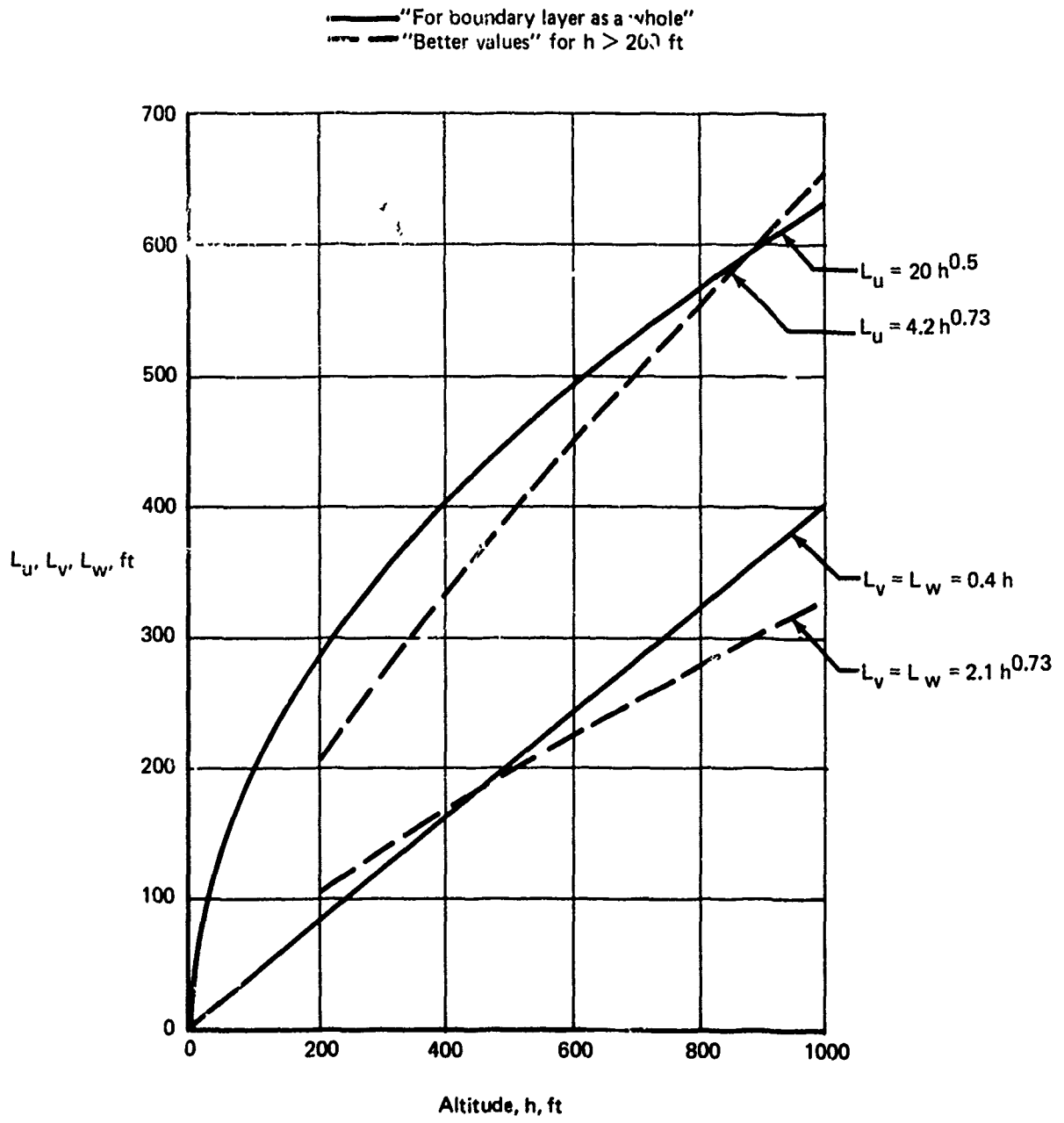

FIGURE 2-59.–INTEGRAL SCALE REPRESENTATION (FROM REF. 2-3, VON KARMAN SPECTRA)

The author qualifies this formula as follows: "This formula should provide acceptable results since it suggests the correct trends, but the formula should be looked upon for what it is–a guess." Combining this equation and Figure 2-57 provides the model on Figure 2-60.

Reference 2-40 provides horizontal turbulence spectra shapes at various levels of stability that indicate the horizontal turbulence integral scales decrease with stability for stable conditions. The trend with stability for unstable conditions is unclear. Reference 2-39 reports similar findings: "The value of the dimensionless integral scale is significantly less (~45%) than the ones . . . for the neutral case. However, for the unstable case, the integral scales . . . depart from the ones [for the neutral case] by only ~20%." Reference 2-39 also reports a change in integral scales' dependence upon altitude with atmospheric stability:

	Unstable	Neutral
Variation of L_u with altitude	$h^{-0.13}$	Invariant
Variation of L_v with altitude	$h^{0.28}$	$h^{0.42}$

In general, there has been little direct measure of the integral scales for horizontal turbulence components. Rather, they have been specified in terms of other parameters. The dominant provision for horizontally isotropic integral scale relationships may not necessarily be support for that assumption but may rather be for the convenience of avoiding scale transformations from the mean wind axis system to the airplane's relative wind axis system.

A test of a different sort on horizontal isotropy is reported in Reference 2-7. An aircraft was flown in various directions relative to the mean wind in unstable air at about 100 meters. The one-dimensional vertical velocity spectrum was found to be essentially independent of direction of flight, indicating that "turbulence in such situations is more or less horizontally isotropic."

2.4.6 Selection of a Low Altitude Turbulence Description

Analytic descriptions of low altitude turbulence and their assumptions have been presented. From these, a description for specific application to the approach and landing maneuver will now be selected.

2.4.6.1 Selected Assumptions

The most fundamental assumption concerning the description of turbulence is that it is a random process superimposed upon a "mean wind" which, though also having frequency-dependent characteristics, occurs at lower and distinct frequencies. This assumption is technically incorrect, as the differential equations governing turbulent motion have been developed, implying a deterministic description. However, the differential equations have not been solved and a stochastic representation must be used. Fortunately, turbulence meets most statistical requirements for a stochastic process. The spectral functions are then selected as the best and most descriptive tools for the particular application to describe the stochastic process.

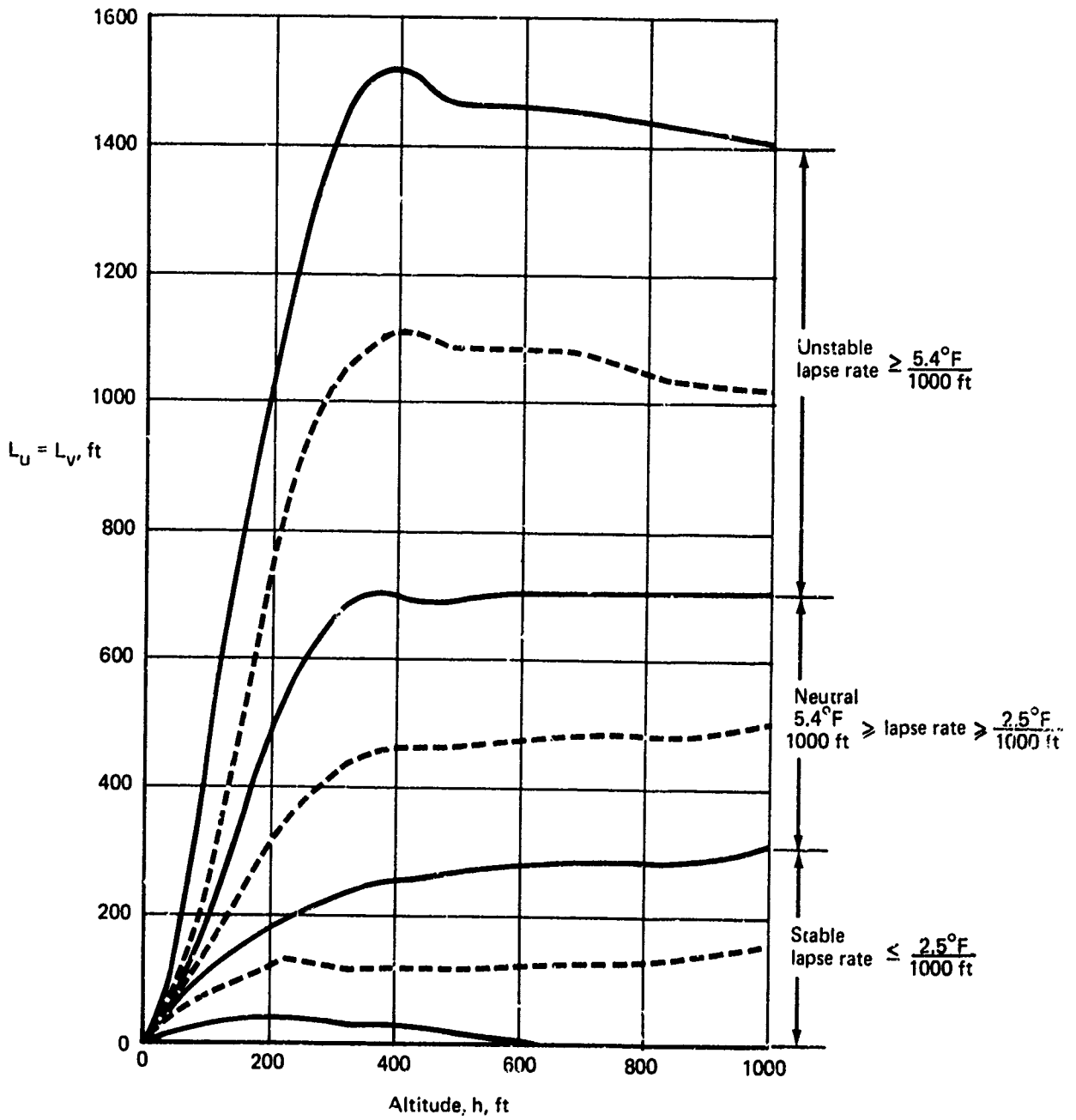

FIGURE 2-60.–INTEGRAL SCALE ESTIMATE FOR HORIZONTAL SPECTRA (FROM REF. 2-49, DRYDEN SPECTRA)

Other assumptions that are either necessary or extremely helpful for developing a quantitative description, and which have been reasonably well substantiated and accepted, are as follows:

1. A patch of turbulence exhibits three-dimensional homogeneity at high altitudes and horizontal homogeneity near the ground. That is, the statistical properties of turbulence within a patch of turbulence are independent of absolute horizontal position at low altitudes and are additionally independent of altitude at high altitudes. The application of the low altitude assumption requires restriction to homogeneous terrain. Homogeneity permits elimination of the absolute displacement coordinates as independent arguments.

2. Turbulence exhibits stationarity. The statistical properties of turbulence are independent of absolute time, leaving relative time or time displacement between two components of turbulence as an independent argument for describing the combined statistical properties of the two components.

3. Turbulence exhibits ergodicity. That is, ensemble and time averages are identical, permitting application of measured data taken by feasible means.

4. The amplitude distribution of a patch of turbulence is Gaussian. Evidence has been presented showing that, for the whole of all turbulence and turbulence patches, the distribution is not Gaussian, but no evidence against the normality of the distribution for a patch of turbulence was discovered. A normal distribution has the greatest theoretical support.

5. A patch of turbulence is sufficiently large to permit sustained flight within the patch of duration that is long with respect to the minimum frequency of interest.

6. For airspeeds sufficiently high, Taylor's hypothesis is applicable. Rates of change of turbulent velocities at a point are assumed to be small compared to the speed of the aircraft so that the field of turbulence velocities may be regarded as frozen. This assumption enables the interchangeability of the time and position displacements along the direction of relative wind, reducing the independent variables to just the position displacement vector. One estimate permits use of this assumption for airspeeds greater than one-third the "mean wind" speed.

7. At a sufficiently high altitude, turbulence exhibits isotropy. That is, the average functions describing the field of turbulence are independent of the orientation of the axis system describing the field of turbulence.

8. At all altitudes, turbulence is isotropic above a sufficiently high spacial frequency.

9. The one-dimensional turbulence power spectra are invariant with frequency at low spacial frequencies and vary with $\Omega_1^{-5/3}$ at high spacial frequencies.

The most descriptive isotropic spectral form that meets the assumptions was found to be the Von Karman models. In keeping with common practice, it shall be assumed that the shapes of the spectra for isotropy hold for the nonisotropic conditions at low altitudes, Integral scales for the transverse (normal to the direction of the relative wind) components of turbulence are redefined to mean twice the area under the respective autocorrelation functions. It remains to establish the integral scales and variances for each of the turbulence components and the cross spectra.

An additional assumption frequently made is that low altitude turbulence is horizontally isotropic (statistical properties invariant with rotations of the axis system about the vertical axis), which would require equal variances and integral scales for the horizontal components of turbulence and definition of only a single cross spectrum.

Only a single non-zero cross spectrum has been found, and the power spectrum for a vertical turbulence has been found to be invariant with measurements at different orientations relative to the mean wind, supporting horizontal isotropy. On the other hand, a greater variance is attributed to the component along the mean wind, eddies are said to stretch in the direction of the mean wind, and atmospheric stability is said to influence each horizontal component differently. However, the nonisotropic character of the horizontal components appears to occur at very low frequencies, perhaps below the minimum frequency of interest. Further, quantitative estimates of the statistical properties of the horizontal components vary widely and are subject to large measurement errors. Thus, the assumption of horizontal isotropy is probably not much worse than any quantitative description for a nonhorizontally isotropic model, and will be accepted.

What little information there is concerning the cross spectrum deals with the amplitude relationship (for the u and w turbulence components). Theory predicts, and is supported, that the cross spectrum is proportional to the mean wind shear and the square root of the product of the u and w power spectra, and is additionally inversely proportional to frequency at high frequencies, combining to cause an $\Omega_1^{-8/3}$ variation at high frequencies. As a consequence, the cross spectrum is most significant at the lower spacial frequencies. There is little alternative but to accept this description.

2.4.6.2 Requirements for Statistical Functions

Acceptance of the Von Karman spectral forms and isotropy at high frequencies for all altitudes leads to

$$\frac{\sigma_u^2}{L_u^{2/3}} = \frac{\sigma_v^2}{L_v^{2/3}} = \frac{\sigma_w^2}{L_w^{2/3}}$$

as shown previously.

Acceptance of the horizontal isotropy requires

$$\sigma_u = \sigma_v$$

$$L_u = L_v$$

At high altitudes turbulence is required to be isotropic. Thus, as $h \rightarrow h_I$,

$$\frac{\sigma_u}{\sigma_w} = \frac{\sigma_v}{\sigma_w} \rightarrow 1, \quad \frac{L_u}{L_w} = \frac{L_v}{L_w} \rightarrow 1.$$

At the surface, the proximity of the ground inhibits the eddy sizes. Thus, as $h \rightarrow 0$, $L_u \rightarrow 0$, $L_v \rightarrow 0$, $L_w \rightarrow 0$. It is generally agreed that the proximity of the ground has a greater influence on the vertical dimensions of the eddies than the horizontal dimensions. Thus, $L_u = L_v \leq L_w$. Since the effect of the proximity of the ground is to decrease the eddy sizes, the integral scales must not be larger than the isotropic values, and

$$dL_u/dh \geq 0$$

$$dL_v/dh \geq 0$$

$$dL_w/dh \geq 0$$

The effect of stability upon turbulence variances is to increase the variance with decreasing stability. At sufficiently high stability, turbulence must disappear. Thus,

$$d\sigma/dR_i < 0$$

$$\lim_{R_i \rightarrow \infty} \sigma = 0$$

It is within this framework that the statistical properties of turbulence are to be specified.

2.4.6.3 Selected Turbulence Variance Description

Of the three components, the vertical component of turbulence has received the most scrutiny. Similarity theory predicts

$$\sigma_w = Cu_* \frac{\sigma_w}{u_*} (h/\ell')$$

The value of the proportionality constant, C, that receives the most agreement and which shall be adopted is 1.3.

The friction velocity at the surface, $u_{*_{REF}}$, may be calculated from a surface wind measured at the same height by

$$u_{*_{REF}} = \frac{k\,\bar{V}_{REF}}{\ln\left(\frac{h_{REF} + z_0}{z_0}\right) + \left(f\,\frac{h_{REF}}{\ell'}\right)}$$

as shown in the discussion on mean wind. Hence, σ_w is altered by small scale roughness. In keeping with the selected mean wind description, measurements shall be assumed to be taken at 20 feet, a value of $z_0 = 0.15$ feet is accepted as typical of airports, and the function $f(h_{REF}/\ell')$ is as was defined for the mean wind. The Von Karman constant, k, is 0.4.

The universal function, $(\sigma_w/u_*)(h/\ell)$, is specified by

$$\frac{\sigma_w}{u_*}\left(\frac{h}{\ell'}\right) = \left[\frac{kh}{u_{*_0}}\,\frac{\partial \bar{V}_w}{\partial h} - 2.2363\,\frac{h}{\ell'}\right]^{1/3}, \frac{h}{\ell'} < 0$$

Where ℓ' has replaced ℓ assuming a constant proportionality between eddy viscosity and eddy conductivity.

At some sufficiently large Richardson's number (or h/ℓ'), turbulence must disappear. There is apparently a hysteresis effect, but a critical Richardson's number of 1/4.5, corresponding to that implied for the selected mean wind description, shall be used.

The function combining the proportionality constant and the universal function for both stable and unstable conditions is presented on Figures 2-61 and 2-62. The shape of the curve up to moderate stable conditions was made to match that of Figure 2-40 and was extrapolated to $\sigma_w = 0$ at $1/\ell' = 1.22$, which, using the relationships provided for the selected mean wind description, is equivalent to the critical Richardson's number. Artistic license was used to remove the objectionable slope reversal at $h/\ell' = 0$. The abrupt change of the curve at $h/\ell' = 1$ was made to correspond to the point where the nondimensional shear changes abruptly.

The complete equation selected to define the rms level of vertical turbulence is given by

$$\sigma_w = \left[\frac{\sigma_w(\frac{h}{\ell'})}{u_*}\right]\left[\frac{u_*}{u_{*_0}}\left(\frac{h}{d}\right)\right] u_{*_0}$$

where $(\sigma_w/u_*)(h/\ell')$ is given by Figures 2-61 and 2-62.

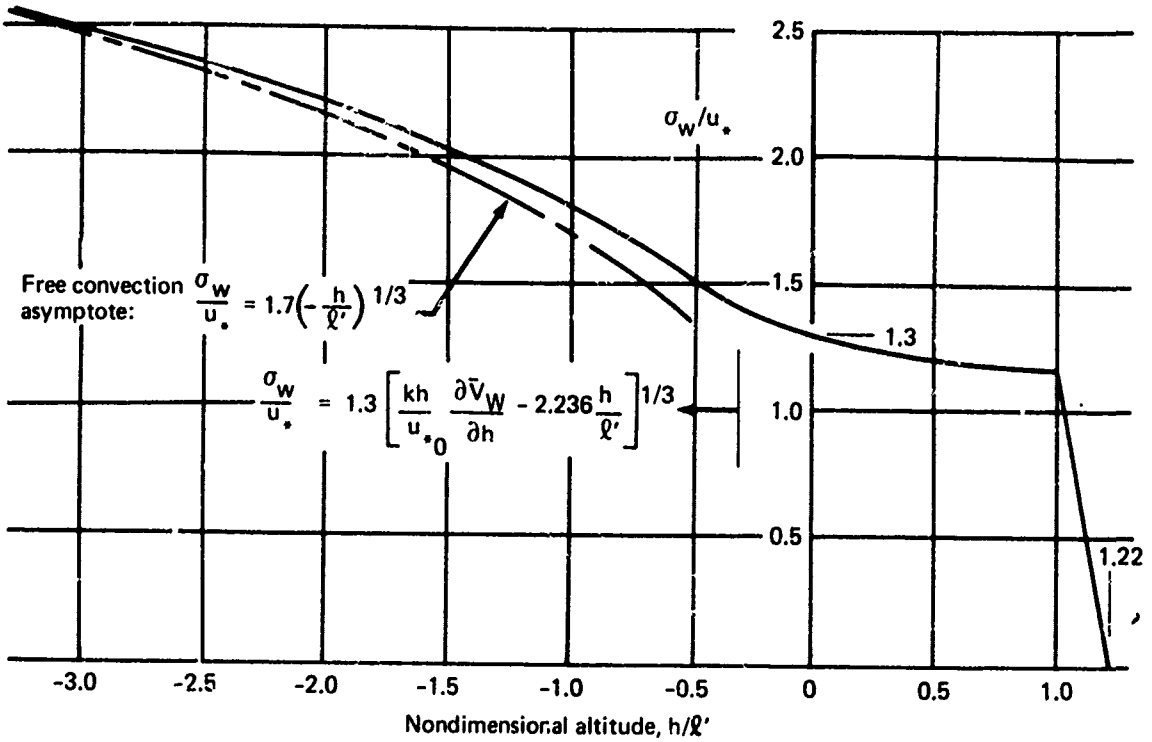

FIGURE 2-61.—σ_W/u_* VARIATION WITH STABILITY

$$\frac{u_*}{u_{*0}} = \begin{cases} 1 - \frac{h}{d}, & h < d \\ 0 \quad , & h \geq d \end{cases}$$

$$d = 2000\, u_{*0}$$

$$u_{*0} = 0.4 \frac{u_{*0}/k}{\bar{V}_{20}} (R_{i_{20}})\ \bar{V}_{20}$$

Resulting profiles of σ_W with altitude for neutral, stable, and unstable conditions are shown on Figure 2-63.

Specification of the variances of the horizontal components is more troublesome since theory, supported by empirical evidence, is not as well developed. The theory does suggest that the rms levels of horizontal turbulence are linearly related to the friction velocity. Thus, the effect of the reduction of friction velocity with altitude is the same for all three components. Additionally, turbulence for all three components must disappear at the same stable condition and must increase with decreasing stability, although the variances of the horizontal turbulence components are not well established. Although there is some

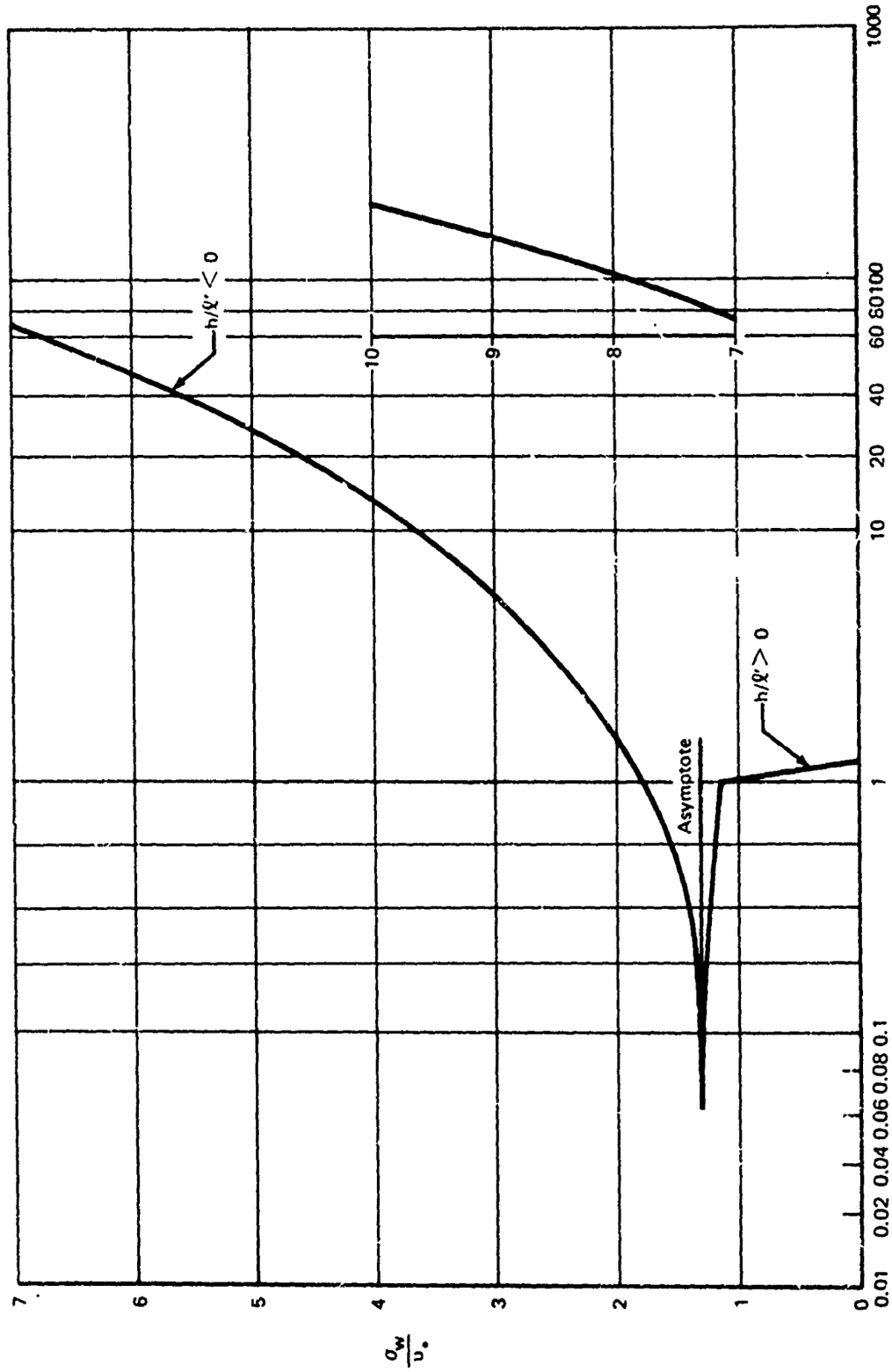

FIGURE 2-62. – $\frac{g\omega}{U_*}$ VARIATION WITH STABILITY, LOG PLOT

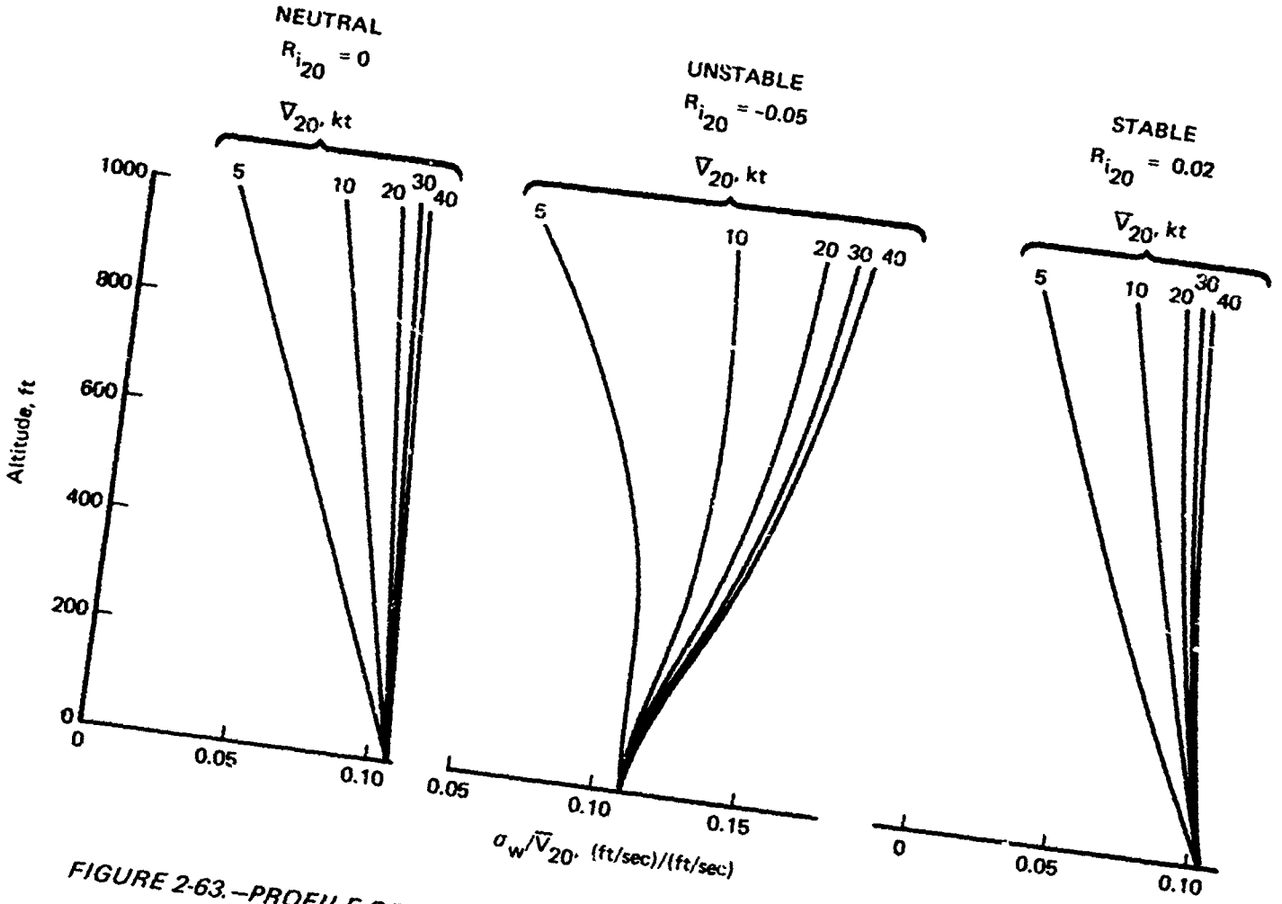

FIGURE 2-63.—PROFILE OF VERTICAL TURBULENCE RMS, SELECTED DESCRIPTION

qualitative evidence to the contrary, it shall be assumed that the shapes of the variations with stability for all three components are the same. Thus, it remains only to establish ratios between the rms levels of the horizontal components to the vertical components.

In keeping with horizontal isotropy, $\sigma_u = \sigma_v$. To assure isotropy at sufficiently high altitudes, σ_u/σ_w and σ_v/σ_w must go to unity with increasing altitude.

The literature does not provide a justification for any variation of the ratios. A linear change of the ratio from a reference altitude, h_{REF}, to a ratio of one at the altitude where isotropy exists, h_I, is provided by

$$\frac{\sigma_u}{\sigma_w} = \begin{cases} \left.\frac{\sigma_u}{\sigma_w}\right|_{REF} + \left[\frac{1.0 - \left.\frac{\sigma_u}{\sigma_w}\right|_{REF}}{h_I - h_{REF}}\right] h, & h < h_I \\ 1.0, & h \geq h_I \end{cases}$$

$$\sigma_v = \sigma_u$$

or, if h_{REF} is sufficiently close to the surface so that it is small compared to the boundary layer thickness

$$\frac{\sigma_u}{\sigma_w} = \begin{cases} \left[\left.\frac{\sigma_u}{\sigma_w}\right|_{REF} + \left(1 - \left.\frac{\sigma_u}{\sigma_w}\right|_{REF}\right)\frac{h}{h_I}\right], & h < h_I \\ 1.0, & h \geq h_I \end{cases}$$

$$\sigma_v = \sigma_u$$

Such a linear model is similar to that proposed in Reference 2-49. However, a linear model does not necessarily enable meeting all the requirements, particularly those for the variance-integral scale interrelationships and those for the integral scales alone. For the time being, the variation of the rms ratios will be considered to be of n^{th} order:

$$\frac{\sigma_u}{\sigma_w} = \begin{cases} \left\{\left(\left.\frac{\sigma_u}{\sigma_w}\right|_{REF}\right)^{1/n} + \left[1 - \left(\left.\frac{\sigma_u}{\sigma_w}\right|_{REF}\right)^{1/n}\right]\frac{h}{h_I}\right\}^n, & h < h_I \\ 1.0, & h \geq h_I \end{cases}$$

This form satisfies the requirements

$$\frac{\sigma_u}{\sigma_w} = \left.\frac{\sigma_u}{\sigma_w}\right|_{REF} \quad \text{for } \frac{h}{h_I} = 0$$

$$\frac{\sigma_u}{\sigma_w} = 1 \quad \text{for } \frac{h}{h_I} \geq 1$$

$$1.0 \leq \frac{\sigma_u}{\sigma_w} \leq \left.\frac{\sigma_u}{\sigma_w}\right|_{REF}$$

$$\frac{d\left(\frac{\sigma_u}{\sigma_w}\right)}{dh} \leq 0$$

What is additionally needed is a ratio of rms's for a horizontal component to the vertical component at some altitude (h_{REF}). A review of the data for σ_u/u_*, σ_v/u_*, and $\sigma_u/\sigma_v/\sigma_w$ indicates that for very low altitudes $\sigma_u/\sigma_w = \sigma_v/\sigma_w = 2$ is a reasonable compromise. It shall be assumed that this ratio holds at the surface as the measurement altitudes are very small compared to the boundary layer thickness. Thus,

$$\sigma_u = \sigma_v = \begin{cases} \sigma_w \left[2^{1/n} + (1 - 2^{1/n}) \frac{h}{h_I}\right]^n, & h < h_I \\ \sigma_w, & h > h_I \end{cases}$$

It should be recalled that these specifications hold for an axis system aligned to the mean wind, not to the airplane.

2.4.6.4 Selected Integral Scale Description

The integral scale for vertical turbulence is that which has been best defined, particularly because it is more easily measured. It shall be accepted that the vertical integral scale is proportional to altitude at low altitudes, as predicted by theory and as is most strongly supported by empirical measurements.

The constant of proportionality has been variously estimated to be from 0.4 to 1, independent of stability and surface roughness, and to be a function of both stability and terrain. A value of unity is selected, even though this is on the high side of the estimates, because it is the value most strongly supported. Trends of variations with large scale roughness also indicate a value near unity for "typical" airport terrain.

The estimates of the proportionality constant near 0.5 might well be due to differences in definition; if the 0.5 estimates were made for defining the vertical turbulence integral scale as the area under the autocorrelation function as opposed to twice the area under the autocorrelation function, the 0.5 estimates would be consistent with a proportionality constant of 1 for the second definition.

Atmospheric stability shall be assumed not to influence the integral scale for vertical turbulence, in keeping with the observation of Reference 2-7 that there is no evidence of systematic variations of the proportionality between the vertical turbulence integral scale and altitude. This is in contradiction to the model of Reference 2-49. However, the latter model uses lapse rate as the stability parameter which, although most easily understood, is not well accepted as the independent parameter. For neutral conditions, the model of Reference 2-49, as indicated on Figure 2-57, shows good agreement with a proportionality constant of one.

Measurements of integral scales for horizontal components are poor and estimates vary widely. They can, however, be derived from the requirements for isotropy at high frequencies and the assumption of the Von Karman spectra using the other parameters already specified:

$$L_u = L_v = L_w \left(\frac{\sigma_u}{\sigma_w}\right)^3 = L_w \left(\frac{\sigma_v}{\sigma_w}\right)^3$$

$$= \left[2^{1/n} + (1 - 2^{1/n}) \frac{h}{h_I}\right]^{3n} \quad \text{for low altitudes.}$$

As $\sigma_u = \sigma_v \geq \sigma_w$, the integral scales for the horizontal components are greater than that for the vertical component. Furthermore, this equation satisfies the requirement that the integral scales be equal (and turbulence isotropic) at h_I. However, σ_u/σ_w and σ_v/σ_w decrease with altitude, indicating that above some altitude the changes of horizontal integral scales with increasing altitude will be negative.

By setting the differential of the equation to zero, the requirement that the integral scales increase with altitude up to the boundary layer is expressed by

$$3n(2^{1/n} - 1) \leq 1$$

The inequality can be replaced by an equality if the maximum is required at the altitude above which turbulence is isotropy (h_I), a mathematical nicelty providing for a continuity of slope. A graphical solution provides a value of n nearly equal to -0.4. Thus,

$$\frac{\sigma_u}{\sigma_w} = \frac{\sigma_v}{\sigma_w} = \begin{cases} \dfrac{1}{\left[0.177 + 0.823\dfrac{h}{h_I}\right]^{0.4}} & , \; h < h_I \\ 1.0 & , \; h \geq h_I \end{cases}$$

$$L_u = L_v = L_w\left(\frac{\sigma_u}{\sigma_w}\right)^3 = L_w\left(\frac{\sigma_u}{\sigma_w}\right)^3 = \begin{cases} \dfrac{h}{\left[0.177 + 0.823\dfrac{h}{h_I}\right]^{1.2}} & , \; h < h_I \\ h_I & , \; h \geq h_I \end{cases}$$

These equations are presented on Figures 2-64 and 2-65, and meet all the stated requirements. These figures represent a model that is similar to that of Reference 2-42 (Figures 2-54 and 2-58) and is derived for similar requirements. The model also agrees with invariance, a linear variation, a square root variation, and a cube root variation for different ranges of altitude. However, it is but one of several representations that meet the stated requirements.

It remains to define h_I, the altitude above which isotropy effectively exists. Estimates exist from about the 300 feet implied by Figure 2-57 (which also implies weak effect of stability on h_I) to the 2500 feet used in the model of Reference 2-42. The value selected is 1000 feet, a number appearing in several aircraft design criteria. The comment in Reference 2-7 referring to the linear altitude dependence of L_w up to a few hundred meters is not incompatible with 1000 feet. The use of an isotropic altitude independent of stability appears to be intuitively justifiable, since the dominant factor for reducing the integral scales at low altitudes is the physical restriction on eddy size caused by the presence of the ground.

Fixing h_I = 1000 feet and $L_w = h$ for low altitudes independent of stability causes $\sigma_u/\sigma_w = \sigma_v/\sigma_w$ and $L_u = L_v$ to be independent of stability, while qualitative trends with stability have been explained. However, the successful attempts to model the dependency of these parameters on stability rather than qualitatively are few and are very restrictive as to the conditions to which they apply. Considering the great diversity of opinion on neutral stability values, any attempt to model effects of stability would be arbitrary and would imply more knowledge than is available.

2.4.6.5 Selected Cospectrum Description

From a Taylor series expansion of a universal expression for the one-dimensional cospectrum developed from similarity theory, Reference 2-7 has postulated and substantiated with empirical data the form

$$\frac{\sigma_u}{\sigma_w} = \frac{\sigma_v}{\sigma_w} = \begin{cases} \left[0.177 + 0.823\, h/h_I\right]^{.4} & , h < h_I \\ 1.0 & , h \geq h_I \end{cases}$$

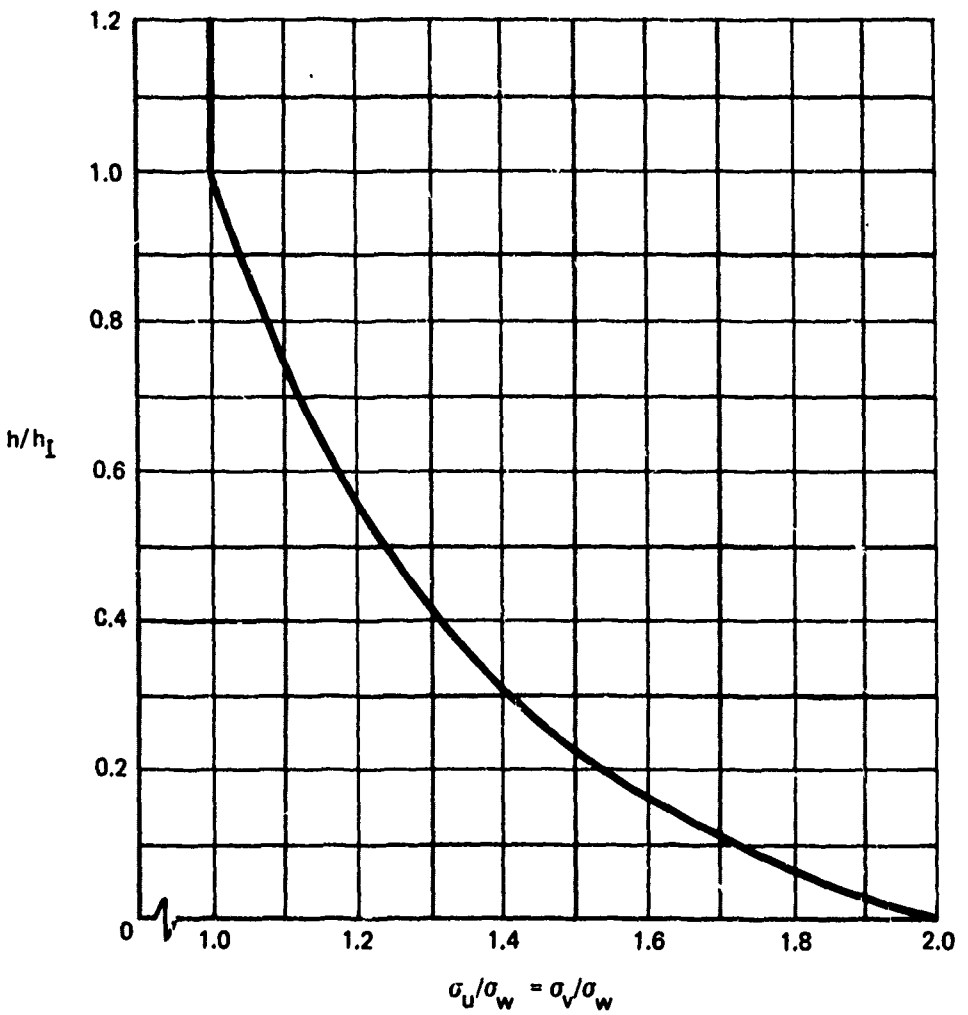

FIGURE 2-64.—SELECTED DESCRIPTION FOR VARIANCES OF HORIZONTAL TURBULENCE COMPONENTS

$$L_w = \begin{cases} h, h < h_I \\ h_I, h = h_I \end{cases}$$

$$L_u = \begin{cases} L_w \left(\frac{\sigma_u}{\sigma_w}\right)^3 = \frac{h}{\left[0.177 + 0.823\, h/h_I\right]^{1.2}} & , h < h_I \\ h_I & , h \geq h_I \end{cases}$$

$$L_v = L_u$$

h_I = Altitude above which turbulence is isotropic

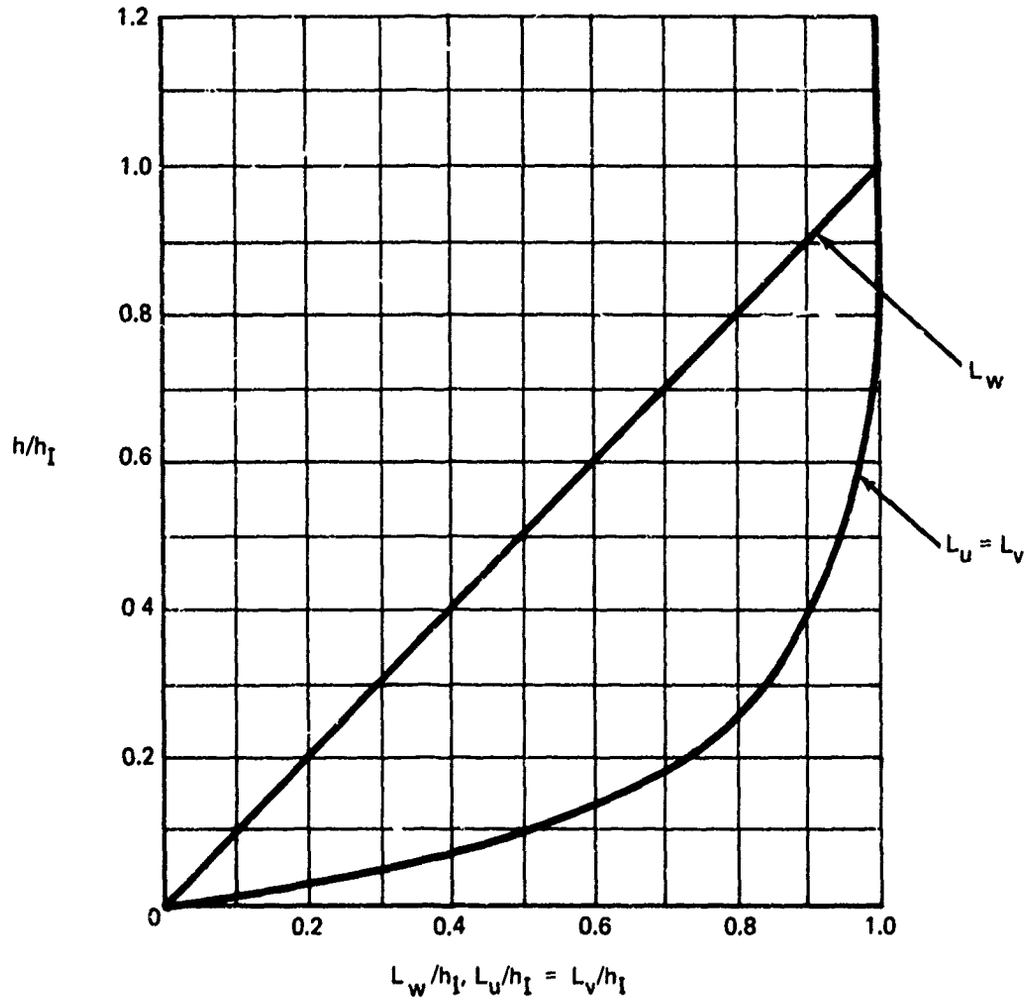

FIGURE 2-65.– SELECTED INTEGRAL SCALE DESCRIPTION

$$\Phi_{uw}(\omega) = A\,\Phi_w \frac{1}{\omega} \frac{\partial \bar{V}_W}{\partial h}$$

which is valid at high frequencies and where the u and w power spectra are proportional to each other. The more general expression was given as

$$\Phi_{uw}(\omega) = \sqrt{\Phi_u \Phi_w}\, G\left(\frac{1}{\omega} \frac{\partial \bar{V}_W}{\partial h}\right)$$

At low frequencies, it is argued that the cospectrum must be invariant or increase with increasing frequency. Presumably, the arguments that require the one-dimensional power spectra to have a constant low frequency asymptote also apply to the cospectrum.

The data on Figure 2-32 suggest a transition from the low frequency to the high frequency region for Φ_{uw}/Φ_w similar to the frequency response of a first order lag. Such a form is represented by

$$\frac{\Phi_{uw}}{\Phi_w} = \frac{C}{\left[1 + (T\omega)^2\right]^{1/2}}$$

Where the time constant, T, would be proportional to $1/(\partial \bar{V}_W/\partial h)$ to satisfy the high frequency requirement. This is the form recommended by Reference 2-3. Using the data of Figure 2-32, a good fit is found for

$$\frac{\Phi_{uw}}{\Phi_w}(\omega) = \left[\frac{2}{1 + \left(\frac{2.5\omega}{\partial \bar{V}_W/\partial h}\right)^2}\right]^{1/2}$$

as shown on Figure 2-66: The break frequency occurs at

$$\frac{1}{T} = 0.4 \frac{\partial \bar{V}_W}{\partial h} = 0.16 \left[\frac{u_{*0}/k}{\bar{V}_{20}}\right] \left[\frac{kh}{u_{*0}} \frac{\partial \bar{V}_W}{\partial h}\right] \frac{\bar{V}_{20}}{h}$$

where

$$\frac{u_{*0}/k}{\bar{V}_{20}} = f(R_{i_{20}}) \qquad \text{Figure 2-15}$$

$$\frac{kh}{u_{*0}} \frac{\partial \bar{V}_W}{\partial h} = f(h/\ell') \qquad \text{Figure 2-18}$$

$$1/\ell' = f(R_{i_{20}}) \qquad \text{Figure 2-16}$$

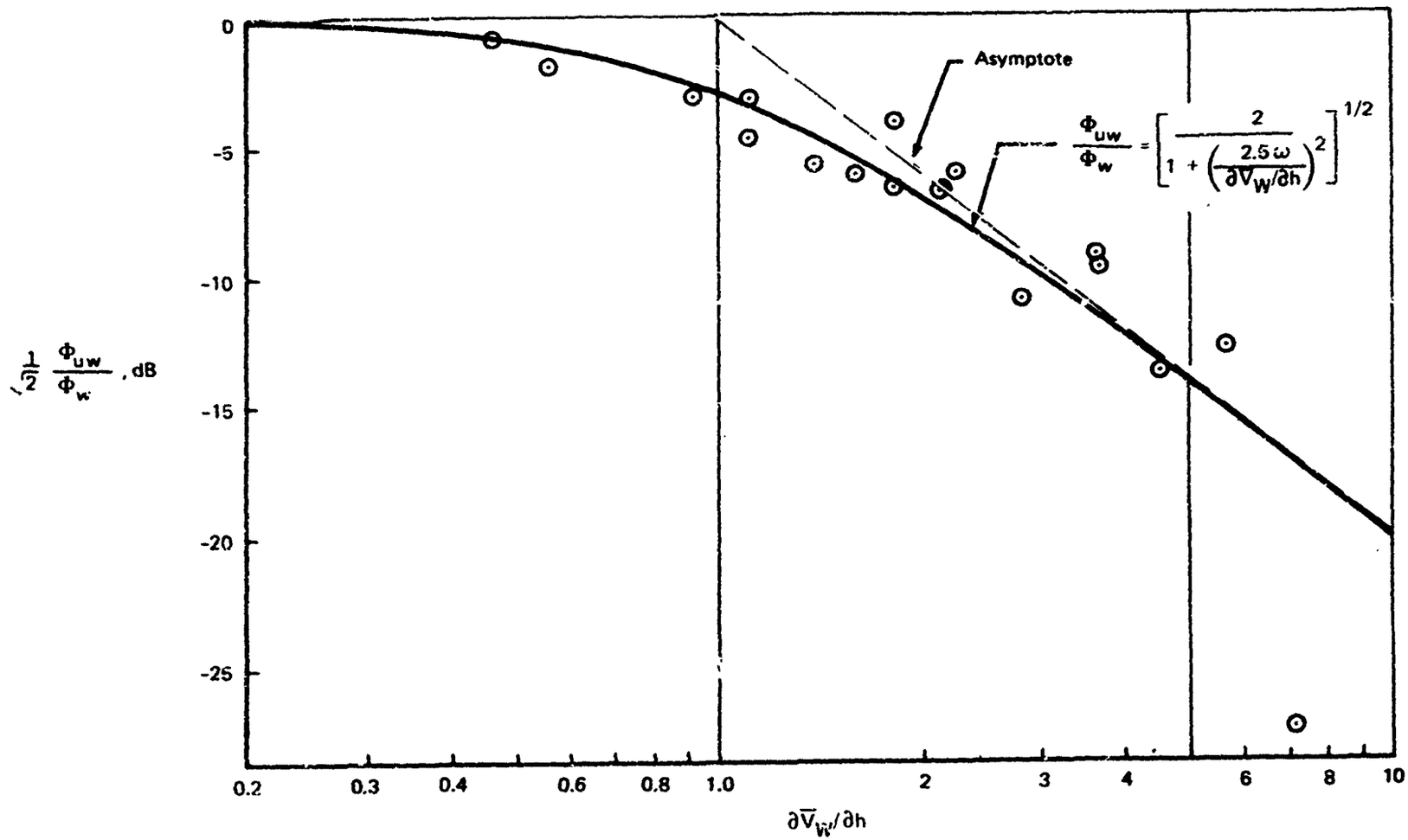

FIGURE 2-66.—COSPECTRUM DATA FITTING (FROM REF. 2-7)

Thus, the break frequency decreases with altitude and increases with surface wind level and stability, as shown on Figure 2-67.

The curve fit of Figure 2-66 implies that the cospectrum is proportional to the vertical turbulence power spectrum, but this is true only when the longitudinal and vertical turbulence power spectra differ only by a constant (at the relatively low and high spacial frequencies). To satisfy the more general expression, the cospectrum must be multiplied by the square root of the ratio of the longitudinal turbulence spectrum to the vertical turbulence spectrum:

$$\Phi_{uw}(\omega) = \frac{A\sqrt{2}\,\Phi\,\omega}{\left[1+\left(\frac{2.5\,\omega}{\partial\bar{V}_W/\partial h}\right)^2\right]^{1/2}}\sqrt{\frac{\Phi_u}{\Phi_w}} = \frac{A\sqrt{2}\,\sqrt{\Phi_u\,\Phi_w}}{\left[1+\left(\frac{2.5\,\omega}{\partial\bar{V}_W/\partial h}\right)^2\right]^{1/2}}$$

The correction factor is presented on Figure 2-68 and has high and low frequency asymptotes of $\sqrt{3/4}$ and $\sqrt{2(\sigma_u/\sigma_w)^5}$, using the power spectra description selected.

From Figures 2-66 and 2-68 the break frequency of the cospectrum relative to those for the power spectra may be found. Figure 2-66 indicates that the cospectrum assumes its low frequency asymptote below about $2.5\,\omega/(\partial\bar{V}_W/\partial h) = 0.1$. The ratio of the power spectra is constant below about $h\Omega_1 = 0.1$ for all cases ($h = 0$ is critical), as indicated on Figure 2-68. Using Taylor's hypothesis, $\Omega_1 = \omega/V_A$, where V_A is total airspeed (equal to the mean wind speed for an observer stationed at the ground), spacial and temporal frequencies can be related. Equating temporal frequencies from the two expressions provides

$$\frac{0.1(\partial\bar{V}_W/\partial h)}{2.5} = \frac{0.01 V_A}{h}$$

as the condition where the cospectrum break frequency is as high as that for the longitudinal power spectrum. For neutral atmospheric stability,

$$\frac{\partial\bar{V}_W}{\partial h} = 0.4\left[\frac{u_{*0}/k}{\bar{V}_{20}}\right]\frac{\bar{V}_{20}}{h} = \frac{0.0816\,\bar{V}_{20}}{h} \qquad \text{(From Figure 2-15)}$$

and the requirement becomes

$$V_A/\bar{V}_{20} = 0.3264$$

For ratios below this value, the cospectrum break frequency will occur below those for the power spectra. Unless an aircraft flies with a negative airspeed, this ratio will always be exceeded, even for hover. This ratio is very near that specified in Reference 2-1 for applying Taylor's hypothesis. Increased stability will shift the cospectrum break frequency higher, but it is reasonable to assume that for all airspeeds at which Taylor's hypothesis holds, the

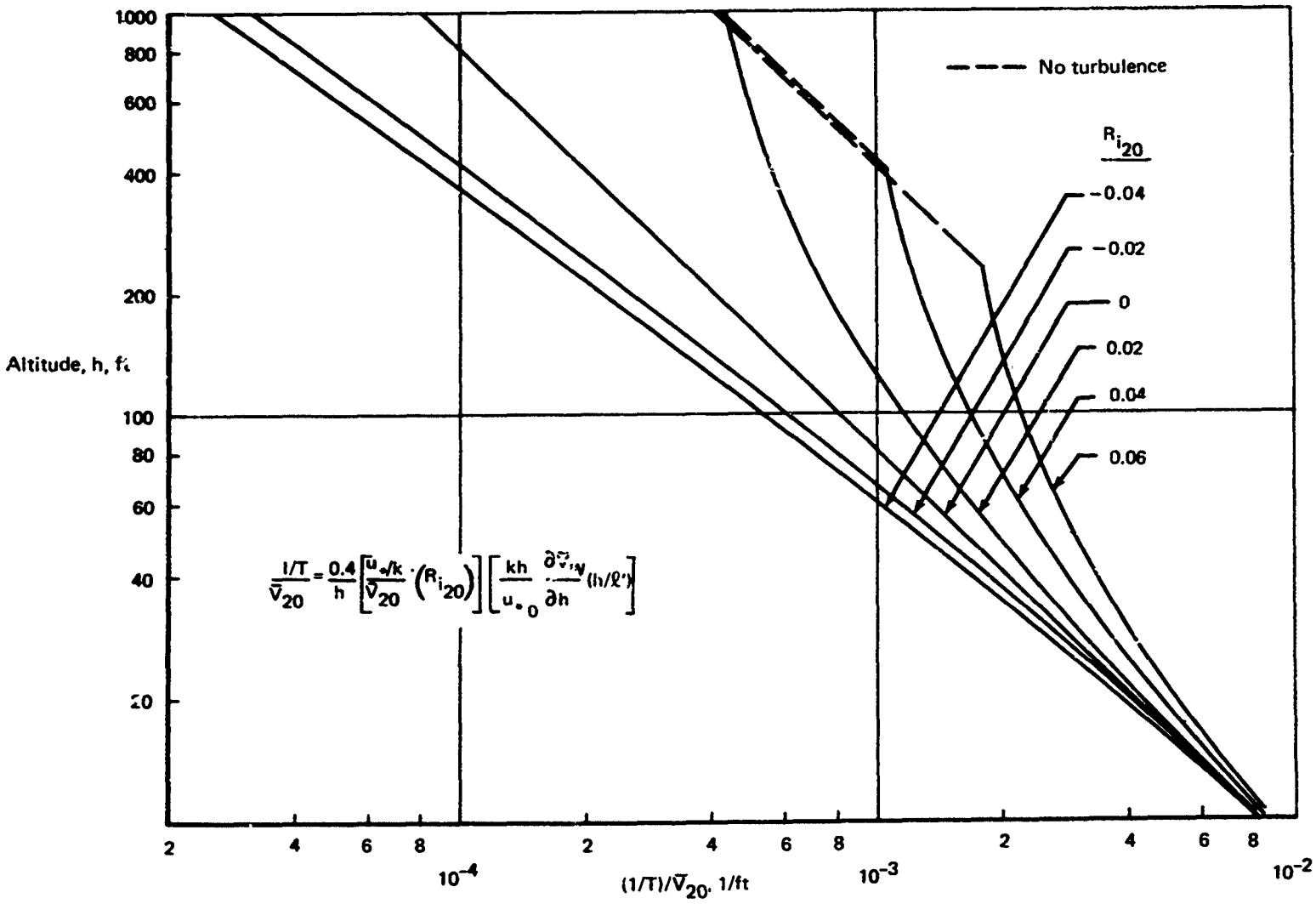

FIGURE 2-67.—COSPECTRUM BREAK FREQUENCY

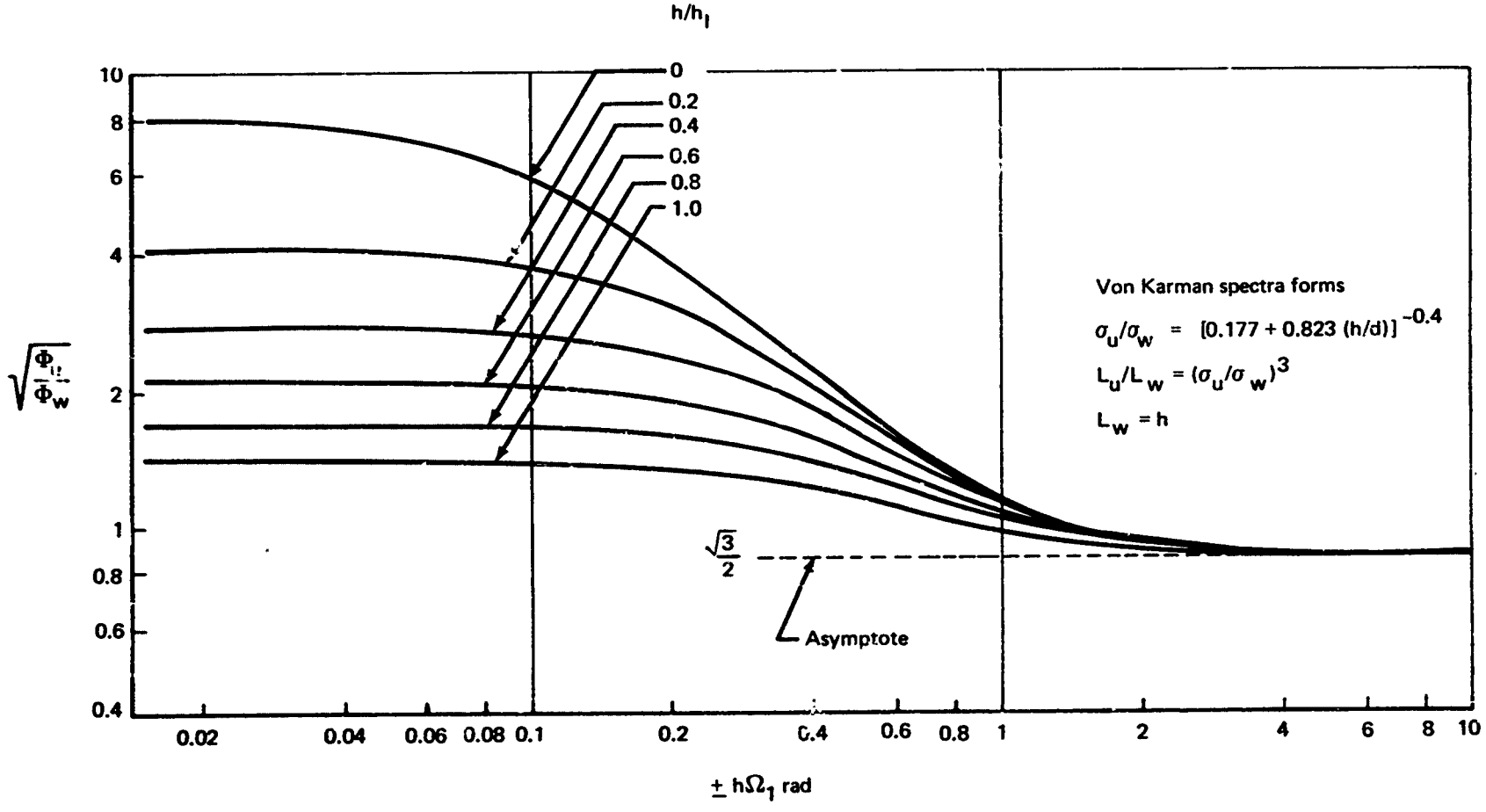

FIGURE 2-68.–COSPECTRUM CORRECTION FACTOR

The cospectrum may be rewritten to recognize the low frequency gain (Von Karman power spectra):

$$\Phi_{uw}(\Omega_1) = \frac{A\,\sigma_u\,\sigma_w\sqrt{L_u\,L_w}}{\pi}\;\frac{\sqrt{\left[\frac{\pi}{\sigma_u^2\,L_u}\,\Phi_u(\Omega_1)\right]\left[\frac{2\pi}{\sigma_w^2\,L_w}\,\Phi_w(\Omega_1)\right]}}{\left[1+\left(\frac{2.5\,\Omega_1\,V_A}{\partial\bar{V}_W/\partial h}\right)^2\right]^{1/2}}$$

or using $L_u/L_w = (\sigma_u/\sigma_w)^3$,

$$\Phi_{uw}(\Omega_1) = \frac{u_*^2\,A\left(\frac{\sigma_w}{u_*}\right)^2\left(\frac{\sigma_u}{\sigma_w}\right)^{5/2}L_w}{\pi}\;\frac{\sqrt{\left[\frac{\pi}{\sigma_u^2\,L_u}\,\Phi_u(\Omega_1)\right]\left[\frac{2\pi}{\sigma_w^2\,L_w}\,\Phi_w(\Omega_1)\right]}}{\left[1+\left(\frac{2.5\,\Omega_1\,V_A}{\partial\bar{V}_W/\partial h}\right)^2\right]^{1/2}}$$

which is the form

$$\Phi_{uw}(\Omega_1) = u_*^2 AKF(\Omega_1)$$

The form presented in Reference 2-7 did not contain functions dependent upon airspeed, V_A, nor of h/d, inherent in this form. However, the form of Reference 2-7 was developed for an observer fixed in an inertial reference system, for which airspeed is not a separate parameter, for the constant shear stress layer where u_* is assumed invariant with h/d, and for the inertial subrange where σ_u/σ_w is not a separate parameter.

Yet to be determined is the "constant," A, a term that has only been specified to be a constant for larger $(\partial\bar{V}_W/\partial h)/\omega$. Its value may be determined by noting that the covariance is identical to the square of friction velocity. Hence,

$$u_*^2 = \int_{-\infty}^{\infty}\Phi_{uw}(\Omega_1)\,d\Omega_1$$

$$AK = \frac{1}{\int_{-\infty}^{\infty}F(\Omega_1)\,d\Omega_1}$$

The use of the Von Karman power spectra compounds the difficulty of solving the integral. Furthermore, the normalized function, $F(\Omega_1)$, contains the independent parameters of Ω_1, h, h/ℓ', h/h_1, and $\bar{V}_{20}/V_A$. However, the function may be approximated by

$$F(\Omega_1) \cong \frac{1}{\left[1+(TV_A\Omega_1)^2\right]^{1/2}}\;\frac{1}{\left[1+(L_u\Omega_1)^2\right]^{1/2}}$$

cospectrum break frequency will be substantially below those of the power spectra. Using this conclusion, the qualitative shape of the cospectrum is expected to be as shown on Figure 2-69.

The area under $\Omega_1 \Phi_{uw}(\Omega_1)$ when plotted against log (Ω_1) represents the covariance. The logarithm of $\Omega_1 \Phi_{uw}(\Omega_1)$ is plotted on Figure 2-69 to show the asymptotic behavior, but Figure 2-69 does demonstrate that the contribution of spacial frequencies above the break frequency for the longitudinal power spectrum (approximately $1/L_u$) to the covariance diminishes rapidly with increasing frequency.

It may be noted that the cospectrum has been presented as a function of temporal frequency, while the power spectra are defined in terms of spacial frequency. The two may be interchanged using Taylor's hypothesis and by requiring the variances and covariance to be the same in either domain:

$$\sigma^2 = \int_{-\infty}^{\infty} \Phi(\Omega_1)\, d\Omega_1 = \int_{-\infty}^{\infty} \Phi\left(\frac{\omega}{V_A}\right) d\left(\frac{\omega}{V_A}\right)$$

$$\sigma^2 = \int_{-\infty}^{\infty} \Phi'(\omega)\, d\omega$$

Thus,

$$\Phi'(\omega) = \frac{1}{V_A}\, \Phi\left(\frac{\omega}{V_A}\right)$$

In the temporal frequency domain, the cospectrum is given by

$$\Phi_{uw}(\omega) = \frac{A\sqrt{2}\sqrt{\left[\frac{1}{V_A}\Phi_u(\Omega)\right]\left[\frac{1}{V_A}\Phi_w(\Omega)\right]}}{\left[1+\left(\frac{2.5\,\omega}{\partial\bar{V}_W/\partial h}\right)^2\right]^{1/2}} = \frac{A\sqrt{2}\sqrt{\Phi_u(\Omega)\,\Phi_w(\Omega)}}{V_A\left[1+\left(\frac{2.5\,\omega}{\partial\bar{V}_W/\partial h}\right)^2\right]^{1/2}}$$

In the spacial frequency domain, the expression is

$$\Phi_{uw}(\Omega) = \frac{A\sqrt{2}\sqrt{\Phi_u(\Omega_1)\,\Phi_w(\Omega_1)}}{\left[1+\left(\frac{2.5\,\Omega_1 V_A}{\partial\bar{V}_W/\partial h}\right)^2\right]^{1/2}}$$

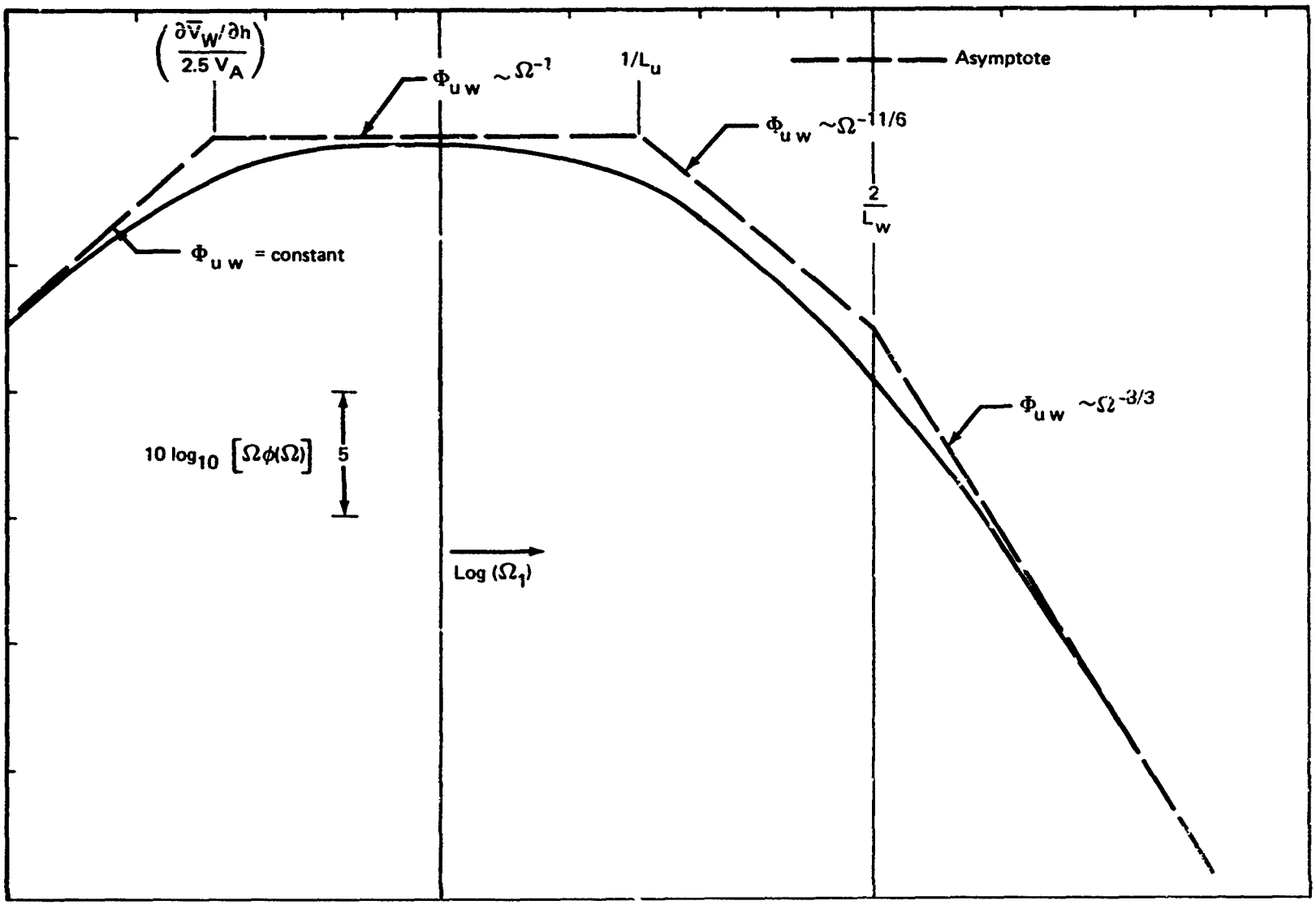

FIGURE 2-69.—QUALITATIVE COSPECTRUM SHAPE

This form ignores the vertical turbulence power spectrum break frequency and provides for a Ω_1^{-2} variation beyond the longitudinal turbulence power spectrum break frequency, which has been approximated by $1/L_u$. However, this is acceptable since it is known that the vertical turbulence break frequency (approximately $2/L_w$) is always greater than that for the longitudinal spectrum and that frequencies beyond $1/L_u$ have a rapidly diminishing contribution to the covariances.

A further approximation is possible by recalling that the cospectrum break frequency is much less than $1/L_u$. Thus, the contribution of frequencies below and about the cospectrum break frequency will also have a small contribution to the covariance, and the normalized function may be approximated by its asymptotic form in this region:

$$F(\Omega_1) \cong \begin{cases} 1. & , \ |\Omega_1| < \frac{1}{TV_A} \\ \dfrac{1}{\Omega_1 \left[1 + (L_u\Omega_1)^2\right]^{1/2}} & , \ |\Omega_1| > \frac{1}{TV_A} \end{cases}$$

This form is readily integrable:

$$\int_{-\infty}^{\infty} F(\Omega_1)\, d\Omega_1 = 2 \int_0^{\infty} F(\Omega_1)\, d\Omega_1 \cong \frac{2}{TV_A}\left\{1 + \ln\left[\frac{\frac{1}{L_u} + \sqrt{\frac{1}{T^2V_A{}^2} + \frac{1}{L_u{}^2}}}{\frac{1}{TV_A}}\right]\right\}$$

or, again recognizing $\frac{1}{TV_A} \ll \frac{1}{L_u}$,

$$\int_{-\infty}^{\infty} F(\Omega_1) \cong \frac{2}{TV_A}\left[1 + \ln\left(\frac{2TV_A}{L_u}\right)\right]$$

This expression has been checked by numerically integrating the exact expression and has been found to be very accurate. It may be substituted into the cospectrum equation to give:

$$\Phi_{uw}(\Omega) = \frac{u_*^2 V_A \sqrt{\left[\frac{\pi}{\sigma_u{}^2 L_u}\Phi_u(\Omega_1)\right]\left[\frac{2\pi}{\sigma_w{}^2 L_w}\Phi_w(\Omega_1)\right]}}{2\left(\frac{1}{T}\right)\left\{1 + \ln\left[\frac{2V_A}{\left(\frac{1}{T}\right)L_u}\right]\right\}\left[1 + (TV_A\Omega_1)^2\right]^{1/2}}$$

This cospectrum provides for a linearly decreasing covariance, with altitude, but because 1/T decreases with altitude, the low frequency portion increases with altitude. It may reasonably be expected that the cospectrum will have significant effects only at the very low frequencies.

2.4.6.6 Composite Turbulence Description Selected

The selection of a turbulence description has been complex. In an effort to provide an overview of the description, a composite of the description is presented as follows:

Power spectra:

$$\Phi_u = \frac{\sigma_u^2 L_u}{\pi} \frac{1}{\left|1 + (1.339\, L_u \Omega_1)^2\right|^{5/6}}$$

$$\Phi_v = \frac{\sigma_v^2 L_v}{2\pi} \frac{1 + \frac{8}{3}(1.339\, L_v \Omega_1)^2}{\left|1 + (1.339\, L_v \Omega_1)^2\right|^{11/6}}$$

$$\Phi_w = \frac{\sigma_w^2 L_w}{2\pi} \frac{1 + \frac{8}{3}(1.339\, L_w \Omega_1)^2}{\left|1 + (1.339\, L_w \Omega_1)^2\right|^{11/6}}$$

$$\sigma_w = \left(\frac{\sigma_w}{u_*}\right)\left(\frac{u_*}{u_{*0}}\right) u_{*0}$$

$$\frac{\sigma_w}{u_*} = f(h/\ell'), \text{ Figure 2-61}$$

$$\frac{u_*}{u_{*0}} = 1 - \frac{h}{d}$$

$$d = 2000\, u_{*0}$$

$$u_{*0} = 0.4\left[\frac{u_{*0}/k}{\bar{V}_{20}}\right]\bar{V}_{20}$$

$$\frac{u_{*0}/k}{\bar{V}_{20}} = f(R_{i_{20}}) \quad , \text{ Figure 2-15}$$

$$\sigma_u = \left(\frac{\sigma_u}{\sigma_w}\right)\sigma_w$$

$$\sigma_v = \sigma_u$$

$$\frac{\sigma_u}{\sigma_w} = \begin{cases} \dfrac{1}{\left[0.177 + 0.823\,\dfrac{h}{h_I}\right]^{0.4}} & , \dfrac{h}{h_I} < 1 \\ 1 & , \dfrac{h}{h_I} \geq 1 \end{cases}$$

(Figure 2-62)

$$\left.\begin{aligned} L_w &= \begin{cases} h & , \dfrac{h}{h_I} < 1 \\ h_I & , \dfrac{h}{h_I} \geq 1 \end{cases} \\ L_u &= L_w \left(\frac{\sigma_u}{\sigma_w}\right)^3 \\ L_v &= L_u \\ h_I &= 1000 \text{ ft} \end{aligned}\right\} \quad \text{Figure 2-65}$$

Cospectrum:

$$\Phi_{uw}(\Omega_1) = \frac{u_*^2 V_A}{2\left(\frac{1}{T}\right)} \frac{\sqrt{\left[\frac{\pi}{\sigma^2 L_u}\Phi_u(\Omega_1)\right]\left[\frac{2\pi}{\sigma_w^2 L_w}\Phi_w(\Omega_1)\right]}}{\left\{1 + \ln\left[\frac{2V_A}{\left(\frac{1}{T}\right)L_u}\right]\right\}\left[1 + \left(\frac{V_A \Omega_1}{\frac{1}{T}}\right)^2\right]^{1/2}}$$

where

$$\frac{1}{T} = 0.4\,\frac{\partial \bar{V}_W}{\partial h} = 0.16\left[\frac{kh}{u_{*0}}\frac{\partial \bar{V}_W}{\partial h}\right]\left[\frac{u_{*0}/k}{\bar{V}_{20}}\right]\frac{\bar{V}_{20}}{h}$$

$$\frac{kh}{u_{*0}}\frac{\partial \bar{V}_W}{\partial h} = f(h/\ell') \quad , \quad \text{Figure 2-18}$$

$$1/\ell' = f(R_{i_{20}}) \quad , \quad \text{Figure 2-16}$$

u, v, w refer to turbulence components along the x, y, and z axes of a system aligned to the mean wind such that x is downwind and w is vertically downward.

2.5 REFERENCES

2-1. Skelton, Grant B., *Investigation of Gusts on V/STOL Craft in Transition and Hover,* AFFDL-TR-68-85.

2-2. Garrison, Jan N., "An Assessment of Atmospheric Turbulence Data for Aeronautical Application," Royal Aeronautical Society, *International Conference on Atmospheric Turbulence Proceedings,* 18-21 May 1971.

2-3. Etkin, Bernard, *Dynamics of Atmospheric Flight,* John Wiley & Sons, 1958.

2-4. Pasquill, F., *Wind Structure in the Atmospheric Boundary Layer,* Philosophical Transactions Society, London A269, 1971.

2-5. Etkin, Bernard, *Dynamics of Flight,* John Wiley & Sons.

2-6. *Glossary of Meteorology,* Edited by Huschke, Ralph E., American Meteorological Society, Boston, Mass., 1959.

2-7. Lumley, John L. and Panofsky, Hans A., *The Structure of Atmospheric Turbulence,* Interscience Publishers.

2-8. Johnson, Walter A., and McRuer, Duane T., *Development of a Category II Approach System Model,* NASA CR 2022.

2-9. Plate, B. J., *Aerodynamic Characteristics of Atmospheric Boundary Layers,* Atomic Energy Commission, Division of Technical Information.

2-10. Tennekes, H. and Lumley, J. L., *A First Course in Turbulence,* The MIT Press, Cambridge, Mass. and London, England, 1972.

2-11. Kurkowski, Richard L., Fichtl, George H. and Gera, Joseph, *Development of Turbulence and Wind Shear Models for Simulation Application,* Vol. I, NASA Aircraft Safety and Operating Problems Conference, NASA SP-270-1971.

2-12. Zbrozek, T. K., "Atmospheric Gusts," *Journal of Royal Aeronautical Society*, Vol. 69.

2-13. Joppa, Robert G., *A Proposed Model of Low Altitude Atmospheric Turbulence for Use in V/STOL Aircraft Handling Qualities Studies*, Boeing Document D6-10738, 1965.

2-14. "Circulation of Proposed Wind Model Appendix for Project 417 Based on UK ARB Regulatory Document," Airlines Electronic Engineering Committee Letter No. 70-2-40, July 17, 1970.

2-15. Fichtl, George H., Kaufman, John W., and Vaughan, William W., *The Characteristics of Atmospheric Turbulence as Related to Wind Loads on Tall Structures*, National Bureau of Standards, Dept. of Commerce Building Science Series 30, 1970.

2-16. Panofsky, H. A. and Townsend, A. A., "Change of Terrain Roughness and the Wind Profile," *Royal Meteorological Society Quarterly Journal*, Vol. 90, April 1964.

2-17. Taylor, P. A., "On Wind and Shear Stress Profiles Above a Change in Surface Roughness," *Royal Meteorological Society Quarterly Journal*, Vol. 95, 1969.

2-18. Appleby, J. F. and Dries, T. H., "Wind Variability Over a Complex Surface," AMS/AIAA Paper No. 66-335, March 1966.

2-19. O'Brien, James J., "An Investigation of the Diabatic Wind Profile of the Atmospheric Boundary Layer," *Journal of Geophysical Research*, Vol. 70, No. 10, May 15, 1965.

2-20. Davenport, A. G., "Rationale for Determining Design Wind Velocities," *Journal of the Proceedings of the American Society of Civil Engineers*, Structural Division, May 1960.

2-21. *Civil Aeronautics Manual*, Vol. 4B, Appendix A.

2-22. Brooke, R. R. and Spillane, K. T., "On the Variation of Maximum Wind Gusts with Height," *Journal of Applied Meteorology*, Vol. 9.

2-23. McVehil, G. E., "Wind and Temperature Profiles Near the Ground in Stable Stratification," *Royal Meteorological Society Quarterly Journal*, Vol. 91, 1964.

2-24. Clark, R. H., "Observational Studies in the Atmospheric Boundary Layer," *Royal Meteorological Society Quarterly Journal*, Vol. 96, 1970.

2-25. Panofsky, H. A., Blackador, A. K., and McVehil, G. E., "The Diabatic Wind Profile," *Royal Meteorological Society Quarterly Journal*, Vol. 86, 1960.

2-26. Webb, E. K., "Profile Relationships: the Log-Linear Range, and Extension to Strong Stability," *Royal Meteorological Society Quarterly Journal*, Vol. 96, 1970.

2-27. Davidson, Ben, and Barad, Morton L., "Some Comments on the Deacon Wind Profile," *Transactions, American Geophysical Union*, Vol. 37, No. 2.

2-28. Hanna, Steven R., and Panofsky, Hans A., *Estimation of the 90M Wind from Low-Level Observations*, U. S. Department of Commerce, Weather Bureau.

2-29. Hanna, R. S., "A Method of Estimating Vertical Eddy Transport in the Planetary Boundary Layer Using Characteristics of the Vertical Velocity Spectrum" *Journal of the Atmospheric Sciences*, November 1968, Vol. 25.

2-30. Batchelor, G. K., *The Theory of Homogeneous Turbulence*, Cambridge University Press, London, England, 1956.

2-31. Jones J. G., *A Unified Discrete Gust and Power Spectrum Treatment of Atmospheric Turbulence*, Royal Aeronautic Society/ASAA/CASI International Conference on Atmospheric Turbulence, London, May 1971.

2-32. Jones J. G., *Similarity Theory of Gust Loads on Aircraft Development of Discrete Gust Theory and Introduction to Empirical Functions*, Royal Aircraft Establishment TR-69171, August 1969.

2-33. Jones, J. G., *Gradient Properties of a Model of Stationary Random Turbulence*, Ministry of Technology, Aeronautical Research Council C.P. No. 998, 1968.

2-34. Reeves, Paul M., *A Non-Gaussian Turbulence Simulation*, Technical Report AFFDL-TR-69-67, December 1969.

2-35. Dutton, John A., "The Probabilistic Structure of Clear Air Turbulence--Some Observational Results and Implications," Boeing Scientific Research Laboratories, *Symposium on Clear Air Turbulence and Its Detection*, Seattle, Washington, August 14-16, 1968.

2-36. Franklin, James A., *Turbulence and Lateral-Directional Flying Qualities*, NASA CR-1718, April 1971.

2-37. Gunter, E. D., Jones, W. G., and Monson, R. K., *Low Altitude Atmospheric Turbulence LO-LOCAT Phases I and II*, Technical Report AFFDL-TR-69-12, February 1969.

2-38. Bowne, N. E., and Anderson, G. E., *Takeoff and Landing Critical Atmospheric Turbulence (TOLCAT) Analytical Investigation*, Technical Report AFFDL-TR-68-23, April 1968.

2-39. Fichtl, George H., and McVehil, George B., "Longitudinal and Lateral Spectra of Boundary Layer at the Kennedy Space Center," *Journal of Applied Meteorology*, February 1970.

2-40. Kaimel, J. C., Wyngaard, J. C., Izumi, Y., and Cote, O. R. "Spectral Characteristics of Surface Layer Turbulence," *Royal Meteorological Society Quarterly Journal*, 1972.

2-41. Etkin, B., *Theory of the Flight of Airplanes in Isotropic Turbulence–Review and Extension*, Advisory Group for Aeronautical Research and Development, Report 372, April 1961.

2-42. Chalk, C. R., Neal, T. P., Harris, F. E., and Pritchard, F. E., *Background Information and User Guide for MIL-F-8785B(ASG), "Military Specification–Flying Qualities of Piloted Airplanes,"* Technical Report AFFDL-TR-69-72.

2-43. Jones, W. T., Mieke, H. R., Jones W. G., et al., *Low Altitude Atmospheric Turbulence LO-LOCAT Phase III*, Technical Report AFFDL-TR-70-10, November 1970.

2-44. Ramsdell, V. T., Powell, D. C., and Sandusky, W. F., *Meteorological Information for V/STOL Operations at Ports in Cities–An Analysis*, Battelle Northwest Report BNW 474 (Interim Report for the Period February-July 1972 for DOT Contract DOT-FA72WA1-263).

2-45. Sandaram, T. R., Ludwig, C. R., and Kinner, F. T., "Modeling of the Turbulence Structure of the Atmospheric Surface Layer," *AIAA Journal*, June 1967.

2-46. Pasquill, F., "Some Aspects of Boundary Layer Description," *Royal Meteorological Society Quarterly Journal*, July 1972.

2-47. Dutton, T. A , Panofsky, H. A., Deaven, D. C., Kerman, B. R., and Mirrabella, V., *Statistical Properties of Turbulence at the Kennedy Space Center for Aerospace Vehicle Design*, NASA CR-1889.

2-48. Zbrozek, K. J., *The Relationship Between the Discrete Gust and Power Spectra Presentation of Atmospheric Turbulence With a Suggested Model of Low-Altitude Turbulence*, R&M No. 3216.

2-49. Pitchard, Francis E., *A Statistical Model of Atmospheric Turbulence and a Review of the Assumptions Necessary for Its Use*. AGARD Stability and Control, Part 2, September 1966, AD-665320.

2-50. Houbolt, J. C., *Design Manual for Vertical Gusts Based on Power Spectral Techniques*, Technical Report AFFDL-TR-70-106, December 1970.

2-51. Lappe, Oscar U., "A Low Altitude Turbulence Model for Estimating Gust Loads on Aircraft," AIAA Paper No. 65-14, 1965.

2-52. A.E.E.C. Letter No. 70-1-24, "Circulation of Douglas Wind Data Report," December 18, 1969.

APPENDIX 2A

EXTENSION OF MEAN WIND MODEL TO BOUNDARY LAYER

General expressior for nondimensional shear:

$$\frac{kh}{u_*}\frac{\partial \bar{V}_W}{\partial h} = \phi\left(\frac{h}{\ell'}\right)$$

Friction velocity:

$$u_* = u_{*0}\,[1 - h/d]$$

Therefore,

$$\frac{kh}{u_{*0}}\frac{\partial \bar{V}_W}{\partial h} = \phi\left(\frac{h}{\ell'}\right)[1 - h/d]$$

or

$$\frac{\partial \bar{V}_W}{\partial h} = \frac{u_{*0}}{k}\,\phi\left(\frac{h}{\ell'}\right)\left(\frac{1}{h} - \frac{1}{d}\right)$$

Logarithmic profile (neutral stability)

$$\phi\left(\frac{h}{\ell'}\right) = 1$$

$$\bar{V}_W = \int_{z_0}^{h} \frac{\partial \bar{V}_W}{\partial h}\,dh = \frac{u_{*0}}{k}\left[\ln\left(\frac{h}{z_0}\right) - \left(\frac{h - z_0}{d}\right)\right]$$

Displace origin so that h = 0 coincides with earth's surface:

Replace h with $h + z_0$

$$\bar{V}_W = \frac{u_{*0}}{k}\left[\ln\left(\frac{h + z_0}{z_0}\right) - \frac{h}{d}\right]$$

For low altitudes,

$$\nabla_w = \frac{u_{*0}}{k} \ln \left(\frac{h + z_0}{z_0} \right)$$

Log-linear profile (h/ℓ′ small)

$$\Phi (h/\ell') \cong 1 + \alpha' h/\ell'$$

$$\frac{kh}{u_{*0}} \frac{\partial \bar{V}_W}{\partial h} = \left[1 - \frac{h}{d} \right] \left[1 + \alpha' \frac{h}{\ell'} \right] = 1 + h \left[\frac{\alpha'}{\ell'} - \frac{1}{d} \right] - \frac{\alpha' h^2}{\ell' d}$$

$$\frac{\partial \bar{V}_W}{\partial h} = \frac{u_{*0}}{k} \left[\frac{1}{h} + \left(\frac{\alpha'}{\ell'} - \frac{1}{d} \right) - \frac{\alpha' h}{\ell' d} \right]$$

$$\bar{V}_W = \int_{z_0}^{h} \frac{\partial \bar{V}_W}{\partial h} dh = \frac{u_{*0}}{k} \left[\ln \left(\frac{h}{z_0} \right) + \left(\frac{\alpha'}{\ell'} - \frac{1}{d} \right) (h - z_0) - \alpha' \frac{\left(h^2 - z_0^2 \right)}{2 \ell' d} \right]$$

Shift origin so that h = 0 coincides with the surface:

Replace h with $h + z_0$

$$\bar{V}_W = \frac{u_{*0}}{k} \left[\ln \left(\frac{h + z_0}{z_0} \right) + \alpha' \frac{h}{\ell'} - \frac{h}{d} - \frac{\alpha'}{2} \frac{h}{\ell'} \frac{h}{d} - \alpha' \frac{h}{\ell'} \frac{z_0}{d} \right]$$

The term $\alpha' h/\ell' z_0/d$ may be ignored as being negligibly small; thus,

$$\bar{V}_W = \frac{u_{*0}}{k} \left[\ln \frac{h + z_0}{z_0} - \frac{h}{d} + \alpha' \frac{h}{\ell'} \left(1 - \frac{1}{2} \frac{h}{d} \right) \right]$$

The increment for nonneutral stability is recognized as $\alpha' \frac{h}{\ell'} \left(1 - \frac{1}{2} \frac{h}{d} \right)$ At low altitudes this equation reduces to that for $u_* = u_{*0}$ = constant:

$$\bar{V}_W = \frac{u_{*0}}{k} \left[\ln \left(\frac{h + z_0}{z_0} \right) + \alpha \frac{h}{\ell'} \right]$$

General profile

$$\frac{kh}{u_{*0}}\frac{\partial \bar{V}_W}{\partial h} = \Phi\left(\frac{h}{\ell'}\right)\left(1-\frac{h}{d}\right) = \left(1-\frac{h}{d}\right) + \left[\Phi\left(\frac{h}{\ell'}\right) - 1\right]\left(1-\frac{h}{d}\right)$$

The term (1 - h/d) is recognized as the neutral stability term. The contribution of the nonneutral term is denoted as f[(h/ℓ'), (h/d)]. For constant friction velocity, equivalent to h/d = 0, $f(h, \ell', h/d)\big|_{h/d=0} = f(h/\ell')$:

$$f\left(\frac{h}{\ell'}\right) = \int_0^h \frac{\left[\Phi\left(\frac{h}{\ell'}\right) - 1\right]}{h} dh, \qquad \left(\frac{h}{d} = 0\right)$$

$$\bar{V}_W = \frac{u_{*0}}{k}\left[\ln\left(\frac{h+z_0}{z_0}\right) - \left(\frac{h}{d}\right) + f\left(\frac{h}{\ell'}, \frac{h}{d}\right)\right]$$

$$f\left(\frac{h}{\ell'}, \frac{h}{d}\right) = \int_0^h \frac{\left[\Phi\left(\frac{h}{\ell'}\right) - 1\right]\left(1-\frac{h}{d}\right)}{h} dh$$

$$= \int_0^h \left[\frac{\Phi(h/\ell') - 1}{h}\right] dh - \frac{1}{d}\int_0^h \left[\Phi\left(\frac{h}{\ell'}\right) - 1\right] dh$$

$$= f\left(\frac{h}{\ell'}\right) - \frac{1}{d}\int_0^h \left[\Phi\left(\frac{h}{\ell'}\right) - 1\right] dh$$

The remaining integral may be written as

$$\int_0^h \left[\Phi\left(\frac{h}{\ell'}\right) - 1\right] dh = \int_0^h \left[\frac{\Phi\left(\frac{h}{\ell'}\right) - 1}{h}\right] h\,dh$$

and integrated by parts:

$$\int udv = uv - \int vdu$$

$$u = h \qquad dv = \frac{\Phi\left(\frac{h}{\ell'}\right) - 1}{h} dh$$

$$du = dh \qquad v = f\left(\frac{h}{\ell'}\right)$$

$$\int_0^h \left[\Phi\ \frac{h}{\ell'} - 1\right] dh = h f\left(\frac{h}{\ell'}\right) - \int_0^h f\left(\frac{h}{\ell'}\right) dh$$

$$f\left(\frac{h}{\ell'}, \frac{h}{d}\right) = f\left(\frac{h}{\ell'}\right) - \frac{h}{d} f\left(\frac{h}{\ell'}\right) + \frac{1}{d}\int_0^h f\left(\frac{h}{\ell'}\right) dh$$

$$= f\left(\frac{h}{\ell'}\right)\left[1 - \frac{h}{d}\right] + \frac{1}{d}\int_0^h f\left(\frac{h}{\ell'}\right) dh$$

if $h/\ell' < 0$

$$f\left(\frac{h}{\ell'}, \frac{h}{d}\right) = f\left(\frac{h}{\ell'}\right)\left[1 - \frac{h}{d}\right] + \frac{h/d \int_0^{-h/\ell'} f(\xi)\, d\xi}{(-h/\ell')}, \quad \left(\xi = -\frac{h}{\ell'}\right)$$

if $h/\ell' > 0$

$$f\left(\frac{h}{\ell'}, \frac{h}{d}\right) = f\left(\frac{h}{\ell'}\right)\left[1 - \frac{h}{d}\right] + \frac{h/d \int_0^{-h/\ell'} f(\xi)\, d\xi}{h/\ell'}, \quad \left(\xi = \frac{h}{\ell'}\right)$$

When $f(h/\ell') = \alpha'(h/\ell')$, the general form must reduce to the log-linear equation:

If $f(h/\ell') = \alpha'(h/\ell')$, then

$$f\left(\frac{h}{\ell'}, \frac{h}{d}\right) = \alpha' \frac{h}{\ell'}\left(1 - \frac{h}{d}\right) + \frac{1}{d}\int_0^h \alpha \frac{h}{\ell'}\, dh$$

$$= \alpha' \frac{h}{\ell'}\left(1 - \frac{h}{d}\right) + \frac{\alpha}{2}\frac{h^2}{d\ell}$$

$$= \alpha \frac{h}{\ell'} - \frac{\alpha h^2}{2d\ell} = \alpha \frac{h}{\ell'}\left(1 - \frac{1}{2}\frac{h}{d}\right)$$

$$= f\left(\frac{h}{\ell'}\right) - \frac{\alpha}{2}\frac{h}{\ell'}\frac{h}{d'}$$

This is the same as obtained for the log-linear profile. The log-linear profile has been described as applicable for the stable region of $0 < h/\ell' < 1$.

For the region $h/\ell' > 1$, $f(h/\ell')$ has been described as

$$f(h/\ell') = \alpha' \left[1 + \ln(h/\ell')\right]$$

Thus,

$$f\left(\frac{h}{\ell'}, \frac{h}{d}\right) = \alpha'\left[1 + \ln\left(\frac{h}{\ell'}\right)\right]\left[1 - \frac{h}{d}\right] + \frac{1}{d}\int_0^h f\left(\frac{h}{\ell'}\right) dh$$

$$= \alpha'\left[1 + \ln\left(\frac{h}{\ell'}\right)\right]\left[1 - \frac{h}{d}\right] + \frac{1}{d}\int_0^{\ell'} \alpha'\frac{h}{\ell'}\, dh + \frac{1}{d}\int_{\ell'}^h \alpha'\left[1 + \ln\frac{h}{\ell'}\right] dh$$

$$= \alpha'\left[1 + \ln\left(\frac{h}{\ell'}\right)\right]\left[1 - \frac{h}{d}\right] + \frac{\alpha'}{d}\left\{\frac{\ell'}{2} + h\ln\left(\frac{h}{\ell'}\right)\right\}$$

$$= \alpha'\left\{1 + \ln\left(\frac{h}{\ell'}\right) - \frac{h}{d}\left[1 - \frac{1}{2}\frac{1}{(h/\ell')}\right]\right\}$$

$$f\left(\frac{h}{\ell'}, \frac{h}{d}\right) = f\left(\frac{h}{\ell'}\right) - \alpha'\left(\frac{h}{d}\right)\left[1 - \frac{1}{2}\frac{1}{(h/\ell')}\right]$$

In summary, the effect of linearly decreasing friction velocity is to change the wind profile from

$$\bar{V}_W = \frac{u_{*0}}{k}\left[\ln\left(\frac{h+z_0}{z_0}\right) + f\left(\frac{h}{\ell'}\right)\right]$$

to

$$\bar{V}_W = \frac{u_{*0}}{k}\left[\ln\left(\frac{h+z_0}{z_0}\right) - \frac{h}{d} + f\left(\frac{h}{\ell'}, \frac{h}{d}\right)\right]$$

where the function $f(h/\ell', h/d)$ is expressed as:

$$f\left(\frac{h}{\ell'}, \frac{h}{d}\right) = f\left(\frac{h}{\ell'}\right) - \frac{1}{d}\int_0^h (\Phi - 1)\, dh$$

where $\Phi = (kh/u_{*_0})(\partial \bar{V}_W/\partial h)$, or

$$f\left(\frac{h}{\ell'}, \frac{h}{d}\right) = f\left(\frac{h}{\ell'}\right)\left(1 - \frac{h}{d}\right) + \frac{1}{d}\int_0^h f\left(\frac{h}{\ell'}\right) dh$$

For stable conditions, $f[(h/\ell'), (h/d)]$ is given by

$$0 < \frac{h}{\ell'} < 1 \quad , \quad f\left(\frac{h}{\ell'}\right) = \alpha' \frac{h}{\ell'}$$

$$f\left(\frac{h}{\ell'}, \frac{h}{d}\right) = f\left(\frac{h}{\ell'}\right) - \frac{\alpha'}{2}\frac{h}{\ell'}\frac{h}{d}$$

$$\frac{h}{\ell'} > 1 \quad , \quad f\left(\frac{h}{\ell'}\right) = \alpha'\left[1 + \ln\frac{h}{\ell'}\right]$$

$$f\left(\frac{h}{\ell'}, \frac{h}{d}\right) = f\left(\frac{h}{\ell'}\right) - \alpha'\left(\frac{h}{d}\right)\left[1 - \frac{1}{2}\frac{1}{(h/\ell')}\right]$$

3.0 PROBABILISTIC DESCRIPTION OF THE LOW ALTITUDE ATMOSPHERE

In this section are presented descriptions of atmospheric conditions in the lower atmosphere as obtained from (1) airports around the U.S., (2) a literature survey of tower measurements, and (3) analysis of measurements from two U.S. towers.

Simulation of atmospheric conditions should be based on knowledge of the real atmosphere and its interactions. While a complete simulation of the lower atmosphere would be a very large task indeed, it is possible to describe in some detail the conditions one might expect and the general form of the relationships between variables of interest.

Perhaps the primary variables of interest to low altitude simulation are wind speed and direction, together called "wind velocity." These are described in some detail, first by a general description obtained by averaging the conditions at 24 U.S. airports for one height, and then by descriptions of the vertical changes (shears) as determined by a literature survey and by actual measurements from two towers.

Another variable of interest is the Richardson's number, R_i, which is a measure of the stability of the atmosphere and is determined by the vertical wind and temperature gradients. Using the two sets of tower observations the interrelationships between wind speed, speed and direction shears, and Richardson's numbers are obtained. This information is analyzed and a description given which is applicable to the simulation portions of this study.

3.1 LIST OF SYMBOLS

h	Height above ground surface, feet (unless otherwise noted)
$\bar{V}_W$	Mean speed in knots
ϕ	Direction from which the wind is blowing
R_i	Richardson's number
$\frac{\partial \bar{V}_W}{\partial h}$	Wind speed shear
$\frac{\partial \phi}{\partial h}$	Wind direction shear

3.2 NEAR-SURFACE WIND AND WIND SHEAR INFORMATION

This section discusses three atmospheric properties: (1) wind speed, direction, and crosswind near the surface, (2) mean wind profiles near the surface, and (3) wind speed and direction shears. Discussion of the first leads to a new model for wind speed, direction, and crosswind at 20 feet elevation, the standard for Weather Service anemometer height at airports.

The second discussion briefly outlines the mean wind speed at several levels in the lower layers of the atmosphere. Three locations are studied indicating the variability between locations and providing an introduction to the wind shears of importance as far as aircraft are concerned. (Mean profiles are seldom realized in nature.)

The third part of this section outlines near-surface wind shear information obtained from the literature for a variety of locations and topographic conditions. This last part provides background information for the analysis of tower data processed for this study and described in Section 3.3.

3.2.1 Evaluation of Surface (20-Foot) Wind Descriptions

3.2.1.1 Wind Speed

This part of the study is the development of a realistic description of the distribution of annual mean wind speed at the local airport anemometer height (approximately 20 feet). Wind speed and its probability distribution at an airport vary with a number of parameters, including, but not limited to:

- Local climate
- Topography and roughness of the surrounding area
- Geographical location
- Frequency and severity of large and small scale storms
- Height of the anemometer
- Peculiarities unique to the site (for example, on-shore and off-shore winds during the summer)
- Types of instruments and location with respect to supporting equipment, wind direction, and method of recording

Thus, a wide variance between airports is to be expected, and any model can only be some average of a number of locations.

Historically, airport anemometer height has varied from less than 20 feet to more than 120 feet above the ground and has been a function not only of the airport but of the period of record at some airports. There has been an attempt to standardize the U.S. Weather Service anemometer height of 20 feet and location between or near the runways since approximately 1938. Unfortunately, Weather Service climatological normals were established before this procedure could be implemented at most airports. Thus, the climatological wind data in the literature (usually Weather Service documents) are given for various heights above the ground. Often 10 year averages and distributions at a particular station were computed from wind speeds at two or three heights because the instrument location and height had been changed during the period of record.

Realizing these difficulties, a representative wind speed distribution description was established from data obtained for all 24 airports across the U.S. where the anemometer height during the period of record was between 20 and 35 feet, as listed in Reference 3-1.

Figure 3-1 is a chart indicating the percent probability of exceedance of wind speeds equal to or greater than the speeds indicated for a composite of the 24 airports. This is assumed to be representative of a greater number of airports nationwide. Figure 3-2 is a histogram of the same information.

A total of approximately 170,000 hourly wind speeds (10 minute averages on the hour) were used in the analysis and description. The ARB model, identical to the present FAA model, Reference 3-2, was also developed from 10 minute averages, but the sample size was about 1000 "worldwide in-service operations of U.K. airlines," and the anemometer heights were assumed to be at 33 feet, or some 6 or 7 feet higher than the average height in our study, Reference 3-3. Some may have been much higher. The descriptions are compared in Figure 3-3.

Another description was derived from all 132 airports provided in Reference 3-1. The The average anemometer height is approximately 55 feet. This height difference is reflected in a wider distribution of wind speeds; for instance, at 1% probability the 24 airport composite speed is 22.3 knots and for all 132 cases it is 24.5 knots.

Watson, in a paper presented to the World Meteorological Organization, produces another description, Reference 3-4. The spread of speed values is much greater. His information was compiled from several world locations, the total number of observations is unknown, anemometer heights varied from the "surface level" to 130 feet, and the estimated curve was derived by weighting the data at each airport by the number of BOAC operations there. Such a single-airline description is not appropriate for this study.

It is apparent that the 24 airport description contains speeds slightly less than the ARB and other models for percent probability of exceedance values less than 50%. However, this is to be expected of a description designed for an anemometer height of 20 feet, the lowest of all the studies.

Recently Marut, et al., of the Weather and Flight Service Station Branch of the FAA, prepared a study in which a composite wind speed table was developed from the wind speeds at 39 U.S. airports during periods of fog with visibility of one-half mile or less and no precipitation, Reference 3-5. These conditions and strong wind shears could be exceptionally dangerous for landing or departing airplanes. Therefore, Marut, et al., data are shown in Figure 3-3 for comparison with the all-weather speed probabilities. It is apparent that wind speeds are light during fog conditions; for instance, less than 1% of the speeds equal or exceed 14 knots. (This may be lower still if the speeds were reduced to the 20 foot height because of the normal decrease in wind speed with decrease in elevation.)

3.2.1.2 Wind Direction

The preceding section describes wind speed. This section will describe wind direction related to runway orientation. One may ascertain from this information the frequency of occurrence of crosswinds.

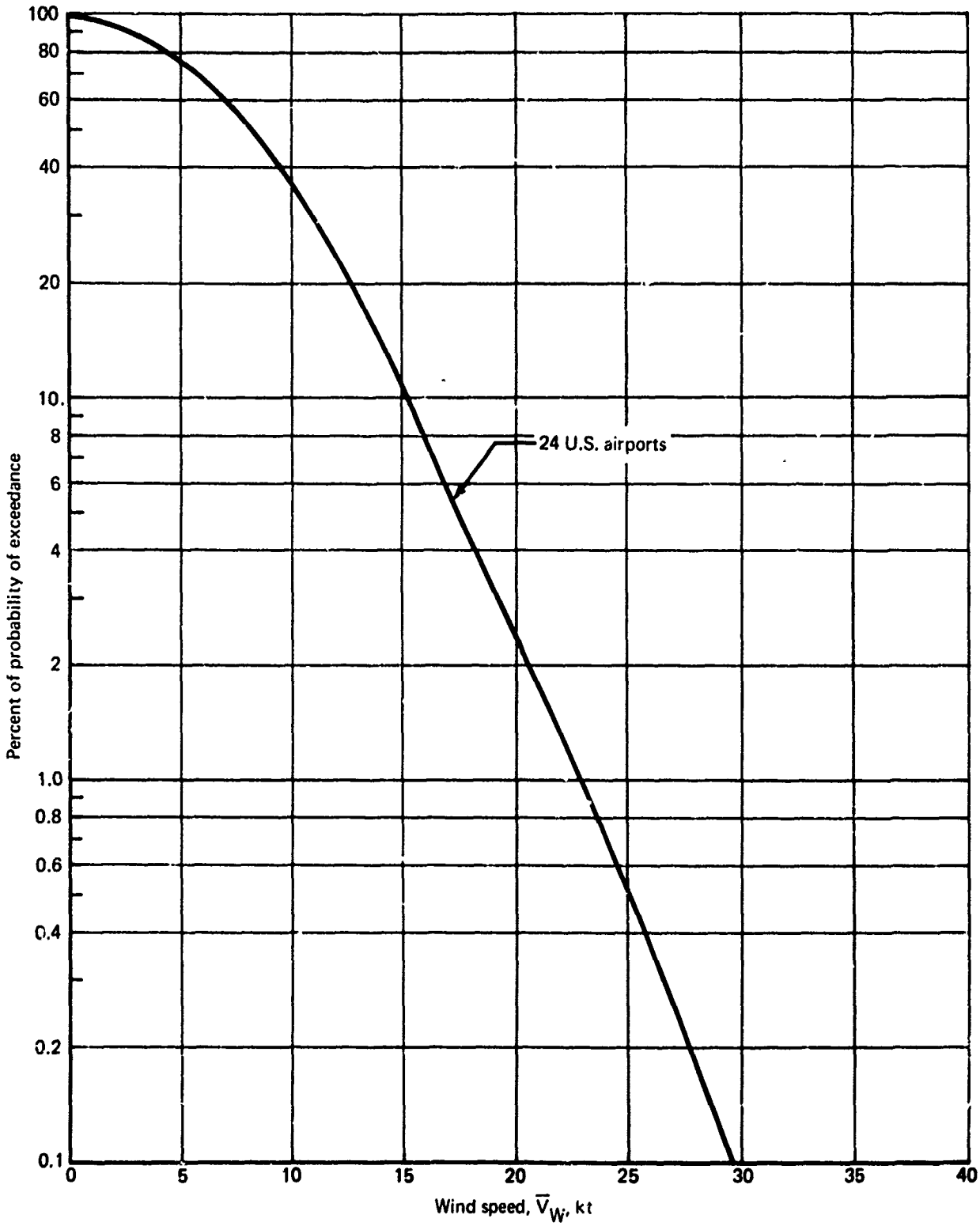

FIGURE 3-1.–ANNUAL PERCENT PROBABILITY OF MEAN WIND SPEED EQUALING OR EXCEEDING GIVEN VALUES

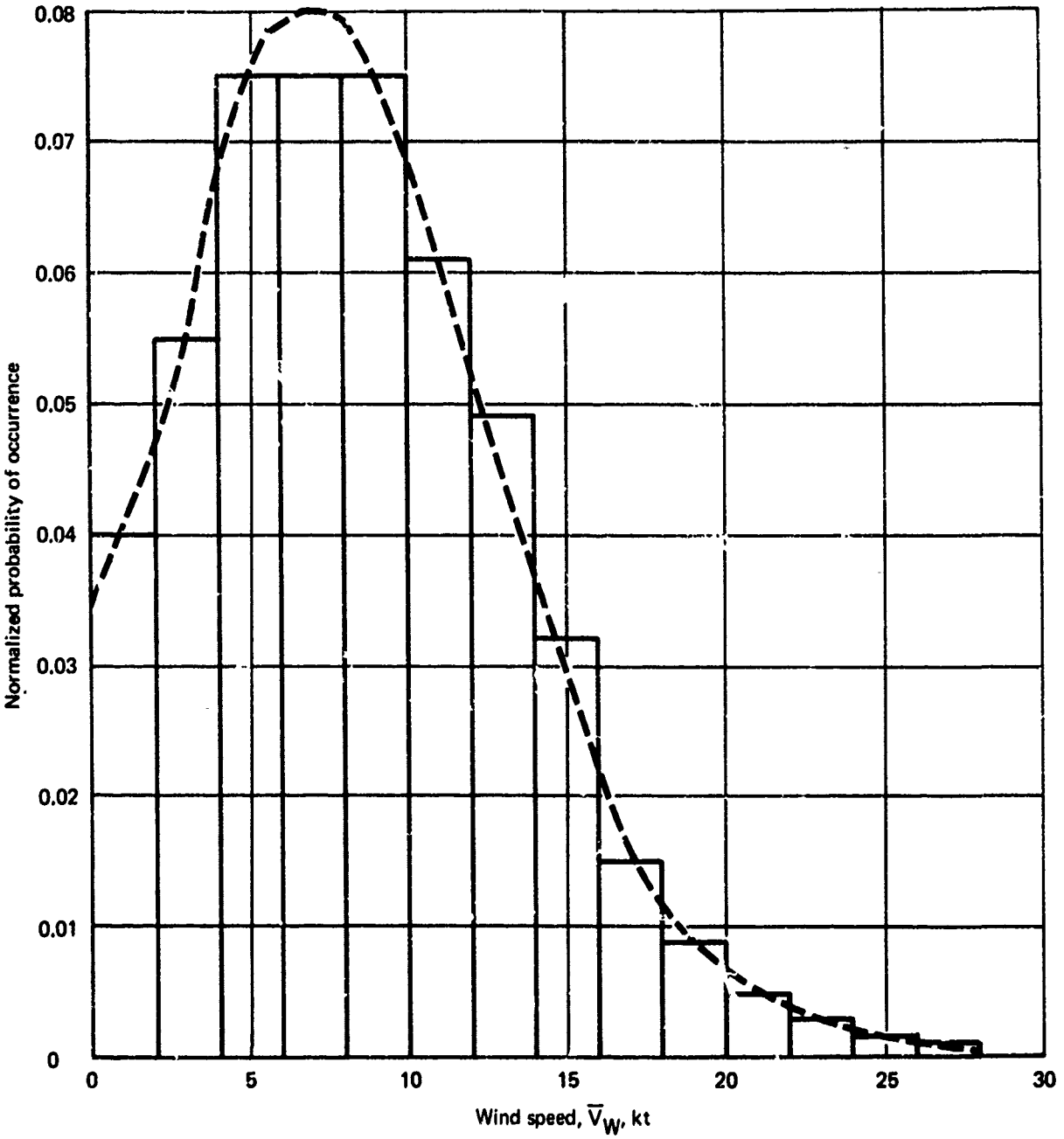

FIGURE 3-2.--WIND SPEED DESCRIPTION, NORMALIZED PROBABILITY OF OCCURRENCE, 24 U.S. AIRPORTS

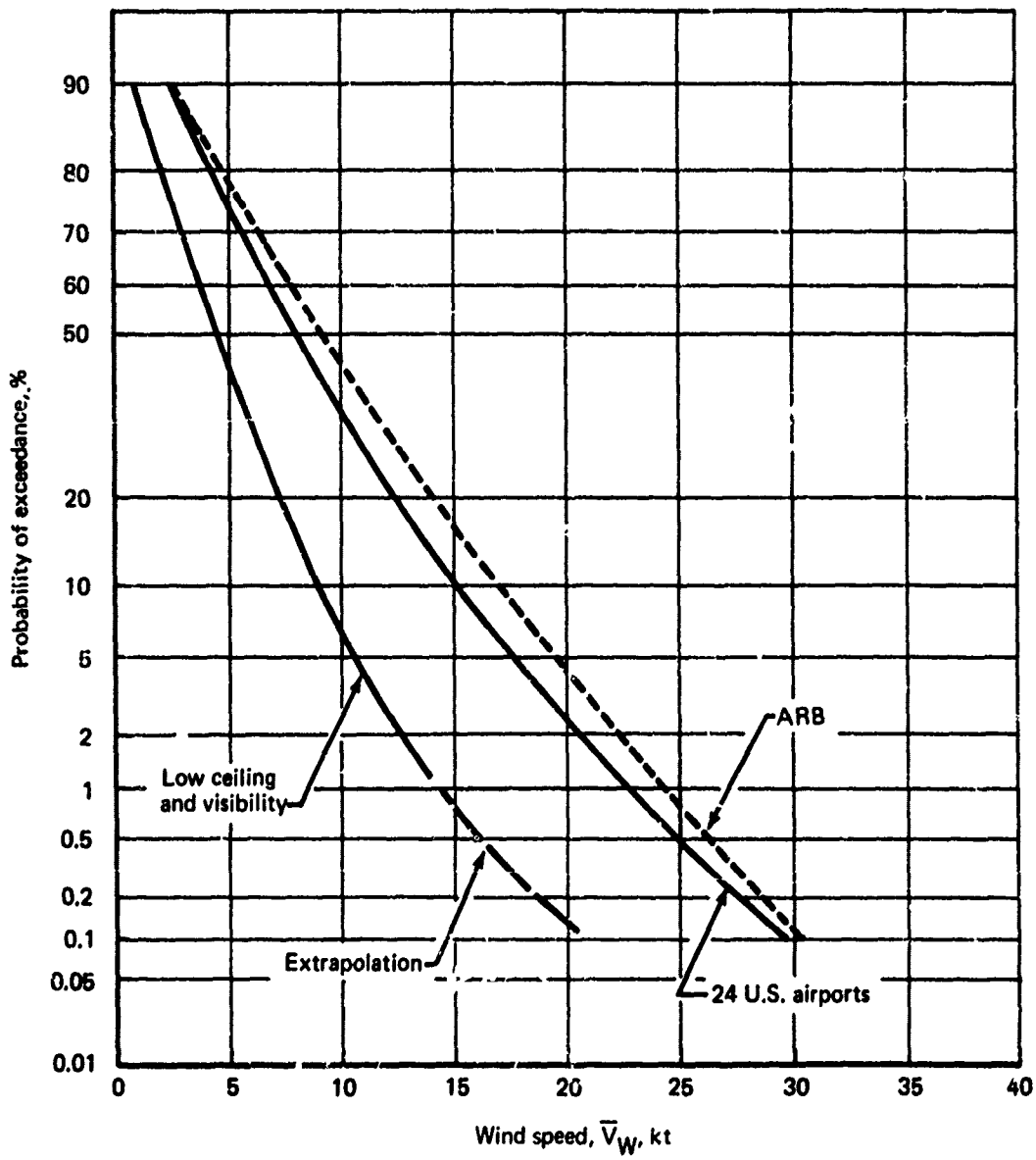

FIGURE 3-3.–COMPARISON OF WIND SPEED DESCRIPTIONS

Wind direction (direction *from* which the wind is coming) is related to the controlling parameters described in the previous discussion concerning wind speed, and no single description will be appropriate at a particular airport. Therefore, the description is only the "general case," an average of directional frequencies from the 24 airports used for the wind speed description.

The general case was developed from the airport wind roses and a knowledge of the major runway orientations at these airports. The wind direction along the runway having the greater frequency of occurrence was given the 0° orientation. (Obviously, the other wind direction along the runway became 180°.) Having oriented all the wind roses in this manner, the average frequencies of occurrence of wind directions relative to the 0° orientation were obtained. These are shown in Figure 3-4. The result indicates that 50% of the time annually the surface wind is either from ±35° of the runway orientation or calm.

A composite runway wind rose, including speed, was also compiled and is shown in Table 3-1.

3.2.1.3 Crosswinds

The probability distribution of crosswinds was computed using a graphical method described by Harold L. Crutcher, of the National Climatic Center, Reference 3-6. The resulting crosswind speed distribution, provided in Figure 3-5, indicates the percentage probabilities from each side of the runway; negative values indicate crosswinds from the left side of the runway in the *upwind* direction, positive values from the right side of the runway in the same direction. Probabilities from both sides may be added to obtain percent frequencies of crosswinds regardless of direction, Figure 3-6. Comparing this last figure with the ARB crosswind model indicates a definite similarity but with slightly lower probabilities for speeds greater than 5 knots. The total probabilities of crosswinds from the right and left are very nearly equal, 0.501 to 0.499, respectively, ignoring calm conditions.

3.2.1.4 Headwind-Tailwind Description

A headwind-tailwind description was computed for directions oriented 90° to those in the crosswind description, and using the same technique, Figure 3-7. Winds from 0° are arbitrarily designated headwinds; those from 180° are designated tailwinds (although they would be headwinds to an airplane landing toward 180°). The total probabilities of headwinds and tailwinds are 0.59 versus 0.41, respectively, ignoring calm conditions. Total headwind-tailwind percent frequencies are shown in Figure 3-8.

3.2.2 Mean Profiles From Instrumented Towers

Mean wind profiles are indicative of average conditions at particular heights. A curve is often drawn through these average values and to some readers this curve indicates an average curve or set of shears to be found at a particular site at a particular time. This is not the case, and the shears indicated in this manner may occur infrequently at any interval and seldom at all tower intervals simultaneously. The important, to aviation, true wind shears for various tower intervals are discussed in Section 3.2.3.

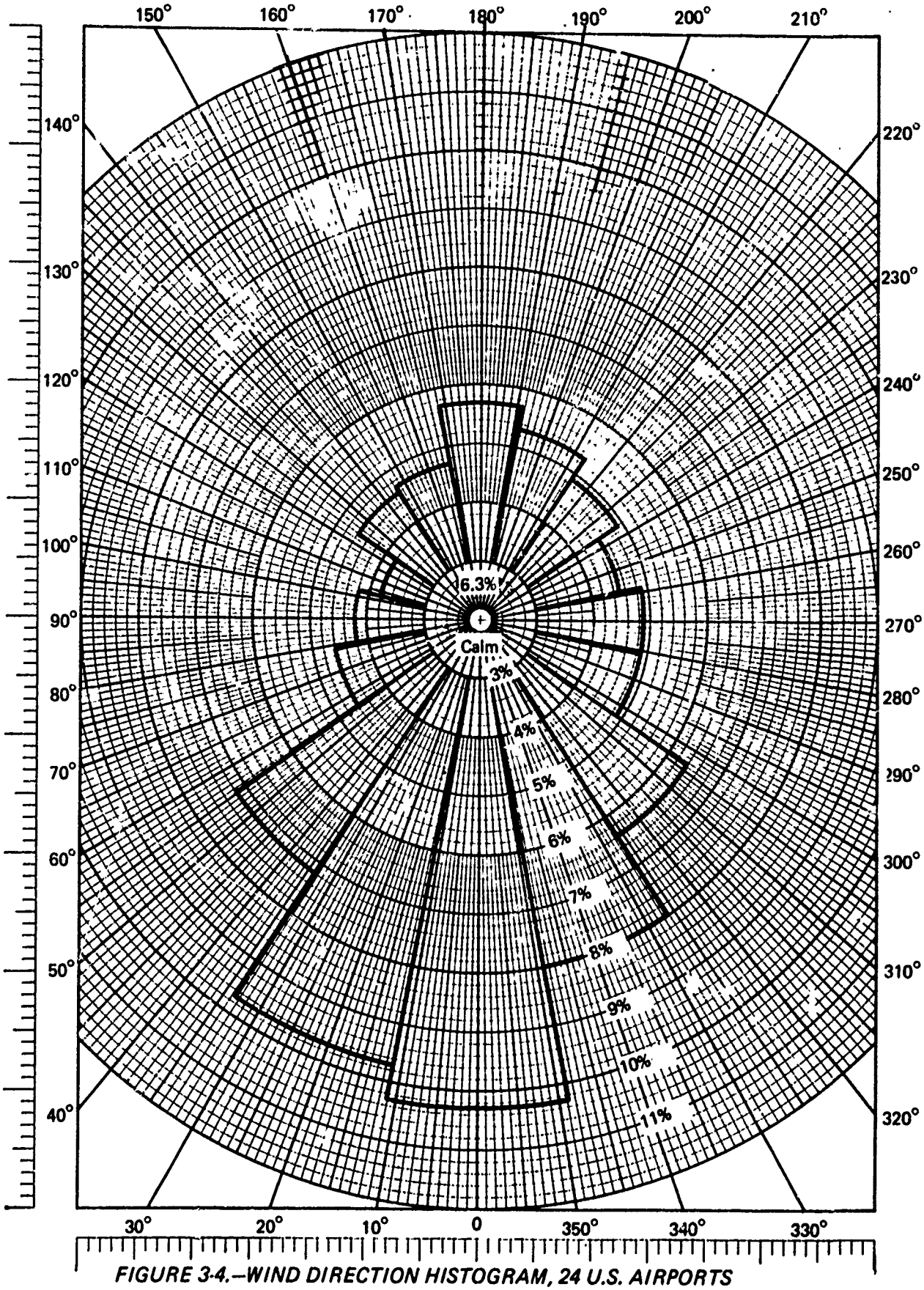

FIGURE 3-4.—WIND DIRECTION HISTOGRAM, 24 U.S. AIRPORTS (PERCENT FREQUENCY OF OCCURRENCE OF DIRECTIONS FROM WHICH WIND IS COMING)

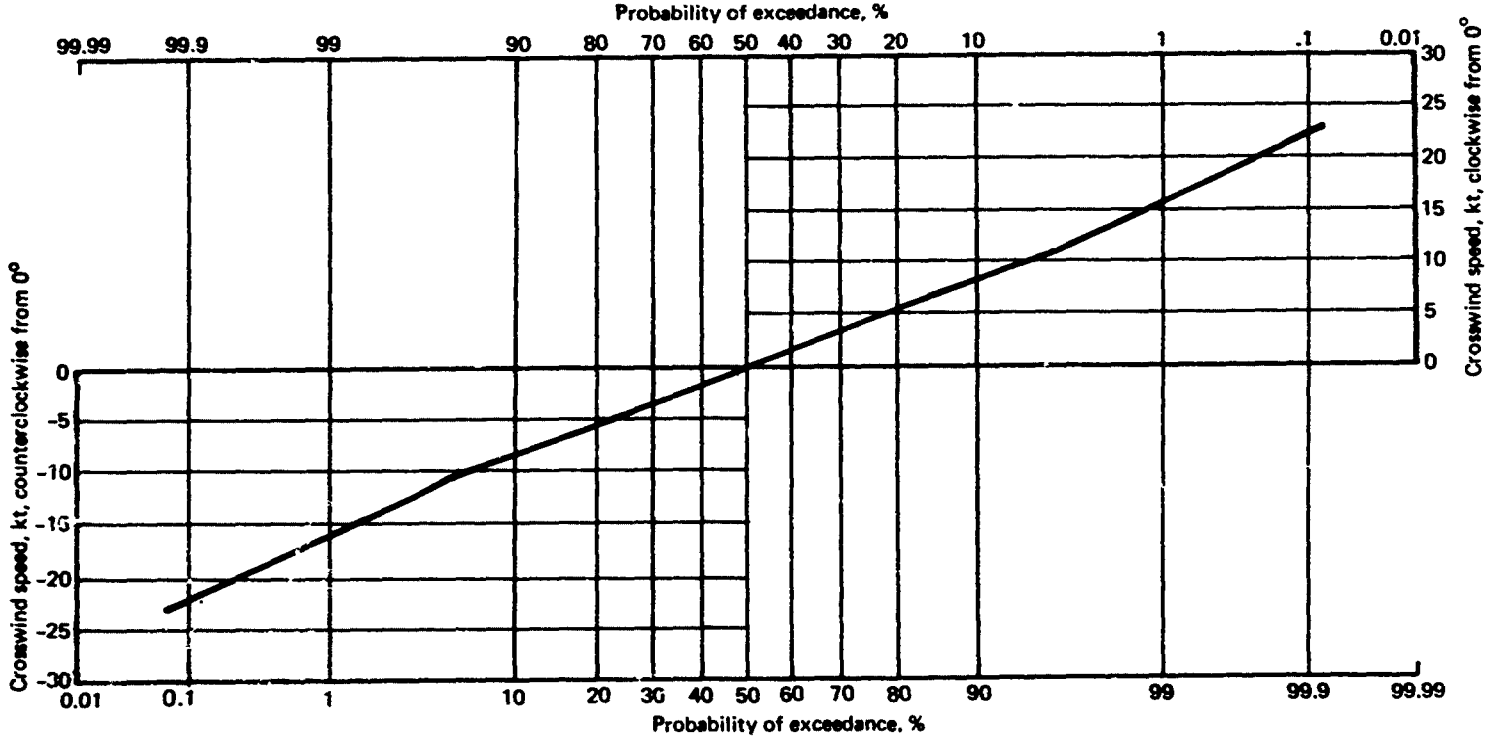

FIGURE 3-5.—CROSSWIND DESCRIPTION COMPILED FROM 24 U.S. AIRPORTS

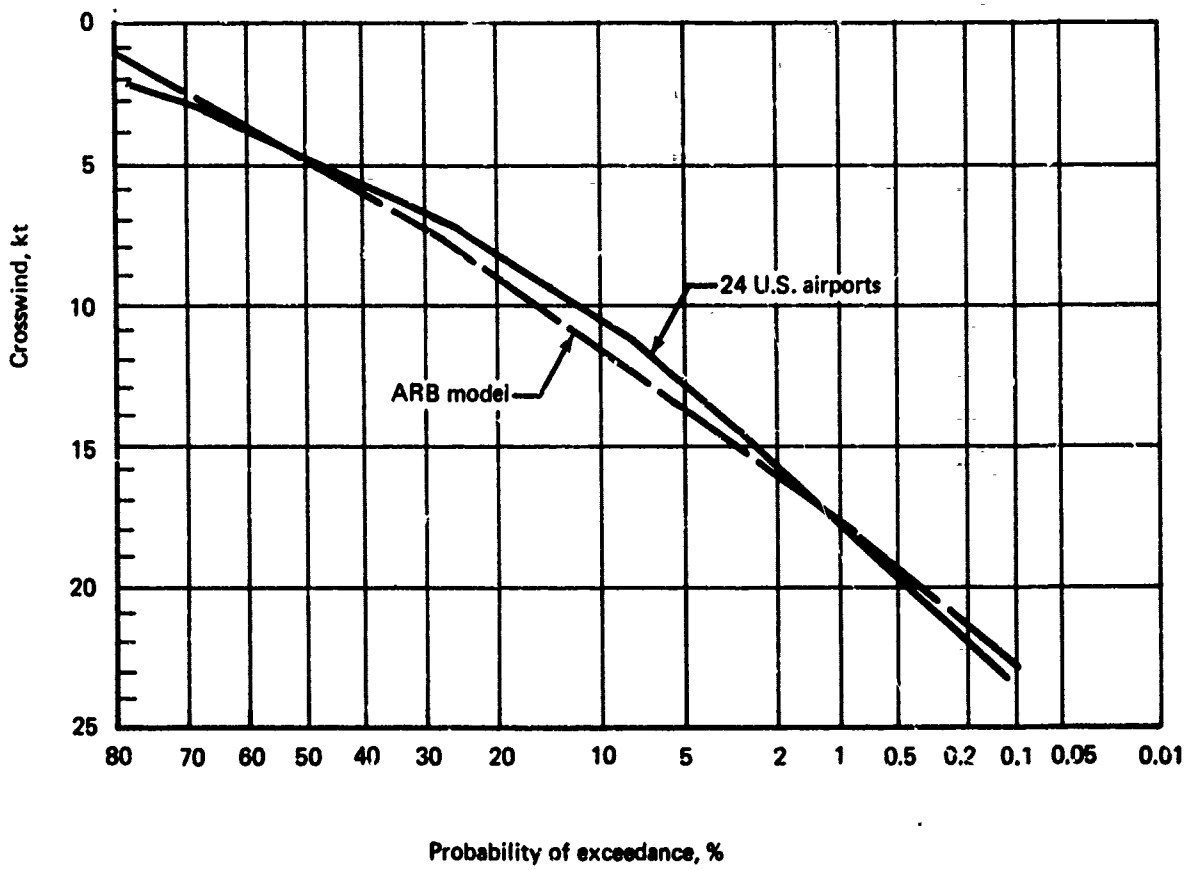

FIGURE 3-6.—TOTAL CROSSWIND INFORMATION COMPILED FROM 24 U.S. AIRPORTS AND ARB MODEL

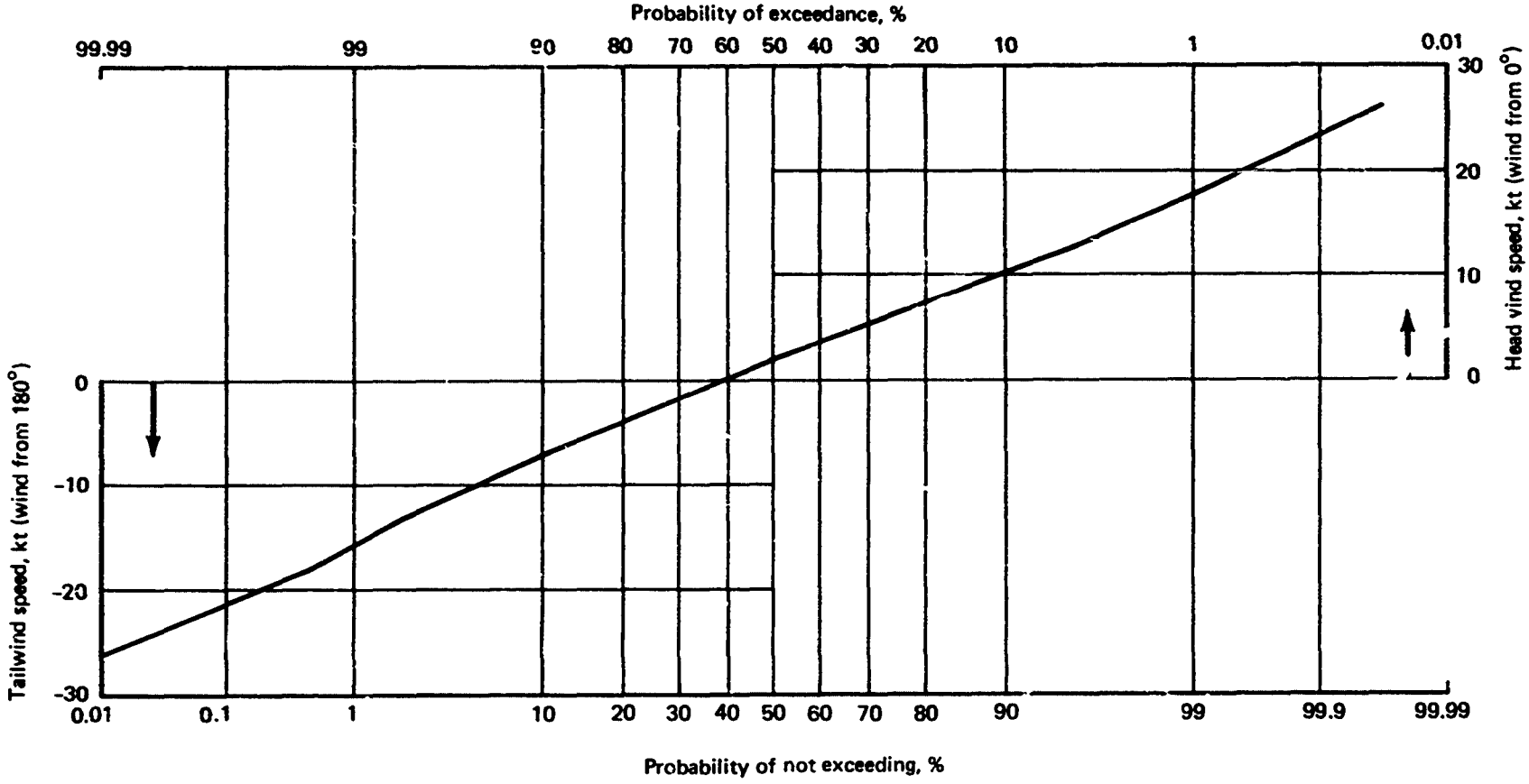

FIGURE 3-7.–HEADWIND–TAILWIND DESCRIPTION COMPILED FROM 24 U.S. AIRPORTS

TABLE 3-1.–WIND ROSE MODEL RELATIVE TO RUNWAY ORIENTATION

Median direction (deg)	1-3	4-6	7-10	11-16	17-21	22-27	28-33	34-40	41	Heading frequency (%)	Average speed (kn)
0	0.8	2.4	3.5	2.6	0.8	0.2	+	+	+	10.3	9.0
22.5	0.6	2.1	3.3	2.9	0.6	0.1	+	+	+	9.7	9.2
45.0	0.6	1.8	2.6	1.8	0.3	+	+	+	+	7.2	8.6
67.5	0.4	1.3	1.6	1.1	0.2	+	+	+	+	4.6	8.5
90.0	0.5	1.3	1.4	0.8	0.2	+	+	+	+	4.2	7.8
112.5	0.4	1.1	1.3	0.8	0.2	+	+	+	+	3.8	7.8
135.0	0.6	1.4	1.5	0.9	0.2	+	+	+	+	4.6	7.8
157.5	0.5	1.4	1.6	1.0	0.2	+	+	+	+	4.7	8.3
180.0	0.7	1.8	1.9	1.1	0.2	+	+	+	+	5.7	8.1
202.5	0.5	1.6	1.8	1.0	0.2	+	+	+	+	5.3	8.4
225.0	0.6	1.4	1.6	1.0	[illegible]	+	+	+	+	4.9	8.1
247.5	0.5	1.3	1.4	1.0	0.3	+	+	+	+	4.5	8.1
270.0	0.6	1.4	1.6	1.0	0.3	+	+	+	+	4.9	7.7
292.5	0.5	1.4	1.7	1.1	0.2	+	+	+	+	4.9	7.9
315.0	0.8	1.8	2.1	1.3	0.3	0.1	+	+	+	6.4	7.9
337.5	0.6	1.9	2.7	2.1	0.6	0.1	+	+	+	8.0	8.7
Calm										6.3	
										100.0	
Wind speed frequency	9.2	25.4	31.6	21.5	5.0	1.0	+	+	+		
Exceedance probability	93.7	84.5	59.1	27.5	6.0	1.0	+	+	+		
+ = ≤0.05											

The curves of Figure 3-9 are provided to indicate the average wind speeds to be expected at heights in the lowest few hundred feet and to show the general increase of speed with height. Examples are provided for three locations.

In the figure is shown the mean annual speed profile for Hanford, Washington, with values given for the 50, 200, and 400 foot levels, Reference 3-7, pages 10.59, 10.63, and 10.67. The difference in average conditions between 400 and 50 feet is 3.2 knots. Composite wind shear data provided on page 10.55 indicate an average shear of 6.1 knots between the 400 and 50 foot heights, or nearly twice that indicated by the mean profile. Thus, the profile of the means is not the same as the mean of the profiles.

Similar annual profiles for Oklahoma City and Cape Kennedy are also shown in the figure, References 3-8 and 3-9. It may be seen that in the lower layers the differences in mean speeds over given height intervals increase as the mean speeds increase.

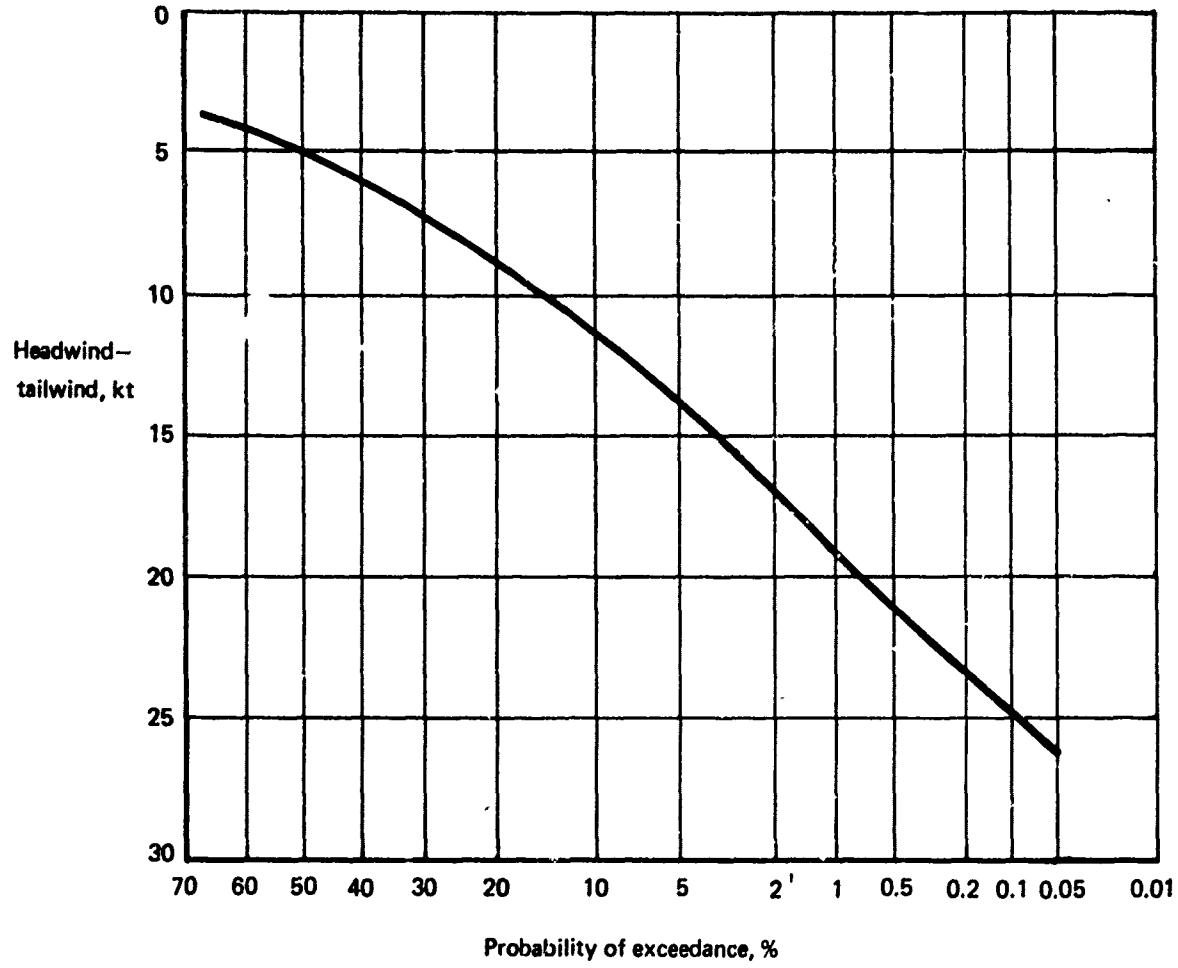

FIGURE 3-8.--TOTAL HEADWIND/TAILWIND, MEAN OF 24 U.S. AIRPORTS

3.2.3 Evaluation of Near-Surface Wind Shear Information From the Literature

The literature search disclosed observations of vertical shears of horizontal mean winds at only a few locations. Few tall towers are instrumented for meteorological purposes, and wind shear frequency information in the open literature is not available even for all of these.

The World Meteorological Organization in 1964 requested member countries to "carry out studies relating to the occurrence of vertical wind shear in the layer between 10 and 100 meters above ground level at appropriate locations, preferably at international aerodromes (airports) on a worldwide basis." Responses to this request have been published in Reference 3-10. Other reports on this subject by these and other investigators were uncovered by the literature search. Results are in widely differing formats, measurement units, and conditions. This handicap has been overcome to some degree, and the results are given here in similar format and units where possible, along with comments on the conclusions of the authors.

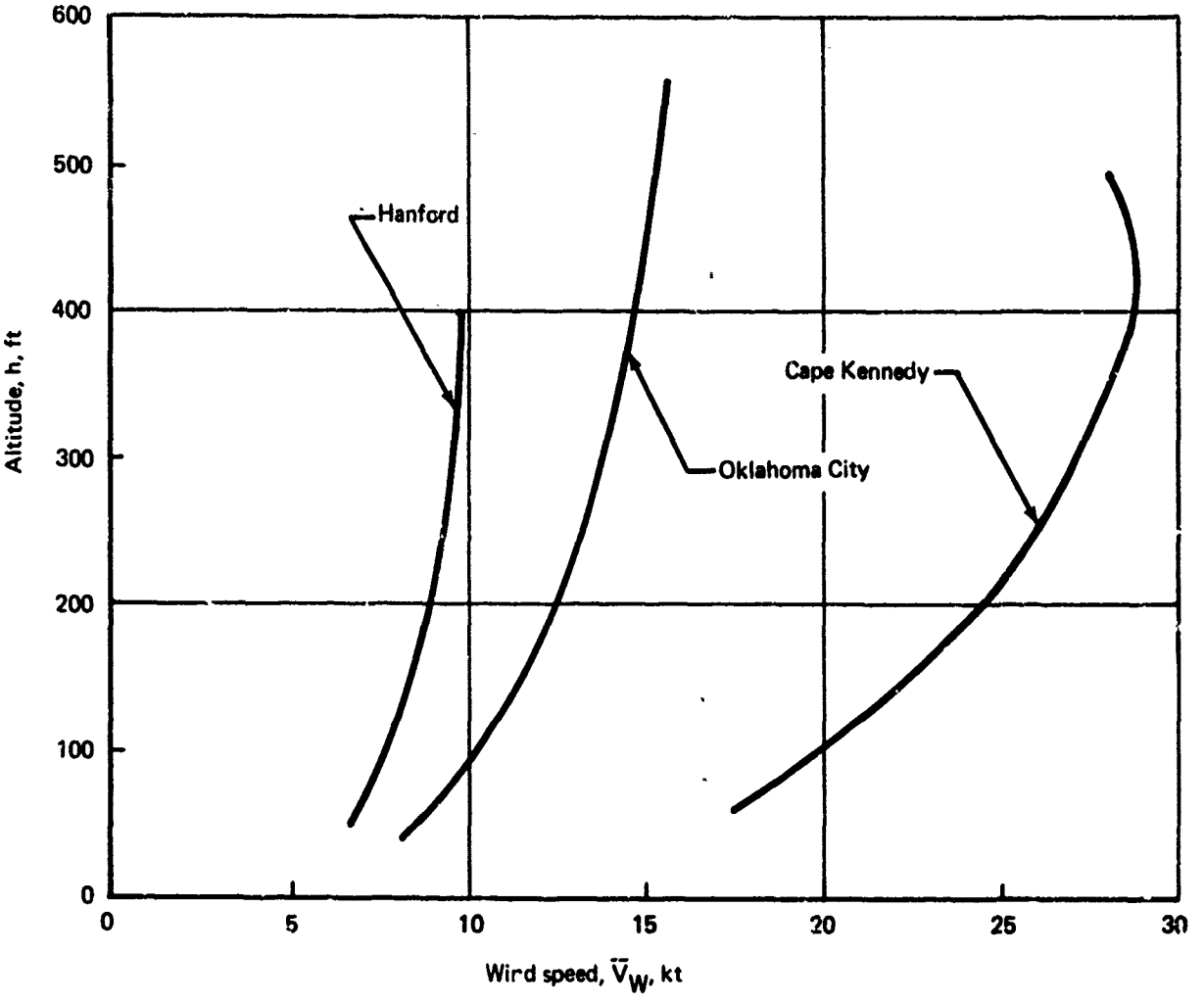

FIGURE 3-9.–MEAN ANNUAL WIND SPEED PROFILES FOR THREE LOCATIONS

While "wind shear" is defined mathematically as a vector quantity, often only the magnitude $\partial\bar{V}_W/\partial h$ or $d\bar{V}_W/dh$ is used, for instance, in the Richardson's number. The quantity given indicates either the scalar or vector magnitude, as the case may be, at a point in the vertical. In actual studies of observations the term has been used interchangeably with a difference term, usually $(\bar{V}_{W2} - \bar{V}_{W1})/(h_2 - h_1)$. Thus, what is shown is an "average wind shear for an interval." Most authors using tower data at height intervals ranging from 10 feet or so to at least 150 feet use the term "wind shear" and the mathematical symbol $\partial\bar{V}_W/\partial h$ even though the data are not related to a point. That is, they assume a linear relationship between observational levels. This loses its accuracy near the ground where the wind profile is least linear.

In the following discussion, therefore, the term "wind shear" is referred to a finite height interval dependent upon instrument locations and given in knots/100 feet for consistency. Often the vector shear is described in terms of its orthogonal components or magnitude and direction shears separately. This often makes difficult the comparison of "shears" studied by different investigators.

Possibly the greatest criticism which might be leveled at the following results obtained from the literature is that they do not represent the true shear conditions to be encountered by arriving or departing airplanes. Muller and Mushkat mention these in their paper, Reference 3-11. Most of the tower shear data given below are for averaging periods of 10 minutes to 1 hour, whereas an airplane takes only a minute or so to pass through the shear height interval. Secondly, the airplane will move horizontally a distance of a mile or so in this time interval, while the shear data are observed vertically at one location. Ideally, nearly instantaneous observations should be taken at different levels on two towers a mile or so apart and separated a minute or so in time. Observations of this nature will be discussed later along with the representativeness of the tower data.

3.2.3.1 Survey of World Locations

The response of various investigators to the WMO call for studies of wind shear in the lowest 100 meters or so resulted in a broad range of replies. These replies are summarized here with similar information gathered from additional sources for other locations.

Pettit and Root studied the 200- to 20-foot wind shear at Montreal and Whiteshell, Canada, for cases when the 200-foot wind speed exceeded 20 mph (17.4 kn), Reference 3-12. The Montreal tower site is in an urban residential area, while Whiteshell is on a relatively flat plane with exposure more typical of an airport. Shears at the two sites are compared in the following table.

	Montreal	Whiteshell
Period of record	12 mo	20 mo
Time that 200 ft speed >17.4 kn	1200 hr	3000 hr
Most probable scalar shear	4.2 kn/100 ft	4.8 kn/100 ft
Extreme scalar shear	10 kn/100 ft	13.5 kn/100 ft
Other probabilities	0.9% $\geq$ 8.4 kn/100 ft	2.0% hr $\geq$ 8.7 kn/100 ft
		0.9% hr $\geq$ 9.6 kn/100 ft
		0.75% hr $\geq$ 9.7 kn/100 ft

There is a larger variation of shear magnitude at Whiteshell, the location with the higher mean wind speed and fewer obstructions to the wind. The probabilities of exceedance of wind shear magnitude are compared for the two locations in Figure 3-10.

In addition to the shears of speed magnitude, the distribution of direction shears is given for Whiteshell, Figure 3-11. Only 1.9% of these cases had directional shear greater than 17°/100 ft (30°/180 ft). At Montreal the directional shear was $\leq$ 27°/100 ft (45°/165 ft) in nearly all cases. The authors conclude that a scalar treatment of speed shears is valid; that is, the speed shear may be obtained in nearly all cases by simply subtracting the wind speed at one level from the speed at the other level, ignoring the directional shear.

Directional shear information is also available for the Hanford, Washington tower located on nearly level desert terrain, Reference 3-7. Data are given for the 400 -50 foot interval in the reference, and these have been reduced to a common 100 foot interval for comparison with the Whiteshell information, Figure 3-12. This linear interval reduction may not be entirely

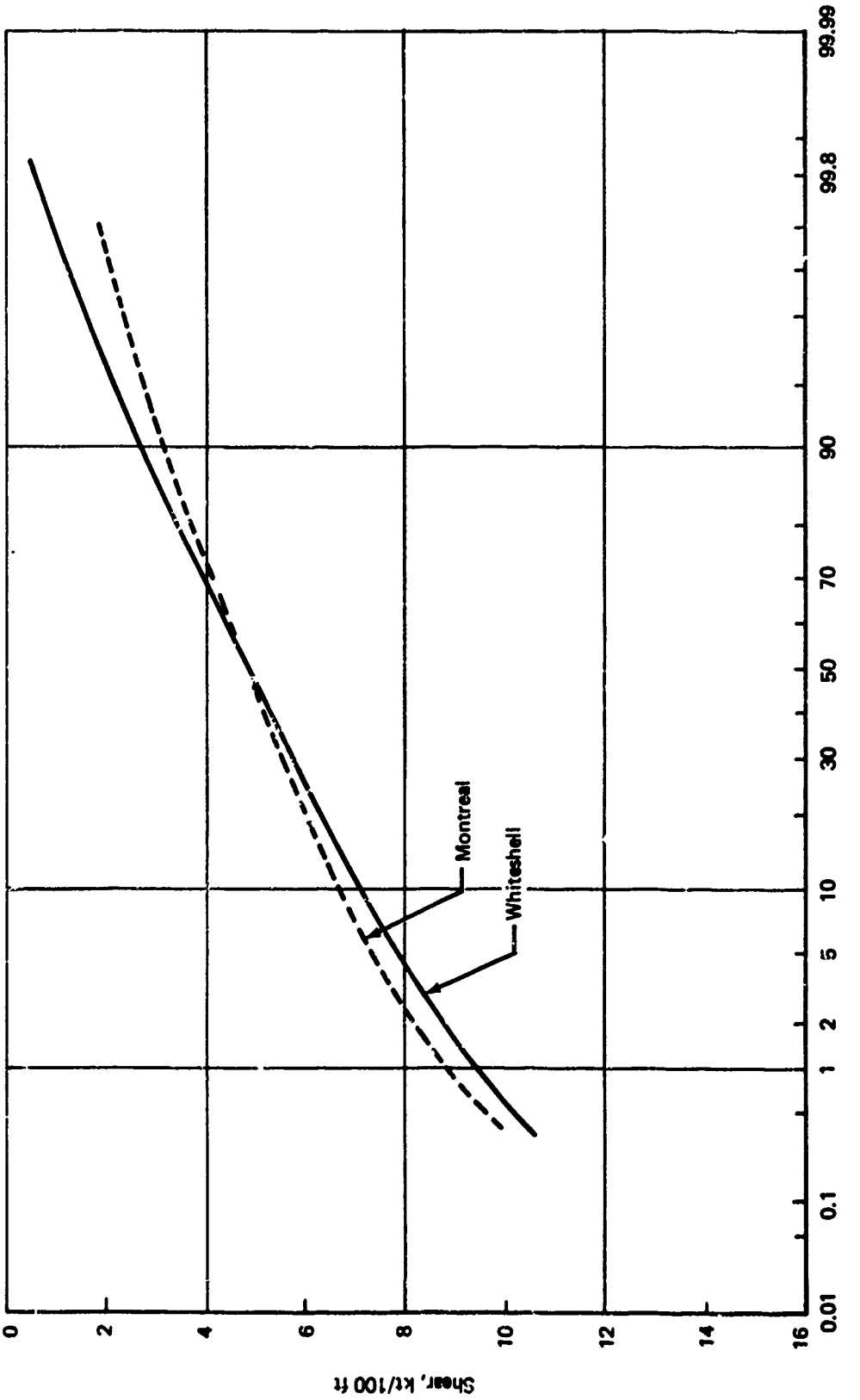

FIGURE 3-10.–WIND SHEAR MAGNITUDES (10 MIN MEANS), MONTREAL AND WHITESHELL, CANADA, 200-FT SPEED > 17.4 KT

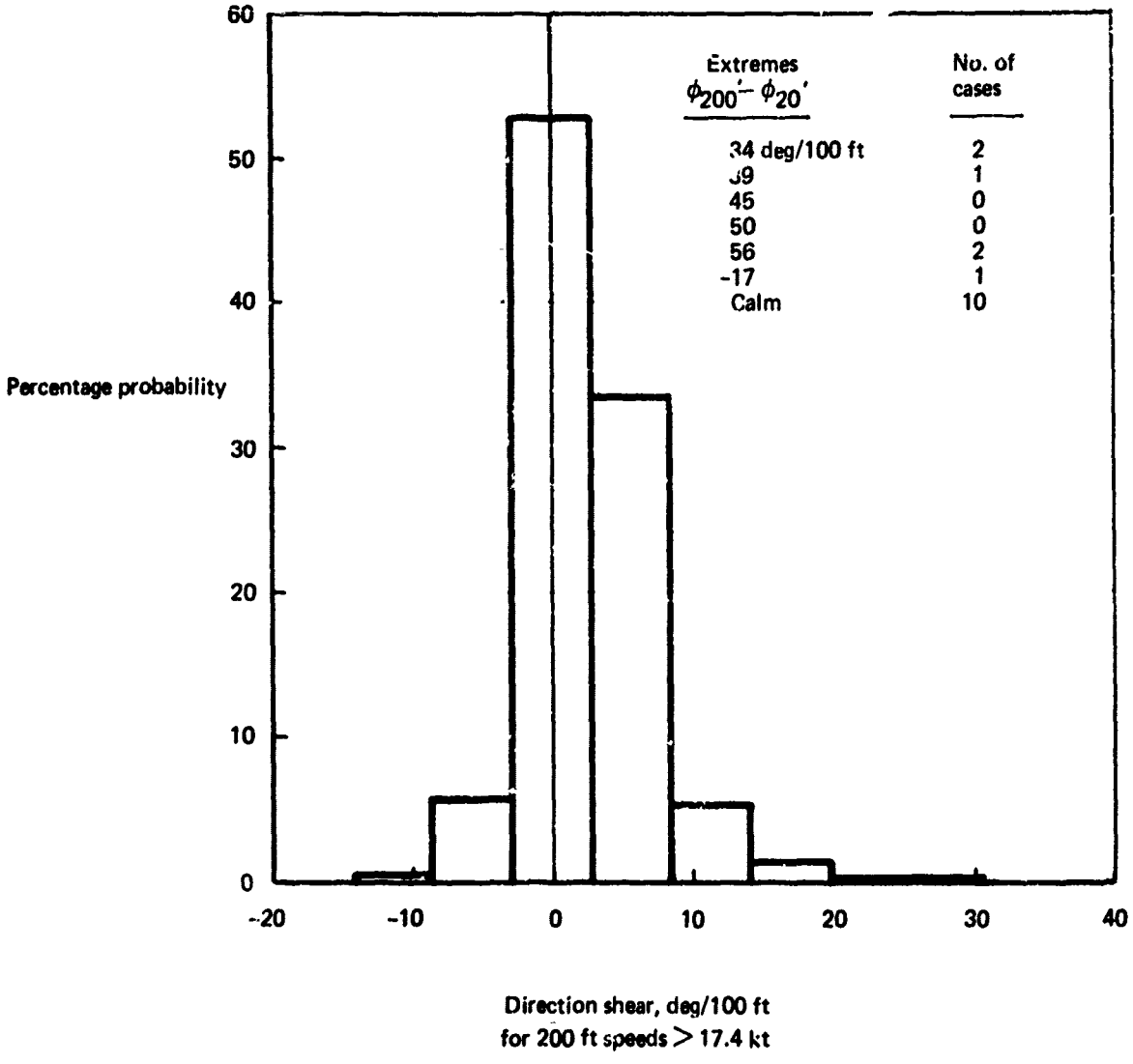

FIGURE 3-11.–DIRECTIONAL SHEAR, WHITESHELL, CANADA ($\phi_{200}' - \phi_{20}'$) IN DEG/100 FT

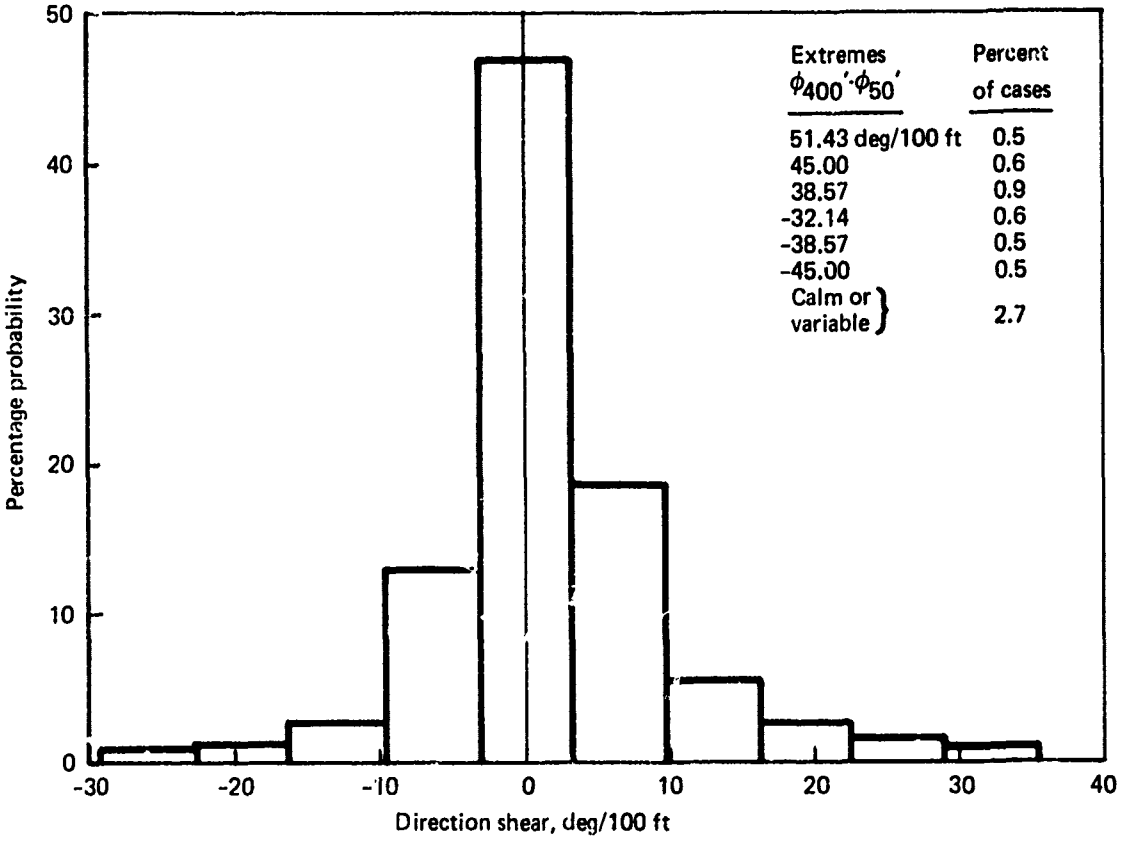

FIGURE 3-12.–DIRECTIONAL SHEAR, HANFORD, WASHINGTON (ϕ_{400}'-ϕ_{50}') IN DEG/100 FT

legitimate for the more extreme shears; however, the implication is clear that large directional shears are the exception. Directional shears are investigated further under the computer study of accumulated tower wind records, Section 3.3.

The following paper in Reference 3-11 by Muller and Mushkat also contains information for Whiteshell but in addition contains 1-hour mean shears for towers at Ottawa and Sarnia. Ottawa's tower is about a mile from an urban area and Sarnia's is in flat, open country. Whereas in the previous paper the data were limited to those observations where the 200-foot wind speed exceeded 17.4 knots, no such limitation was used in this reference. In addition, the period of record was approximately 3 years as versus 1 year in Reference 3-12. An additional difference was that a vector shear was determined for each observation and from this the downwind, crosswind, and vector magnitudes were determined and summarized. "Downwind" was defined as the component of the shear in the direction of the upper-wind vector. No directional shear summaries similar to the previous reference are provided in this reference. The shear magnitudes are compared in Figure 3-13 for the three sites. Whiteshell again has the larger variation; no doubt due, in part, to the shorter wind averaging period (10 vs. 60 minutes for the other two sites). In Figure 3-14 the effect of limiting the cases to 200 foot speeds of greater than 17.4 knots is shown by comparing the Whiteshell shear magnitude from the two papers. It must be recognized that a true

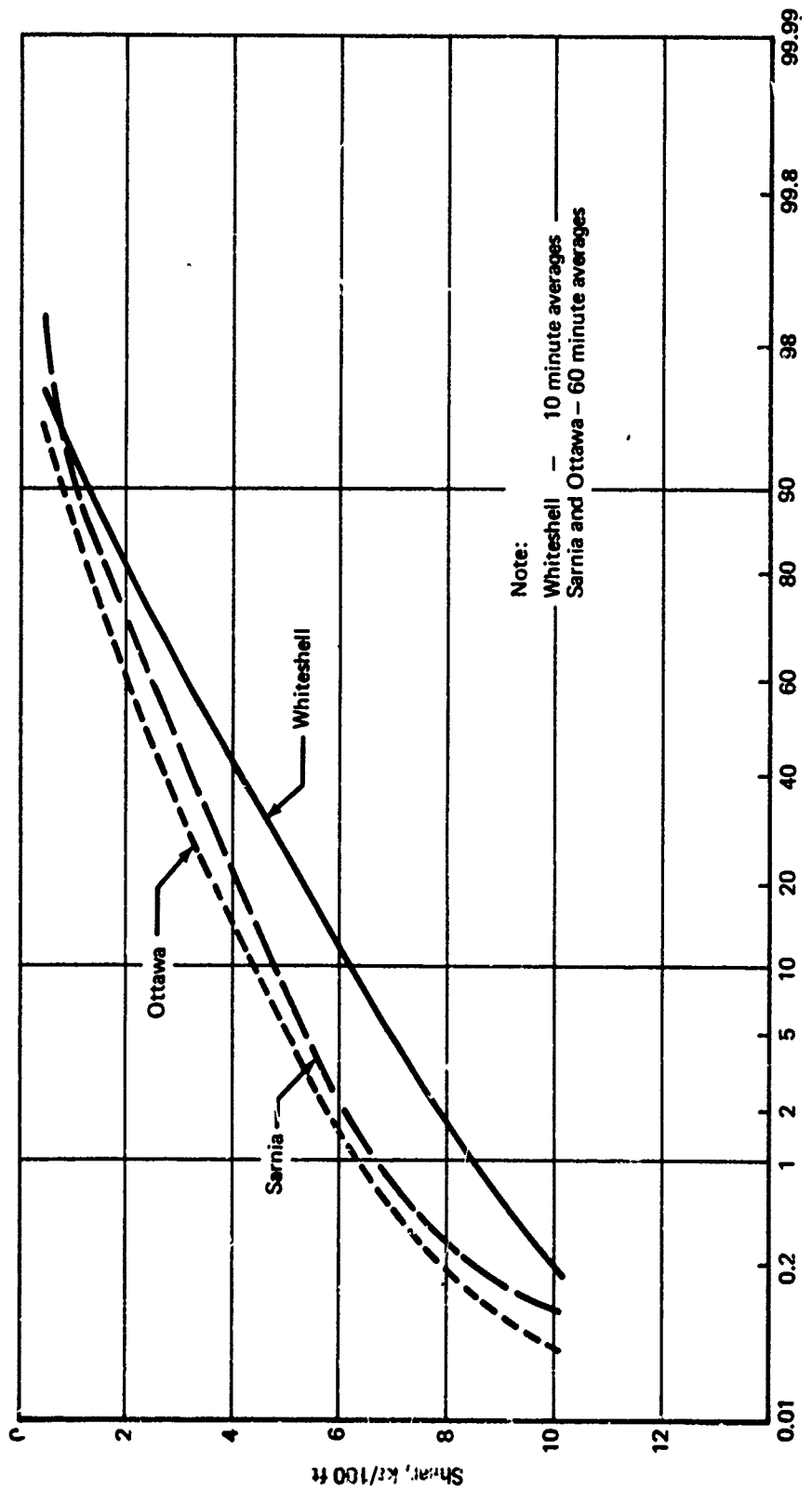

FIGURE 3-13.—WIND SHEAR MAGNITUDES, CANADA

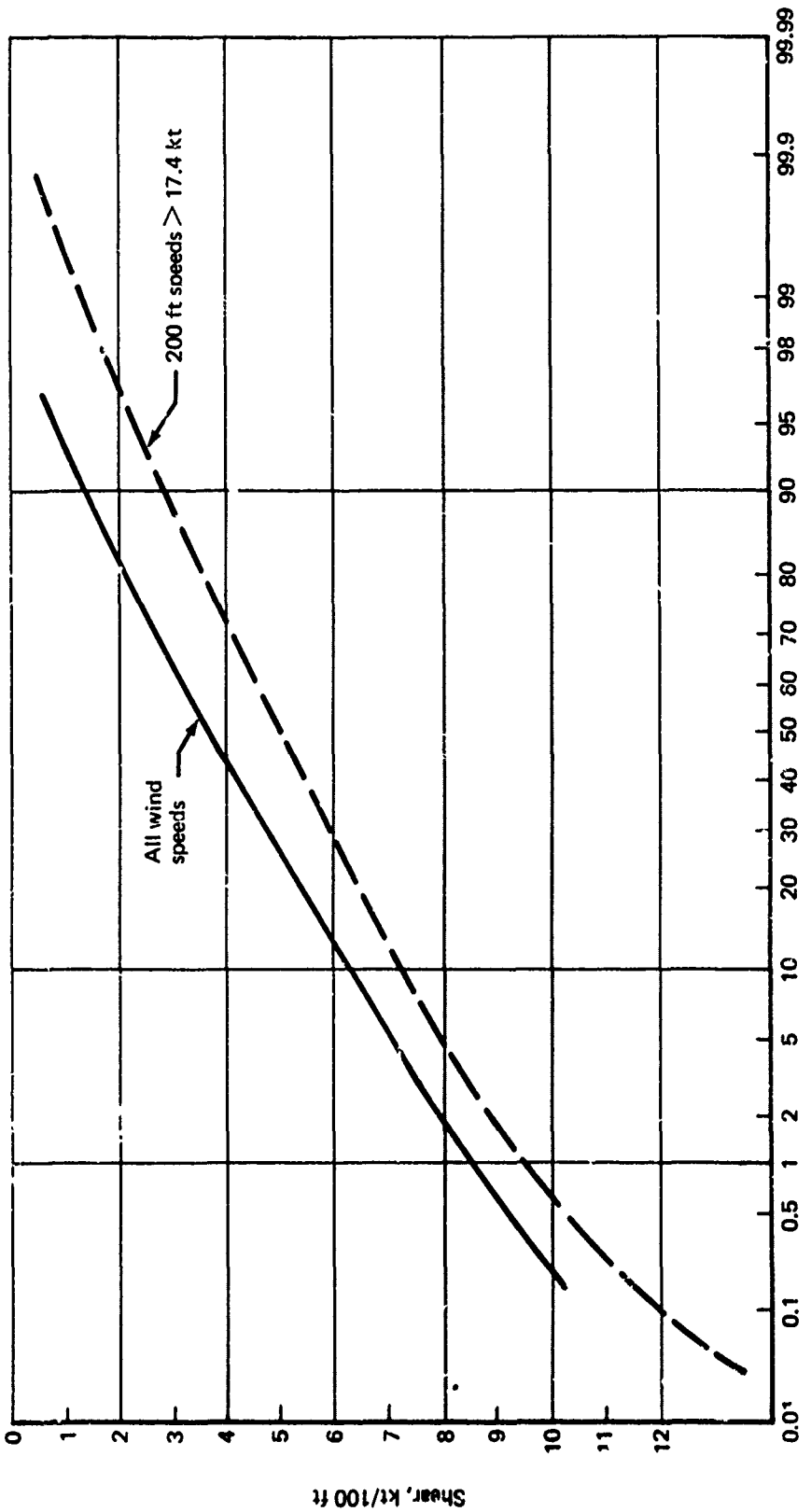

FIGURE 3-14.—WIND SHEAR MAGNITUDES, WHITESHELL, CANADA

comparison is not possible because of the differences between the definition of shear in the two cases and the dissimilarity in periods of record. It is assumed that these differences are minor compared to the speed limitation.

The mean (50%) shear magnitudes for the three locations from Figure 3-12 are:

Whiteshell	3.8 kn/100 ft
Sarnia	2.9 kn/100 ft
Ottawa	2.3 kn/100 ft

In another paper a study of wind shears observed on a 200-foot tower on the coastline near Thumba, India, is discussed, Reference 3-13. Tower intervals studied were small compared to other studies and only two layers near the ground, 33-8 and 58-33 feet, had sufficiently long periods of record for our study. The probability of exceedance distributions for these two intervals are included in this report, Figure 3-15. However, the site is believed not to be representative of airports (shoreline site with trees cleared only within 250 feet of the tower). Observations were at 3-hour intervals between 0000 and 1500 local standard time (LST) and the observational averaging period is not known precisely but is assumed to be 1 hour. Other reservations covering the location and instrumentation could be enumerated; however, the results are provided here because at few other locations are data available for such small height intervals. Care should be exercised in any application of the results to airports.

The summarized shears are provided in component form (North-South and East-West). Assuming that the 50% shear magnitudes in Figure 3-15 can be determined directly from the 50% components, the 50% shear magnitudes are 5.9 kn/100 ft for the 58-33 foot interval and 11.1 kn/100 ft for the 33-8 foot interval. The 50% and 1% component shear values for both intervals are:

		50%	1%
58-33 ft			
	N-S	4.5 kn/100 ft	25.0 kn/100 ft
	E-W	3.8	23.5
33-8 ft			
	N-S	6.5	31.5
	E-W	9.0	38.5

Much shorter periods of record are available for height intervals higher on the tower, but they are not included here because of the uncertainties concerning them. However, it appears that the shears become less extreme with altitude, as would be expected.

As contrast to the previous paper, a study by Kusano, Suzuki, and Takei from an 830-foot tower near the Tokyo International Airport provides S-N and W-E component shear

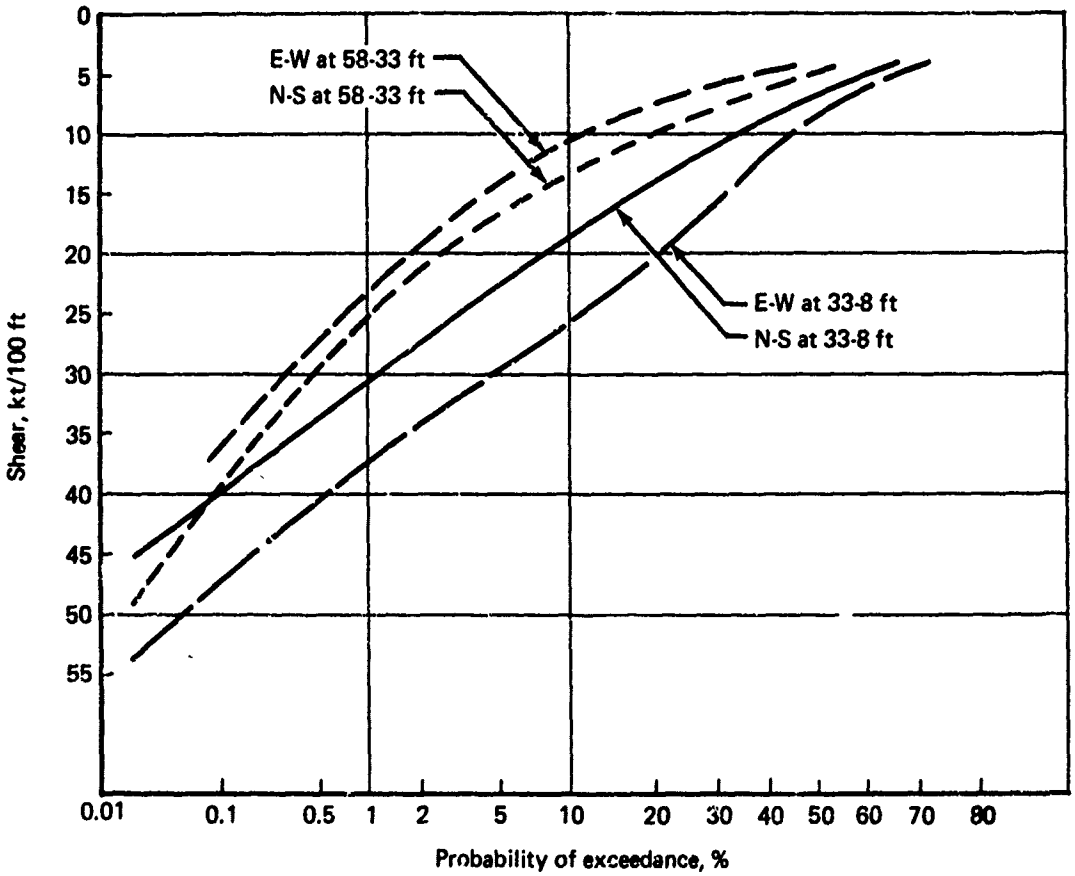

FIGURE 3-15.–COMPONENT WIND SHEAR MAGNITUDES, THUMBA, INDIA

information for large height intervals, Reference 3-14. The averaging time interval of the hourly observations is not given explicitly in the paper but is assumed to be 1 hour. The period of record is 1 year.

The most noticeable feature of the curves in Figure 3-16 is the lower values and the non-Gaussian distribution of the shears compared with similar information from other locations. Fifty percent component values are given in the following table.

		50%
380-350 ft	S-N	1.5 kn/100 ft
	E-W	1.4
350-85 ft	S-N	1.5
	E-W	1.3

The 50% shear vector magnitudes computed as before both equal 2.0 kn/100 ft.

An interesting aspect of this Japanese study is a section discussing wind shear duration. The annual distributions of occurrences are shown for two cases (vector shear magnitude $\geq$ 2.0

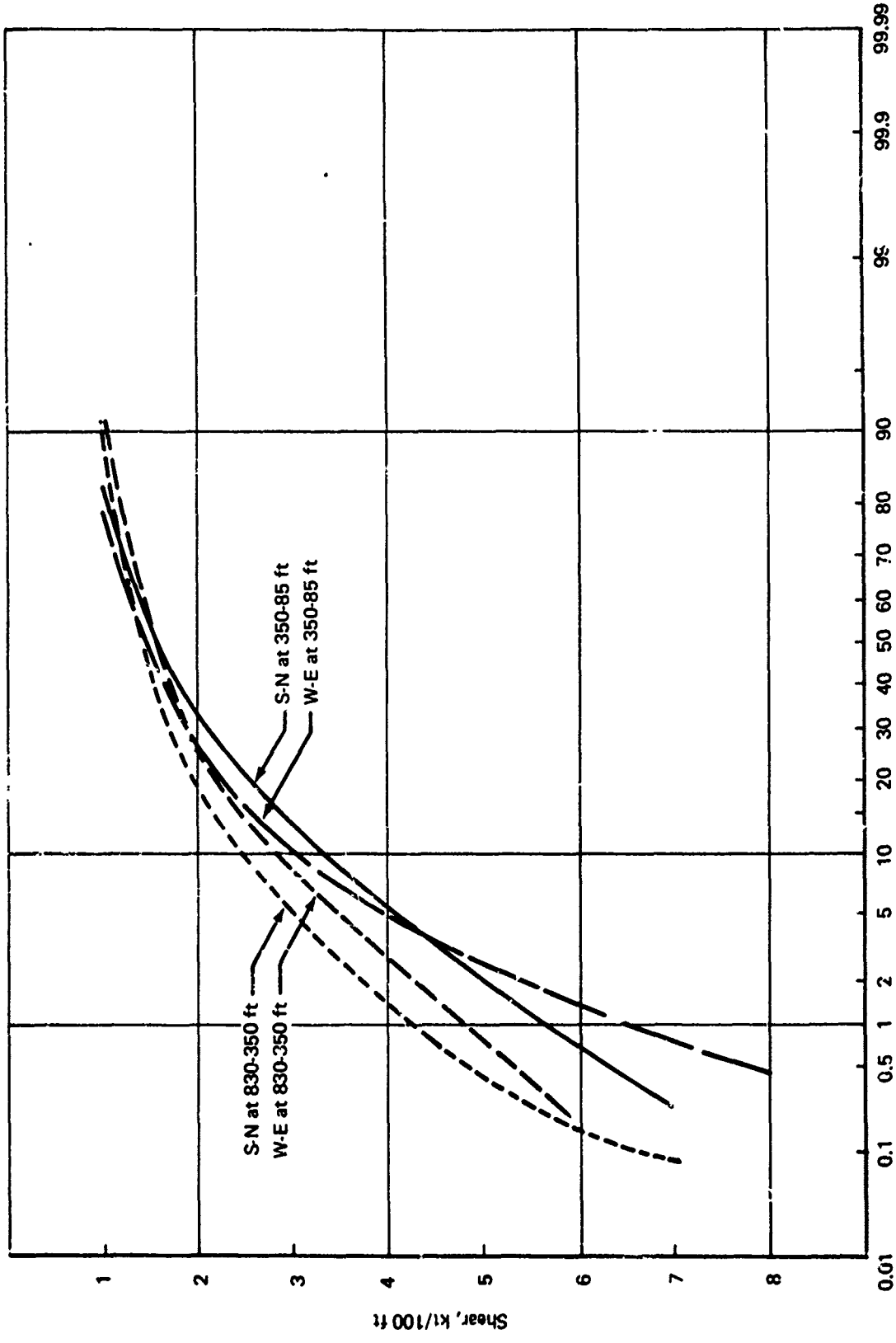

FIGURE 3-16.—COMPONENT WIND SHEAR, TOKYO

and ≥3.2 kn/100 ft) for the 830-350 foot height interval in Table 3-2. Information of this nature for greater shears and shorter time intervals (less than 1 hour) would be more valuable for our study.

TABLE 3-2.–FREQUENCIES OF OCCURRENCE OF VECTOR WIND SHEAR MAGNITUDE DURATIONS FOR 830- TO 350-FT INTERVAL

Shear magnitude (kt/100 ft)	Duration (hr)									Total occurrences	% of total observations
	1-2	3-5	6-8	9-11	12-14	15-17	18-20	21-24	24		
	Frequencies of occurrence										
2.0	403	103	41	12	6	5	2	3	2	577	8.45
3.2	172	33	8	2	2					217	3.18

P. J. Rijkoort reports on an interesting and different study of wind shears obtained at Lopik, Netherlands, with fast response instruments, Reference 3-15. "Momentaneous" speed observations were obtained at 175 and 49 feet at 3-second intervals for 32 14-minute time series spaced over a total of 5 days. These 8960 observations were then statistically analyzed for 3-, 6-, 9- 12-, and 30-second, as well as 14-minute time averages. For example, the average of three successive observations becomes a 9-second observation. The 14-minute mean and extreme shears were also determined. All these data are summarized in Figure 3-17, a semilogarithmic plot of shear versus time for the various statistics. As may be seen, the average shear for the entire record is 3.34 kn/100 ft, approximately the same as other studies. (Shear in this case is defined as a speed shear only, and any directional shear is ignored.) The average maximum and minimum shears for the 32 series are plotted, as are the extreme shears for the entire record. Only the average and extreme shears are available for the 14-minute periods. It is obvious that a positive shear (speed increasing with height) is most common; however, negative shears certainly occurred and with surprising magnitude for the shorter averaging times. Qualitatively these results are valuable to our study since they indicate the problem that results from simulating, for landing conditions, wind shears obtained from 10 minute or longer averages. There is no indication in the reference that the observations were taken when severe shearing was present. Therefore, the extremes obtained in that relatively short study should not be understood to be the extremes that might be found with shear-producing weather situations. For instance, the extreme 10-minute shear indicated in Figure 3-17 is about 7.5 kn/100 ft over the 175 to 49 foot height interval. Other studies for roughly the same height interval indicate 10-minute extreme shears of at least 10 kn/100 ft. More observational studies are required for this facet of the problem.

A Russian paper by Abramovic and Glazunov presents information from both tower and pilot-balloon observations at various locations in the Soviet Union, Reference 3-16. At the tower location, Obinsk, 7-minute average vector wind shear magnitudes were obtained at several levels and are repeated here in Table 3-3.

Extreme vector wind shear magnitudes of 12 kn/100 ft over intervals of approximately 80 feet in the lowest 250 feet were obtained near Moscow during cloudy winter days by using

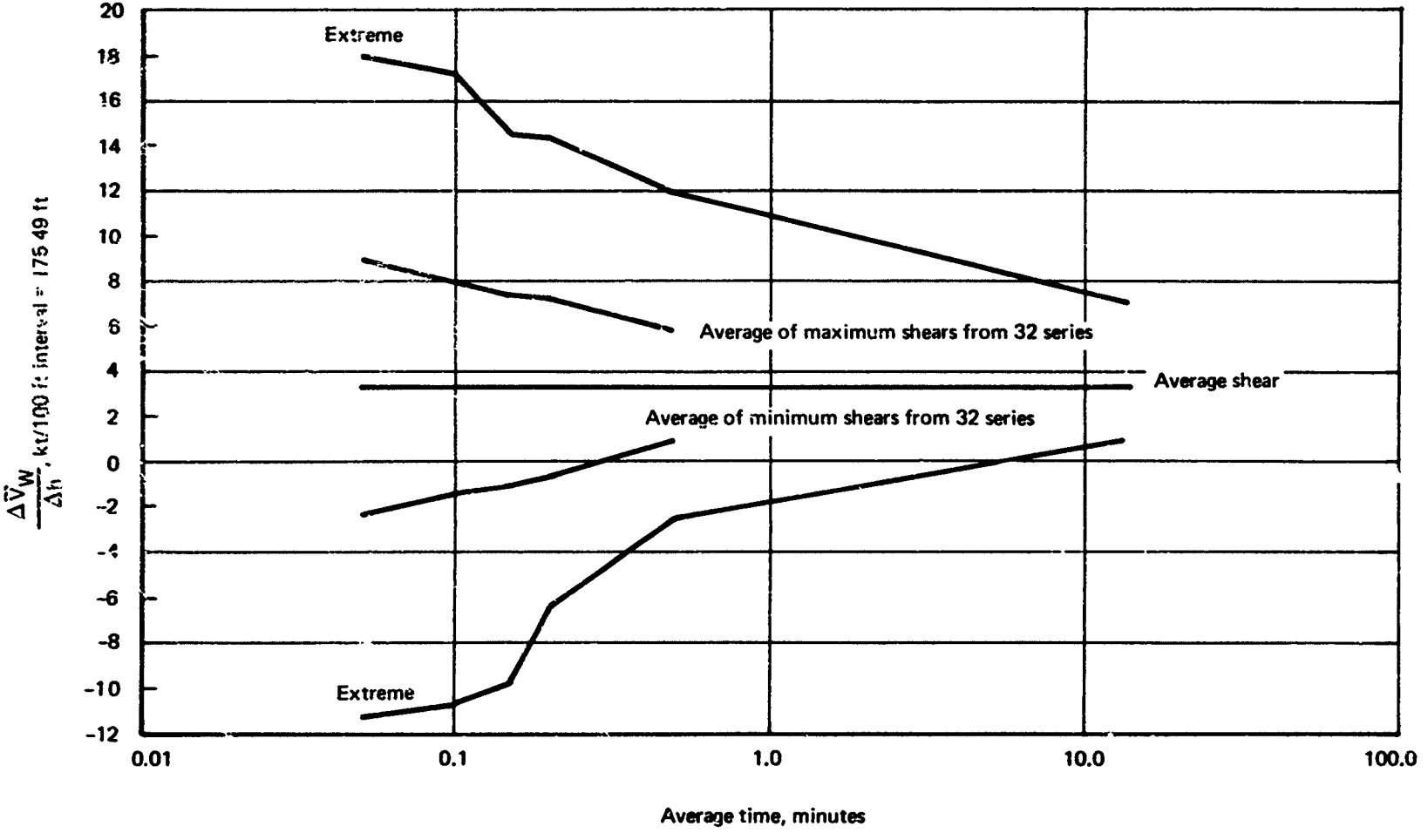

FIGURE 3-17.—WIND SHEAR VS SPEED AVERAGING TIME

TABLE 3-3.–VECTOR WIND SHEAR MAGNITUDES AT OBLINSK, RUSSIA

Layer interval (ft)	Vector shear magnitude (kt/100 ft)	
	Average	Extreme
3-82	3.7	11
82-161	2.2	10
161-240	2.2	10
240-318	2.2	Not given
318-397	2.0	Not given

captive balloons. Average shears were less than 3.3 kn/100 ft and decreased with increasing altitude.

A 5-year period of pilot-balloon observations at 11 airports in the Uzbekistan Republic of the Soviet Union were analyzed for wind shear. Only 1.6% of the shears from various 300-foot height intervals below 1000 meters (3280 feet) provided shears of 3 kn/100 ft or greater. Only seven cases out of 38,092 (or 0.2%) exceeded 9 kn/100 ft. The applicability of these data to our study are questionable because of the large height intervals involved.

Roberts has performed analyses of wind shear in the lower layers of the atmosphere for application to the control of aircraft on approach, Reference 3-17. His conclusions are that characteristic shears (speed only) are 3-5 kn/100 ft in the lowest 100 feet with extreme values of 10 kn/100 ft. Ten minute wind averages were used and the directional shear was ignored since it never exceeded 45° during his selection of 50 days out of the year when shears were favored.

As to a question we raised earlier concerning the usefulness of shears observed vertically, Roberts states, "In surface layers of the atmosphere, the change in the mean wind flow with distance is about two orders of magnitude greater in the vertical direction than in the horizontal. Consequently, it is permissible to neglect these horizontal changes for distances representative of the approach zone of an airport and consider only the vertical change of the wind."

No probability distribution similar to Figures 3-13 through 3-16 was available from the referenced paper; however, for the 110-10 foot interval the average speed shear and the extreme shear are 3.2 and 9.3 kn/100 ft, respectively, and for the 210-110 foot interval the average and extreme shears are 4.4 and 10.0 kn/100 ft.

Roberts provides a chart of the average and maximum wind shears versus surface wind speed, Figure 3-18. It is apparent that the greatest average and extremes occur with surface speeds of 3-4 knots. He also includes a diagram from Ramsey, Reference 3-18, depicting the variation of wind shear with temperature gradient at Lopik, Netherlands, Figure 3-19. It is noticeable that shear increases with a positive temperature gradient but that the highest percentage occurs with a shear of approximately 3 kn/100 ft and an adiabatic temperature gradient.

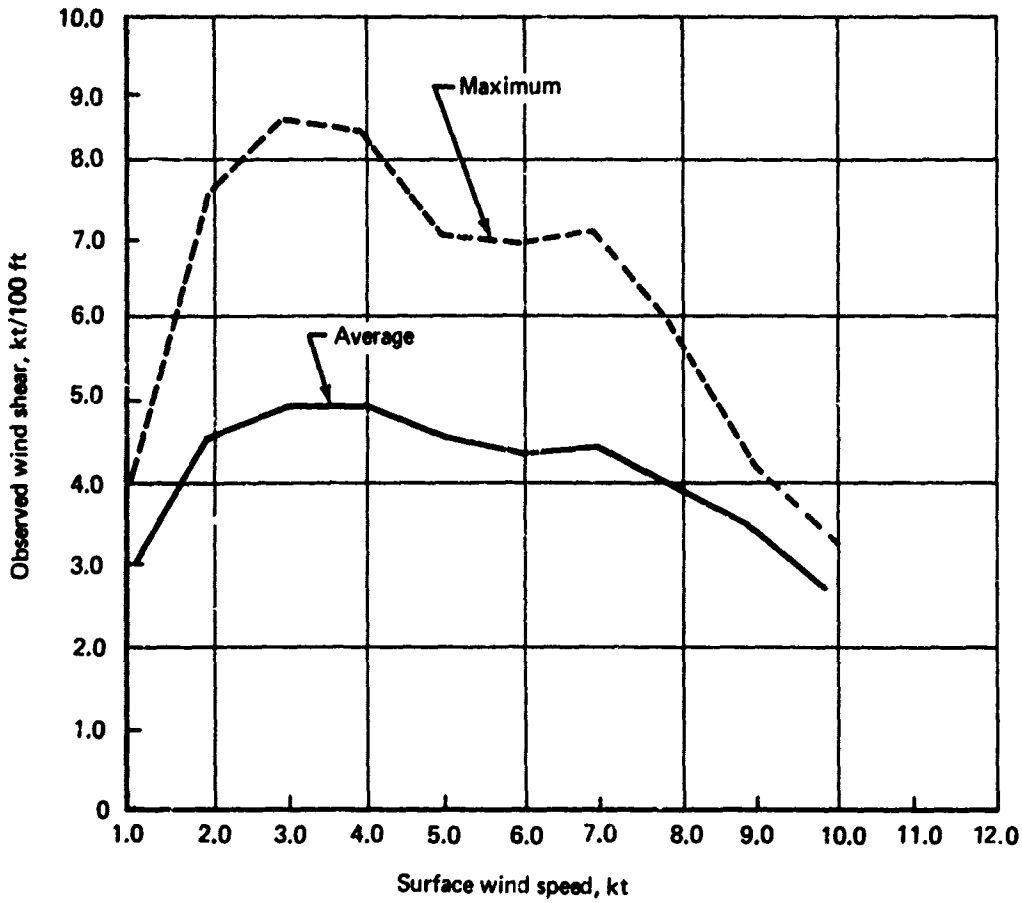

FIGURE 3-18.–DISTRIBUTION OF AVERAGE AND MAXIMUM WIND SHEAR FROM SURFACE LEVEL TO 110 FT AS A FUNCTION OF SURFACE WIND SPEED

One of the interesting conclusions is that there is little difference between the results from his Damascus, Maryland results and the Lopik, Netherlands and Cedar Hills, Texas results.

Watson, Reference 3-4, studying 2-minute-averaged shears from Cardington, England and Lopik, Netherlands as well as other models suggests the following speed shear models for landings:

- During glideslope (down to 100 ft elevation)
  Mean shear = 2.5 kn/100 ft
  Standard deviation = 2.0 kn/100 ft

- During attitude hold and autoflare (less than 100 ft elevation)
  Mean shear = 3.5 kn/100 ft
  Standard deviation = 2.0 kn/100 ft

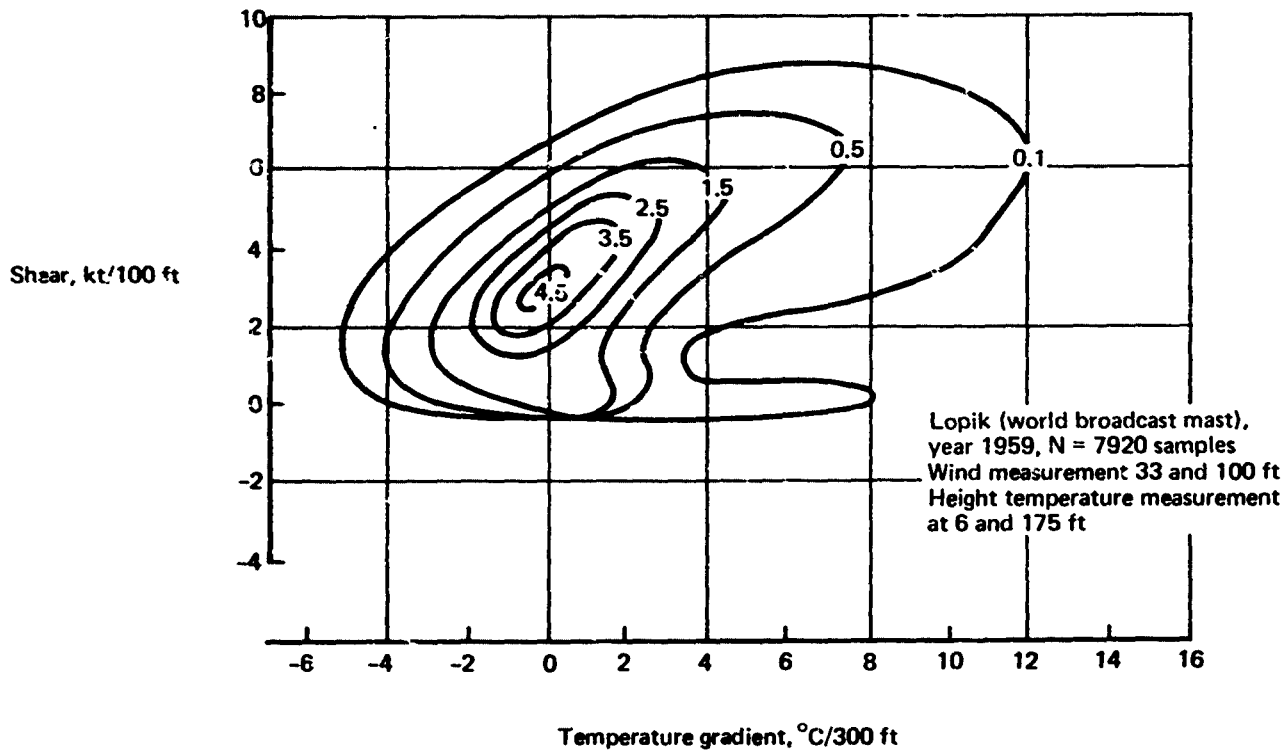

FIGURE 3-19.—RELATIVE FREQUENCIES (IN PERCENT) OF WIND SHEAR AND TEMPERATURE DIFFERENCES ACCORDING TO RAMSEY (REF. 2-18)

In the latter case, the mean plus three standard deviations (he found the distribution of shears to be normal) equals nearly 10 kn/100 ft, which is approximately the same as the extreme shears found by other investigators.

Watson includes an appendix to his paper entitled "Wind Shear in the Lower Layers of the Atmosphere, Observations from a Tethered Balloon at Cardington–1949 to 1954," in which are speed shear frequencies and stability conditions. These are reproduced in probability of exceedance form in Figure 3-20 along with the curve representing the total number of observations. Observations were conducted thrice daily except when strong winds or lightning prevailed. Numbers noted after the stability condition are the percentages of the total observations included in that condition. The range of values is not as great as in other studies, possibly because of the large height interval between observation heights (220 feet).

In a paper by Dubov, Reference 3-19, additional wind shear information from Russia is reviewed. The observations were obtained primarily by balloons and no averaging times are given. One of his figures is interesting in that the dependence of shear and the boundary layer height upon stability is indicated in a general way, Figure 3-21. The top of each curve indicates the geostrophic height. The abscissa is the ratio of the wind speed at height h to that at 10 meters. Other interesting features of wind shear are to be noted in Tables 3-4 and 3-5, developed from radiosonde data. It is uncertain whether the numbers in the tables are vector shear magnitudes or speed shears but it is believed that they are speed shears.

Dubov writes that low level jet streams have been noted in Russia and that jet cores are found just below the inversion height and have speeds sometimes 2-3 times as large as the geostrophic wind. These jets are rare but can occur over various types of terrain. He cites one Russian investigator as observing a jet for 4 days.

Clodman, Muller, and Morrissey, Reference 3-20, in a subsequent paper to Reference 3-11, present additional and more detailed information. The paper is separated into two sections, the first providing shear probabilities from several years of 10-minute or 1-hour average winds. In addition to the data presented earlier they provide important mean and standard deviation information for shear components relative to either the surface or upper wind. Relevant portions of their tables are reproduced here, Tables 3-6 and 3-7. They note, as others have, the Gaussian distribution of the shears for the bulk of the observations but they also present data indicating that the extremes (number of cases with return period of 10,000 hours) are not Gaussian but occur tens (for downwinds) and hundreds (for crosswinds) of times more frequently than predicted by the Gaussian distribution. Perhaps some of these cases are rare low level jet streams. It should be noted that the Whiteshell data with 10-minute mean observations are generally closer to the Gaussian predictions than the 1-hour mean observations at the other locations. The positive crosswind shear is the greatest departure from Gaussian at Whiteshell.

A second section of their paper discusses a short term study of observations from two towers about 1 mile apart in a semideveloped area in the Toronto suburbs. They studied both 60-second and 10-second mean wind shears and components from the 300-foot tower and a smaller 30-foot tower. They reported three shear situations: (1) 300-foot level on the high tower to 30-foot level on the small tower, no time lag; (2) 300-foot level on the high tower to 30-foot level on the small tower, 20-second time lag; (3) 300-foot level to the

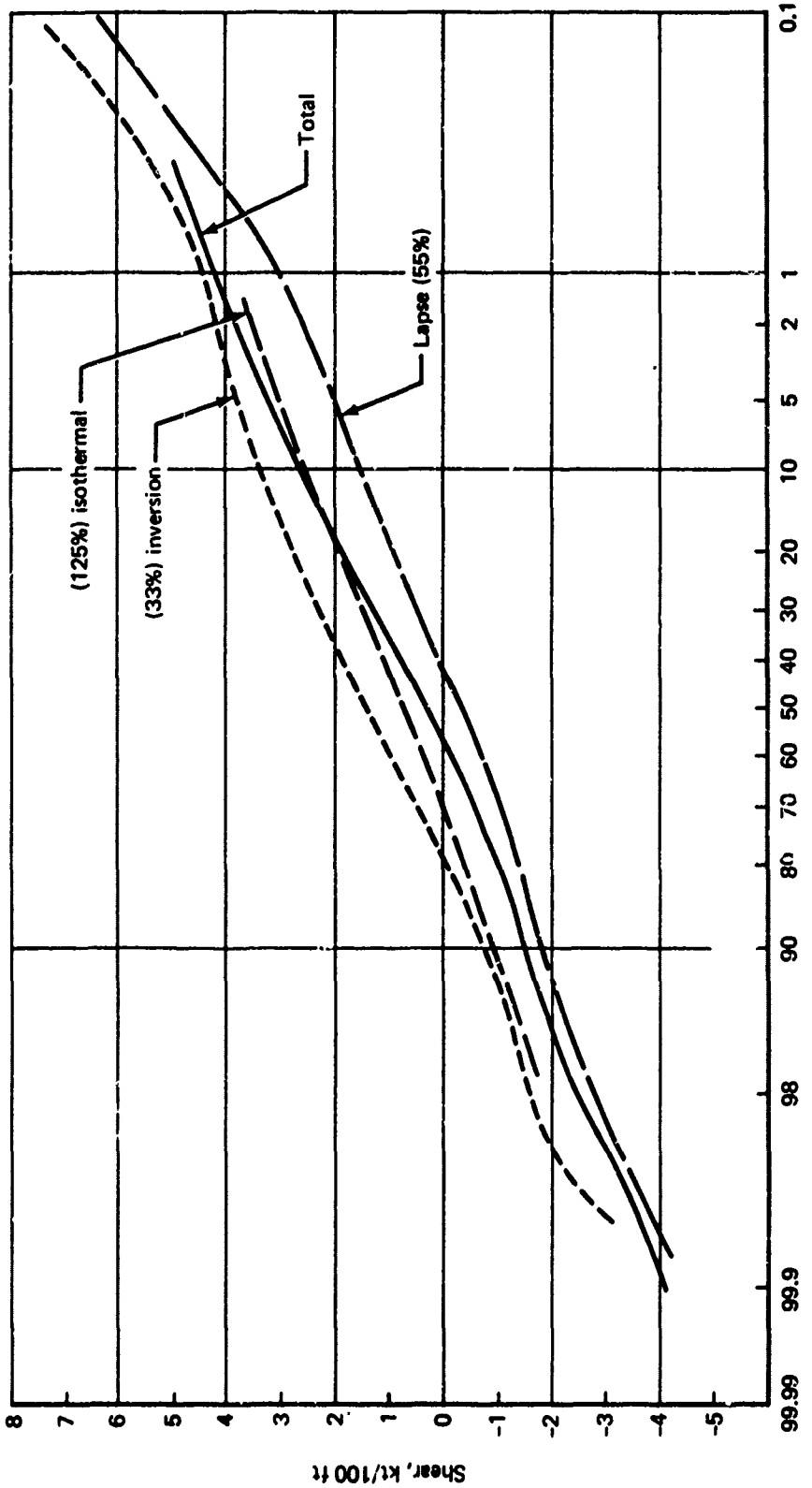

FIGURE 3-20.—WIND SHEAR MAGNITUDES, CARDINGTON, ENGLAND

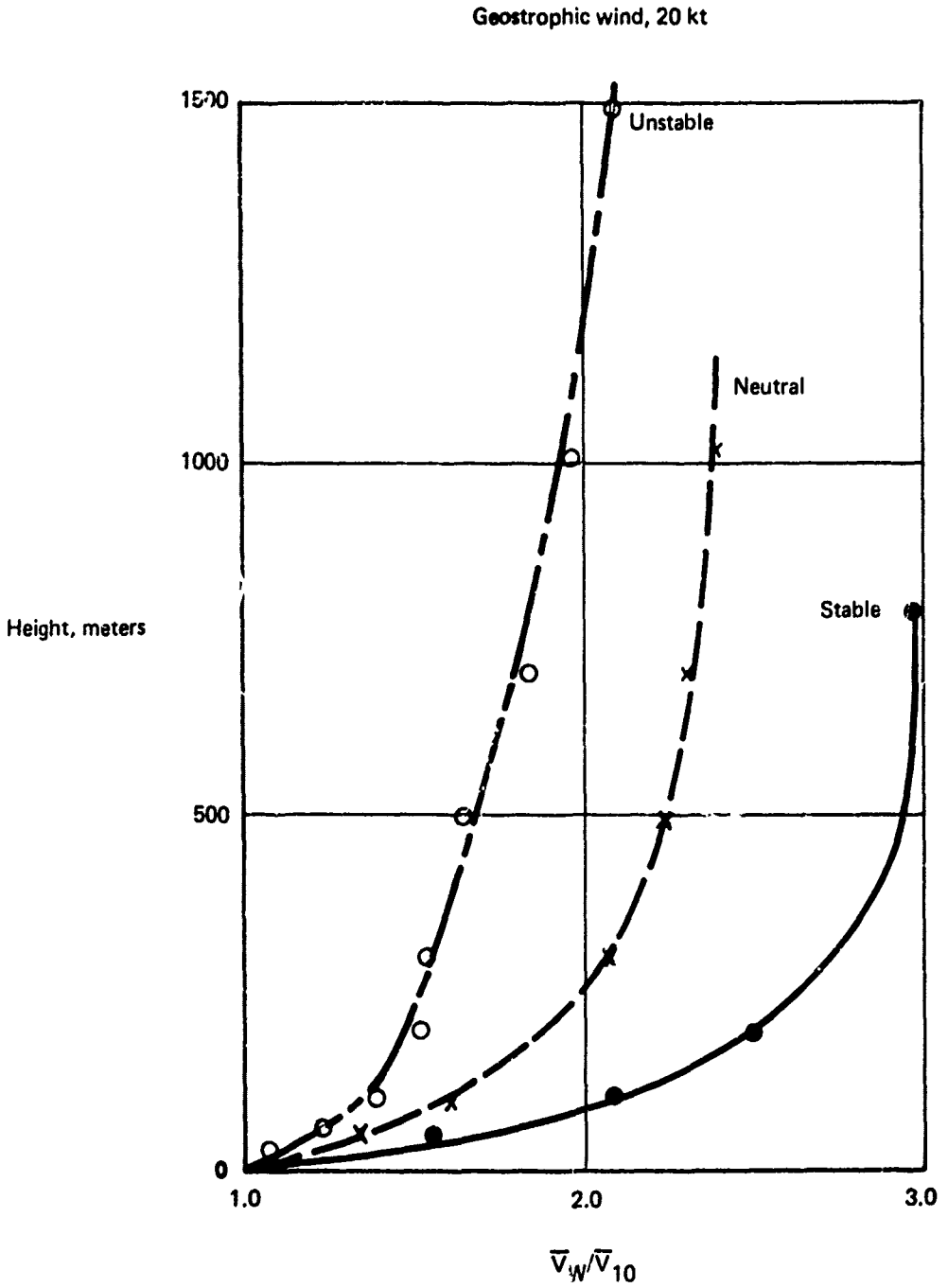

FIGURE 3-21.–WIND SHEAR AND STABILITY FROM RUSSIAN BALLOON DATA

TABLE 3-4.–VARIATION OF WIND SHEAR WITH WINDSPEED AND HEIGHT INTERVAL DURING NEUTRAL CONDITIONS–RUSSIA

Wind speed (kt)	Height intervals (ft)		
	328 to 30	656 to 30	1640 to 30
	Wind shear		
5.8	1.2	0.8	0.4
7.8	1.5	1.0	0.5
9.7	1.8	1.2	0.7
11.7	2.3	1.6	0.9
13.6	2.8	1.8	1.0

TABLE 3-5.–VARIATION OF WIND SHEAR WITH HEIGHT INTERVAL AND STABILITY–RUSSIA

Atmospheric stability[a]	Height intervals (ft)		
	328 to 30	656 to 30	1640 to 30
	Wind shear		
Unstable	0.7	0.4	0.2
Neutral	1.2	0.8	0.4
Unstable	2.4	1.6	0.7

[a] V_{30} = 5.8 kt

30-foot level on the high tower. Their Tables 6 and 7 are reproduced here as Tables 3-8 and 3-9 with the shears converted to kn/100 ft and the wind speeds to knots. The "shear components were calculated relative to the lower wind (crosswind shear being positive when the wind veered with height)."

Their conclusion to this section of their study is that the space and time required for landing an airplane should result in 1-3 kn/100 ft higher shears than detected by single tower data. These results are some of the most appropriate for our study of airplane landing conditions, although the period of record is short and more extreme conditions should be expected for longer observational periods and other locations. It must also be realized that the above conclusions were based on observations from two towers in a particular line which might be assumed to be the same as the runway orientation. Therefore, they may not be entirely valid for some portions of their study where a runway was at some other angle to the tower's orientation. This would be especially true for the study with the 20-second time lag. The effect is probably minor and too detailed for our purpose, considering the other uncertainties (site similarity to airports, differences in roughness and climatology between airports).

TABLE 3-6.–MEANS AND STANDARD DEVIATIONS FOR 20- TO 200-FT SHEARS

Item	Mean (kt/100 ft)	Standard deviation (kt/100 ft)
Ottawa: (4-year, 9-month record of 1-hr mean winds)		
Downwind shear component	2.07	1.31
Crosswind shear component	0.46	0.93
Whiteshell: (3-year, 2-month record of 10-min mean winds)		
Downwind shear component	3.38	1.96
Crosswind shear component	0.46	0.63
Sarnia: (5-year, 7-month record of 1-hr mean winds)		
Downwind shear component	2.60	1.38
Crosswind shear component	0.38	0.77
All relevant to upper wind		

R. R. Brook has written what he terms a preliminary study of boundary layer wind shear at the Melbourne, Australia airport, Reference 3-21. He has studied several aspects of the wind shear problem. One conclusion is that the downwind component of shear exceeds the crosswind component by 3 to more than 10 times. This is borne out by other studies reviewed above. He also tentatively concludes that the variability of the downwind component of shear is related to the mean upper level (150 feet in his case) wind speed and the gustiness. He has developed a table indicating this relationship for wind speed shears exceeding 6 kn/100 ft, which he assumes may present a problem to aviation, Table 3-10. In the table he combines the study data from Melbourne Airport (Tullamarine) with wind and gustiness data from Essendon to obtain the percentage of time during a year that the wind speed and gustiness combinations occur, and the annual number of hours that speed shears greater than 6 kn/100 ft exist for 10 seconds or more. The total number of hours that the shears occurred is approximately 81 per year. (The gustiness classifications are defined in Table 3-11.)

Crawford and Hudson have analyzed wind observations accumulated from a television tower near Oklahoma City in a recent report, Reference 3-8. Their paper discusses various wind facets, the last being shear.

The tower location generally is typical of airport locations; thus, the study results are applicable to this work. The shear values represent 5-minute mean conditions obtained hourly over a 1-year period, June 1966 through May 1967. Several tables and figures from this section of their study are repeated here. Figures 3-22 and 3-23 are histograms and probability of exceedance charts, respectively, of the vector wind shear speeds for six layers on the tower. Only the probabilities for layers 1, 2, and 3 are shown in Figure 3-23 because

TABLE 3-7.—VARIATION OF NUMBER OF EXTREME SHEAR OCCURRENCES FROM GAUSSIAN DISTRIBUTION RELATIVE TO UPPER-WIND DIRECTIONS

Item	Ottawa		Whiteshell		Sarnia	
	Crosswind	Downwind	Crosswind	Downwind	Crosswind	Downwind
Positive shear with probability of 1/10,000 (kt/100 ft)	3.80	6.93	2.80	10.02	3.24	7.75
Predicted number of total observations with this probability	3.4	3.4	2.6	2.6	3.6	3.6
Actual number of total observations with this probability	23	36	155	29	90	51
Negative shear with probability of 1/10,000 (kt/100 ft)	-2.98	-3.28	-2.37	-3.93	-2.46	-2.56
Predicted number of total observations with this probability	3.4	3.4	2.6	2.6	3.6	3.6
Actual number of total observations with this probability	801	6	54	6 (est)	996	7

TABLE 3-8.–MEAN SHEAR VALUES–TWO-TOWER EXPERIMENT

Shear	Averaging period (min)	Shear measurements (kt/100 ft)		
		(a)	(b)	(c)
Downwind	40	1.4	1.5	1.1
Crosswind	40	-2.6	-2.7	0.3
Magnitude from average components	40	3.0	3.1	1.2
Downwind	10	1.4	1.4	1.8
Crosswind	10	-2.7	-2.7	0.5
Total magnitude	10	3.0	3.0	1.9
Average of shear magnitudes:				
40-min runs	40	3.4	3.4	1.7
10-min runs	10	3.1	3.1	2.3

(a) From simultaneously measured data on tall tower and short tower

(b) From data on tall tower and short tower measurements–20-sec lag

(c) Data from two measurements from tall tower taken simultaneously

TABLE 3-9.–PROBABILITIES OF SHEAR*

Shear intervals (kt/100 vertical ft)	Shear probabilities (%)					
	(a)		(b)		(c)	
	Downwind	Crosswind	Downwind	Crosswind	Downwind	Crosswind
-3.2 to -2.9						
-2.9 to -2.6			0.2			
-2.6 to -2.3			0.3			
-2.3 to -1.9	0.1	0.1	0.6			0.1
-1.9 to -1.6	0.7	0.1	0.6	0.1	0.1	0.2
-1.6 to -1.3	1.5	0.4	1.8	0.4	0.6	0.4
-1.3 to -1.0	3.6	1.7	3.6	1.6	1.9	1.4
-1.0 to -0.6	6.2	5.1	6.8	5.0	5.2	6.0
-0.6 to -0.3	13.8	14.6	12.0	14.0	16.0	13.2
-0.3 to 0	22.7	29.8	23.2	28.6	26.9	27.0
0 to 0.3	23.1	26.5	22.7	28.8	25.8	29.9
0.3 to 0.6	14.1	14.7	13.7	14.3	14.2	14.7
0.6 to 1.0	8.1	5.3	7.6	4.9	6.6	4.9
1.0 to 1.3	4.2	1.2	4.4	1.2	1.7	1.5
1.3 to 1.6	1.0	0.3	1.9	0.7	0.8	0.6
1.6 to 1.9	0.8	0.2	0.4	0.3	0.2	0.1
1.9 to 2.3	0.1		0.1	0.1		
2.3 to 2.6			0.1			
2.6 to 2.9						
2.9 to 3.2						
Std deviation (kt/100 vertical ft)	0.62	0.46	0.67	0.47	0.50	0.47

(a) From simultaneously measured data on tall tower and short tower

(b) From data on tall tower and short tower measurements–20-sec lag

(c) Data from two measurements from tall tower taken simultaneously

*From 10-min average

TABLE 3-10.–WINDSPEED RELATIONSHIP TO GUSTINESS AT ESSENDON, ENGLAND

Gustiness classification	Windspeed		
	Less than 20 kt	10 to 20 kt	Greater than 10 kt
Fluctuations of wind direction exceeding 90°	1.0% ND	0.0% ND	0.0% ND
Fluctuations confined to 15° to 45° limits	23.3% (10.0 hr)	19.9% (32.5 hr)	0.6% (3.83 hr)
Fluctuations of wind direction between 45° and 90°	4.9% (1.3 hr)	1.2% (0.0 hr)	0.0% ND
Unbroken solid core through which a straight line can be drawn	3.1% ND	12.1% (28.5 hr)	1.3% (4.5 hr)
Approximates a straight line; short term fluctuations do not exceed 15°	31.3% (0.0 hr)	1.3% (0.0 hr)	0.0% ND

( ) Denotes hours the windspeed difference is greater than 60 kt/100 ft (±50 ft) for 10 sec or more
ND No data

TABLE 3-11.–MEAN LAPSE RATES IN THE BOUNDARY LAYER DEFINED BY SINGER AND SMITH

Gustiness classification	Lapse rate (°C/100 m)	Standard error	Stability
Fluctuations of wind direction exceeding 90°	-1.1	±0.6	Unstable
Fluctuations of wind direction between 45° and 90°	-1.4	±0.4	Very unstable
Fluctuations confined to 15° to 45° limits	-1.1	±0.6	Unstable
Unbroken solid core through which a straight line can be drawn	-0.6	±0.5	Neutral
Approximates a straight line; short term fluctuations do not exceed 15°	+1.8	±2.3	Stable

[a]Singer, I. A. and M. E. Smith, "Relation of Gustiness to Other Meteorological Parameters," *Journal of Meteorology*, vol. 10, p. 121, 1953.

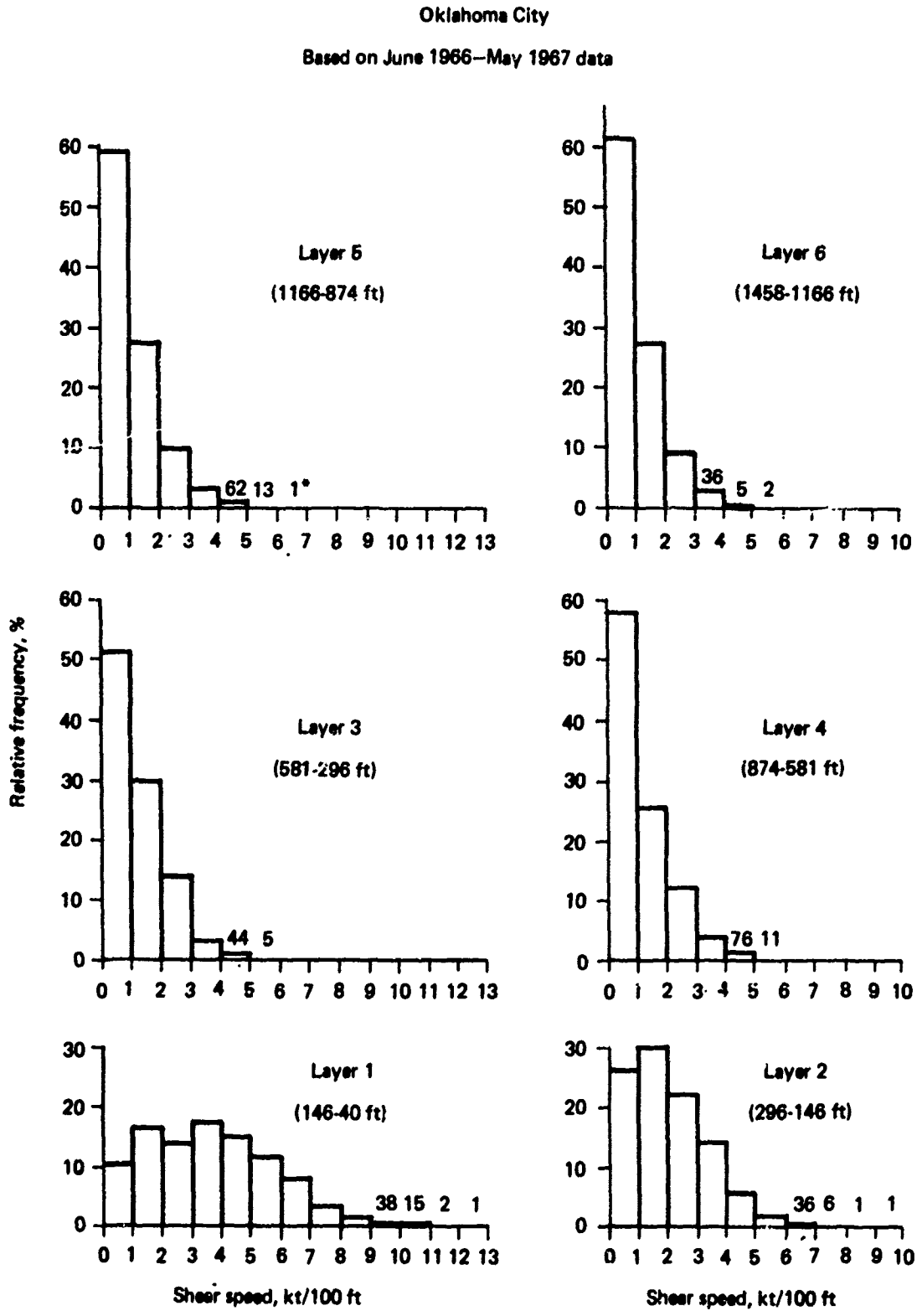

*Number of events for categories with less than 1% of the events

FIGURE 3-22.–ANNUAL RELATIVE FREQUENCY DISTRIBUTION OF WIND SHEAR SPEED

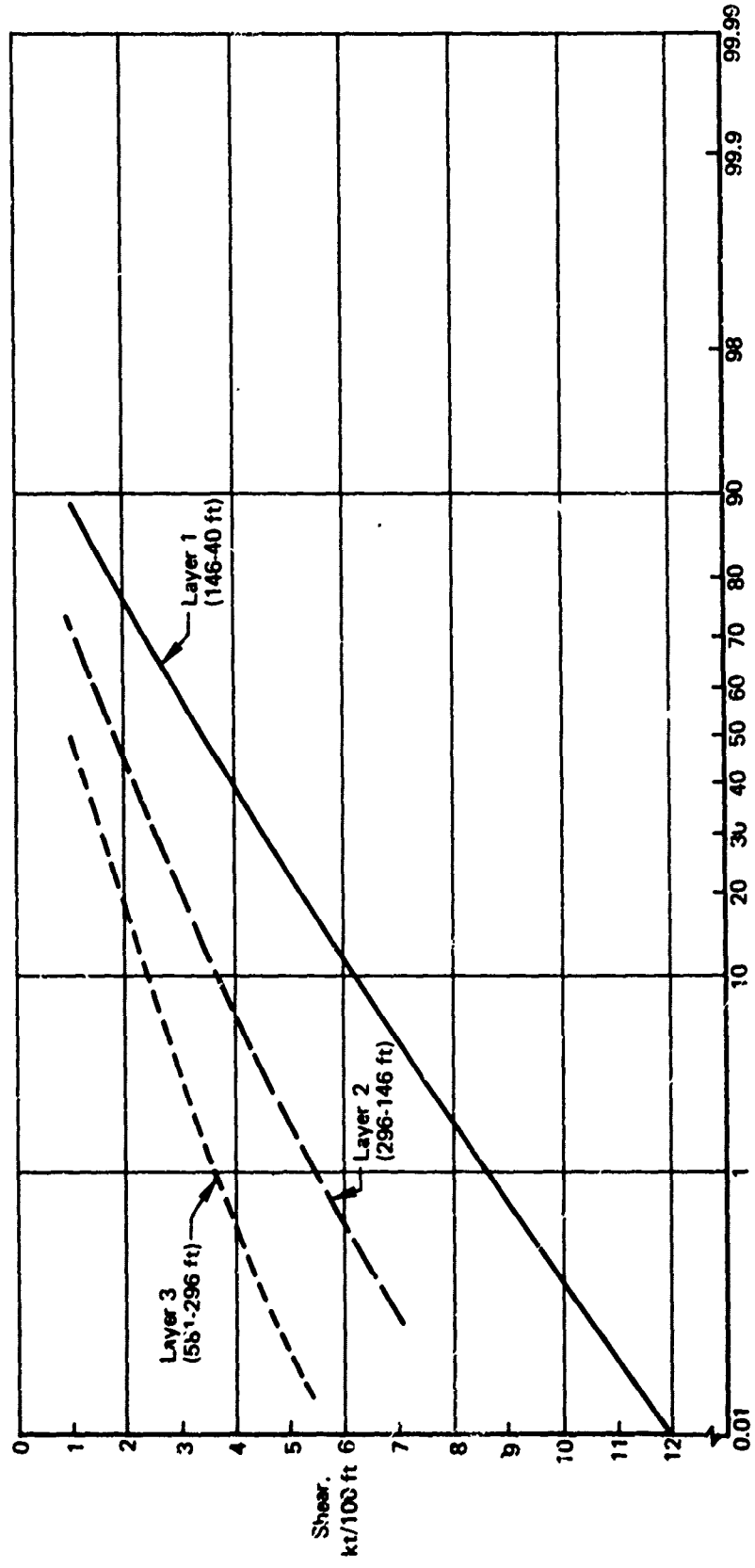

FIGURE 3-23.—WIND SHEAR MAGNITUDE, OKLAHOMA CITY

the curves for layers 3 and higher are virtually identical. This certainly indicates the greater average and variation of shear at the lower layers. The results agree reasonably well with those of other investigators. In the lowest layer there were 17 cases or 0.2% with shears equal to or greater than 10 kn/100 ft. The layer 1 probabilities of exceedance compare very favorably to the curve for the 200-20 foot layer at Whiteshell, Canada in Figure 3-13. From this little evidence it is suggested that shear probabilities at various airports are very similar over the same height intervals; however, more evidence would be desirable.

These authors also found that in the lowest three layers the wind shear is mostly speed shear and the directional shear becomes more important in the upper three layers.

3.2.3.2 Summary

Additional wind shear information is available in a Boeing internal memo for Cedar Hills, Texas and Cape Kennedy, Florida (Ref. 3-22). These data were obtained from the same computer tapes analyzed in greater detail in Section 3.3 of this report. Some of the information from the previous report is presented in Table 3-12, a summary compilation of the shear information discussed in this section. It is obvious that direct comparison between locations is difficult, as was discussed earlier; however, it appears that wind shear magnitudes in the lowest 200 feet or so average 3-5 kn/100 ft and extremes for 100 foot or greater intervals are 13-15 kn/100 ft. However, extremes of 30 kn/100 ft might be expected for short intervals (see Cape Kennedy in Table 3-12). (Data for Thumba, India probably are not appropriate for airport locations.) The extreme shears may be associated with the low level jet stream which has been discussed by various authors (see Izumi, Ref. 3-23). Such jets generally appear within the lowest 2000 feet over specific locations during the late night and early morning hours with particular weather conditions. It is not the purpose of the present study to discuss the low level jet, per se, only the shears that might be expected.

3.3 EVALUATION OF TOWER DATA

Computer tape records of wind and temperature information observed at four tall tower sites (Cape Kennedy, Florida; Cedar Hills, Texas; Oklahoma City, Oklahoma; and Philadelphia, Pennsylvania) were obtained by Boeing at various times. These records have been made available to this study. They have been programmed separately to provide answers to the same set of basic questions, although the tape formats and the observations themselves are quite different. Data from the Philadelphia tower were not analyzed because the lowest observational level is 100 feet, too high for the study of properties below that level. The Oklahoma City data also were found to be deficient in several respects, primarily in that wind and temperature records overlapped for a period of only 6 months.

The tower levels with useful data at the other two locations are:

Cape Kennedy	Cedar Hills
10 feet	30 feet
33	70
59	150

TABLE 3-12.—WIND SHEAR SUMMARY (KT/100 FT)

Location	Monrovia	Whiteshell	Whiteshell	Sarnia	Ottawa	Thumba		Tokyo		Oklahoma City			Cape Kennedy										Cedar Hill									
Height interval (ft)	200-35	200-20	200-20	200-20	200-20	33-8	58-33	350-85	830-380	146-40	286-146	581-286	59-10		98-59		197-98		295-197		394-295		492-394		70-30		150-70		300-150		450-300		600-450	
Averaging period	10 min	10 min	10 min	60 min	60 min	Hrly	Hrly	Hrly	Hrly	5 min	5 min	5 min	10 min		10 min		10 min		10 min		10 min		10 min		10 min		10 min		10 min		10 min	
Other	200 ft speed 17.4 kt	200 ft speed 17.4 kt																														
Probability of exceedance (%)	Scalar		Vector sum			Components							Vector sum			A	B	A	B	A	B	A	B	A	B	A	B	A	B	A	B	A	B
						N-S	E-W	N-S	E-W	N-S	E-W	N-S	E-W																					
0.1	11.5E	12.0	10.4E	9.8	8.7	40.0	48.0	40.0	37.0	8.0	9.4	6.5	8.4E	16.4	7.0	4.8	24	22	32	29	12	11	11	11	9	11	9	11	13	12	7	8	7	6	6	5	5	5
1.0	8.9	9.5	8.5	6.6	6.3	31.0	38.0	26.0	23.0	5.6	6.7	4.2	4.8	8.6	5.5	3.7	11	11	14	14	7	6	5	5	4	4	4	4	7	8	4	6	3	3	2	2	1	1
90.0	4.9	5.0	3.6	2.9	2.3	6.5	9.0	4.3	3.9	1.6	1.4	1.4	1.5	3.6	1.7	1.0	3	3	2	2	2E	2E	1E	2E	1E	1E	1E	1E	4	4	2	3	2	3	2	2	2	1

Notes:
A = Along runway
B = Across runway
E = Extrapolated graphically

Cape Kennedy	Cedar Hills
98 feet	300 feet
197	450
295	600
394	750
	900
	1050
	1200
	1300
	1420

The tapes were evaluated for wind velocity (speed and direction), Richardson's number (R_i), and wind direction and speed shears. Following is a description of the analysis methods and the results from the two sites.

3.3.1 General Description

3.3.1.1 Cape Kennedy

Magnetic tape records containing 3 years (1966 through 1968) of hourly observations of 10-minute average wind velocities and temperatures at approximately 10, 33, and 59 feet (3, 10, and 18 meters) on one tower and 59, 98, 197, 295, 394, and 492 feet (18, 30, 60, 90, 120, and 150 meters) on a second tower displaced 18 meters from the first were in Boeing files. A program was written to extract these records and to determine the desired quantities discussed below. Since no records were available for 20 feet, the standard level for Weather Service instruments, a program was written to fit a curve to the data from which the 20-foot values could be extracted.

The most important winds in determining the 20-foot winds are those closest to the 20-foot height; therefore, in the development of a regression equation the speed data first were weighted inversely with distance from the 20-foot height. Then the weighted speeds were assumed to be related to ln h by a second order regression equation, i.e., $\bar{V}_W = C_1 + C_2 \ln h + C_3 (\ln h)^2$. The constants C_1, C_2, C_3 were determined from a second order least squares fit of the weighted data.

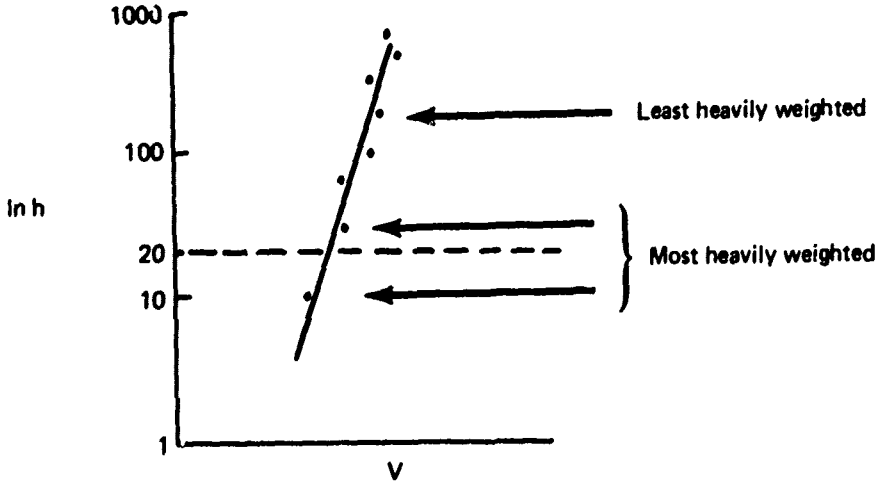

Then the 20-foot values were determined, in each case, by interpolation from the curve. A few cases were chosen at random and actual data plotted along with the derived curves. It was noted that in each case the 20-foot value so determined appeared, by eye, to be a very reasonable estimate and any unknown errors probably were within a small percentage (< 20%) of the true value. Another "spot" check of the data was made by determining for a few cases the 10-foot speed from the known speeds at the other levels and comparing this value to the known 10-foot value. Again, the errors were small and noticeable only when the speeds were light (1-7 knots) at the lowest levels. Then, some slightly negative 10-foot speeds were computed.

This method was not used for determining wind direction shear. Directional shears were determined for the geometric altitude of ~18 feet from the wind directions at 10 and 33 feet.

There were 21,056 records read into the computations; another 2529 were not used because some data were missing. Another 291 records were dropped because of low wind speeds at all levels which caused the model to give erroneous negative speeds. The following process/nonprocess criteria were applied:

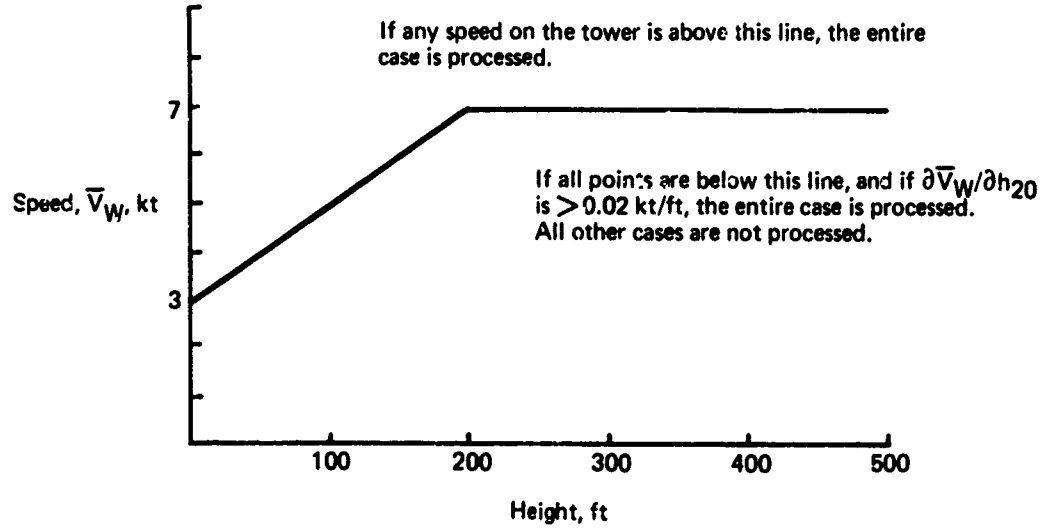

One additional criterion was used in the initial procedure. That entailed not processing those observational periods when the R_i was less than -20 or greater than +20. This included 2282 cases, and was caused by a nearly zero wind speed shear, or very large positive temperature gradient, or both. Another five were dropped because of "out-of-range" data. This was due to one or more data points in an observation being so extreme that it appeared to be in error.

3.3.1.2 Cedar Hills

Magnetic tape records from December 1960 to December 1962 for Cedar Hills contain 10-minute average wind velocities and temperatures from the 12 levels, previously mentioned, on a single 1434-foot-high television tower. As at Cape Kennedy, a computer program was written to extract and analyze the data. Again no records were available for the

20-foot height nor were any available for less than 20 feet, so a program analogous to the Cape Kennedy program was written to obtain estimates for that level (see 3.3.1.1).

Since wind directions were not determined for levels below the lowest tower level (30 feet), wind shear was computed for a geometric altitude of 46 feet from the directions at 30 and 70 feet. This shear was used as an estimate of the true shear at 20 feet. The frequency distribution of shears at 20 and 44 feet at Cape Kennedy are quite similar, Figure 3-54, and it is assumed that holds true for Cedar Hills as well.

There were 39,046 points read into the program out of a total of 66,567, no points dropped because of missing records, 2171 dropped because of low speeds (see previous section), 24,147 dropped because of excessive R_i, and another 1203 dropped because of out-of-range data. Note that a far greater number of points were dropped because of excessive R_i for Cedar Hills than Cape Kennedy.

3.3.2 Wind Speed

3.3.2.1 Evaluation Methods

Wind speed at 20 feet for each hourly observation was determined by the log linear method described in Section 3.3.1.1. The method was adapted to the various formats and observation levels provided by the tapes. Wind speed information for the observing levels were processed directly to histograms.

3.3.2.2 Distribution at 20 Feet Elevation

The distribution of wind speeds at 20 feet is shown in Figures 3-24 and 3-25 for the two locations. Both distributions indicate lighter winds than the descriptions given in Section 3.2.1.1, Figures 3-26 and 3-27. Also note that the Cedar Hills wind speeds are lighter than the Cape Kennedy wind speeds.

3.3.2.3 Distribution with Height

Wind speed distribution at the given tower levels was also determined and the probabilities of exceedance are shown in Figures 3-28 and 3-29 at the individual sites. The Cape Kennedy data are shown also in Table 3-13. This indicates the smooth transition between the 10- and 33-foot levels through the interpolated 20-foot level. A smooth increase in speed with altitude exists through all but the top level, where an unexplained decrease in speed is noted at Cape Kennedy.

3.3.3 Richardson's Number

3.3.3.1 Evaluation Methods

The R_i at 20 feet was determined for all wind speeds and by 2-knot intervals from 2 to 30 knots. Cases processed are the same as for wind speed, and the computer program used for extrapolating to 20 feet is analogous to that used for wind speed.

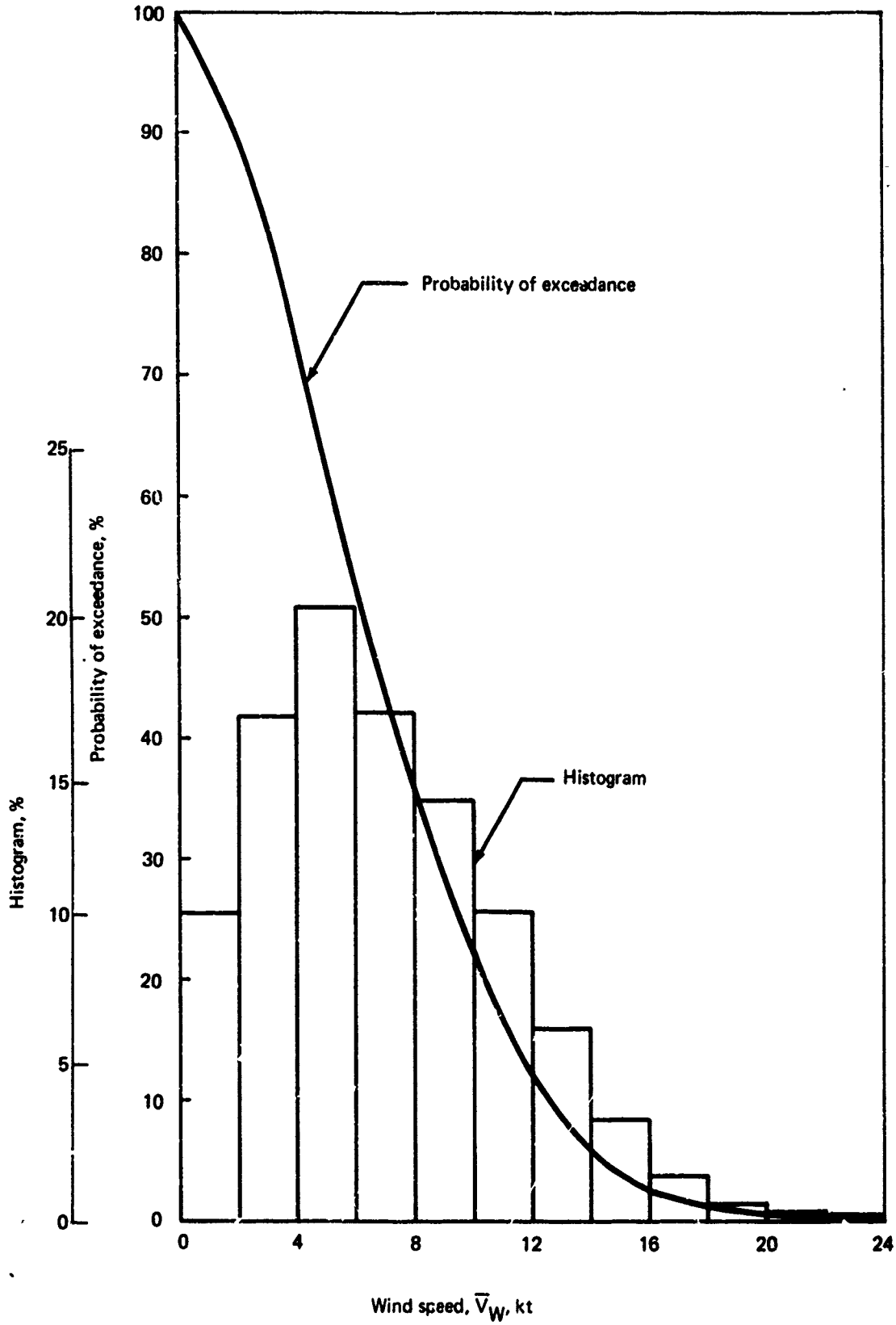

FIGURE 3-24.–WIND SPEED AT 20 FEET, CAPE KENNEDY, 1966-68

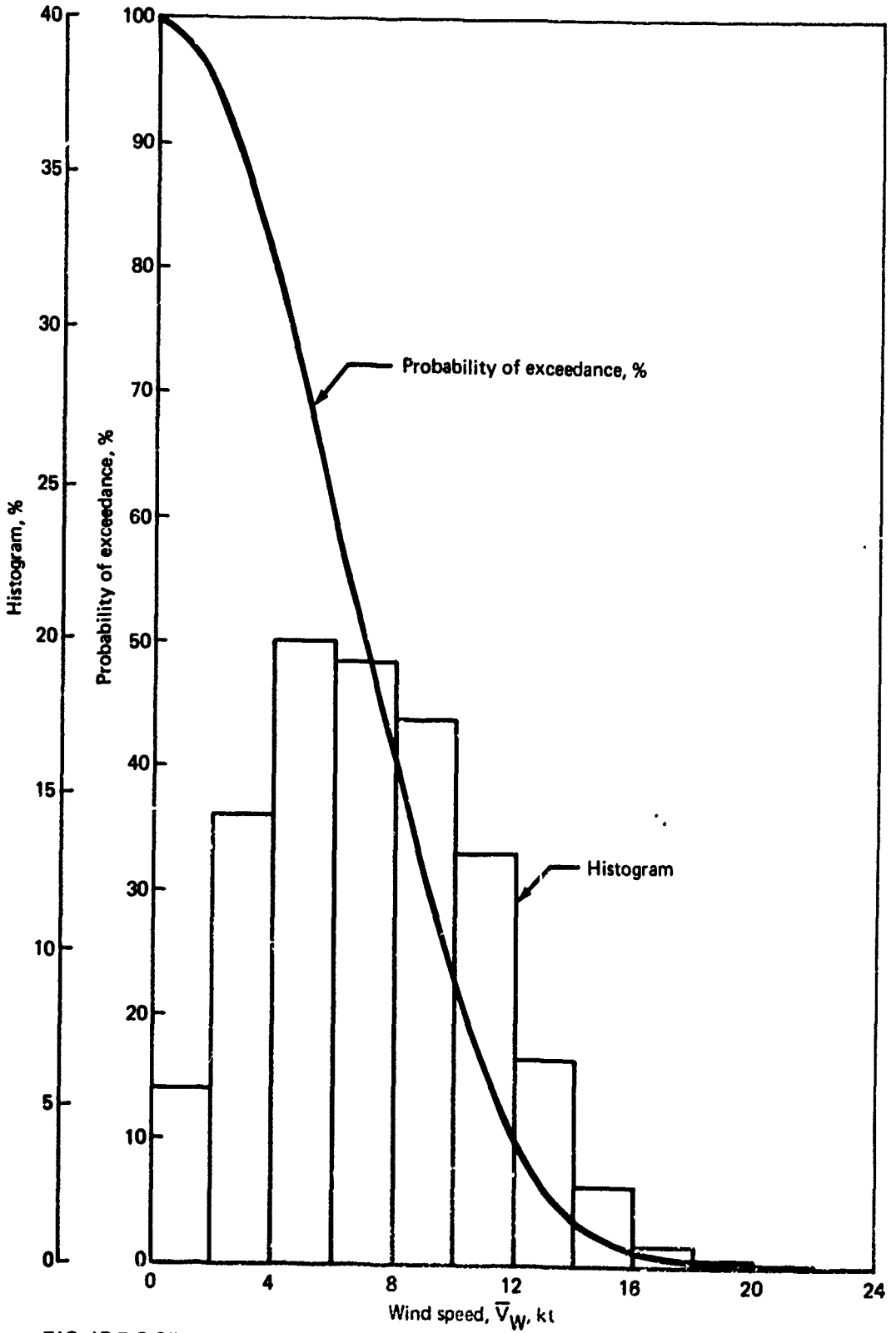

FIGURE 3-25.–WIND SPEED AT 20 FEET, CEDAR HILLS, TEXAS, 1960-62

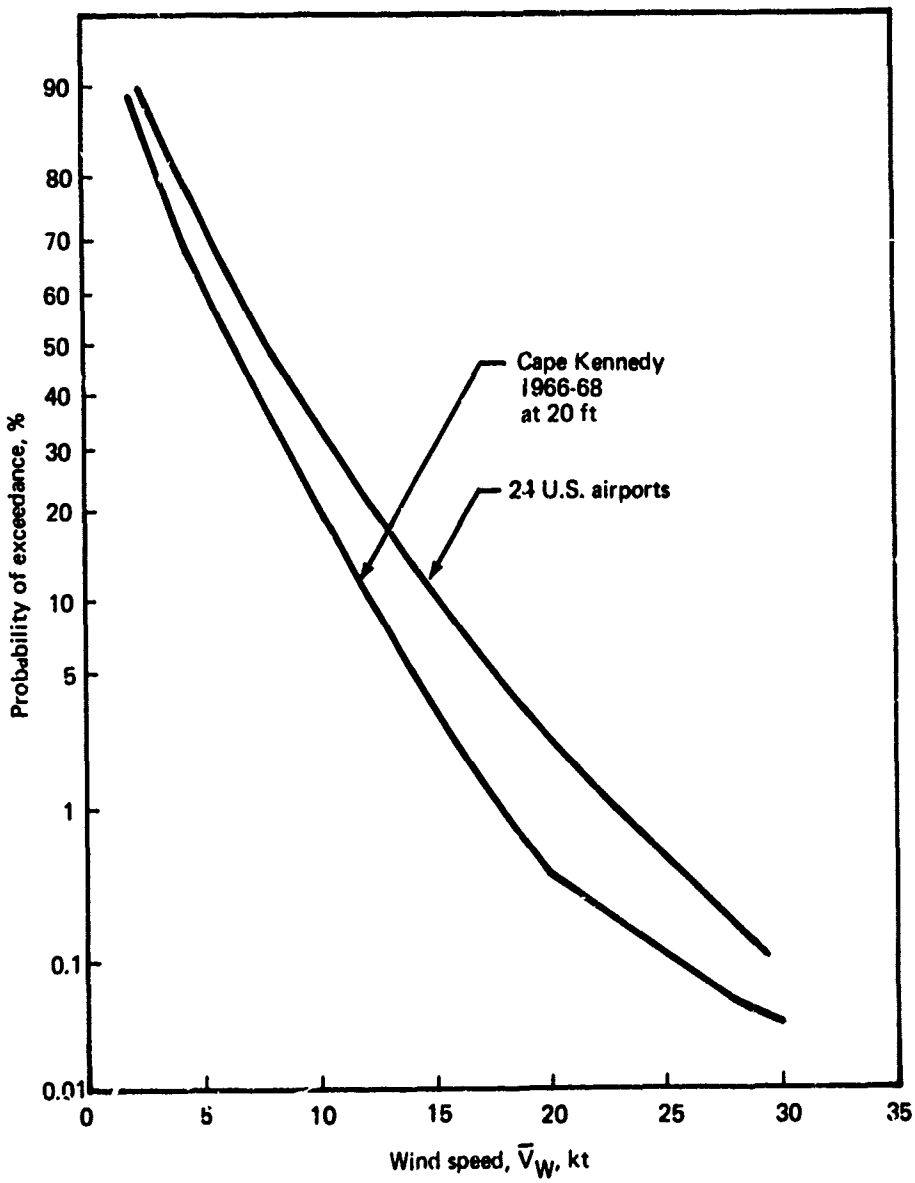

FIGURE 3-26.–COMPARISON OF WIND SPEEDS, CAPE KENNEDY AND 24 U.S. AIRPORTS

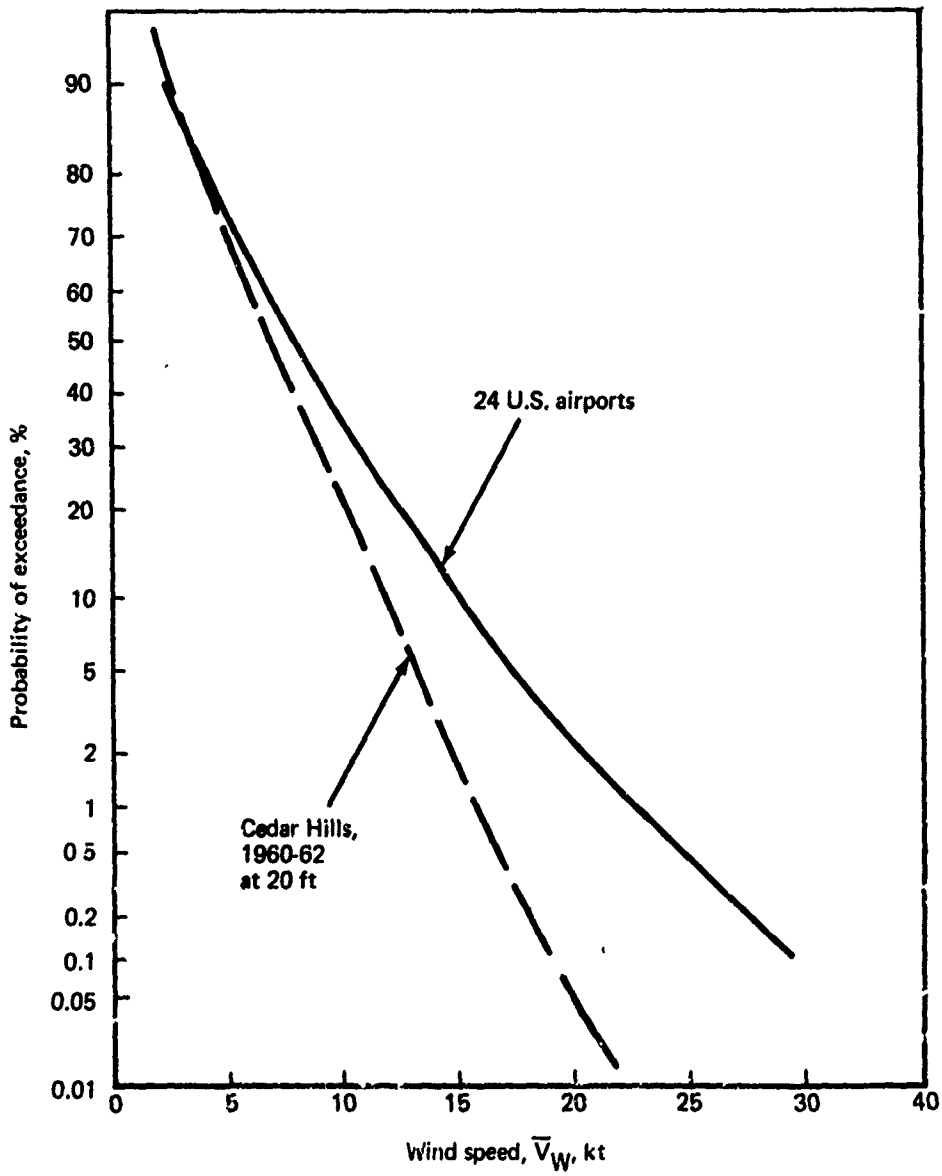

FIGURE 3-27.–COMPARISON OF WIND SPEEDS, CEDAR HILLS, TEXAS AND MEAN OF 24 U.S. AIRPORTS

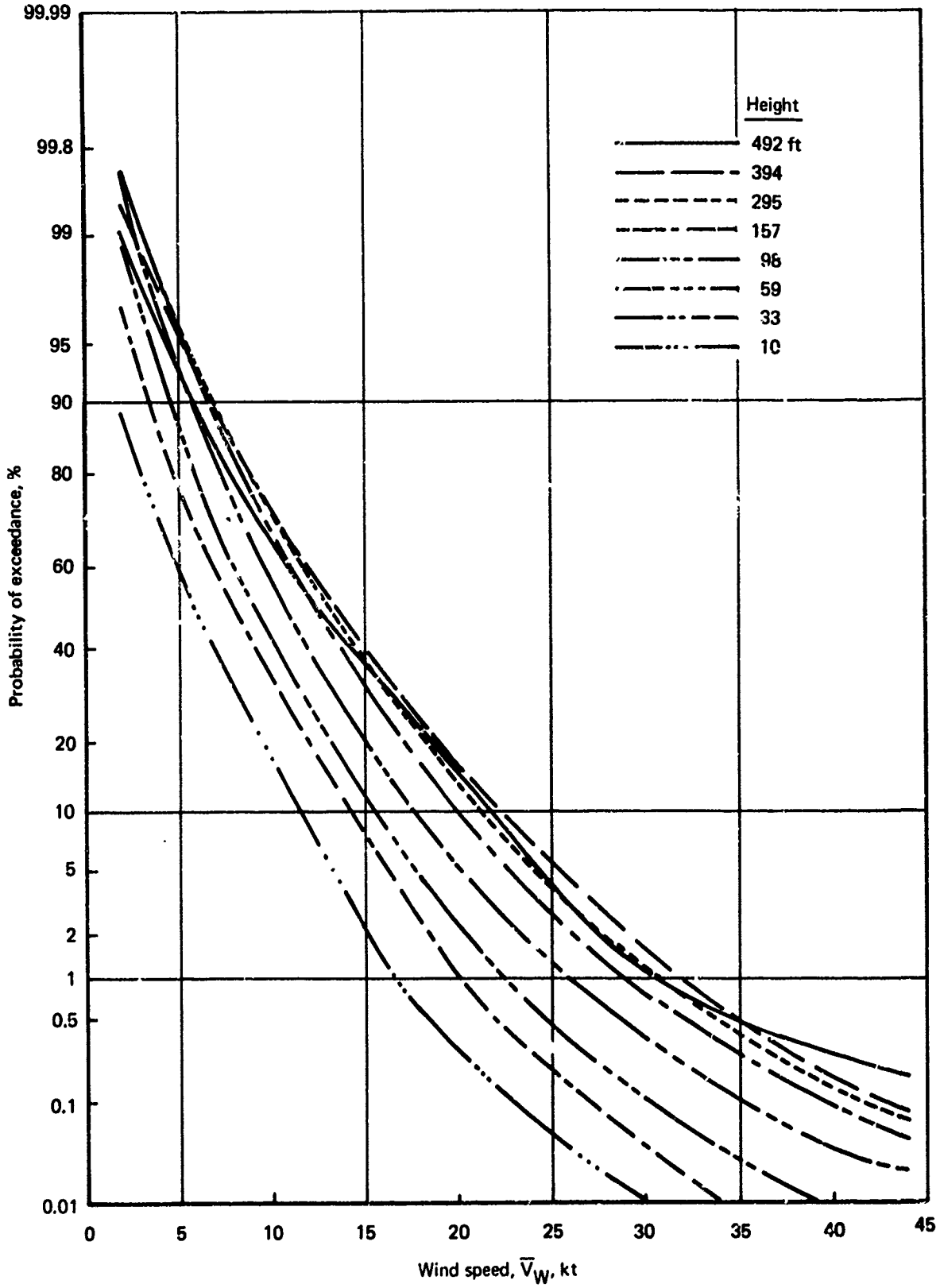

FIGURE 3-28.–PERCENT FREQUENCY OF EXCEEDANCE OF WIND SPEED AT SEVERAL HEIGHTS, CAPE KENNEDY, 1966-68

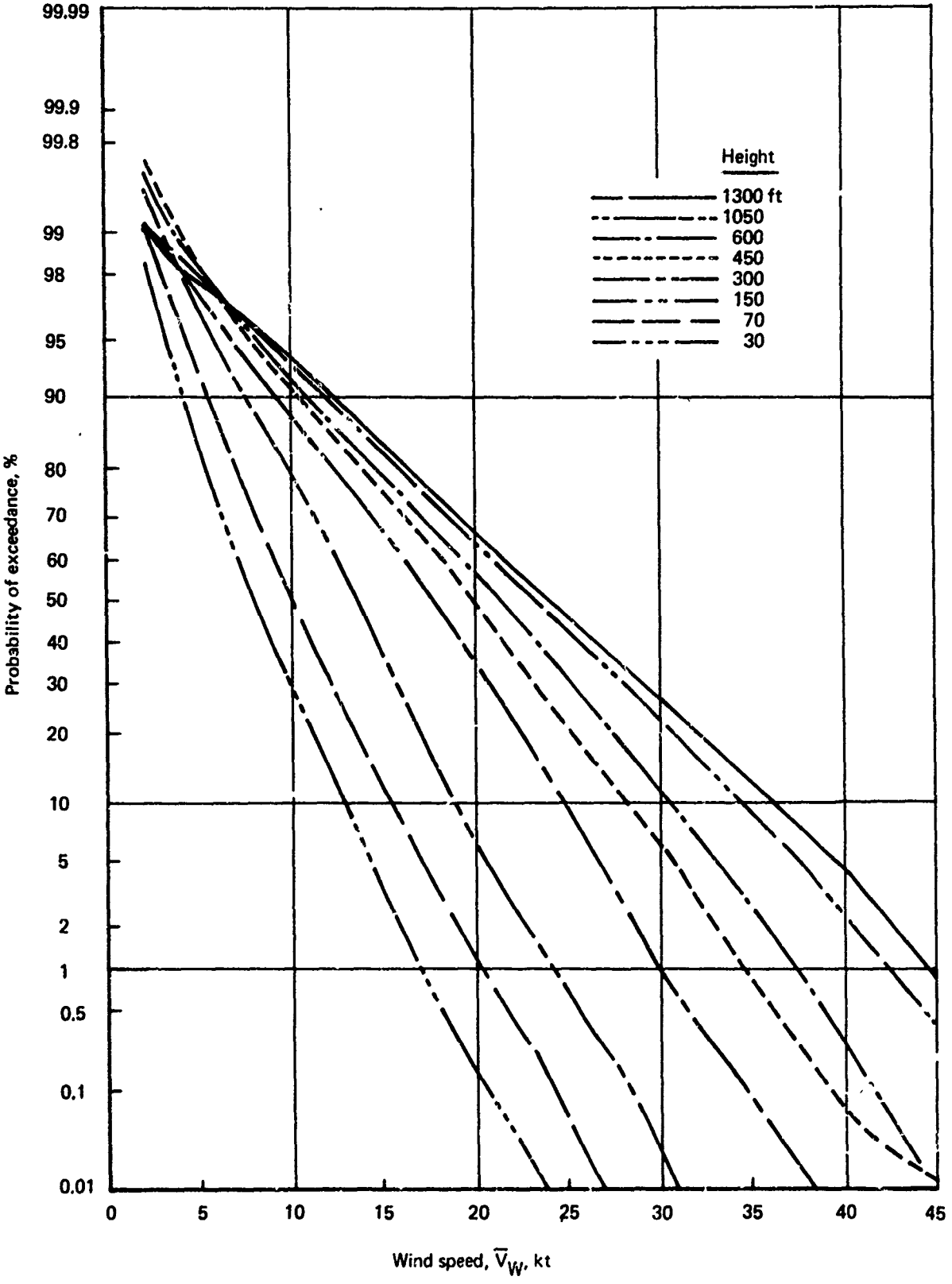

FIGURE 3-29.–PERCENT FREQUENCY OF EXCEEDANCE OF WIND SPEED AT SEVERAL HEIGHTS, CEDAR HILLS, TEXAS, 1960-1962

TABLE 3-13.–PERCENT FREQUENCY OF EXCEEDANCE OF WINDSPEED–CAPE KENNEDY 1966-68

Height (ft)	Probability of exceedance (%)						
	99	95	90	50	10	5	1
	Frequency of exceedance of windspeed (%)						
492	2.0	4.5	5.8	12.3	21.5	24.3	30.5
394	2.7	5.3	7.0	13.5	22.5	25.2	32.4
295	3.3	5.7	7.0	13.1	21.2	24.0	30.6
197	3.5	5.7	7.0	12.3	20.0	22.8	28.8
98	2.6	4.5	5.8	10.8	17.0	20.2	26.0
59	1.8	3.4	4.4	9.0	15.6	17.7	22.5
33	2.0	2.8	3.7	8.0	14.2	16.3	21.0
20	2.0	2.0	2.0	6.3	12.3	14.1	17.6
10	2.0	2.0	1.8	5.8	11.4	13.2	16.5

3.3.3.2 Distribution at 20 Feet Elevation

Probability of exceedance curves for R_i at 20 feet were drawn from the computer printout and are shown in Figure 3-30 as V-shaped curves with negative values to the left and positive values to the right on log-probability paper. The Cape Kennedy distributions between $R_i = -1.5$ and $+1.5$ are quasi-linear on this paper. The same data are presented in a different form on linear paper in Figures 3-31 to 3-46. The upper sections of these later figures are expanded versions of the lower sections for R_i near zero. It is to be noted that there is a difference between the results from the two locations, with Cedar Hills results indicating a larger percentage of high Richardson's numbers and Cape Kennedy results being more log-normally distributed. The former implies a greater frequency of stable conditions at Cedar Hills.

Although no complete answer is available to describe the difference without a rigorous investigation, it may be due in part to lighter wind speeds at Cedar Hills and the consequent greater frequency of inversions. A larger probable factor is the difference in climate and weather conditions between the two sites.

In addition to the R_i difference between the two sites, the speed shears differ in two ways–Cedar Hills has a higher mean shear and a greater spread of shears as noted in the following table.

Cumulative probability	10%	50%	90%
$\partial\bar{V}_W/\partial h$ at Cape Kennedy (kn/100 ft)	1.4	6.5	13.0
$\partial\bar{V}_W/\partial h$ at Cedar Hills (kn/100 ft)	-3.8	10.0	26.8

Since larger speed shears should result in lower Richardson's numbers it is obvious that the other terms, noticeably the temperature gradient, are influencing the results. Apparently, there are a large number of inversions or at least stable conditions at Cedar Hills. Future investigations should determine the reasons for the differences. However, Cedar Hills has a drier climate with a greater range of surface temperatures and intuitively a greater range of temperature gradients. Printouts of the Cape Kennedy results for the 1966-67 and the 1968

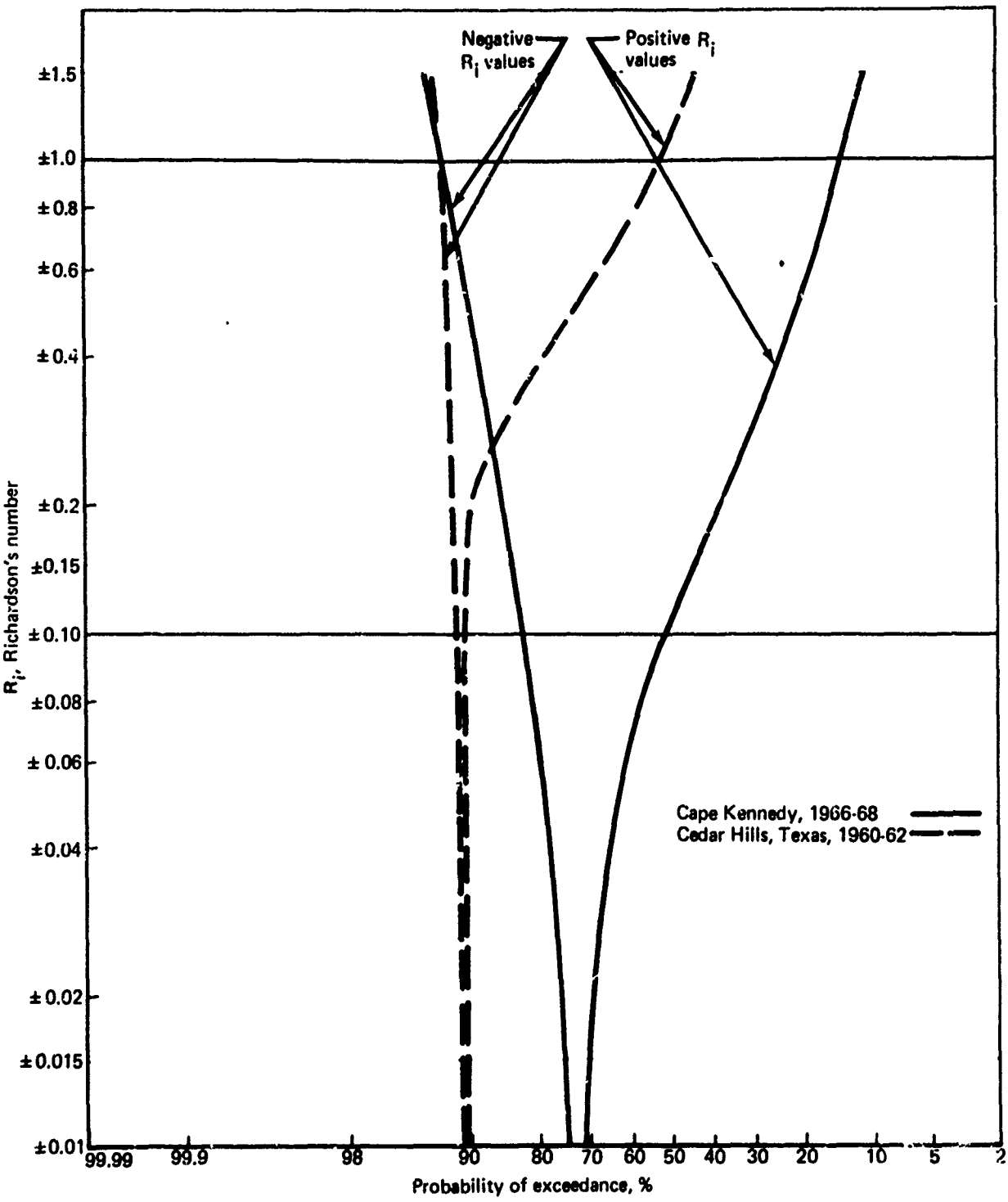

FIGURE 3-30.–PROBABILITY OF EXCEEDANCE OF R_i FOR ALL WIND SPEEDS

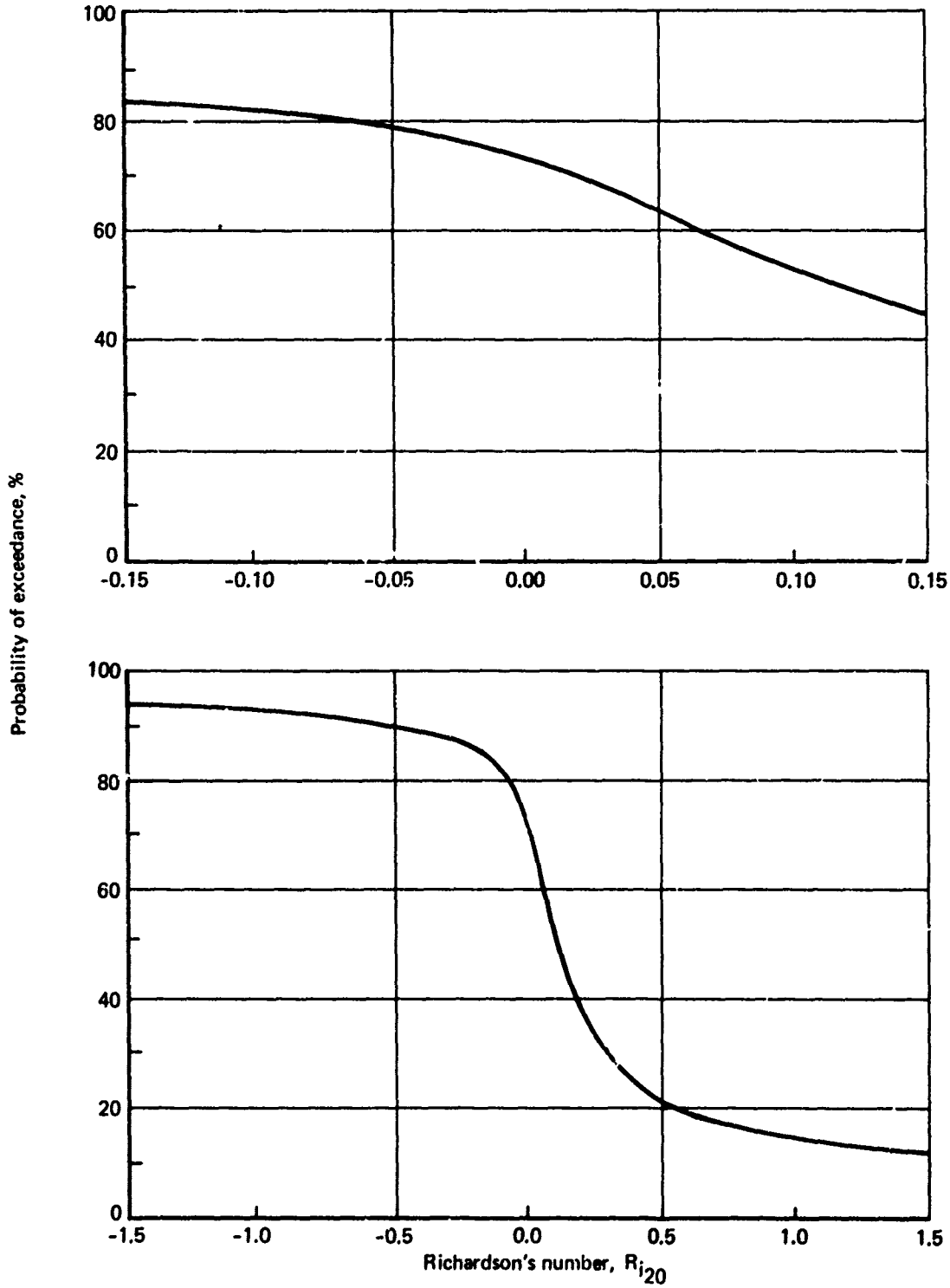

FIGURE 3-31.–R_i AT 20 FEET, CAPE KENNEDY, 1966-68, ALL WIND SPEEDS

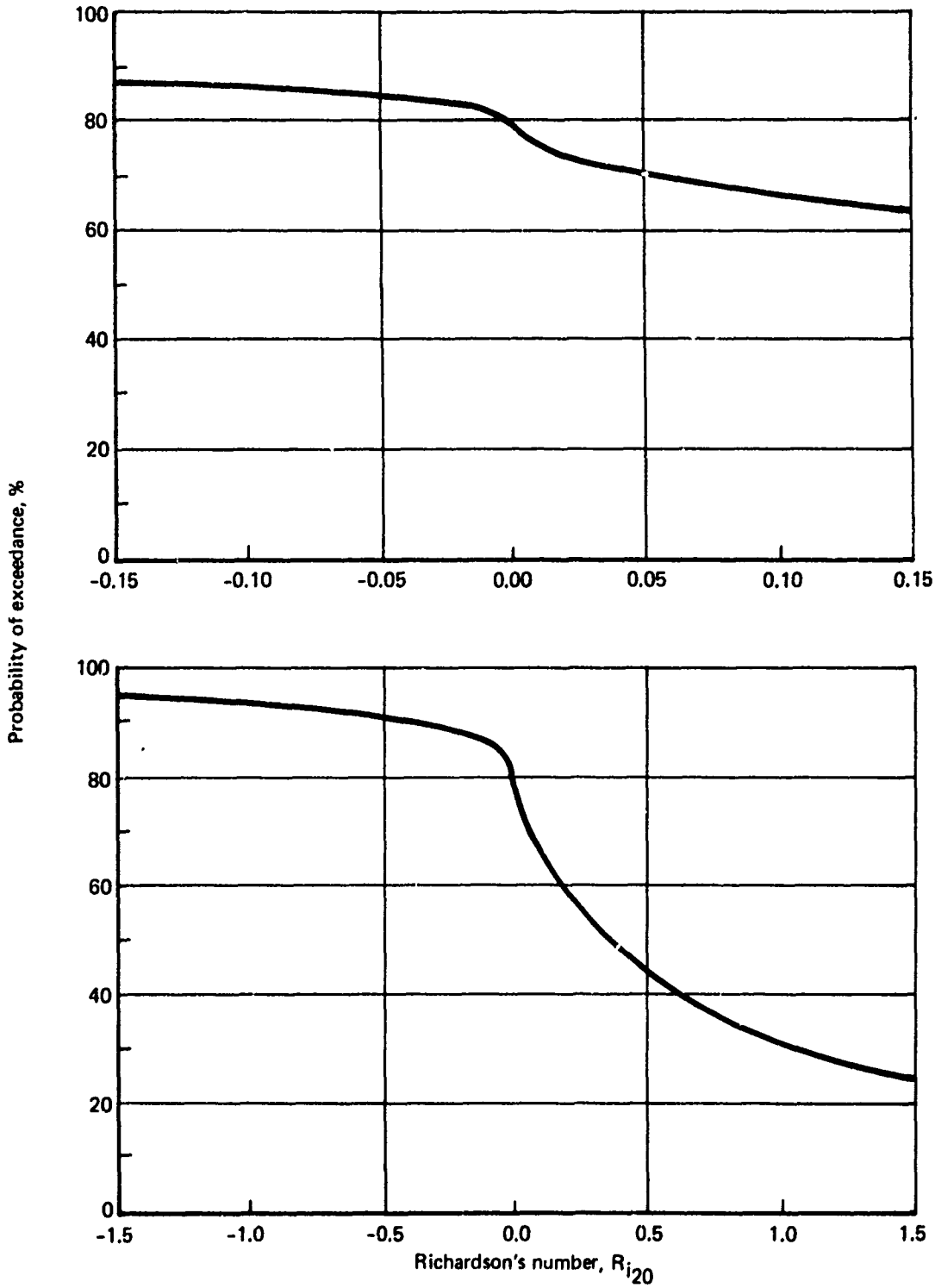

FIGURE 3-32.–R_i AT 20 FEET, CAPE KENNEDY, 1966-68, WIND SPEEDS 0-2 KT

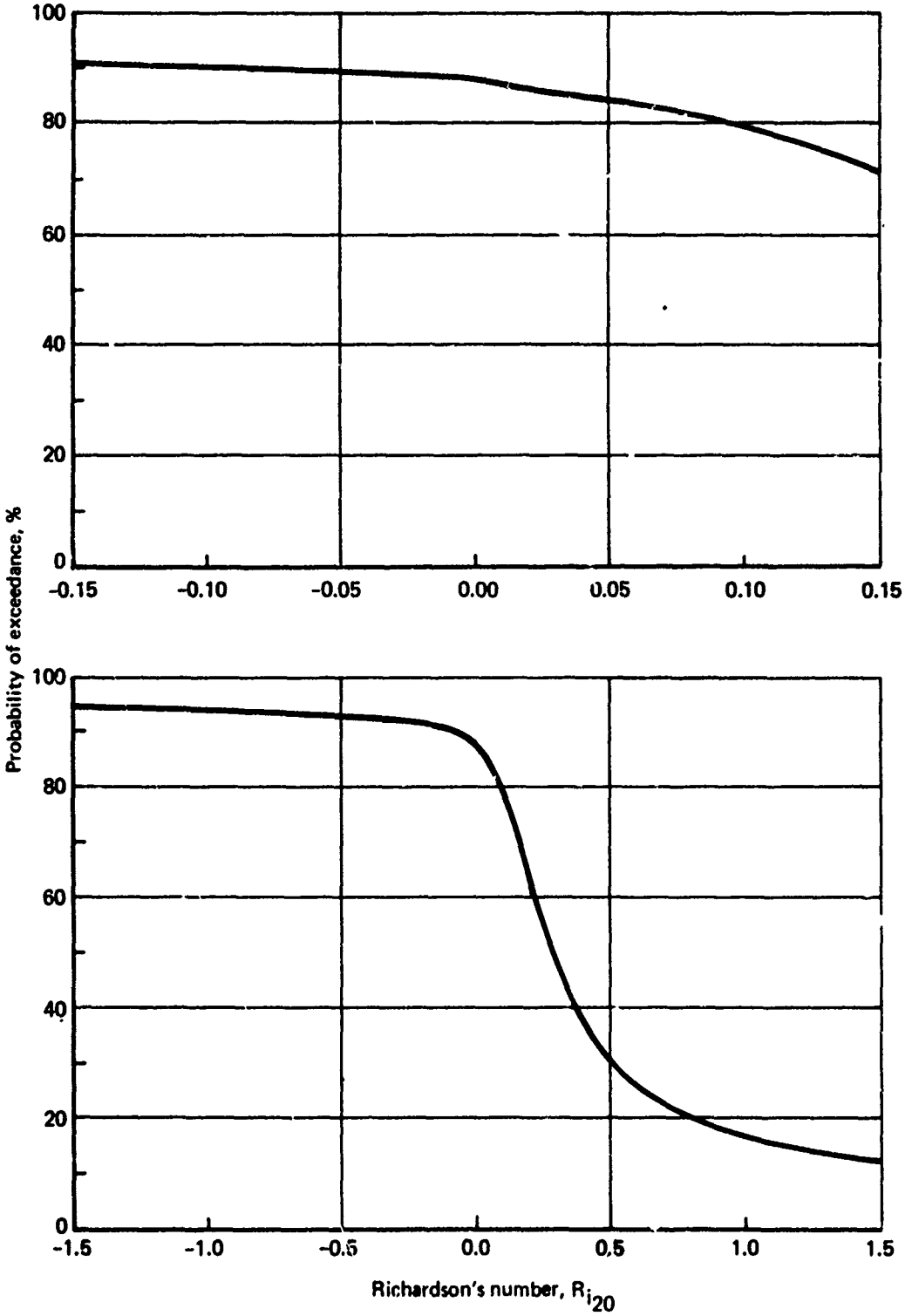

FIGURE 3-33.–R_i AT 20 FEET, CAPE KENNEDY, 1966-68, WIND SPEEDS 2-4 KT

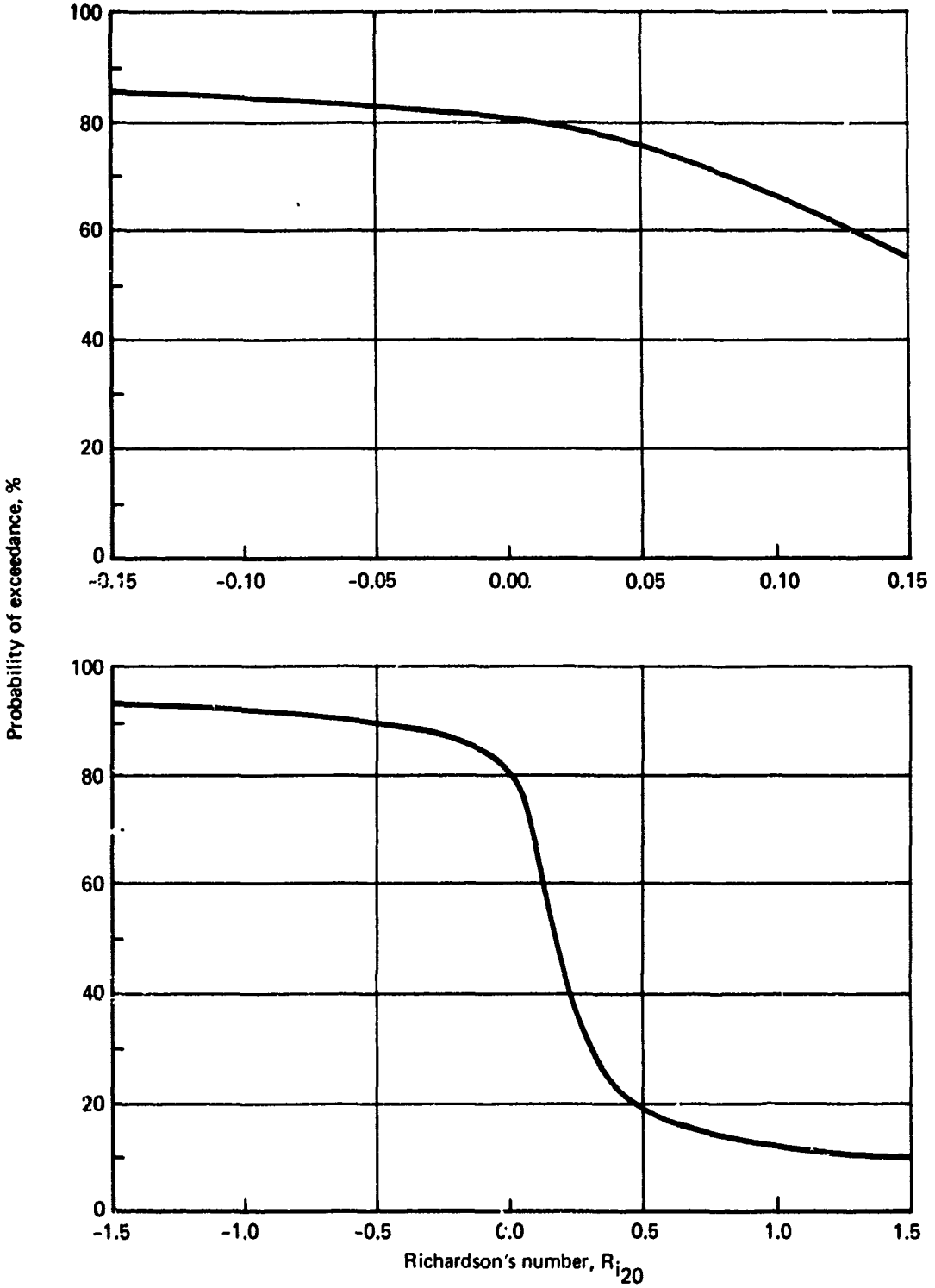

FIGURE 3-34.–R_i AT 20 FEET, CAPE KENNEDY, 1966-68, WIND SPEEDS 4-6 KT

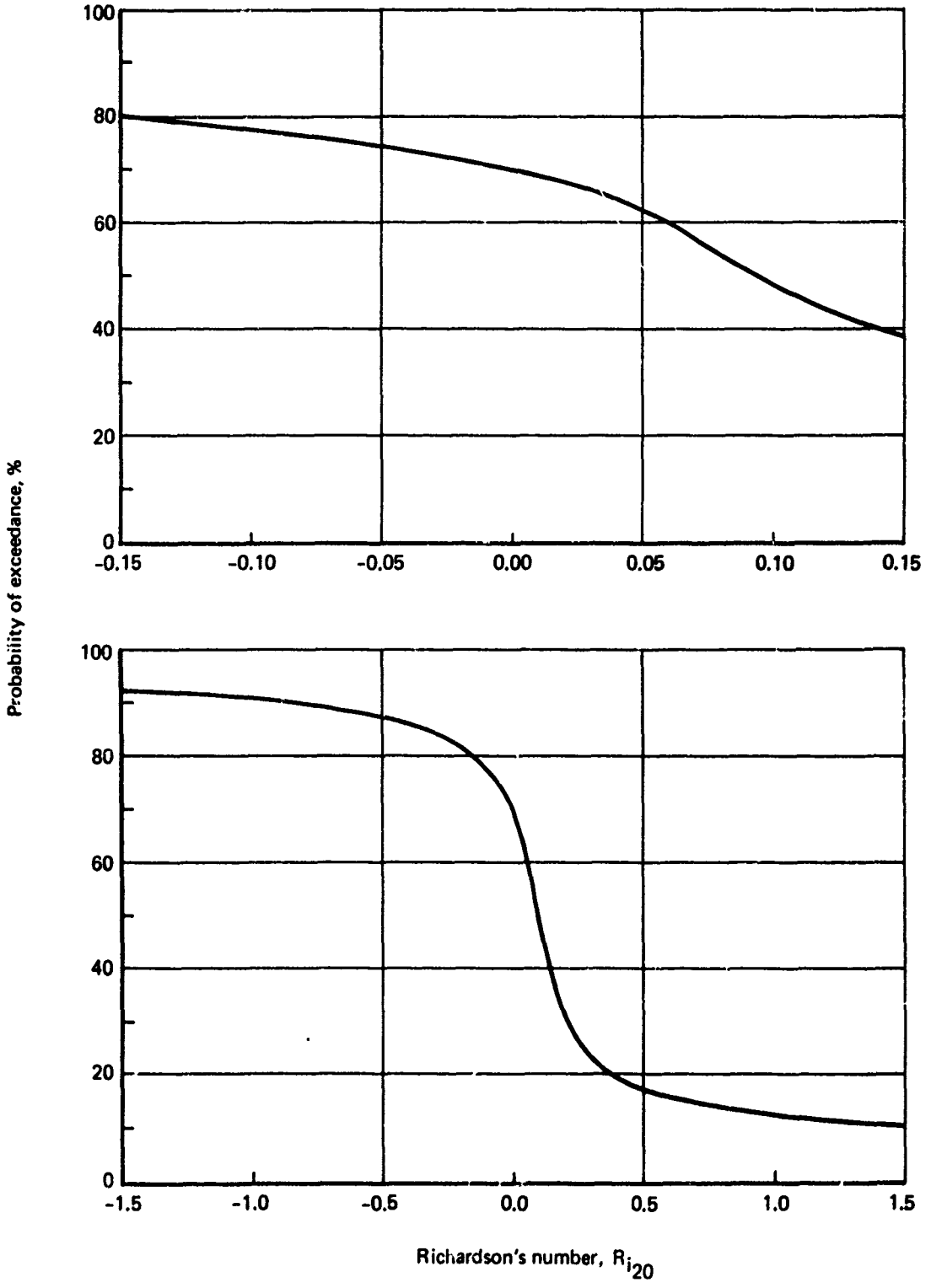

FIGURE 3-35.—R_i AT 20 FEET, CAPE KENNEDY, 1966-68, WIND SPEEDS 6-8 KT

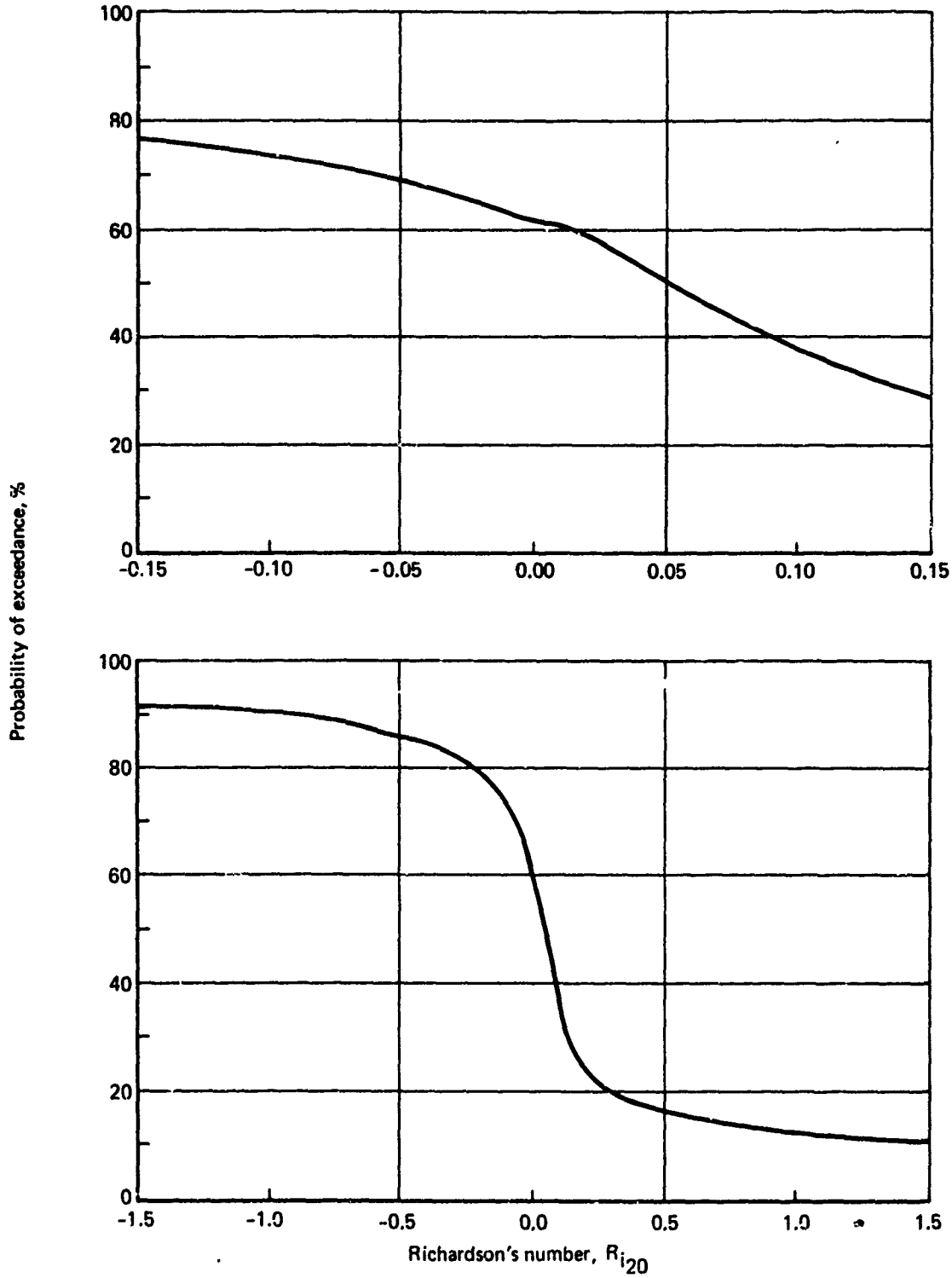

FIGURE 3-36.–R_i AT 20 FEET, CAPE KENNEDY, 1966-68, WIND SPEEDS 8-10 KT

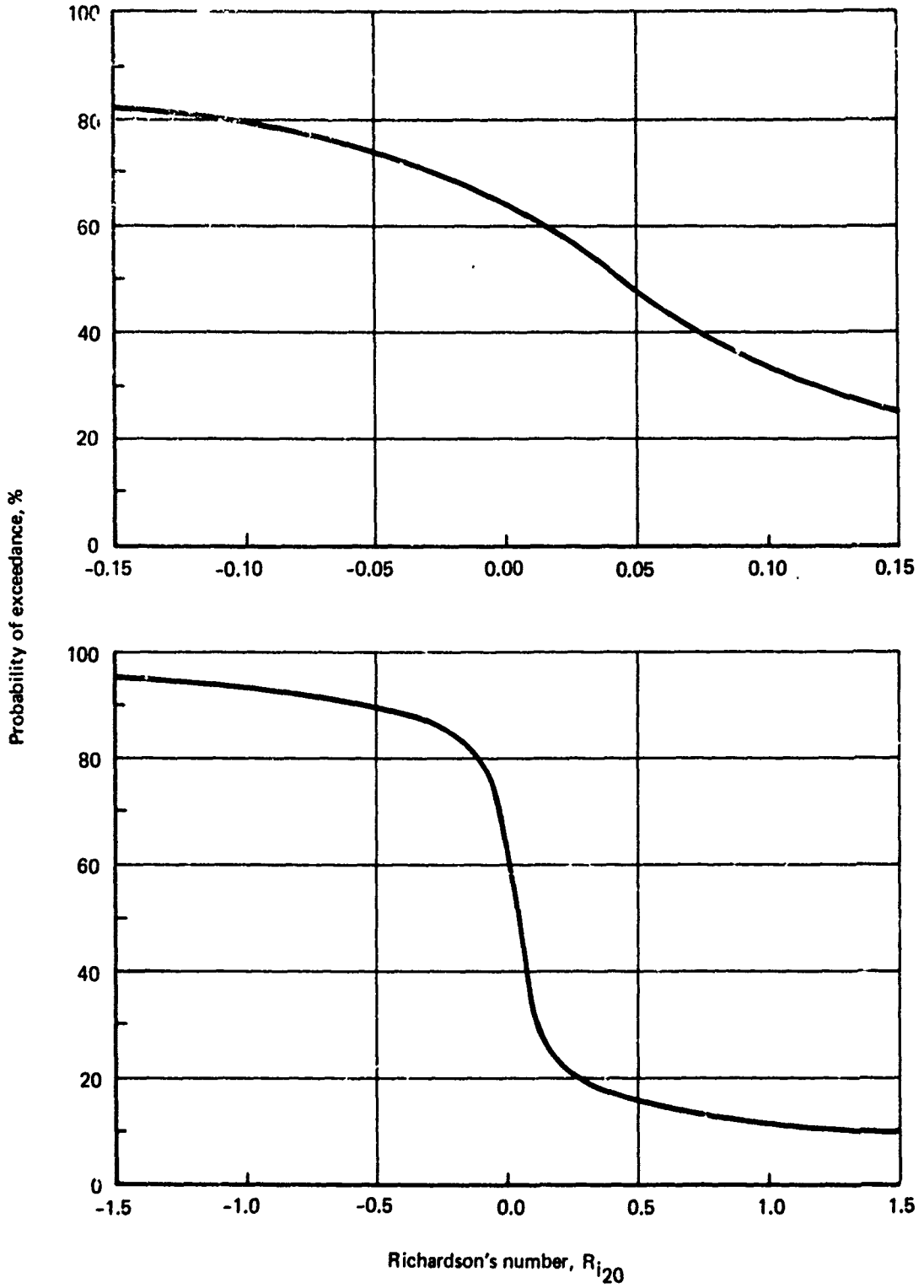

FIGURE 3-37.–R_i AT 20 FEET, CAPE KENNEDY, 1966-68, WIND SPEEDS 10-12 KT

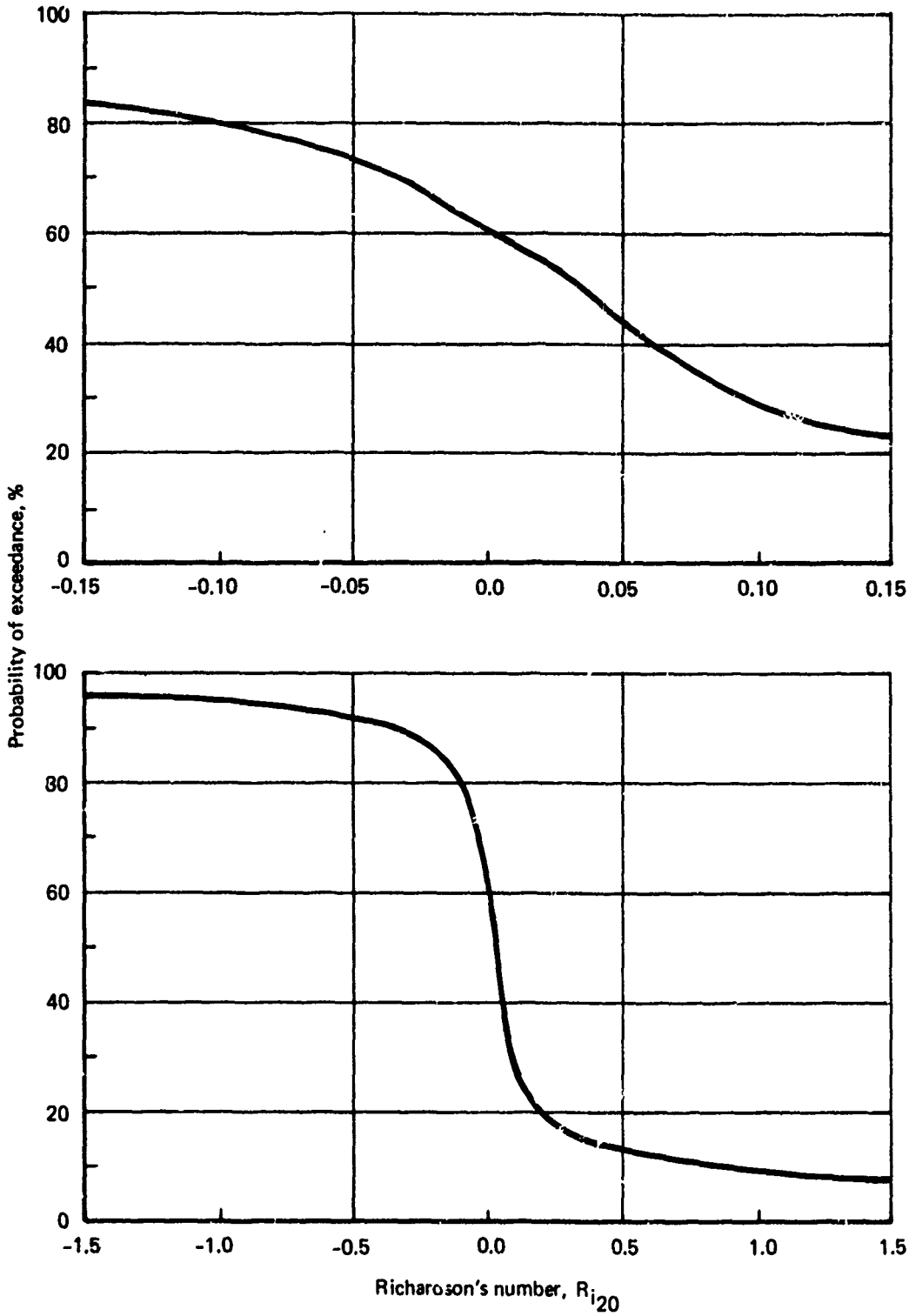

FIGURE 3-38.—R_i AT 20 FEET, CAPE KENNEDY, 1966-68, WIND SPEEDS 12-14 KT

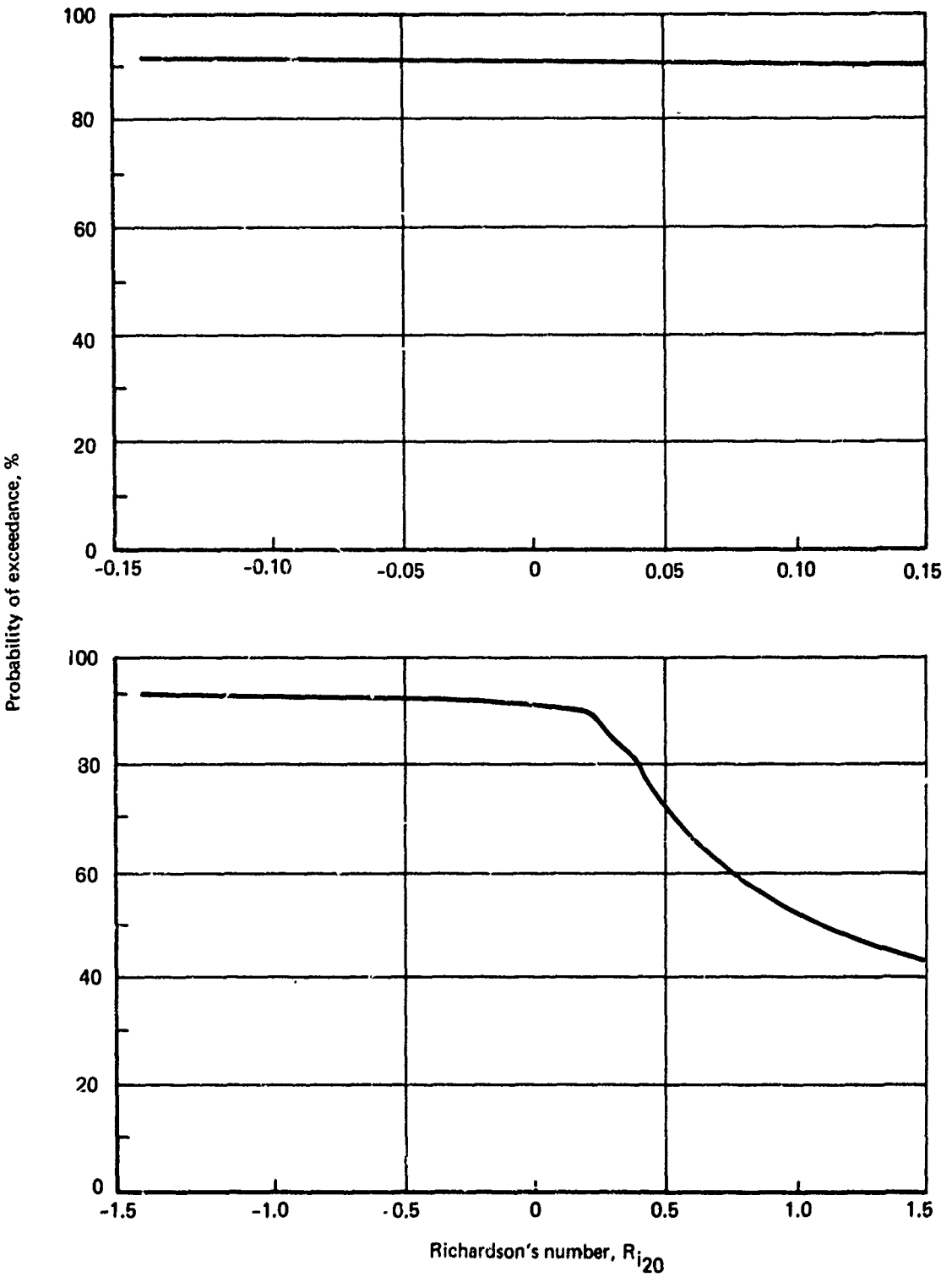

FIGURE 3-39.—R_i AT 20 FEET, CEDAR HILLS, TEXAS, 1960-62, ALL WIND SPEEDS

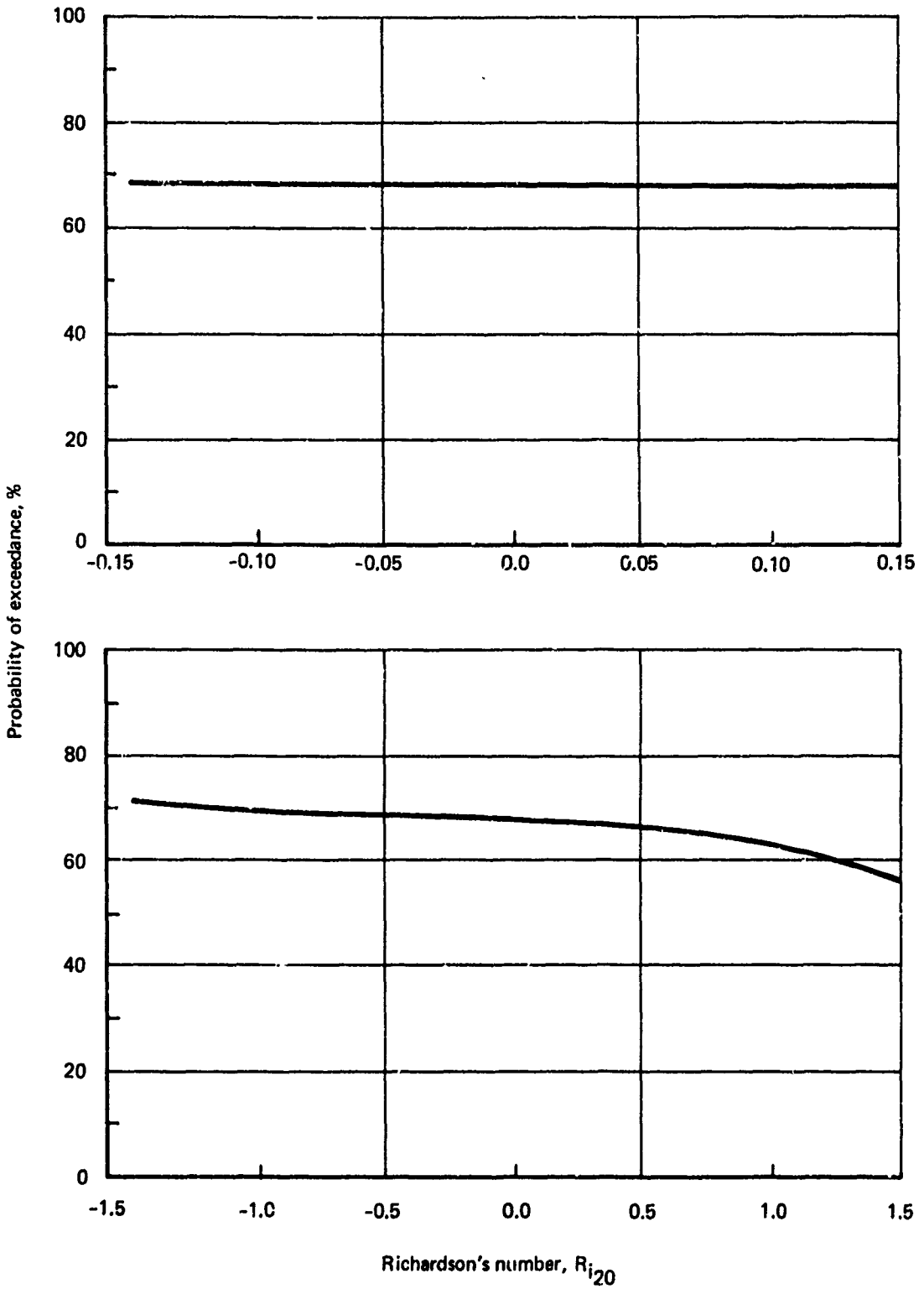

FIGURE 3-40.—R_i AT 20 FEET, CEDAR HILLS, TEXAS, 1960-62, WIND SPEEDS 0-2 KT

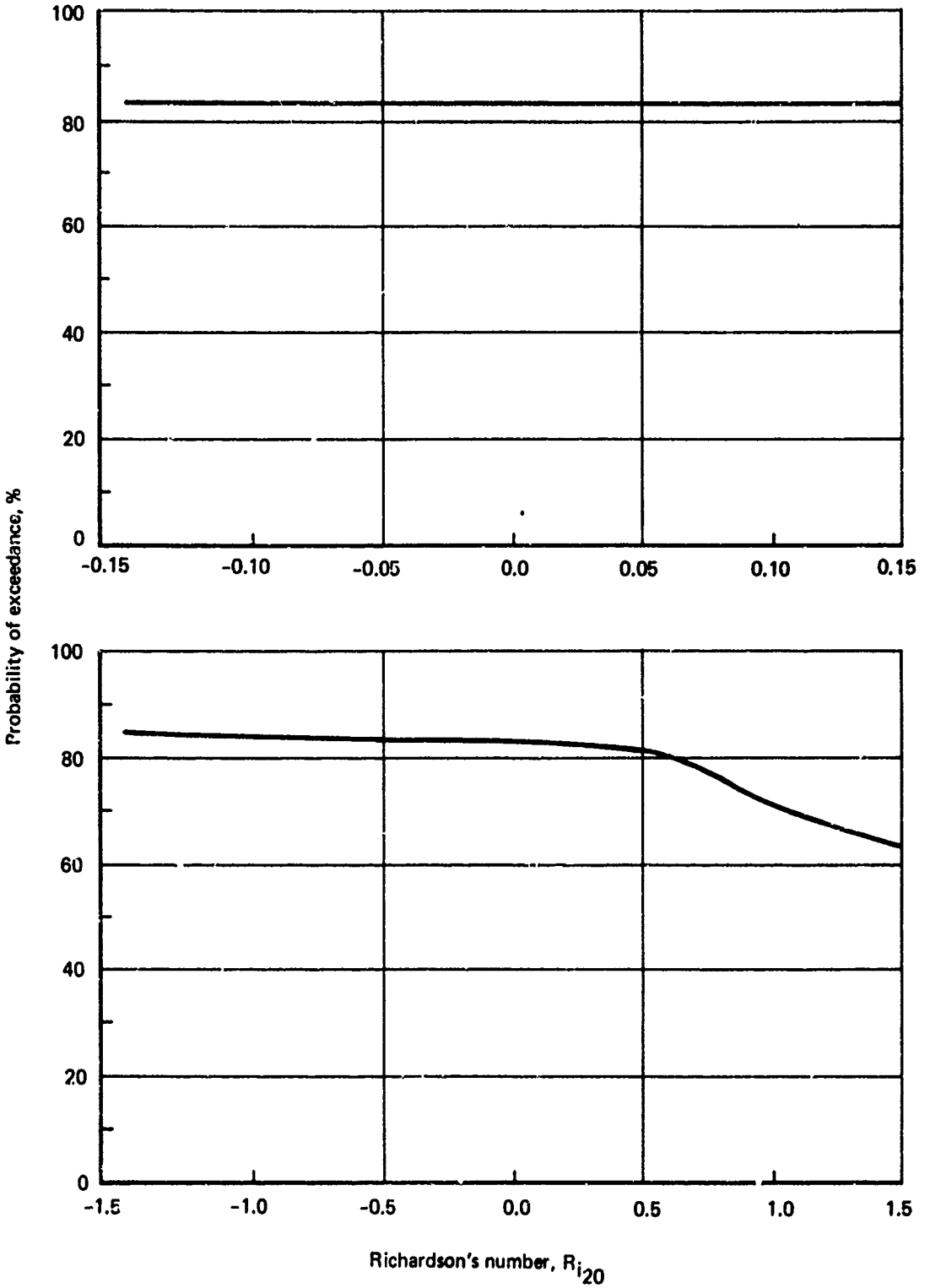

FIGURE 3-41.—R_i AT 20 FEET, CEDAR HILLS, TEXAS, 1960-62, WIND SPEEDS 2-4 KT

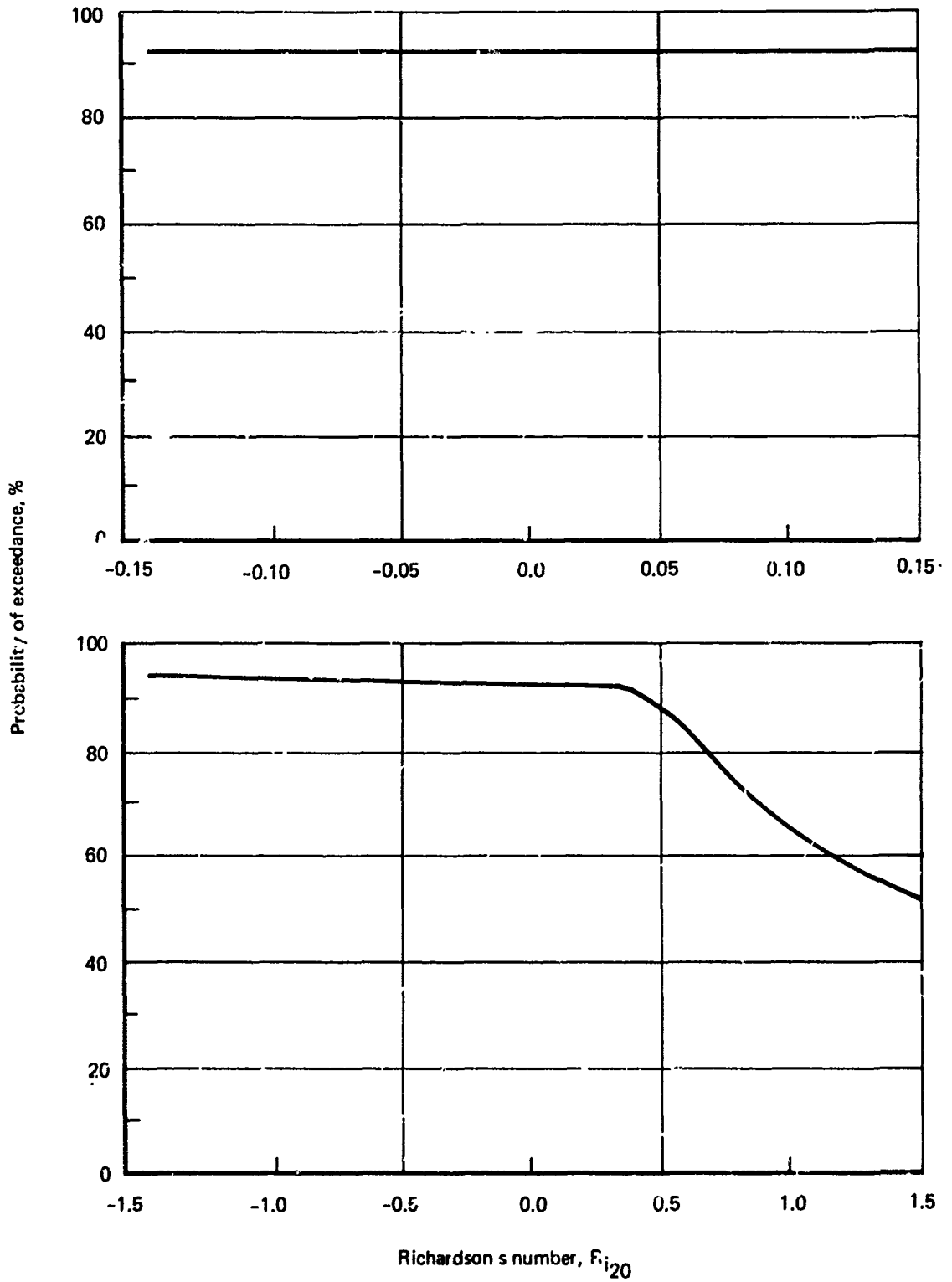

FIGURE 3-42.–R_i AT 20 FEET, CEDAR HILLS. TEXAS, 1960-62, WIND SPEEDS 4-6 KT

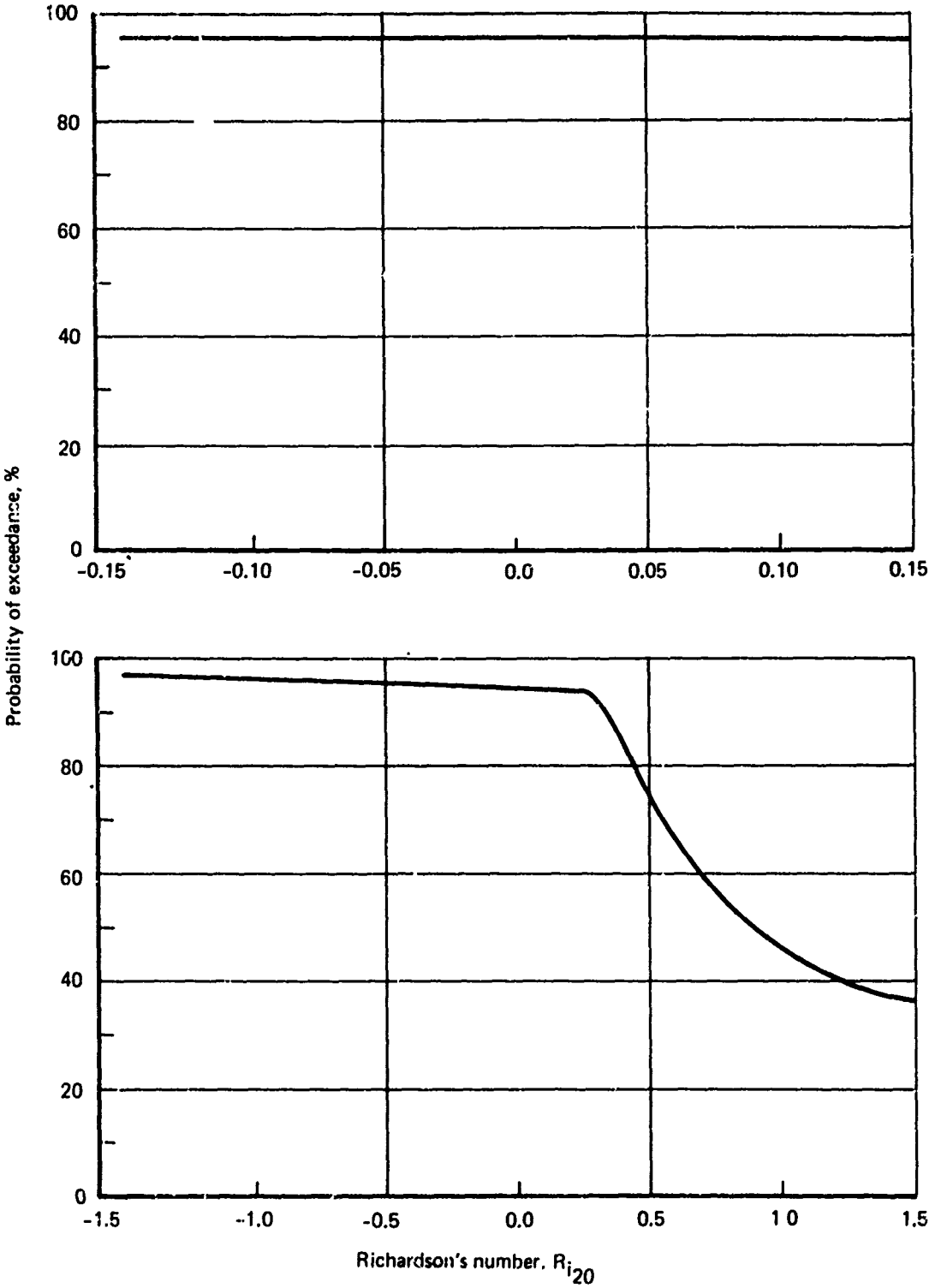

FIGURE 3-43.—R_i AT 20 FEET, CEDAR HILLS, TEXAS, 1960-62, WIND SPEEDS 6-8 KT

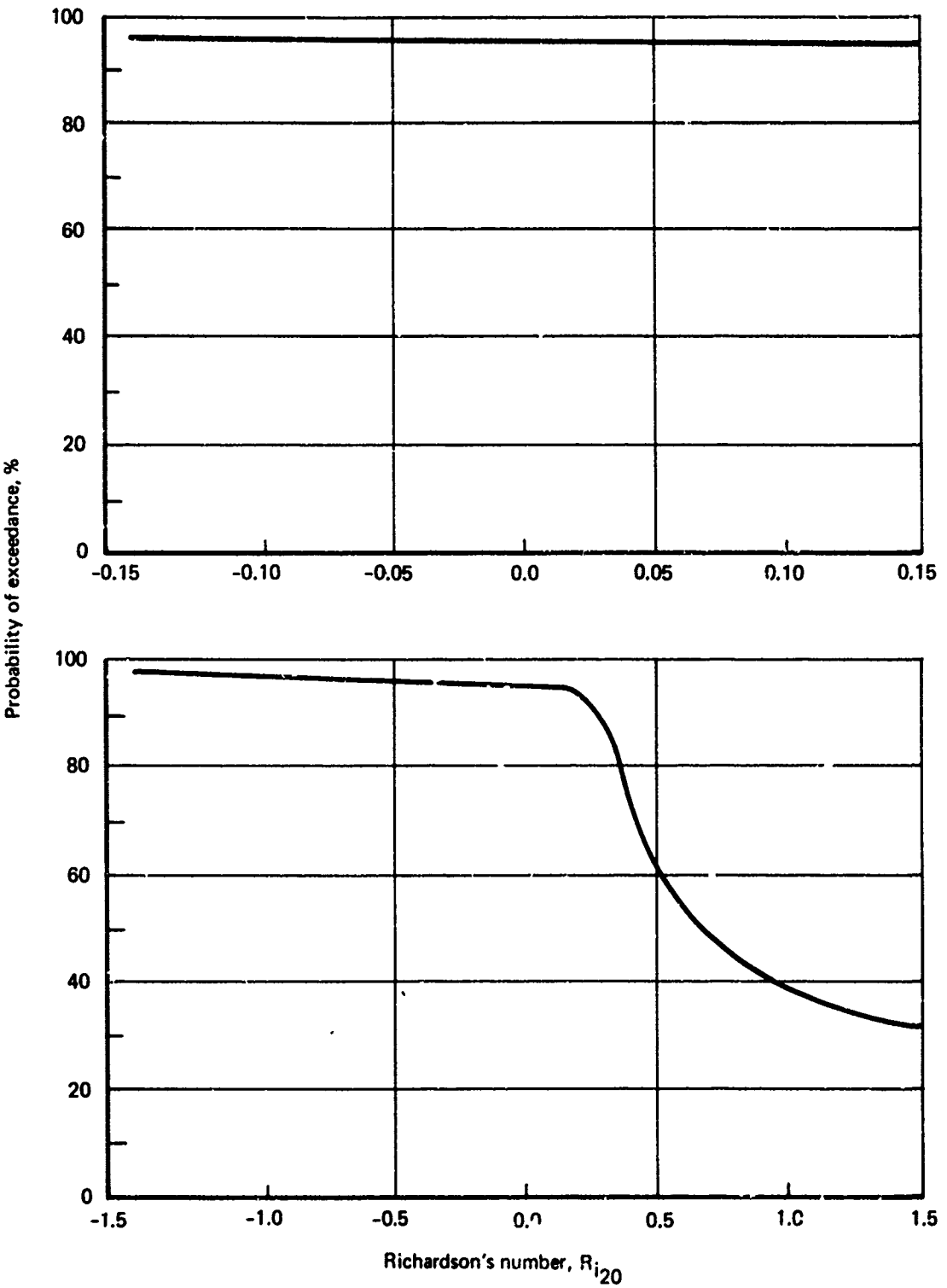

FIGURE 3-44.–R_i AT 20 FEET, CEDAR HILLS, TEXAS, 1960-62, WIND SPEEDS 8-10 KT

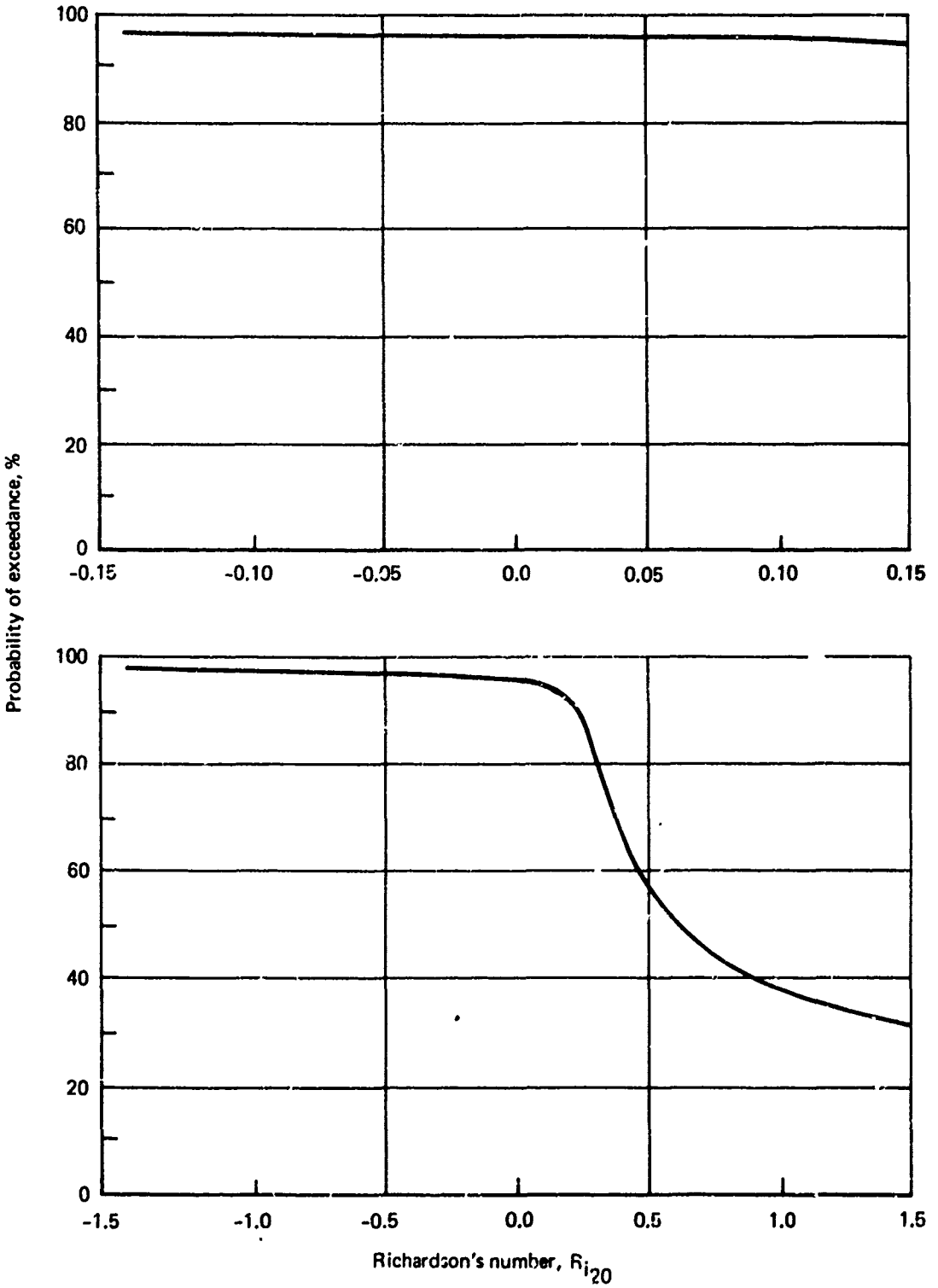

FIGURE 3-45.--R_i AT 20 FEET, CEDAR HILLS, TEXAS, 1960-62, WIND SPEEDS 10-12 KT

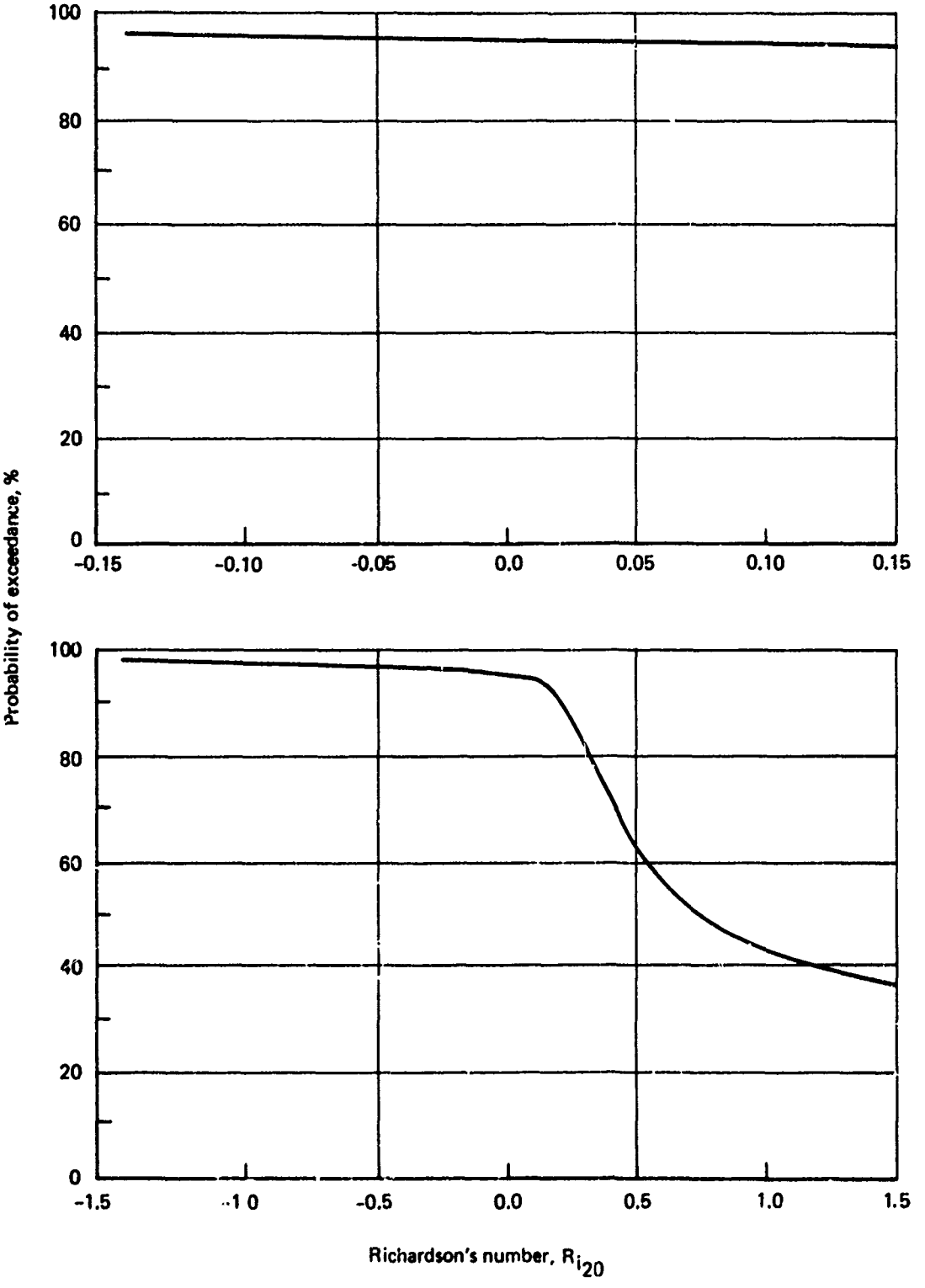

FIGURE 3-46.—R_i AT 20 FEET, CEDAR HILLS, TEXAS, 1960-62, WIND SPEEDS 12-14 KT

periods were compared to ascertain whether the distribution of R_i varied with time. There were differences between the two periods, but not as great as those between sites. The median R_i varied from 0.016 for 1968 to 0.165 for 1966-67—an order of magnitude difference; however, the distribution of values about the median remained about the same. Noting these intra- and inter-site differences, it appears that the distribution of R_i is greatly influenced by the local weather and climate and no single distribution will be representative of all airports. Information from a greater sample of stations is required to ascertain which set of curves, Cape Kennedy or Cedar Hills, is more representative of a large number of airports.

3.3.3.3 Richardson's Number and Speed at 20 Feet Elevation

The distributions of R_i at 20 feet were computed for 2-knot speed intervals as well as for all wind speeds described in the previous section. Percent frequency of occurrence diagrams were determined for each speed interval and plotted at the midpoint of each interval in Figures 3-47 and 3-48. As wind speed increases the spread of R_i decreases at Cape Kennedy. The greater spread of R_i values at Cedar Hills as compared to Cape Kennedy is again seen. At Cedar Hills there is an obvious increase in spread of R_i as wind speed increases above 12 knots. This may be partially due to a rapid decrease in the number of cases of high wind speeds, a larger decrease than at Cape Kennedy, and thus, there is less confidence in the higher speed figures at Cedar Hills.

Data from a larger sampling of stations are required to develop curves representative of a number of airports nationwide, and more data for Cedar Hills are needed to determine whether the results which show an increase in spread of R_i with an increase in wind speed at Cedar Hills are correct.

3.3.4 Wind Direction Shear

3.3.4.1 Evaluation Methods

Wind direction shear was determined for each hourly case by subtracting the wind direction at the lowest given level from that at the next lowest given level and assuming this to be equivalent to the directional shear at the geometric height $(h_1 h_2)^{1/2}$ and further assuming that this was a good estimate of the directional shear at 20 feet. The geometric heights computed for each tower as representative of 20 feet are Cape Kennedy—18 feet, and Cedar Hills—46 feet. Information from Cape Kennedy indicates that there is not much difference in shear distributions over the interval 18 to 44 feet at a given location, Figure 3-53.

3.3.4.2 Distribution With Speed at 20 Feet Elevation

Distributions of directional shears at 20 feet in degrees per 100 vertical feet by 2-knot speed intervals at 20 feet are shown in Figures 3-49 to 3-52. The first two figures depict the percent probability of not being exceeded and the second two figures indicate the variation of specific probabilities with wind speed. There is apparently a small variation with speed except at the extreme probabilites. This is borne out in the correlation coefficients

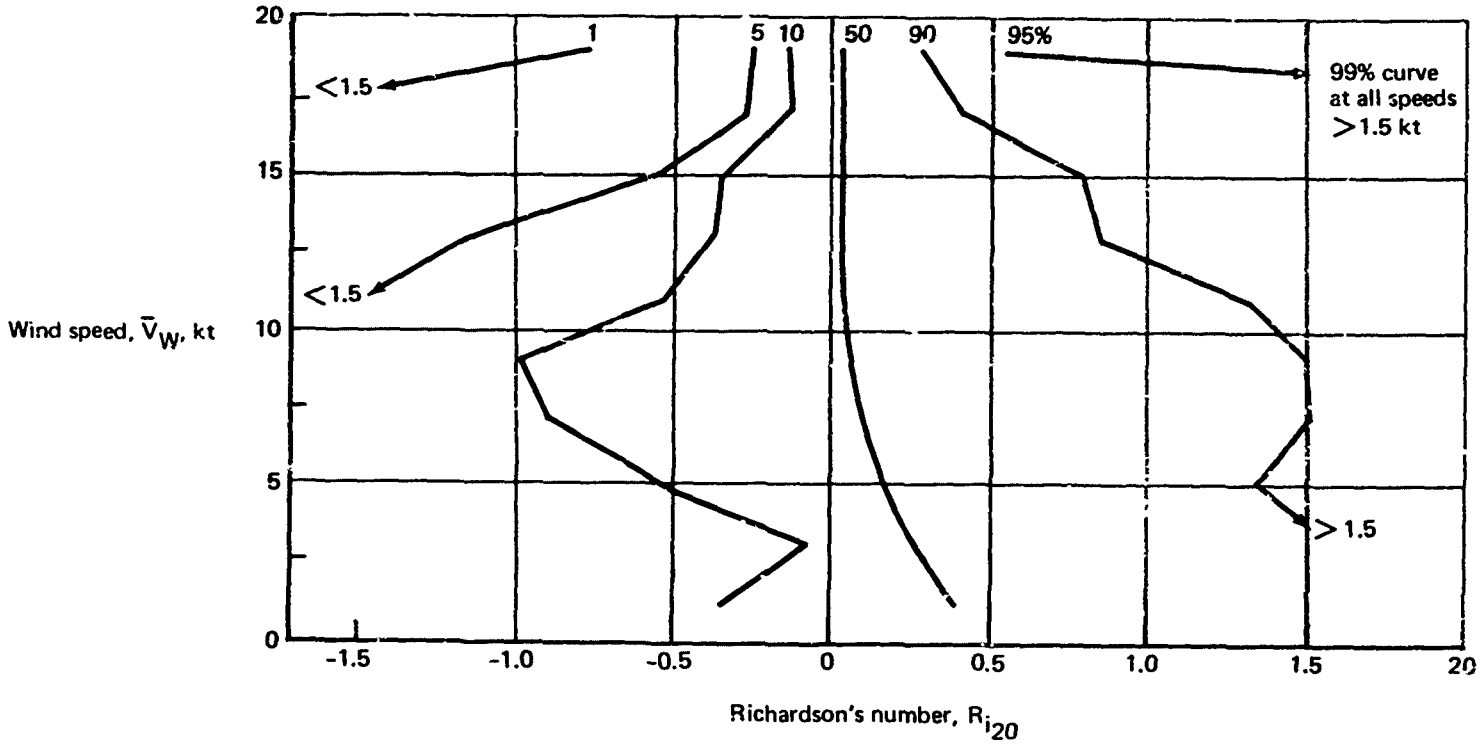

FIGURE 3-47.–PERCENT FREQUENCY OF OCCURRENCE, WIND SPEED VS RICHARDSON'S NO., CAPE KENNEDY, 1966-68

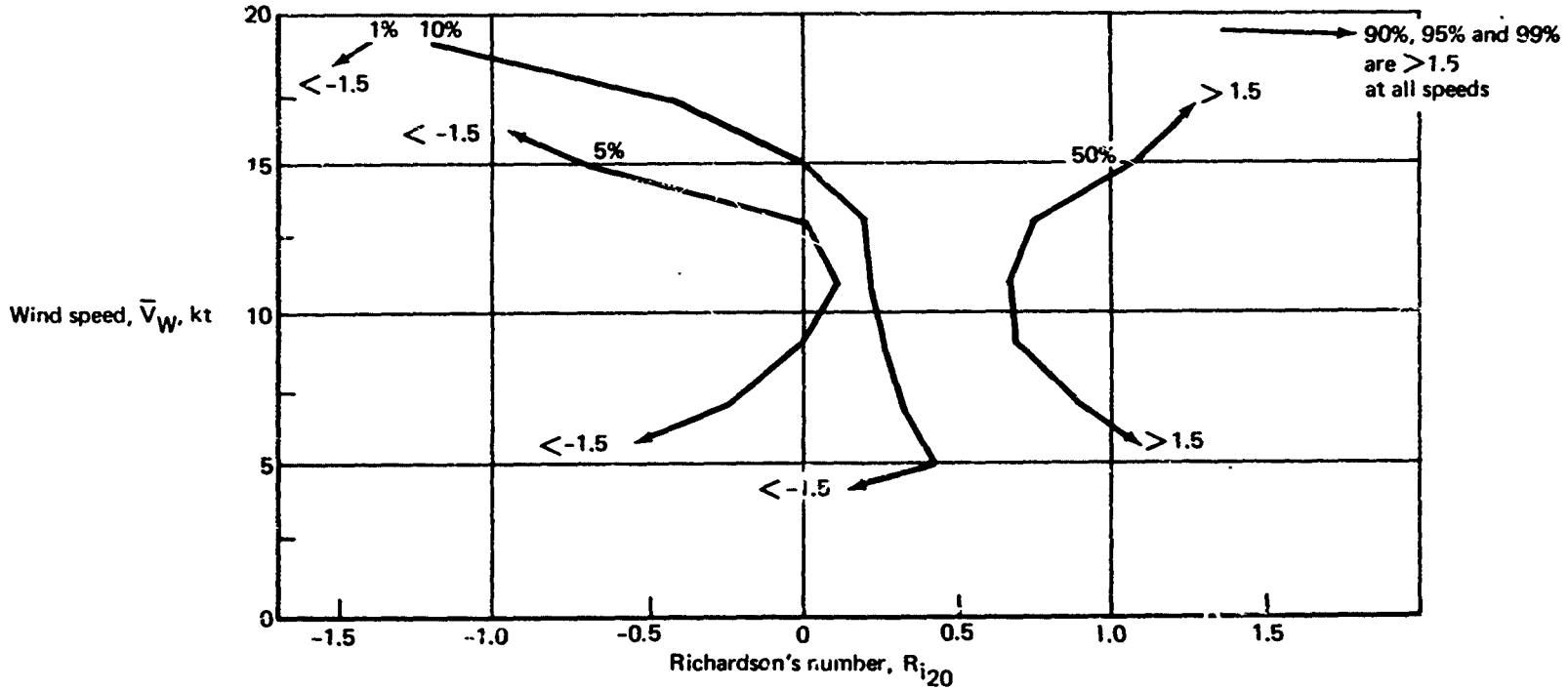

FIGURE 3-48.—PERCENT FREQUENCY OF OCCURRENCE, WIND SPEED VS RICHARDSON'S NO., CEDAR HILLS, TEXAS, 1960-62

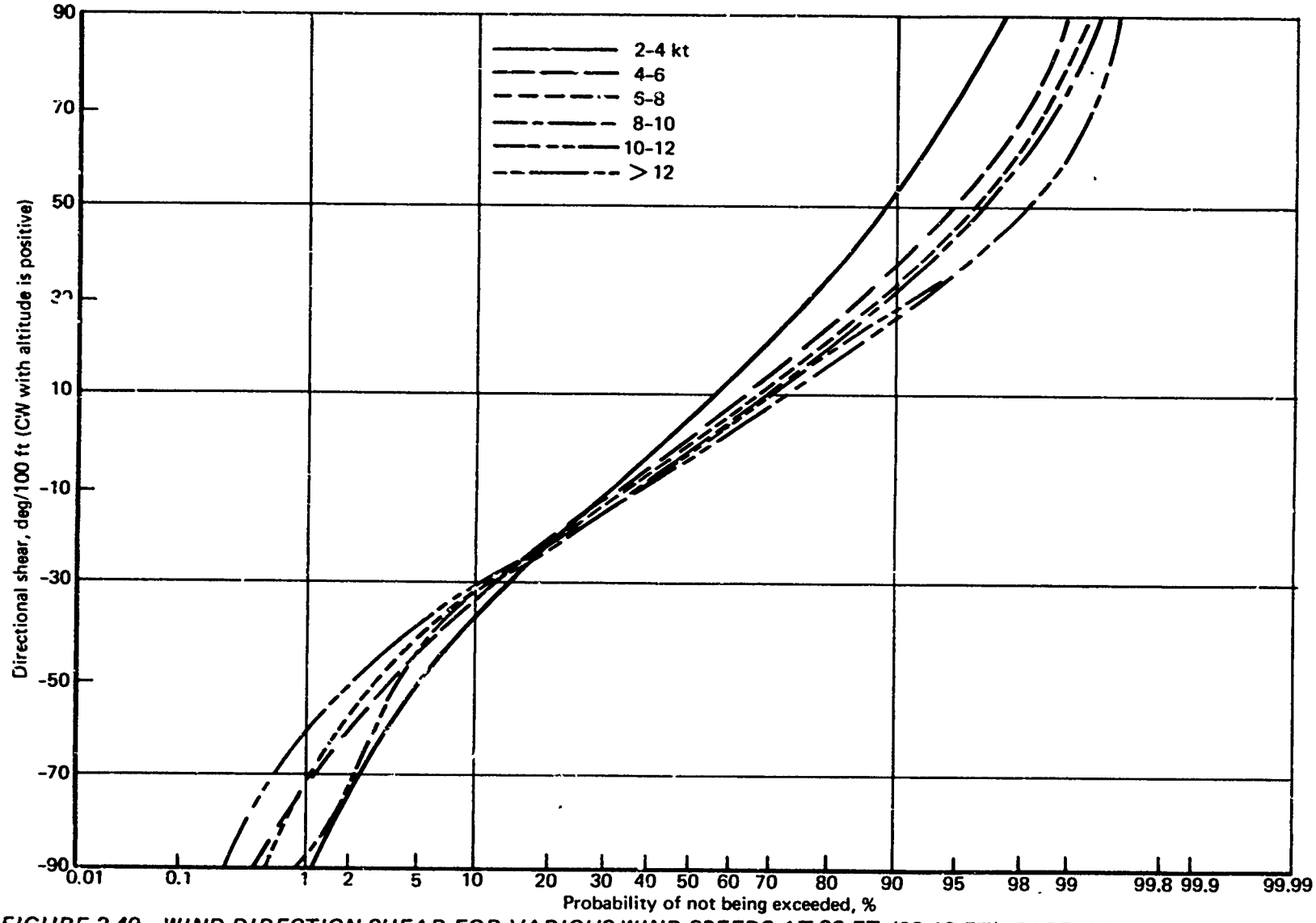

FIGURE 3-49.--WIND DIRECTION SHEAR FOR VARIOUS WIND SPEEDS AT 20 FT (33-10 FT), CAPE KENNEDY, 1966-68

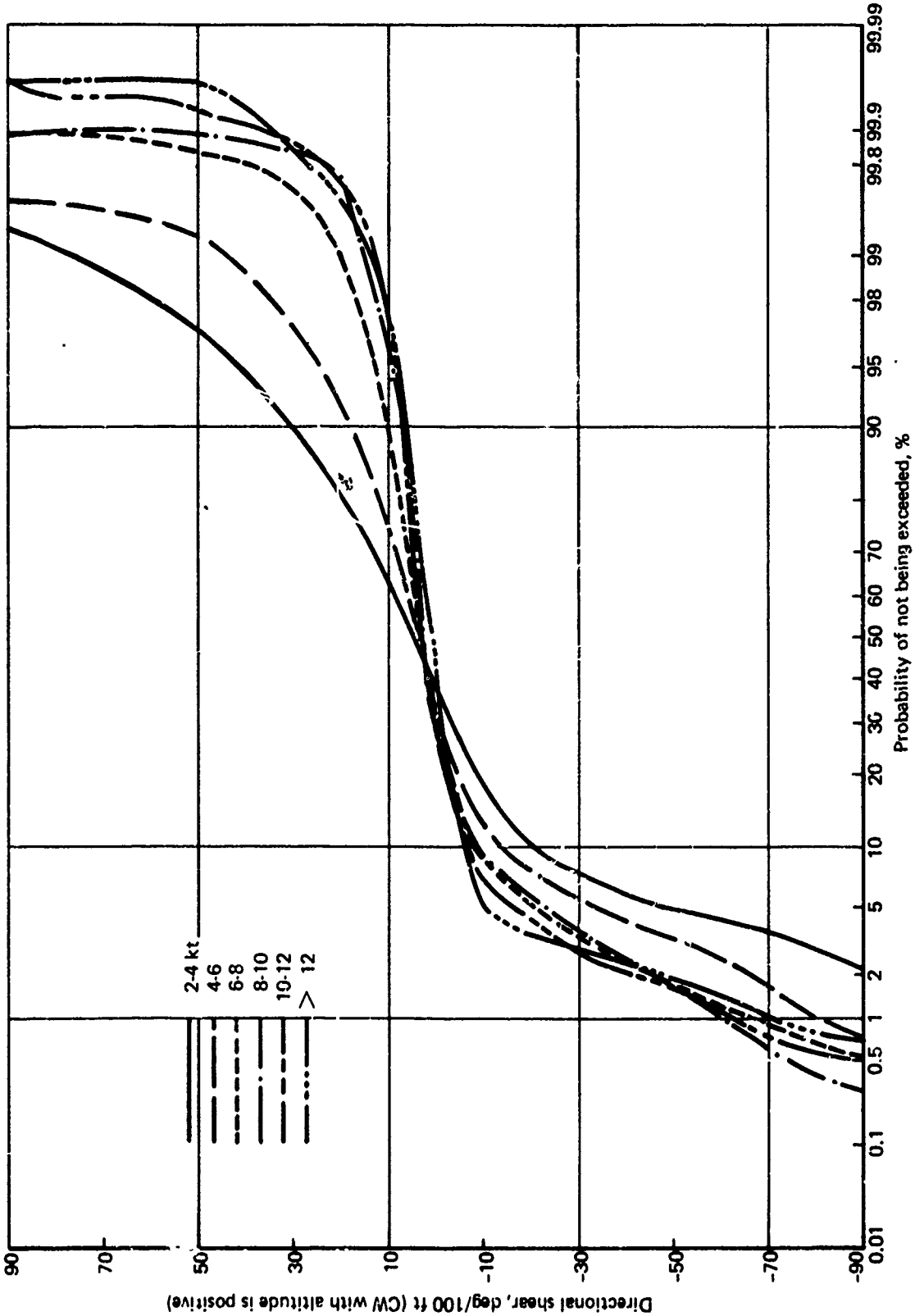

FIGURE 3-50.—WIND DIRECTION SHEAR FOR VARIOUS WIND SPEEDS AT 46 FT (70-30 FT), CEDAR HILLS, TEXAS, 1960-62

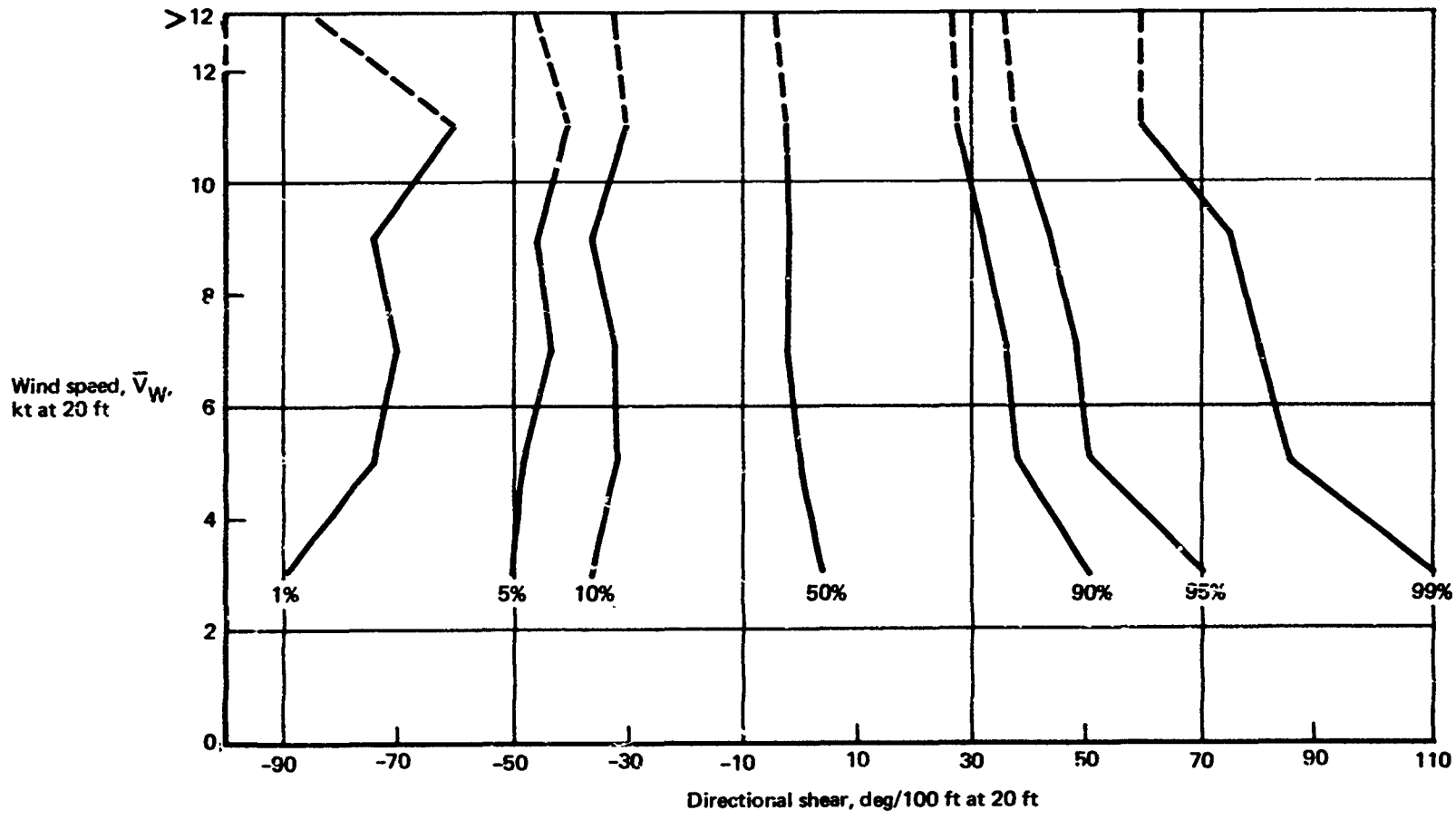

FIGURE 3-51.--PERCENT FREQUENCY OF OCCURRENCE, WIND SPEED VS DIRECTIONAL SHEAR, CAPE KENNEDY , 1966-68

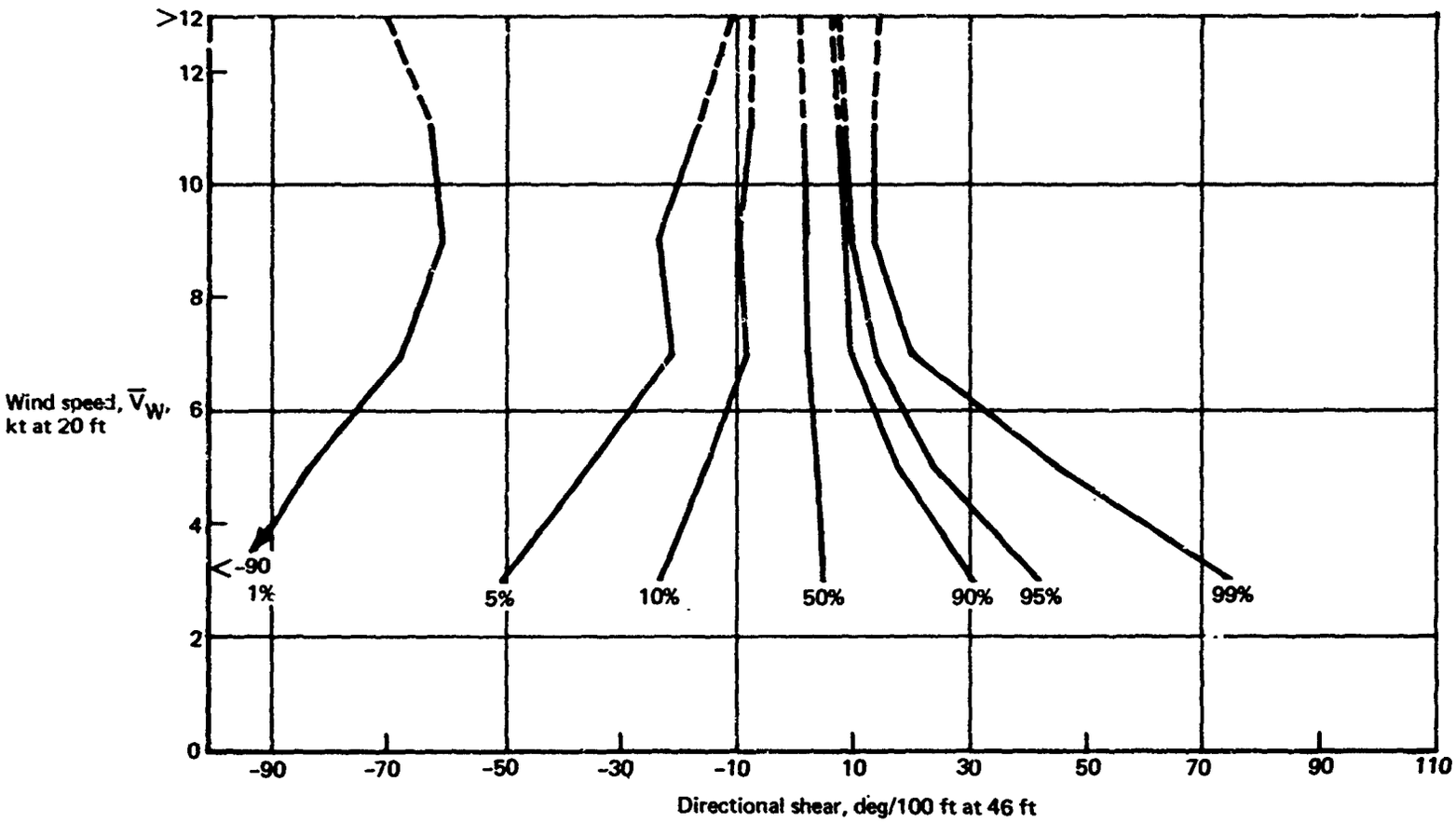

FIGURE 3-52.—PERCENT FREQUENCY OF OCCURRENCE, WIND SPEED VS DIRECTIONAL SHEAR, CEDAR HILLS, TEXAS, 1960-62

described in Section 3.3.6. There is less direction shear variability at Cedar Hills than at Cape Kennedy. The middle 80% of the shears are -10° to +10° per 100 feet and -30° to +30° per 100 feet, respectively.

3.3.4.3 Distribution With Height

Cumulative probability charts showing wind shears at various heights for all wind speeds are provided in Figures 3-53 and 3-54, and the variations of specific probabilities are shown in Figures 3-55 and 3-56. There is a definite decrease in spread of directional shear values with altitude; the smaller range of direction shear variability at Cedar Hills is noticeable in both sets of figures. At Cape Kennedy 80% of the shears at all but the lower two heights are within ±10° per 100 feet; at the lower two heights 80% are within ±30° per 100 feet. By contrast, 80% of the shears at all heights at Cedar Hills are within ±10° per 100 feet, and except for the lowest level 93% of the shears are less than ±20° per 100 feet.

In addition to the differences noted between locations there is also a difference in the shape of the distributions from year to year at the same location. Therefore, establishing long period mean curves is difficult.

Several 10-minute average profiles were selected at random from the records to provide an indication of the magnitudes of directional shears at any time. Four of these are shown in Figure 3-57. In the figures, the $\Delta\phi$ from the lowest level are shown by the curves and the speeds at each height are given numerically. In general, the largest shears occur near the surface and with the lowest wind speeds. As mentioned in Section 3.2.3, many investigators ignore the directional shears in their investigations. This is because directional shears affect the total velocity shears numerically the most at the higher wind speeds. This investigation as well as others (see Fig. 3-11) indicate that in most cases direction shears are low (0-20° per 100 feet) at high speeds. This is especially true when shears are measured over large height differences.

3.3.5 Wind Speed Shear

3.3.5.1 Evaluation Methods

Wind speed shear was determined using the same procedure as wind speed and Richardson's number but only for heights of 20, 100, 200, and 500 feet.

3.3.5.2 Distribution With Speed at 20 Feet Elevation

Wind speed shear at 20 feet by 2-knot intervals is shown in Figures 3-58 and 3-59. At Cape Kennedy there is an obvious normal distribution at all speed intervals between 5% and 95% of the observations. Fewer observations at the extremes may accentuate the lack of normality there.

The curves for Cedar Hills are more normally distributed than those for Cape Kennedy. Also, there is a greater spread between the curves with the higher speeds being associated with a shift to smaller (less positive and more negative) values of shear at constant probabilities. For example, the 50% values at Cape Kennedy are clustered randomly about a

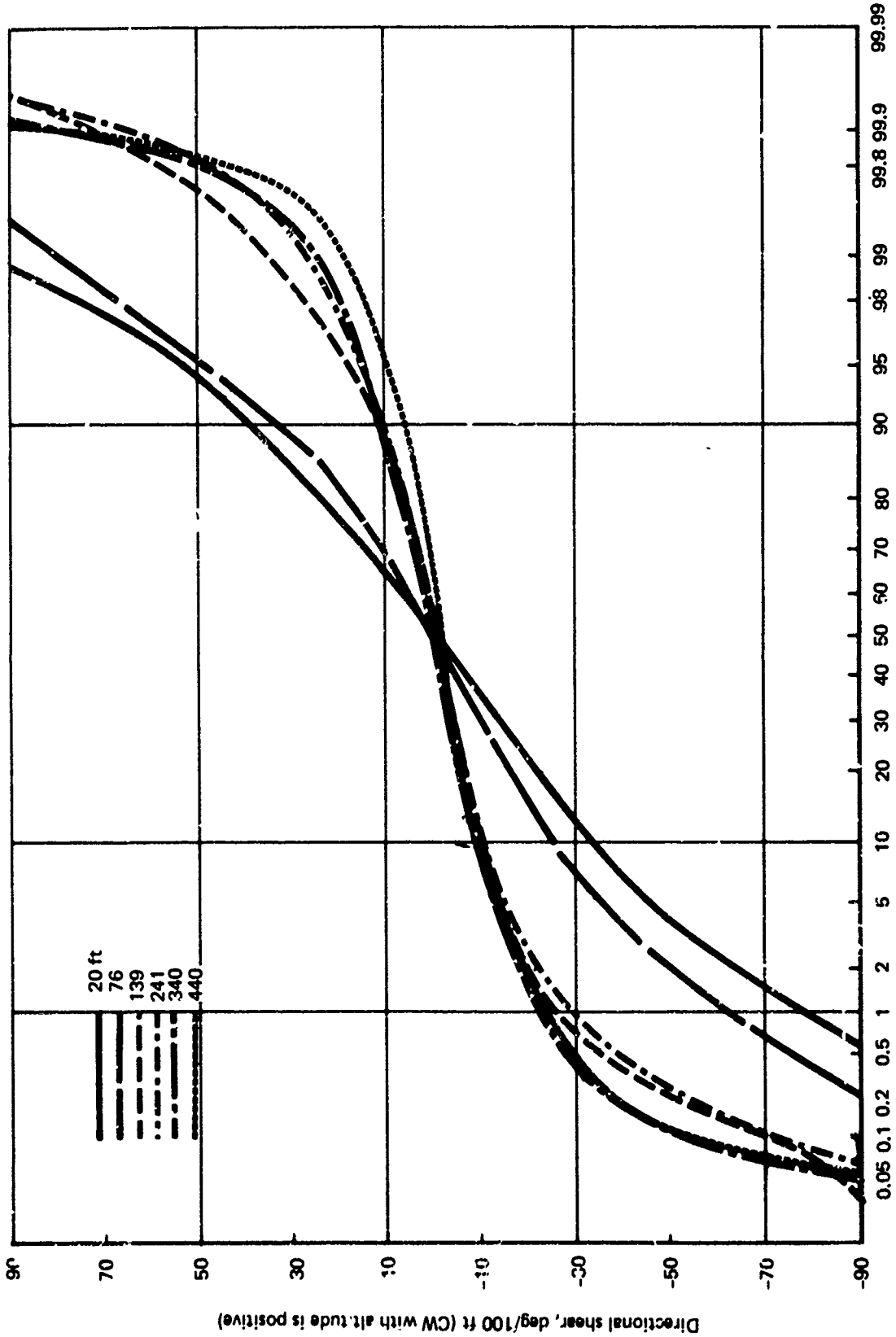

FIGURE 3-53.—WIND DIRECTION SHEAR FOR SEVERAL HEIGHTS, ALL WIND SPEEDS, CAPE KENNEDY, 1966-69

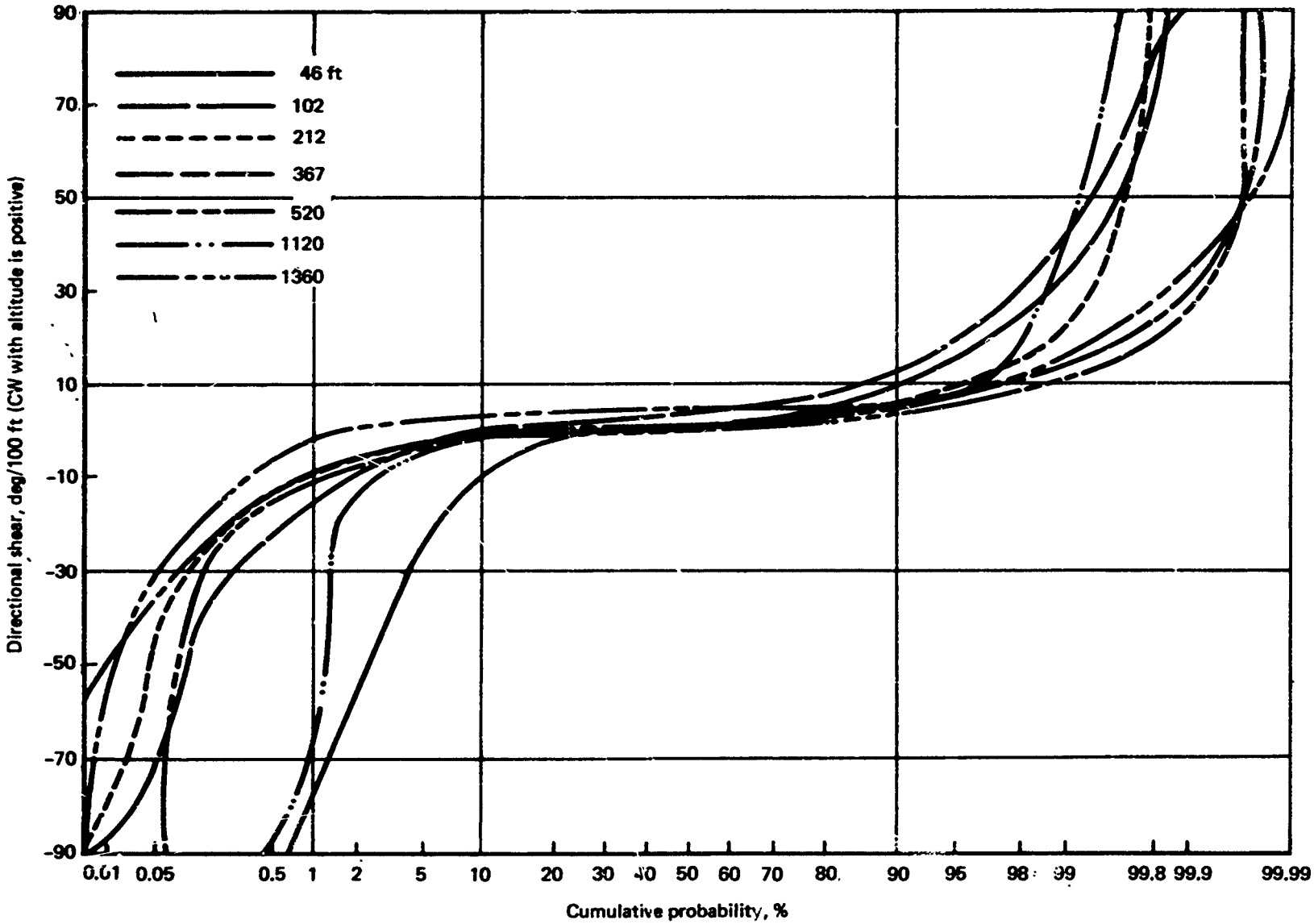

FIGURE 3-54.—WIND DIRECTION SHEAR FOR SEVERAL HEIGHTS, ALL WIND SPEEDS, CEDAR HILLS, TEXAS, 1960-62

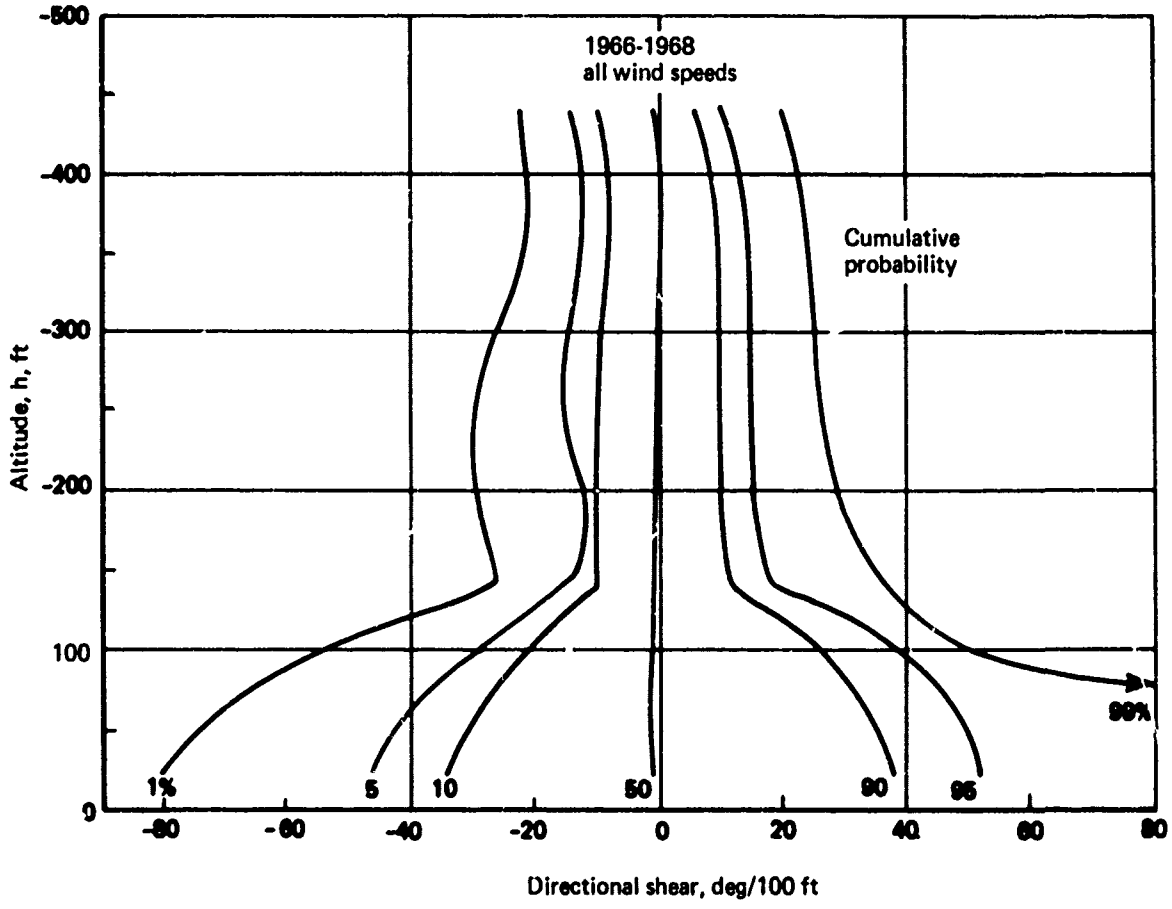

FIGURE 3-55.–DISTRIBUTION OF WIND DIRECTION SHEAR WITH HEIGHT, CAPE KENNEDY

shear of 7 kt/100 ft while the 50% Cedar Hills shears range from 7-17 kt/100 ft with the higher values at lowest wind speeds. This effect may be related to the site location, climatology, and weather. Comparison with information from other locations would be valuable in resolving the differences.

Selected probability percent frequencies for the range of wind speeds are related in Figures 3-60 and 3-61. Values of shear vary little with wind speeds at Cape Kennedy, but the Cedar Hills values indicate a decrease in spread with increasing wind speed and then an increase in spread at still greater speeds. A similar shape was found by Roberts with tower data from the Washington, D.C. area, Figure 3-18. He also included some Cedar Hills data with his report which indicated the same shape of the 50% curve as our analysis. This increase of shear at the higher wind speeds is not obvious in the Cape Kennedy data, although it may occur at wind speeds greater than 12 knots.

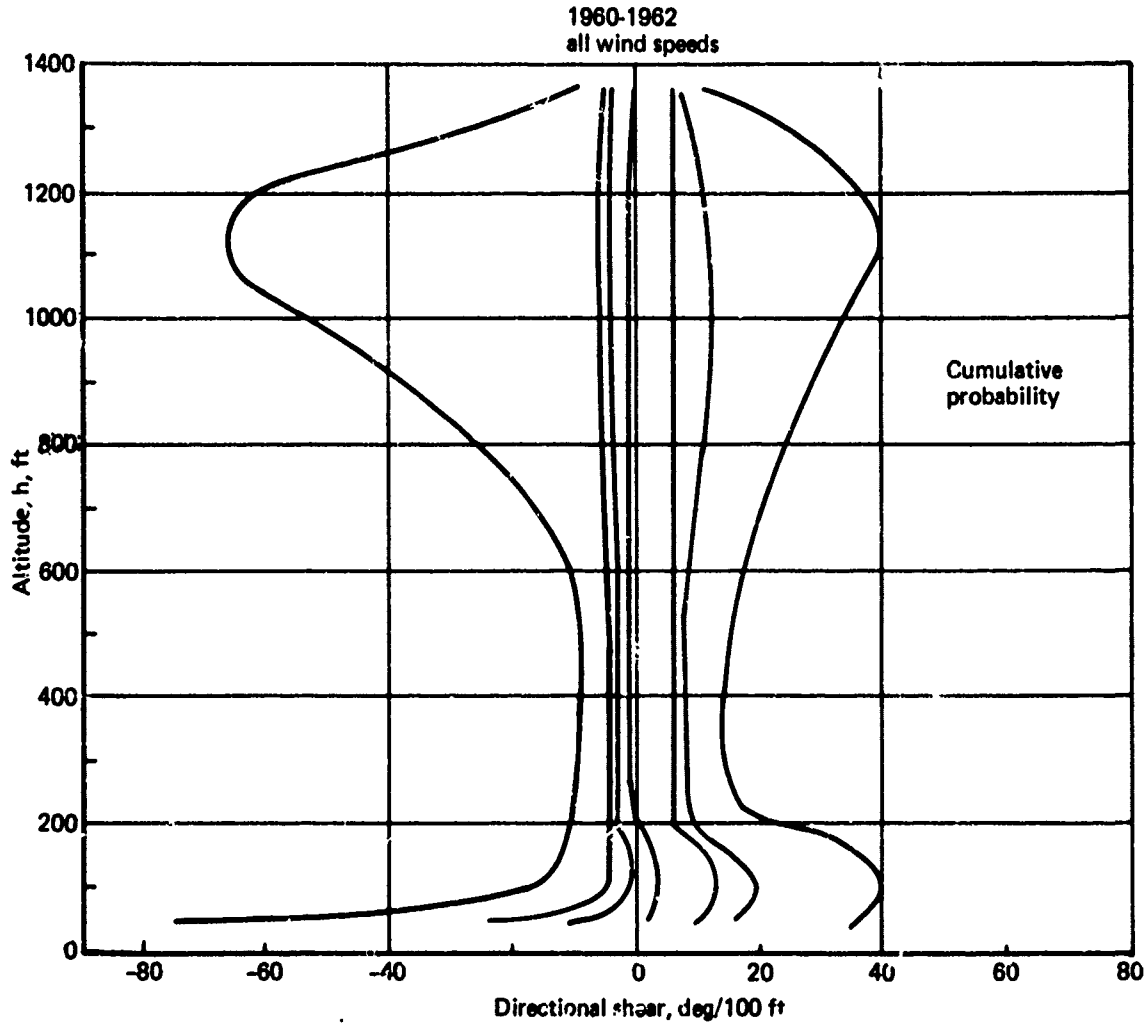

FIGURE 3-56.–DISTRIBUTION OF WIND DIRECTION SHEAR WITH HEIGHT, CEDAR HILLS, TEXAS

3.3.5.3 Distribution With Height for Two Speed Intervals at 20 Feet Elevation

There is a definite decline in the spread of shear values with height as shown in Figures 3-62 to 3-67. The first two figures depict the probability of not being exceeded for the 2-4 knot speed interval. The second and third sets of two figures each compare the spread of specific percent frequencies with height for two speed intervals. Note that the spread of values is very dependent upon height in the lower heights.

Intersite differences are apparent at low heights. The Cedar Hills 20-foot shear curve is more normally distributed than its counterpart at Cape Kennedy, and there is a greater spread to the values at Cedar Hills at low heights, especially at the lower wind speed.

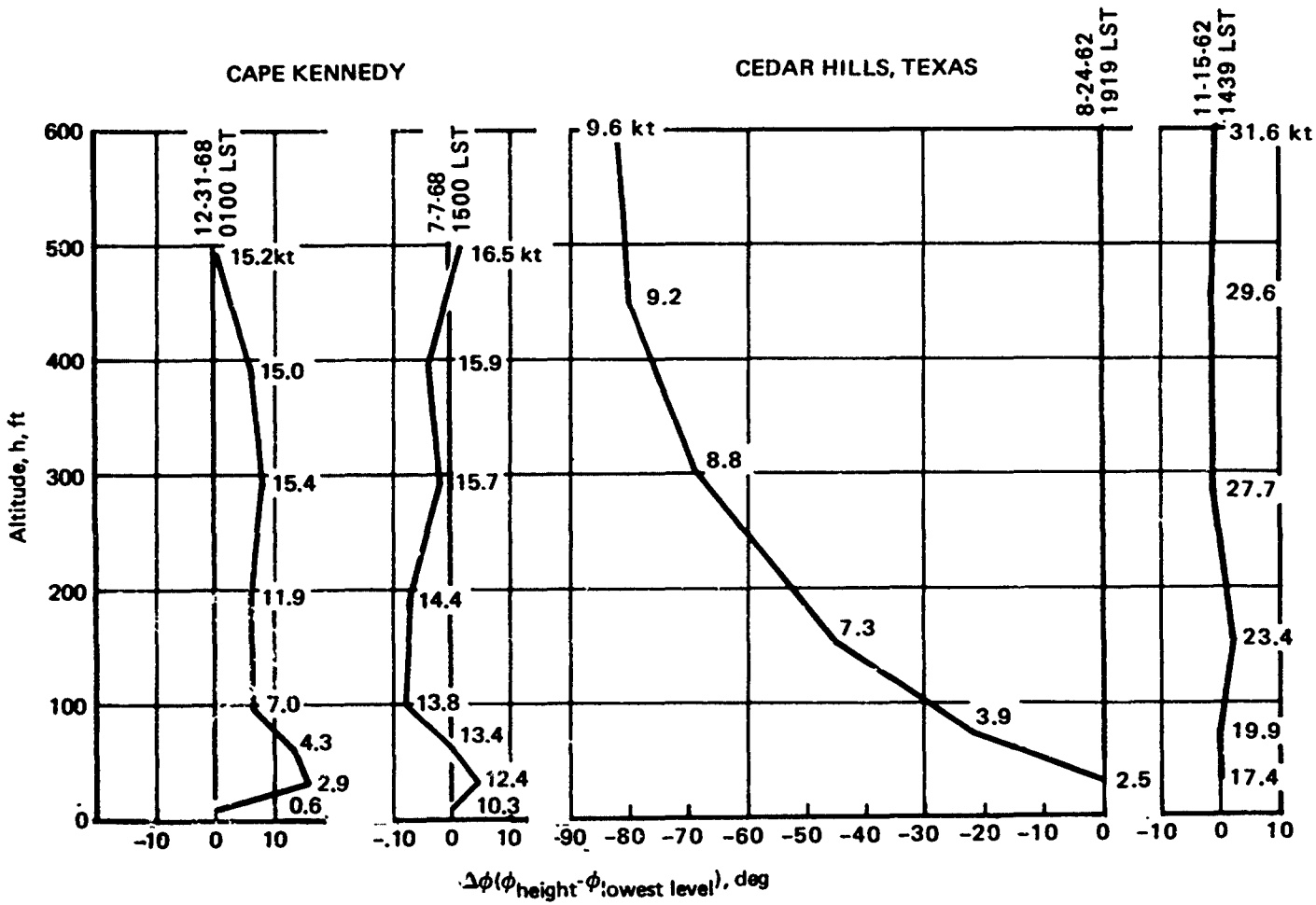

FIGURE 3-57.--EXAMPLES OF WIND DIRECTION PROFILES

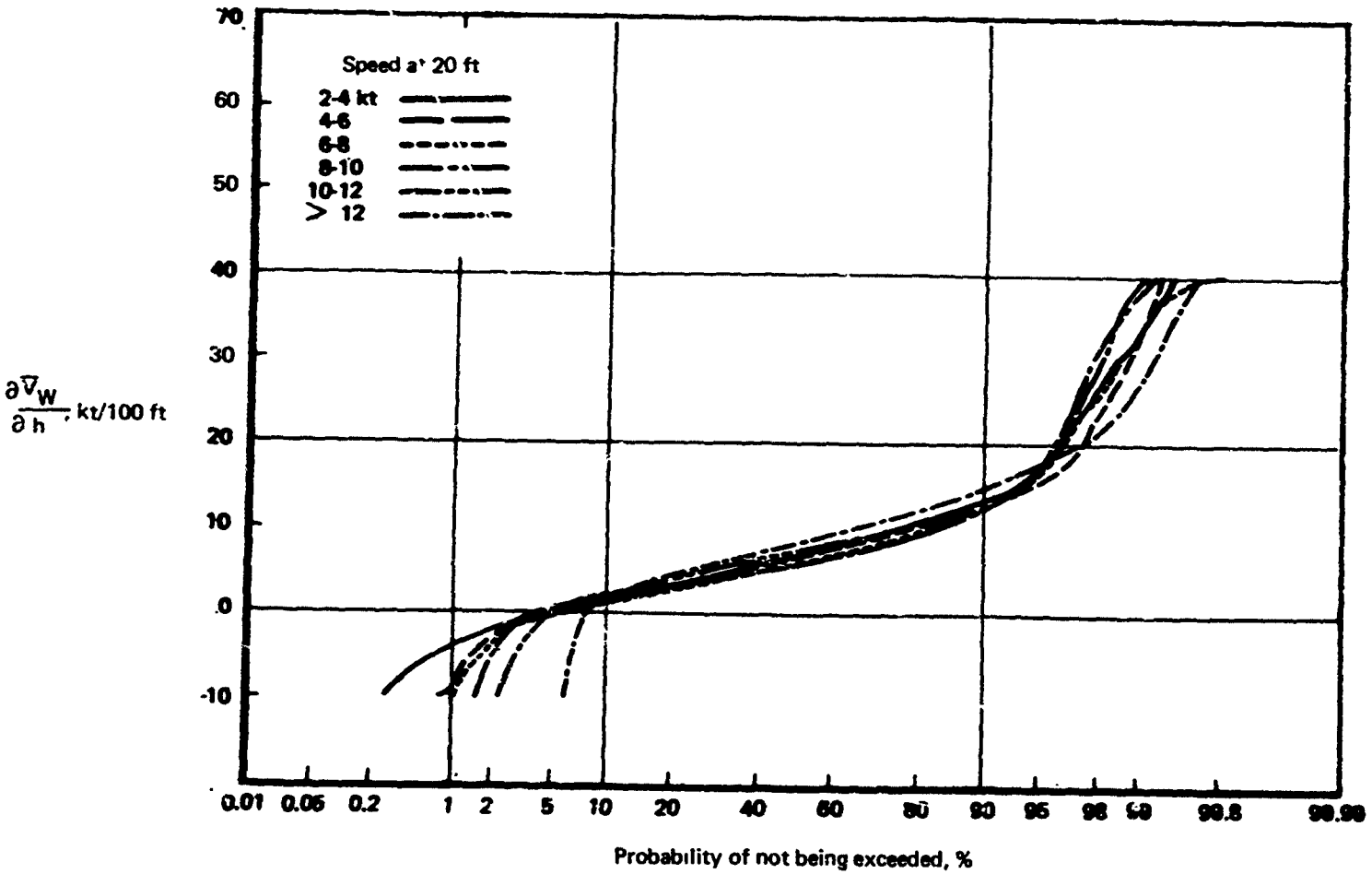

FIGURE 3-58.--CAPE KENNEDY, 1966-68, WIND SPEED SHEAR AT 20 FT

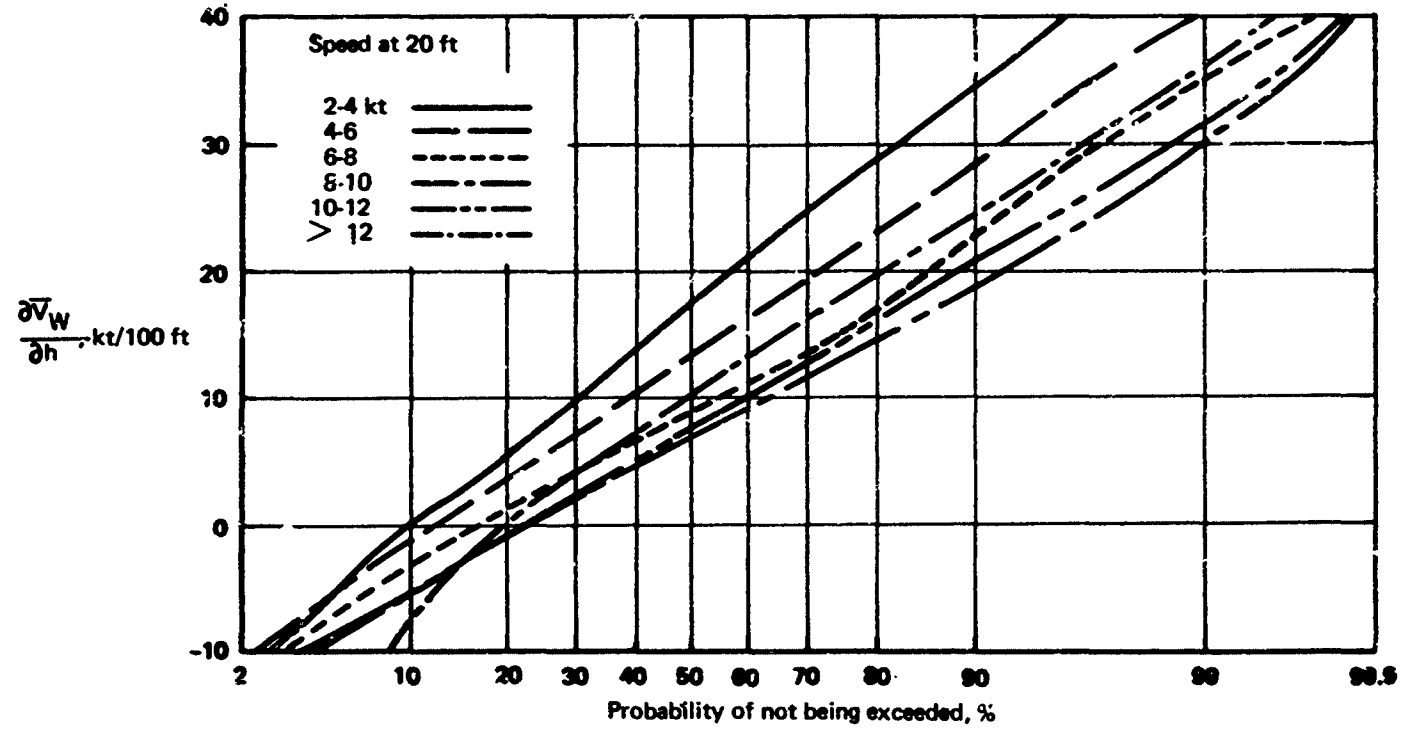

FIGURE 3-59.—CEDAR HILLS, TEXAS 1960-62, WIND SPEED SHEAR AT 20 FT

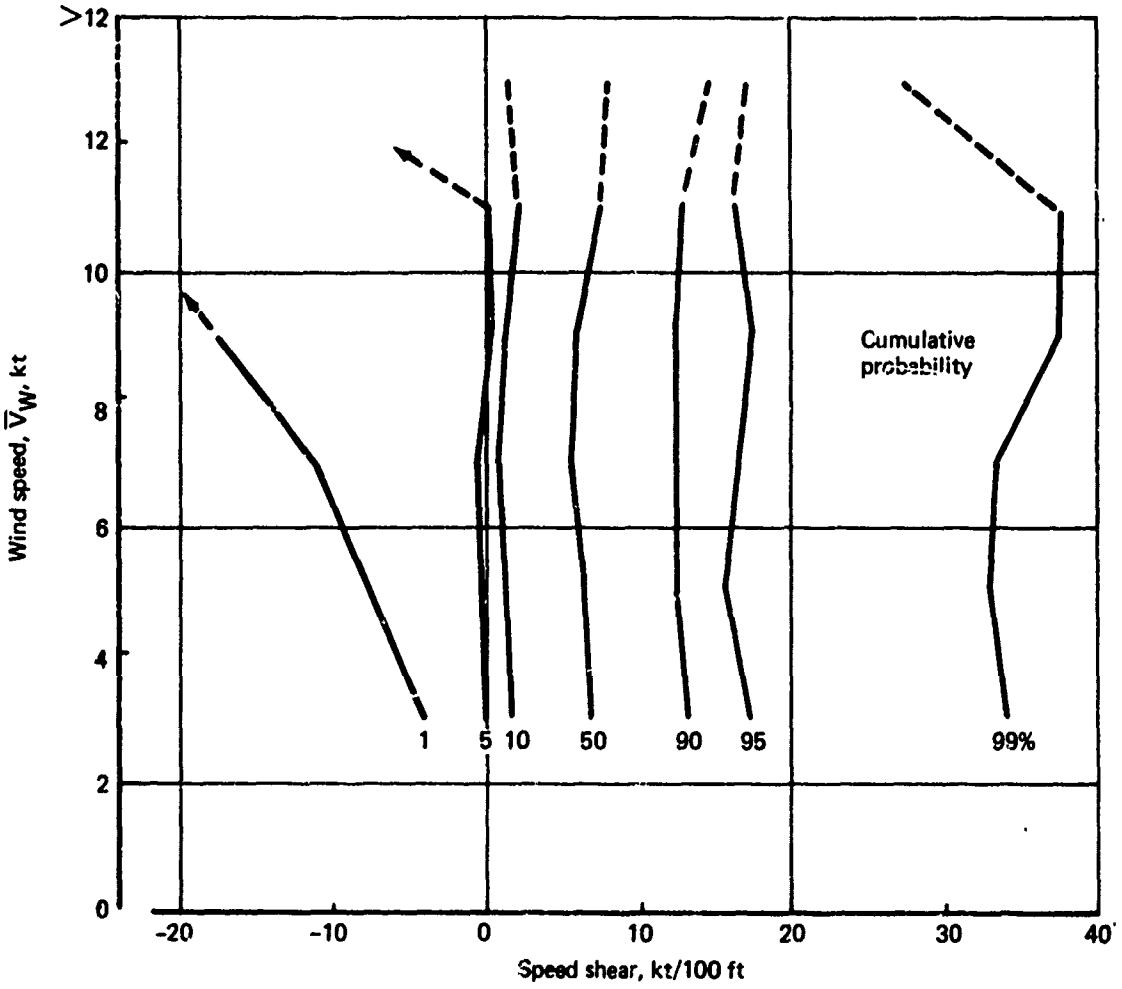

FIGURE 3-60.--PERCENT FREQUENCY OF OCCURRENCE, WIND SPEED VS SPEED SHEAR AT 20 FT, CAPE KENNEDY, 1966-68

3.3.6 Regression Equations and Correlation Coefficients

3.3.6.1 Evaluation Methods

Regression equations and correlation coefficients were determined for four relationships between Richardson's number, wind speed, wind direction shear, and wind speed shear at the 20-foot height by standard statitistical techniques. The equations were fit by a least squares fit that makes the sum of the squares of the Y residuals a minimum in the equation $Y = AX + B$.

3.3.6.2 Richardson's Number and Speed

Regression equations and correlation coefficients of Ri_{20} vs $\bar{V}_{20}$ for the separate sites are:

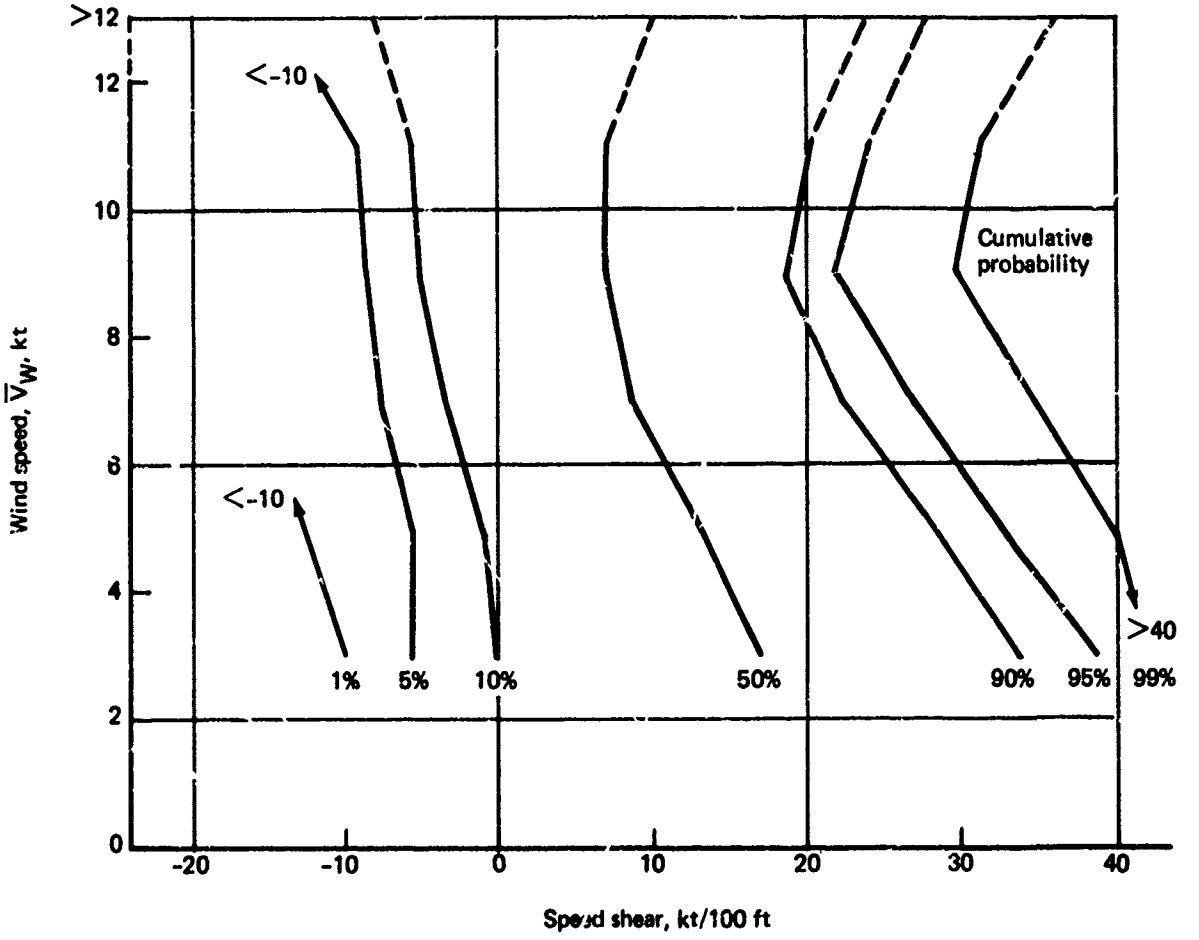

FIGURE 3-61.–PERCENT FREQUENCY OF OCCURRENCE, WIND SPEED VS SPEED SHEAR AT 20 FT, CEDAR HILLS, TEXAS, 1960-62

Cape Kennedy	Cedar Hills
$\bar{V}_{20} = 6.91\ Ri_{20} - 0.08$	$\bar{V}_{20} = 7.25\ Ri_{20} - 0.0008$
$r = 0.86$	$r = 0.90$

It is apparent that there is very little difference between sites and the correlations are high, and therefore the variables are dependent.

3.3.6.3 Speed and Direction Shear

Regression equations and correlation coefficients of $\partial\phi/\partial h_{20}$ versus $\bar{V}_{20}$ for the separate sites are:

Cape Kennedy	Cedar Hills
Not available	$\partial\phi/\partial h_{20} = 0.0036\ \bar{V}_{20} - 0.003$
$r = 0.036$	$r = 0.025$

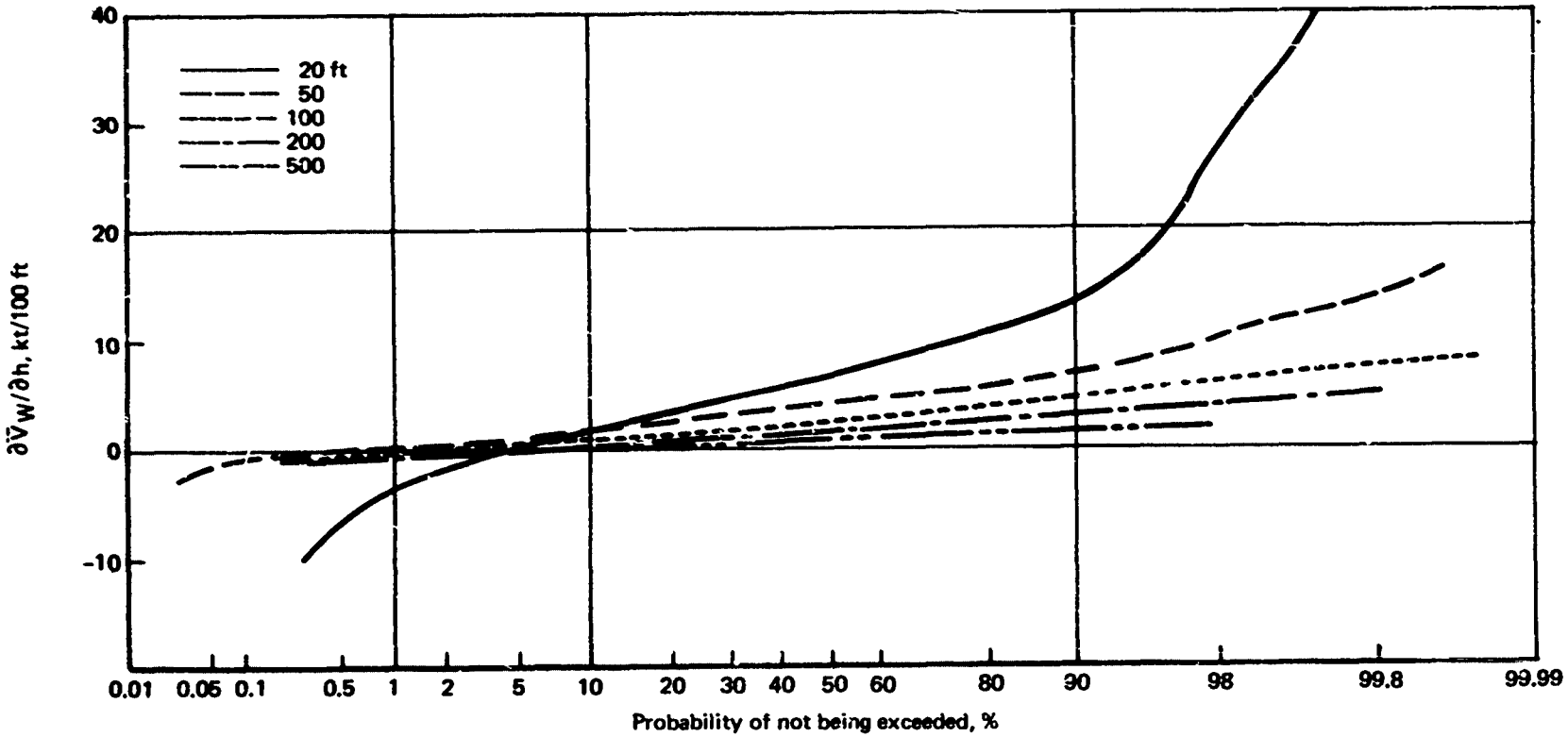

FIGURE 3-62.–CAPE KENNEDY, 1966-68, VARIATION WITH HEIGHT OF WIND SPEED SHEAR, 2-4 KT SPEED AT 20 FT

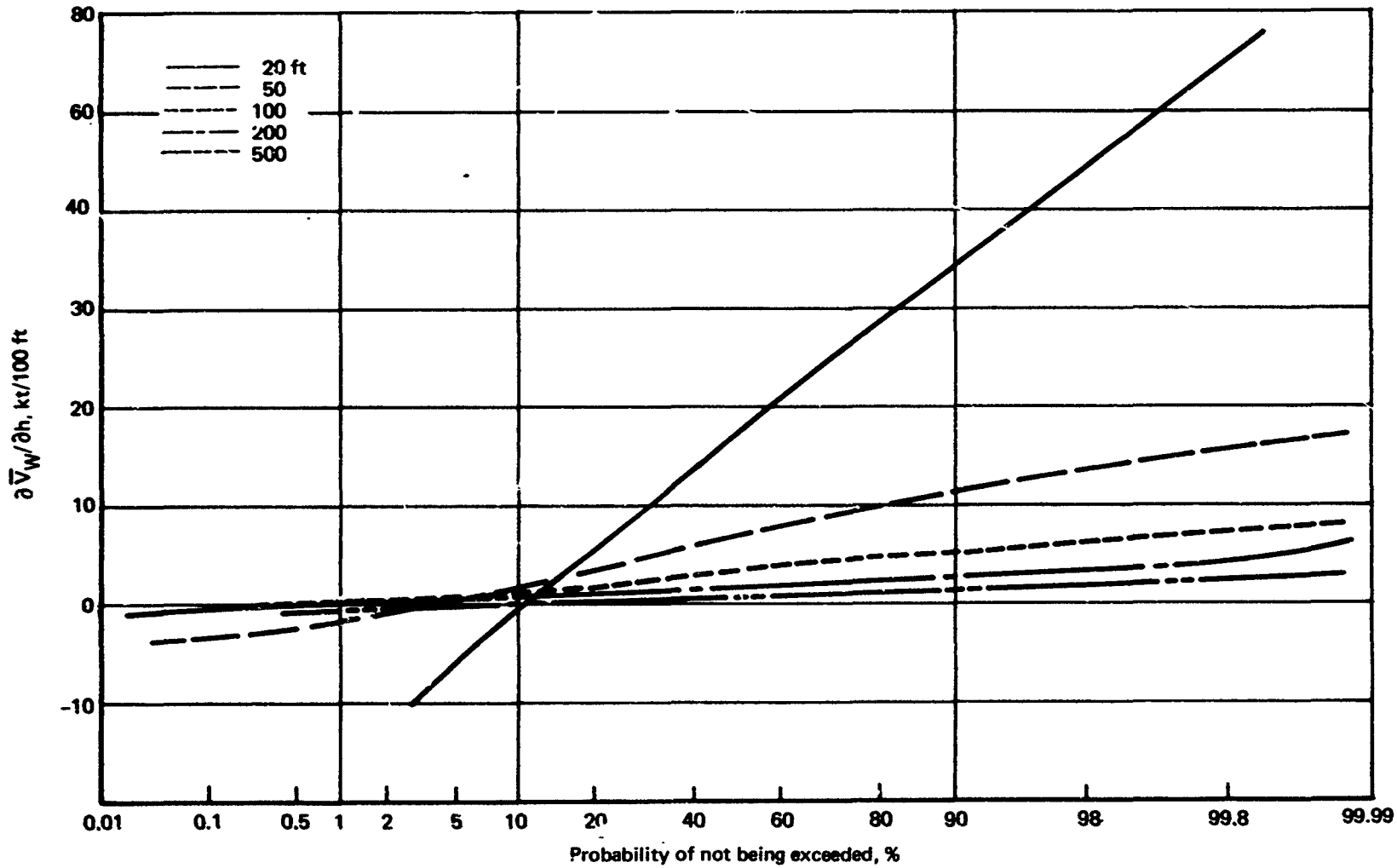

FIGURE 3-63.—CEDAR HILLS, TEXAS, 1960-62, VARIATION WITH HEIGHT OF WIND SPEED SHEAR, 2-4 KT SPEED AT 20 FT

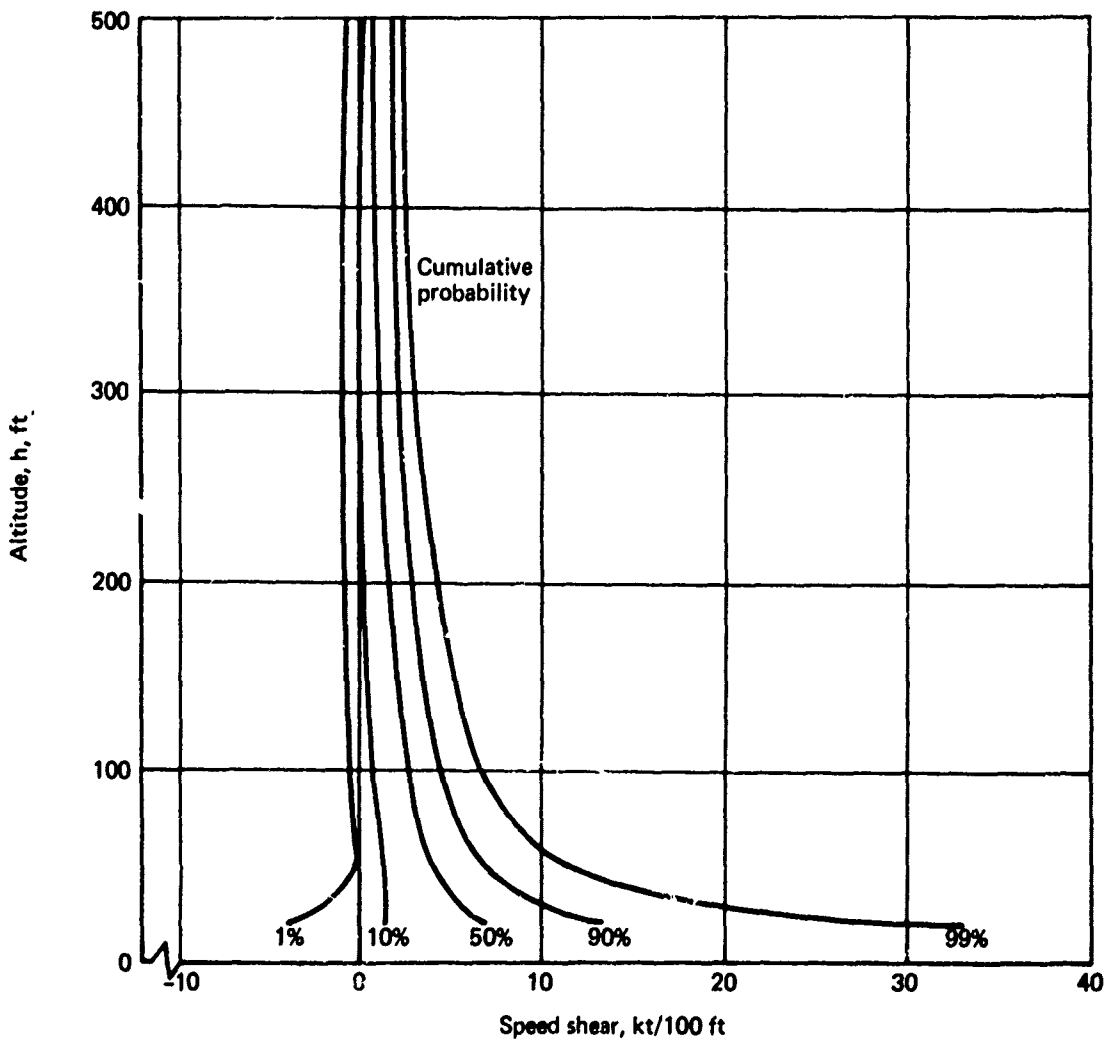

FIGURE 3-64.–CAPE KENNEDY, 1966-68, DISTRIBUTION OF WIND SPEED SHEAR VS HEIGHT, 20 FT WIND SPEED = 2-4 KT

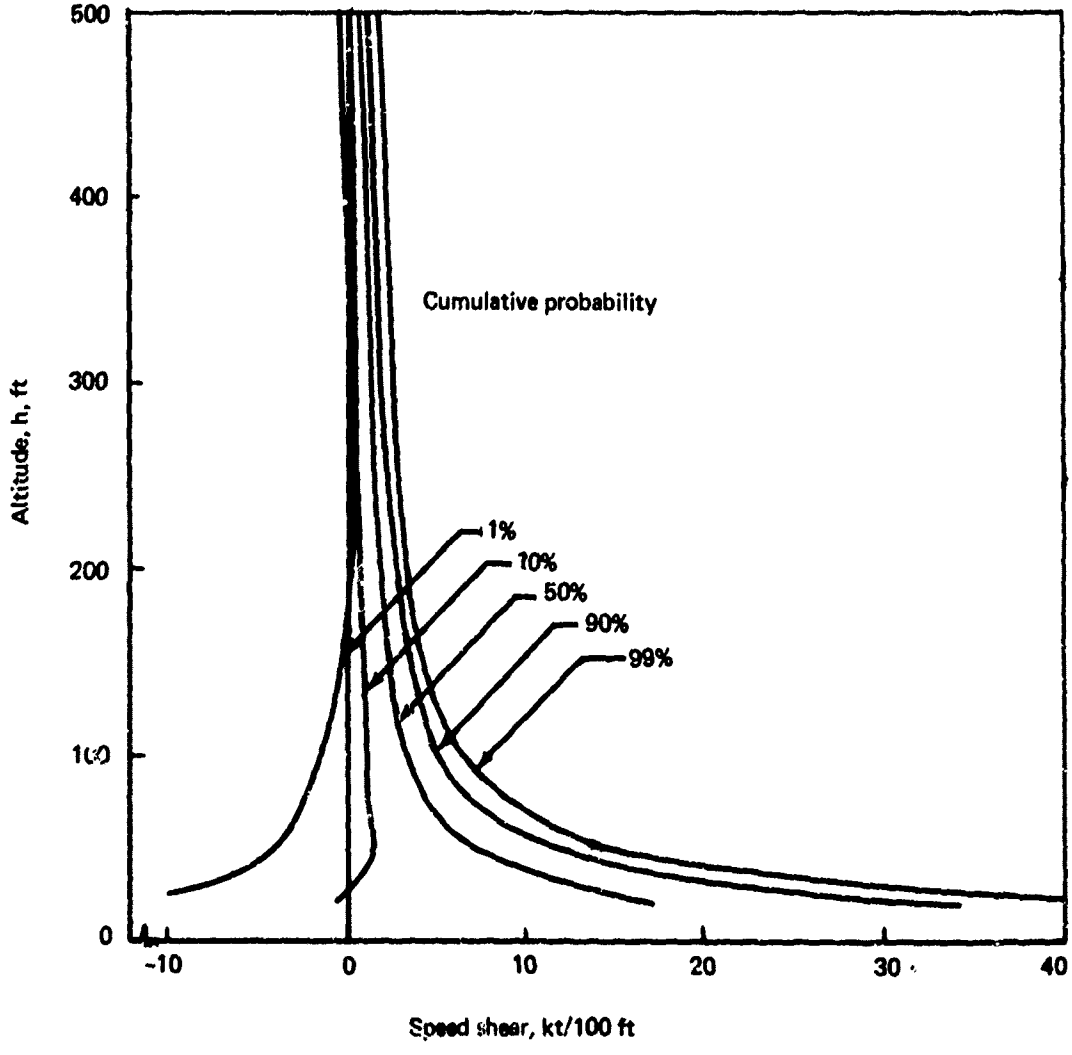

FIGURE 3-65.—CEDAR HILLS, TEXAS, 1960-62, DISTRIBUTION OF WIND SPEED SHEAR VS HEIGHT, 20 FT WIND SPEED 2-4 KT

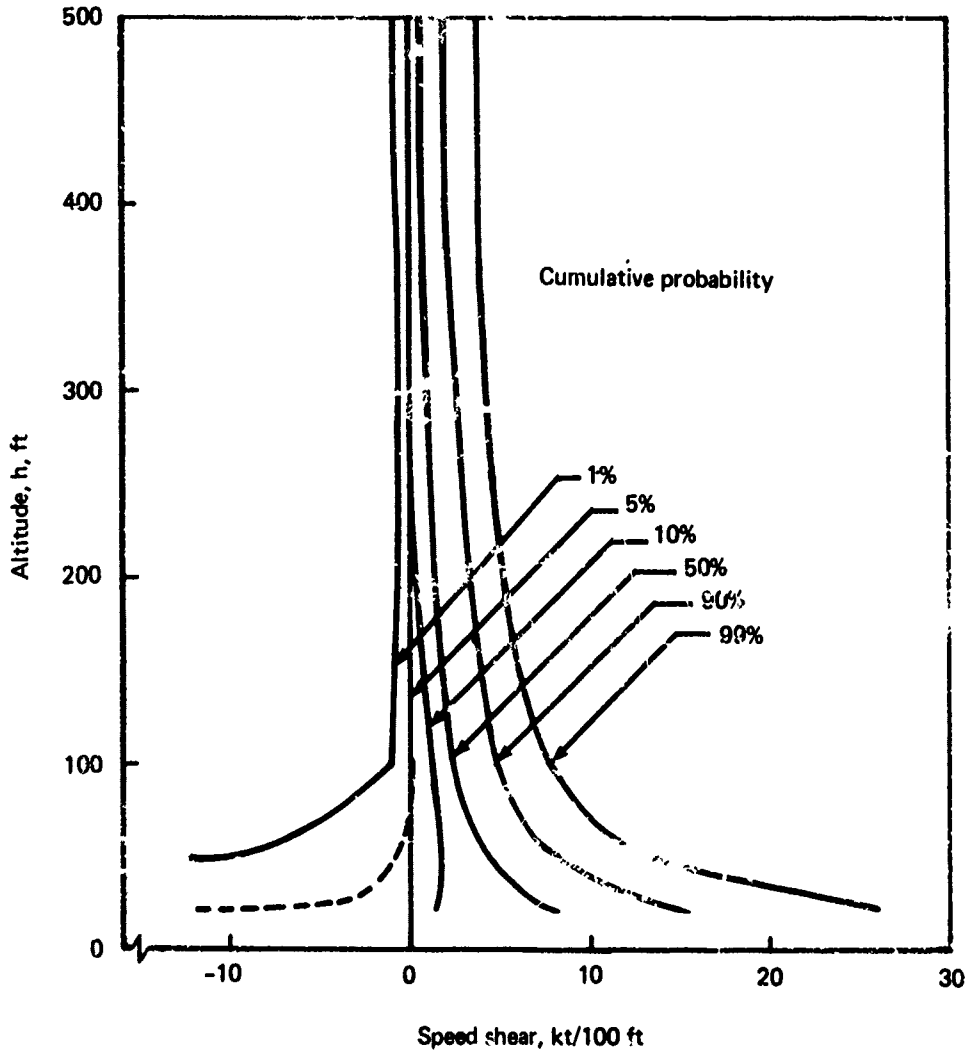

FIGURE 3-66.–CAPE KENNEDY, 1966-68, DISTRIBUTION OF WIND SPEED SHEAR VS HEIGHT, 20 FT WIND SPEED >12 KT

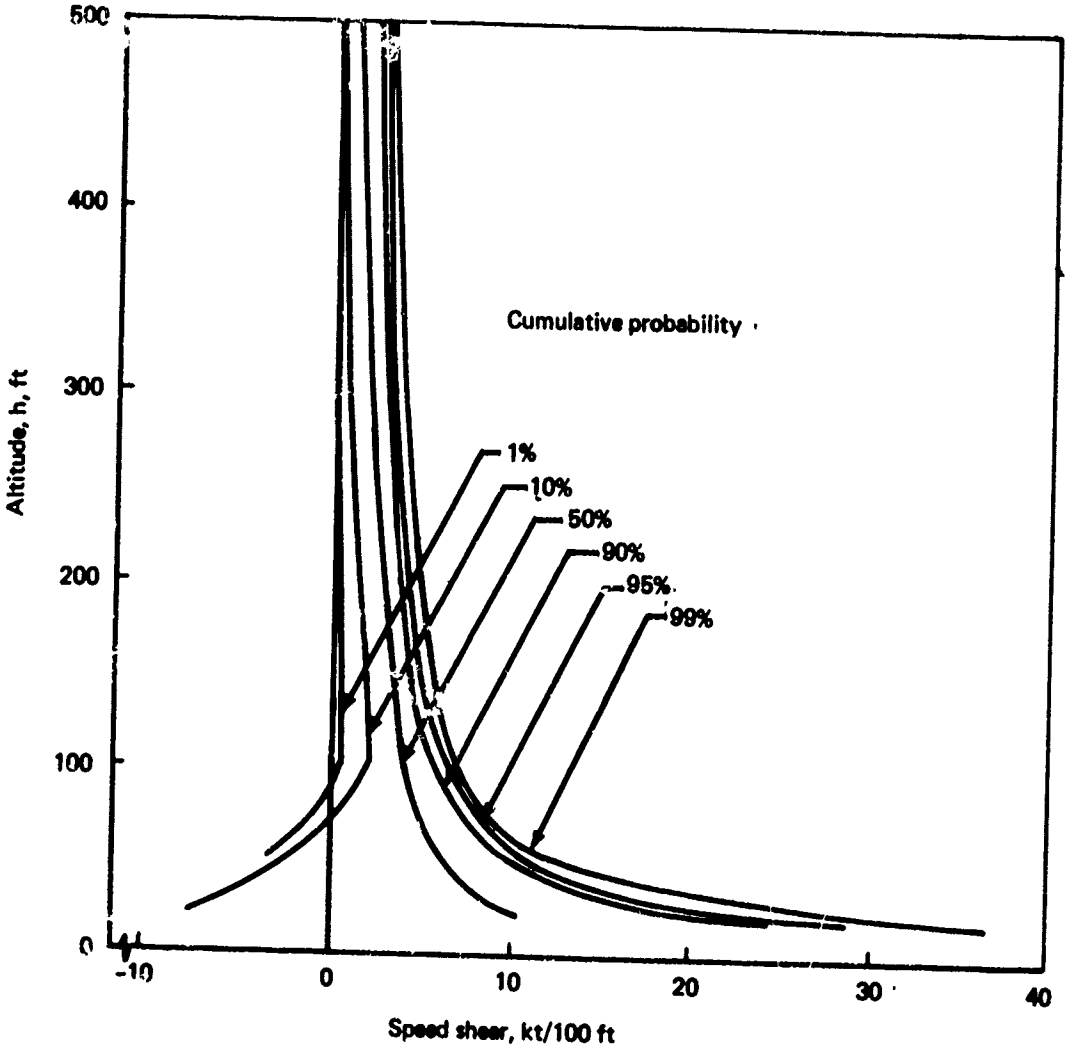

FIGURE 3-67.–CEDAR HILLS, TEXAS, 1960-62, DISTRIBUTION OF WIND SPEED SHEAR VS HEIGHT, 20 FT WIND SPEED > 12 KT

Although the regression equation for Cape Kennedy was not obtained the correlation coefficients are similar–very low–and the two variables are essentially independent.

3.3.6.4 Richardson's Number and Direction Shear

Regression equations and correlation coefficients of $\partial\phi/\partial h_{20}$ versus R_{i20} for the two sites are:

Cape Kennedy	Cedar Hills
Not available	$\partial\phi/\partial h_{20} = -0.018\ R_i + 0.001$
$r = 0.036$	$r = 0.023$

Again in this case the correlation is very low and the regression equation for Cape Kennedy not available. Apparently, there is little dependence between these variables.

3.3.6.5 Speed and Speed Shear

Regression equations and correlation coefficients of $\partial\bar{V}_W/\partial h_{20}$ versus $\bar{V}_{20}$ for the two sites are:

Cape Kennedy	Cedar Hills
$\partial\bar{V}_W/\partial h_{20} = 0.13\ \bar{V}_{20} - 0.0074$	$\partial\bar{V}_W/\partial h_{20} = 0.18\ \bar{V}_{20} - 0.01$
$r = 0.57$	$r = 0.69$

As with R_{i20} and $\bar{V}_{20}$ in Section 3.3.6.2, the regression equations are very similar and the correlation coefficients high, although not as high as in the former case.

3.3.7 Comparison With Literature, Section 3.3.3

The work accomplished in this section differs in many respects from the literature. However, it is possible to compare the wind speed shears described in the two sections. For instance, it may be seen that the average and extreme speed shears are of similar magnitude (see Table 3-12 and Figs. 3-59 to 3-64). Notice particularly column 4 in Table 3-12, which shows a mean shear of 3.6 knots per 100 feet at Whiteshell. These data were taken from 10-minute records for all wind speeds, the nearest conditions to the data processed from Cape Kennedy and Cedar Hills. The Whiteshell records are for a height interval of 20-200 feet, while derived shears are at given tower levels. Although the results cannot be compared explicitly, it appears by visual comparison of the diagrams and tables that the results obtained in both sections are comparable.

Directional shear comparisons are difficult because of differences in the height intervals and other conditions, and only a cursory comparison is possible with the Whiteshell, Canada and Hanford, Washington data (see Figs. 3-11, -12, -53, and -54). It appears that the shears are of the same order of magnitude. The higher shears are near the ground.

3.4 SELECTED DESCRIPTION

Results of a literature search, description of airport winds, and evaluation of winds and stability conditions obtained from two tall towers have been discussed in previous subsections. Now it is possible to select those results or descriptions, either directly or in amended form, applicable to other sections of this study. These include wind speed and direction distributions, wind shear versus altitude, and the Richardson's number distribution at different wind speeds.

3.4.1 Airport Wind Speed Description

A comparison of wind speed descriptions is provided in Figure 3-3. Slightly lower wind speeds are found in the 24 airport descriptions than are presently found in the ARB model. This difference, in part, may be due to the lower height (20 feet) of the observing instruments throughout the 24 airport network. The 24 airport description is selected as being most representative of conditions at a height of 20 feet and for use in other sections of this study.

3.4.2 Airport Wind Direction Description

A wind direction description was obtained from the 24 airport network as being representative of the "average" U.S. airport. This has been selected for use with the speed description of subsection 3.4.1. The description, Figure 3-4, depicts the direction relative to the major runway direction of the composite airport. Crosswinds and headwinds at the composite airport are obtained from the speed and direction descriptions (Figs. 3-6 to 3-8).

3.4.3 Description of Wind Direction Variation With Height

Information outlined in Section 3.3.4 and the literature search, Section 3.2.3.1, indicates that shears greater than $\pm 20^{\circ}$ per 100 feet are unusual and that the majority of these occur at the lower heights, small height intervals, and with small wind speeds. Shears vary from airport to airport and with time at any airport. The great variability in wind shear profiles is shown in Figure 3-57 and no one "average profile" will be indicative of simultaneous conditions at all tower heights. That is, the combined means of the shears at given heights do not indicate the average shear profile. (The average shear at one height does not mean that an average shear at another height occurs simultaneously.) Therefore, no general case description of wind direction variation with height is proposed except to assume zero variation. The errors introduced by this assumption should be small; rare occurrences of combined strong speed and direction shears may occur at some airports.

3.4.4 Richardson's Number-Wind Speed Description

Two descriptions of the Richardson's number-wind speed relationship have been obtained from towers at Cape Kennedy and Cedar Hills, Figures 3-31 through 3-48. These were determined for $-20 < R_i < 20$ at each site. Many other cases with high (< -20 and > 20) R_i at Cedar Hills were not studied because of the limiting R_i's. It is apparent that Cedar Hills has a greater frequency of large temperature gradients and/or very small wind speed shears than Cape Kennedy. In addition to the differences between sites there are annual differences

in the relationship. It is difficult therefore to establish an all-encompassing description from short period records at two sites. By examining the results, however, those for Cape Kennedy appear to behave more rationally (Figs. 3-47 and 3-48), and a far greater percentage of the total observations are included in the study. Therefore, while the Cape Kennedy results are not all-inclusive, they do appear to be more appropriate for this study. Ideally, similar tower information from the 24 U.S. airports, for which surface data were studied in Section 3.2, would be the most valuable in the establishment of an all-inclusive description, if this information existed. Until information is obtained from additional towers as well as Cape Kennedy and Cedar Hills, the Cape Kennedy description in Figures 3-32 through 3-38 is suggested for use in the simulation program. As better descriptions become available they can be substituted for this description.

The information in these figures does not include the distributions for 2-knot speed intervals greater than 12-14 knots because of the paucity of observations at the higher wind speeds. It is evident from Figure 3-47 that the spread of R_i values is rapidly diminishing as the wind speed increases. Additionally, it may be noted that the 50% probability R_i is becoming constant above approximately 14 knots. The other percent frequencies apparently are becoming less variant as well.

In order to establish the distributions for higher wind speeds it is assumed that at high wind speeds (>19 kt) R_i is inversely proportional to the square of the speed. From the analytic description given previously

$$\frac{\partial \bar{V}_W}{\partial h} = \bar{V}_{20} \left(\frac{u_*/k}{\bar{V}_{20}}\right) \phi\left(\frac{h}{\ell'}\right)$$

it may be argued that variability of the product of all terms except $\bar{V}_{20}$ is not a strong function of $\bar{V}_{20}$ when $\bar{V}_{20}$ is large and the subsequent R_i distribution is small. Therefore

$$\partial \bar{V}_W / \partial h \sim \bar{V}_{20}$$

and

$$R_{i_{20}} = \frac{\frac{q}{T}\left(\frac{\partial T}{\partial h} + \frac{q}{C_p}\right)}{\left(\frac{\partial \bar{V}_W}{\partial h}\right)^2} \sim \frac{1}{\bar{V}_{20}^2}$$

Thus, to extrapolate the distribution we assume that the distribution for large $\bar{V}_{20}$ with $R_{i20}\bar{V}_{20}^2$ is invariant with $\bar{V}_{20}$.

Then

$$R_{i'20}\bar{V}_{20}^2 = \text{constant} = R_{i''20}(19)^2$$

where

R_{i20}' = R_{i20} at any speed greater than 19 kt

R_{i20}'' = R_{i20} at 19 kt

19 kt = the highest speed available on Figure 3-47.

The distributions at higher wind speeds can then be obtained, and these are shown in Figure 3-68 as extensions to the lines in Figure 3-47. In addition to these extensions, the 10% and 90% curves have been smoothed in order that they be more representative of a possible distribution which might result from the averaging of data from a number of stations and more years of data from Cape Kennedy. The same method as used for extending the curves to higher winds cannot be used at lower speeds, and therefore the curves were smoothed visually. The largest change in the 10% curve is about 5% at 9 knots as computed using Figure 3-36. This is due to the flatness of the distributions at other than very low Richardson's numbers. The revised exceedance curves are shown in Figures 3-69 to 3-71 with probabilities reversed from those of the Cape Kennedy curves in order that the cumulative probability increase from negative to positive R_i.

3.5 REFERENCES

3-1. U.S. Department of Commerce, Weather Bureau, "Summary of Hourly Observations," *Climatography of the United States,* No. 82, Decennial Census of United States Climate, 1951-1960 or 1956-1960, Superintendent of Documents, Washington, D.C., 1962 and 1963.

3-2. Federal Aviation Administration, DOT, "Automatic Landing Systems (ALS)," Advisory Circular AC No. 20-57A, 12 January 1971.

3-3. Air Registration Board, "Airworthiness Requirements for Automatic Landing in Restricted Visibility Down to Category 3," British Civil Airworthiness Requirements, Paper No. 367, Issue 3, Working Draft, June 1970.

3-4. Watson, I.A., "Report of an Investigation into Low-Altitude Wind Structure for Automatic Landing," *Aeronautical Meteorology,* WMO Technical Note No. 95, World Meteorological Organization, Geneva, Switzerland, October 1969.

3-5. Marut, J. K., E. Van Duyne, F. V. Melewicz, K. A. Kraus, and F. G. Coons: *Statistical Analysis of Meteorological Parameters During Fog at 45 U.S. Airports,* Report No. FAA-RD-72-39, Weather and Flight Service Station Branch, Systems Research and Developmental Service, FAA, Washington, D.C., May 1972.

3-6. Crutcher, H. L., "Project Crosswinds," unpublished paper of the National Climatic Center, U.S. Department of Commerce, NOAA, Environmental Data Services, Federal Building, Asheville, N.C., 28801, no date.

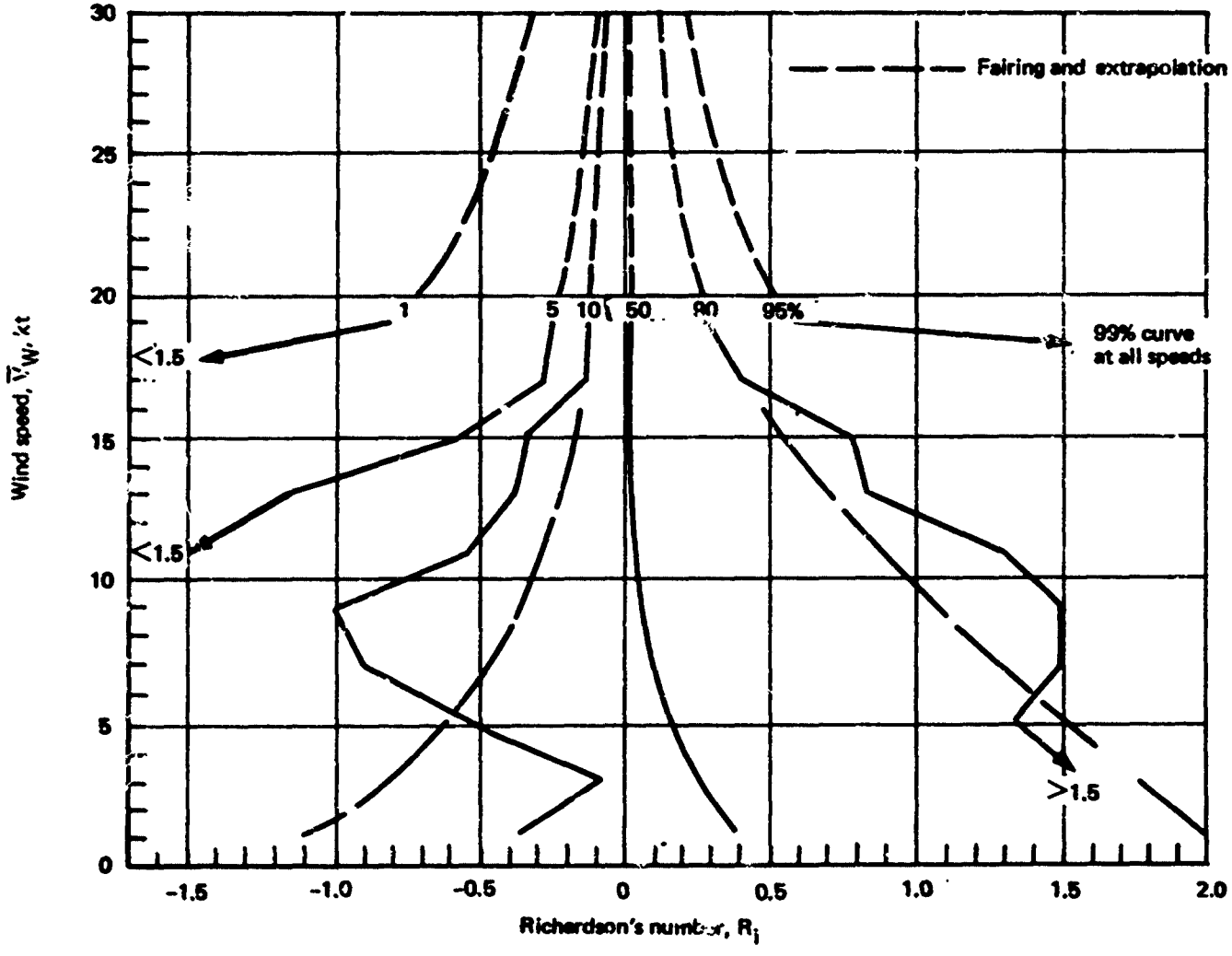

FIGURE 3-68.—PERCENT FREQUENCY OF OCCURRENCE, WIND SPEED VS R_i, CAPE KENNEDY, 1966-68

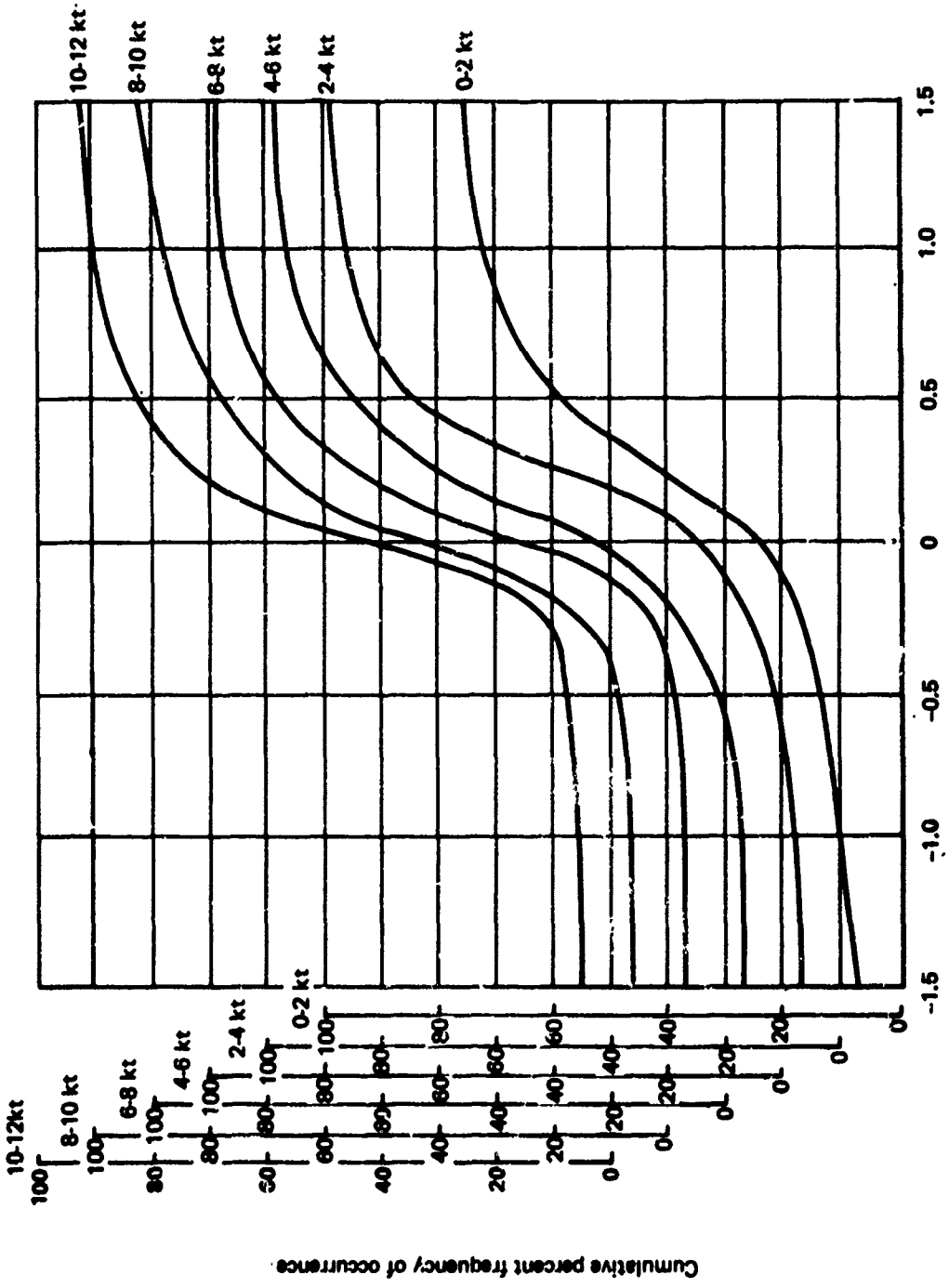

FIGURE 3-69.—CUMULATIVE PERCENT FREQUENCY OF OCCURRENCE OF R_i AT GIVEN WIND SPEEDS, 0 TO 12 KNOTS

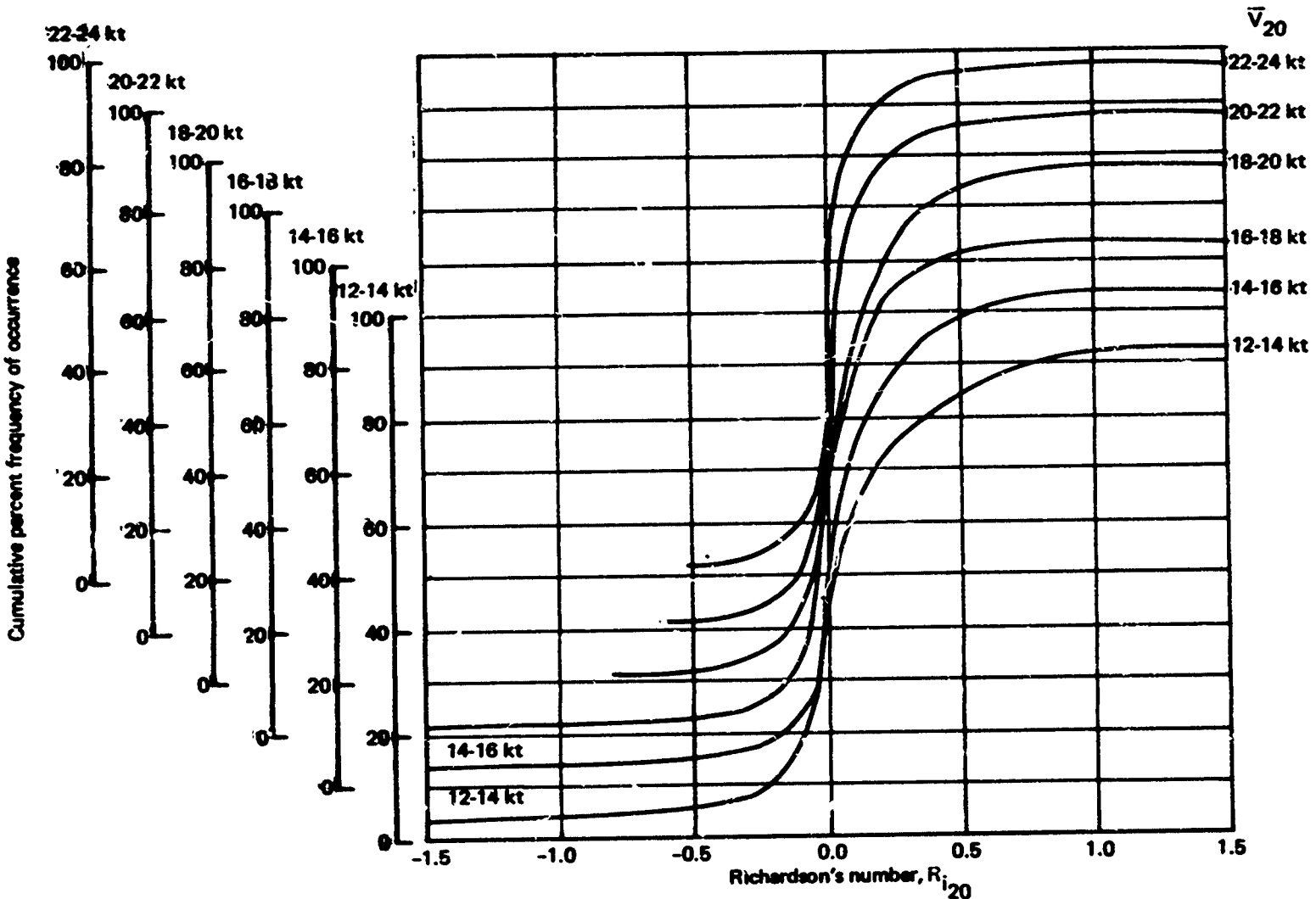

FIGURE 3-70.—CUMULATIVE PERCENT FREQUENCY OF OCCURRENCE OF R_i AT GIVEN WIND SPEEDS, 12 TO 24 KNOTS

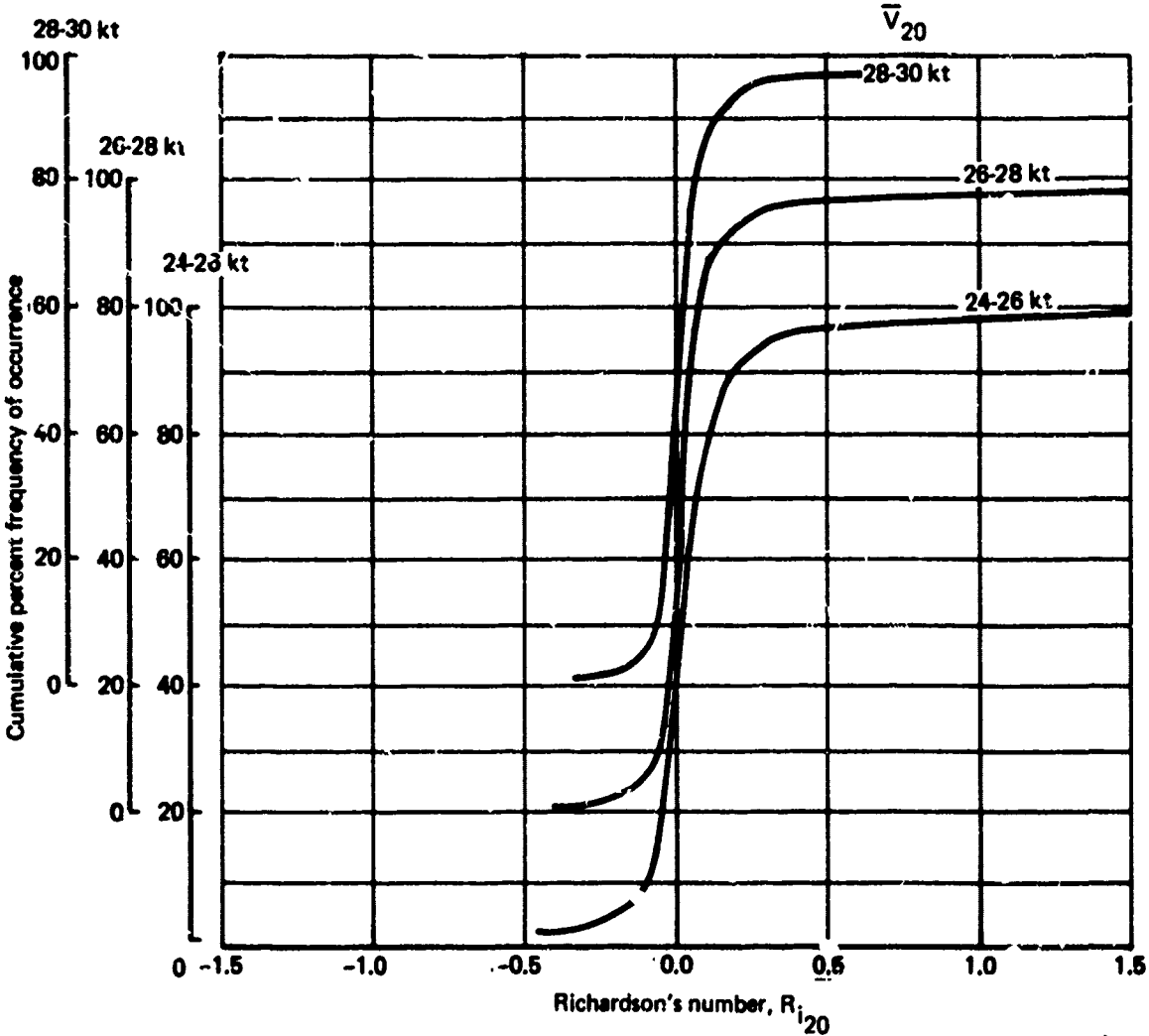

FIGURE 3-71.–CUMULATIVE PERCENT FREQUENCY OF OCCURRENCE OF R_i AT GIVEN WIND SPEEDS, 24 TO 30 KNOTS

3-7. Stone, W. A., D. E. Jenne, and J. M. Thorp: "Climatography at the Hanford Area," BNWL-1605, UC-53, Battelle Pacific Northwest Laboratories, Richland, Washington 99352.

3-8. Crawford, K. C. and H. R. Hudson, *Behavior of Winds in the Lowest 1500 Feet in Central Oklahoma: June 1966–May 1967,* ERLTM-NSSL 48, National Severe Storms Laboratory, Norman, Oklahoma, August 1970.

3-9. McVehil, G. E. and H. G. Commity, *Ground Wind Characteristics at Kennedy Space Center,* NASA CR-1418, Prepared by Cornell Aeronautical Laboratory, Inc., Buffalo, New York, September 1969.

3-10. World Meteorological Organization, "Vertical Wind Shear in the Lower Layers of the Atmosphere," Technical Note No. 93, WMO-No. 230, TP. 123, Secretariat of the World Meteorological Organization, Geneva, Switzerland, 1969.

3-11. Muller, F. B. and C. M. Mushkat, "Preliminary Analysis of Canadian Wind-Shear Data," Reference 3-1 above, pp 31-36.

3-12. Pettitt, R. B. and R. G. Root, "Vertical Wind Shear in the Boundary Layer," Reference 3-1 above, pp. 1-30.

3-13. Author unknown, "A Report of the Statistical Investigations on Vertical Wind Shear in the Lower Layers at Thumba," Reference 3-1 above, pp. 103-168.

3-14. Kusano, K., Y. Suzukik and H. Takei, "Vertical Wind Shear in the Lower Layers at the Tokyo International Airport," Reference 3-1 above, pp. 168-183.

3-15. Rykoort, P. J., "Dependence of Observed Low-Level Wind Shear on Averaging Period and Lapse Rate," Reference 3-1 above, pp. 185-194.

3-16. Abramovic, K. G., and V. G. Glazunov: "Wind Shear in the Lower Atmosphere," Reference 3-1 above, pp. 195-202.

3-17. Roberts, C. F., "A Preliminary Analysis of Some Observations of Wind Shear in the Lowest 100 Feet of the Atmosphere for Application to the Problem of the Control of Aircraft on Approach," Reference 3-1 above, pp. 203-218.

3-18. Ramsey, C. M. "Vertical Wind Shear," Memorandum No. 10, All Weather Operations Panel, ICAO Montreal P.Q., Canada 1964.

3-19. Dubov, A. S., *Variations of Wind, Temperature and Turbulence in the Lowest 1 Km,* CAem STC/Doc. 35, WMO Commission for Aeronautical Meteorology Scientific and Technical Conference, London, March 1968.

3-20. Clodman, J., F. B. Muller and E. G. Morrissey, *Wind Regime in the Lowest One Hundred Metres as Related to Aircraft Take-Offs and Landings,* CAem STC/Doc. 30, WMO Commission for Aeronautical Meteorology Scientific and Technical Conference, London, March 1968.

3-21. Brook, R. R., *Preliminary Study of Wind Shear in the Boundary Layer at Melbourne Airport (Tullamarine)*, N70-30146, Department of the Interior, Melbourne, Australia, February 1970.

3-22. Knechtel, K. B., "Vertical Wind Shear Near the Ground," Boeing Coordination Sheet No. AERO-340, March 25, 1969.

3-23. Izumi, Y. and H. A. Brown, "Temperature, Humidity and Wind Variation During Dissipation of a Low-Level Jet," *Journal of Applied Meteorology*, Vol. 5, No. 1, pp. 36-42, February 1966.

4.0 ANALYSIS AND SIMULATION MODELING

Having described phenomena of wind in its own natural axis system, it remains to define wind phenomena in the airplane's axis system and the effects of winds on aircraft motion. Then, with some qualitative understanding of the effects of the input on the output, a model, representing all the significant parameters and effects for approach and landing, is developed for flight simulation.

Although a number of assumptions and value judgments were involved in the development of the descriptions and wind and turbulence, the descriptions will be accepted as fact and emphasis will be placed on applications.

A qualitative analysis of the effects of winds is first provided to develop an understanding of what effects need to be represented. Criteria are established for evaluating approximate techniques. The more specific subjects of distributed lift effects, unsteady aerodynamics, and the effects of speed and altitude are considered. An attempt is made to provide the means of transforming turbulence from the axis system of the mean wind to that of the airplane. Specific techniques of generating the random noise needed for the production of turbulence are reviewed.

Finally, the model is developed. The model begins with the probabilistic combinations of environmental data and ends with the generation of the effects of the winds on aerodynamic forces and moments.

4.1 NOMENCLATURE

a_x, a_y, a_z	Components of linear body axis acceleration along the x, y, and z body axes
b	Wing span
$\bar{c}$	Mean chord
C_D, C_{D_0}	Drag coefficient and that at an initial condition
C_{D_α}	$\partial C_D/\partial\alpha$
$C_{L_{WB}}$	Wing-body contribution to the lift coefficient
C_L, C_{L_0}	Lift coefficient and that at an initial condition
C_{L_α}, $(C_{L_\alpha})_{ss}$	Lift curve slope ($\partial C_L/\partial\alpha$) and that at steady state conditions
$C_{L_{\hat{u}}}$	$\partial C_L/\partial\,(u/u_0)$
$C_{L_{H_{\alpha_H}}}$	Horizontal stabilizer lift curve slope ($\partial C_{L_H}/\partial\alpha_H$)

C_l	Rolling moment coefficient
C_{l_i}, $C_{l_{i_W}}$, $C_{l_{i_V}}$ ($i = p, \hat{p}, v, \beta$)	$\partial C_l/\partial_i$ and that due to the wing and vertical stabilizer
$(C_{l_{r_{WB}}})_x$ $(C_{l_{r_{WB}}})_z$	Contributions of wing-body forces along the x and z axes to C_{l_r}
C_m, $C_{m_{WB}}$	Pitching moment coefficient and that due to the wing-body
C_{m_i}, $(C_{m_i})_{WB}$ ($i = \alpha, \dot{\alpha}, q$)	$\partial C_m/\partial_i$ and that due to the wing-body
Cy	Side force coefficient
$(Cy_p)V$	$\partial Cy/\partial p$ due to vertical tail
C_N	Yawing moment coefficient
$(C_{N_p})V$	$\partial C_N/\partial p$ due to vertical tail
C_{z_H}	z force coefficient due to horizontal stabilizer
d	Atmospheric boundary layer depth or derivative
e	Exponential function
$f(h/\ell')$	Universal function of h/ℓ' defining contribution of nonneutral atmospheric conditions to the mean wind
$\vec{F}$	Body axis aerodynamic force vector
F_x, F_y, F_z	x, y, and z components of $\vec{F}$
g	Acceleration due to gravity
$g(h/\ell')$	Universal function of h/ℓ' defining contribution of nonneutral atmospheric stability to the mean wind
$\vec{G}$	Body axis aerodynamic moment vector
G_x, G_y, G_z	x, y, and z components of $\vec{G}$

$G(s)$	Transfer function
$G(i\omega)$, $G^*(i\omega)$	Frequency response and its complex conjugate
G_u, G_v, G_w	Filters for producing u, v, and w components of turbulence
h, h_{CG}, h_W	Altitude, altitude at the airplane's center of gravity, and altitude used in wind model
i	$\sqrt{-1}$
$\hat{i}$	Unit vector along x axis
I_{xx}, I_{yy}, I_{zz}	Roll, pitch, and yaw body axis moments of inertia
I_{xz}	Product of inertia
j	Unit vector along y axis
k	Von Karman's constant, 0.4
$\hat{k}$	Unit vector along z axis
$K(s)$	Küssner lift growth function
ℓ	Length
ℓ'	Monin-Obukov scaling length
ℓ_T	Distance from the wing-body aerodynamic center to the tail aerodynamic center along the x body axis, positive aft
L	Aerodynamic roll acceleration, $(G_x I_{zz} + G_z I_{xz})/(I_{xx} I_{zz} - I_{xz}^2)$
L_u, L_v, L_w	Integral scales for u, v, and w components of turbulence
L_H, L_V	Integral scales for horizontal and vertical components of turbulence
L_i, L_{i_W}, L_{i_V} ($i = p, r, v, z, \beta, \theta, \phi, \delta_j, f\theta$)	Roll acceleration derivative, $\partial L/\partial i$, that due to the wing, and that due to the vertical stabilizer
L_L, L_R	Lift on left and right wings
m	Airplane mass

M	Aerodynamic pitch acceleration, G_z/I_{yy}
$M(\omega)$	Frequency response amplitude
M_i (i = q, u, w, $\dot{w}$, z, α, $\dot{\alpha}$, δ_j, θ, $\dot{\theta}$, $\int\theta$,	Pitch acceleration derivative, $M_i = \partial M/\partial i$
M_i'	$M_i - Z_i M_{\delta c}/Z_{\delta c}$
n_z	Normal applied acceleration, F_z/W
N	Aerodynamic yaw acceleration, $(G_x I_{xz} + G_z I_{xx})/(I_{xx} I_{zz} - I_{xz}^2)$
N_i (i=h, p, r, u, w, β, δ_j, θ, $\int\theta$, ψ)	Yaw acceleration derivative, $\partial N/\partial i$, or transfer function numerator for response parameter i
N_{i_W}, N_{i_V}	Contributions of wing and vertical tail to yaw acceleration derivative
N_{h_0}	Altitude to column transfer function numerator for zero mean wind speed
p	Inertial body axis roll rate
$\hat{p}$	Nondimensional body axis roll rate, $pb/2u_0$
p_A, $p_{A_{CG}}$, $p_{A_{TAIL}}$	Effective body axis roll rate relative to the air mass, that at the center of gravity, and that at the tail
p_T	Effective roll rate of the air mass due to turbulence relative to the earth
p_W, $p_{W_{CG}}$, $p_{W_{TAIL}}$	Effective roll rate of the air mass due to wind relative to the earth and that at the center of gravity and the tail
$\bar{p}_W$, $\bar{p}_{W_{CG}}$, $\bar{p}_{W_{TAIL}}$	Effective roll rate of the air mass due to the mean wind relative to the earth and that at the center of gravity and the tail
q	Inertial body axis pitch rate
$\bar{q}$, $\bar{q}_{WB}$, $\bar{q}_{TAIL}$, $\bar{q}_H$	Dynamic pressure and that for the wing-body, the tail, and the horizontal tail
q_{CG}	Dynamic pressure at the center of gravity

$q_A, q_{A_{CG}}$	Effective body axis pitch rate relative to the air mass and that at the center of gravity
q_T	Effective body axis pitch rate due to turbulence with respect to the earth
$q_W, \bar{q}_W$	Effective body axis pitch rate due to the wind and the mean wind relative to the earth
r	Inertial body axis yaw rate
$\vec{r}$	Displacement vector
$r_A, (r_{A_{WB}})_X, (r_{A_{WB}})_Z$	Effective body axis yaw rate relative to the air mass and that for the wing body x and z force contributions to yaw rate derivatives
r_T	Effective body axis yaw rate due to turbulence relative to the earth
$r_W, (r_{W_{CG}})_X, (r_{W_{CG}})_Z$	Effective body axis yaw rate due to wind relative to the earth and that used with x and z force contributions to yaw rate derivatives
$\bar{r}_W, (\bar{r}_{W_{CG}})_X, (\bar{r}_{W_{CG}})_Z$	Effective body axis yaw rate due to the mean wind relative to the earth and that used with x and z force contributions to yaw rate derivatives
$R_i, R_{i_{20}}$	Richardson's number and that at 20 feet altitude
R_{ii}	Autocorrelation function for variable i
s	Laplace transform variable
S	Wing area
S_H	Horizontal tail area
t	Time
t*	Nondimensional time, $\bar{c}/2V_A$
T	Time constant
T_R, T_S	Roll mode and spiral mode time constants

$T_{h_1}, T_{h_2}, T_{h_3}$	Altitude to column numerator time constants
T_{h_0}	T_{h_1} for zero wind speed
T_θ	Pitch attitude to column numerator time constant
$T_{REQ}, (T/W)_{REQ}$	Thrust and thrust to weight required for unaccelerated trim
u, u_0	Inertial linear velocity along the x body axis and that at the initial condition
u_M, u_R	Linear velocity along the x mean wind and relative wind axes
u_{TAIL}	Inertial velocity along the x body axis at the tail relative to the earth, including angular velocity effects
u_*, u_{*0}	Friction velocity (shear stress/density)$^{1/2}$ and that at the surface
u_A, u_{A_0}	Linear velocity with respect to the air mass along the x body axis and that at the initial condition
$u_{A_{CG}}, u_{A_{TAIL}}$	u_A at the center of gravity and the tail
u_E	Inertial linear velocity along the x earth axis
$u_T, u_{T_{TG}}$	Linear turbulence velocity along the x body axis and the x turbulence generation axis, relative to the earth
$u_W, u_{W_{CG}}, u_{W_{TAIL}}$	Linear wind velocity along the x body axis relative to the earth and that at the center of gravity and the tail
u_W, u_{W_0}	Linear mean wind velocity along the x body axis relative to the earth and that at the initial condition
v	Inertial linear velocity along the y body axis relative to the earth
$v_A, v_{A_{CG}}, v_{A_{TAIL}}$	Linear velocity along the y body axis relative to the air mass and that at the center of gravity and the tail
v_E	Inertial linear velocity along y earth axis
v_M, v_R	Linear velocity along the y mean wind and relative wind axes
$v_T, v_{T_{TG}}$	Linear turbulence velocity along the y body axis and the y turbulence generation axis relative to the earth

v_{TAIL}	Inertial velocity along the y body axis at the tail relative to the earth, including angular velocity effects
$\bar{v}_W$	Linear mean wind velocity along the y body axis relative to the earth
$v_W, v_{W_{CG}}, v_{W_{TAIL}}$	Linear wind velocity along the y body axis relative to the earth and that at the center of gravity and the tail
V	Speed
$\vec{V}$	Linear velocity vector
V_A, V_{A_0}	Total airspeed and that at the initial condition
$V_{A_{CG}}, V_{A_{TAIL}}$	Total air speed at the center of gravity and the tail
$V_{E_{GT}}$	Total ground track speed
$\bar{V}_H$	Horizontal tail volume coefficient, $(S_H/S)(\ell_H/c)$
$\bar{V}_W, \bar{V}_{W_0}$	Mean wind speed and that at the initial condition
w	Inertial linear velocity along the z body axis
$w_A, w_{A_{CG}}, w_{A_{TAIL}}$	Linear velocity along the z body axis relative to the air mass and that at the center of gravity and the tail
$w_{\bar{W}}, w_R$	Linear velocity along the z mean wind and relative wind axes
$w_T, w_{T_{CG}}, w_{T_H}$	Linear turbulence velocity along the z body axis relative to the earth and that at the center of gravity and the horizontal stabilizer
w_{TAIL}	Inertial velocity along the z body axis at the tail relative to the earth, including angular velocity effects
$(w_T)_0, w_{T_{CG}}$	w_T at the origin and the center of gravity
w_{T_e}	Effective w_T
$w_W, w_{W_{CG}}, w_{W_{TAIL}}$	Linear wind velocity along the z body axis relative to the earth and that at the center of gravity and the tail
$\bar{w}_W, \bar{w}_{W_{CG}}$	Mean wind velocity along the z body axis relative to the earth
W	Airplane weight

X	Linear aerodynamic acceleration along the x body axis, F_x/m; amplitude
X_i ($i = q, u, w, z, \alpha, \dot{\alpha}, \delta, \theta, \int\theta, \phi, \psi$)	$\partial X/\partial i$
Y	Linear aerodynamic acceleration along the y body axis, F_y/m
Y_i ($i = p, r, v, z, \delta_j, \int\theta, \psi$)	$\partial Y/\partial i$
z_0	Surface roughness length
z_T	Distance from the wing-body aerodynamic center to the tail aerodynamic center along the z body axis, positive down
Z	Linear aerodynamic acceleration along the y body axis, F_z/m
Z_i ($i = q, u, w, z, \alpha, \delta_j, \theta, \int\theta, \phi, \psi$)	$\partial Z/\partial i$

Greek:

α	Log-linear mean wind profile constant = 4.5
$\alpha, \alpha_{WB}, \alpha_{TAIL}, \alpha_H$	Angle of attack and that used for wing-body, tail, and horizontal stabilizer aerodynamics
α_I, α_W	Angles of attack due to inertial and wind velocities
$\alpha_{W_{CG}}$	Rate of change of angle of attack due to the wind at the center of gravity
$\beta, \beta_{CG}, \beta_{TAIL}$	Sideslip angle and that at the center of gravity and the tail
γ, γ_0	Flight path angle relative to the earth and that at the initial condition
δ	Perturbation
δ_j	j^{th} controller or control surface deflection
Δ	Increment
$\Delta(s), \Delta_{LONG}(s), \Delta_{LD}(s), \Delta_{SP}(s)$	Characteristic equation and that for longitudinal, lateral-directional, and short period motion
ϵ	Downwash
$\zeta_{ph}, \zeta_{sp}, \zeta_d, \zeta_\phi$	Damping ratio for the phugoid, short period, Dutch roll, and bank angle to control input transfer function numerator

θ, θ_0	Euler pitch angle and that at the initial condition
$\int\theta$	Integral of θ
σ	Sidewash or standard deviation
σ_i	Standard deviation of the i^{th} component of turbulence
σ_H, σ_V	Standard deviation of horizontal and vertical turbulence
σ_{ij}^2	Covariance of the i^{th} and j^{th} components of turbulence
τ	Transport lag delay time
ϕ	Euler bank angle
$\phi(h/\ell')$	Universal function of h/ℓ' defining the nondimensional mean wind shear
Φ_i	Power spectrum for parameter i
Φ_{ij}	Cospectrum for parameters i and j
Φ_I, Φ_0	Input and output power spectra
ψ, ψ_0	Euler heading angle and that at the initial condition
$\bar{\psi}_W, \bar{\psi}_{W_0}$	Heading to which the mean wind is blowing and that at the initial condition
ω	Temporal frequency (rad/sec)
$\vec{\omega}$	Angular velocity vector
$\omega_N, \omega_d, \omega_{ph}$ ω_{sp}, ω_ϕ	Natural frequency and that of the Dutch roll, phugoid, short period, and the numerator of the bank angle to control transfer function
$\Omega_1, \Omega_2, \Omega_3$	Components of the spatial frequency vector along the x, y, and z axes
Ω'_2, Ω'_3	Maximum values of the lateral and vertical components of spatial frequency at which the first order Taylor-series method of representing distributed lift effects of turbulence is accurate

Dotted terms refer to derivatives with respect to time.

Other nomenclature defined where used.

Schematic Symbology:

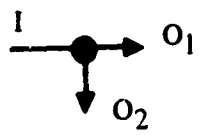

Node: $O_1 = O_2 = I$

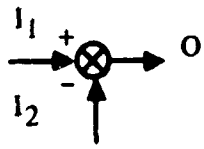

Summing junction: $O = I_1 - I_2$

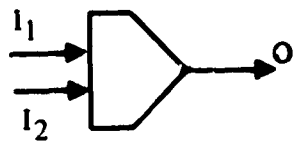

Multiplier: $O = I_1 I_2$

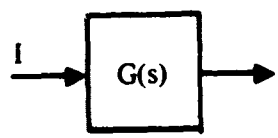

Linear operation: $O = G(s) I$

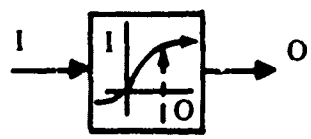

Input-output function (table lookup)

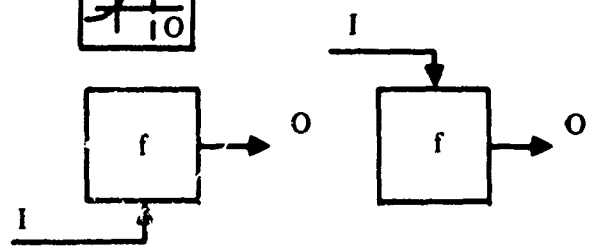

Nonlinear function: $O = f(I)$

4.2 EFFECTS OF WINDS ON AIRCRAFT MOTION

The influence of mean winds and mean wind shears is generally considered in terms of control power requirements (i.e., rudder power for decrab), control actuation rates (i.e., autothrottle and autopilot thrust and control surface rate authority), guidance, and speed margins. Additionally, there are stability considerations that are much less straightforward.

At high altitudes and speeds, the influence of winds and wind shears is generally not considered to be so important because wind speeds are small compared to airspeeds, aerodynamic forces and moments are large compared to inertial effects, speed margins are high, and wind shears are less frequent. In addition, at large distances from the ground there is less need for accurate guidance.

At low altitudes, particularly for approach and landing, the effect of winds is much more critical. The accuracy requirements for simulation modeling are dependent upon the sensitivity of aircraft response to winds and wind shears. An analysis and discussion of these effects is provided in the following for the effects that are less straightforward. The analysis may be divided into linear and nonlinear analysis, depending on what may be determined from the linearized equations of motion.

4.2.1 Small Disturbance Analysis

As is conventional, the linear equations of motion are defined for an axis system attached to the aircraft, or a body axis system. Aircraft symmetry is assumed and the x-y plane coincides with the plane of symmetry. The x axis is oriented forward and is aligned to the airspeed vector in the x-y plane (stability axis), some geometric characteristic (i.e., wind chord plane, waterline, etc.) or some inertial axis (i.e., principal axis). The y axis is oriented toward the right wing and the z axis downward. The equations of motion are the same for any such body axis system, but the forces and moment characteristics are unique to a particular axis system and the orientation in space of the axis system, defined in terms of Euler angles, is dependent upon the axis system selected. Gyroscopic couples, produced by masses rotating with respect to the body axis system, (i.e., rotating engine parts), and Coriolis forces are considered to be negligible. Atmospheric density is assumed to change so slowly with altitude that it may be represented as a constant.

The linearized equations of motion for these assumptions, for a rigid airframe and still air, are presented on Figure 4-1 and are similar to those presented in Reference 4-1. Uncoupling of the longitudinal and lateral-directional sets requires level wings initially as well as uncoupled aerodynamics. If the body axis system selected is the stability axis system, the initial Euler pitch angle is identical to the flight path angle. The equations on Figure 4-1 are written for uncoupled accelerations. Thus, the normalized aerodynamic rolling and yawing moments are written to exclude the appearance of the product of inertia from the equations.

LONGITUDINAL SET

Longitudinal acceleration:

$$(s - X_u)\,u - (X_{\dot{w}}s + X_w)w + \left[\frac{-X_q s + g\cos\theta_0}{s}\right] q = \sum_i X_{\delta_i}\,\delta_i$$

Vertical acceleration:

$$-Z_u u + (s - Z_{\dot{w}}s - Z_w)w + \left[\frac{-(u_0 + Z_q)s + g\sin\theta_0}{s}\right] q = \sum_i Z_{\delta_i}\,\delta_i$$

Pitch acceleration:

$$-M_u u - (M_{\dot{w}}s + M_w)w + (s - M_q)q = \sum_i M_{\delta_i}\,\delta_i$$

LATERAL-DIRECTIONAL SET

Side acceleration:

$$(s - Y_v)v - \left[\frac{Y_p s + g\cos\theta_0}{s}\right] p + \left[\frac{(u_0 - Y_r)s - g\sin\theta_0}{s}\right] r = \sum_i Y_{\delta_i}\,\delta_i$$

Roll acceleration:

$$-L_v v + (s - L_p)p - L_r r = \sum_i L_{\delta_i}\,\delta_i$$

Yaw acceleration:

$$-(N_{\dot{v}}s + N_v)v - N_p p + (s - N_r)r = \sum_i N_{\delta_i}\,\delta_i$$

Linear velocity vector, $\vec{V} = u\hat{i} + v\hat{j} + w\hat{k}$

Angular velocity vector, $\vec{\omega} = p\hat{i} + q\hat{j} + r\hat{k}$

Applied force vector, $\vec{F} = F_x\hat{i} + F_y\hat{j} + F_z\hat{k}$

Applied moment vector, $\vec{G} = G_x\hat{i} + G_y\hat{j} + G_z\hat{k}$

$$X = F_x/m \qquad L = \frac{G_x I_{zz} + G_z I_{xz}}{I_{xx}I_{zz} - I_{xz}^2}$$

$$Y = F_y/m \qquad M = G_y/I_{yy}$$

$$Z = F_z/m \qquad N = \frac{G_x I_{xz} + G_z I_{zz}}{I_{xx}I_{zz} - I_{xz}^2}$$

δ_i = i^{th} control surface deflection

s = Laplace transform variable

$$A_\lambda = \frac{\partial A}{\partial \lambda}, \qquad A = X, Y, Z, L, M\ N \qquad \lambda = u, v, w, p, q, r, \delta_i$$

FIGURE 4-1.—LINEARIZED EQUATIONS OF MOTION FOR STILL AIR

To generalize the equations for flight in winds, the inertial velocity terms that are multiplied by the dimensional derivatives are changed to airspeed component perturbations, which represent the differences between inertial velocity components and wind velocity components. The wind velocity components are in turn the sum of the turbulence components and the mean wind components. That is,

$$\xi_A = \xi - \xi_W$$

$$\xi_W = \bar{\xi}_W + \xi_T$$

where $\xi = u, v, w, p, q, r$.

It is common to see the airspeed defined as the sum of inertial and wind velocities, but this is merely a change in convention where the axis system defining wind motion in space is reversed from that for airplane motion.

It is common to assume that certain derivatives are insignificant or negligible. The derivatives that shall be dropped or ignored and which are dropped in Reference 4-1 are $X_{\dot{w}}$, X_q, $Z_{\dot{w}}$, Z_q, Y_p and Y_r. The stability axis is selected and the initial Euler pitch angle is assumed to be zero, corresponding to level flight. For non-still-air conditions, the pitch attitude and flight path are equal only in level flight. That is, the relationship $\theta = \gamma + \alpha$ holds only for still air. Restricting consideration to level flight permits dropping gravity terms in the vertical and side acceleration equations and enables simplified relationships between the body axis angular velocities and the Euler angles: $p = s\phi$, $q = s\theta$, $r = s\psi$. The linearized equations considered are presented on Figure 4-2.

LONGITUDINAL SET

$$(s - X_u)u - X_w w + g\theta + X_u u_W + X_w w_W = \sum_i X_{\delta_i} \delta_i$$

$$-Z_u u + (s - Z_w)w - u_0 s\theta + Z_u u_W + Z_w w_W = \sum_i Z_{\delta_i} \delta_i$$

$$-M_u u - (M_{\dot{w}} s + M_w)w + (s^2 - M_q s)\theta + M_u u_W + \left[M_{\dot{w}} s + M_w \right] w_W + M_q q_W = \sum_i M_{\delta_i} \delta_i$$

LATERAL DIRECTIONAL SET

$$(s - Y_v)v - g\phi + u_0 r + Y_v v_W = \sum_i X_{\delta_i} \delta_i$$

$$-L_v v + (s^2 - L_p s)\phi - L_r r + L_v v_W + L_p p_W + L_r r_W = \sum_i L_{\delta_i} \delta_i$$

$$-N_v v - N_p s\phi + (s - N_r)r + N_v v_W + N_p p_W + N_r r_W = \sum_i N_{\delta_i} \delta_i$$

FIGURE 4-2.–LINEARIZED EQUATIONS OF MOTION FOR LEVEL FLIGHT IN WIND

That part of the wind terms associated with turbulence is generally placed on the right side of the equations and treated as a forcing function independent of the motion of the airplane. However, the mean wind has been described deterministically as a function of altitude. Thus, the mean wind alters the uncontrolled stability of the airplane as the airplane motion is dependent on the mean wind and the mean wind is dependent upon the airplane motion. Consequently, the mean wind alters the aircraft's characteristic motion or stability.

4.2.1.1 Effects of Mean Wind, Point Lift

The angular components of the mean wind shown on Figure 4-2 are approximate representations of distributed lift effects. If the changes of mean wind heading and magnitude are sufficiently small with respect to the size of the aircraft, the effective angular components may be ignored, resulting in representing all the aerodynamics as if they were concentrated at the center of gravity.

The body axis components of mean wind are found by first transforming from the mean wind axis system to the earth axis system, a rotation in the plane of the earth through $\overline{\psi}_W$, and then by transforming from the earth axis through the Euler angles of the body axis. The resulting nonlinear expressions are shown on Figure 4-3. The small perturbation body axis wind components are computed from first order Taylor series expansions about the initial conditions (equivalent to derivatives) and are shown on Figure 4-3 for wings level, level flight. The mean wind is considered to have both variable heading and magnitude with altitude. Substituting these expressions into the equations of motion (after dropping the δ's with the understanding that all motion variables are small perturbations) results in the equations on Figure 4-4.

From Figure 4-4, some conclusions concerning the effects of winds may be reached:

- Longitudinal and lateral-directional motion appear to be coupled in the presence of a wind although they are not in still air. If the wind is aligned to the flight path, lateral-directional motion will not influence the longitudinal motion, but longitudinal motion will continue to influence lateral-directional motion so long as a mean wind heading shear exists.

- The presence of a mean wind introduces new aerodynamic stiffness derivatives (derivatives with respect to Euler angles and vertical translation) and derivatives proportional to the integral of pitch attitude and which augment the pitch damping derivatives.

- All the derivatives due to the presence of the mean wind are asymmetric with respect to mean wind heading. That is, a derivative that appears statically to be stabilizing for one wind heading will be destabilizing for the wind heading changed by 90°.

If gradients of the mean wind in the horizontal planes or if nonlevel flight were permitted, additional stiffness derivatives caused by the gradients of the mean wind and with respect to horizontal displacements would be introduced. Nonlevel flight also alters the attitude stiffness derivatives.

LARGE DISTURBANCE BODY AXIS COMPONENTS OF MEAN WIND

$$\begin{Bmatrix} u_W \\ v_W \\ w_W \end{Bmatrix} = \begin{Bmatrix} \cos(\psi - \bar{\psi}_W)\cos\theta \\ \cos(\psi - \bar{\psi}_W)\sin\theta\sin\phi - \sin(\psi - \bar{\psi}_W)\cos\phi \\ \cos(\psi - \bar{\psi}_W)\sin\theta\cos\phi + \sin(\psi - \bar{\psi}_W)\sin\phi \end{Bmatrix} \bar{V}_W$$

SMALL DISTURBANCE BODY AXIS COMPONENTS OF MEAN WIND

$$\theta_0 = \phi_0 = 0$$

$$\begin{Bmatrix} \delta u_W \\ \delta v_W \\ \delta w_W \end{Bmatrix} = \begin{Bmatrix} 0 \\ 0 \\ 1 \end{Bmatrix} \cos(\psi_0 - \bar{\psi}_{W_0})\bar{V}_{W_0}\delta\theta + \begin{Bmatrix} 0 \\ 0 \\ \sin(\psi_0 - \bar{\psi}_{W_0}) \end{Bmatrix} \bar{V}_{W_0}\delta\phi$$

$$+ \begin{Bmatrix} -\sin(\psi_0 - \bar{\psi}_{W_0}) \\ -\cos(\psi_0 - \bar{\psi}_{W_0}) \\ 0 \end{Bmatrix} \bar{V}_{W_0}(\delta\psi - \delta\bar{\psi}_W) + \begin{Bmatrix} \cos(\psi_0 - \bar{\psi}_{W_0}) \\ -\sin(\psi_0 - \bar{\psi}_{W_0}) \\ 0 \end{Bmatrix} \delta\bar{V}_W$$

$$\delta\bar{\psi}_W = \frac{d\bar{\psi}_W}{dh}\delta h \qquad \delta\bar{V}_W = \frac{d\bar{V}_W}{dh}\delta h \qquad \delta h = \frac{1}{s}\left[(u_{A_0} + \bar{V}_{W_0})\delta\theta - \delta w\right]$$

$$\delta u_W = -\sin(\psi_0 - \bar{\psi}_{W_0})\bar{V}_{W_0}\delta\psi + \left[\cos(\psi_0 - \bar{\psi}_{W_0})\frac{d\bar{V}_W}{dh}\right.$$

$$\left. + \sin(\psi_0 - \bar{\psi}_0)\bar{V}_{W_0}\frac{d\bar{\psi}_W}{dh}\right]\frac{1}{s}\left[(u_{A_0} + \bar{V}_{W_0})\delta\theta - \delta w\right]$$

$$\delta v_W = -\cos(\psi_0 - \bar{\psi}_{W_0})\bar{V}_{W_0}\delta\psi - \left[\sin(\psi_0 - \bar{\psi}_{W_0})\frac{d\bar{V}_W}{dh}\right.$$

$$\left. - \cos(\psi_0 - \bar{\psi}_{W_0})\bar{V}_{W_0}\frac{d\bar{\psi}_W}{dh}\right]\frac{1}{s}\left[(u_{A_0} + \bar{V}_{W_0})\delta\theta - \delta w\right]$$

$$\delta w_W = \cos(\psi_0 - \bar{\psi}_{W_0})\bar{V}_{W_0}\delta\theta + \sin(\psi_0 - \bar{\psi}_{W_0})\bar{V}_{W_0}\delta\phi$$

FIGURE 4-3.—BODY AXIS MEAN WIND COMPONENTS

LONGITUDINAL SET

$$(s - X_u)u - (X_w + \frac{X_z}{s})w + (s - X_\theta - \frac{X_{\int\theta}}{s})\theta - X_\phi\phi - X_\psi\psi = 0$$

$$-Z_u u + (s - Z_w - \frac{Z_z}{s})w - (u_0 s - Z_\theta - \frac{Z_{\int\theta}}{s})\theta - Z_\phi\phi - Z_\psi\psi = 0$$

$$-M_u u - (M_{\dot{w}}s + M_w + \frac{M_z}{s})w + \left[s^2 - (M_q + \Delta M_{\dot{\theta}})s - M_\theta - \frac{M_{\int\theta}}{s}\right]\theta - (M_{\dot{\phi}}s + M_\phi)\phi - M_\psi\psi = 0$$

LATERAL DIRECTIONAL SET

$$(s - Y_v)v - g\phi + (u_0 - Y_\psi)r - \frac{Y_z}{s}w - \frac{Y_{\int\theta}}{s} = 0$$

$$-L_v v + (s^2 - L_p s)\phi - (L_r + \frac{L_\psi}{s})r - \frac{L_z}{s}w - \frac{L_{\int\theta}}{s}\theta = 0$$

$$-N_v - N_p s\phi + (s - N_r - \frac{N_\psi}{s})r - \frac{N_z}{s}w - \frac{N_{\int\theta}\theta}{s} = 0$$

Wind-induced derivatives:

$$X_z = X_u \frac{d\bar{u}_W}{dh} \qquad X_\psi = -X_u \bar{v}_{W_0} \qquad X_{\int\theta} = -X_u \frac{d\bar{u}_W}{dh}(u_{A_0} + \bar{u}_{W_0})$$

$$Z_z = Z_u \frac{d\bar{u}_W}{dh} \qquad Z_\psi = -Z_u \bar{v}_{W_0} \qquad Z_{\int\theta} = -Z_u \frac{d\bar{u}_W}{dh}(u_{A_0} + \bar{u}_{W_0})$$

$$M_z = M_u \frac{d\bar{u}_W}{dh} \qquad M_\psi = -M_u \bar{v}_{W_0} \qquad M_{\int\theta} = -M_u \frac{d\bar{u}_W}{dh}(u_{A_0} + \bar{u}_{W_0})$$

$$Y_z = Y_v \frac{d\bar{v}_W}{dh} \qquad Y_\psi = Y_v \bar{u}_{W_0} \qquad Y_{\int\theta} = -Y_v \frac{d\bar{v}_W}{dh}(u_{A_0} + \bar{u}_{W_0})$$

$$L_z = L_v \frac{d\bar{v}_W}{dh} \qquad L_\psi = L_v \bar{u}_{W_0} \qquad L_{\int\theta} = -L_v \frac{d\bar{v}_W}{dh}(u_{A_0} + \bar{u}_{W_0})$$

$$N_z = N_v \frac{d\bar{v}_W}{dh} \qquad N_\psi = N_v \bar{u}_{W_0} \qquad N_{\int\theta} = -N_v \frac{d\bar{v}_W}{dh}(u_{A_0} + \bar{u}_{W_0})$$

$$X_\theta = -X_w \bar{u}_{W_0} \qquad X_\phi = X_w \bar{v}_{W_0}$$

$$Z_\theta = -Z_w \bar{u}_{W_0} \qquad Z_\phi = Z_w \bar{v}_{W_0}$$

$$M_\theta = -M_w \bar{u}_{W_0} \qquad M_\phi = M_w \bar{v}_{W_0}$$

$$\Delta M_{\dot{\theta}} = \text{[illegible]} \bar{u}_{W_0} \qquad M_{\dot{\phi}} = M_{\dot{w}} \bar{v}_{W_0}$$

Where

$$\frac{d\bar{u}_W}{dh} = \cos(\psi_0 - \psi_{W_0})\frac{d\bar{v}_W}{dh} + \sin(\psi_0 - \psi_{W_0})\bar{v}_{W_0}\frac{d\bar{\psi}_W}{dh}$$

$$\frac{d\bar{v}_W}{dh} = -\sin(\psi_0 - \psi_{W_0})\frac{d\bar{v}_W}{dh} + \cos(\psi_0 - \psi_{W_0})\bar{v}_{W_0}\frac{d\bar{\psi}_W}{dh}$$

$$\bar{u}_{W_0} = \cos(\psi_0 - \psi_{W_0})\bar{v}_{W_0} \qquad \bar{v}_{W_0} = -\sin(\psi_0 - \psi_{W_0})\bar{v}_{W_0}$$

FIGURE 4-4.–CHARACTERISTIC EQUATIONS, EFFECTS OF MEAN WIND

The effects of the mean wind shear and magnitude on stability will now be examined separately.

4.2.1.1.1 Effects of Mean Wind Magnitude–The longitudinal and lateral-directional equations may be uncoupled if it is assumed that the mean wind is in the direction of flight ($\psi_0 = \bar{\psi}_{W_0}$) and the heading and magnitude are zero. Now, the mean wind magnitude may be permitted to take on positive and negative values where a positive value corresponds to a tailwind and a negative value corresponds to a headwind. The effects of the mean wind magnitude on the characteristic roots can be examined by performing a root locus for mean wind magnitude. If it is assumed that the airspeed remains unchanged no matter what the mean wind speed, a realistic assumption, the aerodynamics remain unchanged. The inertial velocity appearing in the vertical and side acceleration equations may be rewritten as the sum of the initial airspeed plus the initial mean wind speed. The equations that result are shown on Figure 4-5.

When the determinants for characteristic longitudinal or lateral-directional motion are expanded, all terms containing the mean wind magnitude cancel out and the mean wind is seen not to affect characteristic motion (Fig. 4-5). The same result can be obtained no matter what the relative airplane and mean wind headings. In fact, the nonlinear equations of motion may be written completely in terms of airspeed components without the additional appearance of inertial velocity or wind velocity terms. This is to be expected as the motion in one axis system is the same as the motion in another moving at a constant linear velocity with respect to the first axis system.

So long as transfer functions are for parameters measured relative to the air mass, the zeros of the transfer functions will also be invariant with wind speed at constant airspeed. When transfer functions measure an earth-referenced parameter, invariance with mean wind speed is not necessarily true.

The numerators for the longitudinal inertial speed and pitch attitude to control transfer functions can be seen to be independent of wind speed. However, the airplane's inertial vertical velocity is affected.

The vertical velocity response by itself is usually of little importance. However, the altitude response is important and is affected by the vertical velocity response:

$$\frac{h}{\delta_c} = \frac{1}{S}\left[u_0 \frac{\theta}{\delta_c}(s) - \frac{w}{\delta_c}(s)\right] = \frac{N_h(s)}{S\Delta_{LONG}(s)}$$

For a tail aft aircraft, the zeros of the altitude to control transfer form a cubic made of three real roots (Reference 1):

$$N_h(s) = \left(s + \frac{1}{T_{h_1}}\right)\left(s + \frac{1}{T_{h_2}}\right)\left(s + \frac{1}{T_{h_3}}\right)$$

LONGITUDINAL

$$\begin{bmatrix} s - X_u & -X_w & g + X_{\dot{w}} \nabla_{W_0} \\ -Z_u & s - Z_w & -(u_{A_0} + \nabla_{W_0})s + Z_w \nabla_{W_0} \\ -M_u & -(M_{\dot{w}}s + M_w) & s^2 - (M_q - M_{\dot{w}} \nabla_{W_0})s + M_w \nabla_{W_0} \end{bmatrix} \begin{Bmatrix} u \\ w \\ \theta \end{Bmatrix} = 0$$

$$\Delta_{long}(s) \quad + \nabla_{W_0} F_{long}(s) = 0$$

$$F_{long}(s) = 0$$

$\Delta_{long}(s)$ = characteristic equation for still air

LATERAL-DIRECTIONAL

$$\begin{bmatrix} (s - Y_v) & -g & (u_A + \nabla_{W_0})s - Y_v \nabla_{W_0} \\ -L_v & s^2 - L_p s & -L_r s - L_v \nabla_{W_0} \\ -N_v & -N_p s & s^2 - N_r s - N_v \nabla_{W_0} \end{bmatrix} \begin{Bmatrix} v \\ \phi \\ \psi \end{Bmatrix} = 0$$

$$\Delta_{L\text{-}D}(s) + \nabla_{W_0} \; F_{L\text{-}D}(s) = 0$$

$$\text{or} \quad 1 + \nabla_{W_0} \frac{F_{L\text{-}D}(s)}{\Delta_{L\text{-}D}(s)} = 0$$

$$F_{L\text{-}D}(s) = 0$$

$\psi = \psi_W$ (wind in direction of flight)

$$\frac{d\psi_W}{dh} = \frac{d\nabla_W}{dh} = 0 \text{ (no mean wind shear)}$$

$\nabla_{W_0} > 0$, tailwind; $\nabla_{W_0} < 0$, headwind

Conclusion: Mean wind magnitude does not affect characteristic motion

FIGURE 4-5.—EFFECT OF MEAN WIND MAGNITUDE, NO CROSSWIND

Two of the zeros will be approximately equal in magnitude and opposite in sign. The third zero will be much smaller than the other two, and, in still air, will be negative for frontside of the thrust required curve operation ($\partial T_{REQ}/\partial V_A > 0$) and positive for backside of thrust required curve operation ($\partial T_{REQ}/\partial V_A < 0$), as shown in Reference 4-2.

The altitude to control transfer function zero that receives the most attention is $1/T_{h_1}$, the low frequency zero. The significance of this zero may qualitatively be explained in the following. A pilot normally controls altitude through pitch attitude. When he controls pitch attitude, stable, low frequency, closed loop roots exist. When altitude is controlled through attitude, these roots will tend to become less stable until, when the pilot attempts sufficiently tight control, the new closed loop roots become unstable.

The level of tightness of control, or pilot altitude to attitude gain, at which instability occurs is dependent upon the location of $1/T_{h_1}$, with more unstable values providing a greater tendency toward instability. This does not mean, however, that if, after closing on altitude, the roots are unstable the aircraft will be uncontrollable, for the pilot can restablize these roots with throttle activity. However, the more unstable $1/T_{h_1}$ the more throttle activity is required, the more pilot attention is required, and the closer one is to approaching the physical limitations of the pilot.

Much more rigorous and comprehensive descriptions are provided in several publications by Systems Technology, Inc., such as References 4-3 and 4-4. A parallel between the pilot and the autoland system can be drawn. The location of $1/T_{h_1}$ has a strong impact on the design of the attitude, altitude, and airspeed control systems.

To return to the analysis, the effect of mean wind speed on the numerator of the altitude to control transfer function is derived from the equations on Figure 4-6. The numerator is seen to be expressible approximately as

$$N_h = N_{h_0} - \bar{V}_{W_0} \left[(Z_{\delta_c} M_{\dot{w}} + M_{\delta_c}) s^2 + Z_{\delta_c} M_{\dot{w}} s \right.$$

$$\left. + Z_{\delta_c} (X_w M'_u - X_u M_{\dot{w}}) \right]$$

where N_{h_0} represents the altitude transfer function zeros in still air. Using the approximate expression for N_{h_0} and the approximate cubic rooting employed in Reference 4-1, the zero $1/T_{h_1}$ may be expressed as

$$\frac{1}{T_{h_1}} = \frac{1}{T_{h_0}} + \frac{g M'_u}{M'_\alpha} \left[\frac{\bar{V}_{W_0}/u_{A_0}}{1 - \bar{V}_{W_0}/u_{A_0}} \right]$$

$$\frac{h}{\delta_c}(s) = \frac{1}{s}\left[u_0 \frac{\theta}{\delta_c}(s) - \frac{w}{\delta_c}(s)\right] = \frac{N_h(s)}{s\Delta_{long}(s)}$$

$$N_h(s) = u_0 N_\theta(s) - N_w(s)$$

$$N_\theta(s) \neq f(\bar{V}_{W_0})$$

$$N_w(s) = \begin{vmatrix} -X_u & X_{\delta_c} & g + X_w \bar{V}_{W_0} \\ -Z_u & Z_{\delta_c} & -(u_{A_0} + \bar{V}_{W_0})s + Z_w \bar{V}_{W_0} \\ -M_u & M_{\delta_c} & s^2 - (M_q - M_w \bar{V}_{W_0})s + M_w \bar{V}_{W_0} \end{vmatrix}$$

$$= N_{w_0} + \bar{V}_{W_0} F(s)$$

$$N_{w_0} = N_w \text{ at } \bar{V}_{W_0} = 0$$

$$F(s) = \left[M_{\delta_c} + M_{\dot{w}} Z_{\delta_c}\right]s^2 + \left[X_{\delta_c}(M_u + M_{\dot{w}} Z_u) + Z_{\delta_c}(M_w - X_u M_{\dot{w}}) + M_{\delta_c}(X_u + Z_w)\right]s$$

$$+ \left[X_{\delta_c}(Z_u M_w - Z_w M_u) + Z_{\delta_c}(X_w M_u - X_u M_w) + M_{\delta_c}(X_u Z_w - X_w Z_u)\right]$$

Assume X_{δ_c} negligible and let $M'_\xi = M_\xi - \frac{M_{\delta_c}}{Z_{\delta_c}} Z_\xi$

$$F(s) \cong (Z_{\delta_c} M_{\dot{w}} + M_{\delta_c})s^2 + Z_{\delta_c} M'_w s + Z_{\delta_c}(X_w M'_u - X_u M'_w)$$

$$N_h(s) = N_{h_0}(s) - \bar{V}_{W_0} F(s)$$

$$N_{h_0} = N_h \text{ at } \bar{V}_{W_0} = 0$$

FIGURE 4-6.–EFFECT OF MEAN WIND MAGNITUDE ON ALTITUDE TRANSFER FUNCTION ZEROS–NO CROSSWIND

The relevant parameter is the ratio of mean wind speed to airspeed. A tailwind will tend to destabilize the zero and a headwind will tend to stabilize it. However, the term $gM'_u/M\alpha$ may be approximated as

$$\frac{gM'_u}{M'_\alpha} \cong \frac{2gC_{L_0}}{u_{A_0} C_{L_\alpha}}$$

This term is quite small, except for STOL aircraft, and is on the order of 0.1 for conventional aircraft during landing approach. Hence, it may be concluded that the effect of the mean wind speed on altitude control is negligible for conventional aircraft and possibly moderate for STOL aircraft.

This apparent change of the point of operation on the thrust required curve is quite real and can perhaps be explained better physically with the aid of Figure 4-7. As the flight path with respect to the air mass ($\theta - \alpha$) is decreased, the speed at which the change of thrust required with respect to airspeed is zero shifts to lower speed. More generally, as ($\theta - \alpha$) is decreased, the change of thrust required with respect to airspeed at a given airspeed increases. The relationship between the flight path with respect to the earth and $\theta - \alpha$ for small angles is

$$\theta - \alpha = \left[1 + \frac{\bar{V}_W}{V_A} \cos(\psi - \bar{\psi}_W)\right] \gamma$$

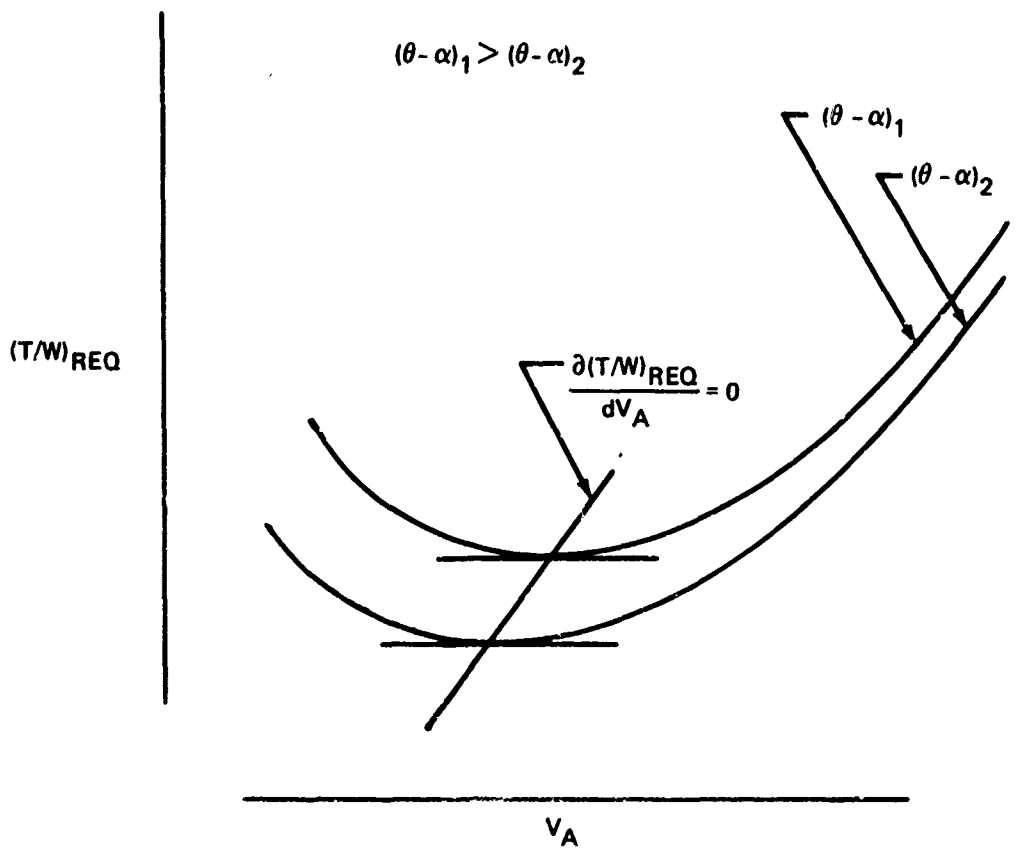

FIGURE 4-7.–CHANGE OF $\partial(T/W)_{REQ}/\partial V_A$ WITH FLIGHT PATH

This relationship is derived in Appendix 4A and is plotted on Figure 4-8. If the same negative glideslope with respect to the earth is maintained, such as for tracking a glideslope beam, an increasing tailwind decreases the glideslope (more negative) with respect to the air and shifts operation to a lower thrust required curve, having a more positive slope at the same airspeed. The increase in $\partial(T_{REQ}/W)/\partial V_A$ corresponds to the increase of $1/T_{h_1}$ for the same tailwind increase.

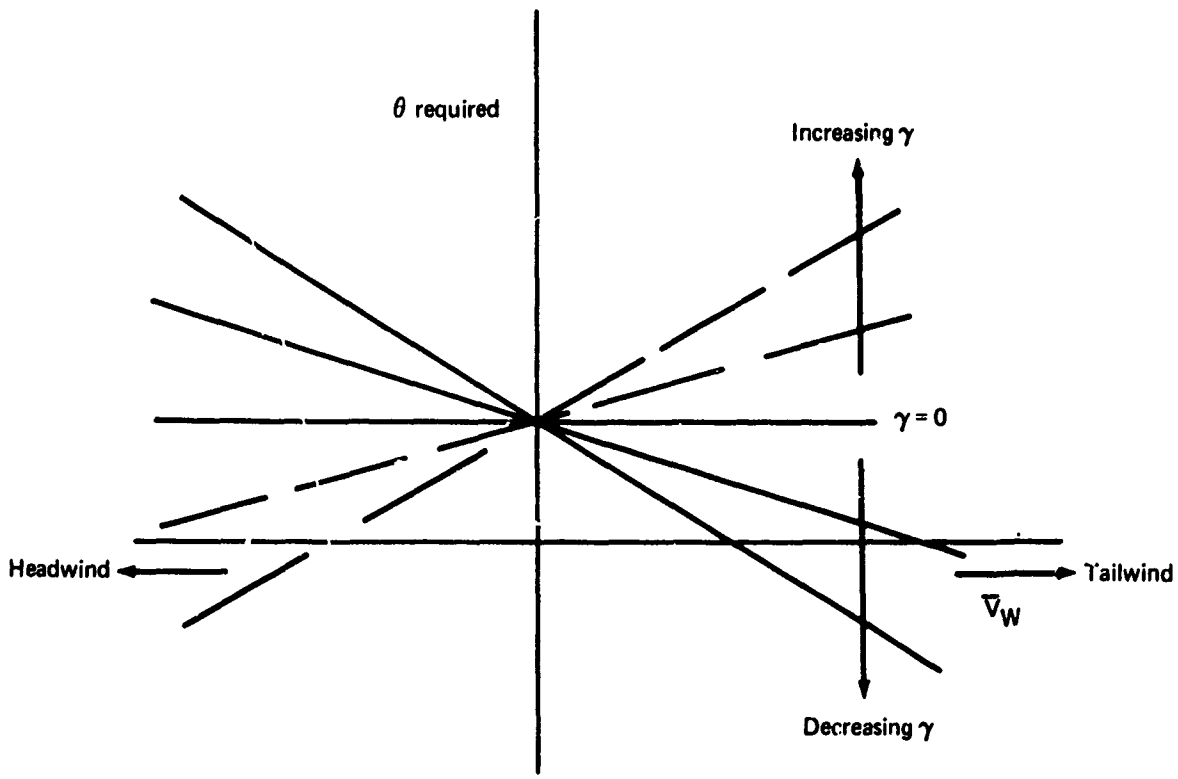

FIGURE 4-8.–PITCH ATTITUDE REQUIRED TO HOLD A GLIDESLOPE

4.2.1.1.2 Effects of Mean Wind Shear–The small perturbation body axis components of the mean wind shear are given by

$$\frac{d\bar{u}_W}{dh} = \cos\left(\psi_0 - \bar{\psi}_{W_0}\right)\frac{d\bar{V}_W}{dh} + \sin\left(\psi_0 - \bar{\psi}_{W_0}\right)\bar{V}_{W_0}\frac{d\bar{\psi}_W}{dh}$$

$$\frac{d\bar{v}_W}{dh} = -\sin\left(\psi_0 - \bar{\psi}_{W_0}\right)\frac{d\bar{V}_W}{dh} + \cos\left(\psi_0 - \bar{\psi}_{W_0}\right)\bar{V}_{W_0}\frac{d\bar{\psi}_W}{dh}$$

The shear components are made up of contributions from the variation of mean wind magnitude with altitude and the variation of mean wind heading with altitude. The latter effect will cause a component of shear even if the mean wind magnitude is invariant with altitude. Nothing can be said about the relative contribution of the two sources of shear without specifying wind heading relative to airplane heading. However, if the heading shear effect dominates, the absolute magnitudes of the shear components are likely to be small.

The mean wind shear introduces effective aerodynamic derivatives proportional to vertical displacement and the integral of pitch attitude. In general, all six degrees of freedom will be coupled in the presence of a shear, even though the longitudinal and lateral-directional degrees of freedom are uncoupled in still air.

Longitudinal motion is uncoupled from lateral-directional motion by assuming a wind heading relative to airplane heading that causes the lateral component of shear to be zero. For reasonable values of the heading shear, this will mean the wind heading is nearly aligned to the flight path. Positive values of the longitudinal shear component now correspond to an increase in tailwind or a decrease of headwind with increasing altitude. The effects of the longitudinal shear will be considered in the absence of a mean wind magnitude. Thus, the condition considered is near the transition from a tailwind to a headwind or from a headwind to a tailwind for changes of altitude. The separate effects of mean wind magnitude and shear can then be considered to be approximately additive.

The longitudinal equations and characteristic equation for the assumptions made are provided on Figure 4-9. Similar to that done for the mean wind magnitude, the characteristic equation can be expressed in terms of the characteristic equation for still air plus a term proportional to the longitudinal component of shear.

The first observation that can be made is that the shear introduces a new, fifth longitudinal root. Unless the aircraft is capable of high L/D at very low speeds (such as for STOL aircraft),

$$X_u Z_\alpha - X_\alpha Z_u < 0$$

and the stability of the new root is governed by the product of the change in pitch acceleration with speed and the longitudinal wind shear. If the airplane is dynamically stable in still air, then, for small components of wind shear,

$$\frac{d\bar{u}_W}{dh} M_u < 0 \quad , \text{ stable fifth root}$$

$$\frac{d\bar{u}_W}{dh} M_u > 0 \quad , \text{ unstable fifth root}$$

For STOL aircraft, where

$$X_u Z_\alpha - X_\alpha Z_u > 0$$

the reverse it true.

At low Mach numbers, the rigid aerodynamic contribution to M_u is generally negligible. The primary effects are from the moment arm of the center of gravity to the engines, the variation of thrust with speed, and aeroelastic effects. The moment arm effect will cause non-zero M_u without thrust changes with speed at constant throttle setting. For engines mounted below the center of gravity, the moment arm effect by itself is positive. If, additionally, thrust decreases with increasing speed, as for high bypass ratio engines, there will be a second negative increment. Positive M_u is considered to be statically stabilizing, since when an airplane speeds up, it will pitch up and cause the airplane to slow down due to the gravity component. At very low speeds, the propulsion effect usually dominates. For

THREE DEGREES OF FREEDOM

$$\begin{vmatrix} s - X_u & -X_w s - X_u \frac{d\bar{u}_w}{dh} & gs + X_u u_0 \frac{d\bar{u}_w}{dh} \\ -Z_u & s^2 - Z_w s - Z_u \frac{d\bar{u}_w}{dh} & -u_0 s^2 + Z_u u_0 \frac{d\bar{u}_w}{dh} \\ -M_u & -M_{\dot{w}} s^2 - M_w s - M_u \frac{d\bar{u}_w}{dh} & s^2 - M_q s^2 + M_u u_0 \frac{d\bar{u}_w}{dh} \end{vmatrix} = 0$$

$$s\Delta_{long_0}(s) + \frac{d\bar{u}_w}{dh} F(s) = 0$$

$$F(s) = -Z_u \left[s^3 - (M_{\dot{\alpha}} + M_q)s^2 + (-M_\alpha + \frac{M_u}{Z_u} Z_{\dot{\alpha}})s + M_u(X_\alpha - \frac{X_u Z_\alpha}{Z_u}) \right]$$

SHORT PERIOD APPROXIMATION

$$\begin{vmatrix} s^2 - Z_w s - Z_u \frac{d\bar{u}_w}{dh} & -u_0 s^2 + Z_u u_0 \frac{d\bar{u}_0}{dh} \\ -M_{\dot{w}} s^2 - M_w s - M_u \frac{d\bar{u}_w}{dh} & s^3 - M_q s^2 + M_u u_0 \frac{d\bar{u}_w}{dh} \end{vmatrix} = 0$$

$$s^2\Delta_{SP}(s) + \frac{d\bar{u}_w}{dh} F(s) = 0$$

$$F(s) = -Z_u \left[s^2 - (M_q + M_{\dot{\alpha}})s + (Z_\alpha \frac{M_u}{Z_u} - M_\alpha) \right]$$

PHUGOID APPROXIMATION

$$\begin{vmatrix} s - X_u & gs + X_u u_0 \frac{d\bar{u}_w}{dh} \\ -Z_u & -u_0 s^2 + Z_u u_0 \frac{d\bar{u}_w}{dh} \end{vmatrix} = 0$$

$$s^2 - X_u s - \left[\frac{g}{u_0} + \frac{d\bar{u}_w}{dh} \right] Z_u = 0$$

$$Z_u \cong \frac{-2g}{u_0}$$

$$X_u \cong \frac{-2g}{u_0} \frac{C_{D_0}}{C_{L_0}}$$

$$s^2 + \frac{2g}{u_0} \frac{C_D}{C_L} s^2 + 2\left(\frac{g}{u_0}\right)^2 \left[1 + \frac{u_0}{g} \frac{d\bar{u}_w}{dh} \right] = 0$$

FIGURE 4-9.—EFFECT OF WIND SHEAR, NO CROSSWIND

STOL aircraft employing propulsive lift concepts, strong propulsion-system-induced aerodynamic effects may occur. For aircraft without irreversible controls, additional effects are introduced by hinge movements and mass balancing. Aircraft with propellers have stabilizing effects due to propeller wash. Due to the difficulty in determining the sign of M_u, many authors assume that it is zero, but rarely is this the case. If M_u should happen to be zero, the fifth root appears at the origin.

More general information, involving fewer restrictions, can be obtained through root locus analysis. That part of the characteristic equation proportional to the wind shear component represents the root locus zeros for variations of the wind shear component. Some information on the nature of these zeros can be obtained from a short period approximation to the equations. When the speed degree of freedom and the longitudinal acceleration equation are dropped for the short period approximation, the characteristic equation is expanded as shown on Figure 4-9. For the wind shear root locus there are two zeros, given by:

$$s_{2,3} = \frac{M_q + M_{\dot{\alpha}}}{2}\left[1 \pm \sqrt{1 - \frac{4\left(Z_\alpha \frac{M_u}{Z_u} - M_\alpha\right)}{\left(M_q + M_{\dot{\alpha}}\right)^2}}\right]$$

Some parameters inside the radical may be rewritten in terms of the airplane's still air characteristics:

$$Z_\alpha \frac{M_u}{Z_u} - M_\alpha = -\frac{u_0 \omega_{sp_0}^2 \omega_{ph_0}^2}{g Z_u}$$

$$\cong \frac{u_0^2 \omega_{sp_0}^2 \omega_{ph_0}^2}{2g^2}$$

Thus, the short period zeros are given by

$$s_{2,3} = \frac{M_q + M_{\dot{\alpha}}}{2}\left[1 \pm \sqrt{1 - \frac{4 u_0^2 \omega_{sp_0}^2 \omega_{ph_0}^2}{g^2 (M_q + M_{\dot{\alpha}})^2}}\right]$$

The quantity $\omega_{sp_0}^2/(M_q + M_{\dot{\alpha}})^2$ is greater than one. A crude approximation to the phugoid natural frequency is given by

$$\omega_{ph_0} \cong \sqrt{\frac{-gZ_u}{u_0}} = \sqrt{2}\frac{g}{u_0}$$

for small M_u and sufficient static stability. Hence, the quantity inside the radical is approximated by

$$1 - \frac{4\omega_{sp_0}^2}{(M_q + M_\alpha)^2}$$

which will be negative for aircraft with stable maneuver margins. The short period zeros for the wind shear root locus are complex with stable real parts. The root locus is shown on Figure 4-10. An increasing tailwind (or decreasing headwind) with altitude will cause an unstable real root. An increasing headwind with altitude will cause a lowly damped oscillatory pair having a positive damping ratio provided

$$\zeta_{sp_0}\omega_{sp_0} - \frac{gC_{L_\alpha}}{C_{L_0}} > 0$$

The short period approximation generally predicts the behavior of the root locus away from the origin. To determine the root locus near the origin. and thus the effects of wi' shear on the phugoid, three-degree-of-freedom analysis must be used. It may be noticed Figure 4-9 that the coefficients for the polynomial representing the short period zeros are the same as the first three coefficients for the coefficient representing the three-degree-of-freedom zeros. This indicates that the third zero is much smaller than the short period zeros and that the short period expression for the high frequency zeros is accurate for the three degree-of-freedom case. The location of the third zero may be approximated by:

$$s_1 \cong -\frac{M_u\left(X_\alpha - X_u\frac{Z_\alpha}{Z_u}\right)}{-M_\alpha + M_u\frac{Z_\alpha}{Z_u}}$$

$$= \frac{gM_u(X_\alpha Z_u - X_u Z_\alpha)}{u_0\omega_{sp_0}^2\omega_{ph_0}^2}$$

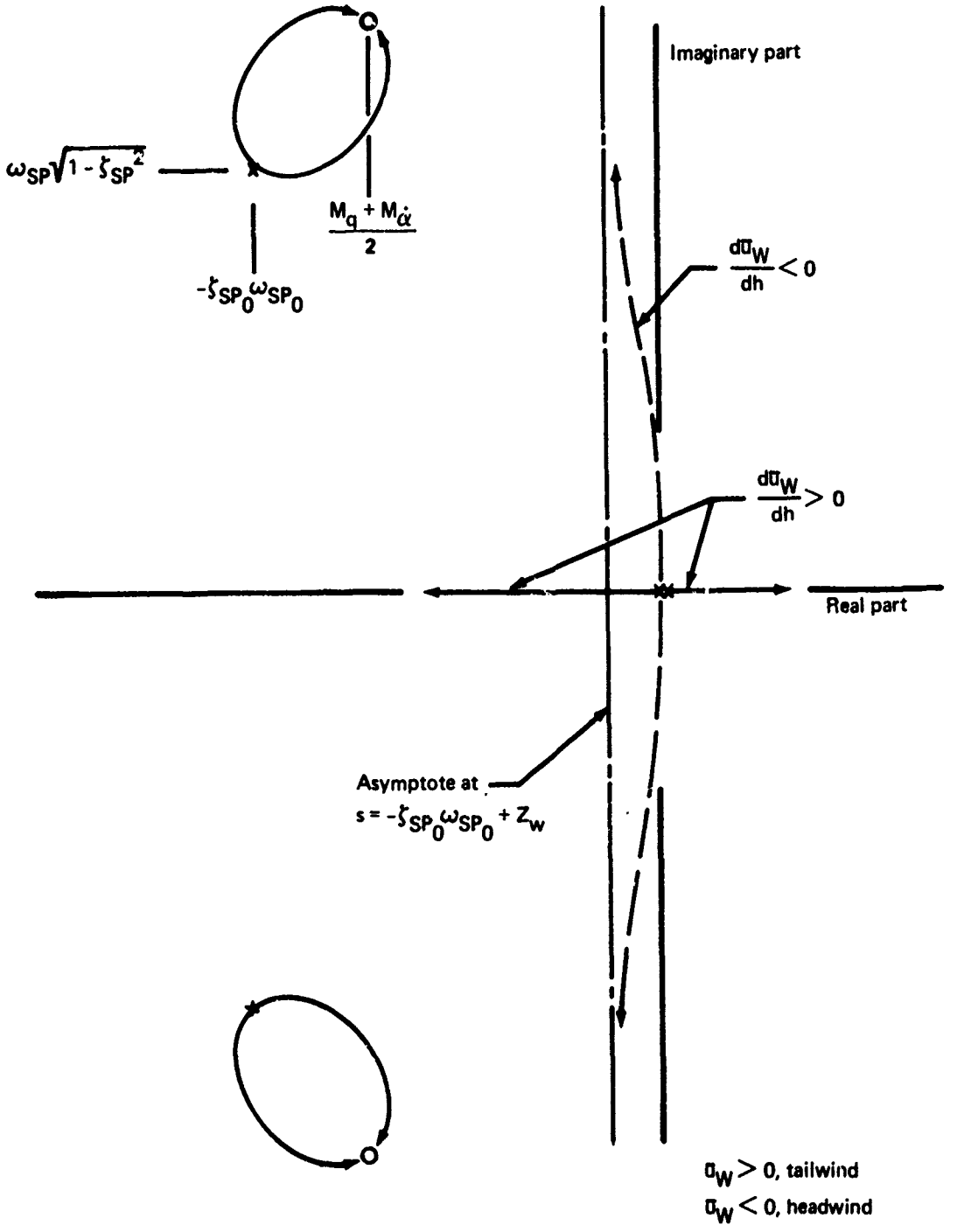

FIGURE 4-10.–WIND SHEAR ROOT LOCUS, SHORT PERIOD APPROXIMATION, NO CROSSWIND

There are many possible relative locations of the phugoid roots and the low frequency zero. The wind shear root loci for some of these combinations are shown on Figure 4-11. Some conclusions that can be drawn from Figure 4-11 are:

- The primary effect of the wind shear on the phugoid roots is to alter the phugoid frequency.

- The effect of the wind shear depends on whether the zero is in a stable or unstable location. For a stable location, increasing $d\bar{u}_W/dh$ (from zero) increases phugoid natural frequency and stabilizes the fifth root and decreasing $d\bar{u}_W/dh$ reduces phugoid natural frequency and destabilizes the fifth root. An unstable zero location reverses the effect.

- Unstable oscillatory roots may form from the joining of one phugoid root and the fifth root.

- The stability of the phugoid roots for high $\left|d\bar{u}_W/dh\right|$ when phugoid natural frequency is increased is determined by whether the asymptote is in a stable or unstable location. The location of the asymptote is given by:

$$s \cong \left|M_q + M_{\dot{\alpha}}\right| + \frac{1}{2}\left[\sum(\text{phugoid roots}) - M_u\left(X_\alpha - X_u\frac{Z_\alpha}{Z_u}\right)\right]$$

  The first term, a measure of the relative locations of the short period roots and zeros, will generally dominate.

For all conditions, an unstable root or roots due to a wind shear is possible. However, there are stability parameters which will maximize the airplane's tolerance to shears:

- Stable still air phugoid roots and

$$\frac{gM_u\left(X_\alpha Z_u - X_u Z_\alpha\right)}{u_0\omega_{sp_0}^2\omega_{ph_0}^2}$$

  positive and small (unstable zero). This minimizes the instability due to negative $d\bar{u}_W/dh$ and maximizes the gain margin for positive $d\bar{u}_W/dh$.

- Large $(M_{\dot{\alpha}} + M_q)$--This assures a stable location for the $\pm 90°$ asymptote.

The sensitivity of the root locations to wind shear has been assessed in Reference 4-5 by employing the phugoid approximation. The angle of attack is assumed to be unaffected by the phugoid and changes of pitching moment are assumed to be negligible. After dropping the vertical velocity degree of freedom and the pitch acceleration equation, the equations reduce to those shown on Figure 4-9. The resulting characteristic equation for phugoid

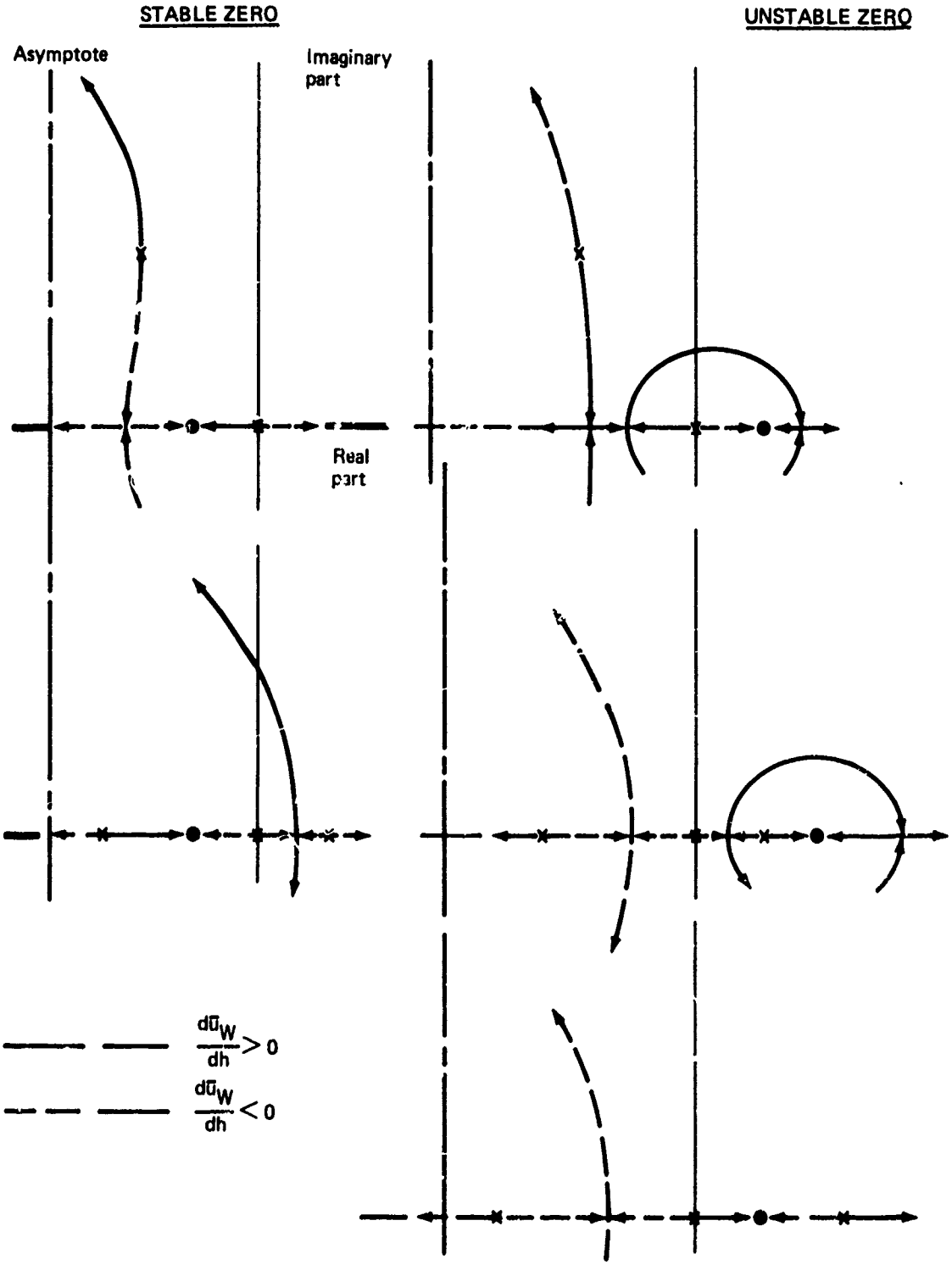

FIGURE 4-11.—WIND SHEAR ROOT LOCUS, LOW FREQUENCY BEHAVIOR, NO CROSSWIND

motion on Figure 4-9 is identical to that derived in Reference 4-5. The phugoid damping ($-\zeta_{ph}\ \omega_{ph}$) is seen to be unaffected by the shear. The phugoid natural frequency can be expressed as

$$\omega_{ph}^2 = \omega_{ph_0}^2 + \frac{2g}{u_0}\frac{d\bar{u}_W}{dh}$$

where $\omega_{ph_0}^2$ is the phugoid natural frequency in still air. The change in the square of the phugoid natural frequency with wind shear is seen to be independent of the aircraft configuration (except when strong aerodynamic contributions to Z_u and X_u exist, such as for powered lift STOL aircraft) and is most sensitive at the lowest speeds. For example, for a still air phugoid natural frequency of 0.1 and an approach speed 120 knots, an increasing headwind with increasing altitude of 18.7 kt/100 ft is predicted to drive one phugoid root unstable. The phugoid root loci for this simplified analysis are shown on Figure 4-12.

A decreasing tailwind (or increasing headwind) with increasing altitude is seen to always tend to cause an unstable or more unstable real root, and the fifth root from the three-degree-of-freedom analysis is missing.

The phugoid approximation leads to a root locus at low frequencies similar to that which would be obtained by the three-degree-of-freedom analysis with $M_u = 0$ (which is an assumption of the phugoid approximation) except that the location of the asymptote for oscillatory phugoid roots is determined by the still air phugoid roots using the phugoid approximation rather than by the short period poles and zeros for the three-degree-of-freedom analysis. The three-degree-of-freedom analysis predicts that the effects of increasing headwind and tailwind with altitude are reversed with the low frequency zero in an unstable position. Additionally, the location of the low frequency zero relative to the still air phugoid roots affects the sensitivity of root locations to a wind shear. In general, the movement of the roots will be less sensitive to wind shears than is predicted by the phugoid approximation.

An analysis on the effects of wind shears has also been conducted in Reference 4-6, using a substantially different set of equations. There, it is implied that wind shears have no effect on the short period for level flight. However, the equations in Reference 4-6 do not provide for the existence of the z or vertical translation derivatives provided on Figure 4-4, and the existence of which is acknowledged in Reference 4-7. The root locus for wind shear is the same as that for the phugoid approximation on Figure 4-11 even though M_u is not assumed to be zero.

For the case where the longitudinal component of shear is zero but the lateral component is non-zero, longitudinal motion will be unaffected by the shear, but lateral-directional motion, from Figure 4-4, appears to be dependent upon both the shear and longitudinal motion. However, when the determinant of the characteristic equations is expanded, all terms containing the lateral component of shear cancel, leaving lateral-directional characteristic motion invariant with shears. The same conclusion can be reached for any heading of the mean wind for the assumptions specified (particular dependence is on the assumption of wings initially level).

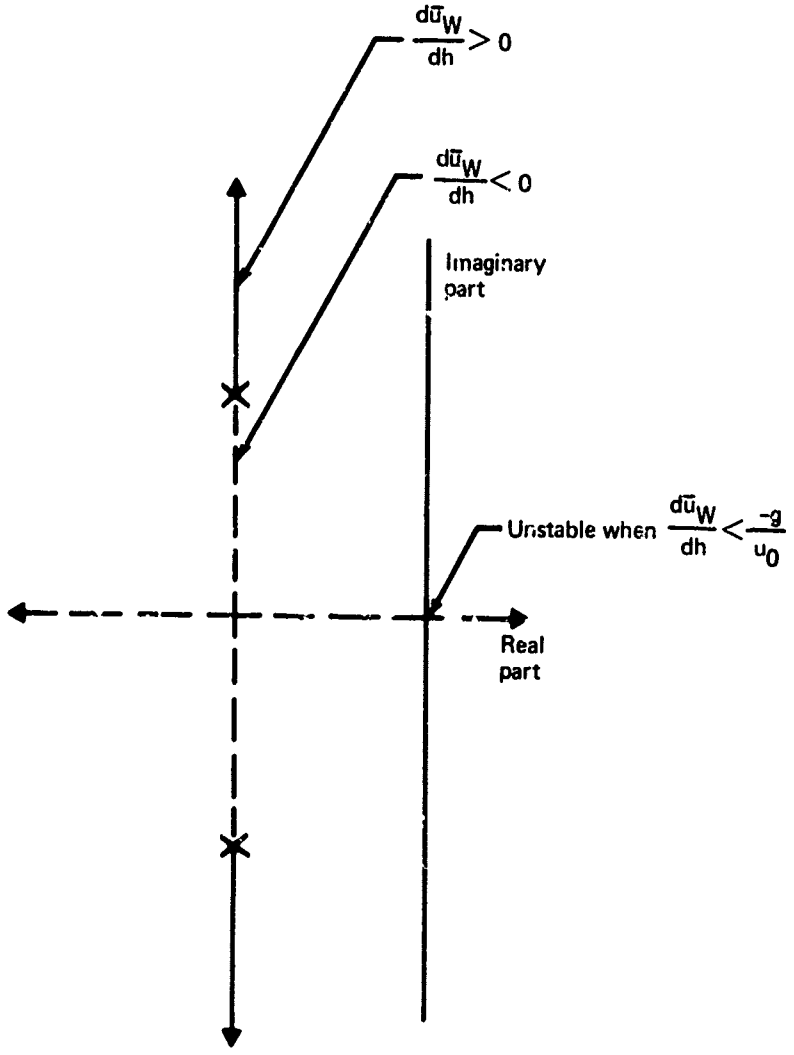

Assumes: Constant angle of attack
No pitch acceleration

$$s^2 + \frac{2g}{u_0}\frac{C_D}{C_L}s + 2\left(\frac{g}{u_0}\right)^2\left[1 + \frac{u_0}{g}\frac{d\bar{u}_W}{dh}\right] = 0$$

FIGURE 4-12.–WIND SHEAR ROOT LOCUS, PHUGOID APPROXIMATION, NO CROSSWIND

The longitudinal component of wind shear also alters the numerators of the longitudinal responses to control input transfer functions. If the control input is considered to be column (or elevator), the speed transfer function has a free s in the numerator as before, but the attitude and vertical velocity numerators are altered.

As shown on Figure 4-13, a positive shear decreases the high frequency zero ($1/T_{\theta_2}$), commonly called "L_α," and is actually approximated by the change of lift with vertical velocity (L_w), but increases the low frequency zero. The former effect is the same as a reduction of the lift curve slope. The high frequency zero governs the amplitude of the pitch attitude response at frequencies near the short period, and too low a value can give the appearance of the airplane being excessively sensitive. The high frequency zero is also the inverse of the flight path to pitch attitude lag time constant, and low values can cause difficult altitude control. However, the change in the θ/γ lag is due solely to the quickening of the attitude response for, as shown on Figure 4-13, the altitude response to control input is unaffected by the longitudinal component of shear.

The low frequency zero influences the ability of the pilot to stabilize the phugoid using pitch attitude feedback. Negative shears can cause closed loop phugoid instability.

Altering the high frequency zero also has the effect of changing the short period attitude to column gain. A positive shear component will provide an apparent increase in stick force per g. Pilots will prefer a higher optimum stick force per g in negative shears (increasing headwind with increasing altitude) than for still air.

The longitudinal component of shear does not affect lateral-directional motion. When the wind heading is such that the longitudinal component is zero and the lateral component is non-zero, the equations, developed from those on Figure 4-4, appear to have lateral-directional motion affected by longitudinal motion (through the z and $f\theta$ derivatives proportional to the lateral component of the shear). However, when the determinants for the characteristic motion and the numerators of the control transfer functions are expanded, all terms containing the shear cancel and lateral-directional motion is left unaffected.

4.2.1.2 Effects of Mean Wind, Distributed Lift

If an airplane is at a non-zero bank angle in the presence of a wind shear, the airspeed on one wing will be greater than that on the other. If the airplane is at a pitch attitude, the airspeeds at the wing and tail will be different. These distributed lift effects introduce forces and moments proportional to the wind shear.

Reference 4-7 has classified the distributed lift effects of a mean wind shear according to those which produce a change in the conventional stability derivatives and those which introduce new effective aerodynamic derivatives. In the former classification fall corrections to the angle of attack, sideslip, and control power derivatives caused primarily by a dynamic pressure at the tail different from that at the center of gravity.

PITCH ATTITUDE

$$\frac{\theta}{\delta_c}(s) = \frac{N_\theta}{\Delta_{LONG}}$$

$$N_\theta = \begin{vmatrix} s - X_u & -X_w - \frac{X_u}{s}\frac{d\bar{u}_W}{dh} & X_{\delta_c} \\ -Z_u & s - Z_w - \frac{Z_u}{s}\frac{d\bar{u}_W}{dh} & Z_{\delta_c} \\ -M_u & -M_{\dot{w}}s - M_w - \frac{M_u}{s}\frac{d\bar{u}_W}{dh} & M_{\delta_c} \end{vmatrix}$$

$$N_\theta = N_{\theta_0} + \frac{d\bar{u}_W}{dh}(M_u Z_{\delta_c} - Z_u M_{\delta_c})$$

$$= N_{\theta_0} + \frac{d\bar{u}_W}{dh} Z_{\delta_c} - Z_{\delta_c} M'_u$$

$$N_{\theta_0} = N_\theta \Big|_{\frac{d\bar{u}_W}{dh} = 0}$$

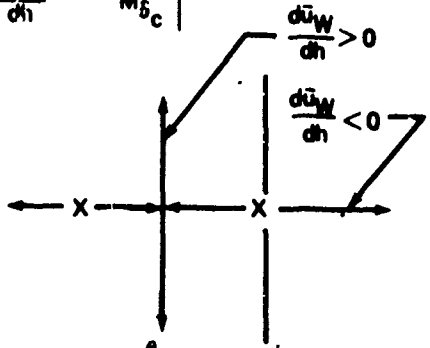

Locus of $\frac{\theta}{\delta_c}(s)$ zeros for changes of longitudinal shear component

VERTICAL VELOCITY

$$\frac{w}{\delta_c}(s) = \frac{N_w}{\Delta_{LONG}}(s)$$

$$N_w = \begin{vmatrix} s - X_u & X_{\delta_c} & g + \frac{X_u u_0}{s}\frac{d\bar{u}_W}{dh} \\ -Z_u & Z_{\delta_c} & -u_0 s + \frac{Z_u u_0}{s}\frac{d\bar{u}_W}{dh} \\ -M_u & M_{\delta_c} & s^2 - Mq s + \frac{M_u u_0}{s}\frac{d\bar{u}_W}{dh} \end{vmatrix}$$

$$N_w = N_{w_0} + u_0 \frac{d\bar{u}_W}{dh}(Z_{\delta_c} M_u - Z_u M_{\delta_c}) = N_{w_0} + \frac{d\bar{u}_W}{dh} u_0 Z_{\delta_c} M'_u$$

$$N_{w_0} = N_w \Big|_{\frac{d\bar{u}_W}{dh} = 0}$$

ALTITUDE

$$\frac{h}{\delta_c} = \frac{N_h}{s\Delta_{LONG}}$$

$$N_h = N_w + u_0 N_\theta = -N_{w_0} + u_0 N_{\theta_0} = N_{h_0}$$

Shear does not affect N_h

FIGURE 4-13.—EFFECT OF LONGITUDINAL COMPONENT OF SHEAR ON CONTROL TRANSFER FUNCTIONS

New derivatives introduced are such as rolling and yawing moment derivatives with respect to bank angle proportional to the shear, and the wing contributions to derivatives with respect to yaw rate (L_r and N_r). Thus, the new terms are equivalent to introducing angular components of wind, as shown on Figure 4-14. When the change of the shear with respect to altitude is small compared to the dimensions of the aircraft, the distribution of the wind across the airplane is well approximated by a linear distribution with a slope computed at the center of gravity. The effect is the same as the airplane rolling in the opposite direction in a uniform wind field. That is,

$$L_p \bar{p}_W \cong (L_p)_{WING} \left(- \frac{\partial \bar{w}_W}{\partial y} \right)$$

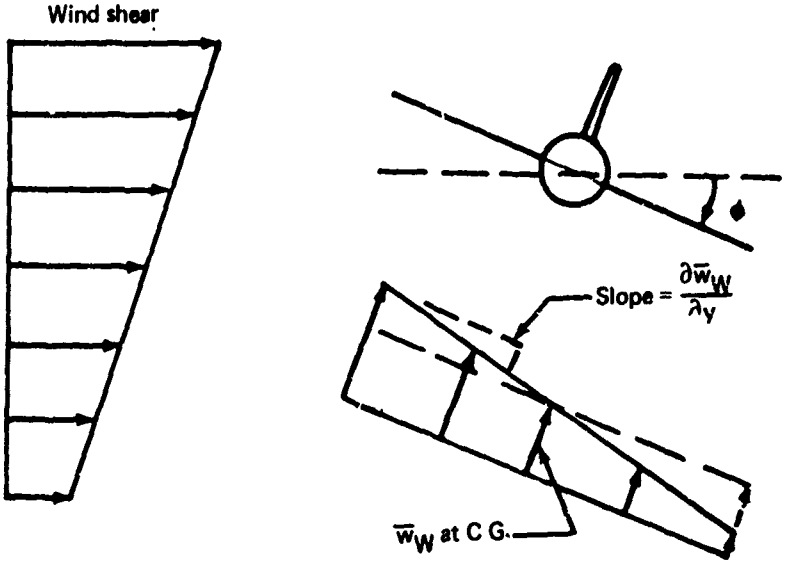

Wind velocity at left wing tip=

$$\bar{w}_{W_{CG}} - \frac{\partial \bar{w}_W}{\partial y} \frac{b}{2} = \bar{w}_{W_{CG}} - \frac{\partial \bar{w}_W}{\partial h} \frac{\partial h}{\partial y} \frac{b}{2} \cong \bar{w}_{W_{CG}} + \frac{\partial \bar{w}_W}{\partial h} \frac{b}{2} \sin \phi$$

Wind velocity at right wing tip =

$$\bar{w}_{W_{CG}} + \frac{\partial \bar{w}_W}{\partial y} \frac{b}{2} = \bar{w}_{W_{CG}} + \frac{\partial \bar{w}_W}{\partial h} \frac{\partial h}{\partial y} \frac{b}{2} \cong \bar{w}_{W_{CG}} - \frac{\partial \bar{w}_W}{\partial h} \frac{b}{2} \sin \phi$$

FIGURE 4-14.—WIND SHEAR DISTRIBUTION ACROSS AN AIRPLANE WING

There will also be a contribution to $L_p\bar{p}_W$ from a vertical distribution of the lateral component of wind over the vertical tail. Thus, the more complete expression is

$$L_p\bar{p}_W = (L_p)_{WING}\left(-\frac{\partial \bar{w}_W}{\partial y}\right) + (L_p)_{VERTICAL}\left(\frac{\partial \bar{v}_W}{\partial z}\right)$$

In general, all three components of angular velocity will be generated from the body axis gradient of wind velocity. The components of the gradient can be expressed by

$$\frac{\partial \bar{\lambda}_W}{\partial \xi} = \frac{\partial \bar{\lambda}_W}{\partial h}\frac{\partial h}{\partial \xi} \quad , \quad \begin{array}{l}\lambda = u, v, w \\ \xi = x, y, z \text{ (body axis)}\end{array}$$

The derivatives of the body axis wind components are developed from the mean wind axis to body axis transformation, and are shown on Figure 4-15. The change of altitude from the center of gravity to any point on the airplane is expressed using the body axis dimensions and the body axis to earth axis transformation.

For linear analysis of stability, the perturbations of the effective angular wind components, or the perturbations of the body axis gradient of wind, are of interest. These are shown on Figure 4-15. For the initial conditions of wings level and level flight ($\theta_0 = 0$ for the stability axis system), the non-zero terms can be expressed in terms of the longitudinal and lateral components of shear and the perturbations of pitch attitude, heading, and bank angle. When these terms are combined to form the effective wind angular velocity perturbances, only the effective yaw and roll rates are non-zero. In general, for arbitrary airplane attitudes, all the terms in the wind angular velocities will be non-zero, but the other terms will be negligibly small.

The perturbation yawing and rolling moments due to wind yaw and roll rates may be written as:

$$\begin{aligned} N_r\bar{r}_W &= N_{r_V}\left(-\frac{\partial \bar{v}_W}{\partial x}\right) + N_{r_W}\left(\frac{\partial \bar{u}_W}{\partial y}\right) \\ &= -N_{r_V}\frac{d\bar{v}_W}{dh}\theta - N_{r_W}\frac{d\bar{u}_W}{dh}\phi \\ &= -N_\theta\theta - N_\phi\phi \end{aligned}$$

$$\begin{aligned} L_r\bar{r}_W &= L_{r_V}\left(-\frac{\partial \bar{v}_W}{\partial x}\right) + L_{r_W}\left(\frac{\partial \bar{u}_W}{\partial y}\right) \\ &= -L_{r_V}\frac{d\bar{v}_W}{dh}\theta - L_{r_W}\frac{d\bar{u}_W}{dh}\phi \\ &= -L_\theta\theta - L_\phi\phi \end{aligned}$$

LARGE DISTURBANCE WIND AND SHEAR COMPONENTS

$$\begin{Bmatrix} \bar{u}_W \\ \bar{v}_W \\ \bar{w}_W \end{Bmatrix} = \begin{Bmatrix} \cos(\psi - \bar{\psi}_W)\cos\theta \\ \cos(\psi - \bar{\psi}_W)\sin\theta\sin\phi - \sin(\psi - \bar{\psi}_W)\cos\phi \\ \cos(\psi - \bar{\psi}_W)\sin\theta\cos\phi + \sin(\psi - \bar{\psi}_W)\sin\phi \end{Bmatrix} \bar{V}_W$$

$$\begin{Bmatrix} \frac{\partial \bar{u}_W}{\partial h} \\ \frac{\partial \bar{v}_W}{\partial h} \\ \frac{\partial \bar{w}_W}{\partial h} \end{Bmatrix} = \begin{bmatrix} \cos(\psi - \bar{\psi}_W)\cos\theta & \sin(\psi - \bar{\psi}_W)\cos\theta \\ \cos(\psi - \bar{\psi}_W)\sin\theta\sin\phi - \sin(\psi - \bar{\psi}_W)\cos\phi & \sin(\psi - \bar{\psi}_W)\sin\theta\sin\phi + \cos(\psi - \bar{\psi}_W)\cos\phi \\ \cos(\psi - \bar{\psi}_W)\sin\theta\cos\phi + \sin(\psi - \bar{\psi}_W)\sin\phi & \sin(\psi - \bar{\psi}_W)\sin\theta\cos\phi - \cos(\psi - \bar{\psi}_W)\sin\phi \end{bmatrix} \begin{Bmatrix} \frac{d\bar{V}_W}{dh} \\ \bar{V}\frac{d\bar{\psi}_W}{dh} \end{Bmatrix}$$

$$\Delta h = h - h_{cg} = x\sin\theta - y\cos\theta\sin\phi - z\cos\theta\cos\phi$$

SMALL DISTURBANCE WIND SHEAR COMPONENTS

$$\theta_0 = \phi_0 = 0$$

$$\begin{Bmatrix} \delta\left(\frac{\partial \bar{u}_W}{\partial h}\right) \\ \delta\left(\frac{\partial \bar{v}_W}{\partial h}\right) \\ \delta\left(\frac{\partial \bar{w}_W}{\partial h}\right) \end{Bmatrix} = \begin{bmatrix} \frac{d\bar{v}_W}{dh} & 0 & 0 \\ -\frac{d\bar{u}_W}{dh} & 0 & 0 \\ 0 & \frac{d\bar{u}_W}{dh} & \frac{d\bar{v}_W}{dh} \end{bmatrix} \begin{Bmatrix} \delta\psi \\ \delta\theta \\ \delta\phi \end{Bmatrix}$$

$$\frac{d\bar{u}_W}{dh} = \cos(\psi_0 - \bar{\psi}_{W_0})\frac{d\bar{V}_W}{dh} + \sin(\psi_0 - \bar{\psi}_{W_0})\bar{V}_{W_0}\frac{d\bar{\psi}_W}{dh}$$

$$\frac{d\bar{v}_W}{dh} = -\sin(\psi_0 - \bar{\psi}_{W_0})\frac{d\bar{V}_W}{dh} + \cos(\psi_0 - \bar{\psi}_{W_0})\bar{V}_{W_0}\frac{d\bar{\psi}_W}{dh}$$

$$\delta\left(\frac{\partial h}{\partial x}\right) = \delta\theta \qquad \delta\left(\frac{\partial h}{\partial y}\right) = -\delta\phi \qquad \delta\left(\frac{\partial h}{\partial z}\right) = 0$$

$$\begin{bmatrix} \delta\left(\frac{\partial \bar{u}_W}{\partial x}\right) & \delta\left(\frac{\partial \bar{u}_W}{\partial y}\right) & \delta\left(\frac{\partial \bar{u}_W}{\partial z}\right) \\ \delta\left(\frac{\partial \bar{v}_W}{\partial x}\right) & \delta\left(\frac{\partial \bar{v}_W}{\partial y}\right) & \delta\left(\frac{\partial \bar{v}_W}{\partial z}\right) \\ \delta\left(\frac{\partial \bar{w}_W}{\partial x}\right) & \delta\left(\frac{\partial \bar{w}_W}{\partial y}\right) & \delta\left(\frac{\partial \bar{w}_W}{\partial z}\right) \end{bmatrix} = \begin{bmatrix} \frac{d\bar{u}_W}{dh}\delta\theta & -\frac{d\bar{u}_W}{dh}\delta\phi & -\frac{d\bar{v}_W}{dh}\delta\psi \\ \frac{d\bar{v}_W}{dh}\delta\theta & -\frac{d\bar{v}_W}{dh}\delta\phi & -\frac{d\bar{u}_W}{dh}\delta\psi \\ 0 & 0 & -\frac{d\bar{u}_W}{dh}\delta\theta + \frac{d\bar{v}_W}{dh}\delta\phi \end{bmatrix}$$

$$\delta p_W = f\left[\frac{d\bar{u}_W}{dh}\delta\psi\right] \qquad \delta q_W = 0 \qquad \delta r_W = f\left[\frac{d\bar{u}_W}{dh}\delta\phi, \frac{d\bar{u}_W}{dh}\delta\theta\right]$$

FIGURE 4-15.–PERTURBATIONS OF EFFECTIVE ANGULAR COMPONENTS OF MEAN WIND

$$N_p\bar{p}_W = N_{p_V}\left(\frac{\partial \bar{v}_W}{\partial z}\right)$$

$$= -N_{p_V}\frac{d\bar{u}_W}{dh}\psi$$

$$= -N_\psi\psi$$

$$L_p\bar{p}_W = L_{p_V}\left(\frac{\partial \bar{v}_W}{\partial z}\right)$$

$$= -L_{p_V}\frac{d\bar{u}_W}{dh}\psi$$

$$= -L_\psi\psi$$

(V and W subscripts on aerodynamic derivatives refer to vertical tail and wing contributions, respectively). The δ prefixes have been dropped with the recognition that variables are small perturbations.

The effective bank angle derivatives are as described in Reference 4-7. The pitch attitude derivatives provide an apparent dependence of lateral-directional motion upon longitudinal motion, but when the determinants of the six simultaneous equations are expanded these derivatives are found to affect neither characteristic motion nor numerators of control transfer functions and can be ignored. The remaining distributed lift derivatives are all proportional to the longitudinal component of the mean wind shear.

The distributed lift effect is the only mean wind effect predicted to alter lateral-directional motion. Substituting the expressions for the effective angular wind velocities into the equations on Figure 4-2 yields the characteristic equations on Figure 4-16. The first effect that may be noted is that the distributed lift effect in a wind shear produces a new, fifth root.

THREE DEGREES OF FREEDOM

$$\begin{vmatrix} s - Y_v & -g & u_0 s \\ -L_v & s^2 - L_p s - L_{r_W} \frac{d\bar{u}_W}{dh} & -L_r s - L_{p_V} \frac{d\bar{u}_W}{dh} \\ -N_v & -N_p s - N_{r_W} \frac{d\bar{u}_W}{dh} & s^2 - N_r s - N_{p_V} \frac{d\bar{u}_W}{dh} \end{vmatrix} = 0$$

$$s\Delta_{L\text{-}D}(s) + \frac{d\bar{u}_W}{dh} F_1(s) + \left(\frac{d\bar{u}_W}{dh}\right)^2 F_2(s) = 0$$

$$\begin{aligned} F_2(s) &= (s - Y_v)(L_{r_W} N_{p_V} - L_{p_V} N_{r_W}) \\ &\cong (s - Y_v)(L_r N_{p_V} - L_{p_V} N_r) \end{aligned}$$

$$\begin{aligned} F_1(s) = {} & (L_{r_W} + N_{p_V})s^3 + [Y_v (L_{r_W} + N_{p_V}) + L_{r_W} N_r \\ & + L_r N_{r_W} + L_p N_{p_V} - L_{p_V} N_p]s^2 + [L_\beta N_{r_W} - L_{r_W} N_\beta \\ & + Y_v (L_r N_{r_W} - L_{r_W} N_r + L_{p_V} N_p - L_p N_{p_V})]s \\ & - g [L_{p_V} N_v + L_v N_{p_V}] \end{aligned}$$

ROLL MODE APPROXIMATION

Retain only roll acceleration equation, neglect v and r terms

$$s^2 - L_p s - L_{r_W} \frac{d\bar{u}_W}{dh} = 0$$

LATERAL OSCILLATION APPROXIMATION

Set $v = -u_0 \psi$, drop side acceleration equation

$$\begin{vmatrix} s^2 - L_p s - L_{r_W} \frac{d\bar{u}_W}{dh} & -L_r s + L_\beta - L_{p_V} \frac{d\bar{u}_W}{dh} \\ -N_p s - N_{r_W} \frac{d\bar{u}_W}{dh} & s^2 - N_r s + N_\beta - N_{p_V} \frac{d\bar{u}_W}{dh} \end{vmatrix} = 0$$

$$s\left(s + \frac{1}{T_{R_U}}\right) \Delta_{L\text{-}D_0}(s) + \frac{d\bar{u}_W}{dh} F_1(s) + \left(\frac{d\bar{u}_W}{dh}\right)^2 F_2(s) = 0$$

$$\begin{aligned} F_2(s) &= L_{r_W} N_{p_V} - L_{p_V} N_{r_W} \\ F_1(s) &= -(L_{r_W} + N_{p_V})s^2 + (L_{r_W} N_r - L_r N_{r_W} + L_p N_{p_V} - L_{p_V} N_p)s \\ &\quad + (N_{r_W} L_\beta - L_{r_W} N_\beta) \end{aligned}$$

FIGURE 4-16.–DISTRIBUTED LIFT EFFECTS OF LONGITUDINAL WIND SHEAR ON CHARACTERISTIC LATERAL-DIRECTIONAL MOTION

For small values of the longitudinal component of wind shear, the terms proportional to the square of the longitudinal component of shear may be ignored. The terms proportional to the shear form a cubic and the signs of the coefficient are given by:

$$F_1(s) = a\left(s^3 + \frac{b}{a}s^2 + \frac{c}{a}s + \frac{a}{d}\right)$$

where

$$\frac{b}{a} > 0$$

$$\frac{c}{a} \begin{cases} > 0, & L_\beta \text{ small negative or positive} \\ < 0, & L_\beta \text{ large negative} \end{cases}$$

$$\frac{d}{a} < 0$$

The roots of the polynomial multiplying the longitudinal shear component form the zeros of the root locus for variations of the wind shear. There must be at least one of these zeros on the real axis in an unstable location.

To gain more understanding of the root locus characteristics, a roll mode approximation is made. The heading and side velocity terms are dropped and only the roll equation is retained. The resulting equation on Figure 4-16 provides for the roll mode and a second root near the origin. The wind shear root locus for the roll mode approximation is shown on Figure 4-17. There it is seen that a positive shear component reduces the roll mode time constant and provides for an unstable real root. A negative shear component provides real roots that eventually join and form an oscillatory pair.

A second approximation that can be made is the lateral oscillation or Dutch roll approximation. For the Dutch roll mode, sideslip and heading are nearly equal and opposite. An approximation to the product of the Dutch roll mode and the roll mode time constant can be made by assuming $\psi = -\beta$ and by dropping the side acceleration equation. The equations for this approximation are shown on Figure 4-16. An investigation of the quadratic for the root locus zeros for the lateral oscillation approximation indicates that the zeros are a stable oscillatory pair for small negative or positive L_β or two real roots, one unstable, for large negative L_β. The root locus for the Dutch roll approximation is shown on Figure 4-17. When L_β is small, the character of the roll mode time constant and the fifth root are as predicted by the root locus for roll mode time constant approximation. A positive shear component decreases Dutch roll natural frequency and may drive the Dutch roll unstable. A negative shear increases Dutch roll natural frequency and damping. When L_β is large negative, the effect of the shear on the Dutch roll mode is reversed. Sufficiently large values of negative shears will drive the Dutch roll mode unstable.

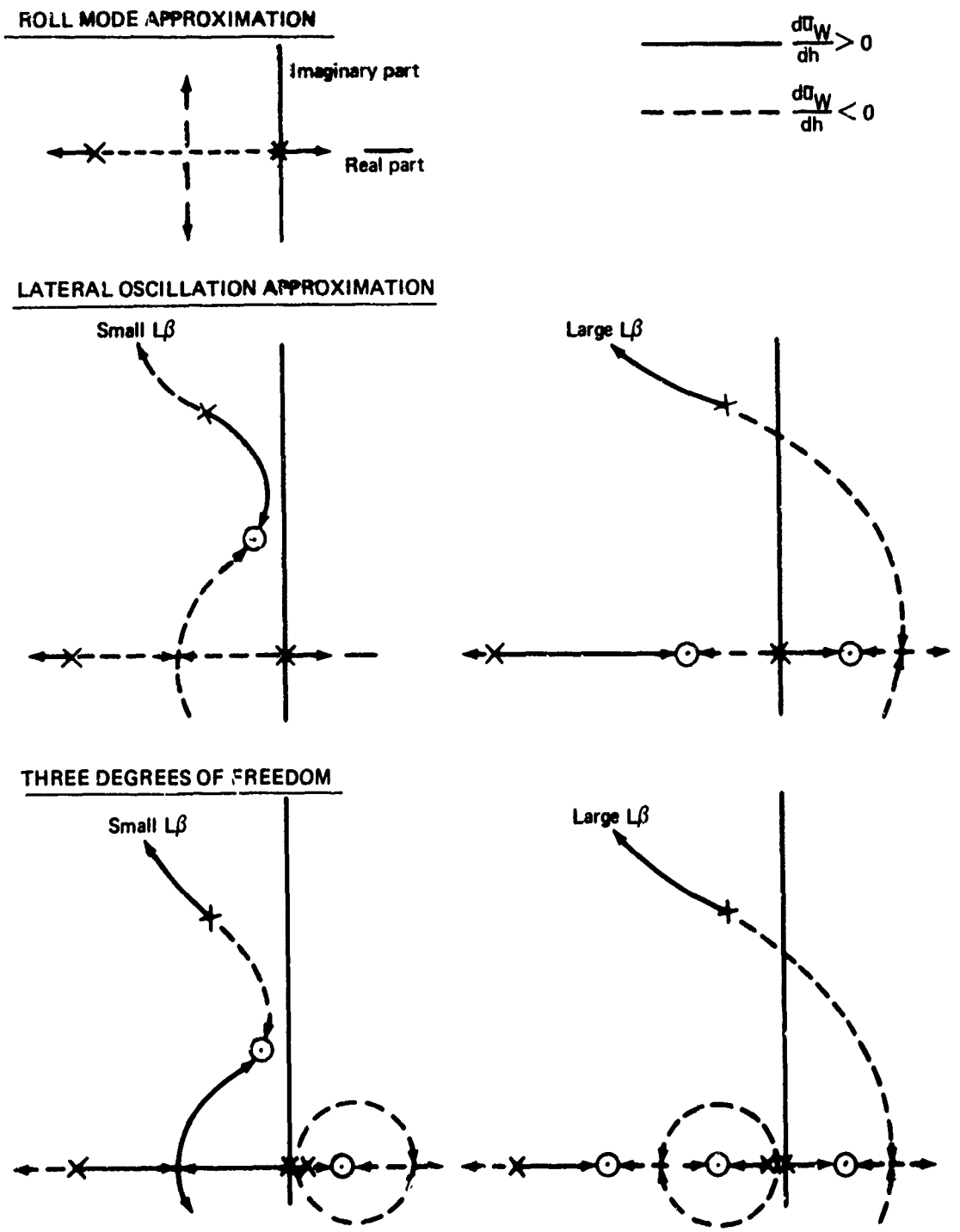

FIGURE 4-17.–ROOT LOCUS OF LATERAL-DIRECTIONAL CHARACTERISTIC MOTION DUE TO WIND SHEAR

Neither of the approximations predicted the third root locus zero. The third zero location may be approximated from the ratio of the constant root locus terms for the three-degree-of-freedom equation and the lateral oscillation approximation equation:

$$s \cong \frac{g}{u_0} \frac{\left(L_\beta N_{p_V} + L_{p_V} N_\beta\right)}{\left(N_{r_W} L_\beta - L_{r_W} N_\beta\right)}$$

For small negative or positive L_β, the location will be unstable. For large negative L_β, the location is unstable. Combined with the zeros from the Dutch roll approximation, there will always be one unstable real zero. Now, the root locus for the three-degree-of-freedom case may be drawn and is shown on Figure 4-17.

For the three-degree-of-freedom analysis, the wind shear root locus exhibits the following characteristics:

- A positive longitudinal shear component increases the Dutch roll natural frequency and damping, increases the roll mode time constant, stabilizes the spiral mode, and provides for an unstable fifth root no matter what the size of L_β. The instability of the fifth root is less than predicted by the lateral oscillation approximation.

- A negative longitudinal shear component decreases Dutch roll natural frequency and damping, decreases the roll mode time constant, and causes the spiral mode and the fifth root to form an oscillatory pair. For small L_β the low frequency oscillatory pair may be unstable and the Dutch roll stable. For large negative L_β the low frequency oscillatory pair will be unstable for a sufficiently large negative shear component.

Clearly, the important parameter governing the stability of the Dutch roll mode is L_β, the dihedral effect. Small L_β stabilizes the still air Dutch roll mode and ensures that the Dutch roll will be stable in wind shears. However, there is a tradeoff between the Dutch roll and the spiral/fifth root. Small L_β destabilizes the spiral in still air and causes an unstable oscillatory pair, formed by the spiral and fifth root, in the presence of a wind shear. The optimum value of L_β for operation in shears is likely to be a compromise, just as it normally is for still air.

The distributed lift effects have not introduced any new explicit terms describing aircraft size. The effects of size are contained within the aerodynamic derivatives.

Perhaps the most important lateral-directional transfer function is the bank angle to control input (wheel) transfer function. The numerator of this transfer function is second order. As shown on Figure 4-18, the distributed lift effects of wind shear introduce a new real root. Positive shears reduce the frequency of the still air oscillatory pair zeros. A fundamental handling qualities requirement for these zeros is that their natural frequency be less than or equal to that for the Dutch roll mode to ensure that closed loop control on bank angle do

$$\frac{\phi}{\delta_c} = \frac{N_\phi}{\Delta_{L-D}(s)}$$

$$N_\phi = \begin{vmatrix} s - Y_v & Y_{\delta_c} & u_0 s \\ -L_v & L_{\delta_c} & -L_r s - L_{p_V} \dfrac{d\bar{u}_W}{dh} \\ -N_v & N_{\delta_c} & s^2 - N_r s - N_{p_V} \dfrac{d\bar{u}_W}{dh} \end{vmatrix}$$

$$N_\phi \cong sN_{\phi_0} + L_{\delta_c}\left(L_{p_V}\frac{N_{\delta_c}}{L_{\delta_c}} - N_{p_V}\right)\frac{d\bar{u}_W}{dh}(s - Y_v)$$

$$\omega_\phi^2 = \omega_{\phi_0}^2 + \left(L_{p_V}\frac{N_{\delta_c}}{L_{\delta_c}} - N_{p_V}\right)\frac{d\bar{u}_W}{dh}$$

$$N_{h_0} = N_h\Big|_{\frac{d\bar{u}_W}{dh}=0} = s^2 + 2\zeta_{\phi_0}\omega_{\phi_0}s + \omega_{\phi_0}^2$$

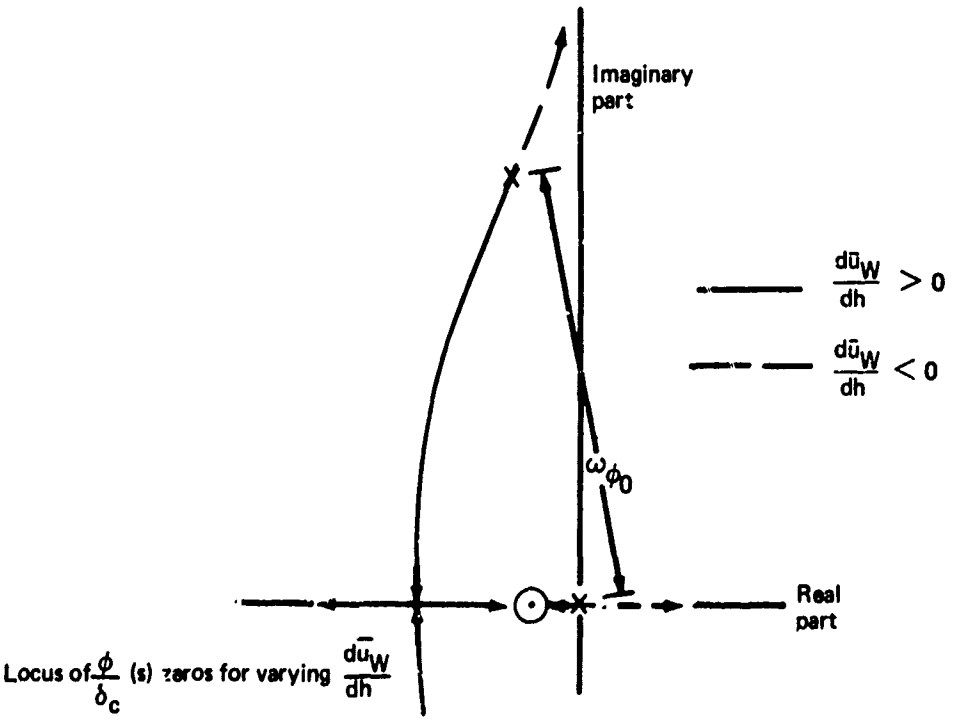

FIGURE 4-18.—BANK ANGLE TO CONTROL TRANSFER FUNCTION ZEROS, EFFECT OF WIND SHEAR

not result in high frequency unstable roots but that the difference not be so large as to cause a roll rate reversal (Ref. 4-4). Figures 4-17 and 4-18 show that a headwind increasing with increasing altitude decreases Dutch roll natural frequency and increases the frequency of the zeros. Thus, for a sufficiently large value of $|d\bar{u}_W/dh|$, $\omega_\phi/\omega_d > 1$ and there will be a tendency towards closed loop instability, equivalent to pilot-induced instability.

The distributed lift effects of the longitudinal wind shear component affect the numerators of all the lateral-directional transfer functions and may need to be considered for the design of feedback systems, either automatic or through the pilot.

4.2.1.3 Effects of Turbulence

Turbulence velocities, unlike the mean wind, are not described uniquely with time or space. Rather, the description is stochastic and affects the linear equations as forcing functions. If once again, a component of wind is equated to the sum of mean wind and turbulence,

$$\lambda_W = \bar{\lambda}_W + \lambda_T$$

where $\lambda = u, v, w$.

The turbulence terms on Figure 4-2 are placed on the right-hand side of the equation. When turbulence and mean wind are both present, the effective aerodynamic derivatives due to the mean wind are included on the left side of the equation.

Assuming the mean wind shear to be zero and representing the airplane at a point (no distributed lift effects), the relevant linear equations for analyzing the effects of turbulence are those on Figure 4-19. From these equations, transfer functions of aircraft motion with respect to turbulence components are computed.

The transfer functions define aircraft motion for arbitrary turbulence input. Together with the turbulence spectra, the airplane motion due to turbulence is defined. The mechanism for relating the two is the "output spectrum."

The transfer functions and the turbulence spectra combine characteristics to permit consideration to a frequency range, outside of which characteristics of turbulence or the transfer functions are less important. This "frequency range of interest" is important for permitting the simplification of models and simulation techniques. Two important parameters which influence airplane response within the frequency range of interest are speed, used to transform spacial to temporal frequency, and altitude, upon which turbulence characteristics are dependent.

The final effects of turbulence considered are the distributed lift effects and their representation. That is, because the aerodynamic characteristics do not exist at a point and because the spacial distribution of turbulence is not uniform over the airplane at a given point of time; representing three linear components of turbulence at the airplane center of gravity, implied in the equations of Figure 4-19, may not be sufficient.

Assumptions: Level flight, wings level
X_q, $X_{\dot{\alpha}}$, Z_q, $Z_{\dot{\alpha}}$, Y_p, Y_r negligible

LONGITUDINAL EQUATIONS

$$\begin{bmatrix} s - X_u & -X_w & g \\ -Z_u & s - Z_w & -u_0 s \\ -M_u & -(M_{\dot{w}} + M_w) & s(s - M_q) \end{bmatrix} \begin{Bmatrix} u \\ w \\ \theta \end{Bmatrix} = \begin{bmatrix} -X_u & -X_w \\ -Z_u & -Z_w \\ -M_u & -(M_{\dot{w}} s + M_w) \end{bmatrix} \begin{Bmatrix} u_T \\ w_T \end{Bmatrix}$$

$$h = \frac{1}{s}[u_0\theta - w],\ \dot{h} = u_0\theta - w,\ a_z = s[u_0\theta - w]$$

$$q = s\theta,\ \dot{q} = s^2\theta$$

$$\Delta x = \frac{u}{s},\ \dot{x} = u;\ a_x = su$$

LATERAL DIRECTIONAL EQUATIONS

$$\begin{bmatrix} s - Y_v & -g & u_0 \\ -L_v & s(s - L_p) & -L_r \\ -N_v & -N_p s & s - N_r \end{bmatrix} \begin{Bmatrix} v \\ \phi \\ r \end{Bmatrix} = \begin{Bmatrix} -Y_v \\ -L_v \\ -N_v \end{Bmatrix} v_T$$

$$\Delta y = \frac{v + u_0 r}{s},\ \dot{y} = v + u_0 r,\ a_y = s[v + u_0 r]$$

$$p = s\phi,\ \dot{p} = s^2\phi$$

$$\psi = \frac{r}{s},\ \dot{r} = sr$$

FIGURE 4-19.—EQUATIONS FOR TURBULENCE RESPONSES

4.2.1.3.1 The Output Spectra–The variance of airplane motion due to turbulence may be determined from the area under the output power spectra in the same manner as the variance of turbulence is determined by the input spectra. When there is a single random input, the output power spectrum is defined (Ref. 4-7) as:

$$\Phi_0(\omega) = M^2(\omega)\,\Phi_I(\omega)$$

where $M(\omega)$ is the amplitude frequency response of the output to input transfer function and $\Phi_I(\omega)$ is the input power spectrum. That is, simply multiply the square of the frequency response by the input power spectrum.

If there are more than one uncorrelated random inputs,

$$\Phi_0 = \sum_{i=1}^{n} M_i^2(\omega)\,\Phi_{I_i}(\omega)$$

For example, if the power spectrum of normal load factor is desired and there are three uncorrelated linear components of turbulence,

$$\Phi_{n_z} = \left|\frac{n_z}{u_T}(i\omega)\right|^2 \Phi_{u_T}(\omega) + \left|\frac{n_z}{v_T}(i\omega)\right|^2 \Phi_{v}(\omega) + \left|\frac{n_z}{w_T}(i\omega)\right|^2 \Phi_{w_T}(\omega)$$

If, in addition, the random inputs are not uncorrelated, the output spectra must include the effects of the cross-spectra. According to Reference 4-7:

$$\Phi_0(\omega) = \sum_{k=1}^{n}\sum_{\ell=1}^{n} G_k^*(i\omega)\,\Phi_{I_{k_\ell}}(\omega)\,G_\ell(i\omega)$$

Where $G(i\omega)$ is the complex frequency response and $G^*(i\omega)$ is its complex conjugate. For three correlated components of turbulence, the normal load factor power spectrum is defined by:

$$\Phi n_z(\omega) = \left|\frac{n_z}{u_T}(i\omega)\right|^2 \Phi_{u_T}(\omega) + \left|\frac{n_z}{v_T}(i\omega)\right|^2 \Phi_{v_T}(\omega)$$

$$+ \left|\frac{n_z}{w_T}(i\omega)\right|^2 \Phi_{w_T}(\omega)$$

$$+ \left\{\left[\frac{n_z^*}{u_T}(i\omega)\right]\left[\frac{n_z}{v_T}(i\omega)\right] + \left[\frac{n_z}{u_T}(i\omega)\right]\left[\frac{n_z^*}{v_T}(i\omega)\right]\right\} \Phi_{u_T w_T}(\omega)$$

$$+ \left\{\left[\frac{n_z^*}{u_T}(i\omega)\right]\left[\frac{n_z}{w_T}(i\omega)\right] + \left[\frac{n_z}{u_T}(i\omega)\right]\left[\frac{n_z^*}{w_T}(i\omega)\right]\right\} \Phi_{u_T w_T}(\omega)$$

$$+ \left\{\left[\frac{n_z^*}{v_T}(i\omega)\right]\left[\frac{n_z}{w_T}(i\omega)\right] + \left[\frac{n_z}{v_T}(i\omega)\right]\left[\frac{n_z^*}{w_T}(i\omega)\right]\right\} \Phi_{v_T w_T}(\omega)$$

The output spectra provide the means for analytically estimating the effects due to turbulence. In particular, the normal load factor spectrum is used in loads analysis. It is generally assumed that all the turbulence cospectra terms are negligible (not necessarily true at low altitudes), that the load factor to lateral turbulence transfer function is zero (not true when spoilers are used for lateral-directional stability augmentation), and that the load factor due to the longitudinal turbulence component is relatively small (not true at very low speeds where it will dominate).

There is no simple rule relating output variance to input variance. If a turbulence spectrum were a constant with all frequencies, thus providing an infinite turbulence variance, the output variance would be finite so long as the output to turbulence frequency response has a high frequency asymptote that decreases with increasing frequency. Furthermore, it is insufficient to use the magnitude of the input variance or covariance to determine whether or not that input has a significant effect. If the input had a large variance but one which was concentrated at a frequency where the appropriate transfer function had a negligible frequency response, the effect of the input may be negligible. To be significant, large contributions to the input variances must occur at the same frequencies where the transfer function frequency response is large. In effect, the input spectrum and the frequency response provide mutual filtering.

4.2.1.3.2 Frequency Range of Interest–The concept of the output spectrum can be used to show that there is a frequency range of interest above and below which accurate representation of the airplane and turbulence is not important.

First, it may be recalled that the contribution of a frequency range to the turbulence variance is the area under the spectrum multiplied by frequency when plotted against the logarithm of frequency. Such plots for the Von Karman spectra are presented on Figure 4-20.

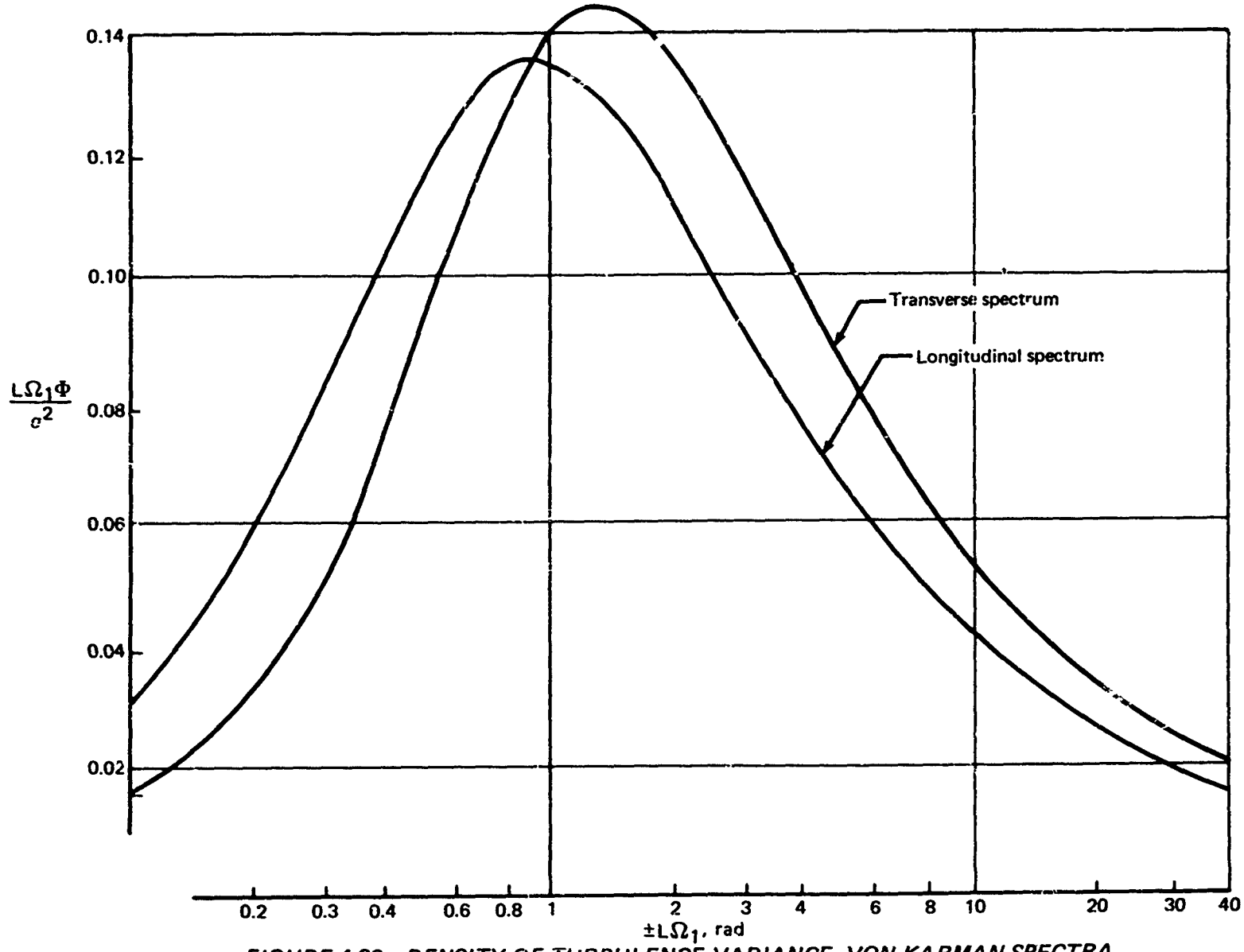

FIGURE 4-20.—DENSITY OF TURBULENCE VARIANCE, VON KARMAN SPECTRA

At high and increasing frequencies, the contribution of successive frequency octaves to the total turbulence variance decreases until, above some frequency, the contribution of all higher frequencies is negligible. Similarly, the contribution of successively lower frequencies at low frequencies diminished until at some low frequency the contribution of all lower frequencies is negligible.

If a transfer function between an output parameter and an input turbulence component were a constant (invariant with frequency), the output spectrum shape would be the same as the input spectrum shape and once again there would be frequencies above and below which the contribution to the output spectrum would be negligible. This argument can be generalized. If, at high frequencies, a transfer function has an asymptote that is constant or decreases with frequency, the output spectrum will decrease with frequency at high frequencies and there will be some frequency above which the contributions of higher frequencies to the output variance will be negligible. Similarly, if the transfer function is constant or increases with frequency at low frequencies, there will be a lower frequency limit below which variance contributions are negligible. The intermediate frequency region in which contributions to the output variance are not negligible constitutes the frequency range of interest for that particular output parameter.

The frequency range of interest for a particular output parameter will, in general, depend on the entire output spectrum shape, but upper and lower frequency limits tend to vary with the high and low asymptotic character of the transfer functions. If an asymptote of a transfer function is given by $O/I = ks^n$, then the output spectra asymptotes are:

$$\omega\Phi_0 = \begin{cases} k\omega^{2n-\frac{2}{3}} & \text{high frequencies} \\ k\omega^{2n+1} & \text{low frequencies} \end{cases}$$

The upper frequency limit decreases as n becomes more negative and the lower frequency limit increases as n becomes more positive.

To ensure there are frequency ranges of interest for all output parameters, it must be ensured that the transfer functions for all parameters do not have frequency responses that increase at high frequencies or decrease at low frequencies. In general, there are position, velocity, and acceleration parameters to be considered. However, upper frequency limits for velocities and accelerations are ensured if the corresponding position transfer functions decrease at least as fast as s^2 (ω^2) at high frequencies.

The high and low frequency asymptotes for the linear and angular position transfer functions derivable from the equations on Figure 4-19 are presented in Table 4-1. All vary at high frequencies as s^{-2} except for the θ/w_T transfer function. However, the high frequency

TABLE 4-1.–ASYMPTOTES OF TURBULENCE TRANSFER FUNCTIONS

Transfer function	Low-frequency asymptote	High-frequency asymptote
$\frac{\Delta x}{u_T}(s)$	$\frac{1}{s}$	$-\frac{X_u}{s^2}$
$\frac{\Delta x}{w_T}(s)$	$\frac{g M_w}{w_{sp}^2 w_{ph}^2}$	$-\frac{\lambda_w}{s^2}$
$\frac{\theta}{u_T}(s)$	$-\frac{s}{g}$	$-\frac{(M_u + Z_u M_{\dot{w}})}{s^2}$
$\frac{\theta}{w_T}(s)$	$\frac{(X_u M_w - X_w M_u)\, s}{w_{sp}^2 w_{ph}^2}$	$-\frac{M_{\dot{w}}}{s}$
$\frac{h}{u_T}(s)$	$-\frac{u_0}{g}$	$\frac{Z_u}{s^2}$
$\frac{h}{w_T}(s)$	$-\frac{1}{s}$	$\frac{Z_w}{s^2}$
$\frac{\Delta y}{v_T}(s)$	$\frac{1}{s}$	$-\frac{(Y_v + N\beta)}{s^2}$
$\frac{\phi}{v_T}(s)$	$\frac{(L_v N_r - L_r N_v)\, s}{w_d^2 \frac{1}{T_R} \frac{1}{T_S}}$	$-\frac{L_v}{s^2}$
$\frac{\psi}{v_T}(s)$	$\frac{(L_p N_v - L_v N_p)\, s}{w_d^2 \frac{1}{T_R} \frac{1}{T_S}}$	$-\frac{N_v}{s^2}$

gain for that transfer function is $M_{\dot{w}}$, which does not actually qualify as a point lift term since it is due to the finite time required for downwash produced by a lifting surface to reach a trailing lifting surface. Hence, for a point lift representation, sw_T should not be considered a turbulence parameter. The distributed lift effects shall be considered separately. It may be noted that there must be an upper frequency limit to ensure a finite output variance.

Three transfer functions on Table 4-1 do not satisfy the low frequency asymptote requirements: h/w_T, $\Delta x/u_T$, and $\Delta y/v_T$, parameters corresponding to inertial linear position. These decrease with increasing frequency at low frequencies. This would appear to invalidate a lower frequency limit. However, these transfer functions are open loop transfer functions. Pilots and reasonable autopilot designs can effectively eliminate the turbulence disturbances at sufficiently low frequencies. Hence, for closed loop considerations, there is a frequency below which the open loop spectrum is unimportant, whether or not the open loop spectrum has a significant contribution to the open loop variances below that frequency.

It is difficult to generalize on a frequency range of interest for all motion parameters. Accelerations are significant at higher frequencies than displacements, and vice versa. To define a single frequency range, the highest and lowest frequencies must be applicable for any of the response parameters and will necessarily be conservative for any single parameter.

In the absence of structural modes, transfer functions will generally not increase much above the short period or Dutch roll frequencies. The upper frequency limit may then be considered as, say, a decade beyond the lesser of the short period/Dutch roll natural frequency or the highest turbulence break frequency.

Pilot or autopilot closed loop turbulence effects are likely to be negligible below about 0.01 rad/sec in the absence of lowly damped oscillatory roots near or below that frequency.

4.2.1.3. Distributed Lift Effects of Turbulence—Up to this point, turbulence has been represented as though the aerodynamics of the airplane were concentrated at the airplane's center of gravity. Alternately, the representation incorporates a uniform turbulence field over the airplane such that the components of turbulence are invariant with position; a temporal change in turbulence at the center of gravity is accompanied by identical changes of turbulence components on all other locations on the airplane. As neither of these descriptions is correct, the point representation is at best an approximation that assumes that the airplane dimensions are "vanishingly small with respect to the wavelengths of all significant spectral components" (Ref. 4-7). That is, the point representation may be expected to be most valid for very long turbulence wavelengths. If the frequency range of interest is only at low frequencies, then the point representation may well be valid.

Reference 4-7 has examined the validity of the point representation. The position is taken that the representation is valid below some frequency. For the longitudinal spacial frequency component of turbulence, the representation is considered valid until the complex amplitude of the lift on a finite wing flying through a sinusoidal inclined wave of upwash deviates too far from the response at zero frequency. From a theoretical solution, the region of validity is given as

$$\Omega_1 \ \bar{c}/2 < 0.05$$

where $\Omega_1 \ \bar{c}/2$ is the nondimensional or reduced frequency, k,

$$k = \omega\bar{c}/2V_A$$

Alternately, the point representation for chordwise distributions of turbulent velocities is good for

$$\lambda_1/\bar{c} > 60$$

For a mean chord of 20 feet, turbulence wavelengths in the longitudinal direction less than 1200 feet must not lie in the frequency range of interest.

The wavelength limitation in terms of mean chord must be considered a rough guide. The limitation is most certainly dependent upon wing geometry. For a wing with a zero taper ratio, the specified wavelength limitation is likely valid for outboard sections but invalid for inboard sections where the chord may be substantially larger than the mean. Also, this guide considers distributed lift effects over the wing only; there are also strong aerodynamic effects due to the nonuniform distribution between the wing and the tail. The length of the aircraft is a sufficient, but perhaps not necessary, dimension for testing the validity of the point representation. In any event, the order of magnitude of the maximum valid wavelength indicates possible error by the point representation in at least the frequency region of short period motion.

For the lateral spacial frequency component, the point representation is found in Reference 4-7 to be accurate within 10% up to the reduced frequency

$$\Omega_2 \, b/2 < 1$$

or

$$\lambda_2/b > \pi.$$

Thus, the point representation for lateral distributions of turbulence is far more restrictive than for longitudinal distributions.

The accuracy of the point approximation for vertical distributions or turbulence is not considered in Reference 4-7 but is often assumed acceptable either through representation of the airplane as being two-dimensional or by assuming that the effects of the vertical distribution are negligible.

Perhaps the most rigorous method of attacking the general problem is the panel method. The surfaces of the aircraft are divided into many small panels having dimensions sufficiently small that the point aerodynamic representation for a single panel is accurate. The aerodynamics of any one panel are coupled with those of all other panels through the aerodynamic influence coefficients (downwash in panel i due to lift on panel j). The total forces and moments are found by summing the contributions of each of the panels. The

force and moment power spectra may then be computed from the output spectrum concept involving input spectra for each of the panels and cospectra between each pair of panels.

The panel method is similar to that used for load analysis and permits the inclusion of unsteady aerodynamic effects and structural modes. Accuracy from this method is limited only by the limitations of the modeling, the capabilities of the computer, the accuracy of the mathematical routines, and the accuracy of linearization. Solution by this technique is, however, quite laborious. A large amount of time is required for modeling, the cospectra tend to be quite complex, and solution of the large number of simultaneous equations is performed in the frequency domain and is quite slow and expensive. Seldom are the full distributed lift effects represented, even for loads analysis. Simplification is possible, however, through recognizing that the input power spectra are the same for each panel and that the input cospectra for all panels separated laterally by the same distance are the same. The cospectra for two paths separated laterally are derived and presented for the Von Karman spectra in Reference 4-8. Physical interpretation is difficult using this method, but Reference 4-9 provides some of the possible mathematical simplifications and some general results.

Direct application of the panel method to simulator usage is out of the question. Computational time and computer storage requirements are beyond the scope of digital real-time solution, particularly for simulation of nonlinearities. The technique may lead to the design of approximate filters or forms of force and moment spectra that could be used in place of turbulence spectra. Such applications are not well adapted for low altitude simulation, where relatively large speed changes and turbulence changes with altitude occur. The applications would also tend to be quite configuration dependent.

A much simpler and more physically understandable technique has been developed by Etkin. As first presented in Reference 4-10, the distribution of a turbulence component over an airplane is expressed using a Taylor-series expansion about the center of gravity. For a two-dimensional representation of the airplane, the vertical component is represented by:

$$w_T(x, y) = (w_T)_0 + \left(\frac{\partial w_T}{\partial x}\right)_0 x + \left(\frac{\partial w_T}{\partial y}\right)_0 y + \frac{1}{2}\left(\frac{\partial^2 w_T}{\partial x^2}\right) x^2$$

$$+ \left(\frac{\partial^2 w_T}{\partial x \partial y}\right)_0 xy + \frac{1}{2}\left(\frac{\partial^2 w_T}{\partial y^2}\right) y^2 + \ldots\ldots$$

All derivatives are evaluated at the center of gravity. The zero order term corresponds to turbulence for a point lift representation. Thus, the method superimposes the distributed lift effects upon the point representation effects.

The first order derivatives are equivalent to introducing angular velocity components of turbulence, just as was done for the mean wind distributed lift effects:

$$\frac{\partial w_T}{\partial x} = q_T \,, \quad \frac{\partial w_T}{\partial y} = -p_T$$

In Reference 4-10, the second order derivatives with respect to x and y are interpreted as a parabolic downwash distribution and the second order xy derivative is described as periodic cambering at each section, with amplitude of the camber proportional to y and antisymmetric with respect to the airplane centerline. Interpretations of higher order derivatives are much more difficult.

In Reference 4-10, Taylor-series derivatives up to the second order are retained, but in his subsequent publications (Refs. 4-11, -12 and -7) Etkin has restricted his attention to the zero and first order terms. From Reference 4-12: "Generally speaking, since the input spectra corresponding to [second order derivatives] are relatively so weak, it appears that rough estimates of the second order derivatives will serve well enough for analysis. A note of caution must be sounded in this connection, however, when elastic modes of the aircraft are involved, for then the second order terms may be more important." The distributed lift effects are thus represented entirely by angular components of turbulence, implying that the turbulence field is linearly distributed about the center of gravity.

If an extension from the two-dimensional representation to the three-dimensional description is made (accounting for the finite size of the vertical tail), the incremental distributed lift effects are represented not only by effective angular velocities acting on the wing, but also by using effective angular velocities acting on the vertical tail:

Wing angular velocities	Vertical tail angular velocities
$q_T = \frac{\partial w_T}{\partial x}$	$q_T = \frac{\partial u_T}{\partial z}$
$p_T = -\frac{\partial w_T}{\partial y}$	$p_T = \frac{\partial v_T}{\partial z}$
$r_T = \frac{\partial u_T}{\partial y}$	$r_T = -\frac{\partial v_T}{\partial x}$

The total effective angular velocity is made up from the wing and tail terms weighted by their relative aerodynamic contributions. For example,

$$C_{l_p} p_T = \left(C_{l_p}\right)_W \left(-\frac{\partial w_T}{\partial y}\right) + \left(C_{l_p}\right)_V \left(\frac{\partial v_T}{\partial z}\right)$$

or,

$$p_T = \frac{\left(C_{l_p}\right)_W}{C_{l_p}} \left(-\frac{\partial w_T}{\partial y}\right) + \frac{\left(C_{l_p}\right)_V}{C_{l_p}} \left(\frac{\partial v_T}{\partial z}\right)$$

The aerodynamic (relative to the air mass) angular velocities are made up from the angular velocity of the airplane relative to the earth less the angular velocity of the wind relative to the earth. For example,

$$p_A = p - p_T$$

This is the same technique as used for the mean wind distributed lift effects.

Having determined that distributed lift effects may be represented by angular components of turbulence, it remains to specify the power spectra of the angular components and their cospectra with the linear components.

In Reference 4-12, it is shown that the three-dimensional power spectrum of a displacement derivative of a turbulence component is given by

$$\theta_{\frac{\partial \lambda_i}{\partial \xi_k} \frac{\partial \lambda_i}{\partial \xi_k}} = -\Omega_k^2 \theta_{\lambda_i \lambda_i}$$

and the cospectra are given by

$$\theta_{\frac{\partial \lambda_i}{\partial \xi_k} \lambda_j} = i\Omega_k \theta_{\lambda_i \lambda_j}$$

where

$i, j, k = 1, 2, 3$

$\lambda_1 = u_T$

$\lambda_2 = v_T$

$\lambda_3 = w_T$

$$\xi_1 = x$$

$$\xi_2 = y$$

$$\xi_3 = z$$

The one-dimensional spectra are obtained by successive integrations with respect to the transverse spacial frequencies. For the cospectra and power spectra involving derivatives with respect to the longitudinal coordinate, the following simple relationships result:

$$\Phi_{\frac{\partial\lambda}{\partial x}\frac{\partial\lambda}{\partial x}}(\Omega_1) = \Omega_1^{\,2}\,\Phi_{\lambda\lambda}(\Omega_1)$$

$$\Phi_{\frac{\partial\lambda}{\partial x}\lambda}(\Omega_1) = i\Omega_1\,\Phi_{\lambda\lambda}(\Omega_1)$$

The one-dimensional expression for derivatives with respect to the transverse components coordinates is more complex. One bad result from this procedure occurs: The variance of the effective angular components of turbulence is infinite due to the $\Omega_1^{1/3}$ asymptote of the power spectra for the turbulence component spacial derivatives. The explanation is that a first order Taylor-series approximation is inadequate at high frequencies. A physical interpretation is provided with the aid of Figure 4-21. At low frequencies, the linear turbulence field representation over the airplane dimensions is accurate and, in fact, exact at zero frequency. At short wavelengths, the linear approximation is poor and estimating the distribution by the slope of turbulence velocities at the origin drastically overpredicts the effects of the distribution. At low frequencies, the updraft on one wing combines with the downdraft on the other wing. At high spacial frequencies, updrafts on one wing are counterbalanced with downdrafts on the same wing as well as downdrafts on the opposite wing. At infinite frequencies, the net rolling moment must be zero. The linear approximation, however, increases the rolling moment with increasing frequencies.

To account for the maximum frequency limitation of the linear gust field representation, the three-dimensional spectra have been truncated at the maximum frequencies before integrating with respect to the transverse spacial frequency components in References 4-10 and 4-12. This is analogous to abruptly reducing the one-dimensional spectra to zero at some frequency.

Truncation of the three-dimensional spectra not only affects the effective angular velocity spectra, but also the linear velocity power spectra. That is, the lift on a finite airplane due to a turbulence field is less than that from a point lift representation. This can be demonstrated by a simple example using the output spectra concept. Consider a two-panel representation of the airplane whereby a panel represents half of the wing. Over each panel, the turbulence is considered to be uniform. The power spectrum of lift due to vertical turbulence is given by:

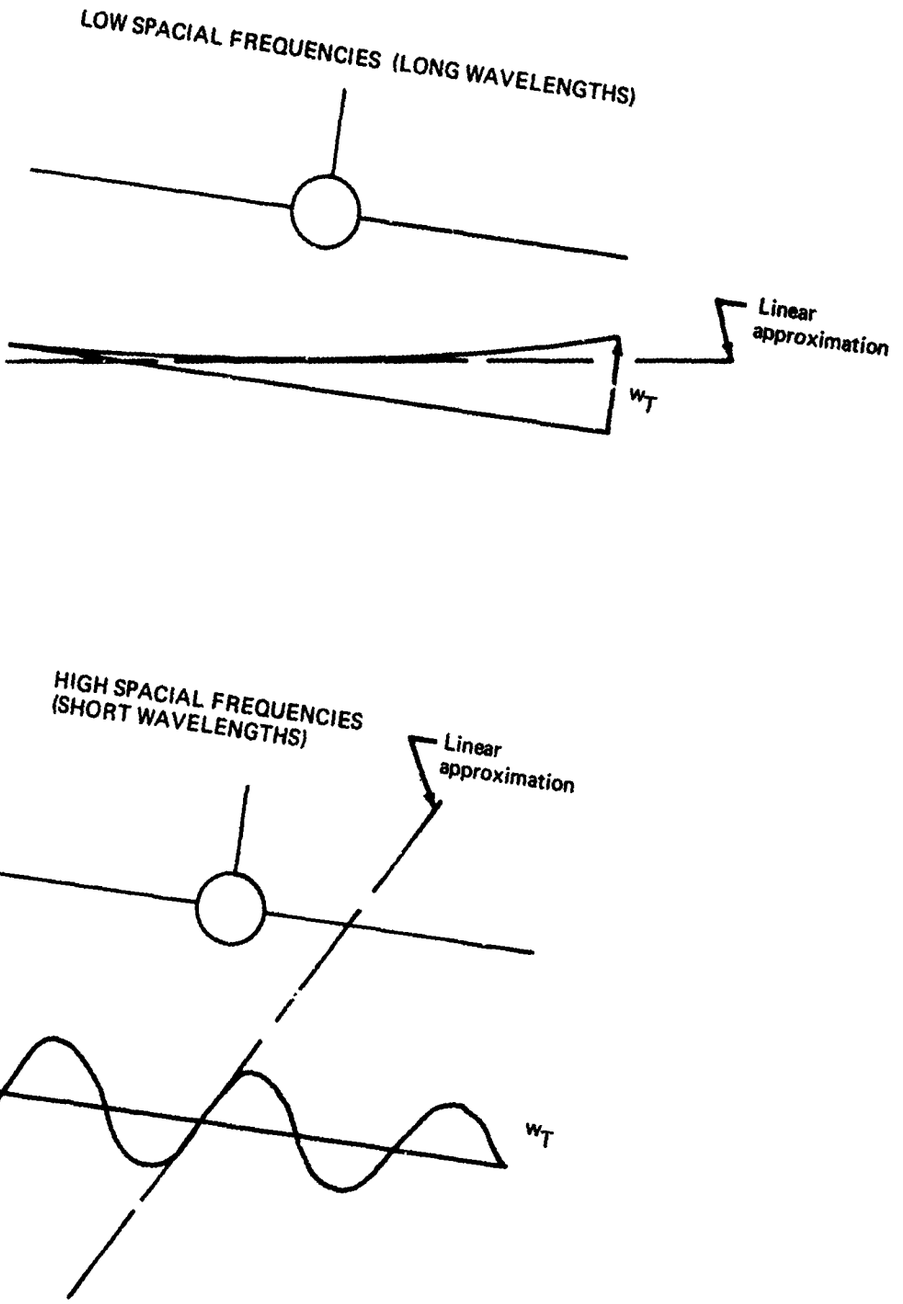

FIGURE 4-21.—FREQUENCY LIMITATION OF LINEAR TURBULENCE FIELD REPRESENTATION

$$\Phi_{LIFT} = \left(\frac{\partial L_L}{\partial w_T}\right)^2 \Phi_{w_L} + \left(\frac{\partial L_R}{\partial w_T}\right)^2 \Phi_{w_R} + \left(\frac{\partial L_L}{\partial w_T}\right)\left(\frac{\partial L_R}{\partial w_T}\right)\Phi_{w_L w_R}$$

The power spectra for turbulence on the left and right wings are equal ($\Phi_{w_{T_L}} = \Phi_{w_{T_R}}$), and the derivatives of lift produced by each half of the wing with respect to vertical turbulence are equal to each other and half the airplane's entire lift derivative:

$$\frac{\partial L_L}{\partial w_T} = \frac{\partial L_R}{\partial w_T} = \frac{1}{2}\frac{C_{L_\alpha} \bar{q} s}{u_0}$$

Thus,

$$\Phi_{LIFT} = 2\left(\frac{C_{L_\alpha} \bar{q} s}{2u_0}\right)^2 \Phi_w \left[1 + \frac{\Phi_{w_L w_R}}{\Phi_w}\right]$$

The point lift representation expression is

$$\Phi_{LIFT} = \left(\frac{C_{L_\alpha} \bar{q} s}{u_0}\right)^2 \Phi_w$$

The two expressions are equal only if $\Phi_{w_L w_R} = \Phi_w$. This can happen only if the two panel centers coincide. It is a sufficient approximation if the distance between the two panel centers is close with respect to the scale of turbulence. The cospectra for two parallel turbulence velocities separated laterally have been developed for the Von Karman spectra in Reference 4-8. The analytic form of these spectra are quite complex, but they are reproduced on Figure 4-22 for various ratios of separation distance to turbulence integral scale. A 20% error at low frequencies occurs for separation of the panel control points equal to about 30% of the integral scale. For straight, untapered wings (mean chord at the middle of the semispan), a significant reduction of the lift spectrum (10% error) occurs when the wing span is greater than 60% of the integral scale.

Of course, a two-panel representation is quite crude and more panels will require knowledge of the section lift curve slopes. The equations that result from more panels are vastly more complicated, but will reduce to the point representation for very small distances. As previously discussed, the panel method is not considered suitable for simulation.

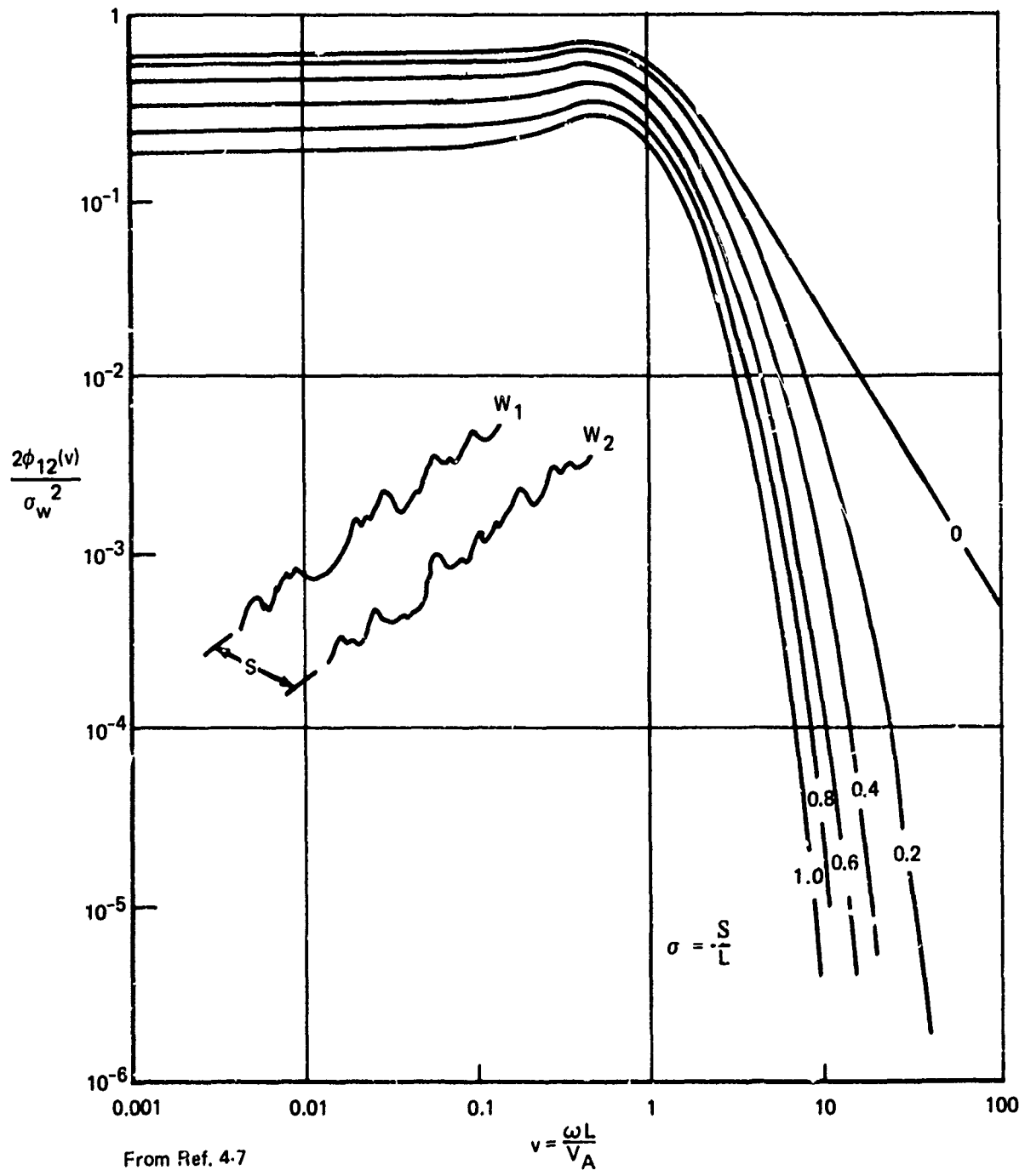

FIGURE 4-22.–CROSS SPECTRA FOR TREATMENT OF NONUNIFORM SPANWISE GUSTS

The Fourier component method treats the effects of distributed lift on the force spectra by truncating the frequencies over which integration of the three-dimensional spectra is performed to achieve the one-dimensional spectra. That is,

$$\Phi_{ij}^{*}(\Omega_1) = \int_{-\Omega'_3}^{\Omega'_3} \int_{-\Omega'_2}^{\Omega'_2} \theta_{ij}(\Omega_1, \Omega_2, \Omega_3)\, d\Omega_2, d\Omega_3$$

where Ω'_2, Ω'_3 = maximum frequencies for which representation is valid to account for the lateral dimensions rather than

$$\Phi_{ij} = \int_{-\infty}^{\infty} \int_{-\infty}^{\infty} \theta_{ij}(\Omega_1, \Omega_2, \Omega_3)\, d\Omega_2\, d\Omega_3$$

as used for the point representation. The spectra $\Phi_{ij}^{*}(\Omega_1)$ then becomes the effective one-dimensional power spectrum associated with the first order Fourier-series approximation. The power spectra that result from finite spanwise dimensions are presented on Figures 4-23, -24, and -25, for the Dryden spectra, taken from Reference 4-12. The spectra are seen to be reduced at high frequencies with decreased maximum transverse spacial frequency. These spectra must be considered as approximate, since truncation eliminates all contributions of higher frequencies while it is likely that higher frequencies have continuously diminishing contribution to the effective turbulence velocity power spectra. This inadequacy of truncation has been noted in Reference 4-7 with reference to the rigid body response to turbulence: "It is probably better, and certainly simpler, to use the basic (not truncated) one-dimensional spectra on the grounds that including the small contribution with an inaccurate theory is better than leaving them out altogether."

The spectra on Figure 4-25 cannot be compared directly with that on Figure 4-22. Rather, the effects of the spectra on Figure 4-25 plus the effects of the spectra for the angular components of turbulence are compared to the effects of the spectra on Figure 4-22.

Reference 4-7 has compared the first order Taylor-series method to a theoretical solution for lift, pitching moment, and rolling moment of a wing in a turbulence field and has concluded that without incorporating unsteady aerodynamics, the first order Taylor-series method is accurate for

$$\Omega_1 < 1/\bar{c} \quad \text{or} \quad \lambda_1 > 2\pi\ell_T$$

$$\Omega_2 < 2/b \quad \text{or} \quad \lambda_2 > \pi b$$

Thus, the first order Taylor-series method represents a factor of 10 improvement for distributions along the x axis over the point approximation, but provides no improvement for spanwise disturbances. That is, although the effective turbulence roll rate may be significant, its inclusion provides no improvement over the results from assuming the

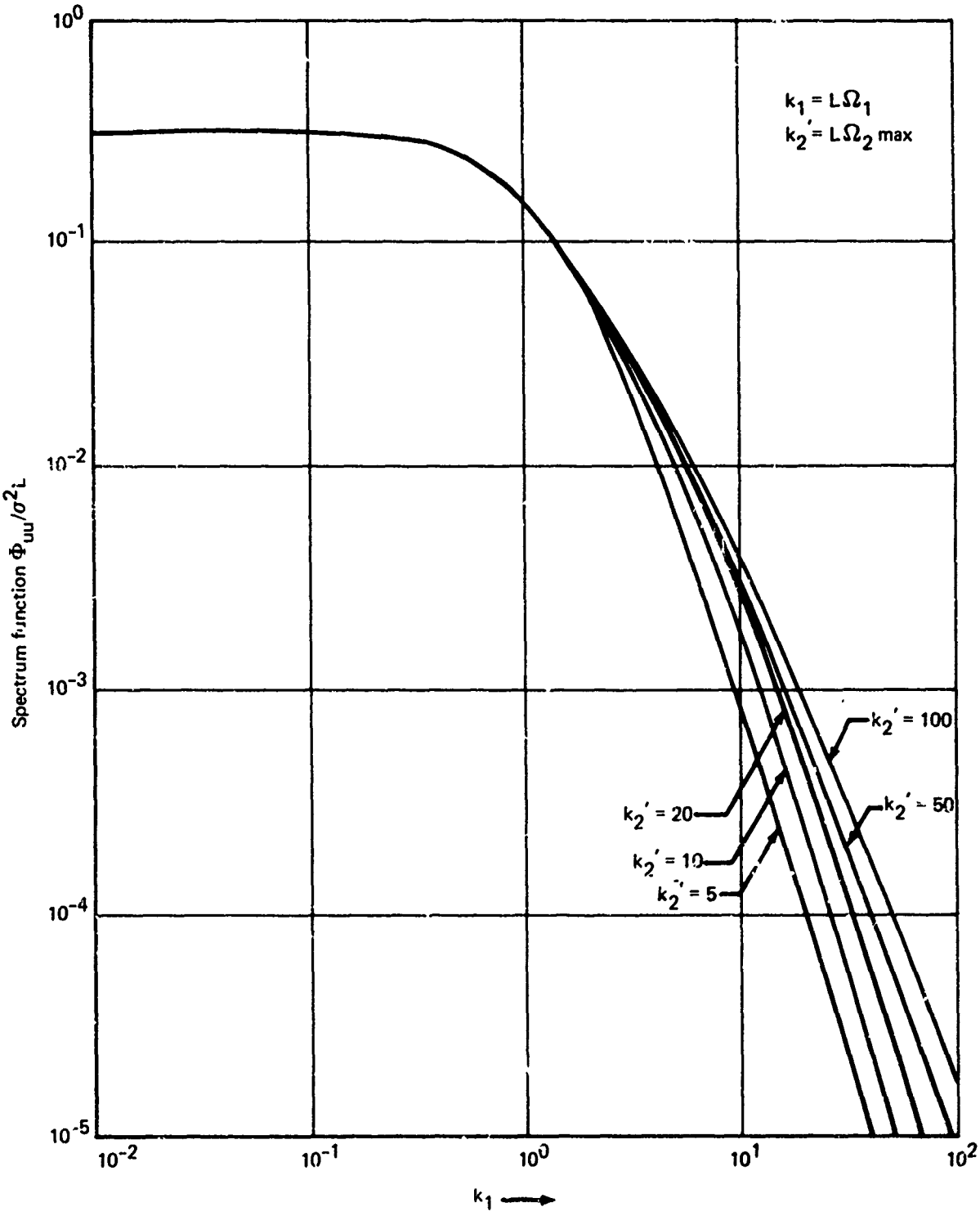

FIGURE 4-23.–SPECTRUM FUNCTION $\Phi_{uu}/\sigma^2 L$ (FROM REF. 12)

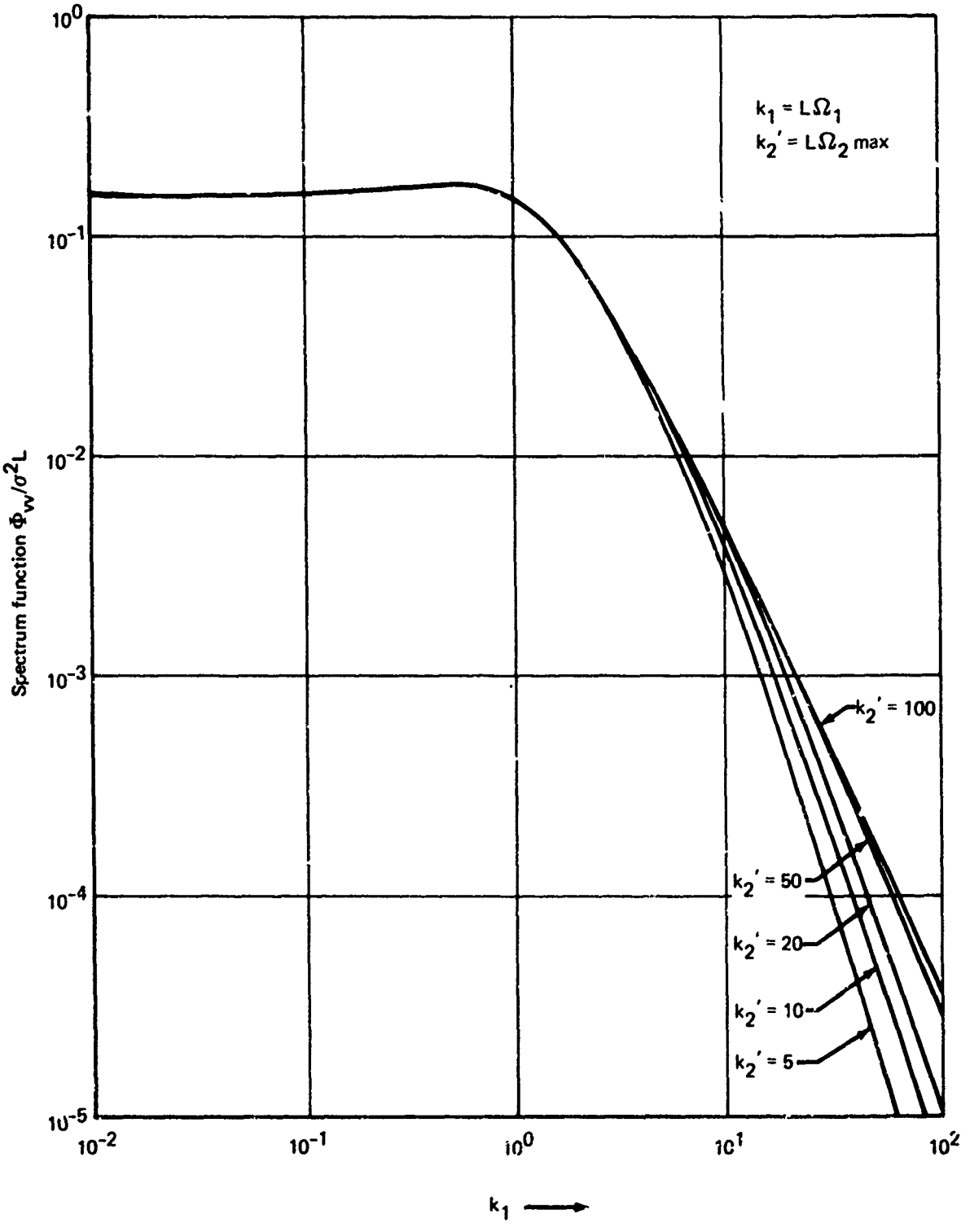

FIGURE 4-24.–SPECTRUM FUNCTION $\Phi_{ww}/\sigma^2 L$ (FROM REF. 12)

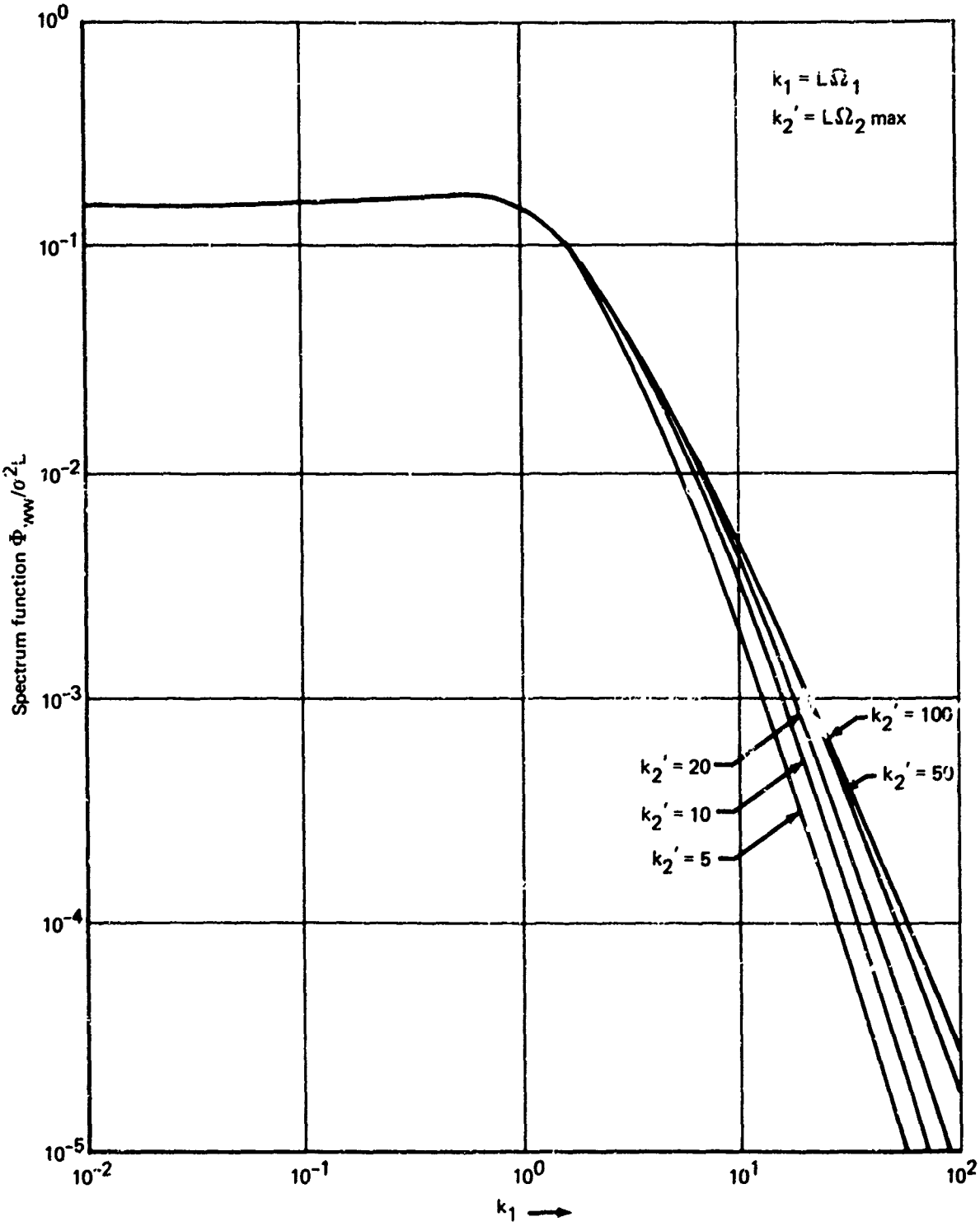

FIGURE 4-25.–SPECTRUM FUNCTION $\Phi_{ww}/\sigma^2 L$ (FROM REF. 12)

spanwise dimensions are zero. Other, more complex methods, can be used to approximate the spanwise distribution but tend to be heavily dependent upon airplane configuration and flight condition. As a consequence, the spanwise lift distribution effects will not be included. This does not mean that turbulence will not produce rolling moments; strong rolling moments due to turbulence are produced through L_β, the dihedral effect, and the lateral component of turbulence.

The significance of the roll component of turbulence at low frequencies can be evaluated by examining the rolling moment spectra, assuming rolling moment is due only to roll rate and sideslip. (Ignore yaw rate terms, the object is to compare the relative importance of roll rate and sideslip.)

$$\Phi_{G_X} = \Phi_v \left[C_{l_v} \bar{q}sb\right]^2 + \Phi_p \left[C_{l_p} \bar{q}sb\right]^2$$

$$\Phi_{G_X} = \Phi_v \left[C_{l_v} \bar{q}sb\right]^2 \left[1 + \frac{\Phi_p}{\Phi_v}\left(\frac{C_{l_p}}{C_{l_v}}\right)^2\right]$$

It may be noted that no correlation between the effective turbulence roll rate and the lateral component of turbulence is included, correctly implying that the two are perfectly uncorrelated.

The aerodynamic derivatives may be written in terms of C_{l_β} and $C_{l_{\hat{p}}}$ ($\hat{p}$ = nondimensional roll state, $\hat{p} = pb/2V$) to remove some of their dependence upon speed:

$$\Phi_{G_X} = \Phi_v \left[C_{l_\beta} \frac{\bar{q}sb}{V_A}\right]\left[1 + \frac{b^2}{4}\frac{\Phi_p}{\Phi_v}\left(\frac{C_{l_{\hat{p}}}}{C_{l_\beta}}\right)^2\right]$$

To conclude that the effective turbulence roll rate is insignificant in the region of validity for the first order Taylor-series representation, it must be concluded that

$$\frac{b^2}{4}\frac{\Phi_p}{\Phi_v}\left(\frac{C_{l_{\hat{p}}}}{C_{l_\beta}}\right)^2 \ll 1$$

At low frequencies, $\Phi_v|_{\Omega_1 = 0} = \sigma_v^2 L_v/2\pi$. The turbulence roll rate spectrum is presented on Figure 4-26, as taken from Reference 4-12. The low frequency gain of this spectrum has been cross-plotted on Figure 4-27 as a function of the lateral cutoff spacial frequency. This gain is on the order of $\Phi_p|_{\Omega 1 = 0} \cong \sigma_w^2/L_w$. Thus

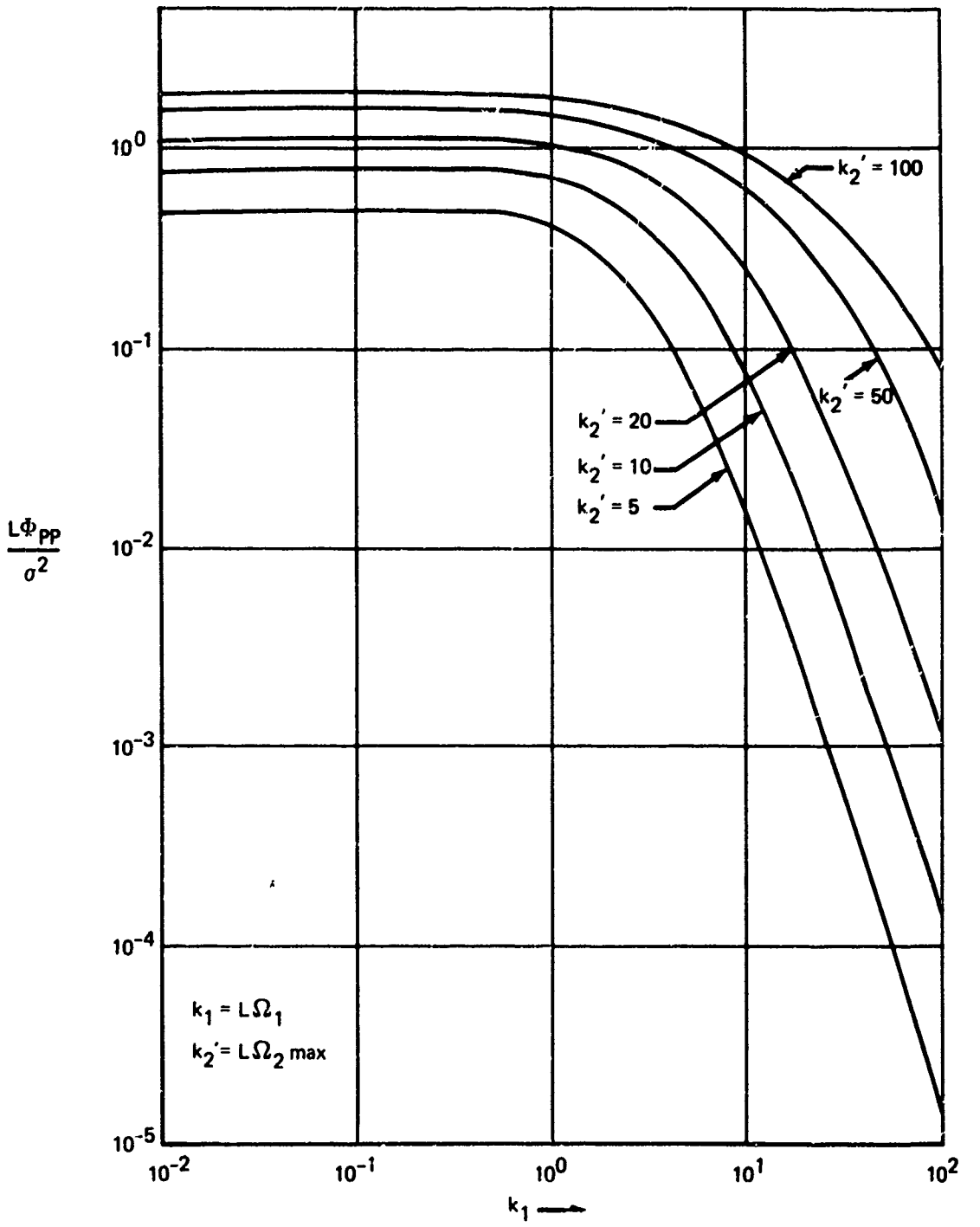

FIGURE 4-26.–EFFECTIVE TURBULENCE ROLL RATE POWER SPECTRUM (FROM REF. 12)

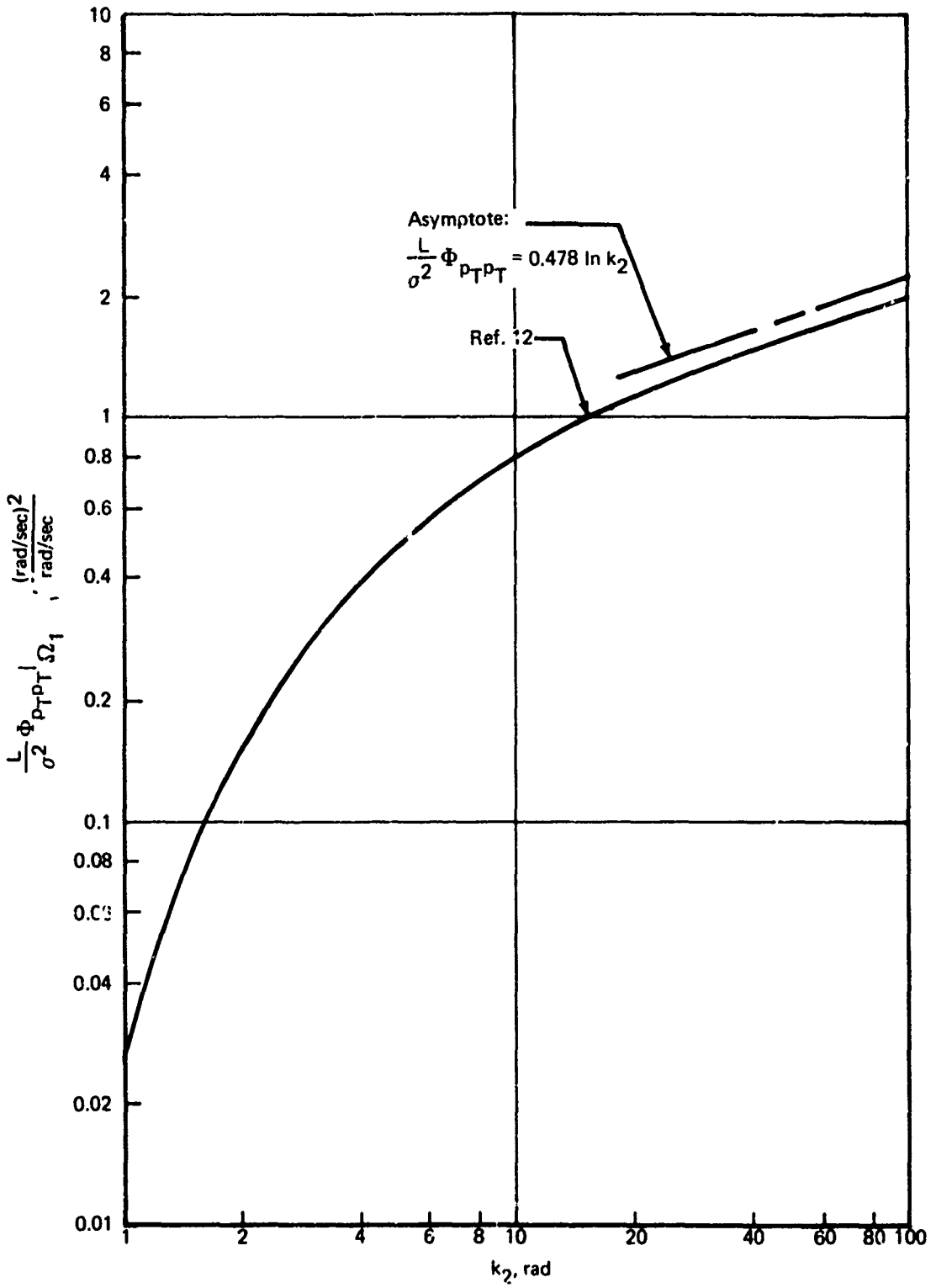

FIGURE 4-27.–EFFECTIVE TURBULENCE ROLL COMPONENT LOW FREQUENCY POWER SPECTRUM

$$\frac{b^2}{4}\frac{\Phi_p}{\Phi_v} \cong \frac{\pi}{2}\left(\frac{\sigma_w}{\sigma_v}\right)^2 \frac{b^2}{L_v L_w}$$

Assuming level flight and using the requirement of isotropy at high spacial frequencies, $L_v/L_w = (\sigma_v/\sigma_w)^3$,

$$\frac{b^2}{4}\frac{\Phi_p}{\Phi_v} = \frac{\pi}{2}\left(\frac{b}{L_w}\right)^2 \frac{1}{(\sigma_v/\sigma_w)^5}$$

At high altitudes, the integral scale of vertical turbulence will be large compared to the span and this term will be very small. At low altitudes, the vertical turbulence integral scale may be less than the span, but the ratio of the lateral to vertical turbulence rms levels will increase from one to two, and the overall effect will once again produce a small term. Thus, so long as $C_{l_{\hat{p}}}/C_{l_\beta}$ is not large, the turbulence roll rate effect will be negligible at low frequencies.

The roll damping derivative is determined by the lift distribution and the wing geometry. Speed effects occur only through compressibility effects. A reasonable number, for $C_{l_{\hat{p}}}$, from the data in Reference 4-11, is -0.4.

The dihedral effect has primarily two parts, one due to the geometric dihedral and another proportional to the lift coefficient and due to the crossflow across the fuselage. The latter term will usually dominate at low speeds. A reasonable estimate for the proportionality constant, from the data in Reference 4-11, is -0.2. Thus

$$C_{l_\beta} \cong -0.2\, C_L = \frac{-0.2\, W/S}{q}$$

For a wing load of 100 lb/ft^2, C_{l_β} will be about the same magnitude as $C_{l_{\hat{p}}}$ for a speed of about 120 knots. This ignores the geometric dihedral effects, which will tend to increase the speed at which $C_{l_{\hat{p}}} = C_{l_\beta}$.

Reduced speeds cause increased C_{l_β}. Thus, it is concluded that the roll damping term is unlikely to be greater than the dihedral effect for landing approach. Even though this conclusion is reached by some very crude analysis, it is unlikely that $C_{l_{\hat{p}}}/C_{l_\beta}$ will become sufficiently large to overcome the smallness of

$$\frac{\pi}{2}\left(\frac{b}{L_w}\right) \frac{1}{(\sigma_v/\sigma_w)^3}$$

at low frequencies.

The result is agreement that the roll rate spectrum is unlikely to have significant effects in the range of frequencies for which it is valid.

It remains to represent gust penetration. As stated, the turbulence pitch and yaw rate spectrum are given by:

$$\Phi_{qq}(\Omega_1) = \Phi_{\frac{\partial w_T}{\partial x}\frac{\partial w_T}{\partial x}} = \Omega_1^2 \Phi_w(\Omega_1)$$

$$\Phi_{qw}(\Omega_1) = \Phi_{\frac{\partial w_T}{\partial x} w_T} = i\Omega_1 \Phi_w(\Omega_1)$$

$$\Phi_{rr}(\Omega_1) = \Phi_{\frac{\partial v_T}{\partial x}\frac{\partial v_T}{\partial x}} = \Omega_1^2 \Phi_v(\Omega_1)$$

$$\Phi_{rv}(\Omega_1) = \Phi_{\frac{\partial v_T}{dx} v_T} = i\Omega_1 \Phi_v(\Omega_1)$$

These relationships are provided in Reference 4-12 but are accurate only for large wavelengths and must be attenuated for decreasing wavelengths. Rather than truncating the spectra, they will be filtered. Reference 4-1 i suggests that the unfiltered spectra are good for wavelengths greater than eight times the relevant length, based on eight straight lines providing a fair approximation to a sine wave. The filter time constant is thus

$$\frac{1}{T} = \frac{2\pi}{\lambda} = \frac{2\pi}{8\ell} = \frac{\pi}{4\ell} \quad -\text{rad/ft}$$

and the pitch and yaw rate power spectra become

$$\Phi_{qq} = \frac{\Omega_1^2}{1 + \left(\frac{4\ell\Omega_1}{\pi}\right)^2} \Phi_w(\Omega_1)$$

$$\Phi_{rr} = \frac{\Omega_1^2}{1 + \left(\frac{4\ell\Omega_1}{\pi}\right)^2} \Phi_v(\Omega_1)$$

These spectra have the same form as those in Reference 4-13 and are presented on Figure 4-28.

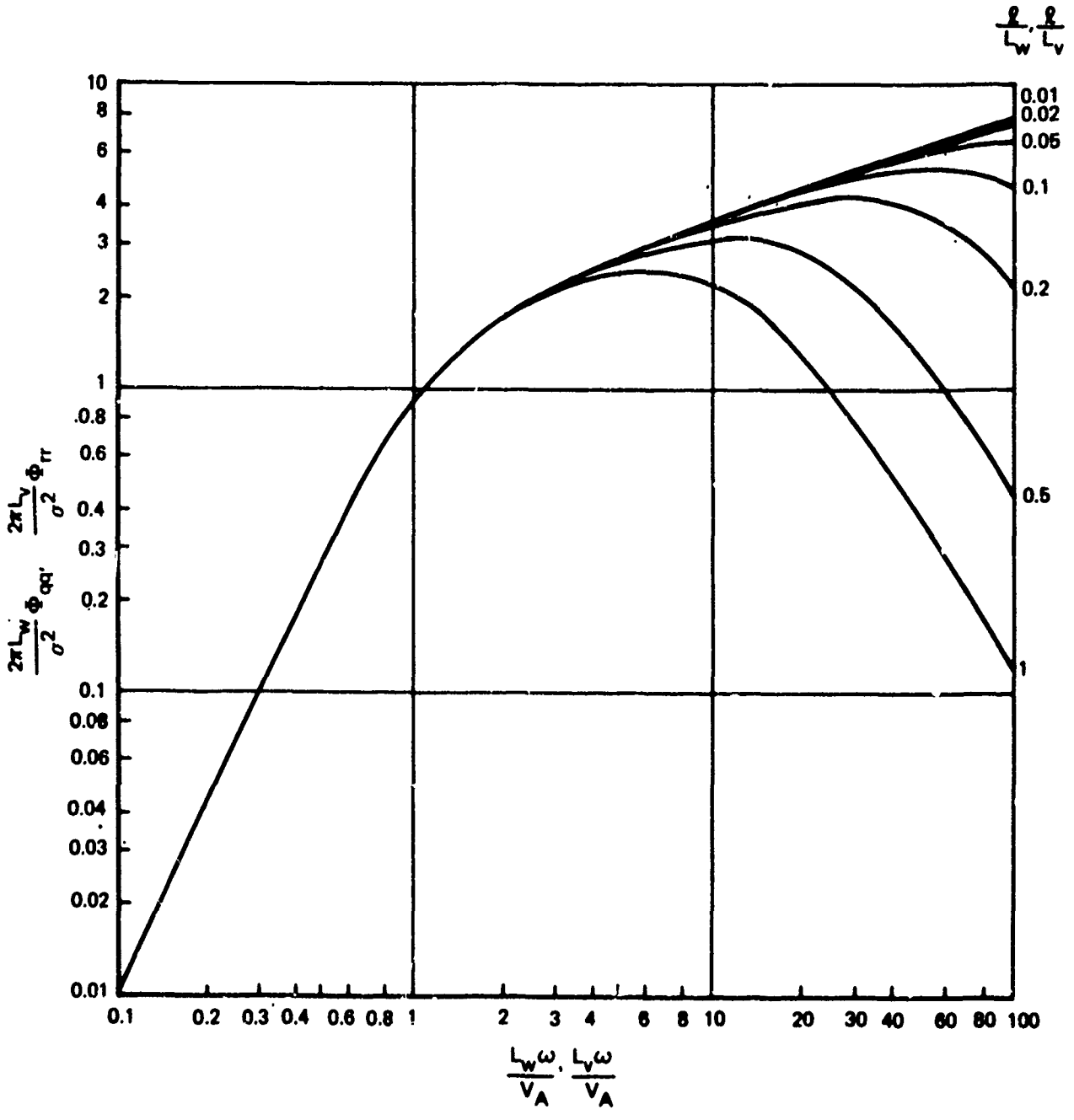

FIGURE 4-28.--TURBULENCE PITCH AND YAW RATE SPECTRA

If the linear components of turbulence are produced by a temporal process, then the correct cospectra and power spectra are produced by

$$q_T = -\frac{1}{V_A}\frac{s}{1+\frac{4\ell}{\pi V_A}s}w_T$$

$$r_T = \frac{1}{V_A}\frac{s}{1+\frac{4\ell}{\pi V_A}s}v_T$$

The time rate of change of linear turbulence velocities is similar to that of the angular velocities:

$$\dot{u}_T = \frac{\partial u_T}{\partial x}\frac{dx}{dt} = \left[\frac{s}{1+(4\ell/\pi V_A)s}\right]u_T$$

$$\dot{v}_T = \frac{\partial v_T}{\partial x}\frac{dx}{dt} = \left[\frac{s}{1+(4\ell/\pi V_A)s}\right]v_T$$

$$\dot{w}_T = \frac{\partial w_T}{\partial x}\frac{dx}{dt} = \left[\frac{s}{1+(4\ell/\pi V_A)s}\right]w_T$$

The angular turbulence velocities are combined with the angular inertial velocities to provide angular velocities of the aircraft with respect to the air mass. These in turn are used to compute the aerodynamic forces and moments. That is,

$$\Delta C_m = C_{m_q} q_A + C_{m_{\dot{\alpha}}} \dot{\alpha}_A$$

$$= C_{m_q}(q - q_T) + C_{m_{\dot{\alpha}}}(\dot{\alpha} - \dot{\alpha}_T)$$

Although the forebody has aerodynamic loads, the major contributions to forces and moments are produced by the wing and tail. Consequently, the relevant length, ℓ, should be the distance from the wing aerodynamic center to the tail aerodynamic center.

An alternate method for representing gust penetration can be developed from the panel method. Using Taylor's hypothesis, the turbulence velocity on any point on the x axis can be described in terms of the turbulence velocity at the center of gravity by:

$$\xi_x = \xi_{CG} e^{s\tau} \quad , \quad \xi = u_T, v_T, w_T$$

$$\tau = \frac{x}{V_A}$$

Where x is the distance from the aircraft, positive forward. This equation simply represents a transport lag; the turbulence velocity remains constant at a fixed point with respect to the air mass and the airplane passes that point.

The transport lag may be approximated by a series of filters, or, for digital computers, a logic statement can store previously computed turbulence velocities. To use the transport lag, the x axis of the airplane is broken into small bands with the airplane's aerodynamics concentrated at the centers of each band. The aerodynamic derivatives of each band are modified by the turbulence velocity at that point and the total forces and moments become the sum of the contributions by each band.

Generally, the distribution of aerodynamics over the length of the airplane is not available for simulation. However, separate wing-body and tail data are often available. The wing-body data may then be modified by the cg turbulence and the tail data modified by the cg turbulence velocity lagged by a time of $= \ell_T/V_A$, where ℓ_T is the distance between the cg and tail aerodynamic center. This method requires that the tail angle of attack be built up. The contribution of vertical turbulence to pitching moment by this method would be:

$$\Delta C_m \cong - \left[\left(C_{m_\alpha} \right)_{WB} \frac{w_{T_{CG}}}{V_A} - C_{L_{H_{\alpha_H}}} \bar{V}_H \left(1 - \frac{\partial \epsilon}{\partial \alpha} \right) \frac{w_{T_H}}{V_A} \right]$$

$$= - \left[\left(C_{m_\alpha} \right)_{WB} \frac{w_{T_{CG}}(t)}{V_A} - C_{L_{H_{\alpha_H}}} \bar{V}_H \left(1 - \frac{\partial \epsilon}{\partial \alpha} \right) w_{T_{CG}} \left(t - \frac{\ell_T}{V_A} \right) \right]$$

or, using Laplace transforms,

$$\Delta C_m = - \left[\left(C_{m_\alpha} \right)_{WB} - C_{L_{H_{\alpha_H}}} \bar{V}_H \left(1 - \frac{\partial \epsilon}{\partial \alpha} \right) e^{-\frac{s\ell_T}{V_A}} \right] \frac{w_{T_{CG}}}{V_A}$$

The effective airplane angle of attack is found by weighting the wing and tail angles of attack by their aerodynamic contributions:

$$\Delta C_m = -C_{m_\alpha} \frac{w_{T_e}}{V_A}$$

$$w_{T_e} = \left[\frac{\left(C_{m_\alpha}\right)_{WB}}{C_{m_\alpha}} - \frac{C_{L_{H_{\alpha_H}}} \bar{V}_H \left(1 - \frac{\partial \epsilon}{\partial \alpha}\right)}{C_{m_\alpha}} e^{-\frac{s\ell_T}{V_A}} \right] w_{T_{CG}}$$

A first order approximation to the transport lag is given by

$$e^{-\frac{s\ell_T}{V_A}} = \frac{e^{-\frac{s\ell_T}{2V_A}}}{e^{\frac{s\ell_T}{V_A}}} \cong \frac{1 - \frac{s\ell_T}{2V_A}}{1 + \frac{s\ell_T}{2V_A}}$$

The effective turbulence velocity can then be found by filtering the cg turbulence velocity:

$$w_{T_e} = \left\{ \frac{1 + \frac{s}{C_{m_\alpha}} \left[\left(C_{m_\alpha}\right)_{WB} + C_{L_{H_{\alpha_H}}} \bar{V}_H \left(1 - \frac{\partial E}{\partial \alpha}\right) \right] \frac{\ell_T}{2V_A}}{1 + \frac{s\ell_T}{2V_A}} \right\} w_{T_{CG}}$$

At low frequencies, the expression is the same as the point representation. Since the wing body pitching moment slope is generally unstable (positive), the high frequency effective turbulence velocity is amplified. This effective turbulence velocity is, however, the effective velocity for computing only pitching moment.

The transport lag method represents the wing and the tail as points. The frequency improvement for a perfect transport lag representation over point airplane representation is a factor of $2\ell_T/\bar{c}$ or is valid for

$$\Omega_1 < 0.1/\bar{c}_R$$

which may not be as good as the first order Taylor-series restriction of

$$\Omega_1 < 0.5/\ell_H$$

depending on the relative magnitude of the mean chord and the tail length. Actually, this comparison is somewhat deceiving, for the criterion was developed for lift distribution over a wing, not between wing and tail.

Additionally, the first order filter approximation to the transport lag is not perfect. If a 15° phase error is tolerable, then the first order approximation is accurate to about

$$\Omega_1 < 1.7/\ell_T$$

as can be determined from Figure 4-29. Accuracy to higher frequencies can be obtained by using higher order terms from the Pade polynomial, shown on Figure 4-29.

The two methods (transport lag and Taylor series) may be combined. The lift distribution over the wing and tail may be provided separately using the Taylor-series method. The turbulence at the cg and the tail aerodynamic center would be related by the transport lag. The tail dimensions are generally small enough that the lift distribution across the tail may be ignored. For example, the pitching moment represented by this method would be:

$$\Delta C_m = -\left[\left(C_{m_\alpha}\right)_{WB} \frac{w_{T_{CG}}}{V_A} + \left(C_{m_q}\right)_{WB} q_{T_{CG}} - C_{L_{H_{\alpha_H}}} \bar{V}_H \left(1 - \frac{\partial \epsilon}{\partial \alpha}\right) \frac{w_{T_{CG}}}{V_A} e^{-\frac{s\ell_T}{V_A}}\right]$$

This combined method is accurate for

$$\Omega_1 < 1/\bar{c}$$

and improvement over the point representation by a factor of $10\,\ell_H/\bar{c}_R$.

If 10 rad/sec is representative of the maximum frequency of interest, the simplest method providing accurate representation of gust penetration may be described in terms of the airplane's dimensions and airspeed:

$\ell_T/V_A < 0.005$	,	point representation
$\ell_T/V_A < 0.05$	,	first order Taylor series
$\bar{c}_R/V_A < 0.01$	,	transport lag
$\bar{c}_R/V_A < 0.1$	,	transport lag and first order Taylor series

For most aircraft, even the best feasible method is marginal.

4.2.1.3.4 Unsteady Aerodynamics- The lift from a surface does not change instantaneously for an instantaneous change of angle of attack. The lift growth over time is subject matter for the field of unsteady aerodynamics.

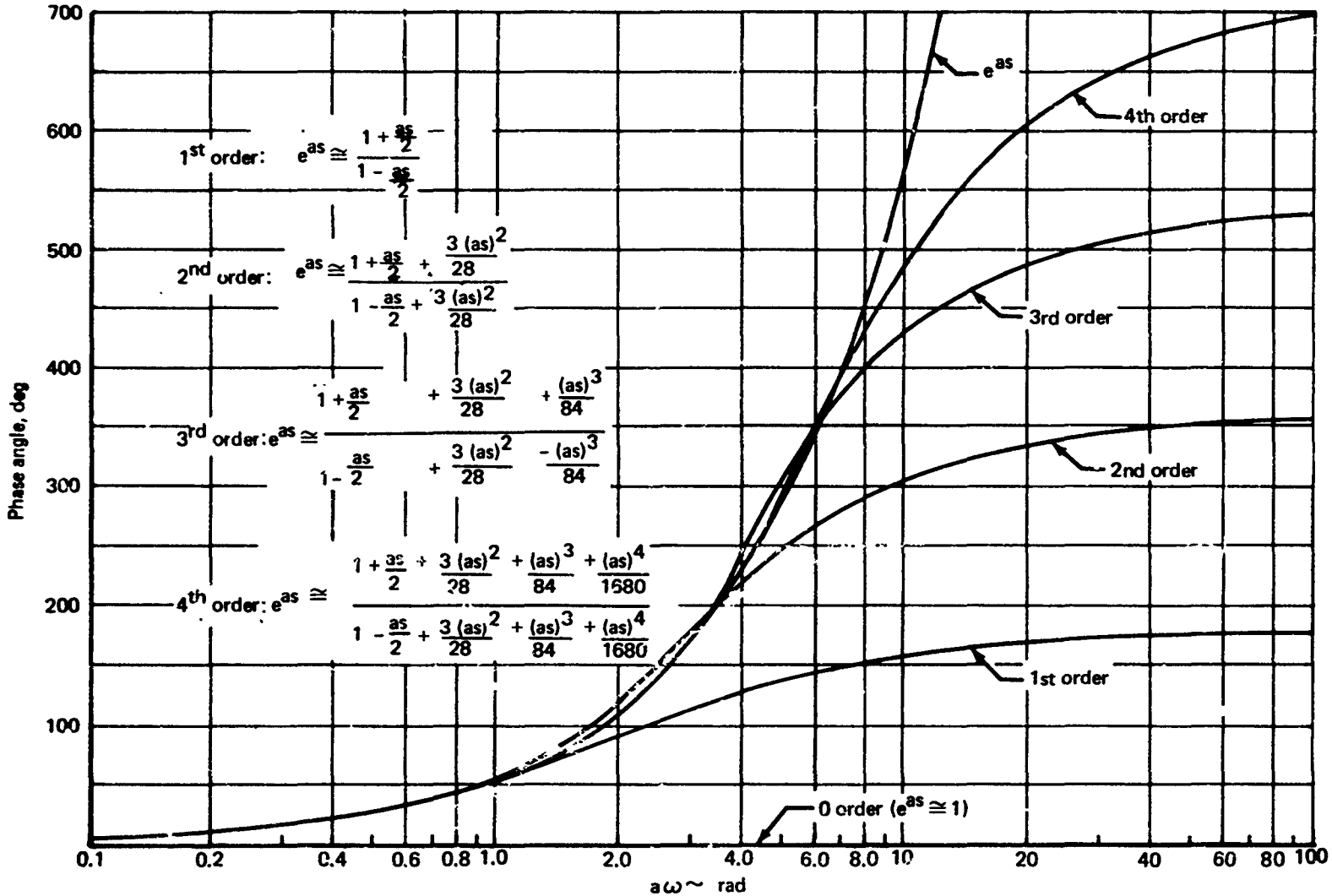

FIGURE 4-29.—TRANSPORT LEAD (LAG) APPROXIMATIONS

Rigorous representation of unsteady aerodynamics is difficult given unlimited time, and can certainly be excluded for application to real time or faster simulation. However, approximate representation for whole wings (as opposed to panels) is possible through the use of the Küssner and Wagner functions.

The need for two different functions reflects the difference in lift growth for angle of attack changes due to airplane motion and winds. Both functions are developed from two-dimensional airfoil theory and are corrected for finite wings by the lift curve slope. Wagner's and Küssner's functions for the nondimensional lift time responses $(\Delta C_L(t))/\Delta C_L(t\rightarrow\infty))$ to step changes of inertial and gust vertical velocities, respectively, are shown on Table 4-2, as taken from Reference 4-14.

The functions of Table 4-2 are for incompressible speeds. The aspect ratio is used merely to reflect the three-dimensional lift curve slope. Thus, the selection of a function should be based on lift curve slope. The normalized lift to angle of attack transfer functions have been derived from the temporal functions and are also listed on Table 4-2.

Although the Küssner and Wagner functions describe the transient lift, the normalized transfer functions may be used to filter the input. That is,

$$\Delta C_L \cong \left[\frac{C_L}{\alpha_I}(s)\right]\frac{w}{V_A} - \left[\frac{C_L}{\alpha_W}(s)\right]\frac{w_W}{V_A}$$

$W(s)$ = Wagner transfer function

$$= \frac{1}{C_{L_\alpha}}\left[\frac{C_L}{\alpha_I}(s)\right]$$

$K(s)$ = Küssner transfer function

$$= \frac{1}{C_{L_\alpha}}\left[\frac{C_L}{\alpha_W}(s)\right]$$

$$\Delta C_L = \frac{C_{L_\alpha}}{V_A}\left[wW(s) - w_W K(s)\right]$$

The Wagner function modifies the inertial vertical velocity and Küssner's function modifies the vertical component of wind. The two are modified to form the modified vertical velocity with respect to the air mass and this in turn determines lift. The same procedure can be used for nonlinear data: the modified aerodynamic angle of attack is used to enter the nonlinear tables.

As shown on Table 4-2, the lift growth functions depend on the mean aerodynamic chord and the airspeed (combined to represent the time required to travel one semichord), as well

TABLE 4-2.–LIFT GROWTH FUNCTIONS FOR MACH = 0

AR	$(C_{L_\alpha})_{WING}$	Wagner's function (inertial α)	Küssner's function (gust α)
Indicial admittances (from ref. 14)			
3	1.2π	$1 - 0.283e^{-0.54\ t/t^*}$	$1 - 0.679e^{-0.558\ t/t^*} - 0.227e^{-3.2\ t/t^*}$
6	1.5π	$1 - 0.361e^{-0.381\ t/t^*}$	$1 - 0.448e^{-0.29\ t/t^*} - 0.272e^{-0.725\ t/t^*} - 0.193e^{-3\ t/t^*}$
∞	2π	$1 - 0.165e^{-0.0455\ t/t^*} - 0.335e^{-0.3\ t/t^*}$	$1 - 0.5e^{-0.13\ t/t^*} - 0.5e^{-t/t^*}$
Approximate transfer functions $\frac{1}{(C_{L_\alpha})_{ss}} \frac{C_L}{\alpha}(s)$			
3	1.2π	$\frac{0.7\ (s + 0.754/t^*)}{s + 0.54/t^*}$	$\frac{0.094\ (s + 1.34/t^*)\ (s + 14.176/t^*)}{(s + 0.558/t^*)\ (s + 3.2/t^*)}$
6	1.5π	$\frac{0.639\ (s + 0.596/t^*)}{s + 0.381/t^*}$	$\frac{0.087\ (s + 0.43/t^*)\ (s + 1.35/t^*)\ (s + 12.5/t^*)}{(s + 0.29/t^*)\ (s + 0.725/t^*)\ (s + 3/t^*)}$
∞	2π	$\frac{0.533\ (s + 0.05374/t^*)\ (s + 0.5078/t^*)}{(s + 0.0455/t^*)\ (s + 0.3/t^*)}$	$\frac{0.565/t^*\ (s + 0.23/t^*)}{(s + 0.13/t^*)\ (s + 1/t^*)}$

$t^* = \frac{\bar{c}}{2V_A}$

as the lift curve slope. The wing and tail have different chords, so there are different functions for the wing and the two tails. Consequently, use of the lift growth functions requires separate wing (or wing-body) and tail aerodynamics and the buildup of tail angle of attack (or sideslip angle).

Angle of attack is not the only term that must be modified: pitch rate, roll rate, yaw rate, and sideslip derivatives have contributions due to the angle of attack and sideslip angle distribution over the wing and tail and can be modified in the same manner as angle of attack.

Representation of the unsteady aerodynamics has the effect of extending the frequency to which the effects of turbulence are accurately represented. Reference 4-7 states that using unsteady aerodynamics with the first order Taylor-series representation of gust penetration extends the maximum frequency at which total lift is correctly represented by one decade. The Küssner and Wagner functions only approximate unsteady effects, and the improvement is likely to be somewhat less.

Above some frequency, the Küssner and Wagner functions are likely to give erroneous answers, no matter what distributed lift effects of turbulence are used. Each panel, or region of the wing, will have unsteady aerodynamic characteristics different from those of other panels and different from the Küssner-Wagner functions. Although using the same lift growth functions for each panel may give correct effects on airplane center of gravity motion, only by coincidence will the effects on high frequency structural modes be correct.

Although approximating unsteady aerodynamics increases the frequency at which the aerodynamic representation is valid, it remains to be determined whether that frequency improvement is necessary.

The amplitude frequency response asymptotes of the lift growth transfer functions are plotted on Figure 4-30. The frequency at which attenuation of the lift response begins is proportional to the airspeed to mean chord ratio and is reduced by an increasing lift curve slope. Greater attenuation of the lift due to gust occurs at the higher frequencies. For an aspect ratio of 6 ($C_{L_\alpha} = 1.5\pi$), attenuation begins at

$$\omega = 0.6V_A/\bar{c}$$

If 10 rad/sec is representative of the maximum frequency of interest, lift growth effects are insignificant for

$$V_A/\bar{c} > 16.7$$

If an airplane has a 15-foot mean chord, lift growth representation is unnecessary for approach speeds above about 150 knots. Lift growth effects become more significant at lower altitudes due to the possible decrease in the maximum frequency of interest, caused by the decreasing integral scales.

For many types of aircraft, whether or not to include lift growth effects is likely a marginal decision. For the Boeing 747, attenuation is expected to begin at about $\omega = 5.2$ rad/sec or

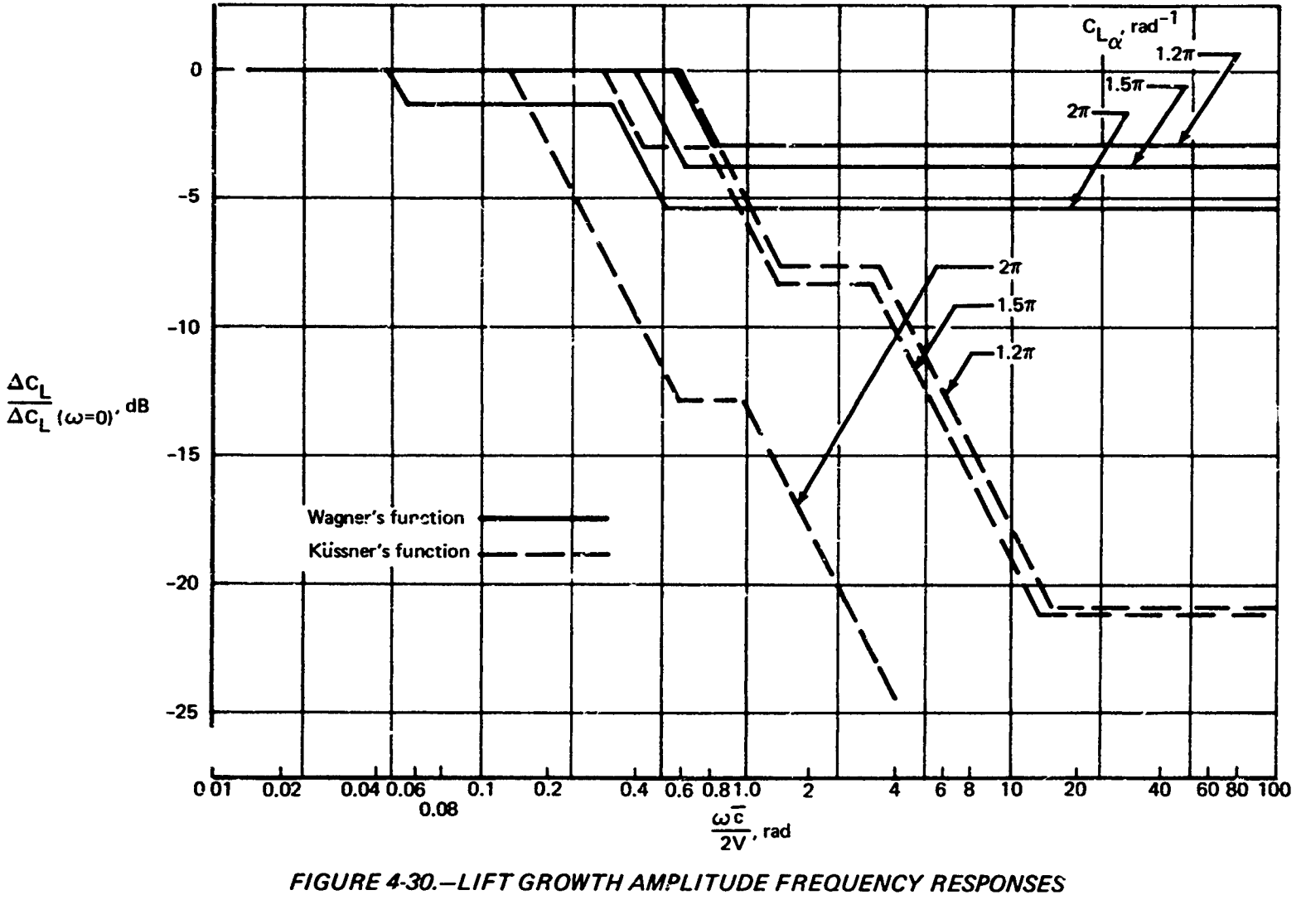

FIGURE 4-30.—LIFT GROWTH AMPLITUDE FREQUENCY RESPONSES

Ω_1 = 0.02 rad/ft. For the Boeing SST, a delta wing aircraft with an unusually large chord, the frequency is about $\omega = 4$ rad/sec or $\Omega_1 = 0.016$ rad/ft. For a commercial STOL configuration, the frequencies are $\omega = 4.7$ rad/sec or $\Omega_1 = 0.035$. Although these aircraft are radically different, their frequencies for the onset of lift growth attenuation are not dissimilar, reflecting tendency of large mean chords and low lift curve slopes to be associated with high approach speeds.

It is concluded that lift growth should be included for the wing unless analysis reveals its effects to be negligible. Lift growth need not be included for tail aerodynamics. Although the inclusion of lift growth attenuates wing lift, it cannot be concluded that excluding lift growth is conservative, for that conclusion depends on the phase between wing and tail terms. A reasonable representation of lift growth may be based on Figure 4-30, interpolating the asymptotes using the lift curve slope.

4.2.1.3.5 Effects of Speed and Altitude–The power spectra of the linear components of turbulence in terms of temporal frequency are found by requiring the variances for the spacial temporal frequency description to be the same:

$$\sigma^2 = \int_{-\infty}^{\infty} \Phi(\Omega_1)\, d\Omega_1 = \frac{1}{V_A} \int_{-\infty}^{\infty} \Phi\left(\frac{\omega}{V_A}\right) d\omega$$

$$= \int_{-\infty}^{\infty} \Phi'(\omega)\, d\omega$$

$$\Phi'(\omega) = \frac{1}{V_A} \Phi\left(\Omega_1 = \frac{\omega}{V_A}\right)$$

The temporal frequency power spectra, normalized by the variances, are described in terms of the temporal frequency and the ratio of airspeed to integral scale (V_A/L). For landing approach, changes of the integral scale are dominated by changes of altitude. If the aircraft's response to gust input transfer functions is independent of altitude (reasonable, except for ground effects) and unaltered by airspeed changes (not true), then the parameters altering a given aircraft configuration to linear turbulence components of a given level are airspeed and altitude.

One comment consistently received from pilots concerning the nature of turbulence is that the level of turbulence appears to diminish rapidly as the ground is approached (Ref. 4-15). The description of turbulence provides for turbulence variances that increase as altitude decreases; thus, the answer must rely to some extent on the effects of speed and scale.

The effects of the speed and integral scale on the normalized power spectra are shown on Figure 4-31. Increasing speed and decreasing scale cause reduced low frequency power and increased high frequency power. That is, power is removed from the frequencies of rigid body response and added to the frequencies of structural mode response. This is perhaps

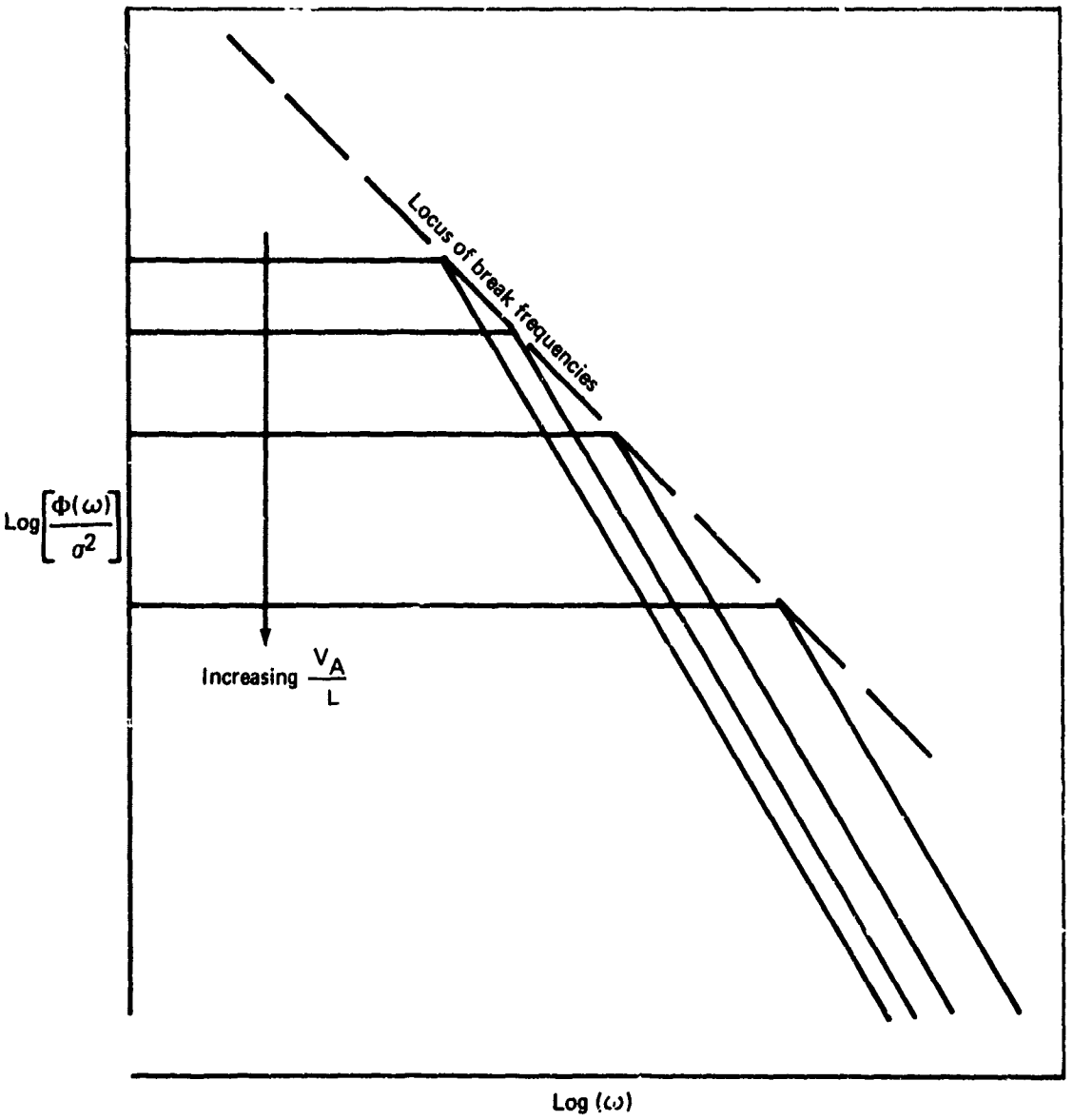

FIGURE 4-31.–SPECTRUM ASYMPTOTES, EFFECT OF SPEED AND SCALE

more evident on Figure 4-32 where the variance density is plotted. The variance remains constant but is concentrated at higher frequencies as the airspeed to scale ratio is increased. Figure 4-32 demonstrates why it is unlikely that flightpath controllability and structural fatigue or ride qualities due to turbulence would be critical at the same flight condition.

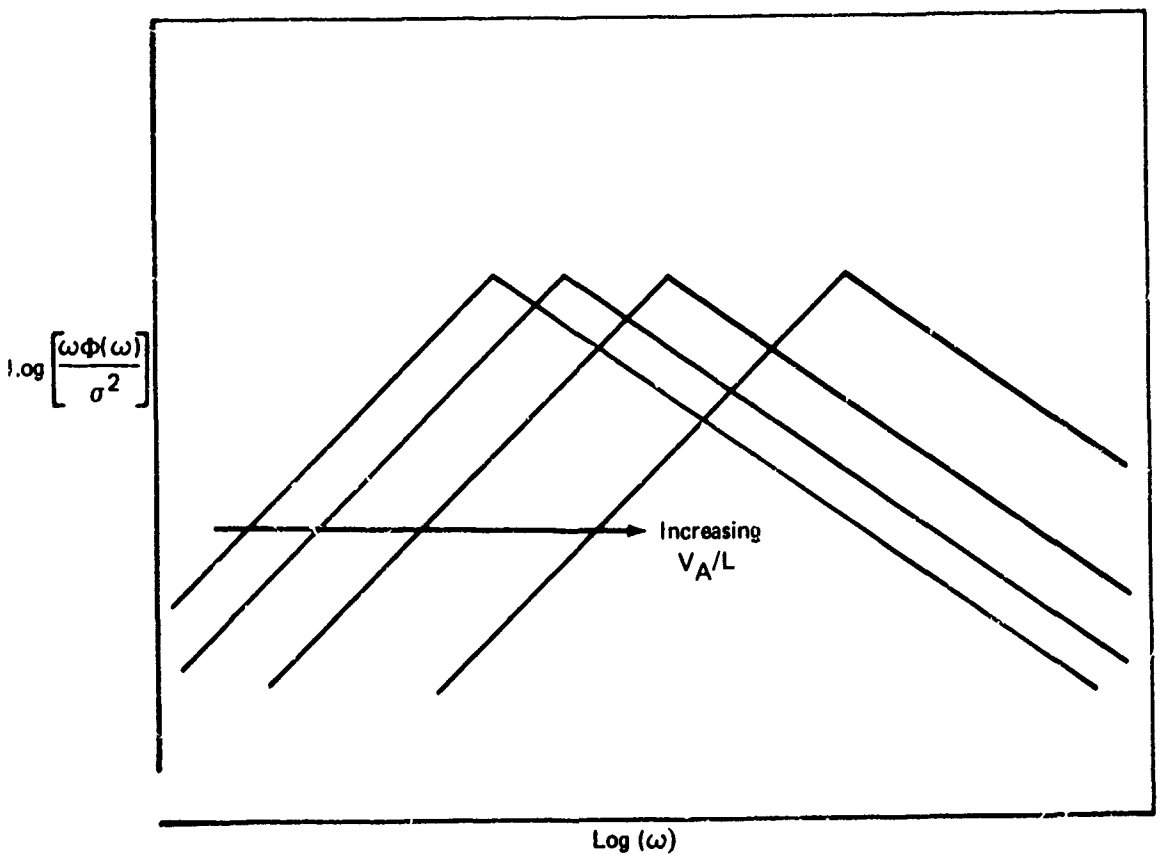

FIGURE 4-32.—VARIANCE DENSITY ASYMPTOTES, EFFECT OF SPEED AND SCALE

The apparent decrease of turbulence as the ground is approached is caused by the decrease of integral scale, which shifts turbulence power to frequencies beyond those at which the airplane responds. The same effect occurs when airspeed is increased. Landing approach, as the lowest airspeed condition, tends to be the most critical for controlling airplane motion in turbulence, not only because the task requires greater precision, but also because the response of airplane motion to gusts tends to be greatest there.

The discussions about transferring power from the rigid body to the structural mode frequencies can, to some extent, be extended to transferring power to different types of rigid body motion. When power is centered about the short period/Dutch roll frequencies, dominant motion consists of angular and vertical velocities. Lower speeds and longer scales cause greater speed and linear and angular displacement responses. For conventional aircraft,

the primary concern is with the control of attitude, through which flight path is maintained. For STOL aircraft, attitude is insufficient to control lateral and longitudinal position.

The variance density for the turbulence angular components is somewhat different, as shown on Figure 4-33. Increasing airspeed shifts the spectra to higher frequencies as before, but the high pass filtering due to the spacial frequency derivative of turbulence used to form the effective angular velocities causes the low frequency character to remain scale length invariant. Increasing the integral scale has the effect of increasing angular velocity variance. After the integral scale becomes large enough with respect to the aircraft's dimensions, the increase of variance is accompanied by a decrease in low frequency power, or a decrease of effect on airplane motion.

Generally, shifting the turbulence spectra to lower frequencies increases the severity of aircraft rigid body (or perhaps more correctly, quasi-static elastic) motion until turbulence power begins to fall below the frequency range of interest, as may occur with extremely large integral scales. Turbulence level (rms or variance) is an insufficient measure of the severity of turbulence unless speed and scale are held constant. At sufficiently high speeds or short scales, the rigid body motion feels only the constant low frequency asymptote on Figure 4-31, and it may be sufficient to represent turbulence with unfiltered noise having the correct low frequency spectrum amplitude but with an infinite variance. It is unfortunate that there is so much difficulty in measuring and so little agreement on the character of the integral scales when their values are so significant for the aircraft's motion.

The effects of speed are made more complex by the variations of the gust transfer functions with speed. If the approximate expressions for longitudinal characteristic motion are expressed in terms of the nondimensional stability derivatives so as to separate out the explicit dependence of airspeed, it can be shown that, assuming the nondimensional derivatives are speed invariant, characteristic motion varies with speed as:

$$\omega_{sp} \sim u_0 \qquad \zeta_{sp} \qquad \text{speed invariant}$$

$$\omega_{ph} \sim \frac{1}{\sqrt{u_0}} \qquad \zeta_{ph} \sim u_0^{3/2}$$

Reducing speed reduces the short period natural frequency, increases phugoid natural frequency, and decreases phugoid damping. Consequently, unaugmented STOL aircraft are more likely to have coupled short period-phugoid motion. Furthermore, because the output spectra are very sensitive to changes of damping ratio for low damping ratios, STOL responses to turbulence may be dominated by the phugoid. Automatic control systems can reduce (or amplify) much of this effect. For one STOL configuration examined by Boeing, phugoid damping augmentation (speed feedback to thrust/drag devices) reduced the rms normal acceleration for a fixed level of turbulence by 30%. For conventional aircraft, the phugoid is assumed to have so little influence on normal acceleration that two-degree-of-freedom analysis is used.

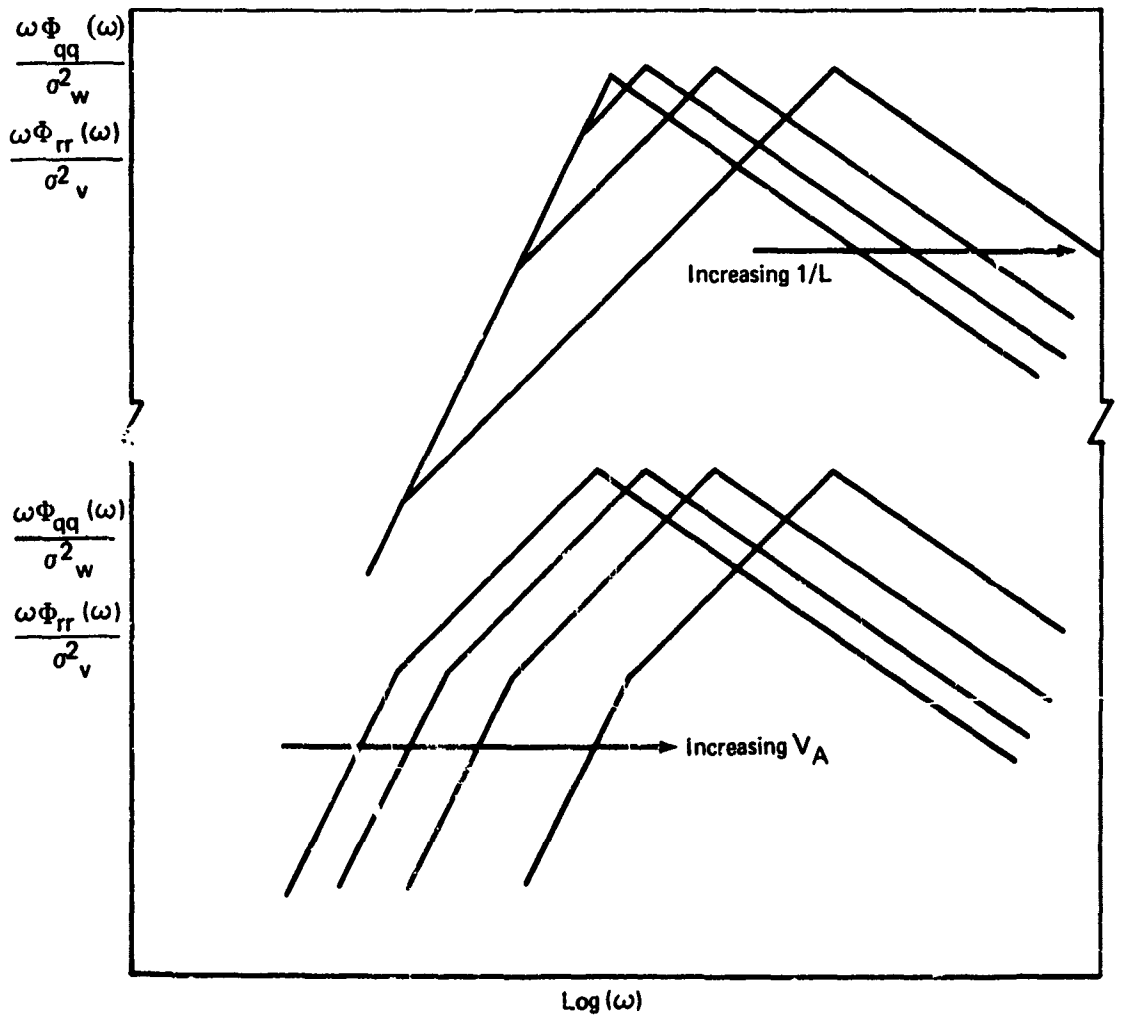

FIGURE 4-33.–TURBULENCE ANGULAR COMPONENTS, EFFECT OF SPEED AND SCALE

The effects of speed on the gust transfer functions are by no means restricted to the characteristic motion. The high frequency asymptotes of the normal acceleration to vertical and horizontal gust transfer functions are given by

$$\left.\frac{n_z}{u_T}\right|_{\omega \to \infty} = z_u = -\left[\frac{2}{u_0} + \frac{C_{L_{\hat{u}}}\rho u_0}{2(W/S)}\right]$$

$$\left.\frac{n_z}{w_T}\right|_{\omega \to \infty} = z_w = -\frac{\rho u_0}{2(W/S)}\left(C_{L_\alpha} + C_{D_0}\right)$$

The shapes of both transfer functions, Figure 4-34, are similar. For conventional aircraft, $C_{L_{\hat{u}}}$ can be expected to be negligible, and for the approach speeds of conventional commercial aircraft, $2/u_0$ is small; thus, the load factor spectrum is represented only by that produced by vertical gusts.

For two-degree-of-freedom approximation (drop longitudinal force equation and inertial speed degree of freedom, but not longitudinal gust forcing function), the variation of the load factor to gust frequency response for a STOL configuration with speed is shown on Figure 4-35. When combined with the vertical turbulence spectrum, the contribution of vertical gusts to the load factor spectrum becomes that on Figure 4-36.

The increase of the load factor to longitudinal gust frequency response is shown on Figure 4-37 and the contribution of the longitudinal gust to the load factor power spectrum is shown on Figure 4-38.

The combined load factor spectrum (the sum of the spectra due to vertical and longitudinal turbulence) is shown on Figure 4-39. By comparing Figure 4-39 to Figure 4-36, it is evident that at low speeds the load factor spectrum is not adequately represented by just the contribution of vertical turbulence, and that at sufficiently low speeds the contribution of the longitudinal turbulence will dominate. A three-degree-of-freedom analysis of the same configuration (including damping effects; asymptotes shown on Figures 4-35 through 4-39) revealed a minimum rigid body motion load factor variance at about 95 knots. For the speeds and integral scales considered, the rigid body contribution to normal acceleration dominates the structural modes contribution.

The power spectrum of rate of sink may be obtained by dividing the load factor spectrum by the square of frequency and is shown on Figure 4-40. The effect of speed is seen to be even more pronounced. If the flight path angle is more relevant than rate of sink, speed effects are even stronger, as shown on Figure 4-41.

The conclusion that can be drawn from this analysis is that representation of only the vertical component of turbulence for landing approach speeds is insufficient, even if concern is only with short period vertical motion. For STOL approach speeds, the use of feedbacks to direct lift control devices to attenuate or control the responses to turbulence is likely to

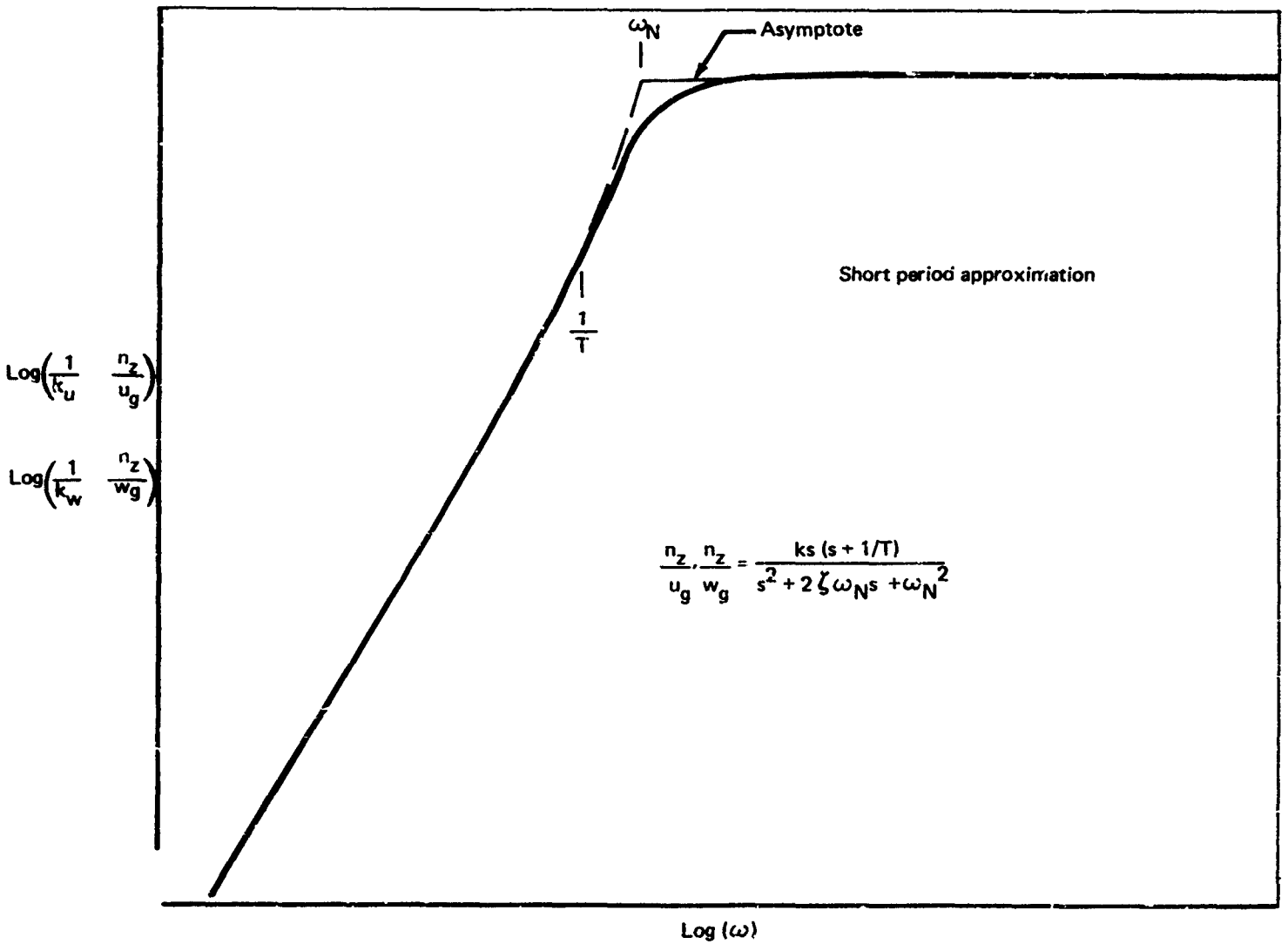

FIGURE 4-34.—LOAD FACTOR TO GUST FREQUENCY RESPONSE

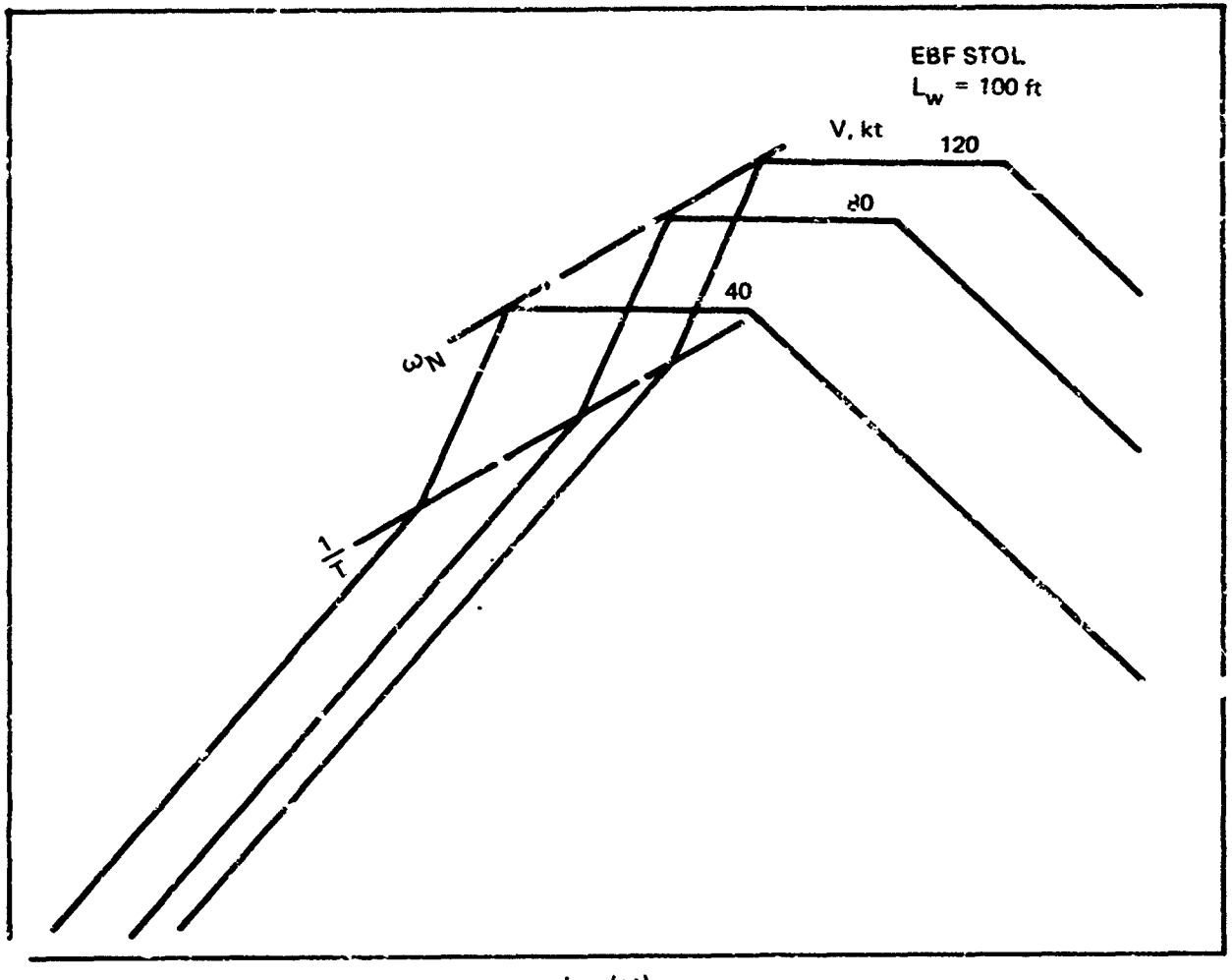

FIGURE 4-35.—NORMAL LOAD FACTOR P.S.D. DUE TO w_g EFFECT OF SPEED

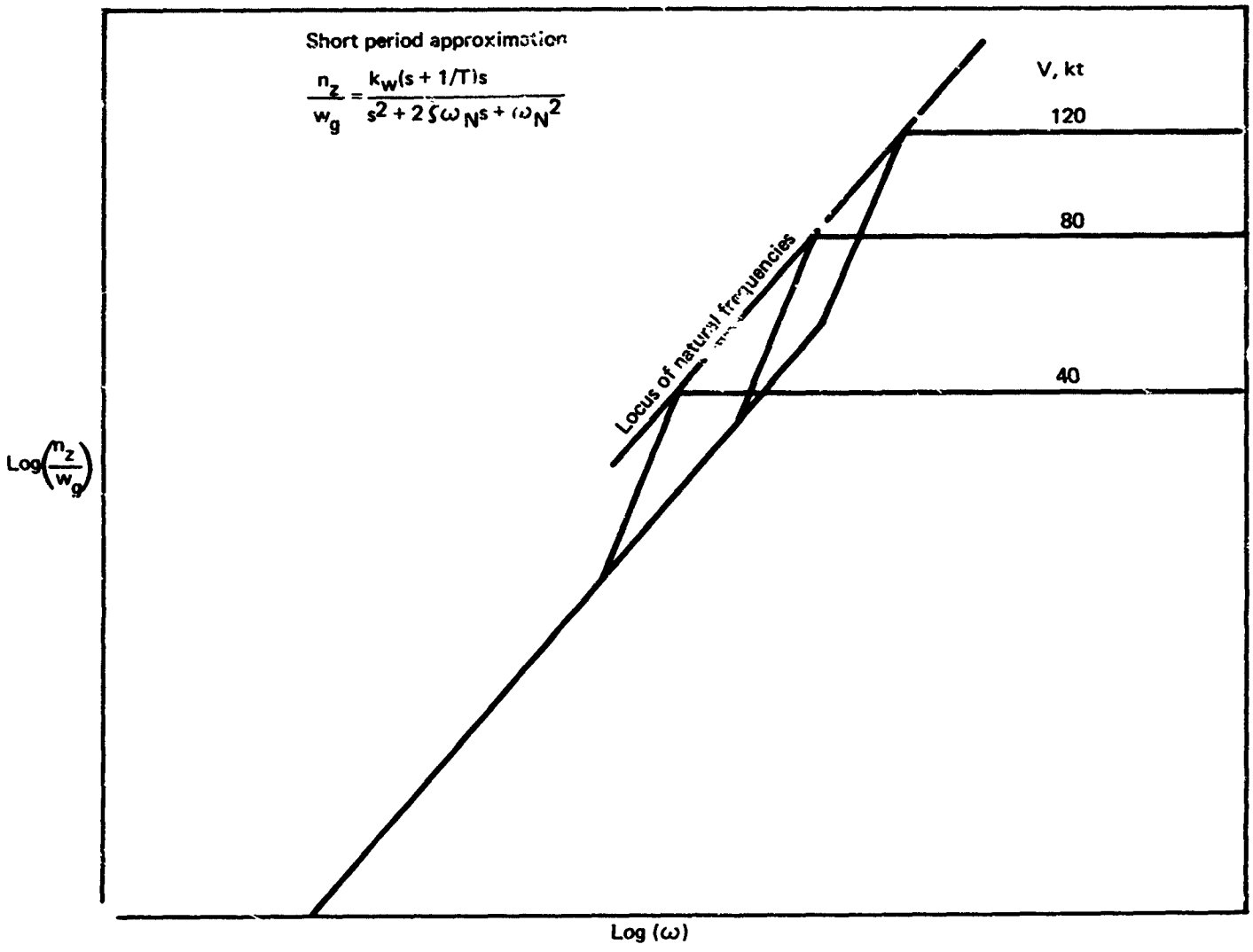

FIGURE 4-36.—LOAD FACTOR RESPONSE TO VERTICAL GUST, EFFECT OF SPEED

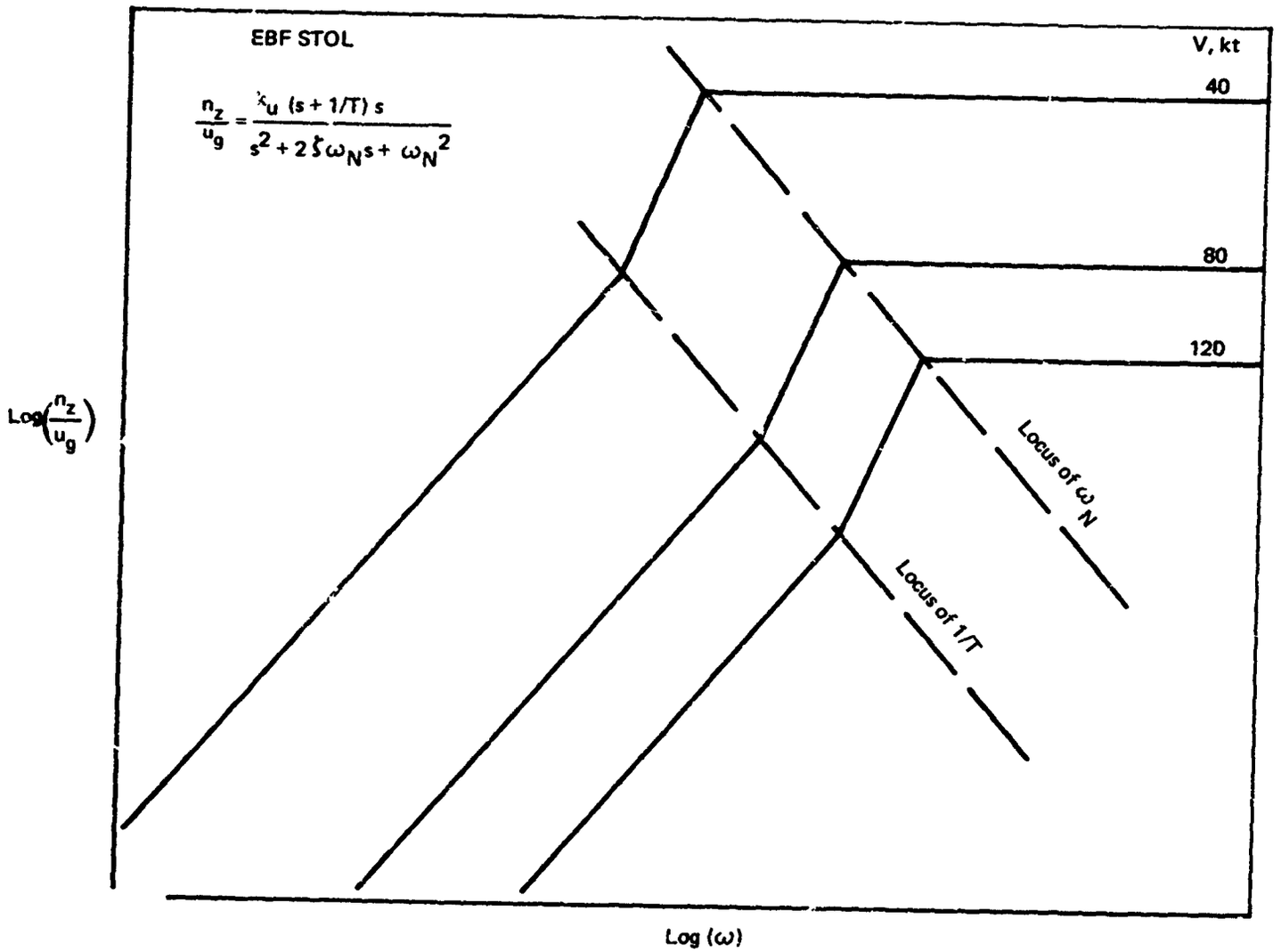

FIGURE 4-37.–LOAD FACTOR RESPONSE TO LONGITUDINAL GUST, EFFECT OF SPEED

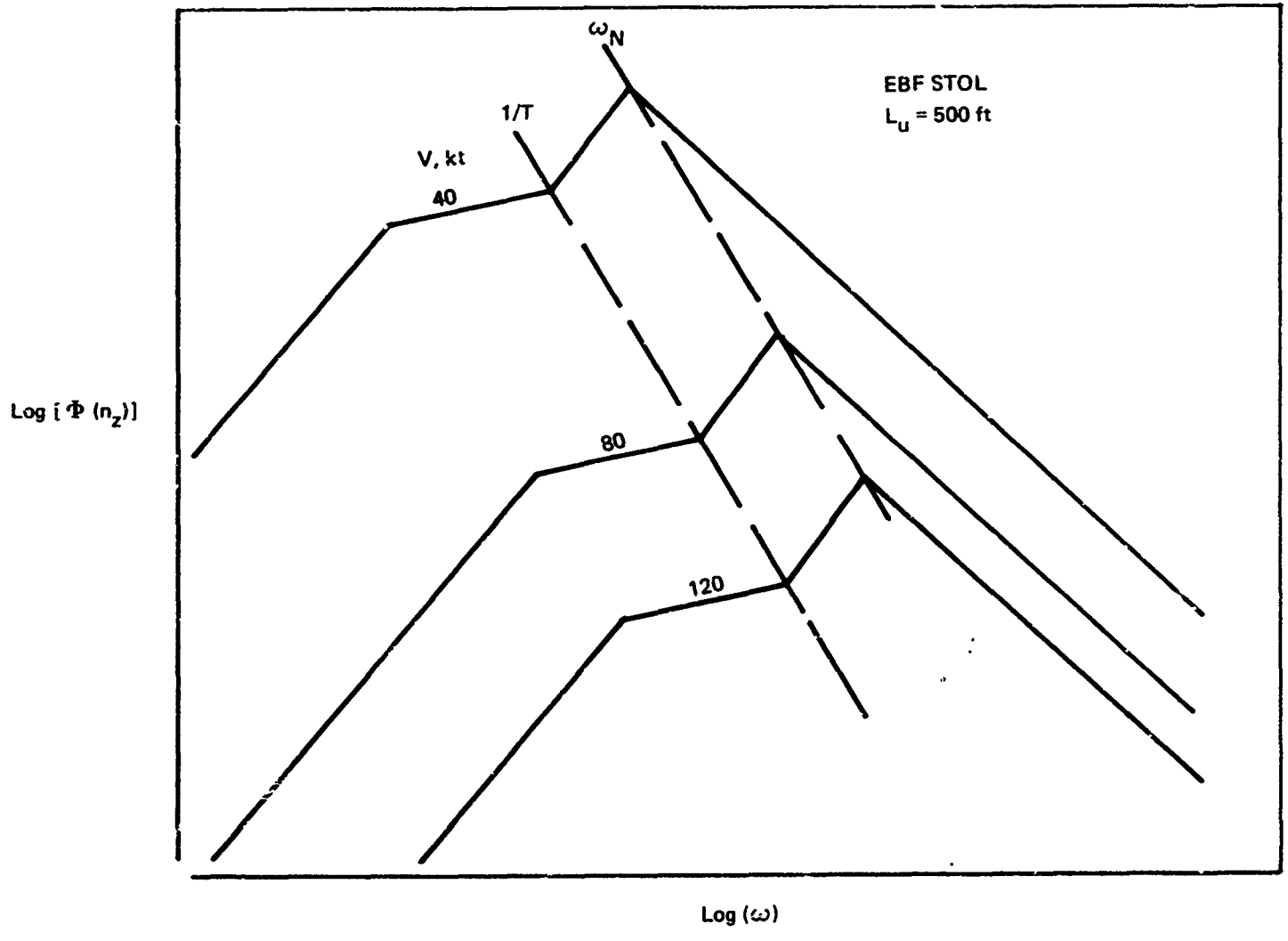

FIGURE 4-33.–NORMAL LOAD FACTOR P.S.D. DUE TO u_g, EFFECT OF SPEED

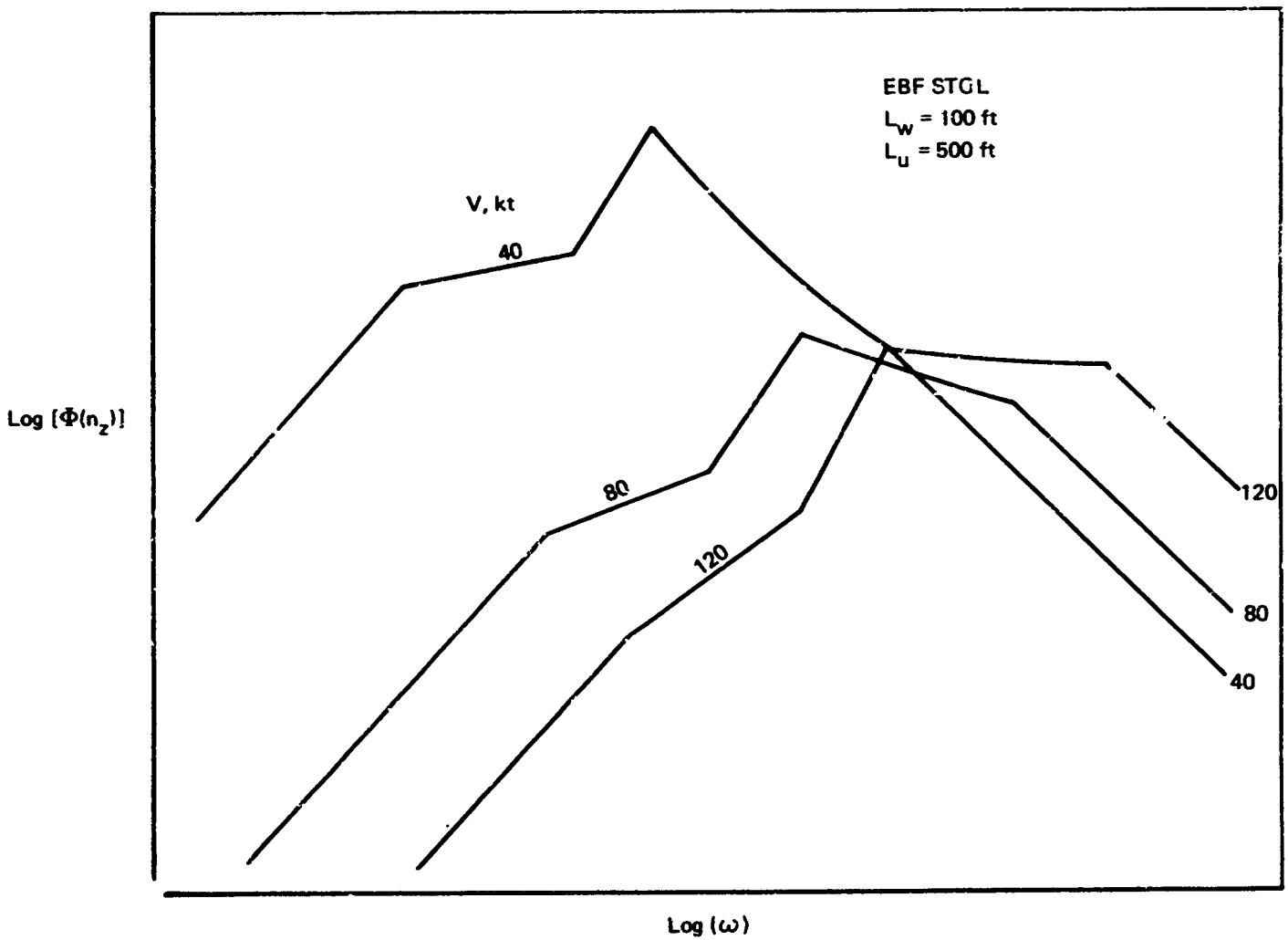

FIGURE 4-39.–NORMAL LOAD FACTOR P.S.D. DUE TO u_g AND w_g. EFFECT OF SPEED

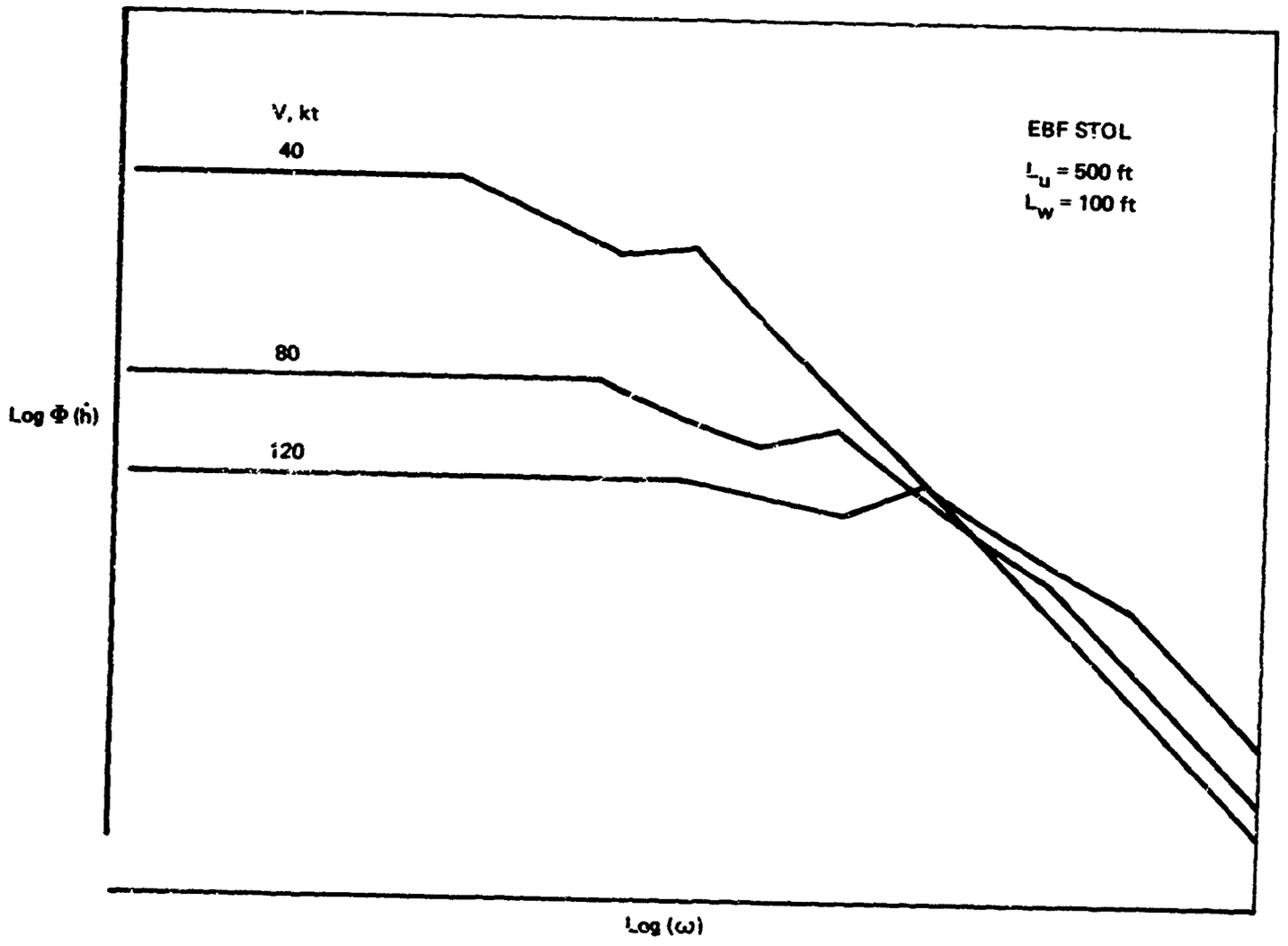

FIGURE 4-40.–POWER SPECTRUM OF ALTITUDE RATE OF CHANGE DUE TO TURBULENCE, EFFECT OF SPEED

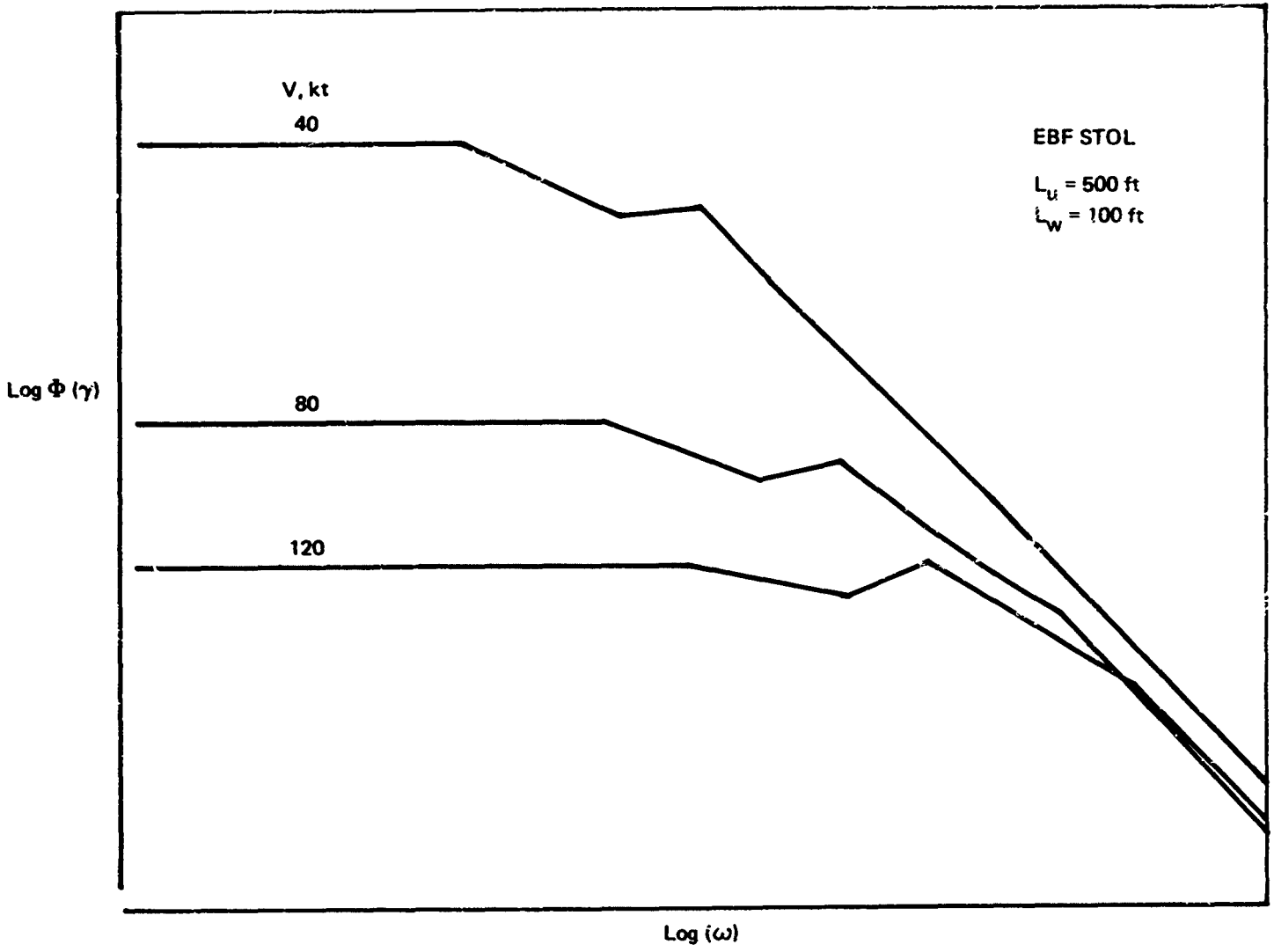

FIGURE 4-41.–FREQUENCY RESPONSE OF FLIGHT PATH ATTITUDE DUE TO TURBULENCE, EFFECT OF SPEED

be ineffective as it would not alter the responses to longitudinal turbulence. For the same reason, wing loading effects may be insignificant. For powered lift STOL configurations, speed feedbacks to thrust or thrust vectoring, providing augmentation of speed derivatives, may be more effective.

4.2.2 Large Disturbance Effects of Winds

Topics that fall under the heading "large disturbance motion effects" essentially consist of all those which violate the assumptions of small disturbance analysis. Some categories are:

1) *Nonlinearities of the equations of motion.* The trends predicted by linear analysis are generally not violated by equations of motion nonlinearities, but reasonable predictions of magnitudes often require that the nonlinear equations be evaluated semiempirically (such as by simulation).

2) *Aerodynamic nonlinearities.* The most significant aerodynamic nonlinearities have been associated with angle of attack variations, particularly C_{D_α} (backside/frontside of the thrust required curve), static stability, stall, control effectiveness, and loss of directional stability at high angles of attack. Particular emphasis has been placed on stall margins required when flying in turbulence. It is not necessary that turbulence be prevented instantaneously from causing the stall angle of attack to be exceeded; rather, it must not be exceeded long enough to affect airplane inertial motion. For powered lift STOL aircraft, strong nonlinearities of aerodynamics with speed are introduced. Ground effects represent an additional important class of aerodynamic nonlinearities.

3) *Coupled motion.* Many aspects of coupled motion may be evaluated by linear analysis, but because of the large number of simultaneous equations, it is difficult to describe response characteristics in parametric form. Dynamically coupled motion problems tend to be specialized, without wide application, and require analytic tools of greater flexibility than are often available for easy use. Hence, the problems are often treated as a large disturbance problem. Dropping the assumption of wings initially level coupled the longitudinal and lateral-directional motion. Lateral-directional forces and moments frequently have non-zero variations with angle of attack. Coupling may be introduced by the multiple use of a control surface for longitudinal and lateral-directional control. Perhaps the greatest coupling is introduced by the pilot, whose action may also be highly nonlinear.

4) *Control system nonlinearities.* Nonlinearities in the control system may either be inherent or intended and are found in the electrical, mechanical, and hydraulic subsystems. These nonlinearities take the form of hysteresis, breakouts, dead zones, authority limits, switching circuits, and gain changes. Many of the nonlinearities are designed into the system for failure protection. Hydraulic-actuator systems have particularly strong nonlinearities that cannot be overcome for linear analysis, particularly when pump flow limits are exceeded and line pressure falls. Hydraulic system design for sufficient control in turbulence is developing as a major simulation task, particularly for supersonic aircraft, STOL

aircraft, and aircraft with flight-critical augmentation systems. When high control surface hinge moments (large actuator bores) combine with high control system rate requirements, as results when dynamic pressure is low or an augmentation system is employed, large hydraulic systems result. Small amounts of overdesign result in large weight penalties, and underdesign may result as loss of system pressure and control power.

5) *Large altitude excursions.* Large variations of altitude cause considerable variation of the mean wind magnitude and shears, turbulence scales, and turbulence levels. Airplane motion over large excursions, particularly airplane position, depends on the past history of airplane motion and cannot be accurately measured using constant wind shears and fixed-gain turbulence filters.

The differences between the small and large disturbance (or linear and nonlinear) responses are what gives rise to the need for simulation.

One particular subject under (5) relevant to autoland systems has received particular attention and is involved in substantial controversy: The effects of mean winds and mean wind shear on touchdown dispersion. Reference 4-16 conducts an analysis that shows a headwind that decreases as the ground is approached causes the touchdown point to be long. Reference 4-6 notes that "... there is a lack of agreement as to what actually takes place during an approach to landing in a headwind that is decreasing with altitude. According to Reference ... an airplane trimmed for a glide at constant airspeed and constant altitude would touch down short of the initial aim point if no control action is taken by the pilot." In contrast, Reference 4-17 asserts that "a trimmed airplane executing an instrument approach in decreasing headwind would overshoot the intended point of touchdown unless the pilot reduces power." The conclusion of the analysis in Reference 4-6 is that "... an undershoot will occur if in a wind shear the airspeed, angle of attack, and throttle setting are kept the same. If on the other hand, the pilot changes the throttle and control settings so that the airspeed, angle of attack, and pitch attitude are the same as in the steady wind, an overshoot takes place."

Reference 4-17 is also up to taking other authors to task: "....certain rules are established which supposedly tell a pilot whether he will overshoot or undershoot in a particular wind shear situation. These rules, which may be correct for certain special circumstances, are not correct for the typically long term wind shears which occur more frequently. Most papers available to pilots concerning wind shear have expressed as a rule that an aircraft will undershoot the runway and have a deficiency in thrust if a decreasing headwind shear is encountered on approach. However, any pilot who has ever flown an ILS with a strong headwind knows it takes a great deal more thrust to fly the glidepath than with no wind. Then it would appear that if a shear to no wind condition should occur, there would be an excess of thrust." The procedure recommended by Reference 4-17 is: 'As the pilot advances the thrust to the required level to compensate for the rate of wind shear he must begin a gradual reduction in thrust to compensate for the changing flight path angle."

With so much conflicting information, one begins to wonder what is going on. Can there really be that many well-published authors who have performed erroneous analyses?

First, it may be concluded that if the required thrust level increases and if the thrust provided is less than that required, the aircraft will tend to undershoot the glideslope and land short. Providing excessive thrust will tend to cause the airplane to land long. The problem reduces to computing the required thrust and then comparing that to the available thrust. Statically, the change of thrust requirements may be determined from the approximate relationship derived in appendix A:

$$\theta \cong \left[1 + \frac{\bar{V}_W \cos(\psi - \bar{\psi}_W)}{V_A}\right]\gamma + \alpha$$

The term $\bar{V}_W \cos(\psi - \bar{\psi}_W)$ is just the horizontal component of wind in the direction of the airplane's orientation. If only wind aligned to the airplane's heading is considered, with $\bar{V}_W > 0$ referring to a tailwind, a tailwind will require a more nose-down pitch attitude and a headwind will require a more nose-up pitch attitude than for still air at the same airspeed. If no attitude or thrust correction is made, a steady tailwind will cause an overshoot, and a steady headwind, as noted in Reference 4-6, will cause an undershoot. The change of pitch attitude at constant airspeed and glideslope is

$$\Delta\theta = \theta_2 - \theta_1 \cong \left[\frac{\bar{V}_{W_2} - \bar{V}_{W_1}}{V_A}\right]\gamma$$

For trimmed flight and constant airspeed, the lift is the same at both conditions, and angles of attack will be the same. Then, if condition 1 is still air and condition 2 is a headwind condition,

$$\bar{V}_{W_2} - \bar{V}_{W_1} < 0$$

$$\theta_2 - \theta_1 > 0$$

The pitch attitude contribution to thrust is W sin θ, thus,

$$\Delta T_{REQ} = T_{REQ_2} - T_{REQ_1} = W(\sin\theta_2 - \sin\theta_1) > 0$$

That is, if the attitude correction is made for a steady headwind, more thrust is required, as noted in Reference 4-17, or the airplane will touch down short.

For a headwind that decreases nearer the ground, the pitch attitude required will decrease, and the thrust required for the attitude change will also decrease. If no thrust correction is made, the attitude effect will cause an overshoot. However, this is not the only effect of a

headwind shear. In order to hold constant airspeed, changes in the wind speed must be equaled by changes in inertial speed, requiring an acceleration. That is

$$V_A \cong V - \bar{V}_W; \frac{dV_A}{dt} = 0 \Rightarrow \frac{dV}{dt} \cong \frac{d\bar{V}_W}{dh}\frac{dh}{dt}$$

$$\Delta T_{REQ} \cong \frac{W}{g}\frac{dV}{dt} = \frac{WV}{g}\frac{d\bar{V}_W}{dh}\gamma$$

For a headwind that diminishes during the approach, $(d\bar{V}_W/dh)\gamma > 0$ and thrust must be increased, as opposed to the attitude effect.

The combined effects require a thrust change of

$$\left(\frac{\Delta T}{W}\right)_{REQ} \cong \gamma\left[\frac{\Delta\bar{V}_W}{V_A} + \frac{(V_A + \bar{V}_W)}{g}\frac{d\bar{V}_W}{dh}\right]$$

So long as the magnitude of the wind increases with altitude, the change of wind on an approach path and the wind shear will be opposite in sign.

The discussion in Reference 4-17 concerning the advancing and retarding of a throttle refers to a wind shear that goes to zero before touchdown. Thus, while the shear is non-zero, the acceleration effect is presumed to dominate. For STOL aircraft, operating at low speeds, the attitude effect may dominate.

The conclusion of Reference 4-6 is compatible with these results for the conditions specified. If a constant airspeed approach is performed in a steady headwind using a still air throttle setting and pitch attitude, an undershoot occurs. The incremental effect of the shear is to cause an increased undershoot. If the attitude and throttle setting are set for a steady wind of 15 knots, the effect of a constant headwind shear of 5 kt/100 ft while flying a constant airspeed of 70 knots is to overshoot, relative to the steady headwind touchdown point (attitude effect dominates).

Reference 4-16 has also performed an analysis for a low airspeed aircraft, but the predicted overshoot for flying a constant airspeed approach is due not only to the dominance of the attitude effect, but also to the fact that inertial speed changes, not airspeed changes, were set to zero. Hence, the acceleration effect was not included.

The effects of airframe configuration on touchdown dispersion are weak except as they affect the approach speed. Whether an overshoot or undershoot occurs will depend on:

- Airspeed
- Mean wind magnitude, heading, and shear

- Control procedure (constant airspeed, constant glideslope, constant attitude, constant throttle, or combinations)

- Initial conditions (trimmed on glideslope for still air, steady wind, or other)

If the wind speed were known at every altitude, it would be possible to determine in advance the column and throttle inputs required at every point in time for a perfect landing. Of course, that information is unavailable to the pilot or autopilot. Fortunately, however, pilots and autopilots do not operate in an open loop manner. Information is supplied to both portraying the deviations from the glideslope and localizer beams and airspeed errors. Advanced display systems even indicate a command for correcting errors. Additionally, the pilot has another inertial reference through his out-the-window vision. Reasonably alert and competent pilots and reasonable autopilot designs are capable of holding constant airspeed and glideslope without knowing the wind profile, but, of course, the closure techniques must reflect a qualitative understanding of the effects of winds. Closed loop performance will not necessarily reflect a tendency to land increasingly short or long with increasing wind speeds and wind shears, so long as control authority is not saturated. The turbulence associated with the mean wind does, however, tend to saturate control authority.

It may be noted that constant airspeed is not required in order to hold the glideslope. A procedure used at Boeing Flight Crew Training School for manual approaches is to increase the initial airspeed by half the surface steady wind plus all of the difference between steady and peak wind, up to a maximum of 20 knots. For example, surface winds reported as 10 knots gusting to 15 knots would result in an initial airspeed increase of 1/2(10) + (15-10) = 10 knots. The increment for the steady wind is bled off during the approach. The peak gust margin provides an additional stall margin. The steady wind margin reflects a rule of thumb that winds at glideslope capture altitude are 50% greater than at the surface. Then, the deficiency in thrust during the approach bleeds off the excess airspeed during the maneuver, reducing the required throttle activity.

Inability to hold the glideslope may not even be the dominant factor for determining touchdown dispersions. Another factor is difficulty in performing the flare. Piloted approach simulations in winds at Boeing have produced comments indicating a tendency to float or to go through a low frequency altitude oscillation just before touchdown. A contributing factor may be the changes of the phugoid:

- Increased L/D due to ground effects reduces phugoid damping

- Reduced airspeed due to throttle chop and headwind shear decreases short period natural frequency and increases phugoid natural frequency

- The shear may cause an increase of phugoid natural frequency.

These factors may combine to cause an increased response at the phugoid frequency when the column input is made. Then, the point of touchdown performance would depend upon the point of oscillation at which touchdown occurred.

4.3 SORTING OUT THE AXIS SYSTEMS

The task of simulating turbulence for flight at low altitudes involves at least three axis systems: mean wind axis, relative wind axis, and body axis.

For the mean wind axis system, the x axis is aligned to the mean wind and the z axis is downward perpendicular to the earth. It is this axis system for which the statistical properties of turbulence and the one non-zero cospectrum have been defined. This axis system does not account for the motion and orientation of the aircraft.

The body axis is that for which the airplane's aerodynamic and inertial properties are known. It is the relationship of this axis system with the earth that defines the airplane's inertial motion. The axis system is attached to the airplane with the origin fixed at the airplane's center of gravity. The x-z plane lies in the airplane's plane of symmetry (assuming that the airplane is symmetric) with the z axis downward. The x axis is oriented with respect to some physical property of the airplane such as the wing chord plane or a waterline.

The relative wind axis also has its origin attached to the center of gravity, but its x z plane does not coincide with the plane of symmetry. Rather, the x axis is aligned to the airspeed vector. The relationship between the relative wind axis and the body axis is defined with the angle of attack and sideslip angle and thus, with the airspeed, defines the airplane motion with respect to the moving air mass.

It is only in the relative wind axis that the transformation from spacial to temporal frequency using Taylor's hypothesis ($\Omega_i = \omega/V_A$) may be applied. It may be recalled that the definition of turbulence began with correlation functions described as a function of displacement vector. A spacial frequency vector resulted from the Fourier integral of the correlation functions. Hence, the components of the spacial frequency vector are aligned to those of the displacement vector. Integrations with respect to the transverse components of spacial frequency were performed to eliminate the dependence of the spectra on those components. The time-distance relationship corresponding to the spacial-temporal frequency relationship is $\xi = V_A \Delta t$. That is, the airspeed vector must be aligned with the displacement vector in order to relate spacial and temporal frequencies. The presumed one-dimensional spectra apply only for turbulence components aligned to the relative wind axis.

The problem is this: the statistical properties of turbulence are known in one axis system, the spectra shapes in another, and the problem must be solved in a third axis system. The misalignment of the axis systems is almost universally ignored for the simulation of turbulence, or it is assumed that the axis systems are sufficiently aligned that the effects of the misalignment are negligible. Consequently, turbulence is usually generated in the body axis using the relative wind axis power spectra shapes and the mean wind axis variances and integral scales. The existence of any cospectra in the body axis is seldom acknowledged.

A straightforward, but complex, procedure would be to transform the statistical properties of turbulence from the mean wind axis to the relative wind axis, where they would be inserted into the spectra and where turbulence components would be generated, and then

transform the components of turbulence to the body axis, where the forces and moments acting upon the airplane could be found. A solution to the problem using this approach is described in the following.

4.3.1 Transformations

There are undoubtedly several methods for developing the transformation for the power spectra, variances, and integral scales. The method proposed is based on the concept of the output power spectrum. Reference 4-7 shows that the output spectrum of multiple filtered random inputs (Fig. 4-42) is given by:

$$\left[\Phi_{y_i y_j}\right] = \left[G^*_{y_i x_j}\right] \left[\Phi_{x_i x_j}\right] \left[G_{y_i x_j}\right]^T$$

When the transfer functions are constants (frequency or time invariant), the frequency responses are just the partial derivatives and the frequency response and its complex conjugate are equal:

$$G_{y_i x_j} = \frac{\partial y_i}{\partial x_j}, \quad G_{y_i x_j} \neq f(\omega)$$

$$G^*_{y_i x_j} = G_{y_i x_j}$$

To apply the output spectra to the task of transformations, consider turbulence generated in one axis system and transformed to another. The frequency responses, or partial derivatives, are just the elements of the axis transformations for vectors. That is, if turbulence is generated in the mean wind axis, the spectra in the body axis are given by

$$\left[\Phi_{y_i y_j}\right]_{\text{BODY}} = \left[\text{M to B}\right] \left[\Phi_{x_i x_j}\right]_{\substack{\text{MEAN} \\ \text{WIND}}} \left[\text{M to B}\right]^T$$

where [M to B] = mean wind axis to body axis vector transformation. Similarly, for turbulence generated in the body axis, the spectra in the relative wind axis system are given by:

$$\left[\Phi_{y_i y_j}\right]_{\substack{\text{REL} \\ \text{WIND}}} = \left[\text{B to R}\right] \left[\Phi_{x_i x_j}\right]_{\text{BODY}} \left[\text{B to R}\right]^T$$

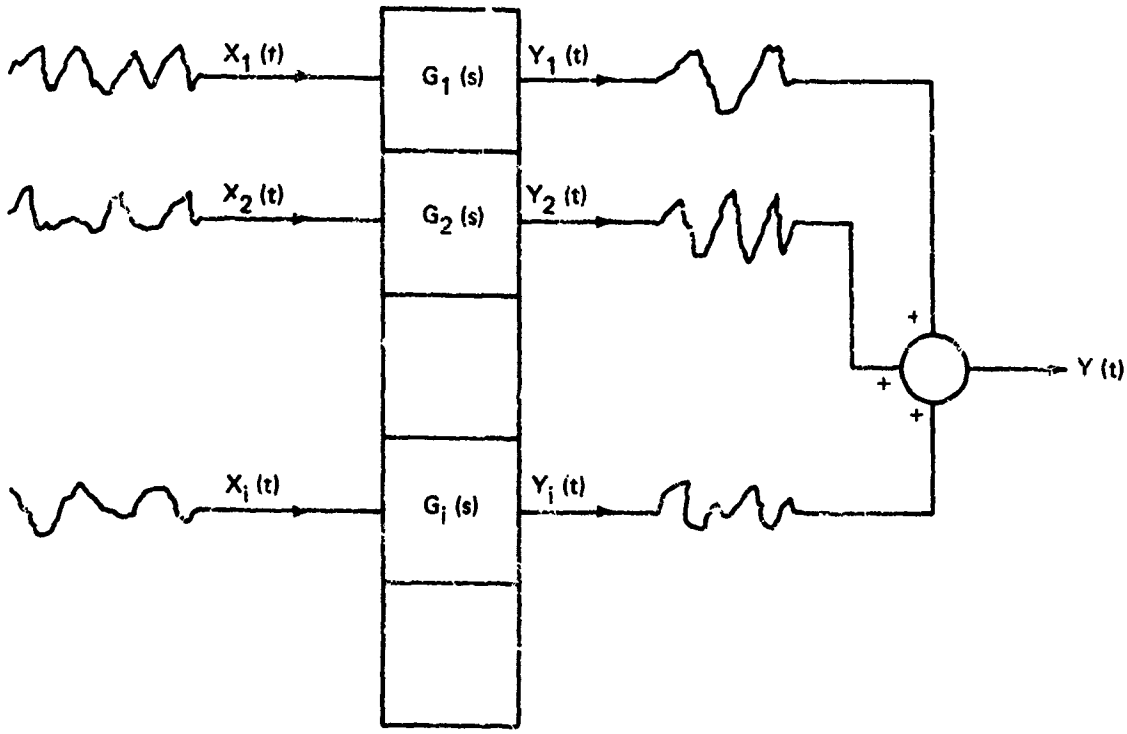

FIGURE 4-42.–RESPONSE TO A SET OF RANDOM INPUTS (FROM REF. 7)

Combining the relationships, the transformation from the mean wind axis to the relative wind axis system is

$$\left[\Phi_{y_i y_j}\right]_{\substack{\text{REL.}\\ \text{WIND}}} = \left[\text{B to R}\right]\left[\text{M to B}\right]\left[\Phi_{x_i x_j}\right]_{\substack{\text{MEAN}\\ \text{WIND}}}\left[\text{M to B}\right]^T\left[\text{B to R}\right]^T$$

The mean wind axis to body axis vector transformation is identical to the well known earth axis to body axis transformation (Ref. 4-11) except that the heading transformation is from the wind heading. The body axis to relative wind axis vector transformation is obtained by first rotating through $-\alpha$ and then through β, and is derived in appendix 4B. The transformations, both of which are orthogonal, are presented on Figure 4-43, and are undoubtedly necessary ingredients for unraveling the axis systems by any approach.

Beginning by assuming that the only non-zero cospectrum in the mean wind axis is $\Phi_{u_m w_m}$, the matrix expressions relating the body axis spectra to the mean wind axis spectra are expanded to provide the transformation matrix on Figure 4-44. Similarly, the transformation relating relative wind axis spectra to body axis spectra is provided on Figure 4-45. Note that the transformations have been rewritten to appear as vector transformations. To go from the mean wind axis to the relative wind axis, the transformation is the product of the matrix on Figure 4-45 times the matrix on Figure 4-44. These transformations certainly cannot be considered simple, and even though only one cospectrum existed in the mean wind axis, all exist in general in both the body axis and the relative wind axis. All will exist in the body and relative wind axes even if there were no cospectra in the mean wind axis.

MEAN WIND AND BODY AXIS

$$\begin{Bmatrix} u \\ v \\ w \end{Bmatrix} = \left[\begin{array}{c}\text{Mean wind to body} \\ \text{axis transformation} \\ \text{(M to B)}\end{array}\right] \begin{Bmatrix} u_M \\ v_M \\ w_M \end{Bmatrix} \; ; \; \begin{Bmatrix} u_M \\ v_M \\ w_M \end{Bmatrix} \left[\begin{array}{c}\text{Mean wind to body} \\ \text{axis transformation} \\ \text{(B to M)}\end{array}\right] \begin{Bmatrix} u \\ v \\ w \end{Bmatrix}$$

$$[\text{M to B}] = [\text{B to M}]^T = \begin{bmatrix} \cos(\psi - \bar{\psi}_W)\cos\theta & \sin(\psi - \bar{\psi}_W)\cos\theta & -\sin\theta \\ \sin(\psi - \bar{\psi}_W)\cos\phi & \cos(\psi - \bar{\psi}_W)\cos\phi & \cos\theta\sin\phi \\ \quad + \cos(\psi - \bar{\psi}_W)\sin\theta\sin\phi & \quad + \sin(\psi - \bar{\psi}_W)\sin\theta\sin\phi & \\ \sin(\psi - \bar{\psi}_W)\sin\phi & -\cos(\psi - \bar{\psi}_W)\sin\phi & \cos\theta\cos\phi \\ \quad + \cos(\psi - \bar{\psi}_W)\sin\theta\cos\phi & \quad + \sin(\psi - \bar{\psi}_W)\sin\theta\cos\phi & \end{bmatrix}$$

RELATIVE WIND AND BODY AXIS

$$\begin{Bmatrix} u_R \\ v_R \\ w_R \end{Bmatrix} = \left[\begin{array}{c}\text{Body to relative wind} \\ \text{axis transformation} \\ \text{(B to R)}\end{array}\right] \begin{Bmatrix} u \\ v \\ w \end{Bmatrix} \; ; \; \begin{Bmatrix} u \\ v \\ w \end{Bmatrix} = \left[\begin{array}{c}\text{Relative wind to body} \\ \text{axis transformation} \\ \text{(R to B)}\end{array}\right] \begin{Bmatrix} u_R \\ v_R \\ w_R \end{Bmatrix}$$

$$[\text{B to R}] = [\text{R to B}]^T = \begin{bmatrix} \cos\alpha\cos\beta & \sin\beta & \sin\alpha\cos\beta \\ -\cos\alpha\sin\beta & \cos\beta & -\sin\alpha\sin\beta \\ -\sin\alpha & 0 & \cos\alpha \end{bmatrix}$$

FIGURE 4-43.–AXIS TRANSFORMATIONS

The axis transformation for the spectra is not particular to spectra functions. The identical axis transformation equation is given in Reference 4-18 for tensors in general. To transform a tensor from axis system B to axis system A,

$$\left|\lambda_{ij}\right|_A = \left|\text{B to A}\right| \left|\lambda_{ij}\right|_B \left|\text{B to A}\right|^T$$

Thus, the transformations on Figures 4-44 and 4-45 should also hold for the variances and covariances. The integral scales may also be thought of as tensor quantities. Integral scales are defined as tensor quantities in Reference 4-7:

$$L_{ij} = \frac{1}{\sigma_i^2} \int_0^\infty R_{ij}(\vec{\xi})\, d\xi_j$$

For isotropic turbulence, where the orientation in space of the displacement vector does not affect the integral scales, the "shear stress" terms are zero. However, at low altitudes where statistical properties of turbulence are dependent upon the orientation of the displacement vector (or, alternately, the direction of flight), the cross-product terms are in general

$$
\begin{Bmatrix} \Phi_{uu} \\ \Phi_{vv} \\ \Phi_{ww} \\ \Phi_{uv} \\ \Phi_{vw} \\ \Phi_{wu} \end{Bmatrix} =
\begin{bmatrix}
\cos^2(\psi - \bar{\psi}_W)\cos^2\theta & \sin^2(\psi - \bar{\psi}_W)\cos^2\phi & \sin^2\theta & -2\cos(\psi - \bar{\psi}_W)\sin\theta\cos\theta \\
\sin^2(\psi - \bar{\psi}_W)\cos^2\phi + \cos^2(\psi - \bar{\psi}_W)\sin^2\theta\sin^2\phi & \cos^2(\psi - \bar{\psi}_W)\cos^2\phi + \sin^2(\psi - \bar{\psi}_W)\sin^2\theta\sin^2\phi & \cos^2\theta\sin^2\phi & -2\sin(\psi - \bar{\psi}_W)\cos\theta\sin\phi\cos\phi \\
-2\sin(\psi - \bar{\psi}_W)\cos(\psi - \bar{\psi}_W)\sin\theta\sin\phi\cos\phi & +2\sin(\psi - \bar{\psi}_W)\cos(\psi - \bar{\psi}_W)\sin\theta\sin\phi\cos\phi & & +2\cos(\psi - \bar{\psi}_W)\sin\theta\cos\theta\sin^2\phi \\
\sin^2(\psi - \bar{\psi}_W)\sin^2\phi + \cos^2(\psi - \bar{\psi}_W)\sin^2\theta\cos^2\phi & \cos^2(\psi - \bar{\psi}_W)\sin^2\phi + \sin^2(\psi - \bar{\psi}_W)\sin^2\theta\cos^2\phi & \cos^2\theta\cos^2\phi & 2\sin(\psi - \bar{\psi}_W)\cos\theta\sin\phi\cos\phi \\
+2\sin(\psi - \bar{\psi}_W)\cos(\psi - \bar{\psi}_W)\sin\theta\sin\phi\cos\phi & -2\sin(\psi - \bar{\psi}_W)\cos(\psi - \bar{\psi}_W)\sin\theta\sin\phi\cos\phi & & +2\cos(\psi - \bar{\psi}_W)\sin\theta\cos\theta\cos^2\phi \\
-\sin(\psi - \bar{\psi}_W)\cos(\psi - \bar{\psi}_W)\cos\theta\cos\phi & \sin(\psi - \bar{\psi}_W)\cos(\psi - \bar{\psi}_W)\cos\theta\cos\phi & -\sin\theta\cos\theta\sin\phi & \cos(\psi - \bar{\psi}_W)[\cos^2\theta - \sin^2\theta]\sin\phi \\
+\cos^2(\psi - \bar{\psi}_W)\sin\theta\cos\theta\sin\phi & +\sin^2(\psi - \bar{\psi}_W)\sin\theta\cos\theta\sin\phi & & +\sin(\psi - \bar{\psi}_W)\sin\theta\cos\phi \\
-\sin(\psi - \bar{\psi}_W)\cos(\psi - \bar{\psi}_W)\sin\theta(\cos^2\phi - \sin^2\phi) & \sin(\psi - \bar{\psi}_W)\cos(\psi - \bar{\psi}_W)\sin\theta(\cos^2\phi - \sin^2\phi) & \cos^2\theta\sin\phi\cos\phi & \sin(\psi - \bar{\psi}_W)\cos\theta(\sin^2\phi - \cos^2\phi) \\
+[\cos^2(\psi - \bar{\psi}_W)\sin^2\theta - \sin^2(\psi - \bar{\psi}_W)]\sin\phi\cos\phi & +[\sin^2(\psi - \bar{\psi}_W)\sin^2\theta - \cos^2(\psi - \bar{\psi}_W)]\sin\phi\cos\phi & & +2\cos(\psi - \bar{\psi}_W)\sin\theta\cos\theta\sin\phi\cos\phi \\
\sin(\psi - \bar{\psi}_W)\cos(\psi - \bar{\psi}_W)\cos\theta\sin\phi & -\sin(\psi - \bar{\psi}_W)\cos(\psi - \bar{\psi}_W)\cos\theta\sin\phi & -\sin\theta\cos\theta\cos\phi & \cos(\psi - \bar{\psi}_W)[\cos^2\theta - \sin^2\theta]\cos\phi \\
+\cos^2(\psi - \bar{\psi}_W)\sin\theta\cos\theta\cos\phi & +\sin^2(\psi - \bar{\psi}_W)\sin\theta\cos\theta\cos\phi & & -\sin(\psi - \bar{\psi}_W)\sin\theta\sin\phi
\end{bmatrix}
\begin{Bmatrix} \Phi_{u_M u_M} \\ \Phi_{v_M v_M} \\ \Phi_{w_M w_M} \\ \Phi_{u_M w_M} \end{Bmatrix}
$$

$$\Phi_{uv} = \Phi_{vu},\quad \Phi_{vw} = \Phi_{wv},\quad \Phi_{wu} = \Phi_{uw}$$

FIGURE 4-44.—MEAN WIND AXIS TO BODY AXIS TRANSFORMATION OF SPECTRA

$$
\begin{Bmatrix} \sigma_{u_R}^2 \\ \sigma_{v_R}^2 \\ \sigma_{w_R}^2 \\ \sigma_{u_R v_R}^2 \\ \sigma_{v_R w_R}^2 \\ \sigma_{w_R u_R}^2 \end{Bmatrix} =
\begin{bmatrix}
\cos^2\alpha\cos^2\beta & \sin^2\beta & \sin^2\alpha\cos^2\beta & 2\cos\alpha\sin\beta\cos\beta & 2\sin\alpha\sin\beta\cos\beta & 2\sin\alpha\cos\alpha\cos^2\beta \\
\cos^2\alpha\sin^2\beta & \cos^2\beta & \sin^2\alpha\sin^2\beta & -2\cos\alpha\sin\beta\cos\beta & -2\sin\alpha\sin\beta\cos\beta & 2\sin\alpha\cos\alpha\sin^2\beta \\
\sin^2\alpha & 0 & \cos^2\alpha & 0 & 0 & -2\sin\alpha\cos\alpha \\
-\cos^2\alpha\sin\beta\cos\beta & \sin\beta\cos\beta & -\sin^2\alpha\sin\beta\cos\beta & \cos\alpha(\cos^2\beta-\sin^2\beta) & \sin\alpha(\cos^2\beta-\sin^2\beta) & -2\sin\alpha\cos\alpha\sin\beta\cos\beta \\
\sin\alpha\cos\alpha\sin\beta & 0 & -\sin\alpha\cos\alpha\sin\beta & -\sin\alpha\cos\beta & \cos\alpha\cos\beta & (\sin^2\alpha-\cos^2\alpha)\sin\beta \\
-\sin\alpha\cos\alpha\cos\beta & 0 & \sin\alpha\cos\alpha\cos\beta & -\sin\alpha\sin\beta & \cos\alpha\sin\beta & (\cos^2\alpha-\sin^2\alpha)\cos\beta
\end{bmatrix}
\begin{Bmatrix} \sigma_u^2 \\ \sigma_v^2 \\ \sigma_w^2 \\ \sigma_{uv}^2 \\ \sigma_{vw}^2 \\ \sigma_{wu}^2 \end{Bmatrix}
$$

$$\sigma_{uv}^2 = \sigma_{vu}^2; \quad \sigma_{vw}^2 = \sigma_{wv}^2; \quad \sigma_{wu}^2 = \sigma_{uw}^2$$

Note: Same transformation used for spectra.

FIGURE 4-45. –RELATIVE WIND AXIS VARIANCES AND COVARIANCES

non-zero and integral scales are represented as a tensor. These off-diagonal integral scale terms are defined in Reference 4-7 as "the j scale of the i velocity component."

It can be shown more rigorously that the spectra transformations do hold for the variance and integral scales. Expanding the first row on Figure 4-44,

$$\Phi_{uu} = \cos^2(\psi - \bar{\psi}_W)\cos^2\theta\,\Phi_{u_m u_m} + \sin^2(\psi - \bar{\psi}_W)\cos^2\theta\,\Phi_{v_m v_m}$$

$$+ \sin^2\theta\,\Phi_{w_m w_m} - 2\cos(\psi - \bar{\psi}_W)\sin\theta\cos\theta\,\Phi_{u_m w_m}$$

Integrating this equation with respect to Ω_1 from $-\infty$ to ∞ yields

$$\sigma_u^2 = \int_{-\infty}^{\infty} \Phi_{uu}\,d\Omega_1 = \cos^2(\psi - \bar{\psi}_W)\cos^2\theta\,\sigma_{u_m}^2 + \sin^2(\psi - \bar{\psi}_W)\cos^2\theta\,\sigma_{v_m}^2$$

$$+ \sin^2\theta\,\sigma_{w_m} - 2\cos(\psi - \bar{\psi}_W)\sin\theta\cos\theta\,\sigma_{u_m}{}^2{}_{w_m}$$

This integral transformation can be applied to every term on Figures 4-44 and 4-45.

The spectra are just Fourier integrals of the correlation functions; hence, Figures 4-44 and 4-45 must also hold for the correlation functions. Since the correlation functions in turn may be integrated with respect to the displacement vector magnitudes to yield the integral scales, the transformation on Figures 4-44 and 4-45 hold also for the integral scales.

The selected description for the statistical properties of turbulence accepted horizontal isotropy. Thus, the transformations on Figure 4-42 for the variances and covariances and the integral scales may be simplified by using

$$\sigma_{u_m} = \sigma_{v_m} = \sigma_H, \quad L_{u_m} = L_{v_m} = L_H$$

The subscript H is used to refer to horizontal components. Similarly, the variance and integral scale for vertical turbulence are rewritten as σ^2_v and L_V. The u-w covariance is identified as u_*^2, but the integral scale for the covariance has not been provided by the literature. With these changes, the transformations for the variances and covariances are simplified on Figure 4-46. The same transformation applies to the integral scales. A corresponding simplification does not exist for the body axis to relative wind axis tensor transformation. Note also, that the simplified form on Figure 4-46 does not apply to the spectra as

$$\Phi_{u_m u_m} \neq \Phi_{v_m v_m}$$

$$
\begin{Bmatrix} \sigma_u^2 \\ \sigma_v^2 \\ \sigma_w^2 \\ \sigma_{uv}^2 \\ \sigma_{vw}^2 \\ \sigma_{wu}^2 \end{Bmatrix} =
\begin{bmatrix}
\cos^2\theta & \sin^2\theta & -2\cos(\psi-\bar{\psi}_W)\sin\theta\cos\theta \\
\sin^2\theta\sin^2\phi + \cos^2\phi & \cos^2\theta\sin^2\phi & 2[\cos(\psi-\bar{\psi}_W)\sin\theta\sin\phi - \sin(\psi-\bar{\psi}_W)\cos\phi]\cos\theta\sin\phi \\
\sin^2\theta\cos^2\phi + \sin^2\phi & \cos^2\theta\cos^2\phi & 2[\cos(\psi-\bar{\psi}_W)\sin\theta\cos\phi + \sin(\psi-\bar{\psi}_W)\sin\phi]\cos\theta\cos\phi \\
\sin\theta\cos\theta\sin\phi & -\sin\theta\cos\theta\sin\phi & \cos(\psi-\bar{\psi}_W)[\cos^2\theta-\sin^2\theta]\sin\phi + \sin(\psi-\bar{\psi}_W)\sin\theta\cos\phi \\
-\cos^2\theta\sin\phi\cos\phi & \cos^2\theta\sin\phi\cos\phi & \sin(\psi-\bar{\psi}_W)\cos\theta[\sin^2\phi-\cos^2\phi] + 2\cos(\psi-\bar{\psi}_W)\sin\theta\cos\theta\sin\phi\cos\phi \\
\sin\theta\cos\theta\cos\phi & -\sin\theta\cos\theta\cos\phi & \cos(\psi-\bar{\psi}_W)[\cos^2\theta-\sin^2\theta] - \sin(\psi-\bar{\psi}_W)\sin\theta\sin\phi
\end{bmatrix}
\begin{Bmatrix} \sigma_H^2 \\ \sigma_V^2 \\ u_e^2 \end{Bmatrix}
$$

$$
\sigma_{uv}^2 = \sigma_{vu}^2 : \sigma_{wv}^2 = \sigma_{vw}^2 : \sigma_{wu}^2 = \sigma_{uw}^2
$$

FIGURE 4-46.—BODY AXIS VARIANCES AND COVARIANCES.

Figure 4-44 reveals that in the absence of pitch and bank angle rotations, the statistical properties of turbulence are invariant with rotations in the plane of the earth, precisely the assumption of horizontal isotropy.

To have found the required transformations does not imply that the problem has been solved. Even though the statistical properties of turbulence and the cospectra are presumed to be known in the mean wind axis system and can be transformed to the relative wind axis system where the power spectra are presumed to be known, the solution remains unknown because the forms of the cospectra in the relative axis system are unknown. With this observation, the initial approach fails. Alternate approaches must be considered or sufficiently accurate approximations found. To gain insight, the condition of isotropy is examined first.

4.3.2 Isotropic Turbulence

For the condition of isotropy, the mean wind axis system is no longer relevant, as the statistical properties of turbulence are independent of the orientation of the flight path. That is, the matrices for transforming various covariances and integral scales reduce to identity column matrices when the variances and integral scales for each component are equal and when the covariances are zero in some one axis system. Additionally, there are only two power spectra in the relative wind axis system; the parallel or longitudinal spectrum and the normal or transverse spectrum. The relative wind axis spectra may be transformed to the body axis as shown on Figure 4-47.

As seen on Figure 4-47, even though the variance and integral scales are invariant and the covariances remain zero for an axis transformation, the spectra for the three body axis components of turbulence are not the same as those for the three components of the relative wind axis system. Furthermore, the cospectra are not zero in the body axis system even though they were in the relative wind axis system. This is comparable to moments of inertia: there is but one orientation of an axis system relative to the airplane for which all the products of inertia are zero–that of the principal axis. Hence, the relative wind axis system is the principal axis for turbulence.

The cospectra, as seen on Figure 4-48, assume both positive and negative values as they must to enable zero covariances. Even though the covariances of turbulence are zero, the covariances of turbulence as seen by the airplane are non-zero because the airplane filters out the effects at high frequencies.

Figure 4-48 gives the illusion of relative significance only at very low frequencies, but when plotted so that the area under the curve is proportional to the contribution of a frequency range to the covariance, Figure 4-49, it is seen that the intermediate frequencies have the greatest impact on the spectra for aircraft motion. The point on Figures 4-48 and 4-49 where the cospectra cross zero ($\pm 1.339\ L\Omega_1 = 1.225$) divides the areas between 0 and $\pm\infty$ into equal parts.

Although using relative wind axis spectra for generating turbulence in the body axis is not precisely correct, it may be sufficiently accurate if the error is small.

ISOTROPY:

$$\Phi_{u_R} = \Phi_P = \frac{\sigma L}{\pi} \frac{1}{[1+\lambda^2]^{5/6}} \qquad \Phi_{v_R} = \Phi_{w_R} = \Phi_N = \frac{\sigma L}{2\pi} \frac{1+8/3\,\lambda^2}{[1+\lambda^2]^{11/6}}$$

$$\lambda = 1.339\, L\,\Omega$$

$$\Phi_{u_R v_R} = \Phi_{v_R w_R} = \Phi_{w_R u_R} = 0$$

$$\left.\begin{aligned} \sigma_u &= \sigma_v = \sigma_w = \sigma \\ L_u &= L_v = L_w = L \\ \sigma_{uv} &= \sigma_{vw} = \sigma_{wu} = 0 \end{aligned}\right\} \text{ Body axis and relative wind axis}$$

$$\begin{Bmatrix} \Phi_u \\ \Phi_v \\ \Phi_w \\ \Phi_{uv} \\ \Phi_{vw} \\ \Phi_{wu} \end{Bmatrix}_{\text{Body axis}} = \begin{bmatrix} \cos^2\alpha\cos^2\beta & 1-\cos^2\alpha\cos^2\beta \\ \cos^2\alpha\sin^2\beta & 1-\cos^2\alpha\sin^2\beta \\ \sin^2\alpha & \cos^2\alpha \\ \cos^2\alpha\sin\beta\cos\beta & -\cos^2\alpha\sin\beta\cos\beta \\ \sin\alpha\cos\alpha\sin\beta & -\sin\alpha\cos\alpha\sin\beta \\ \sin\alpha\cos\alpha\cos\beta & -\sin\alpha\cos\alpha\cos\beta \end{bmatrix} \begin{Bmatrix} \Phi_P \\ \Phi_N \end{Bmatrix} \text{ Relative wind axis}$$

$$\frac{\Phi_u - \Phi_P}{\Phi_P} = -\frac{(1-\cos^2\alpha\cos^2\beta)}{2} \frac{(1-2/3\,\lambda^2)}{(1+\lambda^2)}$$

$$\frac{\Phi_v - \Phi_N}{\Phi_N} = \cos^2\alpha\sin^2\beta\,\frac{(1-2/3\,\lambda^2)}{(1+8/3\,\lambda^2)}$$

$$\frac{\Phi_w - \Phi_N}{\Phi_N} = \sin^2\alpha\,\frac{(1-2/3\,\lambda^2)}{(1+8/3\,\lambda^2)}.$$

$$\Phi_{uv} = \frac{\sigma^2 L}{2\pi}\cos^2\alpha\sin\beta\cos\beta\,\frac{(1-2/3\,\lambda^2)}{(1+\lambda^2)^{11/6}}$$

$$= \Phi_P \frac{\cos^2\alpha\sin\beta\cos\beta}{2}\frac{(1-2/3\,\lambda^2)}{(1+\lambda^2)} = \Phi_N \cos^2\alpha\sin\beta\cos\beta\,\frac{(1-2/3\,\lambda^2)}{(1+8/3\,\lambda^2)}$$

$$\Phi_{vw} = \frac{\sigma^2 L}{2\pi}\sin\alpha\cos\alpha\sin\beta\,\frac{(1-2/3\,\lambda^2)}{(1+\lambda^2)^{11/6}}$$

$$= \Phi_P \frac{\sin\alpha\cos\alpha\sin\beta}{2}\frac{(1-2/3\,\lambda^2)}{(1+\lambda^2)} = \Phi_N \sin\alpha\cos\alpha\sin\beta\,\frac{(1-2/3\,\lambda^2)}{(1+8/3\,\lambda^2)}$$

$$\Phi_{wu} = \frac{\sigma^2 L}{2\pi}\sin\alpha\cos\alpha\cos\beta\,\frac{(1-2/3\,\lambda^2)}{(1+\lambda^2)^{11/6}}$$

$$= \Phi_P \frac{\sin\alpha\cos\alpha\cos\beta}{2}\frac{(1-2/3\,\lambda^2)}{(1+\lambda^2)} = \Phi_N \sin\alpha\cos\alpha\cos\beta\,\frac{(1-2/3\,\lambda^2)}{(1+8/3\,\lambda^2)}$$

FIGURE 4-47.–BODY AXIS SPECTRA, ISOTROPIC TURBULENCE

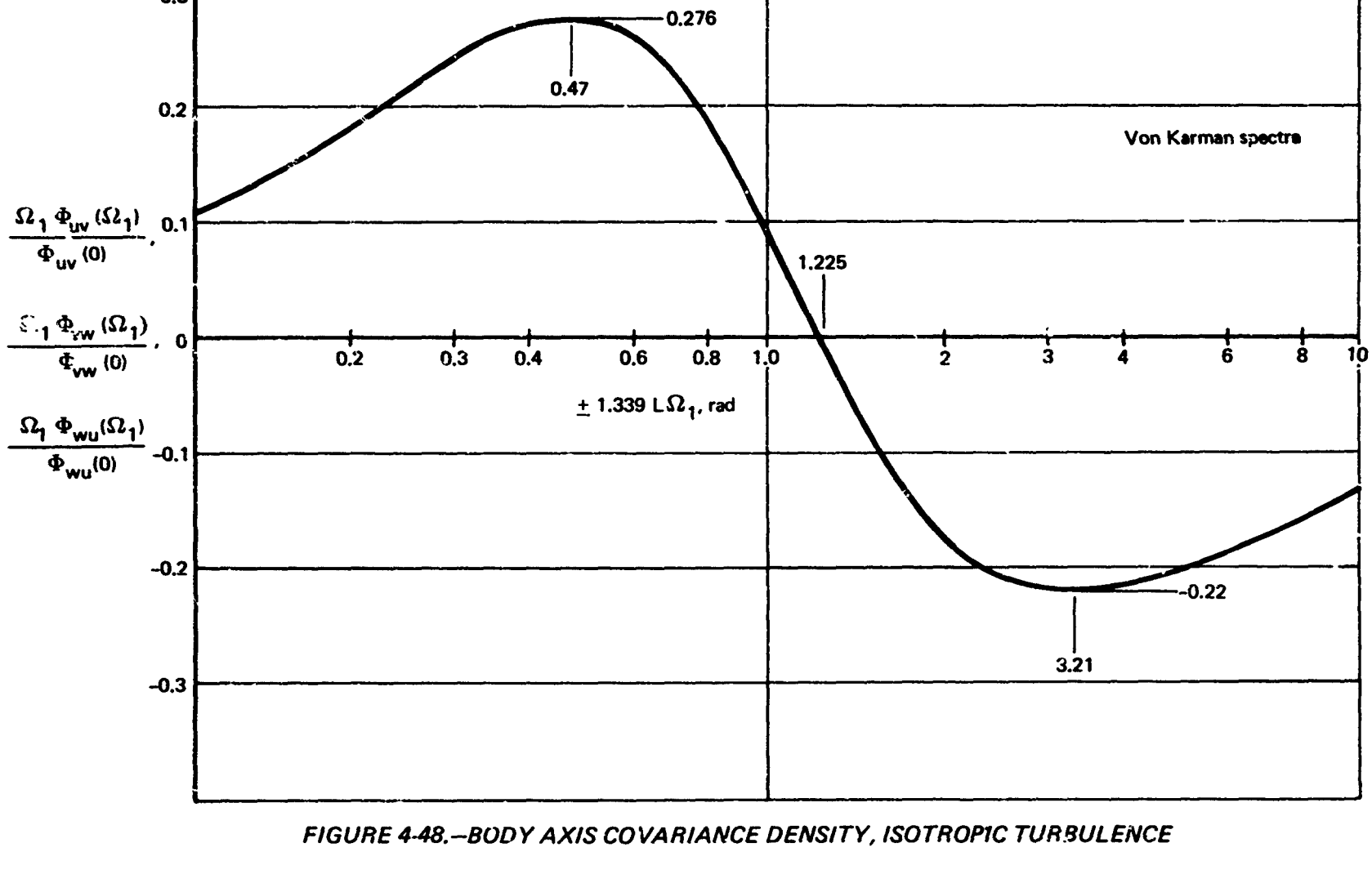

FIGURE 4-48.–BODY AXIS COVARIANCE DENSITY, ISOTROPIC TURBULENCE

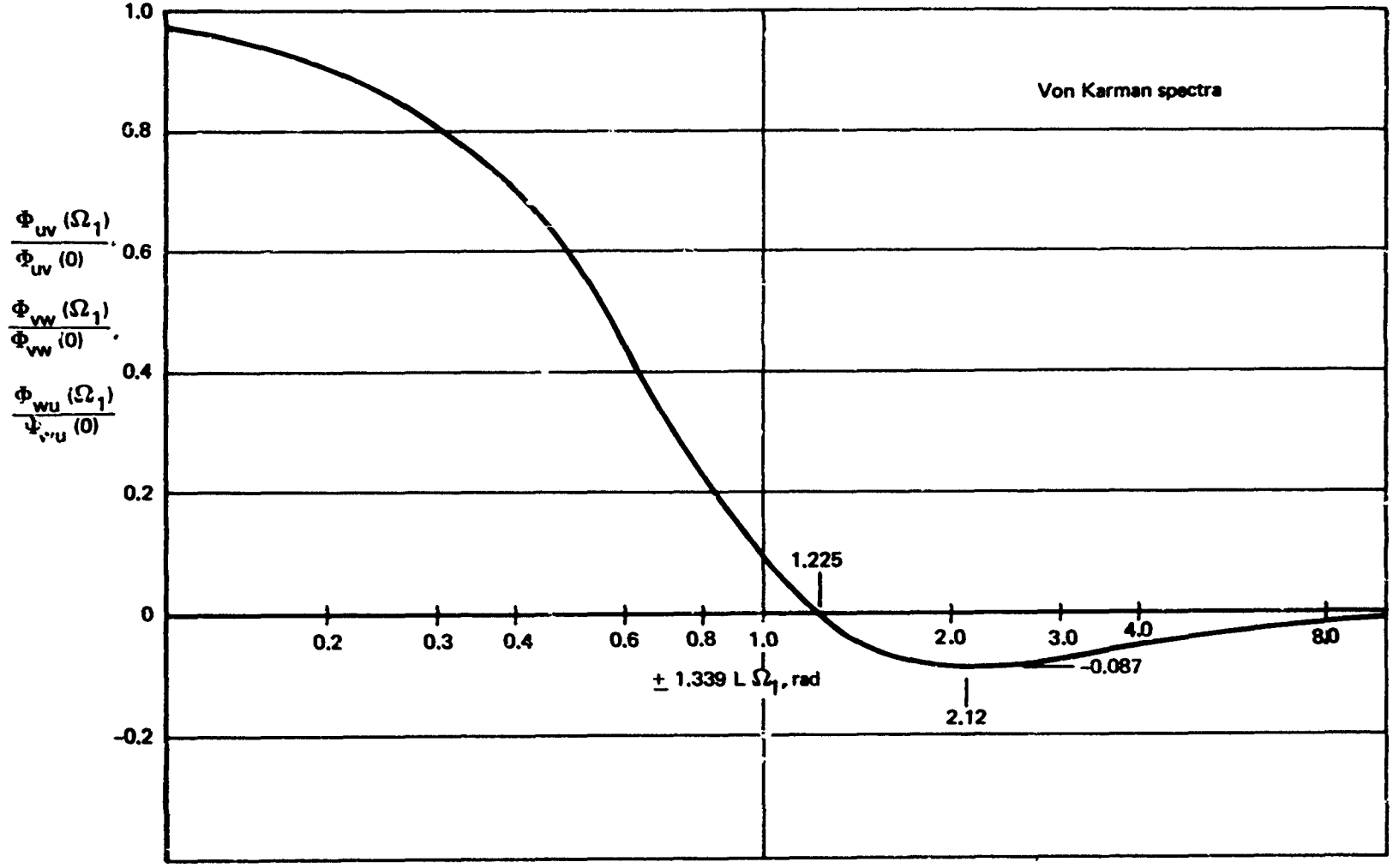

FIGURE 4-49.—BODY AXIS COSPECTRA, ISOTROPIC TURBULENCE

For the case where sideslip angle is zero, the body axis vertical spectrum may be written as:

$$\Phi_w = \Phi_N \cos^2\alpha + \Phi_P \sin^2\alpha$$

At the high frequencies,

$$\frac{\Phi_N}{\Phi_P}\Big|_{\Omega_1 \to \infty} = \frac{4}{3}$$

The difference between the body axis and the relative wind axis vertical turbulence power spectra as a fraction of the relative wind axis spectrum is

$$\frac{\Phi_w}{\Phi_N}\Big|_{\Omega \to \infty} = \frac{4\cos^2\alpha + 3\sin^2\alpha}{4} = 1 - \frac{1}{4}\sin^2\alpha$$

Even for an angle as large as 20°, this error is only about 3%. At the low frequencies,

$$\frac{\Phi_N}{\Phi_P}\Big|_{\Omega_1 \to 0} = \frac{1}{2}$$

and

$$\frac{\Phi_w}{\Phi_N}\Big|_{\Omega_1 \to 0} = \cos^2\alpha + 2\sin^2\alpha = 1 + \sin^2\alpha$$

For an angle as large as 20°, the error is only about 11%. It can easily be shown that the largest effect of the transformation is at zero frequency.

Similar analysis for the longitudinal spectra yields:

$$\frac{\Phi_u}{\Phi_P}\Big|_{\Omega_1 \to \infty} = 1 + \frac{\sin^2\alpha}{3}$$

$$\frac{\Phi_u}{\Phi_P}\Big|_{\Omega_1 \to 0} = 1 - \frac{\sin^2\alpha}{2}$$

The effects at low frequencies for the longitudinal spectrum are even less than those for the vertical spectrum. The lateral spectrum is unaltered by angle of attack rotations. If the angle of attack were zero and sideslip non-zero

$$\left.\frac{\Phi_u}{\Phi_P}\right|_{\Omega\to\infty} = 1 + \frac{\sin^2\beta}{3}$$

$$\left.\frac{\Phi_u}{\Phi_P}\right|_{\Omega\to 0} = 1 - \frac{\sin^2\beta}{2}$$

$$\left.\frac{\Phi_v}{\Phi_N}\right|_{\Omega\to\infty} = 1 - \frac{\sin^2\beta}{4}$$

$$\left.\frac{\Phi_v}{\Phi_N}\right|_{\Omega\to 0} = 1 + \sin^2\beta$$

For reasonable angles of attack and sideslip angles, generating isotropic turbulence directly in the body axis does not introduce significant errors for most engineering applications. Whether or not the cospectra may be ignored is a different question. However, for isotropic turbulence, it is not necessary to generate turbulence directly in the body axis. Turbulence components may be generated in the relative wind axis system, then transformed to the body axis system using the transpose of the body axis to relative wind axis vector transformation on Figure 4-43. The correct body axis power spectra and cospectra will result. The vector transformation is not so complex that its use is prohibitive.

4.3.3 Low Altitude Turbulence

Consider the special case of level flight in the direction of the mean wind, wings level. For horizontal isotropy, the variances and integral scales for the components of turbulence in the relative wind axis system are the same as those for the components in the mean wind axis system.

If, in addition, the airplane is at some angle of attack but zero sideslip angle, the ratio of the relative wind axis power spectra at low frequencies is

$$\left.\frac{\Phi_{u_R}}{\Phi_{w_R}}\right|_{\Omega\to 0} = 2\left(\frac{\sigma_H}{\sigma_V}\right)^2\left(\frac{L_H}{L_V}\right); \quad \frac{\Phi_{v_R}}{\Phi_{w_R}} = \left(\frac{\sigma_H}{\sigma_V}\right)^2\left(\frac{L_H}{L_V}\right)$$

or, from the condition of isotropy at high frequencies,

$$\frac{L_H}{L_V} = \left(\frac{\sigma_H}{\sigma_V}\right)^3$$

$$\frac{\Phi_{u_R}}{\Phi_{w_R}} = 2\left(\frac{\sigma_H}{\sigma_V}\right)^5 \; ; \; \frac{\Phi_{v_R}}{\Phi_{w_R}} = \left(\frac{\sigma_H}{\sigma_V}\right)^5$$

If, additionally, the u_m-w_m cospectrum may be ignored, the effects of angle of attack at low frequencies are:

$$\left.\frac{\Phi_w}{\Phi_{w_R}}\right|_{\Omega_1 \to 0} = \cos^2\alpha + 2\left(\frac{\sigma_H}{\sigma_V}\right)^5 \sin^2\alpha$$

$$\left.\frac{\Phi_u}{\Phi_{u_R}}\right|_{\Omega_1 \to} = \frac{2\left(\frac{\sigma_H}{\sigma_V}\right)^5 \cos^2\alpha + \sin^2\alpha}{2\left(\frac{\sigma_H}{\sigma_V}\right)^5}$$

The effect of angle of attack is greatest at low altitudes where σ_H/σ_V is greatest. At an altitude of 100 feet a mean wind speed of 10 knots at the surface, and neutral atmospheric considerations, the selected description yields

$$\frac{\sigma_H}{\sigma_V} = 1.72, \left(\frac{\sigma_H}{\sigma_V}\right)^5 = 15$$

For the same 20° angle considered for the isotropic case,

$$\left.\frac{\Phi_w}{\Phi_{w_R}}\right|_{\Omega_1 \to 0} = 4.39$$

$$\left.\frac{\Phi_u}{\Phi_{u_R}}\right|_{\Omega_1 \to 0} = 0.887$$

The change of the longitudinal spectrum is small at low frequencies, but the change of the vertical spectrum is enormous. The entire vertical spectra ratio is shown on Figure 4-50. At high frequencies, where turbulence at low altitudes is isotropic, the effects are again quite small. The percentage of error of the vertical spectra ratio at low frequencies for all altitudes is shown on Figure 4-51. Significant errors are not restricted to the altitude and angle considered.

The method of generating turbulence directly in the body axis system using relative wind axis characteristics will become very bad at low altitudes where components of the larger horizontal turbulence variance and integral scale should introduce substantially increased low frequency power into the vertical body axis turbulence components. This error may well account for the lack of "patchiness" found by Reference 4-19 in conventional turbulence generation.

If, for the same flight condition, the angle of attack were zero but sideslip non-zero, then at low frequencies the effects of the sideslip angle are

$$\left.\frac{\Phi_u}{\Phi_{u_R}}\right|_{\Omega_1 \to 0} = \cos^2\beta + \frac{1}{2}\sin^2\beta = 1 - \frac{\sin^2\beta}{2}$$

$$\left.\frac{\Phi_v}{\Phi_{v_R}}\right|_{\Omega_1 \to 0} = \cos^2\beta + 2\sin^2\beta = 1 + \sin^2\beta$$

These are the same relationships as those found for isotropy, which is to be expected since the rotation takes place in the plane of isotropy. Additional effects are introduced when the flight path is non-zero, heading not in the direction of the mean wind, wings not level, and the cospectrum in the mean wind axis nonnegligible.

The simple analysis reveals that it is not sufficient to generate turbulence in the body axis using mean wind axis statistical characteristics and relative wind axis spectra shapes. Turbulence cannot be generated in the relative axis system as for isotropic turbulence because at low altitudes the relative wind axis cospectra are non-zero and are unknown.

Two primary effects exist. One is the change of the spectra due to the difference in shape between the longitudinal and transverse spectra. The other is the change in the spectra due to the differences between the horizontal and vertical mean wind axis variances and integral scales. A comparison of the isotropic and restrictive low altitude analysis of the transformations reveals that the latter effect is by far the more powerful. That is, it is more important to account for the orientations of the variances and integral scales than it is to account for the orientations for the power spectra shapes.

The proposed method is to generate turbulence in the plane of the earth using the relative wind axis spectra shapes but in the direction of the airspeed vector. The components

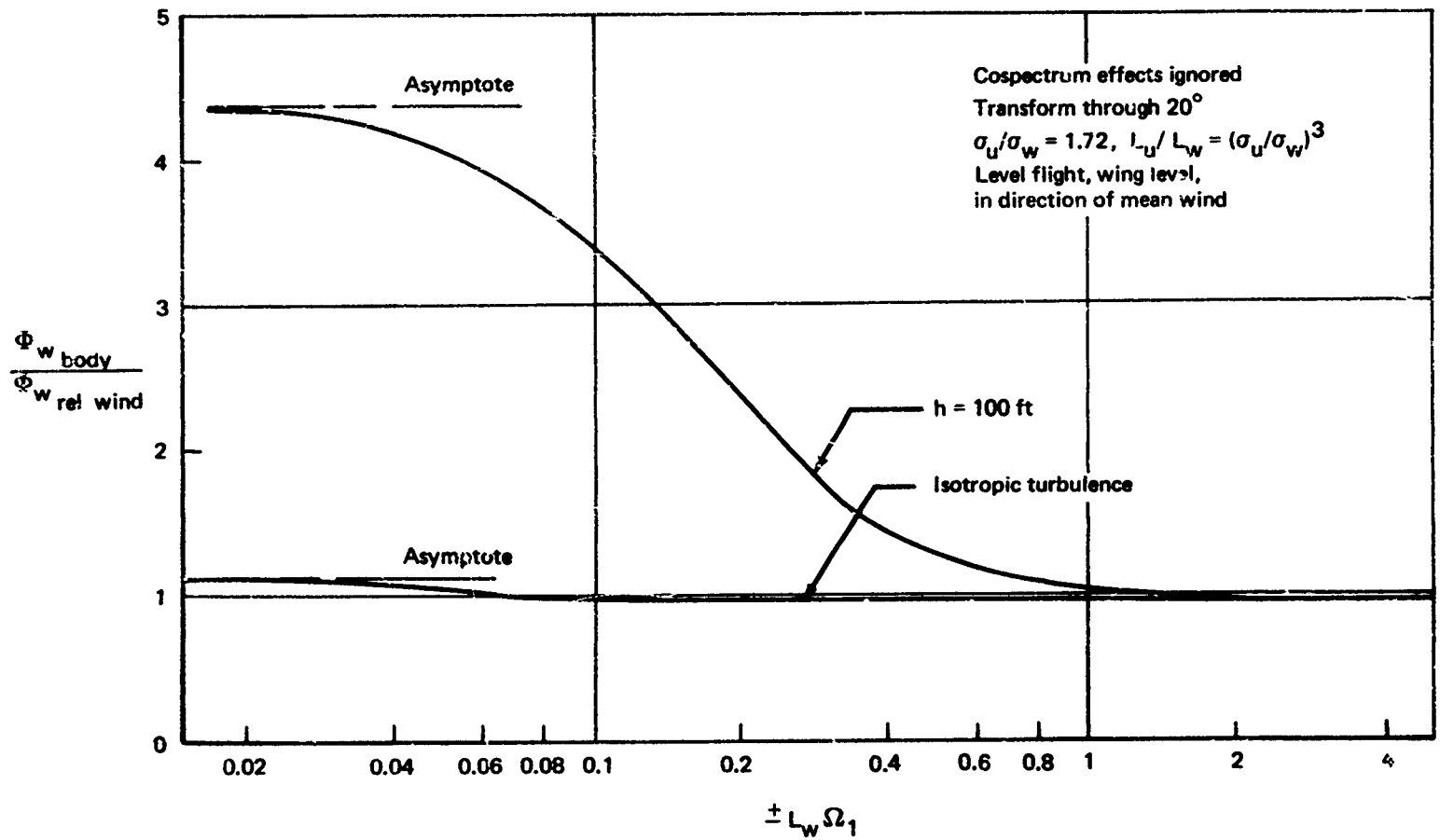

FIGURE 4-50.—RELATIVE WIND TO BODY AXIS TRANSFORMATION EFFECT ON VERTICAL P.S.D.

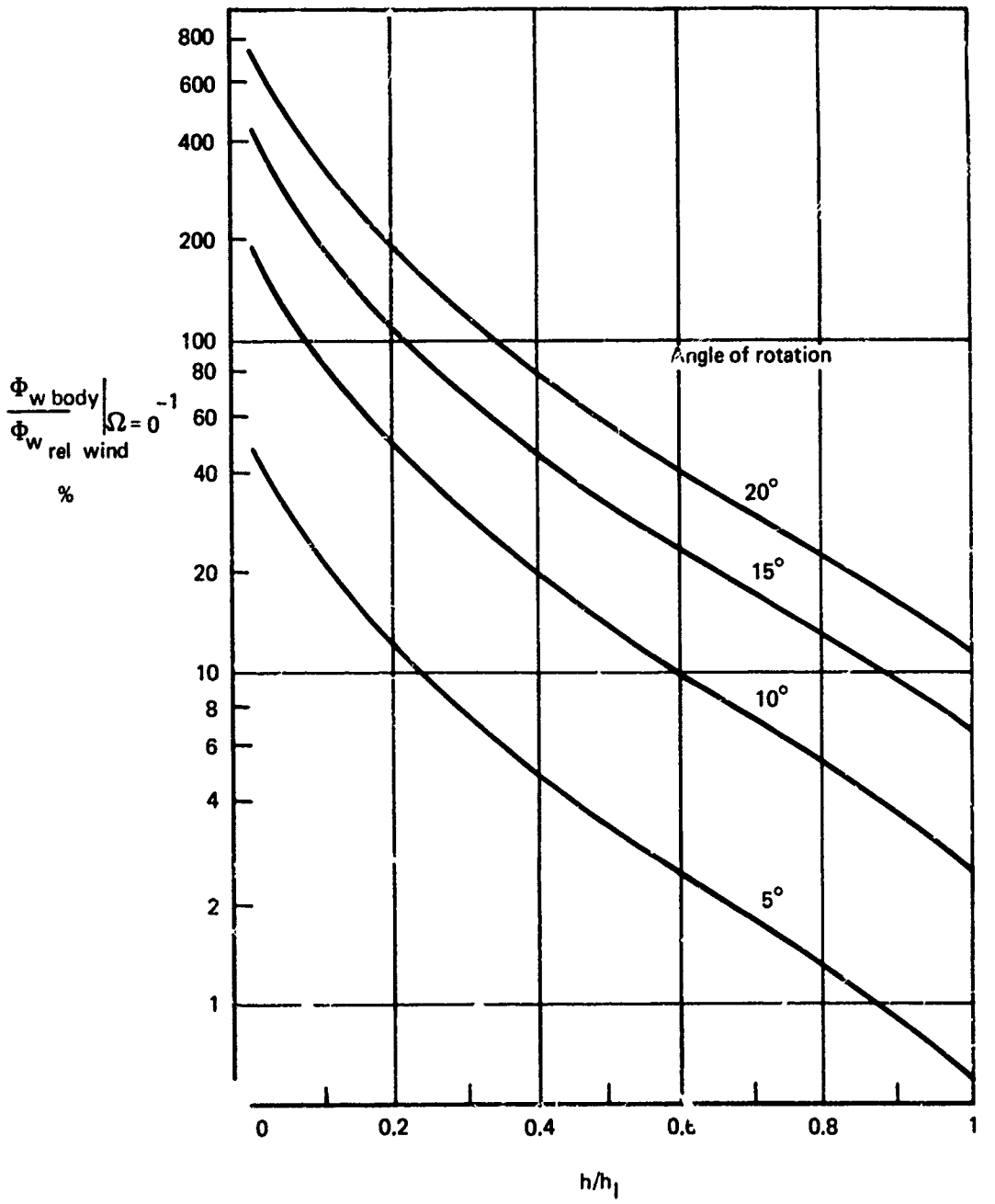

FIGURE 4-51.—LOW FREQUENCY VERTICAL P.S.D. LEVEL, EFFECT OF AXIS ROTATION

generated would then be transformed to the body axis system. This method would have the following effects:

- So long as horizontal isotropy exists, the integral scales and variances would be correctly oriented.
- The error due to the misorientation of the horizontal and vertical spectra shapes depends on the flight path with respect to the air ($\theta - \alpha$).
- Except for small ($\theta - \alpha$) effects, the orientation of the lateral spectra shape would be correct.
- The effect of the u-w mean wind axis cospectrum remains unaccounted for, and large errors could result when the aircraft is not flying in the direction of the mean wind if the u-w cospectrum is significant for any orientation.
- Body axis cospectra will result.

There still is no assurance that this method will not yield significant errors. It can only be stated that the errors will be substantially less than those produced by the other methods. In particular, they will be less than those produced by the conventional method of generating turbulence components in the body axis using relative wind axis spectra shapes and mean wind axis variances and integral scales.

The proposed method is summarized on Figure 4-52. For lack of a better name, the axis system used for the generation of turbulence is referred to as the "turbulence generation" axis system.

4.3.4 Significance of Mean Wind Axis Cospectra

If no cospectra existed in the mean wind axis system, the three linear components of turbulence would be uncorrelated and their statistics would be invariant for rotations in the plane of the earth, assuming horizontal isotropy. However, the literature reveals that cospectra do exist at u-w in the mean wind axis system, and Figure 4-46 shows that the power spectra must be modified and three cospectra must, to be rigorous, be introduced for any deviation from the mean wind heading.

The cospectra can be ignored only if it can be shown that their effects are insignificant. The cospectra have been described as diminishing more rapidly than the power spectra at high frequencies. Thus, at high frequencies, their effects are relatively insignificant. The break frequency of the cospectra has been previously estimated as shown on Figure 4-53. For an extreme surface wind level, say 30 knots, and a minimum altitude of concern, say 30 feet, Figure 4-53 shows the cospectra break frequency to be at 0.003 $\overline{V}_W$ for neutral atmospheric stability (most likely for very high wind speeds and very low altitudes), or about 0.16 rad/sec. This is probably not below the minimum frequency of interest, so it cannot be considered insignificant. The cospectra are likely to have weak effects, however, at least for the majority of the cases.

GENERATE TURBULENCE TO MATCH THE SPECTRA

$$\Phi_{u_{T_{TG}}} = \frac{\sigma_H^2 L_H}{\pi} \frac{1}{\left[1 + (1.339 L_H \Omega_1)^2\right]^{5/6}}$$

$$\Phi_{v_{T_{TG}}} = \frac{\sigma_H^2 L_H}{2\pi} \frac{1 + 8/3 (1.339 L_H \Omega_1)^2}{\left[1 + (1.3339 L_H \Omega_1)^2\right]^{11/6}}$$

$$\Phi_{w_{T_{TG}}} = \frac{\sigma_v^2 L_V}{2\pi} \frac{1 + 8/3 (1.339 L_V \Omega_1)^2}{\left[1 + (1.339 L_V \Omega_1)^2\right]}$$

TRANSFORM TURBULENCE GENERATION AXIS TURBULENCE COMPONENTS INTO BODY AXIS COMPONENTS:

$$\begin{Bmatrix} u_T \\ v_T \\ w_t \end{Bmatrix} = \begin{bmatrix} \cos\Delta\psi \cos\theta & \sin\Delta\psi \cos\theta & -\sin\theta \\ \cos\Delta\psi \sin\theta \sin\phi + \sin\Delta\psi \sin\theta \sin\phi & \sin\Delta\psi \sin\theta \sin\phi + \cos\Delta\psi \cos\phi & \cos\theta \sin\phi \\ \cos\Delta\psi \sin\theta \cos\phi + \sin\Delta\psi \sin\phi & \sin\Delta\psi \sin\theta \cos\phi - \cos\Delta\psi \sin\phi & \cos\theta \cos\phi \end{bmatrix} \begin{Bmatrix} u_{T_{TG}} \\ v_{T_{TG}} \\ w_{T_{TG}} \end{Bmatrix}$$

$\Delta\psi$ = angle from projection of airspeed vector on plane of earth to x body axis projection on plane of earth

$$= -\tan^{-1}\left(\frac{v_{A_P}}{u_{A_P}}\right)$$

$\cong -\beta$ for small $\theta, \phi, \alpha, \beta$

$$u_{A_P} = \left[\cos\alpha \cos\beta \cos\theta + \sin\beta \sin\theta \sin\phi + \sin\alpha \cos\beta \sin\theta \cos\phi\right] V_A$$

$$v_{A_P} = \left[\sin\beta \cos\phi - \sin\alpha \cos\beta \sin\phi\right] V_A$$

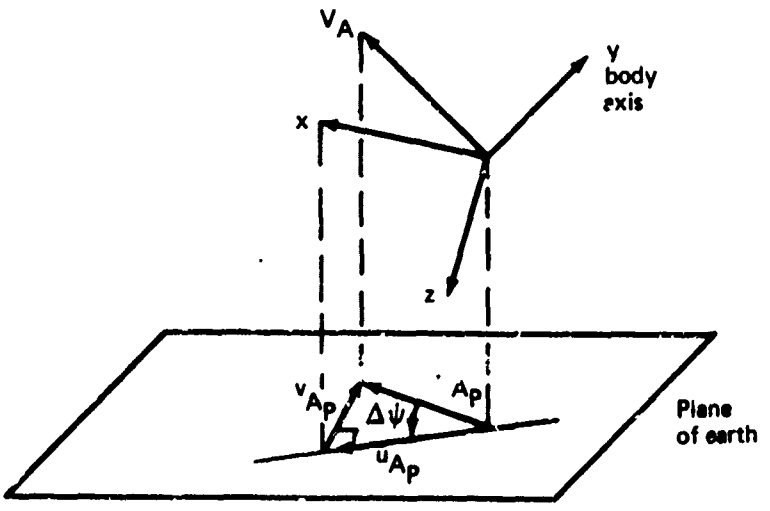

FIGURE 4-52.–GENERATION AND TRANSFORMATION OF TURBULENCE COMPONENTS

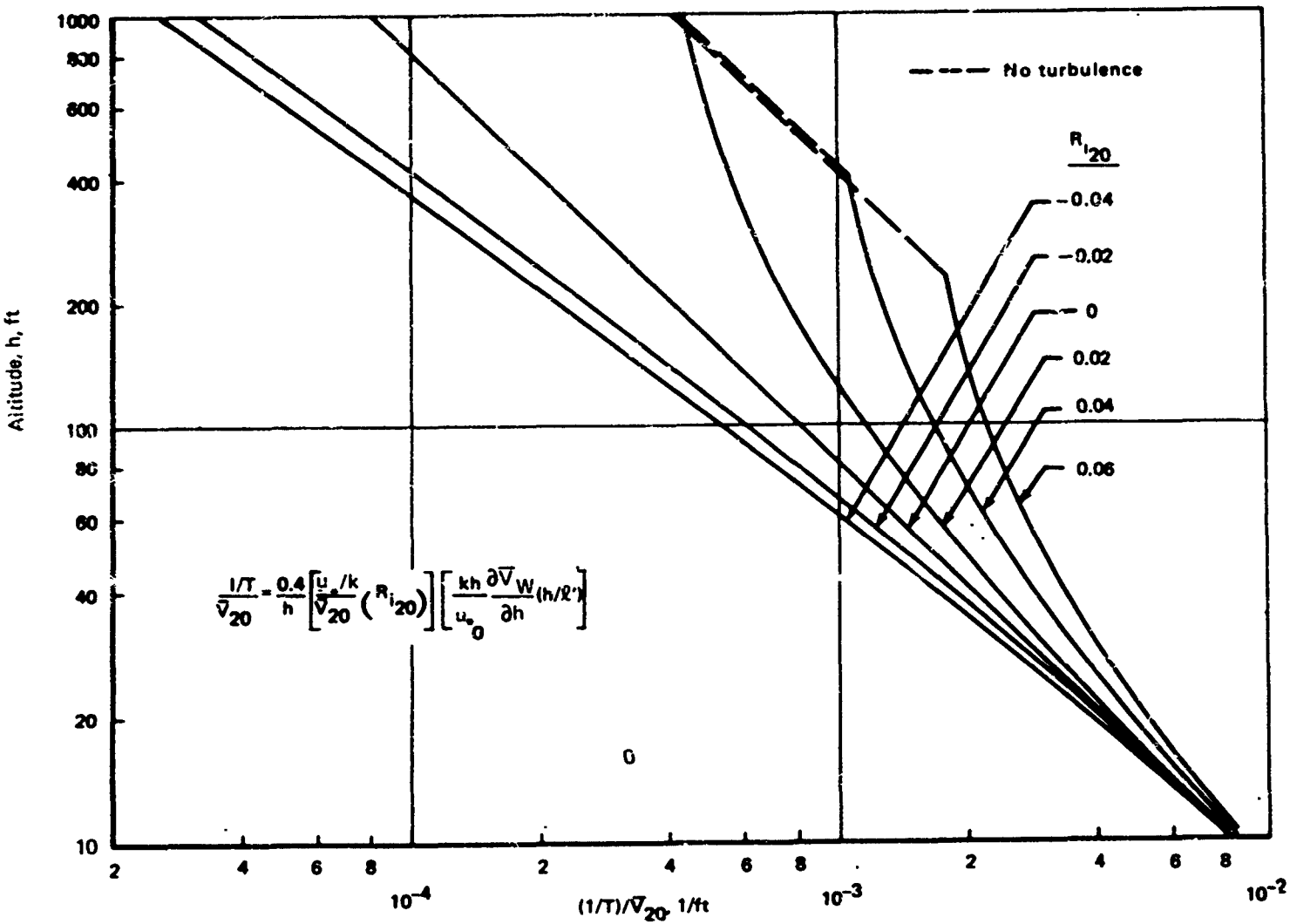

FIGURE 4-53.—COSPECTRUM BREAK FREQUENCY

The general form of the output spectra for a parameter having a constant frequency response has been described as:

$$\theta_\lambda = \left(\frac{\partial\lambda}{\partial u_T}\right)^2 \Phi_u + \left(\frac{\partial\lambda}{\partial v_T}\right)^2 \Phi_v + \left(\frac{\partial\lambda}{\partial w_T}\right)^2 \Phi_w + 2\left(\frac{\partial\lambda}{\partial u_T}\right)\left(\frac{\partial\lambda}{\partial v_T}\right) \Phi_{uv}$$

$$+ 2\left(\frac{\partial\lambda}{\partial v_T}\right)\left(\frac{\partial\lambda}{\partial w_T}\right)\Phi_{vw} + 2\left(\frac{\partial\lambda}{\partial w_T}\right)\left(\frac{\partial\lambda}{\partial u_T}\right) \Phi_{wu}$$

If the effects of the cospectra on all of the force or moment spectra are insignificant, the cospectra are insignificant, even though they may lie within the frequency range of interest.

First, none of the aerodynamic forces and moments are significant with respect to both v_T and u_T or w_T. Thus, the effect of the mean wind axis u-w cospectra on the body axis u-v and v-w cospectra need not be considered further.

For the u-w cospectra to have even a weak effect on a component of force or moment, the force or moment derivatives with respect to longitudinal and vertical gust components must be of the same order of magnitude. If the u_T derivative exceeds the w_T derivative, then the low frequency gain of the cospectra must be large with respect to that of the longitudinal power spectrum:

$$\Phi_\lambda = \left(\frac{\partial\lambda}{\partial u_T}\right)^2 \Phi_u \left[1 + \left(\frac{\partial\lambda/\partial w_T}{\partial\lambda/\partial u_T}\right)^2 \frac{\Phi_w}{\Phi_u} + 2\left(\frac{\partial\lambda/\partial w_T}{\partial\lambda/\partial u_T}\right) \frac{\Phi_{uw}}{\Phi_u}\right]$$

Similarly, if the w_T derivative is large with respect to the u_T derivative, then the low frequency cospectra must be large with respect to the low frequency vertical power spectrum. The same factors that tend to produce a cospectrum break frequency within the frequency range of interest also reduce the low frequency gain ($\Phi_{uw} \sim 1/(1/T)$) so that the low frequency cospectra gain is of the same order of magnitude as the longitudinal, power spectrum when the break frequency is high. It is not at all impossible for the w and u derivatives of a force or moment to be of the same order of magnitude, but it is unlikely and, at most, the effect of the cospectrum will be weak. The number of cases where the cospectra have an effect on aircraft motion does not appear to justify the complexity required to represent them.

4.4 NOISE GENERATION FOR TURBULENCE SIMULATION

The method for generating turbulence by a temporal process is based on the output spectrum. If a single input is filtered, the output power spectrum is defined by:

$$\Phi_{OUT} = \left|G(i\omega)\right|^2 \Phi_{IN}$$

where G(s) is the filter transfer function. Solving for the filter amplitude frequency response gives

$$\left|G(i\omega)\right| = \sqrt{\frac{\Phi_{OUT}}{\Phi_{IN}}}$$

or, if the power spectrum of the input is unity over all frequencies (physically unrealizable as it would imply infinite variance),

$$\left|G(i\omega)\right| = \sqrt{\Phi_{OUT}}$$

That is, the filter can be designed to match the square root of the desired output power spectrum.

It is not actually necessary for the input power spectrum to be unity over all frequencies (white noise), only over the frequency range of interest.

The filtering process does not alter the amplitude distribution of the input; the input power spectrum and the probability density distribution are independent. Thus, the input must have the desired output amplitude distribution.

To meet the requirements of a random process, the correlation between any two elements displaced in time by any amount (serial correlation) must be zero. To match the definition of turbulence, the input random process must have a zero mean.

There are many alternate methods for generating the input random process, both for digital and analog simulation applications. None of them satisfy the requirements exactly. One of the most conceptually simple methods for digital simulation is to load a table of random numbers for the desired probability density distribution into the computer. However, to produce 3 minutes of random noise for three uncorrelated turbulence components and a frame time of 40 milliseconds would require 13,667 random numbers and the same number of storage units. This could be a significant portion of the capacity of most digital simulators, and even the keypunching time would be prohibitive. Thus, an additional requirement of the random process is that it must be efficient, not only in terms of storage requirements, but also in terms of computation time. Other methods for digital, analog, and hybrid applications will be examined.

4.4.1 Analog Computer Methods

4.4.1.1 Analog Random Noise Generators

Semiconductor diodes, photocells, and thyratrons are sources of random noise which have Gaussian probability density distribution. To ensure a zero mean value, the noise signal must go through a dc blocking filter with a sufficiently large time constant to allow passage of the lowest frequency of interest. A bandpass filter selects a frequency band where the noise power spectrum is flat. Using a frequency shifting technique, the flat power spectrum may

start at a desired frequency. An automatic gain-control circuit controlling the mean square output will ensure a stationary noise output.

Binary noise with outputs alternating between two fixed voltages can be produced by a flip-flop triggered by random pulses from some radioactive phenomenon. Such a signal, which sometimes is called a random telegraph wave, may readily be filtered to produce random noise with Gaussian probability distributions and a flat power spectrum.

There are many more random physical phenomena and application techniques which can be used to construct elaborate analog random noise generators. The reader is referred to Reference 4-20 for more complete descriptions.

The output of a given analog noise generator will be affected by variations in ambient temperature, background electromagnetic fields, and any changes in the physical properties of circuit components. The statistical characteristics of the random noise must therefore be verified regularly by the measurement of statistical averages from sufficiently large noise samples.

The analog random noise generator system described in Reference 4-21 is used extensively for low frequency analog computer applications. It offers two stable outputs of band-limited white noise which can readily be filtered to yield other reasonable power spectra. The low frequency output has a flat power spectrum from 0 to 350 hertz, and the high frequency output has a flat power spectrum from 10 to 35,000 hertz. Time-variable filters may be used to produce certain categories of nonstationary noise, and suitable diode function generators can be used to alter the amplitude probability distribution. Since the randomness is derived from nondeterministic physical phenomena, it is impossible to repeat a random sequence of events exactly. This disadvantage may preclude the use of an analog random noise generator in certain applications. Although this type of noise generator has primarily been used with analog computers, they may be used with digital computers by providing a suitable analog-to-digital interface.

4.4.1.2 A Hybrid Analog-Digital Pseudo-Random Noise Generator

The problem of nonrepeatability of random sequences associated with a true analog random noise generator can be avoided by the use of a digital shift register sequence generator, which produces binary pseudo-random noise sequences. A pseudo-random sequence is produced by a deterministic process but satisfies some predetermined set of statistical tests for randomness.

Shift register sequences have been studied quite extensively. Reference 4-20 describes the properties of particular arrangement and shows how a shift register sequence can be applied to produce pseudo-random analog noise. Figure 4-54, which has been reproduced from Reference 4-20, is a block diagram of a practical pseudo-random noise generator system.

Consider an n-bit digital shift register where each bit can either have the state 0 or 1. The register can have 2^n different combinations of 0s and 1s. Starting with any n-bit sequence except all 0s, the states of the n^{th}-bit and, say, the m^{th}-bit are supplied to a modulo-two adder. The output of a modulo-two adder is 1 if the two inputs are different and is 0 if the

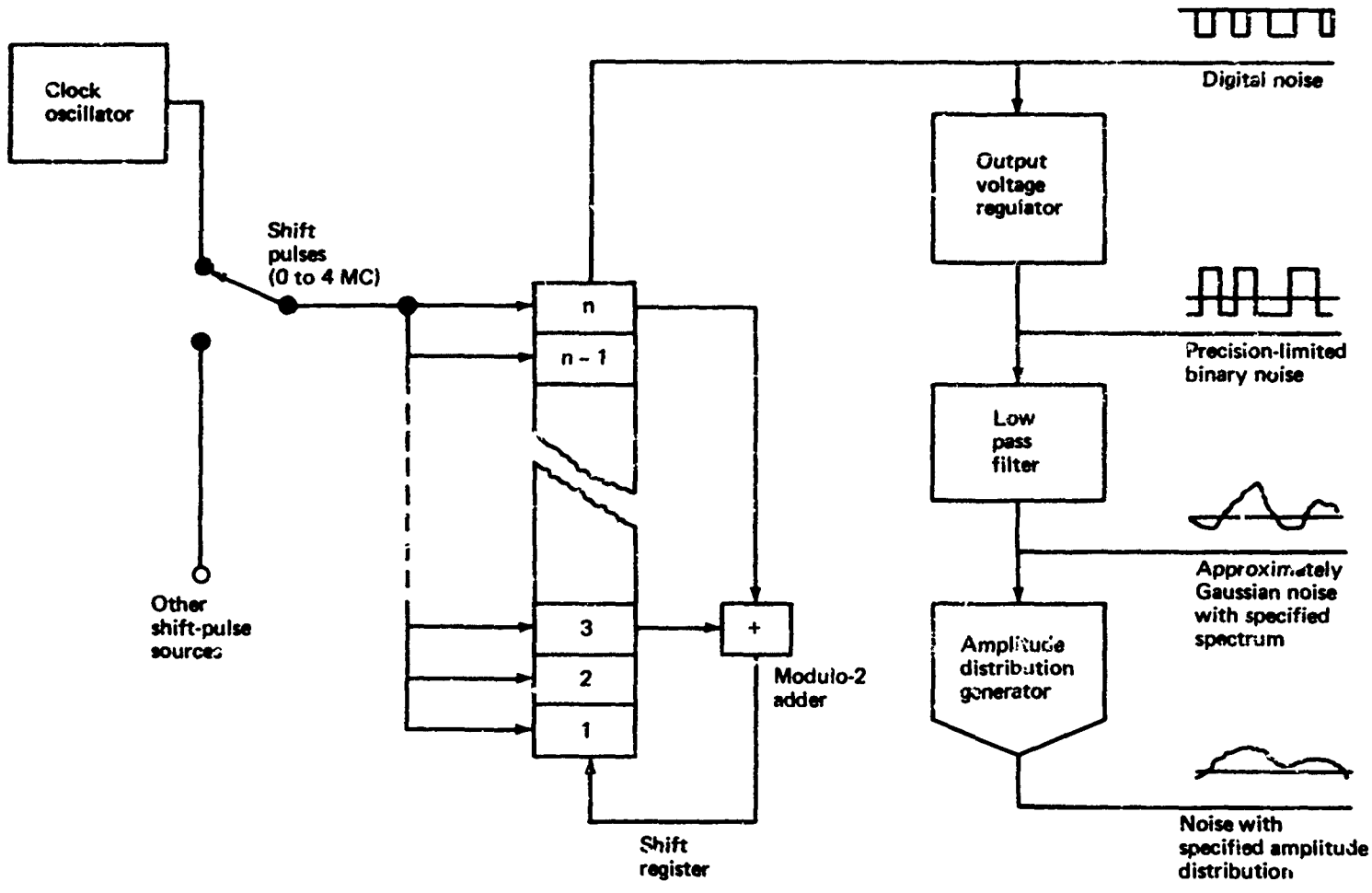

FIGURE 4-54.—A PRACTICAL PSEUDO-RANDOM NOISE GENERATOR SYSTEM

two inputs are the same. Let the modulo-two output state replace that of the first bit and then shift the state of each bit to the next higher order bit in the sequence. Repeating this operation will produce a periodic binary sequence of 0's and 1's. The maximum period obtainable with modulo-two feedback is (2^n-1) if the feedback is selected from the stages specified in Reference 4-20. The all 0's state is excluded from the sequence since it will merely reproduce itself.

The binary sequence is used to produce a pseudo-random square wave x(t) alternating between two values. If there is a shift pulse every Δt seconds, x(t) has a period of $(2^n-1)\,\Delta t$ seconds. When the simulation time is shorter than the shift register period, the first and second order probability distributions of a pseudo-random square wave are essentially the same as those of true random binary noise generated by independent trials yielding one of the two states with equal probability.

The one-dimensional probability distribution of a random square wave assuming one of two equally probable values ($\pm a$) at fixed instants $t = m\Delta t$ consists of two probabilities (see Fig. 4-55).

$$p(x) = \frac{1}{2} \text{ for } x = \pm a$$

$$p(x) = 0 \text{ for } x \neq a$$

This distribution and consequently the mean value of x(t) do not depend upon time. However, the two-dimensional distribution of $x(t)x(t+\tau)$ turns out to be time dependent. Consider the values of x(t) and $x(t+\tau)$ at $t = t_1$, where $|\tau| < \Delta t$ and the time origins have been arbitrarily chosen so that $0 < t_1 < \Delta t$. For a given time displacement τ

$$x(t_1)x(t_1 + \tau) = a^2$$

with a probability of 1 if $(t_1 + \tau) < \Delta t$ and

$$x(t_1)x(t_1 + \tau) = \pm a^2$$

with equal probability of 1/2 if $(t_1 + \tau) < \Delta t$. Therefore, for the same value of the time displacement τ, the ensemble averaged autocorrelation function may have one of two values depending upon the value of the time t_1. Thus the random function considered is nonstationary.

If $|\tau| > \Delta t$, then

$$x(t_1)x(t_1 + \tau) = \pm a^2$$

with equal probability of 1/2 for any value of the time t_1. For time displacements greater than Δt and less than the shift register period $(2^n-1)\,\Delta t$, the pseudo-random square wave x(t) can be considered to represent a stationary random process. The process can also be considered ergodic since successive values of x(t) for time displacements larger than Δt and less than $(2^n-1)\Delta t$ are essentially uncorrelated. The time-averaged mean value and the

n = number of bits in the shift register

$1/\Delta t$ = shift pulse rate

$t_2 = t_1 + \tau$

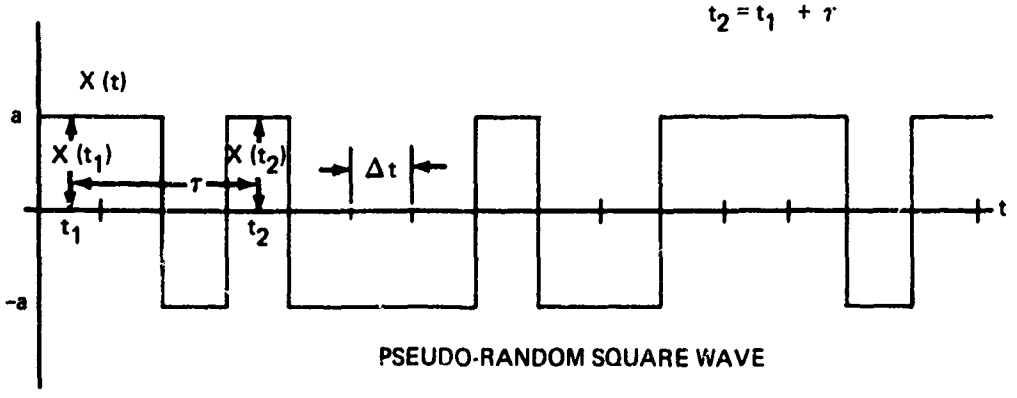

PSEUDO-RANDOM SQUARE WAVE

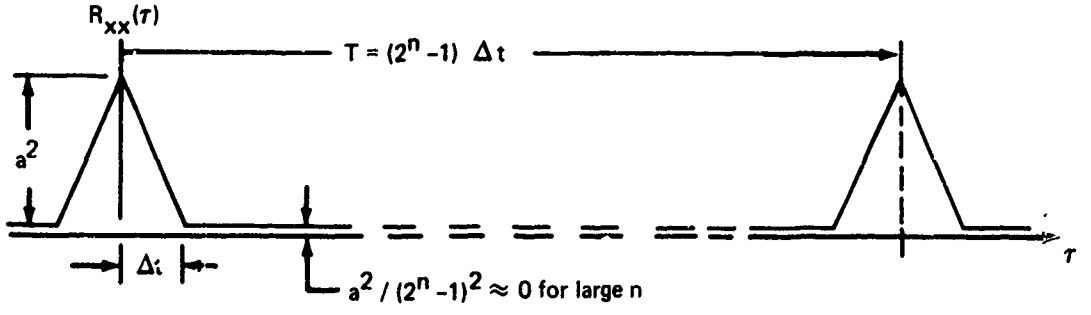

PERIODIC AUTOCORRELATION FUNCTION

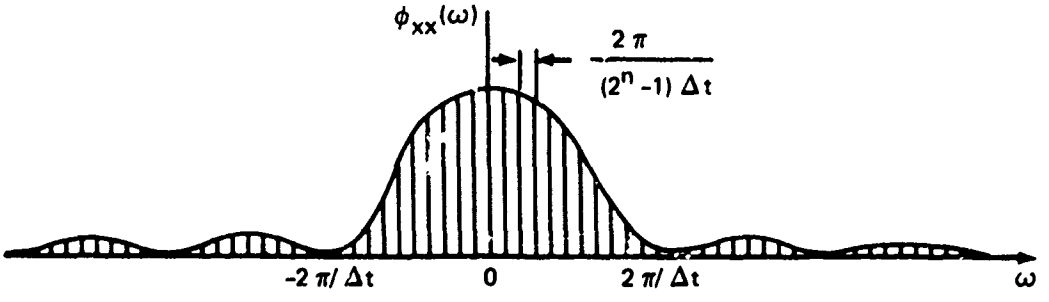

LINE POWER SPECTRUM

FIGURE 4-55.—POWER SPECTRUM AND AUTOCORRELATION FUNCTION OF A BINARY SEQUENCE GENERATOR

autocorrelation function derived from the pseudo-random square wave are then the same as the equivalent ensemble averages.

Referring to Figure 4-55, the time-averaged mean value and autocorrelation function of a pseudo-random square wave alternating between the values +a and -a are as follows:

$$\bar{x} = a/(2^n - 1) \approx 0$$

$$R_{xx}(\tau) = a^2 \left[1 - \frac{|\tau - k(2^n - 1)\,\Delta t|}{\Delta t}\right]$$

when $|\tau - k(2^n - 1)\Delta t| \leq \Delta t$, $(k = 0, \pm 1, \pm 2, \ldots\ldots)$ and

$$R_{xx}(\tau) \approx 0 \text{ otherwise}$$

This autocorrelation function is periodic with time period $(2^n - 1)\Delta t$. For large n the period becomes very long and $a/(2^n - 1)$ tends toward zero. For n = 32 the pseudo-random sequence will repeat after essentially 4,294,967,295 uncorrelated events.

The periodic autocorrelation can be represented by a Fourier series.

$$R_{xx}(\tau) = \frac{a^2}{(2^n - 1)} \sum_{k=-\infty}^{\infty} \left[\frac{\sin(k\omega_0 \Delta t/2)}{k\omega_0 \Delta t/2}\right]^2 e^{ik\omega_0 \tau}$$

where $\omega = 2\pi/(2^n - 1)\Delta t$ is the fundamental frequency.

Transformation of the periodic autocorrelation function yields the power spectral density function:

$$\phi_{xx}(\omega) = \frac{a^2}{(2^n - 1)} \sum_{k=-\infty}^{\infty} \left[\frac{\sin(k\omega_0 \Delta t/2)}{k\omega_0 \Delta t/2}\right]^2 \delta(\omega - k\omega_0)$$

where $\delta(\omega - k\omega_0)$ is the impulse function.

The power spectrum of a periodic pseudo-random square wave is a line spectrum where the spectral lines are separated by the fundamental frequency $2\pi/(2^n-1)\Delta t$. The power contribution from each multiple of the fundamental frequency is proportional to

$$\left[\frac{\sin(k\pi/(2^n-1))}{k\pi/(2^n-1)}\right]^2$$

which is constant within -0.1 dB up to approximately $\omega = k\omega_0 = 0.5/\Delta t$. The shift register period $(2^n-1)\Delta t$ must be large compared to the required simulation time. The fundamental frequency $\omega_0 = 2\pi/(2^n-1)\Delta t$ will then be small compared to the lowest frequency of interest, and adjacent spectral lines cannot be resolved. As the period $T = (2^n-1)\Delta t$ becomes large, the power spectral density function approaches:

$$\phi_{xx}(\omega) = \frac{a^2\,\Delta t}{2\pi}\left[\frac{\sin\frac{\omega\Delta t}{2}}{\frac{\omega\Delta t}{2}}\right]^2$$

the pseudo-random noise approximation band limited white noise, with a specified flat spectrum up to a frequency determined by the shift pulse frequency. The approximate flat spectrum is then

$$\phi_{xx}(\omega) = \frac{a^2\Delta t}{2\pi}$$

and the autocorrelation function is approximated by

$$R_{xx}(\tau) = a^2\,\Delta t\,\delta(\tau)$$

The shift pulse frequency which determines the bandwidth of the white noise must be large compared to the highest frequency of interest in the simulation, but should not be larger than of the order of ten since the power spectral density is proportional to the shift pulse period Δt (Ref. 4-20).

For pseudo-random waveforms with periods greater than $2^{10} \times \Delta t$ (Ref. 4-20) low pass filtering of the pseudo-random waveform will yield random noise with essentially a first-order Gaussian probability distribution, if the filter time constant is large compared to Δt but does not exceed $n\Delta t$. Higher order distributions are not necessarily Gaussian.

It has been shown how a suitably designed pseudo-random binary noise generator will produce approximate band-limited white noise. This method offers many advantages which are not shared by pure analog noise generators discussed in the previous subsection. Since a binary shift register is used to produce the pseudo-random noise, the analog noise output is relatively unaffected by the physical environment. By resetting the initial value of the shift

register, a random sequence of events can be repeated identically. The bandwidth of the flat power spectrum can easily be changed by simply changing the shift-pulse rate. Digital multiplexing can be used to produce multiple uncorrelated noise outputs, and delayed sequences of random noise can readily be obtained.

The mean and mean square outputs of time-invariant linear systems depend only on the autocorrelation function of the random noise input. In the case of the pseudo-random square wave, its triangular autocorrelation function approximates the delta autocorrelation function of white noise very well when the shift period Δt is suitably selected. However, in the case of nonlinear systems, the output will be affected by the second and higher order probability distributions, which are not necessarily Gaussian.

4.4.2 Digital Computer Methods

Methods for providing sequences of random numbers for use on a digital computer can be divided into three groups: generation by a random physical phenomenon, the use of a random number table, and the use of a mathematical process to generate a sequence of pseudo-random numbers. Random numbers that manage to pass a predetermined set of statistical tests for randomness, even though produced by a completely deterministic process, are called 'pseudo-random' numbers.

The first alternative involves attaching a mechanical or electrical random noise generator to the digital computer. By the use of a proper interface, sequences of random numbers can be produced. The analog noise generator described previously may be used for this purpose. This method has the serious disadvantage that a given sequence of random numbers cannot be identically repeated as required in debugging. The associated electronics and other equipment of these devices must be maintained to ensure acceptable invariance of the statistical properties of the output.

The use of random number tables has the advantage that the random number sequences can have almost any desired statistical properties, and that any given sequence of random numbers can be identically repeated. Since generally it would be impractical to store the whole random number table in the memory core, the main problem with this approach is the time required to read the random numbers into the computer. Reference 4-22 describes a random number generator which uses a table but overcomes this problem. The method is considered practical for large computers with buffered inputs.

The third alternative, which will be covered in some detail in this discussion, is the generation of pseudo-random number sequences by a completely specified arithmetic rule which is so devised that certain statistical tests will not detect any significant departure from randomness. Arithmetic methods are normally based on some recurrence relation involving integers. Each new number is generated from the previous one in such a way that the output appears to be drawn at random from the finite population of numbers that the computer can produce.

4.4.2.1 Random Numbers With a Uniform Distribution

Random numbers are normally classified according to their probability density distribution. The following discussion will concentrate exclusively on the generation of random numbers with a uniform probability density distribution. The cumulative distribution function for the standardized uniform distribution is defined as

$$P(X) = \begin{cases} 0, X \leq 0 \\ X, 0 < X < 1 \\ 1, X \geq 1 \end{cases}$$

It will subsequently be shown how random numbers having other distributions can be easily obtained from uniformly distributed random numbers.

The goal is to find a relation that produces sequences of random numbers which are statistically independent, uniformly distributed, reproducible, and nonrepeating for any desired length. Furthermore, the method must satisfy requirements for computational speed and minimum amount of computer memory capacity. The so-called congruential methods, properly applied, have been found to satisfy most of these requirements, and consequently there has been a strong emphasis on their use for digital computations. The fundamental congruence relationship of these methods may be expressed as follows:

$$X_i = aX_{i-1} + C \pmod{m} \quad , \quad (0 < X_i < m)$$

which means that the expression $(aX_{i-1} + C)$ is divided by m, and X_i is set equal to the remainder. X_i is the i^{th} random number and X_{i+1} will be the next. X_i, i, a, C, and m are all positive integers with X_i, a, and C all less than m. Given an initial value X_0, a constant multiplier a, and an additive C, then the congruence relationship given by the above equation will produce the sequence of random integers $X_1, X_2, \ldots, X_i, \ldots$, where all X_i's are less than m. The random integers in the sequence may be transformed to rational random numbers in the interval from 0 to 1 by the relation $r_i = X_i/m$, $0 < r_i < 1$.

The determination of the period of pseudo-random sequences, the statistical testing of given sequences of numbers, and the analytic determination of the statistical properties of sequences of pseudo-random numbers are the three main areas of interest in the studies of arithmetical generators. The parameters which will ensure the maximum period of the sequences have been determined for most of the generators. Statistical tests of the sequences have not been so successful. It is impractical to devise a sufficient set of tests which will ensure randomness for all applications. It is therefore necessary to compromise with statistical properties suitable for most problems. However, cases where the generator properties are incompatible with the particular problem at hand may occur. Therefore, it is important to examine the results to determine whether the simulation is giving a reasonable answer to the problem. The analytic study of the statistical properties of pseudo-random numbers is a difficult task. Significant achievements in this field are presented in References 4-23, -24, and -25.

There are three main congruential methods used for generating pseudo-random numbers, each being a different version of the general relationship. These methods are the multiplicative congruential method, the mixed congruential method, and the additive congruential method. Each of these methods is currently being used on a number of digital computers.

4.4.2.1.1 The Multiplicative Method—The multiplicative congruential method (also called the power residue method) uses the congruence relation

$$X_i = aX_{i-1} \pmod{m}$$

This is a special case where C = 0. Among the three congruential methods the multiplicative method has been found to behave best statistically (Refs. 4-22, -26, and -27). Furthermore, this method offers a relative advantage in terms of computational speed for most cases. Conditions are imposed on the starting value X_0, the constant multiplier a, and the modulus m, to ensure computational speed, a maximum period, and good statistical properties for the sequences generated by this method.

The application of this method in both binary and decimal number systems will be considered.

Binary computers: The multiplicative method for generating pseudo-random numbers on a binary computer is summarized from Reference 4-26 as follows:

(1) Choose $m = 2^b$, where b is the number of binary bits in a computer word.

(2) Choose a positive odd integer as the starting value X_0.

(3) Choose an integer $a = 8t \pm 3$ as the constant multiplier, where t is a positive integer giving a value for a close to $2^{b/2}$.

(4) Compute aX_0 using fixed-point integer arithmetic. This product will consist of 2^b bits, from which the lower order b bits are retained and are equal to the new number X_1.

(5) Compute $r_1 = X_1/2^b$ to obtain a uniformly distributed rational number from the interval 0 to 1.

(6) Each successive random number X_i is obtained from the lower order bits of the product aX_{i-1}.

With the above selection of the modulo m, the multiplicative constant a, and the starting value X_0, the maximum period of 2^{b-2} will be obtained ($b > 2$). The full period includes one-fourth of all the different numbers available.

Decimal computers: The multiplicative method for generating pseudo-random numbers on a decimal computer is summarized from Reference 4-26 as follows:

(1) Choose $m = 10^d$, where d is the number of decimal digits in a computer word.

(2) Choose a positive odd integer not divisible by 5 as a starting value X_0.

(3) Choose an integer $a = 200\,t \pm p$ as the constant multiplier, where p is any of the values 3, 11, 13, 19, 21, 27, 37, 53, 59, 61, 69, 77, 83, 91 and t is a positive integer giving a value for a close to $10^{d/2}$.

(4) Compute aX_0 using fixed-point integer arithmetic. This product will consist of 2d digits, from which the lower order digits are retained and are equal to the number X_1.

(5) Shift the decimal point d digits to the left to convert the random integer number X_1 into a uniformly distributed rational number r_1 from the interval 0 to 1.

(6) Each successive random number X_i is obtained from the lower order digits of the product aX_{i-1}.

With the above selection of the modulo m, the multiplicative constant a, and the starting value X_0, the maximum period of $5 \times 10^{d-2}$ will be obtained ($d > 3$). The full period includes one-fourth of all the different numbers available.

The fact that the value of the multiplicative constant a was chosen to be close to the square root of m in both cases is a necessary but not sufficient condition for minimizing first order serial correlation between the numbers in the sequences. Although the multiplicative method is considered to be the better of the three congruential methods, Reference 4-22 points out several shortcomings. Only empirical testing can establish confidence in the statistical properties of a given sequence generated by the multiplicative congruence method.

4.4.2.1.2 The Mixed Method–The mixed congruential method uses the fundamental congruence relation described where $C \neq 0$. The advantage of this method is that by the proper selection of the multiplier and the additive constant C, the period will cover the full set of m different numbers, m being the modulo. As before, the application of this method in both binary and decimal number systems will be considered.

Binary computers: The mixed method for generating pseudo-random numbers on a binary computer is summarized from Reference 4-26 as follows:

(1) Choose $m = 2^b$ where b is the number of binary bits in a computer word.

(2) Choose a positive integer number for X_0.

(3) Choose a positive odd integer number for C.

(4) Choose an integer $a = (2^S + 1)$ for a constant multiplier ($S \geq 2$).

(5) Compute $(aX_0 + C)$ using fixed-point integer arithmetic. This result will consist of 2b bits, from which the lower order bits are retained and are equal to the number X_1.

(6) Compute $r_1 = X_1/2^b$ to obtain an informally distributed rational random number from the interval 0 to 1.

(7) Each successive random number X_i is obtained from the lower order bits of the result $(aX_{i-1} + C)$.

With the above selection of the modulo m, the multiplicative constant a, the additive constant C, and the starting value X_0, the maximum period of 2^b will be obtained ($b \geq 2$). The full period includes all the numbers available.

Decimal computers: The mixed method for generating pseudo-random numbers on a decimal computer is summarized from Reference 4-26 as follows:

(1) Choose $m = 10^d$, where d is the number of decimal digits in a computer word.

(2) Choose a positive integer number as the starting value X_0.

(3) Choose a positive odd integer number not divisible by 5 for the additive constant C.

(4) Choose an integer $a = (10^S + 1)$ for a constant multiplier ($S \geq 2$).

(5) Compute $(aX_0 + C)$ using fixed-point integer arithmetic. The result will consist of 2d digits. from which d digits are retained and are equal to the number X_1.

(6) Shift the decimal point d digits to the left to convert the random integer number X_1 into a uniformly distributed rational number r_1 from the interval 0 to 1

(7) Each successive random number X_i is obtained from the lower order digits of the result $(aX_{i-1} + C)$.

With the above selection of the modulo m, the multiplicative constant a, the additive constant C, and the starting value X_0, the maximum period 10^d will be achieved ($d \geq 2$). The full period includes all the different numbers available.

Although the preceding conditions will ensure a maximum period of the pseudo-random sequences, they are not sufficient for assuming that the mixed congruential method will be statistically satisfactory. The selection of a value for the constant multiplier close to the square root of m is not sufficient for minimizing first order serial correlation for these sequences. Only empirical testing can establish confidence in the statistical properties of a given sequence generated by the mixed congruential method. Systematic testing of mixed congruential generators with $m = 2^{35}$ and $m = 10^{10}$ has been described in References 4-22

and 4-28. These tests revealed that the value of X_0 has no significant influence on the statistical properties although certain values of C tended to improve the statistical properties of the sequences. For $m = 2^{35}$, $a = (2^7 + 1)$ is a good choice of multiplier when C = 1. For $m = 10^d$ with $d \geq 8$, a good choice of a multiplier is a = 101 when C = 1. All the digits in the random numbers generated by this method have the full period. This makes small word sizes and higher speeds possible when the length of the period is of little significance.

4.4.2.1.3 The Additive Method–The additive congruential method is described by the recursion relation

$$X_i = (X_{i-1} + X_{i-n}) \pmod{m}$$

where the X_is, i, n, and m are positive integers with $n \geq 2$ and $X_i < m$. As for the other congruential generators, the values normally chosen for the modulo m are 2^b for binary computers and 10^d for decimal computers where b is the maximum number of bits and d is the maximum number of decimals.

The starting values $X_0, X_{-1}, \ldots X_n$ must be provided in an original storage. This method can produce sequences with periods longer than m since a given number is determined by the combinations of two predecessors. For a binary computer the pseudo-random numbers generated by this method will have a period equal to $P \times 2^{b-1}$, where P_n depends on n and the word size b. Several values for P_n, when b is equal to 35, are tabulated in Reference 4-29. For example, for n = 16 the period is 255×2^{34}. In general, $n \geq 16$ is necessary but not sufficient to ensure good statistical characteristics. Discarding every second number from the sequence produces reasonable random numbers with n = 6 and with a period equal to 63×2^{34} (Ref. 4-26). Additive generators were originally proposed because addition is faster than multiplication on most computers. However, the computational speed depends upon the particular programming codes used, and the indexing operations tend to reduce the speed advantage. As in the case of the two methods discussed earlier, the determination of the statistical properties of random number sequence produced by an additive congruential generator will require empirical tests.

The multiplicative method has generally been found to behave well statistically, while the mixed and additive generators do not always do as well. Several papers have been published indicating that some correlation exists between successive numbers produced by the multiplicative and mixed generators. These correlations are suspected to occur less frequently for the multiplicative method. However, Reference 4-25 claims that the difference in correlation results from using a less than optimum fixed multiplier for the mixed generators, and concludes that there is no significant difference in the statistical properties of the sequences produced by the multiplicative and mixed generators. The correlations appear as patterns and periodicities in the random number sequences and may give poor results in problems where order statistics are important.

4.4.2.1.4 Advanced Congruential Methods–Reference 4-22 maintains that the commonly used tests for randomness in pseudo-random number sequences have little relevance to actual applications and have therefore limited value. Instead a series of more stringent tests on multiplicative and mixed generators and on two improved generators were conducted. It

was concluded that the mixed methods are not satisfactory and the multiplicative methods are suspect at best. The alternative generators developed passed all the devised tests for randomness.

One of the improved methods uses a stored table of random numbers derived from the Rand Corporation table of random digits (Ref. 4-30). As a number is used, it is replaced by a transformed version of itself provided by the relation

$$X_i^1 = aX_i + C \pmod{m}$$

so that when the original table is exhausted a new table is available. This can be repeated for several cycles by using a different value for a and C in each cycle. Thus, the problem of a finite table is avoided. Reference 4-22 used the transformation

$$X_i^1 = (2^{15} + 5)\, X_i + 3 \pmod{2^{27}}$$

for the second run, and

$$X_i^1 = (2^7 + 1)\, X_i + 1 \pmod{2^{27}}$$

for the third run. This method is only practical for large computers using a buffered input.

The second improved method suggested in Reference 4-22 uses two congruential generators, where one shuffles the order in which the numbers from the other generator are chosen. Reference 4-22 used the following relations to describe this method

$$X_i = (2^{17} + 3)\, X_{i-1} \pmod{2^{35}}$$

$$Y_i = (2^7 + 1)\, Y_{i-1} + 1 \pmod{2^{35}}$$

where $X_0 = 1$, $Y_0 = 0$. The first 128 random numbers produced from the first relation were stored in the memory core. The first seven bits produced by the second relation were used as an index to pick one number from one of the 128 core locations. The location of the chosen number was then refilled with the next number produced by the first relation. The time used to generate a random number by this method is about twice the time required with a single congruential generator. Reference 4-22 concludes that the method does have better statistical properties than any of the other congruential generators.

4.4.2.1.5 Selected Congruential Methods--It appears that the multiplicative congruential method is a good, simple choice with few pitfalls. For some applications, the mixed method or the additive method may be faster, but their parameters must be chosen with care to ensure equivalent statistical properties. However, the sequences produced by these three generators display certain nonrandom serial patterns and periodicities which may or may not have a measurable effect on the results from turbulence simulations. For applications where the additional computational time and storage requirements of more complex methods are acceptable, the use of a random number table or the combination of two generators as suggested in Reference 4-22 should be adopted.

4.4.2.2 Random Numbers with Nonuniform Distributions

This section discusses how uniformly distributed random numbers from the interval 0 to 1 may be transformed into random numbers drawn from other probability distributions. Random numbers which are uniformly distributed between 0 and 1 are denoted by r_i. There are three basic methods, or some variation of them, for simulating nonuniform distributions: the inverse transformation method, the rejection method, and the composition method. Following is a brief general description of these methods based on Reference 4-26.

4.4.2 2.1 Inverse Transformation Method–To generate the random numbers X_i from a particular population whose probability density function is given by f(x), it is necessary to obtain the cumulative distribution function

$$F(x) = \int_{-\infty}^{x} f(x)\,dx$$

F(x) is defined over the range 0 to 1. Therefore, x_i, which is a random number from the distribution f(x), is uniquely determined by the relation

$$r_i = F(x_i)$$

where, as before, r_i is a uniformly distributed number from the interval 0 to 1. For any value of r_i it is possible to find a value x_i determined by

$$x_i = F^{-1}(r_i)$$

if the inverse function F^{-1} of the function F is known. For many probability distributions it is impossible to obtain an analytic expression for the inverse function of the cumulative distribution function. This problem can be overcome by the use of a numerical approximation to the distribution function, as illustrated in Figure 4-56. This method is very suitable for generating random numbers having empirical distributions.

4.4.2.2.2 The Rejection Method–If the nonuniform probability density function f(x) is bounded and the corresponding random numbers have a finite range $a \leq x \leq b$ the following method may be used:

(1) Multiply f(x) by a scale factor c, such that

$$cf(x) \leq 1 \quad a \leq x \leq b$$

(2) Express x as a linear function for r,

$$x = a + (b - a)r$$

(3) Generate pairs of random numbers (r_1, r_2)

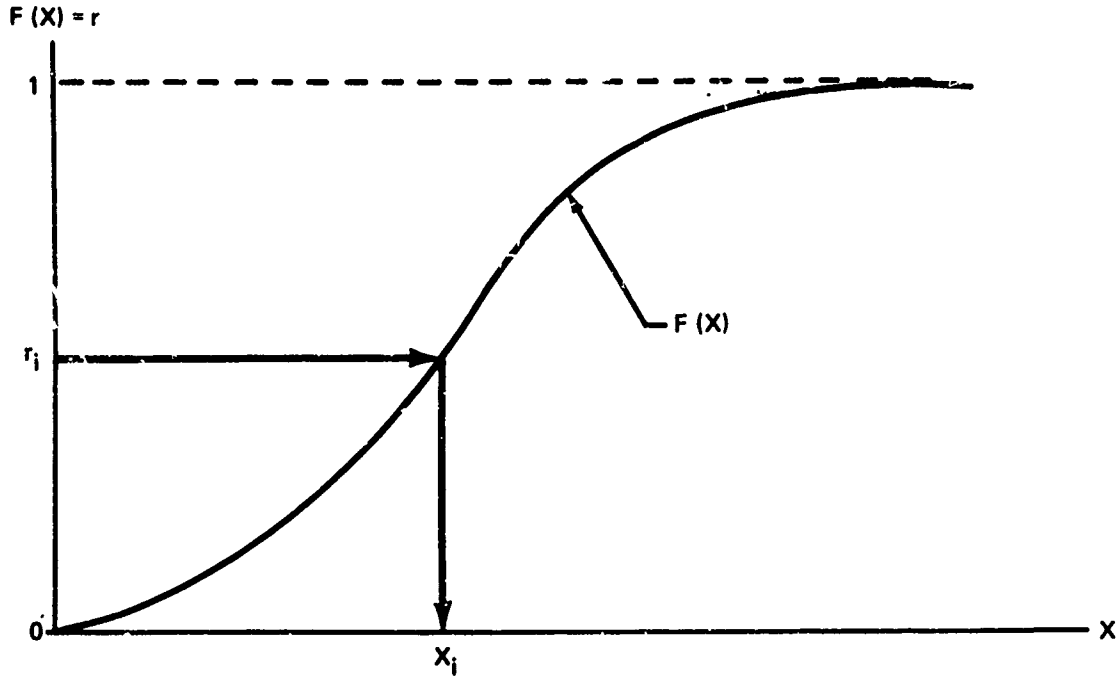

r_i = random number from uniform distributed numbers in the interval 0 to 1

X_i = random number from a population with cumulative probability distribution F(X)

FIGURE 4-56.–NUMERICAL APPROXIMATION TO OBTAIN THE INVERSE OF A CUMULATIVE DISTRIBUTION FUNCTION

(4) If a pair of random numbers that satisfy the relationship

$$r_2 \leq cf[a + (b - a)r_1]$$

are encountered, then "accept" the pair and use $x = a + (b - a)r_1$ as the random number generated. If this relationship is not satisfied, reject the pair and continue to generate another pair.

The theory behind this method is based on the fact that probability of

$$[r \leq cf(x)] = cf(x)$$

If x is selected at random from the range a to b according to step 3 and rejected or accepted according to step 4, then the probability density function of the accepted values of x will be f(x). The mean number of trials before a successful pair of random numbers (r_1, r_2) is found is 1/c and therefore the method may be inefficient for certain probability density functions.

4.4.2.2.3 The Composition Method -Random numbers having a probability density function f(x) may be generated by combining random numbers having simpler but properly selected probability density functions $g_i(x)$. The proportion from each of the approximate distributions $g_i(x)$ is such that

$$f(x) = \sum_{i=1}^{n} g_i(x) P_i$$

P_i and $g_i(x)$ are selected with the purpose of minimizing the sum

$$T = \sum_{i=1}^{n} T_i P_i$$

Where T_i is the average computation time for generating random numbers from $g_i(x)$.

4.4.2.3 The Normal Distribution

In statistical work the normal distribution is the best known and most frequently used probability density distribution. Both mathematical proof and statistical experience indicate that this distribution is to be expected when dealing with complex natural physical phenomena. The assumption of normally distributed gust velocities has been commonly used in the modeling of turbulence fields. For this reason, the generation of normally distributed random numbers will be covered in some detail in the following discussion.

If a random variable x has a probability density function

$$f(x) = \frac{1}{\sigma_x \sqrt{2\pi}} e^{-1/2 \left[\frac{x - \bar{x}}{\sigma_x}\right]^2} \quad , \quad -\infty < x < \infty$$

Where σ_x is the standard deviation and $\bar{x}$ is the mean value, then x has a Gaussian or normal probability density function. The cumulative Gaussian distribution function F(x) only exists in integral form, but its values are tabulated in almost any book on statistics. There are four methods commonly used to generate normally distributed random numbers: the central limit method, Teichrow's approximation, the direct method, and the composition method.

4.4.2.3.1 Central Limit Method–The central limit theorem states that the probability distribution of the sum of n independently but identically distributed random numbers with respective mean values $\bar{x}_i$ and variances σ_i^2 will approach the normal distribution asymptotically with a mean value and variance equal to

$$\bar{x} = \sum_{i-1}^{n} x_i$$

$$\sigma_x^2 = \sum_{i-1}^{n} \sigma_i^2$$

when n becomes large. Summing uniformly distributed numbers having the same mean values and variances, a value for n as low as 10 will provide a good approximation to the normal distribution for values of x less than $3\sigma_x$ from the mean value.

If r_1, i = 1, 2 .... n, are n uniformly distributed numbers from the interval 0 to 1, the central limit theorem yields the following relationship

$$x = \sigma_x \left[\frac{12}{n}\right]^{1/2} \left[\sum_{i=1}^{n} r_i - \frac{n}{2}\right] + \bar{x}$$

where x is a random number from an approximately Gaussian population with mean value equal to $\bar{x}$ and standard deviation equal to σ_x. The value of n is normally selected to be 12 to simplify the computations, in which case this equation reduces to

$$x = \sigma_x \left[\sum_{i-1}^{n} r_i - \frac{n}{2}\right] + \bar{x}$$

This approach leads to a relatively fast program, but the value of n = 12 truncates the distribution at $\pm 6\ \sigma_x$, and values of x greater than $\pm 3\ \sigma_x$ from the mean value have been found to be unreliable (Ref. 4-26).

It can be seen from Figures 4-57, -58, and -59 that the central limit method with n = 12 will produce probability distributions where deviations beyond three times the standard deviation are considerably less likely than would be predicted by the Gaussian distribution. The turbulence generated by these methods will therefore contain fewer large peak gusts than would be predicted by the Gaussian distribution. To obtain better accuracy, larger values of n may be considered, but in these cases the efficiency of the central limit method decreases and other approaches should be considered.

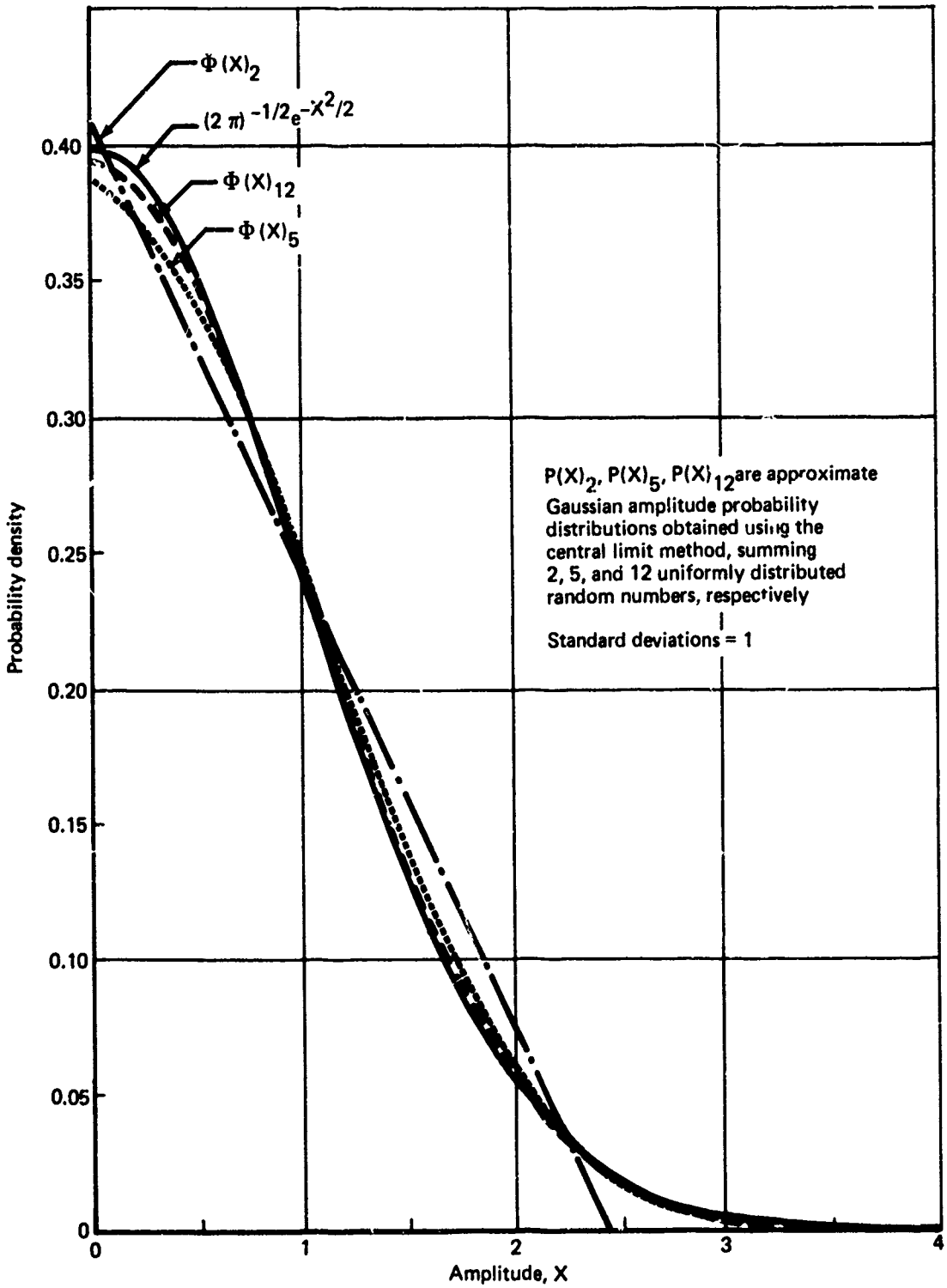

FIGURE 4-57.--APPROXIMATE GAUSSIAN AMPLITUDE DISTRIBUTIONS, LINEAR PLOT

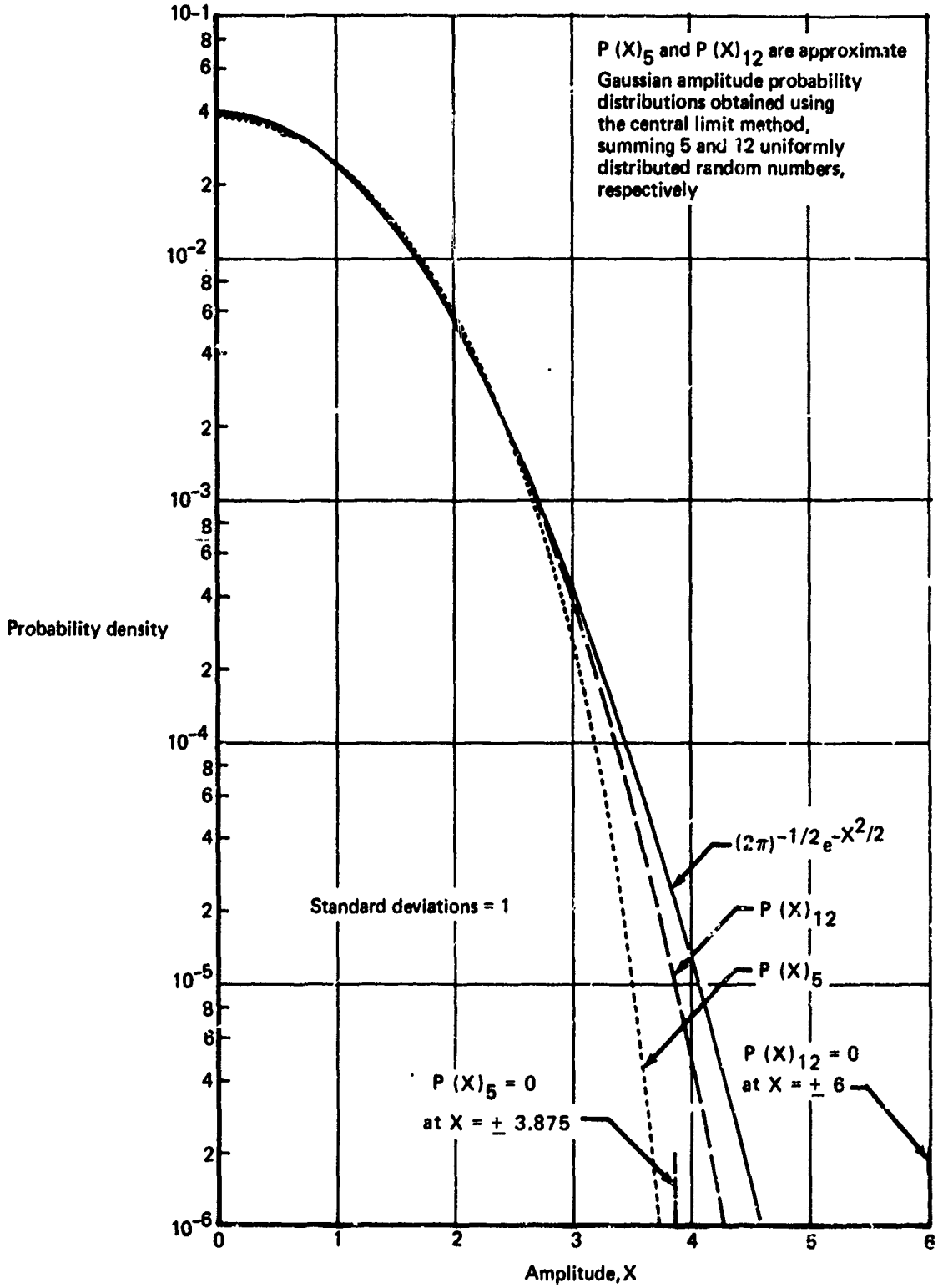

FIGURE 4-58.–APPROXIMATE GAUSSIAN AMPLITUDE DISTRIBUTIONS, LOG PLOT

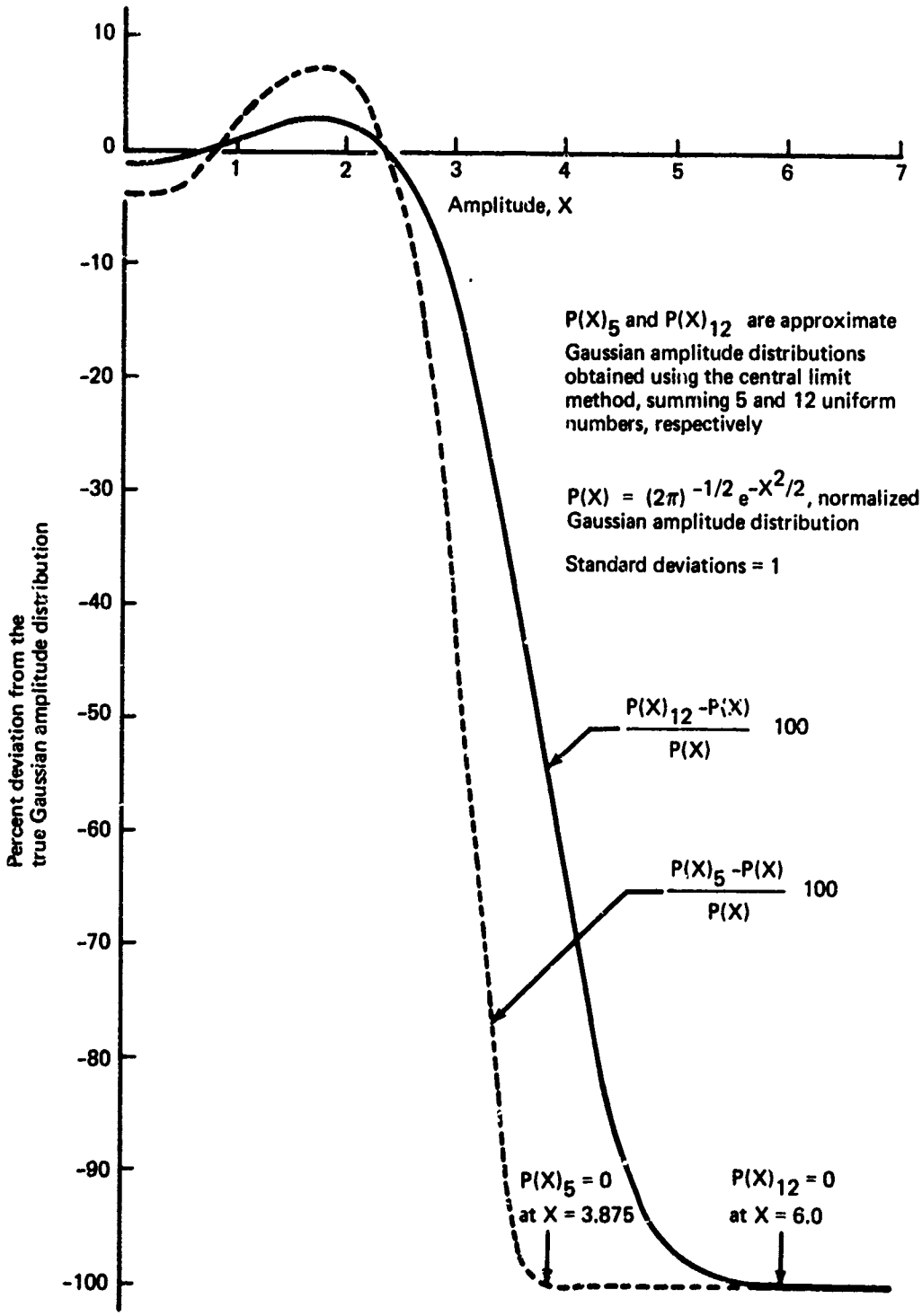

FIGURE 4-59.–DEVIATIONS OF APPROXIMATE GAUSSIAN AMPLITUDE DISTRIBUTIONS FROM THE TRUE GAUSSIAN DISTRIBUTION

4.4.2.3.2 Teichrow's Approximation–This is a variation of the central limit method that improves the accuracy of the sequences obtained but is fairly inefficient. From Reference 4-20 let

$$y = \frac{1}{4}\left(\sum_{1}^{12} r_i - 6\right)$$

then a random number x drawn from a normally distributed population with mean value equal to 0 and standard deviation equal to 1 is given by

$$x = y\left|a_1 + y^2\left(a_3 + y^2\left(a_5 + y^2\left(a_7 + a_9 y^2\right)\right)\right)\right|$$

where

$a_1 = 3.949846138$

$a_3 = 0.252408784$

$a_5 = 0.076542912$

$a_7 = 0.008355968$

$a_9 = 0.02989776$

4.4.2.3.3 The Direct Method–Let r_1 and r_2 be two independent random numbers from a uniform distribution in the interval 0 to 1. Then

$$x_1 = (-2 \log_e r_1)^{1/2} (\cos 2\pi r_2)$$

$$x_2 = (-2 \log_e r_1)^{1/2} (\sin 2\pi r_2)$$

are two random numbers from a population with a normal distribution, with mean value equal to 0 and standard deviation equal to 1. This transformation is exact, and the speed of calculations compares well with that of other methods if the required function subroutines are efficient.

4.4.2.3.4 Composition Method–The normally distributed random numbers are derived from three populations having different densities, $g_1(x)$, $g_2(x)$, and $g_3(x)$. The normal density function is approximated by

$$f(x) = 0.9578 g_1(x) + 0.395 g_2(x) + 0.027 g_3(x)$$

This method is faster than the direct method but requires approximately 500 storage locations for specified constants. The equation implies that $g_1(x)$ is used 95.78% of the time, $g_2(x)$ is used 3.95% of the time, and $g_3(x)$ is used 0.27% of the time. The generation

of random numbers from the population having density functions $g_1(x)$ is fast, while the generation of random numbers from the two populations having density functions $g_2(x)$ and $g_3(x)$ is relatively slow. Reference 4-31 describes this method in detail.

4.4.2.3.5 Comparison of Normal Distribution Methods–The selection of a digital method for generating a normal distribution involves a tradeoff between accuracy, computation time, and storage requirements. This tradeoff is a strong function of the computer's characteristics. Even for a given computer, the tradeoff between computation time and storage will lead to different optimum solutions for different simulations, depending whether memory or computation time is most critical.

The composition method can be rejected out of hand as it involves large computation storage requirements without superior accuracy. A comparison of the computation time requirements for the other methods is made on Table 4-3. Time required for mathematical operations will vary tremendously from computer to computer, particularly time required for table lookups and nonarithmetic operations. Table 4-3 is provided only as an illustration, and the time requirements are based on a relatively modern digital computer. The linear distribution is presumed to be generated by the multiplicative congruential method, and the time required by nonarithmetic operations is not considered.

Table 4-3 shows that the inverse transformation method requires the least time. However, a table accurately representing the inverse of the cumulative probability requires a very large number of values, depending on how much of the tails is represented.

The next fastest method is the central limit method, depending on how the number of elements from a linear distribution are to be used. However, as shown on Figure 4-59, the central limit method drastically underpredicts the tails of the normal distribution. Teichrow's method is a more accurate version of the central limit method.

Two estimates are made for the direct method. The differences depend on whether table lookup or series are used to compute the logarithm, square root, and cosine functions. Table lookups are feasible for these functions because the numbers operated upon are either scaled or can be scaled to reduce the number of points required to represent the function accurately. When storage requirements are critical, the series representations of the functions is used. The accuracy of the direct method is limited only by the number of bits in a word.

The figures on Table 4-3 are misleading because neither the storage requirements nor the accuracy is held constant between the methods. This is not possible, as the accuracy of the direct method cannot be duplicated by the other methods. The choice of the optimum method depends heavily upon how much of the normal distribution tails must be represented.

The significance of the tails depends on both the response variable and the criteria applied to that variable. For example, the infrequent high velocity samples of turbulence are more important for acceleration variables, having a more nearly instantaneous response to turbulence, than for the position variables. The large amplitudes have greater influences on the tails of the response distribution than on the amplitudes near the response mean. Hence,

TABLE 4-3.–GAUSSIAN DISTRIBUTION GENERATION: COMPARISON OF COMPUTATION TIME

		Central Limit theorem				Inverse transformation		Tiechrow's approximation		Direct method	
		5 samples		12 samples							
Operation	Time operation (μsec)	Number	Time (μsec)	Number	Time (μsec)	Number	Time (μsec)	Number	Time (μsec)	Number	Time (μsec)
Additions	3	6	18	13	39			17	102		
Multiplications	6							6	36	1	9
2-D table lookup or nonarithmetic functions	50					1	50			3	180 / 396
Random numbers	15	5	75	12	180	1	15	12	180	2	30
Totals			93		219		65		318		189 / 435

the tails are more important when performance limits (rate of sink, touchdown dispersion, nacelle strike, etc.) cannot be exceeded more often than, say, once in 10^9 landings than when performance limits cannot be exceeded more often than once in 10^3 landings.

It is usually desirable to have a standard noise generation technique for all simulations. An intuitive estimate for approach and landing is that the distribution should be accurately represented to three standard deviations. This would rule out the central limit method using less than 12 samples. The method that appears to be most suitable as a standard is the direct method. Use of the direct method eliminates accuracy considerations without the severe core requirements of the inverse transformation method. The tradeoff then needs to be performed only when constraints on time are severe. Even then, the additional time over the central limit method, for three turbulence components and the numbers on Table 4-3, is only 0.00065 second.

4.4.2.4 The Power Spectrum of a Digital Noise Generator

The preceding discussion shows how periodic sequences of pseudo-random numbers with a given probability density distribution may be generated on digital computers. The following analysis will derive expressions for the autocorrelation function and the power spectral density function. Referring to Figure 4-60, consider a random function x(t), which represents the random variations in a particular turbulence component. The time axis is divided into equal intervals Δt. In successive time intervals the random function assumes independent values which are kept constant over the time increment Δt. If x_1 is the magnitude of x(t) at $t = t_1$, the probability that $x(t_1)$ lies between the value x_1 and $x_1 + dx_1$ is given by

$$\text{Probability of } \left[x_1 < x(t_1) < x_1 + dx_1\right] = f(x_1)\, dx_1$$

where f(x) represents the probability density functions of the random function x(t). It can be seen that f(x) values do not depend upon the time t_1.

The two-dimensional probability density distribution of $x(t)\, x(t + \tau)$ turns out to be time dependent. Consider the values of x(t) and $x(t + \tau)$ at $t = t_1$, where $|\tau| < \Delta t$ and the time origin has been chosen so that $0 < t_1 < \Delta t$. For a given time displacement τ, let $x(t_1 + \tau) = x_2$. Then,

$$x(t_1)\, x(t_1 + \tau) = x_1^{\,2}$$

with probability

$$g(x_1\, x_2)\, dx_1\, dx_2 = f(x_1)\, \delta(x_1 - x_2)\, dx_1\, dx_2,$$

if $(t_1 + \tau) < \Delta t$, i.e.,

$$x(t_1) = x(t_1 + \tau) = x_1,$$

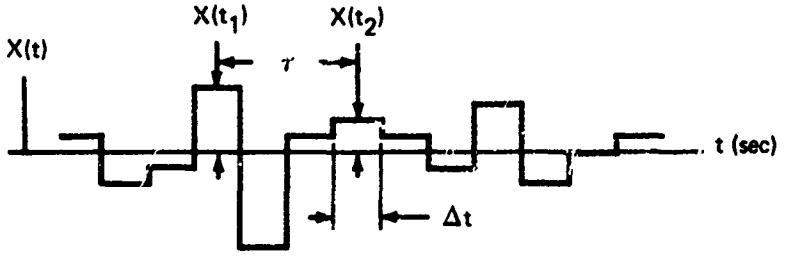

RANDOM WAVE

σ_X = standard deviation
Δt = simulation frame time
$t_2 = t_1 + \tau$

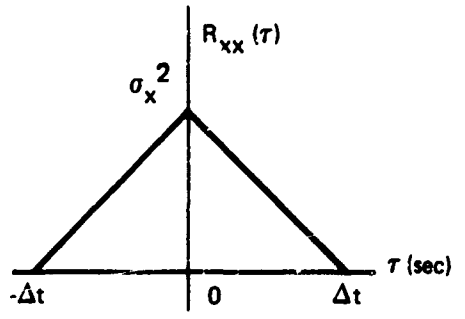

AUTOCORRELATION FUNCTION

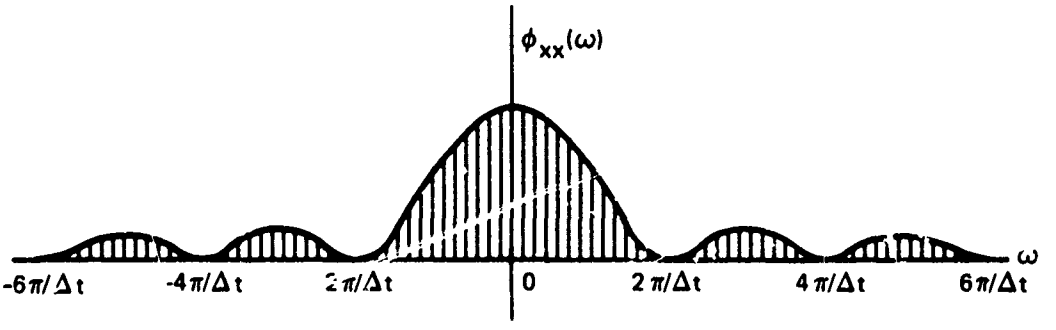

POWER-DENSITY SPECTRUM

FIGURE 4-60.--POWER SPECTRUM AND AUTOCORRELATION FUNCTION OF A DIGITAL RANDOM NUMBER GENERATOR

and

$$x(t_1)\, x(t_1 + \tau) = x_1\, x_2$$

with probability

$$g(x_1,x_2)\, dx_1\, dx_2 = f(x_1)\, f(x_2)\, dx_1\, dx_2,$$

if $(t_1 + \tau) > \Delta t$, i.e.,

$$x(t_1) = x_1,\ x(t_1 + \tau) = x_2$$

where $g(x_1 x_2)\, dx_1\, dx_2$ is the joint probability that $x(t_1)$ has a value between x_1 and $x_1 + dx$, and $x(t_1 + \tau)$ has a value between x_2 and $x_2 + dx_2$. For the same time displacement τ the joint probability distribution has two different expressions, depending upon the sampling time t_1. Thus, the random function considered is nonstationary.

If $|\tau| > \Delta t$, then

$$x(t_1)\, x(t_1 + \tau) = x_1\, x_2$$

with probability

$$g(x_1,x_2)\, dx_1\, dx_2 = f(x_1)\, f(x_2)\, dx_1\, dx_2$$

for any value of the time t_1.

For time displacements greater than Δt and less than the period T, the periodic pseudo-random function x(t) can be considered to represent a stationary random process. The function can also be considered ergodic since successive values of x(t) for time displacements greater than Δt and less than T are essentially uncorrelated. The time-averaged mean value and the time-averaged autocorrelation derived from x(t) may be considered the same as the equivalent ensemble averages.

The probability that $x(t) = x(t + \tau)$ is the probability that t and $t + \tau$ are both in the same interval Δt, which is evidently $(1 - (|\tau| \div \Delta t))$ if $|\tau| < \Delta t$ and zero if $|\tau| \geq \Delta t$. The time-averaged autocorrelation function $R_{xx}(\tau)$ of the periodic pseudo-random function x(t) with a mean value equal to zero and variance equal to σ_x^2 is

$$R_{xx}(\tau) = \sigma_x^2 \left[1 - \frac{|\tau - kt|}{\Delta t}\right]$$

when $|\tau - kt| \leq \Delta t$, $(k = 0, \pm 1, \pm 2 \ldots)$

and

$$R_{xx}(\tau) = 0$$

otherwise.

This autocorrelation function is periodic, having the same period T as the random function x(t). However, for the purpose of turbulence simulation the period T may be made sufficiently larger than the time delays of interest so that the periodicity may be neglected.

Transforming the autocorrelation function yields the power spectral density function

$$\phi_{xx}(\omega) = \frac{\sigma_x^2 \Delta t}{2\pi} \left[\frac{\sin \omega \Delta t/2}{\omega \Delta t/2}\right]^2$$

This power spectrum which is shown graphically in Figures 4-60, -61, and -62 is constant within -0.1 dB up to approximately $\omega = 0.5/\Delta t$.

The effect of the periodicity of x(t) is to make the power spectrum a line spectrum where the spectral lines are separated by fundamental frequency $\omega_0 = 2\pi/T$. The power contribution from each multiple of the fundamental frequency is proportional to

$$\left[\frac{\sin (k\pi\Delta t/t)}{k\pi\Delta t/T}\right]^2$$

However, since the period T will be sufficiently larger than the time delays of interest, the spectrum will appear continuous.

The pseudo-random function x(t) approximates band-limited white noise with a specified flat spectrum up to a frequency determined by the frame time Δt. The approximate flat spectrum is

$$\phi_{xx}(\omega) \simeq \frac{\sigma_x^2 \Delta t}{2\pi}$$

and the corresponding autocorrelation function is approximated by

$$R_{xx}(\tau) = \sigma_x^2 \Delta t \, \delta(\tau)$$

The frame time Δt which determines the bandwidth of the white noise must be small compared to the smallest time constant and oscillation period of interest in the simulation. The power spectral density is proportional to the frame time Δt and the variance σ_x^2, but is independent of the form of the particular probability density function.

Any random process used on a digital computer or any digital pseudo-random process, even when used with an analog computer, has the above spectrum characteristics, and the elements of the process must be multiplied by $2\pi/\Delta t$ to give bandwidth-limited white noise.

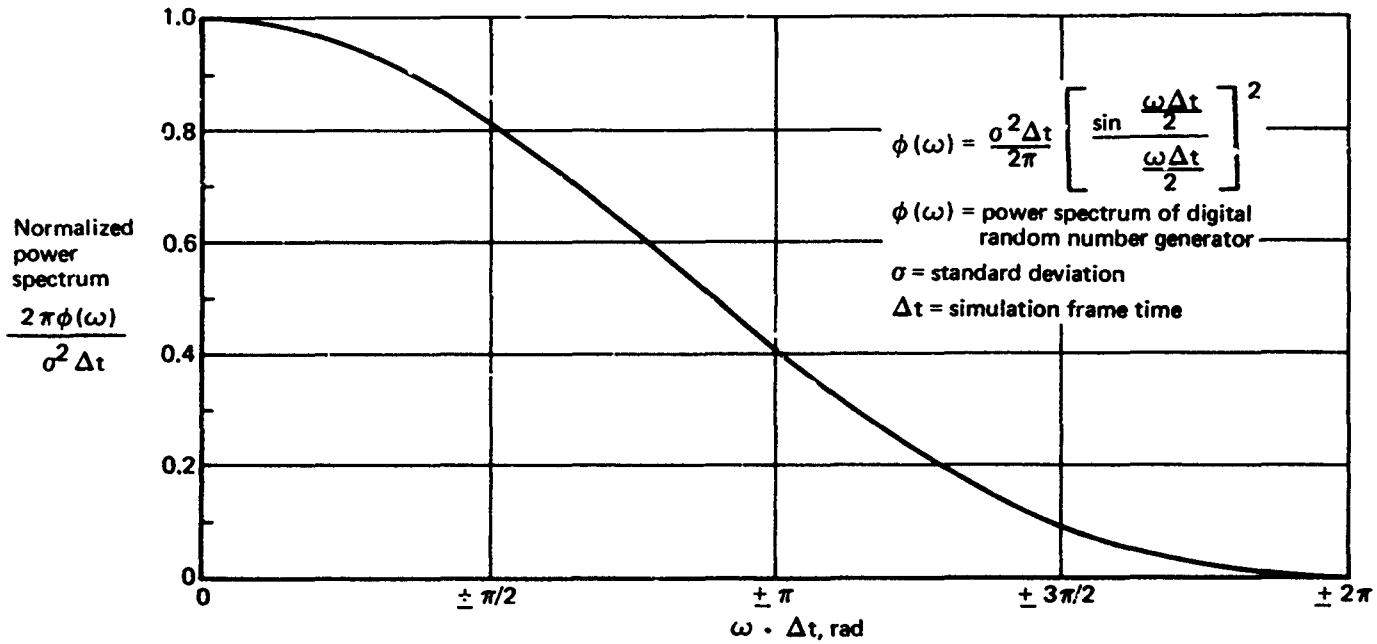

FIGURE 4-61.--DIGITAL RANDOM NUMBER GENERATOR POWER SPECTRUM

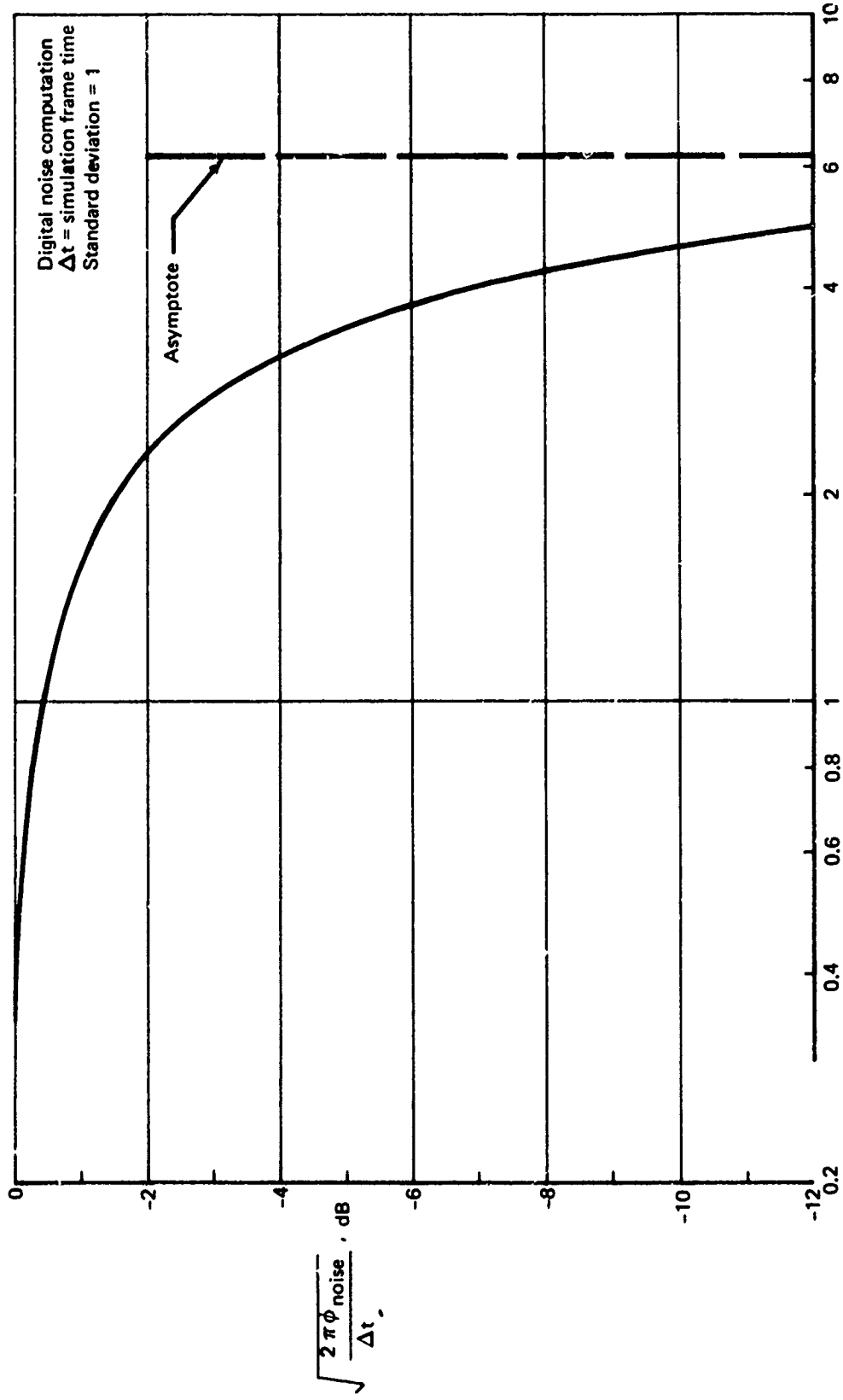

FIGURE 4-62.–NOISE POWER SPECTRUM, LOG-LOG SCALE

4.4.2.5 Digital Computer Application

Programming of digital simulators is not generally performed by the test engineer. Software techniques for generating noise are not as well understood as analog techniques, and digital simulation does not lend itself so well to noise spectral analysis. For these reasons, the digital simulation test engineer often has little knowledge of noise generation. Consequently, a brief review and discussion of pitfalls is pertinent.

The objective is to provide uncorrelated noise with a spectrum of unit amplitude over the frequency range of interest, referred to as "band-limited white noise." There are three basic steps required to achieve this result by software, as shown on Figure 4-63:

- Generation of a uniform distribution, having unit amplitude between 0 and 1.
- Generation of a normal or Gaussian distribution from samples of the linear distribution.
- Division of the samples from the normal distribution by the square root of low frequency unadjusted spectrum gain.

The uniform distribution generation controls the statistical randomness of the noise. The most common methods are variations of the congruential relationship. The basic procedure requires multiplication of the previously generated unadjusted random number by a constant, to which another constant may be added. The resulting number is stored in two registers. The unadjusted random number is equal to the lower order bits in the second register. This number is then adjusted to provide an element from a uniform distribution between 0 and 1. The resulting uniform noise distribution has a mean of 1/2 and a variance of 1/12.

The randomness of the noise may be strongly dependent upon proper selection of the multiplicative and additive constants. When using the multiplicative congruential method (power residue method), too low a multiplicative constant can introduce strong correlation between successive samples. When a small random number occurs, a small constant will cause the next number in the overflow register to be small compared to the size of the register. The overflow will then increase monotonically until the capacity of the register is exceeded, after which the numbers will tend to be random until another small number is generated.

Correlation between successive numbers introduces high frequency harmonics, with the frequency of the harmonics proportional to the multiplicative constant. This serial correlation appears as strong, long period "fluctuating shears," and may be observed by the slow buildup of the signal standard deviation to the desired level when computing a cumulative signal standard deviation. The effect may be masked by judicious selection of the starting number. However, the selection of the starting number does not alter the correlation. A more relevant test of a bias is the lack of a running standard deviation (say, over the previous 10 seconds) to build up slowly.

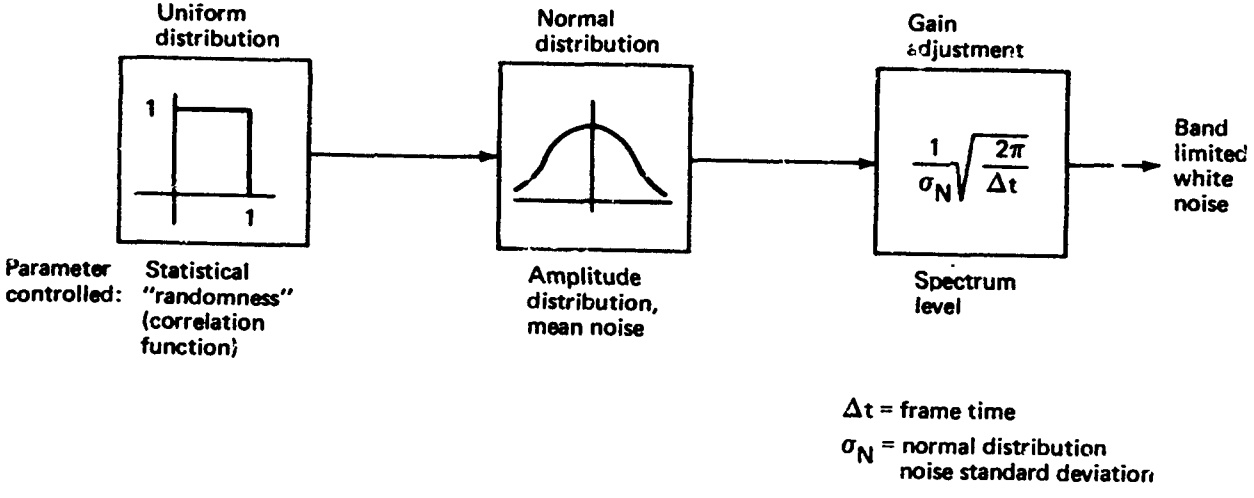

FIGURE 4-63.—WHITE NOISE GENERATION STEPS

The probability density distribution of the white noise is controlled by the generation of the normal distribution from elements of the linear distribution. If the peak output noise never exceeds, say, twice the noise standard deviation, the error is likely to be in this step. This step is also where the non-zero mean of the linear distribution is corrected to produce zero mean. The level of the noise is frequently adjusted at this step to provide output noise with a unity standard deviation. The objective is not, however, to provide noise with a standard deviation of one. Rather, adjustment for the noise standard deviation is more correctly considered as part of the next step, the adjustment of the low frequency spectrum level.

The output of the Caussian generation produces a spectrum with low frequency gain of

$$\lim_{\omega \to 0} \Phi_{NOISE} = \frac{\sigma_N \Delta t}{2\pi}$$

Where Δt is the sampling interval and σ_N is the standard deviation of the Gaussian noise. The noise spectrum is 10% within a constant spectrum up to about $\omega \Delta t = 1.15$. On digital computers, computational stability for feedback loops exists for time constants as short as 50% greater than the frame time. Thus, the noise spectrum is essentially flat for the maximum frequency that can be represented.

Since the noise spectrum is flat, band-limited white noise is achieved by multiplying the unadjusted spectrum by a constant k,

$$\Phi_{N_{OUT}} = k^2 \Phi_{N_{IN}}$$

$$k = \sqrt{\frac{\Phi_{N_{OUT}}}{\Phi_{N_{IN}}}} = \sqrt{\frac{1}{\frac{\sigma_N^2 \Delta t}{2\pi}}} = \frac{1}{\sigma_N} \sqrt{\frac{2\pi}{\Delta t}}$$

This factor may be conveniently combined with the filter gain to give low frequency gains of:

Component	$\sqrt{\Phi_{N_{OUT}}\big\vert_{\omega \to 0}}$	Combined Gain
u	$\sigma_u \sqrt{L_u/\pi V_A}$	$\frac{\sigma_u}{\sigma_N} \sqrt{2L_u/V_A \Delta t}$
v	$\sigma_v \sqrt{L_v/2\pi V_A}$	$\frac{\sigma_v}{\sigma_N} \sqrt{L_v/V_A \Delta t}$

Component	$\sqrt{\Phi_{N_{OUT}}}\ \omega \to 0$	Combined Gain
w	$\sigma_w \sqrt{L_w/2\pi V_A}$	$\frac{\sigma_w}{\sigma_N} \sqrt{L_w/V_A \Delta t}$

The combined gain should not be confused with a change of units of the spectrum being modeled. That is, the spectrum of turbulence that eventually results has units of $(ft/sec)^2/(rad/sec)$, not $(ft/sec)^2/(cycles/sec)$.

To provide uncorrelated turbulence components, three white noise generators are generally specified. However, when software is used to produce the pseudo-random number, it is undesirable to use different techniques for each component. Then, the same routine may be used for all three components by simply using different starting numbers for generating the uniform distributions.

Software noise generation eventually repeats, so care must be taken in the selection of the three starting numbers so that they are not displaced over too short a time period. That is, the correlation between two turbulence components may be perfect if the noise sequences are shifted in time. If the time shift required is too short, the effective aerodynamic coupling occurs.

A safer and more efficient method for generating uncorrelated turbulence components is to simply make three passes through the noise generator in one computation frame. If the constants for the noise generator are correctly selected, the sequences for the three components are separated in time by at least one-third the period of the noise generator.

4.5 MODELING FOR SIMULATION

The model providing the effects of wind is described in terms of six basic parts, as shown on Figure 4-64:

- The probability model, which is not used on line or during the running of the simulation, is used to determine the combinations of parameters defined deterministically.
- Using the probabilistic parameters, the mean wind speed and mean wind shear are determined at the airplane's altitude.
- The turbulence associated with the mean wind is generated at the airplane's altitude and for the airplane's airspeed.
- Using the Euler angles describing the airplane's attitudes, the wind heading, and the horizontal components of airspeed, the mean wind and the turbulence components are transformed into components along the airplane's body axis and are assigned to the airplane's center of gravity.

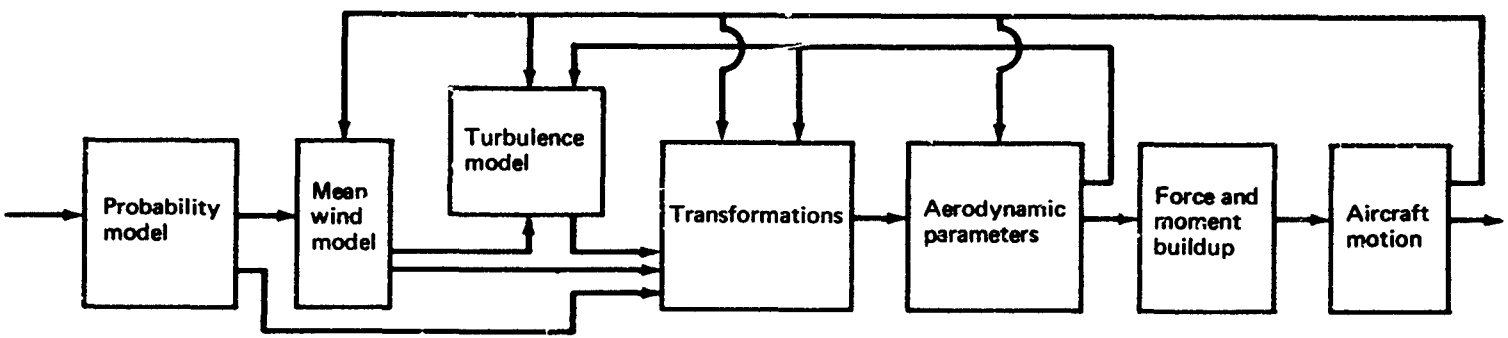

FIGURE 4-64.—WIND MODEL SCHEMATIC

- The airplane's inertial velocities and the components of wind are combined to form the parameters required for determining aerodynamic forces.

- The aerodynamic forces are developed in a manner compatible with the technique required to accurately reflect the effects of the wind and turbulence.

A last step, the determination of aircraft motion from the forces and moments, is unaltered by the presence of wind and turbulence.

4.5.1 Probability Model

Frequently there are two probabilities to be dealt with, an input and an output probability. For example, a criterion may state that for a headwind having a magnitude equal to or less than that occurring 90% of the time, the airplane may not have a lateral dispersion greater than such or such value for more than 1% of the landings.

The input and output criterion may be stated qualitatively, as in Reference 4-32: "... analysis should show that under realistic environmental conditions ... the touchdown performance will be such that landing outside the prescribed dispersion area will be improbable."

The output probability is used to ensure that an accident will occur very infrequently. The use of the input probability is less clear. If a known relationship exists between the input and the output (i.e., higher surface wind speeds cause exceeding touchdown position limits to be more probable), the input probability may be used to reduce the number of parameters and/or to reduce the output probability while maintaining constant the likelihood of an accident. This approach is most suitable when a single input is described probabilistically and least suitable when multiple inputs are described probabilistically, particularly when the combination of inputs that are successively more critical is unknown.

When surface conditions are severe enough, an airplane need not land at a specific airfield, but has recourse to diverting to an alternate field. The input probability may be used to reflect the severity of conditions that should be met or to restrict the severity of conditions that must be met.

The descriptions of a mean wind and turbulence that have been selected provide for three parameters defined probabilistically: wind heading at the surface, wind speed at the surface, and atmospheric stability measured at the surface. A fourth parameter that could have been included is the heading shear, or the profile of wind heading. However, no analytic description, matching empirical measurements, nor any empirical description could be found and the parameter shall not be described.

All other parameters have been described deterministically in terms of the probabilistically defined parameters, even though distributions about the deterministic descriptions are likely.

Increases in the surface wind cause more severe wind conditions for aircraft during approach and landing. Although more stable atmospheric conditions cause more severe mean wind shears up to a point, they also reduce the severity of turbulence for a fixed surface wind speed, making it difficult to define the probability of being at a more severe stability condition. It is also quite difficult to define the most and least severe surface wind headings for all aircraft.

It is concluded that a ranking of combinations of probabilistically defined parameters according to increasing severity is not possible for all aircraft. Consequently an input probability is not used. Rather, combinations of parameters shall be provided according to the weighting provided by the joint probability densities.

One simplification to the joint distribution function is immediately available: evidence that the wind heading (as measured from the heading of the prevailing wind) is correlated with either the mean wind speed or atmospheric stability is very weak, and wind heading will be assumed to be uncorrelated with stability and wind speed. On the other hand, evidence that the distribution of atmospheric stability is dependent upon the wind speed is quite strong, and a joint description must be provided. A joint description of the surface mean wind speed and atmospheric stability is generated by providing a unique probability density distribution of atmospheric stability at the surface for each surface wind speed.

A means must be provided to generate the desired joint probability density distributions. First, the distribution for two correlated parameters is considered (such as atmospheric stability and wind speed at the surface). As an example, all the wind speeds are divided into two groups, say, those that are less than 10 knots and those that are greater than 10 knots. Let the probability of having a wind speed less than 10 knots be 0.65 and the probability that the wind speed is greater than 10 knots be 0.35. Similarly, all conditions of stability are divided into groups of stable and unstable and assigned probabilities as follows:

	$P\{R_{i_{20}} < 0\}$	$P\{R_{i_{20}} > 0\}$
$\bar{V}_{20} < 10$ kt	0.3	0.7
$\bar{V}_{20} > 10$ kt	0.45	0.55

The joint probabilities of the four possible outcomes are computed as shown on Figure 4-65. The case of uncorrelated parameters can be evaluated in the same manner, but the result reduces to the joint probability equal to the product of the unconditional probabilities:

$$P\{A, B\} = P\{A\}\, P\{B\}, \quad A \text{ and } B \text{ uncorrelated}$$

The outcome of Figure 4-65 is represented if first all wind speeds or Richardson's numbers within an interval are assigned the mean of the interval. The interval means are plotted

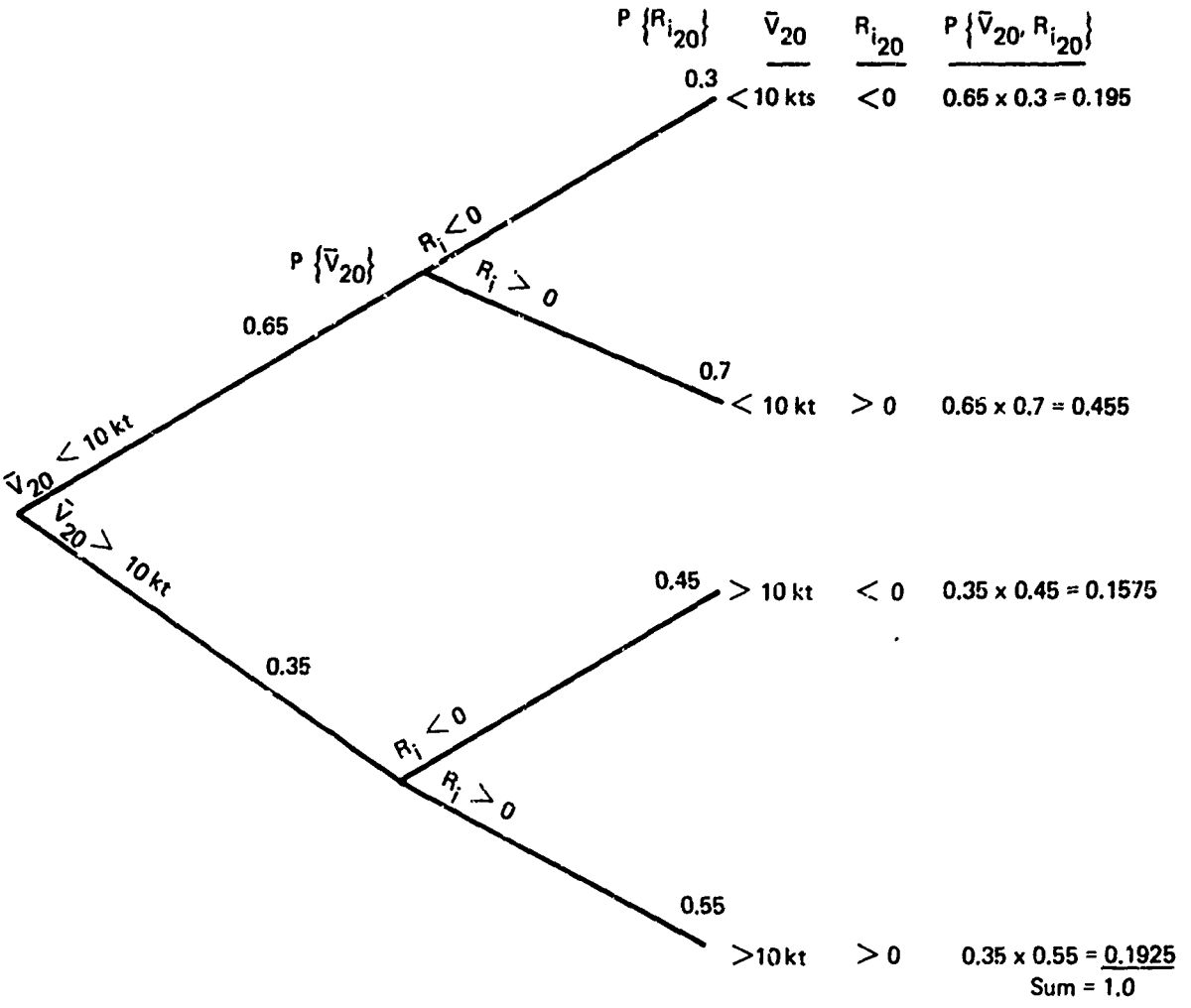

FIGURE 4-65.–EXAMPLE: JOINT PROBABILITY FOR CORRELATED PARAMETERS

against a 0 to 1.0 argument so that the percentage of the 0 to 1.0 space occupied by an interval mean is equal to the probability of the interval. The plots corresponding to the example are shown on Figure 4-66.

A random number from a 0 to 1.0 uniform distribution is generated and the first curve is entered to obtain a $\bar{V}_{20}$. Depending on the $\bar{V}_{20}$ obtained, a second curve is entered with a new random number to obtain R_{i20}. As the procedure is repeated many times, the joint distributions obtained are those in Figure 4-65.

The example described is quite crude, but better joint probability representations are obtained as more intervals are used for each parameter. As the number of intervals approaches infinity, the curves in Figure 4-66 approach the inverses of the cumulative probability curves, with the 0 to 1.0 argument equal to the cumulative probability (the exceedance probability curves could be used just as well).

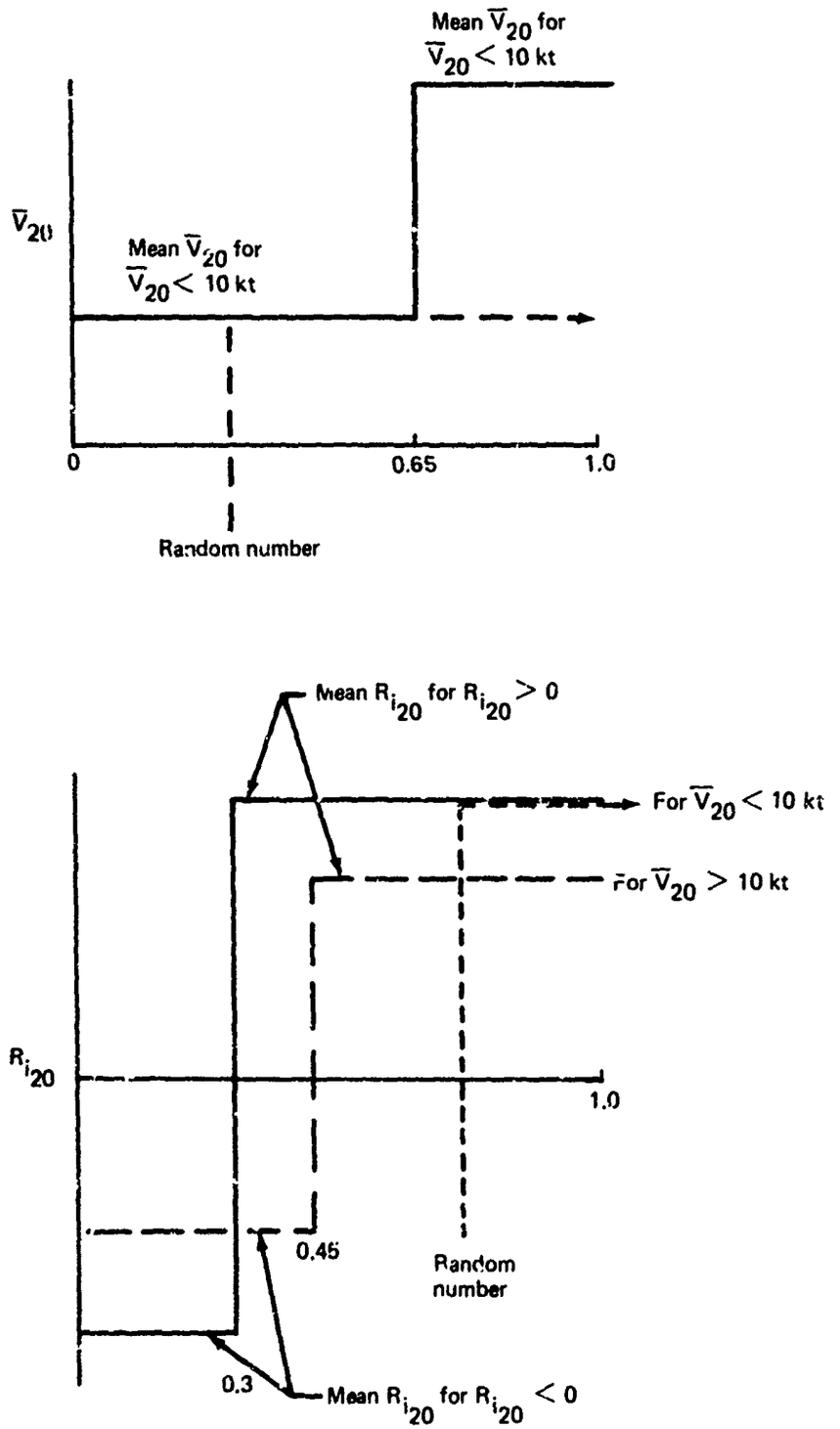

FIGURE 4-66.—EXAMPLE: GENERATION OF JOINT DISTRIBUTION

The probability model that results is that on Figure 4-67. The procedure is as follows:

1) Generate three random samples from a uniform probability density distribution defined between 0 and 1.

2) Using the first random sample, enter the cumulative (or exceedance) probability curve for $\overline{V}_{20}$ to find the surface wind speed.

3) Using the second random sample, enter the cumulative (or exceedance) probability curve for $R_{i_{20}}$ to find the atmospheric stability at the surface.

4) Using the third random sample, enter the cumulative (or exceedance) probability curve for $\overline{\psi}_W$ to find the wind heading.

5) Compute the down-runway component of mean wind at the surface. If it exceeds +10 knots (positive downwind component is a tailwind), return to 1). This corresponds to the FAA requirement (Ref. 4-32) that aircraft need demonstrate approaches and landings for tailwinds only up to 10 knots.

The cumulative wind heading probability is derived by integrating the selected wind heading probability density function and is provided in Figure 4-68. Wind heading is used to mean the direction to which the wind is blowing, relative to the runway heading (assumed to be aligned to the prevailing wind), which is opposite the meteorological convention.

Describing mean winds and Richardson's numbers for all cumulative (or exceedance) probabilities between 0 and 1 is more difficult as the maximum surface winds or Richardson's numbers that ever have or ever will be reached are unknown.

The problem associated with wind speed is alleviated by the FAA requirement (Ref. 4-32) implying that wind speeds only up to some maximum value need be considered. Presumably, greater winds result in a diversion to an alternate field or perhaps even a manual approach. If a maximum value is specified, then random numbers associated with the greater wind speeds should be discarded and a new sample generated. This amounts to ratioing the curve so that the maximum wind speed corresponds to a cumulative probability of 1.0 (that is, use the cumulative or exceedance probabilities of surface wind speeds, given that the surface wind speed is less than the maximum). The wind speed probabilities are presented on Figure 4-69.

The problem associated with wind speed may also be alleviated by using an input probability to determine a single surface wind speed to be used. However, as mean wind speed increases, the Richardson's number distribution narrows and it is possible that the highest surface wind speed is not the most severe one.

Limitations on the maximum levels of atmospheric stability and instability that must be considered are not provided. This may in part be due to relative ignorance about the effects of atmospheric stability, the paucity and variability of empirical data, and simply the fact that stability is not a parameter measured and reported by airport towers.

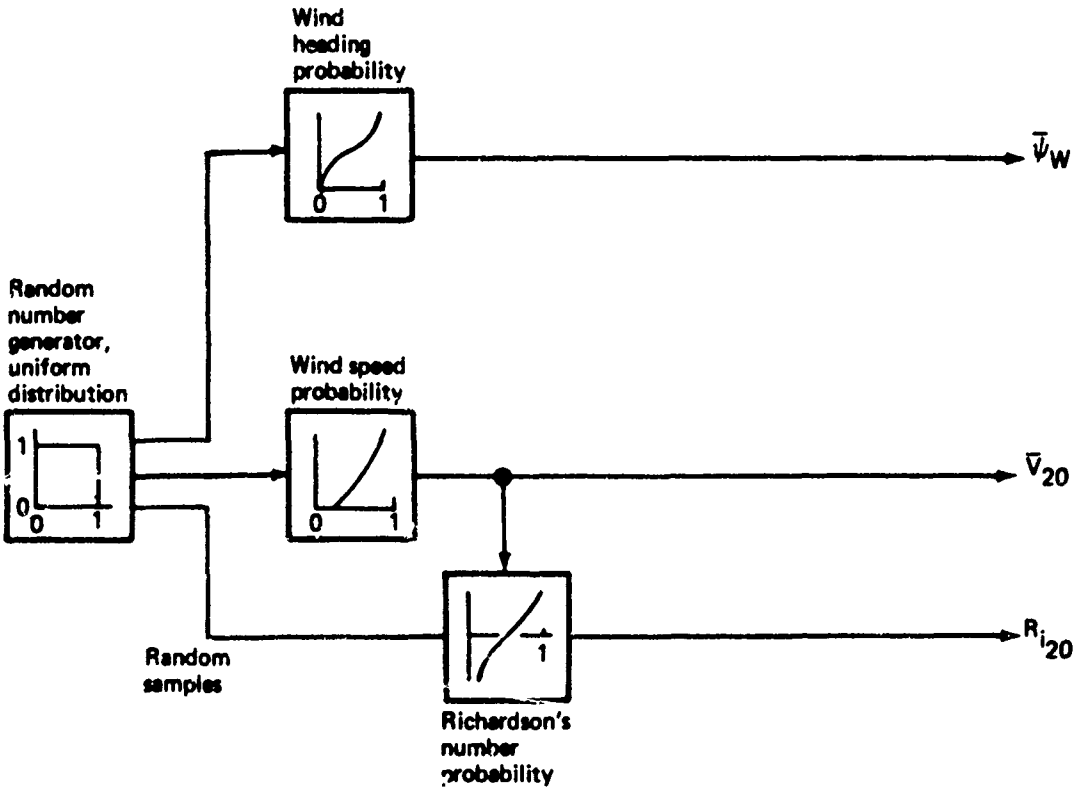

FIGURE 4-67.--PROBABILITY MODEL SCHEMATIC

Extreme levels of instability may result in extreme levels of turbulence, even for reasonable mean wind speeds. It is likely that there is some extreme turbulence level in which an approach would not be performed. Hence, a restriction resulting in a maximum level of instability is feasible and greater instabilities need not be considered.

The extremely stable conditions present a different problem. As stability increases, turbulence decreases until it disappears altogether. As discussed in the next subsection, the mean wind speed and speed shear at altitude at first increase as a ratio times the wind speed at the surface then decrease as stability increases. Also, at extremely stable conditions, the likelihood of atmospheric discontinuities, such as low altitude inversion layers which are difficult to model, increases, invalidating models providing continuous variations for altitude changes.

It can be argued that, rather than discarding all random samples corresponding to cumulative or exceedance probabilities for which Richardson's numbers are not defined, the last stated value should be used. This at least would be more representative of the more extreme value that should be used and can be expected to frequently give the same result in terms of success or failure. This is the suggested approach to be used with Figures 4-70, -71, and -72, obtained from the selected descriptions. Fortunately, the most extreme levels of stability occur at the lowest surface wind speeds, thus reducing their effect.

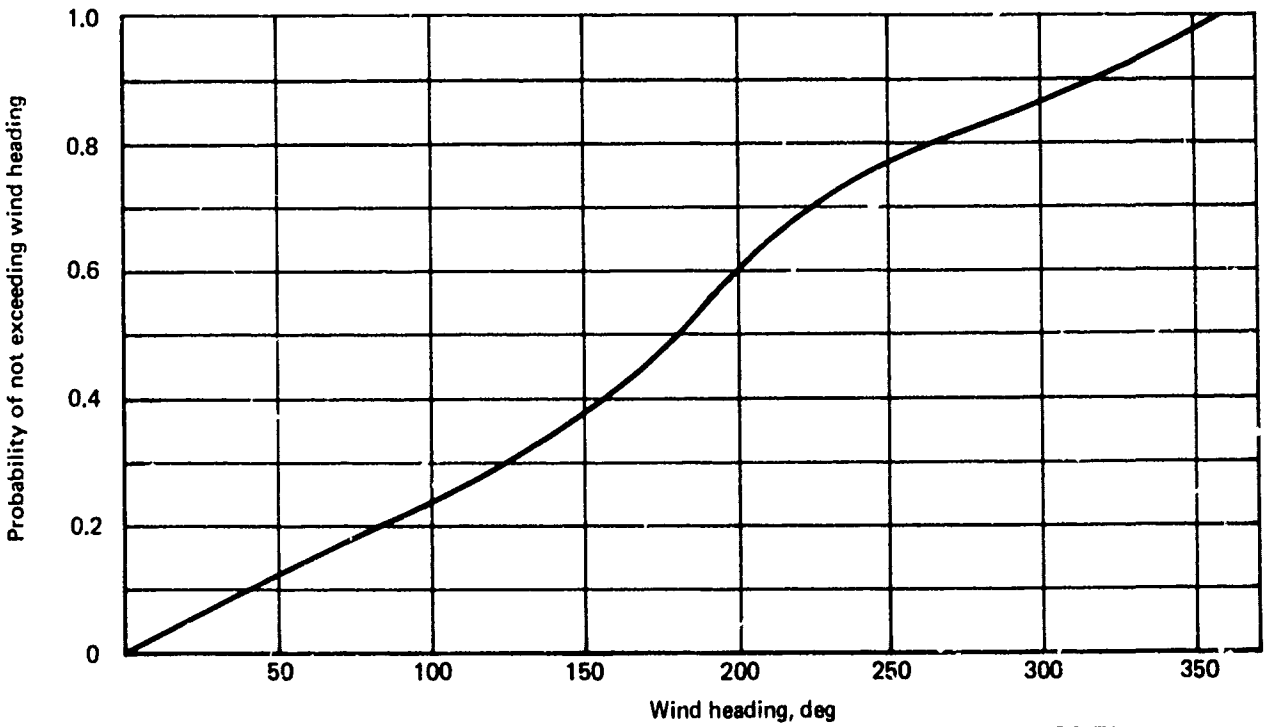

FIGURE 4-68.–WIND HEADING CUMULATIVE PROBABILITY MODEL

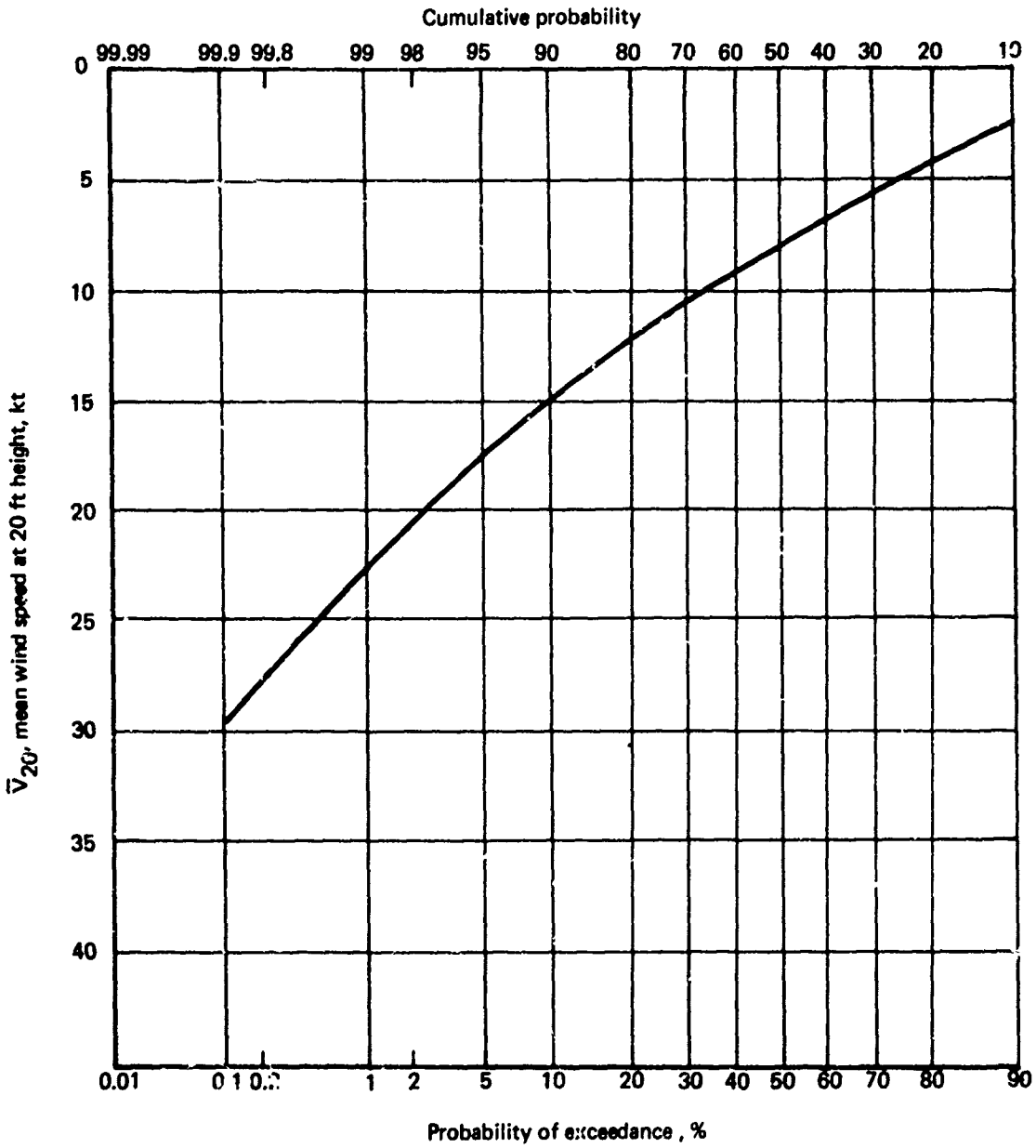

FIGURE 4-69.—MEAN WIND CUMULATIVE/EXCEEDANCE PROBABILITY

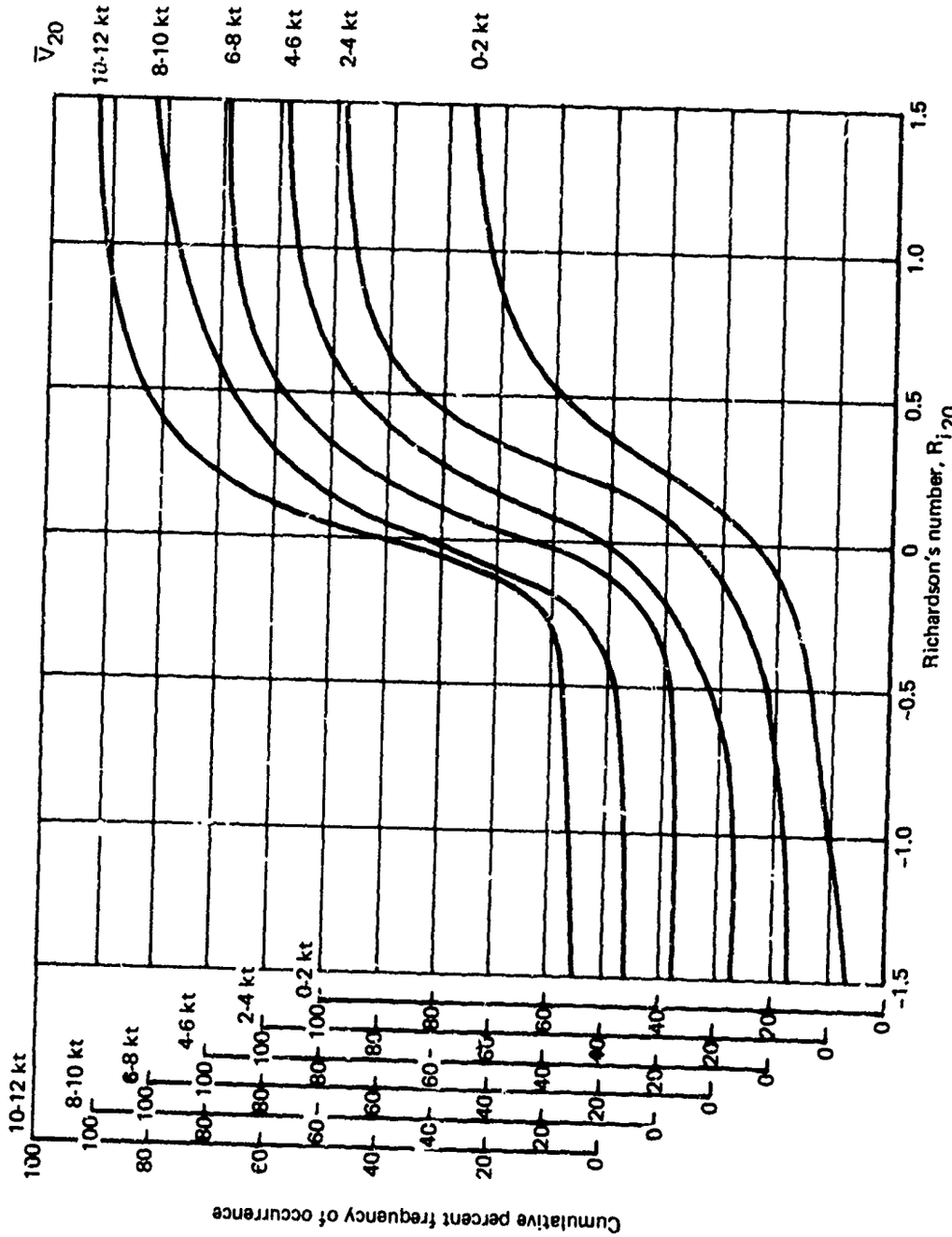

FIGURE 4-70.—CUMULATIVE PROBABILITY OF R_i AT GIVEN WIND SPEEDS, 0 TO 12 KT

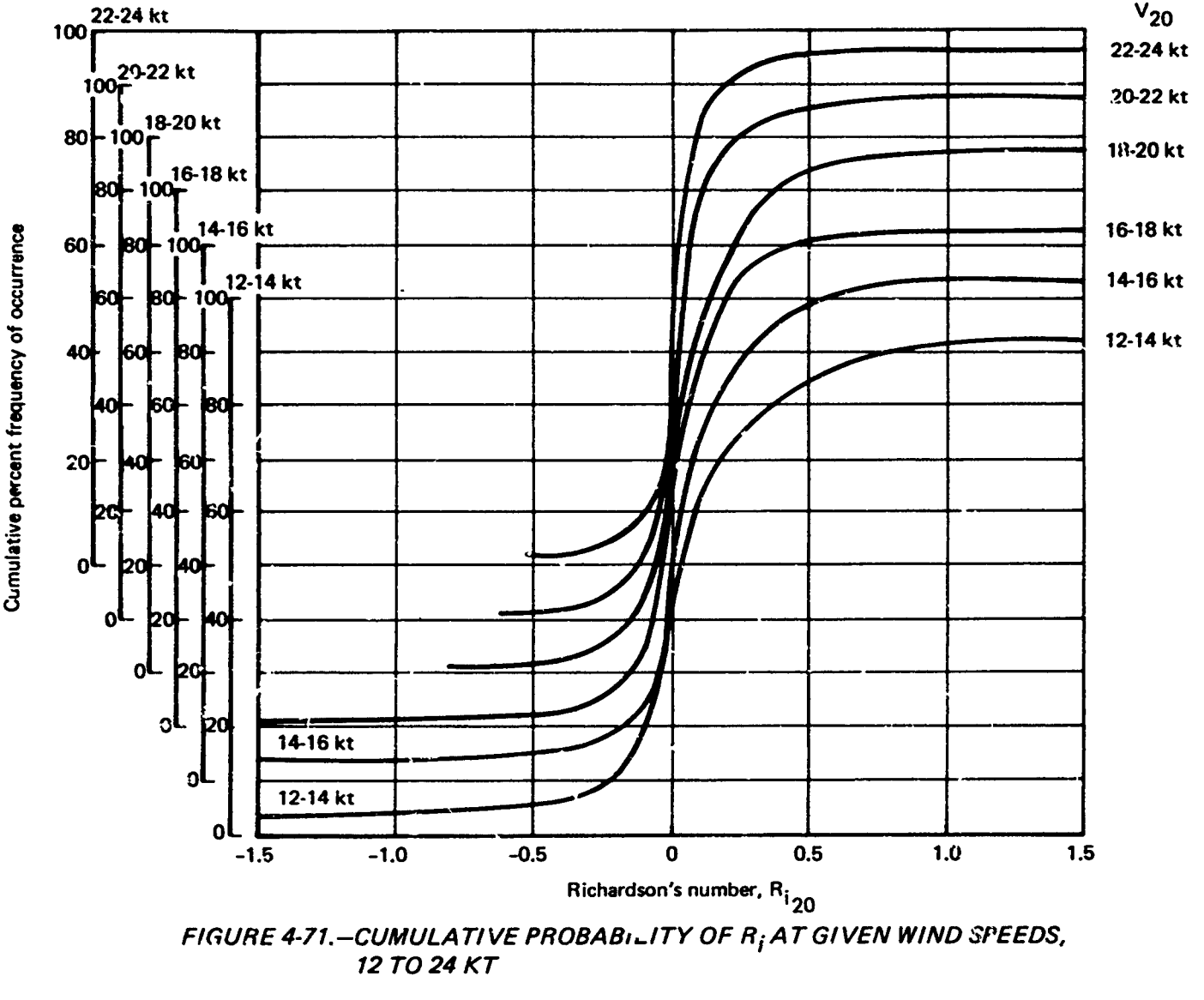

FIGURE 4-71.—CUMULATIVE PROBABILITY OF R_i AT GIVEN WIND SPEEDS, 12 TO 24 KT

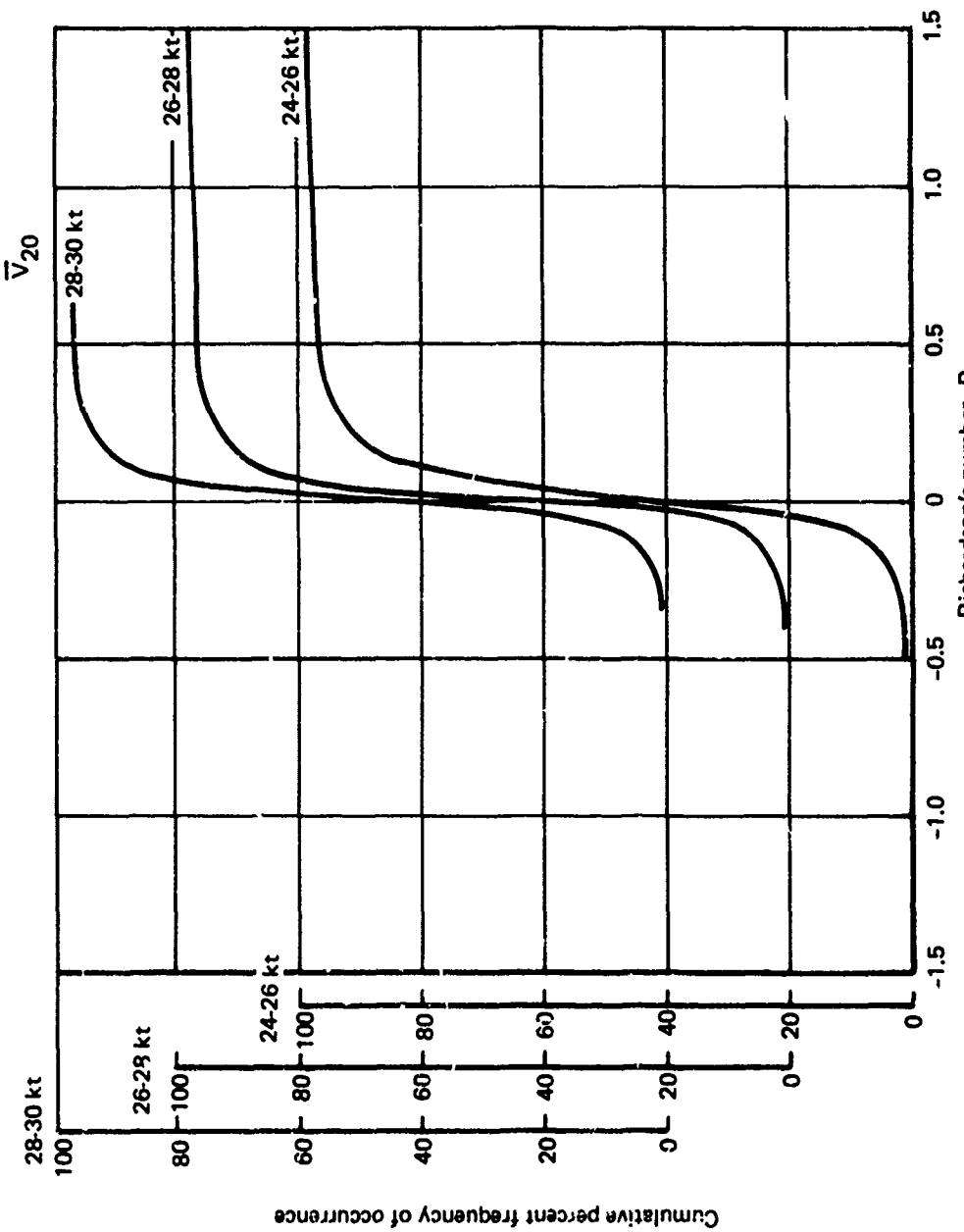

FIGURE 4-72.—CUMULATIVE PROBABILITY OF R_i AT GIVEN WIND SPEEDS, 24 TO 30 KT

4.5.2 Mean Wind Model

The descriptions of the mean wind profile and the mean wind shear, selected from alternative descriptions provided by the literature, are:

$$\bar{V}_W = \bar{V}_{20}\left(\frac{u_{*0}/k}{\bar{V}_{20}}\right)\left[\ln\left(\frac{h_W + 0.15}{0.15}\right) + f\left(\frac{h_W}{\ell'}\right) - \frac{h}{d}\, g\left(\frac{h_W}{\ell'}\right)\right]$$

$$\frac{\partial \bar{V}_W}{\partial h} = \bar{V}_{20}\left(\frac{u_{*0}/k}{\bar{V}_{20}}\right)\left(1 - \frac{h_W}{d}\right)\phi\left(\frac{h_W}{\ell'}\right)$$

$$h_W = \begin{cases} h, h < d \\ d, h \geq d \end{cases}$$

Where $\phi(h_W/\ell')$, $f(h_W/\ell')$ and $g(h_W/\ell')$ are given on Figures 4-73, 4-74, 4-75, and 4-76, which describe the functions:

$h/\ell' < 0$:

$$\phi\left(\frac{h}{\ell'}\right) = \frac{R_i}{[1 - 18\, R_i]^{1/4}},\ R_i = \frac{\phi\,(h/\ell')}{(h/\ell')}$$

$$f\left(\frac{h}{\ell'}\right) = \int_0^{-h/\ell'} \left[\frac{\phi\,(\xi) - 1}{\xi}\right] d\xi$$

$$g\left(\frac{h_W}{\ell'}\right) = f\left(\frac{h}{\ell'}\right) - \frac{1}{(-h/\ell')}\int_0^{-h/\ell'} f\,(\xi)\, d\,\xi$$

$1 > h/\ell' > 0$:

$$\phi\left(\frac{h}{\ell'}\right) = 1.0 + 4.5\left(\frac{h}{\ell'}\right)$$

$$f\left(\frac{h}{\ell'}\right) = 4.5\left(\frac{h}{\ell'}\right)$$

$$g\left(\frac{h}{\ell'}\right) = 1 + 2.25\left(\frac{h}{\ell'}\right)$$

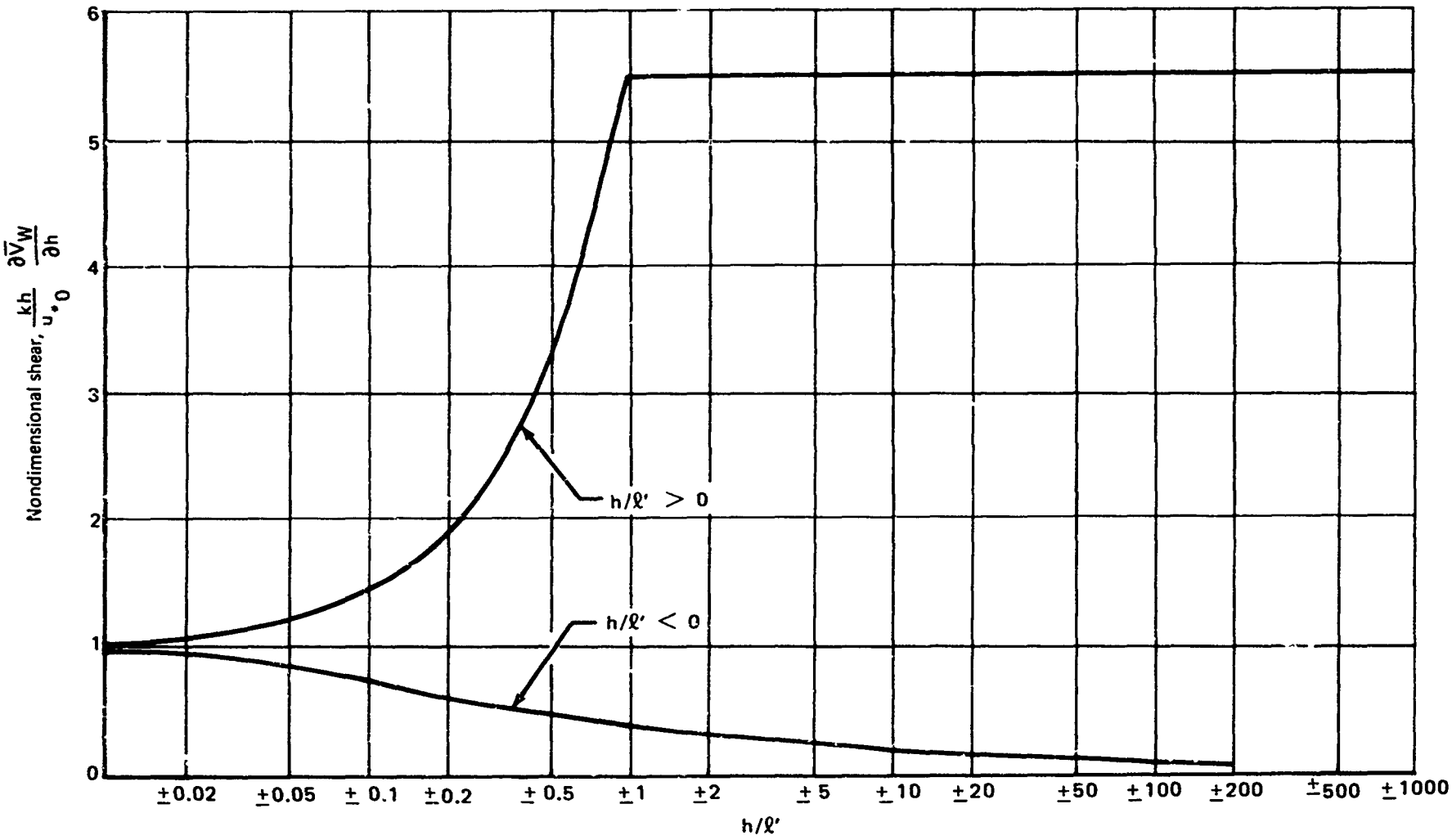

FIGURE 4-73.—NONDIMENSIONAL SHEAR

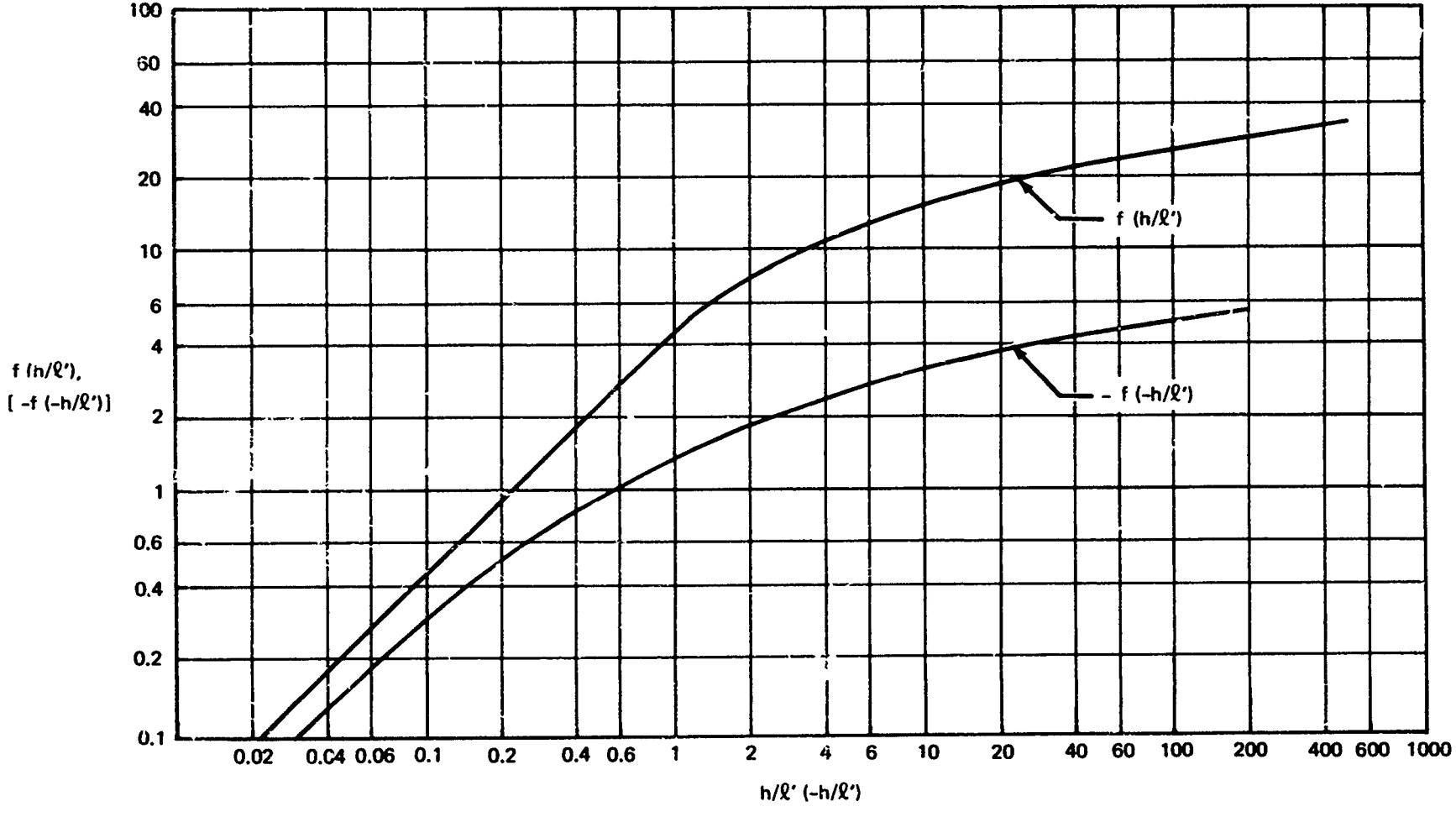

FIGURE 4-74.—CONTRIBUTION OF NONNEUTRAL STABILITY TO MEAN WIND

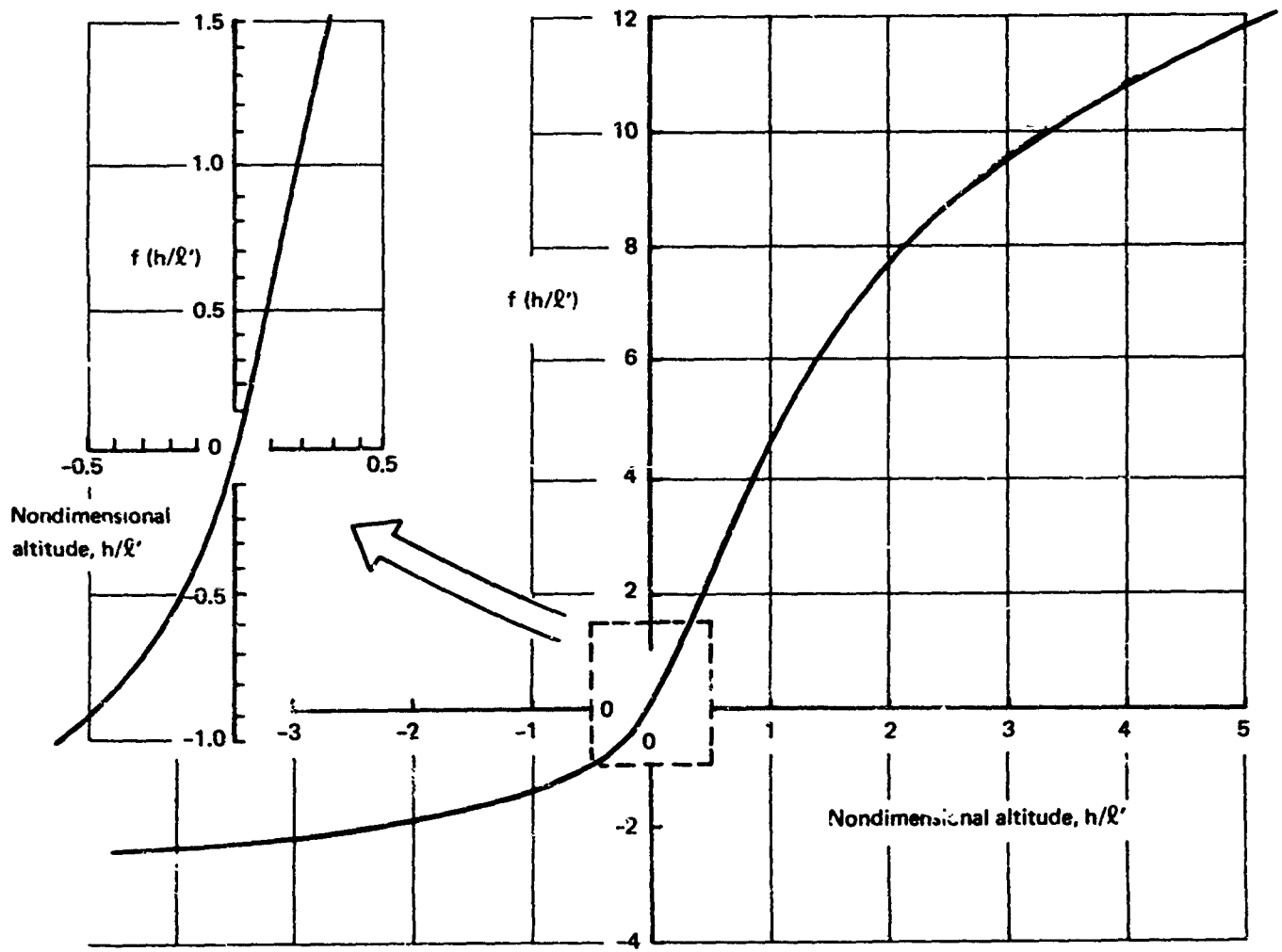

FIGURE 4-75.—CONTRIBUTION OF NON-NEUTRAL STABILITY TO MEAN WIND

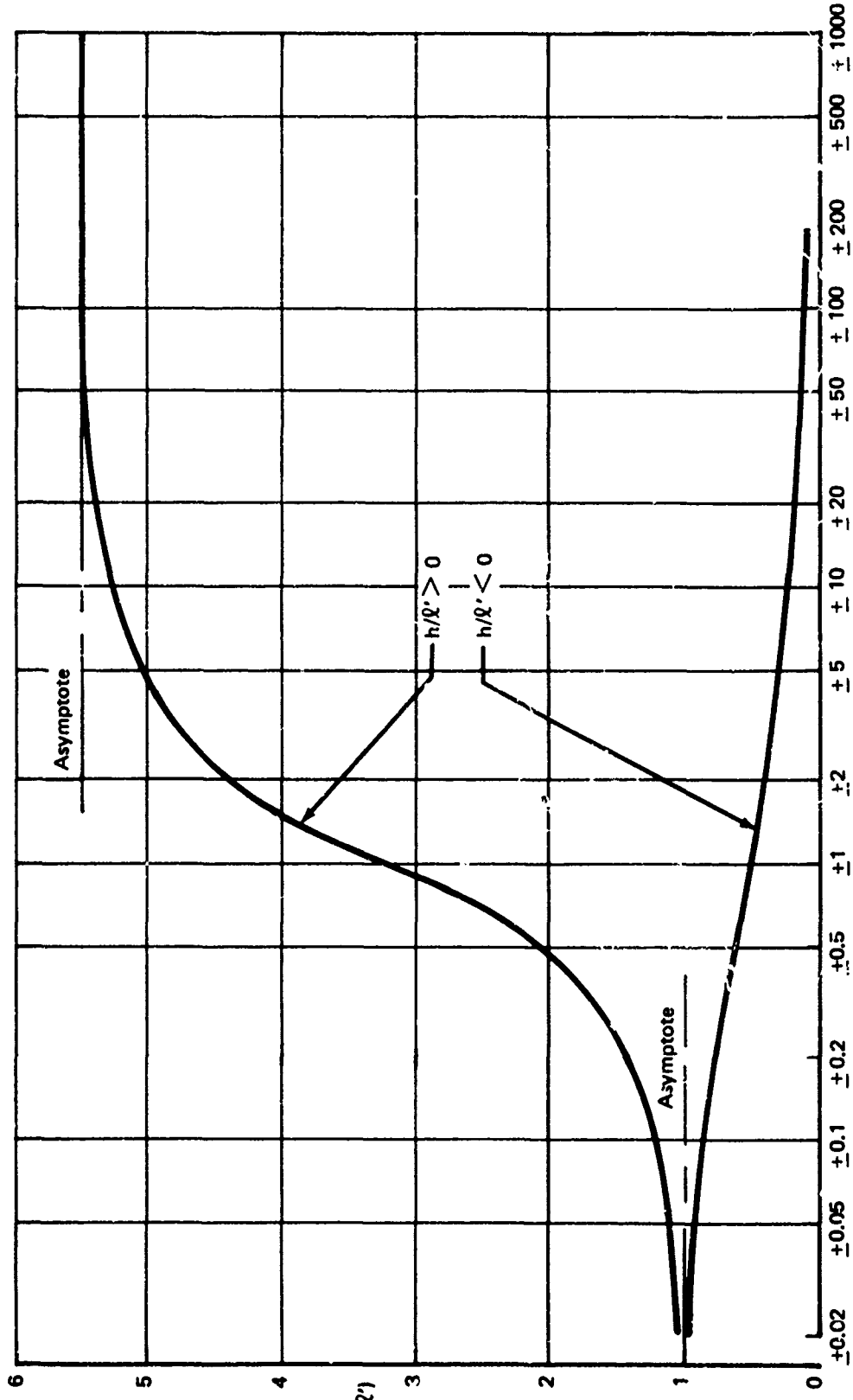

FIGURE 4-76.—VARIABLE SHEAR STRESS CORRECTION TO WIND PROFILE

$h/\ell' > 1$:

$$\phi\left(\frac{h}{\ell'}\right) = 5.5$$

$$f\left(\frac{h}{\ell'}\right) = 4.5\left[1 + \ln\left(\frac{h}{\ell'}\right)\right]$$

$$g\left(\frac{h}{\ell'}\right) = 5.5 - \frac{2.75}{(h/\ell')}$$

All other terms required for generating the mean wind profile and mean wind shear remain constant throughout a simulation and may be computed prior to the running of the simulation:

- Combinations of $\bar{V}_{20}$ and R_{i20} are determined from the probability model or may be user specified.
- $\frac{u_{*0}/k}{\bar{V}_{20}}$ presented on Figure 4-77 as a function of $R_{i_{20}}$, which describes

$$\frac{u_{*0}/k}{\bar{V}_{20}} = \frac{1}{\ln\left(\frac{20.15}{0.15}\right) + f\left(\frac{20}{\ell'}\right)}$$

- $1/\ell'$ presented on Figure 4-78 as a function of $R_{i_{20}}$, which describes

$$\frac{1}{\ell'} = \begin{cases} \frac{1}{20}\frac{R_{i_{20}}}{[1 - 18\,R_{i_{20}}]^{1/4}} & , \frac{20}{\ell'} < 0 \\ \frac{1}{20}\frac{R_{i_{20}}}{1 - 4.5\,R_{i_{20}}} & , 0 < \frac{20}{\ell'} < 1 \\ \frac{5.5\,R_{i_{20}}}{20} & , \frac{20}{\ell'} > 1 \end{cases}$$

$$d = 800\,\bar{V}_{20}\left(\frac{u_{*0}/k}{\bar{V}_{20}}\right)$$

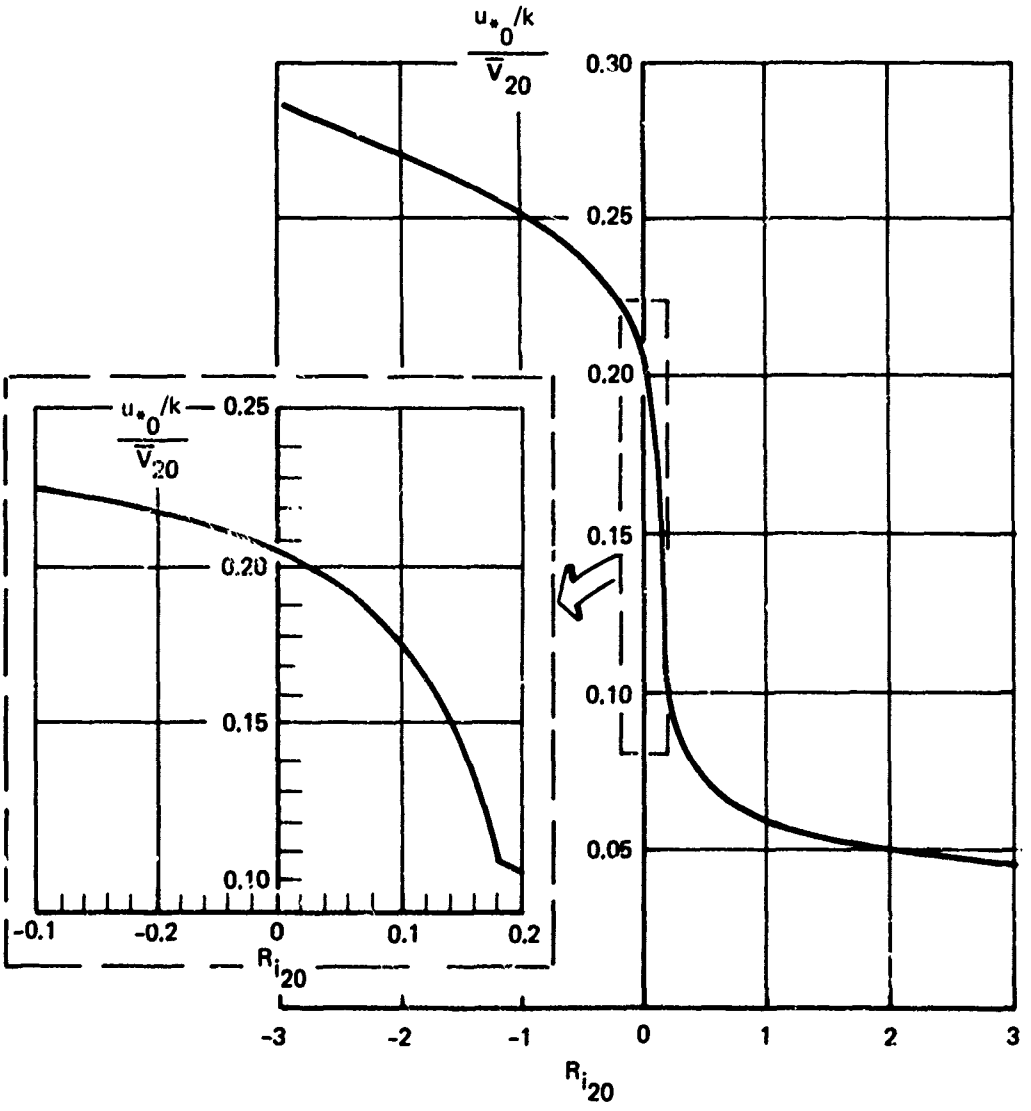

FIGURE 4-77.–MEAN WIND PROPORTIONALITY CONSTANT

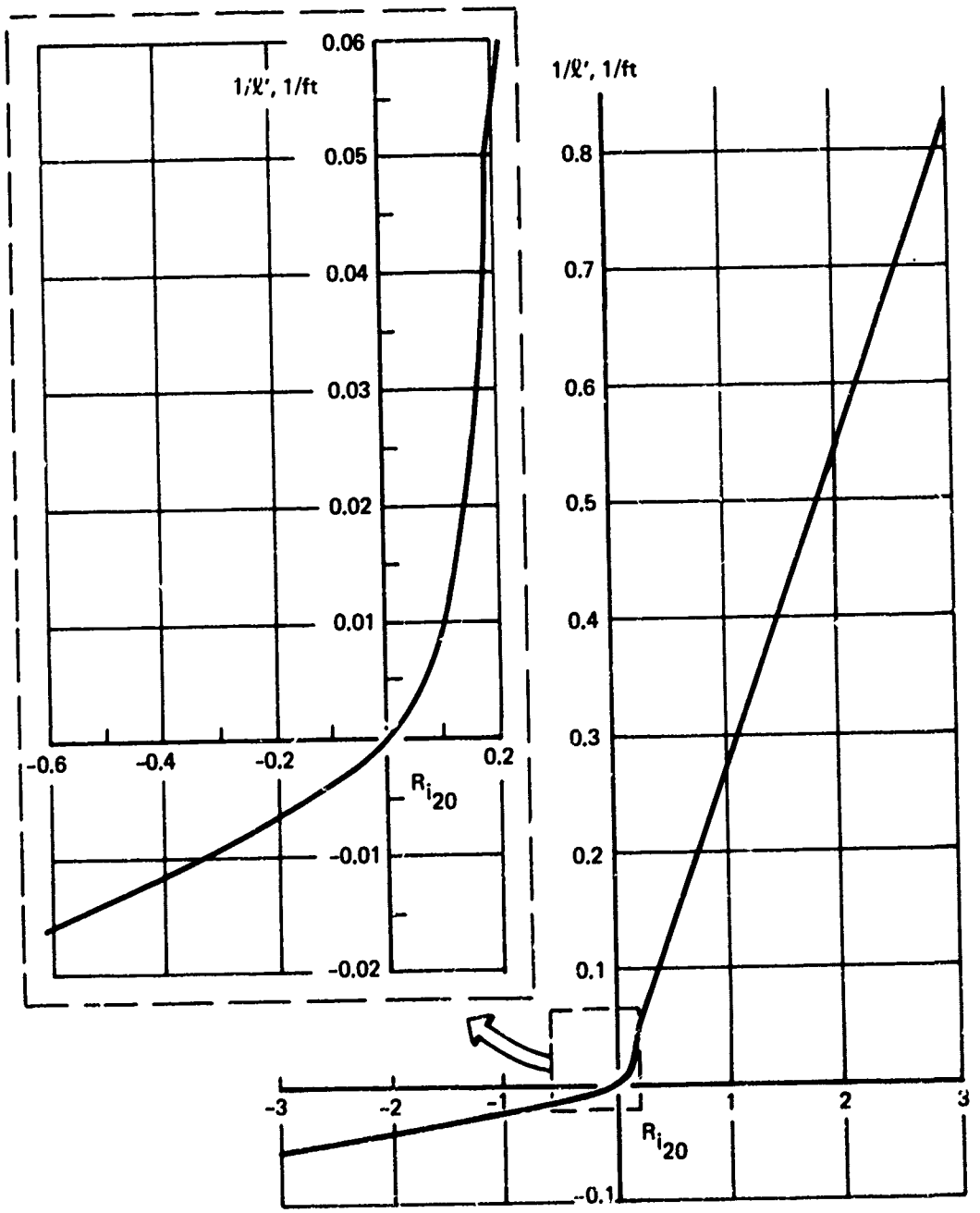

FIGURE 4-78.—SCALING LENGTH

The mean wind profile and the mean wind shear could have been specified directly in terms of Richardson's number at each altitude without introducing the explicit dependence on h/ℓ'. However, it then would have been necessary to compute Richardson's number at each altitude, a computation that would require a table lookup. Using h/ℓ' eliminates the table lookup during the simulation, simplifying the simulation; table lookups for determining h/ℓ' from $R_{i_{20}}$ are performed before the running of the simulation.

The detailed procedure for computing the wind and turbulence model parameters is provided schematically on Figure 4-79 and is described as follows:

- Initial condition calculations
  - Determine $1/\ell'$ from $R_{i_{20}}$ using Figure 4-78
  - Determine $(u_{*0}/k)/\bar{V}_{20}$ from $R_{i_{20}}$ using Figure 4-77
  - Compute $u_{*0}/k = [(u_{*0}/k)/\bar{V}_{20}]\ \bar{V}_{20}$ and $u_{*0} = 0.4(u_{*0}/k)$
  - Compute $d = 800(u_{*0}/k)$
- On-line calculations
  - Compute h_{CG}/d
  - Compute $h_W/d = \begin{cases} h_{CG}/d, & h_{CG} < d \\ 1, & h_{CG} \geq d \end{cases}$

    where h_W is the altitude used in the wind and turbulence models. Limiting h_W/d to one ensures that the mean wind will be constant above the boundary layer.
  - Compute $1 - (h_W/d)$, h_W/ℓ', and $h_W = (h_W/d)d$

The detailed calculations for determining the mean wind (used for point aerodynamic effects) and the mean wind shear terms (used for distributed lift effects) are presented schematically on Figure 4-80 and are described as follows:

- Compute $\ln(1 + (20/3)\ h_W)$, or use table lookup. This is the adiabatic contribution to the mean wind.
- Determine $f(h_W/\ell')$, the contribution of nonadiabatic thermal conditions to the mean wind, from Figures 4-74 or 4-75.
- Determine $g(h_W/\ell')$, the contribution of the altitude variation of shear stress to the mean wind, from Figure 4-76.

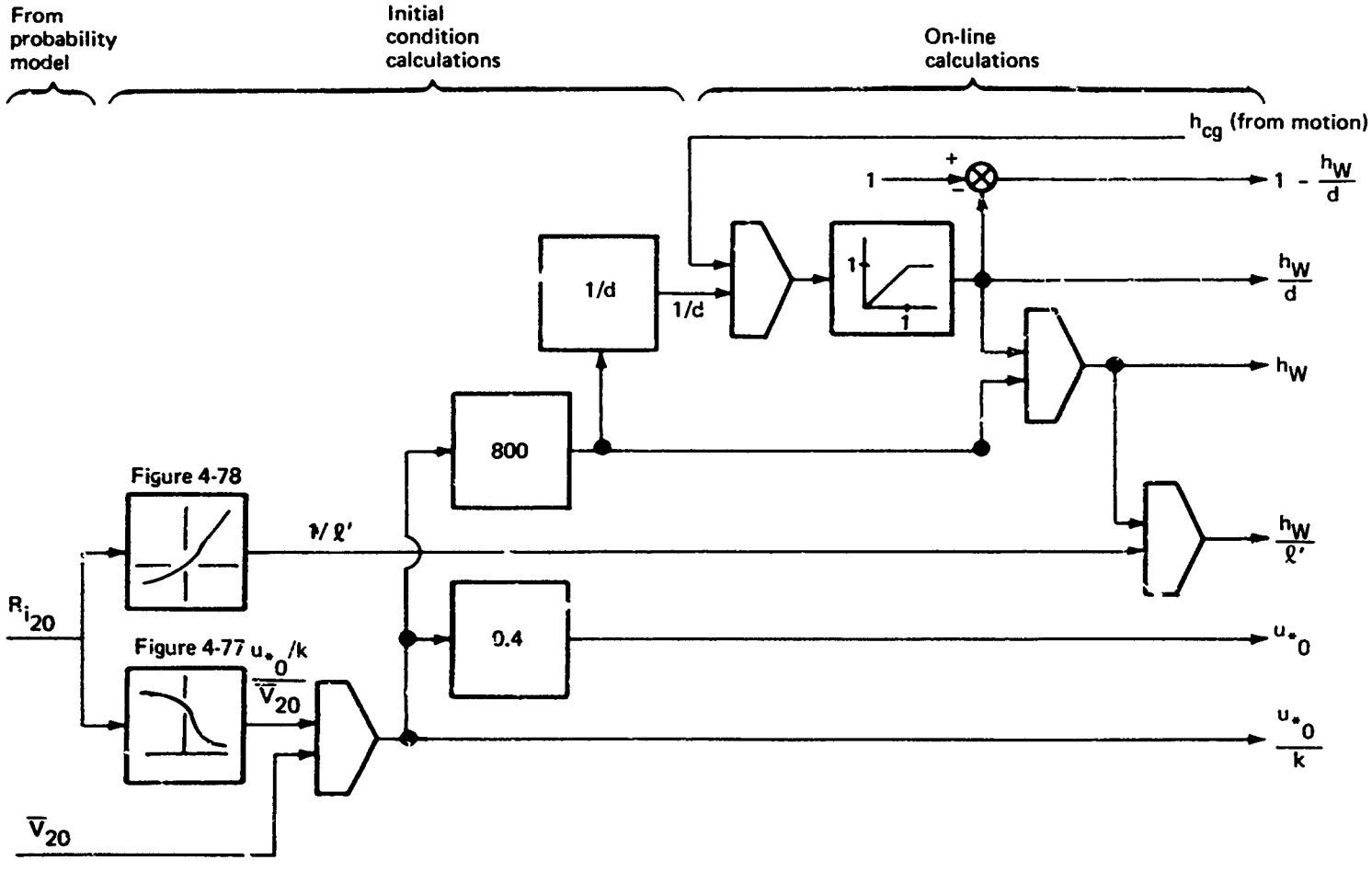

FIGURE 4-79.—SCHEMATIC OF CALCULATIONS OF PARAMETERS

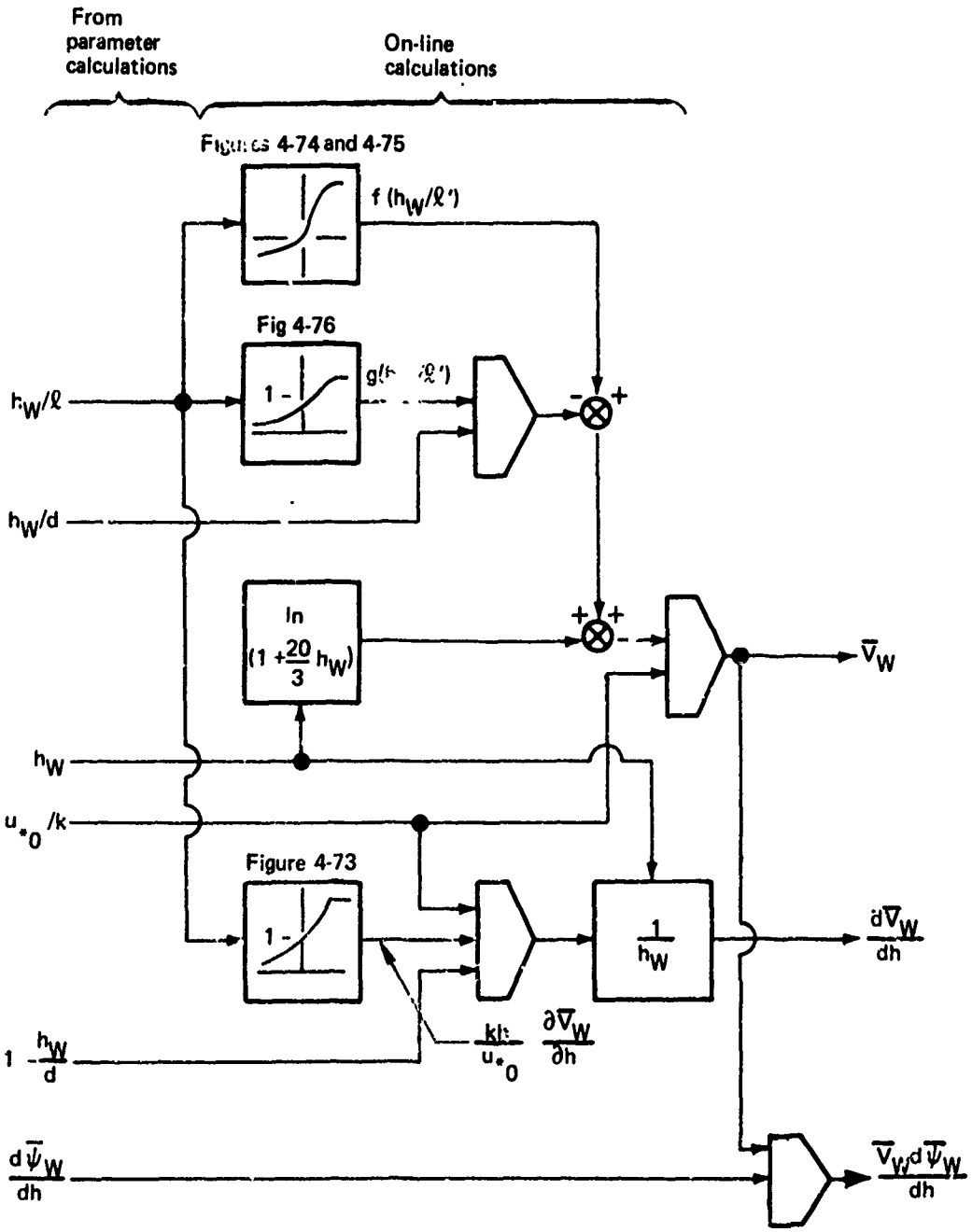

FIGURE 4-80.—MEAN WIND AND WIND SHEAR MODEL SCHEMATIC

- Compute

$$\bar{V}_W = \frac{u_{*0}}{k}\left[\ln\left(\frac{20}{3} h_W\right) + f\left(\frac{h_W}{\ell'}\right) - \frac{h_W}{d} g\left(\frac{h_W}{\ell'}\right)\right]$$

- Determine $(kh/u_{*0})(\partial \bar{V}_W/\partial h)$, the constant shear stress nondimensional shear, from Figure 4-73 using h_W/ℓ'.

- Compute

$$\frac{d\bar{V}_W}{dh} = \frac{u_{*0}}{k}\left(\frac{kh}{u_{*0}} \frac{\partial \bar{V}_W}{\partial h}\right)\left(1 - \frac{h_W}{d}\right)\frac{1}{h_W}$$

This is the wind speed shear.

4.5.3 Turbulence Model

Three uncorrelated components of mean wind axis system turbulence, all measured at the same point, are produced by passing samples of band-limited white noise having a Gaussian probability density distribution through gains and filters which cause the outputs to have power spectra approximating the Von Karman spectral shapes. The filter time constants and the gains are dependent upon the airspeed, integral scales, and turbulence variances. A qualitative description of this procedure is provided on Figure 4-81.

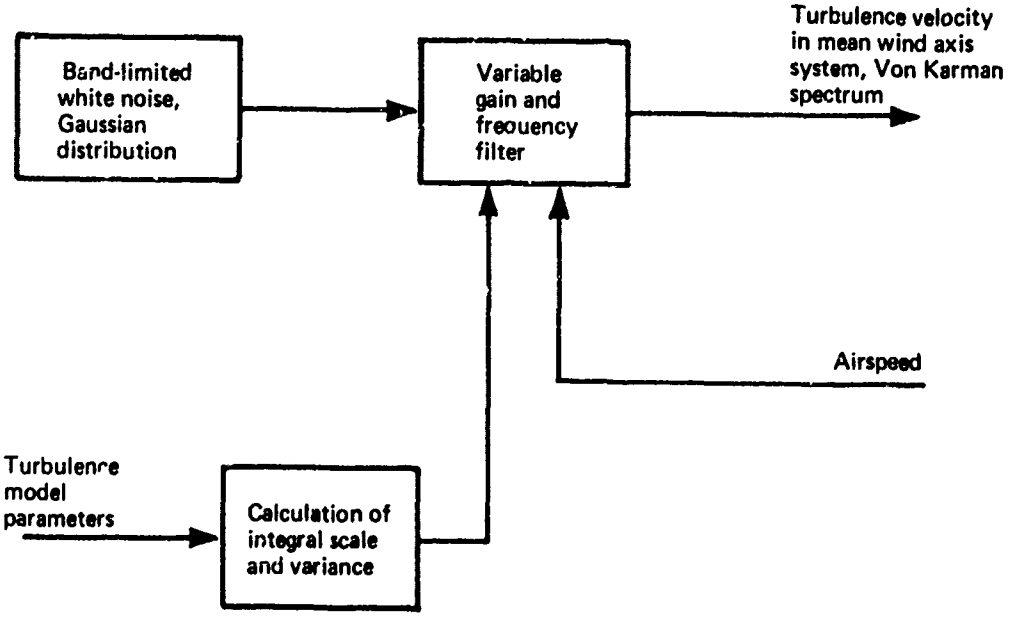

FIGURE 4-81.–GENERATION OF TURBULENCE VELOCITY SCHEMATIC

The Von Karman spectra for the components in the direction of the mean wind, perpendicular to the right of the direction in the mean wind in the horizontal plane, and vertically downward, respectively, are given by

$$\Phi_u = \frac{\sigma_H^2 L_H}{\pi} \frac{1}{\left[1 + (1.339\, L_H \Omega_1)^2\right]^{5/6}}$$

$$\Phi_v = \frac{\sigma_H^2 L_H}{2\pi} \frac{1 + 8/3\,(1.339\, L_H \Omega_1)^2}{\left[1 + (1.339\, L_H \Omega_1)^2\right]^{11/6}}$$

$$\Phi_w = \frac{\sigma_V^2 L_V}{2\pi} \frac{1 + 8/3\,(1.339\, L_V \Omega_1)^2}{\left[1 + (1.339\, L_V \Omega_1)^2\right]^{11/6}}$$

where $\Omega = \omega/V_A$, and where the variances and the power spectra are related by

$$\sigma_i^2 = \int_{-\infty}^{\infty} \Phi_i(\Omega_1)\, d\Omega_1$$

4.5.3.1 Noise Generator

Any procedure producing noise with a flat unit amplitude power spectrum over the frequency range of interest, thus implying negligible serial correlation, and having a probability density distribution that does not deviate significantly from a Gaussian distribution for amplitudes up to $\pm 3\sigma$ is an acceptable noise generator.

A particular routine for use on digital binary computers that provides a good combination of efficiency (computation time and memory requirements) and accuracy is described as follows:

(1) Generation of uniform distribution between 0 and 1

(a) Choose positive odd integer for x_0

(b) Choose an integer $K = 8t \pm 3$, where t is a positive integer giving a value for k close to $2^{b/2}$ and where b is the number of binary bits in a computer word.

(c) Compute kx_0 using fixed point integer arithmetic. The product is stored on two registers. The lower order b bits are retained and are equal to the new number x_1.

(d) Compute $r_1 = x_1/2^b$. The term r_1 is a random number from a uniform probability density distribution between 0 and 1.

(e) Each successive random number x_i is obtained from the b lower order bits of the product kx_{i-1}.

(2) Generation of Gaussian distribution
From two successive samples from a uniform distribution, r_1 and r_2, compute a sample from a Gaussian distribution, g, by: $g = (-2 \ln r_1)^{1/2} \cos(2\pi r_2)$

(3) Spectrum adjustment
Adjust the magnitude of g to provide a spectrum of unit amplitude by multiplying g by $2\pi/\Delta t$, where Δt is the computation frame time. The product is the input to the turbulence filter.

(4) Multiple components of turbulence
Perform the entire process (1, 2, and 3) three times within each computation cycle, once for each of the three components, using six successive samples from the uniform distribution.

The method for generating the uniform distribution is known as the "multiplicative congruential" or the "power residue method." The method for generating the Gaussian distribution from the uniform distribution is known as the "direct method."

4.5.3.2 Turbulence Statistics, Mean Wind Axis

The standard deviations and integral scales for the components of turbulence aligned to the mean wind axis system are generated in accordance with the selected description as presented on Figure 4-82 and as described in the following:

Determine $\sigma_V/u_*(h/\ell')$ from Figures 4-83 or 4-84

Calculate $\sigma_V = (\sigma_V/u_*)(1 - h/d)\, u_{*0}$

Determine $\sigma_H/\sigma_V(h_W)$ from Figure 4-85

Calculate $\sigma_H = (\sigma_H/\sigma_V)\sigma_V$

Identify $L_V = h_W \leq 1000$ ft

Calculate $L_H = L_V(\sigma_H/\sigma_V)^3$

4.5.3.3 Turbulence Filters

Upon assurance that the random noise has a flat spectrum of unit amplitude, it remains to develop filters having frequency responses equal to the square roots of the turbulence power spectra.

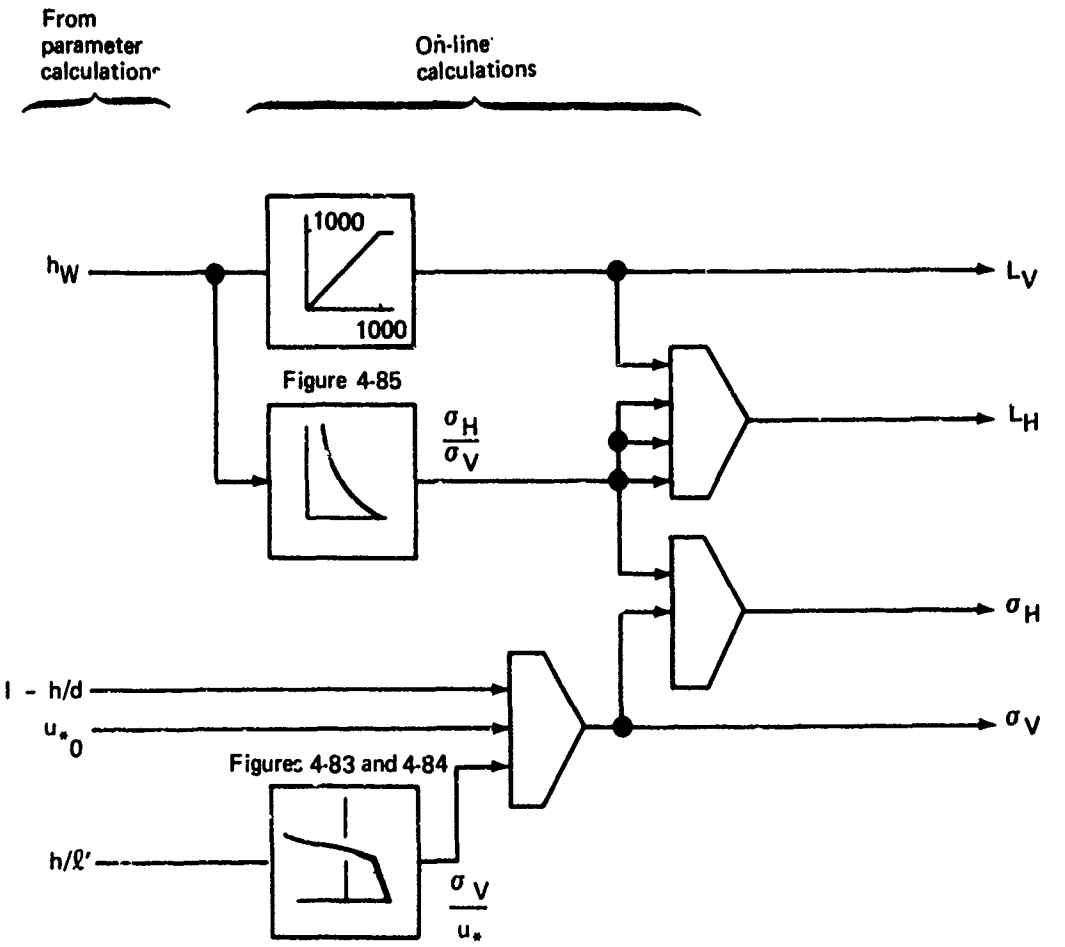

FIGURE 4-82.–SCHEMATIC OF CALCULATION OF MEAN WIND AXIS TURBULENCE STATISTICS

First, it must be ensured that the spectrum being matched is two sided. That is,

$$\sigma^2 = \int_{-\infty}^{\infty} \Phi(\Omega_1)\, d\Omega_1$$

not

$$\sigma^2 = \int_{0}^{\infty} \Phi(\Omega_1)\, d\Omega_1$$

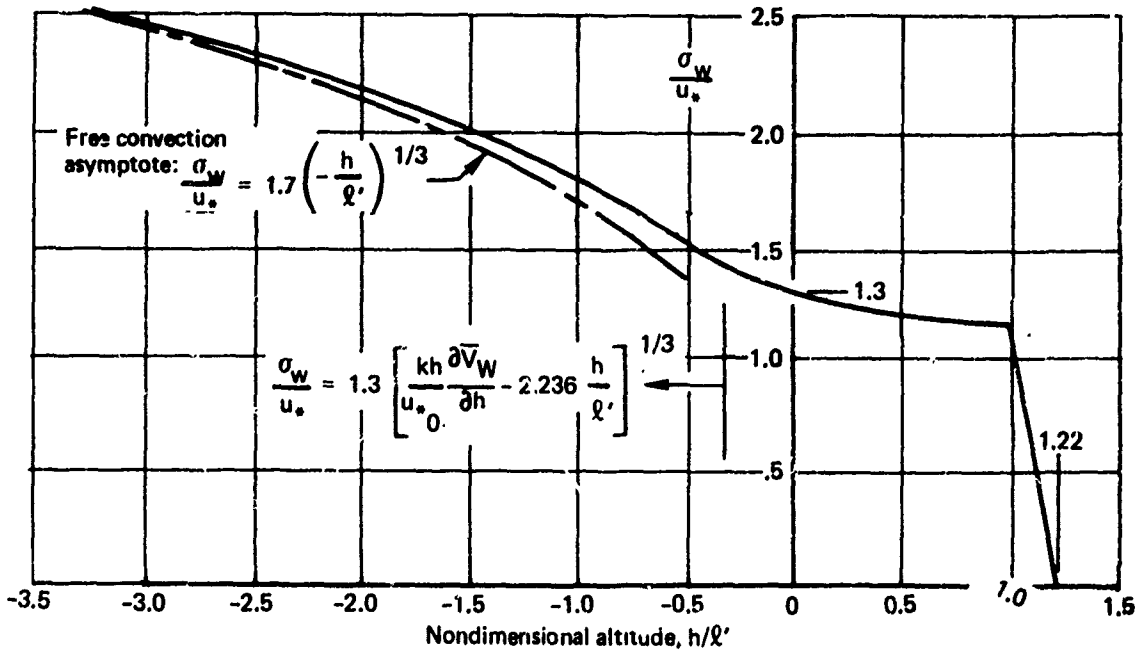

FIGURE 4-83. $-\sigma_w/u_*$ VARIATION WITH STABILITY

The latter form has twice the amplitude of the former and is used when output variances are computed from the output spectrum by numerical integration. The knowledge that the spectrum is even is used to enable integration over half the frequency domain. The variance is then twice the integral. However, rather than defining the variance as twice the integral from 0 to ∞, a one-sided spectrum has been defined, with twice the amplitude of the two-sided spectrum. Unfortunately, the one-sided spectrum has been carried over to simulation. The effect is turbulence with twice the intended variance since, by the Fourier integral inversion theorem,

$$x(t) = \int_{-\infty}^{\infty} x(\omega)\, e^{i\omega t}\, d\omega\,,$$

all frequencies from -∞ to ∞ transform into time; there is no way to restrict a temporal process to producing a half-plane power spectrum.

A second point of confusion is the units of the spectrum. The appearance of the gain of $1/\pi$ in the spectra is often erroneously assumed to represent a conversion of units from $(\text{velocity})^2/(\text{rad/sec})$ to $(\text{velocity})^2/(\text{cycles/sec})$. The Von Karman spectra presented are in terms of $1/(\text{rad/sec})$.

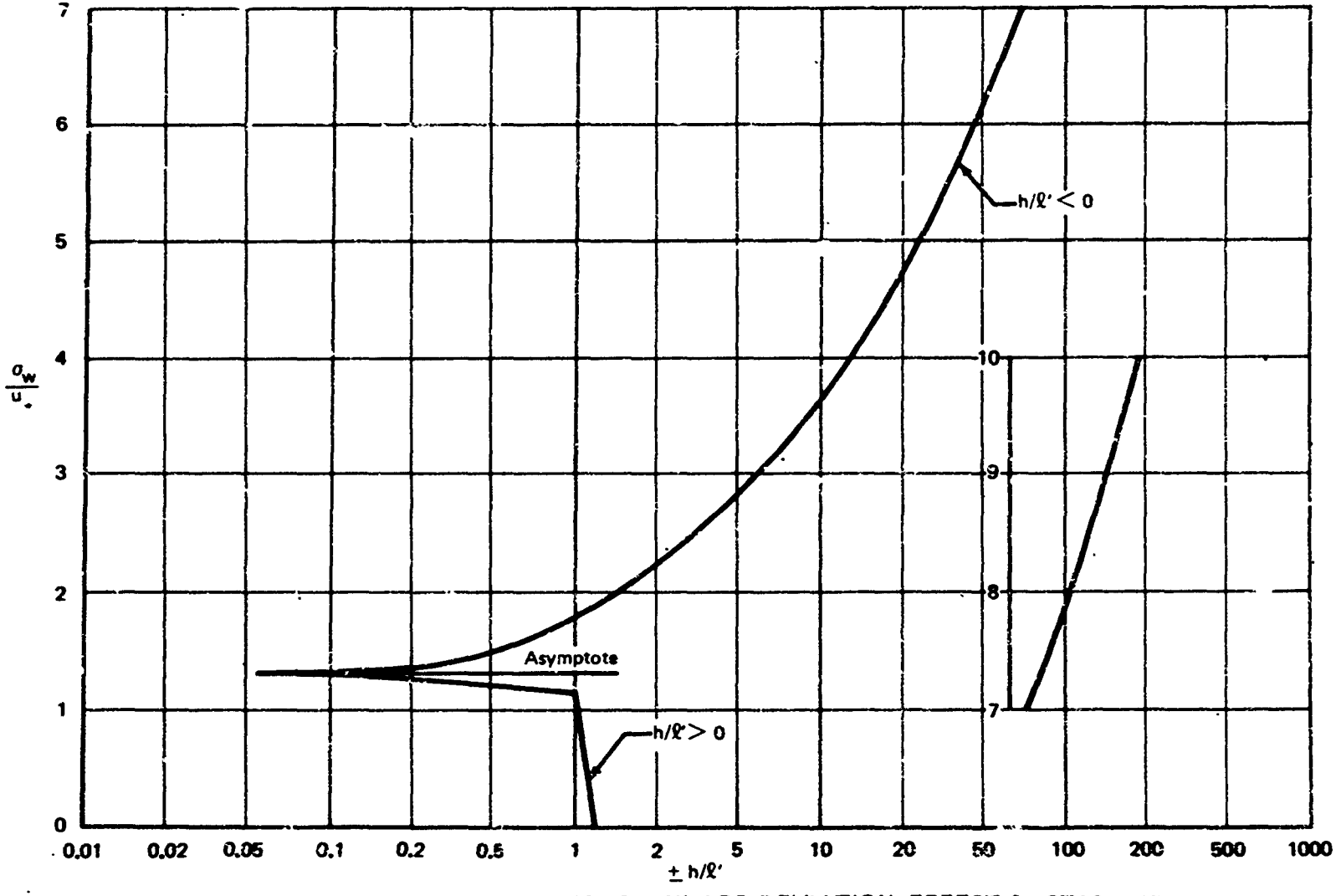

FIGURE 4-84.—VERTICAL TURBULENCE STANDARD DEVIATION, EFFECT OF STABILITY

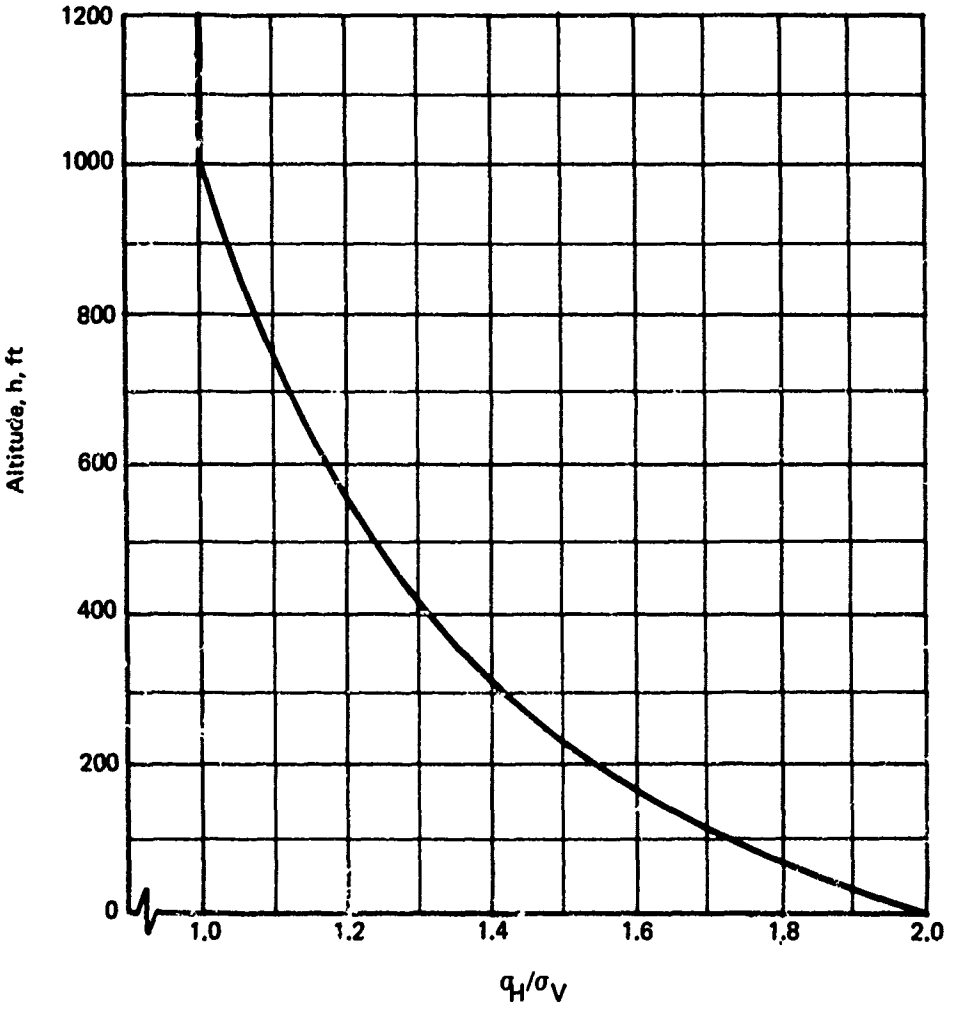

FIGURE 4-85.–SELECTED DESCRIPTION FOR VARIANCES OF HORIZONTAL TURBULENCE COMPONENTS

To convert from spacial frequency to temporal frequency, Taylor's hypothesis, $\Omega_1 = \omega/V_A$, requiring the variance to be the same in either domain, is used:

$$\sigma^2 = \int_{-\infty}^{\infty} \Phi(\Omega_1)\, d\Omega_1 = \frac{1}{V_A} \int_{-\infty}^{\infty} \Phi(\Omega_1)\, d\omega$$

$$\sigma^2 = \int_{-\infty}^{\infty} \Phi'(\omega)\, d\omega$$

$$\Phi'(\omega) = \frac{1}{V_A}\, \Phi(\Omega)$$

To approximate the Von Karman spectra, filters must approximate

$$\sqrt{\Phi_u(\omega)} = \sigma_H \sqrt{\frac{L_H}{\pi V_A}} \frac{1}{\left[1 + \left(1.339 \frac{L_H}{V_A}\omega\right)^2\right]^{5/12}}$$

$$\sqrt{\Phi_v(\omega)} = \sigma_H \sqrt{\frac{L_H}{2\pi V_A}} \left\{ \frac{1 + 8/3 \left(1.339 \frac{L_H}{V_A}\omega\right)^2}{\left[1 + \left(1.339 \frac{L_H}{V_A}\omega\right)^2\right]^{11/16}} \right\}^{1/2}$$

$$\sqrt{\Phi_w(\omega)} = \sigma_V \sqrt{\frac{L_V}{2\pi V_A}} \left\{ \frac{i + 8/3 \left(1.339 \frac{L_V}{V_A}\omega\right)^2}{\left[1 + \left(1.339 \frac{L_V}{V_A}\omega\right)^2\right]^{11/16}} \right\}^{1/2}$$

These square roots of the temporal frequency Von Karman power spectra are shown on Figure 4-86.

The ultimate test as to whether a filter correctly represents a given power spectrum is to test the contribution of each frequency to the total variance within the frequency range of interest. This is not the same as ensuring that the total variance is the same.

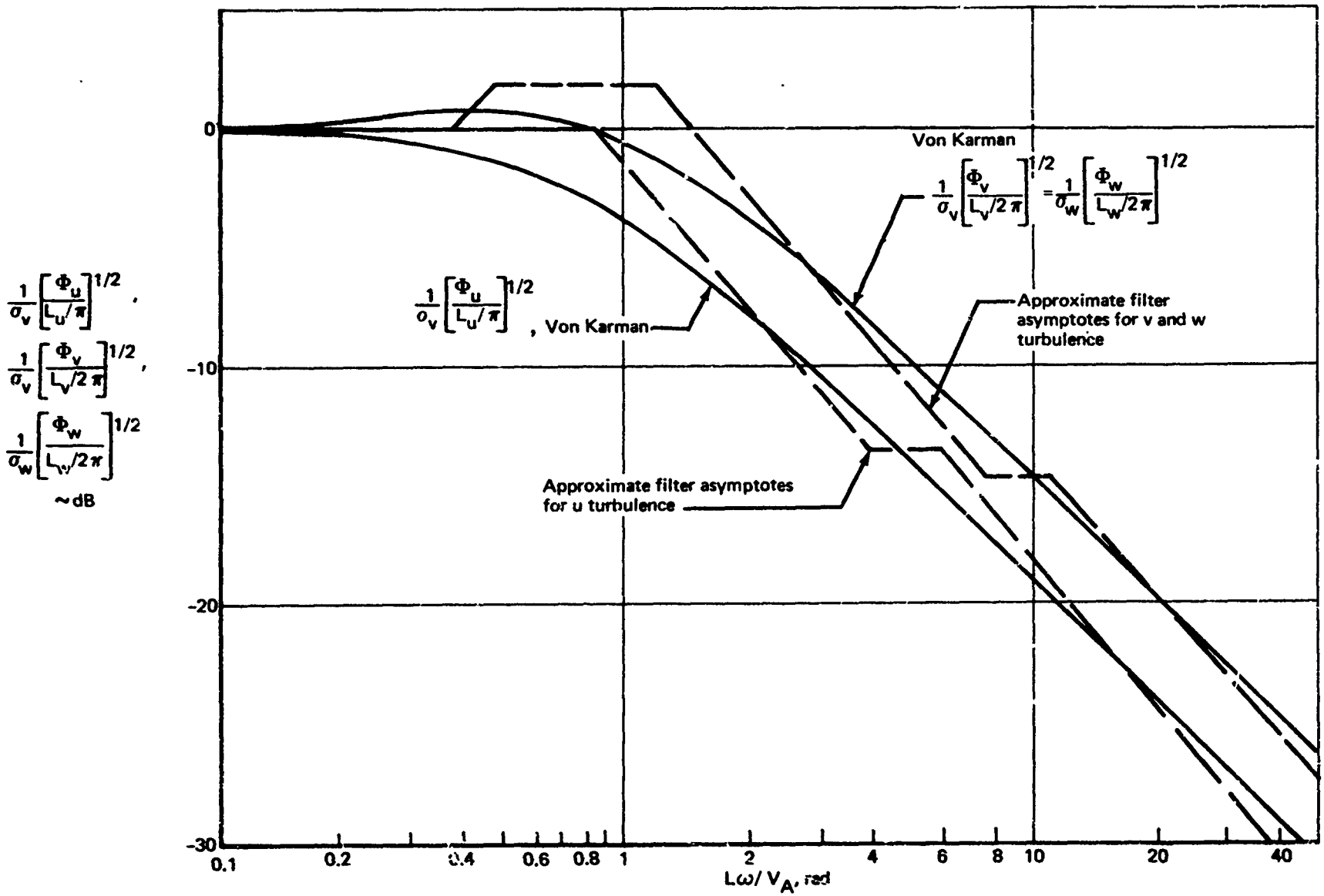

FIGURE 4-86.—TURBULENCE FILTER DESIGN

It is often assumed that the filters that exactly produce the Dryden spectra represent the Von Karman spectra well. This does not appear to be the case, as seen on Figure 4-87, unless the maximum frequency of interest is below

$$\omega < 0.05 \frac{V_A}{L_H}$$

and

$$\omega < 0.09 \frac{V_A}{L_V}$$

which is quite unlikely for landing approach. The Dryden spectra, although having the correct variance, overpredicts the Von Karman spectra by as much as 25% at the frequencies having the greatest contribution to the variance. The greater contribution to the variance at the intermediate frequencies by the Dryden spectra is compensated by a lesser contribution at the very high frequencies. The very high frequencies, however, will be beyond the maximum frequency of interest; they have a negligible contribution to the output response or variance. It is most likely that use of the Dryden spectra will overpredict the airplane's responses to turbulence.

Much better filter approximations are obtainable. Examples are those on Figure 4-88, whose asymptotes are shown on Figure 4-87, and which are compared to the Von Karman spectra on Figures 4-89 and 4-90. The error on Figures 4-89 and 4-90 is reduced to less than 3%, except at very high frequencies. The high frequencies can be matched better as higher order filters are used, but the filters on Figure 4-88 are expected to satisfy the simulation requirements for almost all aircraft during approach and landing. No first order filter for the longitudinal spectrum, comparable to the Dryden filters, could be found that would adequately represent the right side of the peak on Figure 4-89. Similarly, second order filters could not be found for the transverse spectra.

The filters must be reduced to first order lags, with the Laplace transform variable, s, appearing only as integrator (1/s). A series of first order lags may be used, but the parallel arrangement on Figure 4-91, obtained by a partial fraction expansion, is preferred, as it is considered easier to implement and check out.

4.5.4 Transformations

Axis system transformations provide the interrelationship between the mean wind axis system, in which the characteristics of the wind and turbulence are defined, and the airplane's body axis system, in which aircraft motion is defined. Specifically, transformations are needed to define:

- Body axis components of the mean wind
- Body axis components of the mean wind shear
- Body axis components of turbulence.

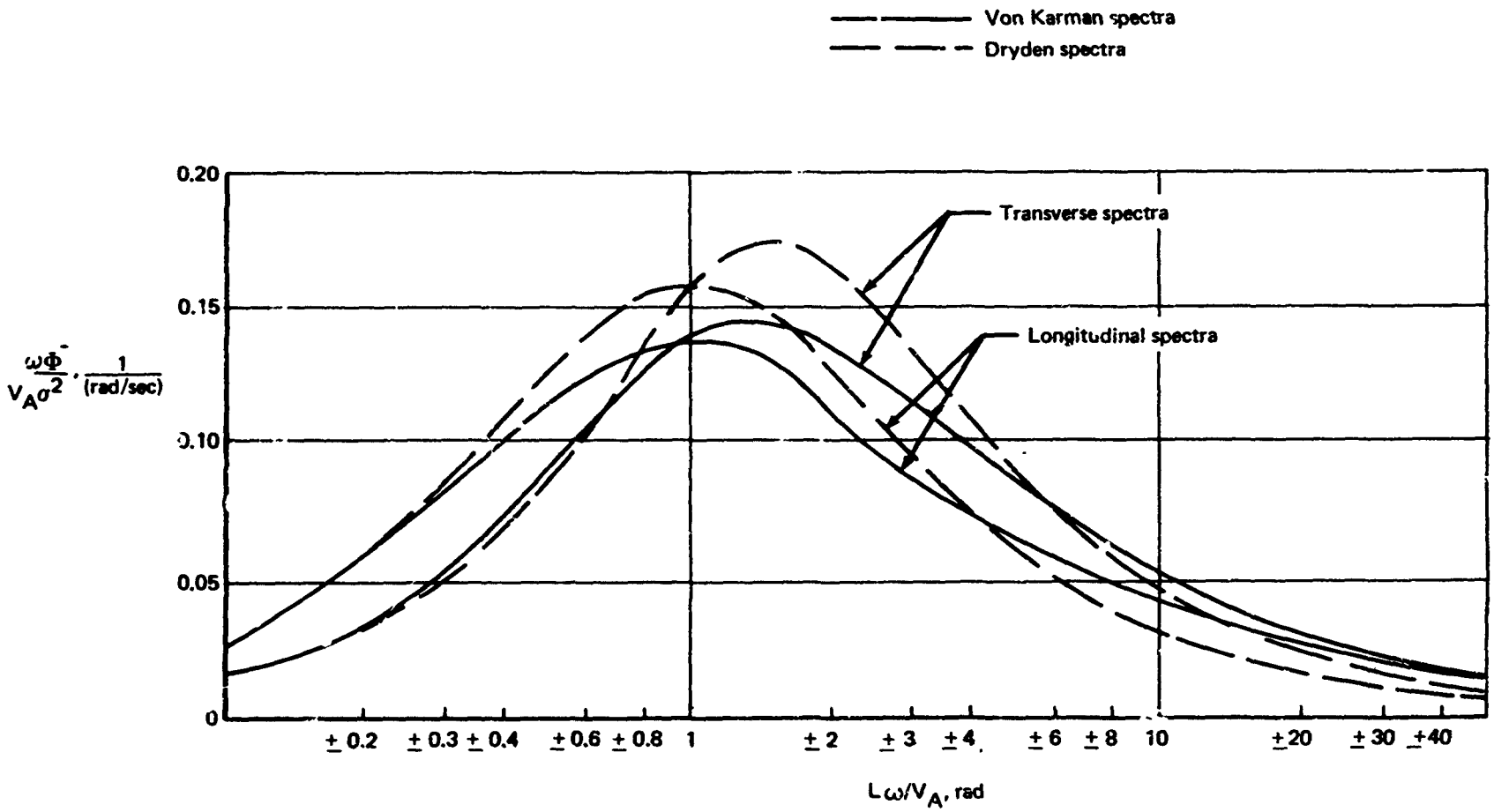

FIGURE 4-87.—COMPARISON: DRYDEN AND VON KARMAN VARIANCE DENSITY

$$G_u(s) = \sigma_H \sqrt{\frac{L_H}{\pi V_A}} \quad \frac{1 + 0.25\frac{L_H}{V_A}s}{(1 + 1.19\frac{L_H}{V_A}s)(1 + 0.167\frac{L_H}{V_A}s)}$$

$$G_v(s) = \sigma_H \sqrt{\frac{L_H}{2\pi V_A}} \quad \frac{(1 + 2.618\frac{L_H}{V_A}s)(1 + 0.12981\frac{L_H}{V_A}s)}{(1 + 2.083\frac{L_H}{V_A}s)(1 + 0.823\frac{L_H}{V_A}s)(1 + 0.08977\frac{L_H}{V_A}s)}$$

$$G_w(s) = \sigma_V \sqrt{\frac{L_V}{2\pi V_A}} \quad \frac{(1 + 2.618\frac{L_V}{V_A}s)(1 + 0.12981\frac{L_V}{V_A}s)}{(1 + 2.083\frac{L_V}{V_A}s)(1 + 0.823\frac{L_V}{V_A}s)(1 + 0.08977\frac{L_V}{V_A}s)}$$

FIGURE 4-88.—TURBULENCE FILTERS

The required transformations have been discussed previously and are presented on Figure 4-92.

4.5.5 Aerodynamic Parameters

The aerodynamic parameters are those upon which aerodynamic forces and moments are dependent and can be represented by suitable modifications of the velocity distributions over the airplane.

The velocity distribution about the airplane is represented by four parts, made up of combinations of mean wind or turbulence, and point lift or distributed lift effects. It is generally necessary to provide separate buildups of wing-body (where the primary body effects are considered to come from the carryover of wing lift) and tail forces and moments for turbulence simulation during landing approach.

The effective linear velocities at the center of gravity used for wing-body aerodynamics are made up of the sum of the mean wind components and the turbulence components:

$$u_{W_{CG}} = u_W + u_T$$

$$v_{W_{CG}} = v_W + v_T$$

$$w_{W_{CG}} = w_W + w_T$$

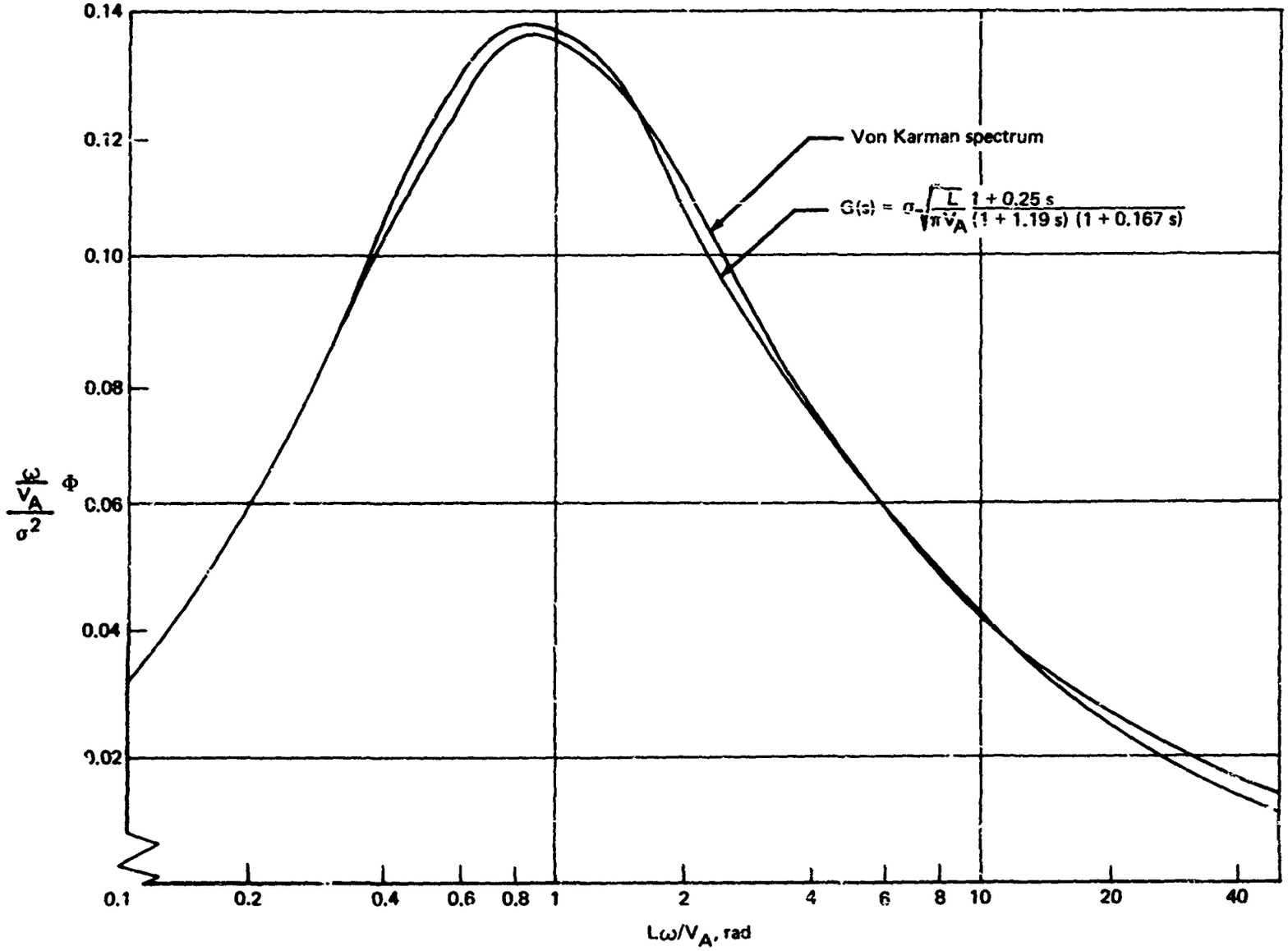

FIGURE 4-89.—APPROXIMATE LONGITUDINAL TURBULENCE FILTER ACCURACY

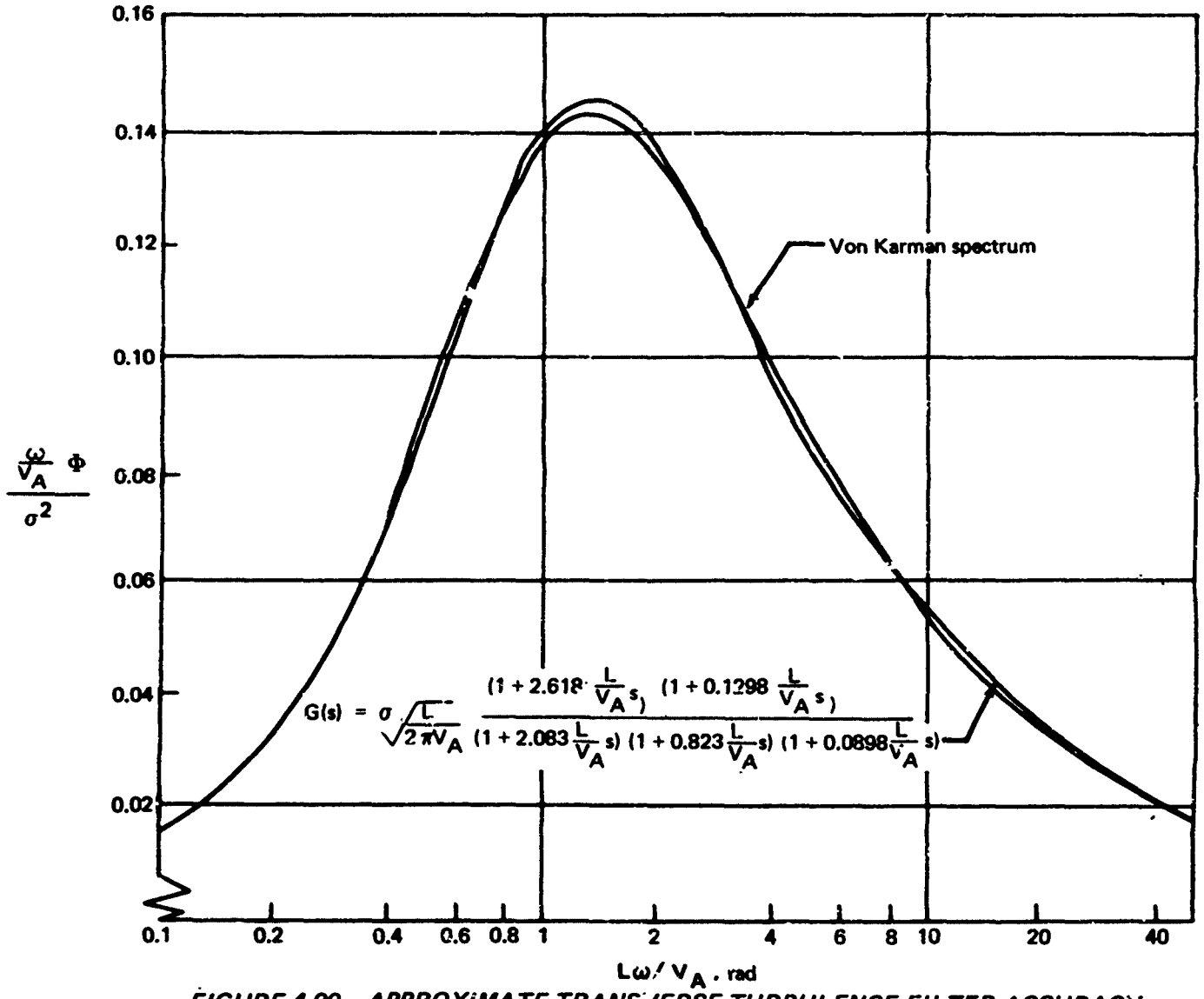

FIGURE 4-90.—APPROXIMATE TRANSVERSE TURBULENCE FILTER ACCURACY

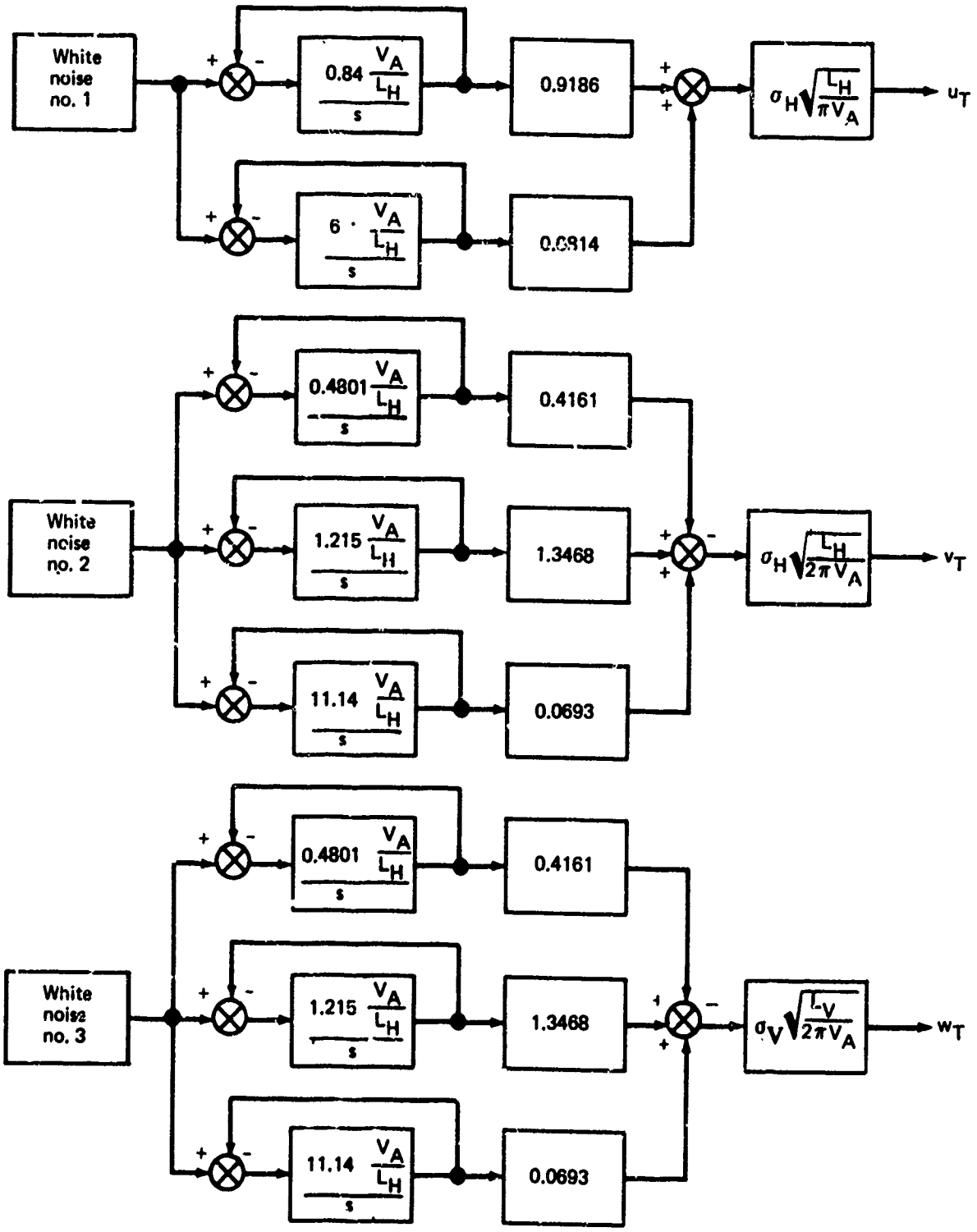

FIGURE 4-91.–SCHEMATIC FOR TURBULENCE FILTERS

BODY AXIS MEAN WIND COMPONENTS

$$\begin{Bmatrix} \bar{u}_W \\ \bar{v}_W \\ \bar{w}_W \end{Bmatrix} = \begin{Bmatrix} \cos(\psi - \bar{\psi}_W)\cos\theta \\ \cos(\psi - \bar{\psi}_W)\sin\theta\sin\phi - \sin(\psi - \bar{\psi}_W)\cos\phi \\ \cos(\psi - \bar{\psi}_W)\sin\theta\cos\phi + \sin(\psi - \bar{\psi}_W)\sin\phi \end{Bmatrix} \bar{V}_W$$

BODY AXIS MEAN WIND SHEAR COMPONENTS

$$\begin{Bmatrix} \frac{\partial \bar{u}_W}{\partial h} \\ \frac{\partial \bar{v}_W}{\partial h} \\ \frac{\partial \bar{w}_W}{\partial h} \end{Bmatrix} = \begin{bmatrix} \cos(\psi - \bar{\psi}_W)\cos\theta & \sin(\psi - \psi_W)\cos\theta \\ \cos(\psi - \bar{\psi}_W)\sin\theta\sin\phi - \sin(\psi - \bar{\psi}_W)\cos\phi & \sin(\psi - \psi_W)\sin\theta\sin\phi + \cos(\psi - \psi_W)\cos\phi \\ \cos(\psi - \bar{\psi}_W)\sin \quad \cos + \sin(\psi - \bar{\psi}_W)\sin\phi & \sin(\psi - \psi_W)\sin\theta\cos\phi - \cos(\psi - \psi_W)\sin\phi \end{bmatrix} \begin{Bmatrix} \frac{d\bar{V}_W}{dh} \\ \bar{V}_W \frac{d\bar{\psi}_W}{dh} \end{Bmatrix}$$

BODY AXIS TURBULENCE COMPONENTS

$$u_{A_p} = \left[\cos\alpha\cos\beta\cos\theta + \sin\beta\sin\theta\sin\phi + \sin\alpha\cos\beta\sin\theta\cos\phi\right] V_{A_{CG}}$$

$$v_{A_p} = \left[\sin\beta\cos\phi - \sin\alpha\cos\beta\sin\phi\right] V_{A_{CG}}$$

$$\Delta\psi = -\tan^{-1}\frac{v_{A_{TG}}}{u_{A_{TG}}}$$

$$\begin{Bmatrix} u_T \\ v_T \\ w_T \end{Bmatrix} = \begin{bmatrix} \cos\Delta\psi\cos\theta & \sin\Delta\psi\cos\theta & -\sin\theta \\ \cos\Delta\psi\sin\theta\sin\phi + \sin\Delta\psi\sin\theta\sin\phi & \sin\Delta\psi\sin\theta\sin\phi + \cos\Delta\psi\cos\phi & \cos\theta\sin\phi \\ \cos\Delta\psi\sin\theta\cos\phi + \sin\Delta\psi\sin\phi & \sin\Delta\psi\sin\theta\cos\phi - \cos\Delta\psi\sin\phi & \cos\theta\cos\phi \end{bmatrix} \begin{Bmatrix} u_{T_{TG}} \\ v_{T_{TG}} \\ w_{T_{TG}} \end{Bmatrix}$$

FIGURE 4-92.—TRANSFORMATIONS

Effective body axis wind angular velocities for wing-body terms are related to the first order Taylor-series terms and have mean wind and turbulence contributions:

$$p_{W_{CG}} = \bar{p}_{W_{CG}} + p_T$$

$$q_{W_{CG}} = \bar{q}_{W_{CG}} + q_T$$

$$r_{W_{CG}} = \bar{r}_{W_{CG}} + r_T$$

where

$$\bar{p}_{W_{CG}} = \frac{\partial \bar{w}_W}{\partial y} = \frac{\partial \bar{w}_W}{\partial h}\frac{dh}{dy} = -\frac{\partial \bar{w}_W}{\partial h}\cos\theta \sin\phi$$

$$\bar{q}_{W_{CG}} = \frac{\partial \bar{w}_W}{\partial x} = -\frac{\partial \bar{w}_W}{\partial h}\frac{dh}{dx} = -\frac{\partial \bar{w}_W}{\partial h}\sin\theta$$

There are two contributions to wing-body effective yaw rate: one due to the normal force variation in the chordwise direction and one due to the spanwise distribution of the longitudinal force.

$$\left(\bar{r}_{W_{CG}}\right)_Z = \frac{\partial \bar{v}_W}{\partial x} = \frac{\partial \bar{v}_W}{\partial h}\frac{dh}{dx} = \frac{\partial \bar{v}_W}{\partial h}\sin\theta$$

$$\left(\bar{r}_{W_{CG}}\right)_X = -\frac{\partial \bar{u}_W}{\partial y} = -\frac{\partial \bar{u}_W}{\partial h}\frac{dh}{dy} = \frac{\partial \bar{u}_W}{\partial h}\cos\theta \sin\phi$$

Only the penetration distributed lift effects of turbulence are represented. Thus,

$$P_T = 0$$

The remaining angular turbulence terms are obtained by filtering the linear turbulence components:

$$q_T = -\frac{1}{V_A}\frac{s}{1 + 2\bar{c}/\pi V_A s} w_T$$

$$(r_T)_Z = \frac{1}{V_A}\frac{s}{1 + 2\bar{c}/\pi V_A s} v_T$$

Linear wind accelerations are determined from the mean wind shear components and filtered derivatives of turbulence velocities, as done for the angular components, by recognizing that turbulence is represented as being variable only with distance:

$$\dot{u}_W = \frac{\partial u_W}{\partial x}\frac{dx}{dt} = \frac{\partial}{\partial x}\left[\bar{u}_W + u_T\right] V_{A_{CG}}$$

$$= \frac{\partial \bar{u}_W}{\partial h} \sin\theta \, V_{A_{CG}} + \left(\frac{s}{1 + 2\bar{c}s/\pi V_{A_{CG}}}\right) u_T$$

$$\dot{v}_W = \frac{\partial \bar{v}_W}{\partial h} \sin\theta \, V_{A_{CG}} + \left(\frac{s}{1 + 2\bar{c}s/\pi V_{A_{CG}}}\right) v_T$$

$$\dot{w}_W = \frac{\partial \bar{w}_W}{\partial h} \sin\theta \, V_{A_{CG}} + \left(\frac{s}{1 + 2\bar{c}s/\pi V_{A_{CG}}}\right) w_T$$

The effect of turbulence on the velocities at the tail derives from two sources: the direct effect of the turbulence velocities plus the effect of the wing-body on the tail, as measured in terms of downwash and sidewash.

No wing-body effect is provided for the longitudinal wind component. The turbulence at the tail is described in terms of that at the center of gravity, delayed by the amount of time required to traverse the distance equal to the tail length. Thus,

$$u_{W_{TAIL}} = \bar{u}_{W_{CG}} - \frac{\partial \bar{u}_W}{\partial x} \ell_T + \frac{\partial \bar{u}_W}{\partial z} z_T + u_T e^{-s\ell_T/V_A}$$

$$\frac{\partial \bar{u}_W}{\partial x} = \frac{\partial \bar{u}_W}{\partial h} \sin\theta$$

$$\frac{\partial \bar{u}_W}{\partial z} = -\frac{\partial \bar{u}_W}{\partial h} \cos\theta \cos\phi$$

Downwash and sidewash reduce the magnitude of angle of attack and sideslip at the tail and are assumed to be linearly related to wing lift and side force, respectively. Wing lift and side force are in turn assumed to be determined significantly only by angle-of-attack and sideslip angle. That is, the wing-body effects on the tail due to turbulence are:

$$(\Delta w_T)_{TAIL} \cong -(\Delta\epsilon)\, u_T\, e^{-s\ell_T/V_A}$$

$$\Delta\epsilon = \frac{\partial\epsilon}{\partial\alpha_{WB}}\left[\frac{C_{L_{WB}}}{\alpha_{WB}}(s)\right]\frac{w_T}{u_T} = \frac{\partial\epsilon}{\partial\alpha}\frac{w_T}{u_T}\,K(s)$$

$$(\Delta w_T)_{TAIL} = -\frac{\partial\epsilon}{\partial\alpha}\, w_T\, K(s)\, e^{-s\ell_T/V_A}$$

Similarly,

$$(\Delta v_T)_{TAIL} = -\frac{\partial\sigma}{\partial\beta}\, v_T\, K(s)\, e^{-s\ell_T/V_A}$$

The transport lag accounts for the time required for the downwash to reach the tail, and no additional contributions of the tail to $\dot{\alpha}$ and $\dot{\beta}$ derivatives are to be used. The total expressions for the wind velocity vertical and lateral components are:

$$v_{W_{TAIL}} = \bar{v}_W - \frac{\partial\bar{v}_W}{\partial x}\,\ell_T + \frac{\partial\bar{v}_W}{\partial z}\,z_T + \left[1 - \frac{\partial\sigma}{\partial\beta}K(s)\right] v_T\, e^{-s\ell_T/V_A}$$

$$\frac{\partial\bar{v}_W}{\partial x} = \frac{\partial\bar{v}_W}{\partial h}\sin\theta \quad , \quad \frac{\partial\bar{v}_W}{\partial z} = -\frac{\partial\bar{v}_W}{\partial h}\cos\theta\cos\phi$$

$$w_{W_{TAIL}} = \bar{w}_W - \frac{\partial\bar{w}_W}{\partial x}\,\ell_T + \frac{\partial\bar{v}_W}{\partial z}\,z_T + \left[1 - \frac{\partial\epsilon}{\partial\alpha}K(s)\right] w_{T_{CG}}\, e^{-s\ell_T/V_A}$$

$$\frac{\partial\bar{w}_W}{\partial x} = \frac{\partial\bar{w}_W}{\partial h}\sin\theta \quad , \quad \frac{\partial\bar{w}_W}{\partial z} = -\frac{\partial\bar{w}_W}{\partial h}\cos\theta\cos\phi$$

When the lengths from the wing-body aerodynamic center to the aerodynamic centers of the vertical and horizontal tails are significantly different, the side velocity should be based on the vertical tail arm, the vertical velocity should be based on the horizontal tail arm, and two longitudinal velocity terms should be computed. Generally, unless the horizontal and vertical tails are on opposite ends of the airplane, the tail arms will be close enough to warrant using an average length (for canards, tail lengths are negative).

Neither tail lift growth nor the distribution of turbulence over the tail surfaces are accounted for, as their presumed relatively small dimensions make these effects insignificant.

One additional tail term has not yet been accounted for: the effective wind roll rate due to the vertical distribution of the lateral component of mean wind over the vertical tail. This term is:

$$p_{W_{TAIL}} = \bar{p}_{W_{TAIL}} = -\frac{\partial \bar{v}_W}{\partial z} = \frac{\partial \bar{v}_W}{\partial h} \cos\theta \cos\phi$$

From the wind and inertial velocity components, the effective velocities with respect to the air mass are developed:

Linear components	Angular components
Wing-body terms	
$u_{A_{CG}} = uW(s) - u_{W_{CG}} K(s)$	$p_{A_{CG}} = pW(s) - p_{W_{CG}} K(s)$
$v_{A_{CG}} = vW(s) - v_{W_{CG}} K(s)$	$q_{A_{CG}} = qW(s) - q_W K(s)$
$w_{A_{CG}} = wW(s) - w_{W_{CG}} K(s)$	$(r_{A_{CG}})_X = rW(s) - (r_{W_{CG}})_X K(s)$
$\dot{u}_{A_{CG}} = \dot{u}W(s) - \dot{u}_W K(s)$	$(r_{A_{CG}})_Z = rW(s) - (r_{W_{CG}})_Z K(s)$
$\dot{v}_{A_{CG}} = \dot{v}W(s) - \dot{v}_W K(s)$	$\dot{w}_{A_{CG}} = \dot{w}W(s) - \dot{w}_W K(s)$
Tail terms	
$u_{A_{TAIL}} = u_{TAIL} - u_{W_{TAIL}}$	$p_{A_{TAIL}} = p - p_{W_{TAIL}}$
$v_{A_{TAIL}} = v_{TAIL} - v_{W_{TAIL}}$	
$w_{A_{TAIL}} = w_{TAIL} - w_{W_{TAIL}}$	

Tail inertial and effective wind angular velocities for the use with rate derivatives, other than roll rate, do not appear explicitly but are involved in the computation of linear velocities at the tail.

The angle of attack and its time derivative, sideslip angle, airspeed, and dynamic pressure at both the wing and tail are determined from the linear airspeed components by:

Wing	Tail
$V_{A_{CG}} = \sqrt{u_{A_{CG}}^2 + v_{A_{CG}}^2 + w_{A_{CG}}^2}$	$V_{A_{TAIL}} = \sqrt{u_{A_{TAIL}}^2 + v_{A_{TAIL}}^2 + w_{A_{TAIL}}^2}$
$\bar{q}_{CG} = \frac{\rho}{2} V_{A_{CG}}^2$	$q_{TAIL} = \frac{\rho}{2} V_{A_{TAIL}}^2$
$\alpha_{CG} = \tan^{-1} \frac{w_{A_{CG}}}{u_{A_{CG}}}$	$\alpha_{TAIL} = \tan^{-1} \frac{w_{A_{TAIL}}}{u_{A_{TAIL}}}$
$\beta_{CG} = \sin^{-1} \frac{v_{A_{CG}}}{V_{A_{CG}}}$	$\beta_{TAIL} = \sin^{-1} \frac{v_{A_{TAIL}}}{V_{A_{TAIL}}}$

$$\dot{\alpha}_{CG} = \frac{u_{A_{CG}} \dot{w}_{A_{CG}} - w_{A_{CG}} \dot{u}_{A_{CG}}}{u_{A_{CG}}^2 + w_{A_{CG}}^2}$$

$$\dot{\beta}_{CG} = \frac{\left(u_{A_{CG}}^2 + w_{A_{CG}}^2\right) \dot{v}_{A_{CG}} - v_{A_{CG}} \left(u_A \dot{u}_{A_{CG}} + w_A \dot{w}_{A_{CG}}\right)}{V_{A_{CG}}^2 \sqrt{u_{A_{CG}}^2 + w_{A_{CG}}^2}}$$

The appropriate Küssner and Wagner lift growth filters, K(s) and W(s), are determined from Table 4-2 and/or Figure 4-30, according to the three-dimensional wing-body lift curve slope. The Küssner lift growth function can correctly modify the total center of gravity wind components, or the sum of turbulence and mean wind, rather than just the turbulence component. The difference will be negligible as the mean wind along the flight path will not change fast enough to cause significant attenuation.

The transport lags are perhaps easiest to represent in a digital computer by storing past values. The maximum error, by this method, is an error of the time delay equal to half the frame time. Then, if 10 rad/sec is representative of the maximum frequency of interest, the error can be expressed as a phase angle:

$$\Delta\phi = \omega\Delta t/2 = 5\Delta t$$

for $\Delta t = 40$ milliseconds and $\Delta\phi = 0.2$ rad = 11.5°.

An alternate technique, if it is known that large percentage changes of airspeed do not occur, is to use two deterministic processes for generating the noise. The starting numbers are adjusted so the noise sequences are displaced by time equal to the transport lag. Then, one noise source is used for wing-body turbulence and the delayed source for turbulence at the tail. This method may be particularly attractive for analog simulations using digital shift register noise generators.

If neither of the above transport lag methods is feasible, filter approximations to the transport lag, such as those on Figure 4-29, may be used.

The equations for the aerodynamic parameters for th wing-body and the tail are collected and presented on Figures 4-93 and 4-94, respectively.

4.5.6 Aerodynamic Forces and Moments

The aerodynamic forces and moments are built up by first building up the separate wing-body forces and moments, based on their respective aerodynamic parameters. For example, pitching moment may be built up by

$$M = C_{M_{WB}}(\alpha_{CG}, \delta_{c_{WB}}, q_{WB})\,\bar{q}s + \ell_H\, C_{Z_H}(\alpha_H, \delta_{c_H})\, q_H S_H$$

The subscript H refers to horizontal tail characteristics and $\delta_{c_{WB}}$ and δ_{c_H} refer to control surfaces assigned to the wing-body and the tail. With the exception of the effective tail roll rate, caused by the vertical gradient of wind over the vertical tail, tail contributions to moments are found from the tail forces and the moment arms. The contributions of the tail roll rate, in terms of linear derivatives are

$$\Delta Y = \left(C_{Y_p}\right)_V p_{A_{TAIL}}\, \bar{q}_H S$$

$$\Delta L = \left(C_{l_p}\right)_V p_{A_{TAIL}}\, \bar{q}_H S b$$

$$\Delta N = \left(C_{N_p}\right)_V p_{A_{TAIL}}\, \bar{q}_H S b$$

where the subscript V refers to the vertical tail contribution and where the coefficients ar. based on wing area.

There are two wing-body yaw rate effects: the chordwise change of the wing normal force, and the spanwise force distribution change due to the difference in forward speed along the span, referred to as the Z and X effects. Wing-body yaw rate derivatives are identified as to their source and combined by

$$\Delta C_{l_{WB}} = \left(C_{l_{r_{WB}}}\right)_X \left(r_{A_{WB}}\right)_X + \left(C_{l_{r_{WB}}}\right)_Z \left(r_{A_{WB}}\right)_Z$$

When it is determined that the aerodynamics are sufficiently linear, the inertial velocity effects on motion may be represented by total airplane coefficients and the incremental effects of winds by separate wing-body and tail effects.

Upon development of the aerodynamic forces and moments, their application in the equation of motion is conventional.

	Airspeed components		Inertial contribution		Wind contribution				
			Inertial velocities	Wagner lift growth filter	Mean wind components		Turbulence components		Küssner lift growth function
Linear components	$u_{A_{CG}}$	=	u	$W(s)$	$-[\bar{u}_W$	+	u_T	]	$K(s)$
	$v_{A_{CG}}$	=	v	$W(s)$	$-[\bar{v}_W$	+	v_T	]	$K(s)$
	$w_{A_{CG}}$	=	w	$W(s)$	$-[\bar{w}_W$	+	w_T	]	$K(s)$
Angular components	$p_{A_{CG}}$	=	p	$W(s)$	$-\left[\frac{\partial \bar{w}_W}{\partial h}\cos\theta \sin\phi\right.$			]	$K(s)$
	$q_{A_{CG}}$	=	q	$W(s)$	$-\left[-\frac{\partial \bar{w}_W}{\partial h}\sin\theta\right.$	-	$\frac{1}{V_{A_{CG}}}\left(\frac{s}{1+2\bar{c}s/\pi V_{A_{CG}}}\right)w_T$	]	$K(s)$
	$(r_{A_{CG}})_x$	=	r	$W(s)$	$-\left[\frac{\partial \bar{v}_W}{\partial h}\cos\theta \sin\phi\right.$			]	$K(s)$
	$(r_{A_{CG}})_z$	=	r	$W(s)$	$-\left[\frac{\partial \bar{v}_W}{\partial h}\sin\theta\right.$	+	$\frac{1}{V_{A_{CG}}}\left(\frac{s}{1+2\bar{c}s/\pi V_{A_{CG}}}\right)v_T$	]	$K(s)$
Linear accelerations	$\dot{u}_{A_{CG}}$	=	$\dot{u}$	$W(s)$	$-\left[\frac{\partial \bar{u}}{\partial h}V_{A_{CG}}\sin\theta\right.$	+	$\left(\frac{s}{1+2\bar{c}s/\pi V_{A_{CG}}}\right)u_T$	]	$K(s)$
	$\dot{v}_{A_{CG}}$	=	$\dot{v}$	$W(s)$	$-\left[\frac{\partial \bar{v}}{\partial h}V_{A_{CG}}\sin\theta\right.$	+	$\left(\frac{s}{1+2\bar{c}s/\pi V_{A_{CG}}}\right)v_T$	]	$K(s)$
	$\dot{w}_{A_{CG}}$	=	$\dot{w}$	$W(s)$	$-\left[\frac{\partial \bar{w}}{\partial h}V_{A_{CG}}\sin\theta\right.$	+	$\left(\frac{s}{1+2\bar{c}s/\pi V_{A_{CG}}}\right)w_T$	]	$K(s)$

$$V_{A_{CG}} = \sqrt{u^2_{A_{CG}} + v^2_{A_{CG}} + w^2_{A_{CG}}} \qquad \bar{q}_{CG} = \frac{\rho}{2}V^2_{A_{CG}}$$

$$\alpha_{CG} = \tan^{-1}\left(\frac{w_{A_{CG}}}{u_{A_{CG}}}\right) \qquad \dot{\alpha}_{CG} = \frac{u_{A_{CG}}\dot{w}_{A_{CG}} - w_{A_{CG}}\dot{u}_{A_{CG}}}{u^2_{A_{CG}} + w^2_{A_{CG}}}$$

$$\beta_{CG} = \sin^{-1}\left(\frac{v_{A_{CG}}}{V_{A_{CG}}}\right) \qquad \dot{\beta}_{CG} = \frac{\left(u^2_{A_{CG}} + w^2_{A_{CG}}\right)\dot{v}_{A_{CG}} - v_{A_{CG}}\left(u_{A_{CG}}\dot{u}_{A_{CG}} + w_{A_{CG}}\dot{w}_{A_{CG}}\right)}{V^2_{A_{CG}}\sqrt{u^2_{A_{CG}} + w^2_{A_{CG}}}}$$

FIGURE 4-93.–WING-BODY BODY AXIS AERODYNAMIC PARAMETERS

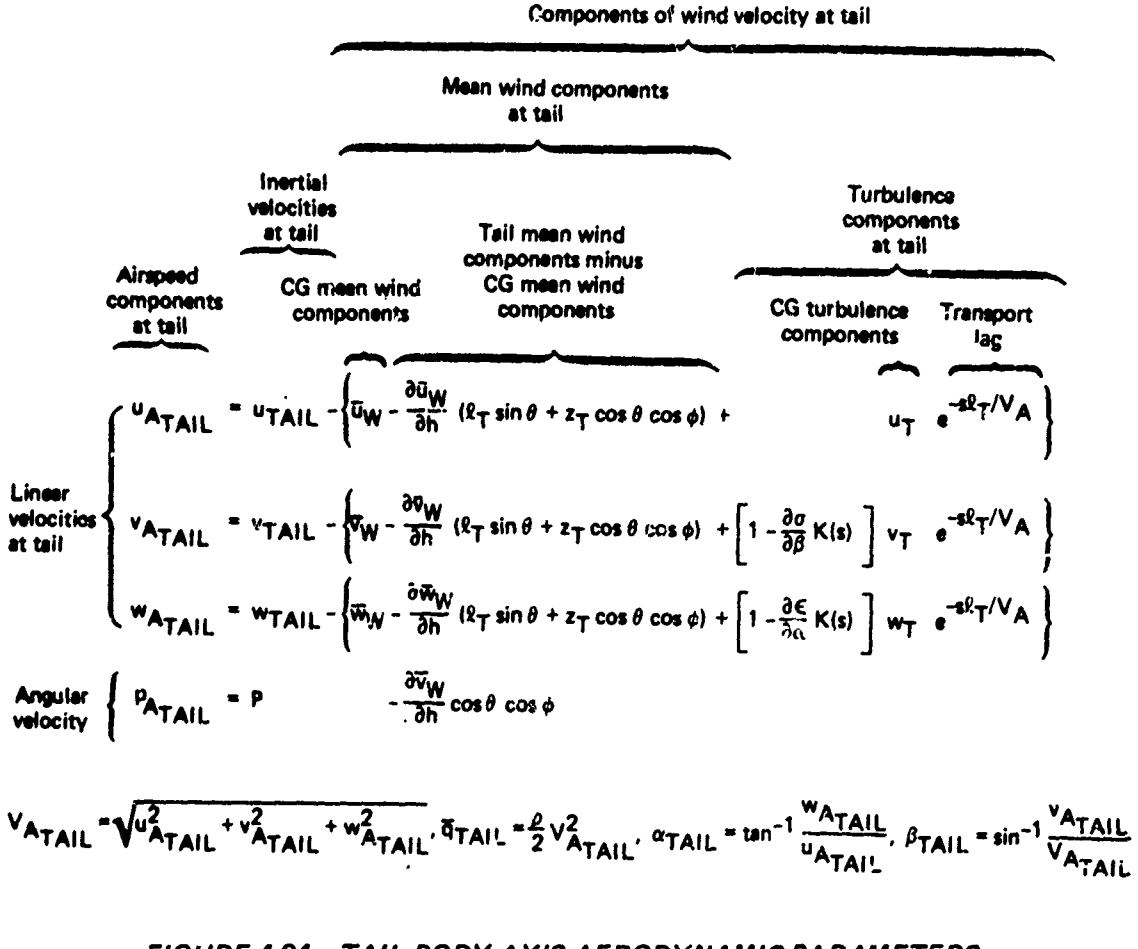

$$u_{A_{TAIL}} = u_{TAIL} - \left\{ \bar{u}_W - \frac{\partial \bar{u}_W}{\partial h} (\ell_T \sin\theta + z_T \cos\theta \cos\phi) + u_T \, e^{-s\ell_T/V_A} \right\}$$

$$v_{A_{TAIL}} = v_{TAIL} - \left\{ \bar{v}_W - \frac{\partial \bar{v}_W}{\partial h} (\ell_T \sin\theta + z_T \cos\theta \cos\phi) + \left[1 - \frac{\partial \sigma}{\partial \beta} K(s) \right] v_T \, e^{-s\ell_T/V_A} \right\}$$

$$w_{A_{TAIL}} = w_{TAIL} - \left\{ \bar{w}_W - \frac{\partial \bar{w}_W}{\partial h} (\ell_T \sin\theta + z_T \cos\theta \cos\phi) + \left[1 - \frac{\partial \epsilon}{\partial \alpha} K(s) \right] w_T \, e^{-s\ell_T/V_A} \right\}$$

$$p_{A_{TAIL}} = p - \frac{\partial \bar{v}_W}{\partial h} \cos\theta \cos\phi$$

$$V_{A_{TAIL}} = \sqrt{u^2_{A_{TAIL}} + v^2_{A_{TAIL}} + w^2_{A_{TAIL}}}, \quad \bar{q}_{TAIL} = \frac{\rho}{2} V^2_{A_{TAIL}}, \quad \alpha_{TAIL} = \tan^{-1} \frac{w_{A_{TAIL}}}{u_{A_{TAIL}}}, \quad \beta_{TAIL} = \sin^{-1} \frac{v_{A_{TAIL}}}{V_{A_{TAIL}}}$$

FIGURE 4-94.–TAIL BODY AXIS AERODYNAMIC PARAMETERS

4.5.7 Model Simplifications

A great number of simplifying assumptions have been applied to develop the model for two reasons:

1) The assumption was necessary to develop any model.

2) It was reasonably certain that making the assumption would not significantly alter the output spectrum and the output probability density distribution within the frequency region of concern for any aircraft.

For any particular airplane, there are undoubtedly additional suitable assumptions. The criteria for determining the suitability of an assumption continue to be the same: a simplification of assumption is acceptable, provided they do not cause significant changes of the probability distribution of the output motion nor cause significant changes of the output spectra for the relevant motion parameters.

There is one assumption in particular that is used almost universally for simulation–the assumption of neutral atmosphere. If this assumption can be made, a great number of wind

and turbulence model simplifications become possible. However, from the probability model, a narrow distribution of atmospheric stability at the surface about neutral occurs only for very high wind speeds. To ensure small levels of nonneutral stability, it must be valid to either consider only the mean level of stability at high wind speeds or to assume that only the altitudes very close to the surface are significant.

Using only mean conditions, or conditions very near the mean, implies that interest is in the mean response, or the responses near the mean, not in the whole of the distribution. Assuming mean conditions implies either that interest is not in failure probabilities or the more remote events, or it implies that the relationship between the mean response and the rest of the response distribution is known.

For those applications that are concerned with high mean wind levels, the following functions are simplified:

$$R_j = 0$$

$$l/\ell' = h/\ell' = 0$$

$$\phi(h/\ell') = \phi(0) = 1$$

$$f(h/\ell') = f(0) = 0$$

$$g(h/\ell') = g(0) = 1$$

$$\frac{u_{*0}/k}{\bar{V}_{20}}(R_j) = \frac{u_{*0}/k}{\bar{V}_{20}}(0) = \frac{1}{\ln \frac{20 + 0.15}{0.15}} = 0.20407$$

$$\sigma_V/u_{*0}(h/\ell') = \sigma_V/u_{*0}(0) = 1.3$$

$$d = 800 \frac{u_{*0}/k}{\bar{V}_{20}} \bar{V}_{20} = 163.3 \bar{V}_{20}$$

$$\frac{u_*}{u_{*0}} = 1 - \frac{h_W}{d} = 1 - \frac{h_W}{163.3 \bar{V}_{20}}$$

The model for the mean wind and the statistical turbulence parameters reduce to:

$$\frac{\partial \bar{V}_W}{\partial h} = \bar{V}_{20}\left(\frac{u_{*0}/k}{\bar{V}_{20}}\right)\frac{1}{h_W}\left(1 - \frac{h_W}{d}\right)$$

$$= 0.20407 \bar{V}_{20}/h - 0.00125$$

$$\bar{V}_W = \bar{V}_{20}\left(\frac{u_{*0}/k}{\bar{V}_{20}}\right)\left[\ln\left(\frac{h_W + 0.15}{0.15}\right) + f\left(\frac{h_W}{d}\right) - \frac{h_W}{d}\, g\left(\frac{h_W}{\ell'}\right)\right]$$

$$= 0.20407\, \bar{V}_{20} \ln\left(\frac{h_W + 0.15}{0.15}\right) - \frac{h_W}{800}$$

$$\sigma_V = \frac{\sigma_V}{u_*}\left(\frac{h}{\ell'}\right)\frac{u_*}{u_{*0}}\left(\frac{u_{*0}/k}{\bar{V}_{20}}\right) k\bar{V}_{20}$$

$$= 0.1061\, \bar{V}_{20} - h_W/1538.5$$

$$h_W = \begin{cases} h & , \ h < 163.3\, \bar{V}_{20} \\ 163.3\, \bar{V}_{20}, & h \geq 163.3\, \bar{V}_{20} \end{cases}$$

$$\sigma_H = \left(\frac{\sigma_H}{\sigma_V}\right)\sigma_V$$

$\frac{\sigma_H}{\sigma_V}$ given on Figure 4-85

$$L_V = \begin{cases} h & , \ h < 1000 \\ 1000, & h \geq 1000 \end{cases}$$

$$L_H = L_V\left(\frac{\sigma_V}{\sigma_H}\right)^3$$

For those applications for which it can be shown that the winds and turbulence at the higher altitudes have an insignificant effect, simplification results from assuming $h_W/d \cong 0$. Then, the function $g(h_W/\ell')$ is not needed and $h = h_W$. If this assumption is combined with the assumption of high wind levels, the mean wind, mean wind shear, and rms level for vertical turbulence reduce to:

$$\frac{\partial \bar{V}_W}{\partial h} = 0.20407\, \frac{\bar{V}_{20}}{h}$$

$$\bar{V}_W = 0.20407\, \bar{V}_{20} \ln\left(\frac{h_W + 0.15}{0.15}\right)$$

$$\sigma_V = 0.1061\, \bar{V}_{20}$$

Two other classes of simplifications are possible: those which can be shown to be conservative and those which can be shown to not significantly affect aircraft response.

Simplifications that normally would be conservative include:

- Deletion of lift growth (unsteady aerodynamics) representation.
- Use of the Dryden spectra.
- Deletion of h/d effects in the mean wind, mean wind shear, and the rms turbulence models.
- Constant rms levels for horizontal turbulence equal to that at the surface, but without corresponding changes of the horizontal integral scales.
- Assignment of the probability of exceeding $R_{i_{20}} = 1.0$ to the probability of incurring $R_{i_{20}} = 1.0$ (no turbulence exists for $R_{i_{20}} > 1.0$ and the shear at any altitude reduces for more stable conditions).

This list is not intended to be exhaustive. Conservatism imposes an economic penalty associated with overdesign. The list does not include the assumption of integral scales invariant with altitude. Although a single worst integral scale may be found for a single touchdown parameter and a particular airplane, the critical integral scale will vary from airplane to airplane, with approach speed, and with different touchdown parameters. When normal acceleration feedbacks are in danger of saturation due to turbulence, short integral scales are critical. When touchdown rates of sink are near those causing structural failure of the landing gear, integral scales causing maximum turbulence power near the short period become critical. For touchdown dispersions, critical integral scales tend to be longer. For excessive attitudes at touchdown, still another critical integral scale (or scales) would be specified.

Simplications that might be shown to not significantly affect airplane response or touchdown performance for a particular airplane include:

- Small angle approximations to the transformations.
- Separate longitudinal and lateral-directional simulations.
- Represent gust penetration (longitudinal distributed lift effects) by effective turbulence pitch and yaw rates rather than separate wing and tail buildups with a transport lag or use a point representation rather than using any distributed lift representation. Simpler distributed lift representations are possible with higher airspeeds and shorter tail lengths.

These simplifications are generally nonconservative and would require substantiation. Linear analysis might be sufficient for substantiating distributed lift simplifications.

4.6 ANALYSIS OF TOUCHDOWN PERFORMANCE

Traditionally, adequate touchdown performance has been demonstrated by generating distribution curves for each of the parameters. Then it is shown from these distribution curves that the probability of exceeding a critical value is more remote than required. For example, compliance for longitudinal touchdown dispersion may be shown by generating from a simulator the probability distribution for touchdown points relative to a nominal point. If the probability of exceeding 1500 feet from the nominal point is less than 0.01, the airplane-autoland system is acceptable.

This procedure should then be repeated for all significant parameters:

- Longitudinal touchdown dispersion
- Lateral touchdown dispersion
- Rate of sink at touchdown to ensure structural limits are not exceeded
- Pitch attitude–excessive angles at touchdown can cause structural problems due to the tail or the nose gear striking first
- Bank angles–excessive angles of touchdown may cause wing tip or nacelle strikes
- Crab angles–excessive angles may cause structural failure due to excessive side loads on the landing gear.

Data for each of the parameters may be collected singly or in combination with data collected for other parameters. A 3° longitudinal simulation may be run to collect data for the longitudinal parameters and another separate three-degree-of-freedom simulation may be run for the lateral-directional parameters. Even further breakdowns may occur: landings in mean wind and turbulence may be performed separately; separate landings for longitudinal and vertical turbulence may be performed.

For each type of simulation about 2,000 runs are required. For example, for a longitudinal simulation, 10 wind speeds with 100 runs each, plus 1000 runs at the maximum wind speed is likely. This gives at least 100 points associated with probabilities more remote than 10^{-2}. If the simulation is broken down only into longitudinal and lateral-directional simulations, 4000 runs are required. In order to perform this number of runs, it is necessary to use analog simulation so that time can be scaled. A common time scaling is 100 to 1.

In theory, a simulation of any complexity can be performed with analog simulators. In practice, the complexity of the simulation is restricted by the amount of time and equipment available. Hence, it is necessary to use analog simulation to enable the number of runs required, but in order to perform an analog simulation, it is necessary to simplify complex simulations. The choice may well be between an insufficient number of data points with an accurate model on a digital computer or a sufficient number of data points with an inaccurate model. The solution often results in a simplified model that is conservative. Conservatism, however, results in overdesign, which in turn results in economic penalties.

This procedure is objectionable because it does not account for the correlation of parameters. For example, do excess lateral dispersions occur at the same time that excess longitudinal dispersions occur? The acceptability of the airplane-autoland system is likely to be much different when they occur independently than when they appear together, for the number of unsafe landings for the number of total landings is altered.

Additionally, when the simulation is broken down into too many subsimulations, the dependence one performance parameter has upon more than one wind parameter may be ignored. For example, if longitudinal turbulence and the mean wind are simulated only to determine longitudinal dispersion and vertical turbulence is used only to determine rate of sink at touchdown, the dependence of dispersion upon vertical turbulence (caused because touchdown dispersion is the measure of longitudinal position at a specific altitude, altitude = 0) and the dependence of rate of sink on the horizontal winds (drag rise causes rate of sink to change with airspeed) are ignored.

All these problems may be alleviated if a sufficient number of points can be obtained efficiently from a digital simulation for which increased complexity does not impose so severe a problem. The following presents an approach that can be used with a digital simulator.

Consider each landing to be measured in terms of a success or a failure rather than in terms of quantitative measures of each parameter. A success occurs when each touchdown parameter is within its prescribed bounds. The objective is to ensure that the rate of failure (number of failures/number of landings) does not exceed a prescribed level. This objective is achieved if it can be shown that the probability of an airplane having a failure rate greater than a specified amount is remote.

Alternately, the question is: What is the probability that there will be r failures in n tests? The question is answered by the binomial distribution, which describes the probability of obtaining r occurrences in n tests when it is known that the average rate of occurrence for all possible tests is b:

$$P(r \text{ occurrences in } n \text{ tests}) = \frac{n!}{r!(n-4)!}\, b^r (1-b)^{n-r}$$

Now, to devise a test whereby n successive landings must be made without a failure, r is set to zero and the equation is solved for n

$$P = \frac{n!}{0!n!}\, b^0 (1-b)^{n-0} = (1-b)^n$$

$$n = \frac{\log(P)}{\log(1-b)}$$

For example, if unsafe landings may occur only once in 100 landings (b = 0.01), and we do not want the probability of accepting an airplane having a failure rate greater than 0.01 to be greater than 10%,

$$n = \frac{\log(0.1)}{\log(0.99)} = 229$$

That is, at least 229 landings must be performed without any failures to ensure an acceptable airplane-autoland system for a simulation containing six-degree-of-freedom motion and all wind and turbulence parameters.

Figure 4-95 shows that the probability of accepting a configuration with an excessive failure rate can be reduced substantially with a moderate rise in the number of landings that must be performed. For example, the number of runs required for 0.01 probability is 459. A very low probability of accepting a configuration with an excessive failure rate is not required, for if such a configuration were erroneously accepted, the probability that the failure rate for such a configuration was much greater than that required would be remote.

The choice of a 10% probability of accepting a configuration having an unacceptably large failure rate was arbitrary and implies that the probability of rejecting a configuration having a better-than-required failure rate is as much as 90%. The selection of a probability of accepting an unsatisfactory failure rate should result by balancing the costs of overdesign against the consequences of not meeting a specific failure rate. It is conceivable that a higher probability is appropriate. Allowing a finite probability for accepting a configuration with excessive failure rates is not a relaxation of requirements compared to the traditional method; the dispersion associated with a specified exceedance probability is not known with certainty. The probability of accepting a configuration having a greater actual dispersion at the specified exceedance probability can be calculated.

The computer time comparison for the digital simulation example requiring 229 runs and the analog simulation requiring 4000 runs with a 100-to-1 time scaling is

$$\frac{\text{Digital simulation time}}{\text{Analog simulation time}} = \frac{229}{4000/100} = 5.725$$

No accounting for any time scaling on digital computers was made, although some time scaling is generally possible. A time saving occurs if the tolerances on other items are run simultaneously with the wind simulation. For example, winds and turbulence may be run simultaneously with a simulation of localizer and glideslope errors.

For a 130-knot approach speed on a 3° glideslope, the mean rate of sink will be 11.5 ft/sec. For an approach begun from 500 feet, each approach and landing requires 43.5 seconds plus some additional time for the trim and flare. Using 50 seconds per landing, 229 runs can be performed in 3.18 hours. This amount of time is certainly feasible for a digital simulation, particularly because no on-line monitoring is required. In fact, a number 10 or 20 times as large would be feasible for certification.

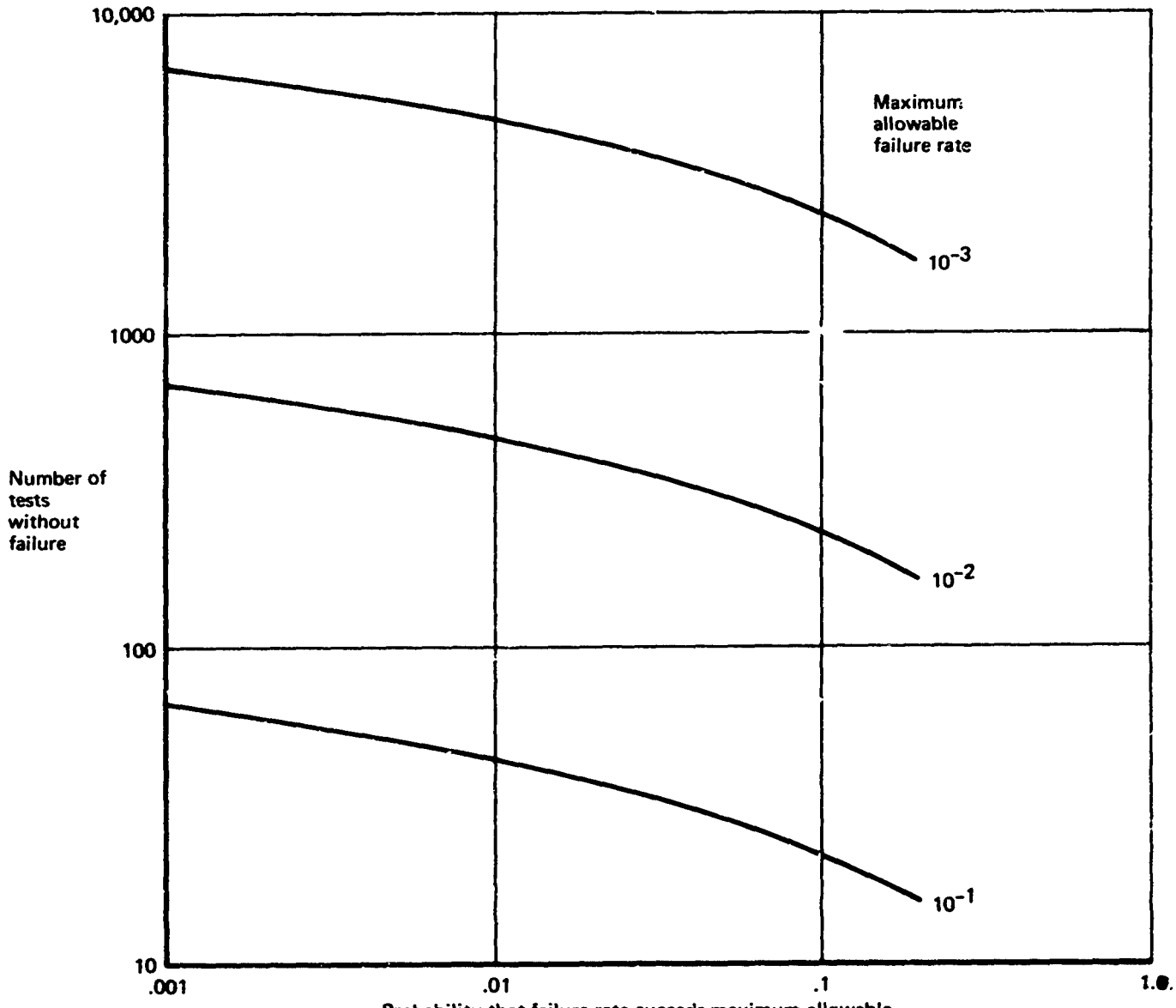

FIGURE 4-95.—NUMBER OF DIGITAL SIMULATION RUNS REQUIRED FOR SIMULATION

With a little more sophisticated thinking, the number of digital simulator runs required can further be reduced. When Richardson's number at an altitude of 20 feet exceeds 1.0, there is virtually no turbulence. Then, results are repeatable for a given wind speed, heading, and level of stability. With a few runs, boundaries for heading, wind speed, and Richardson's number can be determined such that inside the boundary there will never be a failure and outside the boundary there will always be a failure. From the data defining the probability distributions of heading, wind speed, and Richardson's number, the probabilities of being inside and outside the boundary can be determined, say P_1 and P_2. From the data in Section 3.3.3.1, the probability of exceeding $R_{i_{20}} = 1.0$ at Cape Kennedy is 53%. Then

$$\text{Probability of failure} = b = 0.47\, P_3 + 0.53(0 \cdot P_1 + 1 \cdot P_2)$$

$$P_3 = \frac{b - 0.53P_2}{0.47}$$

For $b = 10^{-2}$, $P_3 = 0.0212 - 1.129\, P_2$ = probability of failure for $R_{i_{20}} < 1$.

If it turned out that $P_2 = 0.005$, the number of runs required to evaluate all cases for which $R_{i_{20}} < 1.0$ would be

$$n = \frac{\log (0.1)}{\log [1 - (0.0212 - 1.129 \cdot 0.005)]} = \frac{\log (0.1)}{\log (0.9844)}$$

$$= 147 \text{ runs}$$

If fewer than 82 runs are required to establish the probability of failure given Richardson's number is greater than 1, a net savings in the number of runs required is realized.

The problem may also be partitioned according to wind speed. For high wind speeds, the distribution of Richardson's number at the surface is quite narrow about neutral conditions. Then, for high wind speeds, the neutral atmospheric stability model is applicable and the simulation model is greatly simplified. The low wind speed conditions may then be run on a digital simulator and the high wind speed conditions would be run on either digital or analog simulators.

In conclusion:

1) Evaluation of touchdown performance need not be performed by computing the exceedance probabilities for each touchdown parameter. Rather, each touchdown may be considered as a failure or success, depending on whether all parameters are within specified bounds. The latter approach leads to a significant savings of the number of landings required to ensure a satisfactory airplane-autoland system.

2) The reduced number of required runs enables the use of digital simulation.

3) The use of digital simulators enables simultaneous evaluation of all six degrees of freedom in the presence of all components of wind and turbulence and in the presence of other factors influencing touchdown performance, such as beam errors. This results in a reduction of the number of runs and time required.

4) The number of runs required can be reduced by partitioning the problem such as according to the level of atmospheric stability.

5) The time required to perform the evaluation on a digital computer as compared to traditional methods using an analog is efficient.

4.7 REFERENCES

1. Ashkenas, Irving L., and McRuer, Duane T., *Approximate Airframe Transfer Functions and Application to Single Sensor Control Systems,* Wright Air Development Center TR 58-82, June 1958.

2. Chalk, C. R., Neal, T. P., Harris, T. M.. and Prichard, F. E., *Background Information and User Guide for MIL-F-8785B (ASG), "Military Specification–Flying Qualities of Piloted Airplanes,"* Air Force Flight Dynamics Report AFFDL-TR-69-72, August 1969.

3. Stapleford, R. L., and Ashkenas, I. L., "Effects of Manual Altitude Control and Other Factors on Short-Period Handling Quality Requirements," AIAA Paper No. 579, 1967.

4. Ashkenas, I. L., and McRuer, Duane T., "A Theory of Handling Qualities Derived From Pilot-Vehicle System Considerations," IAS Paper No. 62-39, 1962.

5. Zbrozek, J. K., "Aircraft Behavior in a Vertical Gradient of Wind Velocity," *Aeronautical Quarterly,* Vol. XIV, Part 3, August 1963.

6. Gera, Joseph, *The Influence of Vertical Wind Gradients on the Longitudinal Motion of Airplanes,* NASA TND-6430, 1971.

7. Etkin, Bernard, *Dynamics of Atmospheric Flight,* John Wiley and Sons.

8. Houbolt, John C., and Sen, Asim, *Cross-Spectral Functions Based on Von Karman Spectral Equation,* NASA Contractor Report, NASA CR-2011, March 1972.

9. Franklin, James A., *Turbulence and Lateral-Directional Flying Qualities,* NASA Contractor Report, NASA CR-1718, April 1971.

10. Etkin, Bernard, *A Theory of the Response of Airplanes to Random Atmospheric Turbulence,* Institute of Aerophysics, University of Toronto, UTIA Report No. 54, May 1958.

11. Etkin, Bernard, *Dynamics of Flight*, New York, N Y., John Wiley and Sons, Inc., 1959.

12. Etkin, Bernard, *Theory of Flight of Airplanes in Isotropic Turbulence–Review and Extension*, Advisory Group for Aeronautical Research and Development, North Atlantic Treaty Organization, Report No. 372. April 1961.

13. Chalk, C. R., Neal, T. P., Harris, F. E., and Prichard, F. E., *Background Information and User Guide for MIL-F-8785B (ASG), "Military Specification–Flying Qualities of Piloted Airplanes,"* Technical Report AFFDL-TR-69-72.

14. Fung, Y. C., *An Introduction to the Theory of Aeroelasticity*, New York, N. Y., John Wiley and Sons, Inc., 1955.

15. Schaeffer, D. R., *Determination of Landing Approach Design Turbulence Levels for the Boeing 2707-300*, Boeing Document D6A12039-1TN, 1970.

16. Etkin, Bernard, "Effect of Wind Gradient on Glide and Climb," *Journal of Aeronautical Sciences*, Vol. 14, June 1947.

17. Melvin, W. W., "Effects of Wind Shear on Approach Couplers and Flight Directors," AIAA Paper No. 69-796, July 1969.

18. Thelander, J. A., *Aircraft Motion Analysis*, FDL-TDR-64-70, March 1965.

19. Reeves, P. M., *A Non-Gaussian Turbulence Simulation*, Technical Report AFFDL-69-67, December 1969.

20. Granino, A. K., *Random-Process Simulation and Measurements*, McGraw-Hill, Inc., 1966.

21. Elgenco, Inc., *Instruction Manual Model C1-66 Noise Generator.*

22. MacLaren, M. D., and Marsaglia, G., "Uniform Random Number Generators," *JACM*, Vol. 12, No. 1, January 1965, pp. 83-89.

23. Greenberger, M., "A Priori Determination of Serial Correlation in Computer Generated Random Numbers," *Math. of Comp.*, Vol. 15, 1961.

24. Greenberger, M., "Method in Randomness," *Comm. of ACM*, Vol. 8, No. 3, March 1965.

25. Coveyou, R. R., and MacPherson, D. R., "Fourier Analysis of Uniform Random Number Generators," *Journal of ACM*, Vol. 14, No. 1, January 1967.

26. Naylor, H. T., Balintfy, L. H., Burdick, S. D., and Chu, K., *Computer Simulation Techniques*, John Wiley and Sons, Inc., 1966.

27. Chambers, P. R., "Random-Number Generation," *IEEE Spectrum*, February 1967, pp. 48-55.

28. Hull, T. E., and Dobell, A. R., "Mixed Congruential Random Number Generators for Binary Machines," *Comm. of ACM*, VIII, No. 3, 1965, pp. 177-179.

29. Green, B. F., *Digital Computer in Research*, New York, McGraw-Hill, Inc., 1963.

30. Rand Corporation, *A Million Random Digits with 100,000 Normal Deviates*, New York, Free Press, 1955.

31. Marsagiia, G., and MacLaren, M. D., "A Fast Procedure for Generating Normal Random Variables," *Comm. of ACM*, Vol. VII, January 1964, pp. 4-10.

32. Advisory Circular No. 20-57A, *Automatic Landing Systems*, Department of Transportation, Federal Aviation Administration, January 1971.

APPENDIX 4A

DERIVATION OF GENERAL RELATIONSHIP BETWEEN INERTIAL AND AERODYNAMIC ANGLES

The ground track velocity vector (velocity vector in the plane of the earth) is equal to the u velocity component in the earth axis when heading is zero or the v velocity component in the earth axis when heading is 90°. Thus, the magnitude of velocity in the earth axis can be found from the body axis to earth axis transformation:

$$V_{E_{GT}} = u_E \big|_{\psi=0} = v_E \big|_{\psi=90°}$$

$$= u \cos\theta + v \sin\theta \sin\phi + w \sin\theta \cos\phi$$

Rate of sink is also found by transforming body axis inertial velocity components to the earth axis:

$$\dot{h} = -w_E = u \sin\theta - v \cos\theta \sin\phi - w \cos\theta \cos\phi$$

By definition:

$$\tan\gamma = \frac{\dot{h}}{V_{E_{GT}}} = \frac{u \sin\theta - v \cos\theta \sin\phi - w \cos\theta \cos\phi}{u \cos\theta + v \sin\theta \sin\phi + w \sin\theta \cos\phi}$$

or

$$\sin\theta \,[v \tan\gamma \sin\phi + w \tan\gamma \cos\phi - u] = \cos\theta \,[-u \tan\gamma - v \sin\phi - w \cos\phi]$$

$$\tan\theta = \frac{[u \tan\gamma + v \sin\phi + w \cos\phi]}{u - v \tan\gamma \sin\phi - w \tan\gamma \cos\phi}$$

For components of wind defined in the body axis system (tail wind is $+u_W$, wind from left is $+v_W$ wind down is $+w_W$), inertial velocity and airspeed components are related by:

$$u = u_A + u_W$$

$$v = v_A + v_W$$

$$w = w_A + w_W$$

Airspeed components can be expressed in terms of angle of attack, sideslip angle, and total airspeed through the definition of the latter:

$$\tan\alpha = \frac{w_A}{u_A} \; ; \; -u_A^2 \tan^2\alpha + w_A^2 = 0$$

$$\sin\beta = \frac{v_A}{V_A} \; ; \; v_A^2 = V_A^2 \sin^2\beta$$

$$u_A^2 + v_A^2 + w_A^2 = V_A^2$$

In matrix form,

$$\begin{bmatrix} -\tan^2\alpha & 0 & 1 \\ 0 & 1 & 0 \\ 1 & 1 & 1 \end{bmatrix} \begin{Bmatrix} u_A^2 \\ v_A^2 \\ w_A^2 \end{Bmatrix} = \begin{Bmatrix} 0 \\ \sin^2\beta \\ 1 \end{Bmatrix} V_A^2$$

Solving simultaneously for u_A^2, v_A^2, and w_A^2 using Cramer's rule gives:

$$u_A^2 = V_A^2 \cos^2\alpha \cos^2\beta$$

$$v_A^2 = V_A^2 \sin^2\beta$$

$$w_A^2 = V_A^2 \sin^2\alpha \cos^2\beta$$

Thus,

$$u = u_W + V_A \cos\alpha \cos\beta$$

$$v = v_W + V_A \sin\beta$$

$$w = w_W + V_A \sin\alpha \cos\beta$$

The exact expression for pitch attitude is given as follows:

$$\tan\theta = \frac{\left\{\begin{array}{l}\frac{1}{V_A}\left[u_W \tan\gamma + v_W \sin\phi + w_W \cos\phi\right] + \left[\tan\gamma \cos\alpha \cos\beta\right. \\ \left. + \sin\beta \sin\phi + \sin\alpha \cos\beta \cos\phi\right]\end{array}\right\}}{\left\{\begin{array}{l}\frac{1}{V_A}\left[u_W - \tan\gamma\,(v_W \sin\phi + w_W \cos\phi)\right] + \left[\cos\alpha \cos\beta\right. \\ \left. - \tan\gamma\,(\sin\beta \sin\phi + \sin\alpha \cos\beta \cos\phi)\right]\end{array}\right\}}$$

For small $\alpha, \beta, \gamma, \theta, \phi$

$$\theta \cong \frac{\gamma + \alpha + \dfrac{u_W\gamma + v_W\phi + w_W}{V_A}}{1 + \dfrac{u_W}{V_A}}$$

Note that for still air conditions, this reduces to $\theta = \gamma + \alpha$.

If the body axis components of mean wind are due entirely to a wind whose vector lies in a horizontal plane, the body axis components are given by:

$$\begin{Bmatrix} u_W \\ v_W \\ w_W \end{Bmatrix} = \begin{Bmatrix} \cos(\psi - \bar{\psi}_W)\cos\theta \\ \cos(\psi - \bar{\psi}_W)\sin\theta\sin\phi - \sin(\psi - \psi_W)\cos\phi \\ \cos(\psi - \bar{\psi}_W)\sin\theta\cos\phi - \sin(\psi - \psi_W)\sin\phi \end{Bmatrix} \bar{V}_W$$

where $\bar{V}_W$ and $\bar{\psi}_W$ are the magnitude and heading of the wind, respectively ($\bar{\psi}_W = 0$ is a wind from the south, to the north).

Substituting these expressions into the exact expression for $\tan\theta$ gives:

$$\tan\theta = \frac{\left\{\begin{array}{l}\frac{\bar{V}_W \cos(\psi - \bar{\psi}_W)}{V_A}\left[\tan\gamma\cos\theta + \sin\theta\right] \\ \left. + \tan\gamma \cos\alpha \cos\beta + \sin\beta \sin\phi + \sin\alpha \cos\beta \cos\phi\right]\end{array}\right\}}{\left\{\begin{array}{l}\frac{\bar{V}_W \cos(\psi - \bar{\psi}_W)}{V_A}\left[\cos\theta - \tan\gamma \sin\theta\right] \\ \left. + \cos\alpha \cos\beta - \tan\gamma\left[\sin\beta \sin\phi + \sin\alpha \cos\beta \cos\phi\right]\right]\end{array}\right\}}$$

This is not a closed form expression for tan θ. Assuming small α, β, θ, ϕ, and γ yields:

$$\theta = \left[1 + \frac{\bar{V}_W \cos(\psi - \bar{\psi}_W)}{V_A}\right]\gamma + \alpha$$

Thus, for still air or a pure crosswind, $\theta = \gamma + \alpha$. A tail wind reduces the pitch attitude required to hold a glideslope (negative γ).

The exact equation for pure longitudinal motion ($\phi = \beta = \psi - \bar{\psi}_W = 0$) reduces to

$$\bar{V}_W \tan\gamma = V_A [\sin(\theta - \alpha) - \tan\gamma \cos(\theta - \alpha)]$$

or

$$\tan\gamma = \frac{\sin(\theta - \alpha)}{\frac{\bar{V}_W}{V_A} + \cos(\theta - \alpha)}$$

and the body components of wind are

$$\bar{u}_W = \bar{V}_W \cos\theta$$

$$\bar{w}_W = \bar{V}_W \sin\theta$$

The differential relationship is

$$\delta\bar{V}_W \tan\gamma_0 + \frac{\bar{V}_{W_0}}{\cos^2\gamma_0}\delta\gamma = \delta V_A [\sin(\theta_0 - \alpha_0) - \tan\gamma_0 \cos(\theta_0 - \alpha_0)$$

$$- \frac{V_{A_0} \cos(\theta_0 - \alpha_0)}{\cos^2\gamma_0}\delta\gamma + V_{A_0} [\cos(\theta_0 - \alpha_0) + \tan\gamma_0 \sin(\theta_0 - \alpha_0)] (\delta\theta - \delta\alpha)$$

or

$$\delta\bar{V}_W \tan\gamma_0 - \delta V_A \frac{\bar{V}_{W_0} \tan\gamma_0}{V_{A_0}} + \delta\gamma \left[\frac{\bar{V}_{W_0} + V_A \cos(\theta_0 - \alpha_0)}{\cos^2\gamma_0}\right]$$

$$= V_{A_0} [\cos(\theta_0 - \alpha_0) + \tan\gamma \sin(\theta_0 - \alpha_0)] (\delta\theta - \delta\alpha)$$

APPENDIX 4B

BODY AXIS-RELATIVE WIND AXIS VECTOR TRANSFORMATION

Rotate through β, from stability axis to relative wind axis

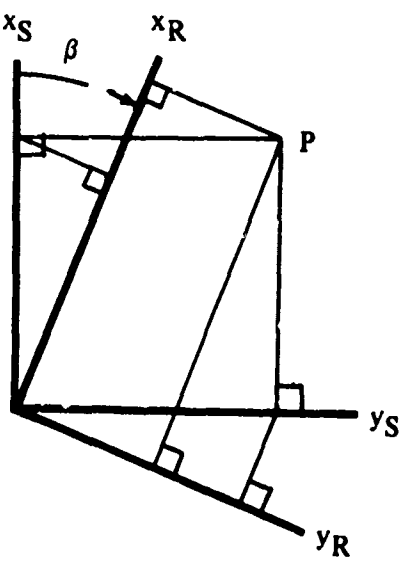

$$x_R = x_S \cos\beta + y_S \sin\beta$$

$$y_R = x_S \sin\beta + y_S \cos\beta$$

$$z_R = z_S$$

or,

$$\begin{Bmatrix} x_R \\ y_R \\ z_R \end{Bmatrix} = \begin{bmatrix} \cos\beta & \sin\beta & 0 \\ -\sin\beta & \cos\beta & 0 \\ 0 & 0 & 1 \end{bmatrix} \begin{Bmatrix} x_S \\ y_S \\ z_S \end{Bmatrix} = \begin{bmatrix} \text{S to R} \end{bmatrix} \begin{Bmatrix} x_S \\ y_S \\ z_S \end{Bmatrix}$$

combine transformations:

$$\begin{Bmatrix} x_R \\ y_R \\ z_R \end{Bmatrix} = \begin{bmatrix} \text{S to R} \end{bmatrix} \begin{Bmatrix} x_S \\ y_S \\ z_S \end{Bmatrix} = \begin{bmatrix} \text{S to R} \end{bmatrix} \begin{bmatrix} \text{B to S} \end{bmatrix} \begin{Bmatrix} x \\ y \\ z \end{Bmatrix} = \begin{bmatrix} \text{B to R} \end{bmatrix} \begin{Bmatrix} x \\ y \\ z \end{Bmatrix}$$

$$\begin{bmatrix} \text{B to R} \end{bmatrix} = \begin{bmatrix} \cos\alpha\cos\beta & \sin\beta & \sin\alpha\cos\beta \\ -\cos\alpha\sin\beta & \cos\beta & -\sin\alpha\sin\beta \\ -\sin\alpha & 0 & \cos\alpha \end{bmatrix}$$

Angle of attack is the angle between the x body axis and the projection of the velocity vector on the x-z body axis plane. Sideslip angle is the angle the velocity vector makes with the x-z body axis plane. Hence there is an ordered sequence of rotations: rotate through α first, then through β.

Rotate through α, from body axis to stability axis

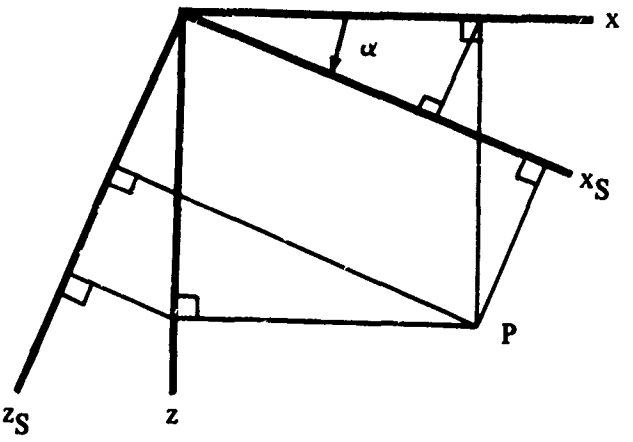

$$x_S = x \cos\alpha + z \sin\alpha$$

$$y_S = y$$

$$z_S = -x \sin\alpha + z \cos\alpha$$

or,

$$\begin{Bmatrix} x_S \\ y_S \\ z_S \end{Bmatrix} = \begin{bmatrix} \cos\alpha & 0 & \sin\alpha \\ 0 & 1 & 0 \\ -\sin\alpha & 0 & \cos\alpha \end{bmatrix} \begin{Bmatrix} x \\ y \\ z \end{Bmatrix} = \begin{bmatrix} \text{B to S} \end{bmatrix} \begin{Bmatrix} x \\ y \\ z \end{Bmatrix}$$